NASA SP-76

FACILITY FORM 602

N66-10226 (ACCESSION NUMBER)
749 (PAGES)
(NASA CR OR TMX OR AD NUMBER)

N66-10261 (THRU)
1 (CODE)
31 (CATEGORY)

FINAL REPORT ON THE RELAY I PROGRAM

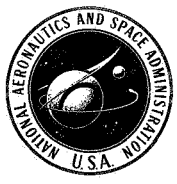
GPO PRICE $ 4.25
CFSTI PRICE(S) $
Hard copy (HC)
Microfiche (MF) 3.50
ff 653 July 65

NATIONAL AERONAUTICS AND SPACE ADMINISTRATION

NASA SP-76

FINAL REPORT ON THE RELAY I PROGRAM

Prepared by Goddard Space Flight Center,
Greenbelt, Maryland



Scientific and Technical Information Division 1965
NATIONAL AERONAUTICS AND SPACE ADMINISTRATION
Washington, D.C.

For sale by the Superintendent of Documents, U.S. Government Printing Office
Washington, D.C. 20402 Price $4.25

Contents

Chapter		Page
	Introduction	1
	PART I	
1	The Relay System	5
2	The Relay Spacecraft	21
3	Structural and Dynamic Considerations in the Spacecraft Design	29
4	Spacecraft Performance	63
5	The Microwave Repeater	91
6	The Telemetry System	129
7	The Command System	153
8	The Spacecraft Power Supply System	171
9	Spacecraft Environmental Testing	191
10	Ground Support Equipment	207
11	Systems Integration	227
12	Reliability Program	261
	PART II	
1	The Relay Experiment Plan	275
2	GSFC Relay Communications Satellite Test Station	289
3	The Relay Test Station Low Noise Receiving and Demodulation Systems	329
4	Relay System Operations	359
5	Spurious Signals in Satellite Command Systems	383
6	The Energetic Particle Environment of Relay I	403
7	Relay I Trapped Radiation Measurements	429
8	The Relay I Radiation Effects Experiment	449
9	The Andover Ground Station	469

Chapter		Page
10	Communications Experiments Conducted at Andover, Maine	477
11	The Nutley Ground Station	515
12	Results of Relay I Narrowband Experiments	525

PART III

1	GSFC Demonstrations	549
2	Rio de Janeiro Space Communications Station	561
3	The Pleumeur-Bodou Space Communications Station	575
4	Results of Tests Performed with Relay I at the Pleumeur-Bodou Space Communications Station	597
5	The Raisting Space Communications Station	633
6	Results of Tests Performed with Relay I at the Raisting Space Communications Station	641
7	Description and Results of Tests Performed at Fucino Earth Station with Relay I	647
8	The KDD Space Communications Station	657
9	Results of Tests Performed with Relay I at the KDD Space Communications Station	663
10	The Goonhilly Downs Space Communications Station	671
11	Results of Tests Performed with Relay I at Goonhilly Downs Space Communications Station	753

INTRODUCTION

Project Relay is the National Aeronautics and Space Administration's low-altitude, active repeater communication satellite project. The objectives of this program were to carry out communications experiments by satellite, to detect radiation particles in the Van Allen belt, and to determine the extent of radiation damage to solar cells and electronic components.

This report describes the history, technical developments and events concerned with Project Relay.

The application of satellites for providing long distance communication capabilities had been forecast for some time. Prior to 1960 NASA had pursued the development of passive satellites and demonstrated the feasibility of microwave satellite communications with the successful launch of the Echo satellite. The Department of Defense had conducted communication experiments using the active repeater satellites SCORE and Courier.

In November of 1960 NASA awarded a contract to the Space Technology Laboratories to conduct an accelerated study which would determine the technical characteristics of an experimental low-altitude, active communications satellite system capable of providing technology leading to a commercial communications satellite system. This study examined satellite equipment, modulation systems, satellite structure, thermal control, attitude control, power systems, tracking, telemetry, command, ground station configurations, and antennae for a communications satellite system. In addition, numerous orbit studies were conducted to examine viewing times between station pairs of possible ground station locations. Specifications were developed from this work for the Relay satellite.

In January of 1961, industry was briefed on the requirements of Project Relay and in May of 1961 a contract was awarded to the Radio Corporation of America, Astro-Electronics Division for the development of three flight spacecraft for Project Relay.

In addition to the primary communications equipment, instrumentation was also designed to measure the intensity and distribution of high and low energy electrons and protons in the space environment and to determine the extent of damage that these particles would cause to diodes and solar cells. Bell Telephone Laboratories and the State University of Iowa developed and built the radiation monitoring equipment under a NASA contract. Diode and solar cell damage experiments were developed by NASA/Goddard Space Flight Center.

During this period, great international interest was shown in the Relay program and foreign governments were invited to participate in communications experiments using the Relay satellite. Under agreements approved by the respective countries, communications organizations in the United Kingdom, France, West Germany, Italy, Brazil and Japan developed ground stations for participating in the Relay experiments. An International Ground Station Committee was formed for coordination and definition of the Relay system and communication experiments. The Ground Station Committee is chaired by L. Jaffe, Director of Communication and Navigation Programs, NASA Headquarters with D. G. Mazur of NASA/Goddard Space

Flight Center as alternate chairman. This membership includes the Relay Project and Assistant Project Managers, and a representative from each participating ground station. The capabilities and experiment requirements of the various countries represented an important contribution to the design of the Relay communication system, including the communications transponder in the spacecraft.

In addition to the participating overseas ground stations, the NASA contracted with the American Telephone and Telegraph Company and the International Telephone and Telegraph Company for their services and facilities at Andover, Maine, and Nutley, New Jersey, respectively, for performing experiments as defined by NASA.

Two NASA test stations, located at Mojave, California, and at the IT&T facility, Nutley, New Jersey, were developed for the Relay Project. These stations are utilized for commanding, receiving telemetry from the spacecraft, and running communications tests and experiments. These test stations were designed, built and operated by the Space Technology Laboratories under contract to NASA.

The first Relay spacecraft was launched on December 13, 1962 from the Atlantic Missile Range by a Delta vehicle. A near nominal orbit with a perigee of 712 nautical miles, apogee of 4020 nautical miles, inclination of 47.5 degrees, and a period of 185 minutes was achieved.

After experiencing some difficulty with one of the communication transponders, the spacecraft was brought successfully under control, and in January of 1963 technical tests and demonstrations were begun. These tests have continued for the lifetime of the satellite, and the objectives of the program have been met. Test results show that a satellite can be successfully used as a microwave repeater and that the results obtained are in full agreement with theory. Radiation has gradually affected the spacecraft power system, and damage measurements to selected solar cells have shown that N on P solar cells are more resistant to radiation than P on N cells. Some mapping of the electron and proton fields in the Relay orbit was also accomplished.

The papers which follow in the body of this report describe in detail the basic elements of the Relay system and the technical information gained from the project. This report is intended to satisfy the objective of enabling broad dissemination of information concerning Project Relay to the scientific and engineering community.

Part I of this report describes the major elements of the overall Relay system and the technical considerations leading to the design and development of the Relay satellite.

In Part II, the operational problems associated with an experimental satellite are discussed, and a detailed description is given of the Relay test stations, the U.S. communication stations, and the spacecraft radiation monitoring and damage experiments. This volume also contains the communications experiment results obtained by the U.S. ground stations in addition to giving results of the radiation experiments.

Part III of this report is a compilation of reports submitted to NASA by the international ground stations. These show the technical considerations and problems encountered in the development and operation of the overseas ground stations. The separate reports contained in this volume are substantially as submitted by the various international participants and provide station descriptions and results of experiments as conducted with the Relay satellite.

PART I

N66-10227

The Relay System

INTRODUCTION

The Relay project under the direction of NASA, Goddard Space Flight Center, has resulted in the successful operation of an experimental, active repeater, communication satellite for over a year. Results of the system studies started in November 1960 by STL preceded the project development and led to valid engineering compromises between the communication satellite performance objectives and the various system constraints and parameters discussed herein.

In the following material, relationships between the system parameters, constraints, and desired objectives will be discussed. Included are: a) the system design tradeoff areas, b) requirements of the orbit, c) communication system performance objectives, and d) the spacecraft transponder specification interface with the widely varied facilities and capabilities of the ground and test stations. Finally, typical link calculations are given with predicted performance margins for both wideband and narrowband operation.

Papers found in Parts II and III describe communication experiment results, facilitating comparison between predicted and actual values of signal levels and performance margins.

SYSTEM DESIGN TRADEOFFS

The Relay system design evolved with the solution of the interface problems and system tradeoffs related to the following major areas.

1. Ground station and test station design characteristics, including their geographical locations, antenna characteristics and receiving system noise temperatures.

2. Communication system baseband to baseband performance in accordance with minimally modified CCIR and CCITT requirements as necessitated by 1. above.

3. Spacecraft transponder configuration, effective radiated power output and antenna characteristics consistent with minimum weight and maximum efficiency.

4. Selection of an orbit that would provide:

   (a) Acceptable mutual visibility times between the stations for both East to West and North to South links consistent with spacecraft power system capability.

   (b) Traversal through radiation fields of sufficient intensity to permit assessment of radiation damage to semiconductor materials carried in the spacecraft radiation experiments.

   (c) Both (a) and (b) above to be consistent with the booster-vehicle capability when launched from the Atlantic Missile Range.

By virtue of almost two years of successful operation of the Relay system, it can be said that the major design tradeoffs had been adequately considered.

GROUND STATION AND TEST STATION DESIGN CHARACTERISTICS

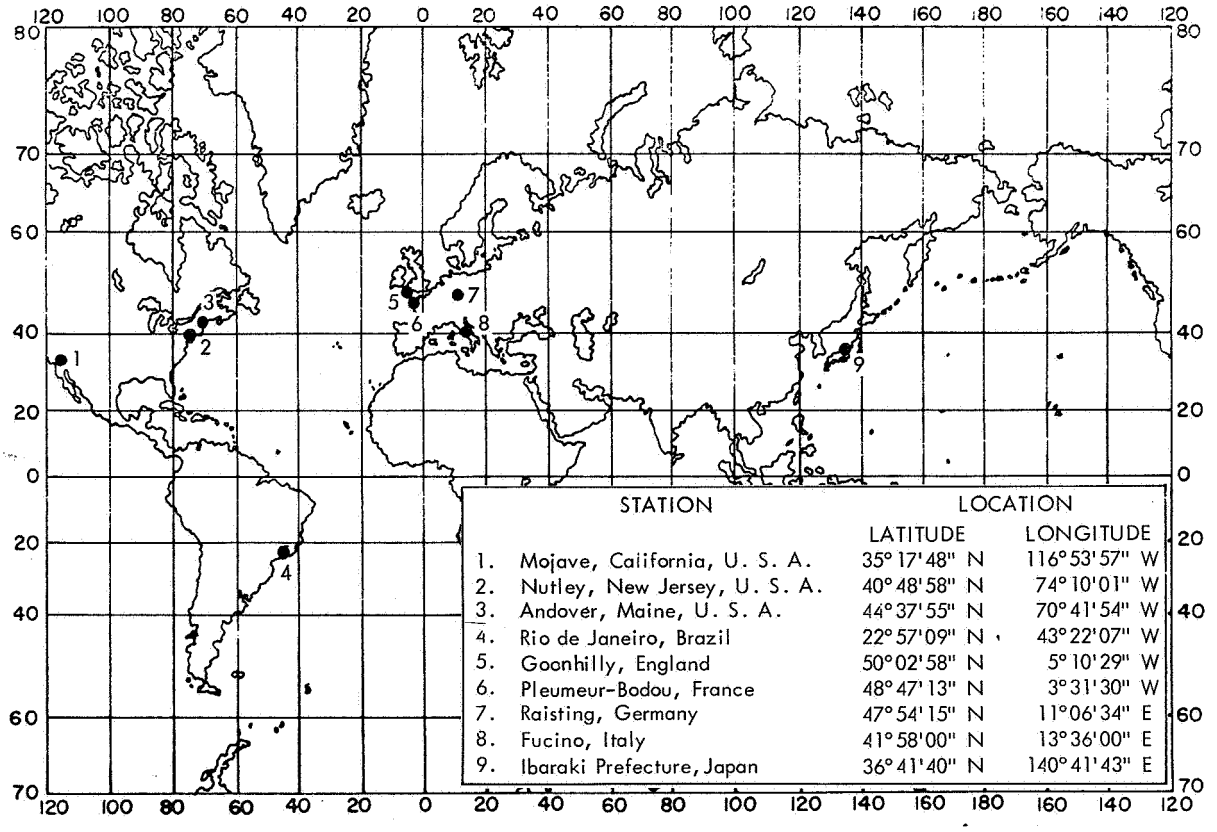
Figure 1–1 provides a means of viewing the geographical locations of the stations participating in the Relay program. Typical great-circle distances involved in the N–S link are in the order of 5000 statute miles, 4200 statute miles in the E–W link.

Table 1–1 lists the major station design characteristics upon which the system link calculations were based. Of particular note is the wide variation of system noise temperatures and antenna gains among the stations, within which bounds the varied communication requirements were to be met. It is appropriate to note that in the early design phases of the program only "best estimates" for antenna gains and noise temperatures were available in some cases. It was expected that as the stations became operational and refinements in equipment and measuring techniques were made, that the criteria of Table 1–1 would appear slightly pessimistic, thus adding to the system performance margins.

Since individual papers in Parts II and III provide details of all the participating stations, only the major station design characteristics and the manner in which they interfaced with the Relay system design are discussed here.

Frequency Selection

One major consideration given to the choice of the uplink frequency was that of minimizing the collimation error of ground transmitting and receiving antenna beams. It should be noted that, chronologically speaking, the stations were not operational at the time of frequency selection. Potential tracking error sources (servo system angular resolution, gear backlash, wind gust induced servo error, nonorthogonality of antenna



STATION		LOCATION	
		LATITUDE	LONGITUDE
1.	Mojave, California, U. S. A.	35° 17' 48" N	116° 53' 57" W
2.	Nutley, New Jersey, U. S. A.	40° 48' 58" N	74° 10' 01" W
3.	Andover, Maine, U. S. A.	44° 37' 55" N	70° 41' 54" W
4.	Rio de Janeiro, Brazil	22° 57' 09" N	43° 22' 07" W
5.	Goonhilly, England	50° 02' 58" N	5° 10' 29" W
6.	Pleumeur-Bodou, France	48° 47' 13" N	3° 31' 30" W
7.	Raisting, Germany	47° 54' 15" N	11° 06' 34" E
8.	Fucino, Italy	41° 58' 00" N	13° 36' 00" E
9.	Ibaraki Prefecture, Japan	36° 41' 40" N	140° 41' 43" E

FIGURE 1–1.—Geographical locations of stations participating in Project Relay.

TABLE 1–1.—*Relay Ground Station and Test Station Design Characteristics*

Station	Transmit and receive capability	Antenna	Receiver	Gain		Total system noise temp. at 7.5° elev.
				1725 Mc	4170 Mc	
Andover, Maine Ground Station.	One-way television and 300-channel telephony; two-way, 12 channel telephony	3600-ft² aperature horn, AZ–EL mount, under radome	4°K maser	50.2 db	57.6 db	50.8°K
Fucino, Italy Ground Station.	Receive 12-channel telephony	30-ft diam. Cassegrainian parabola, AZ–EL mount	Cooled parametric amplifier		48.6 db	220–250°K
Goonhilly Downs, England Ground Station.	One-way television and 300-channel telephony; two-way, 12 channel telephony	85-ft-diam. parabola, AZ–EL mount	Maser	50.7 db	58.4 db	100°K
Mojave, California Test Station.	Wideband test signals	40-ft-diam. parabola, X–Y mount	100°K cooled parametric amplifier	44 db	52 db	175°K
Nutley, New Jersey Test Station.	Wideband test signals	Same as Nutley Ground Station	120°K cooled parametric amplifier	42.9 db	51.1 db	200°K
Nutley, New Jersey Ground Station.	Two-way, 12-channel telephony	40-ft-diam. Cassegrainian parabola, AZ–EL mount	290°K parametric amplifier	42.9 db	51.1 db	420°K
Pleumeur-Bodou, France Ground Station.	One-way television and 300-channel telephony; two-way, 12-channel telephony	3600-ft² aperature horn, AZ–EL mount under radome	4°K maser	50.2 db	57.6 db	50.8°K
Rio de Janeiro, Brazil Ground Station.	Two-way 12-channel telephony	35-ft diam. Cassegrainian parabola, AZ–EL mount	290°K parametric amplifier	40.2 db	48.2 db	420°K

axes) were not finitely known. Compounding this was the variety in size and type of antennas which the Relay system had to accommodate.

Whereas the downlink (wideband) center frequency was prearranged by agreement between GSFC/NASA and BTL to be 4169.72 Mc, compatible with Telstar I 4 kMc tracking beacon, it was decided to utilize a lower uplink frequency to take advantage of the wider antenna beamwidth that results. Thus, tracking at 4 kMc and transmitting on the up-link at 2 kMc with twice the antenna beamwidth materially eased the beam collimation requirements.

The tracking geometry is illustrated in Figure 1–2; the analysis of this problem along with other tracking and acquisition considerations is available.*

**Project Relay Ground Station Acquisition and Tracking Considerations*, STL Document No. 8949–0012–NU–000.

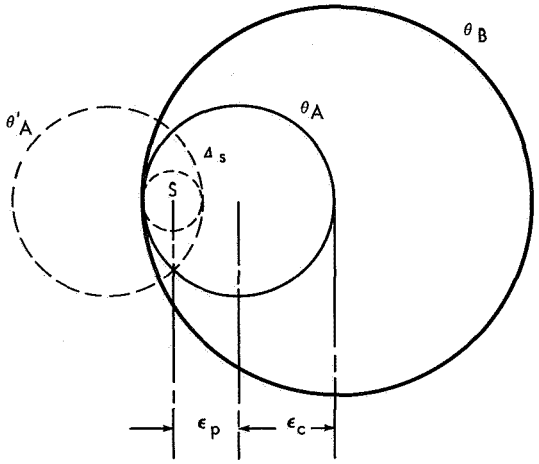


FIGURE 1–2.—Antenna pointing geometry.

S = Satellite uncertainty in the plane normal to antenna line of sight
Δ_S = Nominal satellite position
θ_A = Antenna beamwidth A (tracking), θ_B = antenna beamwidth B (transmitting)
θ'_A = Beamwidth A positioned at opposite limit
ϵ_P = Allowable pointing error
ϵ_c = Allowable RF collimation error for beamwidths A and B, $\theta_B > \theta_A$

$$\epsilon_c \leq \frac{\theta_B - \theta_A}{2}$$

The exact frequencies selected were therefore:

UPLINK (Ground-to-spacecraft)
1725.000 Mc for one-way television
1723.333 Mc for East-to-West and North-to-South } two-way
1726.667 Mc for West-to-East and South-to-North } telephony

DOWNLINK (Spacecraft-to-ground)
4169.72 Mc for one-way television
4164.72 Mc for East-to-West and North-to-South } two-way
4174.72 Mc for West-to-East and South-to-North } telephony

The additional advantage to be gained by the choice of a lower uplink frequency for transmission was that any 4 kMc waveguide used in a ground station receiving antenna system would be operating well below cutoff at the 2 kMc transmitting frequency, thus providing increased isolation for the sensitive receivers. Antenna feed systems could then be made simpler, obviating the need for diplexers and filters in some cases.

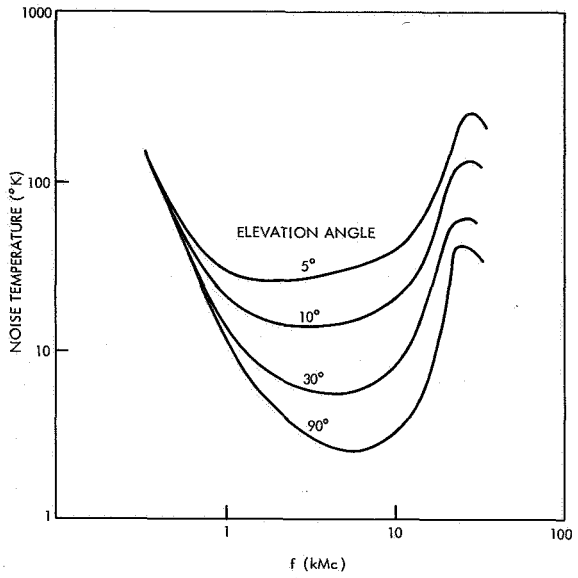


FIGURE 1–3.—Sky temperature.

Selection of these frequencies, as can be seen from Figure 1–3, is compatible with lower noise contributions from galactic and sky sources as well as water vapor and oxygen absorption effects.*

Power Level Considerations

During the system study phase of Relay, the link calculations were subjected to an iterative process as the requirements of ground and spacecraft transmitter power levels were being finalized. Previously, an extensive state-of-the-art study had been conducted by STL for GSFC in the field of power amplifying devices for spacecraft applications.** The applicability and availabil-

**Ground Station Factors Affecting Wideband Relay Link Parameters of the NASA Communications Satellite,* STL Document No. 8949–0001–NU–000.

***Project Relay Airborne Equipment Survey,* STL Document No. 8949–0010–NU–000.

ity of TWT's, planar triodes, and voltage tunable magnetrons were investigated.

Finally selected were a specially developed 10 kw Eimac klystron for the ground transmitter and a 10 w RCA traveling wave tube for the more critical downlink. The former was selected on the basis of minimizing any noise contribution on the uplink, thus providing some margin for spacecraft receiver noise figure degradation, with the adjunctive consideration that the weight penalty could be most conveniently carried in the ground equipment. The choice of TWT for the spacecraft was based on bandwidth, efficiency and low weight characteristics coupled to a power level that would enhance performance margins.

Both devices were engineering development tasks that could be completed and tested in consonance with the schedule for ground station and spacecraft completion. Therefore, NASA/GSFC outfitted both ground and test stations with identical 10 kw transmitters.

SPACECRAFT SPECIFICATION SUMMARY

There were four possible configurations for the overall Relay spacecraft proposed to NASA/GSFC in April 1961 as a result of STL studies.* Included were studies on a number of suggested configurations for the transponder.** A linear-translator, a frequency-multiplier and demodulator-remodulator were among those examined. Analyses of modulation systems, link parameters and satellite antennas, as outlined in the study reports were given considered judgement by NASA/GSFC. The redundant, multiplier transponder configuration was finally selected.

As design and development proceeded within the facilities of the spacecraft contractor, the detailed configuration of Figure 1–4 evolved.

A brief summary of the major spacecraft performance requirements is given below. Later papers in this volume will describe the spacecraft in detail.

Weight: 172 lb.

Stabilization: Spin, 150 rpm nominal (longitudinal), spin axis nominally 90 degrees to the sun vector.

Power System: P on N solar array (Relay I only) 60 mil silica shielding, 10.5 percent minimum efficiency cells at 30°C, AMO; sealed Ni-Cad batteries, 9 AH capacity, matched cells; unregulated output 28^{+5}_{-4} vdc with maximum 20 mv ripple; individual regulators for transponders, 22.5 vdc ± 1 percent; low power regulator for radiation experiment, 22.5 ±1 percent, common negative ground system. Continuous load requirements 5.5 watts, transponder load 92 watts for 36 minutes of operation in an orbital period of 163 minutes.

Telemetry System: Dual 136 Mc (nominal frequency) transmitters, individually commanded, with switchable modulation; 200 mw output with minimum of 24 to 33 vdc input, PCM/PM modulation, continuous operation capability at 0°C to +30°C, 0 to 5 volt telemetry data input signal level, with 2 to 5 volt range input causing RF carrier phase shift to 140 ±5 degrees; RFI performance requirements in accordance with MIL–I–26600. Antenna system to be shared with command system. Telemetry system inputs to be obtained via an encoder preceded by suitable signal conditioning circuits. Encoder contains 1–128 channel main multiplexer (primarily radiation experiment data inputs), 1–64 channel submultiplexer (primarily spacecraft instrumentation), 1–32 channel submultiplexer (solar cell radiation damage experiment data input), 1152 bits/sec data rate, split phase NRZ output format.

Command System: Frequency (about 150 Mc; redundant, 1μv sensitivity receivers and decoders; compatible with NASA PCM/PDM/AM/AM command format, 20 command capability with telemetered command verification; antennas shared with telemetry transmitters; continuously operable at tem-

---

**Ground Station Factors Affecting Wideband Relay Link Parameters of the NASA Communications Satellite,* STL Document No. 8949–0001–NU–000.

***Final Report—Project Relay Active Communications Satellite System Study, Volume I,* STL Document No. 8949–0004–RU–000.

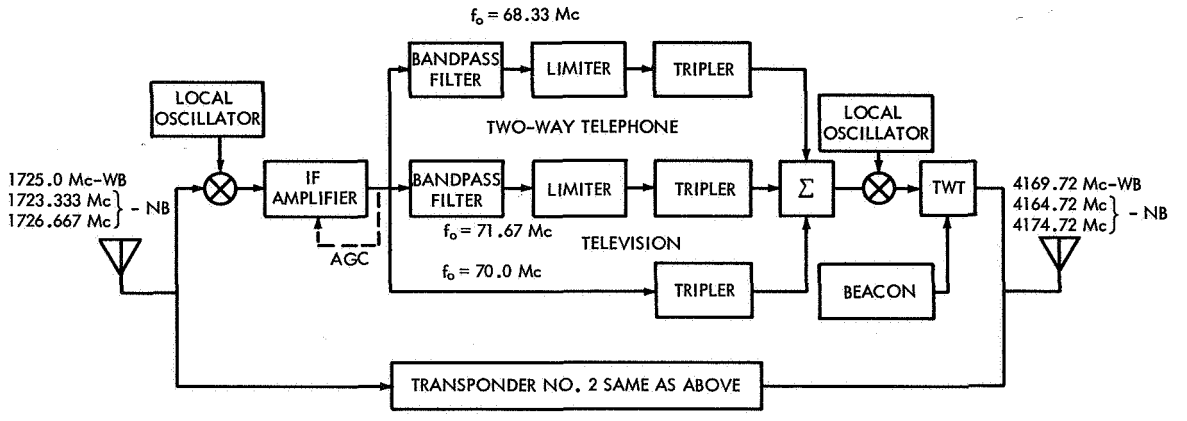


FIGURE 1–4.—Relay satellite transponder configuration.

peratures of 0 to 30°C with input voltage between 20 and 34 vdc. RFI performance compatible with MIL–I–26600 standards.

Wideband System: Two completely redundant systems, switchable on command; uplink frequency 1.725 kMc nominal center frequency; downlink frequency 4.170 kMc nominal center frequency; input signal dynamic range —40 to —80 dbm; output signal 10 watts nominal for TV, 4 watts for each carrier for two-way, twelve-channel telephony; hard-limiting, tripler configuration (Figure 1–4); FM modulation. Antenna polarization circular, right hand for receiving, left hand for transmitting, 70 db minimum isolation between transmitter and receiver; antenna gain greater than —1 db for look angles (θ) between 35 and 120 degrees; antenna VSWR's less than 2:1; receiver noise figure less than 14 db including 3 db input hybrid coupler; image rejection greater than 20 db; crosstalk in narrowband channels to be less than —55 dbm0 in CCIR group A or B channel; phase delay response over 23 Mc output bandwidth less than 50 nsec parabolic, 7 nsec linear, 5 nsec ripple, with ±5 percent matching characteristics from transponder to transponder; 4 kMc ±20 kc tracking beacon of 40 mw minimum effective radiated power.

Thermal Control: Both active (actuator-vane type) and passive. Component average temperature to be maintained between +5°C and +30°C.

*Attitude Control:** Active, torquing coil.

RELAY ORBIT CHARACTERISTICS

The Relay orbit was designed to meet the following requirements:

1. To maximize satellite mutual visibility above a 5-degree horizon between U.S. and Europe. A minimum of 100 minutes per day during the first 30 days was the achieved design objective.

2. To provide acceptable mutual visibility times for the test stations and smaller ground stations (see Figure 1–1 and Table 1–1).

3. To traverse a radiation environment suitable for evaluation by the on-board radiation experiments.

4. To minimize the simultaneous occurrence of mutual visibility times and eclipses.

5. The sun look angle was to lie between 90 ±15 degrees for the first 30 days in orbit with a maximum deviation of ±31 degrees for a year's orbit.

6. The launch trajectory was to be consistent with the range safety requirements at AMR.

Based on launch vehicle economics, payload weight and reliability, Relay was launched by a vehicle consisting of a Thor-Delta Block II first stage, an AJ10–118 second stage and an ABM–248 third stage, utilizing a low drag nose fairing.

*Perturbations in the spacecraft attitude were of so minor a nature that this system was not actively used.

Within the constraints outlined above, few orbital parameters were really open for judgment, as each minimized parameter choice. In general, operating time as a variable absorbed the influences of the various system constraints.

Allowable launch azimuths at AMR, within range safety boundaries, extend from nearly due east to about 108 degrees true. Using this southernmost pitch plane would lead to an orbital inclination of approximately 30 degrees.

Since a greater inclination was needed, a dog-leg launch trajectory was flown. Giving the upper stages a yaw angle-of-attack to the right caused the final velocity vector to be rotated such that the resulting orbit plane inclination was 47.5 degrees.

Several ground stations are at north latitudes in the 40–50 degree region, therefore, the 47.5 degree inclination was an acceptable compromise.

The Delta launch sequence involves two stages of powered flight, coasting to apogee of a transfer ellipse, then an injection burn of the final stage increases the velocity to greater than that required for a circular orbit at that altitude. Apogee on the transfer orbit becomes perigee on the final orbit, and the altitude of apogee in the final orbit is a function of the velocity in excess of circular velocity achieved at final burnout. Apogee and perigee altitudes for the resulting orbit are therefore influenced by the amount of energy used for rotating the velocity vector to control the inclination.

The 172 pound spacecraft was thus placed in a 4000 nautical mile apogee – 700 nautical mile perigee orbit which was inclined 47.5 degrees with respect to the equator. These three orbit parameters represent a good compromise between communication operation time and booster capability, with adequate launch vehicle performance and stability margins to insure a high probability of launch success.

Point-to-point communication via the Relay satellite is available only when the spacecraft is 5 degrees above horizons of both stations. It can be readily visualized that the farther the satellite is from either station the higher its altitude must be for mutual visibility. With ground stations in England, France, Germany, Italy, and the U.S. it is easy to visualize those periods when communication might be available across the Atlantic Ocean. The latitude of the ground track must be close to the latitude of the stations, depending upon the coincident altitude. At the same time the longitude of the ground track must be between the longitudes of the participating stations, again depending upon the altitude. With a ground station in South America, a similar discussion applies for mutual visibility to North America or to Europe.

For the Relay I satellite in the orbit previously discussed, the latitude, longitude, and altitude requirements for mutual visibility were met at least two or three times each day on successive revolutions. Adjacent communication passes were separated by the orbital period of approximately three hours, consistent with spacecraft power supply recharging capability. The exact amount of useful communication operation time was different on each pass, and the time of occurrence followed no simple pattern but was predicted by using computer computation for the orbit.

From the nature of the launch trajectory it is apparent that injection (perigee) occurs near the equator. Initially, therefore, apogee is also near the equator. One significant orbit perturbation, due to the oblate earth, is the motion of apogee. From its starting position, apogee progresses northward in the orbit plane at a rate which is a function of the size, shape, and inclination of the orbit, and of the oblateness of the gravitational potential field. For this orbit the apsidal rate was 1.2 degrees per day. Apogee therefore occurred at northern latitudes throughout the first five months in orbit. Obviously, the longest mutual visibility periods for the Atlantic link were available during this favorable interval, but a few months later with perigee at northern latitudes, operating time

on this link was greatly reduced.

Another feature of the Relay orbit which can be described in general terms is the occurrence of eclipse periods during some revolutions. On-board component temperatures and power supply capacity (maintained by solar cell energy conversion) are reduced during eclipse seasons. Since the most useful mutual visibility occurred when the spacecraft was near apogee, and most eclipses occur when near perigee, little communication time was lost due to coincidence of eclipse.

The other orbit perturbation resulting from the oblate gravity field is a rotation of the orbit plane about the polar axis. This nodal regression amounted to 1.3 degrees per day for the Relay orbit. A rather complex combination of nodal regression, apsidal rotation, and the earth's motion around the sun causes the length of eclipse seasons and the duration of eclipse on particular revolutions to be difficult to predict unless machine computations are used. It is nevertheless possible to visualize two other features of the eclipse geometry.

Due to the size of the orbit and the inclination of the orbit plane, there were periods when this plane made a large (maximum) angle with the earth-sun line. No eclipsing occurred for a time, the duration of which depended on whether apogee or perigee was nearest to the umbra. Also, consistent with other known constraints, when selecting the launch time, the eclipse experiences which were to affect system operation during the early weeks in orbit were somewhat controlled by specifying the lift-off time in the launch window, thus minimizing eclipses during early revolutions.

Relay, a spin-stabilized spacecraft, essentially maintained the same attitude it was given at injection. So far as the utilization of ambient solar energy is concerned, it would be preferred that this orientation be always normal to the ecliptic plane. Actually the orientation with respect to the earth is controlled by powered flight considerations. It is then a matter of accepting the annual sinusoidal variation in orientation angle between the spin-axis and the sun line which arises. A time-of-day for injection can be selected for any launch date in order to minimize this fluctuation in available solar energy. It was this parameter, rather than eclipse considerations, which governed the actual launch time.

With the inertially fixed spin-axis orientation, there arose one significant geometrical constraint on the communication usage of the Relay spacecraft: the satellite antenna gain pattern could limit the amount of mutual visibility time available for operations. As the vehicle moved along its orbit, the line-of-sight between ground and airborne antenna changed length and orientation with respect to the spin axis. Detailed planning of operating periods therefore required the selection of those sections of the geometrical mutual visibility periods when favorable antenna look angles were also available. The task of selection was given to the personnel of the Operations Center.

It is of interest to compare the prelaunch orbital element data with early tracking and elements computed by GSFC Data Systems Division after several days in orbit. It can be seen from Table 1–2 that the desired orbit was achieved with only minute deviation, to the credit of all concerned.

COMMUNICATION SYSTEM CHARACTERISTICS AND PERFORMANCE OBJECTIVES

The basic communication objective for Relay I was the transmission of television and telephony across the Atlantic and the transmission of telephony between North and South America via a satellite relay. In order to achieve this objective, certain system standards were adopted for the communication link.* Because the Relay program involved the cooperative efforts of many countries, as well as many industrial organizations within these countries, the standards selected for use in this system were the recommendations of the International Radio

**Project Relay I System Requirements*, GSFC/STL Document No. R1–0000.

TABLE 1-2.—*Relay Orbital Elements*

Elements	Prelaunch	Early tracking	Post launch	Units
Epoch	11 Dec. 62; 2350	13 Dec. 62; 2350	13 Dec. 62; 2350	----------
Semi-major axis	1.681	1.686	1.68673	earth radii
Eccentricity	0.285	0.2843	0.28427	----------
Inclination	47.77	47.47	47.48	degrees
Mean anomaly	00.00	0.8	0.754	degrees
Argument of perigee	176.43	177.5	177.543	degrees
Motion plus	1.20	1.212	1.2151	deg/day
R.A. of ascending node	217.22	218.74	218.742	degrees
Motion minus	1.28	1.278	1.2788	deg/day
Anomalistic period	184.36	185.09	185.09	minutes
Height of perigee	1296	1322	1321.94	km
Height of apogee	7407	7439	7438.59	km
Velocity at perigee	29408	----------	29353	km/hr
Velocity at apogee	16371	----------	16359	km/hr

Consultative Committee (CCIR). In particular, the CCIR document guiding the definition of the baseband-to-baseband system performance was *Documents of the IXth Plenary Assembly, Los Angeles 1959, Volume I, Recommendations.*

Due to certain pecularities of satellite systems in general and Project Relay in particular, some exceptions to CCIR recommendations were necessary. It is these exceptions, primarily, which will be emphasized in the following review of system characteristics and performance objectives.

System Characteristics

The primary characteristics of the Relay communication system involve the type of signals to be transmitted, along with their baseband structure, and the configuration of the link over which the transmission occurs.

Signal Structure

The two principal types of signals transmitted via the satellite are television and multi-channel telephony. The telephony transmissions may be further divided into a wideband, 300 channel, one-way mode and two narrowband, 12 channel, two-way mode.

Television transmission consists of a 3 Mc video signal accompanied by an audio channel on an FM subcarrier. The video portion of the signal conformed to the 525-line characteristics specified in CCIR Report No. 126, except for the reduction in baseband width from 4 Mc to 3 Mc. The peak-to-peak RF carrier deviation at the ground receiver due to the picture portion of the signal was made 9.6 Mc instead of the 5.6 Mc specified by CCIR Recommendation No. 276 in order to make maximal use of the threshold reduction properties of modulation-following demodulators.

The accompanying sound channel differs in several respects from CCIR Recommendation No. 272. The subcarrier on which the audio is transmitted was placed at 4.5 Mc in the baseband instead of the recommended 7.5 Mc. Such a change was necessary in order to compress the total RF bandwidth so that a klystron transmitter could be employed. Furthermore, a reduced baseband permits carrier demodulation with modulation-tracking receivers of reasonable bandwidth. Also, the deviation of the RF carrier produced by the unmodulated subcarrier was increased from ± 300 kc *rms* to 2.7 Mc peak-to-peak. This insures that the audio subcarrier discriminator operates above threshold whenever the RF demodulator is above threshold. In addition, the audio 3-db band-

width was reduced to 50–8000 cps and a standard 75 μ sec pre-emphasis was provided for optional use.

The multichannel telephony baseband structure is composed of either two separate groups of 12 two-way frequency division multiplex voice channels for narrowband operation or 300 one-way frequency-division multiplex voice channels for wideband operation. The baseband interconnections are made in accordance with CCIR Recommendation No. 269. For 12 channel operation, basic group A occupies the frequency band of 12–60 kc and basic group B the band from 60–108 kc. For 300 channels the baseband is 60–1300 kc. In order to make maximal use of the modulation-tracking demodulator in reducing spacecraft power, greater carrier deviations were required than those specified in CCIR Recommendation No. 274. Table 1–3 lists the deviations used for Project Relay. Pre-emphasis was used in accordance with CCIR Recommendation No. 275.

Link Description

The up-link portion of the satellite relay link operates at 1725 Mc. The ground transmitter has an output power capability of 10 kw and supplies an FM signal with the deviations listed in Table 1–3.

The satellite transponder, shown in Figure 1–4, receives this signal, amplifies and triples it, and then retransmits it to the ground at 4170 Mc. Simultaneous reception and transmission from two different ground stations, as required in two-way telephony, is accomplished in the transponder with two narrowband channels separated by 3.333 Mc in center frequency. The separation was accomplished on the ground with one terminal station shifting its transmitting frequency by 1.667 Mc, while the other station lowered its frequency by an equal amount. The use of separate amplifying channels insures that both signals enter the TWT at equal power levels, thereby preventing suppression of the weaker channel. Without this provision, differences in range and look angle between stations would make it necessary to program transmitter power to equalize the received power levels at the spacecraft.

TABLE 1–3.—*Frequency Deviations*

Television	Peak-peak deviation	
	Up-link	Down-link
Video, picture only	3.2 Mc	9.6 Mc
Video, picture plus sync	4.57 Mc	13.7 Mc
Audio subcarrier on carrier	0.90 Mc	2.7 Mc
Audio on subcarrier	200 kc	200 kc
Telephony	**RMS deviation per channel**	
	Up-link	Down-link
300 Channels	225 kc	673 kc
12 Channels (60–108 kc)	105 kc	314 kc
12 Channels (12–60 kc)	29.6 kc	88.8 kc

The frequency tripler in the spacecraft was chosen to provide a match between a high-power, narrowband ground transmitter and a lower-power, wideband spacecraft transmitter. Overall link performance is determined by the critical downlink, where limited transmitter power required the trading of bandwidth for power through high deviation FM. The ground transmitter, on the other hand, was limited by the bandwidth capability of its klystron. Deviation tripling in the spacecraft satisfied both constraints. A necessary consequence of the tripler was an increase in the up-link noise contribution by a factor of $(3)^2 = 9$ over its normal value. However, unlike typical microwave links, the up-link and down-link were not equal contributors to system noise because of the wide disparity in received carrier-to-noise density ratio at the spacecraft and ground receivers. Because of this disparity the up-link noise typically contributed less than 1–2 db to the total even though magnified by a factor of nine. The increase in output signal was 9.55 db so that the total performance quality was improved by 7–9 db through the use of the tripler.

On the ground the incoming signal is received at 4170 Mc and demodulated with either a conventional discriminator, a wideband phase-lock demodulator, or an FM

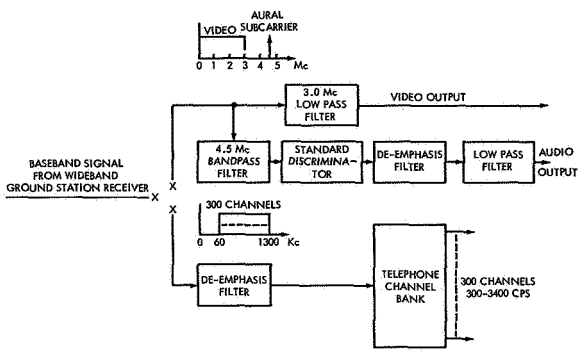


FIGURE 1–5.—Baseband arrangement for wideband mode.

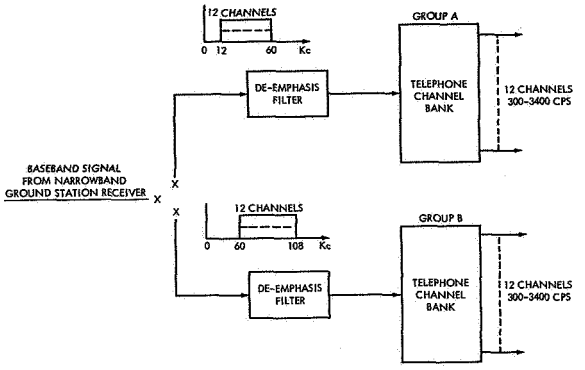


FIGURE 1–6.—Baseband arrangement for narrowband mode.

feedback demodulator. Following this demodulator is the baseband equipment shown in Figures 1–5 and 1–6 for the wideband and narrowband modes, respectively.

System Performance Objectives

The performance objectives for Relay I communication system coincided with the recommended CCIR requirements wherever possible. In some instances, however, the CCIR requirements could not be met by all ground stations, so that reduced objectives applicable to these stations had to be defined. Also, for the television audio channel it was necessary to define additional objectives to apply to parameters not covered by CCIR specifications.

Television

For the video channel, CCIR Recommendation No. 267 applied with two exceptions: the number of television lines and the signal-to-noise ratio for continuous random noise. The primary transmission for Project Relay was 525-line television. However, due to the limited spacecraft transmitter power and the resultant difficulty in attaining a wide baseband with comfortable margins, the communication link baseband-to-baseband was judged adequate for the 525-line signal of Project Relay if the transmission objectives for the 405-line system were met. The 405-line standard for required video signal-to-weighted-noise ratio could not be achieved by all ground stations at extreme spacecraft range and 7.5 degree elevation angle. As a consequence, instead of 50 db, a 43 db signal-to-weighted-noise ratio was considered acceptable for the Relay I experiment for these smaller stations. Provision was made for the optional use of video pre-emphasis for experimentation. When used, the 525-line pre-emphasis characteristic to CCIR Recommendation No. 277 applied.

At present CCIR has no specifications for performance of the television sound channel. However, using the video channel requirements of CCIR Recommendation No. 267 as a guide, reasonable objectives for the audio channel were established. Between the audio-to-audio interconnection points an insertion gain of 0 $\pm$1 db was specified with allowable short period variations of $\pm$0.3 db and medium period variations of $\pm$1.0 db. The minimum audio signal-to-noise ratio without pre-emphasis was set at 50 db when using a 9 dbm0 sinusoidal test tone (100 percent modulation). The peak-to-peak signal to peak-to-peak noise was specified as 50 db for periodic noise, while for impulsive noise it was specified as 25 db. The objective for harmonic distortion with modulation indices between 0.25 and 1.0 was 2 percent from 100–5000 cps and 3 percent from 5000 to 8000 cps.

Multi-Channel Telephony

Considering Project Relay an initial experiment in satellite communication, and further considering spacecraft power limita-

tions and the small size of certain ground installations, CCIR Recommendations Nos. 287 and 288 were viewed only as guides to system noise objectives for telephony. To accommodate the wide disparity in ground receiver capabilities, a double standard was established for telephony channel quality. For 12-channel operation, the thermal noise objective for Andover, Goonhilly, and Pleumeur-Bodou at 5000 nautical miles and 7.5 degrees elevation was 7500 pw, psophometrically weighted, measured at a point of zero relative level. For the remaining stations this objective was increased to 50,000 (psoph) pw. The objective for 300-channel operation was 20,000 (psoph) pw. Total intermodulation noise in any telephone channel at a point of zero relative level was limited to 7500 (psoph) pw for all stations. A summary of the total telephony noise objectives at 5000 nautical miles and 7.5 degrees elevation is given in Table 1–4.

COMMUNICATION LINK PERFORMANCE MARGINS

The expected performance of the communication link operating between the various Relay stations will now be evaluated. This performance is determined using the station parameters listed in Table 1–1 at the extreme spacecraft range of 5000 nautical miles and an elevation of 7.5 degrees above the horizon. It is assumed that each station employs a frequency-following demodulator and that the threshold of this receiver occurs at a signal-to-noise ratio of 6 db within the demodulator noise bandwidth for television and 7 db for telephony.*

TABLE 1–4.—*Telephony Total Noise Objectives at 5000 Nautical Mile Range and 7.6 Degree Elevation Angle*

Receiving station	Number of channels	Total noise objective, psophometrically weighted (picowatts)
Andover	12 Two-way	15,000
	300 One-way	27,500
Goonhilly	12 Two-way	15,000
	300 One-way	27,500
Pleumeur-Bodou	12 Two-way	15,000
	300 One-way	27,500
Nutley	12 Two-way	57,500
Rio de Janiero	12 Two-way	57,500
Fucino	12 Two-way	57,500

TABLE 1–5.—*Television Power Budget Goonhilly to Andover*

	Ground-spacecraft			Spacecraft-ground		
	Nominal	+	−	Nominal	+	−
Frequency, Mc	1725	-----	-----	4170	-----	-----
Transmitter power, dbm	70.0	0.0	0.0	40.0	0.7	0.5
Diplexer and cable loss, db	0.5	0.0	0.0	1.0	0.0	0.0
Transmitter antenna, gain, db	50.0	0.5	0.5	0.0	3.5	12.0
Space loss, db	176.5	0.0	0.0	184.2	0.0	0.0
Ellipticity loss, db	1.0	0.0	0.5	1.0	0.0	0.5
Receiver antenna gain, db	−1.0	1.0	6.0	57.6	0.5	0.5
Receiver signal power, dbm	−59.0	2.0	6.5	−88.6	5.2	13.0
Receiver noise density, dbm/Mc	−100.0	1.0	0.5	−122.4	3.4	0.0
Up-link noise contribution, db	----------	-----	-----	4.3	1.6	3.5
Receiver noise bandwidth, Mc	23	-----	-----	24.3	-----	-----
Total receiver noise power, dbm	−86.4	1.0	0.5	−104.2	5.0	3.5
Predetection S/N, db	27.4	2.5	7.5	15.6	5.1	18.0
Threshold, db	12.0	-----	-----	6.0	-----	-----
Margin, db	15.4	2.5	7.5	9.6	5.1	18.0

Picture quality: 51.9 db, weighted*
Audio quality: 60.7 db
Range: 5000 nautical miles
Elevation: 7.5 degrees
Frequency deviation, downlink
  Video: 9.6 Mc peak-peak, picture only
  Audio subcarrier on carrier: 2.7 Mc peak-peak
  Audio on subcarrier: 200kc peak-peak
Noise bandwidths
  Video: 3.0 Mc
  Audio: 8.0 kc

*CCIR 405—line weighting factor = 12.3 db.

Television

A power budget for transmission of television from Goonhilly Downs, England to Andover, Maine is shown in Table 1–5. The signal transmitter from the ground is received at the spacecraft at a nominal level of —59.0 dbm with a possible variation of 8.5 db. This variation is due primarily to the dependence of spacecraft antenna gain upon the radiation look angle within the "typical" look angle extremes of 20 degrees and 150 degrees (and can range from —7 db to 0 db). The noise figure of the transponder is 14 db so that the spacecraft noise density is —100.0 dbm/Mc and the pre-detec-

*Develet, Jean A., *Coherent FDM/FM Telephony Communication*, Proceedings of IRE, Volume 50, September 1962, pp. 1957–1966.

tion signal-to-noise density ratio is nominally 41.0 db. For the downlink the 10 watt transponder output arrives at the ground station antenna terminals at a level of —88.6 dbm, and again the 17.2 db tolerance is due mainly to the look angle of the spacecraft antenna. In clear weather the total system noise temperature of the Andover station is 42°K, thus producing a receiver noise density of —122.4 dbm/Mc. In addition to this ground station noise there is an uplink contribution from the transponder which is magnified by a factor of $(3)^2$ due to the tripler. The total noise density at the ground receiver is given as

$$\Phi_T = 10 \log \left[1 + 9\left(\frac{\Phi_v}{S_v}\right)\left(\frac{S_g}{\Phi_g}\right)\right] + 10 \log \Phi_g$$
$$= 4.3 - 122.4 = -118.1 \text{ dbm/Mc}$$

where

Φ_v, Φ_g = Noise power density due to the spacecraft and the ground receiver, respectively, dbm/Mc

S_v, S_g = Signal power at the spacecraft and ground receiver, respectively, dbm

The predetection S/N within the demodulator noise bandwidth of 24.3 Mc is then 15.6 db. Threshold of the demodulator occurs at approximately 6 db so that the nominal breaking margin for the entire link is 9.6 db.

The margin tolerance of +5.1 db and —18.0 db indicates the large variation in link performance which can occur from pass to pass. For those revolutions having antenna look angles of 25 degrees or less, the breaking margin at 5000 nautical miles is negative and reliable communication is not always possible.

The quality of the television transmission is obtained by adding the CCIR 405-line weighting factor of 12.3 db to the ratio of peak-peak picture signal-to-mean square noise. This ratio is given by

$$\frac{S}{N}_{TV} = \frac{3 f_{pp}^2 S_g}{f_v^3 \Phi_g \left[1 + 9\left(\frac{\Phi_v}{S_v}\right)\left(\frac{S_g}{\Phi_g}\right)\right]}$$

where

f_{pp} = Peak-peak picture signal deviation

f_v = Video bandwidth

With a predetection S/N of 15.6 db the weighted video S/N is 51.9 db.

The audio portion of the signal is transmitted as FM on a subcarrier. Its quality is defined as the full-load average tone power-to-average noise power ratio

$$\frac{S}{N}\text{audio} = \frac{3}{4} \frac{\phi_{sc}^2 f_{pa}^2 S_g}{f_a^3 \Phi_g \left[1 + 9\left(\frac{\Phi_v}{S_v}\right)\left(\frac{S_g}{\Phi_g}\right)\right]}$$

where

ϕ_{sc} = Modulation index of subcarrier

f_{pa} = Peak audio deviation

f_a = Audio bandwidth

The nominal audio S/N is 60.7 db.

Table 1–6 lists similarly calculated qualities and margins for television transmission between each of the Relay participants. In each case the elevation angle is 7.5 degrees, but for the smaller stations the spacecraft range has been reduced from 5000 nautical miles to the maximum range for that station.

Telephony

The power budget for 12-channel telephony transmission from Rio to the Nutley Ground Station is given in Table 1–7. Ground station received signal power and total noise density are calculated in the same manner as for television transmission with a change in bandwidths and transponder power output for the narrowband mode. The link margin for telephony is determined by both the allowable thermal noise limit in any channel and the breaking threshold of the demodulator, since both typically occur at the same carrier-to-noise ratio.

For the Nutley ground station the thermal noise requirement for the worst channel is a maximum of 50,000 psophometrically weighted picowatts referred to zero relative level. The ratio of test tone to psophometrically weighted noise power in the top channel for an FDM/FM system is given by

$$\frac{S_o}{N_o} = \frac{10^{0.25} F_{drms}^2}{3100\left[N^2\left(\frac{\Phi_v}{S_v}\right) + \left(\frac{\Phi_g}{S_g}\right)\right] F_2^2}$$

where

TABLE 1-6.—*System Performance for Television Transmission*

Transmitting station	Receiving station	Range nautical miles	Quality video weighted, db	Quality audio (db)	Margin (db)
Andover	Goonhilly	5000	49.2	58.0	7.1
Andover	Pleumeuer-Bodou	5000	52.3	61.1	10.0
Andover	Fucino	3500	41.7	50.5	—0.4
Goonhilly	Andover	5000	51.9	60.7	9.6
Pleumeur-Bodou	Andover	5000	52.3	61.1	10.0
Nutley Test	Nutley Test	3000	42.0	50.8	—0.3
Mojave	Mojave	2500	42.6	51.4	0.3

NOTE:
1. The margin indicated is a breaking margin only, not a performance margin.
2. Elevation angle is 7.5 degrees above horizon.

TABLE 1-7.—*Narrowband Telephony Power Budget Rio to Nutley Ground Station*

	Ground-spacecraft			Spacecraft-ground		
	Nominal	+	−	Nominal	+	−
Frequency, Mc	1725			4170		
Transmitter power, dbm	70.0	0.0	0.0	36.0	0.5	1.5
Diplexer and cable loss, db	0.5	0.0	0.0	1.0	0.0	0.0
Transmitter antenna gain, db	40.2	1.0	1.0	0.0	3.5	12.0
Space loss, db	176.5	0.0	0.0	184.2	0.0	0.0
Ellipticity loss, db	1.0	0.0	0.5	1.0	0.0	0.5
Receiver antenna gain, db	−1.0	1.0	6.0	49.3	0.8	0.8
Received signal power, dbm	−68.8	2.5	7.0	−100.9	5.3	14.3
Receiver noise density, dbm/Mc	−100.0	1.0	0.5	−112.2	0.7	0.0
Up-link noise contribution, db				0.4	0.2	0.3
Receiver noise bandwidth, Mc	2.3			1.3		
Total receiver noise power, dbm	−96.4	1.0	0.5	−110.7	0.9	0.3
Predetection S/N, db	27.6	3.0	8.0	9.8	5.6	15.2
Threshold, db	12.0			7.0		
Margin, db	15.6	3.0	8.0	2.8	5.6	15.2

Range: 5000 nautical miles
Elevation: 7.5 degrees
Baseband frequency limits: 12–60 kc
Down-link frequency deviation: 88.8 kc RMS/channel for 0 dbm0 test tone at 800 cps
CCIR/CCITT pre-emphasis
Thermal noise performance: 50,000 pw (psoph) per channel at zero relative level

F_{drms} = RMS deviation due to a 800 cps test tone
F_2 = Highest channel frequency, cps
N = Frequency multiplication in transponder

If F_{drms} is caused by a 0 dbm0 test tone, the noise power in the worst channel can be expressed in psophometrically weighted picowatts referred to zero relative level as

$$N_{pw} = \frac{3.1\left[N^2\left(\frac{\Phi_v}{S_V}\right)+\left(\frac{\Phi_g}{S_g}\right)\right]F_2^2 \times 10^{12}}{10^{0.25}\,F_{\text{drms}}^2\,I}$$

where I is the improvement factor due to pre-emphasis. From this expression, the relation between received carrier power and worst channel noise power is obtained:

$$\left[\frac{N^2\,\Phi_v}{S_v}+\frac{\Phi_g}{S_g}\right]=\frac{10^{0.25}\,F_{\text{drms}}\,I}{3.1\,F_2^2 \times 10^{12}}\,N_{pw}$$

For Group A transmission we have $F_2 = 60$ kc, $F_{\text{drms}} = 88.8$ kc, and $I = 2.4$ as given by GSFC/STL Document No. R1-0000. Substituting these values into the above equation with $N_{pw} = 50{,}000$ we find the threshold value of noise density-to-carrier power ratio. This is

$$\left[N^2\left(\frac{\Phi_v}{S_v}\right)+\left(\frac{\Phi_g}{S_g}\right)\right]_T = 153 \times 10^{3-}\ \text{rad}^2/\text{Mc}$$
$$= -8.1\ \text{db/Mc}$$

Returning to the power budget we have

$$10 \log \frac{\Phi_g}{S_g}\left[1+N^2\left(\frac{\Phi_v}{S_v}\right)\left(\frac{S_g}{\Phi_g}\right)\right]$$
$$= -112.2 + 0.4 + 100.9$$
$$= -10.9\ \text{db/Mc}$$

for nominal system parameter values. The

nominal performance margin is thus —8.1 —(10.9) = +2.8 db. The difference between this performance margin and the predetection S/N is 7.0 db, the demodulator threshold. The margin is thus both a performance and a breaking margin. Note that it is possible in bad weather on a pass with an unfavorable spacecraft look angle to be as much as 12.4 db below threshold.

TABLE 1–8.—*System Performance for 12 Channel Telephony, Group A*

Transmitting station	Receiving station	Range (nm)	Thermal noise pw (psoph. wtd.)	Margin (db)
Nutley	Goonhilly	5000	7,500	1.9
Nutley	Rio	5000	50,000	1.1
Nutley	Nutley	5000	50,000	2.1
Goonhilly	Nutley	5000	50,000	2.7
Goonhilly	Rio	5000	50,000	1.5
Rio	Nutley	5000	50,000	2.8
Rio	Goonhilly	5000	7,500	3.9
Rio	Fucino	5000	50,000	3.7

NOTES: 1. The margin indicated is both a performance and a breaking margin except for Goonhilly receiving, which is performance only.
2. Elevation angle is 7.5° above horizon.

In Table 1–8 the expected performance for 12 channel Group A transmission for each Relay participant is presented. Tables 1–9 and 1–10 extend the performance calculations to 12 channel Group B and 300 channel modes, respectively.

TABLE 1–9.—*System Performance for 12 Channel Telephony, Group B*

Transmitting station	Receiving station	Range (nm)	Thermal noise pw (psoph. wtd.)	Margin (db)
Andover	Goonhilly	5000	7,500	11.3
Andover	Pleumeur-Bodou	5000	7,500	15.1
Andover	Fucino	5000	50,000	0.1
Goonhilly	Andover	5000	7,500	15.0
Pleumeur-Bodou	Andover	5000	7,500	15.1

NOTES: 1. The margin indicated is both a performance and a breaking margin, except for Fucino which is breaking only.
2. Elevation angle is 7.5° above horizon.

TABLE 1–10.—*System Performance for 300 Channel Telephony*

Transmitting station	Receiving station	Range (nm)	Thermal noise pw (psoph. wtd.)	Margin (db)
Andover	Goonhilly	5000	18,750	5.9
Andover	Pleumeur-Bodou	5000	18,750	9.0
Goonhilly	Andover	5000	18,750	9.0
Pleumeur-Bodou	Andover	5000	18,750	9.0

NOTES: 1. The margin indicated is both a performance and a breaking margin.
2. Elevation angle is 7.5° above horizon.

AUTHORS. *This chapter was written by* B. N. ABRAMSON, W. LITTENBERG, M. R. SKINNER, *and* C. M. THOMAS *of Space Technology Laboratories, Inc., Redondo Beach, California, U.S.A. under Contract NAS 5–1302 with NASA/Goddard Space Flight Center.*

N66-10228

Chapter 2

The Relay Spacecraft

INTRODUCTION

Occasionally the horizon of man is brightened and widened by the contributions of the scientific and engineering community. Communications satellites, when peacefully used, can be a boon to mankind by furthering international understanding through greater speed and capacity of transoceanic communications. Relay I and her sister satellites have contributed significantly to this end. The Telstars, Syncoms, and Relays have all had their own noteworthy "firsts" in communications progress, but of more importance, they have laid the groundwork for an embryonic technology. Today this technology is "Thursday's Child"—it has far to go. With intelligent direction, it will achieve the desired goals.

The credit for our present position is due to many governments, companies and persons; so many that they must go unnamed. To each of them we sincerely say—It was an honor to have worked by your side.

GENERAL

The Relay I spacecraft was built for NASA/GSFC by the Astro-Electronics Division of the Radio Corporation of America. After contract award in May of 1961, RCA embarked upon a six week study phase during which time changes were made and additional details were resolved between RCA and GSFC. The process of building, testing, redesign, and retesting followed. In December 1962 this effort was culminated in the successful launch of the final design—Relay I. Figure 2–1 illustrates that awesome moment of truth that we had worked for so long, when no further redesign was possible. The details of this story are told in other chapters in Part I.

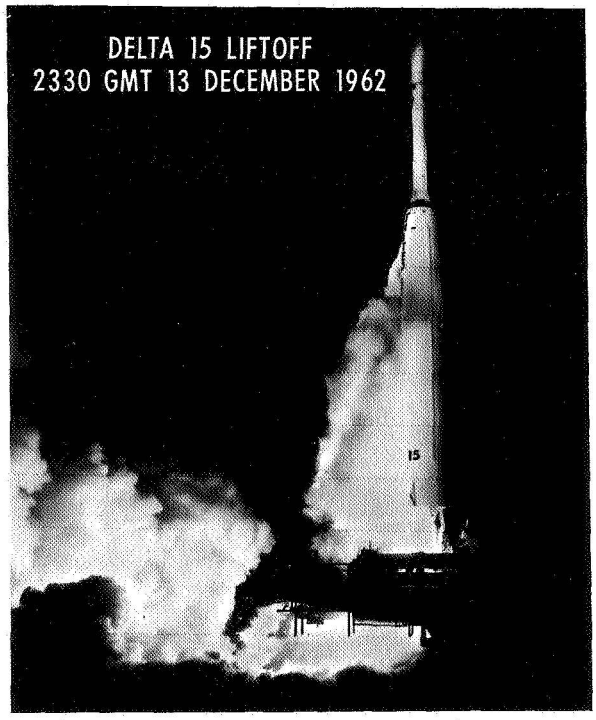


FIGURE 2–1.—Delta 15 launch.

THE SPACECRAFT

Structure

The size of the envelope of the spacecraft was dictated by the low drag nose fairing of the Delta launch vehicle. This has resulted in an eight sided prism with a maximum diameter of 29 inches and a height of 19 inches, topped by an octagonal truncated pyramid 16 inches high. The 18 inch long, mast-like structure mounted on its narrow end is the transmitting and receiving antenna assembly for the microwave communications experiments. A photograph of the spacecraft and a cutaway drawing detailing the various subsystems are shown in Figures 2–2 and 2–3. The structure is fabricated of riveted sections of lightweight aluminum channels. Panels for support of the solar cells are epoxy-bonded, aluminum-honeycomb construction. Attachment to the launch vehicle third stage is by means of a machined aluminum attachment ring.

Power Subsystem

The power supply consists of a solar cell array, hermetically sealed nickel-cadmium storage batteries, charge-controlling electronics, and a 1-year timing device. The solar cells are boron-doped silicon cells, P/N, gridded and covered with 60 mil thick fused sheets. The cover sheets provide protection from energetic particles in space. Every possible square inch of the spacecraft ex-

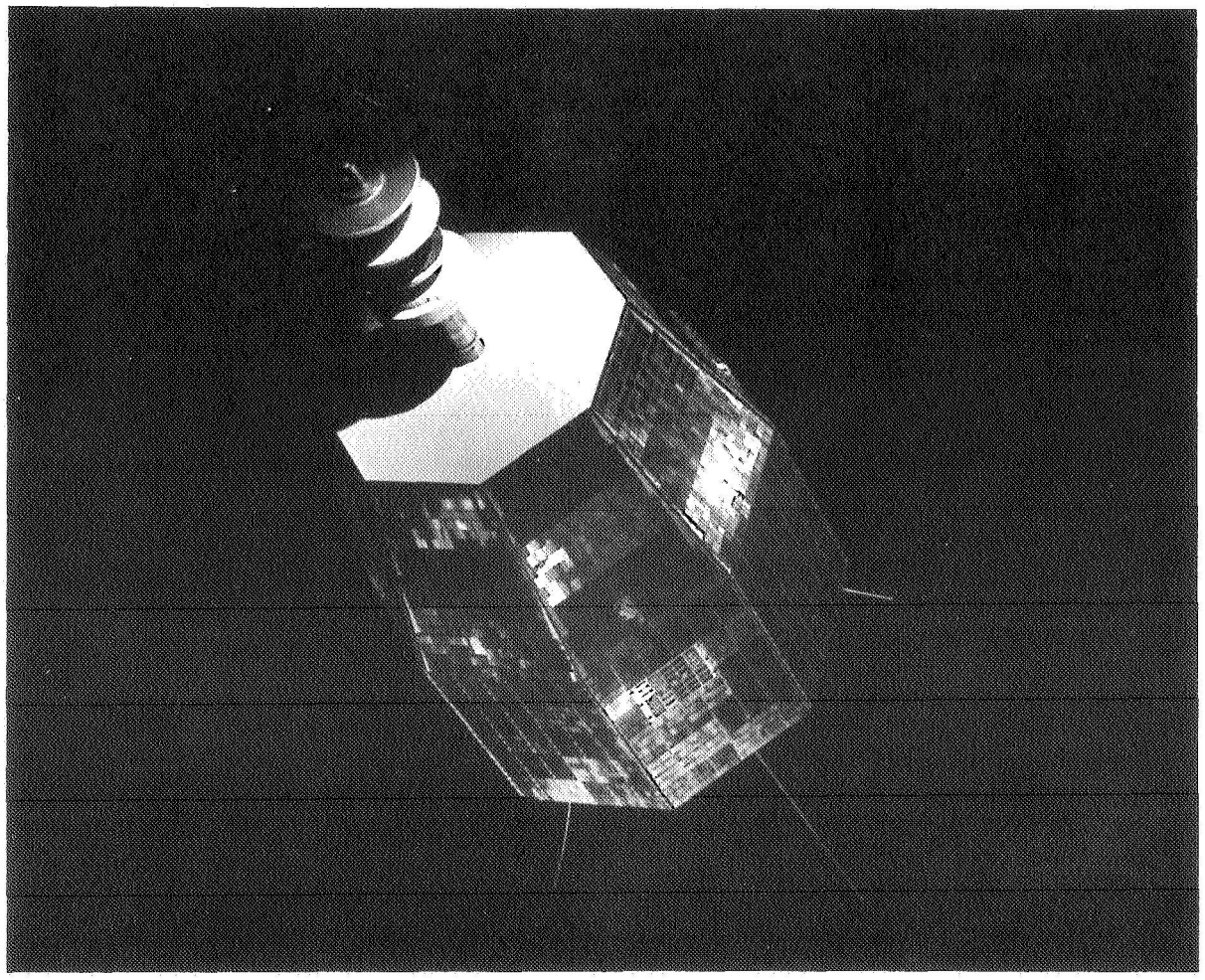
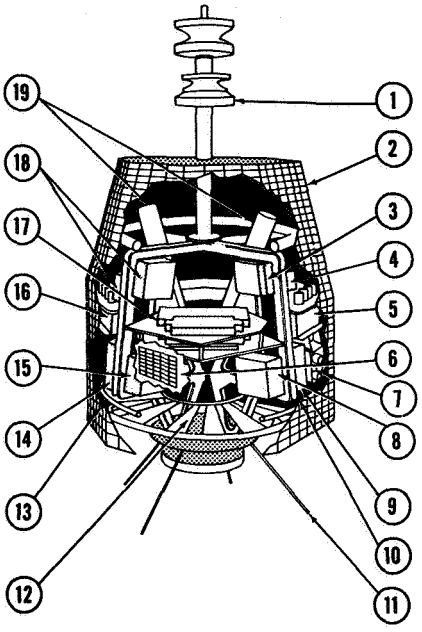


FIGURE 2–2.—The Relay spacecraft.



1. WIDE-BAND ANTENNA
2. SOLAR PANELS
3. TELEMETRY TRANSMITTERS
4. BATTERY CHARGE CONTROLLER
5. BATTERY BOX
6. RADIATION DAMAGE PANEL
7. SOLAR ASPECT INDICATOR & HORIZON SCANNER
8. COMMAND CONTROL
9. RADIATION DETECTOR
10. RADIATION MONITOR (HIDDEN)
11. TT&C ANTENNA
12. THERMAL CONTROLLER
13. TWT POWER SUPPLY (HIDDEN)
14. HEAT CONTROLLER
15. COMMAND RECEIVERS
16. BATTERY BOX
17. WIDE-BAND RECEIVERS
18. COMMAND DECODERS
19. TRAVELING WAVE TUBE

FIGURE 2–3.—Cutaway drawing of Relay spacecraft.

terior is covered with solar cells to provide the power necessary for operating the spacecraft. When the communications system is in operation, the power requirement is about 120 watts. Under typical operating conditions, the solar array is capable of generating an average power of 40 watts. The remaining power is provided by a 250 watt-hour storage battery. Battery depth of discharge is not permitted to exceed 50 percent except during special experiments with the spacecraft.

Telemetry, Tracking and Command Equipment

The telemetry, tracking and command subsystem provides three basic functions in the spacecraft:

1. A VHF cw signal, from which the Minitrack stations provide orbital data.
2. Telemetry of performance data from the communication system and the radiation experiments.
3. A command system, which receives the commands and converts them into a desired switching function.

The telemetry transmitters can be switched on and off by means of the command system. Operationally, one of the transmitters is left on continuously to provide the tracking signal. The Minitrack ground stations utilize this signal to track the satellite and provide orbital measurements. The alternate transmitter is commanded on when telemetry or horizon scanner data are desired. A modulation switch selects the transmitters to be modulated and the source of modulation (telemetry encoder or horizon scanner subcarrier oscillator). This switch is under the control of the command system.

The transmitters are crystal controlled, solid state, and are phase-shift keyed by the modulating signals. In the event of a failure of one transmitter the other would provide both tracking and telemetry signals.

The telemetry encoder accepts digital, high and low level analog data inputs for conversion to a PCM format for transmission. The main commutator provides 128 channels which are sampled each second. Two subcommutators are provided, one, a 32 channel unit and the other, a 64 channel subcommutator. Three of the main channels are used for frame synchronization.

The command system consists of a redun-

dant set of command receivers, subcarrier demodulators, and decoders. A pulse width-modulated subcarrier is transmitted via a VHF carrier to the command receivers which demodulate the carrier and send the subcarrier to the subcarrier demodulators where the pulse code is reconstituted. The code output is then fed to both decoders through a cross coupling network in such a fashion that either demodulator can activate either decoder. Thus, in the event of failure of receiver No. 1, subcarrier demodulator No. 1, and decoder No. 2, the command system will still function. The decoder uses a magnetic core shift register to transform the pulse code into a command signal. The command signals from the two decoders are "paralleled" so that either or both decoders can activate the control function. Twenty separate commands are provided to switch the spacecraft into its various modes of operation.

The VHF antenna comprises four monopoles extending out from the separation ring face of the spacecraft. For command reception, the antennas are fed in phase to produce a dipole-like pattern. For telemetry and tracking transmission, the monopoles are fed in phase quadrature to produce a circularly polarized wave in the plane perpendicular to the spin axis. A diplexer harness is used to couple the two receivers and two transmitters to the antennas.

Microwave Communication Equipment

The purpose of this system is to provide an experimental repeater suitable for transmission of one TV signal (plus its sound channel) or 600 one-way voice channels; or of high-speed data, facsimile, or teletype traffic with bandwidths of up to 4 megacycles. Two-way telephony transmission tests through the repeater can be made, using 12 channels in each direction. (This number is determined by the available ground-station equipment, rather than a limitation of the satellite repeater, which can handle several times this number.)

Two completely independent microwave repeaters (except for the common antenna) are provided for increased reliability. Either one may be selected for operation by ground command.

The basic performance requirements of the satellite repeaters are similar to those used for conventional ground-based microwave links, so far as power output, bandwidth, gain, noise figure, and intermodulation are concerned. There are radical differences, however, in the size, weight, and power drain.

The system parameters were initially chosen to meet international (CCIR) standards (for a 2500-km reference circuit) between Europe and the United States. The sound channel is transmitted by frequency-modulating a 4.5-Mc subcarrier, which is added to the video signal, and the combination is then used to frequency-modulate the ground transmitter.

The satellite transmitter output power of 10 watts gives a margin of at least 6 db for TV transmission over a maximum slant range of 5000 nautical miles.

The receiver is completely solid state, using separate crystal-controlled transistor oscillators and varactor multipliers for both the input and output oscillator sources. Incorporated in the repeater is a microwave beacon which is used for tracking by the ground communications stations. The beacon is a completely self-contained unit with a crystal-controlled transistor oscillator and varactor multipliers. The receiver and beacon outputs are combined and fed to a traveling wave tube for amplification to 10 watts power output. The microwave beacon signal at 4080 megacycles, as amplified by the traveling wave tube, has a radiated power out of the antenna of more than 100 milliwatts.

The traveling wave tube has been designed for long life, light weight, and high efficiency. A solid-state dc-dc converter is used to raise the 22.5 volts regulated input to the high voltages needed by the traveling wave tube.

The microwave antenna receives at 1725 Mc and transmits at 4170 Mc. It is contained

in one mechanical assembly, consisting of a coaxial receiving antenna above a coaxial transmitting antenna. The whole assembly is located on top of the spacecraft, coincident with the spin axis. Both antennas are circularly polarized but of opposite sense. Vertical coverage extends from 40 to 115 degrees (—1 db points).

Figure 2–4 shows the general configuration of the Relay communications transponder. The incoming 1725 Mc signal is translated to a 70 Mc intermediate frequency where most of the amplification is accomplished, frequency tripled, and then translated up to 4170 Mc for power amplification and retransmission.

The reasons for tripling the signal are that with 10 watts RF power output, the required bandwidth for the spacecraft-to-ground link is 25 Mc. Available high power klystron amplifiers with 25 Mc bandwidths were not available for the ground-to-spacecraft link during the time schedule required for the Relay Project. The required down-link deviation was divided by three, which yielded a 14 Mc bandwidth occupancy for the up-link signal. This was an achievable bandwidth for the state of the klystron art at that time.

Two modes of operation are available with the transponder. The first mode or wideband mode, as it is called, is utilized for one-way wideband communications such as television or 300 channels of telephony.

The second mode available is called the narrowband mode. This is utilized for two-way narrowband communications such as 12

WIDE-BAND RECEIVER, BLOCK DIAGRAM

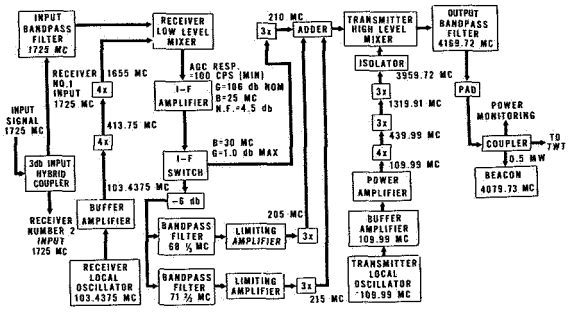


FIGURE 2–4.—Wideband receiver block diagram.

channel two-way telephony. In the narrowband mode, two ground stations communicate with each other, one transmitting on 1723.33 Mc, the other transmitting on 1726.67 Mc. The spacecraft transponder converts these frequencies to 4165 Mc and 4175 Mc respectively.

In the two-way telephony mode, the incoming signals from two communicating ground stations are separated after intermediate frequency amplification and then clipped to the same level by hard limiting. The deviation is tripled, and the two signals enter the TWT at the same level. This prevents suppression of the weaker signal by the stronger one. This is especially important when the spacecraft is much closer to one of the ground stations than to the other, and the antenna look angles to both stations are sufficiently different so that even controlling the transmitted power at the ground stations would not equalize the received power levels. This feature of the transponder has been highly successful in operations conducted with Relay I.

Two approaches were investigated for the tripler design, one using varactors, the other using transistors. The advantage of a varactor design, that no dc input power is required, was offset by the disadvantage of an extremely difficult tuning procedure, and that the units were not easily reproducible. The varactor design was used during the prototype period but was then abandoned in favor of the transistor version which was much easier to tune and reproduce.

The IF amplifier design proved to be more difficult than originally anticipated. The first design utilized triple-stagger-tuned stages which were necessary to achieve the required bandwidth. During electrical testing, however, it was found that the crosstalk for multichannel telephony was excessive. This was caused by AM to PM conversion on the passband skirts of the individual stages. The solution to this problem was to build a broadband video amplifier and then limit the bandwidth with a passive 70 Mc bandpass filter. Performance of this design was most

satisfactory, and it was selected for use.

The traveling wave tube development was well under way when short term (millisecond) fluctuations were noticed in the power output of some of the tubes when they were operated in vacuum. Also there was an occasional helix current runaway on a tube in vacuum; the tubes operated in a normal manner at atmospheric pressure. Yet the vacuum anomalies were not repeatable. At first the power fluctuations were thought to be defective RF cables leading to the vacuum chamber. At times it appeared that tightening the connectors cured the problem. Helix current runaway also was not always repeatable. At this point a very serious design problem was evident. The TWT design would work at sea level conditions but not in the high vacuum of space. Innumerable design modifications were tried; some seemed to work temporarily and then when the problems appeared to be solved, they reappeared. This caused delays in the launch schedule and it was finally decided to seal the TWT in a container pressurized at one atmosphere. The pressurized TWT models would be used in the first flight spacecraft, and the problem would be further pursued in hopes of producing an unpressurized TWT for the remaining two spacecraft. This was done, and the presently orbiting Relay spacecraft contains pressurized tubes. These are functioning normally and have shown no indication of instability.

The continuing design effort on the TWT has finally yielded a design that will perform just as well in vacuum as in air. Helix current runaway was found to be caused by insufficient thermal sinking of the helix. In air, there was enough convection cooling of the helix area of the bulb that runaway did not take place. The thermal design was modified to provide adequate removal of heat from the helix.

The resolution of the power fluctuation problem was simple but took many months to perfect. The potential difference between the helix and collector is about 1000 volts, which creates a region of high electrical field in this area of the bulb. Local outgassing was ionized by the field and would occasionally break down, momentarily reducing power output. The answer to this problem was to apply thin lines of silver paint directly on the exterior of the bulb between the area of the end of the helix and the beginning of the collector. The lines were electrically connected to the collector. They served to provide a low impedance leakage path which eliminated the high field in this area. This design has performed very well in all tests and will be used in the next Relay spacecraft.

Radiation Experiments

In addition to the communications repeaters and other subsystems needed to support the principal mission of Relay, the spacecraft carries a group of components to obtain data on particle radiation in space. These consist of six radiation detectors and a collection of isolated solar cells and semi-conductor diodes. The latter are accumulated on a "radiation damage effects" panel.

The radiation detectors are included to monitor proton and electron spectra by measuring flux density in various domains of intensity levels. Two of them are scintillation counters; four are PN junctions. One of the detectors is omnidirectional; the others are restricted to a small solid angle and are gated by an on-board magnetometer to measure only that flux normal to the earth's magnetic field. Accumulators in the telemetry encoder count and store the detectors' outputs. One hundred of the 128 telemetry channels are reserved for high-speed measurements of the outputs of the short-circuited cells. Thirty specially selected solar cells make up the radiation damage panel. Effects of radiation are observed by measuring short circuit current. The radiation damage panel contains, in addition to the solar cells, six selected diodes that are used to measure minority-carrier lifetime as affected by radiation.

Miscellaneous Equipment

In order to reduce the limits of tempera-

ture variation in the spacecraft, a thermally controlled radial vane assembly is located in the base of the spacecraft. It is operated by a temperature sensor connected to the battery assembly. When the batteries are warm the vanes open; as the battery temperature decreases the vanes close. In this manner the thermal radiation coupling to space is varied. This simple form of active temperature control reduces the mean spacecraft variation 5 degrees centigrade at each end of the range, providing operating limits of 0°C to +25°C.

Solar aspect and horizon transit time are measured by detectors located in the spacecraft. The data are telemetered, and spacecraft spin axis attitude is computed on the ground. If necessary, commands can be sent to tilt the spin axis to a desired orientation by applying a current to the magnetic torquing coil.

Relay Ground Facilities

Relay ground facilities include stations for communications experiments, test stations for checking out the satellite in advance of performing communications experiments and commanding transponders on and off, and the NASA Minitrack network for tracking and acquiring data from the spacecraft.

The ground stations that conduct experiments in intercontinental and transoceanic communications are located at: Goonhilly Downs, England; Pleumeur-Bodou, Britanny, France; Fucino, Italy; Rio de Janeiro, Brazil; and in the United States at Andover, Maine; and Nutley, New Jersey.

The test stations check out the Relay satellite, including operation of the communications transponder, prior to the start of communications experiments. They select the transponder and the mode for the type of transmissions scheduled, and turn the transponder off when the experiment is concluded. If the satellite is out of range of the test station, an automatic timer will turn the equipment off two minutes after spacecraft illumination ceases, to conserve the satellite's power supply. The test stations are located at Nutley, New Jersey and Mojave, California.

NASA's world-wide Minitrack network periodically tracks the satellite and acquires data on performance and condition of equipment and on radiation levels in space.

All stations transmit information for processing and dissemination to NASA's Goddard Space Flight Center, Greenbelt, Maryland.

SUMMARY

We have thus seen the Relay spacecraft as an integrated system, comprising major interrelated subsystems including: structure; power; communications; telemetry, tracking and command. A short description of the radiation experiments carried on board has also been given.

Chapters that follow will provide details of the subsystems described.

It is gratifying to note that solutions to the design problems encountered has resulted in a spacecraft system which has been in active operation for almost two years and gives every sign of continuing indefinitely.

AUTHOR. *This chapter was contributed by* R. H. PICKARD, *NASA/Goddard Space Flight Center, Greenbelt, Maryland, U.S.A.*

N66-10229

Chapter 3

Structural and Dynamic Considerations in the Spacecraft Design

INTRODUCTION

The size, weight, and shape of the Relay I spacecraft were controlled by factors and constraints resulting from analysis of mission requirements and project specifications. In particular, the relevant parameters included a weight limit imposed by the required altitude and the capacity of the launch vehicle, stabilization by spin momentum with its corollary limit on inertia distribution, and the surface area needed for solar power. The final configuration accommodated these requirements. The use of a shroud of fixed dimensions led to extensive topological considerations to satisfy the maximized surface area and the inertia ratio necessary for spin stabilization. Other general specifications included relatively severe vibration testing, especially the 10.7 g sine wave input in the 50–500 cps range, the axial, transverse, and torsional loads from the booster, and the eccentricity and dynamic balance limits. Adequate strength and stiffness were provided to meet these loads within the constraints of an ultra-light structural design. The structural weight target was 10 percent of the spacecraft total.

During qualification testing it was found that the wideband receiver and the telemetry encoder experienced vibrational forces which these components could not withstand. A unique coulomb damper was developed which reduced the forces applied to levels compatible with the capabilities of these components. The development of the damper is described in detail on page 39.

CONFIGURATION

The configuration of the Relay I spacecraft (see Figures 3–1 and 2–3) had to satisfy the following primary conditions: (1) spin stabilization, (2) compatibility with an existing fairing, and (3) maximized surface area. The first condition, basic control of spin axis attitude in inertial space, required the mass distribution to be that of a disc, regardless of the external shape of the payload. Dynamically, the ratio of the mass moment of inertia about any transverse axis to the maximum inertia about the spin axis must be less than one; that is, $I_{trans}/I_{spin} < 1$, or $I_{trans} < I_{spin}$. Control of this parameter was a stringent requirement since any unbalanced moment at separation or dynamic unbalance would eventually lead to tumbling, preventing the necessary orientation of the directional antennas.

Achieving a component arrangement that would result in the required inertia condition was a major problem because of the limitation of the second condition; that is, the maximum diameter of the fairing was fixed. After calculating the inertia ratios for several layouts, it was found that the required

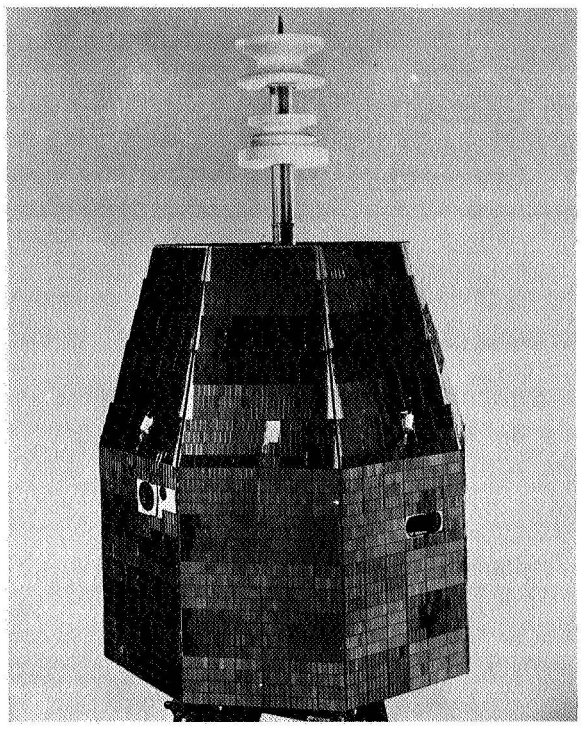


FIGURE 3–1.—The Relay spacecraft.

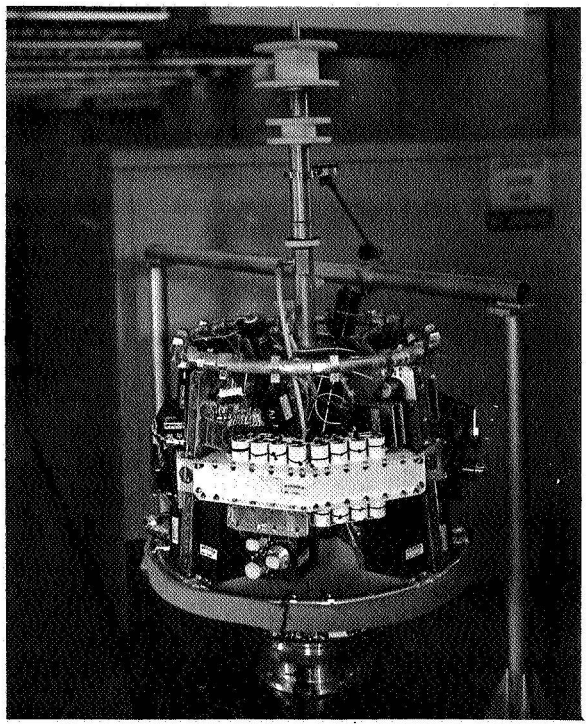


FIGURE 3–2.—Structure of Relay spacecraft.

inertia condition was achieved by a basic cruciform structure of four vertical elements supporting most of the components and an equatorial belt or ring formed by the four heaviest components (see Figure 3–2). The combined weight of the two battery packs, the wide-band receiver, and the telemetry encoder was approximately 50 pounds. Each of these components was mounted in or on beam structures which bridged two adjacent cruciform elements to form the equatorial ring. Longitudinally, these assemblies were placed in the plane of the center-of-gravity.

Since the final weight and center-of-gravity location of the individual components were uncertain, it was decided that the I_{trans}/I_{spin} inertia ratio should not exceed a design goal of 0.95. This 5-percent margin was arbitrarily allowed to ensure that the theoretical limit for the inertia ratio (1.00) would not be exceeded. A bifilar pendulum with a demonstrated accuracy of 0.3 percent minimum was utilized to measure the inertia ratio of Relay I. The measured value for I_{trans}/I_{spin} was 0.963. The high accuracy and consistency of the pendulum measurements gave confidence in this value.

The third primary condition, that of maximized surface area, was defined as a maximum in terms of the surface area for mounting silicon solar cells to support a given power requirement, but not necessarily in terms of total area. Relay I was not basically a power-limited design; that is, the balance of limitations was well established among such items as power, temperature-rise of the traveling wave tube, altitude, weight, and mutual-visibility time. However, power duty-cycle requirements necessitated extensive design attempts to attain sufficient solar-cell mounting area within the fixed values of diameter and inertia ratio. Finally, the geometric and electrical arrangement of the solar cells was established and this criterion determined the number of panels, (eight), and the panel length necessary to provide the required solar-array area. Later it was found that a slight increase of solar-array

area could be provided by extending the length of the solar array panels. This did not violate the dynamic stability criterion of the limiting inertia ratio.

The final configuration was an eight-sided polyhedron consisting of a short cylindrical section surmounted by a truncated conical section (see Figure 3–1). The essentially cylindrical wideband antenna was mounted at the top of the spacecraft (as viewed in the launching position) co-linearly with the spin axis. The four narrowband antennas were attached to a collar just above the separation ring and projected downward at an angle of 45 degrees to the axis. The ends of the polyhedron were closed with Mylar sheets painted for proper thermal emissivity and attached by nylon zippers. The planned in-orbit orientation of the spacecraft was such that the heat to be dissipated could be radiated to outer space through the lower (larger) end. To reduce the range of temperature fluctuation within the spacecraft, an adjustable-vane heat controller was installed just above this lower closure.

LOAD ANALYSIS

The basic load-carrying structure was a vertical, four-element truss (see Figure 3–3). The majority of the component boxes were bolted to this truss or frame. Tubular rings encircling the truss were attached at the upper and lower corners of each quarter-frame to position the frames and to provide support for other components. The eight solor panels were attached in tension to the upper ring, the attachments between the panels and the lower ring being designed to support lateral loads only. This arrangement was designed to avoid column loading in the panel substrate. A bending moment was developed in the panel due to the geometric impossibility of reacting the load vector through the vertical centroid of the substrate. One panel supporting a sensor and four other panels containing irregular holes unsymmetrically located, contributed to the lack of symmetry in load distribution. Other components, such as the precession damper, attitude coil, lower collar, and antennas, were mounted as functional requirements dictated. Essentially all loads were supported by the frame as shear loading into the flanges, and compression in the webs of the members above H, H′, J and J′ (see Figure 3–4). The latter four members then supported the total load in compression and shear from the separation ring and the third-stage interface.

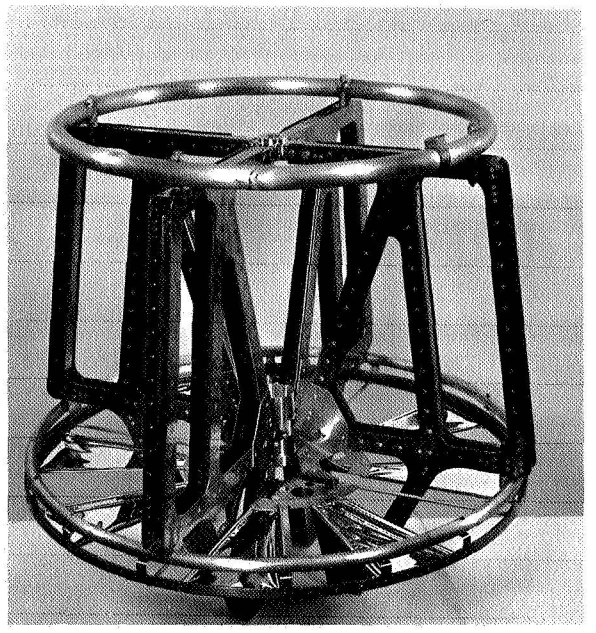


FIGURE 3–3.—Basic load carrying structure.

The vibratory forces required by the specified qualification tests defined the most severe stresses the structure would have to withstand. Evaluation of the effects of these required inputs in conjunction with the constant accelerations led to the choice of the following equivalent design load factors (see Figure 3–5):

Vertical:	n_z	=	30 g
Radial:	n_r	=	10 g
Lateral:	n_x	=	n_y = 5 g
Tangential:	n_t	=	3 g

The several loads applied to the structure according to the direction of the input were found by taking the vectorial (nW), where W was the weight of the individual component. Calculations for the applied loads, the

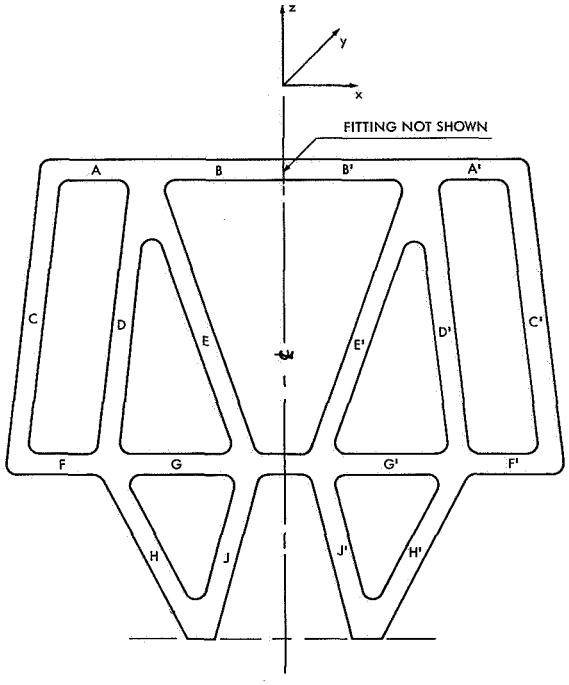


FIGURE 3–4.—Spacecraft loading.

TABLE 3–1.—*Summary of Loads and Margin Safety for Basic Design Conditions*

Truss member	Conditions: 30 g vertical loading (lb)	5.0 g side loading (lb)	10 g radial loading (lb)	L/ρ	Allowable load: ρ_{ty} Tension (lb)	ρ_{cy} Comp (lb)	Margin of safety
A,A′	-------	-------	-------	15.22	6096	1530	-------
B,B′	+395	-------	+151	23.66	------	1460	+14.43
C,C′	-------	-------	-------	49.53	------	1429	-------
D,D′	+ 50	± 234	Neg.	49.53	------	1429	+ 5.11
E,E′	−555	± 258	Neg.	54.57	------	1403	+ 1.53
F,F′	-------	-------	-------	15.22	------	1530	-------
G,G′	+ 73	± 340	+145	24.05	------	1505	+ 3.43
H,H′	−460	± 267	Neg.	33.49	6096	1486	+ 2.23
J,J′	−549	±1092	Neg.	31.71	8757	4652	+ 3.26
Lower central fitting arm							+ 0.96
Lower central fitting AN–4 bolt							+ 1.89

F_{ty} = 48,000 psi

Symbols used are as defined in MIL Handbook No. 5.

crippling stresses, and the margins of safety based on ultimate strength are summarized in Tables 3–1, 3–2, and 3–3. See the following illustration for identification of items refer-

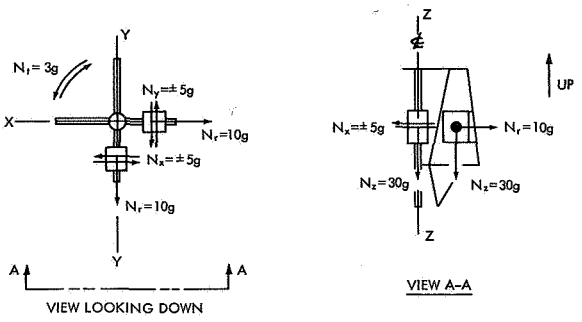


FIGURE 3–5.—Equivalent design load factors.

TABLE 3–2.—*Crippling Allowable Stress .025 Channel + Plate*
(Members A thru I)

Item	No. of items	b	t	b/t	Edges free	Area	Stress F_{cc}	Load P_c
1	2	0.500	.032	-----	1	.06400	*4,750	304
2	2	.7875	.025	31.50	1	.03630	4,750	172
3	2	------	----	-----	-----	.01080	50,800	549
4	1	.7610	.025	30.44	0	.01590	32,600	518
Total						0.12700		1543

$$F_{cr} + \frac{\text{Load}}{\text{Area}} + 12{,}150 \text{ psi}$$

Symbols used are as defined in MIL Handbook No. 5.

*Adjusted to F_{cc}[2]

TABLE 3–3.—*Crippling Allowable Stress .050 Channel + .032 Plate*
(Member J)

Item	No. of items	b	t	b/t	Edges free	Area	Stress F_{cc}	Load P_c
1	2	.50	.032	15.6	1	.06400	*18,000	1,152
2	2	.875	.050	17.5	1	.05750	18,000	1,035
3	2	-----	R/t = 5	R/t = 5	-----	.04414	47,700	2,105
4	1	.936	.050	18.7	0	.01680	43,000	722
Total						0.18244		5,014

$$F_{cr} = \frac{\text{Load}}{\text{Area}} = 27{,}485 \text{ psi}$$

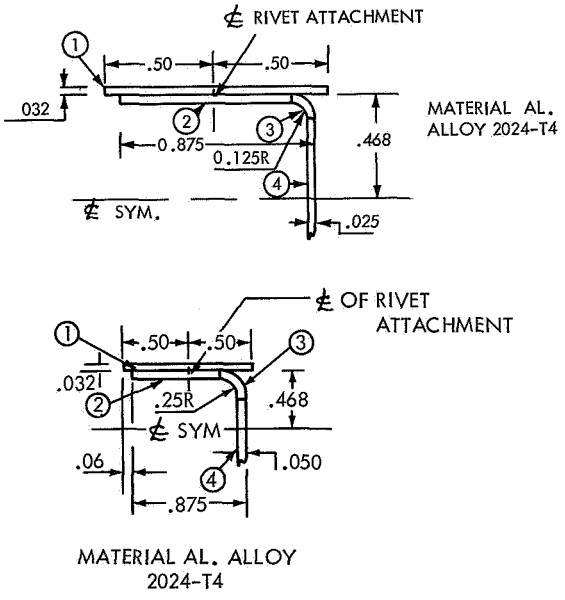
Symbols used are as defined in MIL Handbook No. 5.

*Adjusted to F_{cc}[2]

enced. Margins of safety for elements where stiffness was critical were based on the yield strength.

STRUCTURAL DESIGN

The essential details of the basic structure are shown in Figure 3–6. The frame sub-



assembly is composed of two cap sheets riveted to a formed channel. Flush-head rivets were used to permit complete utilization of available component mounting area for optimum thermal conduction. For accuracy of fit, and to provide adequate rivet bearing area, the sheets and channels were dimpled at assembly. The gap between the sheet surface and the rivet head was held between +0.000 and —0.005. Finishing after assembly was not permitted.

As shown in Figures 3–7 and 3–8, the four quarter-frames were bolted to the central fittings to establish the cruciform configuration. The upper and lower rings (see Figures 3–9 and 3–10) provided the required angular location, rigidity, and mounting locations for the solar panels. The upper and lower central fittings as well as the separation ring (see Figure 3–11) were machined from solid stock. The upper fitting provided a pilot for centering the wideband antenna. The original structural design of the lower fitting was modified by increasing the wall thickness to enable it to serve as a heat sink for the traveling wave tube, thus eliminating the need for a dead-weight heat sink. The

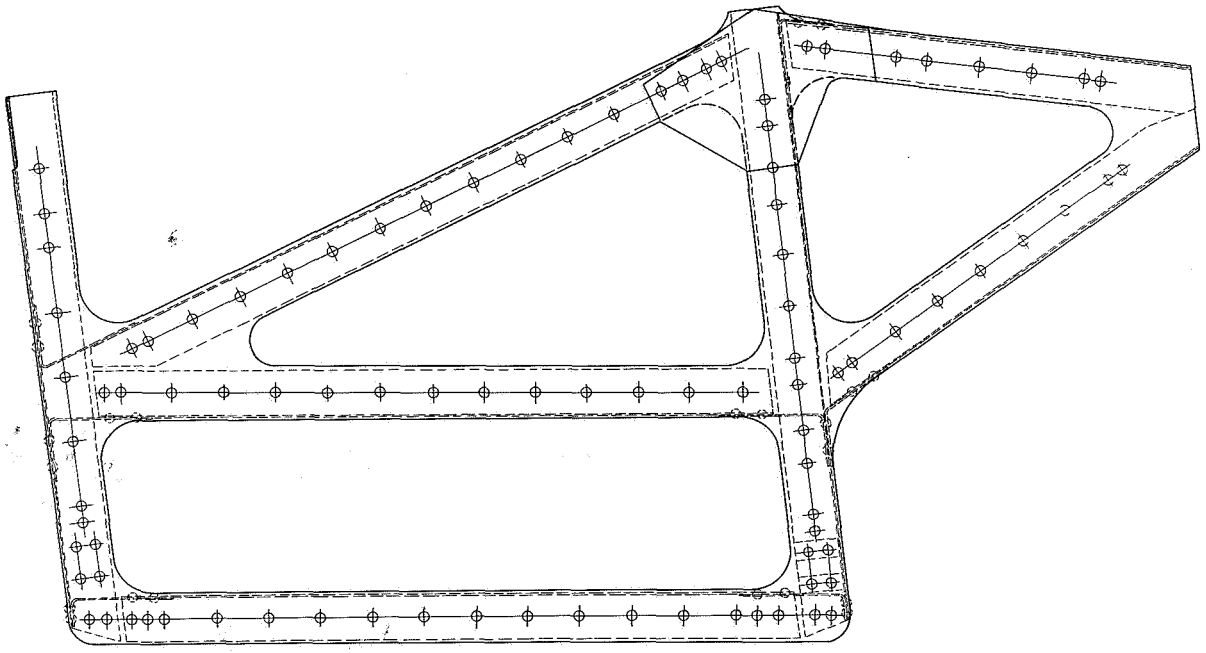


FIGURE 3–6.—Details of basic structure.

upper and lower rings were of formed aluminum tubing cut into four quadrants and epoxy-bonded into sleeve fittings for attachment to the frame by bolts. The bonding method of fabrication proved superior to welding in regard to strength and accuracy of shape. In addition, the fixtures used for bonding were less expensive than those required for welding.

The solar-panel substrate was an all-aluminum sandwich composed of a honeycomb core of quarter-inch cells of 0.001 inch, 5052 alloy, which was epoxy-bonded to faces of 5052 alloy 0.003 inch thick (see Figure 3–12). The bend between the two planar portions was formed by crushing, then filling the deformed cells with epoxy adhesive to provide the required shear strength. A doubler sheet was applied on the inside face across the bend line to increase stiffness. All panel support brackets were attached by bonding. The bare substrate weighed 0.0022 lb/in^2, and the final panel assembly complete with cells, covers, and wiring weighed

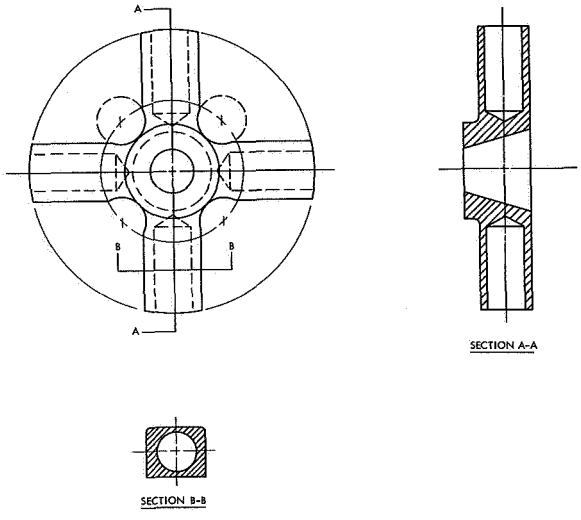


FIGURE 3–7.—Upper central fitting.

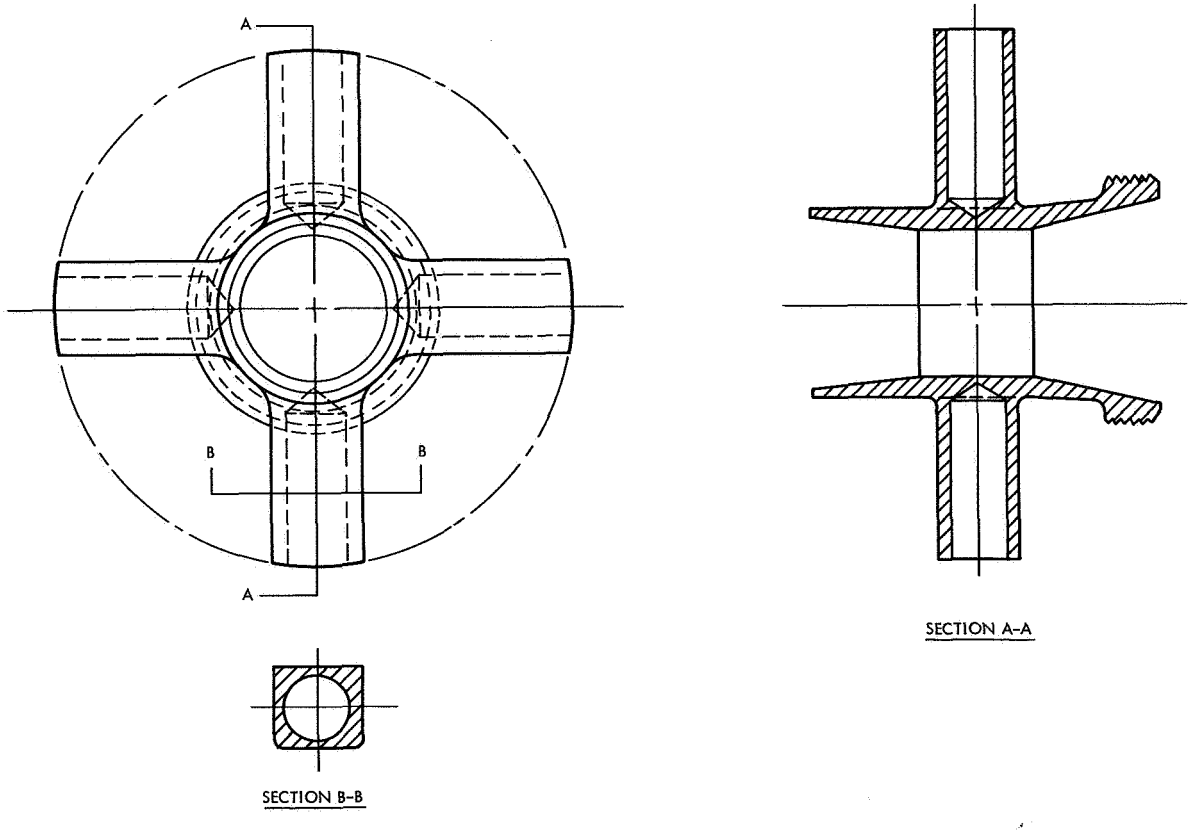


FIGURE 3–8.—Lower central fitting.

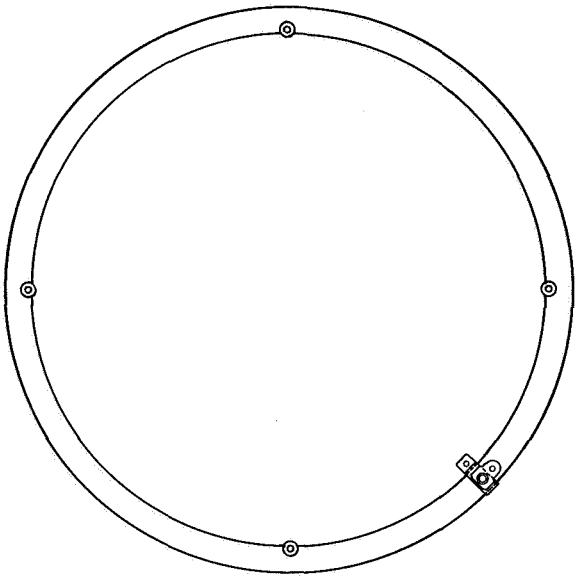


FIGURE 3–9.—Upper ring.

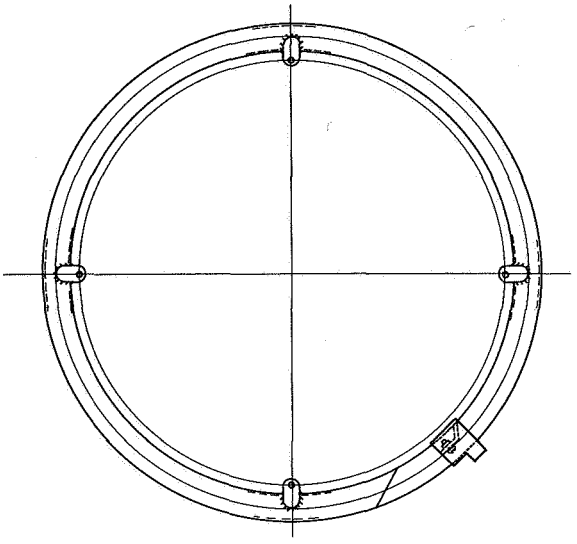


FIGURE 3–10.—Lower ring.

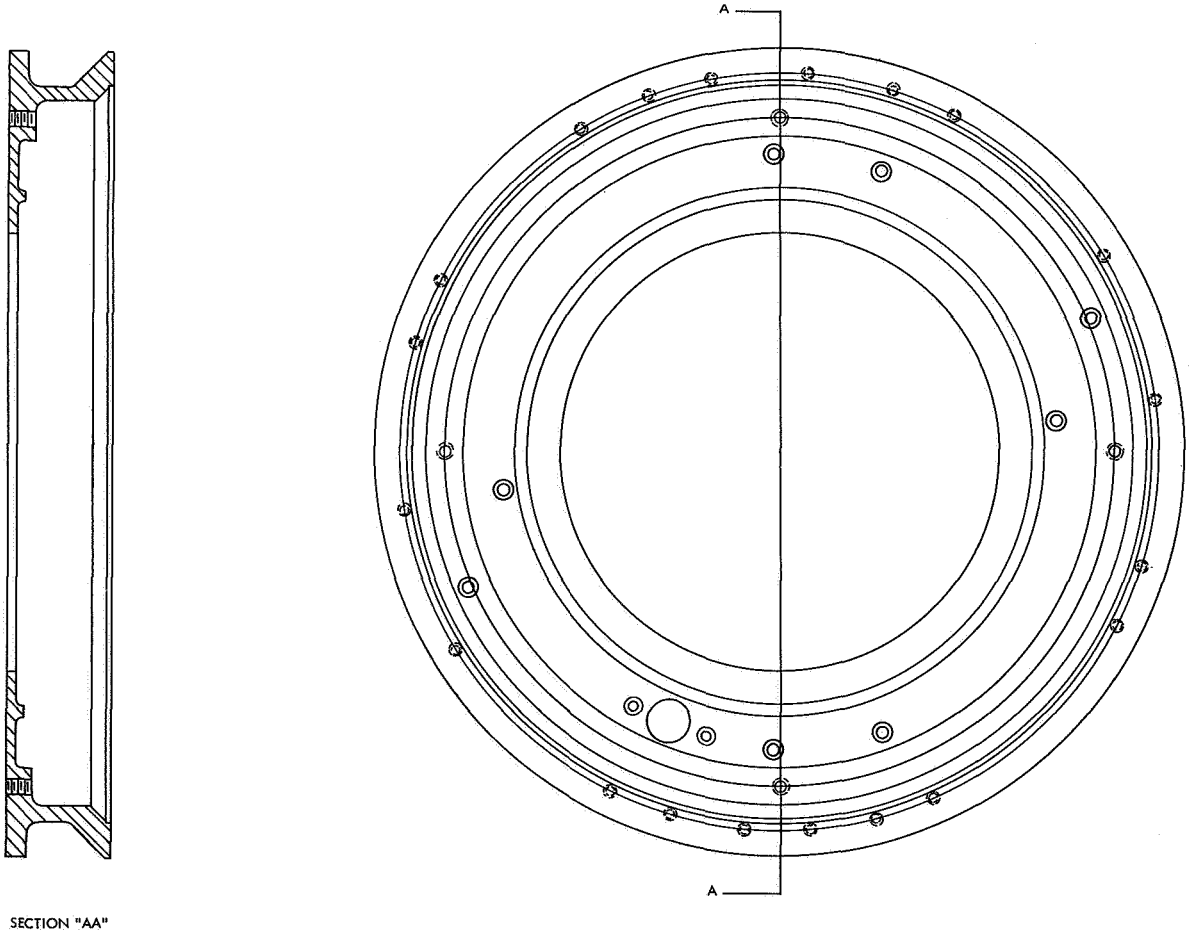


FIGURE 3–11.—Separation ring.

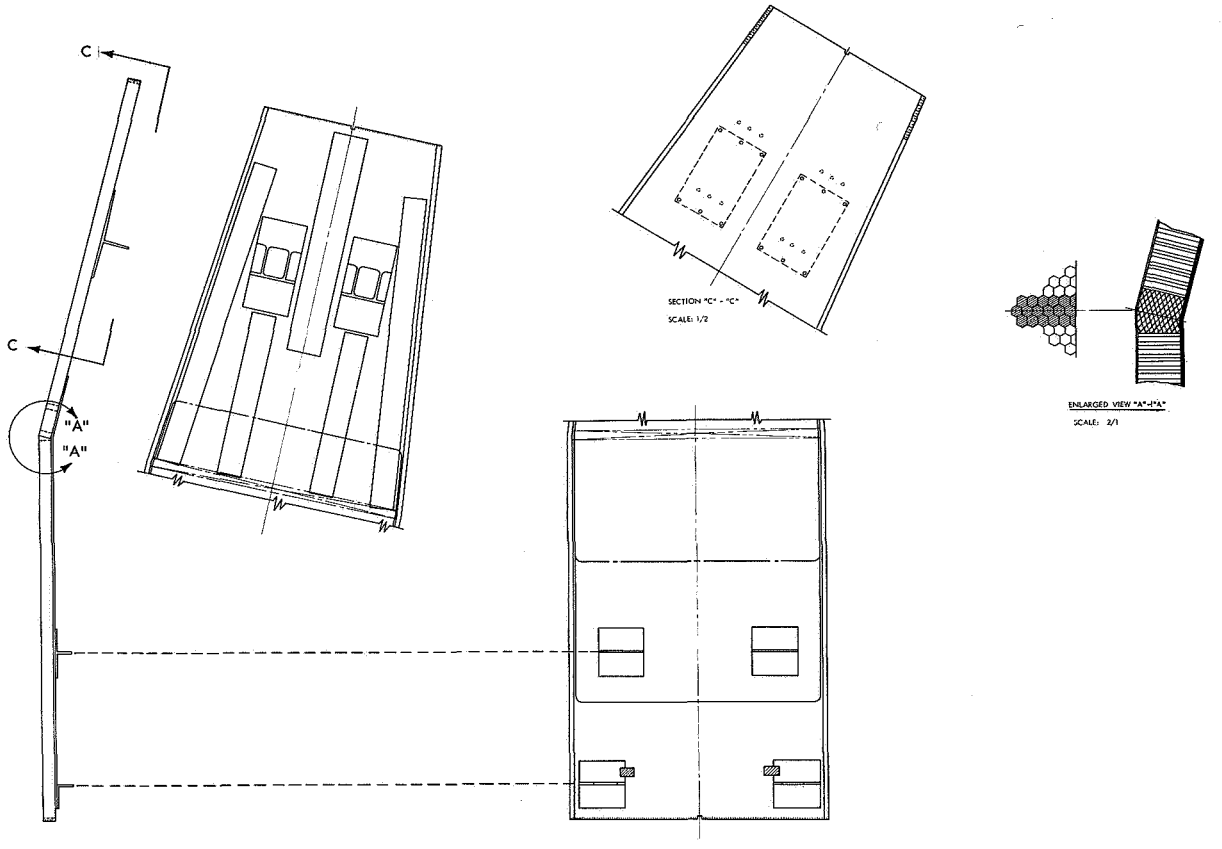


FIGURE 3–12.—Solar panel substrate.

0.0125 lb/in^2, for a ratio of about 6 to 1. The panels were treated as vertical loads through the upper ring to the frame.

WEIGHT CONSIDERATIONS

The initial structural weight allotment for Relay I was 11.25 pounds, or 9 percent of the estimated total. Structure was defined as that material which was present solely for the purpose of carrying a load. The only exception was the lower central fitting which also acted as a heat sink. Mounting brackets were not included in this definition. Increases in component weight and number during the course of the project forced the structural weight up to a final value of 18.94 pounds. This was 11 percent of the 172-pound total spacecraft weight. Since the majority of spacecraft are designed with a structural weight in the range of 15 to 30 percent of the total, the Relay I structure is, by comparison an extremely lightweight design.

The design effort to minimize spacecraft weight took a number of forms. Calculations of required material sizes for all load-bearing members were based on the lower limit of acceptable margins of safety. Weight was then increased only when necessary to accommodate deficiencies indicated by test results. A specific example was the addition of doublers in truss member "J" when it was found that static loading of that member, as initially designed, produced stresses close to the yield point. Since the mounting bolts and other hardware constituted two percent of the total spacecraft weight, and, since the use of non-magnetic material was specified, aluminum bolts were used in almost all cases. Only where the anticipated load exceeded the practical load limits of aluminum was stainless steel used. As another example of weight reduction, the container for the individual

cells of the battery pack was designed as a double channel beam which eliminated most of the brackets associated with conventional pack design.

SPACECRAFT DYNAMICS

Establishing the configuration of the spacecraft required consideration of a number of parametric relationships. A plot of inertia ratio versus solar cell area (see Figure 3–13) was made to determine the limiting values for these design parameters. Similarly, the allowable dynamic unbalance as related to inertia ratio was worked out for several configurations (see Figure 3–14).

Spacecraft attitude in space is controlled primarily by providing spin momentum. Ideally, a spin stabilized configuration designed within the limits mentioned above, and accurately injected, would maintain its injection attitude throughout the required operational period of one year. However, experience has shown that small injection errors cannot be avoided and that a slow drift of the attitude axis will result from magnetic torques. Therefore, a counter torquing system is required. The torquing system designed for Relay I was a magnetic coil having a capacity of approximately 1.5 amp-turn-(meters)^2 (700 turns of 32-gage aluminum wire on a 28-inch diameter with a current of 0.05 amp at 24 vdc). Counter torque produced by current flow through the coil will adjust the spin axis attitude at the rate of approximately one degree per day. A solar aspect indicator and an Earth horizon scanner provide the two angles required to determine spacecraft attitude at any given time. From this angular information the amount and direction of the correctional torque may be calculated and the proper commands programmed.

The above method of attitude control requires that the residual magnetic dipole moment in the spacecraft be zero. Since this value is rarely obtainable, the magnitude and sign of the residual magnetic dipole moment must be measured. The measurement must be made with a threshold sensitivity of approximately 0.05 amp-turn-(meters)^2. A compensating magnet can then be introduced so that, under its average operating condition, the spacecraft will produce a near zero dipole.

A precession damper in the form of an

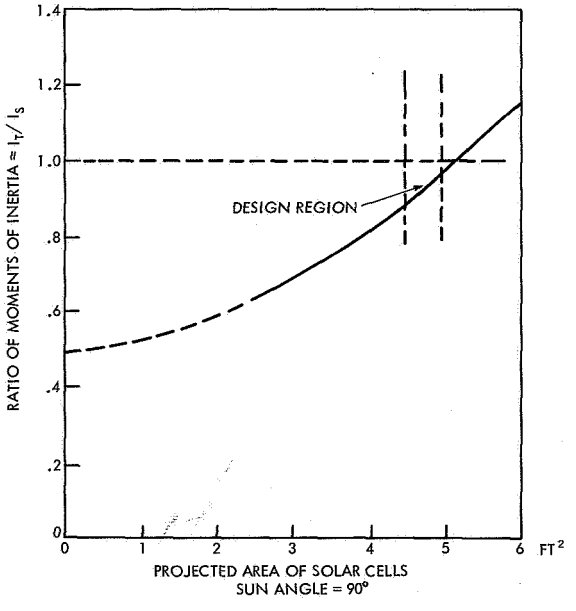


FIGURE 3–13.—Inertia ratio vs. solar cell area.

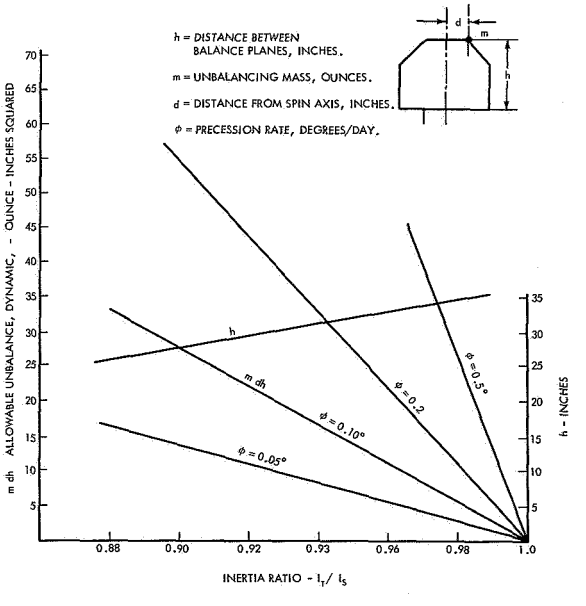


FIGURE 3–14.—Allowable dynamic unbalance for various configurations.

oil-filled toroidal tube was added to aid in damping out spin axis precession caused by unbalance and orbit-injection errors. Design curves are shown in Figures 3–15 and 3–16.

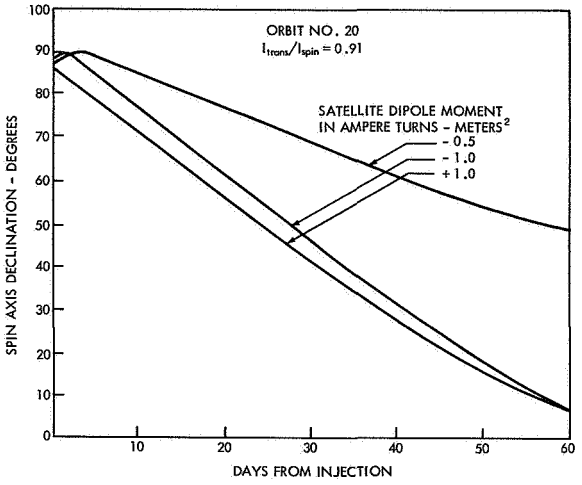


FIGURE 3–15.—Spin axis declination vs. time.

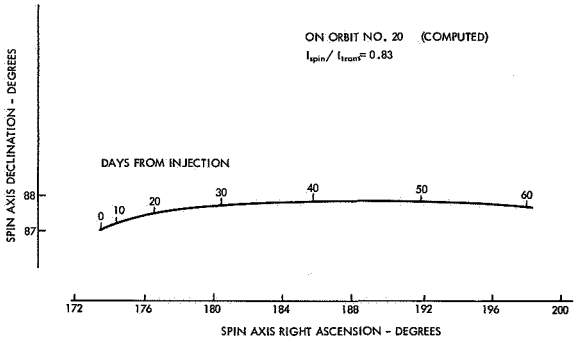


FIGURE 3–16.—Spin axis precession.

MATERIALS

The primary properties required of the structural materials were:

1. Low magnetic permeability
2. Low weight-to-strength ratio
3. Reasonable formability
4. Immediate availability.

The choice of aluminum alloys was justified because that material met all design requirements adequately, and, in the final form provided a design which constituted only 11 percent of the total spacecraft weight. High-strength steels were ruled out for magnetic reasons, and magnesium alloys, with a theoretically lower value for the weight-to-strength ratio, were not considered practical because of weight penalties arising from formability and size-availability considerations.

Formability and availability considerations were controlling factors in the selection of material for the solar-panel substrates. The use of titanium alloys offered no appreciable advantage because the required temperature range was well within the capabilities of aluminum. Furthermore, a design in titanium would have greatly increased material costs and fabrication time.

The bonded joints in the panel substrates and in the rings were made up using an epoxy adhesive, type M–688. Individual components were secured to printed circuit boards with Stycast 1095 Staking Compound.

METHODS OF FABRICATION

The decision to use a combination of riveting, bonding, and bolting for assembly of Relay I was based on the needs for accessibility, multiple removals of components from a partial assembly, and maximizing the slip-joint damping of vibrational input energy. While these parameters were inherently qualitative in nature, the developmental character of much of the equipment made it obvious that the first few assemblies would have to be repeated several times. Thus, the need for easy access arose, and, as it turned out, the cruciform configuration was most efficient in this respect. Its nearest competitor was the base-plate configuration, but this would have required component mounting area, and access to inner locations would have entailed considerable difficulty.

The choice between the use of riveting or bolting methods for a particular joint depended on the relative permanence of the joint. Riveting was used for assembling the four quarter-frames and adhesive bonding was used for the fabrication of solar panel substrates and ring joints. Bolting was used for the assembly of all other joints.

The requirement that the spacecraft withstand high vibrational inputs (10.7g sine wave) in the frequency range which included the natural frequency of the spacecraft made it necessary to absorb or damp out as much of this vibrational energy as possible. This condition required, wherever possible, the use of a joint which would maximize the dry-friction or coulomb damping while maintaining adequate structural stiffness. Bolted or riveted joints satisfy both conditions. A comparison of damping and transmissibility characteristics for these joints is given in Figure 3–17. These semi-quantitative curves indicate that an aluminum structure, having the majority of its joints assembled by bolting and riveting methods, should produce a transmissibility of 10 or less at the fundamental frequency. This condition was true in general for the Relay I assembly. However, high stiffness of the cruciform in the vertical plane tended to raise the transmissibility to values of 12 to 16 at some locations. These high-level inputs degraded the performance of only the wideband receivers and the encoder. The additional protection required by these sensitive devices was provided by specially-designed coulomb dampers, described in the following section.

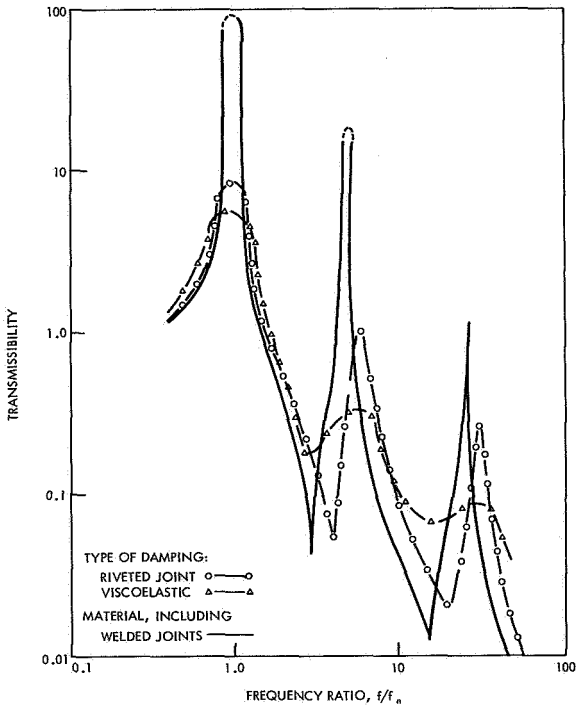


FIGURE 3–17.—Comparison of types of damping.

DESIGN OF COULOMB DAMPERS

To meet the inertia ratio required by spin stabilization, the electronic components were physically arranged to place the component masses at the maximum possible radius and at the minimum displacement from the longitudinal plane of the center-of-gravity; that is, to make a short ring. The controlling components in the effort to obtain a value of inertia ratio of less than 0.95 were the widebrand receiver, the encoder, and the two battery packs. To optimize the location of these heavy components, the local enclosure for each was developed as a box beam to bridge circumferentially between adjacent elements of the cruciform.

Of these four heaviest components, however, both the receiver and encoder showed considerable sensitivity to the high forces developed during vibration testing. The vibratory input forces at the separation ring were multiplied some 12 to 16 times by the transmissibility of the structural path from the ring, up through the vertical legs of the cruciform, and along the bridge beam. The design of the battery packs and the nature of the components were such that they did not show a similar sensitivity.

Of the several vibration tests to which the components and assemblies were subjected, the qualification test specified the most severe inputs. Because the first natural frequency, or resonance, of the entire assembly as a mass-spring system turned out to be 110 cps, the frequency range of greatest interest was from 50 to 500 cps with its 10.7g input.

Since the electronic design of the receiver and encoder had been well established, it was deemed advisable to determine the vibratory-force capacity of the units as they existed. Separate exploratory vibration tests of the components indicated that they could probably survive 80 to 100g peaks. During system test they would experience these high

inputs only as the frequency sweep passed through their local resonance. Thus, they would absorb relatively small amounts of energy. Vibration tests on the components had indicated that these resonances occurred at approximately 150 cps and that the problem could be solved by providing a constraint on transmissibility of the 10.7g input at the separation ring to a value of 10 or less in the frequency range which included both 110 and 150 cps. The design goal was a transmissibility value of 3 to 5.

It had been observed during vibration tests of the assembly that the relative stiffness of the beams was higher than that of the cruciform elements, the beam motion being nearly that of a rigid body. Therefore, one approach to solving the transmissibility problem was to increase the stiffness of the cruciform. But a preliminary redesign of the cruciform, with the increased stiffness necessary to raise the resonance of the cruciform-beam system significantly above the 110-cps fundamental frequency, resulted in an intolerable weight increase. Reducing the stiffness in order to lower the resonant frequency of the cruciform-beam system was not attractive because of the enhanced potential of buckling the cruciform skin at a number of locations. The general approach in isolating the entire satellite from the booster by means of a spring was, of course, invalid because: (1) tremendous displacements are involved and, (2) such a spring would impart an indefinite change to the separation velocity. Thus, the alternatives were reduced to the introduction of an energy-absorbing element between the booster and payload. The four foot-blocks which form the contact and load-carrying elements between the separation ring and the cruciform were originally solid aluminum alloy (2024–T3). Several trial sets of blocks were made from structural plastics having high compressive strength but low elastic modules. Among those tested were the epoxy-bonded glass laminates. The results of transmissibility measurements made during vibration tests indicated only minor reductions with no discernable change in resonant frequency. The substitution of material was made for weight reduction and improved thermal isolation of the ring.

Returning to the cruciform-beam system, it was decided to limit the vibration amplitude at the center of the beam by decreasing its span through the introduction of a brace or post from the beam center to the separation ring. At the same time the force input to the beam and its electronic component was reduced by designing the brace to be an energy-absorbing element.

The use of viscous friction as a means of energy dissipation was denied by the project specification which prohibited the presence of any liquids outside of sealed containers. Thus, coulomb, or dry-friction, damping was the most practical means available. The dimensions of the physical arrangements were such that a column brace of reasonable slenderness (L/r) could be designed within tolerable weight limits, although it would increase total spacecraft weight (see Figure 3–18). In choosing the materials, the paramount consideration was retention of initial friction load throughout the operating life. This was taken as 100 times the duration of the vibration test, or about 3 hours. As the required friction force, or load was not precisely known, the design of the damper included a means for adjusting this force. Consideration of all the requirements led to the choice of a polished, phenolic, fiberglass rod sliding in a stainless steel tube (see Figure 3–19). The tube was longitudinally slit in the region of the overlap.

The general design approach was based on that of Den Hartog* and may be used for any type of damping as long as its action can be expressed either analytically or graphically. For forced vibrations with non-linear damping, the differential equation of motion is

$$m\ddot{x} + f(\dot{x}) + kx = P_0 \sin \omega t \qquad (3.1)$$

where $f(\dot{x})$ is not equal to the $c\dot{x}$ term of

*Den Hartog, J. P., *Mechanical Vibrations*, Fourth Ed., McGraw-Hill Book Co., Inc., New York.

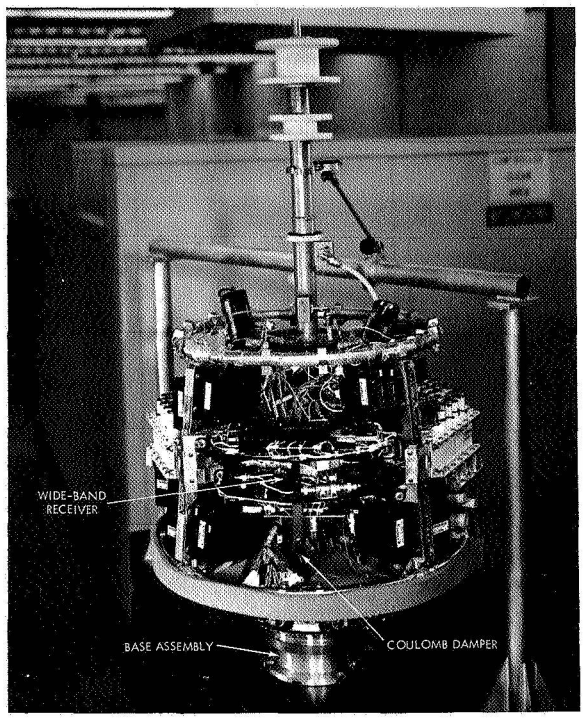


FIGURE 3–18.—Coulomb damper in Relay I assembly.

the equation for linear damping. The motion is not harmonic because of the nonlinear term $f(\dot{x})$. An exact solution for this equation is known only for the case of coulomb, or dry-friction type, damping, where $f(x) = \pm F + cx$. Even though the damping for this design is greater than that usually assumed for this approach, the curve of motion is sufficiently close to sinusoidal that it may be used as a base for an approximate analysis. Basically, the analysis assumed that equal work per cycle will be done in both the sinusoidal and in the equivalent system. The term $f(\dot{x})$ is replaced by an equivalent $c\dot{x}$, and an *equivalent damping constant* $\underline{c}$ is determined such that the actual damping force $f(\dot{x})$ does the same work per cycle as the equivalent damping force $c\dot{x}$. Then $\underline{c}$ is not strictly a constant, but a function of ω and of x_o. Thus the non-linear coulomb system represented by the differential equation can be replaced by a linear one, with the concomitant approximation.

The motion is given by

$$x = x_0 \sin \omega t \tag{3.2}$$

and the work per cycle, of the general damping force $f(\dot{x})$ *is*:

$$u_1 = x_0 \int_0^{2\omega} f(\dot{x}) \cos \omega t \, d\omega t \tag{3.3}$$

The work per cycle of the equivalent damping force $c\dot{x}$ is:

$$u_2 = \pi \, c\omega x_0^2 \tag{3.4}$$

The equivalent damping constant $\underline{c}$ is found by equating (3.3) and (3.4),

$$\underline{c} = \frac{1}{\pi \, \omega x_0} \int_0^{2\pi} f(\dot{x}) \cos \omega t \, d\omega t \tag{3.5}$$

and the amplitude of the now-linearized system is:

$$x_0 = \frac{P_0}{k} \frac{1}{\sqrt{\left[1 - \frac{\omega}{\omega_n}\right]^2 + \frac{\underline{c}\omega}{k}}} \tag{3.6}$$

The amplitude is found by substituting the value of $\underline{c}$ from Equation (3.5), but first the integral must be evaluated. From a plot of

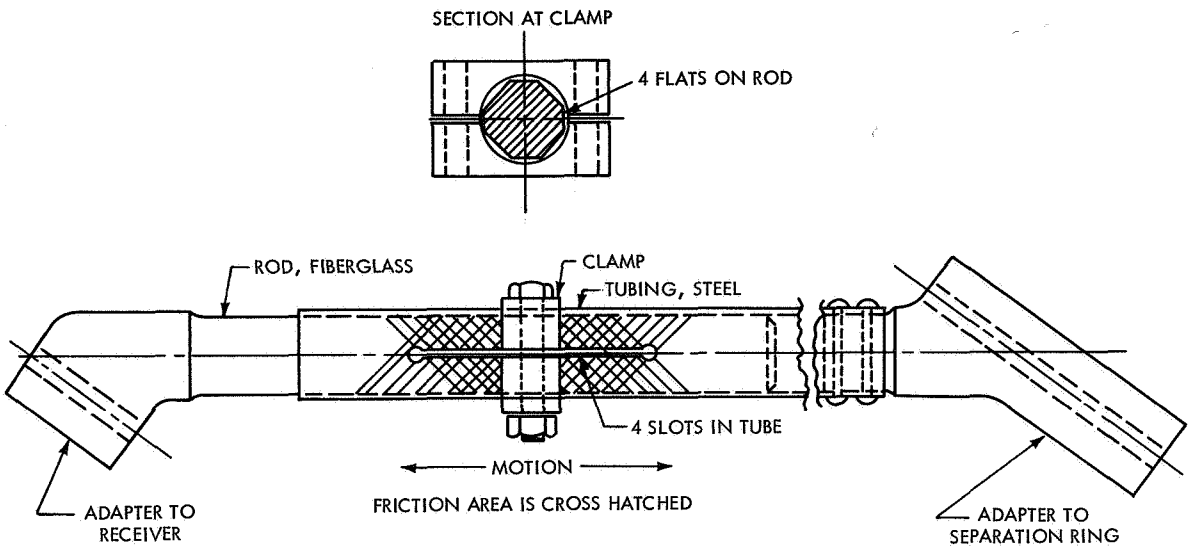


FIGURE 3–19.—Coulomb damper.

damping force and velocity versus ωt, it can be observed that the integral consists of four equal parts

$$4\int_0^{\pi_2} F\cos\omega t\, d\omega t = 4F \tag{3.7}$$

Thus

$$\underline{c} = 4F/\pi\omega x_0 \tag{3.8}$$

and substituting $\underline{c}$ from Equation (3.8) into Equation (3.6) yields

$$x_0 = \frac{P_0}{k}\,\frac{\sqrt{1-[(4/\pi)(F/P_0)]^2}}{1-\left(\frac{\omega}{\omega_n}\right)^2} \tag{3.9}$$

With coulomb friction in the region of $F/P_0 = \pi/4$, the amplitude at resonance is infinite and independent of the damping.

This *linearized* approach was applied in the design of the coulomb damper as a single-degree-of-freedom system at resonance. Thus, critical damping at resonance was required.

Preliminary vibration experiments were performed to determine the natural frequency of the encoder (as typical of these components) when mounted on a rigid brace. This resulted in a value of $f_n = 150$ cps. The weight of the encoder is taken as 11 pounds, and the critical damping at resonance is

$$c_{cr} = \sqrt{\frac{4kW}{g}} = 2\,\omega_n\frac{W}{g} = 2(2\pi f_n)\frac{W}{g} \tag{3.10}$$

or

$$c_{cr} = 4\pi(150\text{ cps})\,\tfrac{11}{386} = 54\text{ lb-sec-in}^{-1}$$

Taking the transmissibility value as 5, for a trial, and assuming that the force on the center of the encoder beam from the brace is relatively high, causing the beam to act as a rigid body, the acceleration at the encoder center and the velocity across the friction elements may be found. The acceleration is:

$$\begin{aligned} a &= \text{input} \times \text{transmissibility} \\ a &= (10.7\text{g})\,(5) = 53.5\text{ g} \end{aligned} \tag{3.11}$$

and the velocity: $V_0 = a/w = a/(2\pi f_n)$

$$\begin{aligned} &\doteq (53.5)\,(386)/2\pi\,150) \\ &= 22\text{ in-sec}^{-1} \end{aligned} \tag{3.12}$$

The critical friction force at resonance is then:

$$\begin{aligned} F_{cr} &= V_0 c_{cr} \\ &= (22\text{ in-sec}^{-1})\,(54\text{ lb-sec-in}^{-1}) \\ &= 1190\text{ lb} \end{aligned} \tag{3.13}$$

This critical-friction force must be developed by the normal force acting through the coefficient of friction at the interface between the fiberglass rod and the steel tube. It is not necessary to know the value of the coefficient of friction, but it is required that the friction force and the break-away force not differ widely. It is also required that the wear and

surface characteristics of the mating materials be such that the friction force remains reasonably constant for the operating period. This is a condition best demonstrated by experiment. The combination of fiberglass and stainless steel proved admirable since no detectable wear nor change in friction force occurred during the extensive experimental operations. The slits in the tube and the adjustable clamp provided the means of setting the normal force which controls the friction force.

The proper value of the friction force is found through the use of the damping ratio. One may take the approximation:

$$\frac{F_{FR}}{F_{cr}} \approx \frac{c}{c_{cr}} \tag{3.14}$$

and, since the amplification is to be 5 (or preferably less), the value of the damping ratio, 0.13, may be read from standard resonance curves for a linear system.* Then from Equation (3.14):

$$\begin{aligned} F_{FR} &= 0.13\, F_{cr} \\ &= 0.13(1190) = 150 \text{ lb} \end{aligned} \tag{3.15}$$

The clamp on the brace was torqued to provide the corresponding normal force, and the axial friction force was measured by experiment. The relationship between this axial friction force and the torque applied to the clamping bolts was established so that the experimental measurement could be omitted in future production.

Direct use was made of the rigidity inherent in the brace even though its major function and design are those of a damper. The introduction of the axial force essential to the dissipation of input energy acts to increase the stiffness of the encoder support and thus to raise its natural frequency. This overall action (i.e., to reduce the energy input to a sensitive component and to move its resonance away from the frequency of maximum energy input) was the primary reason for using the damper.

The increase in stiffness was difficult to calculate because of the unknown spring rate —the k of Equation (3.9)—of the supporting cruciform elements of the encoder. The overall spring rate for the cruciform assembly had been determined during static load tests as approximately 200,000 pounds per inch. This value approximates the value of 211,000 pounds per inch derived from the experimental data of a 110-cps resonance at 172 pounds load, by the relation:

$$\begin{aligned} k_{\text{spacecraft}} &= (2\pi f_n)^2 \frac{W}{g} \\ &= [2\pi(110)]^2 \tfrac{172}{386} \\ &= 211{,}000 \text{ lb-in}^{-1} \end{aligned} \tag{3.16}$$

For the encoder alone:

$$\begin{aligned} k_e &= [2\pi(150)]^2 \tfrac{11}{386} \\ &= 24{,}500 \text{ lb-in}^{-1} \end{aligned}$$

The displacement of the encoder without the brace would be (11 lb)/(25400 lb-in) or about 0.004 inch. With the brace added, the force on the cruciform supports was 11 pounds plus 150 pounds, for a new displacement of about 0.006 inch. However, the displacements with the brace had been measured at about 0.0010 to 0.0015 inch, for a ratio of 6 to 1.2, or 5. Since the natural frequency is related to the square root of the spring constant or displacement, it would be expected to change by a ratio of about 2.2. The results of vibration testing indicate that the damper increased the resonance from 150 cps to 215, for a ratio of 1.4 (see Figure 3–20). No particular precision was expected of these calculations, but it was important that the inevitable increase in stiffness due to the additional force of damping be accounted for by approximating the increase in resonant frequency.

The benefit gained from the installation of the damper is readily seen by a comparison of transmissibilities at resonance. Without the damper the encoder transmissibility was 12 at 150 cps; with the damper it was 7 at 215 cps. The peak force inputs to the encoder were thus reduced to values which were within its capacity of about 10 transmissibility at 10.7g input. The secondary

*Den Hartog, J. P., *Mechanical Vibrations*, Fourth Ed., McGraw-Hill Book Co., Inc., New York.

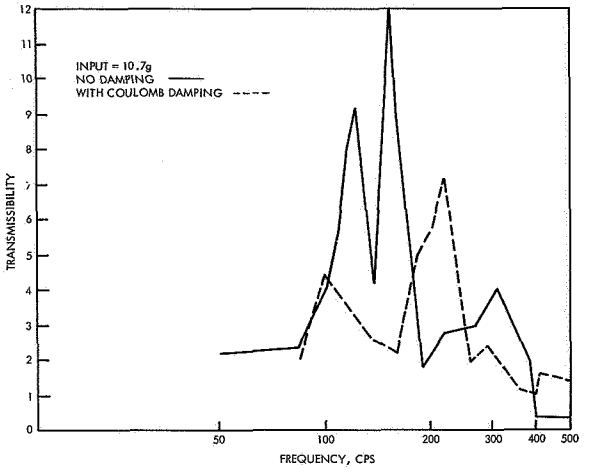


FIGURE 3–20.—Transmissibility vs. frequency for Relay encoder.

peaks, near the 100-cps region for both conditions, were excited by the resonance of the entire assembly and represent a similar reduction in force. The wideband receiver responded even better to a similar treatment. Its transmissibility at resonance was reduced from 16 to 6.

The data gathered during the tests was used to calculate the actual damping and transmissibility on the assumption that the damping was proportional to the square of the velocity, i.e., $f(\dot{x}) = c_1\dot{x}^2$. The equivalent viscous damping is:

$$c = \frac{4\omega_n^2}{\pi a}\int_0^{\pi/2\omega} c_1\dot{x}^2 \cos \omega t \, dt \qquad (3.17)$$

Recalling that $\dot{x} = a/\omega_n \cos \omega t$ and that $c_1 = F_0/\dot{x}^2$

Equation (3.17) yields

$$c = \frac{8F_0\omega}{3\pi a} \qquad (3.18)$$

The data yielded the following values:

F_0, the frictional force = 150 lb
a, the maximum acceleration = 77 g
f_n, the resonant frequency of the component with damper = 215 cps

Substituting these values in Equation (3.18)

$$c = \frac{8(150 \text{ lb})\ 2\pi(215 \text{ sec}^{-1})}{3\pi(77g)\ (386 \text{ in-sec}^{-2})} = 5.5 \text{ lb-sec-in}^{-1}$$

The damping ratio is then:

$$\frac{5.50}{54.0} \approx 0.1$$

which, when entered on standard resonance curves, indicates a transmissibility of about 6, comparable to the measured value of 7.

The energy dissipated per cycle* was also calculated from the expression:

$$D_0 = \frac{2}{3}\left[\frac{1-2k}{k_s}\right]\frac{(F_{\max} - F_{\min})^3}{q} \qquad (3.19)$$

where D_0 is energy, (in in-lb/cycle)

q = force per unit length of the slipped interface
k = $k_s/(k_s+k_t)$
k_s = A_sE_s, (s indicates shaft)
K_t = A_tE_t, (t indicates tube)

Substituting the data values:

$$D_0 = \frac{2}{3}\left[\frac{1-2(0.7)}{10^6}\right]\left[\frac{(175-135)^3}{(150/1)}\right]$$
$$= 2 \times 10^{-6} \text{ in-lb/cycle}$$

which is considered an acceptable value.

In summary, the presence of rather sensitive electronic components, in addition to a configuration dictated by the dynamic-stability criterion, required additional vibration damping, which was furnished by large-capacity coulomb dampers designed specifically for that purpose. This is believed to be the first application for dampers of this type in a spacecraft.

BASIC SPACECRAFT THERMAL DESIGN

Design Requirements

While the thermal design was in progress, requirements were continuously being revised and updated. The following are representative of the values that were used in the design.

Many parameters were from an orbit computed by STL, commonly referred to as *Orbit 32*. The orbit had an inclination of 54

*Pian, T. T. H., and Holowel, F. C. Jr., *Structural Damping in a Single Built-up Beam*, ASME Proc. First National Congress Appl. Mech.

degrees, and an altitude that ranged from a minimum of 800 nautical miles to a maximum of 3000 nautical miles. This resulted in an orbit period of 163 minutes and a suntime that varied from 75 to 100 percent; hence, the maximum eclipse time was 40 minutes. For thermal design purposes, this orbit was similar to the final orbit of Relay I, which had an inclination of 47.5 degrees, altitudes from 700 to 4000 nautical miles, and a period of 185 minutes.

The spacecraft was spin stabilized, with the angle between the sun and the spin axis (sun angle) equal to $90\pm30°$. The maximum duty cycle for the wideband equipment was 36 minutes during each orbit, with operation possible on three consecutive orbits. The orbit average power dissipation was estimated to be from a 16-watt minimum (no wideband operation) to a 90-watt maximum (36-minute wideband operation), in addition to the heat dissipated by the batteries and power regulation equipment.

Trade-offs in Approach

General

Some spacecraft are built around the thermal design, with the best shape (spherical) and structural support dictated to facilitate the thermal design. The basic philosophy in the design of the Relay I spacecraft was different. A configuration was first set by other considerations, and then changes required for adequate thermal control were introduced where necessary. This philosophy resulted in a little weight being required for thermal control and eased the design problems in other areas.

The spacecraft shape was the result of maximizing the area for mounting solar cells within the space limitations of the shroud. The internal equipment was arranged so that the maximum moment of inertia occurred about the spin axis, and the structure was then designed to support the equipment. The only locations dictated by thermal considerations were those of the voltage-limiter resistors, and the two TWT's. The addition of an active thermal controller, of low emittance surfaces on the inside of the solar panels, and of thermal shields at the ends of the spacecraft essentially completed the thermal design.

Internal Coupling

Several considerations indicated a need for maximum thermal coupling within the electronic package. Most of the internal electronic component, including the batteries, had similar temperature requirements. Some components, especially the two TWT's and their power supplies, dissipated large amounts of heat, while other components had negligible dissipation. There were frequently large variations in the power dissipated in any particular piece of equipment. Also, if one component was not on, then either another would be or an equivalent amount of power would be dissipated in the power supply equipment.

Conduction paths were improved where possible, and all electronic boxes were painted to insure maximum radiation coupling. Thermally connecting the interior equipment permits the high power-dissipating components to receive the benefit of the thermal mass of the other components, and the temperature variations caused by switching power from one component to another are thus minimized.

Insulation to Exterior

Since the spacecraft would be subjected to 40-minute eclipses where the equilibrium temperatures would be around —100°C, provisions were required to prevent excessively low internal temperature. The temperature drop in eclipse can be estimated from:

$$\Delta T \approx \frac{\epsilon A \sigma T^4 \Delta t}{mc} =$$

$$\frac{\epsilon(3500 \text{ in}^2)\ (0.3 \text{ w/in}^2)\ (2400 \text{ sec})}{(125 \text{ lb})\ (380 \text{ w-s/lb deg K})} = \epsilon \cdot 53 \text{ deg} \tag{3.20}$$

where: ϵ is the emittance; A, the total surface; T, the absolute temperature; m, the mass; and c, the specific heat. If the internal equipment were well coupled to the outside (emittance equal to one), the temperature

drop would be of the order of 50°C, which is excessive.

The internal equipment was insulated from the exterior by means of a low emissivity coating on the inside of the solar-cell panels. Initially, the inside surface of the honeycomb aluminum was left uncoated. When this proved insufficient, aluminum foil and, later, aluminized mylar were applied to the surface. The effective emittance of the exterior was thus reduced by a factor of ten, and the temperature drop during eclipse was a satisfactory 5°C.

Thermal Coupling to Spacecraft Bottom

The exterior of the solar panels was designed to yield a minimum absorptivity-emissivity ratio and the lowest possible solar-cell temperature. This resulted in an estimated solar-cell temperature of approximately 20°C in the sunlight. While this is satisfactory for the solar panels, excessively high temperature would result within the internal components to dissipate the required amount of heat through the solar panels. To lower the average temperature of the internal equipment, the thermal coupling to the bottom of the spacecraft was maintained high. The bottom surface is colder than the solar panels because the sun does not shine perpendicularly on this surface. By adjusting the coupling to this surface, the average temperature can be set above or below the solar panel temperature of 20°C.

Passive Versus Active Thermal Control

Both in the study phase (STL) and in the initial thermal design, the advantages and disadvantages of an active thermal control were studied. A completely passive system has a low initial cost, low weight penalty, and high reliability; however, the degree of temperature control was, to some extent, marginal. It was difficult to prove that the passive design would be adequate, in view of the inevitable changes that could be expected to arise during final design and construction.

The final choice was a basically passive system, with the use of active control as a small adjustment, or vernier, to decrease the temperature excursions. Considerable latitude was thus allowed for changes. The active control could have been eliminated if the passive control had proved sufficient, or the degree of active control could have been increased if necessary. The final design did include the initial active controller proposed. This was sufficient to reduce temperature excursions, but was small enough that the equipment would probably operate properly even if the active controller failed. Thus, high reliability was assured.

The logical place for the active thermal controller was between the equipment and one of the ends. The bottom end was chosen because it had more surface. Location of the active controller on the exterior of the spacecraft was desirable from a thermal viewpoint. However, the ratio of moments of inertia was critical, and any weight on the spacecraft ends affected the radio adversely. The controller was therefore mounted in the interior, several inches closer to the center of mass of the spacecraft. The interior mounting also facilitated thermal testing of the spacecraft.

A circular type of controller with open pie-sections instead of louvers was chosen because the particular spacecraft area was circular, more experience had been obtained with this type of control, and less friction was involved. Actuation by expanding gas was chosen because it provided more power to overcome friction than a comparable weight of bimetallic strips. The sensor was located on a battery because this component was not critically sensitive to temperature extremes. Finally, hydraulic linkage between the sensor and controller was used for flexibility, ease of installation, and reliability.

Location of High Power Components

The components that generated significant amounts of heat were the batteries, the traveling wave tubes, the TWT power supplies, the TWT power regulators, and the voltage limiter. The batteries generated excessive heat only under overcharge conditions, and a temperature-actuated charge cut-off lim-

ited their temperature to 32°C. The traveling wave tubes were located where their heat could best be distributed throughout the spacecraft. The TWT power supplies were located with the other electronic equipment and generated high, but not excessive, temperatures. The temperature requirements of the remaining two sets of components were less severe, allowing these components to be located away from the main equipment. This prevented the heat generated by these components from affecting the main equipment.

The transistors associated with the TWT power regulators were located on a collar near the bottom of the spacecraft. Because of small size and high power dissipation, a substantial temperature rise was expected. Therefore, they were located at the coldest part of the spacecraft, where the heat dissipation was adequate at an operating temperature below the maximum limit.

The resistors associated with the voltage limiter presented a special problem. The power supply was overdesigned in power capability to allow for solar-cell degradation expected from particle radiation in space. This required excess power to be dissipated in the voltage limiter during the early life of the spacecraft and the amount of dissipation would decrease as the solar cells degraded. If the resistors had been located inside the spacecraft, the gradual decrease in heat dissipated would have produced a long term cooling effect on the spacecraft. For this reason, the resistors were mounted externally on the solar cell panels, where the heat could be dissipated directly into space without affecting spacecraft temperatures.

Initial Thermal Design

General Theory

Based on the considerations outlined in the previous section, an initial heat balance for the spacecraft was formulated. This initial concept was later refined and modified, and calculations were performed in much greater detail. However, it does contain the basic formulation of the thermal design.

To obtain a mean interior-spacecraft temperature, it is assumed that the interior is one isothermal mass and is coupled by radiation to the three external surfaces. These couplings by radiation are constant, except for the coupling to the bottom surface that will be a function of the position of the active thermal controller. The heat balance on each of the three external surfaces can then be written as:

$$\epsilon_B A_B \sigma T_B^4 = a_B A_B (S_B + \rho_B) + \epsilon_B A_B \mu_B + K_B (\sigma T^4 - \sigma T_B^4) \quad (3.21)$$

$$\epsilon_s A_s \sigma T_s^4 = a_s A_s (S_s \rho_s) + \epsilon_s A_s \mu_s + K_s (\sigma T^4 - \sigma T_s^4) \quad (3.22)$$

$$\epsilon_T A_T \sigma T_T^4 = a_T A_T (S_T \rho_T) + \epsilon_T A_T \mu_T + K_T (\sigma T^4 - \sigma T_T^4) \quad (3.23)$$

and the heat balance for the interior package is:

$$K_T(\sigma T_T^4 - \sigma T^4) + K_s (\sigma T_s^4 - \sigma T^4 + K_B (\sigma T_B^4 - \sigma T^4) + Q = 0 \quad (3.24)$$

The definition of the quantities and some numerical values are listed in Table 3–4.

From these four equations, the temperatures of the three external surfaces can be eliminated, and the result solved for the temperature of the interior package. It is useful to define various secondary constants to simplify the expression for the internal temperature. The equivalent radiation input to any surface is defined by

$$I = \frac{a}{\epsilon} (S + \rho) + \mu \quad (3.25)$$

The fractional coupling constant to space is a function only of the spacecraft and, for the top surface, is

$$A = \frac{K_T}{1 + \frac{K_T}{\epsilon_T A_T}} \left[\frac{K_T}{1 + \frac{K_T}{\epsilon_T A_T}} + \frac{K_s}{1 + \frac{K_s}{\epsilon_s A_s}} + \frac{K_B}{1 + \frac{K_B}{\epsilon_B A_B}} \right]^{-1} \quad (3.26)$$

with similar equations for the sides and bottom surfaces. Finally, the constant electrical power term is defined by

$$D = \frac{Q}{\frac{K_T}{1 + \frac{K_T}{\epsilon_T A_T}} + \frac{K_s}{1 + \frac{K_s}{\epsilon_s A_s}} + \frac{K_B}{1 + \frac{K_B}{\epsilon_B A_B}}} \quad (3.27)$$

TABLE 3–4.—*Thermal Design Parameters*

Symbol	Quantity	Initial design value*
A_T	External area, top	300 in^2
A_S	External area, sides	2600 in^2
A_B	External area, bottom	600 in^2
A	Coupling constant to space, top	0.20 and 0.07
B	Coupling constant to space, sides	0.69 and 0.44
C	Coupling constant to space, bottom	0.21 and 0.49
D	Constant electrical power term	0.067 and 0.101 w/in^2
I_T	Equivalent radiation input, top	0.027 w/in^2
I_S	Equivalent radiation input, sides	0.202 and 0.231 w/in^2
I_B	Equivalent radiation input, bottom	0.020 and 0.155 w/in^2
K_T	Radiation coupling, interior to top	25 in^2
K_S	Radiation coupling, interior to sides	165 in^2
K_B	Radiation coupling, interior to bottom	50 and 250 in^2
Q	Electrical power input	15 and 35 w
S_T	Direct solar radiation, top	
S_S	Direct solar radiation, sides	
S_B	Direct solar radiation, bottom	
T	Temperature of spacecraft interior	4°C and 23°C
T_T	Temperature of surface, top	
T_S	Temperature of surface, sides	
T_B	Temperature of surface, bottom	
α_T	Surface absorptance to sunlight, top	0.9
α_S	Surface absorptance to sunlight, sides	0.9
α_B	Surface absorptance to sunlight, bottom	0.27
ϵ_T	Surface emittance, top	0.9
ϵ_S	Surface emittance, sides	0.9
ϵ_B	Surface emittance bottom	0.9
μ	Average earth thermal radiation	0.017 w/in^2
ρ	Average earth reflected radiation	0.010 w/in^2
σ	Stefan-Boltzmann constant	3.657×10^{-11}w/in^{2}degK^4
τ	Spacecraft time constant	

*Where two values are given, the first corresponds to minimum spacecraft temperature conditions (75 percent suntime and 90° sun angle) and the second corresponds to maximum temperature conditions (100 percent suntime and 120° sun angle).

With the above definitions, the temperature of the spacecraft interior can be written as:

$$\sigma T^4 = AI_T + BI_S + CI_B + D \quad (3.28)$$

where the effects of the external inputs and the effects of the spacecraft parameters have been separated. The constants A, B, C, and D are functions of the spacecraft geometry, surface properties, and electrical operation. The equivalent radiation inputs (I) are functions of the external environment (except for the α/ϵ ratio of the surfaces). The spacecraft constants were measured experimentally in various tests and adjusted when necessary to tolerable values.

Using the initial design values given in Table 3–4, the calculated temperature for the spacecraft interior was between 4°C and 23°C. The actual battery temperature would increase under overcharge conditions to the temperature cut-off, which was set at 32°C. The minimum temperature would be lower than 4°C due to transients, which are estimated below.

Transients

Temperature fluctuations from two sources were expected to be important: (1) duty

cycles of the equipment, and (2) eclipses of the sun. Initially it was expected that when the wideband equipment was turned on and dissipated two to three times the average power, the spacecraft temperature would rise. To counteract this effect, the transistors of the wideband power-supply regulators were removed to the bottom of the spacecraft, and the traveling wave tubes were positioned so that much of their heat would go directly to the spacecraft bottom. The result of these efforts was that the temperature actually decreased slightly when the wideband equipment was operated.

The temperature drop when the spacecraft enters the shadow of the earth depends primarily on the time in eclipse and the spacecraft time constant. It was shown earlier that this would be over fifty degrees unless the spacecraft was insulated. With the assumed radiation couplings between the interior and the external surfaces, the temperature drop was estimated at only four degrees, which is tolerable. The actual drop was affected by cut-off of solar power which decreased internal dissipation and tended to increase the temperature drop. However, the mass of the solar-cell panels, neglected so far, delayed the falling-off of temperature, and therefore the transient was small. The expected temperature drop was therefore about four degrees, and the spacecraft time constant was slightly over ten hours.

Conclusions

The final thermal design resulted from modifications necessitated by refinements in the calculations and inputs from other areas. Probably the most important change was that the thermal coupling to the solar panels had to be increased due to structural difficulties, and this had several results. Little effect was produced on the average temperature since the panels and interior are close in temperature. The increase in the temperature drop during eclipse was partially offset by the increase in spacecraft weight to 172 pounds. The fractional thermal coupling to the bottom decreased since the coupling to the sides had increased. This factor, with several other necessary changes, decreased the effect of the active thermal controller to a value smaller than had been anticipated, but it was still adequate.

The average battery temperatures were expected to be in the 0°C to 30°C range, with most of the interior of the spacecraft also in the same range. This was accomplished with relatively minor modifications (determined mainly by structural and solar power considerations) to the spacecraft design. The weight for thermal control was 3.70 pounds, about two percent of the spacecraft weight, which included the active thermal controller and the twenty-two thermistors for reporting temperatures. While a smaller temperature range is always desirable, the range achieved was a satisfactory compromise in view of the equipment requirements as well as the weight and cost of additional temperature control.

COMPONENTS

Coatings and Finishes

General

The critical surfaces for spacecraft thermal control and the measured properties of these surfaces are listed in Table 3–5. The other spacecraft surfaces were those of the unfinished aluminum structure, and most of

TABLE 3–5.—*Thermal Properties of Surfaces*

	ϵ		α/ϵ	
	Value	Method	Value	Method
External surfaces				
Solar cells, individual	.91	C–T	.91	C–T
Solar cells, panel	.86	S–P	.98	S–S
PV–100 paint sprayed on aluminized mylar.	.90	C–T	.35	C–T
Internal surfaces				
Inside of solar cell panels	.13	C–S	------	--------
Insde of thermal model panels	.14	C–S	------	--------
Aluminized mylar on active thermal controller.	.08	C–S	------	--------
	.07	S–P	------	--------

Test Methods

C–S Calorimetric Steady State
C–T Calormetric Transient
S–P Spectrometer
S–S Solar Simulator

the electrical subsystem housing surfaces which were painted black. The batteries were painted white for reasons other than thermal.

The thermal design goal was maximum emittance on all external and internal surfaces, except for the inside of the solar panels and the active thermal controller surface. The absorptivity/emissivity ratio was minimized on the top and bottom surfaces of the spacecraft. In most cases the measured values were in close agreement with the values upon which the original thermal design was based.

External Surfaces

The spacecraft sides consisted of eight aluminum honeycomb panels covered with solar cells having a total area of 2900 square inches. The P-on-N silicon solar cells (Hoffman) were 1×2 centimeters and were covered with 0.060-inch thick Corning fused silica glass (7940). The cover glass included a blue filter having a cut-on at 435 ± 15 millimicrons. The thermal properties of the solar cells were measured for individual cells and also, as will be described later, for a complete panel.

The spacecraft bottom (larger end) was covered with a thermal shield of 0.001-inch thick mylar, fastened with *zippers*, and slit to allow for vibration flexing of the panels. Its area was 560 square inches. The mylar was aluminized on both sides for adhesion purposes and then painted with PV–100. The composition of the PV–100 paint and the results of an ultraviolet test are shown in Table 3–6. The data shows an increase of approximately 15 percent in α/ϵ for a one-year equivalent of normal solar radiation. since the solar radiation would usually strike this surface at a low angle of incidence (maximum of 30° from surface), much less browning of the PV–100 was expected in orbit.

The spacecraft top (wideband antenna end) was covered with a similar mylar shield having an area of 185 square inches. However, the inside surface was aluminized but not painted. A low emittance of the inner top surface was needed to minimize the radiative coupling to the top.

TABLE 3–6.—*Composition and Ultra-Violet Test of PV–100*

Composition of PV–100

Titanium dioxide (rutile, non chalking)	26.1%
Calcined clay	30%
Silicone alkyd (60% non volatile)	22.3%
Mineral spirits	11.7%
Xylol	4.4%
Bentone 34	.03%
Following are mixed together and ground in pedestal:	
Manganese naphthanate	.17%
Lead naphthanate, 6%	1.09%
Mineral spirits	2.3%
Xylol	11.4%
Anti-skimming agent	.27%

Ultraviolet test of PV–100

Equivalent months in space	α/ϵ	α	ϵ
0	.35	.33	.94
3	.35	.31	.87
6	.37	.35	.93
12	.41	.35	.85

Test lamp = 4-watt G.E. germicidal ultraviolet lamp

Internal Surfaces

The active thermal controller was covered with aluminized mylar to provide a radiation heat shield when closed. The covering was mylar film, type C, 0.001-inch thick, aluminized to a maximum visual reflectivity specification on both sides. For low friction in a vacuum environment, some aluminum parts of the controller were anodized and then coated with Emvalon 310 (thickness 0.0005 inch nominal to 0.0007 inch maximum).

About half of the inner surface area of the solar-cell panels was covered with a radiation heat shield. This shield consisted of a sheet of mylar aluminized on one side. The mylar was bonded to the panel in spots to minimize direct contact with the panel.

Test Methods

The technique used for each measurement is indicated in Table 3–5. For the steady state calorimetric method, an electrical heater is

contained inside the sample, and the emittance is determined from the electrical power input, the sample equilibrium temperature, and the temperature of the vacuum chamber walls. The transient calorimetric method requires the use of a carbon arc solar simulator. The thermal emissivity is determined from the rate of change of sample temperature, and the absorptivity-emissivity ratio is determined from the equilibrium temperature.

In the spectrometer method, the normal reflected light from a surface illuminated with total hemispherical illumination was measured as a function of wavelength. The final value used was the average over the spectral band of interest.

A solar simulator test on a larger scale was used to measure the absorptivity of a solar-cell panel since this factor was especially critical in the thermal design of the spacecraft. A typical panel was suspended in a six-foot diameter, ten-foot deep vacuum chamber, and its solar-cell surface was illuminated by a pair of carbon arc lamps used in solar simulation tests on the Relay I spacecraft. The thermally black chamber walls were maintained at a temperature of −110°C. The average intensity incident on the panel was measured by reading the short-circuit current of four pre-calibrated solar cells suspended in front of the panel in the path of the arc-lamp beam. The equilibrium temperature of twenty-five evenly distributed points on the front and back surfaces of the panel were measured. The back and side surfaces of the panel were coated with a paint of known emissivity. The solar cell emissivity of 0.86 had been obtained by using the spectrometer. The solar absorptivity, a, of the outside of the solar panel was then determined from:

$$a = \frac{\sum_i \epsilon_i A_i (\sigma T^4 - \sigma T_w^4)}{A_n S} \qquad (3.29)$$

where i designates front, side, or back surface of panel; and

ϵ_i = the emissivity ($\epsilon_F = 0.86$, $\epsilon_S = 0.9$, $\epsilon_B = 0.80$),

A_i = the surface area ($A_F = 325.6$ in^2, $A_S = 41.3$ in^2, $A_B = 315.6$ in^2),

σ = the Stefan-Boltzman constant (3.66×10^{-11} w/in^2 degK^4),

T^4 = the fourth power average of surface temperature,

T_w = the chamber-wall temperature (−110°C),

A_n = the projected area of the panel to the incident light beam ($A_n = 322$ in^2), and

S = the intensity of the incident light beam.

Three tests were conducted, using different values of intensity, S, by chopping the incident light beam. The following results were obtained:

S (w/in^2)	a
0.954	0.825
0.865	0.825
0.740	0.870

The average panel absorptivity is 0.840, and the average absorptivity/emissivity ratio is 0.975. This agrees with results from previous measurements on a single cell.

Temperature Sensors

General

Twenty-two temperature sensing circuits are included in the telemetry subsystem to evaluate spacecraft performance and for diagnostic purposes. The six circuits associated with the batteries are also used to prevent charging of a battery when its temperature is above 32°C. No discussion is included in this section of the seven temperature sensing circuits (E39 and E41 through E46) of the radiation effects panel which was government furnished equipment.

Description

Each temperature sensing circuit was made up of one or more thermistors and resistors. Each circuit operates from a 9-volt supply, and, for the desired temperature range, supplies the required 0 to +5 volts needed for telemetry. The thermistors are disc-type elements, coated with either red

glyptol or RTV–20 silicon rubber. The finished component is a bead approximately 3/32 inch in diameter. The thermistor parameters are: a maximum operating temperature of 150°C, a dissipation constant of 3 mw/°C at 25°C, a time constant of 10 seconds, and a temperature coefficient of 44%/°C. All resistors are RB55CE–F wirewound, one-percent resistors. The typical sensing circuit is shown in Figure 3–21, where RT1 is the thermistor with a resistance that varies with temperature. One special circuit uses two thermistors to extend the range down to −130°C. The resistance values used for each range of temperatures are shown in Table 3–7.

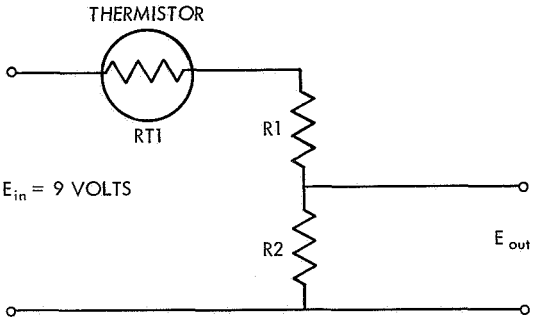


FIGURE 3–21.—Temperature sensor circuit.

TABLE 3–7.—*Temperature Sensor Resistor*

Sensors	Range deg C	R 1 ohms	R 2 ohms
A8–A11	−50 to 40	7,150	9,760
A12–A17	−20 to 66	2,740	4,320
C1	0 to 120	12,400	17,400
C2–C10, C12	−2 to 40	0	25,500

Location

The thermistor locations are listed in Table 3–8 and are shown in the diagram of Figure 3–22. Five thermistors (C1, C3, C4, C5, and C6) are mounted on the spacecraft structure. The mounting bracket is a terminal board centrally drilled to accommodate the thermistor. The thermistor is held in place with epoxy. Table 3–8 also shows that the telemetry sensors are sampled once every 64 seconds, except sensor C8, which is sampled once per second.

Calibration

Each temperature sensing circuit was calibrated as a unit because the nominal accuracy of commercial thermistors does not approach the desired circuit accuracy. Also, the calibration serves as a verification of the circuit design.

TABLE 3–8.—*Specifications on Temperature Sensors*

Sensor	*T/M* comm.	Function	Data range	Accuracy
A8	28/49	Solar panel No. 3B–1	−50 to +40°C	±2.5°C
A9	28/57	Solar panel No. 3B–2	−50 to +40°C	±2.5°C
A10	28/2	Solar panel No. 4A–1	−50 to +40°C	±2.5°C
A11	28/10	Solar panel No. 4A–2	−50 to +40°C	±2.5°C
A12	28/18	Battery temp. 1–1	−20 to +66°C	±2.5°C
A13	28/26	Battery temp. 1–2	−20 to +66°C	±2.5°C
A14	28/34	Battery temp. 2–1	−20 to +66°C	±2.5°C
A15	28/42	Battery temp. 2–2	−20 to +66°C	±2.5°C
A16	28/50	Battery temp. 3–1	−20 to +66°C	±2.5°C
A17	28/58	Battery temp. 3–2	−20 to +66°C	±2.5°C
C1	28/12	TWT collector temp.	0 to 120°C	±5°C
C2	28/20	TT and C transmitter	−2 to 40°C	±2.5°C
C3	28/28	Structure (beac.)	−2 to 40°C	±2.5°C
C4	28/36	Structure (enc.)	−2 to 40°C	±2.5°C
C5	28/44	Structure (WB rec.)	−2 to 40°C	±2.5°C
C6	28/52	Structure (ring)	−2 to 40°C	±2.5°C
C7	28/60	Battery structure temp.	−2 to 40°C	±2.5°C
C8	22	Controller sensor	−2 to 40°C	±2.5°C
C9	28/5	TWT power supply No. 1	−2 to 40°C	±2.5°C
C10	28/13	TWT power supply No. 2	−2 to 40°C	±2.5°C
C11	28/21	Lower surface temp.	−130 to +5°C	±5°C
C12	28/64	Battery structure temp.	−2 to 40°C	±2.5°C

The accuracy of the temperature sensing circuits in the integrated spacecraft was tested during the prototype thermal gradient test by comparing the telemetered temperatures with the readings of thermocouples placed near each thermistor. Comparisons were made at eleven locations where the thermistors were not located inside components. The temperatures were compared over as wide a temperature range as possible, during periods when the time-rate of change of temperature (as indicated by the thermocouple) was small. The results of the comparisons are summarized in Table 3–9. The representative average difference is +0.2°C,

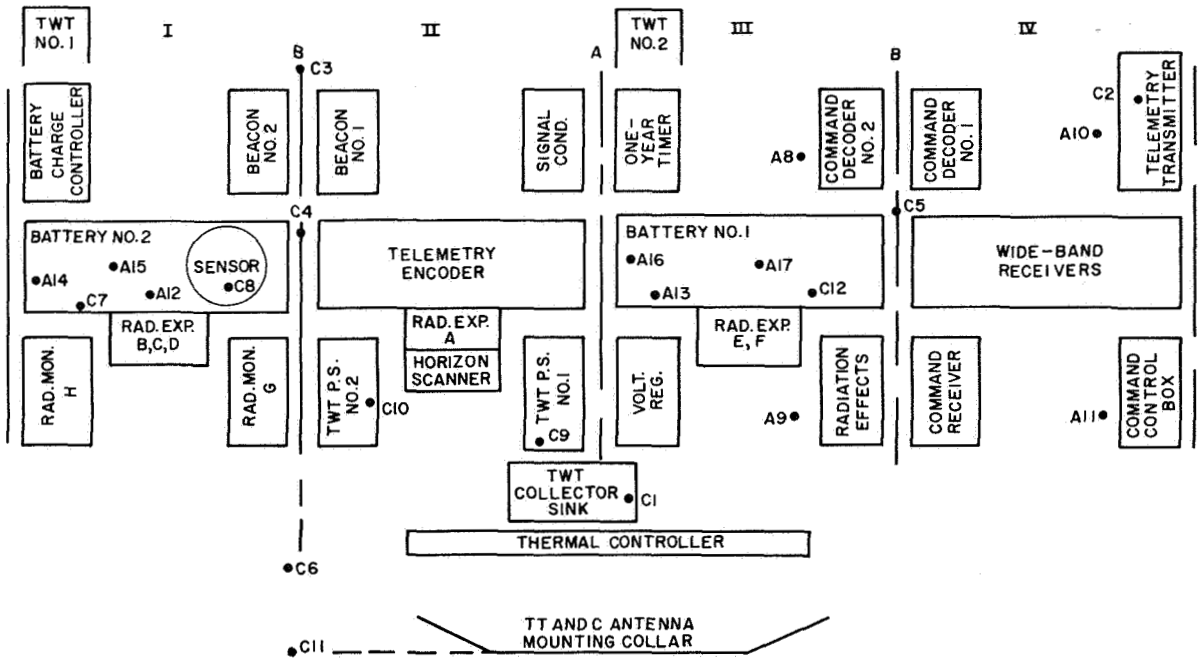


FIGURE 3–22.—Thermistor locations in prototype spacecraft.

a small difference which proves that there is no significant systematic error in the calibration procedure. The two and three degree differences found for a few pairs can be attributed to the difference in the mounting of a thermistor and its corresponding thermocouple. The compounded standard deviation of $\pm 0.6°C$ was much better than the specification requirement of $\pm 2.5°C$.

TABLE 3–9.—*Thermistor–Thermocouple Comparison*

Battery thermistor	Thermocouple	Average difference degrees C.	Standard deviation degrees C.
A13	T21	0.3	±0.1
A14	T25	−0.5	±0.7
A15	T25	−0.5	±0.7
A16	T21	0.2	±0.3
A17	T21	−0.4	±0.3
C12	T23	0.1	±0.6
Average		−0.1	±0.5
Structure thermistor			
C1	T42	−2.0	±0.8
C3	T41	−2.9	±0.3
C5	T43	−1.1	±0.9
C6	T44	2.9	±0.6
C8	T24	0.1	±0.5
Average		−0.8	±0.7
Grand Average of All Readings		−0.2	±0.6

Active Thermal Controller

Design Philosophy

The spacecraft thermal design is basically a passive one, with the active controller reducing the temperature range and providing an extra margin of safety. High reliability is provided, since the spacecraft probably would operate even if the controller failed. After the first model of the active thermal controller was built and tested in a spacecraft, the design was reviewed and careful consideration given to: (1) providing a second controller at the other end of the spacecraft, and (2) omitting the active controller. It was concluded that the controller provided a significant and measurable reduction in temperature range and, thus, contributed to the system reliability. While additional control would have been desirable, a second controller installation was not considered to be warranted.

In orbit, the spacecraft spin axis is nomi-

nally perpendicular to the sun's rays making the ends of the spacecraft colder than the sides. The active thermal controller changes the amount of heat radiated from the components to the colder bottom surface of the spacecraft. When the battery temperature is above 20°C, the controller is open, permitting the heat to flow. Battery temperatures below 6°C cause the controller to close, preventing excessive heat loss from the spacecraft. The mylar covering next to the spacecraft mounting ring is coated with a highly emissive paint and is used as a sink for the heat radiated from the payload. The thermal coupling from the payload to the bottom is thus changed by the action of the controller.

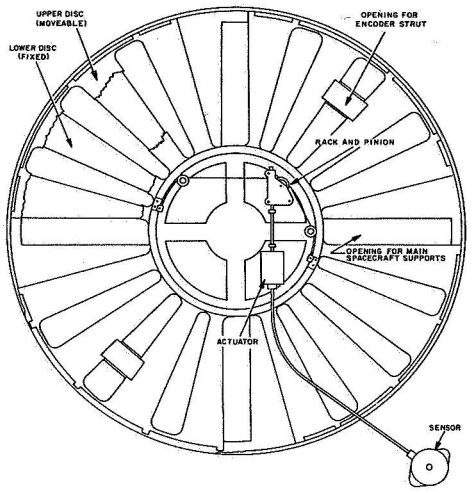


FIGURE 3–24.—Drawing of active thermal controller.

Description

The controller is a flat, circular device weighing 3.6 pounds, mounted perpendicular to the spacecraft spin axis, 7 inches above the bottom surface. The major components are a shutter, an actuator for the shutter, and a temperature sensor. The controller is shown in Figures 3–23 and 3–24.

The shutter consists of two 24.6-inch diameter discs parallel to each other and separated by 1/16 inch. Each disc is made of aluminum tubing supports with 32 pie-shaped sectors. Alternate sectors are covered with one-mil mylar which has been coated with a thin layer of aluminum on each side. The remaining sectors are left uncovered. The lower disc is fixed to the spacecraft structure, and the upper disc is fastened to a movable central ring coupled by a lever mechanism to the actuator rod. The periphery of the upper disc is supported at several points in a groove 3/16 inch wide. All contact points are coated with a special paint (Emvalon) to avoid direct metal-to-metal contact and to reduce friction.

The shutter is opened or closed by the rotation of the upper disc relative to the lower. This rotation is produced by linear motion of the actuator shaft. The total controllable area is 180 square inches.

The temperature sensor (see Figure 3–25) is mounted on one of the battery boxes (box

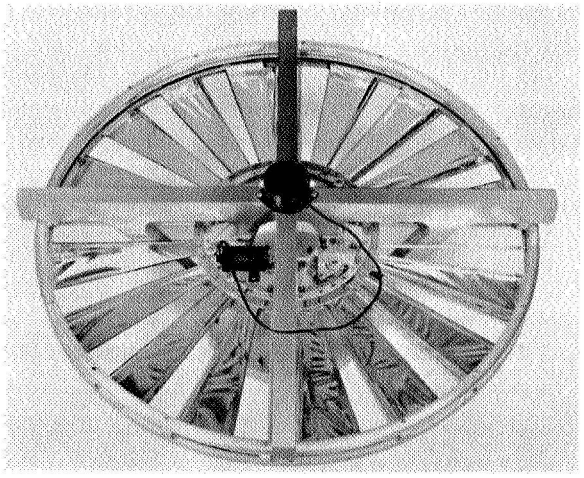


FIGURE 3–23.—Active thermal controller.

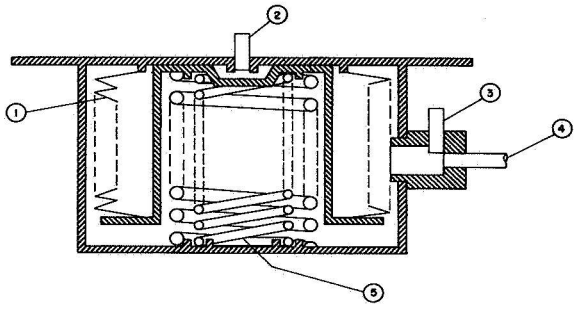


FIGURE 3–25.—Temperature sensor.

2) since the battery temperature is critical in the thermal design. The sensor consists of a bellows containing saturated sulfur dioxide liquid gas. The SO_2 provides the prime force required to move the shutter. Since the SO_2 pressure is always positive, springs are required for a counteracting force. The bellows and springs are housed in a cylindrical container 2–5/16 inches in diameter and 1–3/8 inches high. The cylinder volume outside of the bellows is fllled with N-butyl alcohol. This hydraulic fluid transmits the bellows displacement to the actuator mechanism via a capillary tube having an outside diameter of 1/8 inch and a length of 18 inches.

The actuator (see Figure 3–26) consists of a bellows within a cylinder 1–1/2 inches in diameter and 2–3/32 inches long. As the pressure exerted by the alcohol outside the bellows is increased, the bellows contracts, imparting a linear motion to a rod attached to its free end. When the pressure is decreased, the bellows and rod are forced in the opposite direction by the action of a coil spring located inside the bellows and mounted concentrically with the rod. The total rod displacement is limited by an adjustable stop to 0.362 inch. The rod drives one end of a lever, pinned in the middle. The other end of the lever is hinged to a member which drives the movable shutter disc.

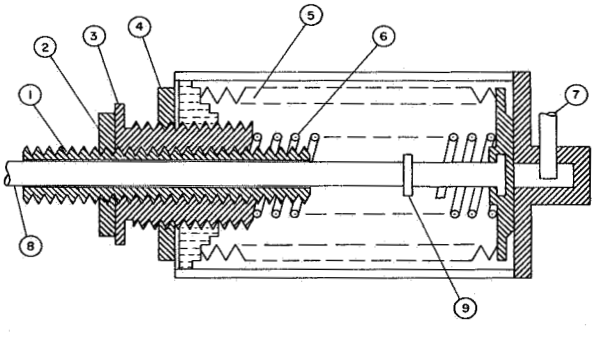


FIGURE 3–26.—Actuator.

Mechanical Performance

Actuator displacement as a function of sensor temperature was measured before mounting the actuator on the shutter. Tests were conducted in vacuum with the actuator rod moving against a two-pound dead load; the measured hysteresis curves are shown in Figure 3–27. Further tests of the complete system were conducted in which the actual rotation of the controller shutter was measured as a function of sensor temperature, resulting in similar hysteresis curves. Then, conducted in air, the curves were translated to higher temperatures, since the effective pressure of the SO_2 is reduced by the atmospheric pressure against which the sensor-actuator system must work. Performance was predicted from test data obtained in air by use of the temperature conversion chart shown in Figure 3–28. This conversion data was calculated from the SO_2 vapor pressure curve.

In addition to measurements made in air, hysteresis curves in vacuum have been obtained from thermal gradient tests and solar simulation tests for several controllers. The controllers for the prototype and flight model No. 1 spacecraft were completely closed at 9 ± 2°C and completely open at 18 ± 2°C.

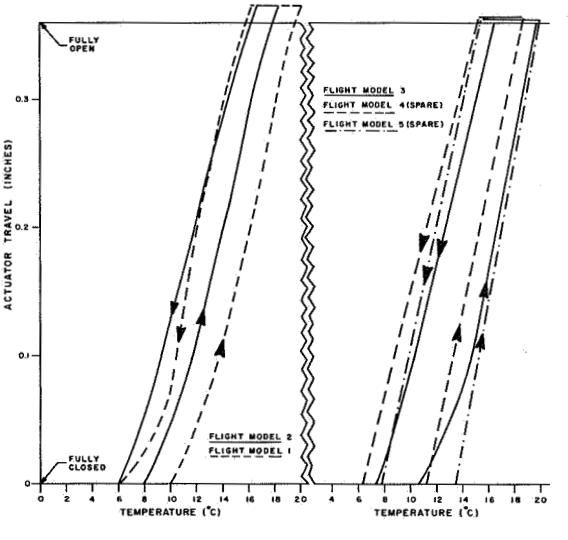


FIGURE 3–27.—Temperature range for thermal controllers.

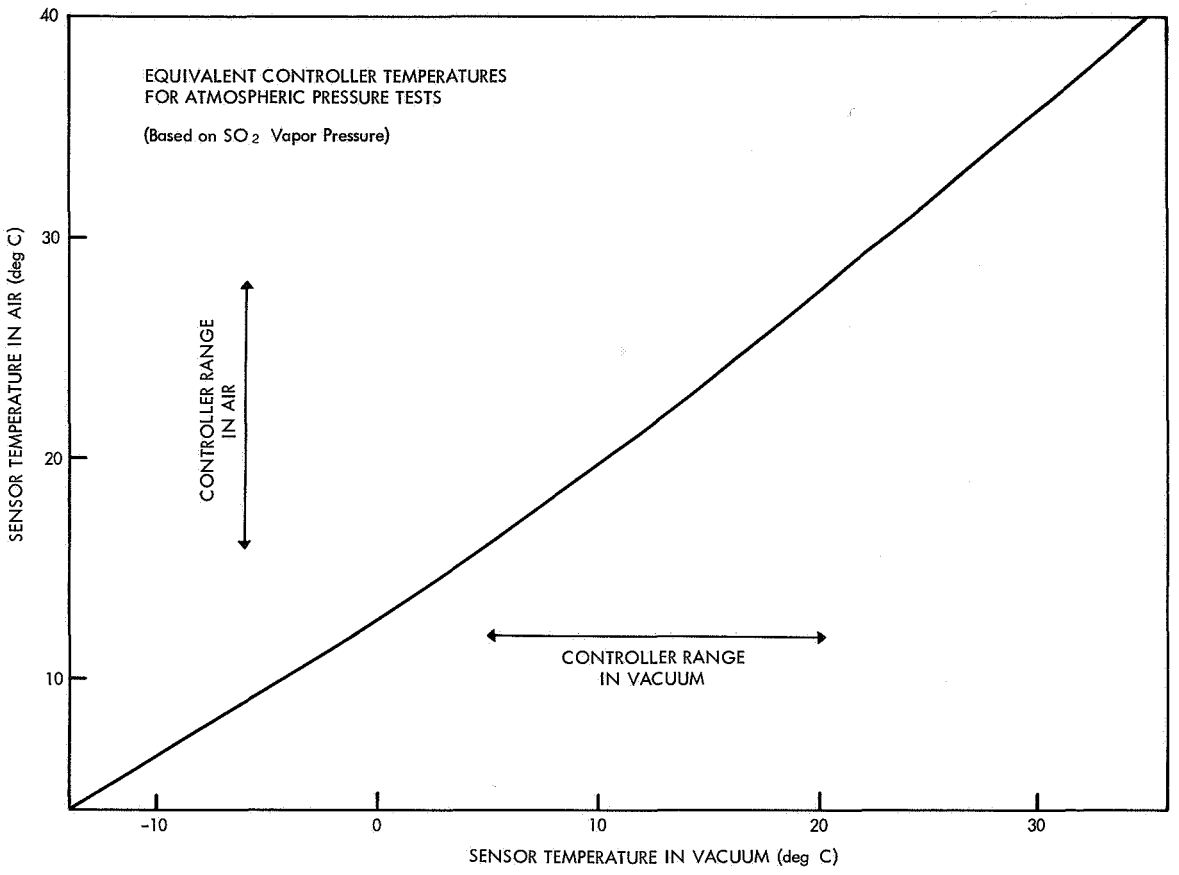


FIGURE 3–28.—Equivalent controller temperatures for atmospheric pressure tests.

Thus, these controllers performed within the required 6°C to 20°C range.

Thermal Performance

A measure of the effectiveness of the thermal controller is the degree to which it changes the thermal coupling between components and the bottom surface. (This coupling, C, can be defined as the rate of change of σT^4 of the components with respect to the thermal irradiance on the bottom.) The values of thermal coupling obtained in thermal gradient tests of the thermal model and the prototype are listed in Table 3–10 for the controller in both the open and closed positions. In all cases the fractional coupling increased with the controller open. The actual increase ranged from a maximum of 0.11 to a negligible 0.008, yielding an average of 0.06. The change is smaller than average for the telemetry transmitter and larger than average for the TWT Power Supply, as expected, since they are respectively farther from, and closer to, the bottom than are the other components. This change in coupling to the bottom, with some secondary effects from other coupling factors, produces the

TABLE 3–10.—*Effect of Controller on Thermal Coupling*

Component	C (open)		C (closed)		ΔC	
	Thermal model	Prototype	Thermal model	Prototype	Thermal model	Prototype
Telemetry	.22	.18	.18	.18	.04	.00
Sensor	-------	.27	-------	.20	-------	.07
Battery center	.24	.27	.20	.17	.04	.10
Battery, edge	.24	------	.18	------	.06	------
Encoder	.23	------	.19	.16	.04	------
WB recorder (1)	.26	.22	.19	.16	.07	.06
TWT power supply	.29	.28	.24	.22	.05	.06
Average	.246	.243	.200	.181	.046	.058

desired temperature change. The agreement among the different tests is satisfactory, considering the final modifications to spacecraft design. The increase in ΔC from the model to the prototype reflects the modifications made to improve controller effectiveness.

The total coupling from the components to space is about 800 square inches. Multiplying this by the fractional coupling C, the coupling to the bottom is 190 square inches for the controller open and 140 square inches with the controller closed. The difference of 50 square inches can be compared with the 180 square inches of controller area that actually opens and closes. The decrease is due to: (1) location of the controller inside the spacecraft to minimize the ratio of moments of inertia, (2) the structural members through the controller, (3) the necessary increase in area of the collar for mounting transistors, and (4) struts through the controller to support the encoder and wideband receiver. Because of internal reflections, the coupling from the painted mylar surface to the lower fitting increases when the controller is closed. A network calculation of the coupling from the components to outer space results in 230 and 160 square inches, respectively, for the controller open and closed—in rough agreement with the 190 and 140 square inches derived experimentally.

Table 3–11 lists temperatures calculated for the probable extreme thermal conditions which the batteries would experience in orbit. The coupling factors obtained from the prototype thermal gradient test were used in these calculations.

TABLE 3–11.—*Calculated Battery Temperatures*

Sun angle degrees	Thermal condition	Battery temp. with controller open degrees C	Battery temp. with controller closed degrees C
60	Hot	16.5	20.6
90		14.2	21.0
120		16.6	17.0
60	Cold	5.2	6.9
90		3.4	7.2
120		3.8	4.3

While the effect of the thermal controller at the 120° sun angle is small, its value increases significantly at lower sun angles. It is most effective at the 90° sun angle, an attitude experienced more often by the spacecraft than the 60° and 120° extremes. Since extreme temperatures have a pronounced effect on battery performance, the average decrease of 5°C by the active thermal controller is significant in improving spacecraft life and reliability.

Traveling Wave Tube

Introduction

During wideband operation, the collector end of the traveling wave tube dissipates more heat (50 w) than any other spacecraft component. The required duty cycle is 36 minutes during each of three consecutive orbits (the orbit period is 163 minutes).

The initial thermal design, during both the study phase and the initial spacecraft design, included a heat sink for the tube such that the combination was a self-contained unit. The design required a thermal mass of one or two pounds and a relatively small radiating area of 25 to 50 square iches. The thermal mass absorbed the heat during the 36 minutes of operation and radiated it during the two hours between operations.

The alternate design finally chosen was radically different. The tube was relocated, and the spacecraft structure was used as both heat sink and radiator. Relocation of the tube was decided after careful consideration of the vibration analysis and the moment of inertia of the spacecraft as well as the thermal requirements. The result was an equivalent thermal mass with no weight penalty, plus a greatly increased radiating area (350 square inches).

The interface with the tube design (RCA, Electronic Components and Devices, Harrison, N. J.) was set by mutual agreement, with consideration given to the thermal problems in both the tube design and in the spacecraft design. The basic requirement

was that the maximum temperature of the collector inside the tube be less than 220°C, and preferably less than 180°C. The interface decision was that the lower fitting, to which the tube was to be attached by a flexible metal strap, was to be held below 80°C for power dissipation up to 50 watts.

Theory

Most of the spacecraft heat was dissipated by the 12 struts of the spacecraft frame which were connected to the lower fitting. An analysis of the temperature along a uniform strut shows that it can be characterized by an effective length l_e, given by

$$l_e^2 = \frac{KA}{\epsilon_p (4\sigma T_0^3)}$$
$$= \frac{(5.4 \text{ w/deg-in})\ (0.15 \text{ in}^2)}{(0.2)\ (6 \text{ in})\ (0.004 \text{ w/deg-in}^2)} = (13 \text{ in})^2$$

where K is the thermal conductivity; A, the cross section area; ϵ, the emissivity; p, the perimeter; T_0 a nominal temperature, and σ the Stefan-Boltzmann constant.

In the steady state, the difference between the temperature on the strut and the surrounding temperature can be approximated by an exponentially decreasing function; the distance over which this difference falls to $1/e$ of its value is defined as the effective length.

The effective radiating area R for the 12 struts is:

$$R = 12\, \epsilon\, p\, l_e \approx 200 \text{ in}^2$$

and the effective thermal mass* is:

$$mc = 12\, \rho\, l_e\, Ac \approx 1000 \text{ w-sec/deg}$$

where c is the specific heat, and ρ is the density of aluminum (0.098 lb/in³).

Some heat will also be absorbed and radiated by the lower fitting itself, by parts of the tube, and by other adjacent parts. The actual effective area and mass would be expected to be larger than these calculated numbers, since, during the design phase, these numbers were used as a conservative approach.

The steady state rise in temperature can then be calculated to be:

$$T_E - T_L = \frac{q}{R\,(4\sigma T_0^3)} = 60°$$

where q is the power dissipated (50 w).

However, this temperature would not be reached during the normal duty cycle; the calculated maximum temperature rise of the lower fitting is only:

$$T_M - T_L = (T_E - T_L)\left[1 - e^{-\frac{tR\,(4\sigma T_0^3)}{mc}}\right]$$
$$= 45°$$

Since the maximum surrounding temperature is expected to be 25°C, the calculated maximum temperature of the lower fitting is 70°C, or ten degrees below the upper limit.

Test Results

The temperature rise and fall of the lower fitting during wideband operation was monitored in many tests, both with a thermocouple and a thermistor. The numbers used for the calculations were:

1. The initial temperature, T_L
2. The initial rate of temperature rise S when the wideband sub-system was turned on,
3. The maximum temperature, T_M, and
4. The initial rate of temperature drop S when the wideband sub-system was turned off.

Assuming a simple isothermal mass, the thermal mass and radiating area are then given by:

$$mc = \frac{q}{S_h}$$
$$R = q\frac{S_c}{S_h}(\sigma\, T_M{}^4 - \sigma\, T_L{}^4) \text{ in}^2$$

where q, the electrical power, was taken as 50 watts.

The parameter values calculated from various tests are presented in Table 3–12. For the flight model No. 1 spacecraft, the average measured thermal mass is 4800

*The temperature-time curve will not be that of an isothermal mass; this value is obtained by equating the area under the two curves.

TABLE 3–12.—*Traveling Wave Tube—Thermal Parameters Analysis at Lower Fitting*

Test		S_h	S_c	T_L	T_M	mc	R
		deg C sec	deg C sec	deg C	deg C	w–sec deg	in2
Thermal gradient tests							
Therm. mod.	5 Dec 61	0.008	0.004	0	15.5	6200	490
Prototype	10 Apr 61	0.016	0.009	−9	14	3100	390
Prototype	24 Aug 62	0.024	0.015	35	53.5	2100	360
Solar simulation tests							
Prototype	Day 3	0.009	0.004	18.5	37	5500	340
FM 1	Day 1	0.011	0.004	23	40	4500	330
FM 1	Day 2	0.011	0.005	23	40	4500	340
FM 1	Day 3	0.010	0.005	23	42	5000	350

w–sec/deg, which corresponds to over ten pounds of aluminum; this is considerably greater than 1000 w–sec/deg calculated theoretically. The measured average radiating area of 340 square inches is also larger than the theoretical 200. Part of this is due to the conservative assumptions that were made, and part of it reflects the fact that not all of the 50 watts are being dissipated at the lower fitting. The use of a pressurized TWT in the flight model No. 1 spacecraft requires a capsule which radiates more heat in the tube case, and therefore less is conducted to the lower fitting.

The net result is that the expected maximum temperature of the lower fitting is 45°C, compared with the 80°C to which the tube is tested. This margin allows for the use, in other spacecraft, of unpressurized tubes or for extended operation of the wideband sub-system beyond the 36 minutes required. The latter actually occurred in the Relay I spacecraft and no harm was done to the tube.

Design Verification

Thermal Model

The initial thermal design was improved with subsequent refinement of the detailed mathematical calculations. The calculations, however, were always subject to limitations in the number of bodies that could be taken and in the calculation of the thermal coupling between each pair of bodies. As a physical verification of the thermal design, a thermal model of the spacecraft was built and tested in a vacuum chamber. This test, plus subsequent tests with the prototype and flight model spacecraft, yielded data that could be used to predict flight temperatures with increasing accuracy.

The thermal model was built with a structure identical to the actual spacecraft and duplicated, as closely as possible, the thermodynamic and geometric properties of the actual spacecraft. All the black boxes were of the same general shape and weight as the actual components, with internal electrical heaters in operation to simulate the electrical heat sources. Figure 3–29 illustrates the nearly completed thermal model. It was then covered with panels of sheet aluminum painted black on the outer surface to simulate the solar cell panels. An active thermal controller was installed complete physically but not in active operation, and the tests were run with the controller either in the open or the closed position.

Thermal-Vacuum Tests

The spacecraft was mounted in the vacuum chamber, as shown in Figure 3–30, for the thermal model test. The vacuum chamber was equipped to permit control of the side wall temperatures. Two special plates were installed in the chamber to control heat inputs to the ends of the spacecraft. Aluminum foil was fastened from the edges of the plates to the spacecraft edges to insure that each spacecraft surface would be exposed only to radiation of the appropriate temperature.

Temperature measurements were made at 30 locations during the tests and were recorded automatically. The pressure was maintained at 10^{-5} mm Hg. While later tests of actual spacecraft were aimed at duplicating the external radiation inputs of actual flight, the thermal model test was directed toward measuring the basic spacecraft thermal constants. Transient tests were used to determine the spacecraft time constant. Steady state tests were used to determine the

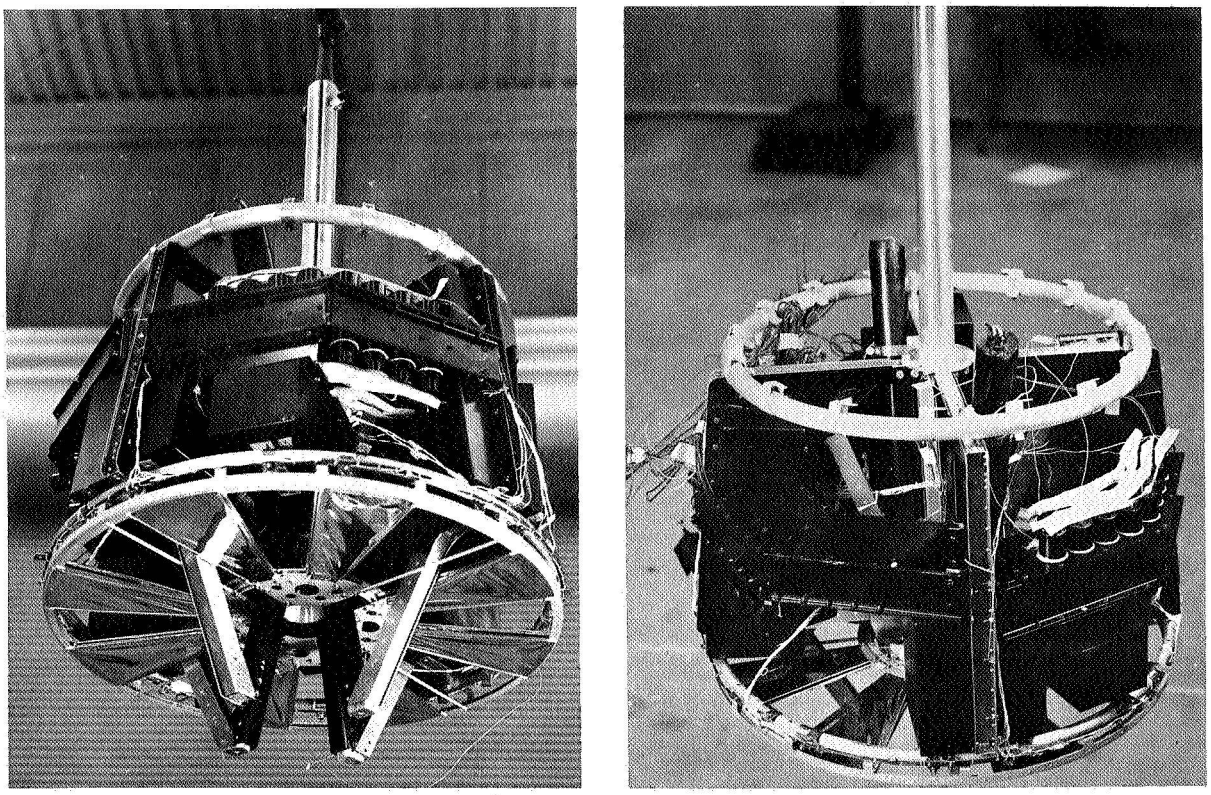


FIGURE 3–29.—Project Relay thermal model.

fractional coupling constants, from the equation:

$$\sigma T^4 = AI_T + BI_S + CI_B + D$$

which was derived on page 47. The equivalent radiation inputs (I) for each surface are determined by the corresponding chamber wall temperatures (σT^4), and, if the interior temperature is measured, a relation is obtained between the four constants: A, B, C, and D. By conducting a series of tests, these constants may be uniquely determined. When these constants are known, predicted temperatures can be calculated for any desired condition in space.

Some of the fractional coupling coefficients calculated from temperatures measured during the testing are listed in Table 3–13. The method of calculation was slightly different for the two tests. Thus, for the thermal model, the three coefficients do not necessarily add to unity, due to experimental errors. For the prototype test, the coefficients were constrained to add to unity. Averaging the results over the equipment, the correlation with the initial design value is good, and the agreement between the thermal model and the prototype tests is excellent.

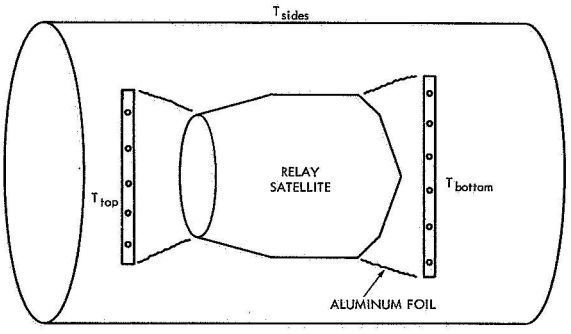


FIGURE 3–30.—Orientation of the spacecraft in the test chamber.

Conclusions

The test results essentially confirmed the thermal design except for minor modifications. After the thermal model test, the design em-

TABLE 3–13.—*Fractional Coupling Coefficients—Test Results*

	A		*B*		*C*		*D*	
							watts/in^2	
	Model	Proto.	Model	Proto.	Model	Proto.	Model	Proto.
Tel. transmitter	.10	.08	.74	.74	.18	.18	.087	.059
Sensor	------	.05	------	.75	------	.20	------	.058
Battery, center	.10	.05	.81	.78	.20	.17	.050	.055
Battery 1, edge	.08	------	.73	------	.18	------	.058	------
Encoder	.06	.05	.79	.79	.19	.16	.064	.060
Battery 2	.08	.05	.78	.77	.22	.18	.046	.056
WB rec. (1)	.09	.07	.72	.77	.19	.16	.046	.051
TWT pow. supply	.12	.06	.76	.72	.24	.22	.047	.048
Test average	.09	.06	.76	.76	.20	.18	.057	.055
Initial design	.10		.69		.21		.067	

phasis did shift away from the traveling wave tube. The 50 watts dissipated by the TWT had been of considerable concern, both in the effect on the tube and on the other components. The test showed that the temperature rise in the tube was below the temperature limit of the tube, and the effect of this rise in temperature on the other electronic components was negligible.

From the test results, predictions of flight temperatures were made. The sources of error were estimated and are listed in Table 3–14. The absorptivity-emissivity ratio of the solar-cell panels was thought to be the most important source of error, although later comparison with flight data indicates this error was probably exaggerated. The error for the properties of the other surfaces was less and was significant only when the sun was shining on the ends. While there are uncertainties in the earth-reflected and earth-emitted radiation, the value for total radiation incident on the spacecraft is probably accurate to two percent.

Measurements of internal spacecraft temperatures were probably accurate to 1°C, but the average wall temperatures were more difficult to determine and may be in error by 2°C. Electrical power differences were included to allow for any differences in dissipation during test or during flight. The

TABLE 3–14.—*Accuracy*

	ΔT°C
Solar cell panels	±4.3°
α/ϵ ±10% σT^4 ±6%	
Top and bottom surfaces	±1°
α/ϵ ±10% σT^4 ±1.7%	
Radiation inputs ±2%	±1°
Test errors	
Temperature measurements	±2°
Electrical power differences	±3°
Vacuum chamber heat leaks	±3°
Extrapolation errors	±2°
Differences in Models	±2°
$\sqrt{\Sigma(\Delta T)^2}$	= ± 7°
Transients (eclipse)	+0°, −2°
Error	= +7°, −9°

vacuum chamber heat leaks were due to imperfections in the radiation baffles and to the support required to hold the spacecraft. The extrapolation errors are those resulting from the use of Equation (3.21), which was derived by assuming that heat transfer is primarily by radiation; this introduces no error for those particular flight conditions that were simulated, but in using the results for other flight conditions, a slight error is introduced. Finally, some differences can be expected between one spacecraft model and another. The total error was equal to the

square root of the sum of the squares, and was 7°C.

Transients during eclipse were not included in the 7°C. The original estimate of the temperature drop during a 40-minute eclipse, based on an isothermal model, was 5°C. During test transients, drops of 4 deg/hr were observed when all the walls were cooled to —70°C. However, considerable lag occurred initially, so that about two hours elapsed before this cooling rate was established. The small coupling between the solar cell panels and the internal package reduced the drop in battery temperatures. The final estimate was about 2°C and may be even smaller. The final estimated error in the temperature predictions for the batteries was +7°, —9°, as given in Table 3–14.

The predicted temperatures for 100-percent suntime are shown in Figues 3–31 for various thermistor locations. These are compared with the range of flight temperatures during the first month of normal operation (January 1963) of Relay I. An absorptivity/emissivity ratio for the solar panels of 0.975 was used, as measured for an entire solar-cell panel. Locations that did not have any strong sources of heat nearby exhibited only a narrow range of temperatures; for these locations the agreement between the predicted and observed values was two or three degrees. The batteries and TWT power supplies have wider variations of temperature, due to their internal heating, but the lower end of the temperature range was in reasonable agreement with the predicted values. The temperature of each thermistor was well within the +7°C, —9°C accuracy anticipated before launch. In conclusion, the comparison of the predicted and observed temperatures was considered excellent.

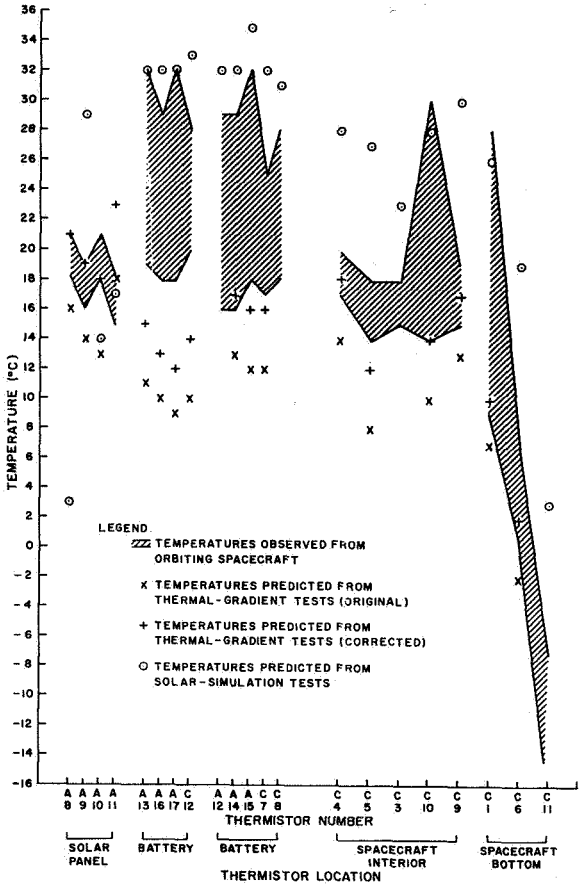


FIGURE 3–31.—Observed and predicted spacecraft temperatures in orbit during 100 percent suntime periods.

AUTHOR. *This chapter was written by* C. C. OSGOOD *and* G. D. GORDON *of the Radio Corporation of America, Princeton, New Jersey, U.S.A. under contract NAS 5–1272 with NASA/Goddard Space Flight Center.*

N66-10230

Chapter 4

Spacecraft Performance

INTRODUCTION

The Relay I satellite was launched and injected into a near nominal orbit at 2330 GMT, 13 December 1962. Except for some early difficulties encountered with the power system and for many command system anomalies, the spacecraft performed essentially as designed. Table 4–1 gives a comparison of the actual and nominal orbits for Relay.

TABLE 4–1.—*Relay Orbit Characteristics*

Item	Nominal	Actual
Height of apogee	3999.48 nm	4020.70 nm
Height of perigee	699.92 nm	712.13 nm
Period	184.36 min	185.09 min
Eccentricity	0.28475	0.28462
Inclination	47.766 deg	47.496 deg
Right ascension of ascending node	217.22 deg	218.74 deg
Argument of perigee (injection)	176.426 deg	177.5 deg
Nodal rate	−1.2845 deg/day	−1.2779 deg/day
Perigee rate	1.2030 deg/day	1.2123 deg/day

The Relay spacecraft* consists of a redundant wideband communications system, a radiation experiment package, electrical power system, command and telemetry system and necessary supporting structure (see Figure 4–1). The spacecraft has horizon and sun sensing devices, attitude control system, a precession damper, and an active thermal controller. It has the general shape of an octagonal cylinder, and with the exception of the top and bottom, the outer surface is completely covered with solar cells. Table 4–2 lists some physical characteristics of Relay I.

TABLE 4–2.—*Spacecraft Physical Characteristics*

Weight	172 lb.
Moments of inertia	
I_{roll}	17,925 lb-in^2
I_{pitch}	15,952 lb-in^2
I_{yaw}	17,124 lb-in^2
$\frac{I_{roll}}{I_{yaw}}$	1.104
Measured residual magnetic dipole moment	0.06 amp-turn-meter^2
Torquing coil	−1.68 amp-turn-meter^2
Measured magnetic dipole moment	+1.53 amp-turn-meter^2

This paper will discuss the performance of each system, with the exception of the radiation experiment package. Observed performance is compared with prelaunch or expected data, where available; the observed anomalous performance is discussed, and some possible explanations are given. The data used here were reduced by the Relay Test Stations and were provided to the Communications Operations Center at Goddard Space Flight Center (GSFC). Figure 4–2, a functional block diagram of Relay, shows the major telemetry points used to monitor

*"Relay I Spacecraft," GSFC Doc. No. R1–0100, 11 August 1961.

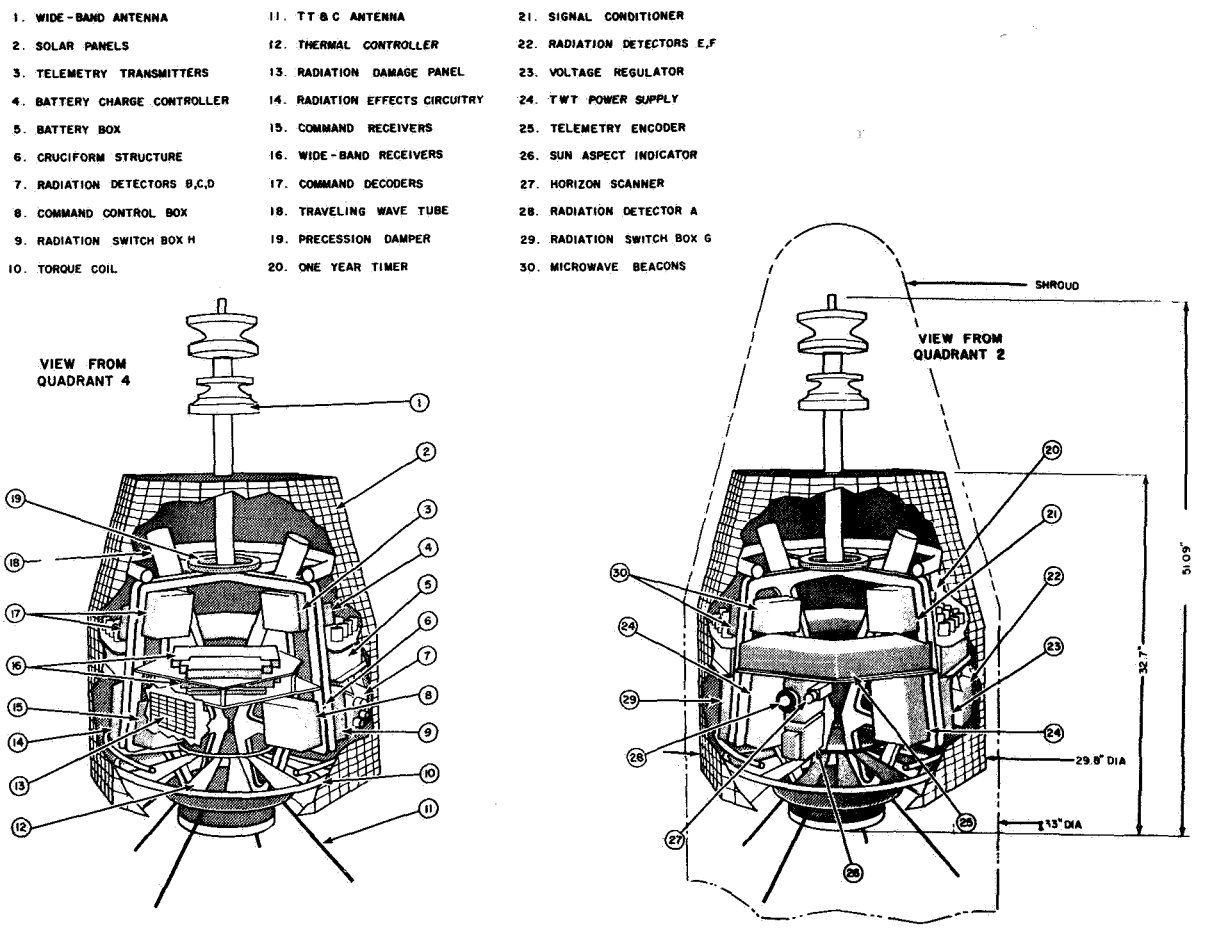


FIGURE 4–1.—Cutaway drawing of Relay spacecraft.

performance. Table 4–3 itemizes these quantities. The spacecraft temperature history, orientation, and spin rate characteristics of Relay are discussed.

ELECTRICAL POWER SYSTEM PERFORMANCE

The electrical power system consists of a P/N solar array and nickel-cadmium battery combination which supplies power to loads on an unregulated power bus and three regulators. A block diagram of the electrical power system is given as part of Figure 4–2, which also indicates the voltage, current, and temperature instrumentation. One of the power regulators supplies the radiation experiment, while the other two supply redundant transponders. During normal operation of the spacecraft with the transponder off, all current provided by the solar array is used to support the continuous spacecraft loads and to charge the batteries. During conditions of light load, and when the batteries are in trickle charge, the excess solar array power is dissipated in a voltage limiter. During operation of the wideband subsystem, the solar array cannot support the loads entirely and the solar array power is supplemented by the batteries. During an eclipse, of course, all power is furnished by the batteries.

Immediately after launch, faulty operation of the regulator for transponder No. 1 caused the spacecraft to be in a low-voltage condition which precluded any operation of the communications system. A means was found to avoid this undesired situation, and as of February 1964 the communications system had been operated for a total of 300 hours

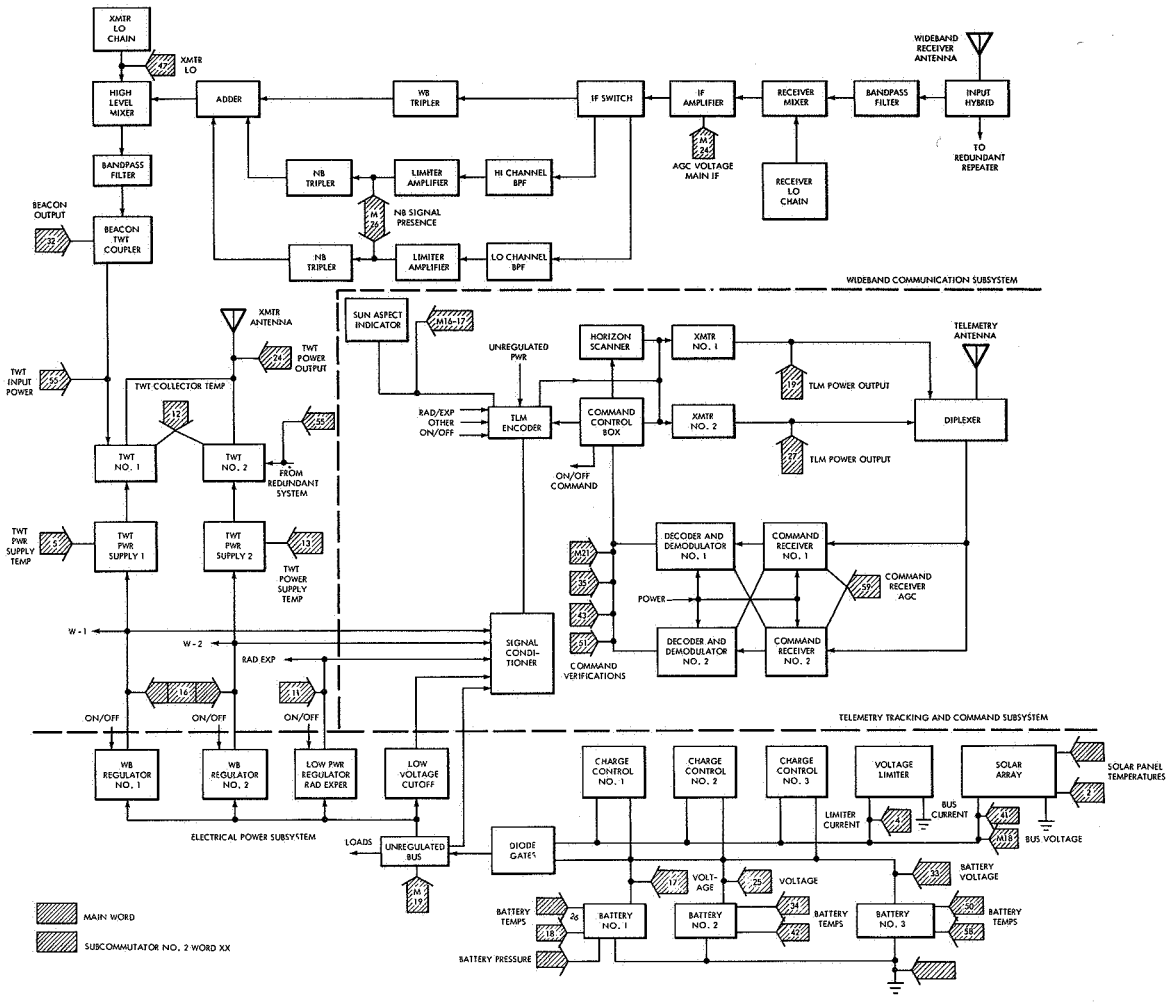


FIGURE 4–2.—Location of major telemetry points.

and the radiation experiments for 500 hours. The transponder operations were typically of 30 minutes duration, although some 45-minute passes were performed as late as December 1963.

The solar array has degraded essentially as expected. The only failure apparent in the electrical power system was that following Rev 548, battery No. 2 failed to charge. From that time, the telemetry indicated a steady decrease of battery No. 2 voltage until it reached zero. This indicates an open-circuit failure in the charge control circuitry for this battery.

Transponder No. 1 Regulator Failure

After the successful launch of the satellite, radiation experiment data was gathered on the first orbit revolution. The radiation experiment was commanded off after gathering approximately four hours of data. It was planned to conduct communication experiments on Revs 004, 005, and 006 of the first operational day, but before the first scheduled communication test on Rev 004, the spacecraft telemetry transmitters were observed by some ground stations to be turning off and on. When the spacecraft telemetry encoder was turned on during Rev 004, it was found that transponder No. 1 was ON and could not be commanded off, and that the spacecraft was in a low voltage condition. Unsuccessful attempts were made on the following revolutions to command the transponder off. Some usable telemetry data was obtained on Revs 029 and 035, but not until

TABLE 4–3.—*Primary Spacecraft Performance Telemetry Items*

TM word	Item	TM word	Item
19	Unregulated bus voltage	28–21	Lower surface Temperature
20	Total battery current	28–24	TWT output power
21	Command verification	28–25	Battery no. 2 voltage
22	Active thermal controller sensor temperature	28–26	Battery No. 1–2 temperature
24	WB-AGC-Main if voltage	28–27	Telemetry transmitter No. 2 power output
26	NB signal present	28–32	Beacon output power
28–2	Solar panel temperature	28–33	Battery No. 3 voltage
28–3	Battery pressure	28–34	Battery No. 2–1 temperature
28–4	Voltage limiter current	28–35	Command verification
28–5	TWT No. 1 power supply temp	28–41	Solar cell bus current
28–10	Solar cell panel temperature	28–42	Battery No. 2–2 temperature
28–11	Radiation experiment regulated bus	28–43	Command verification
28–12	TWT collector temperature	28–44	Wideband baseplate temperature
28–13	Power supply No. 2 temperature	28–47	Transmitter L.O. output
28–16	Regulated bus voltage	28–50	Battery No. 3–1 temperature
28–17	Battery No. 1 voltage	28–51	Command verification
28–18	Battery No. 1–1 temperature	28–55	Transmitter imput signal power
28–19	Telemetry transmitter No. 1 power output	28–58	Battery No. 3–2 temperature
		28–59	Command receiver AGC
		16–17	Sun aspect indicator

orbit Rev 107 did the spacecraft appear in a normal state. Another operation of transponder No. 1 was planned for Rev 108 to obtain additional data in an effort to understand the regulator failure.

Figure 4–3 is a diagram of the high power regulator for transponder No. 1, which is also used as the switch to turn the system ON and OFF. If either or both of the series transistors, Q2 or Q3, is partially conducting, a load will be partially on the bus. A failure of either of these transistors or in the driving transistor Q4, or of the regulator control circuitry, could cause partial conduction or full load. Laboratory tests by RCA* showed that the transistors in question, Q2 and Q3, exhibited a high leakage condition at low temperature. It was felt that by operating the transponder on Rev 108 and thereby increasing the transistor temperature, this condition could be alleviated and thereby restore the spacecraft to normal health.

The planned operation was performed with the resulting condition that transponder No. 1 was fully on and could not be commanded off, as had been observed on Revs 004, 005, and 006. The batteries discharged, as on the earlier occasion, to the point where no useful telemetry could be received. Telemetry data taken some days later, on Revs 138, 139, 146, 154, and 155, indicated that the spacecraft was once again in a normal state. On orbit Revs 161, 162, and 163 transponder No. 2 was successfully operated and the first successful communication experiments were performed with a ground station.

It was noted that some steady leakage was apparent whenever the spacecraft was observed, and that a high leakage was observable immediately following turn-off of the transponder. The transponder would turn off smoothly and the regulated output voltage would drop to some intermediate value and then slowly decrease. It was observed at this time that the higher the spacecraft temperature (as monitored at the thermal sensor) the higher the leakage at the time of shutting off the transponder. It was hypothesized, from the meager data available, that the "disastrous ON" condition would be possible if the spacecraft temperature was above 28°C. In another section, it is shown that the spacecraft temperature is highly dependent upon the degree of overcharge of the batteries. It was therefore decided to maintain the temperature below 25 degrees by operating transponder No. 2 as much as possible, thereby reducing the overcharge.

After a large quantity of data had been accumulated on the leakage characteristics, it was decided to determine whether there was a positive correlation between the spacecraft temperature and the leakage condition. The "disastrous ON" condition was observed initially at a time when the sun aspect angle was such that the base of the spacecraft was not being illuminated; transistors Q2 and

*"Quarterly Technical Report No. 7, Dec. 1962–Feb. 1963", RCA Doc. No. AED R–1859, 30 Apr 1963, pp. III–41–43.

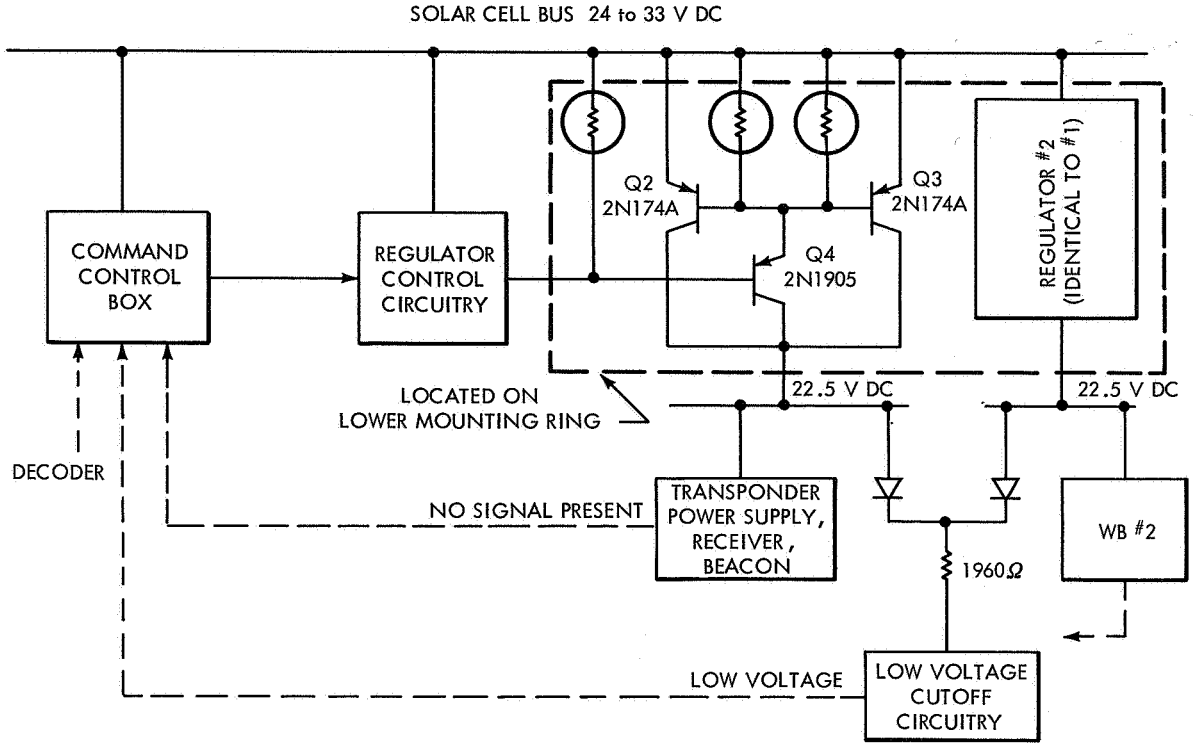


FIGURE 4–3.—Schematic block diagram of wideband No. 1 regulator.

Q3 are located on the bottom of the spacecraft. Passes which had the same sun aspect angle were considered to see whether a correlation could be found between the steady-state leakage condition and temperature, and between the "disastrous ON" condition and temperature. The temperature at the thermal sensor was taken as an average maximum spacecraft temperature, and it was assumed that during the revolutions considered in the analysis, the thermal gradients through the spacecraft remained consistent.

Orbit revolutions from launch to 339 and between the period 1700 to 1932 were considered in this analysis. The first orbit pass of a given day was examined and taken as a case where the spacecraft was in thermal equilibrium. The batteries were always in a state of overcharge at this time, and the spacecraft temperatures stable. Leakage values of the regulator output voltage were compared with the spacecraft temperatures. These results are shown in Figure 4–4. Passes were selected carefully to assure (1) that no anomalous command states existed, or (2) no other subsystems were on, to affect the thermal gradient. Figure 4–4 shows that the steady-state leakage condition is definitely affected by temperature and appears to be greatest when the temperature is lowest.

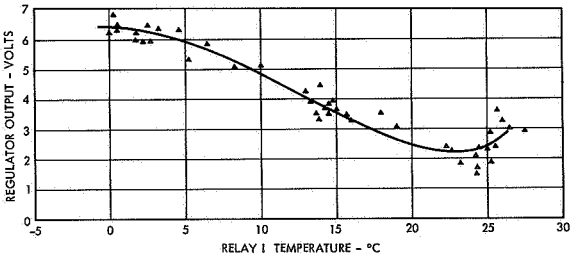


FIGURE 4–4.—Steady-state leakage of transponder regulator vs. temperature.

Test results* obtained on the prototype spacecraft power regulator No. 2 were examined and the leakage characteristic of that

*"Quarterly Technical Report No. 7, Dec. 1962–Feb. 1963", RCA Doc. No. AED R–1859, 30 Apr 1963, pp. III–41–43.

regulator was compared with the steady-state leakage condition observed on Relay I. The two curves are given in Figure 4–5; they appear to have essentially the same slope.

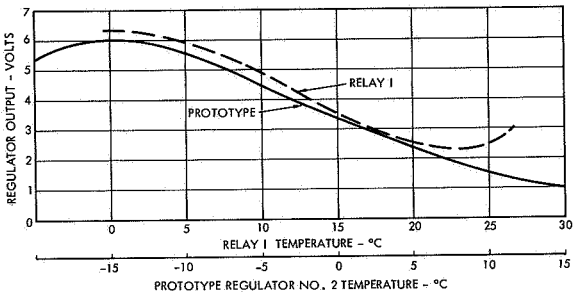


FIGURE 4–5.—Comparison of steady-state leakage and measurements made on prototype spacecraft.

For the prototype, regulator temperatures were 15°C lower than spacecraft temperatures, but since the power transistors are located on the base of the spacecraft, it is expected that when the sun is not shining on the base, these transistors can be 15 to 20°C lower than the thermal sensor temperature.

As previously stated, the turn-off of the wideband system was followed by some transient leakage rate different from the steady-state value. The values noted immediately after transponder shutdown are given in Figure 4–6 versus spacecraft temperature. It can be seen that high leakage rates are apparent at low temperature, but are even greater at high temperatures. The "disastrous ON" situation occurred when the spacecraft temperature was near or above 25°C. The transponder has never been observed to be in an undesired full ON condition at low temperatures. It can be seen from Figure 4–34 that the "disastrous ON" condition existed when the spacecraft temperature was above 27°C. The steady-state leakage curve, determined in Figure 4–4, is also shown in Figure 4–6 for comparison.

These data indicate that the low temperature and transient leakage condition could have the same slope as the steady-state case. These results confirm that some characteristic of the Q2 and Q3 transistors causes high

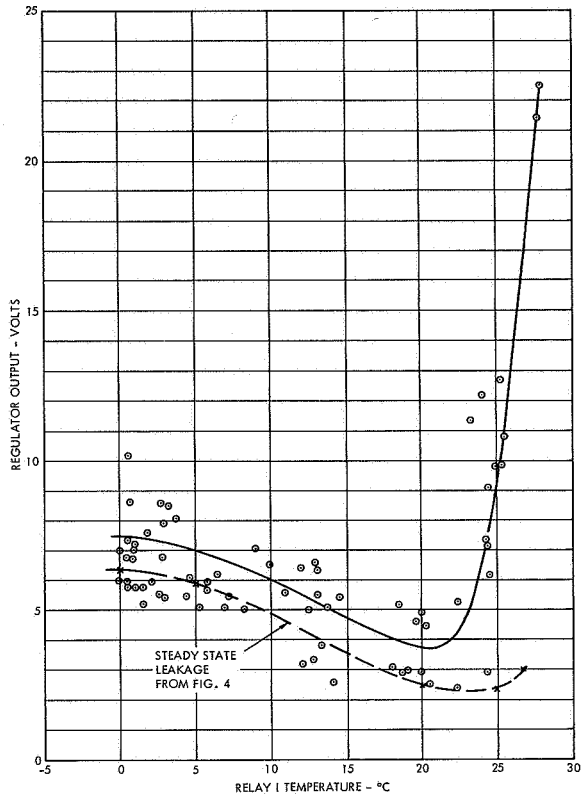


FIGURE 4–6.—Instantaneous leakage of regulator at shutdown of transponder No. 2 vs. temperatrue.

leakage rates at low temperatures. However, these data also show that aside from these high values at low temperatures, a "disastrous ON" condition occurs in the regulator as a result of high temperature. Without detailed test data on the regulator in question, it is impossible to determine whether the malfunction of transponder regulator No. 1 was caused by the launch environment.

The leakage condition of the regulator, regardless of whether it is caused by power transistors Q2 or Q3, the driving transistor Q4, or the control circuitry, demonstrated a need for a positive on-off switch in the spacecraft. This change was incorporated in Flight Model II and has completely eliminated the possibility of the problem occurring in that spacecraft (Figure 4–38).

Load Verification

Figure 4–7 shows the load current result-

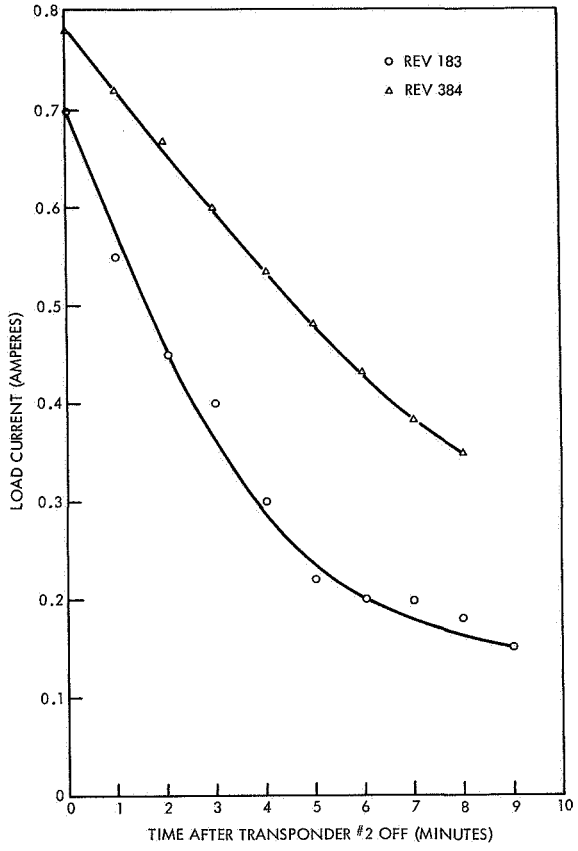


FIGURE 4–7.—Load current vs. time after wideband No. 2 shutdown.

ing from the leakage after a typical shutoff of transponder No. 2. Numerous calculations were performed to verify the electrical loads observed in orbit and to compare these with expected values. After determination of the load current due to the wideband leakage, fair correlation between the observed and expected values was found as listed in Table 4–4.

TABLE 4–4.—*Comparison of Expected and Observed Electrical Loads*

Loads	Current (amps)	
	Expected	Observed
Continuous and telemetry	0.55	0.55
Continuous, telemetry, radiation experiment	0.80	0.90
Transponder warmup	1.61	1.45
Transponder full on	3.80	3.75

Solar Array Performance

From the test data available prior to the launch of Relay, it was anticipated that the solar array output current would be nominally 2.0 amps. In-orbit measurements, however, yielded an initial value of 1.7 amps. The solar array has since then deteriorated with respect to time as expected. This is shown in Figure 4–8, which shows solar array output current versus orbit revolution. The predicted deterioration is also indicated, and fair correlation is apparent between the two values. A 9-volt power supply which supplies power to all the current transducers and to some of the temperature transducers on the spacecraft has performed in an erratic fashion. This is partly responsible for the fact that some of the data points deviate from the nominal value. The current transducer also is temperature-sensitive, which requires the indication of solar array output current to be corrected for temperature. The output current must also be corrected for sun aspect or the sun incident angle of sunlight with respect to the spin axis of the spacecraft. Other variations apparent in the solar array output result from variations in solar array temperatures and distance from the sun.

The array temperature falls during the eclipse seasons, and as array temperature decreases, the output current likewise decreases. Figure 4–9 presents the solar array temperature as a function of duration of eclipse. Figure 4–10 gives the solar array output current at 28 volts as a function of time after a 40-minute eclipse. This curve was derived at a time when the array was at 20°C and at an output of 1.15 amps.

The full-sunlight stabilized temperature of the solar array is 20°C. When orbit revolutions were examined to determine the array output versus temperature characteristics, slopes of 0.0037 to 0.0030 were found. A factor of 0.0035 amp/°C was used to correct the output current to the 20°C stablized condition.

Since the P/N cells deteriorate markedly due to the radiation environment, it was recommended before launch of Relay I that

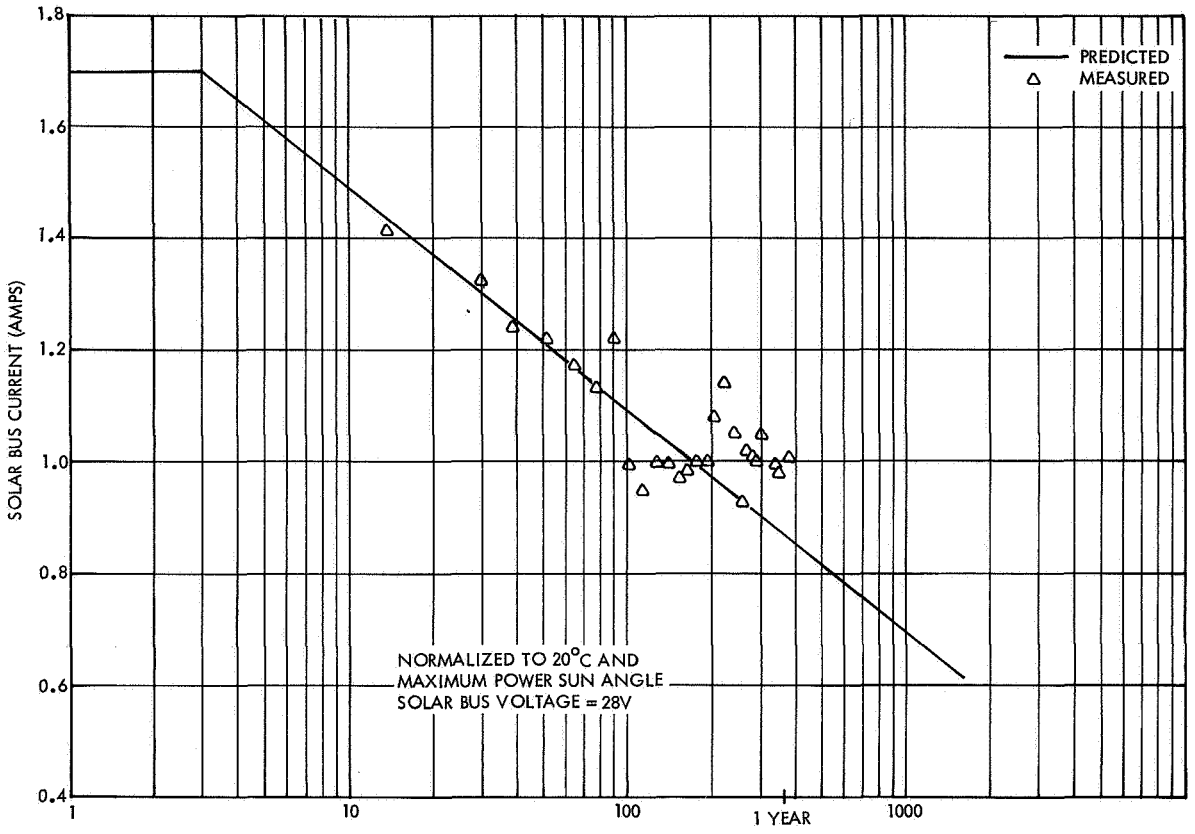


FIGURE 4–8.—Predicted vs. measured solar cell array output current.

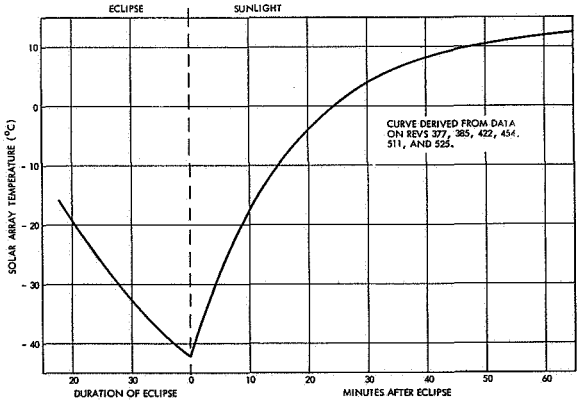


FIGURE 4–9.—Solar array temperature as a function of eclipse.

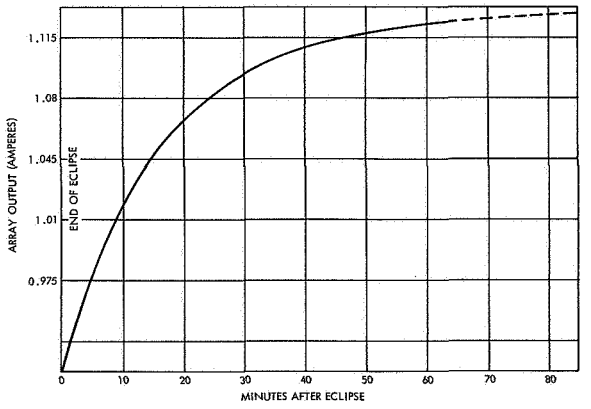


FIGURE 4–10.—Solar array output at 28 volts vs. time after 40-minute eclipse.

N/P cells be utilized on Flight Models 2 and 3. The N/P cells are more resistant to the radiation levels encountered by Relay and could provide an extremely long lifetime for Flight Model 2. Figure 4–11 gives a comparison of solar array versus days in orbit for the P/N cells as measured on Relay I and for N/P cells as derived from calculations based on the results obtained on Relay I.

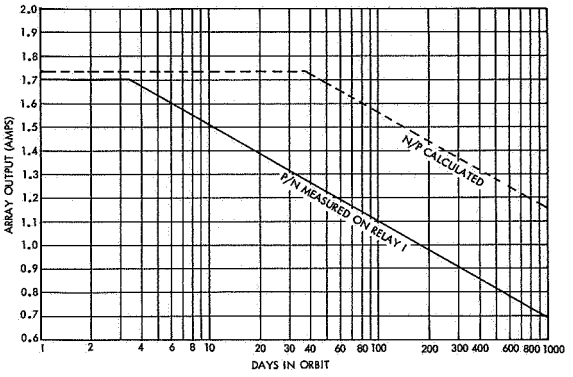


FIGURE 4–11.—Solar array output for P/N cells compared with N/P cells.

Shortly after launch it was estimated that Relay I was encountering 0.75×10^{13} omnidirectional electrons with energies of 0.5 to 8 Mev per cm^2 per day and 1.1×10^8 omnidirectional protons with energies greater than 30 Mev per cm^2 per day. Of the total electrons, 0.5×10^{13} are with energies from 0.5 to 1 Mev*. These estimates were made for January 1963 and it should be noted that the electron field has since lessened. The N/P cells are approximately 20 times more resistant to electron damage and 2.5 times more resistant to proton damage than the P/N cells used on Relay I.

BATTERY PERFORMANCE

With the exception of the failure of the No. 2 charge controller (Rev 548) adequate battery performance has been observed. The loss of battery No. 2 reduced the available capacity; however, during the early full-sunlight periods, four 30-minute operations of the wideband transponder could be supported daily. The spacecraft was operated during these initial full sunlight periods to the maximum extent possible to reduce the amount of overcharge. This in turn reduced the spacecraft temperature to prevent the full ON condition of transponder No. 1. After the first eclipse season there was no difficulty in keeping the spacecraft temperature at a desirable value. The only concern then was that the battery temperatures were as low as —5°C. Overcharge of the batteries at these low temperatures could cause gas formation in the cells which in turn could explode the batteries. Three battery cells are instrumented with a pressure switch set at 500 psi and at no time during the operation of Relay has the switch actuated. The primary guide to normal operation was an end-of-discharge voltage of 23.5 as the cutoff point for transponder operation. This value was established from the known voltage drops in the transponder regulators, so that a full regulated output voltage of 22.5 could be maintained.

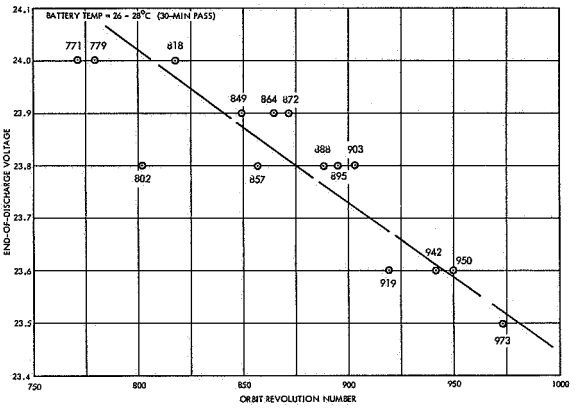


FIGURE 4–12.—End-of-discharge voltage vs. orbit.

One characteristic exhibited by the batteries has been the so-called memory effect, or the apparent decrease of battery capacity with respect to charge and discharge cycles. Figure 4–12 shows a decrease of almost 0.5 volt in the end-of-discharge voltage over a period of 200 orbit revolutions or slightly less than one month. These values were selected from 30-minute passes for which the battery temperatures were in the range of 26°C to 28°C. The memory effect decreased the capacity of the batteries after continued cycling to a point where the 23.5 volt cutoff level was reached after 15 minutes of transponder operation. Normally the spacecraft could be operated 30 to 35 minutes before reaching the cutoff voltage.

*Courtesy of Mr. E. G. Stassinopoulos, GSFC Theoretical Division.

It had been theorized that a deep discharge of the batteries would eliminate the memory effect. The loss of capacity of the cells was blamed on a reduction in the effective plate surface area due to loss of activity of the cadmium plate surface. A deep discharge of the batteries supposedly would remove the inactive cadmium and thereby restore the lost capacity.

Shortly after an eclipse on Rev 625, the spacecraft was found to be in a low-voltage condition, indicating that some load, such as a transponder, had been ON and had discharged the batteries to a very low level. After the spacecraft had been allowed to charge for one orbit revolution, the transponder was turned on. After eight minutes of normal operation, the system voltage dropped rapidly, causing the low-voltage cutoff device (which operates when the voltage is 20 volts or lower) to function, turning off the transponder. The bus voltage and battery voltage for this operation (Rev 626) are shown in Figure 4–13.

After the batteries were fully recharged, it was observed after a 30-minute operation of the transponder that the capacity of the batteries had increased. A 30-minute pass prior to this low voltage cutoff (Rev 602) showed an end-of-discharge voltage of 23.5 after 30 minutes, while on Rev 633 the end-of-discharge for that same operation time was 24.2 volts (see Figure 4–14).

On Rev 663 the spacecraft was operated for 39 minutes when the temperatures were near the upper critical level. This caused the

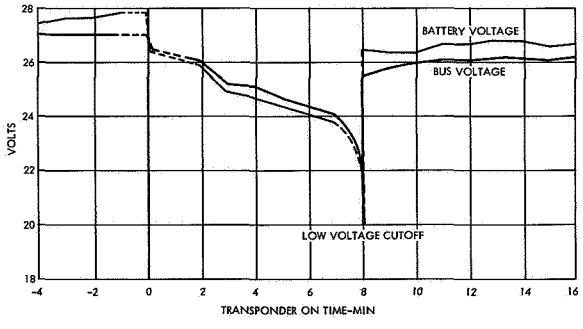


FIGURE 4–13.—Battery and solar bus voltage vs. transponder ON time—orbit 626.

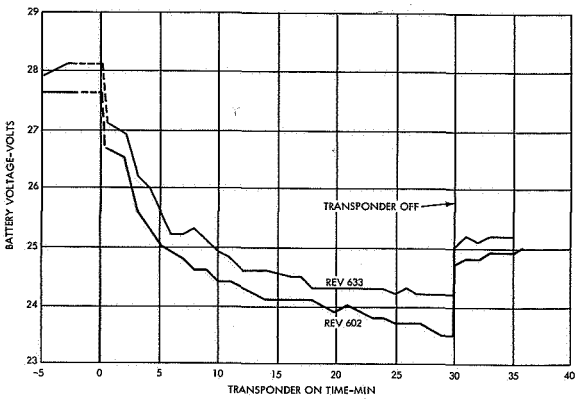


FIGURE 4–14.—Battery improvement after low voltage cutoff—orbit 626.

spacecraft temperature to increase further, and once again the full ON condition of transponder No. 1 resulted. After the spacecraft temperature had decreased and the spacecraft once again returned to a normal condition, it was observed by comparing Revs 657 and 711 that the capacity of the batteries had once again been restored (see Figure 4–15).

During the period of orbit Rev 1127 when the spacecraft entered its deepest eclipse season, a continuous trickle charge condition resulted. The trickle charge feature of the

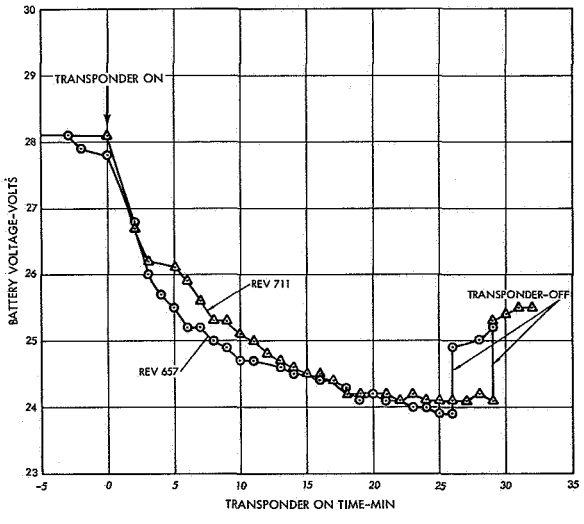


FIGURE 4–15.—Battery improvement after recovery full ON condition—orbit 663.

power system is activated by any of the following three conditions:

- Battery temperature above 32°C.
- Battery voltages below 25 v.
- Actuation of the pressure switch

During the period in question, the batteries would discharge to a low level during an eclipse, possibly as a result of additional loads due to anomalous performance of the command system. The normal continuous loads were also sufficient to discharge the batteries excessively during these long eclipse periods. The resulting condition was that the batteries could not be trickle charged sufficiently to change to the full charge mode at 25 volts, and therefore could not be fully charged before another eclipse occurred. It was necessary to send a series of off commands to the spacecraft whenever it was visible from the Relay Test Stations and Minitrack Stations. This evidently reduced the number of anomalous command states and the batteries were able to charge fully. After this recovery, it was observed that once again an increase in battery capacity was apparent. A comparison of the battery discharge curves for Revs 1112 and 1160 (Figure 4–16) shows an improvement of 0.7 volts in the end-of-discharge voltage after a 25-minute pass.

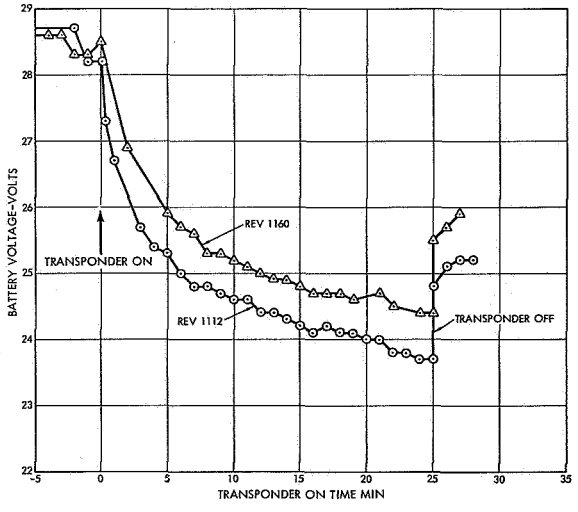


FIGURE 4–16.—Battery discharge curves before and after continuous trickle mode.

Realizing that a deep discharge of the batteries could improve the available capacity, attempts were successful on several occasions to run the transponder for a period of sufficient duration to lower the voltage and therefore reduce the memory effect. These deep discharges resulted in a pronounced increase in battery capacity, even though the low-voltage cutoff level was never reached. Figures 4–17 and 4–18 give comparative battery discharge characteristics before and after a deep discharge for two different time periods. Once again the improvement in battery capacity is apparent.

The nickel-cadmium batteries used on Relay exhibit a lower end-of-discharge voltage

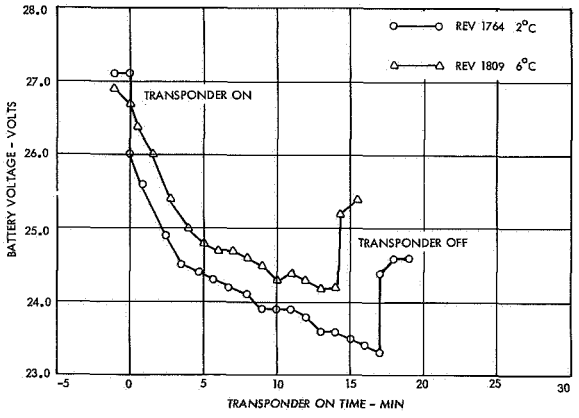


FIGURE 4–17.—Battery characteristics before and after deep discharge—orbits 1764 and 1769.

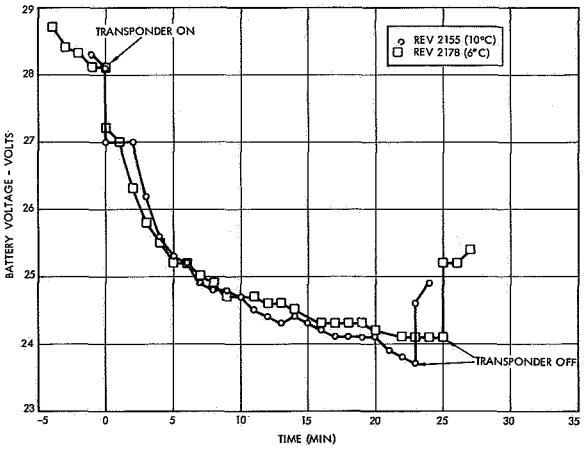


FIGURE 4–18.—Battery characteristics before and after deep discharge—orbits 2155 and 2178.

and higher end-of-charge voltage at lower temperatures. Figures 4–19 give some typical charge-discharge characteristics of nickel-cadmium cells and shows the dependence of available capacity on temperature. This temperature dependence has been observed on Relay I, but is apparent only upon close scrutiny. It is necessary to examine orbit passes sufficiently similar that memory effects are eliminated. Likewise, one must make certain that charging rates, leakage rates and percent of charge are equal. Figure 4–20 illustrates how a comparison of Revs 1237 and 1369, when the battery temperatures were 1.5° and 8°C respectively, fails to reveal a temperature effect. The discharge curve for Rev 1369 has the same shape as that for 1237, but is slightly lower. This illustrates that there is less capacity available for Rev 1369, although the temperature indicates that it should be greater than

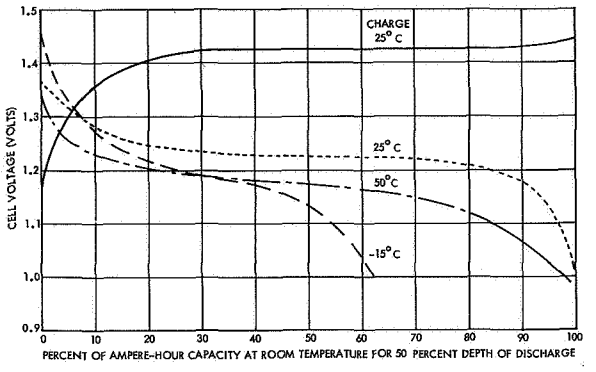


FIGURE 4–19.—Nickel Cadmium cell—typical charge—discharge characteristics.

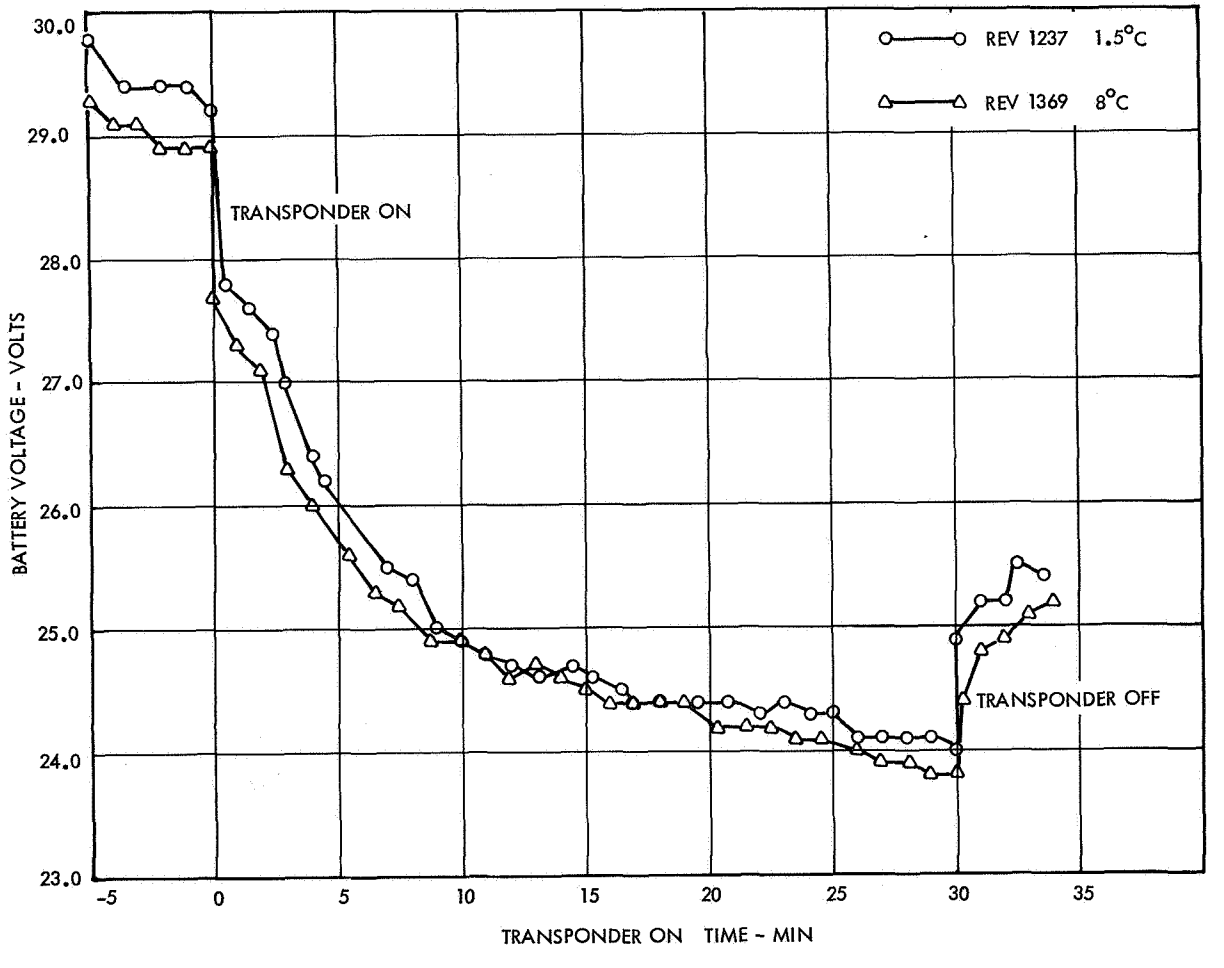


FIGURE 4–20.—Battery characteristics on orbits 1237 and 1369.

for Rev 1237. This is a case where the memory effect predominates, even though the two points in question are only 132 orbit revolutions apart.

A case of maximum battery temperature excursion was examined. Orbit Rev 988 was compared with 1112, where the temperatures were 26° and —3° respectively. The results are illustrated in Figure 4–21 and show that a higher end-of-charge and lower end-of-discharge voltage is apparent when battery temperatures are lower.

The performance of the batteries in Relay has been good; the only changes incorporated in the Relay II were lowering the trickle charge voltage level to 20 volts and the addition of one cell to each battery. Observation of the so-called memory effect indicates a need for closer examination of the phenomenon and possibly laboratory tests to provide a better understanding of it. It appears at present that the greatest improvement in battery capacity is obtained by repeated cycles of deep discharges, such as occurred during the long trickle charge condition around Rev 1130.

Power System Duty Cycle

The duty cycle originally intended for Relay consisted of 100 minutes per day of transponder operation over three or four consecutive orbit revolutions and three to six hours per day of radiation experiment operation. However, due to the initial failure and to continuous command system anomalies through the operational lifetime of Relay I, this planned operation scheme was not followed.

As soon as the temperature-dependent "full-on" load condition of transponder No. 1

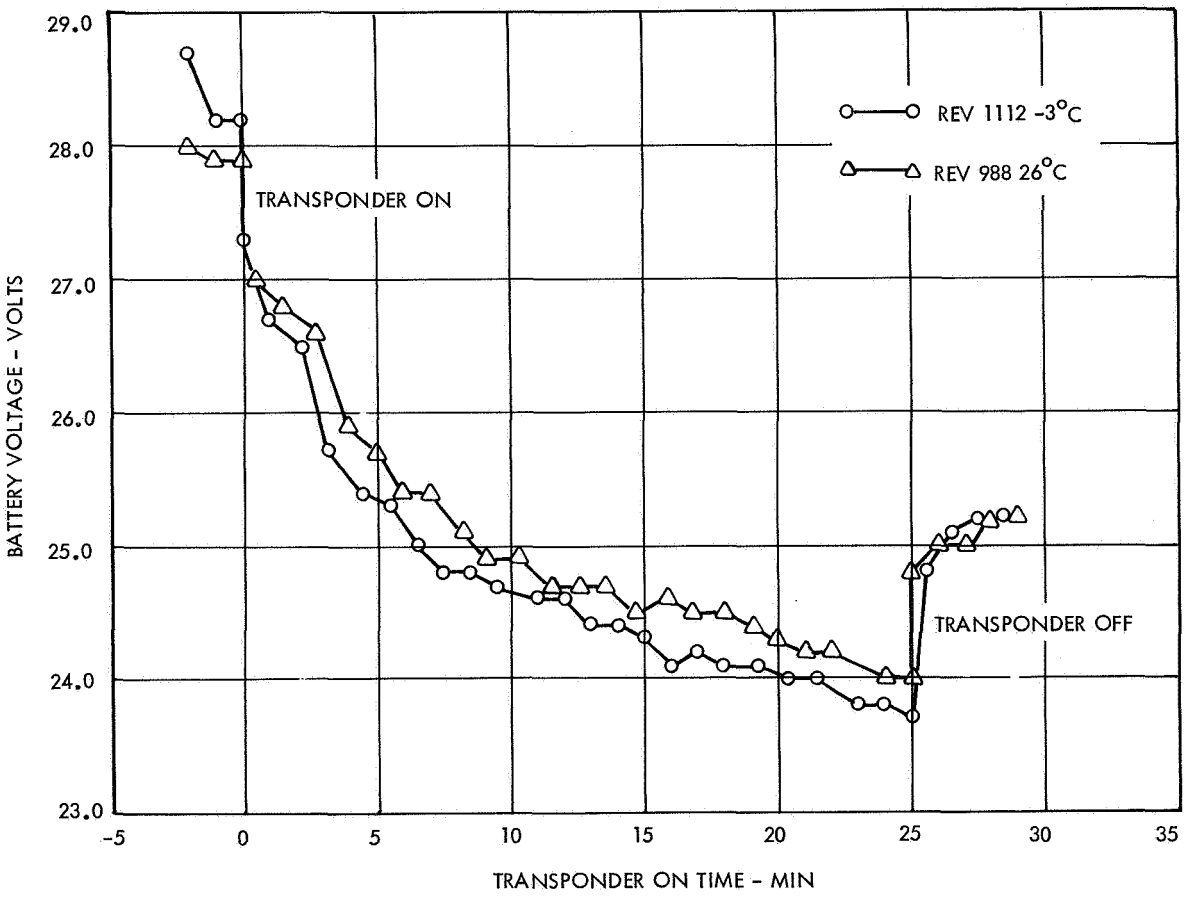


FIGURE 4–21.—Battery discharge characteristics—effects of temperature—orbits 988 and 1112.

was apparent, the spacecraft was operated to reduce the amount of overcharge and thus the spacecraft temperature. When the first eclipse season was reached and temperatures were no longer a problem, the spacecraft was operated for only one wideband pass per day. There was some concern at this time that excessive overcharge at the lower spacecraft temperatures might cause gas formation in the cells, causing the batteries to fail. Much lower spacecraft temperatures were encountered during the second eclipse season; during this phase the spacecraft was operated to reduce the amount of overcharge. The second full sunlight period, which began in early March, showed that the temperature-dependent failure mode of the transponder No. 1 regulator still existed. Once again the spacecraft was operated to the maximum extent possible. Even though battery No. 2 was no longer operable, four 30-minute transponder operations daily were possible. Figure 4–22 shows the accumulated operating time of transponder No. 2 compared with the eclipse history. Eclipse seasons result in the compounded problem of less solar energy available to charge the batteries and at the same time lower temperatures, which are caused partly by the shorter charging time of the batteries, but primarily by the eclipse itself. The rate of transponder operation is obviously affected by the eclipse season. This effect can be seen in Figure 4–22 where the rate of accumulation of operating time decreases with time even during the full sunlight periods. There is less total daily ampere-hour capacity, but operations of 30 to 45 minutes duration are still possible, if

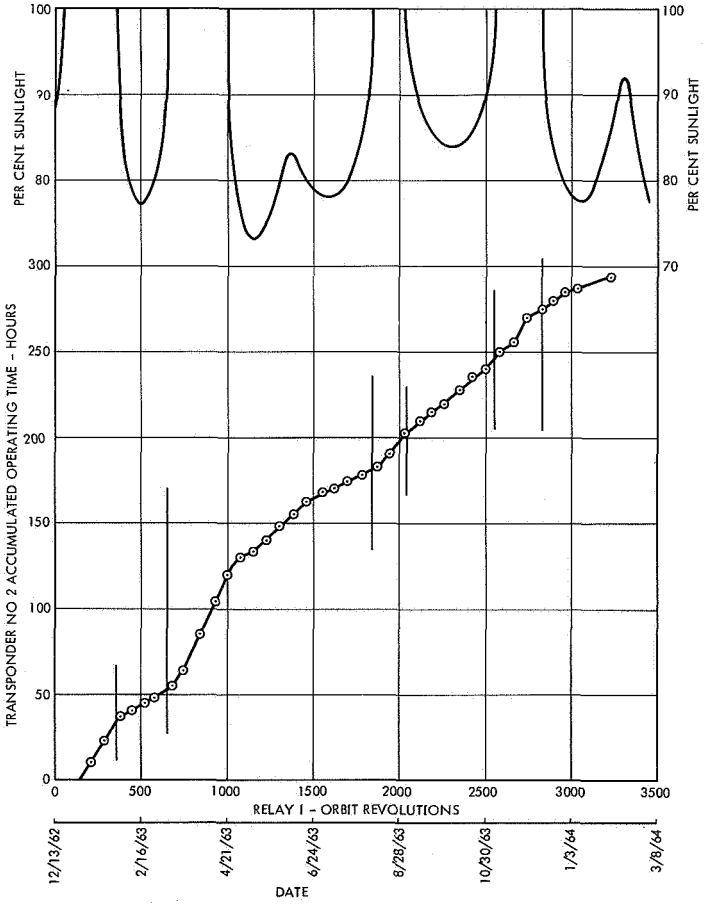


FIGURE 4–22.—Accumulated transponder No. 2 operating time compared with eclipse history.

only one such operation per day is attempted.

Relay I is equipped with an electrolytic timer which has a nominal operation time of one year. This timer will disconnect the solar bus when it functions, thus disabling the spacecraft. The timer is temperature dependent, and it is estimated that for the temperatures it has encountered the nominal operation time may have been increased by as much as a year. The nominal cutoff time was December 1963, but in November 1964, the spacecraft was still functioning.

WIDEBAND COMMUNICATION SYSTEM

The Relay Communication system consists of two completely redundant transponders. Each receives the 1725 Mc signal, triples the modulation index, and retransmits the signal at a frequency of 4169.720 Mc. Figure 4–23 shows the wideband transmitter. The transponder has a narrowband mode in which it can receive two simultaneous signals at 1723.33 Mc and 1726.66 Mc and retransmit them at 4164.720 and 4174.720 respectively. There is also a 40 mw cw output at 4079.73 Mc which serves as a tracking beacon. In the wideband mode, the transponder transmits a nominal power of 10 watts over a bandwidth of 23 Mc. In the narrowband, or two-way mode, the bandwidth is divided into two 1.5 Mc channels.

Transponder system No. 1 was not operated to any appreciable extent, due to the failure noted in the preceding section. The data discussed here covers the operation of transponder No. 2.

By the end of January, 1964, transponder No. 2 was used for over 745 operations in the conduct of wideband communication experiments with the Relay participating ground stations. Three hundred hours of operating time had been accumulated on transponder No. 2 with no apparent difficulties. The results from the communication experiments and from all telemetry data available indicate that the transponder performance was essentially unchanged throughout the operational year. Table 4–5 lists the specified electrical performance of transponder No. 2 along with measured values made prior to launch*.

The only anomalous performance observed was on Revs 989, 1417, and 1710. On Rev 989 the input signal to the TWT dropped to a very low value during the operation and then recovered and rose to a normal value at the end of the pass. The main IF AGC voltage decreased in an almost identical fashion and the TWT power output likewise

*"Completed Electrical Acceptance of Wideband Repeater No. F1A (System No. 2, Flight Model 1)," RCA Document, 11 Dec. 1962.

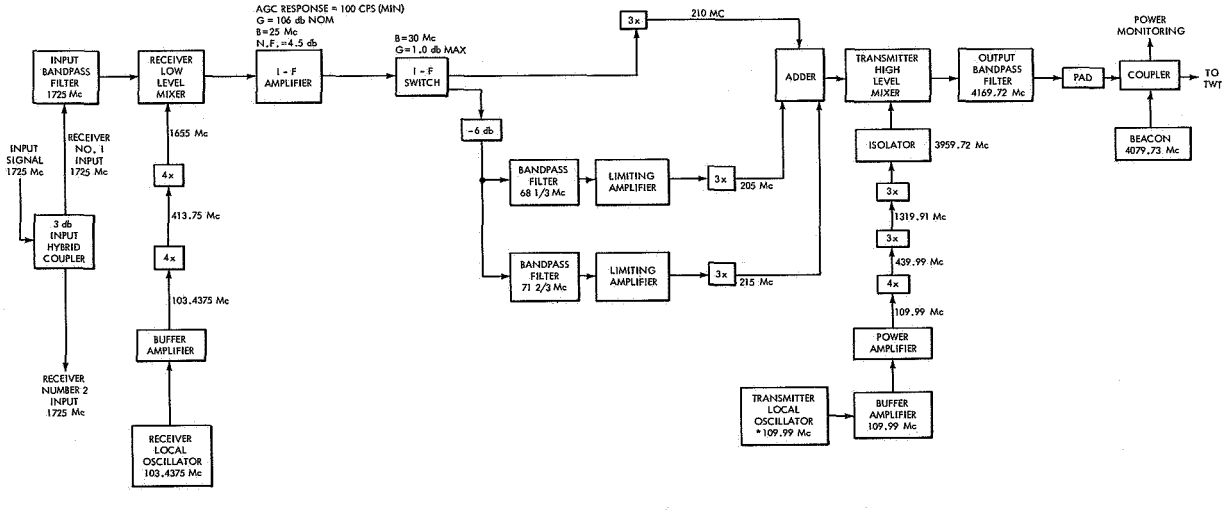


FIGURE 4–23.—Spacecraft wideband receiver block diagram.

TABLE 4–5.—*Electrical Performance Specifications*

Measurement	Specified	Measured
Input power (dc)	90 w	88.8 w
RF output power (at output of TWT)		
Wideband mode	10 dbw	10.65 dbw
Narrowband mode (weakest NB channel)	3.54 dbw	3.67 dbw
Beacon	23 dbm	23.2 dbm
Bandwidth (wideband mode), 1 db	23 Mc	34 Mc
Noise figure	14 db	14 db
Transmission tests		
Wideband mode		
300-channel noise loading	7500 pw*	2290 pw*
Noise power in top channel (with pre-emphasis and weighting). Ground delay.**		
Linear	0.294 ns/Mc	−0.35 ns/Mc
Parabolic	0.378 ns/Mc^2	0.27 ns/Mc^2
Television		
Video	As a design goal, spacecraft shall be transparent for television transmission.	No visible effect on video.
Audio	Crosstalk shall be 50 db down.	No visible distortion; crosstalk on audio 65 db down.
Narrowband mode		
Narrowband noise loading	7500 pw*	1380 pw*
Noise power 24th channel (with pre-emphasis and weighting)		
Crosstalk	31 db	41 db
Spurious check	All spurious products shall be 30 db below wideband output.	All products 30 db below wideband output.

*This includes ground station and repeater.
**Wideband repeater only.

varied. These telemetered items are shown in Figure 4–24. Normally there is enough AGC to maintain transmitter drive level high enough for the TWT output power to be 10 watts. It is reasoned, therefore, that the drop in transmitter drive, TWT output power, and main IF AGC voltage, as indicated in Figure 4–25, was the result of some intermittent behavior in the receiver local oscillator. It also appears that the TWT was functioning normally during this period and was only following the input drive.

On Rev 1417 the 4080 Mc tracking beacon was observed to be erratic. The output power of the beacon L. O. and the TWT remained constant and at the normal level. However, the transmitter drive varied considerably during the period of erratic behavior, as shown in Figure 4–26. The receiver main IF AGC and TWT power output for this revolution are given in Figure 4–27. The command receiver AGC is also included in Figure 4–27, showing that during the period of erratic output of the beacon, the command receiver AGC was high. The command receiver AGC is considered to be a measure of RF interference in the spacecraft. It was observed that when difficulties were encountered in commanding the transponder off, the command receier AGC was excessively high. The Andover, Maine, ATT Ground Station was tracking the spacecraft on Rev 1417 when the beacon exhibited the erratic behavior. The beacon output was extremely noisy and varied considerably in power output. This power variation was reflected in the antenna servo loop error and caused the ground station antenna to oscillate. This oscillation required switching to the programmed tracking mode.

As already mentioned, the command receiver AGC has been taken as a measure of RF interference in the spacecraft. Most of the time the interference has no effect whatever on the function of the spacecraft, but it appears to interfere with reception of the transponder OFF command. For this reason, the transponder is commanded off while the participating ground station is still transmitting a carrier to the spacecraft. The carrier presence quiets the transponder system, reducing RF interference in the command receiver. Figures 4–28 and 4–29 show plots of transmitter input and command receiver AGC versus transponder ON time, and main IF AGC voltage and TWT output power versus transponder ON time, for Rev 1440. During this revolution the command receiver AGC was observed to increase to a high level near the end of the pass. However, the increase had no effect on the functioning of the transponder or the tracking beacon.

Prior to operations on orbit Rev 1710, the TWT output power as telemetered from the spacecraft was nominally 10 watts. After

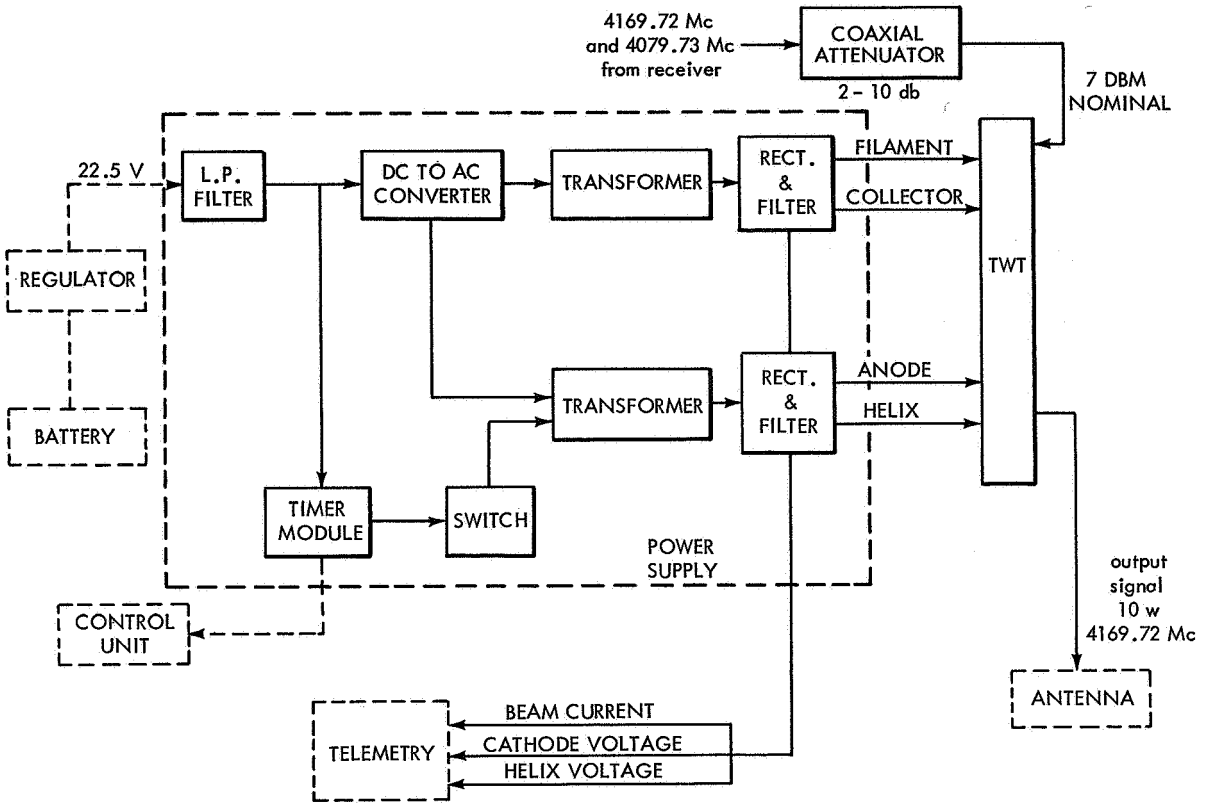


FIGURE 4–24.—Spacecraft wideband transmitter block diagram.

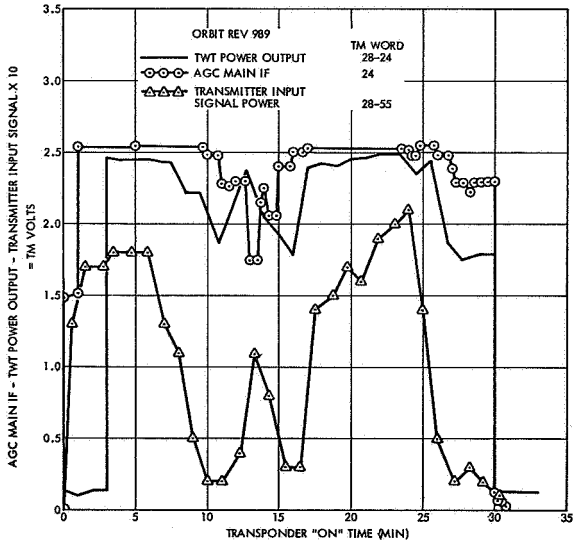


FIGURE 4–25.—TWT power out, AGC main IF, transmitter input, telemetry voltage versus transponder ON time—orbit 989.

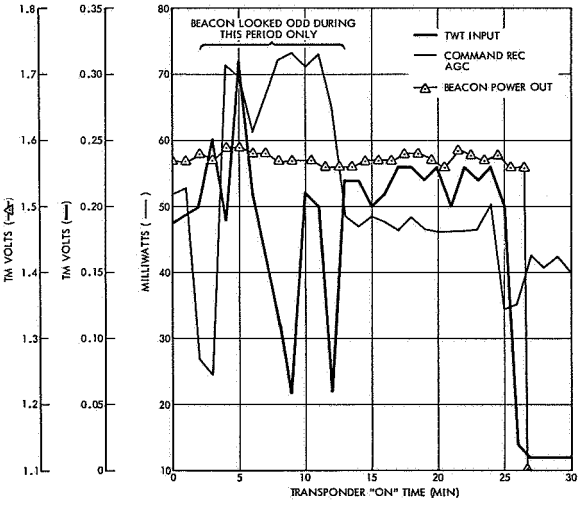


FIGURE 4–26.—TWT input signal, command receiver AGC 4080 beacon output versus transponder ON time—orbit 1417.

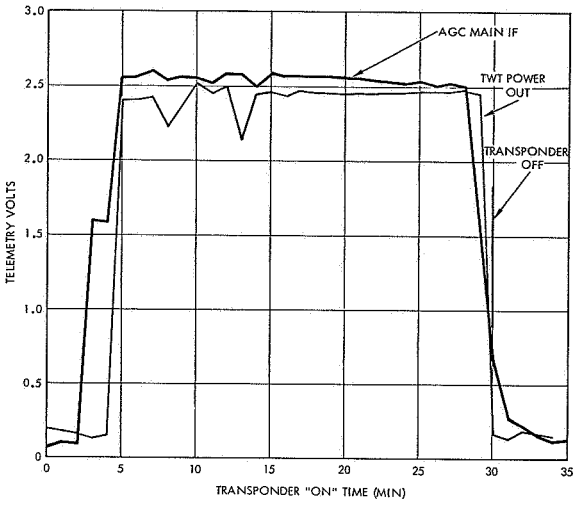


FIGURE 4–27.—TWT power output, AGC main IF telemetry voltage versus transponder ON time.

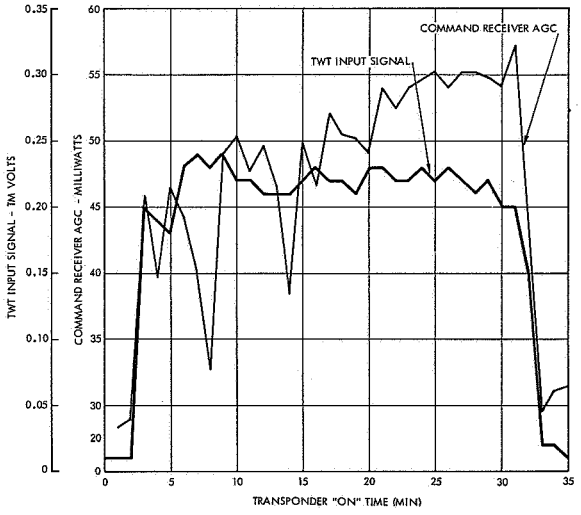


FIGURE 4–28.—Command receiver AGC, TWT input signal versus transponder ON time—orbit 1440.

this period of time (22 July 1963) the output power measurement varied somewhat from the nominal 10-watt value to as low as 8 watts. This condition has persisted since, and efforts were made to confirm whether the TWT output power had actually decreased of whether the characteristics of the power sensing diode had changed. Correlation of received signal strength at the ground stations with the telemetered TWT output power was not very close and generally it was believed, on the basis of ground station

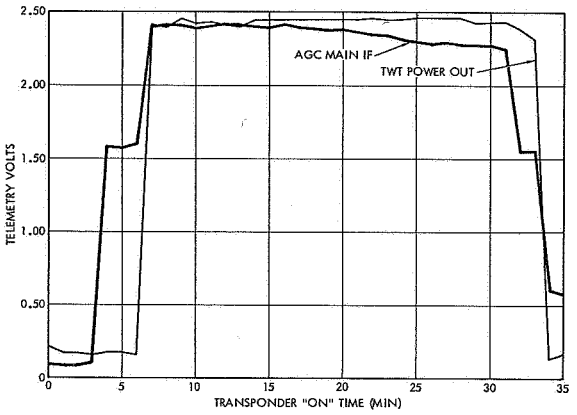


FIGURE 4–29.—TWT power output, AGC main IF telemetry voltage versus transponder ON time—orbit 1440.

data, that the TWT output was still nominally 10 watts. The power sensing diode used to monitor this function is located in a port of the wideband antenna and therefore monitors the power output from either transponder system. Transponder No. 1 was operated for a short period and it was observed that the power output measurement was equally low for system No. 1. It was concluded from this exercise that the telemetry sensing diode characteristic had changed, by giving erroneous power output indications. Since that time the power output measurement has decreased further, although it appears from ground observations that the TWT output power is essentially unchanged. Table 4–6 shows telemetered TWT voltages from early orbit revolutions of January 1963 compared with orbit revolutions in January 1964. These indicate the TWT characteristics have remained essentially constant during the operational lifetime of Relay I.

Difficulty has been encountered in measuring the TWT cathode voltage because the leakage of transponder regulator No. 1, while system No. 2 is operating, causes a change in the telemetry voltage for this item. This is also true of several other telemetered items from the spacecraft. Cathode voltage measurements observed from Revs 2900 to 3100 were examined and it was shown that measurement likewise reflects the sum of the

TABLE 4–6.—*TWT Parameters for Early and Recent Relay Passes Transponder No. 2*

Orbit rev	Cathode voltage (volts)	Helix voltage (volts)	Collector current (ma)
231	950	2000	43.7
262	950	2000	42.5
285	950	2000	42.5
230	950	2000	42.5
2970	950	2000	44.5
3001	950	2000	44.5
3017	950	2000	44.0
3094	950	2000	44.5

the cathode telemetry voltage was indeed a function or regulated bus voltage. Calibration data which gives cathode telemetry voltage as a function of regulated bus voltage for constant values of cathode voltage were compared with the measured data. This comparison is shown in Figure 4–30 and shows that the cathode voltage has an essentially constant value of 950 volts.

The partially ON condition of transponder No. 1 is also reflected in the main IF AGC telemetry voltage. This effect led to difficulty in accurately determining from telemetry the received signal level at the spacecraft. When both transponders are off it is readily apparent that some AGC voltage is indicated, with the value dependent on the regulated bus voltage measurement. The regulated bus voltage measurement gives the sum value of the voltage output from both high-power regulators. The AGC telemetry

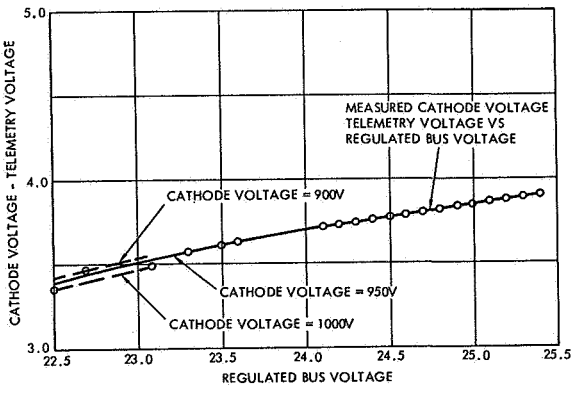


FIGURE 4–30.—Comparison of TWT cathode voltage and regulated bus voltage for orbits 2900 to 3100.

AGC voltage present in both transponders. Examination of many revolutions where leakage was apparent and when transponder No. 2 was on with no carrier illuminating the spacecraft yielded the data indicated in Figure 4–31. The spacecraft was illuminated by a ground station utilizing programmed steering, in order to determine whether this transmitted signal was reflected in the AGC during the time when both transponders were off although the leakage rates were sufficiently high to indicate a relatively high level of AGC voltage. The ground transmission test showed that the carrier presence had no effect. Considering that the no-carrier-present level of AGC voltage for transponder No. 2 is 1.5 volts (pre-launch value), it was reasoned that any AGC voltage above this value was contributed by leakage of the regulator for transponder No. 1. On this basis, a linear correction factor was derived, as shown in Figure 4–32, from which the appli-

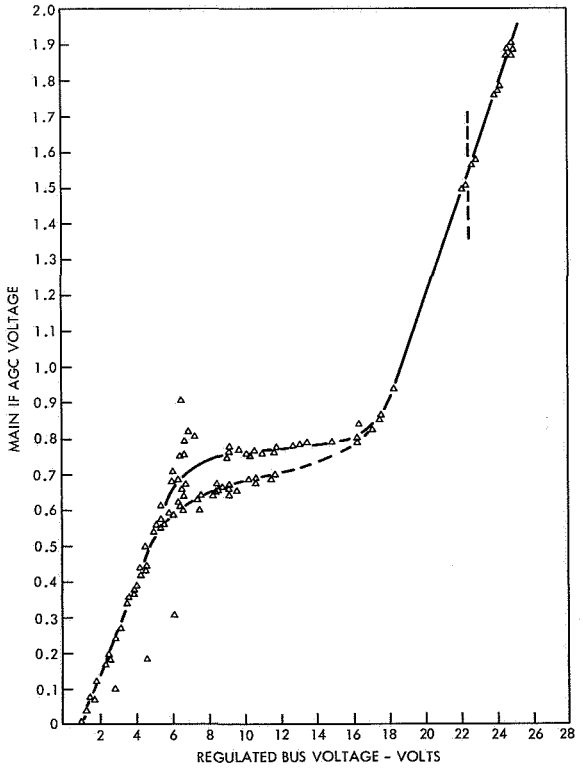


FIGURE 4–31.—Main IF AGC (no carrier present) voltage versus regulated bus voltage.

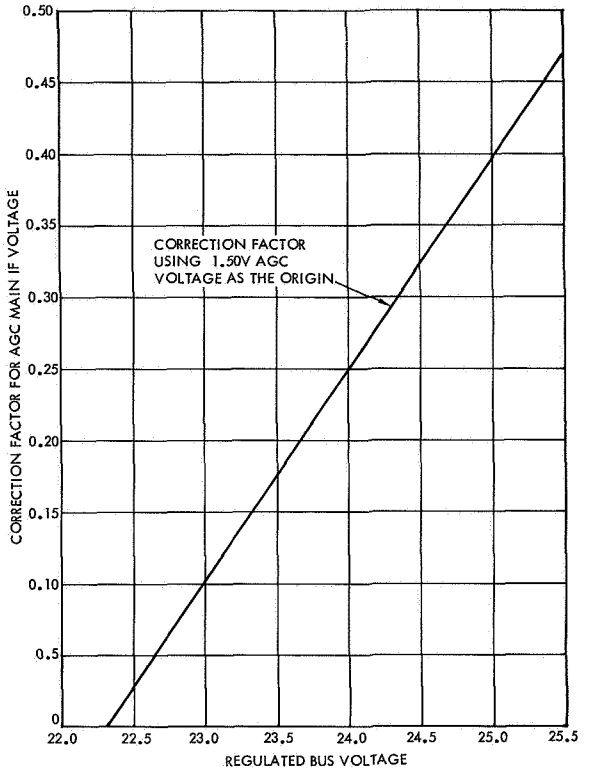


FIGURE 4–32.—Correction factor for AGC main IF voltage.

cable correction could be determined in relation to the telemetered value of the regulated bus voltage. The correction determined in this way is subtracted from the telemetered AGC voltage, yielding a correct indication of the power of the signal received at the spacecraft.

To determine the validity of this correction factor, up-link power tests were performed with a ground station and the spacecraft. Calculated signal strength values were plotted versus the corrected AGC telemetry, and these in turn were compared with the AGC calibration curve. The ground station transmitted power was varied from a low level (250 watts) when the slant range distances were the greatest and increased to the normal 10 kw level when the ranges were the closest. This procedure yielded a maximum excursion of the received signal at the spacecraft. This exercise was performed on several occasions.

The received radiated power at the spacecraft was calculated using the following relationship:

$$S_r = P_t G_t \left(\frac{\lambda}{4\pi R}\right)^2 \frac{G_a}{L}$$

where

S_r = Received signal strength
P_t = Ground transmitted power
G_t = Transmitter antenna gain
λ = Wavelength
R = Slant range (ground station to satellite distance)
G_a = Spacecraft receiving antenna gain
L = Losses

The results of this exercise are shown in Figure 4–33 and indicate that the method of correcting the AGC telemetry voltage is accurate and also that the AGC calibration is essentially unchanged from the time of launch.

Several other telemetered wideband functions were examined for the period of January 1963 and January 1964 indicating that the wideband system performed essentially without change. Table 4–7 shows the telemetered signal-present indications for sev-

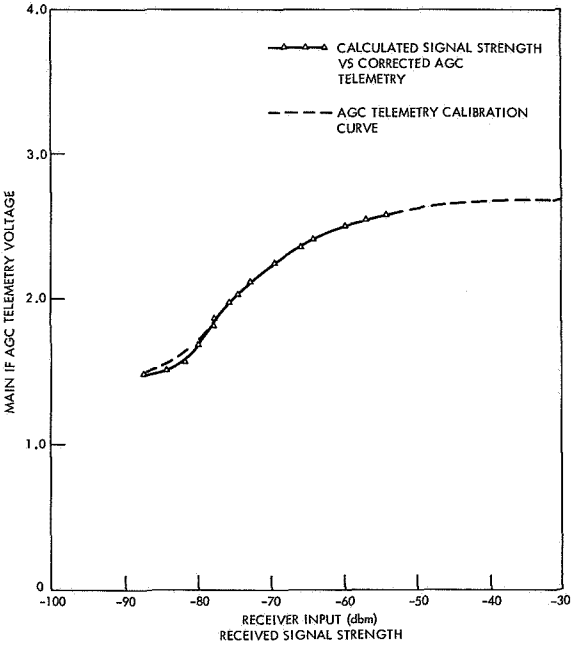


FIGURE 4–33.—Corrected AGC voltage versus calculated signal strength compared with AGC calibration.

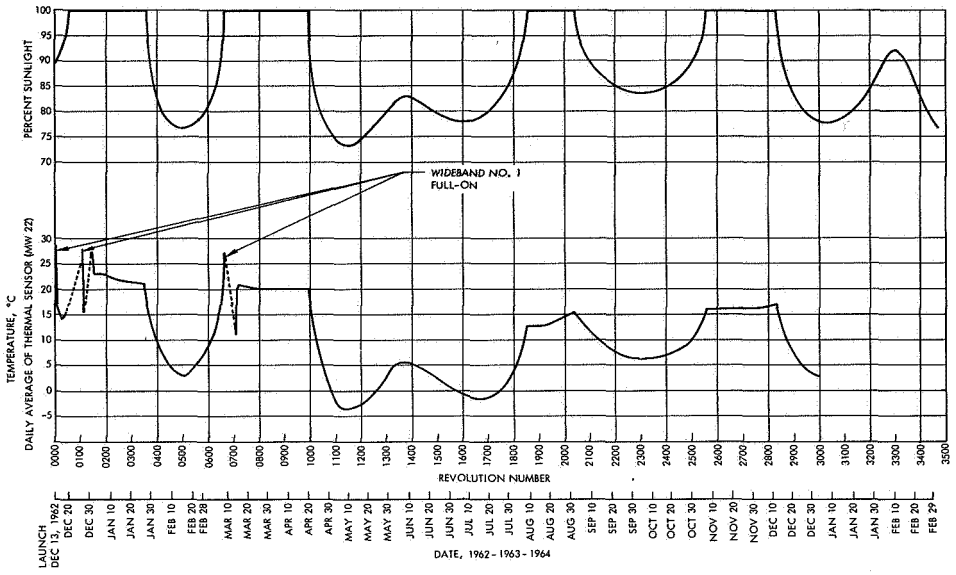


FIGURE 4–34.—Relay I temperature and eclipse history.

eral wideband functions for selected orbit revolutions over the operating lifetime as compared with the prelaunch nominal values.

TABLE 4–7.—*Comparison of Signal Presence Indication for Some Wideband Items*

Item	Prelaunch		Rev 230	Rev 238	Rev 3109	Rev 3258
Beacon output to TWT.		1.54	1.50	1.49	1.57	1.56
Transmitter						
Local Oscillator	1.75	1.64	1.70	1.70	1.76	1.72
TWT input						
Signal power	0.20–0.235	0.13–0.14	0.14	0.16	0.23	0.14
Temperature	0	25	22.5	20.0	7.0	13.7

TEMPERATURE AND ECLIPSE HISTORY

The spacecraft temperature is a function of many parameters; the most important of these is the fraction of time the spacecraft spends in the shadow of the earth. Other significant parameters are amount of energy reflected and emitted from the earth, operational duty cycle of spacecraft, orientation of the spacecraft with respect to the sun, and the variation of the earth-sun distance. All of these parameters, but particularly operational duty cycle, influence the temperature distribution within the spacecraft and temperature variations during an operational day in addition to the average overall temperature. Figure 4–34 gives the temperature and eclipse history for Relay I. The temperature indicated represents an average value for the thermal sensor (batteries are almost the same).

The amount of shadow or eclipse encountered by the spacecraft during the year varied from full sunlight to maximum eclipse durations of 50 minutes (73 percent sunlight) out of an orbital period of 185 minutes (Figure 4–34). This variation was sufficient to cause a change of about 20°C in the spacecraft temperature. Long eclipse periods also limited the duty cycle of Relay I due to reduced total power from the solar cells. Since the primary variation of the spacecraft temperature is the overcharge state of the batteries, the reduced solar power was partly responsible for lower temperatures. These factors have an additional effect on the temperature distribution of the spacecraft as well as on the variation in temperatures seen during an operational day.

The spacecraft has an active temperature control system which consists of louvers controlled by a temperature sensor; the louvers move from fully open to fully closed in response to a temperature change of 15°C. This is not instrumented in Relay I so that

there is no telemetry indication of the operation of the thermal controller.

During the operation of either the communications subsystem or radiation experiment, the spacecraft temperature varies by several degrees. Figure 4–35 gives the temperatures of the thermal controller sensor and batteries during three typical operating days, and also shows the influence of the degree of overcharge on the temperatures. The temperatures are highest when the spacecraft is acquired on the first pass of an operational day, after the batteries have been in overcharge for several hours. The significance of the overcharge-temperature is illustrated on Rev 810 (Figure 4–35) when the spacecraft was acquired with the radiation experiment ON, thereby eliminating the overcharge condition of the batteries. The decrease in temperatures from pass to pass during an operational day can be seen to result primarily from discharge of the batteries which removes the overcharge heat-producing condition.

During a normal operating day the spacecraft is acquired with fully charged batteries, having been in overcharge for perhaps several hours. This period of overcharge causes increased temperatures of the batteries and adjacent items. In the "normal operating day" examples of Figure 4–35, the highest temperature is at the battery, the thermal sensor is next, and most of the rest of the spacecraft is at around 13°C. It is assumed that the temperature of the batteries at acquisition, about 27°C on the first pass of the operational day, is near the overcharge-equilibrium temperature of the batteries. The transponder is then operated, causing partial discharge of the batteries and therefore eliminating the overcharge condition. The batteries do not change temperature appreciably during the first transponder operation of the day. The rest of the spacecraft heats up during the operation as a result of normal component operation and thermal dissipation.

During the time between the end of the

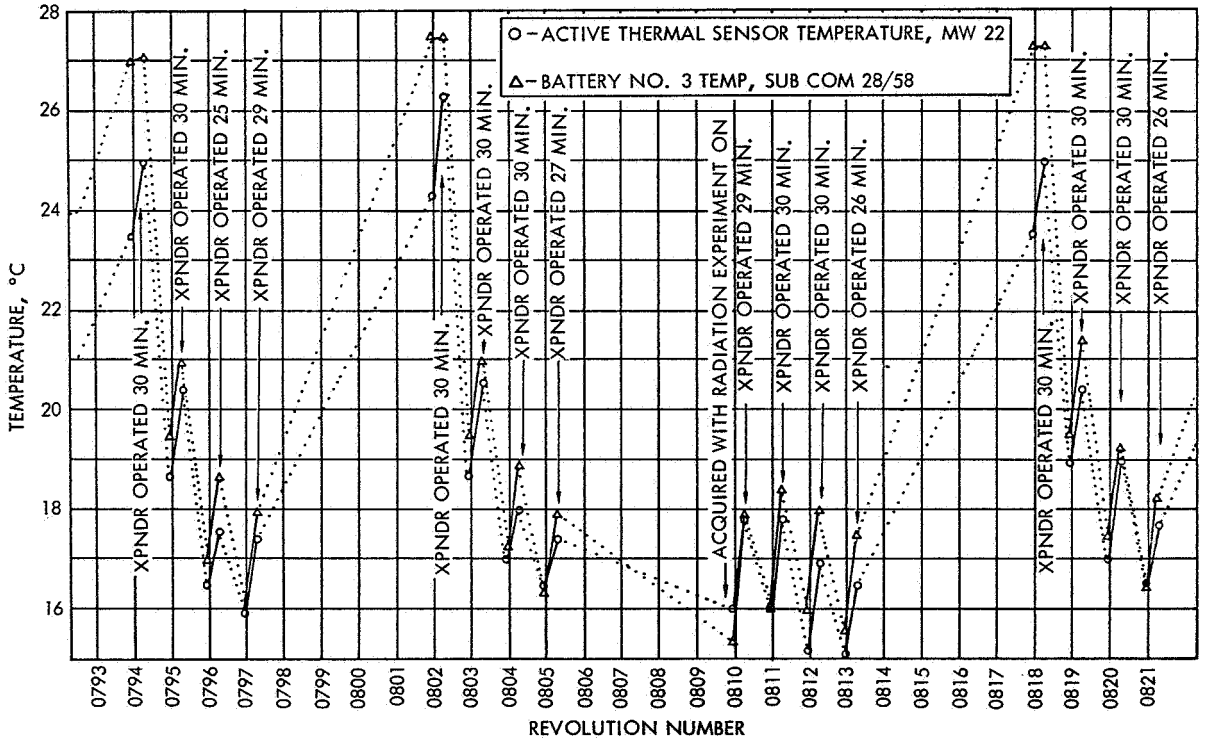


FIGURE 4–35.—Effect of duty cycle on spacecraft temperature.

first operation and the start of the second, the batteries are being charged but do not reach the overcharge condition with its attendant heating. They cool by 7° or 8°C during this 2½-hour period. The temperature variations during the rest of the operational day can be accounted for by the same mechanism.

Some time before Rev 810, the radiation experiment was turned on by anomalous command. The consequent electrical load prevented the batteries from reaching the overcharge condition, and the acquisition temperatures were much lower than usual (Figure 4–35). A similar effect has been noted at various other times. Unusual and/or anomalous duty cycles of the spacecraft are reflected in the temperatures.

The spacecraft temperature variations of Figure 4–35 illustrate the effect of duty cycle on temperature during the period of March 25 through March 28 and are similar to the trends seen at all other times. During other full sunlight periods and during eclipse seasons, the average temperatures may not be as high nor the daily variations as great, but the pattern is similar.

The daily variation of the active thermal sensor temperature during a three-day period for each of the four full sunlight seasons is shown in Figure 4–36. The daily variation during the March season was greater than during other seasons and was caused by a longer duty cycle. The lower overall temperatures seen during the August full sunlight season were caused by decreased solar cell efficiency (with consequent lower battery charge and reduced overcharge) and by the change in spacecraft attitude which removed sunlight from the lower surface. The above

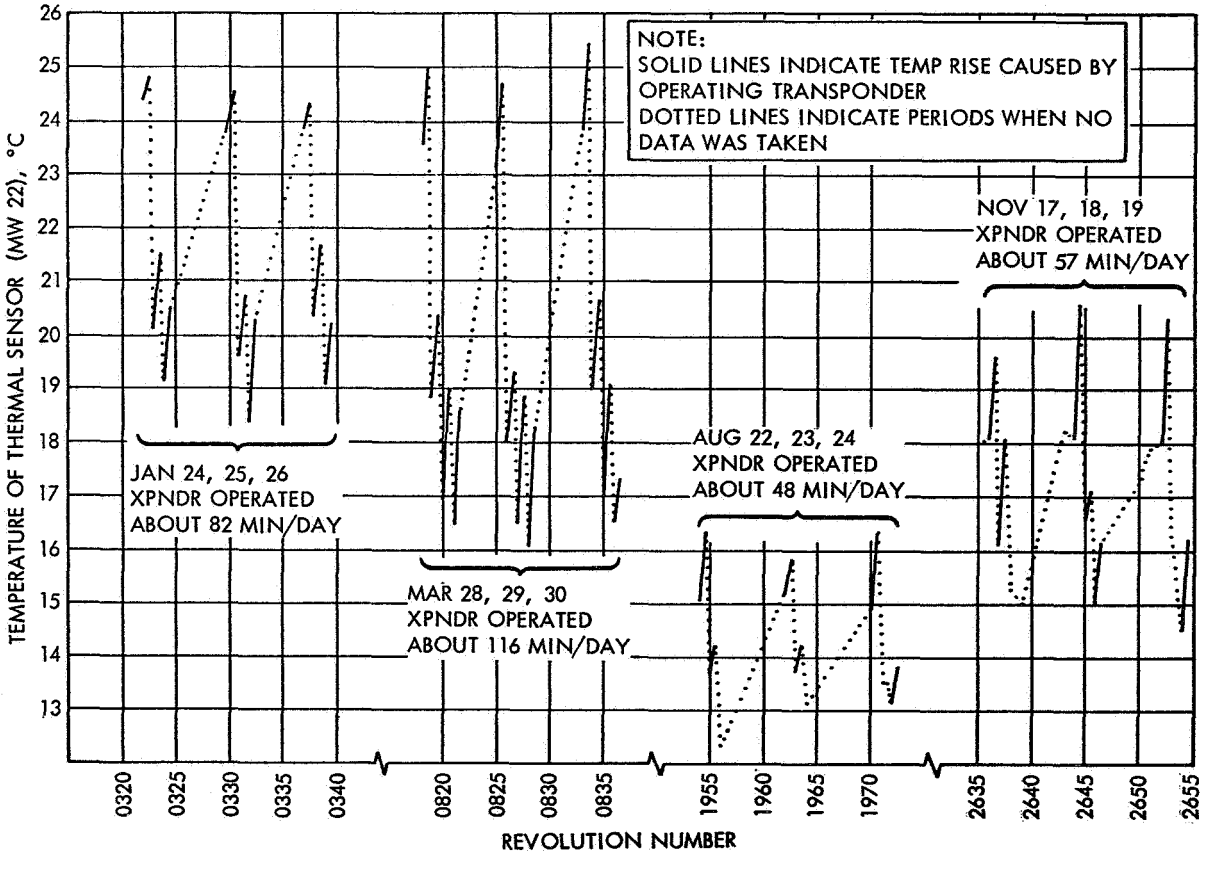


FIGURE 4–36.—Temperature variations during typical three-day periods of each of the four full-sunlight periods.

two factors did not change appreciably from the August to the November full sunlight season, but the thermal sensor temperature during the latter season was about 4°C higher. Other spacecraft temperatures did not show this 4°C difference but were about the same. The fact that the batteries and thermal sensor were warmer during the latter period indicates increased electrical activity (charge and discharge of batteries). This might be attributed in part to different battery characteristics (variation in battery capacity due to so-called memory effect) but more probably the increased electrical activity was possible due to a change of reflected solar energy from the earth (albedo). The coincidence of a sub-satellite perigee point and subsolar point causes a significant increase in albedo radiations. Since the precession of perigee does not have a one-year period, the spacecraft should show a long-term variation in temperature depending on how the lattitude of perigee varied with respect to the latitude of the sub-solar point (i.e., time of year). The latitude of perigee was closer to the sub-solar latitude during the November full-sunlight season than during the August full-sunlight season.

TELEMETRY, TRACKING AND COMMAND SYSTEM PERFORMANCE

The telemetry system consists of an encoder and two transmitters on frequencies of 136.140 and 136.620 Mc. Both transmitters can be on simultaneously, with one providing a cw signal for tracking purposes and the other the encoded telemetry data. The horizon scanner can also modulate the telemetry carrier, although not while the encoder is on.

The telemetry system is Pulse-Code-Modulated (PCM) at a rate of 1152 bits per second. Each telemetry word consists of nine bits, so that there are 128 main telemetry words. Most of these are used to telemeter information from the radiation experiments. Only 10 of the main frame words are used for monitoring spacecraft performance. One of these is subcommutated into 64 channels, which are all primary spacecraft measurements.

Two PCM/PDM/AM command receivers in a redundant configuration are used in the spacecraft to control power to the experiments and to switch spacecraft systems. The carrier frequency is approximately 150 Mc. The command system has provision for receiving 20 different commands. Two redundant decoders within the command system allow normal execution of the received commands with either or both decoders operative.

From the time of launch, command system anomalies have been persistent. A command state anomaly is defined as a state of the spacecraft system not resulting from transmitted commands. Observations of these anomalies has led to the belief that the primary causes are:

1. RF interference generated internally in the spacecraft, primarily from the wideband system.
2. The command and telemetry systems share a common antenna through a hybrid, and insufficient rejection allows the telemetry signal to feed back into the command system.
3. The command receiver sensitivity is such that any signals near 150 Mc will open the squelch circuit allowing any internally generated noise to enter the system.
4. The command system requires a positive voltage for maintaining an OFF command state. A system voltage decrease to a low level, as occurred during deep eclipses, often resulted in command state changes.

Figure 4–37 gives a frequency histogram of all command anomalies observed from launch through Rev 2850. These are compared with the spacecraft temperature and eclipse history; there does not appear to be any relationship between the temperature eclipse environment and the anomalies. Each bar indicated in the histogram represents a period of 20 orbit revolutions. It can be seen that beginning in September 1963, an increasing number of command anomalies occurred. The situation became so serious that NASA Minitrack Stations were utilized to send a series of normalizing and OFF

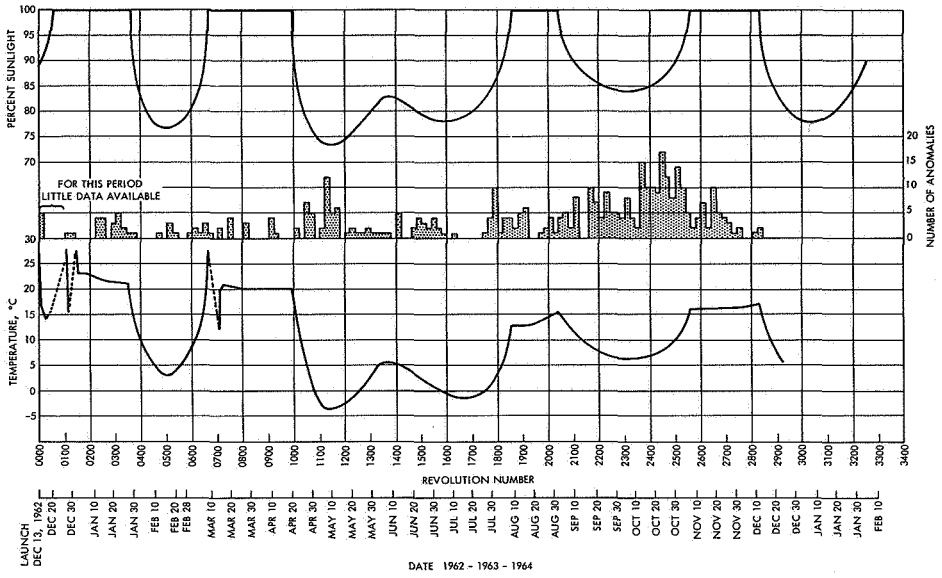


FIGURE 4–37.—Relay I—command anomaly frequency distribution with reference to temperature of spacecraft and eclipse.

commands to the spacecraft whenever visibility existed. This procedure was instituted in December 1963 and only six command anomalies were observed during that month. Table 4–8 gives a summation of the command state anomalies for each month through December 1963.

The command system performance on Relay I led to several recommendations for Flight Model 2. These were as follows:

1. A rejection filter added to the command and telemetry antenna to prevent any telemetry signals from reaching the command receiver.

2. Ferrite beads and braided shielding incorporated on the input leads to the TWT to eliminate the primary source of RFI.

3. Modifications in the squelch circuit to desensitize the command receivers.

4. System changes to provide a positive voltage for an ON command state and zero voltage for an OFF command state.

These changes have been effective in eliminating command system anomalies on Flight Model 2. As of the time of writing, Relay II, after well over a month in orbit, experienced no command system anomalies. It was noted in the section covering the electrical system performance that changes were made in Flight Model 2 to provide a positive OFF command for the wideband system. This was accomplished by the inclusion of magnetic latch relays that must be energized to provide the unregulated bus input to the voltage regulator for the transponder.* Figure 4–38 is a block diagram of the regulator and command system interface. It can be seen that a positive ON command will provide a signal to the solid-state switch in the regulator and also provide a pulse for latching the relay in the ON position. Likewise removal of the positive ON state will turn off the solid state switch and provide a pulse for disconnecting the relay.

SPACECRAFT ORIENTATION

It was intended to determine the orientation of Relay periodically from the horizon scanner and sun aspect sensor. This information was to be used to update the predictions of the spacecraft look angles. The wideband antenna gain, both receive and transmit, is a function of look angle. The look angle is

*"Quarterly Technical Report No. 8, March 1963–May 1963," RCA Document No. AED R–1978, 22 July 1963, pp. II–43–45.

TABLE 4–8.—*Summary of Command Anomalies*

Anomaly	Dec 13 1962	Jan	Feb	Mar	Apr	May	June	July	Aug	Sept	Oct	Nov	Dec	Total
Radiation ON		2	1	3	1	7	3	1	3	6	13	7		47
Radiation OFF									1					1
Horizon scanner ON	1					1	1		2	2	11	6	1	26
Narrowband mode						1	1		2	4	10	5		23
Wideband mode						1			1	1	4	4		11
Transponder No. 1 ON	2	1		1		2				1	2	1		10
Transponder No. 2 ON							1		1	2		2		6
Load cutoff override	1	2	2	4	3	4	2	2	3	7	7	5		42
Mod TLM XMTR No. 1		3	2		1	3	3	1	3	6	13	3		38
Mod TLM XMTR No. 2														
Current coil positive		3			3	4	3			4	9	5		31
Current coil negative		1			2	2		1	2	4	8	5	2	27
Encoder ON		2			3	1	1	1	7	4	5	4	1	29
Encoder OFF									1	2		2		5
Both TLM transmitters ON	1	4		3	2	3	3	1	8	8	12	5	2	51
Both TLM transmitters OFF	1	1	1	4	1		2	2	5	5	5	10		37
TLM transmitter No. 1 ON/ No. 2 OFF	1	1		2	1	4		1	1	1	3			15
Transponder No. 2 OFF											1	1		2
Total	7	20	6	16	17	33	20	11	40	57	103	65	6	401

the angle between the spacecraft spin axis and the range vector from any ground station. Had the look angles deteriorated to the point where adequate communication experiments could not be performed the attitude control system on Relay would have been operated to obtain a more desirable orientation. However, with the exception of Rev 155, the horizon scanner never yielded useful data. Sun aspect data and horizon scanner data on orbit 155 yielded a spin axis declination of —68.3 degrees, and a right ascension of —56 degrees. The nominal values are —69.7 degrees and —63.5 degrees respectively. The data from this examination gave an attitude that differed from the nominal predicted attitude by 2.5 degrees. Fortunately, the orientation of Relay through its operational lifetime has been such that it has provided excellent radar look angles for all stations, agreeing closely with those calculated before launch.

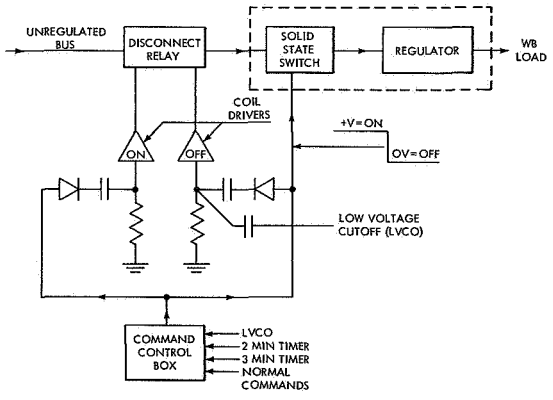


FIGURE 4–38.—Block diagram of interface of HP regulator (flight model 2) with command system.

The attitude control system, which consists of a torquing coil, was never employed although the coil was found to be ON in both positive and negative modes occasionally due to command system anomalies. Due to the long operation time constant and since the coil was turned on randomly in both the positive and negative directions, it was felt that this had no net effect on the spacecraft orientation. The measured magnetic dipole moments of the torquing coil when operating are —1.68 and +1.53 ampere-turn meter^2.

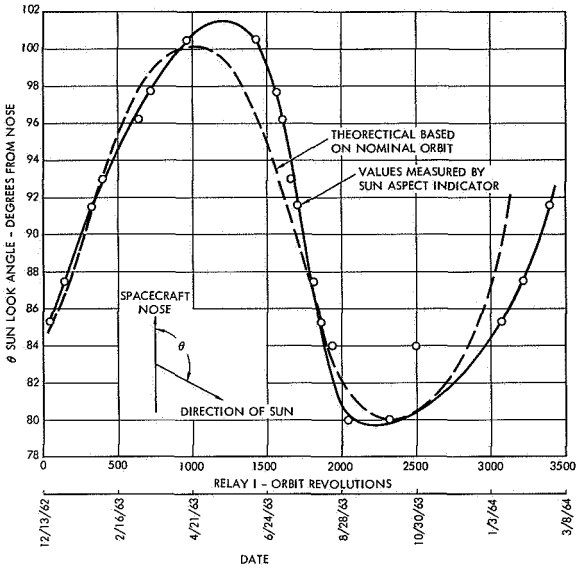


FIGURE 4–39.—Relay I sun aspect.

The sun aspect indicator is used to measure the angle between the sun direction vector and the spacecraft spin axis. The values measured over the first 3500 revolutions are given in Figure 4–39. The two data points at 84 degrees have been ignored since it is obvious that the value for Rev 2500 is in error. Also indicated in this figure is the nominal nonperturbed sun aspect, for comparison. The nominal curve is derived from the following relationship

$$\cos\theta = \sin\delta_s \sin\delta_R + \cos\delta_s \cos\delta_R \cos(\sigma_s - \sigma_R)$$

where

θ = Sun look angle
δ_s = Declination of the sun
σ_s = Right ascension of the sun
δ_R = Declination of spacecraft spin axis
σ_R = Right ascension of spacecraft spin axis

The prelaunch nominal values given above for the spacecraft spin axis declination and right ascension were used to generate the nominal curve. Analysis of the error between the predicted and actual sun aspect angles is difficult, since the error can be due to a drift in either the right ascension or declination of the spin axis. If minimum errors in declination and right ascension are assumed, the total can be as great as 3.5 degrees. If the error is considered to be in declination only, it can be as much as 5 degrees.

The observed error, or difference in the actual and nominal attitude, can be equated to the angular momentum of Relay. If one considers the error to be in declination only, the resultant momentum required to produce it can be expressed as a function of time. The derivative of this function will then yield the torque required to produce the resultant error. This type of analysis yields a maximum disturbance torque of 2×10^{-6} foot-pounds. Considering the configuration of the Relay spacecraft, it is apparent that solar pressure could cause some deviation of the attitude. However, the most probable cause is the effect of gravity gradient. It is reasonable to assume that the total error in the spacecraft attitude is primarily due to gravity gradient with solar pressure responsible for some effect.

SPIN RATE

The spin rate of Relay has decayed from the initial value of 167.3 rpm to 151.85 rpm over a period of 3284 orbit revolutions or 1.15 years (see Figure 4–40). The principal mechanisms which cause spin rate decay are hysteresis losses in magnetic material and induced eddy currents. The results given below assume that the primary cause of the decay is damping from eddy currents. Explicit expressions have been developed which describe retarding torques due to eddy currents in a thin shell of conducting material rotating in the earth's magnetic field. These show the spin rate to decay exponentially with time. Because most satellites have a complex structure, a segmented outer skin with broken current paths, and numerous small metallic containers, it is extremely difficult to predict analytically the exponential time constant.

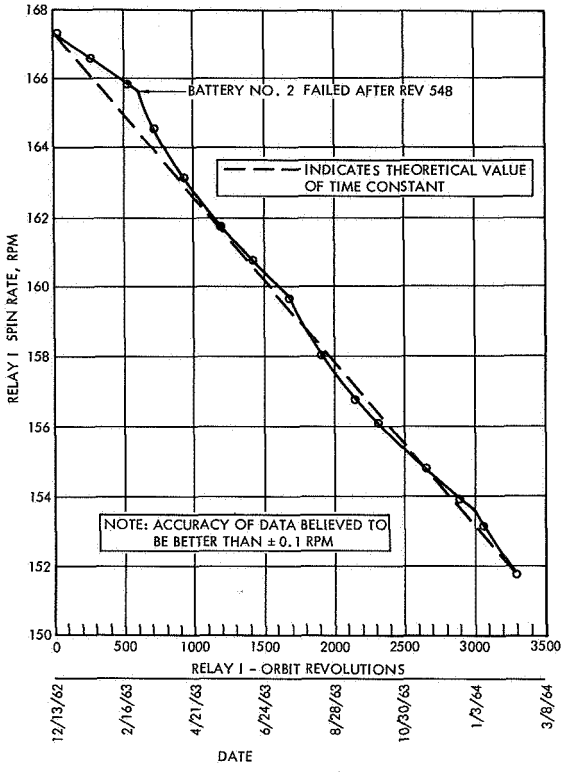


FIGURE 4–40.—Spin rate decay of Relay I.

Assuming the spin rate decay indicated in Figure 4–40 is primarily from eddy current damping, the following expression results

$$\omega = \omega_o e^{-t/r}$$

where

ω = Spin rate at time t
ω_o = Initial spin rate, 167.3 rpm
t = Time in years
r = Time constant 11.9 years

Examination of the spin rate curve shows that around Revs 600, 1700, and 3000 a pronounced change in the decay rate occurred. The first rate change was evidently caused when the battery No. 2 charge controller failed, eliminating Battery No. 2 from the system. This apparently had the effect of changing the eddy current situation in the spacecraft. As it turns out, this failure occurred when perigee was in the extreme southern latitude. The other two points of change comparison, Revs 1700 and 3000, are at times when perigee was in the extreme northern then again southern latitude (see

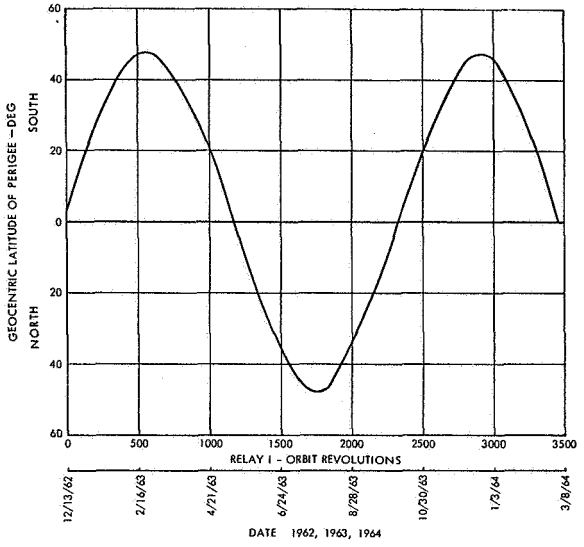


FIGURE 4–41.—Geocentric latitude of perigee.

Figure 4–41). The spacecraft experiences maximum interaction with the earth's magnetic field when perigee is in the extreme northern and southern hemispheres. This circumstance apparently has been responsible for the changes in decay rate. However, the spin rate decay examined over the 11.9 year time constant, would show an exponential decay and the minor variations due to perigee location would not be apparent.

AUTHOR. *This chapter was written by* D. E. KENDALL *of Space Technology Laboratories, Inc., Redondo Beach, California, U.S.A. under contract NAS 5–1302 with NASA/Goddard Space Flight Center.*

N66-10231

Chapter 5

The Microwave Repeater

GENERAL DESCRIPTION

The Communications Mission

The main objective of Project Relay was to provide a high quality communications link to experimentally verify the feasibility of microwave communications via an active spacecraft repeater.

Thus, it was decided that the Relay I spacecraft would be used in either of two ways. The first was to transmit traffic in one direction, where the specific traffic objectives were 300 voice channels or one 3-Mc video channel with sound subcarrier. The second was to transmit two-way traffic (24 total voice channels) originating at two different ground stations through the same repeater. The baseband associated with this narrowband mode traffic extended from 12 kc to 108 kc. The spacecraft specification required transmission of twelve voice channels in one direction, using a baseband of 12 kc to 60 kc. An additional twelve channels were transmitted in the reverse direction through the second narrowband using a baseband of 60 kc to 108 kc.

To meet the latter objectives, a dual-mode, active, heterodyne repeater was designed to maintain near CCIR transmission standards.

Repeater Functions

The microwave repeater received frequency-modulated signals from one or two ground stations, amplified these signals, tripled their deviation and retransmitted them. A block diagram of the wideband subsystem is shown in Figure 5–1. The weight allocation of the total spacecraft, plus the low weight designs achieved for individual elements, permitted redundant design in which all active repeater elements were supplied in duplicate.

The microwave antenna received the right-hand circularly-polarized carriers, transmitted from one (or two) ground stations, at 1725 Mc (or 1723.33 Mc and 1726.67 Mc). These carriers were divided in a 3-db hybrid and fed to each of two receivers. The receivers converted the carriers to a 70-Mc intermediate frequency (IF) using AGC to control the IF level.

Each receiver had dual modes of operation. In the first (single-station mode), the amplified IF signal was tripled to 210 Mc, translated to approximately 4170 Mc, fed to the traveling wave tube, amplified, and transmitted through one of the two parts of the microwave transmitting antenna. The output of a beacon oscillator, for use in tracking, operating at approximately 4080 Mc, was fed into the beacon coupler and was also amplified by the TWT. Each of the wideband subsystems was served by a separately regulated power supply, to achieve redundancy of the active elements.

In the second (or two-station) mode of operation, the two signals which are offset in frequency were separated into different

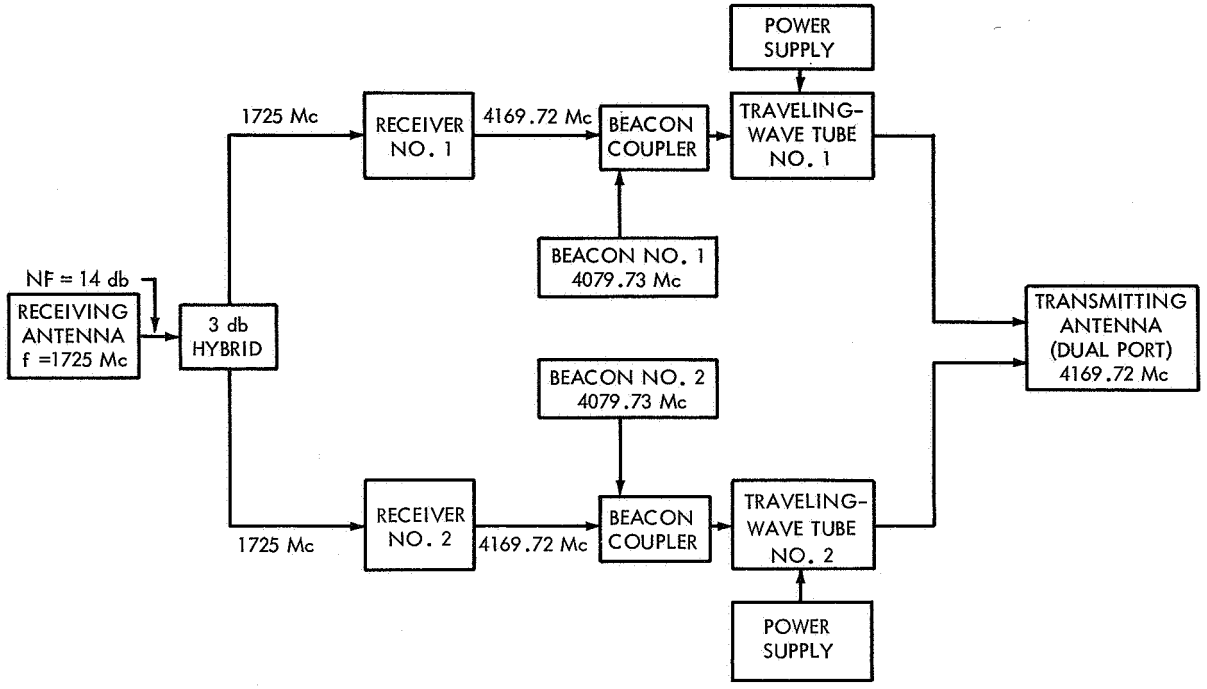


FIGURE 5–1.—Wideband subsystem block diagram.

channels at the output of the 70-Mc IF amplifier. Each channel included a limiter to set the level. After limiting, the signals were tripled to 205 or 215 Mc, depending on the channel, and then recombined. The combined signal was then translated back to the 4170-Mc band and subsequently amplified by the traveling-wave tube. The purpose of the dual-channel mode was to set the level of each channel, and avoid unwanted products which would occur if the two signals were tripled together.

Specifications

The repeater performance specification* is summarized in Table 5–1. The items covered in this specification include the general configuration and the detailed performance specifications.

Basic Design Considerations

General

The block diagram of an individual repeater (minus the traveling wave tube and its power supply) is shown in Figure 5–2. The following basic considerations resulted in this specific configuration.

Heterodyne Repeater

A heterodyne repeater provided controlled amplitude and group-delay characteristics in the IF capable of amplifying and retransmitting FM with very low distortion of the baseband information. It also allowed maximum use of solid-state components for low power drain and high reliability.

The state-of-the-art did not permit achievement of the desired 10-watt amplitude power-level required, using all solid-state components. Also, earlier work* had demonstrated the feasibility of designing light-weight, high-gain, high-efficiency traveling-wave tubes capable of withstanding spacecraft launch environment and of operating reliably

*These specifications are described in detail in the NASA/GSFC DOCUMENT, "Project Relay Performance Requirements," R1–0130.

*H. R. Mathwich, J. D. Kiesling, "A Reliable Wideband Transmitting Amplifier for Space Application," Conference Proceedings 1962 National Winter Convention on Military Electronics, p. 378 and appendix.

TABLE 5–1.—*Summary of Performance Requirements—Microwave Repeater*

I. EQUIPMENT	
The Microwave Repeater will consist of two complete separate transponders, a single-port receiving antenna, and a two-port transmitting antenna. Only one transponder shall operate at a time, with the second unit available as a back-up.	
Each transponder will contain the following major units:	
a. Receiver	
b. Transmitter	
c. Tracking Beacon	
II. GENERAL SYSTEM CONSIDERATIONS	
A. Received signal (at spacecraft antenna)	
1. One-way (wideband) transmission	
Signal strength	−40 to −60 dbm
Frequency	1725 Mc
Bandwidth	14 Mc max.
Modulation	FM
Polarization	RH circular
2. Two-way (narrowband transmission	
Signal strength (each carrier)	−40 to −80 dbm
Max. differential signal strength	10 db
Frequency	1723.333 Mc
	1726.667 Mc
Bandwidth (each carrier)	1.5 Mc
Modulation	FM
B. Radiated signal	
1. One-way transmission	
Effective radiated power	5 watts min. over the ϕ look angle from 40° to 115°
Frequency	4169.72 Mc
Bandwidth (obtained by multiplying the received signal modulation index by a factor of three).	23 Mc max.
Polarization	LH circular
2. Two-way transmission	
Effective radiated power (each carrier)	1.6 watts min. over the ϕ look angle from 40° to 115°
Frequency	4164.72 Mc
	4174.72 Mc
Bandwidth (each carrier—obtained by multiplying the received signal modulation index by a factor of 3).	2.5 Mc
Polarization	LH circular
3. Tracking beacon	
Effective radiated power	10 mw, referred to a linear antenna at any orientation normal to direction of propagation over the look angle of 40° to 115° (200 mw into an antenna with a 13 db axial ratio)
Frequency	4169.72 Mc
Polarization	LH circular

III. ANTENNA SUBSYSTEM	
Radiation pattern	−1 db, with respect to isotropic, for ϕ from 40° to 115°
Assymetry about spin axis	1 db (peak-to-peak gain variation)
Feed losses	1 db max
Polarization	
Receive	RH circular
Transmit	LH circular
Axial ratio	5 db max. over look angle 35° to 120°
VSWR	
Receive	2.0:1
Transmit	1.5:1
Isolation	16 db min. between transmit and receive ports
IV. RECEIVER UNIT	
A. Input characteristics	
Input frequency	
One-way	1725.00 Mc
Two-way	1723.333 Mc and 1726.667 Mc
Frequency stability	±.002%
Bandwidth (referred to input)	
One-way transmission	
1 db BW	14 Mc min.
3 db BW	20 Mc min.
Two-way transmission	
1 db BW	1.5 Mc min.
3 db BW	2.0 Mc min.
Image rejection	20 db min.
Noise figure (including input hybrid)	14 db max.
Dynamic range	−40 to −80 dbm
B. Output characteristics	
Output frequency	
One-way	4169.72 Mc
Two-way	4164.72 Mc and 4174.72 Mc
Bandwidth (1 db) after tripling	23 Mc
Group-delay (over 23 Mc output bandwidth)	
Parabolic	50×10^{-9} sec.
Linear	5×10^{-9} sec.
Ripple	5×10^{-9} sec.
Spurious response	30 db below desired signal
V. TRANSMITTER UNIT	
Saturated RF power output	10 w min.
TWT efficiency	21%
High voltage P.S. efficiency	80%
Spurious outputs	25 db (min) below desired signal
VI. BEACON UNIT	
Frequency	4079.73 Mc
Power output	+23 dbm typical
Incidental phase modulation	
at less than 100 cps rate	less than 0.1 rad.
above 100 cps rate	less than 0.4 rad.

in the space environment. Thus, a traveling-wave tube was used as the final RF amplifier and power-output device.

The use of a 70-Mc IF center frequency permitted maximum use of existing design art. Also, the frequency was high enough to permit reasonable filtering for image rejection and sideband filtering at RF consistent with the wide bandwidth required for low group-delay distortion.

Deviation Tripling

Deviation tripling was employed to compensate for the bandwidth-limited transmit-

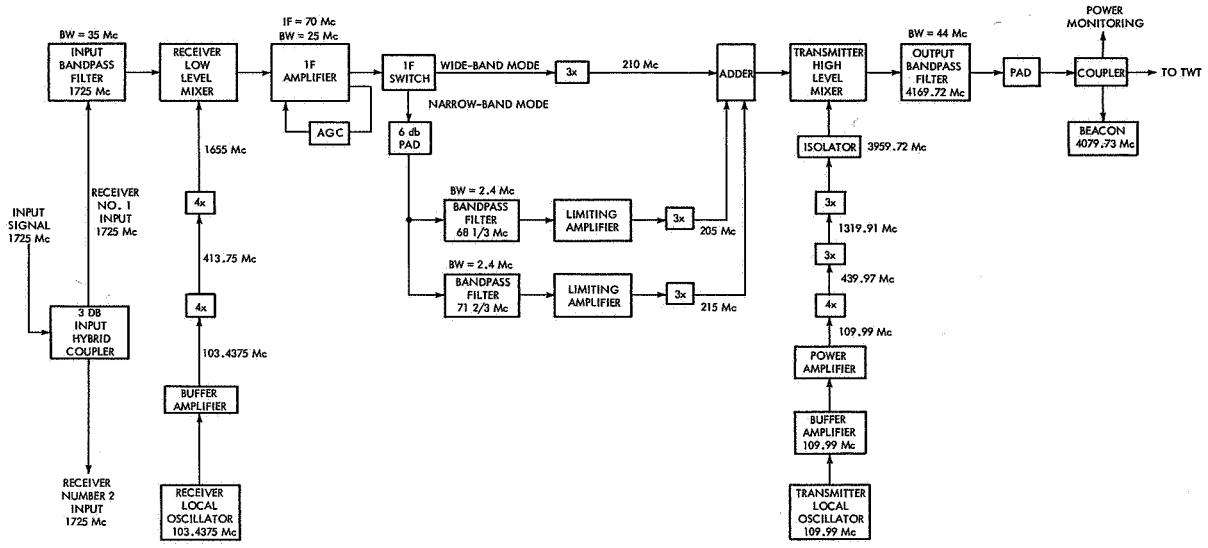


FIGURE 5–2.—Block diagram of receiving and transmitting circuit.

ting klystron used in the ground stations. In this manner, the transmitting klystron could be used over a restricted bandwidth (less than 14 Mc) to maintain reasonable phase linearity, while the critical downgoing link (from spacecraft to ground) could employ larger deviations and obtain the required baseband signal-to-noise by virtue of FM improvement.

Dual-Mode Operation

One wideband or two narrowband channels were specified. In the wideband mode (one wideband signal present), the IF output was tripled, and converted to 4 Gc for retransmission. In the narrowband mode, individual tripling had to be provided for each carrier, to prevent signal suppression, and to keep the intermodulation products to a reasonable level.

Placing the narrowband frequencies within the wideband bandwidth permitted the change from wideband to narrowband modes by switching only the triplers (with a filter preceding each narrowband channel). This switching technique also required that the IF amplifier have a linear transfer characteristic to the point where the two narrowband carriers were separated.

Input Circuitry

In the RF input circuitry, a hybrid was used between the microwave antenna and the two receivers. This split the incoming carrier equally between the two receivers, causing an increase in the effective noise figure of each receiver. Since the ground-to-spacecraft link has a high carrier-to-noise ratio, this design philosophy was preferable to the use of an RF switch in terms of reliability.

IF Amplifier

To meet the phase linearity requirements for the transmission of 300 FDM voice channels in the wideband mode, and to minimize crosstalk due to FM-to-AM-to-PM conversion in the narrowband mode, the IF amplifier was built video-style. In this way, the individual amplifier stages were built like video amplifiers with gain determined by the ratio of feedback impedances. The overall bandwidth of the IF amplifier was determined by a double-tuned circuit at the input (to optimize the first-stage noise figure) and a single-tuned stage at the output (for efficient RF amplification at the 100 mw level).

Microwave Antenna

In the repeater output, a breakthrough in

antenna design made possible the combination of the outputs of the two traveling-wave tube amplifiers without the use of switches, without power loss, and consistent with operational requirements regarding polarization. Functionally, the microwave transmitting antenna accepted the output of either of the two TWT's, providing at least 18 db of decoupling between the tubes, and radiated either carrier left-hand circularly polarized. The degree of freedom used to provide the decoupling was in the sense of the phase rotation of the radiation as a function of angle around the spacecraft spin axis.

Traveling-Wave Tube

The traveling-wave tube used as the RF power amplifying and output device was a most significant part of the repeater. Its design and performance characteristics are described starting on page 106.

MICROWAVE ANTENNA

General Description

During system planning, a broadband disc-cone type antenna was proposed for the Relay I microwave antenna. This would have had linearly-polarized radiation patterns. The two transmitters would have been connected selectively to the antenna by an RF switch. During the early development period, the present antenna was proposed as being superior in several respects: First, both transmit and receive patterns could be circularly polarized with consequent transmission gain in each of 3 db. Second, the two transmitters could be permanently connected to the antenna without loss and with much greater reliability than could be achieved through a switch. Although unproven experimentally, this concept had sufficient promise to be accepted, and it was carried through to successful completion.

The antenna mast was located along the spin axis to avoid signal amplitude modulation during spinning. The apertures on the mast were located as far as possible from the spacecraft body, to avoid pattern distortion by re-radiation or refraction by the spacecraft.

A photograph of the flight model antenna is shown in Figure 5–3. Figure 5–4 is a sketch showing the assembly in cross-section.

The assembly consists of a 1–3/4-inch cylindrical mast, approximately 27 inches high. This mast supports the two pairs of spaced, circular, metal discs which are the apertures for the receiving and transmitting functions. Within this mast are two coaxial tubes which separate the energy fed from the transmission line connecting points J1, J2, and J3 to the two apertures. Connection J1 is the output from the 7-inch diameter receiving aperture at the top. Connectors J2 and J3 are the two inputs to the 5-inch diameter transmitting apertures. Immediately

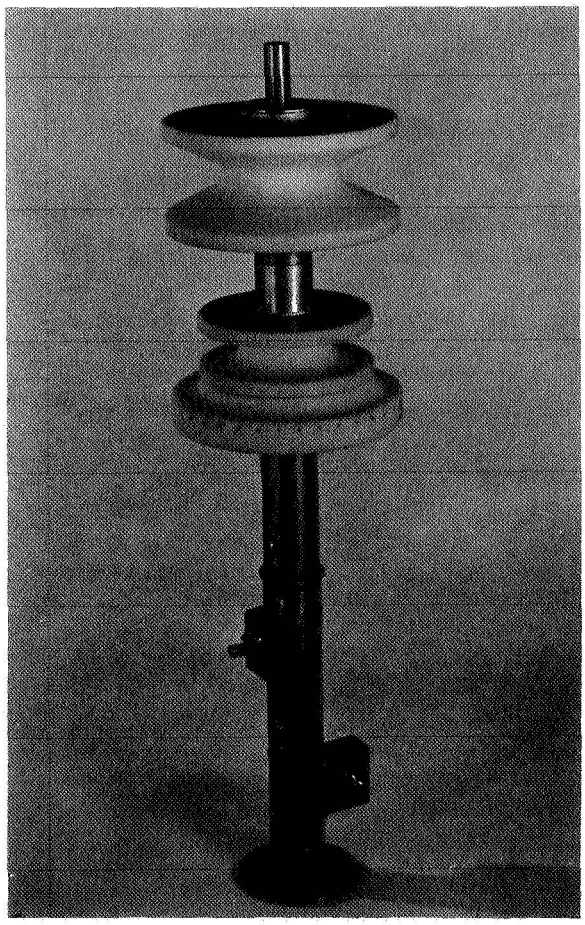


FIGURE 5–3.—The microwave antenna.

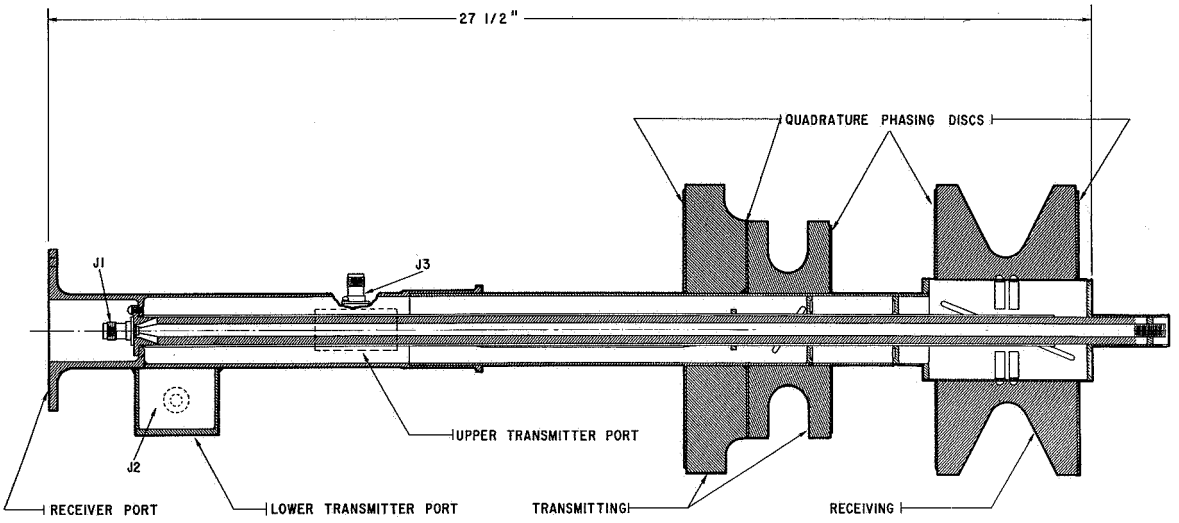


FIGURE 5–4.—Wideband antenna, mechanical configuration.

below the transmitting aperture is the 7-inch diameter, radial-wire, grid assembly. The grid assembly and the four aperture discs are supported by polyurethane-foam spacers. A crystal-detector, transmitter-power-monitoring probe is located midway between the two transmitter input connectors. The metallic portions of the antenna are constructed of aluminum alloys. The complete assembly weighed 2.1 pounds, and the center of gravity was located 11.4 inches from the base.

Transmitting Antenna

Electrically, the transmitting antenna consists of five parts: the mode transducer, the coaxial waveguide tranmission line, the quarter-wave plate, the inclined-slot exciters, and the radial waveguide. A detailed description of these parts follows (refer to Figure 5–4).

The mode transducer consists of two decoupled input ports at the base of the antenna. With this the input coaxial TEM-mode line can feed the coaxial TE_{11}-mode line in the mast. Each input port consists of a short section of rectangular waveguide coupled to the coaxial waveguide through a narrow longitudinal slot cut in the outer conductor of the coaxial waveguide. The coaxial line from the TWT amplifier excites a short probe through the broad face of the rectangular waveguide section. The probe length and location, the positioning of the shorting plate in the rectangular waveguide, the slot dimensions, and the positioning of the slot from the shorting disc in the coaxial waveguide are adjusted to provide an impedance match through the transitions.

The two ports were oriented at right angles so that the TE_{11} modes excited in the coaxial waveguide would be orthogonal, as required for proper operation. In addition, the ports were one guide wavelength apart to reduce direct cross-coupling between ports. For this condition, the cross-coupling isolation had been measured at more than 20 decibels. Experimental measurements on orthogonal ports without offsets have shown the cross-coupling isolation to be not more than 8 decibels.

The coaxial waveguide consists of the 1–3/4-inch outer conductor, which is the principal part of the mast, and the 3/4-inch inner conductor. The quarter-wave plate for polarization conversion, used in the final design, consists of two longitudinal metal ridges attached on opposite sides of the coaxial waveguide inner conductor. The plane of the ridges is at 45-degrees with respect to the orthogonal input ports. The ridges are seven inches long, with the ends tapered to prevent reflections. Dimensions of the ridges were adjusted to convert line-

arly polarized waves from either of the input ports to circularly polarized waves traveling toward the radiating section. Thus, the waves exciting the radiating slots are circularly polarized.

The radiator consists of eight, equally-spaced slots cut in the outer conductor of the coaxial waveguide above the quarter-wave plate. The slots are approximately one-half wavelength in length and are inclined at an angle of 55-degrees, with respect to the waveguide axis, to provide both axial and tangential radiation components. These components were found to be in-phase by experimental measurements.

The required quadrature phasing of these components, so that the radiated field would be circularly polarized, was obtained by using two, parallel, metal discs. The phase velocity of the axial component was unaffected by these discs. The phase velocity of the tangential component, however, was a function of the spacing. Hence, by proper choice of spacing and diameter, a differential phase-shift of 90-degrees between these two components was obtained, to produce circular polarization in the plane normal to the spin axis ($\theta = 90°$).

It became evident during the development phase that the antenna location alone was not a complete solution to the pattern distortion problem. Re-radiation from the spacecraft created a pattern hole, particularly in the transmit patterns.

An eight-db null on one port at θ equal 50 degrees was particularly offensive, being well within the desired coverage region. Considerable effort was taken to eliminate, or at least reduce, the effect. At the beginning of the project, it was anticipated that this type of reflection could cause trouble and it was suggested that RF absorbing material might be required on the top surface. But thermal needs, material considerations, and weight problems made this less than a perfect solution. However, the effect of absorbing material on the top surface was tried experimentally. The desired effect in reducing the pattern hole was obtained, but this did not provide a full-coverage pattern. The pattern, without the reflected signal, tended to be symmetrical about the equatorial plane and not sufficiently broad to encompass system look-angle specifications.

The need was either to tilt the pattern toward the nose or to broaden the pattern. The spacing and the diameters of the radial discs were determined by the method of forming circular polarization. Thus, the aperture could not be varied independently to control beamwidth. Efforts to tilt the pattern for the desired asymmetry (by reshaping the planar discs into double, nonflared cones) seemed to be ineffective. Similarly, the pattern width was not affected, nor the beam tilted, by extending the lower disc.

The most sensitive method of controlling the pattern entailed controlling the spacecraft's top-surface re-radiation.

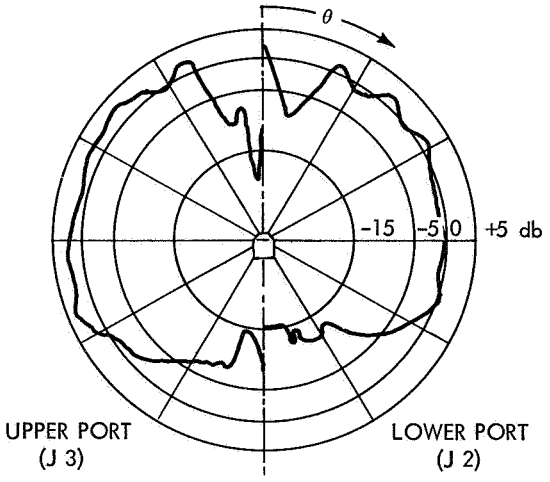
The most satisfactory results were obtained by using a polarization-sensitive, reflecting disc. The primary radiation from the transmitter was circularly polarized and, upon reflection from the spacecraft top surface, the sense of circularity was reversed. Thus, to be most useful for filling in the pattern in the nose region, the energy had to be reflected without this reversal. This was accomplished with a polarization-sensitive reflector, located just below the transmitting antenna, as shown in Figures 5–3 and 5–4. This reflector consisted of a radial wire grid and a metal sheet. Each of these was circular in shape and spaced a quarter-wavelength from each other. The wire grid consisted of 36 equally-spaced, radial, 0.032-inch-diameter wires. The incident-field component, parallel to an individual wire, was reflected, while the orthogonal component passed through and was reflected by the metal sheet. The added half-wavelength of travel for the one component insures that the over-all reflection process does not reverse the sense of circular polarization as is normally the case for metallic reflection. Thus, this reflected signal reinforces the primary radiation toward the nose region and, inasmuch as the reflected signal and primary

signal are effectively originating from points close together, this reinforcement holds over a wide angle.

The radiation patterns of the transmitting antenna are shown in Figures 5–5 and 5–6. These patterns were taken with the antenna in place on the spacecraft. The gain is referenced to a circularly-polarized isotropic radiator.

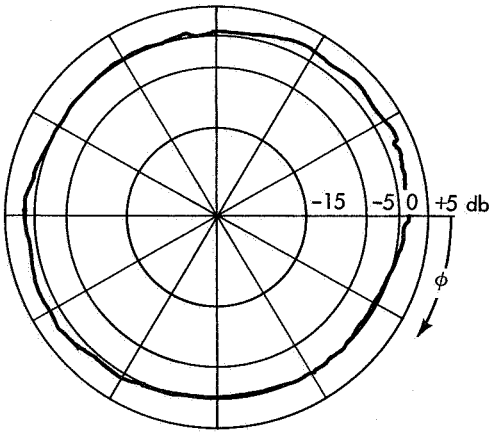
The specifications required a gain of greater than —1 db for angles of ϕ between 40° and 115°.

The VSWR and cross-coupling of the transmitting and receiving antennas are shown in Tables 5–2 and 5–3.



F = 4170 Mc. GAIN REFERENCE IS ISOTROPIC CIRCULAR TO CIRCULAR.

FIGURE 5–5.— Microwave transmitting antenna radiation pattern, polar plot.



F = 4170 Mc , GAIN REFERENCE IS ISOTROPIC CIRCULAR TO CIRCULAR

FIGURE 5–6.—Microwave transmitting antenna radiation pattern, equatorial plot.

TABLE 5–2.—*VSWR*

Freq.	1725 Mc	4080 Mc	4170 Mc
J_1	1.42		
J_2		1.08	1.25
J_3		1.85	1.08

TABLE 5–3.—*Cross-Coupling*

Freq.	4080 Mc	4170 Mc
J_2 to J_3	18.4 db	21.3 db
J_2 to J_1	> 50 db	> 50 db

The axial ratio of the radiated energy from the top port (J_3) of the transmitting antenna is shown in Figure 5–7. The two curves shown (θ_1 and θ_2) were taken in a common plane through the spin axis.

A probe for sampling the field in the transmitter transmission line was developed and

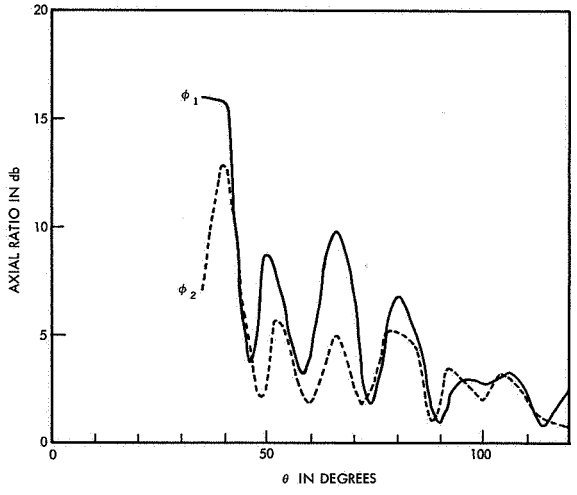


FIGURE 5–7.—Microwave transmitting antenna.

incorporated into the flight model. This probe is located midway between the two transmitter input ports so that it samples both approximately equally. The probe is lightly coupled to the line so that there is no degradation to the impedance match or port isolation. The crystal output is dc and is used to modulate a telemetry channel.

Receiving Antenna

The receiving antenna consists of three electrical parts: the transmission line, the inclined radiating slots, and the radial waveguide. The coaxial transmission line carries the TEM mode energy, excited at the base at J_1, to the inclined half-wavelength slots cut in the outer conductor.

A pair of capacitive probes are located adjacent to each slot to increase the coupling of the slot to the TEM mode. A short-circuited stub at the end of the transmission line assists in matching the slots to the line. The receiving radial waveguide acts similarly to that of the transmitter in causing a 90-degree phase shift between the orthogonal, axial and tangential electric-field components. The slots are oppositely inclined to those of the transmitter, resulting in opposite-sense, circular polarization.

A considerable amount of time and effort was expended in attempting to construct the receiver radiating slots in the same diameter tube as that employed for the transmitting antenna. The objective was to decrease the weight and size and to simplify the mechanical assembly. Such a design was to give the desired circular polarization and θ-plane pattern. However, it was not possible to obtain sufficient impedance bandwidth. This is believed to have occurred because the antenna, inherently a high-Q device, was much too small electrically, at the receiving frequency. After some difficulty, the receiver channel was successfully matched over the 14-Mc bandwidth. The use of a larger diameter coaxial section feeding the slots aided materially, but it was necessary to further increase the coupling of the slots to the guide. This was done by placing capacitive stubs between the slots and the inner line of the coax. After fabrication, a final adjustment with a tuning stub at the top end of the antenna was made to set the receiver frequency at the center of the matched band.

The polar-radiation pattern of the receiving antenna, in place on the spacecraft, is shown in Figure 5–8. Primarily due to the symmetry of the receiving antenna feed system about the spin axis, the polar radiation pattern at $\theta = 90°$ was indistinguishable from a perfect circle (with the scale used).

Fabrication

The wideband antenna was fabricated by using welding, knurling, rolling, and epoxy to join the various sections. In the concept review, it was evident that special techniques would have to be developed to meet environmental requirements and to achieve the weight requirement associated with the

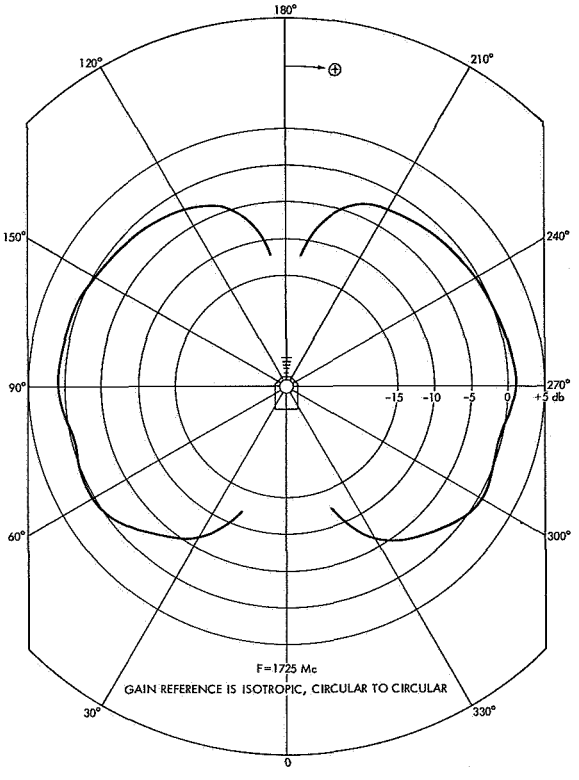


FIGURE 5–8.—Microwave receiving antenna radiation pattern, polar plot.

physical location of the antenna on the spacecraft. Because of structural and fabrication needs, the unit was subdivided into three major parts: (1) base, (2) center conductor, and (3) outer conductor.

The base, having waveguide sections welded to it, presented a problem in maintaining concentricity of the inner diameters. The use of castings was considered, but no assurance could be given that a sound casting could be provided with the wall thickness required. If the wall thickness were increased, casting would have been possible, but the increase in weight would have adversely affected the over-all spacecraft. The base was made from a 4-inch bar of 6061–T6 aluminum. After turning the outer diameters, the waveguide sections were welded, the assembly was stress-relieved, and the inner diameters of the base were bored. This achieved the desired result: a strong, uniform, light-weight base.

Attachment of two, thin, polarizer bars to the outer diameter of the center conductor was necessary. Consideration was given to welding, casting, plating, and metal spraying to build up the strength of these bars. The end products were fabricated by welding, while using another bar inside the tube as a heat sink to eliminate warpage. The weld and bars were then machined to the desired shape.

The outer conductor was welded, using a mandrel to hold the pieces. The assembly was then machined to the required dimension.

Joining the outer conductor to the base was accomplished by using a knurled junction, to achieve good electrical contact, and by using epoxy bonding to assure a good mechanical joint.

Discs required for the apertures were tested on a breadboard assembly. It was determined that excessive thickness would be required to meet the vibration requirements if the plates were unsupported. Because of the location of these discs, not only would the weight increase be undesirable, but the antenna center-of-gravity would also be farther from the base and consequently farther from the center-of-gravity of the spacecraft. This condition would create problems involving the spacecraft moment-of-inertia. Therefore, it was necessary to make the discs as thin as practicable. The discs were made of 0.005-inch aluminum and were bonded to polyurethane foam for support. The necessary electrical contact was accomplished by using a fillet of silver-loaded epoxy.

The result of the above techniques was an antenna weighing only 2.1 pounds which met environmental, electrical, and interface requirements.

THE MICROWAVE RECEIVER

Design Philosophy

The design of the wideband receiver was the result of careful consideration of the dominant factor of reliability. For example, the frequency plan was the result of interference considerations, and an attempt to minimize the number of multiplier stages used in generating microwave signals. Beside applying the specified de-rating of electrical components, the following rules were observed:

1. Complexity of circuits had to be kept to a minimum.
2. All circuits had to be stable beyond the anticipated temperature range and component variation values
3. Power drain had to be kept to a minimum
4. The number of adjustable components had to be minimized.

Observation of the above rules sometimes led to unorthodox circuit designs. For example, in trying to conform to rule (1), it was decided that dissipation in the crystal in the local oscillator (LO) circuit should exceed the manufacturers recommendation, rather than use an additional transistor. This was decided after establishing, beyond doubt, that the dissipation rating given by the manufacturer for one hundred-megacycle quartz crystals was extremely conservative. Dissipations of three to four milliwatts were used, instead of the recommended

maximum of 1 milliwatt. Observation of rule (3) led originally to the choice of varactor triplers for the IF multiplier section because they do not require dc power. Early production testing showed that this type of wideband multiplier had questionable stability over a wide temperature range. It was decided, therefore, that transistor triplers would be substituted with less economy of dc power. Observation of rule (4) led to a lengthy production testing cycle. This unquestionably added to the reliability of the equipment.

In the course of the development, several simplifications were made possible in the original block diagram. These changes mainly affected the varactor multiplier chains. For example, after successful experiments with a quadrupler circuit, it was realized that the number of multiplier stages could be reduced. The receiver oscillator became a chain of two quadruplers and the transmitter local oscillator chain became a quadrupler followed by two triplers. Thus a very small number of multipliers are used to achieve relatively high frequencies. A similar change was made in the beacon transmitter, where the multiplication scheme became a quadrupler followed by a 9-times multiplier.

Circuit Description

Introduction

The wideband receiver was essentially a heterodyne repeater. The input and output frequencies were 1725 Mc and 4170 Mc respectively. As shown in the System Block Diagram (see Figures 5–1 and 5–2) independent LO's were used at the input and output mixers. A detailed description of each sub-unit follows.

Input Filter

The input filter acted as a preselector to permit passage of the 1725 Mc input signal. Other interfering signals, such as the TWT output signal and receiver image frequencies, were rejected. The filter consisted of three mutually-coupled, quarter-wave, tuned, transmission-line cavities. Input and output coupling was achieved by inductive coupling loops. The filter had a 3-db bandwidth of approximately 35 Mc and an insertion loss of approximately 0.4 db (see Table 5–4). The output signal was applied to the crystal mixer.

TABLE 5–4.—*Input Band Pass Filter Characteristics*

Frequency	Insertion loss
1725 Mc (mid band)	0.4 db
1725 ± 10 Mc	0.5 db
1725 ± 17.5 Mc	3.4 db
1725 ± 37.5 Mc	20 db
1725 ± 52.5 Mc	30 db

Crystal Mixer

The crystal-mixer subassembly was secured to the input filter and contained the filter coupling loop. The 1725 Mc signal received by this loop was fed via a built-in coaxial impedance transformer to a type MA449F mixer crystal. The receiver LO signal (1655 Mc) was capacitively coupled into the crystal mixer by means of an adjustable probe set to produce 0.5-ma crystal current. The 1725 Mc and 1655 Mc signals, applied to the crystal mixer, produced an IF signal of 70 Mc which was fed to the IF amplifier. The crystal mixer 70-Mc output terminal consisted of a built-in quarter wave choke assembly which prevented RF and local-oscillator signals from feeding into the IF amplifier. The choke assembly was readily removable from the remainder of the crystal-mixer assembly to permit crystal replacement. Conversion loss of the crystal mixer was approximately 5.5 db.

Receiver LO Transistor Section

The receiver LO transistor section consisted of an oscillator and an amplifier stage with power output of 160 mw at 103.4375 Mc. Power consumption was 800 mw. Frequency stability over the environmental range was better than 2 parts in 10^5.

The oscillator consisted of a grounded-

base, RCA 34290, UHF transistor, and a 5th-overtone crystal. This stage was inductively coupled to the RCA 34290 transistor amplifier through a series-tuned network. The amplifier operated Class A in the grounded emitter configuration. A 1N251 diode rectifier coupled to the output provided a dc telemetry voltage.

Receiver LO 1st Quadrupler

The input matching circuit to the receiver LO 1st quadrupler provided the varactor with a drive of about 150 mw, as supplied by the receiver oscillator and amplifier at a frequency of 103.4375 Mc. The idler circuit was series-tuned to provide a low impedance path at 207-Mc idler frequency and to obtain maximum efficiency at the fourth harmonic.

The output circuit was series-tuned at 414 Mc. This inductor was mutually coupled to a transmission line which was tapped to provide maximum output power of about 70 mw to drive the next quadrupler.

Bias for the varactor was obtained by the use of a resistor which provided a dc path to ground and thus permitted self-bias to develop.

Receiver LO 2nd Quadrupler

The receiver LO 2nd quadrupler was matched at the input by a transmission line transformer. The varactor was placed in a cavity tuned to 1655 Mc by means of a tuning slug that served the dual purpose of output matching. The varactor mount had a built-in bypass capacitor to provide the required path for the 1655-Mc current circulating in the cavity. Bias was obtained by the use of a resistor which provided a dc path to ground and thus permitted self-bias to develop at the varactor.

IF Amplifier

The IF amplifier subassembly received the incoming 70-Mc signal from the crystal mixer and amplified it to an output level of 100 mw. AGC action adjusted the gain of the amplifier to maintain the output constant, within ± 0.5 db, for an input variation of 40 db, which was a —86 to —46-dbm signal level at the input terminal. An input T network acted as a matching transformer between the crystal mixer and the 2N1405 IF-input transistor. In addition, the network provided sufficient selectivity to limit the IF noise bandwidth to the specified maximum of 30 Mc. The two 2N1405 input transistors were low-noise, conventional, common-emitter, amplifier stages with an overall gain of approximately 20 db. The signal was then amplified by eight AGC-controlled stages. These were 2N700A and 2N1141 transistors. Basically these stages were wideband, RC-coupled stages with each stage having a selective, degenerative, feedback loop to improve response. The remaining four stages were conventional synchronously-tuned amplifiers. Two 2N1692 transistors were driver and power amplifier stages, respectively. An AGC detector was connected to the collector of the last transistor and detected changes in output level. Three AGC amplifier transistors applied corrective bias to the signal amplifier stages maintaining constant noise figure and power output level. A schematic of a section of the IF amplifier is shown in Figure 5–9.

IF Switch

The IF Switch permitted the 70-Mc signal to be routed to the wideband tripler or to the narrowband filters. The path was selected by

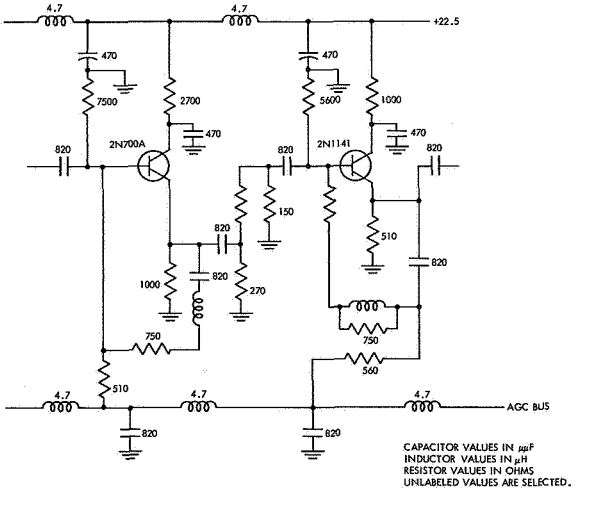


FIGURE 5–9.—Section of IF amplifier.

two identical diode switches operated by a control voltage. The circuit configuration was such that the on-state of the narrowband path switch coincided with the off-state of the wideband path switch, or vice versa.

70-MC Narrowband Bandpass Filters

Three major designs were possible in attempting to meet the performance requirements of these filters:

1. Classical image parameter method.
2. Modified image parameter method.
3. Network synthesis.

The modified image parameter method was chosen.

Experiments were carried out with different types of inductance structures. Detailed plots were obtained of Q, inductance and stray capacitance. Of all the types studied, a toroidal form of specific shape factor, fabricated from Rexolite, was finally chosen.

Detailed calculations were then performed, plotting various filter parameters such as, characteristic impedance, insertion loss slope, band-width, etc., as functions of Q, L, and C. From these and from the experimental data on the toroids, the optimum design parameters were chosen.

From the necessity of having to bridge the two filters for parallel operation, a series-derived structure was chosen. Out-of-band impedance calculations were made, showing how the two filters could be made to work together.

The characteristic impedance of 20 ohms for the filters was chosen for two reasons. From the curves, it was determined that optimum requirements of L, C, Q, etc., for a given size and performance specification, would be obtained from this impedance level. Further, the outputs of the filters were required to work into a load originally specified to be 20 ohms.

This left the problem of matching the bridged input of the two filters to 75 ohms. A mutually-coupled, inductive type of transformer was designed and tried. While its electrical performance was satisfactory, it appeared to have certain difficulties with respect to mechanical reliability and temperature stability. This type of transformer also reflected the impedance of the filters such that the reactive component at the input was still present and the return loss at this point remained the same. As the return loss required was greater than obtained, it was decided to use an RLC matching network in place of the transformer. The ratio of resistance-to-reactance transformation was decided on the basis of insertion loss and resultant return loss of the network.

Special considerations were given to mechanical design and component density. Each tuned circuit was built on a separate subassembly and tested. Two types of mechanical joints were involved:

1. Screw type
2. Chemical (i.e., adhesive)

Whenever parts were joined by screw type devices they were designed to pull against (e.g., the coils to the boards), special test jigs were devised to apply a known stress to each bond after proper aging time.

Components were mounted so that the distance of their centers-of-gravity to mounting surface was kept to a minimum. Component density was high, and mutual coupling was kept at minimum by shielding partitions and the self-shielding properties of toroid coils.

Group delay in the pass bands of the two filters was measured and found to be satisfactory. Typical filter characteristics are shown in Figure 5–10.

Limiter Amplifiers

Each limiter amplifier consisted of two cascaded, common base, tuned amplifiers. The first stage operated in a non-limiting mode, while the second stage was designed to have constant output over the expected narrowband input range of −10 dbm to 0 dbm. The actual limiter output was variable up to a level of 50 mv by the adjustment of a potentiometer.

IF Transistor Triplers

There were one wideband and two narrowband triplers required. The initial design for

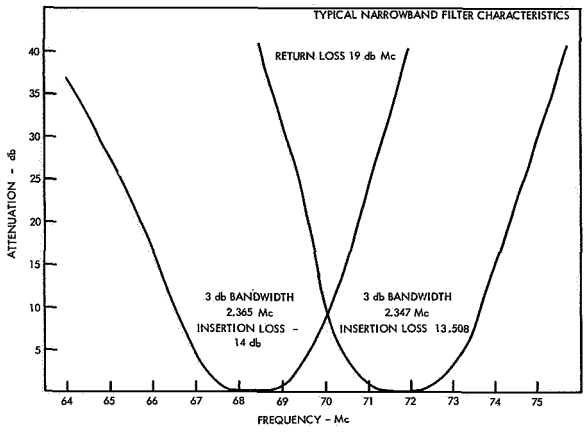


FIGURE 5–10.—Typical narrowband filter characteristics.

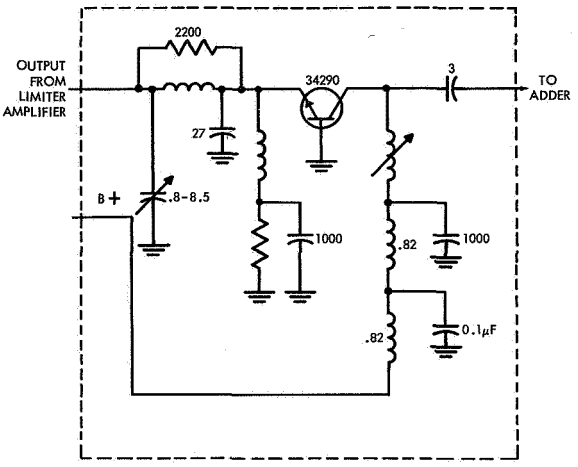


FIGURE 5–11.—Transistorized narrowband tripler, schematic diagram.

these triplers involved varactors. This design had excessive regeneration when adequate bandwidth and efficiency were achieved. The final design employed RCA 34290 UHF transistors in a grounded-base configuration. The circuitry for the three triplers was essentially the same.

The narrowband triplers received signals from their associated limiter-amplifiers through input matching networks. These pi-networks were tuned to 68⅓ Mc and 71⅔ Mc by variable capacitors. The required bias voltage for tripling was provided by the voltage drop across resistors which, with inductors, formed the dc return path.

The collector tank circuit, tuned to three times the input frequency by variable inductors, was capacitively coupled to the input of the adder circuit. Isolation from the power source was provided by a decoupling network. A schematic of a narrowband tripler is shown in Figure 5–11.

The 70-Mc signal received from the IF switch for the wideband mode was coupled through a pi-type matching network to the emitter of an RCA 34290 transistor. The network was tuned for optimum return loss by a variable capacitor and inductor. A coupling capacitor with the inductive component of the input impedance of the transistor, formed a series tuned circuit of low Q, which was further reduced by a shunt resistance. The collector, tuned to three times the input frequency by a variable inductor, was coupled through a capacitor to the adder circuit.

Adder

The adder circuit was provided for two purposes. In the narrowband mode, it provided a method of combining the two signals to drive the high-level mixer, and at the same time it provided reasonable isolation (measured at 16 db or better) between the two triplers. Secondly, on both wideband and narrowband modes, it provided a means of matching the output of the triplers to the high level mixer.

Two common-base amplifier transistors (type 2N1493) were coupled together at the collector and drove a double-tuned circuit. The primary and secondary loads of this circuit were the output resistance of the transistors in parallel with resistors.

The narrowband tripler outputs were connected to individual arms of a resistive attenuation pad as shown in Figure 5–12. Each transistor was therefore driven independently and the outputs were combined. In the wideband mode, the transistors were effectively driven in parallel. Since the adder normally limits when driven in the wideband mode, this resulted in an effective 1 db bandwidth of greater than 35 Mc. This, combined with the limiting characteristics of the high

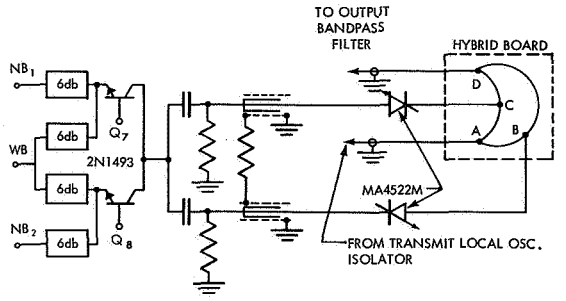


FIGURE 5–12.—Adder—high level mixer.

level mixer, gave the system 1 db bandwidth of 35 Mc.

High Level Mixer

The high level mixer used two MA4522M pill varactor diodes mounted on a stripline hybrid (see Figure 5–12). The IF signal from the adder was mixed with energy from the transmitter local oscillator to produce several sidebands. The first upper sideband at F + IF was selected by the output filter for transmission to the TWT.

The basic operation of the hybrid mixing may be understood in the following way: If a short-circuit at the LO frequency is placed at B and an open-circuit at C, all the LO power entering at A leaves via arm D after a delay of 180°. If the short-circuit and open-circuit are interchanged, all the LO power still leaves at D, but there is now a delay of 360°. If the open and short-circuits are switched at an IF rate of 210 Mc, then the output signal at D contains several sidebands but no carrier. The strongest sidebands are at ($F_{LO} \pm 210$) Mc.

The 210 Mc IF was supplied from the adder through an RC network which developed self-bias voltages on the varactors. The value of R was chosen to obtain optimum drive to the varactors.

The varactors were switched in a push-pull manner, i.e., when the varactor at B was being driven into forward conduction and was acting like a short-circuit, the one at C was being heavily reverse-biased and acted like a high impedance and vice versa. A small section of short-circuited strip-line, shunting the varactors, was used to parallel-resonate with the varactor capacitance in the reverse-biased state to better simulate an open-circuit. The varactors were mounted in holders which were designed to be microwave choke joints at 4170 Mc to prevent RF radiation at this frequency. This restricted the RF operation to the stripline and provided freedom from random external loading and tuning effects.

Another feature of the mixer was the use of a limited amount of negative-resistance type of parametric conversion to increase the available power output. This could occur because the second harmonic of the LO was generated in the non-linear capacitance of the varactors. This energy mixed parametrically with lower sideband energy at F_{LO}–210 Mc reflected back from the output filter, to produce energy at $2\ F_{LO} - (F_{LO} - 210) = F_{LO} + 210$ Mc, which was the desired output frequency. The phase of this energy was set by the length of line between D and the output filter so that it added to the upper sideband energy produced by the primary mixing action. A conversion loss of from seven to eight-db from F_{LO} to (F_{LO}+210) was obtained under normal operating conditions.

Transmitter LO Transistor Section

The transmitter LO transistor section consisted of oscillator, driver, and power amplifier stages. It had a power output of 1.3 to 1.5 watts at 109.9922 Mc. Power consumption was 5 watts. Frequency stability over the environmental range was better than 2 parts in 10^5.

The oscillator consisted of an RCA 34290 transistor operating in the grounded base configuration and a crystal operating at the 5th overtone. A Zener diode provided the base bias voltage. The oscillator delivered about 40 mw to the driver stage.

The driver was inductively coupled to the oscillator by the series-tuned circuit. The buffer transistor was an RCA 34253 UHF transistor operating Class A in the grounded-emitter configuration. It delivered about 500 mw through a pi-coupler to the PA stage.

Base bias was provided by a Zener diode.

The power amplifier was another RCA 34253 UHF transistor operating Class C in the common-emitter configuration. The coupling capacitor from the driver was selected to tune out the transistor lead inductances.

A series-tuned trap, between the collector and the output pi-coupler, improved collector current waveform, increasing the stage efficiency.

Transmitter LO Quadrupler

The quadrupler consisted of an input-matching circuit providing the drive for the varactor of 1.2 to 1.5 watts at 110 Mc. An idler circuit provided a low-impedance path for the idler current at 220 Mc circulating through the varactor, thereby providing high-efficiency operation. The output primary circuit delivered 500 to 600 mw of power at 440 Mc.

Transmitter LO Double Tripler

This unit multiplied the input frequency of 440 Mc at a level of 500 to 600 mw, to the output LO frequency of 3960 Mc at a power level of 50 to 80 mw, in two cascaded tripler stages.

Output Filter

Since the high level mixer normally produced a variety of harmonics, the purposes of the output filter were to allow passage of the desired 4170 Mc signal and sidebands and to reject all other frequencies. An important function of the output filter was to reflect the unwanted lower sideband of 3750 Mc back to the high level mixer with a suitable phase relationship so that it would mix with the generated second harmonic of the local-oscillator signal to produce a 4170-Mc resultant that added to the main 4170-Mc sideband. Thus, the lower sideband signal was reconverted to the upper sideband signal with a consequent improvement of mixer efficiency. The output filter consisted of three mutually-coupled, halfwave diameter, slug-tuned cavities with inductive-coupling loops for input and output terminals. It had a flat bandwidth of approximately 44 Mc and a 20 db bandwidth of approximately 110 Mc. It was center-tuned at 4169.72 Mc. Nominal insertion loss of the filter was approximately 0.4 db. The characteristics of this filter are shown in Table 5–5.

Performance Summary

A tabular presentation of the measured performance of the two receivers is shown in Table 5–6. Photographs of the wideband receiver are shown in Figures 5–13 and 5–14.

TABLE 5–5.—*Output Bandpass Filter Characteristics*

Characteristic	Value
Center frequency	4170 Mc
Insertion loss	0.4 db
Bandwidths:	
3 db	44 Mc
20 db	110 Mc
30 db	200 Mc

TABLE 5–6.—*Performance Summary of Microwave Receivers F4 and F6*

Function	Measurement			
	Receiver F4		Receiver F6	
	0°C	25°C	0°C	25°C
Wideband output power (dbm)	10.6	7.1	12.4	9.4
Narrowband output power (dbm)	8.7	5.8	9.8	7.0
"Beyond the horizon" AGC switch operate point				
Wideband (−dbm)	81.5	83.0	80.5	81.5
Narrowband low (−dbm)	80.0	82.0	79.5	80.5
Narrowband high (−dbm)	80.0	81.5	78.5	79.5
Nominal output frequency error (kc).	−6	+15	+32	−18
Group delay				
Linear (nsec)	−7	−4	−9	−8
Parabolic (nsec)	−7	−7	+2	+2
IF Bandwidth (1 db)				
f^1 (Mc)		65.1		65.3
f^2 (Mc)		73.8		75.0
Δf (Mc)		8.7		9.7

TRAVELING WAVE TUBE

Introduction

General

The RF-power output of the transmitter section of the wideband subsystem was furnished by an RCA Type A–1245 traveling

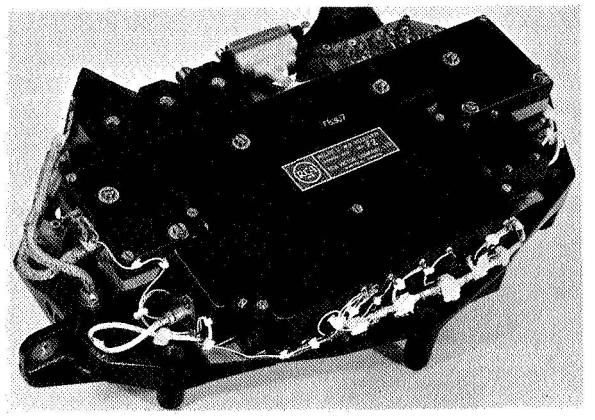


FIGURE 5–13.—Relay I—wideband receiver.

wave tube (TWT). This tube amplified, simultaneously, the wideband, high-level, 4170-Mc, communications signal and the low-level, 4080-Mc beacon signal, providing a minimum of 11 watts of RF power to the line feeding the wideband antenna. Since it was the final RF power amplifier, the traveling wave tube was the major power-consuming element of the spacecraft and, as such, was one of the major controlling factors in the spacecraft design. Requirements for the tube appear in Table 5–7.

Selecting The Tube

A TWT was selected for the transmitter output stage because it could be designed with the best balance between efficiency, power, bandwidth, gain, weight, and ruggedness. Intrinsically, and from operational history, such a tube offered the greatest assurance of reliability in long-term, unattended service.

In June, 1961, when the basic requirements for the Relay I tube were first set down, no history existed for traveling wave tubes operating in a space environment. A period of approximately one year was available for the design, design proof, and delivery of tubes for flight use. It was necessary to reach the primary design freeze in approximately six months.

The needs of Relay I imposed upon the output-stage tube a set of performance, environmental, and reliability requirements,

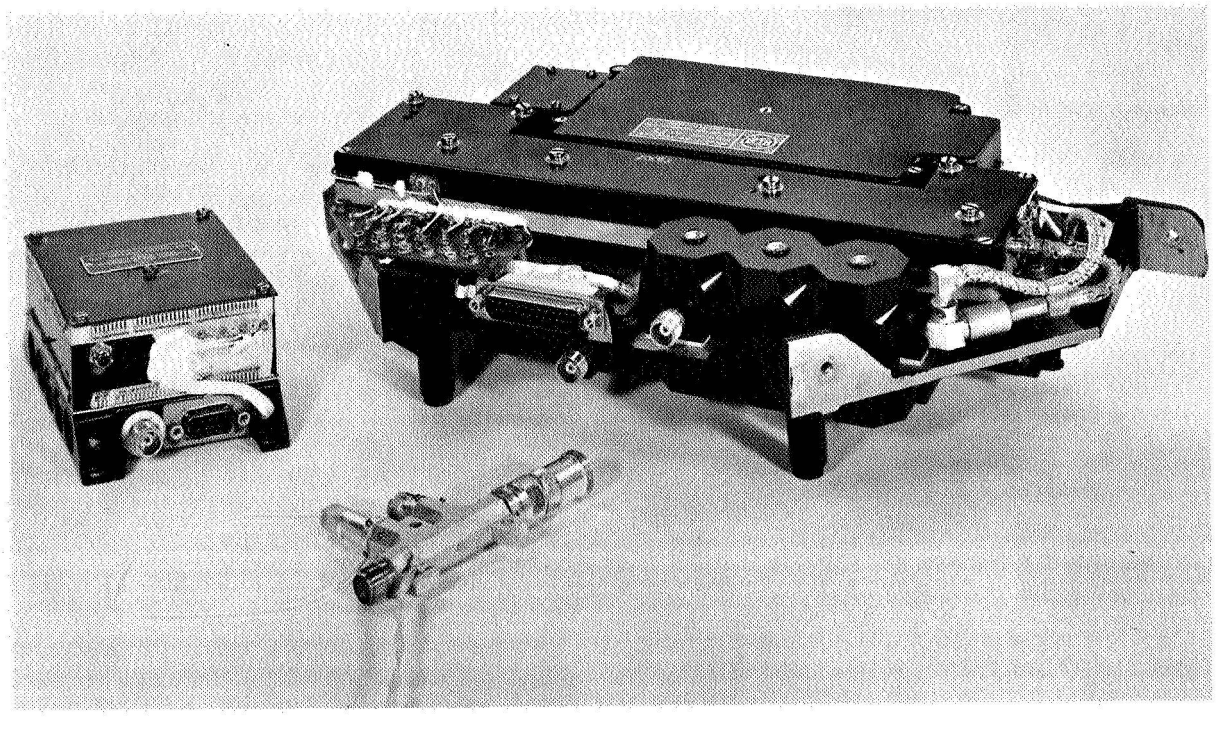


FIGURE 5–14.—Relay I wideband receiver, microwave beacon and beacon coupler.

TABLE 5-7.—*Basic TWT Requirements for Relay I*

Electrical	
Frequency range	4050–4250 Mc
Operating bandwidth	100 Mc
RF power output (fundamental, saturated).	11 watts (40.14 dbm)min.
RF input drive	3.5 mw (5.4 dbm) nominal
Gain (at 11 watts)	35 db min.
dc power available for TWT	55 watts max.
Overall efficiency (at 11 watts RF output).	21% min.
Hot match	
Input (50 ohms coax)	1.8:1 VSWR
Output (50 ohms coax)	3.0:1 VSWR
Output stability (10:1 VSWR any phase with ± 3% helix voltage change, no RF signal in).	2 mw max. output
Spurious output (any 20–Mc band)	−40 dbm max.
Duty cycle	(100 minutes out of any three continuous consecutive 3-hour orbits is the system requirement)
Physical	
Weight/size	Minimum consistent with reliability. Weight not to exceed 4½ lb.
Connectors	Coax (type TNC)
Cooling	Conduction and radiation
Environment	
Temperature (operating)	−10°C to 80°C heat sink −10°C to 35°C ambient
Pressure	Sea level or high vacuum
Vibration	
Sinewave, thrust direction	
20–500 cps	5 g peak
2 sweeps, 50–500 cps	25 g peak
20 octave/min., 50–2000 cps	40 g peak
Dwell, 30 sec., 550–650 cps	60 g peak
Sinewave, lateral direction	½ the thrust-direction levels.
Random	11g RMS, 20–2000 cps, 4 minutes
Life expectancy	Greater than 5 years

none of which could be met by any existing TWT. Nearly all of these requirements, however, had been separately demonstrated in different RCA TWT's. The problem then confronting the TWT designer was how to combine these requirements with the best possible balance (reliability being the controlling factor) within a restricted time schedule.

In the interest of achieving reliability, a general ground rule was established at the start of the program: the tube should incorporate only those design practices, technology, and manufacturing methods which had been proven reliable in actual field use.

Starting Point

With the decision that the new tube must be designed and built only with field-proven materials and techniques, capabilities of existing traveling wave tubes were examined. The ability of TWT's to provide high-quality repeater performance had already been demonstrated. The RCA-designed 7642, an 18-watt 2–Gc tube, was successfully operating in the MM600 Ground Relay system; the Bell Telephone type M1789, a 5-watt, 6–Gc tube was performing well in the bell System transcontinental radio relay. But both types were designed for long, reliable life in ground operation; they did not have the high efficiency, light weight, conduction cooling, and the rugged features needed by a tube to be used in space.

RCA, however, had also completed the design and flight-qualification testing of a TWT intended for spacecraft operation in a pressurized environment. This tube, the RCA Type A–1228, provided 11 watts of power output at 2 Gc. It was a medium-weight, rugged, conduction-cooled tube designed for high efficiency, depressed-collector operation. It operated with the same power output, gain, voltages, and currents as the tube that was projected for use in Relay I. At the start of the Relay I program, five completed A–1228's had been in aging racks for some time.

Most of the design of the A–1228 was applicable to the Relay I program but it was necessary to reduce weight, to improve efficiency while doubling the frequency, and to provide different methods of mounting and conduction cooling. The A–1228, however, served as the prototype from which the Relay I tube was scaled, and the work that had been done on the A–1228 formed a basis for technological and manufacturing methods that would endow the new tube with high reliability.

Design

Major Characteristics

At the start of the program, only the major characteristics of the tube were known, such as frequency, power output, gain, efficiency, maximum weight, length, etc. As the pro-

gram progressed, many other characteristics were specified. These characteristics were derived from those of the forerunners of the A–1245, the 7642, and the A–1228, and they are described below. The major characteristics of the A–1245 are listed in Table 5–8.

At the start of the TWT development program, an unpressurized tube was planned. However, during testing, anomalies in tube performance were revealed which were induced by vacuum environment. On the basis of these test results, and to ensure meeting the schedule for delivery of an acceptable TWT, it was necessary to pressurize the tube (see Figure 5–15). Work continued on the design of the unpressurized version of the tube, the unpressurized TWT (see Figure 5–16) was incorporated in the Relay II spacecraft.

TABLE 5–8.—*Major Characteristics of The RCA A–1245 Pressurized TWT*

Electrical	
Frequency	4.05 to 4.25 Gc
Power output	11 watts (min.)
Overall efficiency (η_o) (including heater power).	21%
Gain (at 11 watts)	35 db
Helix voltage (V_w)	2100 volts
Helix current (I_w) (with RF)	0.25 ma
Collector voltage (V_c)	1000 volts
Collector current (I_c)	45 ma
Grid No. 1 (anode) voltage	1400 volts
Grid No. 1 (anode) current	0.01 ma
Heater voltage (E_h)	4.25 volts
Heater current (I_h)	1.6 amperes
Mechanical	
Weight	4.5 lb
Length	18¾ inches
Diameter	1.7 inches



FIGURE 5–15.—RCA type A–1245 pressurized traveling wave tube.

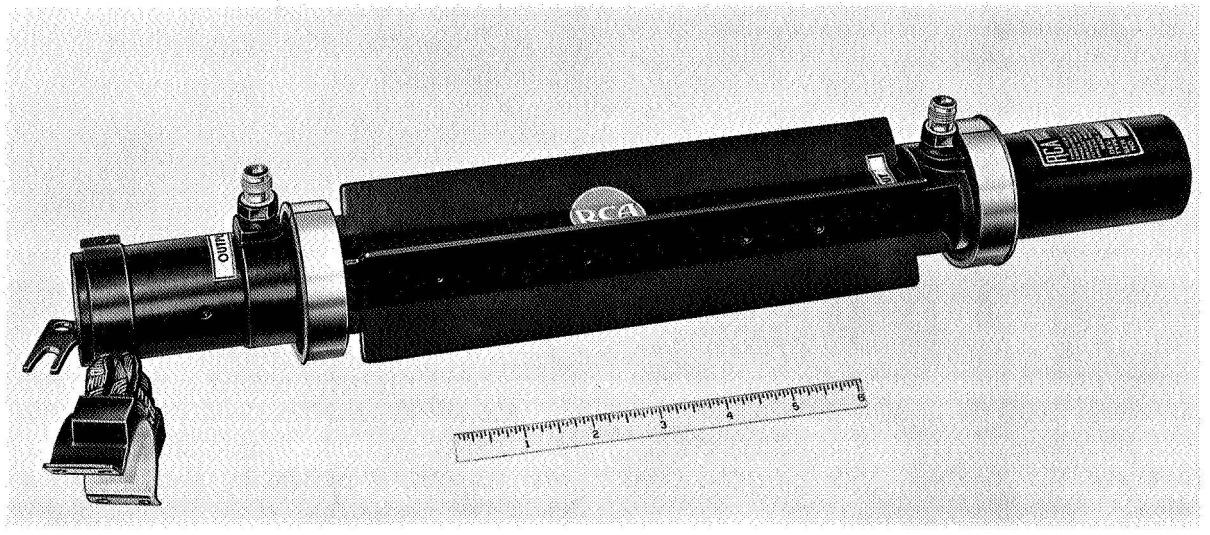


FIGURE 5–16.—RCA type A–1245 unpressurized traveling wave tube.

Major Tasks

The three tasks that converted the A–1228 into the A–1245, mechanically, were: (1) finding a new method of mounting to guard against damage by shock and vibration; (2) development of a new cooling method and (3) reducing the weight. A comparison of the A–1245 and its forerunners, the A–1228 and the 7642, is shown in Table 5–9.

TABLE 5–9.—*Comparison of Prime Design Parameters Between the A–1245 and its Forerunners*

Parameter	RCA 7642	RCA A–1228	RCA A–1245
Freqency (Gc)	1.7–2.3	2.0–2.4	4.05–4.25
Power output (watts)	18–24	11	11
Gain (db)	28	35 at 11 watts	35 at 11 watts
Electronic efficiency (η_e%)	15	14	12
γa	1.25	1.25	1.75
QC	0.30	0.295	0.4
b/a	0.5	0.5	0.6
PHeater(watts)	11.0	7.0	5.5
I_k(ma)	70	46	46
Cathode temperature (°C)	800	740	710
Cathode current density ma/cm^2).	83	57	55

EFFICIENCY

General—The overall efficiency of a TWT can be expressed as follows:

$$\text{Overall efficiency} = \frac{P \text{ output}}{P\,dc + P \text{ heater} + P \text{ output}} = \frac{1}{\frac{1}{\eta_e}\frac{V_c}{V_w} + \frac{I_w}{I_c} + \frac{P \text{ heater}}{P \text{ output}} + 1}$$

where

η_e = electronic efficiency
P = power
V_c = collector voltage
I_c = collector current
V_w = helix voltage
I_w = helix current

The ways in which the A–1245 was made to meet the environmental requirements of shock, vibration, cooling, and certain other problems are described below. The weight was reduced by making the periodic stack permanent magnets of lightweight platinum cobalt, while preserving the integrity of the critical magnet design. The helix interception current had to be reduced practically to the vanishing point to reduce heating of the helix structure. This could be done only by designing the magnets with extreme precision.

The equation shows that to raise the overall efficiency, the following things must be done:

1. Increase electronic efficiency.
2. Increase beam-current transmission.
3. Decrease collector voltage.
4. Decrease heater power.

The electronic efficiency of the A–1245 was actually made lower than that of the A–1228.

Design of the Helix—One of the most important parameters that must be chosen in the design of a TWT is the diameter of the helix. For a given beam diameter, the smaller the diameter of the helix, the closer the helix is to the beam and the greater is the conversion of dc energy into RF power output (and therefore the higher the efficiency).

If the helix is too close to the beam, however, higher interception of the beam, greater losses in the helix, and lowered efficiency result. Thus, when a helix of small diameter is used, the design burden is shifted to the sharp magnetic focusing of the beam. A useful relationship is the ratio of the diameter of the beam to that of the helix or b/a.

The numeric γa is a quantity that is basic in the design of the helix. It is defined as follows:

$$\gamma a = \frac{2\pi a\ 505\ dlf}{\lambda_o \sqrt{V_w}}$$

where:

γ = Radial propagation constant
a = Mean radius of helix
dlf = Dielectric loading factor
λ_o = Free-space operating wavelength
V_w = Helix voltage

Table 5–9 shows that the value of γa chosen for the A–1245 was higher than that of the A–1228. This was to be expected because of the higher operating frequency of the A–1245. But the value of 1.75 was also somewhat higher than the value that would give maximum electronic efficiency. Using a smaller value of γa would have been accomplished by using a smaller helix diameter, but this would have involved the difficulties described above. The larger helix diameter (and wire size) results in the RF and dc dissipation per unit area being about that of the A–1228, despite the higher operating frequency.

The table also shows that the electronic efficiency of the A–1245 is lower than that of the A–1228. This is mainly due to the higher value of γa that is used. But the effect of the lower electronic efficiency on overall efficiency is more than made up by the lower heater power used by the A–1245 and by operating its collector at a depressed potential—at about half that of the helix voltage.

The helix interception current was 0.25 ma of the total beam current. This indicates a beam transmission of over 99 percent.

With a value of γa set at 1.75, and a helix operating voltage of 2000 to 2100 volts, the design parameters of the helix are as shown in Table 5–10.

TABLE 5–10.—*Design Parameters of the Helix*

V_{helix}	2050 volts
V space-charge reduction	100 volts
γa	1.75
ka	0.15
Dielectric loading factor	0.9
C	0.0575
Length	10.9 inch
Mean diameter	0.135 inch
Wire size	0.014
TPI	26.1

The overall length of the helix was determined by the conservative design approach chosen for the tube—low beam-flow perveance (0.5 μperv) and the correspondingly low gain parameter. The length finally selected was 10.9 inches. This length produced the required saturation gain (35 db at 11 watts) and offset all of the recognized RF losses.

Construction of the Helix—Physically, the electronic efficiency of a traveling wave tube depends upon the design of the helix, the kind and placement of its dielectric supports, and the kind and placement of the attenuators. See Figure 5–17, which shows the A–1245 and its components.

The helix was wound of molybdenum wire which was firmly embedded in precision-made, low-loss, fluted-glass tubing (Corning 7070). The fluted glass was shrunk over each turn of the helix to provide a good mechanical bond as shown in Figure 5–18.

The use of rugged, small-diameter, glass tubing to support the helix brought with it certain other advantages as follows:

1. It allowed helical couplers to be used as input and output transducers; this type of coupler did not need to be supported by the vacuum envelope and did not require a vacuum seal. Waveguide couplers at 4 Gc would have been too large, while cavity couplers would not have permitted the use of small-size periodic magnets.

2. Some movement of the helix was permitted to effect a good match during the fabrication of the tube.

3. External RF attenuators could be used, which eliminated the dissipation problem and outgassing associated with internal attenuators.

4. The small radial dimensions permitted the use of small-size, light-weight, periodic, focusing magnets.

Rigid inspection techniques were required to determine the acceptability of the self-supported helix assembly. Each assembly was subjected to accurate measurement of the pitch deviation between turns of the helix. Any helix assembly with a deviation greater than 12 microns was rejected. The RCA-designed device in which these measurements were made is called the HELPER, an acronym for HELix Pitch Error Resolver (shown in Figure 5–19). This inspection technique made it possible to reduce problems of match, stability, and fine-grain gain variation in the A–1245.

Stability

The system performance objectives required stable tube performance with wide-band integrated noise and spurious power output held to less than 5mw, while the output of the tube was subjected to a variable phase VSWR mismatch of 10:1. Further, this operation had to be achieved while simultaneously varying the helix voltage ±3 percent (see Figure 5–20). Attaining this specification becomes difficult with depressed-collector operation, wherein reflected pri-

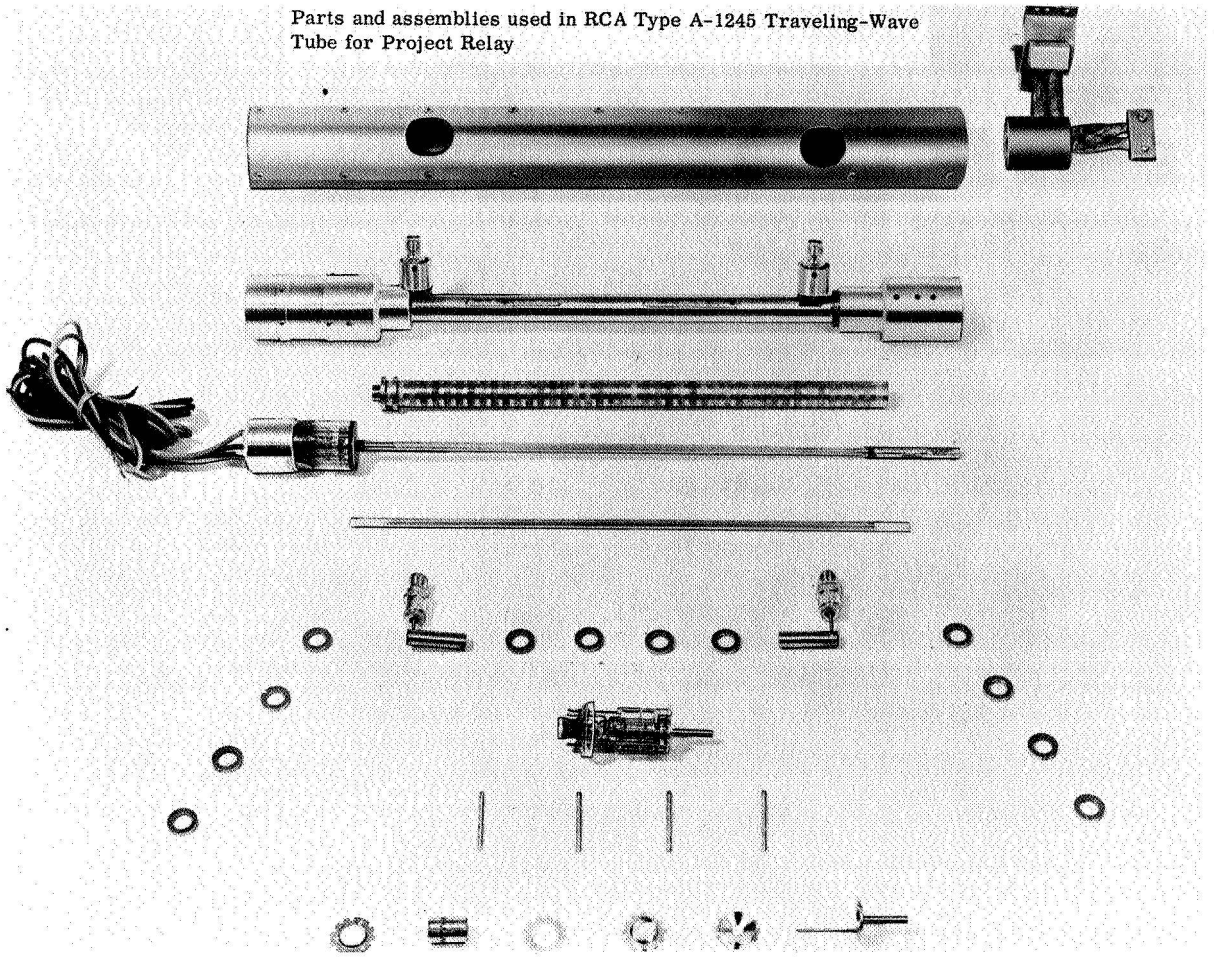


FIGURE 5–17.—Parts and assemblies used in RCA type A–1245 traveling wave tube.

mary or secondary electrons can conceivably initiate a growing wave leading to oscillation.

To meet these stability criteria under all operating conditions, including vacuum environment at elevated temperatures, an external, helical, center attenuator was developed.

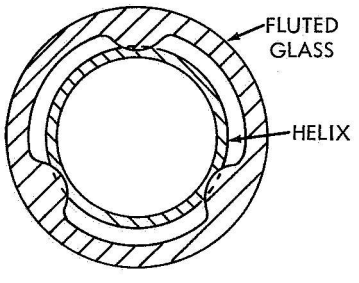


FIGURE 5–18.—Radial cross-section of helix.

The VSWR of the center attenuator was better than 1.05:1; total loss was greater than 50 db in the operating band; and it provided for loss in excess of gain from 2 to 8 Gc, to ensure against instability outside the band where the coupler match degraded. The main portion of the RF attenuator is bifilar wound of 0.5-mil Karma wire, in reverse pitch when compared with the helix winding.

The aquadag tapers, on both sides of the attenuator, were density sprayed to spread RF dissipation and prevent hot spots. The entire assembly was then coated with Eccoceran and baked to provide a durable, protective coating.

An attenuator one-half inch long, con-

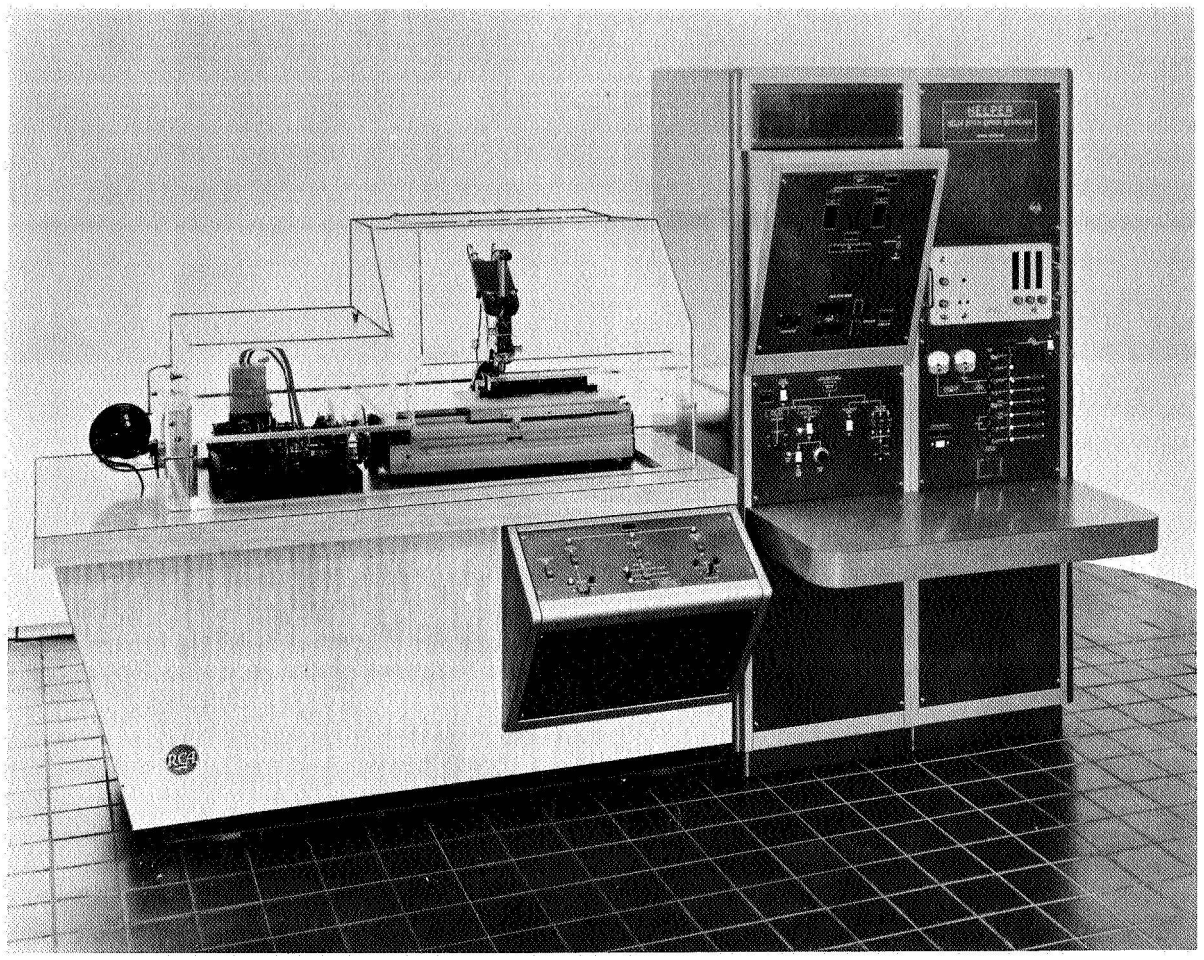


FIGURE 5–19.—The RCA HELPER

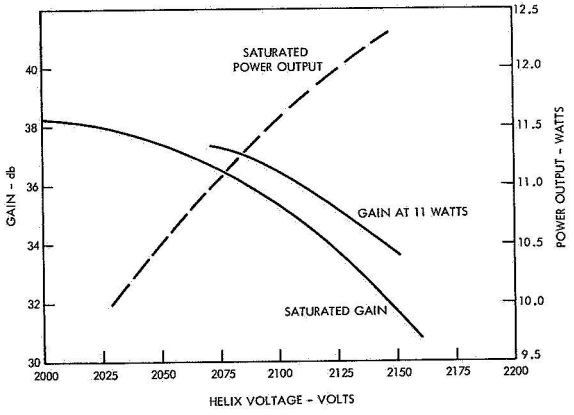


FIGURE 5–20.—Type A–1245 TWT (unpressurized version); saturated power output, saturated gain, and gain at 11 watts vs. helix voltage.

structed in the same fashion as the center attenuator, was placed at the input end of the helix to absorb any RF wave which is coupled in the wrong direction at the input. A $\frac{3}{8}$" Lava-wound end attenuator, positioned off the helix support glass, is used to absorb any uncoupled RF energy in the output coupler region. Extensive tests made on this assembly in a vacuum environment, dissipating rated RF energy, indicated that the temperature of the attenuator was less than 175°C at the hottest point.

Reliability

One of the requirements of the TWT,

which influenced all aspects of its design and fabrication, was the reliability with which it was expected to perform: The specifications called for reliable operation for a minimum of 50,000 hours. This requirement affected every fabrication step: specifying materials, purchasing, testing, manufacturing subassemblies in rigorously clean areas, testing the subassemblies, assembling the tubes in the clean areas, and retesting. Some of the procedures followed are given below.

The Electron Gun—Analysis showed that the electron gun of the A–1228 tube, with some modifications, would be suitable for the A–1245. The gun, similar to the Pierce convergent type, supplied a beam with an excellent laminar flow. Gun features are listed in Table 5–11.

TABLE 5–11.—*Features of the Electron Gun*

Beam current	46 ma
Beam diameter at minimum convergence	0.080 inch
Beam current density	55 ma/cm^2
Beam-area convergence ratio	23:1
Cathode temperature	710°
Gun perveance	0.84 microperv
Anode voltage	1420 volts
Anode current	10 microamp (max.)
Heater voltage	3.75 volts
Heater current	1.5 amperes
Heater temperature	1150° C
Cathode base metal	N1 32
Emissive coating	Barium-strontium carbonate

An important feature of the gun is the dark heater; its use permitted lowering the heater power 20 percent below that of the A–1228.

The Cathode—A major determinant of the life of a TWT is the cathode. A long-lasting emitter, such as thoriated tungsten, could not be used because it would have required too much heater power.

The choice for the A–1245 cathode was a barium-strontium carbonate over vacuum-fired base metal N132. Both of these materials were of proven performance. The cathode was operated so that the current density of the beam was the lowest in any know TWT. This, in turn, enabled the cathode to operate at the lowest possible temperature.

The low operating temperature not only decreased the rate of depletion of the emissive material, it also enabled the operating point of the tube to be placed well beyond the knee, or space-charge saturation point, of the cathode-current versus heater-voltage curve. Operating at this point on the curve helps to ward off damage from any possible momentary cathode poisoning process. The life records of tubes prove the validity of this approach to reliability and longevity.

Performance

For a rigorous evaluation under simulated space conditions, the TWT's were given extensive vacuum-thermal tests. Each tube was subjected to at least three vacuum-thermal operating runs under conditions identical with those anticipated for the spacecraft in orbit.

In anticipation of the slight power fade (approximately 0.2–0.3 db) which is normal and expected, each tube was operated with an input power 2 db above the input power required to produce saturation power output. This also causes greater RF and dc losses in the helix and serves to indicate the degree of operating margin of each tube.

During all thermal-vacuum runs, the pressure was maintained at 10^{-5} mm Hg and the temperature of the radiator was allowed to rise to approximately 95°C. The operation in space was simulated by making each vacuum-thermal run last for 35 minutes. And after each run, the RF drive and heater power were shut down and the tube was allowed to cool for 1½ hours.

Table 5–12 shows data taken in sea-level and vacuum-thermal tests on a group of typical flight-model A–1245's. It can be observed that the average power fade was approximately 0.2 db with an attendant insignificant change in gain.

Environmental Considerations

Requirements

The Relay I orbit and launch conditions established the environmental requirements for the TWT. The major environmental effects were vibration (See Table 5–7), me-

TABLE 5–12.—*Typical Performance of Flight-Model Tubes*

Sea-level run (f = 4.17 Gc)			Thermal-Vacuum Runs P_{in} = Sat P_{in} + 2 db (35 min. duration)									
Pressurized tubes				Run No. 1			Run No. 2			Run No. 3		
Serial No.	Power out(w)	Gain (db)		Po fade (db)	Power out (dbm/w)	Gain (db)	Po fade (db)	Power out (dbm/w)	Gain (db)	Po fade (db)	Power out (dbm/w)	Gain (db)
WC–48	11.45	35.4	Start		40.3/10.75	33.1		40.3/10.75	33.1		40.4/11.0	33.2
			Finish	+0.2	40.5/11.25	33.3	+0.2	40.5/11.25	33.3	+0.1	40.5/11.25	33.3
WC–36	12.3	34.2	Start		40.6/11.5	32.9		40.7/11.75	33.0		40.9/12.3	33.2
			Finish	− .05	40.55/11.35	32.85	0	40.7/11.75	33.0	−0.2	40.7/11.75	33.0
WC–32	11.0	35.2	Start		40.1/10.25	32.4		40.0/10.0	32.3		39.95/9.75	32.25
			Finish	−0.2	39.9/9.75	32.2	−0.2	39.8/9.55	32.1	−0.15	39.8/9.55	32.1
WC–21	10.9	34.7	Start		39.9/9.75	36.8		39.9/9.75	36.8		40.0/10.0	36.9
			Finish	0	39.9/9.75	36.9	0	39.9/9.75	36.8	−0.1	39.9/9.75	36.8
WC–11	11.75	35.5	Start		40.65/11.6	33.05		40.65/11.6	33.05		40.6/11.5	33.0
			Finish	−0.15	40.5/11.25	32.9	−0.15	40.5/11.25	32.9	−0.1	40.5/11.25	32.9

chanical shock (30 g peak, 8 milliseconds duration, sawtooth), vacuum environment, and Van Allen Radiation Belt exposure.

The environmental evaluation of the TWT was accomplished by making separate evaluations of components and subassemblies. Tests were conducted on heaters, gun assemblies, helix assemblies, and magnet assemblies. These tests were then followed by testing completely packaged tubes both at sea level and in a thermal-vacuum environment simulating the conditions in space.

Mounting and Cooling The Tube

In modifying the A–1228 TWT for the Relay I application, new methods of mounting and cooling the tube were necessary. The new mounting method was needed to protect the tube from shock and vibration during launch. The new method of cooling the tube was needed because of the lack of convection. Heat could be removed only by radiation and conduction.

The isolation mounting—Each TWT was mounted in the spacecraft on a structural member of the frame with two mounting isolators used on each tube to limit the vibration amplitudes actually transmitted from the frame to the tube. Each isolator was a molded urethane rubber ring 0.500″ wide and 0.233″ thick, bonded to the capsule, and a split stainless-steel ring was bonded to the outer surface of the isolator. The ring was split to permit application of the proper, predetermined amount of torque by the clamp with which the isolators were fastened to the spacecraft frame. These rings may be seen next to the input and output connectors in Figures 5–15 and 5–16.

Cooling—The main source of heat in the TWT was the 35 to 45 watts of power dissipated in the radiator by the collected beam. This heat was conducted away from the tube by six flexible, stranded-copper cables (0.005-inch strands) each 0.275 inch in diameter and attached to two copper clamps (shown in Figures 5–15 and 5–16). Two cables were fastened to the small clamp and four cables to the large clamp. The larger of the clamps was attached to the main spacecraft heat sink, which extended vertically in the center of the spacecraft, and the smaller clamp was attached to a gusset plate on the spacecraft frame.

The cables were attached to the radiator end of the tube capsule and to the clamps with silver-loaded epoxy to provide a strong, thermally efficient bond. Vibration tests of

a tube in a simulated spacecraft proved the suitability of this flexible strap-and-clamp arrangement for conducting the heat away from the tube radiator. The glass bottle and the magnet stack were cooled by methods described as follows.

The TWT bottle-and-magnet assembly were enclosed in a stainless steel capsule which was, in turn, enclosed in a stainless-steel pressurized envelope. To accomplish this, pressurized TNC connectors and a vacuum-tight metal-ceramic stem were used. The outer pressurized envelope consisted of two stainless-steel, open-ended semi-cylinders. The tube-and-magnet assembly in its stainless-steel capsule was placed in one semi-cylinder and was potted in place with rigid epoxy. Copper straps were used to connect the inner capsule to the inside of the outer envelope to make a good thermal bond between the two. The two semi-cylinders were then heliarc-welded together making a vacuum-tight joint.

A vacuum-tight, metal-ceramic stem was attached to the leads of the tube and heliarc-welded in place in the end of the envelope. Pressurized metal-ceramic TNC connectors were attached to the tube capsule and also heliarc-welded in place. A copper disc with a stainless-steel flange was bonded to the radiator and this was heliarc-welded in place, thus making a pressurized envelope.

This envelope was baked at 100°C, leak tested, and pure nitrogen was pumped into the envelope through a copper tubulation in the stem. The stem tubulation was then pinched off, effecting a coldmetal weld and a pressurized envelope. The completed tube was placed in a vacuum chamber for 24 hours and operated at 35-minute intervals every 2 hours to ensure that the tube was properly pressurized and was leak tight.

The helix glass was cooled by convection through the gas in the pressurized container. The collector, magnet assembly, etc., were cooled by conduction through the stranded copper straps to the spacecraft heat sink. The pressurized tube was protected against shock and vibration by the isolation mounting described earlier.

Environmental Test Results—The prototype TWT was qualification-tested according to the following tests and performed satisfactorily during all the tests:

1. Thermal-Vacuum Test — 30 days at pressure of 5×10^{-5} mm Hg. Temperature cycling from —10°C to +35°C.
2. Vibration—Tested in a dynamic model of the Relay I spacecraft to qualification levels for the spacecraft.
3. Acceleration—Tested on a centrifuge to the qualification levels for the spacecraft.

Fabrication

General

The fabrication procedures and controls adopted for the A–1245 were designed to ensure maximum tube-to-tube uniformity (see Figure 5–21). Rigidly enforced acceptance criteria were established for parts and subassemblies, and a documentation system was established to ensure that a complete record of all parts and processing steps was kept for each tube package. A series of inspection points was established to eliminate non-uniform components during assembly.

In addition, the tube-making practices emphasized special controls on the tube operating parameters which were found to be related to the tube stress points, either through theoretical analyses or during the development phase of the program. Thus, tests were performed during the fabrication cycle on cathode activity and beam transmission characteristics, because these were judged of extreme importance in predicting the reliability of a particular tube. Great emphasis was placed on thermal-vacuum testing of tubes, because this type of test was shown to flush out weak design areas during the later stages of the development phase of the program, prior to the fabrication phase.

Fabrication Steps

The following were the major steps in the preparation of the tubes for the acceptance or design proof tests:

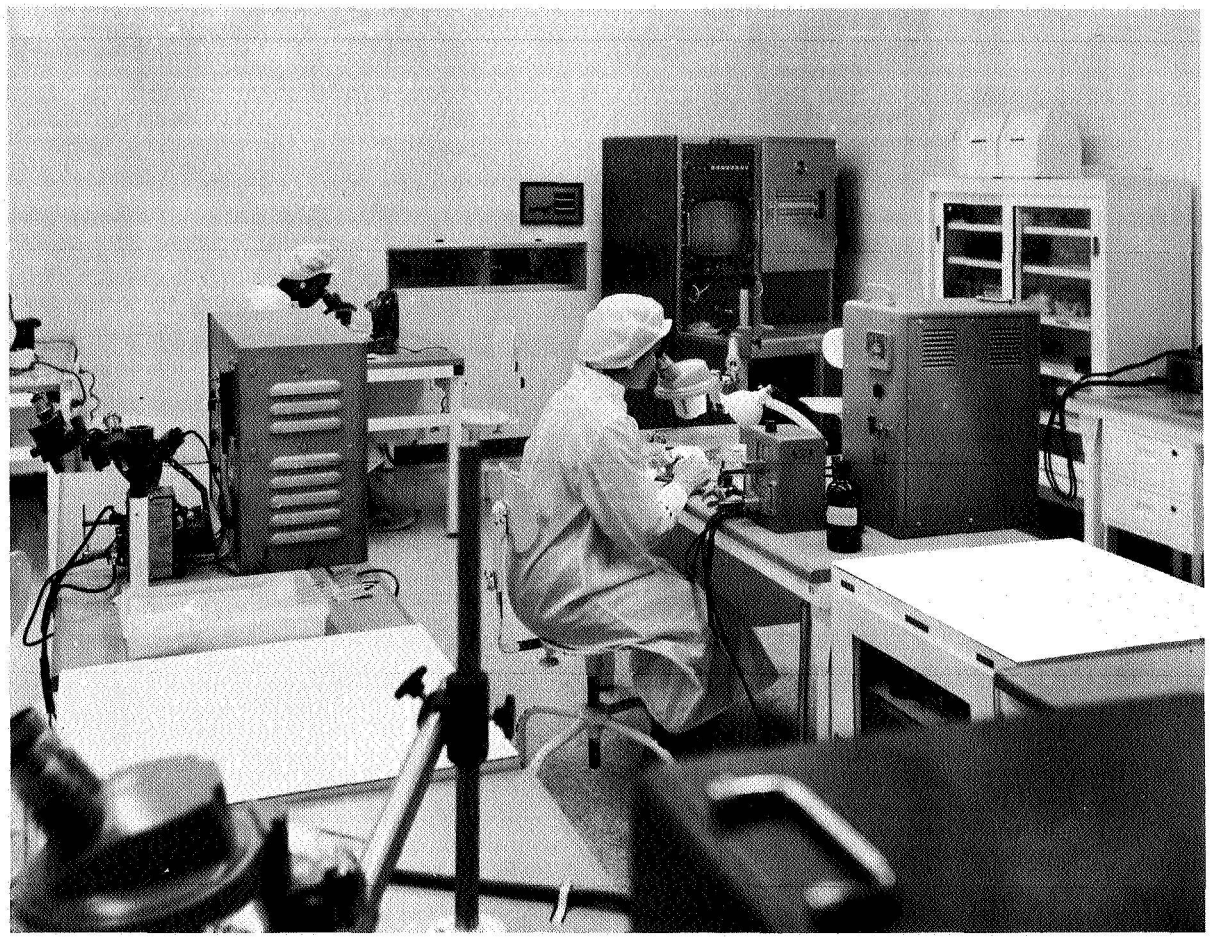


FIGURE 5–21.—Clean Room in which satellite tubes are assembled.

1. After a tube was assembled and processed through the exhaust cycle, it was evaluated electrically in a standard package, containing known focusing and RF components. This was the first screening of the new tube, and peculiarites associated with beam transmission, sensitivity to voltage changes, and RF performance were carefully noted. Variations of these parameters outside predetermined limits or peculiarities of performance resulted in the "bottle" being eliminated.

2. The tube was next focused and locked in a specific package with which it remained mated. It was subjected to the pre-aging bench test (at room temperature, in air), during which it had to pass all RF requirements at the rated voltage and currents.

3. During the next step (aging in air environment—300 hours minimum), any tube which showed anomalous emission-stabilization trends was eliminated. Refocusing the tube after the aging cycle eliminated a substantial portion of the helix current rise. The helix current rose 500 microamperes (typical) during the aging cycle. Refocusing reduced the helix current by this amount and kept the subsequent rise to extremely low levels. This fact is illustrated in Figure 5–22.

Cathode emission was monitored during aging, and any tube displaying a measurable decrease in cathode current was eliminated. An increase in cathode current of up to 5% was accepted.

4. After aging, each tube was again tested

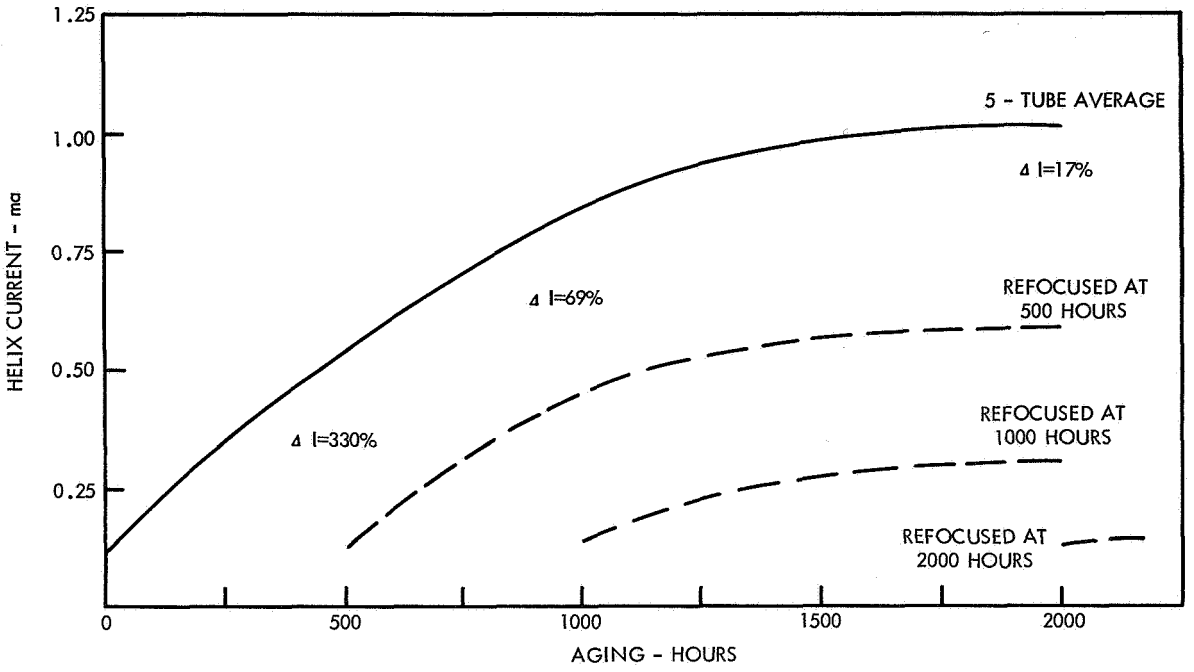


FIGURE 5–22.—Effect of refocusing during aging on helix current.

for electrical performance (post-aging bench test). Except for the rise in cathode current, no change in performance from that observed during the pre-aging test was expected.

5. A cathode activity test was performed next. Figure 5–23 is a plot of cathode current as a function of heater voltage. As shown in the figure, the cathode current change was limited to 1 milliampere maximum when the heater voltage was dropped from 3.75 volts to 3.25 volts.

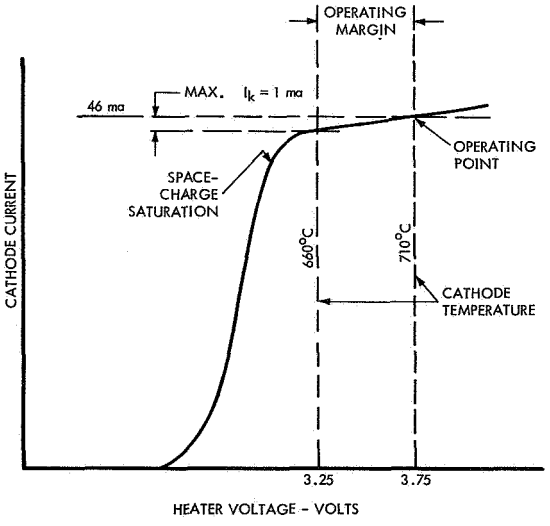


FIGURE 5–23.—Cathode activity test.

6. The first thermal-vacuum test was next performed. The tube was mounted in a vacuum chamber (having a pressure of 10^{-5} mm Hg or less) so that the tube was thermally stressed to limits equal to, or greater, than those expected in flight. The tube was operated for one hour and allowed to reach maximum flight temperatures. Performance within specifications with related voltages applied was required. No performance anomalies were tolerated.

7. Cycled thermal-vacuum test: Each tube was operated for 24 hours minimum (some tubes were operated for 48 hours for this test) at specified cycled conditions of temperature and RF drive. During this test, all tube voltages and currents, the temperature of the tube mounting sink, the vacuum pressure, the tube input and output RF values, and RF spectrum were monitored. No degradation in performance for the specified period and no observable change in emission

or focusing over that established at the beginning of the test was allowed.

8. Tubes passing all the foregoing tests were completely packaged. After this step, adjustments of the tube within its package (e.g., focusing and related adjustments) were not possible.

9. Electrical testing, a preliminary vibration run, and an electrical retest followed packaging. Tubes which met all performance became candidates for design proof or acceptance tests.

The Test Program

In addition to the various screening tests described previously, several formalized sets of tests were used during the development and fabrication phases of the A–1245 traveling wave tube. The purpose and scope of these tests were as follows:

Qualification (Design Proof) Tests

The purpose of this series of tests was to evaluate the capability of the design to meet all requirements except life. The tests included random and sinusoidal vibration, shock and acceleration, and thermal-vacuum, usually at levels 1½ times the maximum stress expected in flight. RF performance was expected to be unchanged before, during, and after the tests.

Acceptance Tests

These tests were performed to ensure conformity of a particular production tube with the qualified design prototype that underwent design proof testing. The tests were generally similar to the design proof tests, except that stresses usually equalled the maximum levels expected during flight.

Special Tests

These were tests devised to prove particular aspects of the tubes' performance. Of particular value during the A–1245 program was a special *design confidence* test, during which tubes were subjected to 30 days of operation in vacuum, with both thermal and RF conditions cycled to simulate conditions expected in flight. The test was used to give a first estimate of the tube life in a relatively short period of time.

Life Tests

The Relay I traveling-wave tube was designed to stay within the stress levels (cathode emission, helix current interception, thermal levels, etc.) previously established for its forerunner, the A-1228. By doing this, reliability data, particularly life data, could be carried forward with validity and combined with A–1245 data to give a much more comprehensive life evaluation. The calculations for MTBF and Confidence utilized the confidence equation:

$$\text{Confidence} = \left\{1 - \sum_{c=0}^{r}\left[\frac{(Nt)^c}{(m)}\frac{\exp -(Nt)}{e(m)}\right]\right\}$$

where:

N = number of units on test
t = time of each unit tested
m = mean-time-before-failure
r = number of failures on test

This equation assumes that the failure rate will be constant; that is,

$$\frac{\text{Number of failures during time interval}}{\text{Number of units operating at start of time interval}} = \text{constant};$$

and that the *wearout point* is beyond the projected mean-time-to-failure. The constant-failure assumption has been found to be valid from electron tube life test plans and is commonly accepted by military agencies. Also, the most likely wearout factor, cathode emission, has been shown to be well beyond seven years at the levels used. Thus, the two assumptions appear valid. The MTBF quoted is based on information from tests which were still continuing. The MTBF projections were expected to increase as more life-hours were accumulated.

TWT POWER SUPPLY

The traveling-wave tube power supply consisted of a low-pass input filter, a dc-to-

ac inverter, two transformer-rectifier-filter circuits, a timer module and switch, and telemetry circuitry. The unit performed the functions of: (1) converting the regulated 22.5 volts dc to the proper filament, collector, helix, and anode voltages for the TWT; (2) supplying a 3-minute time delay between the application of filament-plus-collector voltages to the TWT, and the application of the anode-plus-helix voltages; (3) supplying an output to the command control unit for use in the beyond-the-horizon-turn-off switch; and (4) supplying telemetry outputs related to the TWT operating parameters. A block diagram of the unit is shown in Figure 5–24.

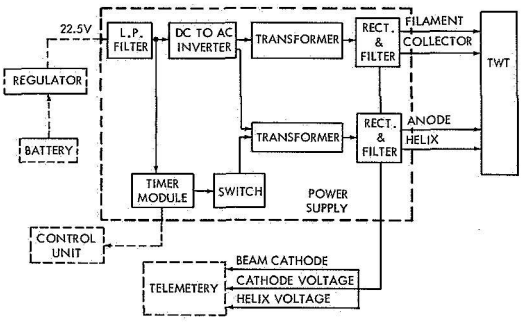


FIGURE 5–24.—TWT power supply, block diagram.

The wideband subsystem power supply design philosophy was to provide a separate power supply regulator for each microwave repeater. A nominal 22.5 ± 1 percent bus was supplied to each repeater. The actual design realized for these regulators provided better than the allowed ±1 percent tolerance including all effects. In tests run with engineering-model TWT power supplies and sample TWT's the TWTs were found to tolerate variations of the power supply input of up to ±3% with a result of no more than a 0.5 db variation in TWT output. Thus, no additional regulation was needed in the TWT power supplies.

To minimize weight it was determined early in the design effort that an unpressurized design would be attempted. The question remained as to whether or not potting should be used for high-voltage components. The overall spacecraft specifications did not require operation of these supplies during launch or during the first orbit of the spacecraft. Bell-jar tests revealed that the pressure inside the unit, with its multi-holed cover (see Figure 5–25), lagged only five minutes behind the outside pressure. Also,

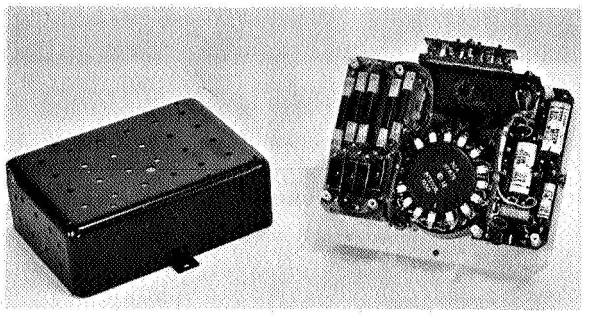


FIGURE 5–25.—Relay I TWT power supply.

similar tests on unpotted development models did not show corona activity when the units were turned on one-half hour following evacuation of the enclosure. Thus, the unit was not pressurized and did not include potted components.

The dc-to-ac inverter used two 2N1016B n–p–n transistors. Operation started at approximately 14-volts input. Inversion took place at a 2.5-kc rate. The output of the inverter was essentially a square wave and drove the two high-voltage transformers. These transformers are oil impregnated (DC–710). Dry-type transformers with toroidal cores were found to have excessive corona. The final transformer design, which was corona-free, used oil-impregnated windings potted in epoxy. After rectification and filtering, filament and collector voltages were applied to the TWT from one transformer circuit while helix and anode voltages were supplied from the other.

A three-transistor timer module delayed by three minutes energization of the helix-anode supply following application of input power, so that full warm-up of the TWT cathode was provided before beam current flowed. De-energization of the timer took

place 10 milliseconds following removal of input power, requiring execution of a new 3-minute cycle. This ensured that power removals of short duration would not result in beam-current flow from a partially heated cathode.

The dc (load-line) regulation of the unit helix-anode supply required special attention. During turn-on of the TWT at low helix-anode voltage, the helix drew current much higher than normal (7 to 10 ma). This caused the tube to behave as a non-linear resistor, with a negative resistance region over a portion of its voltage-current characteristic. If the combination of dc regulation and negative resistance is improper, the tube can "lock-up" at low voltage in non-operating condition. The helix-anode supply had a regulation of 20 volts per milliamp in the zero to 7-milliamp load range which was adequate to avoid this difficulty with most tubes.

The ability to supply the exact voltages needed by a particular TWT was provided by high-voltage transformer taps. These allowed for variation of the nominal helix and anode voltages over ±6 percent total range with a 1 percent variation between successive taps.

The major parameters of the power supply are shown in Table 5–13.

TABLE 5–13.—*TWT Power Supply Parameters*

Parameters	Value
Input voltage	22.5 volts ± 1 percent
Input power	
Operate	70 watts
Warm up	15 watts
Efficiency	75 percent
Output voltages and currents*	
Filaments*	4.25* v. @ 1.6 amps
Collector	950* v. @ 45 ma
Helix	2030 v. @ 1 ma (2½ ma max)
Anode	1500 v. @ 0.1 ma
Turn-on time delay	3 minutes
Weight	4.4 lb
Size	4″ × 7″ × 2½″

*Nominal value.

MICROWAVE BEACON

The microwave beason unit provided an unmodulated carrier at 4079.73 Mc for use as a tracking signal by the ground stations. This was applied to the TWT input via the beacon coupler. A block diagram of the unit is shown in Figure 5–26. A photograph of the unit is included in Figure 5–14.

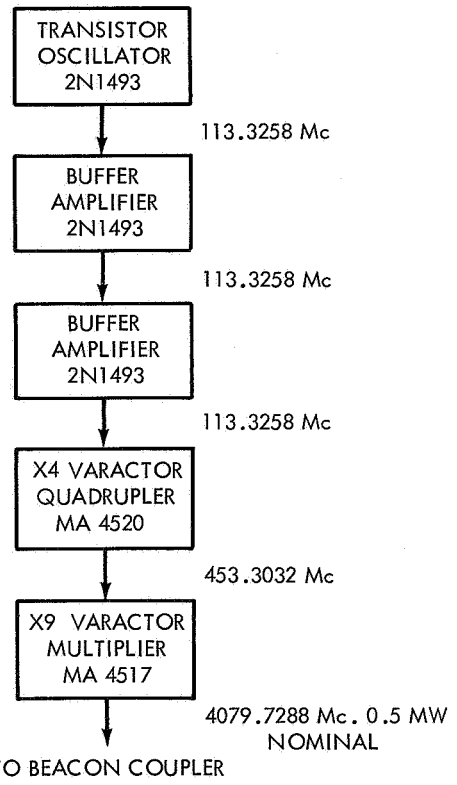


FIGURE 5–26.—Microwave beacon, block diagram.

PERFORMANCE

General

A comprehensive set of measurements was made on each finished repeater. The purpose of these tests was to verify proper operation within design objectives and to establish a set of reference measurements for possible later comparison with actual in-orbit operation. In general, these measurements revealed no anomalous behavior and demonstrated performance essentially within the specifications and objectives. The following material will describe actual measurements made on one of the Relay I wideband repeaters, Serial No. F1A.

Output Power

In the wideband mode, the output power, measured at the TWT output, was 11.6 watts over the expected operating range of input power. Figure 5–27 shows the output power level versus repeater input level for the wideband mode. The block diagram (see Figure 5–28) shows the test set-up for measuring output power. The input levels referred to in this report were measured at the spacecraft antenna terminals and include the effect of the input hybrid.

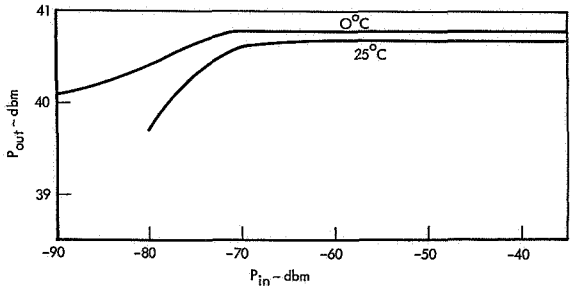


FIGURE 5–27.—Output power vs. reference input level, wideband mode.

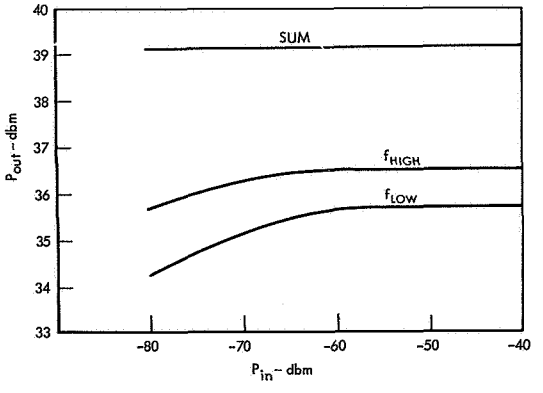


FIGURE 5–28.—Output power vs. repeater input power, narrowband mode.

From no signal conditions to about —80 dbm input, the AGC allowed essentially full gain. There is enough noise in the front-end to cause nearly full power output under this condition. Under signal conditions, noise quieting comes into effect and the noise output decreases.

In the narrowband mode, the output power was measured for equal input levels, and for unbalanced input levels. Figure 5–29 shows the individual carrier levels for equal

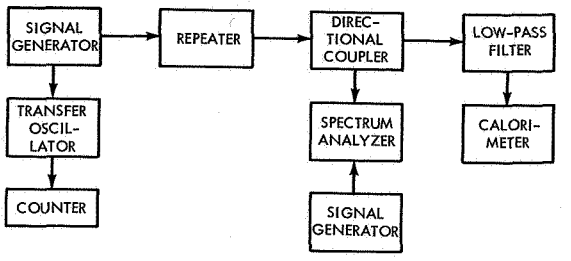


FIGURE 5–29.—Test setup for output power, frequency and spurious signal measurement, block diagram.

carrier-input levels. Also shown is the sum power. It should be noted that this sum power was less than that of the wideband mode single carrier. When two carriers are applied to a saturating amplifier, harmonics and intermodulation products are formed. Part of the available power is lost in these products, lowering the available carrier power. It is noted that at low-input powers (—80 dbm) the individual carrier powers decreased, but the sum power remained constant at a value higher than the RMS of the individual carrier powers. This was due to the measurements technique. The sum power was measured by a total power measuring device, while the individual carrier powers were measured using a spectrum analyzer and calibrating signal generator. The individual carrier-power values plotted were, therefore, the carrier only, exclusive of the noise power associated with the carriers.

The low C/N ratio at —80 dbm most likely accounted for the additional power appearing in the sum measurement.

The repeater was also checked for proper limiting when the two narrowband signals were differing by 10 db in level. Table 5–14 lists the results for several combinations of input levels. The beacon output power was 24.7 dbm at 25°C and 23.2 dbm at 0°C.

Frequency Response

The repeater was swept in frequency in both the wideband and narrowband modes

TABLE 5–14.—*Results of Narrowband Mode Compression Check*

Input power, dbm		Output power, dbm	
f_L	f_H	f_L	f_H
−70	−70	35.47	36.37
−70	−80	35.47	35.47
−70	−60	35.57	36.27
−60	−70	35.57	36.27
−80	−70	35.67	36.27

to insure that the receiver bandpass characteristics were adequate and not a function of signal level (see Figure 5–30). The wideband mode bandwidth was 34 Mc at 1-db and 36 Mc at 3-db down. The bandwidth was measured through the whole repeater and included the effects of tripling and limiting.

The narrowband swept response included the effects of limiting and tripling. The ap-

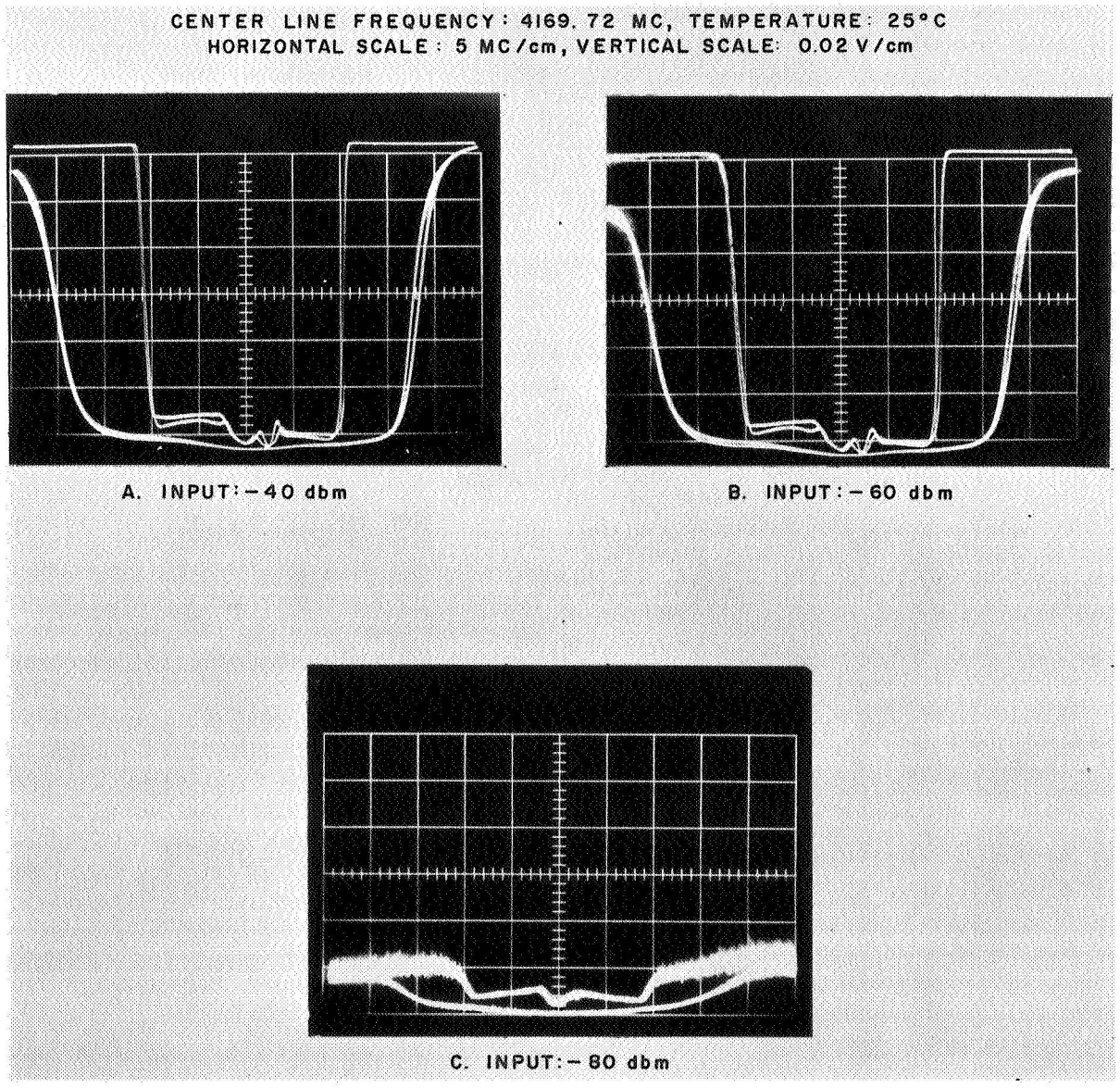


FIGURE 5–30.—Frequency response TWT—wideband and narrowband modes.

parent lack of separation between the two channels is explained as follows, referring to Figure 5–31: As the swept carrier, increasing in frequency, reached the top edge of the bandpass filter, centered at 68.33 Mc, the limiting amplifier tended to keep the power into the low-frequency tripler constant. Simultaneously, power started to appear at the output of the high-frequency tripler. These two powers varied in phase, in accordance with the transfer characteristics of the total networks. Thus, the two powers added vectorially and produced a total output which rose above the individual channel output and varied rapidly with frequency.

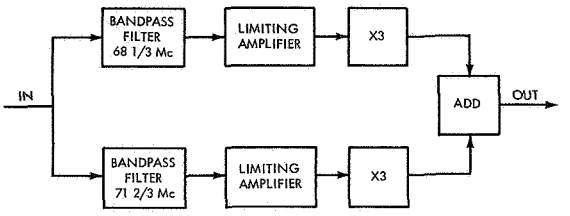


FIGURE 5–31.—Narrowband mode block diagram.

Noise Figure

The small signal noise figure of the repeater was 14 db. Figure 5–32 shows the variation of noise figure with input level. The high measured readings at —80-dbm input were a result of the measurement method. Noise quieting tests showed that the actual noise figure was constant, down to —80 dbm. The slight increase in noise figure with increase in signal strength was a result of the decrease in gain of the early IF stages as the AGC increased. As the gain decreased, the noise contributions from stages past the first two (which have no AGC) increased, increasing the noise figure. This increase did not impair the operation of the repeater, since the carrier power increased at a much faster rate, resulting in a net increase in carrier-to-noise ratio.

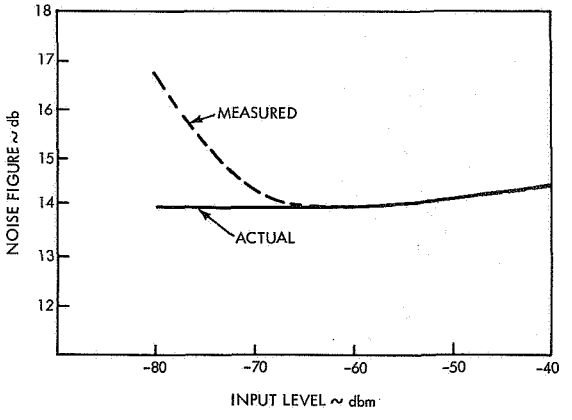


FIGURE 5–32.—Noise figure vs. input level.

Transmission Tests

A series of tests were run in both the wide and narrowband modes to determine the effect of the repeater on the transmitted signals. In the wideband mode the repeater was measured for group delay and the noise-power ratio (NPR) for an FM signal carrying the noise equivalent of 300 frequency-division-multiplex (FDM) voice channels. Standard TV patterns were transmitted and crosstalk measured in the audio channel. In the narrowband mode, NPR and crosstalk measurements were made for 12-channel loading.

Wideband Mode

Intermodulation noise measurements were made, using a flat-baseband noise spectrum extending from 60 kc to 1300 kc, to represent 300 FDM voice channels. This baseband was used to frequency modulate the carrier. Test tone deviation for 0-dbm0 was 225 kc RMS. The repeater triples this deviation to 675 kc RMS. Figure 5–33 shows the test set-up used in the measurements.* A slot filter was placed in the baseband at 1248 kc, and the noise measured in this slot after transmission and demodulation. The resulting NPR was then weighted to determine test-tone-to-noise and converted to picowatts.

*The MM–600 units, referred to in the block diagram, are modulator and demodulator units of an RCA high-capacity microwave relay design. See C. G. Arnold, et al., "A High Capacity Microwave Relay System" Communications and Electronics, Vol. 45, pages 712–722, November 1959.

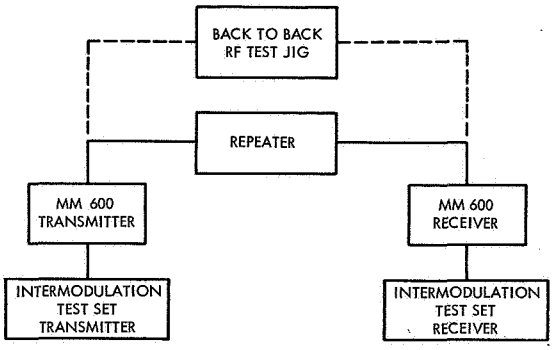


FIGURE 5–33.—300 channel noise loading test setup.

Pre-emphasis was not used in the measurements, so that an allowance of 4 db was made in the weighting. Table 5–15 shows the results for an input level of —40 dbm.

Group-delay (differential time delay) measurements were also made. Table 5–16 lists the linear and parabolic components of the group delay. Back-to-back measurements are also included for correction purposes. Figure 5–34 shows the measured group delay. The group-delay measurements can be correlated with the NPR measurements. Using the uncorrected group delay 0°C, the calculated weighted noise power is 3,150 picowatts, compared to 2,290 picowatts measured. (The measured NPR included the test equipment contributions.)

A television test pattern (staircase or white-window) was transmitted through the repeater. Comparison with back-to-back tests showed no visible deterioration of picture quality for input levels of —40 and —60 dbm.

Measurement of crosstalk from the video portion into the audio subcarrier gave a peak-to-peak reference tone to peak-to-peak noise ratio of 66 db. The noise appeared as a modulation of the audio subcarrier by the 15-kc line rate of the video. The effect is caused by group delay.

TABLE 5–15.—*300-Channel Noise-Loading Test*

Item	25°C			0°C
Slot frequency	70 kc	270 kc	1248 kc	1248 kc
NPR (db)	49.2	45.6	36.2	33.5
0 dbm0 TT/noise (flat) (db)	65.6	62.0	52.6	49.9
Noise in picowatts with 4 db Pre-emphasis and 2.5 db psophometric weighting			1230 pw	2290 pw

Input = — 40 dbm

TABLE 5–16.—*Wideband Group Delay Measurements*

Source	Parabolic component 10^{-9} sec/mc^2		Linear component 10^{-9} sec/mc	
	25°C	0°C	25°C	0°C
Overall measurement	0.5	0.56	+0.06	−0.19
Back-to-back reference	0.29	0.29	+0.16	+0.16
Repeater group delay	0.21	0.27	−0.1	−0.35

Narrowband Mode

Noise-loading tests were run in the narrowband mode to simulate 12 voice channels, in each direction. The specifications called for 12 channels in the baseband of 12 kc to 108 kc. Because of test equipment limitations, the measurements of the Relay I repeater included the effects of thermal noise which tended to obscure the intermodulation and crosstalk performance. The measuring equipment subsequently was modified to eliminate thermal noise. The measurements listed in Tables 5–17 and 5–18 are typical of the narrowband performance. It should be noted that substantially the same performance has been measured on the Relay I spacecraft by the ground stations. For NPR measurements, the baseband was set to give a 0-dbm0 test-tone deviation of 105 kc RMS at the repeater input (315 kc at the output), the required deviation for a 12-channel system. Table 5–17 lists the measured NPR of a typical repeater for baseband frequencies of 70 kc and 105 kc. The measurements were made with a CW signal in the second RF channel to properly load the repeater.

Crosstalk was measured in the unmodulated RF channel. Table 5–18 lists the results for a typical repeater. The crosstalk ranged from about 58.4 to 67.9 dbm0.

Spurious Outputs

The output of the repeater was examined for spurious outputs in both modes. In the

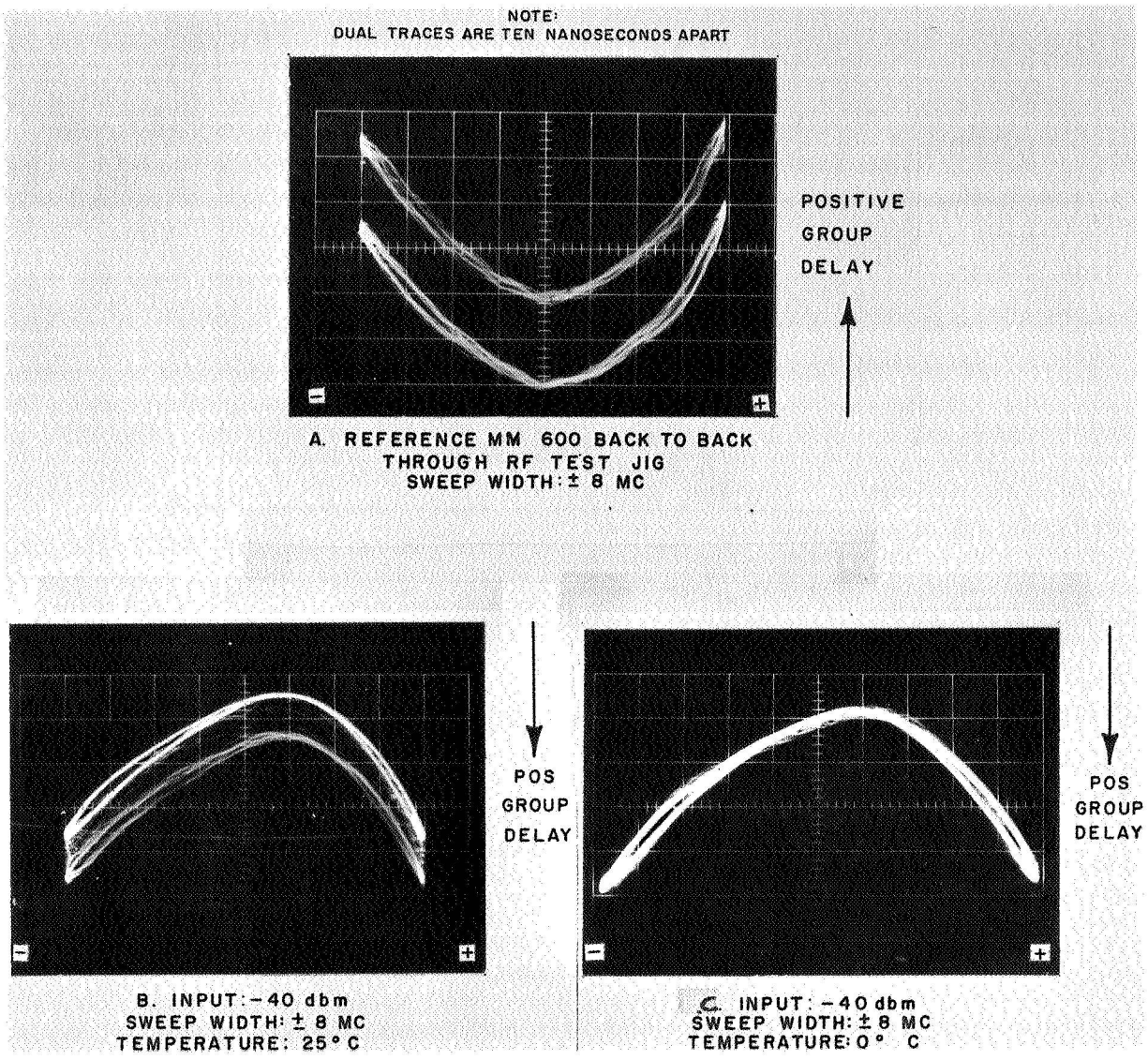


FIGURE 5–34.—Group delay measurements.

TABLE 5–17.—*Narrowband Noise-Loading Test of a Typical Repeater*

Item	Low channel		High channel	
Notch frequency	70 kc	105 kc	70 kc	105 kc
NPR (corrected) (db)	54	52	59.7	58.7
0-dbm TT/noise (flat) (db)	62.6	60.6	68.3	67.3
Noise in picowatts 4 db pre-emphasis and 2.5 db CCIR weighting	123 pw	190 pw	34 pw	55 pw

TABLE 5–18.—*Narrowband Crosstalk in a Typical Repeater*

Channel modulated	Channel measured	Mod. freq.	Crosstalk
Low	High	105 kc	> 59.6 dbm
High	Low	105 kc	= 65.6 dbm

wideband mode, the largest spurious product was at 4193 Mc and was 36 db below the carrier. This is the 37th harmonic of the beacon crystal frequency. This same spurious output was observed during narrowband mode measurements.

In the narrowband mode, the noise level

rose toward the edges of the channels to about 26 db below carrier level when the repeater was exposed to the temperature extreme of —10°C or lower. This noise rise was due to the presence of some regeneration in the receiver. It was not present at normal operating temperatures.

AUTHORS. *This chapter was written by* J. KIESLING, H. R. MATHWICK, T. WAKEFIELD, W. WILKINSON, *and* I. E. PODRACZKY *of the Radio Corporation of America, Princeton, New Jersey, U.S.A. under contract NAS 5–1272 with NASA/Goddard Space Flight Center.*

N66-10232

Chapter 6

The Telemetry System

GENERAL

The Relay I spacecraft telemetry system provided four basic functions:

1. Radiation experiment data transmission
2. Housekeeping data transmission
3. Diagnostic data transmission
4. Beacon signal for Minitrack tracking.

A block diagram of the telemetry system is shown in Figure 6–1. The telemetry encoder, horizon-scanner subcarrier oscillator, and telemetry transmitter were switched on and off by means of ground command. Operationally, one transmitter provided a continuous tracking signal, while the other was commanded on as telemetry or horizon-scanner data was desired. The modulation switch (located in the command control circuit described in Chapter 7) selected the transmitter to be modulated and the source of modulation. Only one transmitter could be modulated at any one time with either telemetry or horizon-scanner data.

A 3-db coupler provided isolation between the telemetry transmitters. Output of the 3-db coupler fed a diplexer, where telemetry signals were decoupled from the command receiving systems. The diplexer fed the four monopoles of the antenna in phase progression to provide a circularly polarized wave in the plane perpendicular to the spin axis. In any plane parallel to the spin axis, the wave was linearly polarized. The polarization sense produced by one transmitter opposed that produced by the other.

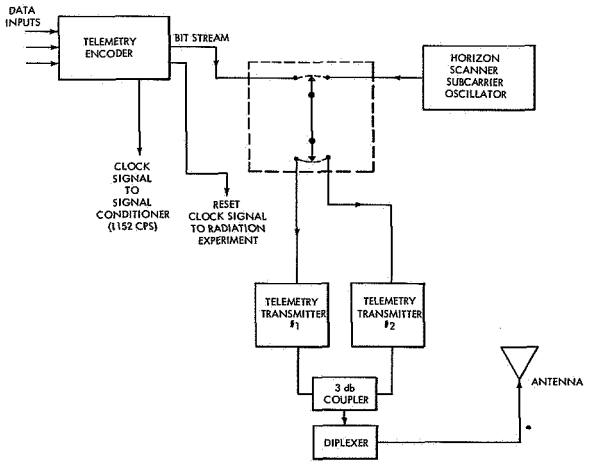


FIGURE 6–1.—Telemetry system block diagram.

THE RELAY I SIGNAL CONDITIONER

Introduction

The function of the signal conditioner was to provide the following:

1. A 9-volt, regulated, non-switched output for battery telemetry
2. A 9-volt, regulated, switched output (actuated by the 1152-pps clock pulses from the telemetry encoder)
3. Solar array and battery current telemetry
4. Battery pressure telemetry
5. Battery temperature and pressure cut-off signals for the charge controller.

Design Approach

The switched telemetry sensor circuits were energized only when telemetry information was being transmitted. When clock pulses from the telemetry encoder were received in the signal conditioner, the 9-volt switched regulator was energized. This regulator applied power to all the telemetry sensor circuits except the battery pressure and temperature sensors. These two sensors were energized by the 9-volt non-switched regulator, since they provided signals for the battery charge-current cut-off circuits when normal battery temperature or pressure was exceeded. To conserve array or battery power, series losses were minimized by using current transducers in the return lines of the solar array and batteries.

The signal conditioner, shown in Figure 6–2, consisted of five printed circuit boards fastened to a mounting plate. Four of the boards were stacked on one side of the mounting plate, while the fifth, containing the current transducers, was on the other side. The power transistor for the 9-volt switched regulator was mounted on the plate to provide an adequate heat sink. Finally the mounting plate was fastened to the spacecraft structure.

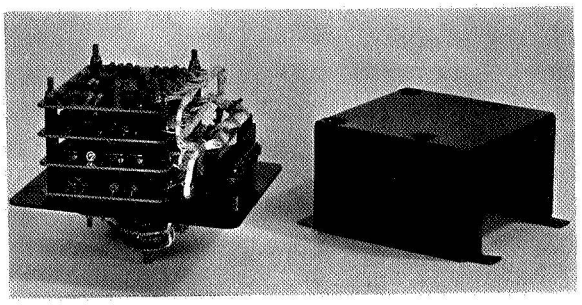


FIGURE 6–2.—Signal conditioner.

Operational Description

General

A block diagram shown in Figure 6–3 indicates the various stages in the signal conditioner.

9-Volt Regulators

Both 9-volt regulators were series type regulators, with a series resistor and transistor between the unregulated bus and the 9-volt output. The output was fed back to a differential amplifier, one side of which contained a zener reference. One collector of the differential amplifier drove an emitter follower connected to the series output transistor.

The switched 9-volt regulator was turned on and off by controlling the base voltage of the emitter follower. The control voltage was obtained from the square-wave supply.

Square-Wave Supply

The input to the square-wave supply, a

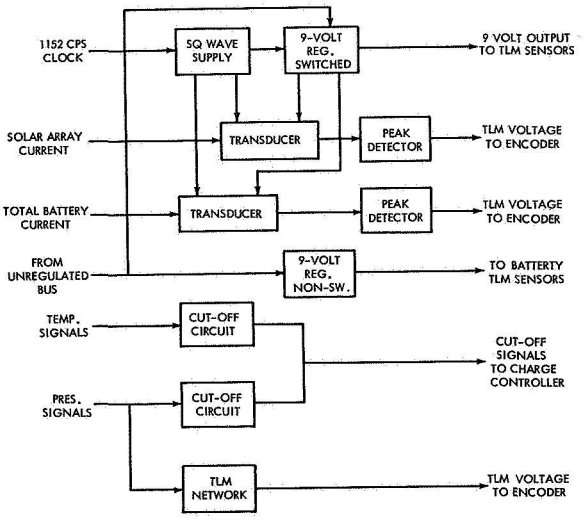


FIGURE 6–3.—Signal conditioner block diagram.

0-to-10-volt pulse at a frequency of 1152 pps, was applied only when the encoder was on. The input pulses charged a capacitor in an RC circuit, which turned on a transistor to energize the 9-volt switched regulator. When the input was removed, the capacitor discharged, and the transistor and 9-volt switched regulator were turned off.

The other square-wave supply output was obtained from a zener diode, which was turned off each time the input pulse grounded the diode through a transistor switch. The output, 0-to-15-volt pulses at the same repetition rate as the input, was capacitively coupled to the current transducers.

Solar-Array and Battery-Current Telemetry

Solar-array and battery currents were passed through one winding of separate current transducers. A current transducer consisted of two tape-wound cores with a current winding of few turns and an output winding of many turns. One end of the output winding was connected to the pulse output of the square-wave supply and the other to the peak-detector input. Since the impedance of the output winding was proportional to the dc current in the current winding, an ac voltage was produced at the input to the peak-detector, proportional to the array or battery current.

The positive half of the voltage input to the peak-detector charged a capacitor in an RC circuit. Because the RC circuit had a long time-constant, the capacitor tended to charge to the peak value of the input. The output of the peak-detector was fed to the telemetry encoder.

Battery Pressure Telemetry

The pressure signals were either zero or 9 volts depending on whether battery pressure was normal or high, respectively. The signals from the three pressure sensors (one per battery) were applied to an arrangement of resistors. From the output voltage level of the resistor matrix, the pressure status of each of the three batteries could be telemetered.

Battery Charge Cut-Off

The signal conditioner included the battery pressure and temperature cut-off circuitry. Because these circuits pertain to the power supply rather than to telemetry functions, they are described in Chapter 8.

Equipment Performance

Unregulated bus input current
1. Encoder off: 24 milliamperes
2. Encoder on: 66 milliamperes

Telemetry signal range
1. Solar-array current,
   0 to 2 amps: 0.7 to 4 volts
2. Battery current,
   −2 to +5 amps: 0.7 to 4 volts

Regulated voltage for telemetry sensors
1. Encoder on: 9 volts ± 0.8 volts*
2. Encoder off: less than 1 volt

Regulated voltage for
battery sensors: 9 volts + 0.8 volts*

Telemetry signal for
battery pressure: 0.57 to 4.5 volts

THE RELAY I TELEMETRY ENCODER

Introduction

The function of the telemetry encoder was to accept the necessary spacecraft data and to multiplex it into a form suitable for transmission to the ground via the telemetry transmitter. Thus, the encoder was interfaced with various data transducers, sensors, and signal conditioners at its input, and the telemetry transmitter at its output.

The following describes the factors which contributed to the development of the encoder specifications.

Telemetry Data Requirements

Commensurate with the established mission objectives, the telemetry data requirements were analyzed on the basis of two major functional areas: (1) Diagnostic and spacecraft status data necessary for efficient and controlled operation of the spacecraft; and (2) Scientific experiment data for de-

*Initial tolerance only, regulation was better than 0.1 volt.

termining environmental survival capabilities of critical spacecraft components (solar cells and silicon diodes), as well as establishing radiation environment parameters at orbital altitudes. A summary of the channel requirements is shown in Table 6–1.

Diagnostic and spacecraft status data included information associated with power, thermal, wideband-communication, and tracking-and-command subsystem operational parameters. These were voltages, currents, temperatures, power levels, command verification, battery pressures, and telemetry calibration signals. The form of this data presented to the encoder was exclusively high-level analog, with the signals at uniform 0-to-5-volt levels.

Scientific data included information from experiments that determined the extent of radiation damage to various types of solar cells and silicon diodes, and from particle detectors that measured the intensity, direction, and type of radiation encountered by the spacecraft. Data forms included analog, digital, and pulse signals. Analog signals were both high level (0 to 5 volts) and medium level (0 to +200 mv), while the digital signals were either 0 or 4 volts. Pulse signals were specified at a maximum input rate of 100 kc at a minimum amplitude of 5 volts.

Telemetry encoder information flow requirements, as established by detailed analysis of the above data requirements, are shown in Figure 6–4. To meet the accuracy requirements and to provide capability for handling the quantity and various forms of data, a time-multiplexed PCM system was

TABLE 6-1.—*Relay I Telemetry Channel Allocations*

Description	Analog		Digital bits	Sampling rate	Words per second	Bits per second
	High level (0–5v)	Medium level (0–200 mv)				
Diagnostic and status						
Power subsystem	3			1 sample per sec.	3	27
	17			1 sample per 64 sec.	17/64	153/64
Thermal subsystem	1			1 sample per second	1	9
	11			1 sample per 64 sec.	11/64	99/64
Wideband communications subsystem	2			1 sample per second	2	18
	12			1 sample per 64 sec.	12/64	108/64
Tracking and command subsystem	1			1 sample per second	1	9
	6			1 sample per 64 sec.	6/64	54/64
Scientific experiments						
Radiation monitor experiments			113	1 sample per second	113/9	113
	1			1 sample per second	1	9
	4			1 sample per 64 sec.	4/64	36/64
Radiation effects experiments (includes two medium level calibration channels)		32		100 samples per 32 sec.	100	900
	13			1 sample per 64 sec.	13/64	117/64
Sun aspect indicator			6	1 sample per second	6/9	6
Miscellaneous data						
Frame sync			27	1 sample per second	3	27
Subcommutator identification			6	1 sample per second	6/9	6
Calibration voltages	2			1 sample per second	2	18
				1 sample per 64 sec.	1/64	9/64
Separation signal	1		1	1 sample per second	1/9	1
Totals	74	32	153		128	1152

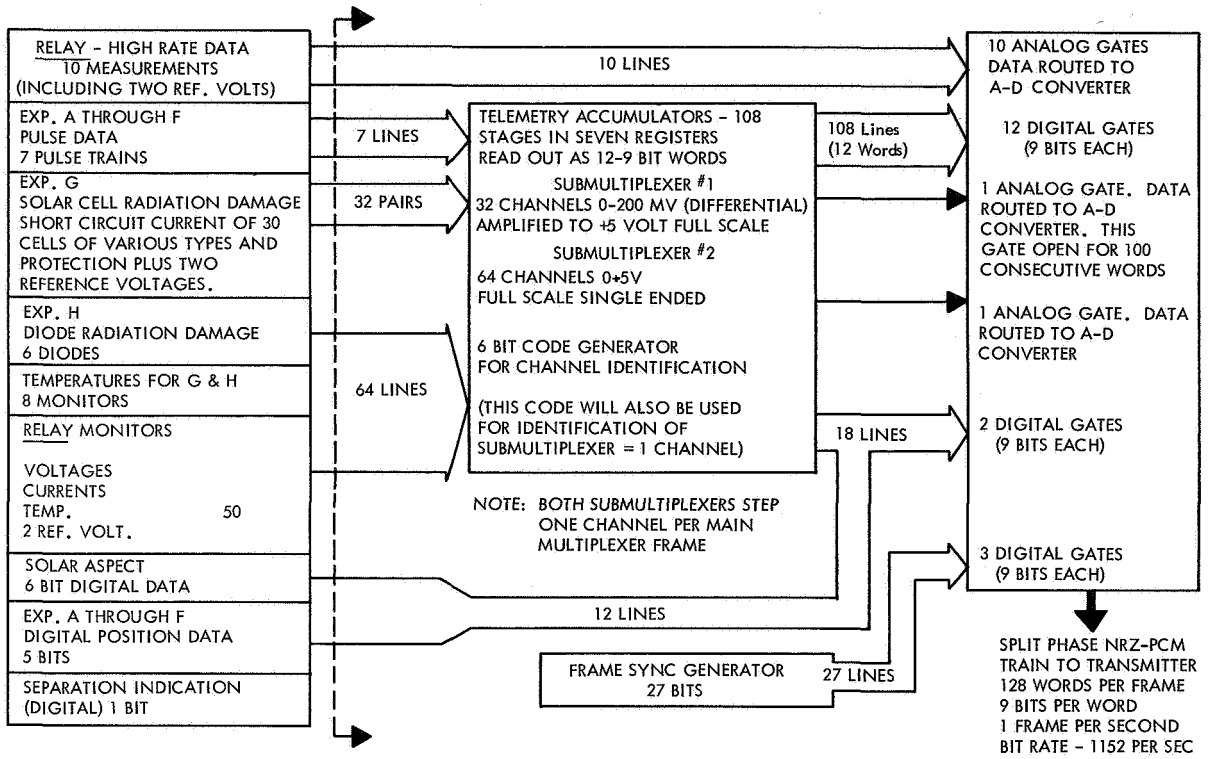


FIGURE 6–4.—Telemetry encoder information flow diagram.

chosen. The system utilized a word format of nine bits per word.

Functional System Description

A block diagram of the system configuration is shown in Figure 6–5. High level (0 to 5 volts) analog signals were fed through single-ended transistor commutator switches to a nine-bit analog-to-digital (A–D) converter, while medium level (0 to 200 mv) signals were fed through a differential commutator and amplifier before being converted to nine-bit words by the A–D converter. Digital signals were grouped into nine-bit words and presented in parallel to transfer registers which stored the information for subsequent serial transmission. Pulse signals from the radiation experiments were counted in binary accumulators that were sampled periodically and multiplexed with other spacecraft data.

The main commutator was a 128-channel commutator with a time-slot configuration, as shown in Figure 6–6. Of particular note is that 100 of the 128 time slots were occupied by one channel of the 32-channel, medium-level subcommutator. This supercommutation technique was a result of the high sampling rate required by the solar-cell experiment.

The solar-cell experiment consisted of measuring peak voltage outputs of solar cells mounted on the external surface of the spacecraft. With the orbiting spacecraft spinning at approximately 150 revolutions per minute, this sampling technique ensured the measurement of peak voltage output as the cells rotated from sunlight to darkness. This experiment could be used also as an indirect check on the spin rate of the spacecraft by measuring the time between output voltage peaks of a single solar cell.

The main commutators frame rate was one frame per second, while the subcommutators stepped one channel per revolution of the main commutator.

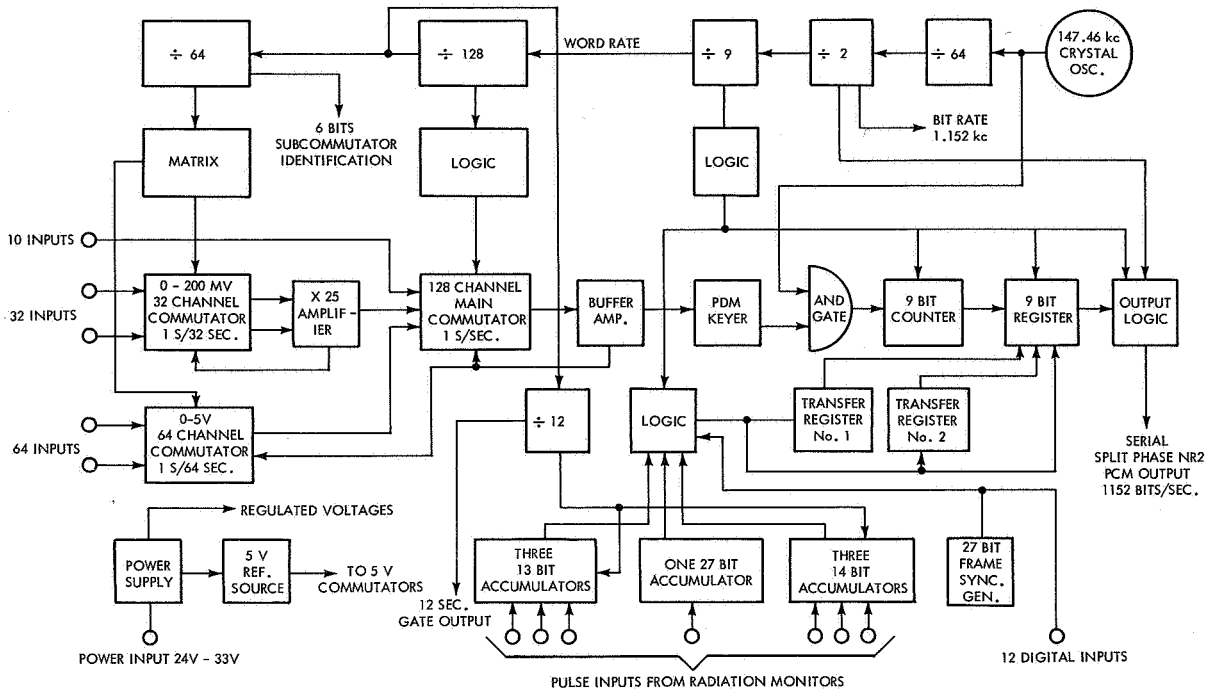
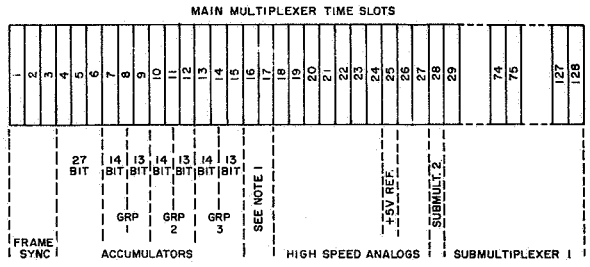


FIGURE 6–5.—Telemetry encoder block diagram.



NOTE 1: FIRST SIX BITS OF 16 — SUBMULTIPLEXER IDENTIFICATION LAST THREE BITS OF 16 AND FIRST THREE OF 17 — SUN ASPECT BITS 4 — 8 OF 17 — DIGITAL POSITION FROM RADIATION MONITOR LAST BIT OF 17 — SEPARATION SIGNAL

NOTE 2: ALL DIGITIZED ANALOG INFORMATION IS TRANSMITTED MOST SIGNIFICANT BIT FIRST.

NOTE 3: ALL ACCUMULATOR DATA IS TRANSMITTED MOST SIGNIFICANT BIT FIRST.

FIGURE 6–6.—Frame timing for telemetry encoder.

Accumulators were divided into three 13-bit, three 14-bit, and one 27-bit binary counters. The 14- and 13-bit accumulators counted for 10 seconds, after which input pulses were inhibited and the fixed parallel outputs were sampled for two seconds prior to resetting the six counters in preparation for another 10-second count. The 27-bit accumulator operated continuously, whether the prime encoder power was on or off. Accumulator inputs were derived from the radiation monitor experiments.

The five-volt reference source was used for calibration of high-level analog channels on the main and 64-channel subcommutators. Calibration voltages for the medium-level subcommutator were supplied from radiation effects experiments.

System Implementation and Performance Characteristics

The telemetry encoder embodied solid state circuitry exclusively to accomplish its functional requirements. Over-all performance characteristics are listed in Table 6–2.

Basic timing for the encoder was derived from a crystal-controlled oscillator, followed by a chain of counters. Outputs of the counters were used to drive transistor logic gates, from which all timing requirements were realized.

TABLE 6–2.—*Encorder Characteristics*

Output code	
Frame format	128 words per frame
Word format	9 data bits per word
Frame sync	Three 9-bit words (27 bits), adaptable to various codes
Frame rate	1 frame per second
Bit rate	1152 bits per second
Output signal	
Format	Serial split phase NRZ–PCM
Output level	The output signal consists of two voltage levels defined as follows: Low voltage 0 to 0.5 v High voltage 3.5 v to 4.5 v
Output impedance	5000 ohms
Clock stability	0.01%
System transfer accuracy	
High-level input (0–5 v)	±0.5% over-all
Low-level input (0–200 mv)	±1.0% over-all
Main multiplexer	
Total channels	128
Sample rate	One sample per second for each channel
Analog inputs	0–5 volts
Channel input impedance	Analog: 1 megohm minimum Digital: 100 kilohms minimum
Back current during sample period.	0.25 microampere maximum
Leakage current during non-sampling period.	0.05 microampere maximum
Submultiplexer No. 1	
Total channels	32
Sampling rate	One sample per 32 seconds for each channel supercommutated to 100 channels of main commutator
Analog inputs	0 to 200 millivolts
Channel input impedance	100 kilohms minimum
Back current during sample period.	0.25 microampere maximum
Leakage current during non-sample period.	0.05 microampere maximum
Submultiplexer No. 2	
Total channels	64
Sample rate	One sample per 64 seconds for each channel
Channel input impedance	1 megohm minimum
Back current during sample period	0.25 microampere
Leakage current during non-sample period.	0.05 microampere
Input power	9.0 watts maximum, with an input voltage range of 24 to 33 volts
Mechanical characteristics	
Weight	8 pounds
Volume	140 cu. in. (approx.)
Operating temperature range	−20°C to +60°C

High-level commutator switches were single transistor circuits with bootstrapping to obtain high input impedance. Medium-level switches were matched transistor pairs to reduce differential offset voltages to values consistent with accuracy requirements.

The output of the medium-level commutator was fed through a differential amplifier, that had a gain of 25. This amplifier provided both a uniform 0-to-5-volt signal to the main commutator and 60-db common-mode rejection.

Binary counters capable of operating at rates of 100 kc were utilized as pulse accumulators.

A PDM keyer and a pulse counter to convert 0-to-5-volt analog signals to a nine-bit word were included in the A–D converter. A significant feature of the converter design was that dc voltage drifts and offsets in the system were corrected automatically for each word. This was accomplished by sampling a zero correction voltage before sampling the analog signal. The offset from true zero was subtracted from the encoded output.

Frame synchronization utilized a 27-bit truncated pseudo-random code. This code occupied the first three word slots of the main commutator. Subcommutator channels were identified by a six-bit code derived from the divide-by-64 counter used to drive the subcommutator channel selection matrix. Subcommutator identification was transmitted once for each revolution of the main commutator.

A dc-to-dc converter was also included in the telemetry encoder to supply the necessary regulated voltages from the unregulated bus.

Physical Characteristics

The unit contained a total of 5600 subminiature components and utilized a cordwood construction packaging technique with printed boards. This technique made possible a significant reduction in volume resulting in a unit of less than 140 cubic inches. The final unit was completely encapsulated in a silicone rubber compound for high resistance to shock and vibration. A picture of the complete unit prior to encapsulation is shown in Figure 6–7. The weight of the potted unit was 8 pounds.

Reliability

Due to the telemetry encoder's complexity and spacecraft physical constraints, no re-

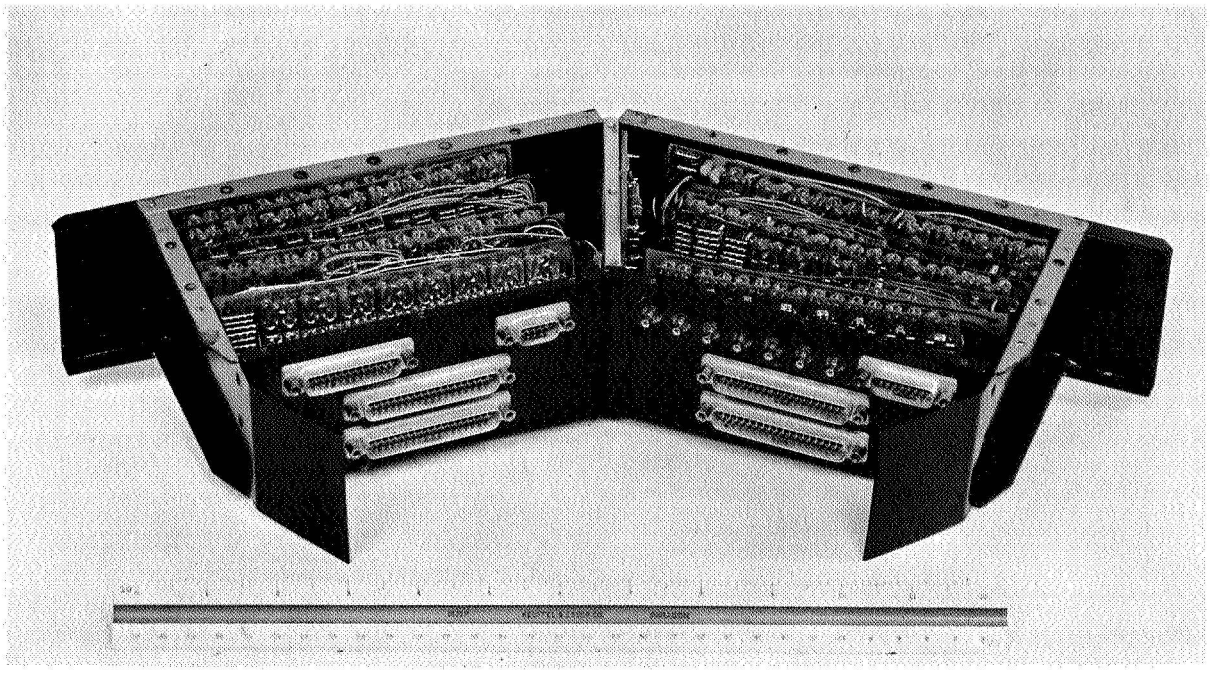


FIGURE 6–7.—Telemetry encoder.

dundancy was used in the design. In order to achieve reliability goals, preferred component parts for space applications were used along with a stringent pre-conditioning program. The calculated mean-time-before-failure was 10,500 hours considering all parts in series and in continuous operation.

THE RELAY I TELEMETRY TRANSMITTER

Introduction

The following paragraphs describe the development, design and construction of an all-solid-state, phase-modulated, telemetry transmitter used in the Relay I telemetry system. The system employs pulse code modulation which results in a PCM/PM transmission, and yields a transmitted signal of high-order frequency stability with a minimum of transmitter input power.

Transmitter output frequencies are 136.140 and 136.620 megacycles. Power output is a minimum of 250 milliwatts for supply voltages of 24 to 33 volts and 200 milliwatts minimum at 22 and 35 volts. Power input is specified as 2.0 watts at 28 volts.

The transmitter developed to meet this specification is shown in block diagram form in Figure 6–8. Specification highlights appear in Table 6–3.

Development Program

General

Originally it was planned that the telemetry transmitter for Project Relay would consist of an off-the-shelf unit chosen because of compatible performance characteristics and successful completion of a field test program. A number of vendors were contacted concerning their products. A tabular list of the performance obtainable and the field history of each unit was made.

A review of the data indicated that none of the available equipment would operate over the specified wide range of supply voltages while meeting the specified power input requirements. Furthermore, most available equipment did not meet MIL–I–26600 with regard to antenna conducted interference without using an additional RF filter.

Results of this survey and specification changes necessary to permit procurement of

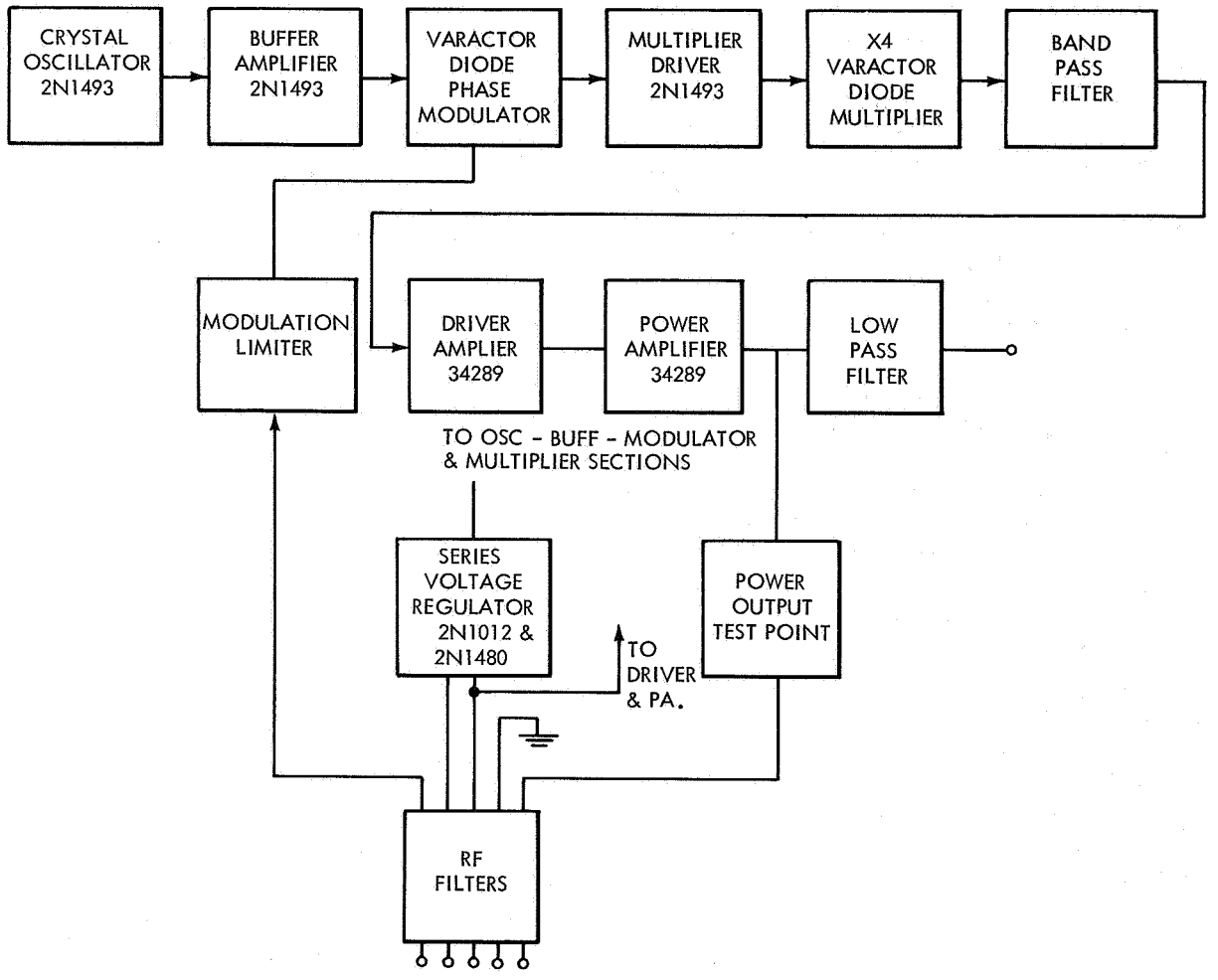


FIGURE 6–8.—Relay telemetry transmitter block diagram.

TABLE 6–3.—*Transmitter Specification Highlights*

Frequency	136.140 Mc and 136.620 Mc
Frequency stability	±.003%, −10°C to +35°C
Power output	200 milliwatts min., 22v and 35v
	250 milliwatts min., 24v to 33v
Modulation-phase	120° to 150° for modulation rates of 600-1200 cps and inputs of 0.0 ± 0.5 volts for mark and +3.3 to +5.0 volts for space
Spurious RF output	74 db down minimum
Power input	2.0 watts maximum at 28v
Supply voltage	+24 to +33 specified operation
	+22 and +35 Limited performance
Weight	2.0 lb. Maximum
Size transmitter	4.01 × 4.031 × 1.26
Transmitter set	4.01 × 4.031 × 2.45 (not including flanges and plug protrusions)

an off-the-shelf transmitter were evaluated. After consideration of all factors involved, it was decided that a new transmitter should be developed, tailored to the needs of the Relay I spacecraft.

It was recognized initially that obtaining the necessary efficiency of the driver and power amplifier was the most difficult problem to overcome. Further, variation characteristics of the supply voltage were not optimum for suitable transistors available in this frequency range and power output level. Therefore, a design program of the following two parallel approaches was initiated.

The first approach consisted of using 2N1493 silicon mesa transistors in a conventional, Class C, driver-PA configuration. In this approach the problem concerned obtaining suitable operating conditions over the

required range of operating voltages. Since the 2N1493 operates with higher supply voltages, operation could not be guaranteed, at that time, at lower power supply voltages. Conversely, transistors such as 2N706 and 2N743 cannot withstand a supply voltage of 22 to 35 volts without adding dropping resistors to dc-to-dc converters. Voltage conversion would have resulted in intolerable power losses.

Accordingly, an alternate scheme for the driver and power amplifier was tried in which dc parameters of the two were in series while ac circuits were in cascade. Figure 6–9 shows how such an arrangement was made and compares with selected circuits. Thus, the entire voltage of the power supply was utilized without extensive voltage dropping networks or power conversion circuitry.

Along with the plan to solve the most critical problem, that of the driver-PA, a parallel effort was started to design the oscillator and modulator section as well as the multiplier driver and ×4 multiplier section of the transmitter. Performance data was summarized daily to establish a final approach to the driver-PA configuration and to determine the possibility of ultimately meeting the specification.

Data taken on two types of driver-PA configurations is shown in Table 6–4. Note that 2N1493's yielded the desired performance and represented circuit simplification over the 2N743 approach. In addition, the circuit was inherently more reliable, since a parallel application of supply voltage was better than a stabilized series circuit. The alternate scheme also depended on using zener diodes to stabilize operating points. Zeners consumed power and consequently lowered the circuit efficiency. Figure 6–10 is a block diagram of the breadboard circuit. This was the basis from which the prototype transmitter was developed.

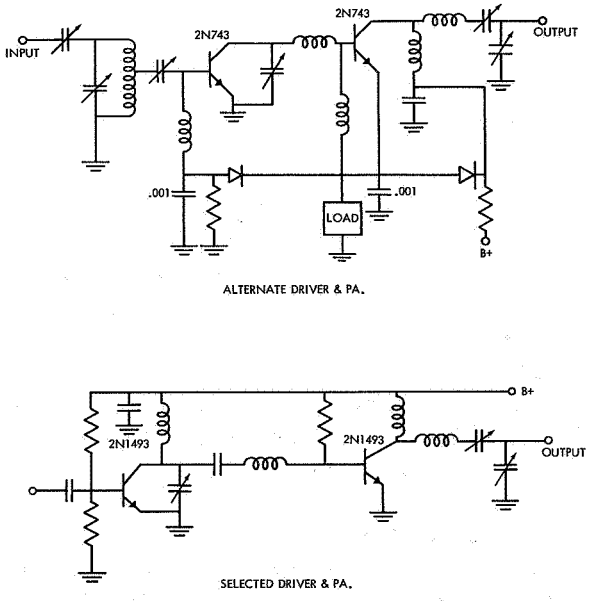


FIGURE 6–9.—Alternate and selected driver and power amplifier circuits for telemetry transmitter.

TABLE 6–4 —*Breadboard Transmitter Performance*

E supply volts	I Supply ma.	P_{in} watts	Power output mw
Alternate driver—PA			
22	62.0	1.30	200
28	77.0	2.15	330
33	92.0	3.04	340
Selected driver—PA			
22	46	1.01	220
28	68	1.91	350
33	74	2.44	420

Oscillator

A grounded-base 2N1493 circuit was selected for the oscillator. This circuit employed a third-overtone crystal as the stabilizing feedback element from collector output tuner circuit to emitter. The crystal selected was a glass encased unit chosen for high accuracy of initial finishing tolerance, broad turning point (±.0005% drift maximum over a temperature range of —10° to +60°C), and low aging. Oscillator output had to be loosely coupled to the phase modulator to reduce phase modulation of the oscillator itself and resultant spurious transmitter outputs.

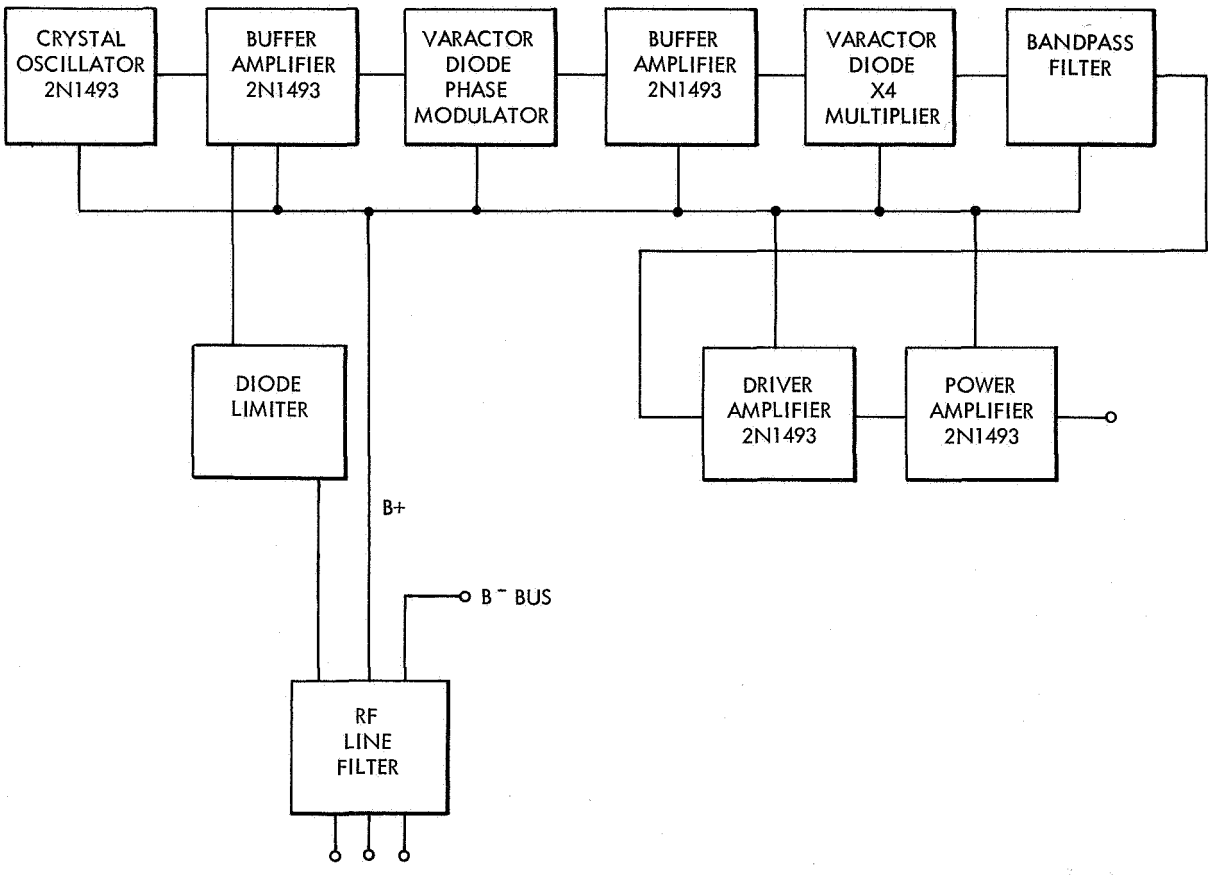


FIGURE 6–10.—Breadboard telemetry transmitter.

Phase Modulator

The phase modulator circuit consisted of a varactor diode acting in series resonance with a fixed inductance. Modulation varied the bias applied to the varactor diode, thus changing the tuned circuit resonance curve. This resulted in a linear phase shift.

Buffer Amplifier and Multiplier

Output of the phase modulator drove a buffer amplifier which increased the power level to about 250 milliwatts at 34 Mc. Output of the buffer drove the varactor $\times 4$ multiplier.

Filter Power Amplifier

A three-pole LC synchronous filter followed the $\times 4$ multiplier, and is used to attenuate adjacent harmonic outputs of the multiplier ($\times 3$ and $\times 5$). Filter output drove an RCA type 34289 (high gain 2N1493 at 24 v) UHF driver-amplifier that employs a combination of fixed and self-biasing. Output of the driver-amplifier, in turn, drove the 34289 class C power amplifier achieving an RF-output-to-collector-input efficiency of about 60 percent at the 300 milliwatt level.

Output Circuit

A two-section low-pass filter was used to reduce second and higher order harmonics which were generated in the power output stage. A diode rectifier connected to the transmitter output provided power output indication which was fed as a signal to the telemetry system encoder.

Signal Processing

Modulation input to the transmitter was clamped at $+0.5$ and $+3.3$ volts. Clamping

at these levels provided additional limiting which further increased system reliability. Initially a 0 to 2.0-volt input was specified, but this resulted in an input impedance that was too low for system applications.

Regulators

Finally, a series regulator circuit controlled the drive over the input supply voltage range of 24 to 35 volts to keep the transmitter within the 2.0 watt input power limit. (Figure 6–11).

Lead Filters

Power leads as well as modulation input and test point output leads were filtered by Allen Bradley Type SMFO–1 filters. This unit was essentially a ceramic feedthrough capacitor with a ferrite bead that acted as a low resistance at radio frequencies. The ac resistance of the bead and the capacitor formed a filter that had the inherent ability to extend filtering action to cover high order harmonics.

Temperature Monitoring

A thermistor was used to sense temperature on the case of the transmitter.

Mechanical

Flight model telemetry equipment consisted of two transmitters that were identical except for frequency. These were mounted together with a common center cover plate, a top cover for the upper transmitter, and a bottom cover for the lower. The bottom cover also served as a mounting plate. This mechanical arrangement permitted both transmitters to be mounted in the spacecraft with a minimum of weight and volume.

The individual transmitter chassis was compartmentized and fabricated of dip-brazed aluminum. This type of construction was chosen for minimum weight and good heat conduction.

Point-to-point wiring using pressed and soldered ground lugs, and teflon insulated feedthrough terminals formed the basis of secure mounting points for the components. Point-to-point wiring was an effective expedient which permitted maximum flexibility to accommodate the changing requirments of the program.

Transistors were mounted on the chassis by passing their leads through the teflon-insulated feedthrough terminals. A beryllium oxide washer was used to insulate the transistor case from the chassis and, at the same time, to permit good heat flow from the transistor case to the metal chassis. The washer and transistor cases were further secured by use of an epoxy resin. No failures, in either qualification tests (vibration, acceleration, and thermal vacuum) or acceptance tests, were attributed to mechanical damage or thermal failure.

The remaining components and wires were selectively potted with epoxy resin. This technique saved weight by reducing moisture retention, a fault of complete encapsulation.

The Allen Bradley, Type SMFO–1, RF line filters required extreme care in mounting. A special mounting bar was designed which permitted assembly (soldering the filter into the mounting bar) in a special fixture. The fixture held the filters in alignment without mechanical strain while heat was applied. This special mounting bar could be removed from the transmitter for easy filter replacement.

The covers for the transmitter had finger stock soldered to the edges which minimized RF leakage.

Major Problems

After product design began, following the breadboard phase, the problem of obtaining transistors with high-gain at 22 and 24 volts and 139 Mc presented itself. A power gain of 7 to 10 db minimum was required of the driver and power amplifier. Part of the solution to this problem was a change in design concept of the coils which were, for the most part, fixed-tuned. Tunable coils, as well as trimmers, permitted more flexibility in matching the impedance variations at these low voltages.

The second part of the solution consisted of developing a transistor test fixture. Selec-

tion of 2N1493 transistors in this test circuit produced a yield of almost 50 percent and resulted in obtaining transistors which matched the transmitter range of circuit impedance at low voltages and possessed sufficient power gain at 137 Mc.

Another design problem, which required considerable effort, was that of minimizing the reaction of the phase modulator on the crystal oscillator. The reflections of the phase modulator, when modulation was applied, fed back to the oscillator resulting in an unstable condition. As a result, more isolation was required between the oscillator output and the buffer amplifiers associated with the phase modulator.

The reduced drive made it mandatory to optimize the efficiency of the multiplier and reduce to a minimum the insertion loss of the bandpass filter which allows the multiplier.

Early in the design phase it became apparent that higher order harmonics generated in the driver and power amplifier section of the transmitter would not be sufficiently attenuated to meet MIL–I–26600 antenna-conducted interference. requirements. Accordingly, a two-section, low-pass, 0.5 db insertion loss output filter was designed. This caused a power decrease of approximately 20 percent which, when multiplied by a factor of two to allow for the efficiency of the driver and power amplifier, required a transmitter power input of more than the design goal of 1.5 watts at 28 volts.

The transmitter design, in fact, could not at first meet the required 200 milliwatts output at 22 volts and stay within the power input requirement of 2.0 watts at 28 volts. Certain selected transistors could be used to accomplish this; however, the selection would have resulted in a very low yield. Test data showed that power output (and corresponding power input) could be obtained by limiting the drive to the output stages of the transmitter. Accordingly, a series voltage regulator (see Figure 6–11) was designed to regulate the drive-governing circuits and also minimize loss of power above the point

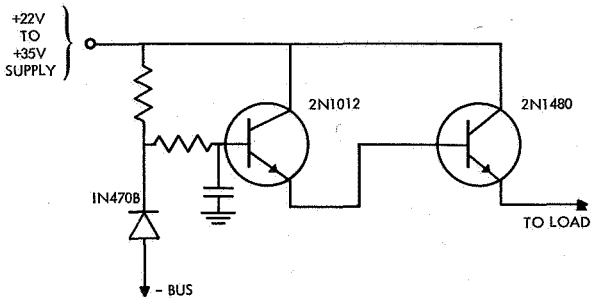


FIGURE 6–11.—Final regulator circuit added to transmitter.

of regulation (22 volts).

A minor problem was that of poor signal-to-noise ratio. It was found that zener diodes, used to establish voltage references, were apt to cause a relatively large amount of noise. Additional RC filtering of the zener diodes feeding sensitive points remedied this problem. Figure 6–12 shows the points of additional filtering required to reduce the noise modulation caused by the zener diodes.

Another major problem encountered early in the design concerned measurement of phase deviation with square-wave displace-

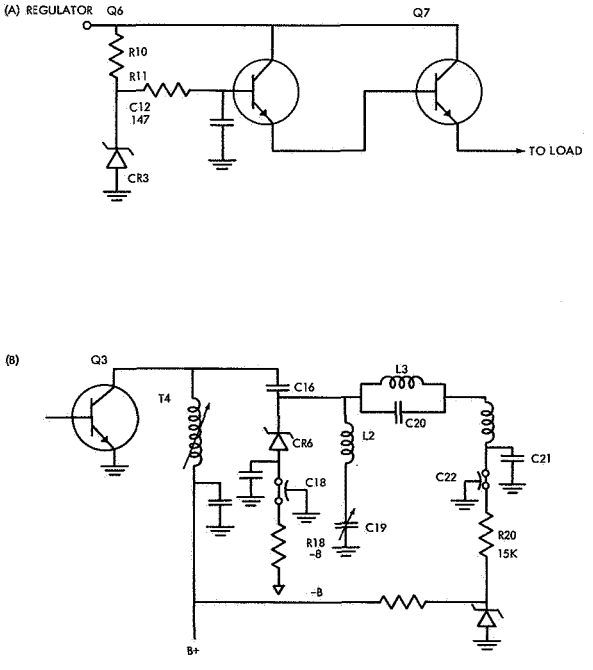


FIGURE 6–12.—Zener filter points.

ment. The most convenient method of phase measurement makes use of the principle that a sinusoidal phase modulation produces a peak deviation identical to that of FM. The formula, $f=Mp$ times the modulating frequency, is used to express the relationship (f=peak deviation from mean carrier frequency and Mp=peak phase shift in radians). This relationship makes phase modulation measurement simple, and an FM deviation meter such as the Marconi 791D can be used.

The relationship, however, does not hold for square-wave modulation. Two other means can be used, however. One method is to employ a phase-lock receiver with a calibrated phase detector, and make a comparison of shifted signals with the phase-lock carrier, as shown in Figure 6–13. The other method uses a spectrum analyzer, with Bessel zero analysis. Since it was found desirable to use the phase-lock receiver not only to measure phase shift, but also to observe the demodulated transmitter output, the phase-lock receiver test setup that was used is shown in Fgure 6–14.

The transmitter deviations were measured

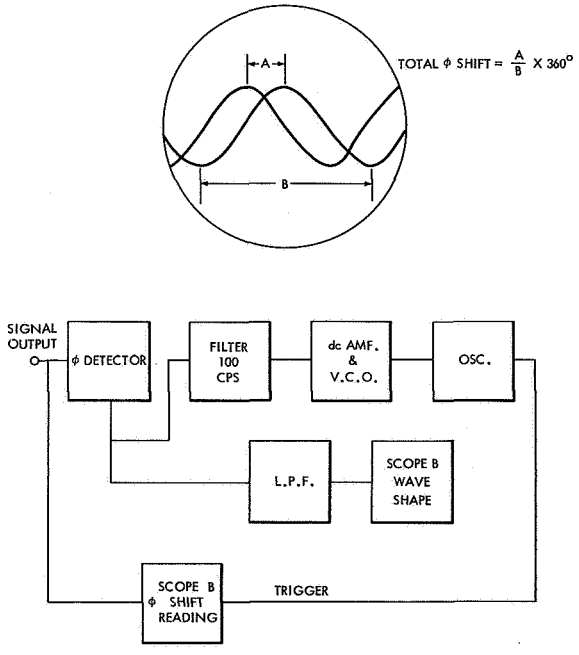


FIGURE 6–13.—Phase comparison.

using this receiver prior to, during, and after qualification testing. Shortly after the qualification tests were completed, the transmitters were checked at Goddard Space Flight Center for compatibility with the ground receivers. Phase calibration between Goddard and RCA was compared, and results agreed to within 2°. The tests did reveal, however, that the demodulated waveshape showed evidence of poor low frequency response. This was subsequently traced to audio feedback to the oscillator circuit, and subsequent further decoupling of the oscillator circuit eliminated this trouble.

During qualification tests, the spurious output of the transmitters at frequencies below the transmitter center frequency was not down by 74 db as required. Tests disclosed that these frequencies (68 Mc and 103 Mc) appeared on the —B line via a ground loop in the ×4 varactor-multiplier bypass return (see Figure 6–12). These frequencies then passed through the RF amplifier and the low pass filter to the antenna. Removal of the coupling path resulted in bringing the output to specified levels.

A preliminary integration with the gating circuits of a simulated spacecraft command control box was made. The tests verified that the modulation input of the transmitter was compatible with the preliminary control box units.

Qualification vibration tests revealed difficulty in one component attachment: a coil lead on one transmitter broke. The coil was potted, retested and passed. Previously, this component had not been potted.

Flight Model Program

The transmitter output sensing circuit was changed during the course of the flight model program. Originally, it was conceived that this signal was to be within the limits of 0 to 5 volts at a power supply voltage of 28 volts. Since the outputs of the power output and voltage sensors of most transmitters were near 5 volts with a 28-volt supply voltage, sensor outputs of over 5 volts were experienced at 33 and 35 volts. Figure 6–15

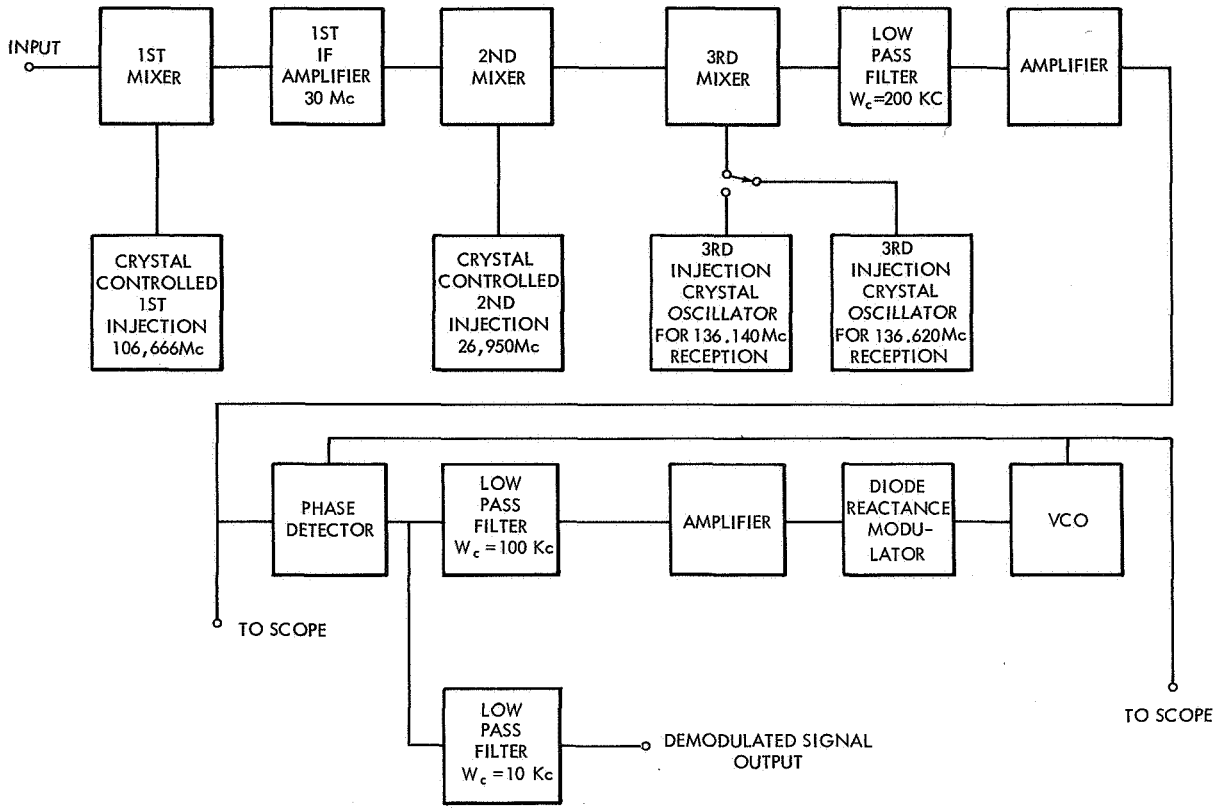


FIGURE 6–14.—Laboratory phase lock receiver.

shows the circuit before and after the modification made to reduce this output voltage.

It was also discovered at this time that this circuit caused the generation of second harmonics which affected antenna conducted interference. While rearranging the circuits for reducing voltage, the diode and resistors were also rearranged to control the second harmonic output. After this modification, the second harmonic output of all transmitters was down by 74 db or better.

A circuit change was incorporated during the flight model program to facilitate production. Some units emitted spurious outputs at frequencies relatively close to the center frequency while other units did not. These outputs were traced to regeneration due to feedback between the high-level stages (Q4 and Q5) and the low-level stages. Additional filtering in the form of a resistor corrected this condition and did not affect other performance characteristics.

The summary of data, from tests of the revised prototype model and dual flight models, indicates the capability of the circuit (refer to Tables 6–3 and 6–4). Table 6–5 summarizes the antenna conducted RFI, and indicates that the units met this requirement with only a minor deviation. Table 6–6 shows power, output supply voltage, and power input.

The specified stability for the telemetry transmitter is ±.003 percent with temperature range of −10° to +35°C. The design goal was ±.0015 percent over the temperature range of −10°C to +35°C, and with supply voltage variations of 24 to 33 volts.

An additional design goal was to hold stability to ±.0015 percent drift maximum (in addition to drift caused by temperature and voltage variation) for a period of 1 year. Table 6–7 shows frequency variations measured in the prototype tests to +60°C. Table 6–8 lists frequency error measurements of

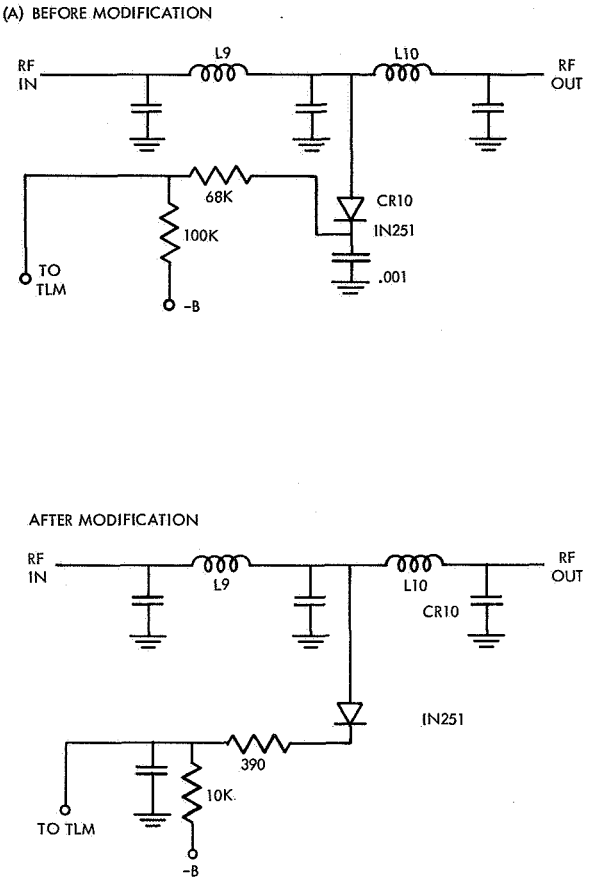


FIGURE 6–15.—Test point circuit.

TABLE 6–5.—*Spurious RF Outputs From Project Relay Telemetry Transmitters*

Assy. No.	Trans. No.	$\frac{f}{4}$	$\frac{f}{2}$	$\frac{3f}{4}$	$\frac{5f}{4}$	$\frac{3f}{2}$	$\frac{7f}{4}$	$2f$	$3f$
1	1	82.5	87	91	87	-----	-----	79	79
1	2	87	89	80	85	-----	-----	70	80
2	3	93	83	81	90	-----	-----	67	74
2	4	91	82	72	83	-----	-----	72	77
3	5	89	89	77	86	102	-----	74	77
3	6	88	75	74	83	98	-----	80	78
4	7	93	84	78	89	98	102	67	83
4	8	83	96	74	74	102	102	79	81
5	9	108	78	88	80	95	-----	68	75
5	10	93	86	79	81	98	-----	81	76

NOTE: All values shown are in db and relative to desired transmitter output.

10 transmitters before and after environmental tests. This data indicates that the requirement of .0015 percent drift stability with supply voltage and temperature was met.

A capacitor from the base of the power output transistor (C52) to ground was found to improve efficiency at Table 6–9 shows. This change was made on all units.

A problem was noted in phase modulation distortion and has since been observed on other FM transmitters employing reactance modulated crystal oscillators. This was the effect of the oscillator tending to oscillate in spurious modes near the desired crystal mode. Since there is a reaction on the crystal oscillator from the phase modulator, perhaps the oscillator may be pulled in frequency momentarily. If a suprious mode is present and not attenuated from the main mode of oscillation, the oscillator will tend to jump, particularly when modulation is applied. Two crystals were found to possess spurious modes of operation sufficiently close in frequency to the desired mode to cause a phase modulated output. The crystal manufacturer verified the existence of spurious modes in the first crystal returned for analysis. Additional crystal tests were specified to eliminate such crystals.

System

Two systems integration problems occurred with the telemetry transmitters. The first problem occurred when the charging current of the tantalum filter capacitor (C23) in the transmitter caused a transmitter failure in the control box. The peak charging current, at the instant the unit was turned on, was too great. It was decided to insert a limiting resistance in series with the filter capacitor.

The second problem was discovered in further integration tests. Occasionally the test receiver could not lock onto the transmitter output. It was found that the control circuit gates were providing pulses exceeding five volts in amplitude. This caused a phase deviation greater than 150° which caused the receiver to fall out of lock. The sensitivity of the transmitter was reduced to provide a compatible system (refer to Table 6–10).

TABLE 6–6.—*Power Output and Power Input as Functions of Supply Voltage and Temperature in Acceptance Tests*

Transmitter assy. #	Transmitter #	Min power output			Max P_{IN} 24v watts	Max P_{IN} 28v watts	I line ma
		P_o 22v milli-watts	P_o 24v milli-watts	P_o 28v milli-watts			
1	1	223	250	300	1.20	1.58	56.5
1	2	200	252	310	1.44	1.81	64.6
2	3	207	290	370	1.49	1.88	67.2
2	4	205	270	320	1.44	1.91	68.2
3	5	215	252	320	1.46	1.96	70.0
3	6	205	260	360	1.44	1.80	64.3
4	7	230	278	350	1.44	1.91	68.2
4	8	225	270	320	1.34	1.71	61.0
5	9	228	290	350	1.49	1.91	68.2
5	10	210	264	320	1.25	1.63	58.2

TABLE 6–7.—*Maximum Frequency Variations for Project Relay Prototype Telemetry Transmitters*

Set #	From nominal f_n at 28v+25°C	$\%\Delta f$ from nominal	Δf at −10° C altern.	$\%\Delta f$ at 10° C	Δf at +35° C altern.	$\%\Delta f$ at +35°C	Δf at +60°C	$\%\times f$ at +60°
1	−1113	.00081	+1129	.00082	−138	.0001	−379	.00028
2	−550	.0004	+592	.00043	−349	.00025	+810	.00059

TABLE 6–8.—*Maximum Frequency Variations for Project Relay Telemetry Transmitters*

Telemetry set No.	Xmtr No.	Δf from nominal cps	$\%\ \Delta f$ from nominal	Maximum cps frequency drift during acceptance test	Maximum % frequency drift during acceptance test	Frequency from nominal after environ. acceptance test (cps)	% Frequency difference between acc. and environmt.	Time period between accept. test and final after environmt.
1	1	+184	.00013	+1254	.00092	----------	----------	----------
1	2	+353	.00026	+1116	.00085	----------	----------	----------
2	3	− 39	.00003	− 165	.00012	−174	.00013	9 days
2	4	−100	.00007	+ 631	.00046	−236	.00010	9 days
3	5	− 23	.00002	− 327	.00024	− 75	.00004	9 days
3	6	+ 69	.00005	+1327	.00096	− 98	.00012	9 days
4	7	+260	.00019	+1380	.00110	−484	.00054	32 days
4	8	+152	.00011	+1072	.00078	−433	.00043	32 days
5	9	+ 10	----------	+1226	.00040	− 30	.00003	38 days
5	10	− 5	----------	+ 531	.00039	− 20	.00002	38 days

TABLE 6–9.—*Power Amplifier Efficiency Improvement Data*

Trans. #	No capacitor base to ground				20*uu* base cap. added			
	V_{dc}	I_C (ma)	P_o (mw)	Col. Eff.(%)	I_C (ma)	P_o (mw)	Col. Eff.(%)	Change in gain (db)
119	22	33	325	44.8	19	264	63	− .90
	28	50	505	36.0	27	426	56.4	− .75
113	22	34	325	43.5	16	246	70.0	−1.20
	28	52	525	36.0	24	448	65.2	− .70
116	22	28	314	51.0	17	246	66	−1.00
	28	40	494	44.0	26	460	63.2	− .32
128	22	28	302	49.0	18	235	59.3	−1.10
	28	51	570	40.0	28	404	51.4	−1.50
118	22	27	280	47.1	19	246	58.9	− .56
	28	52	515	35.3	26	393	54.0	−1.10
102	22	33	325	44.7	15	224	67.8	−1.60
	28	49	515	37.5	24	436	65.0	− .70
107	22	33	246	34.0	18	224	56.6	− .40
	28	49	570	41.5	26	370	50.9	−1.90
No #	22	33	280	55.4	15	224	68.0	−1.00
No #	28	35	481	49.0	22	415	67.3	− .65
115	22	28	281	45.7	18	247	62.5	−1.30
	28	50	571	40.8	25	381	54.5	−1.70
101	22	34	291	38.9	20	246	56.0	− .70
	28	54	505	33.5	27	380	50.3	−1.20
123	22	33	325	44.7	17	235	63.0	−1.40
	28	51	550	38.5	27	470	62.4	− .70

TABLE 6–10.—*Transmitter Deviation Data*

Transmitter #	Low	High	Variation maximum
1	122°	150°	28°
2	120°	146°	26°
3	120°	142°	22°
4	120°	148°	28°
5	122°	140°	18°
6	120°	144°	24°
7	126°	148°	22°
8	120°	140°	20°
9	125°	144°	19°
10	126°	150°	24°

Limits set at 120° to 150°.

THE TT&C ANTENNA SYSTEM

Description of Unit

A block diagram of the antenna system for the telemetry and command is shown in Figure 6–16. The radiators consisted of four whips equally spaced in a truncated cone arrangement of 60-degrees apex angle, mounted at the base of the spacecraft. For the 148-Mc command-receive function, the four whips were fed in-phase to create a linearly-polarized pattern. For the 136-Mc telemetry

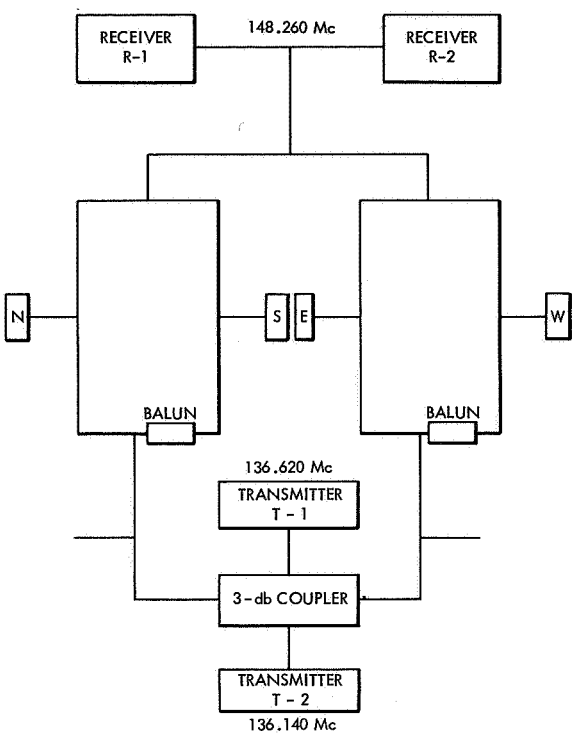


FIGURE 6–16.—TT&C antenna system, block diagram.

function, the whips were fed as a modified turnstile, with counter-clockwise phase progression for one tranmitter and clockwise for the other. Radiation patterns were predominantly circularly polarized, and the two transmitters were isolated. Simultaneous match for the two frequency regions was obtained by a proper configuration of whip length, selected cable lengths, and adjusted open-circuit stubs.

The TT&C antenna system consisted of:

1. Four whip elements
2. One 3-db directional coupler
3. Two baluns
4. A cable-harness assembly consisting of ten coaxial tees and twenty-five cables.

A photograph of this network feeding system is shown in Figure 6–17. Figure 6–18 is a schematic wiring diagram.

The radiators were four monopole whips (N, S, E, W). Each consisted of an aluminum TM panel receptacle with the center conductor extended by the attachment of a

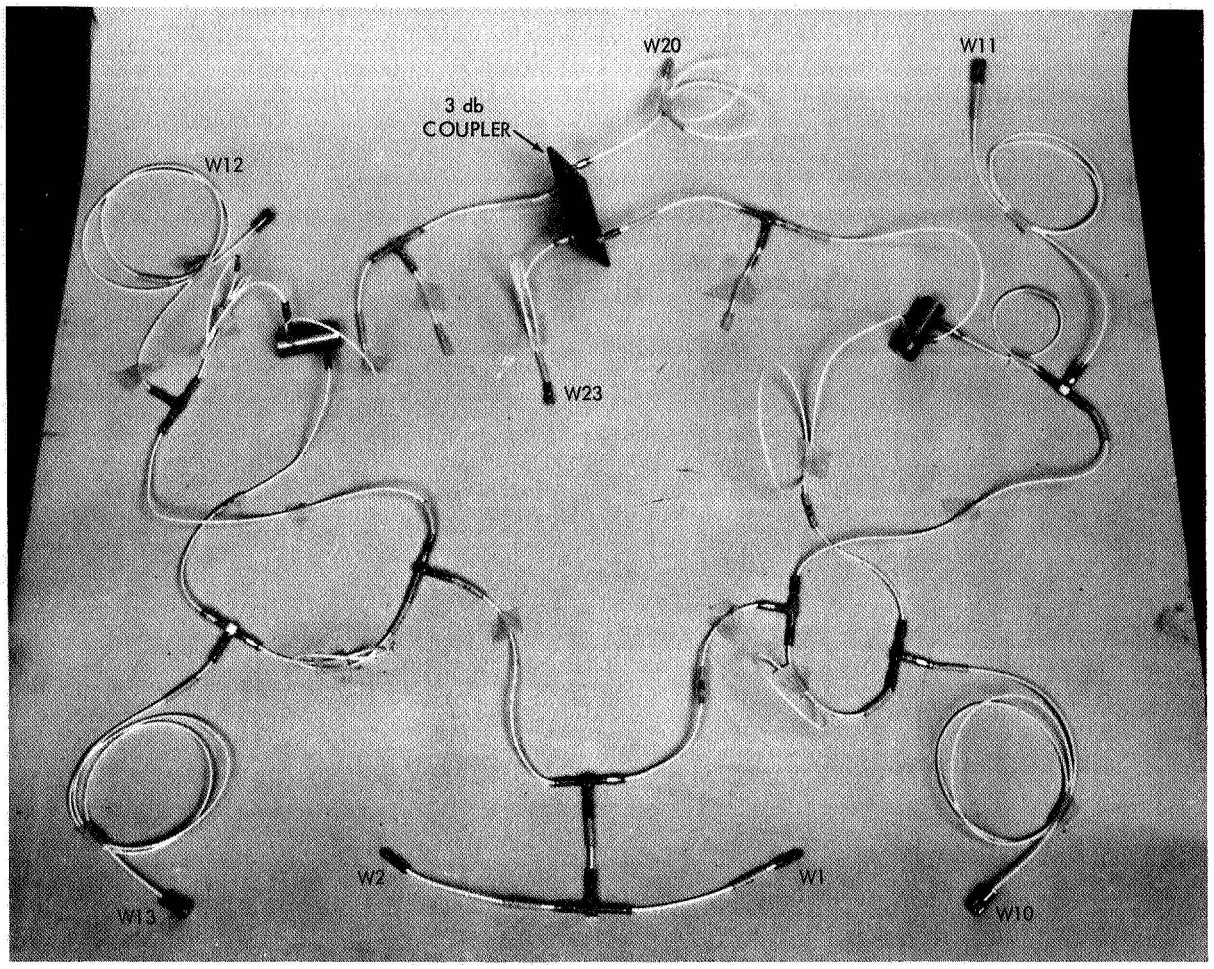


FIGURE 6–17.—Network feeding system.

length of beryllium wire (see Figure 6–19). The weight of each radiator was 0.05 lb.

The 3-db printed-circuit coupler consisted of two 1/16-inch-thick, diclad teflon fiberglass printed boards, separated by a 1/64-inch sheet of teflon fiberglass material to form a four-port coupler. The four ports were Conhex printed-board receptacles. The assembly was protected by a moisture and fungus-resistance coating. The weight of each 3-db coupler was 0.156 lb. (See Figure 6–20.)

The balun consisted of a quarter-wavelength coil of RG–188/U 50-ohm cable inserted into a coaxial phenolic and aluminum tube assembly as shown in Figure 6–21. After the electrical checkout, the tube assembly was filled with polyurethane foam to insure mechanical stability during shock and vibration. The weight of each balun was 0.009 lb. The cabling consisted of RG 188/U cable with Conhex-type connectors.

History of Unit

The TT&C antenna system was originally conceived to be similar to that developed and successfully used on the Tiros series of spacecraft. However, as finally developed, it differs in a number of respects because of the differing spacecraft configuration, frequency separations, and improved components.

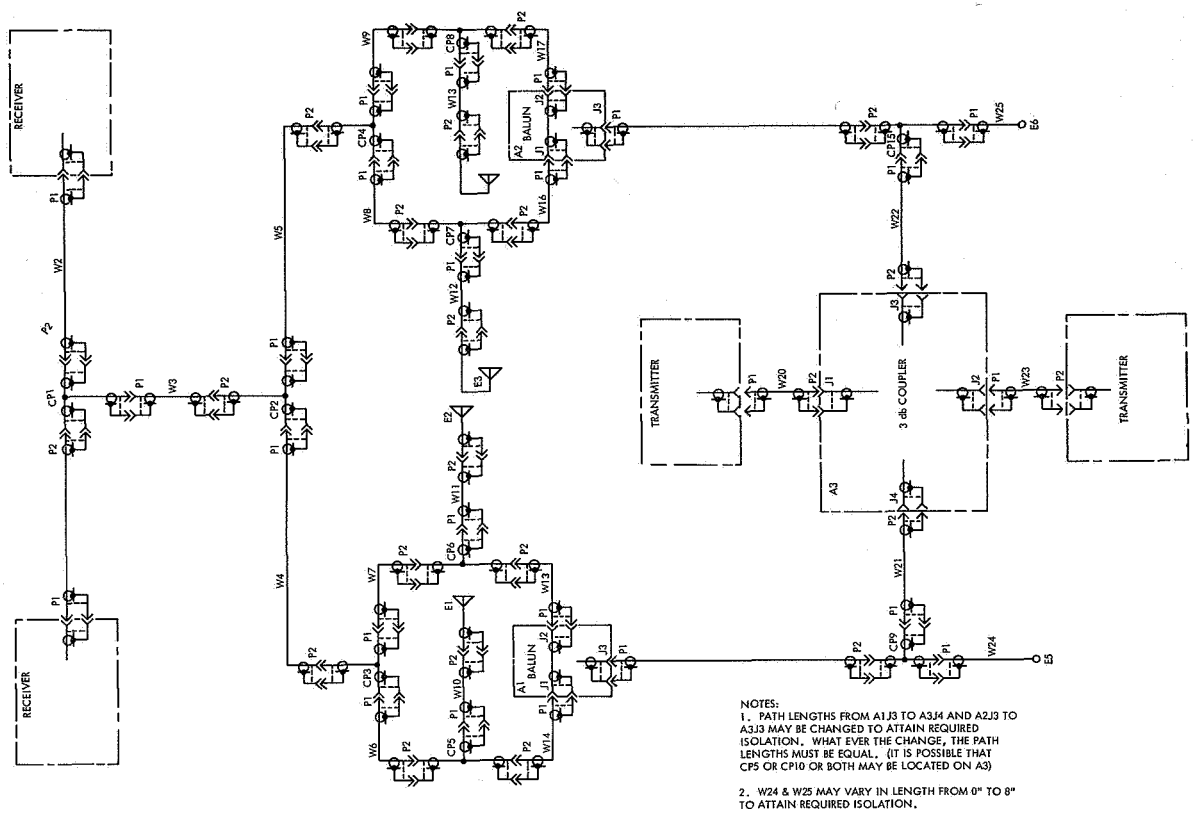


FIGURE 6–18.—Narrowband antenna, schematic wiring diagram.

Design Requirements, Problems, Changes

The requirements of the TT&C antenna system were:

1. Frequency:
   Transmit 136–137 Mc
   Receive 148 Mc
2. Polarization: elliptical with axial ratio not greater than one db on spin axis
3. Pattern: as nearly isotropic as possible
4. Isolation:
   (a) transmitter-transmitter, 25 db (reduced to 20 db later)
   (b) receiver-to-transmitter, 30 db
   (c) receiver-to-transmitter, 20 db
5. Insertion loss 1.5 db or less
6. VSWR:
   (a) not more than 1.5 at 136 Mc
   (b) not more than 2.5 at 150 Mc.

The first concept of the TT&C antenna system visualized the 136-Mc and 148-Mc regions by filters.

These filters were to be constructed using printed-circuit techniques to reduce size and weight. However, an inherent problem of losses arose in the experimental development of these filters. Because of the relatively close spacing of the command and telemetering frequencies, it was not possible to design such a filter using printed-circuit techniques without prohibitive insertion loss and accompanying crosscoupling. Any improvement in the design would have had to be made with air dielectric, which would increase the weight and mechanical complexity of the filter.

It was decided to employ the modified feed circuitry already described (Figure 6–16). Different antenna excitation and radiation modes were used for the two frequencies. Thus, inherent decoupling was gained between the two functions. The advantage ob-

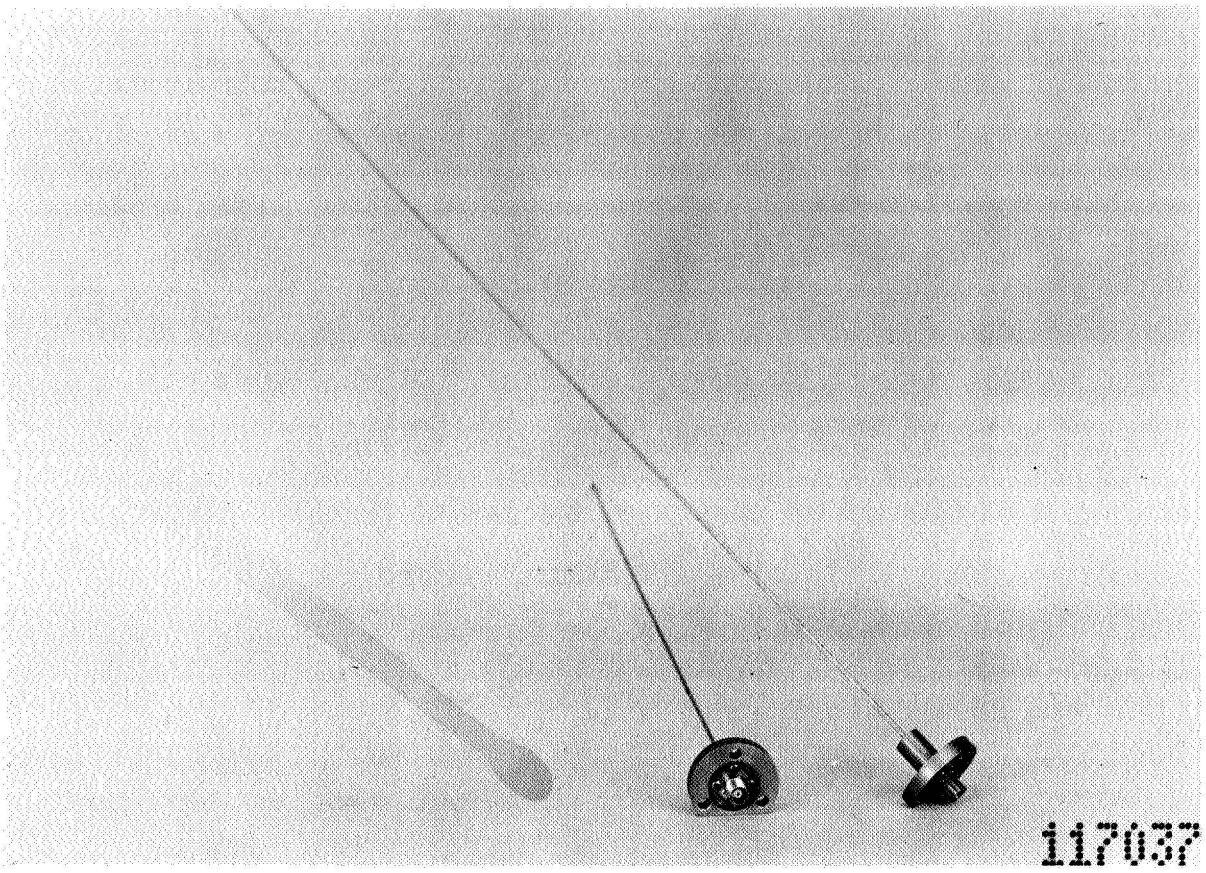


FIGURE 6–19.—Narrowband antenna element (two views).

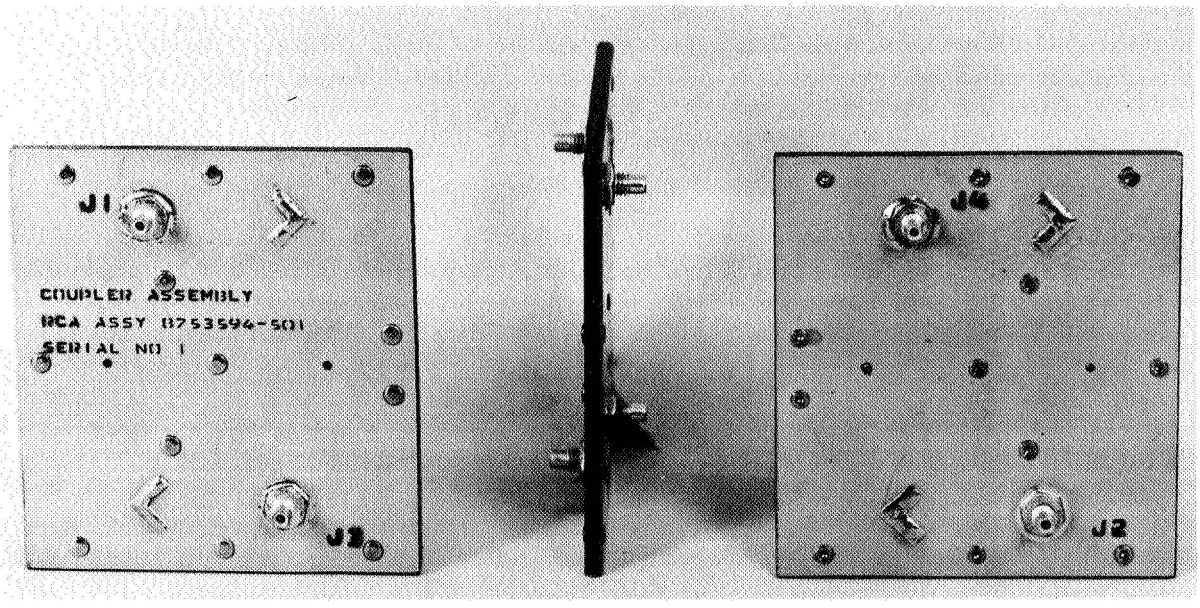


FIGURE 6–20.—Coupler assembly (three views).

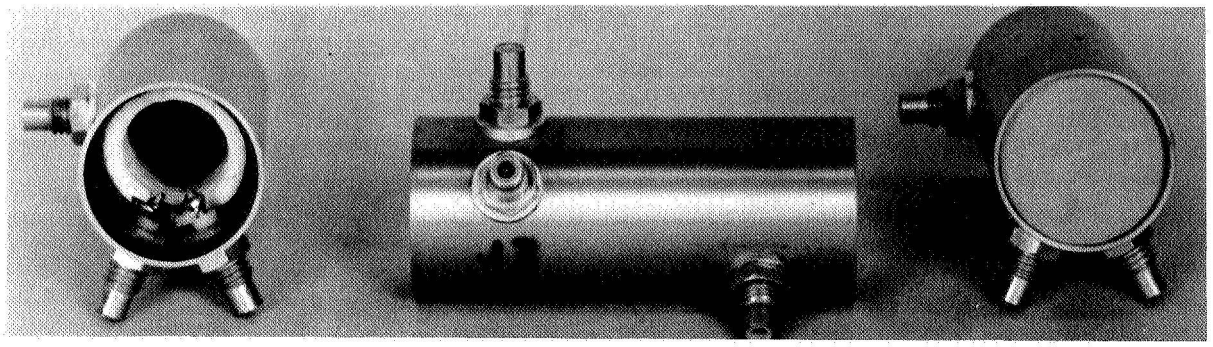


FIGURE 6–21.—Balun Assembly (three views).

tained were the elimination of the filters and a considerable reduction in the weight and complexity of the spacecraft equipment.

During the course of the project, three materials were used for the whips. The original material was C–1085 steel. This was changed to non-magnetic beryllium copper to minimize residual magnetism. The change in material of the whips increased their deflection under spacecraft spin. The earlier steel whips deflected about four inches, while the non-magnetic beryllium-copper whips deflected about eight inches. A rough approximation of this type of deflection at the whip tip showed no severe change in impedance or isolation. However, for reliability reasons this amount of deflection could not be tolerated. A solution was found in the use of pure beryllium.

The feeding and matching network was developed on a mock-up of the spacecraft made of screen-covered wood. This metallic covering was a good conductor. Later, a representative model of the final spacecraft configuration was used to assess its effect on patterns and antenna performance. This model was different from the mockup built at the beginning of the program. The solar panels were electrically insulated from each other and from the structural assembly. The aluminized-mylar sheets at both ends of the spacecraft were insulated from the antennas and from the solar panels. The surface of the aluminized-mylar at the wideband end was not regular ar flat, having an accordion pleat which, under acceleration or pressure variation, could move relative to the antenna.

First tests with the TT&C antennas showed that the impedance was changed markedly and in an erratic manner, indicating circulating currents within the spacecraft. A bonding arrangement was worked out in which sixteen thin aluminum straps joined the eight solar panels to the whip mounting collar. This made an effective ground for currents induced by the radiating whips and established a stable condition. The matching arrangement for the quadrature-fed whips at the telemetry frequency had to be modified, however, to achieve the desired isolation between the two transmitter ports. Patterns were essentially unchanged at the telemetry (136-Mc) frequency. At the command-receive frequency of 148, there was a difference, however. A new set of patterns was taken at this frequency.

Performance Evaluation

After a matching harness design had been achieved, the complete assembly was constructed without further cable changes other than trim adjustments to the two open-circuit stubs, W24 and W25 in Figure 6–18. It was necessary to adjust this length to achieve transmitter isolation. A further adjustment in the location and length of these stubs was necessary on the spacecraft.

The measured values of the antenna characteristics are shown in Table 6–11. Representative patterns are shown in Figures 6–22 through 6–25.

TABLE 6–11.—*Measured Values of TT&C Antenna Characteristics*

Function	Measured value					
	Port on 3-db coupler		Cables to command receiver			
	J1	J2	W1 and W2			
VSWR						
at 135.88 Mc	1.11	1.15				
at 136.88 Mc	1.15	1.15				
at 148.26 Mc	-------	-------	3.15			
Insertion loss						
at 136.38 Mc	0.97 db					
at 148.26 Mc	1.38 db					
	Between points					
	J1 and J2	J1 and W2	J2 and W2	J1 and W3	J2 and W3	
Isolation						
at 135.88 Mc	22	52	36	-------	-------	
at 163.88 Mc	26	51	37	-------	-------	
at 148.26 Mc	-------	-------	-------	40.5	41	
	ϕ					
	—	0°	45°	90°	135°	180°
Axial ratio						
at Θ = 15°	-------	6.0 db	5.3 db	-------	-------	-------
at Θ = 150°	-------	-------	-------	5.9 db	7.3 db	5.5 db
at Θ = 180°	0.8 db	-------	-------	-------	-------	-------

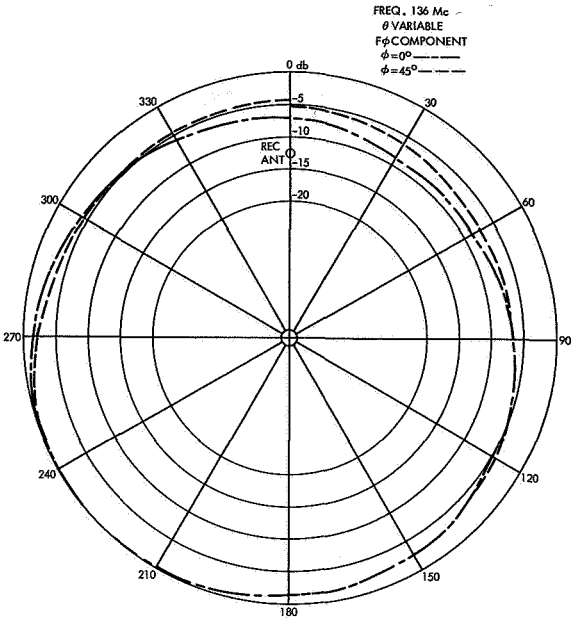


FIGURE 6–23.—ϕ plane telemetry patterns F_ϕ component.

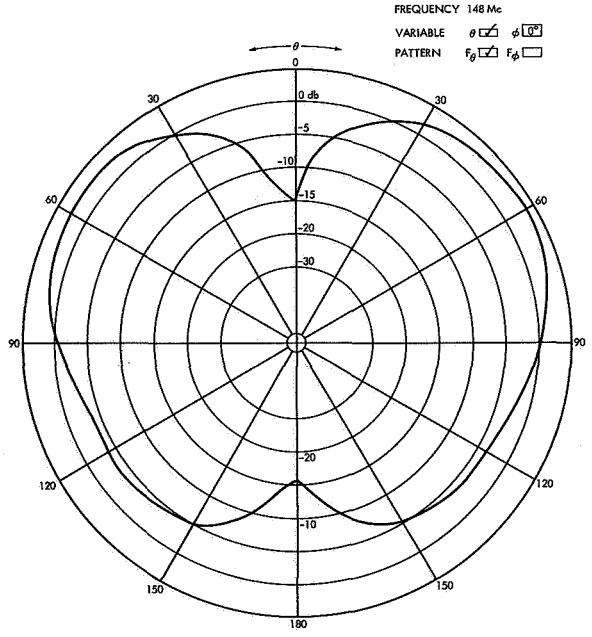


FIGURE 6–22.—Command Receive Pattern.

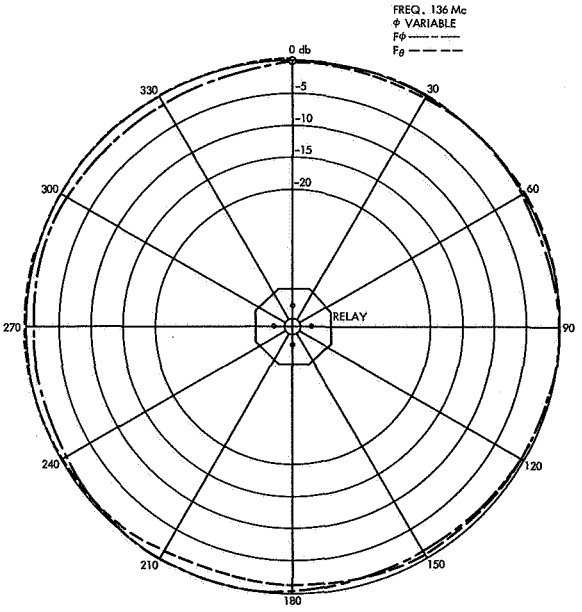


FIGURE 6–24.—ϕ plane telemetry patterns, $F\theta$ $F\phi$ components.

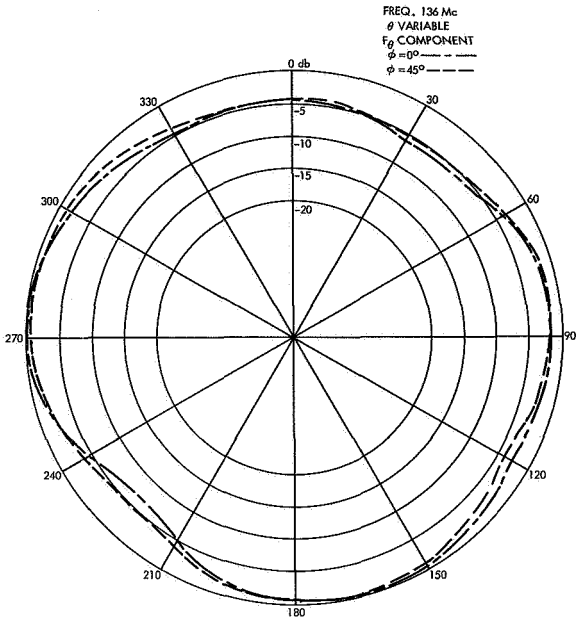


FIGURE 6–25.—ϕ plane telemetry patterns, $F\theta$ component.

AUTHORS. *This chapter was written by* E. MOZZI *and* S. ROTH *of the Radio Corporation of America, Princeton, New Jersey, U.S.A. under contract NAS 5–1272 with NASA/ Goddard Space Flight Center.*

N66-10233

Chapter 7

The Command System

GENERAL

The command system provided support for the radiation experiments, and the communications and attitude control subsystems. This chapter describes the functions performed by the spacecraft command subsystem, both for ground transmitted commands and internal logic. The block diagram of Figure 7–1 illustrates the major elements or functions of the spacecraft command subsystem. For reference, ground elements are also shown.

A VHF signal, containing a coded eight-bit command word, was directed at the spacecraft by the ground antenna. The first two bits were used for word sync and the remaining six bits, constrained to combinations of 3 ONES and 3 ZEROS, contained the command information. The code was applied as a quantized PDM signal in which discrete pulse widths were used to represent SYNC, ONE, and ZERO signals. The PDM signal amplitude modulated a subcarrier which in turn amplitude modulated the VHF carrier.

The VHF signal was received by the spacecraft TT&C (Telemetry, Tracking & Com-

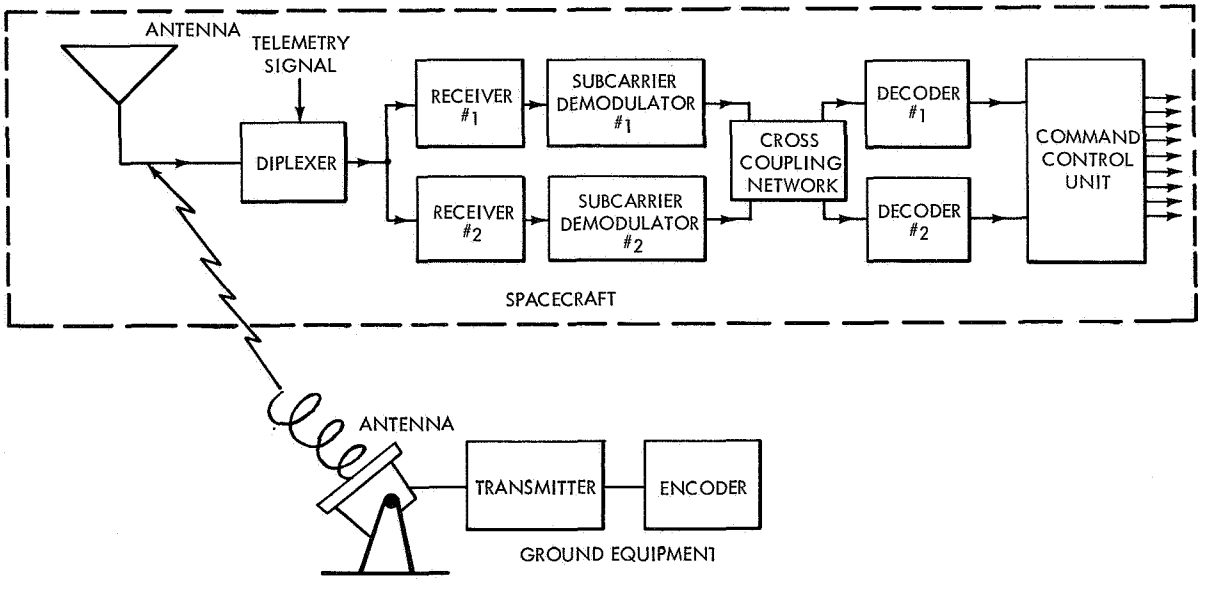


FIGURE 7–1.—Relay I command link, functional block diagram.

mand) antenna (*refer to Chapter 6*). This antenna consisted of an array of four monopoles projecting from the underside of the spacecraft (separation plane). Command and telemetry signals shared the antenna. For the command function the antenna pattern was essentially that of a linearly polarized dipole.

A diplexer performed the function of combining the telemetry and command signals at the antenna. It also provided isolation between telemetry transmitter and command receiver.

The signal was routed to the redundant receivers, which operated independently and in parallel. The receiver detected the VHF carrier and fed the demodulated, PDM modulated subcarrier to the next stage.

The subcarrier demodulator filtered the incoming signal, then demodulated and, finally, reconstructed the original PDM waveform. The cross-coupling network routed the output of each subcarrier demodulator to both decoders. This provided additional reliability, since either receiver and either decoder could simultaneously fail without degradation of the command system.

The decoder accepted the PDM coded signal, verified that the format was correct, and then provided an output pulse corresponding to the desired command. The corresponding pulses from the two decoders were gated at the input to the command control unit. The pulse was then routed to one or more bistable memory elements, setting this memory to the desired state. The outputs of the control unit were either switch closures or dc bias signals controlled by the associated memory elements.

Table 7–1 lists all the direct commands with their respective control circuit outputs. In three cases more than one function is accomplished by a single command, i.e.,:

Command No. 5—Turn off both transponder systems

Command No. 8—Turn on both telemetry transmitters

Command No. 18—Turn off attitude control and horizon scanner

System design also required that repeaters would be turned off automatically after a two-minute delay following removal of the microwave carrier from the repeater. This provided an automatic over-the-horizon turnoff capability which served as backup in the event of direct-command failure.

THE RELAY I COMMAND RECEIVER

Introduction

The function of the RELAY I command receiver was to receive, amplify, and demodulate coded command information received from the control ground station. The PDM commands amplitude modulated the 5.4 kc subcarrier which, in turn, amplitude modulated the 148.26 Mc radio-frequency carrier. The spacecraft employed two command receivers connected in parallel to the command antenna. Each receiver was connected to a command decoder which demodulated the subcarrier command information. The use of reundant command systems increased reliability.

The command receiver was an all-transistorized AM unit employing single conversion and a 20 Mc IF frequency. The receiver occupied two printed circuit boards. One board contained the RF amplifier, crystal oscillator, and mixer; while the other contained the IF amplifier, AGC detector and amplifier, AM demodulator, and power supply regulator (see Figure 7–2). To minimize weight and volume the two receivers were housed in one case.

Design Approach

Some of the major factors considered in the design of the command receivers were:

1. Maximum reliability
2. Minimum power consumption
3. High rejection of suprious signals
4. Minimum weight
5. High sensitivity

Since the receiver was designed to be used in a spacecraft which had to operate successfully for one year or longer, a philosophy of design was adopted which tended to maxi-

TABLE 7-1.—*Direct Commands*

Command		Control circuit output	Remarks
No.	Designation		
1	Load cutoff normal	Open circuit to battery low-voltage cutout sensor	Allows low-voltage cutout circuit to operate normally
2	Load cut-off override	Short circuit to battery low-voltage cutout sensor	Disables low-voltage cutout circuit
3	Transponder #1 ON	Provides turn-on bias signal to transponder #1 voltage regulator	In the event transponder #2 was on when this command was executed transponder #2 will be turned off after the completion of transponder #1 TWT power supply warm-up cycle.
4	Transponder #2 ON	Provides turn-on bias signal to transponder #2 voltage regulator	In the event transponder #1 was on when this command was executed transponder #1 would be turned off after the completion of transponder #2 TWT power supply warm-up cycle.
5	Transponder OFF	Provides turn-off bias signal to both transponder #1 and #2 voltage regulators	
6	TV ON	Provides switch closure to transponders #1 and #2, routing regulated voltage to TV gate	Sets both transponders into the wideband or television mode of operation.
7	Phone ON	Provides switch closure to transponders #1 and #2, routing regulated voltage to phone gate	Sets both transponders into the narrow band or duplex mode of operation.
8	Telemetry transmitters 1 & 2 ON	Provides switch closures which route primary power to both telemetry transmitters	
9	Telemetry transmitter #1 OFF	Opens switch controlling primary power to Tel Xmtr. #1	
10	Telemetry transmitter #2 OFF	Opens switch controlling primary power to Tel. Xmtr. #2	
11	Radiation experiment ON	Provides turn-on bias level to rad. exp. voltage regulator	
12	Radiation experiment OFF	Provides turn-off bias level to rad. exp. voltage regulator	
13	Telemetry encoder ON	Provides turn-on bias to telemetry encoder	Automatically opens power switch to Horizon scanner
14	Telemetry encoder OFF	Provides turn-off bias to telemetry encoder	
15	Horizon scanner ON	Provides switch enclosure which applies primary power to horizon scanner	Automatically applies turn off bias to telemetry encoder
16	Attitude control current positive	Provides current source to attitude control coil in POS direction	Automatically locks out 17
17	Attitude control current negative	Provides current source to attitude control coil in NEG direction	Automatically locks out 16
18	Attitude control off and horizon scanner off	Removes current source from attitude control coil. Remove primary power from horizon scanner.	
19	Modulate tel. Xmtr #1	Gates the outputs from the tel. encoder and horizon scanner to tel. Xmtr. #1	
20	Modulate tel. Xmtr. #2	Gates the outputs from the tel. encoder and horizon scanner to tel. Xmtr. #2	

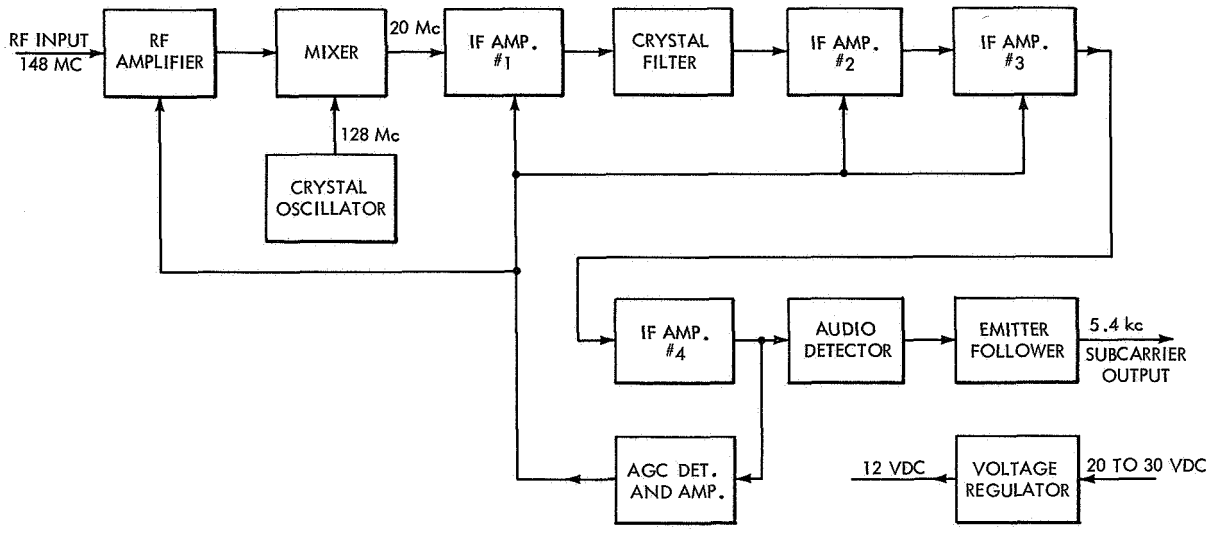


FIGURE 7–2.—Relay I command receiver, block diagram.

mize the reliability of the unit. Only proven reliable parts, thermally aged before assembly, were used. For improved life, components were operated at 10 percent of rated dissipation, while circuit designs were chosen to produce the desired electrical operation with a minimum of parts. Printed circuits were employed to ensure the receiver's uniformity in manufacture and electrical performance.

To minimize the dc power consumption of the command receiver, IF amplifier stages were designed to operate in a starved condition with an emitter current of 0.5 ma. The 2N384 drift transistors were used in the IF amplifier because they exhibited desirable reverse AGC properties. Reverse AGC was chosen over forward AGC because the transistors could be operated with about one quarter the quiescent current required for forward AGC. The only disadvantage of reverse AGC is a tendency to overload due to strong input signals; however, the strongest received RF signal was expected to be in the order of 100 microvolts. AGC was also applied to the RF amplifier to increase the strong signal capability of the receiver resulting in an overload level of 50,000 microvolts.

Extremely sharp selectivity of the receiver was obtained by using a crystal filter in the IF amplifier. The 6 db bandwidth of the filter was 40 kc, and the 60 db bandwidth was less than 100 kc. Each IF amplifier was designed with a bandwidth of about 700 kc; thus the overall bandpass characteristic of the IF amplifier was determined only by the crystal filter. This design eliminated shift in bandwidth and IF center frequency due to AGC action, temperature, and transistor variations.

The receiver included an RF amplifier preceding the mixer to obtain a low noise figure, (7 db) and high input-frequency selectivity. To obtain selectivity, some sensitivity was sacrificed in the input RF filter. A loss of 1.5 db in the input network was tolerated to obtain image and spurious repection of 50 db minimum.

To minimize weight, two receivers are enclosed in one case. The weight of the receiver package was 2 pounds.

Receiver Description

A block diagram of the Relay I command receiver is shown in Figure 7–2. The 148.26-Mc signal from the antenna (divided between the two receivers) was first amplified by the RF amplifier which consisted of a 2N1405 transistor in a grounded emitter

circuit. This amplifier provided 15 db gain with an average noise figure of 7 db. RF selectivity was provided by three single tuned circuits which resulted in a 3-db bandwidth of 4 Mc at the input frequency. All spurious responses were down 50 db or more.

The amplified RF signal was fed into the transistor mixer where it was heterodyned with the 128.26-Mc, 5th overtone, crystal oscillator to produce the 20-Mc IF. The mixer included a 2N1405 transistor biased near cutoff to produce mixing action along with a 15-db gain at 20 Mc. The collector contained a 20-Mc tuned transformer to separate the IF and feed this signal into the IF amplifier.

The IF amplifier consisted of four stages utilizing 2N384 transistors as common emitter amplifiers. Interstage coupling was accomplished by single tuned transformers, and a crystal filter was inserted between the first and second IF amplifier. The bandwidth of each IF amplifier stage was 700 kc and all were synchronously tuned to 20 Mc. The crystal filter, having a 6-db bandwidth of 40 kc and a 60-db bandwith of 100 kc maximum, determined the over-all frequency response of the IF amplifier. Reverse AGC was applied to the first three stages of the amplifier, which were biased to draw 0.5 ma of current each. The fourth IF amplifier was a driver for the AGC detector and audio detector, and was not connected to the AGC control.

Separate detectors were used for AGC and for demodulation of the carrier information to optimize each for its particular function. Carrier demodulation was accomplished by the base-to-emitter diode of a transistor. The transistor, biased close to cutoff, demodulated the signal and amplified the demodulated information. Low-frequency feedback from the transistor collector reduced demodulator distortions. A graph of total receiver harmonic distortion for inputs modulated 50 percent and 90 percent is shown in Figure 7–3. Frequency response of the demodulator and audio amplifier, as shown in Figure 7–4, extended out to 20 kc.

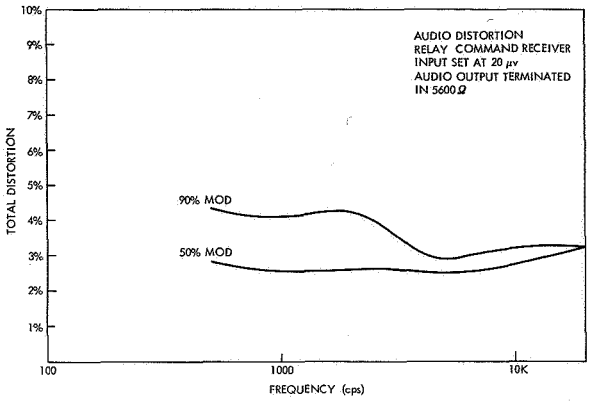


FIGURE 7–3.—Audio distortion, Relay I command receiver.

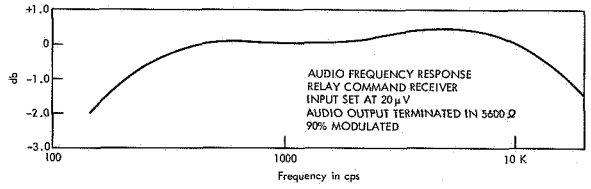


FIGURE 7–4.—Audio frequency response Relay command receiver.

The audio output from the demodulator was fed to an emitter follower amplifier and then to an isolation transformer.

AGC voltage was developed by a transistor using the base-to-emitter diode as a peak detector. No bias was applied to the transistor so that conduction occurred only when the peak IF signal rose above 0.7 volts. This detected voltage was filtered, amplified and applied to the RF and IF amplifiers to control the receiver gain. The AGC was designed to reduce amplifier gain by decreasing transistor emitter current. Figure 7–5 shows the receiver AGC operation at temperatures of −15°, +25° and 35°C. AGC action started for input signals between 1 and 2 microvolts and held the receiver output constant ±1.5 db for input signals between 2 and 10,000 microvolts.

A voltage regulator was incorporated which supplied −12 volts dc to all stages of the receiver. This regulator permitted operation of the command receiver from an unregulated voltage of 20 to 35 volts. A

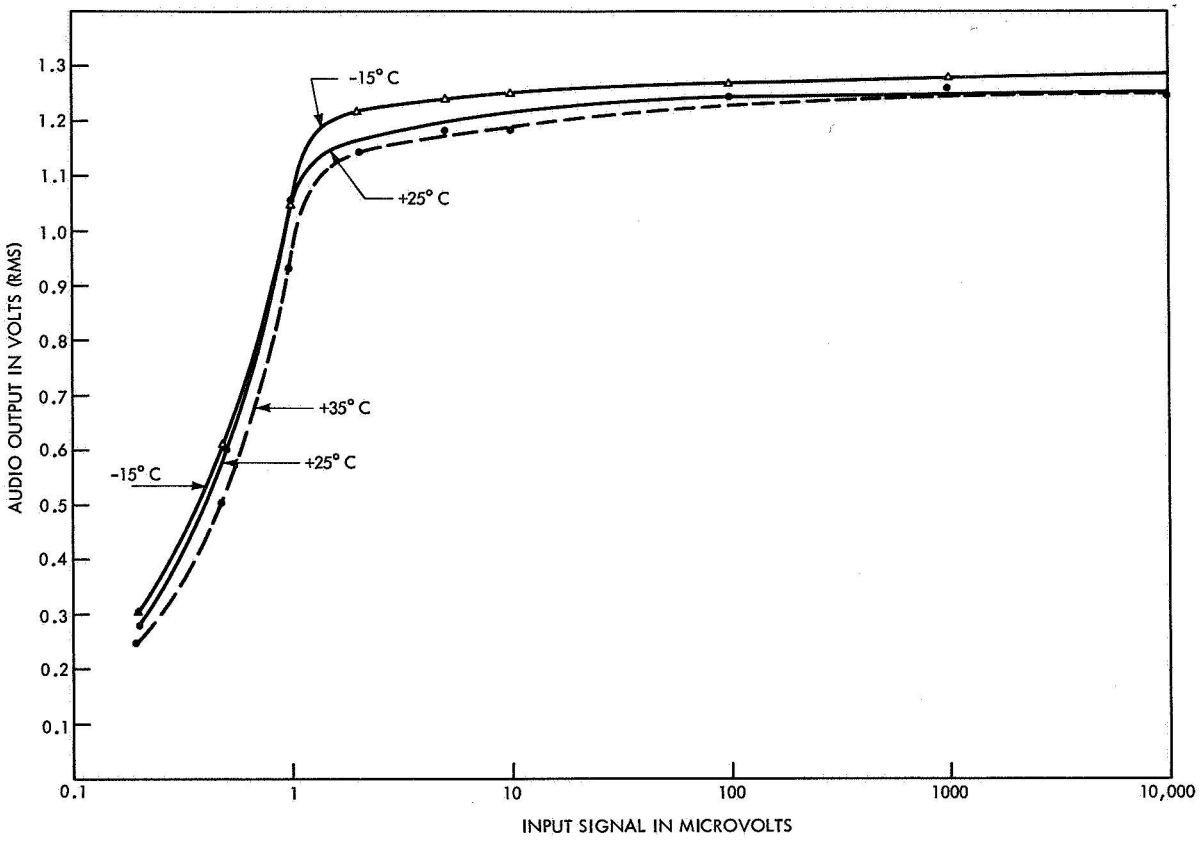


FIGURE 7–5.—Audio output vs. input signal.

TABLE 7–2.—*Parameters for the Relay Command Receiver*

Input frequency band	148 megacycles
Modulation	AM
Noise figure	Typical, 7 db; maximum 10 db
IF frequency	20 megacycles
IF selectivity	40 kc bandwidth, 6 db down; 100 kc bandwidth, 60 db down
Spurious rejection	Down 50 db or more
Input impedance	50 ohms
Audio output impedance	2000 ohms
Voltage gain	120 db ± 3 db over temperature range from −10°C to +60°C
Audio output voltage for 90% modulation at 1 kc	1 volt, RMS
Oscillator stability (−10°C to +60C)	±0.005%
AGC dynamic range	Audio output constant to ±1.5 db for input signal between 2.0 and 10,000 microvolts
Overload level	50,000 microvolts
Power supply	15 milliamperes at 24 volts, dc
Power-supply regulation	Receiver has internal regulator to permit operation from 20 to 35 volts
Operating temperature range	−15° C to +60° C
Weight	2 pounds (two receivers)

summary of command receiver specifications in presented in Table 7–2.

Command Receiver Packaging

The command receiver was divided into two sections, each employing printed circuit boards. The RF amplifier, mixer, and crystal oscillator were assembled on one (see Figure 7–6); while the IF amplifier, AGC and audio detectors, audio amplifier, and voltage regulator were assembled on the other (see Figure 7–7); and both were assembled into one case (see Figure 7–8). A

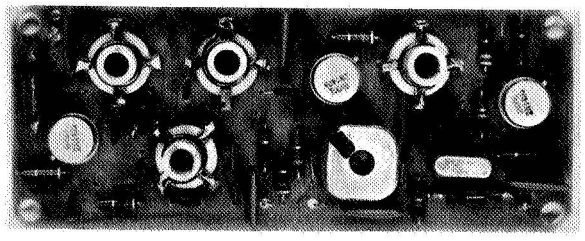


FIGURE 7–6.—RF amplifier, mixer and crystal oscillator board.

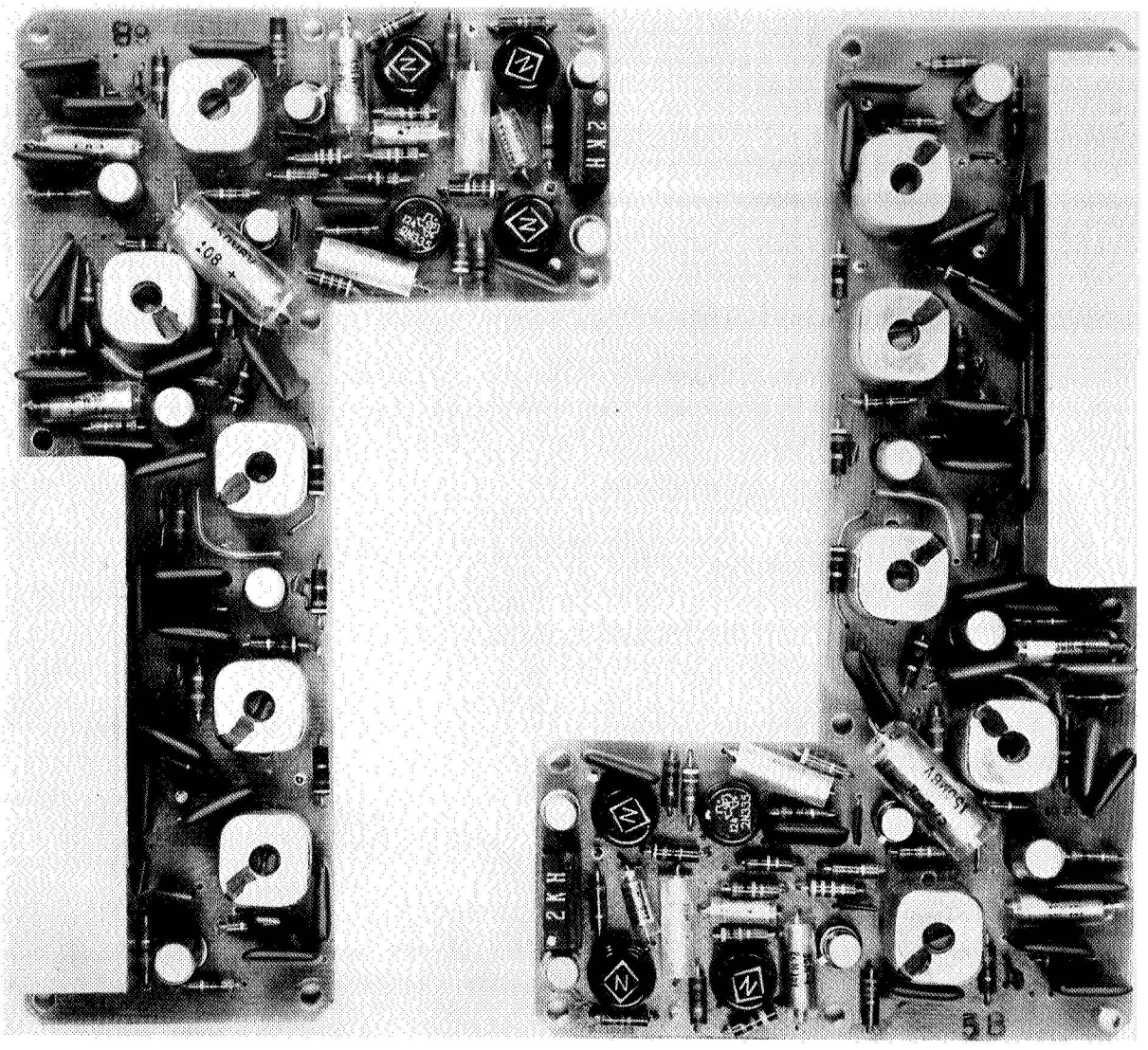


FIGURE 7–7.—IF amplifier, AGC and audio detectors, audio amplifier and voltage regulator board.

center partition, serving as a ground plane for each receiver, was bypassed to the metal case through capacitors, thus providing isolation between the receiver power supply and the case. Positive or negative power supply could be used with the command receiver.

Environment Testing

Prior to environmental testing all components on the printed circuit boards were secured with Thiokol Solithane 113. A description of the protoype and acceptance environmental tests for the RELAY I command receiver are described in Chapter 9.

THE COMMAND DEMODULATOR AND DECODER

To command satellites, the National Aeronautics and Space Administration (NASA) developed a coded message sequence consisting of discrete, pulse-duration-modulated (PDM) tone bursts. The message consisted of a sync pulse, followed by some combination of six pulses, containing three each of ZERO'S and ONE'S. This code permitted

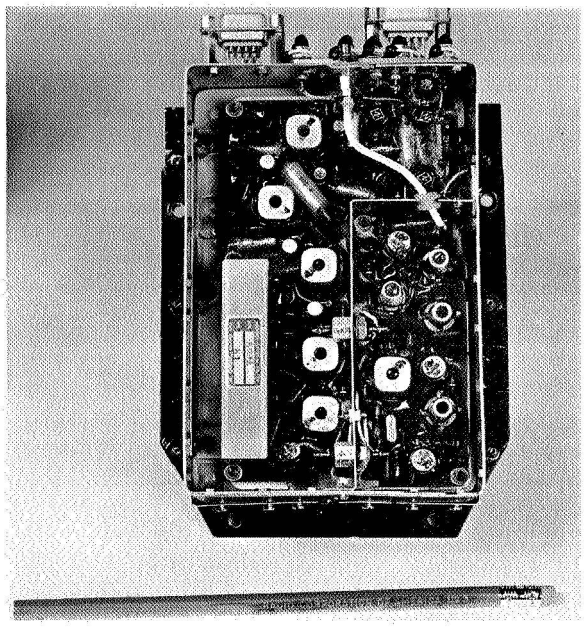


FIGURE 7–8.—Command receiver assembly.

twenty commands.

Equipment developed for the Relay satellite program demodulated the tone bursts, converted the pulse-duration modulation into a binary code, and then decoded the message into twenty discrete commands. The demodulation and PDM-to-binary code conversion functions were accomplished by conventional transistorized circuitry. The circuitry for converting the code into command pulses was a novel utilization of magnetic circuitry. Magnetic cores, used to provide a shift register function, also performed the decoding; and thus eliminated the conventional diode matrix usually employed.

Introduction

The function of the Relay space vehicle command decoder was to accept the command code from the command receiver, demodulate, decode, and provide signals to the control circuit in a form to actuate bistable memory elements. The code was specified by NASA; and was designed to provide a maximum of protection against spurious triggering of command circuits while employing a relatively narrow bandwidth. The basic code consisted of a sync signal, followed by a combination of three one's and three zero's, which permitted twenty commands. The basic code was then transformed into a sequence of pulse - duration - modulated (PDM) bursts of 5451-cps subcarrier tone. A representative (PDM) code sequence is shown in Figure 7–9.

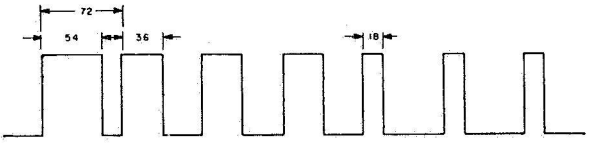


FIGURE 7–9.—PDM subcarrier CPS.

The sequence consisted of eight equal time slots (T) ; the first containing no modulation. The second time slot contained the sync signal, a tone burst three quarters of the time T in duration. This was followed by the three ONE'S and three ZERO'S (ZERO being one quarter of T and a ONE, one-half T in duration). The basic time T was 72 cycles of the subcarrier, or 13.2 msec. This code sequence was then repeated five times to a complete command signal.

The subcarrier tone ampliture-modulated a VHF carrier for transmission to the vehicle. The command receiver demodulated the VHF carrier, and provided the PDM subcarrier tone to the decoder.

Design Objectives

The objective was to design a circuit providing maximum utilization of the noise-immunity properties of the code within the familiar constraints of space vehicle equipment:

1. Maximum reliability
2. Minimum weight
3. Minimum power consumption
4. Minimum volume

These constraints obviously dictated the use of solid-state circuitry. Silicon transistors and diodes were used throughout to minimize the effects of temperature variations. Printed circuits were employed to minimize weight and volume. Conformal

coating was applied to all components to provide protection from vibration during the launch phase. The most reliable components known were used, and inprocess inspections were employed at many steps in fabrication.

Design Approach

In the initial phase, the unit was broken down into three major functions: (1) the subcarrier demodulator, which stripped the PDM from the subcarrier tone; (2) the PDM-to-PCM converter, which transformed the PDM pulses into sync, ONE and ZERO pulses; and (3) the decoder, which transformed the pulse combinations into unique command pulses to drive the memory elements in the control circuit.

In the demodulator, the signal was filtered, amplified, demodulated, and regenerated by means of a Schmitt trigger circuit. The Schmitt circuit output was cross-coupled to a redundant decoder. The Relay vehicle contained redundant command receivers and decoders; and the cross-coupling allowed the command system to function with any receiver and decoder combination. A squelch circuit was incorporated into the demodulator, operating on the average power level in the subcarrier tone. This squelch circuit operated a switch supplying power to the succeeding stages in its own unit and to the corresponding stages in the redundant unit. The squelch had two purposes: (1) to increase the life of the affected stages by removing electrical stress from the components, and (2) to remove the possibility of a spurious command due to noise when a subcarrier tone is not present. The squelch circuit held a time constant of about 10 percent of a message sequence; therefore, the first of the five identical sequences would not get through. However, there was a high probability that one of the succeeding four sequences would activate the command.

In the PDM-to-PCM converter, the pulse from the Schmitt trigger gated-on a free-running multivibrator. The output of the multivibrator was fed to a binary counter, determining whether the PDM pulse was a ZERO, ONE, or a SYNC signal.

In the decoder stages, the ZERO'S and ONE'S were fed into a magnetic shift register. Simultaneously, the ZERO'S and ONE'S were counted in separate counters to insure that the message contains three ONE'S and three ZERO'S. The sync pulse reset these counters and activated a delay circuit. The outputs of the counters and gate circuit associated with the delay circuit were *anded* together to activate the read switch for the shift register. This insured that a message sequence contain three ZERO'S and three ONE'S within a specified length of time—otherwise the message was rejected. (The only way for a false command to be effected on a proper command's transmittal, is the unlikely probability that a ONE be transformed into a ZERO, and a ZERO into a ONE) . . . The conventional means of decoding the message would employ a transistor shift register operating into a diode matrix. Using the magnetic shift register in a novel configuration eliminated the need for the decode matrix, thus considerably reducing the number of semi-conductors required in the unit.

Operational Description

A functional block diagram of the decoder is shown in Figure 7–10. The PDM-modulated subcarrier tone from the receiver was fed to a 5451-cps band-pass filter with a 15 percent bandwith. Then the signal was amplified and applied to a slicer amplifier stage, wherein the power level of the subcarrier tone was detected for application to the squelch circuit. Sliced at approximately the 50 percent level, the signal was then demodulated in a transistor collector detector, and fed to the Schmitt trigger for PDM signal regeneration. At that point, the signal was cross-coupled to the redundant decoder.

The PDM pulse was then amplified and used to activate a free running multivibrator. The PDM pulse was *and* gated with the output of the multivibrator to produce one, two, or three pulses according to the ZERO, ONE or SYNC signal of the PDM pulse.

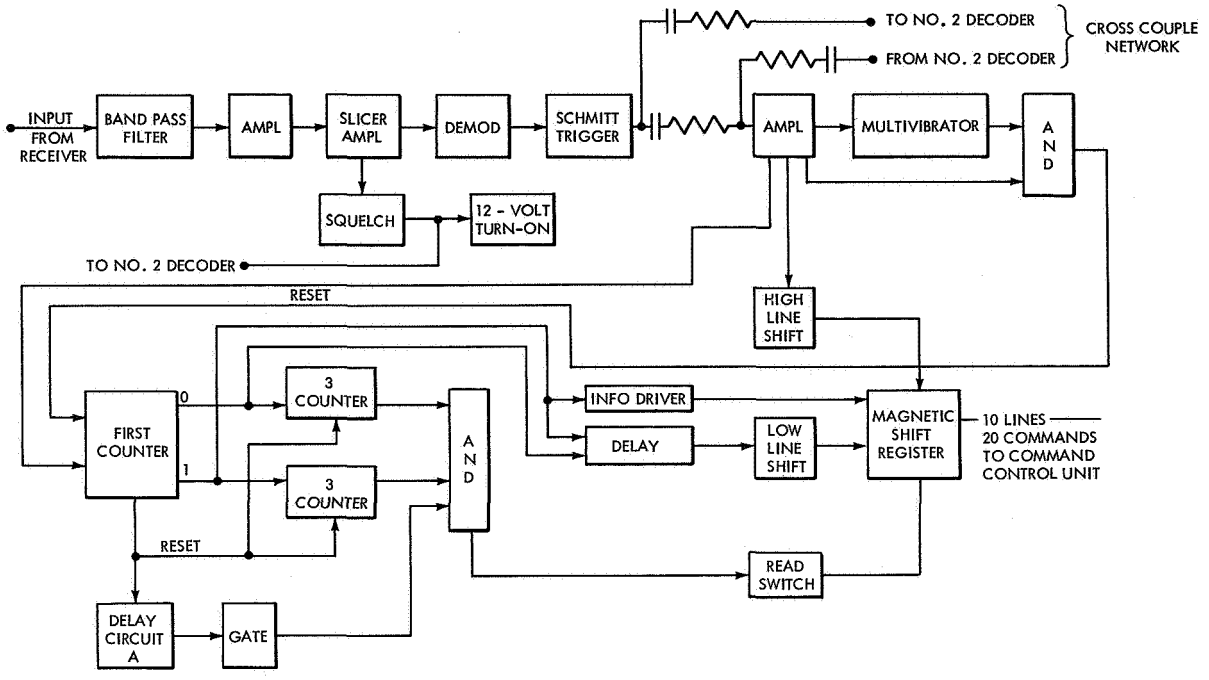


FIGURE 7–10. Decoder block diagram.

The pulses from the multivibrator were fed to a counter having three outputs corresponding to ZERO, ONE, or SYNC. The counter was reset by the leading edge of the original PDM pulse.

Each of the ZEROS and ONES were fed to 3 counters. The 3 counter emitted the proper signal level only when three pulses had been counted. The SYNC signal reset the 3 counters at the beginning of each message sequence. Also the sync signal actuated a delay circuit whose output was *anded* together with the outputs of the 3 counters, to trigger the read switch.

Then ZERO'S and ONE'S are fed to a 2-cores-per-bit magnetic shift register. A circuit diagram illustrating 2 of the 6 bits of the shift register is shown in Figure 7–11.

The timing diagram (see Figure 7–12) shows the order in which each pulse was received. Receipt of a ONE triggered CR2 (see Figure 7–11). This discharged C2 through the 10-turn winding on Core 1, setting that core to state one. When C2 was fully discharged, CR2 opened up, allowing C2 to charge through R2; and the circuit was readied for the next reset pulse. The negative pulse from C2 was delayed and inverted, then used to trigger CR3. When C3 discharged through the 2-turn shift windings, all transistors on the low line whose cores were in state ONE, conducted, setting the core immediately above and to the right of state ONE. When the high-line trigger pulse activated CR_1, this process repeated, moving the ONE'S down to the low line. When a transistor conducted, its own core was set to state ZERO. Through this procedure, all information (ZERO'S and ONE'S) advanced one position whenever a low- and high-line trigger pulse was received. (In the timing diagram, the high-line trigger is shown to occur at the leading edge of the PDM code pulses. This pulse is obtained by differentiating the leading edge of this PDM pulse, and is equivalent to another delay circuit after the low-line trigger pulse.)

The decoding function was accomplished in the magnetic shift register by the use of readout windings on low-line cores. Each core had ten readout windings. These windings were connected as shown in Figure

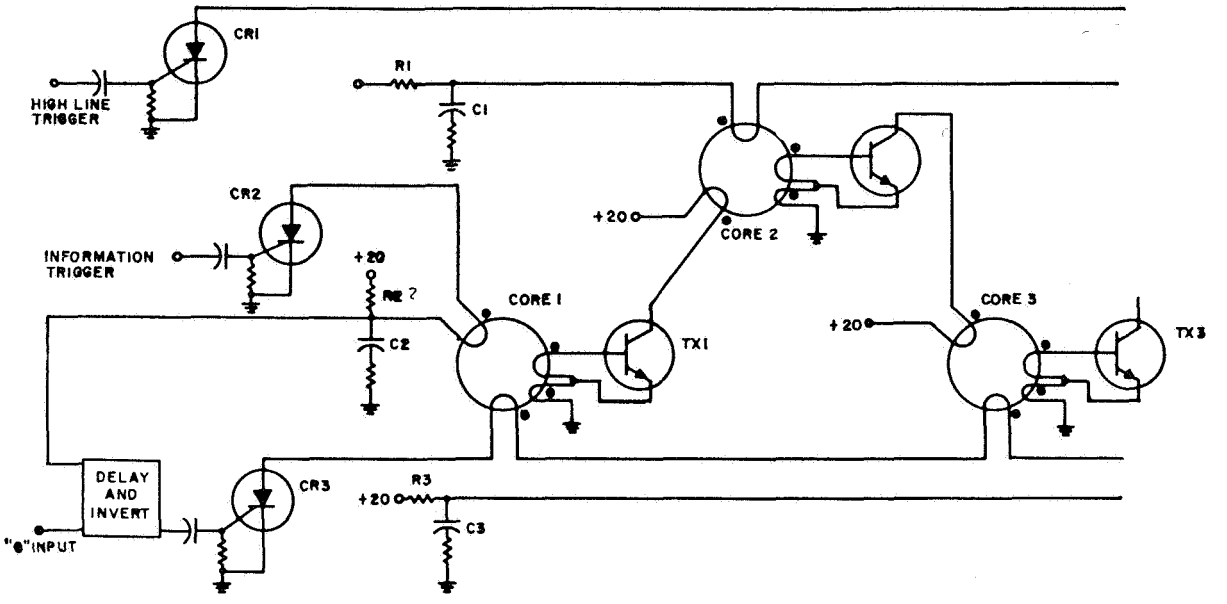


FIGURE 7–11.—Two stages of shift register.

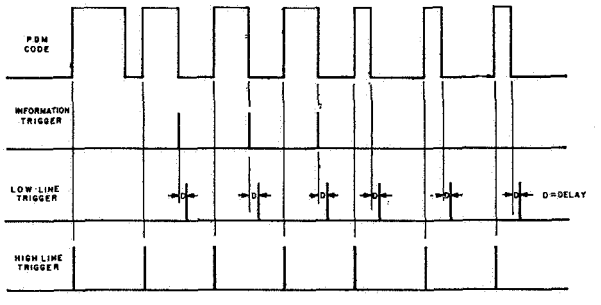


FIGURE 7–12.—Timing diagram for decoder, shift register.

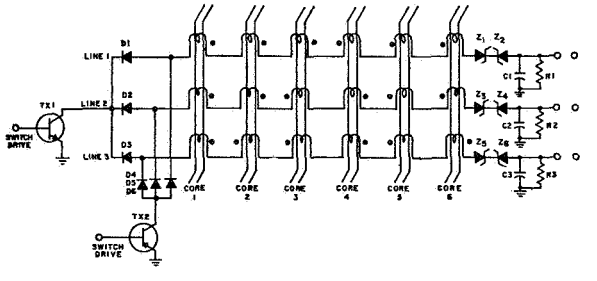


FIGURE 7–13.—Schematic diagram of three readout lines.

7–13. (For simplicity, only three of the ten lines are shown.) Only ten lines and not twenty were required, since a particular code and its complementary code used the same set of windings. The complementary code produced a pulse of opposite polarity. Thus, ten output lines, each capable of producing a positive or negative pulse, yielded twenty command pulses.

In each line of windings, three of the windings were wound in one direction on the cores, and three in the opposite. When a shift pulse occurred, those cores storing a ONE changed state and induced a voltage in all of the output windings on that core, the polarity determined by the direction of winding. To explain the operation of the decoding process, assume that in Figure 7–13, the first three cores store ONE'S, and the last three, ZERO'S. When the cores shifted, one unit of voltage was induced in each core winding with a ONE. Therefore, +3 units of voltage were induced on line 1. A +1 unit of voltage was induced on line 2. Core 3 is wound opposite to cores 1 and 2. On line 3, the voltage was a −1 unit. In every core, where there were three ONES and three ZEROS stored in the register, only one line held a three-unit voltage and all other lines had induced either a plus or minus-one unit voltage. Zener diodes at the end of each line blocked the one-unit volt-

ages, allowing only voltages of the three-level to pass. A code of 000111 meant that ONE'S stored in the last three cores would produce a negative pulse on line 1, of 3 units in amplitude. Codes 110100 and 001011 would produce positive and negative pulses, respectively, on line 2. The codes for line 3 would be 100101 and 011010. The read windings were normally open, that is, transistors TX1 and TX2 were cut off, inhibiting pulses on the output lines during the shifting of a code into the register. (To illustrate, when the two "3" counters on Figure 7–10 have each been set, and the sync-delay-circuit gate has been set, the transistors TX1 and TX2 will be conducting and the output command can be read out.)

Equipment Performance

The performance of the equipment in the presence of noise is indicated by the oscillo-

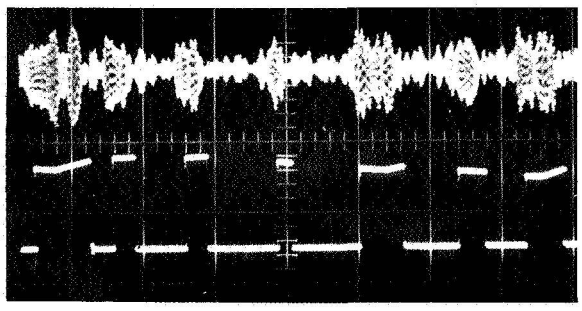


FIGURE 7–14.—Waveforms in the presence of noise.

grams of Figure 7–14. The upper trace shows the PDM-modulated subcarrier after the band-pass filter. The lower trace shows the regenerated PDM pulse out of the Schmitt trigger. In an oscillogram of the signal prior to filtering, the signal would have been indistinguishable since the receiver had approximately 10-kc response. The filter had an 810-cps bandwidth, providing an 11-db improvement in SNR. Other performance characteristics of the finished equipment are summarized in Table 7–3.

The layout of the components was made on three printed-circuit boards, each one corresponding roughly to the three functions of demodulation, PDM-to-PCM conversion and decoding. Figure 7–15 shows the demodulation board at the upper left, the PDM-to-PCM board at the right, and the magnetic decoder at the lower left.

TABLE 7–3—*Summary of Equipment Performance Characteristics*

Weight	1.5 pounds
Size	4 × 4 × 2.5 inches
Supply voltage	20 to 36 v
Power consumption at 28 v	
Idle	225 mw
When commanded	560 mw
Input impedance	10 K at 5451 cps
Input signal level	0.25 to 1 v RMS Threshold of the squelch circuit can be set anywhere in this range.
Output signal amplitude	4 v minimum 8 v maximum
Output pulse shape	Discharge of a 0.002 μf capacitor. width determined by resistive load.
Reliability	MTBF (calculated) 20,000 hours
Temperature range	−30°C to +80°C

COMMAND CONTROL UNIT

Introduction

The function of the command control unit was to accept the decoded commands from the decoder, and to initiate the performance of the command. This was accomplished by storing the decoded commands in bistable memories and by operating transistor power switches according to the state of the memories. In most cases, and on-off command function was accomplished by directly switching the power to the desired subsystem. However, in the wideband subsystem, the radiation experiments, and the telemetry encoder, the command control circuit supplied only an on-off signal.

Beyond the switching functions performed in the control circuit, several other outputs were provided:

1. *Command verification* — Four discrete telemetry voltages indicating the state of the command control memory.

2. *Third stage separation indication* — A telemetry voltage indicating separation of the third stage.

3. *Command Receiver AGC*—The voltage from the command receiver amplified in the

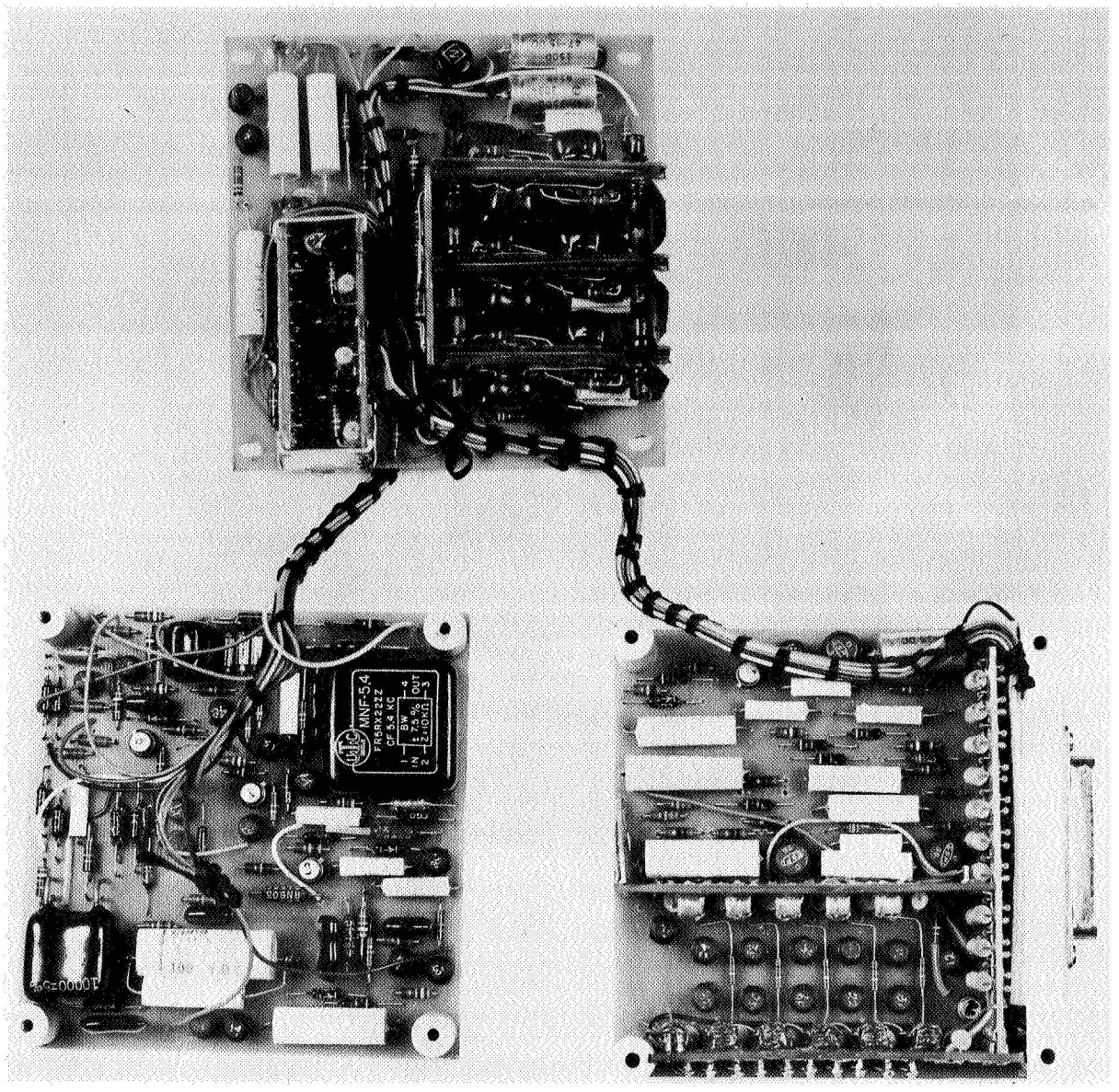


FIGURE 7-15.—Circuit boards showing layout of components.

command control unit and presented as a telemetry voltage.

4. *Initial state set*—An arrangement by which the command control circuit might be reset to its initial state prior to launch. (This was done manually rather than by command.)

Also, certain logic was incorporated within the control circuit to perform the following functions:

1. *Wideband subsystem shutdown*
   a. *Low Voltage*—Shutdown would occur when the unregulated bus fell below some nominal preset level. (Shutdown could be inhibited by command from earth).
   b. *Low Signal Received* — Shutdown would occur when signal strength in the receiver fell below some nominal level

for a period of more than two minutes. (The timers which provided the shutdown signal could be reset by repeating the "ON" command to the respective wideband subsystem.)

2. *Pulse steering* logic which assured that only one wideband subsystem could be on at a time, and that the telemetry transmitter was modulated by only one signal.

Design Approach

Certain trade-offs in weight, volume and power consumption were made to emphasize reliability. Unlike the command decoder and receiver, only one command control unit was included in the command system. Since spacecraft operation depended upon the ability of the control unit to perform reliably, certain circuits contained an augmented number of components where the added components provided an extra margin of safety. For example, the design of a redundant voltage regulator for the command control unit eliminated the possibility of the voltage regulator failing from a single component failure. Additional considerations for higher reliability included:

1. *Power Dissipation*—Not to exceed 10 percent in any component.

2. *Minimum Beta Assumed* — The minimum transistor beta assumed in the design was 10, i.e., the circuits would continue to operate as designed for betas as low as 10 in the transistors. (All transistors actually used had betas of greater than 30.)

3. *Parts Tolerance*—Within ± 5 percent of design value following preconditioning. All circuits were designed to operate reliably with a drift not to exceed ± 10 percent from the design value.

Power consumption was minimized within limits consistent with reliable design. Since the majority of the transistors in the command control unit were operated in either a saturated or cut-off condition, the minimum-beta assumption resulted in more drive current being supplied than required. This provided an added reliability margin; and the additional power required was not significant in relation to over-all spacecraft requirements.

Control Box Description

A block diagram of command control circuits, illustrating the operational description of the command control box is shown in Figure 7–16); a functional listing of commands is provided in Table 7–1. Note that input lines are paired, with redundant signals supplied from the two decoders. The flip-flop inverts incoming data: the number 1 output (upper line) is negative and number 2 (lower line) is positive when the number 1 input is positive. Similarly, both the level-detector and power-switch circuits invert the relative polarity: grounding the input results in a positive output while a positive input (above +6.8 vdc) results in zero output.

Command Inputs to the Command Control Unit

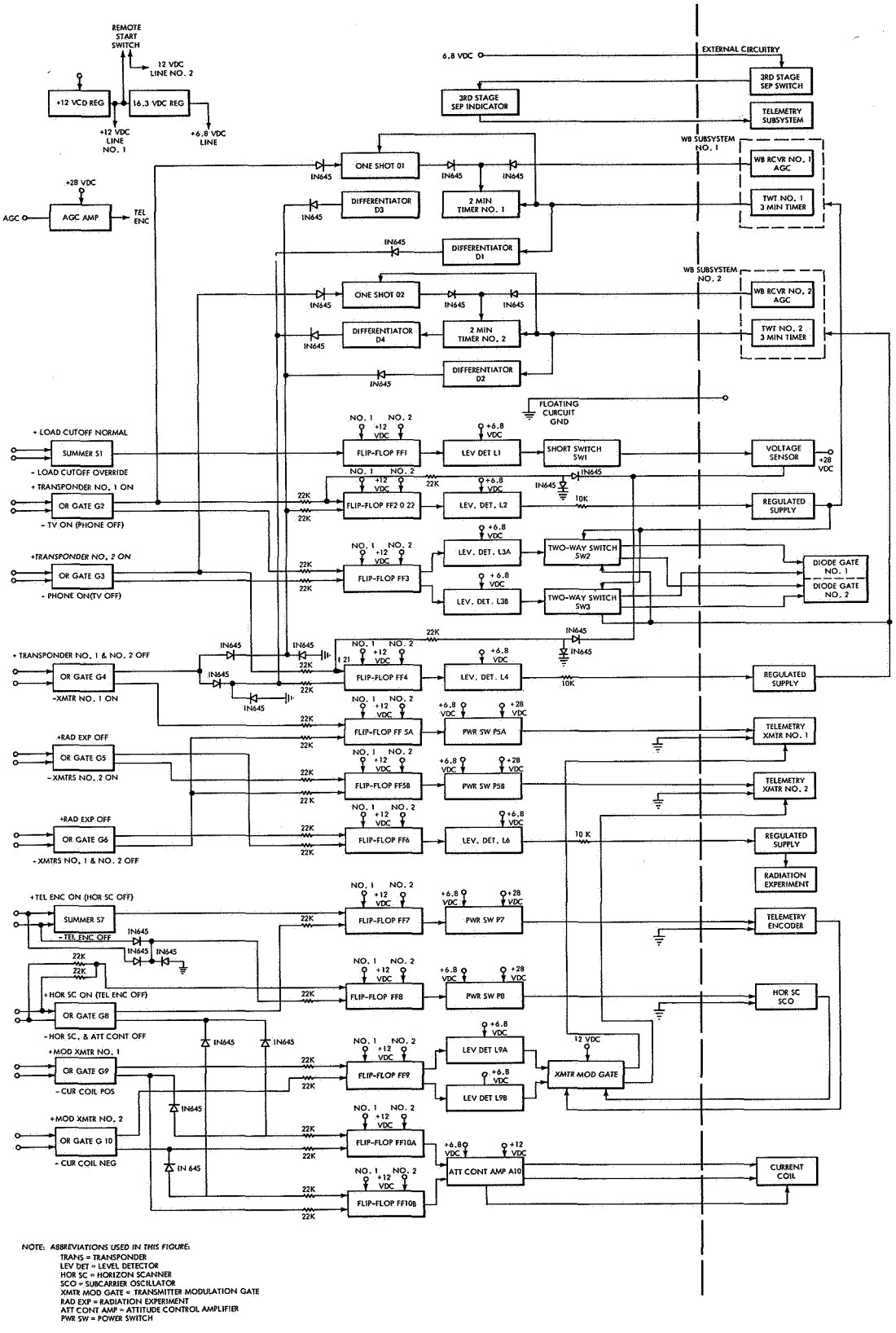
Each of the ten input channels of the command control unit served two commands, receiving inputs and producing corresponding outputs:

1. *Input Channel 1*—A positive input pulse, the Load-Cutoff-Normal signal, resulted in an open circuit (to ground) on the output lead. A negative input pulse, the Load-Cutoff-Override signal, resulted in a short circuit to ground on the output lead.

2. *Input Channel 2*—A positive input pulse, the Transponder 1 ON signal, provided a signal of zero volts to turn on the regulated supply. A negative input pulse, the TV ON-Phone OFF signal, reversed the polarity of the voltages supplied to the wideband system diode mode gate.

3. *Input Channel 3*—A positive input pulse, the Transponder 2 ON signal, provided a signal of zero volts to turn on the regulated supply. A negative input pulse, the Phone ON-TV OFF signal, provided the opposite polarity to the wideband system diode mode gate.

4. *Input Channel 4*—A positive input pulse, the Transponders 1 and 2 OFF signal, provided a 6 vdc output level signal to turn off both regulated power supplies for the trans-



NOTE: ABBREVIATIONS USED IN THIS FIGURE:
TRANS = TRANSPONDER
LEV DET = LEVEL DETECTOR
HOR SC = HORIZON SCANNER
SCO = SUBCARRIER OSCILLATOR
XMTR MOD GATE = TRANSMITTER MODULATION GATE
RAD EXP = RADIATION EXPERIMENT
ATT CONT AMP = ATTITUDE CONTROL AMPLIFIER
PWR SW = POWER SWITCH

FIGURE 7–16.—Command control unit, functional block diagram.

ponders. A negative input pulse, the Transmitter No. 1 OFF signal, removed input power from telemetry tranmitter No. 1.

5. *Input Channel 5*—A positive input pulse, the Radiation Experiment OFF signal, provided +6 vdc output signal to remove power from the radiation experiment regulated supply. A negative input pulse, the Transmitter No. 2 OFF signal, removes input power from telemetry transmitter No. 2.

6. *Input Channel 6* — A positive input pulse, the Radiation Experiment ON signal, cuts off the radiation experiment regulator. A negative input pulse, the Transmitters No. 1 and No. 2 ON signal, provided +28 vdc power input to each of the telemetry transmitters.

7. *Input Channel 7*—A positive input pulse, the Telemetry Encoder ON-Horizon Scanner OFF signal, provided +28 vdc to the telemetry encoder, and removed power from the horizon scanner and subcarrier oscillator. A negative pulse, the Telemetry Encoder OFF signal, removed power from the telemetry encoder.

8. *Input Channel 8*—A positive input pulse, the Horizon Scanner ON and Telemetry Encoder OFF signal, provided +28 vdc input power to the Horizon Scanner and Subcarrier Oscillator, and removed power from telemetry encoder. A negative pulse, the Horizon Scanner and Attitude Control OFF signal, removed power from the horizon scanner and subcarrier oscillator, and inhibited a flow of current in the attitude control coil.

9. *Input Channel 9*—A positive input pulse, the Modulate Transmitter No. 1 signal, grounded the modulation input to telemetry transmitter No. 2 and ungrounded the input to transmitter No. 1. A negative pulse, the Current-Coil-Positive signal, supplied a positive direction current to the attitude control coil.

10. *Input Channel 10*—A positive input pulse, the Modulate Transmitter No. 2 signal, grounded the modulation input to telemetry transmitter No. 1 and ungrounded the input to transmitter No. 2. A negative pulse, the Current-Coil-Negative signal, supplied a negative direction current through the attitude control coil.

Other Signals

Signals utilized by the command control unit which did not originate in the decoder and were applied to other than the input channels were:

1. *Third Stage Separation Indicator*—The signal supplied was a switch closure. The output was supplied to telemetry as a +5V signal prior to separation and zero volts after separation.

2. *Zero-signal Shutdown Circuit*—An input of +22.5 vdc (nominal) was supplied immediately following the 3-minute TWT warm-up period in the transponder to operated two-minute timer. The timing cycle was initiated as soon as the carrier was lost in the transponder IF amplifier. At the end of the timing cycle, the wide-band subsystem was turned off.

3. *Voltage Sensor* — The voltage sensor supplied a negative pulse to turn off the transponders if the battery voltage fell below a predetermined level. This function could be inhibited by the load-cutoff override circuit.

4. *Telemetry Data*—Signals from either the telemetry encoder or the horizon scanner and subcarrier oscillator were fed to the transmitter modulation gate. The gate determined which transmitter was to be modulated.

5. *Remove Start Switch*—The remote start switch delayed application of +12 vdc to the appropriate input of each flip-flop circuit until the flip-flops were in the desired initial turn-on state. Once in orbit, this circuit was inhibited.

Command Control Box Packaging

Early design attempts favoring the stacking of four printed circuit boards were ruled out by the volume restrictions placed on the command control unit ($4 \times 4 \times 2\frac{1}{2}$ inches). The final unit package consisted of three high component density, printed circuit boards stacked on top of each other, and is shown in Figure 7–17; the three boards are shown in Figure 7–18.

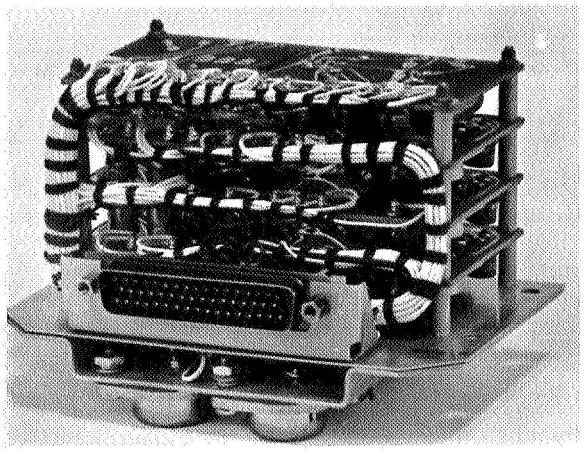


FIGURE 7–17.—Command control unit printed circuit boards assembled to baseplate.

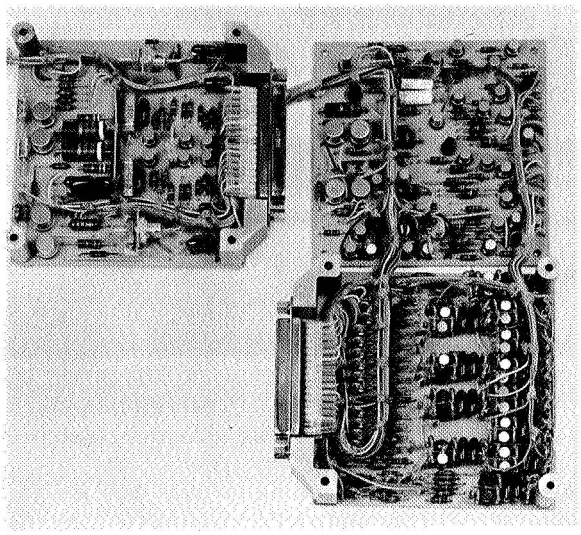


FIGURE 7–18.—Command control unit printed circuit boards wired in harness.

Testing

The command control unit was subjected to the same schedule of environmental testing required of all subsystems and components in the Relay I spacecraft. During these tests, all inputs and loads to the command control box were simulated and operational tests performed. During the tests, the unit's performance was satisfactory.

AUTHORS. *This chapter was written by* S. ROTH, H. GOLDBERG, *and* J. BLAIR *of the Radio Corporation of America, Princeton, New Jersey, U.S.A. under contract NAS 5–1272 with NASA/Goddard Space Flight Center.*

N66-10234

Chapter 8

The Spacecraft Power Supply System

INTRODUCTION

General

The Relay I power supply was a solar-array, storage-battery system with control and protective devices. Solar cells converted solar radiation to electrical energy while the spacecraft was illuminated by the sun but during eclipse periods power was supplied by the storage battery. Battery power was also used to supplement solar power when necessary.

Spacecraft Loads

In orbit, it was planned that one telemetry transmitter, the command receivers, and the command decoders would operate continuously. All other loads were to be commanded only when required.

The four major spacecraft load systems were:

1. Continuous loads: 10.4 watts at 28 volts
2. Telemetry loads: 7.3 watts at 28 volts
3. Radiation experiment loads: 4.25 watts at 22.5 volts; 1.25 watts at 28 volts
4. Microwave communications loads: 85.6 watts at 22.5 vols; 1.6 watts at 28.0 volts

The four major modes of operation planned were:

(1) continuous loads only;
(2) continuous plus telemetry loads;
(3) continuous, telemetry, and radiation experiment loads;
(4) continuous, telemetry and microwave communication loads.

The nominal current required from the solar array and/or battery to support these four modes of operation are shown below:

1. Mode 1: 0.372 amperes
2. Mode 2: 0.630 amperes
3. Mode 3: 0.860 amperes
4. Mode 4: 4.440 amperes

The power supply system was designed to allow a minimum of 100 minutes of microwave communication per day under the following conditions:

1. Orbital period: 150 minutes
2. Maximum eclipse time: 40 minutes
3. Microwave transmission during eclipse: 20 minutes in each of two successive orbits
4. Sun angle: 90 ± 15 degrees
5. Maximum transmission time per orbit: 36 minutes
6. Telemetry operation: beginning 10 minutes before and continuing through 10 minutes after each microwave transmission period.

A typical three-orbit program defined above is shown in Figure 8–1.

There was no restriction against other programs. The capability of the power supply allowed programming flexibility and microwave communication could exceed 100 minutes per day, if sufficient time for battery recharge was allowed between transmissions. While orbiting in sunlight, allowable microwave communication time was about seven hours per day, provided continuous transmission time was less than 90 minutes and sufficient battery recharge time was allowed

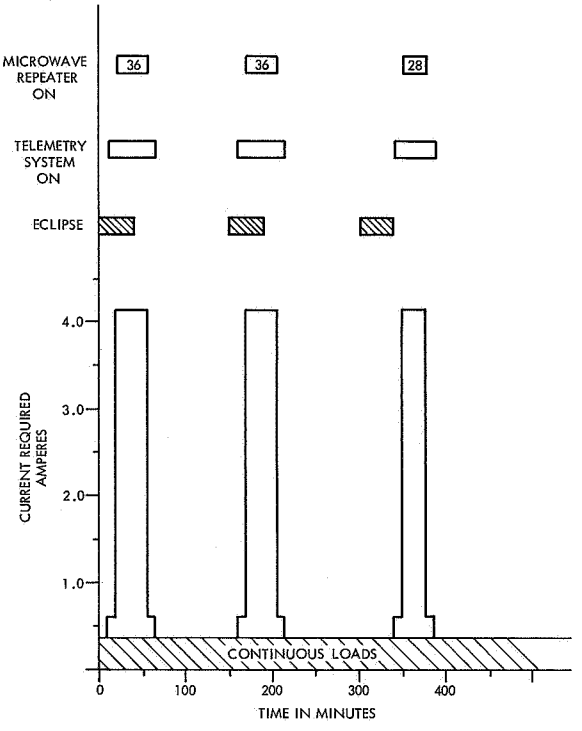


FIGURE 8–1.—Typical three orbit load profile.

between transmissions. As the output of the solar array decreased, due to radiation damage, the maximum allowable programming was also reduced. Figure 8–2 shows the approximate relation between solar-array degradation and maximum permissible microwave system operation times for 100-percent suntime orbits.

Design Considerations

The design philosophy of the Relay I power supply was to provide a basic system with redundancy, whenever possible and practical. This followed the basic Relay design in which two microwave communication systems, completely separate except for a common antenna, were provided. Where redundancy was provided, fault isolation techniques were utilized to isolate defective components. For example: three battery strings were provided, each with its own charge controller and discharge diode, and circuitry to prevent charging a failed battery.

Each microwave communication system

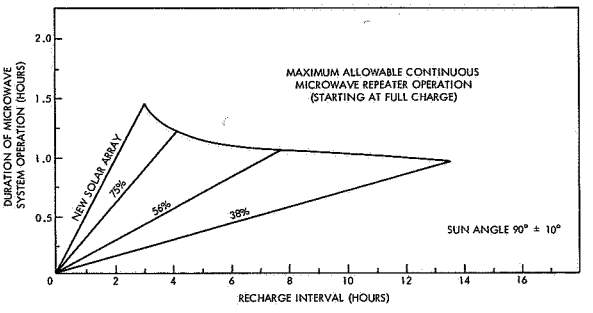


FIGURE 8–2.—Effect of solar array degradation on permissible duration of microwave repeater operation.

had its own voltage regulator, designed to turn off in the event of a short circuit in that system. A separate, low-power voltage regulator supplied power for radiation experiments.

Description of Power System

Silicon solar cells were the primary power source in the Relay I power system. A nickel-cadmium battery provided power for peak loads and eclipses. A block diagram of the power system is shown in Figure 8–3.

The solar array consisted of 8215 1×2-cm, P-on-N, cells. The cells were assembled in 5-cell shingles. These were then bonded to the eight solar panels which formed the sides of the spacecraft. The diode, D1, represents the 16 blocking diodes which prevent loading of the solar bus by a fault in any of the 16-plane sections of the solar array. The one-year timer was employed to disconnect the solar array from the bus after one year in orbit.

The voltage limiter was a shunt regulator which prevented the occurrence of solar bus voltage in excess of 33.0 volts. The three storage batteries were charged through their respective charge controllers. Bypass diodes allowed the batteries to discharge into the unregulated bus when required by peak loads or eclipses. The low-voltage load cutoff sensed the voltage of the unregulated bus and would turn off the microwave systems if the voltage fell below a pre-set level. Each microwave system was powered at 22.5 volts

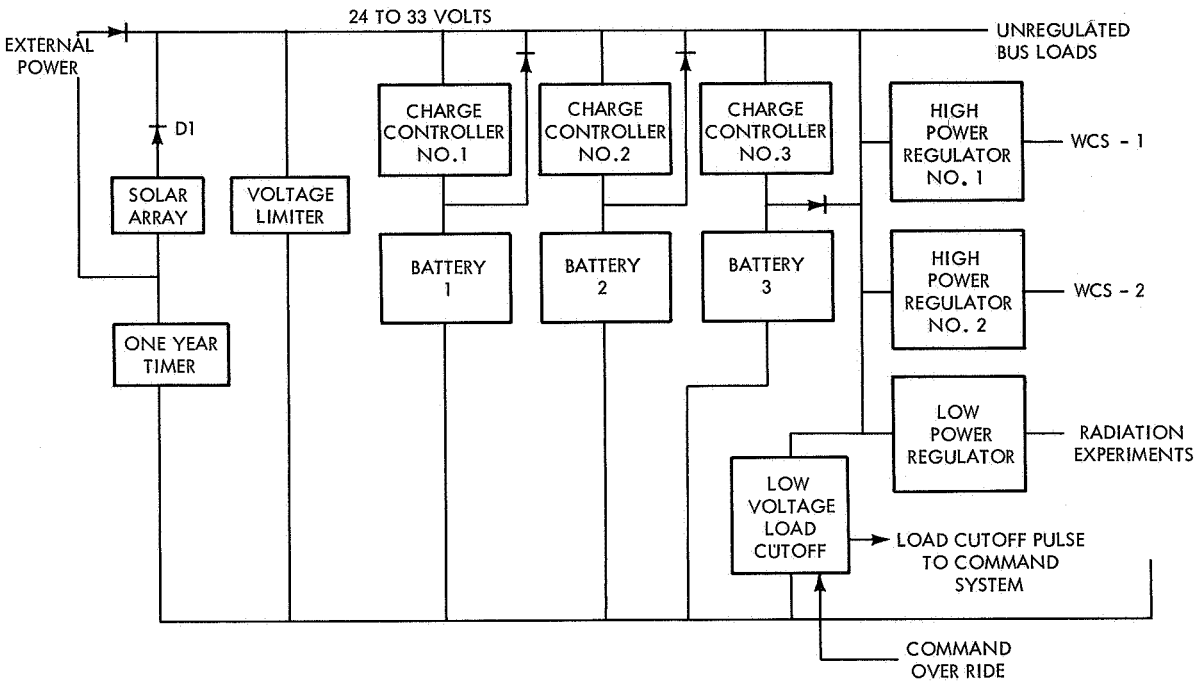


FIGURE 8–3.—Simplified block diagram of Relay I power system.

from its respective high-power regulator. The low-power regulator supplied power at 22.5 volts to a number of the radiation experiments. Other spacecraft systems were connected directly to the unregulated bus.

Telemetry

Twenty channels of telemetry provided information on power supply operation. Included were the following:

1. Solar-bus voltage
2. Battery voltages (3)
3. Total battery current
4. Solar-panel temperatures (4)
5. Battery temperatures (6)
6. Battery pressure
7. Regulated voltages (3)
8. Voltage limiter current.

Subsystem Testing

Following all environmental tests, the power supply subsystem, except the solar panels, was given a final test. The various components were connected together by a harness which duplicated the interconnections of the spacecraft harness.

The subsystem was operated through several simulated orbits, with a power supply replacing the solar array. All possible load and operating conditions were simulated to ensure that no undesired interaction existed between the components. The proper operation of the battery high-temperature, trickle-charge circuits; the battery low-voltage, trickle-charge circuits; and the low-voltage, load-cutoff circuits were verified. In addition, all telemetry readout voltages were compared with measured values and verified to be within the specified accuracy.

SOLAR ARRAY

Introduction

The function of the solar-cell array was to provide primary power for the spacecraft during its lifetime. The array performed this function by direct conversion of solar energy to electrical energy, using light-sensitive, silicon, solar cells. Energy from the array was fed directly to the loads or diverted to the storage battery during light-load conditions. Power requirements under

peak-load conditions were met by utilizing energy from the storage battery in conjunction with energy from the solar array.

Design Objective

The amount of radiation damage expected in space was not finitely known. Therefore, the overall design objective was to provide maximum power and greatest possible protection against radiation damage, within reasonable weight limitations.

Design

Cell

Boron-doped, P-on-N, silicon, 1 × 2-cm solar cells were selected for the array. Each cell had a 0.040-inch positive strip along one 2-cm edge and the negative surface was covered with a solder coating. Grid lines on the positive surface and the solder coating on the negative surface reduced the internal resistance of the cell and provided higher efficiency.

Shingle

Five solar cells were soldered, in series, to make a shingle. Maximum dimensions for each shingle were 1.800 inches in length by 0.798 inch in width. The thickness of any shingle, including filter, was 0.125 inch maximum. Positive and negative tabs, formed from 0.016-inch, silver-plated copper wire, were soldered to the shingle. The shingles were specified to be 9.6 percent efficient in space.

Filter

The cover material for the cells was selected after considering several factors. But the two best materials considered for the application were sapphire and fused silica (Corning 7940). Properties of the two materials which influenced the selection are listed in Table 8–1.

The advantages of fused silica were its higher transmission and emissivity as compared to sapphire. Cost of fused silica was approximately half that of sapphire. The lower density of fused silica required that the thickness be doubled to obtain radiation protection equivalent to that of sapphire at approximately the same weight.

TABLE 8–1.—*Solar-Cell Cover Properties*

Property	Sapphire	Fused silica (Corning 7940)
Density	3.98 grams/cm^3	2.202 grams/cm^3
Specific heat	.18 calories/gram (0° to 20° c)	.16 calories/gram (0° C to 25° C)
Percent transmission (room temperature) 0.4 to 1.1 microns	85%	93%
Thermal conductivity (cal/sec)(cm^2) (°C/cm)	0.065 at 100°C	0.0032 at 25°C
Radiation protection equivalence	30 mils thick	30 mils thick

Fused silica was therefore selected as the filter material, and an ultraviolet filter coating was applied to the surface and bonded to the cell. Properties of the filter coating are listed in Table 8–2. The two-centimeter edges of each filter were polished to decrease shading of the cell when the angle of incidence of the sun vector was not normal to the cell.

TABLE 8–2.—*Solar-Cell Filter Transmission Properties*

Wavelength, millimicrons	Transmission
300 to 370	1% maximum
380 to 420	50% average
500 to 1000	90% minimum average
600 to 800	90% minimum average

Panel Substrate

The solar array for the spacecraft consisted of eight panels of aluminum honeycomb construction (see Figure 8–4). Each panel was composed of a rectangular section, 11.025 inches wide by 16.45 inches long, and an isosceles trapezoidal section whose base was 11.025 inches; its upper side was 7.756 inches long, and its height was 15.75 inches. Four of the eight panels contained cut-outs in the rectangular section which decreased the area available for the solar array. The total projected area of the solar array, at a sun angle of 90 degrees, varied between 5.4 and 5.8 square feet as the spacecraft rotated about its spin axis. The total solar-array weight was 32.42 pounds.

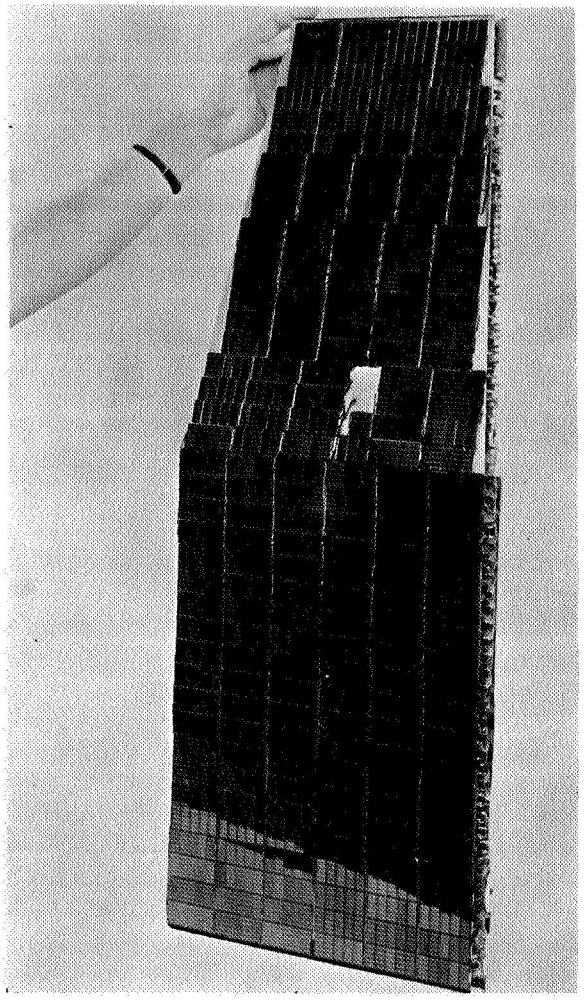


FIGURE 8–4.—Relay I solar panel.

Array Arrangement

A total of 75 solar cells connected in series were required to provide the proper voltage for charging the batteries and supplying the load. The 75 series-connected cells provided a safety factor to ensure that voltage output would be sufficient during the specified spacecraft life. Fifteen 5-cell shingles were connected in series to provide the desired voltage. The shingles were arranged on the panel so that several series strings were connected in parallel at each potential level for increased reliability.

All panels without cutouts had a total of 206 five-cell shingles and 4 each of two and three-cell shingles for an equivalent of 210 five-cell shingles. Two and three-cell shingles were used on the trapezoidal section of the panels for more efficient utilization of available panel area. Based on the maximum shingle dimensions of 1.800 by 0.798 inches, the average packing factor for the entire spacecraft was 91.7 percent.

Array Assembly

Each panel was carefully cleaned with acid etch solution and then neutralized as the first step in assembly. A coating of insulating material (SMP 62/63) was then applied to the cleaned surface to a thickness of approximately 0.008 inch. Primer (General Electric SS–4004) was applied to the insulated surface of the panel and the solder surface of the shingle. The shingles were then bonded to the panel, using silicone-base, room-temperature, vulcanizing rubber.

Shingle-to-shingle, series-parallel connections were made, using silver plated, 0.016-inch diameter copper bus wire. Leads were provided from the arrays on the rectangular and trapezoidal sections of the panel to blocking diodes on the rear surface of the panel. Diodes were provided for each panel section to prevent any loss to shorted or non-illuminated panels. A connector is provided on each panel to facilitate installation on the spacecraft.

Array Power Output

Theoretical

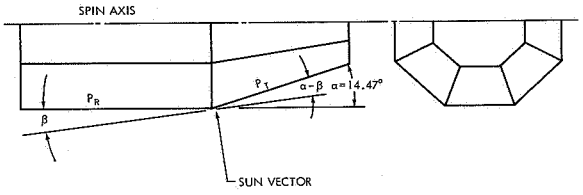
The theoretical power from the solar array, under illumination by an equivalent air mass zero spectrum, and at a temperature of 27 degrees centigrade, was calculated for each of the two projected array areas at the optimum angle between the sun vector and the surfaces of the array. The following assumptions were made in the calculation:

1. Power output was a function of the cosine of the angle between the normal to the sun vector and the solar array.
2. Shingle efficiency was 9 percent.
3. Power output from the trapezoidal sections of each panel was equal to 10.7 watts.

4. Power output from the rectangular section of each panel was uniform and equal to 13.75 watts.

Determination of Optimum Sun Angle

The parameters used to determine the optimum sun angle for the solar array as shown in Figure 8–5. The optimum sun angle was determined as follows:



P_R = POWER FROM RECTANGULAR SECTION
P_T = POWER FROM TRAPEZOIDAL SECTION
β = ANGLE BETWEEN NORMAL TO SUN VECTOR AND SPIN AXIS OF SPACECRAFT (SUN ANGLE)
α = ANGLE BETWEEN RECTANGULAR AND TRAPEZOIDAL SECTIONS OF ARRAY

$$P = P_R \cos\beta + P_T \cos(\alpha-\beta)$$

$$\frac{dP}{d\beta} = P_R \sin\beta - P_T\left[\frac{d\alpha}{d\beta} - 1\right]\sin(\alpha-\beta) \; ; \; \frac{d\alpha}{d\beta} = 0$$

$$\frac{dP}{d\beta} = -P_R \sin\beta + P_T \sin(\alpha-\beta)$$

TO FIND MAXIMUM POWER, SET $\frac{dP}{d\beta} = 0$

$$P_R \sin\beta = P_T \sin(\alpha-\beta)$$
$$P_R \sin\beta = P_T(\sin\alpha\cos\beta - \cos\alpha\sin\beta)$$
$$P_R/P_T = \sin\alpha\cot\beta - \cos\alpha$$
$$\cot\beta = \frac{P_R/P_T + \cos\alpha}{\sin\alpha}$$

$$\cot\beta = \frac{13.75/10.7 + .968}{.25} = 9.0$$

$$\beta = 6.33°$$

THE OPTIMUM ANGLE BETWEEN THE SUN VECTOR AND SPIN AXIS IS 83.67°.

FIGURE 8–5.—Solar array sun angle parameters.

Assuming that the power output of the array can be considered as the average of the values obtained for the two positions relative to the sun vector indicated in Figure 8–6, the following analysis will apply:

$$P = \tfrac{1}{2}[(P_R\cos 6.33° + P_T\cos 8.14°)(1+2\cos 45°) + (2\cos 22.5° + \cos 67.5°)(P_R\cos 6.33° + P_T\cos 8.14°)]$$

$$P = \frac{(2.414+2.612)[(13.75)(.994)+(10.7)(.99)]}{2}$$

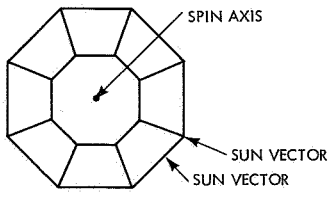


FIGURE 8–6.—Top view of solar array.

$$P = (2.513)(13.7 + 10.69)$$

P average = 61.0 watts at 33 volts

Tungsten Measurements

The power output of each panel assembly was measured under tungsten illumination with the angle of incidence normal to the section of panel under test. The light source was 2800°K ± 50°K color-temperature, tungsten, reflector-type, sealed lamps. The intensity of illumination at the surface of the array was 100 ± 10 milliwatts per square centimeter as determined by an approved standard cell. The minimum outputs when measured at a temperature of no lower than 26°C at 34.5 volts were at least:

1. Trapezoidal section, all panels: 8.0 watts
2. Rectangular section with 8 fifteen-shingle strings: 10.7 watts
3. Rectangular section with less than 8 fifteen-shingle strings: 9.3 watts

Sunlight Measurements

The solar panels were assembled on a satellite structure and illuminated under sunlight. Panel temperature during illumination was approximately 35 degrees centigrade. Solar intensity, measured with a pyrheliometer, was 92 milliwatts per square centimeter. Current-voltage curves were made with the angle of incidence normal to the spin axis of the structure. Seventeen curves were plotted with the initial and final curves indicating the power output of the array with the sun vector bisecting the angle between panels 2A and 3A (see Figure 8–7). The other curves were plotted with the structure rotated in 22.5-degree steps, thus alternately illuminating three or four panels. Figure 8–7 shows the current-voltage curve for measurement number 11 and is typical of all the current-voltage curves.

Table 8–3 shows the current at 33.0 volts, the short circuit current and the open circuit voltage taken from the 17 current-voltage curves.

STORAGE BATTERY

General

The storage battery supplied power during

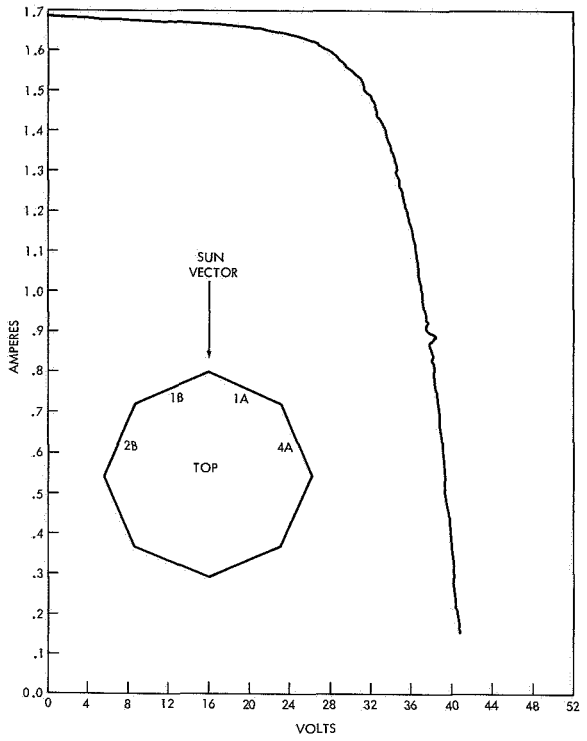


FIGURE 8–7.—Typical solar array I–V curve.

TABLE 8–3.—*Solar-Array Output Measurements*

Position	I@33 v (amperes)	Isc (amperes)	Voc (volts)
1	1.41	1.68	41.0
2	1.31	1.55	41.0
3	1.37	1.65	41.0
4	1.28	1.49	41.5
5	1.37	1.61	41.5
6	1.29	1.49	41.5
7	1.43	1.65	41.5
8	1.34	1.52	42.0
9	1.43	1.69	41.5
10	1.38	1.60	41.5
11	1.42	1.68	41.0
12	1.33	1.52	41.5
13	1.38	1.64	41.5
14	1.28	1.56	41.5
15	1.39	1.66	41.5
16	1.31	1.52	41.5
17	1.41	1.69	41.5

eclipses and during peak load periods, such as wideband communication. The battery was recharged by the solar array.

Sealed nickel-cadmium cells were selected for the Relay power system as they are capable of accepting continuous overcharge and providing long life when operating in the expected temperature range of 0°C to 32°C.

Battery Capacity

The battery was required to meet the requirements of the load profile shown in Figure 8–1 with a maximum depth of discharge of 50 percent. Figure 8–8 shows the battery charge-discharge cycle for the load profile of Figure 8–1 with nominal solar array current of 1.5 amperes.

The required ampere-hour capacity was determined as shown below:

$$\text{ampere-hour capacity required} = \frac{D_d}{60 \times 0.5}$$

where

D_d = maximum depth of discharge in ampere minutes
60 = minutes per hour
0.5 = 50 percent maximum depth of discharge

From Figure 8–8, D_d was found to be 209 ampere minutes. Ampere-hour capacity required was therefore: $\frac{209}{60 \times 0.5}$ or 6.97 ampere hours.

Since the battery consisted of three parallel strings of cells, the individual cell capacity required was: $\frac{3}{6.97}$ or 2.32 ampere hours.

To provide a margin of reserve capacity, a cell with a capacity of 2.75 ampere-hours, at room temperature, and a discharge current of 1.5 amperes, was selected.

Battery Design

The Relay battery system had three battery circuits with 20 cells in series in each circuit. Each battery was individually charged from the solar array through separate charge controllers shown in Figure 8–3.

The maximum battery charging current was limited to approximately 0.5 amperes by the charge controllers. Temperature-sensing thermistors were physically connected to two cells in each battery circuit. If either of these elements exceeded 90°F, the charging current to this particular circuit dropped to a maximum of 50 ma. There

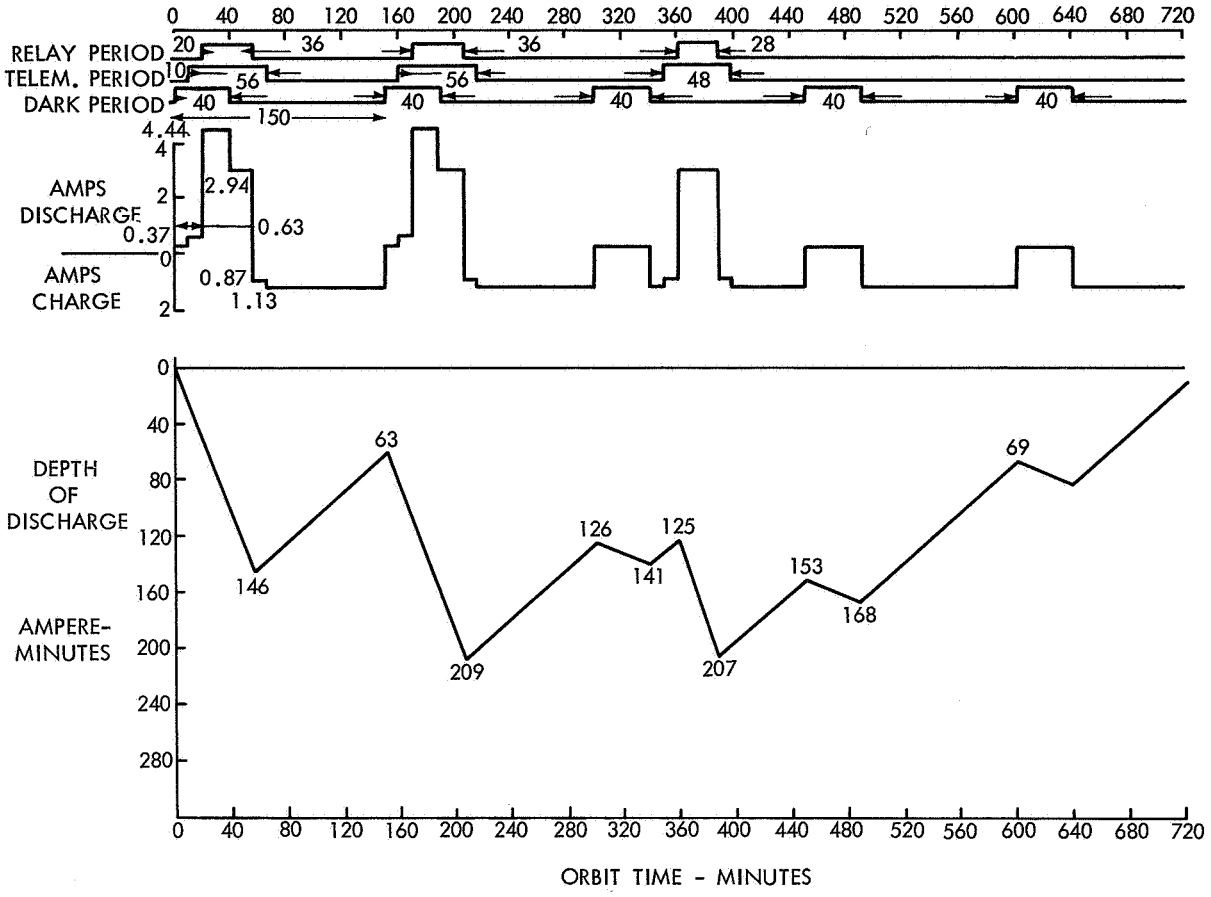


FIGURE 8–8.—Battery charge—discharge profile.

was also one cell in each battery circuit equipped with a pressure switch set to operate at about 500 psi. Operation of a pressure switch also lowered the charging current of that particular battery circuit to 50 ma maximum. There was one other charge-limiting feature. The maximum solar array voltage at the charging system input was limited to 33.0 volts by the voltage limiter (also shown in Figure 8–3).

Before maximum charging commences, (trickle charging is always present) the battery voltage is sampled and, if the total voltage is not above 25 volts, the trickle charge is maintained. The trickle charge continues until the total battery circuit reaches 25 volts at which time the current rises toward its maximum of 0.5 amps. This feature is included to prevent charging a shorted or partially shorted battery circuit.

During eclipse, or peak load periods, the batteries discharge to the unregulated bus through separate diodes.

Cell Description

The battery cells are sintered-plate, nickel-cadmium type. The negative plates consist of sintered, porous nickel impregnated with cadmium-hydroxide active material. The positive plates are likewise sintered, porous nickel plates, but are impregnated with the nickel-hydroxide active material. Positive and negative plates are separated and insulated from each other by a cellulose separator. The positive plates, negative plates, and separator are spirally wound and placed in a cylindrical cell case, hermetically sealed by heliarc weld. The positive terminal of

the cell is insulated from the negative cell cover by a ceramic annular disk brazed to the terminal and cover.

The cell diameter is 1.272 to 1.296 inches; the overall length, including terminals, is 2.950 to 2.990 inches; and the weight is 145 to 163 grams. At temperatures between 25° and 30°C this cell has an electrical capacity of 2.75 ampere-hours when discharged at 1.50 amperes to a final voltage of 1.20 v.

The nickel-cadmium cells were procured from the Sonotone Corporation of Elmsford, New York. Sonotone tested the cells prior to delivery. These tests consisted of a vibration test, a 0°C electrical capacity test, a minimum of one 25°C electrical capacity test, an internal-resistance test, an internal-short test, and an electrolyte leak test.

At RCA, the cells were subjected to an electrolyte leak test, 60 hours of charge-discharge cycling at 25°C, 8 hours of cycling at +5°C, a post-cycling discharge, and a final electrolyte leak test. The charge-discharge cycling followed the schedule shown in Table 8–4.

It was required that all cells remain between the voltage limits of 1.60 and 1.20 during cycling, and that during post-cycling discharge, the cell voltage remain at 1.20 (or higher) for a minimum of 60 minutes. Any cells exhibiting erratic voltage variations during the tests were rejected.

Battery Box Assembly

Three battery circuits, totaling 60 cells and their related circuitry, were contained in two assemblies, designated Battery Box 1 and Battery Box 2.

Battery box 1 (see Figure 8–9) contains 30 cells, 10 cells for half of battery circuit 1 (including one cell equipped with a pressure switch), and 20 cells for battery circuit 2 (including one cell equipped with a pressure switch). In addition, box 1 includes three battery and one temperature-sensing thermistors and two 9-volt Zener diodes. The diodes supply the power for the thermistors on battery circuits 1 and 2 and on the structure.

Battery box 2 also contains 30 cells, 10 cells for half of battery circuit 1, and 20 cells for battery circuit 3 (including one cell equipped with a pressure switch). In addition to the three battery-sensing thermistors and the structure temperature-thermistor, box 2 contains a temperature-thermistor, located under the thermal controller which is mounted on this box. The resistors and a 9-volt Zener diode are also mounted on this box. The diode supplies power for the thermistors on battery circuit 3 and the structure.

The cells are secured to the battery boxes with an alumina-loaded, epoxy bonding compound. Each cell is bonded in a hole in either the top or bottom mounting plates, sixteen cells being fixed to the top plate and fourteen to the bottom plate. All cells, except the two end cells on the top plate, are bonded at the approximate center of the cell, whereas these two cells are bonded to the mounting plate one-eighth inch from the top of the cell. Each battery box is equipped with a 25-pin and a 50-pin connector. The 25-pin connector contains all the interconnections between the battery box and the spacecraft. The 50-pin connector is for test purposes only and is not used in the spacecraft. This connector permits the sensing of each cell voltage during the testing of the battery boxes.

The total weight of both boxes is 28.73 pounds.

TABLE 8–4.—*Storage Cell Charge-Discharge Cycling Schedule*

Operating mode	Duration (minutes)	Current (amperes)	Total elapsed time (minutes)
Discharge	20	1.00	20
Discharge	10	1.50	30
Charge	50	0.50	80
Discharge	20	0.25	100
Charge	50	0.50	150

BATTERY CHARGE CONTROLLER

Introduction

The main function of the charge controller was to limit the amount of charge current

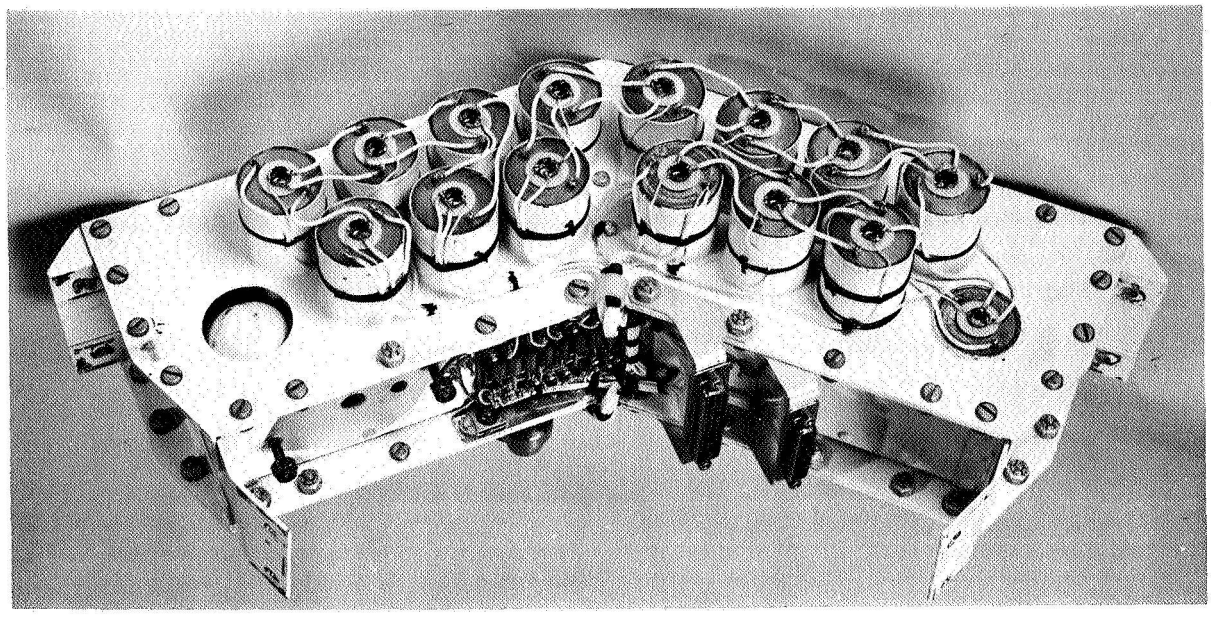


FIGURE 8–9.—Relay I battery pack.

to the batteries. Other functions performed were:

1. Allow battery current to flow to power supply loads whenever battery voltages exceed the solar bus voltage.
2. Cut off battery charge currents when the voltage falls below a pre-set value, but allow a small trickle-charge current.
3. Cut off charge current to battery when temperature or pressure of the battery is above pre-set levels.
4. Produce an output pulse when the unregulated bus voltage falls below a pre-set value.
5. Provide a telemetry voltage of each battery voltage and of the unregulated bus.

The charge controller is located in the current paths between the unregulated bus and each of the three batteries. The unregulated bus provides power to the regulators and to other directly connected loads. The solar array provides primary power to the unregulated bus, part of which goes to the batteries through the charge controller. When peak power is required, or the satellite is in eclipse, the batteries discharge through diodes in the charge controller to the unregulated bus.

Performance Specifications

The performance requirements were as follows:

1. A battery charge current shall be controlled to 500 ± 100 milliamps, as the unregulated bus operates up to a maximum of 33 volts, provided the battery terminal voltage is 1.5 volts less than the unregulated bus.
2. Battery low-voltage cut-off shall be adjustable and set for 25.5 volts.
3. A 0.2 ma temperature or pressure (cut-off) signal shall reduce the battery charge current to a trickle charge current of 50 ma.
4. The pulse generator portion of the charge controller shall produce a negative-going pulse of 5 to 7 volts peak amplitude when the unregulated bus falls to 22 ± 0.25 volts.
5. The telemetry voltage output shall be 0 to 5 volts equivalent to 0 to 36 volts for each battery and the unregulated bus voltage.
6. Operating temperature range shall be 0 to 30°C.

Design Approach

The charge controller unit is shown in Figure 8–10. It has an aluminum mounting

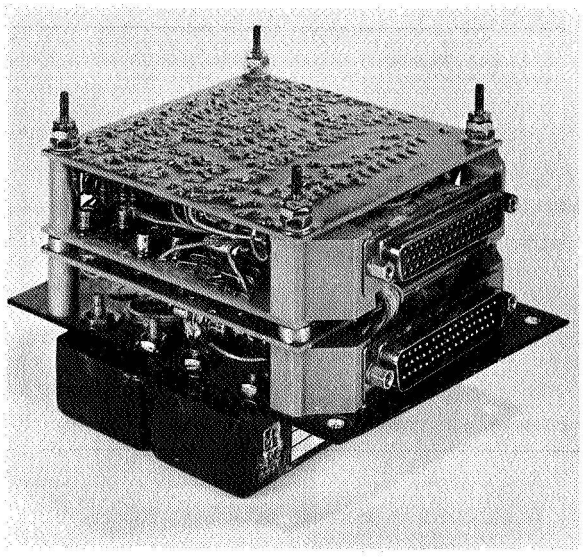


FIGURE 8–10.—Relay I charge controller.

plate to which six power-transistors are mounted. Stacked beneath are four printed-circuit boards, three of which are charge controllers, and the fourth is a pulse generator. The entire unit is essentially enclosed by a radiation shield of 0.060-inch brass. The mounting plate was fastened to the satellite structure, facilitating dissipation of heat from the transistors. Two power transistors are associated with each charge controller circuit, but one is used as a diode and therefore dissipates very little power.

The charge controller acts as a current regulator when the difference in voltage between the unregulated bus and the battery voltage exceeds approximately 1.5 volts. Below this voltage difference, the main pass transistor starts to saturate, reducing the output current. A reference constant current is produced by a combination of unregulated bus voltage and battery voltage into a differential amplifier with one side of the amplifier returning to a Zener diode. This constant current is amplified by two emitter-follower stages and becomes the charge current to the battery. The amount of output current is sensed in a resistor and fed back through amplifiers to subtract from the constant current source. All of the various charge current cut-off features act to reduce the reference constant current to zero, thereby reducing the output charge current to minimum.

The pulse generator consists of a differential amplifier with a common connection between the collector of one transistor to the base of the other followed by an emitter follower. The emitter follower is connected to the normally-off transistor of the differential amplifier. When the unregulated bus falls below 22 volts, the transistor switches on, reducing the voltage to the emitter follower, which has a capacitively coupled output, thus producing a pulse.

One thermal problem involved designing the proper heat sink for the power transistors. It was decided to use Berlox wafers with Indium washers, the Berlox acting as the electrical insulators.

Operational Description

Charge Controller — The block diagram (see Figure 8–11) shows various elements of the charge controller. The constant current source is shown in Figure 8–12. The unregulated bus voltage operates the Zener diode CR1 and turns on Q1. When the base voltage on Q2, developed by the battery, is sufficient to turn on Q2, then Q1 turns off. The base of Q2 is clamped to the Zener voltage of CR1 by CR2. The collector current of Q2 is then constant. Battery voltage below the desired level will tend to turn Q2 off, thereby achieving the low battery voltage cut-off provision. Temperature or pressure signals will turn on Q3 thereby loading the base of Q2 and cutting off Q2.

The differences in current between the constant current and the feedback current is amplified by two transistors in a Darlington connection and fed to the battery.

The feedback amplifier consists of a differential amplifier and an output transistor.

Battery Pressure and Temperature Cut-off Circuits—The battery pressure and temperature cut-off circuits are described in this

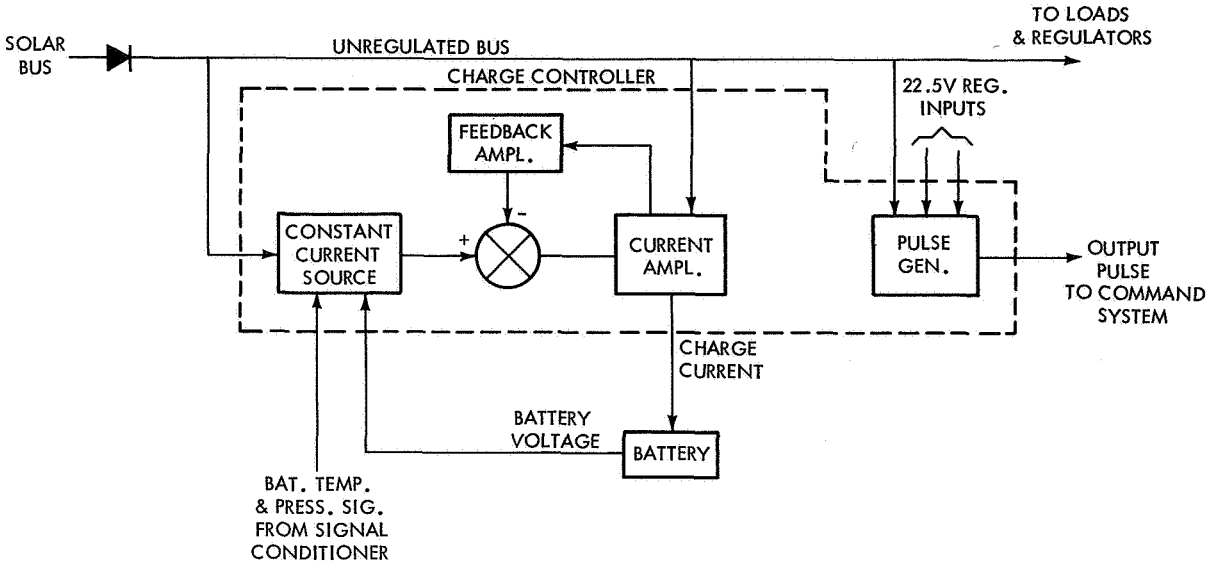


FIGURE 8–11.—Charge controller, block diagram.

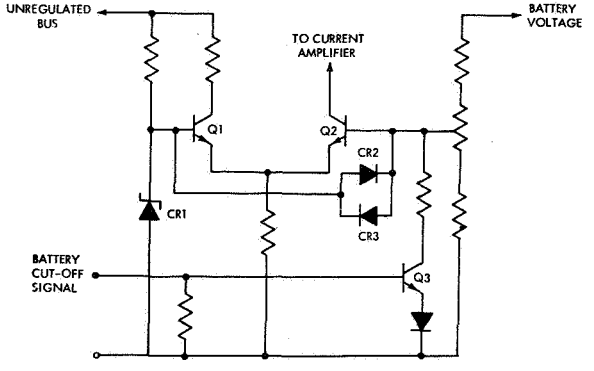


FIGURE 8–12.—Charge controller constant current source.

chapter although they are physically part of the signal conditioner. Signals are received from the pressure and temperature sensor circuits in the battery packs and the output is fed to the charge controller when allowable pressure and temperature limits are exceeded. The output of the circuit will cut off battery charge currents when high temperature or high pressure conditions exist.

The temperature cut-off circuit consists of two stages: The first stage amplifies the dc signal from the battery sensor and turns on the second stage when the input reaches a predetermined level. A small additional change in input level will then saturate the second stage. The output voltage of the first stage is adjustable to allow for exact matching with each battery temperature sensor.

The battery pressure charge cut-off circuit consists of a diode circuit connected in parallel with the output of the temperature circuit. The pressure signal input has two levels, either a zero-volt level for normal pressure or a 9-volt level for high pressure.

Pulse Generator — The pulse generator shown in Figure 8–13 consists of a normally-on stage, Q1, and normally-off stage, Q2, and an emitter follower, Q3. When the unregulated bus falls to a pre-set value, the base voltage of Q1 reduces and Q1 starts to turn off. Since Q2 base is biased near the same value of Q1, Q2 starts to turn on and begins to saturate, rapidly dropping the voltage on the collector of Q2, which reduces the base voltage on Q1, turning it off. The drop in voltage on the collector of Q2 is coupled through the emitter follower Q3 and is the output pulse. In order to reset the circuit, the collector current of Q2 must be reduced by turning off the voltage regulators.

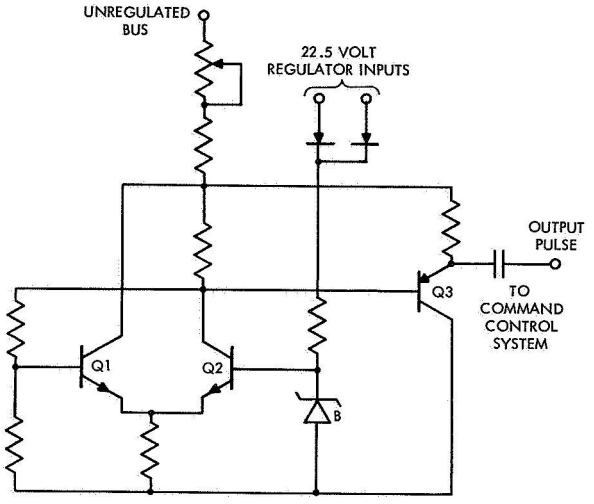


FIGURE 8–13.—Pulse generator schematic.

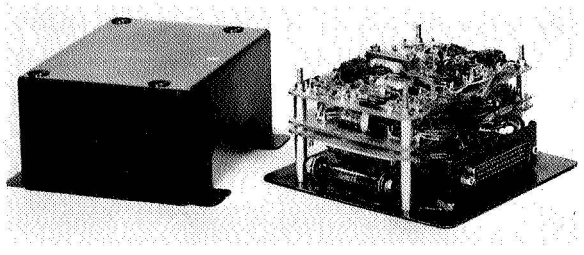
VOLTAGE REGULATORS AND VOLTAGE LIMITER

General

All of the regulator and limiter circuitry, with the exception of the power transistors, is packaged in one assembly (see Figure 8–14). The voltage regulator and the limiter assembly has a volume of 50 cubic inches and weighs 1.4 pounds.

The power transistors for the voltage limiter, the low power regulator, and both high power regulators are mounted on the spacecraft mounting collar assembly. This location was selected because it allows heat from the transistors to be radiated directly into space without heating the interior of the spacecraft.

Stainless steel caps are bonded to the transistors to protect them from radiation. Figure 8–15 shows the mounting collar assembly before the stainless steel caps are bonded on.



FIGURER 8–14.—Relay I voltage regulator.

HIGH POWER VOLTAGE REGULATOR

Introduction

The High Power Voltage Regulators Nos. 1 and 2, supply regulated voltage of +22.5 volts ±1 percent to wideband communications systems Nos. 1 and 2, respectively. The regulators are operated from the unregulated bus. The power required for wideband system operation is partially supplied by the batteries, therefore the unregulated voltage excursions during this time are from 28 volts to 23.5 volts.

The regulators can also be switched on and off; that is, the power to the wideband systems can be supplied or interrupted by ground-station command. Each supplies a load current of about 3.5 amperes when switched on. The circuits are designed to withstand 50 percent overload and tests have shown that 100 percent overload can be tolerated. A short-circuit load will turn the regulator off, since the feedback drive is interrupted. This is a distinct advantage of the collector output series regulator configuration and obviates the necessity for complex protective circuitry.

Since the major portion of regulator losses occur in the series path between unregulated input and regulated output, no dropping elements except the series pass transistors were placed in this path. This allows the

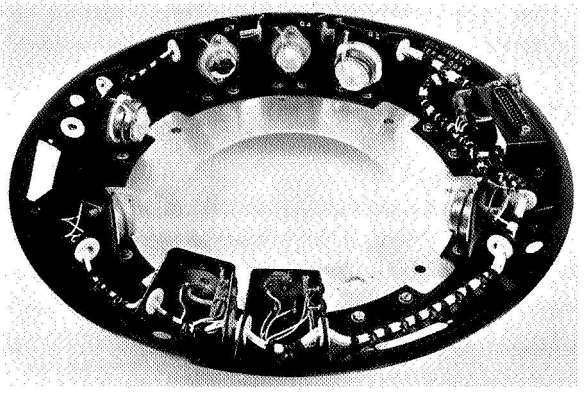


FIGURE 8–15.—Collar assembly.

unregulated voltage to fall to the point where the series pass transistor becomes saturated before regulation is lost. The input voltage high limit is set by the battery discharge characteristic which starts at a level of about 28 volts and decreases fairly rapidly to a level slightly above the transistor saturation point. The overall efficiency during the period of wideband systems operation is therefore very high.

Design Objectives

The performance specifications of the high power voltage regulator are as follows:

Input Voltage—23.5 to 28.0 vdc

Output voltage—22.5 vdc ±1%

Output current—0 to 5.5 amperes

Line regulation—±0.2% under the input-voltage conditions of 23.5 to 28.0 vdc

Load regulation—±0.5% under the output-current conditions of 0 to 5.5 amperes

Ripple and noise—10 mv RMS

Line transient response—Output voltage shall recover to 2 percent of nominal (for steps in line voltage of ±4 v, within the input-voltage limits of 23.5 to 28.0 vdc) within 50 μsecs.

Load Transient response—Output voltage shall recover to 2 percent of nominal (for step-load changes from 0 to full load) within 100 μsecs.

Output Impedance—0.2 ohms, or less, over a frequency range of 0 to 10 kc.

Polarity—Negative side may be grounded.

Temperature Requirements — The unit shall maintain the above electrical performance specifications while operating in an ambient temperature of −10°C to +45°C.

Controls—A level control shall be provided to adjust the output voltage to 22.5 vdc ±1 percent.

In addition to the performance specifications, other design objectives were: light weight and small size compatible with the aforementioned specifications, low power consumption, and high reliability.

Design Approach

The high-power voltage regulator block diagram is shown in Figure 8–16. A series-regulator configuration was chosen because the battery flat discharge characteristic allows high overall efficiency during wideband transmission. The requirements for regulation, transient response, and output impedance over a wide frequency range are much easier to attain with this configuration than with a controlled-pulse-width input switching-regulator. In addition, small physical size and low weight were realized, since large L–C filter sections are not required.

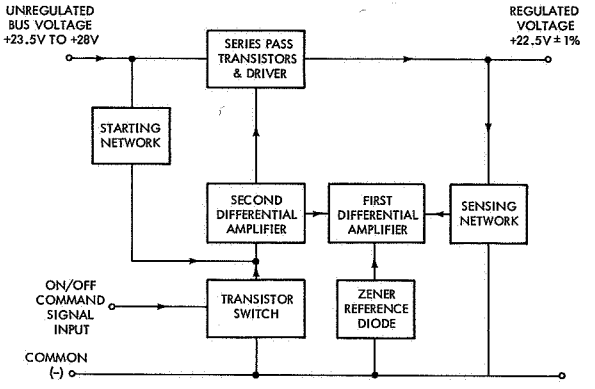


FIGURE 8–16.—High-power voltage regulator, block diagram.

The regulator consists of an output voltage sensing network, a temperature- compensated, Zener reference diode, two cascaded differential amplifiers, a parallel pair of series pass transistors driven by a third power transistor in a Darlington connection, and a transistor switch to effect the turn-on and off of the regualtor.

Two series-pass transistors, in parallel, are used to share the power dissipation and also provide lower minimum voltage drop than is obtainable with a single transistor. Cascading two differential amplifiers allows the first amplifier to operate with a balanced output. The net result is increased linearity, due to restricted collector voltage excursions, and more complete cancellation of V_{BE} and I_{CBO} mismatching, as a result of temperature changes. Temperature effects at the input to the first differential amplifier are held to a very low level by a temperature-compensated reference diode, and low tem-

perature-coefficient resistors in the sensing network.

An effective method of allowing the regulator to supply either 0 volts or the regulated 22.5-volt level to the load is to produce an open-circuit in the feedback path. This was done by using a transistor as a switch and placing it in parallel with the input to the second differential amplifier. Upon receiving the proper dc level from the command subsystem, signifying an off condition, this transistor becomes saturated and shunts the feedback drive to ground, effectively open circuiting the series pass transistor. When the feedback drive is restored, the regulator delivers 22.5 volts to the load.

Operational Description

A change in output or load voltage, due to either load resistance or input voltage fluctuations, is applied to the input of the first differential amplifier by the resistive divider sensing network. A small load voltage change appears as a large error voltage at the input to the second differential amplifier, since it is compared to the Zener reference voltage and amplified by the first stage. The second amplifier further amplifies the error and produces a change in the base drive, or bias level, of the drive transistor. Due to the beta multiplication of the Darlington-connected driver and series pass stages, the small current change at the base of the driver results in a sufficiently large change in current to the load to restore the load voltage to its pre-disturbance level. The phase of the error signal is such that negative feedback is introduced in a closed loop.

Without internal gain/phase compensation, these same deviations would trigger the circuit into oscillation. This is because the cutoff frequencies of the various transistors are sufficiently close to produce an additional 180° of phase shift at a frequency where the loop gain is greater than unity. Phase-lag compensation networks in the circuit start the gain roll-off at a frequency much lower than the transistor cut-off frequency, with a controlled rate of decrease. The output capacitor provides a low output impedance at frequencies beyond the point where the normal regulator impedance increases because of loop gain reduction.

Equipment Performance

The data in Table 8–5 was taken from a flight model high power voltage regulator. It is considered typical data and is included to show the performance versus specifications.

LOW POWER VOLTAGE REGULATOR

Introduction

The low-power voltage regulator supplies +22.5 volts, ± 1 percent, to the radiation experiments loads. The regulator is supplied voltage from the unregulated bus and may be operated during the time the batteries are being charged from the solar array. For this reason, the low power regulator must withstand input voltage excursions of 23.5 to 34.5 volts.

This regulator can also be commanded on and off and delivers 0 volts to the load when its output terminals are short-circuited. The regulator delivers 300 milliamperes to the load under normal operation and is designed to accept constant overloads of at least 50 percent. The major difference between this circuit and the high power voltage regulators is increased load capability.

Design Objectives

The performance specifications for the Low Power Voltage Regulator are as follows:

Input Voltage—23.5–34.5 vdc.

Output Voltage—22.5 vdc ± 1%.

Output Current—0–0.5 amperes.

Line Regulation—± 0.2% under the input-voltage conditions of 23.5 to 34.5 vdc.

Load Regulation—± 0.5% under the output-current conditions of 0 to 0.5 ampere.

Ripple and Noise—10 mv RMS.

Line Transient Response—Output voltage will recover to within 2 percent for steps in line voltage of ± 5v within the input-voltage limits of 23.5 to 34.5 vdc.

TABLE 8-5.—*High Power Voltage Regulator Electrical Test Data*

Test	Conditions	Performance	Comparison with specifications
Line regulation	Vin = 23.5v to 28v (I_L = 4.5A)	$\triangle V$o = 14 mv	Better
Load regulation	I_L = 0 to 4.5A (Vin = 27v)	$\triangle V$o = 31 mv	Better
Ripple	V_{in} = 1v P–P @ 20 cps	V_o = 1 mv P–P	Better
Output impedance	0 to 10 kc	Z_o < 0.1Ω	Better
Transient response (line)	$\triangle V_{in}$ = 5v step	V_o recovers to 2% in 5 μsecs	Better
Transient response (load).	I_L = 4. 5A step	Vo recovers to 2% in 75 μsecs	Better
Short circuit current.	R load = 0 ohms	20 ma	Not specified
On/off control		Operates	As specified
Temperature stability.	$\triangle T_{amb}$ = 45°C	$\triangle V_o$ = 43 mv	Better

Load Transient Response—Output voltage will recover to within 2 percent of nominal for step load change from 0 to full load within 100 μsecs.

Output Impedance—0.2 ohms, or less, over a frequency range of 0 to 10 kc.

Polarity—Negative side may be grounded.

Temperature Requirements — The unit shall maintain the above electrical performance specifications while operating in an ambient temperature of −10°C to +45°C.

Controls—A level control shall be pro-

vided to adjust the output voltage to 22.5 vdc ± 1 percent.

An additional design objective was to meet the aforementioned performance requirements with minimum size and weight, minimum power consumption, and maximum reliability.

Design Approach and Operational Description

The design approach and operation of the low power voltage regulation is the same as that previously discussed for the high power regulator. The block diagram of Figure 8–16 applies to the low power regulator as well. But the series pass configuration for the low power regulator contains only one series transistor, instead of two in parallel, and the driver transistor is eliminated.

Equipment Performance

The data in Table 8–6 was taken on a flight model low power voltage regulator. It is considered typical and is included to show the performance versus specifications.

Voltage Limiter

Introduction

The voltage limiter is a shunt regulator that provides protection for all circuitry connected to the solar bus. It limits the maximum array voltage.

The circuit was designed to shunt current from the solar array and begin limiting the solar array voltage only when it exceeds the threshold of 32.5 volts. This could have occurred at any time during the solar day if

TABLE 8–6.—*Low Power Voltage Regulator Electrical Test Data*

Test	Conditions	Performance	Comparison with specifications
Line regulation	V_{in} = 23.5v to 34.5v (I_L = 500 ma)	ΔVo = 14 mv	Better
Load regulation	I_L = 0 to 500 ma (V_{in} = 27v)	ΔVo = 14 mv	Better
Ripple	V_{in} = 1v P–P @ 20 cps	Vo = 2 mv P–P	Better
Output impedance	0 to 10 kc	$Zo < 0.01\ \Omega$	Better
Transient response (line)	ΔV_{in} = 5v step	Vo recovers to 2% in 20 μsecs.	Better
Transient response (load)	I_L = 500 ma step	Vo recovers to 2% in 50 μsecs. 2% in 50 μsecs.	Better
Short circuit current	R load = 0 ohms	I_L = 35 ma	Not specified
On/off control		Operates	As specified
Temperature stability	ΔT_{amb} = 45°C	ΔVo = 15 mv	Better

the load on the solar bus was very light, but was most likely to occur when the satellite emerges from the earth's shadow into the sunlight. The array at this time is at the lowest temperature, possibly as low as −58°C, and generates maximum voltage. Typically, the voltage would be higher than 50 volts at −58°C. Since this voltage would cause excessive dissipation in the voltage regulators, charge controllers, and other equipment, the voltage had to be limited. The dissipated power to lower the solar array down to 32.5 volts is approximately 48 watts. This corresponds to drawing 1.35 amperes from the array.

Design Objectives

The design objectives were basically the same as for other satellite components, namely, maximum reliability, minimum weight, and minimum power consumption. In order to accomplish all of these objectives, the need for semiconductor circuitry was obvious. Although the purpose of this circuit is to dissipate excessive, unwanted power (this is only true when the solar array exceeds the threshold of 32.5 volts), it must draw minimum power below this threshold to prevent adverse effects on the energy balance of the satellite. This objective is fulfilled in the basic design by utilizing a sharp *I–V* characteristic at the threshold voltage. Finally, reliability was assured by use of the most reliable parts, process inspections during fabrication, and rigorous environmental testing conditions, beyond those encountered in launch and actual space operation.

Design Approach

The circuit is designed to utilize the very sharp *I–V* characteristics of a low-power, Zener diode, multiplied in power capability by several transistor stages. This type of limiter has several advantages over the simple, high-power Zener diodes. The resulting *I–V* characteristic is much sharper than that of a high-power, Zener diode; a larger power-handling capacity is possible; there is greater ease in handling the dissipated power (since it is distributed among four power resistors as compared to one Zener diode); and the breakdown voltage can be set to any desired value.

Operational Description

A block diagram of the limiter is shown in Figure 8–17.

The limiter compares the solar array bus voltage to that of a Zener diode and then amplifies the difference voltage in a comparison amplifier. The comparison amplifier produces an output voltage when the voltage divider output voltage exceeds the Zener diode breakdown voltage. This signal is then amplified further by the final two transistor stages, resulting in a much higher power dissipation capability than that of a Zener diode design. The power resistors are mounted on the outside surfaces of four separate solar panels to effectively radiate the dissipated power on the outer surface of the satellite. The power transistor used in the final amplifier stage is mounted on the spacecraft mounting collar assembly (see Figure 8–15).

Equipment Performance

The electrical *I–V* characteristic of the voltage limiter is shown in Figure 8–18. Table 8–7 is a summary of its electrical and mechanical characteristics.

ONE-YEAR TIMER

The one-year timer is provided to open the solar array bus and thus deactivate the spacecraft after one year in orbit.

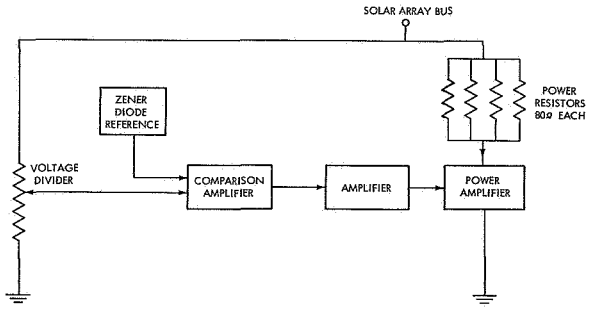


FIGURE 8–17.—Voltage limiter, block diagram.

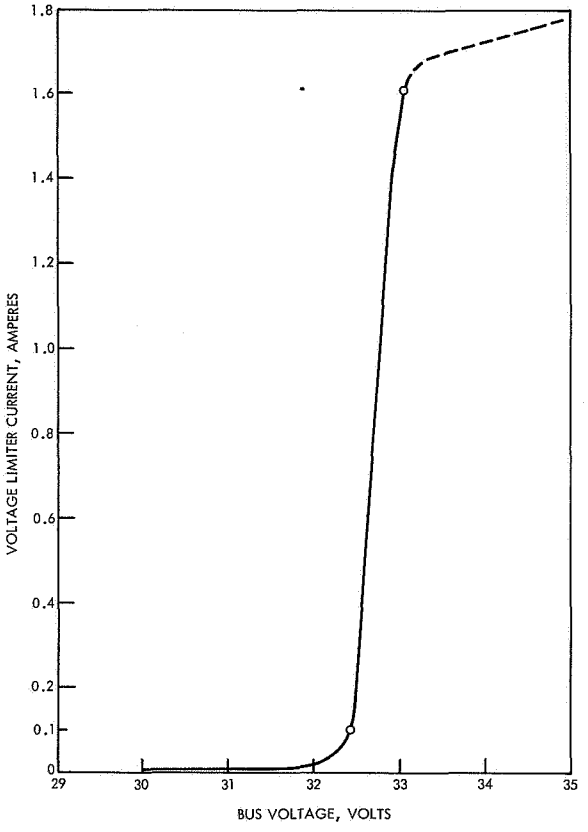


FIGURE 8–18.—Bus voltage vs. voltage limiter current.

The timer is an electro-chemical device which functions by deplating a lead pellet from a silver wire. The silver wire is spring-loaded and after the lead pellet is deplated, the wire is decomposed by chemical action and breaks, thus opening a switch which is connected in the ground return leads of the solar array.

The timer is powered by a 9-volt Zener power supply and draws 15 microamperes. The timer weighs 0.3 lb. and occupies a volume of 5 cubic inches.

TABLE 8–7.—*Electrical Test Results Summary*

Test	Current	Voltage
Threshold voltage at room temperature	$I=100$ ma.	$V=32.51$
Full load voltage at room temperature	$I=1.35$ Amps $I=1.60$ Amps	$V=+32.84$ $V=+32.91$
Temperature stability	$I=100$ ma $T=+34°C$ $I=1.35$ Amps $T=-10°C$	$V=+32.80$ $V=+33.34$
Off current	11 ma Total	$V=30.0$

AUTHORS. *This chapter was written by* T. R. WYLIE, P. J. CALLEN, G. ZIELINSKI, E. HOLLOWAY, L. PESSIN, *and* H. THIERFELDER *of the Radio Corporation of America, Princeton, New Jersey, U.S.A. under contract NAS 5–1272 with NASA/Goddard Space Flight Center.*

N 56-10235

Chapter 9

Spacecraft Environmental Testing

INTRODUCTION

General

The physical tests specified for Project Relay approximated the environments and stresses expected for the spacecraft during handling, launch, and orbital flight.

Environmental Qualification Tests

Environmental qualification tests were intended to ensure and verify the design of the prototype before flight testing similar spacecraft.

The test conditions for the prototype were intended to be more severe than field conditions in order to provide assurance in locating faults, and thus compensating to some extent for the statistical limitation of the small sample size. However, the conditions were not intended to be so severe as to exceed reasonable safety margins or to excite unrealistic modes of failure. The prototype was subjected to the following tests:

1. Spin
2. Temperature
3. Vibration
4. Solar Simulation
5. Humidity
6. Thermal Gradient
7. Acceleration.

Environmental Acceptance Tests

The flight model spacecraft was subjected to only the first four tests listed above. Environmental acceptance tests were intended to improve reliability of the spacecraft by providing a "break-in" period and by disclosing workmanship defects prior to flight. While comparable to field environment in severity, the conditions were intended to be mild enough to avoid fatiguing or wearing out the equipment.

Unit Tests

All flight units were subjected to Environmental Acceptance Tests, with applicable electrical tests, prior to delivery for assembly to the spacecraft. No prototype or other equipment subjected to Environmental Qualification Tests was used for flight spacecraft.

RELAY SPACECRAFT EXPECTED ENVIRONMENT

General

The spacecraft was expected to encounter a wide range of environmental conditions during its lifetime. For convenient classification in design and test, the total lifetime environment was divided into three phases: Phase I concerned earth events (long term), i.e., manufacture, assembly, test, handling, storage, shipment, standby, and prelaunch checkout. Phase II concerned launch events (short term), i.e., boost and separation. Phase III concerned the orbital flight (long-term).

The significant conditions of environment in the various phases are:

1. *Phase I*: mainly climatic (temperature, humidity, pressure, sand and dust,

fungus, salt spray, sun and rain), also shock, vibration, and spacecraft equipment operation.

2. *Phase II*: mainly aerodynamic and propulsion sources of temperature, vibration, acoustic noise, shock, spin, and acceleration; also vacuum conditions.

3. *Phase III*: mainly temperature and vacuum; also solar irradiation, cosmic rays, charged particles, and micrometeoroids.

Environment During Phase I

Temperature

Temperature extremes for unprotected spacecraft during air transport and unsheltered ground conditions were expected to reach −37°C and +70°C respectively. During standby and prelaunch tests, the temperature of the spacecraft (combined effects of heat generated by spacecraft equipment, solar radiation on the nose fairing, and temperature of the atmosphere) usually ranges from 0°C to +35°C at Cape Kennedy. After the spacecraft was mated to the third stage, during *on-stand* operations prior to removal of the gantry (at approximately *T*—90 minutes), conditioned air at 15 to 24°C, less than 30 percent RH, was supplied beneath the third stage nose fairing via a plastic shroud. After removal of the gantry and conditioned air lines, the third stage, at a uniform temperature of approximately 20°C acted as as a heat sink to moderate the temperature within the fairing during subsequent operation of the spacecraft equipment and solar heating.

Humidity

Humidity (up to 100 percent) was expected, at temperatures allowing condensation to take place in the form of water or frost, in both shipping and handling.

Vibration

Complex vibration (including sinusoidal and random) was expected during shipment, the level of which varies with the kind of vehicle used and the extent of care exercised. The estimated maximum effect of vibration during careful transport by truck can be represented by sinusoidal vibration, applied to the shipping container of less than 2 g RMS from 1 cps to 500 cps. Vibration transmitted to the spacecraft assembly was minimized by careful design of the isolator system which supports the assembly in the shipping container.

Shock

Special handling, packaging, and care during transportation of the spacecraft were expected to preclude shock of sufficient magnitude to damage the components. To minimize shock, transportation by special air-ride van (at controlled speeds over a preplanned and checked route) was provided. Recording accelerometers were installed on the floor of the van and on the isolation system of the shipping container. These strip charts were examined to insure compliance with the handling procedure.

Pressure

Atmospheric pressure was expected to range from 30.5 inches of mercury at sea level to 28 inches during transport.

Sand and Dust

The spacecraft was expected to be subjected to sand and dust particles encountered in beach and desert areas.

Salt Spray

Salt sea atmosphere in coastal regions was an expected environment.

Fungus

Fungus growth encountered in tropical climate was an expected environment.

Solar Radiation

The spacecraft, when not protected, was subjected to the complete spectrum of solar radiation at a maximum level of 360 Btu, per square foot, per hour, for periods of two hours per day.

Rain

Special care was exercised to minimize rain penetration.

Environment During Phase II

Temperature

The maximum temperature of the spacecraft assembly during launch and prior to fairing jettison was expected to be 165°F, based on a maximum fairing interior surface temperature of 150°C and a fairing jettison time and altitude of approximately 160 seconds and 400,000 feet, respectively. (These values were based on most severe 165-thousand-pound-thrust Thor trajectory.)

Humidity

Humidity up to 95 percent was expected at lower altitudes during launch.

Vibration

Complex vibration to relatively high values was expected in the spacecraft assembly during the launch phase. The main sources of vibration are: engine acoustic noise at liftoff; aerodynamic forces near Mach 1 and near maximum dynamic pressure; a strong 600 cps combustion resonance of the third stage; and shock forces at ignition, burn out, and separation of each stage. The values in Table 9–1 represent estimated vibration conditions of the maximum severity which were expected by the Relay spacecraft.

Acceleration

Values of axial and side load factors, due to sustained accelerations, which were expected, are given in Table 9–2.

TABLE 9–1.—*Vibration Frequency Sweep Schedule*

Vibration axis	Frequency range, cps	Test Duration, min.	Acceleration g 0-to-peak
Thrust (*Z–Z*)	5–50	0.83	1.5
	500–50	0.83	7.1
	500–2000	0.50	14
	2000–3000	0.15	36
	3000–5000	0.18	14
		≈2.5 min.	
Lateral (*X–X*) and (*Y–Y*)	5–50	0.83	0.6
	500–50	0.83	1.4
	500–2000	0.50	2.8
	2000–5000	0.33	11.3
		≈2.5 min.	
Grand total		≈7.5 min.	

TABLE 9–2.—*Acceleration Load Factors Expected*

Time of flight	Axial load factor	Side load factor
T+120 sec.	4.3g	1.2g
First-stage burnout	12.4g	0.8g
Third-stage spinup	4.8g	0 g (*)
Third-stage burnout	20.6g	0 g (**)

*Does not include centrifugal loads due to spin.
**Based on 180-lb. weight at third-stage burn-out and a maximum ABL X–248 thrust of 3700 lb

Spin

Maximum nominal spin rate, which was expected to occur simultaneously with the axial acceleration listed in Table 9–2, was 2.75 rps.

Pressure/Vacuum

Ambient pressure in the atmosphere and in space during the launch phases were expected to vary approximately as listed in Table 9–3.

TABLE 9–3.—*Ambient Pressure Ranges Expected*

Phase	Pressure (inches of mercury)
First-stage boost	30.5 to 5×10^{-5}
Second-stage boost	2×10^{-9} to 8×10^{-10}

Shock

Shocks caused by ignition, cut-off, staging, etc., occurring during vehicle operation, were considered less severe than the vibration during launch.

Environment During Phase III

Temperature

The internal mean temperature of the spacecraft equipment mounting surface during the orbit phase was expected to be maintained between +4°C and +30°C with the aid of the spacecraft thermal controller. Temperature at extreme locations of internal equipment components was expected to reach limits of −1°C and +38°C, except in the immediate vicinity of the traveling wave tube, where the maximum temperature would exceed +38°C. The external surfaces of the spacecraft would be subjected to radi-

ation from the sun (442 Btu per square foot per hour), radiation from the earth (including reflected sunlight), and radiation from space. The temperature of the external surfaces was expected to vary between the limits of −100°C and +38°C.

Vacuum

Space vacuum at pressure of less than 4×10^{-10} inches of mercury was expected.

Charged Particle Radiation

The boost trajectory was such that the spacecraft would traverse the inner Van Allen zone of trapped radiation as well as encountering radiation from the Starfish experiment.

Micrometeoroids

Micrometeoroids were considered unlikely to penetrate the spacecraft and thus become hazards to internal components. The space densities of the micrometeoroid stream or shower (Geminid) and of singular (Sporadic) micrometeoroids about 80 km altitude are shown by expressions (a) and (b) when

$$10^{-13} \leq m \leq 10^{-3}$$

where m = mass of micrometeoroid in grams. The average density of the material is approximately 3.4 grams per cubic centimeter.

(a) $4 \times 10^{-19} \left(\frac{10^{-3}}{m}\right)$ per cubic centimeter (Geminid)

(b) $\frac{3.5 \times 10^{-22}}{m}$ per cubic centimeter (Sporadic)

Micrometeoroid velocities under the conditions stated above are:

Geminid: approximately 36 km/sec; direction in the equatorial plane

Sporadic: 10 to 70 km/sec; any direction except from the approximate direction of the earth.

Micrometeoroid densities were best estimates, based on the small amount of data available at the time of issuance of the environmental specification.

QUALIFICATION TESTS

Spin

The spacecraft was spun up to 206 rpm during the spin test, corresponding to 1¼ times the maximum spin rate of the vehicle (see Figure 9–1) anticipated during third stage powered flight. The spacecraft was operated for two simulated orbits of wideband mode, i.e., 36 minutes of repeater operation followed by 127 minutes of standby operation per orbit. Power was supplied to the spacecraft from an external power supply via slip rings; all other signals were via radio links.

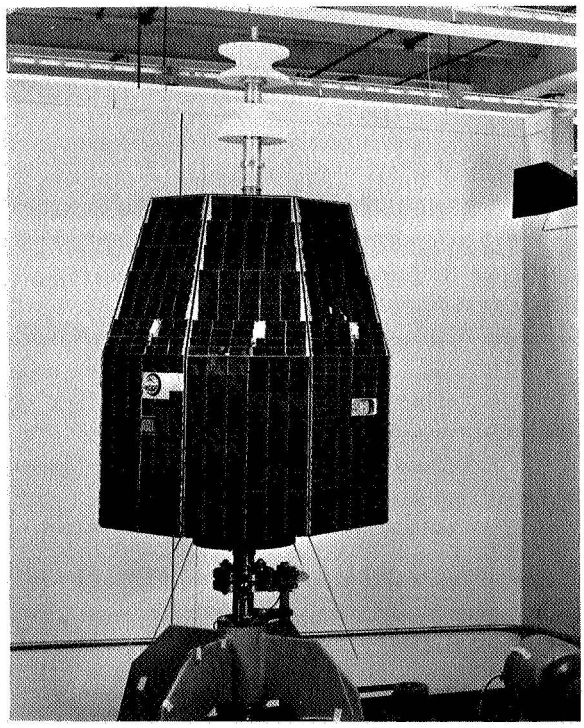


FIGURE 9–1.—Relay I spacecraft mounted on spin test fixture.

Temperature

This test was performed in air instead of vacuum as an expedient measure to prevent excessive expense for thermal-vacuum retest in the event of a seriously defective unit. The spacecraft was installed in a 14′×14′×17′ Tenney chamber (see Figure 9–2) capable of producing temperatures from −80°F to +250°F, and relative humidity from 20 percent to 95 percent over a temperature

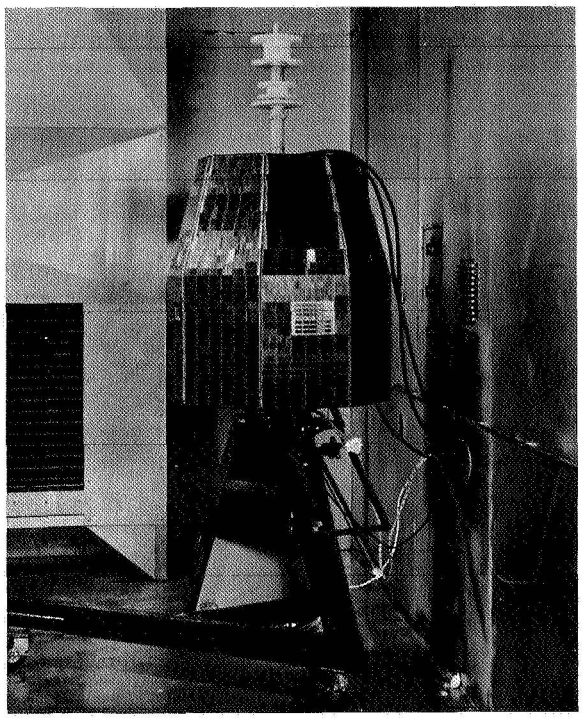


FIGURE 9–2.—Relay I spacecraft installed in Tenny chamber.

range from 33°F to 185°F. All connections to the spacecraft were made via hard-lines.

Following an electrical checkout of all subsystems, the battery packs were removed from the spacecraft, and the inoperative spacecraft was subjected to a temperature soak of 6 hours at −30°C, followed by 6 hours at +60°C. After removal from the chamber, the battery packs were reinstalled, electrical performance was verified, and the spacecraft reinstalled in the test chamber. The spacecraft was then operated for two simulated orbits in wideband mode at temperatures of −5°C and +35°C.

Thermocouples were installed at various significant points within the spacecraft and at specific reference locations indicated by thermal analysis.

Vibration

General

Prior to test, an electrical performance check was made of all spacecraft subsystems. The spacecraft was then attached to an MB–C210 vibration generator by means of a rigid jig fabricated with a spacecraft adapter. The adapter duplicated the vehicle mating surface.

Description of Vibration Facility

1. *Capability*—The MB–C210 vibration machine is capable of producing 28,000 pounds peak force (sine) or 25,200 pounds force (random) with a maximum displacement of ± ½-inch over a frequency range of 5 cps to 2000 cps. The control console can provide sinusoidal, logarithmic-sweep, wideband oscillation with automatic frequency cycling, and servo control to provide constant acceleration, velocity or displacement with varying frequency. The random frequency exciter contains a parallel 80-channel-filter spectrum analyzer and manual/automatic spectrum equalization (± 3 db), facilitating narrow bandwidth scanning, manual/automatic system compensation, and spectrum shaping.

2. *Protective Devices*—Protective devices presently incorporated into the shaker system include the following:

a. An amplitude limiting device which limits the shaker amplifier input drive.

b. A displacement limiter, to prevent excessive displacements from occurring.

c. An acceleration discriminator, which removes the drive to the machine in the event a pre-set peak g-level is exceeded.

d. A safety monitor which overtakes control of the machine in the event of loss of servo control signal from the control accelerometer.

e. An automatic random protective cutout which protects the machine in the event of a random failure in the servo system.

Instrumentation

1. *Installation*—For purposes of controlling vibration applied to the spacecraft, a calibrated accelerometer was attached rigidly to the jig near the spacecraft-jig interface and aligned with the axis of applied vi-

bration. Two other accelerometers were mounted on the jig, close to the spacecraft-jig interface, to monitor uncontrolled lateral crosstalk. The sensitive axis of both accelerometers were mutually perpendicular to the first.

2. *Calibration* — All accelerometers were calibrated on a two-inch thick aluminum adapter plate bolted to the vibration machine. To eliminate noise, the accelerometers were cemented with Kodak HK910 adhesive. The primary accelerometer was a secondary NBS standard. Calibrations were run at 1g, 5g and 20g (all peak), over the frequency range.

Sinusoidal

Sinusoidal vibration is used to simulate the third stage effects. This portion of the test was conducted by sweeping the range from the lowest to the highest frequency, once for each range specified in Table 9–4.

TABLE 9–4.—*Sinusoidal Frequency Sweep Schedule*

Vibration axis	Frequency range cps	Test duration (min.)	Acceleration g, 0-to-peak
Thrust (Z–Z)----	5–50	1.66	2.3
	50–500	1.66	10.7
	500–2000	1.0	21.0
Lateral (X, Y)---	5–50	1.66	0.9
	50–500	1.66	2.1
	500–2000	1.66	4.2

Time-rate-of-change of frequency was proportional to frequency at the rate of two octaves per minute.

Combustion Resonance Dwell

This test simulated a measured combustion oscillation observed in the X–248 solid-propellant rocket motor. The range of the sinusoidal vibration test was from 550 cps to 650 cps. The test was conducted by traversing this 100-cps band slowly, over a one-half minute period. Rate of change of frequency with time was proportional to frequency. The vibration level achieved was the maximum available from the vibration equipment (C210) for the thrust axis, and 14.5 g, peak, for each lateral axis.

Random

Random vibration is considered to occur during launch and maximum dynamic pressure flight. During the random noise vibration tests, signals from the control accelerometer were passed through a bandpass-filter type analyzer that was adjusted to scan the test frequency spectrum. The filter bandwidth was narrowed as required by the test requirements.

Gaussian random vibration was applied to the spacecraft with g-peaks clipped at three times the root-mean-square acceleration, according to the schedule shown in Table 9–5.

TABLE 9–5.—*Random Vibration Sweep Frequency Schedule*

Vibration axis	Frequency range (cps)	Test duration (minutes)	PSD level (g^2/cps)
Thrust (Z–Z)----	20–2000	4	0.07
Lateral (X–X and Y–Y)-----	100–2000	4 (each axis)	0.07

With the spacecraft installed on the vibration machine, the control accelerometer response was equalized with a peak/notch filter system, so that the specified peak-spectral-density values were within ± 3 db within the frequency band; the filter roll-off characteristic above 2000 cps was 40 db per octave or greater.

Thrust Axis

A cylindrical-bodied fixture was bolted to the adapter plate of the C210 vibration machine. This fixture was equipped with the lower mate to the 3rd stage separation ring. The spacecraft was then mounted on the fixture (see Figure 9–3). The two mating halves of the separation ring were held together by a Marman-type clamp designed for vibration loads. Three orthogonal accelerometers were then cemented to the vibration fixture as close to the separation ring as possible.

Following the connection of test and instrumentation cables, an operational check of the spacecraft's various subsystems was

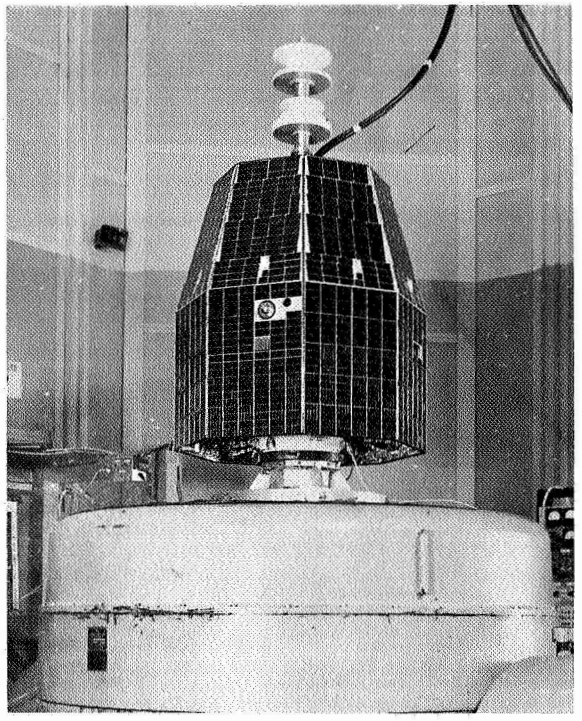


FIGURE 9–3.—Spacecraft mounted on C210 vibration machine for thrust axis vibration test.

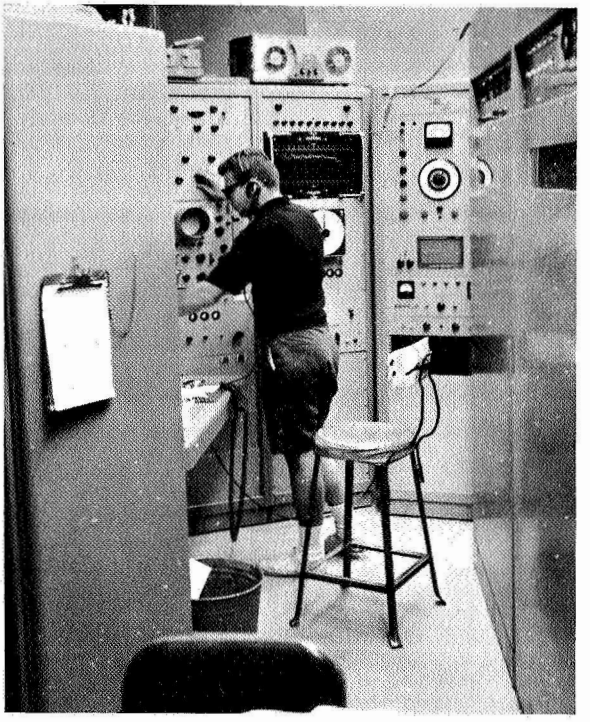


FIGURE 9–4.—Vibration machine spectrum equalization equipment.

made. For survey purposes a preliminary vibration run was made using servo-controlled sinusoidal inputs as follows:

Run A: 2g peak, 50–500 cps, 2 octaves/minute.

Run B: 4g peak, 500–2000 cps, 2 octaves/minute.

This survey acquainted test personnel with timing of tests, and checked the servo control of sweep rate, accelerometer outputs, and instrumentation recording.

Following a review of the survey data, the sinusoidal and the combustion resonance tests were carried out. All spacecraft electrical systems expected to be operating during launch were exercised during these tests and results were recorded and analyzed.

Upon completion of the above tests, a low level random vibration (1g RMS) was applied to the spacecraft. The response spectrum was observed on a scope, and equalization was varied on an MB N–300 spectrum equalizer until the response was flat to within ±3 db (see Figure 9–4). An X–Y plotter was used to record equalized response. Following equalization, the spacecraft electrical systems were checked and the random vibration test of Table 9–5 was carried out.

Lateral

After removal of the spacecraft and thrust-axis fixture from the adapter plate, the vibration machine head was rotated 90° from its normal position and the lateral-axis fixture was attached. The spacecraft was placed on this fixture and secured by a Marman clamp (Figure 9–5). One accelerometer was cemented near the separation ring to monitor input levels. Two other accelerometers (previously cemented near the c.g. of the spacecraft) were used as the control accelerometers during the first phase of the lateral vibration test.

The spacecraft was laterally vibrated as noted in Table 9–5. The accelerometer located at the c.g. of the spacecraft was moni-

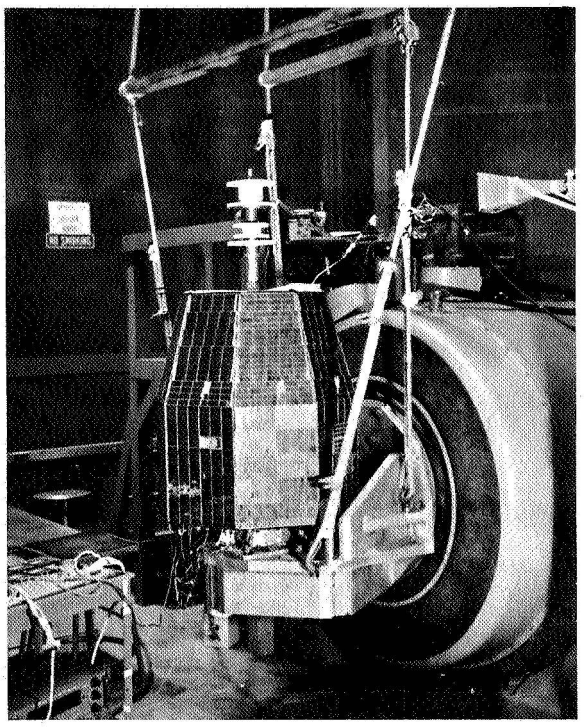


FIGURE 9–5.—Spacecraft mounted on C210 vibration machine for lateral axis vibration test.

tored, up to and including the fundamental structural mode frequency so that the force measured at the c.g. did not exceed 3g peak. This part of the test was not servo-controlled, due to the sharp rise of c.g. acceleration as resonance is approached. Above the first-mode resonance, the test was continued under servo control at a sweep rate of two octaves per minute.

All spacecraft electrical subsystems normally operating during launch were commanded on and the performance was observed. At the completion of the sinusoidal, combustion resonance dwell, and random vibration tests in the X axis, the spacecraft was rotated 90° and the tests repeated for the "Y" axis.

Solar Simulation

General

The solar simulation test was designed to reproduce, as closely as possible, the environment expected during Phase III, i.e., orbital flight. This included temperature, vacuum, and solar irradiation, but excluded radiation and the effects of micrometeoroids.

Installation

The spacecraft was mounted in a thermal-vacuum chamber on a fixture designed to support it in a nearly vertical position, free to rotate about its spin axis (Figure 9–6 and 9–7). A set of slip-rings were provided to facilitate external application of dc power to augment the solar-array output. The satellite was rotated throughout the 5-day test at twelve rpm.

Test Plan

Prior to the start of rotation, chamber pressure was reduced from room ambient to 5×10^{-5} mm mercury or less. With the spacecraft operating, the chamber walls were cooled by liquid nitrogen to —175°C. During this period, radiant energy equivalent to a solar intensity of 442.4 Btu per hour, per square foot, was applied to the spacecraft from the direction corresponding to that of the sun in space. The radiant energy spectral distribution approximated the solar spectrum. Orientation of the spacecraft with respect to the "sun" was selected to provide the most severe temperature conditions and thermal gradients as determined by the thermal design analysis. The spacecraft operation duty cycle was a simulation of the most severe operation in orbit. Solar radiation conditions and test duration are shown in Table 9–6.

TABLE 9–6.—*Solar Simulation Test Conditions*

Condition	Solar simulation	Duration (days)
Maximum sunlight orbit.	Simulator on for maximum time in sun at 100% of solar intensity, off for minimum time in eclipse.	3
Maximum eclipse.	Simulator on for minimum time in sun at 100% of solar intensity, off for maximum time in eclipse.	2

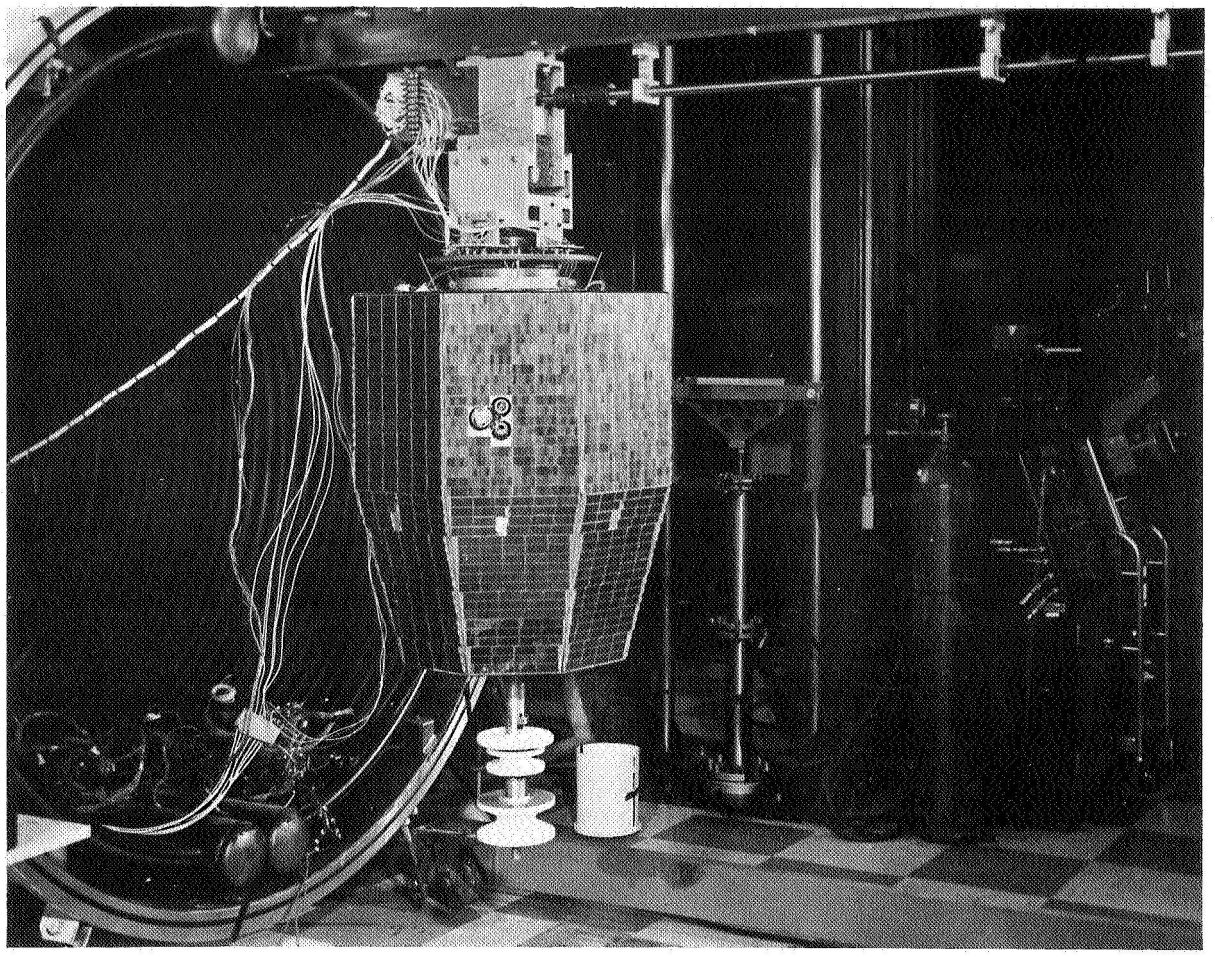


FIGURE 9–6.—Method of mounting spacecraft in thermal-vacuum chamber for solar simulation test.

Solar Simulator

The solar simulator consisted of two carbon arc lamps with optical outputs added together. This solar simulator had the uniformity of field and the spectral output to match approximately the Johnson Spectral Curve, which is the spectral irradiance of the sun's rays outside the atmosphere (air mass zero). A more detailed description of the solar simulator is presented in Chapter 10.

Calibration

An Eppley pyrheliometer, Model 50, was suspended in the vacuum chamber, normal to the solar energy field and in the same plane that the front surface of the spacecraft would eventually be located. Four solar cells were located on the rear wall of the chamber, connected thermally to the chamber wall and shielded from reflected radiation. These cells were located so that the satellite would not place them in shadow when it was suspended in the test position.

Pressure in the vacuum chamber was reduced to 1×10^{-5}mm mercury, the temperature of the walls was reduced to —110°C, and the solar simulator was activated. Solar intensity at the vehicle plane was recorded by the pyrheliometer and also by the solar-cell output current. The intensity recorded by the pyrheliometer was used to calibrate the solar-cell output current. Calibrations were made at 0.154 watts per square centi-

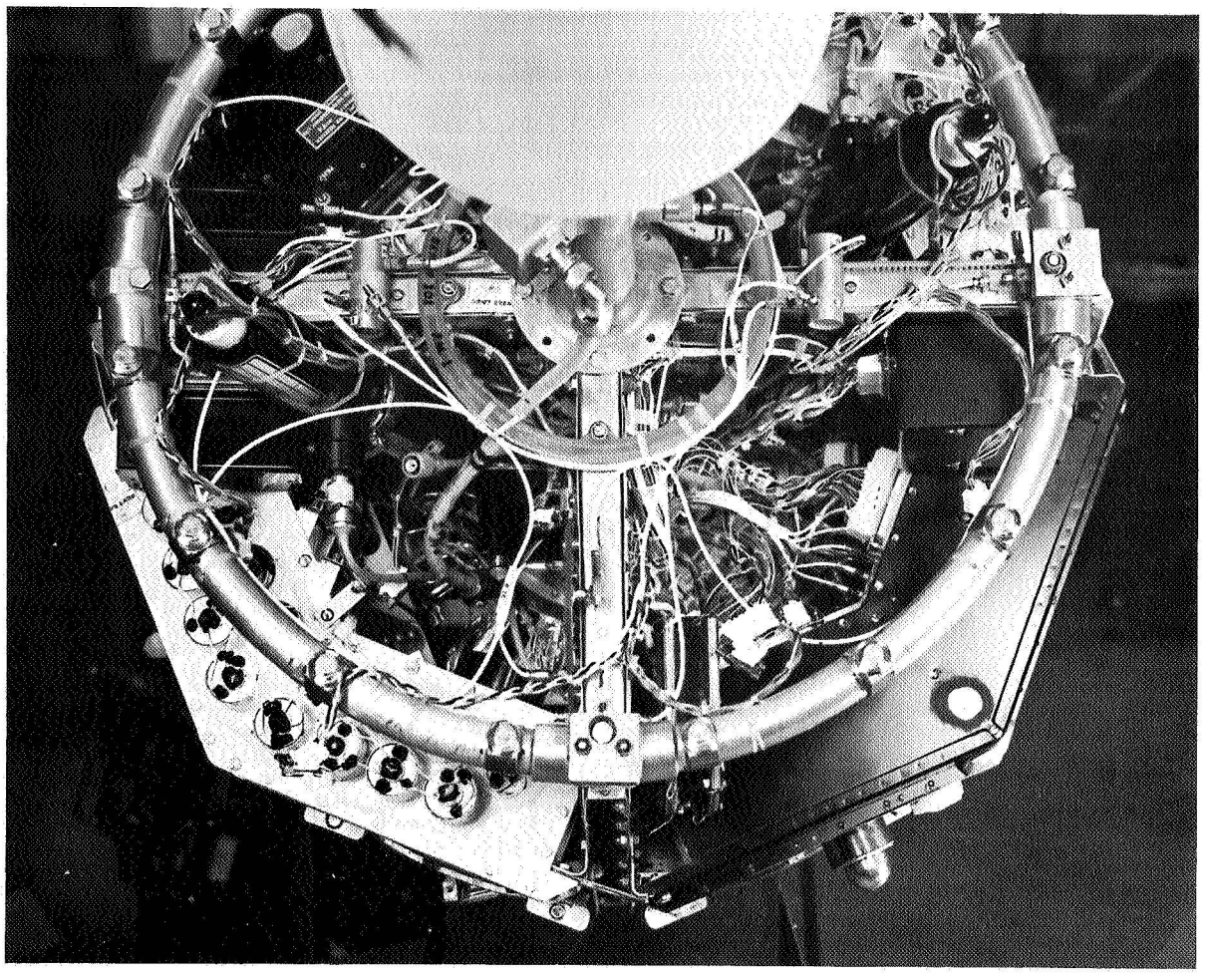


FIGURE 9–7.—Antenna end view—in preparation for solar simulation—solar panels removed.

meter, 0.140w/cm², and 0.126w/cm². Intensity variation was effected by use of a light chopper (Figure 9–8) located outside the vacuum chamber. The calibrated solar cells were used to monitor drifts of solar intensity during the spacecraft tests.

Test Schedule

The solar-simulation test schedule is outlined in Table 9–7.

Humidity

The humidity test was designed to duplicate that portion of the Phase I-expected environment, and to determine if a "drying" period was necessary to re-establish proper operation. The non-operating spacecraft was placed in the 14′ × 14′ × 17′ Tenney chamber (Figure 9–2) and subjected to a chamber temperature of +30°C, and relative humidity of 95 percent ±5 percent for 24 hours. At the end of the 24-hour period, the spacecraft was operated under these conditions for one duty cycle and the performance of all subsystems was verified.

Thermal Gradient

General

The thermal-gradient test duplicated temperature and vacuum conditions expected during Phase III. Chamber heat sinks were adjusted to simulate the thermal gradients expected within the spacecraft in a non-

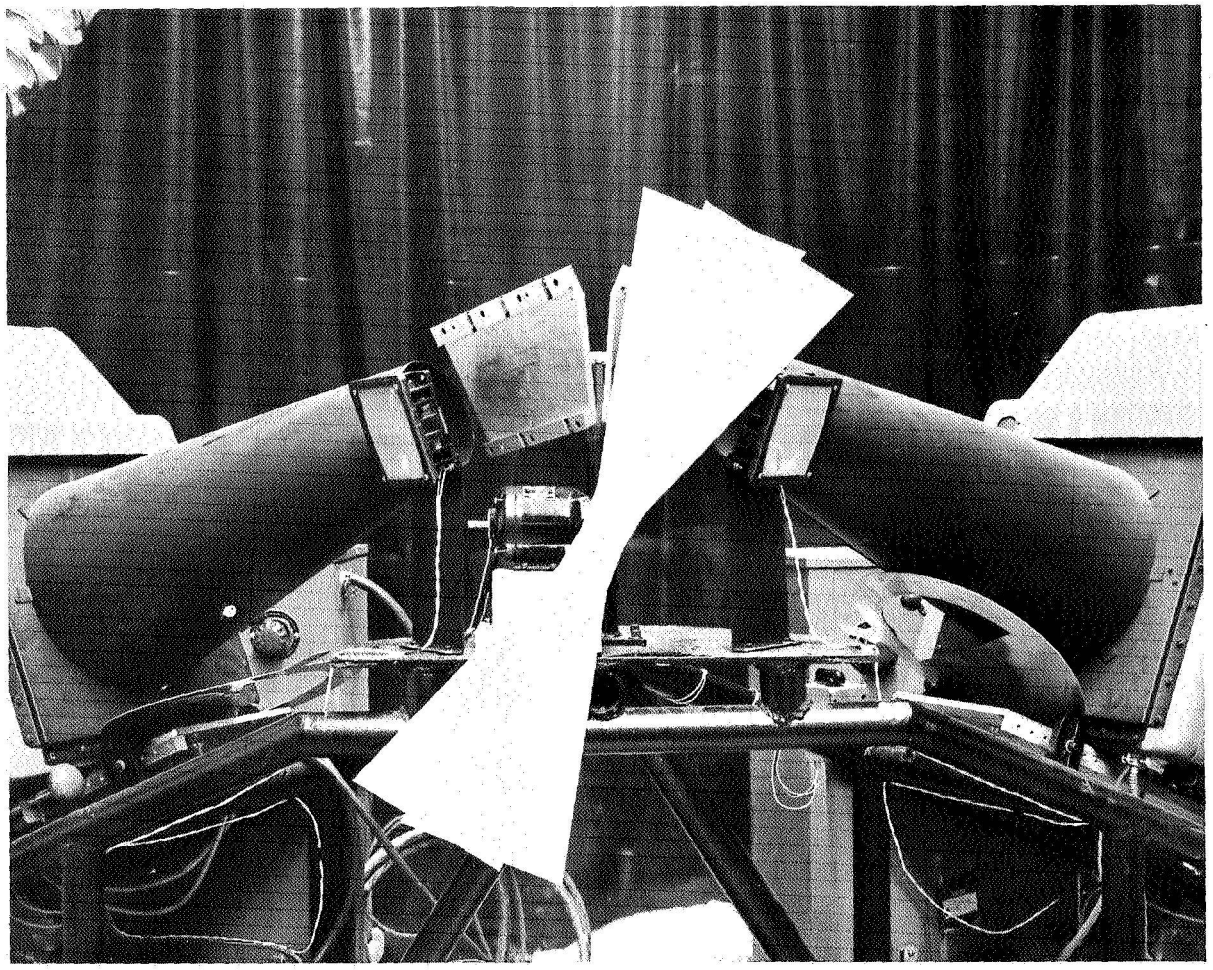


FIGURE 9–8.—Chopper installed between lamps and thermal vacuum chamber to control light density.

operative state during orbital flight (Figure 9–9). Influences of direct sunlight, absorptivity, emissivity, and attitude were considered in establishing these temperatures.

Facility

The thermal-gradient test was performed in the large thermal-vacuum chamber with inner dimensions of 26 feet (diameter) by 20 feet (height). The entrance door is 7 feet in diameter (Figure 9–10) and a removable top cover, 24 feet in diameter, allows entry of large test vehicles.

The vacuum system is capable of establishing a pressure of 5×10^{-6} mm mercury in less than 24 hours. The pumping system is composed of two 375-cubic-feet-per-minute roughing pumps, two 5000 cfm blower pumps, and sixteen oil diffusion pumps having combined capability of 300,000 liters per second. The minimum pressure obtainable with these pumps is 5×10^{-7} mm mercury, whereas the walls are designed to support internal pressures as low as 1×10^{-9} mm mercury.

The thermal system is composed of six separate heating and cooling copper-tube heat sinks. Four of these sinks divide the walls into quadrants and the other two are on top and bottom of the chamber. Using brine coolant, the temperature can range from +275°F to −125°F; with liquid nitrogen,

TABLE 9–7.—*Solar Simulation Test Schedule*

Maximum Temperature Test—72 hours
Solar Input = .154 W/cm² on continuously

Orbit	Operation	Total time
First day	Continuous mode	136 min.
1	Wideband No. 1. 36 min. on, 127 min. off	163 min.
2	Wideband No. 2, 36 min. on, 127 min. off	163 min.
3	Wideband No. 1, 14 min. on. Wideband No. 2, 14 min. on.	163 min.
4–7	Continuous mode 163 min. each orbit	652 min.
8	Continuous mode*	163 min.
	24 hr	=1440 min.
Second day	Continuous mode	136 min.
1	Wideband No. 1, 36 min. on, 127 min. off	163 min.
2	Wideband No. 1, 36 min. on, 127 min. off	163 min.
3	Wideband No. 1, 28 min. on, 135 min. off	163 min.
4–7	Radiation mode 163 min. each orbit	652 min.
8	Radiation mode*	163 min.
	24 hr	=1440 min
Third day	Radiation mode	136 min.
1	Wideband No. 2, 36 min. on, 127 min. off	163 min.
2	Wideband No. 2, 36 min. on, 127 min. off	163 min.
3	Wideband No. 2, 28 min. on, 135 min. off	163 min.
4–7	Continuous mode 163 min. each orbit	652 min.
	24 hr	=1440 min.

Minimum temperature test—48 hours
Solar Input each orbit: 15 min. on, 40 min. off, 108 min. on; equal to .126 watt/cm².

Fourth day	Continuous mode, solar input off 24 min.; on 108 min.	136 min.
1–4	Continuous mode, 163 min. each orbit	652 min.
5	Wideband No. 1, 36 min. on, 127 min. off	163 min.
6	Wideband No. 1, 36 min. on, 127 min. off	163 min.
7	Wideband No. 1, 135 min. off, 28 min. on	163 min.
8	Radiation mode*	163 min.
	24 hr	=1440 min.
Fifth day		
1	Radiation mode	163 min.
2–5	Radiation mode, 163 min. each orbit	652 min.
6	Wideband No. 2, 36 min. on, 127 min. off	163 min.
7	Wideband No. 2, 36 min. on, 127 min. off	163 min.
8	Wideband No. 2, 135 min. off, 28 min. on	163 min.
9	Continuous mode; solar input 15 min. on, 40 min off, 81 min. on	136 min.
	24 hr	=1440 min.

*Necessary adjustments for the next 24 hr. period (such as cleaning mirrors) were made during 8th orbit. Adjustments for fourth and fifth days were made during solar simulator "off" periods.

the lower temperature limit can be dropped to −280°F. The heat capacity is 141,000 Btu per hour at −100°F.

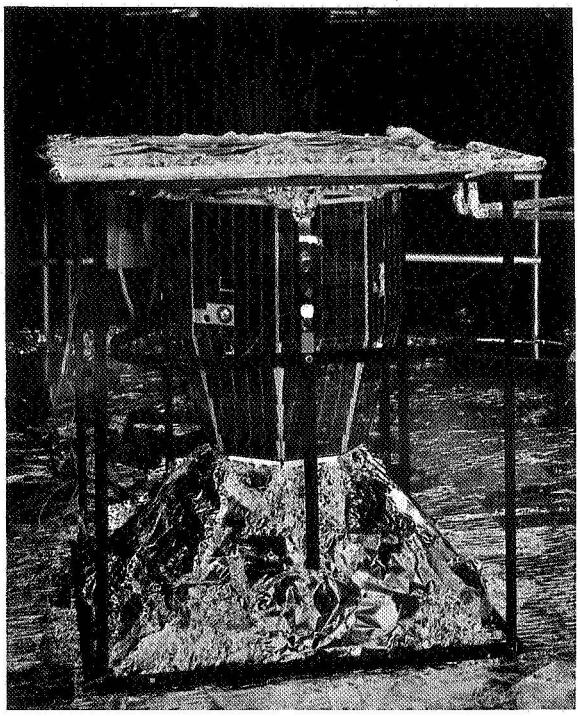


FIGURE 9–9.—Spacecraft installed in the thermal-vacuum chamber for the thermal gradient test.

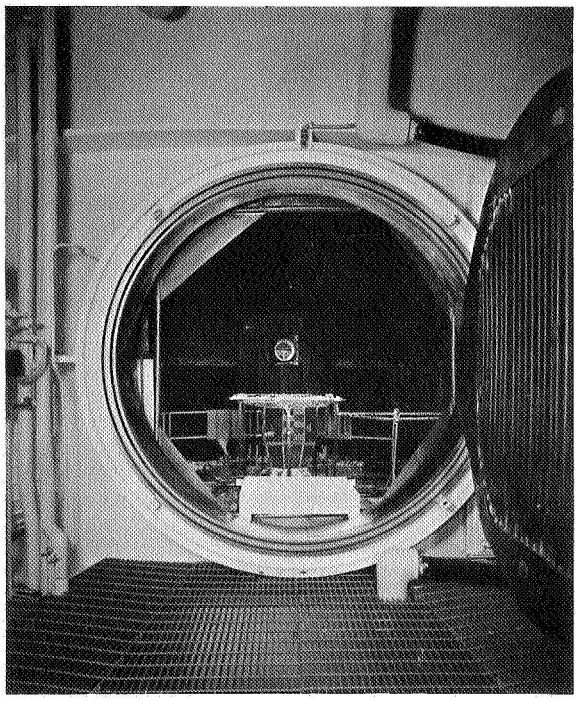


FIGURE 9–10.—View of spacecraft mounted for thermal gradient test.

Test Plan

The spacecraft was exercised under the conditions listed in Table 9–8.

The test commenced when the spacecraft temperature was stabilized at the designated temperature with a rate of change less than 1°C per hour.

Spacecraft temperatures were monitored in all critical areas and duplicate sensors were added to provide and verify calibration of the telemetry temperature channels.

TABLE 9–8.—*Thermal-Gradient Test Conditions*

Condition	Sunlight	Duration (days)
Cold soak	75%	1
Minimum temperature with equipment operating on a duty cycle with low charging rate on the batteries	75%	2
Maximum temperature with equipment operating on a duty cycle with high charging rate on batteries	100%	3

Acceleration (Steady State)

This test was designed to simulate the axial and side load accelerations expected during Phase II, the launch phase. (See Figures 9–11 and 9–12). The tests were conducted separately along each of three coordinate axes and measured at the center-of-gravity. The centrifuge selected for this test was large enough to prevent the g-gradient along the thrust axis from exceeding +15% at the forward end, +10% at

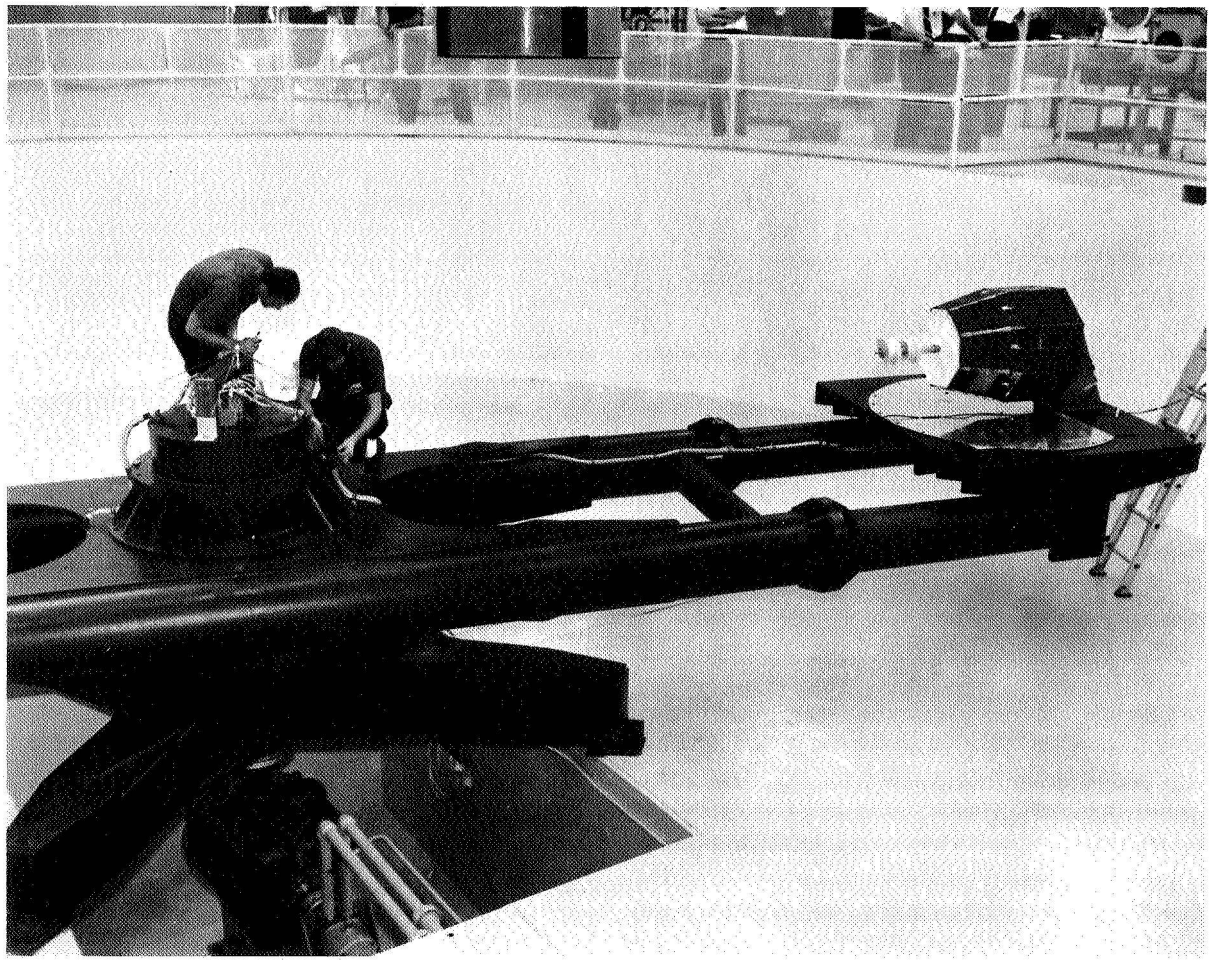


FIGURE 9–11.—Spacecraft mounted on centrifuge for thrust axis acceleration test.



FIGURE 9–12.—Spacecraft mounted on centrifuge for lateral axis acceleration test.

the aft end, and +10% in the transverse direction measured at the c.g. The centrifuge accelerated the spacecraft for a period of three minutes at 29.2 g in the thrust direction and for periods of one minute at 29.2 g in each of four transverse directions ($\pm X$, $\pm Y$).

During the test, two telemetry transmitters and two receivers were used. One of the transmitters was modulated by the spacecraft encoder, and the output from the associated receiver was recorded on magnetic tape. The second transmitter was not modulated, but the frequency of the receiver phase-lock oscillator (associated with the second transmitter) was recorded on paper tape. The magnetic tape recording was made for later analysis in the event of difficulty. The paper tape recording was made to check the frequency stability of the second transmitter during simulated launch.

ACCEPTANCE TESTS

General

The flight model spacecraft were subjected to only the first four environmental tests previously described, but with lower stress limits.

Spin

The spin rate was 165 rpm for acceptance tests; spacecraft operation was the same as in qualification tests.

TABLE 9-9.—*Vibration Acceptance Test Inputs*

Vibration axis	Frequency range, cps	Test duration, min.	Acceleration g, 0-to-peak
	Sinusoidal		
Thrust (Z–Z)	20–50	0.32	1.5
	50–500	0.83	7.0
	500–2000	0.50	14.0
Lateral (X–X) (Y–Y)	20–50	0.32	0.6
	50–500	0.83	1.4
	500-2000	0.50	2.8
	Combustion resonance dwell		
Thrust (Z–Z)	550–650	15	57, or max avail. from C210 machine, whichever is less
Lateral (X–X) (Y–Y)	550–650	15	9.4
	Random (PSD level = 0.03 g^2/cps)		
Thrust (Z–Z)	20–2000	2	7.7
Lateral (X–X) (Y–Y)	100–2000	2	7.7

Temperature

The tests were run at temperatures of +5°C and +25°C.

Vibration

The vibration tests consisted of the inputs listed in Table 9–9.

Solar Simulation

Solar simulation was performed with a solar input of 0.140 watts per square centimeter with the same schedule as in the qualification tests (see Table 9–7).

AUTHORS. *This chapter was written by* W. SCHREINER, R. NEWMAN, M. GITTLER, *and* S. RUMMEL *of the Radio Corporation of America, Princeton, New Jersey, U.S.A. under contract NAS 5–1272 with NASA/Goddard Space Flight Center.*

N66-10236

Chapter 10

Ground Support Equipment

INTRODUCTION

The ground support equipment for Project Relay consisted of spacecraft checkout equipment, environmental simulation facilities, and handling fixtures. Spacecraft checkout equipment was subdivided into four groups. The system groups were:

1. Microwave repeater
2. Telemetry
3. Command
4. General support equipment.

Environmental simulation equipment to be described includes the solar simulator, designed and built by the spacecraft contractor. Other equipment used for environmental simulation were commercially built vibration machines, thermal-vacuum test chambers, etc., previously described.

The ground support handling fixtures constitute the mechanical equipment designed to lift, hold, support, and protect the spacecraft reliably and safely.

SPACECRAFT CHECKOUT EQUIPMENT

General

The spacecraft checkout equipment was assembled from standard electronic test equipment and installed in either a 32-foot semi-trailer van or within the contractor's spacecraft laboratory, RCA–AED, Princeton, N. J.

The van was supplied by NASA/GSFC. Table 10–1 lists data regarding the van:

TABLE 10–1.—*GSE Van Data*

Nameplate data:
Freuhauf Model SSVV 532, S/N FW 113084
Gross weight: 35,000 pounds
Capacity: 24,000 pounds
Manufactured: 15 October 1956

Dimensions	Outside	Inside
Height:	146 inches	86 inches (80 inches clear of ducts)
Width:	96 inches (max.)	87 inches
Length:	384 inches	370 inches (331.5 inches clear of air conditioner)

The van exterior surfaces were made of spot-welded stainless steel panels. The wall cross-section included three inches of glass-wool insulation with an aluminum-foil vapor barrier and an internal facing of ¼-inch plywood. The floor consisted of 1½-inch plywood, plus three inches of insulation. The work surface of the floor was asphalt tile.

The rear doors were mounted on offset hinges to give access to the full inside width (87 inches). The personnel door was on the curb side of the forward half and measured 38.5 inches wide by 7 feet high.

The van air conditioner had a rated cooling capacity of 7 tons. Cooling air was carried through two ducts on the ceiling; one discharging over the personnel area and the other along the equipment area.

A pair of plug-in heaters were installed to provide for personnel comfort during inclement weather.

Input power consisted of two independent 208 v, 3 phase, 60 cycle services; one for the air conditioner and the other for remaining equipment.

The trailer contained eight racks of equipment and four work benches. (See Figures 10–1, 10–2, and 10–3.)

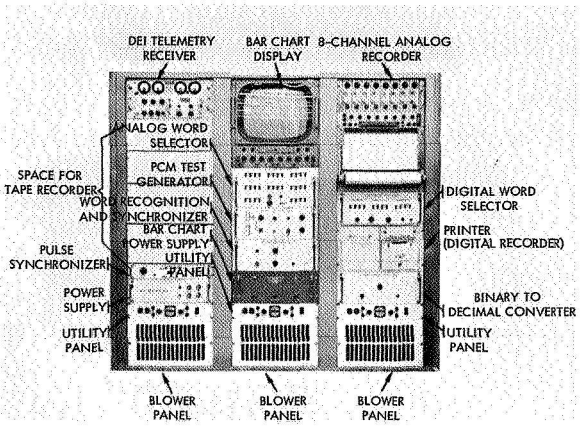


FIGURE 10–1.—Telemetry ground checkout equipment.

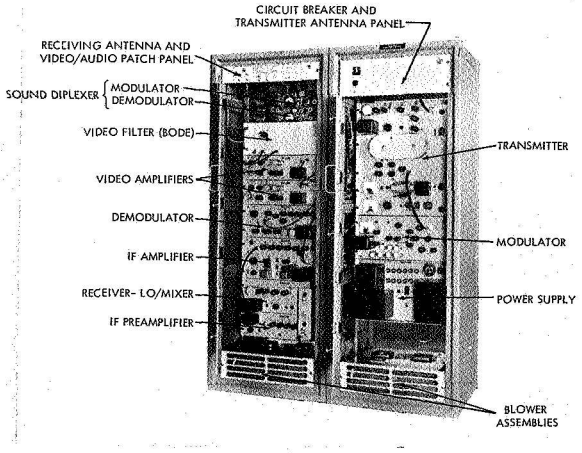


FIGURE 10–2.—Wideband microwave transmitter and receiver racks.

MICROWAVE REPEATER CHECKOUT EQUIPMENT

The microwave repeater checkout provided for transmission and reception of video test signals (stairstep, stairstep with superimposed signal, multiburst, white window,

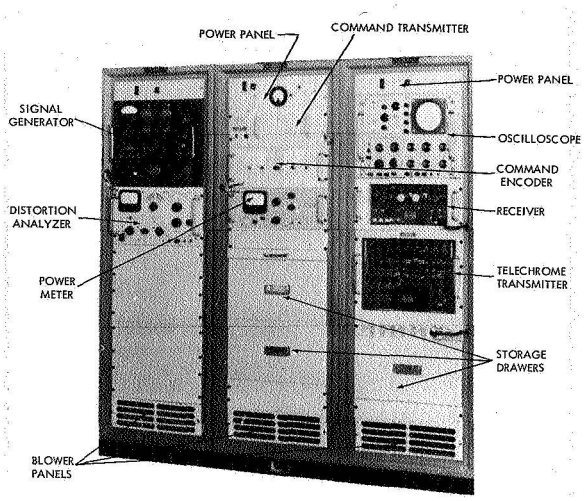


FIGURE 10–3.—Command, video, and general test equipment racks.

and audio test signals (0 to 20-kc sine waves). These signals provided means for determining differential phase, differential gain, and low and high frequency characteristics.

Equipment required for transmitting test signals to the microwave repeater comprises the following:

- Swept-frequency oscillator (GR type 1300 AR)
- Video-test-signal generator (Telechrome 1003–D1)
- Group delay transmitter (RCA MI–24365B)
- MM–600 transmitter (see Figures 10–4, 10–5, and 10–6)
- Antenna (lab built 1.7-KMC horn).

Reception of microwave signals from the spacecraft repeater was accomplished with the following equipment:

- Antenna
- MM–600 receiver (see Figures 10–7, through 10–12)
- Video-test-signal receiver (Telechrome 1004B)
- Group delay receiver (RCA MI–24366A)
- Oscilloscope
- Waveform analyzer (HP Model 302AR).

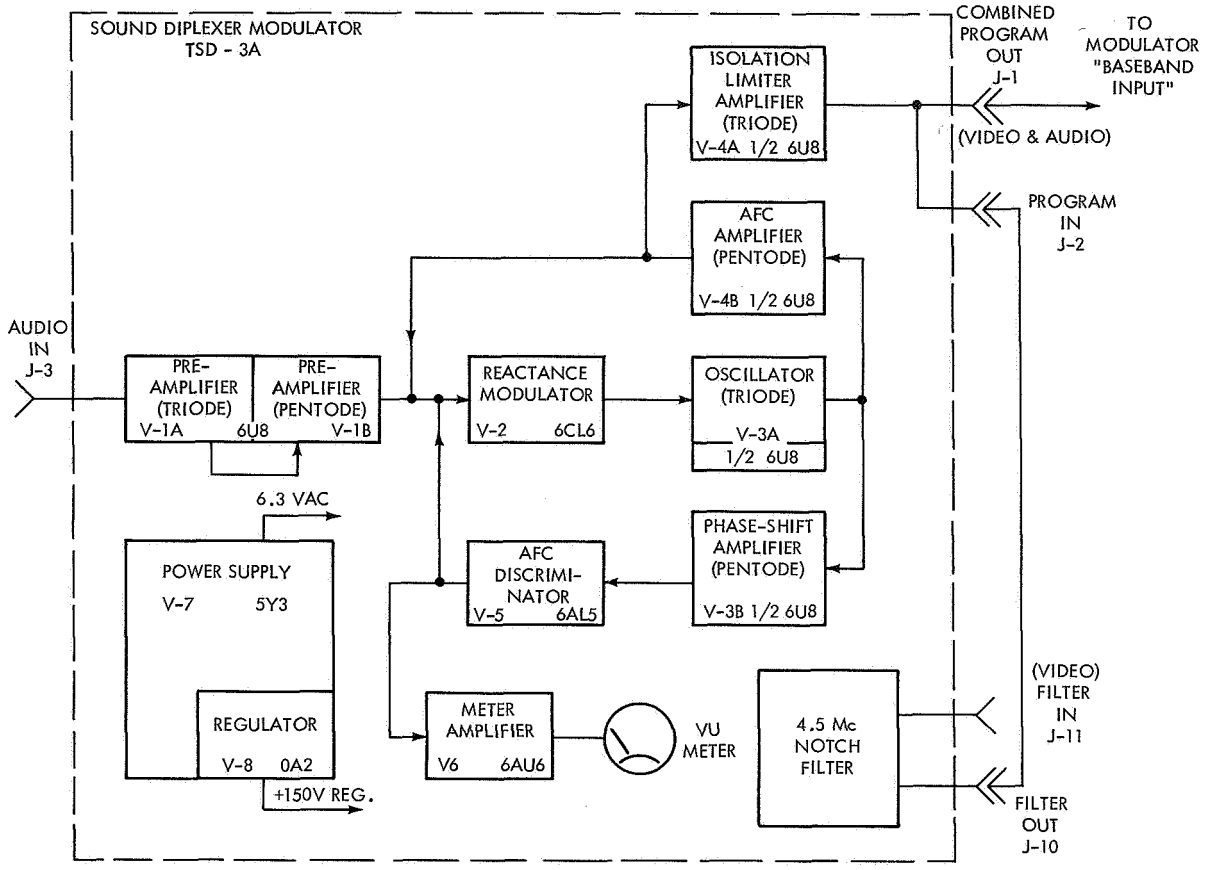


FIGURE 10–4.—Transmitter—sound diplexer modulator section, block diagram.

Telemetry Checkout Equipment

General

Reception of telemetry data from the spacecraft was accomplished with the following equipment:

- Antenna (Taco yagi, 148 Mc)
- Receiver (DEI—see Figure 10–13)
- Decommutator (DSC—see Figure 10–14)
- Oscilloscope
- Magnetic tape recorder (Ampex FR–1100).

Much of the Relay testing concerned itself either directly or indirectly with the reduction of telemetry data. This was necessary to test the satellite encoder and other subsystems. Because of this need, a relatively complete telemetry decommutation station was purchased. Since simultaneous readout of all 128 telemetry channels was not needed, a compromise against an overwhelming volume of equipment was reached by providing for reduction of any eight words in analog form and any three in printed binary format. Alternately, any one word is available in decimal equivalent along with any other additional word in binary form. This last arrangement has been exploited by reducing channel 28 (a word subcommutated 64 times) in decimal printout, along with its binary identification (word 16).

The units of the telemetry decommutation station (see Figure 10–14) included a sensitive, 136-Mc, phase lock, PM receiver (DEI); a seven-track, magnetic-tape recorder (Ampex-used exclusively in the direct recording mode); a signal simulator (test generator); a pulse synchronizer; a word sync and recognition unit; an analog word selector; a digital word selector; a binary-

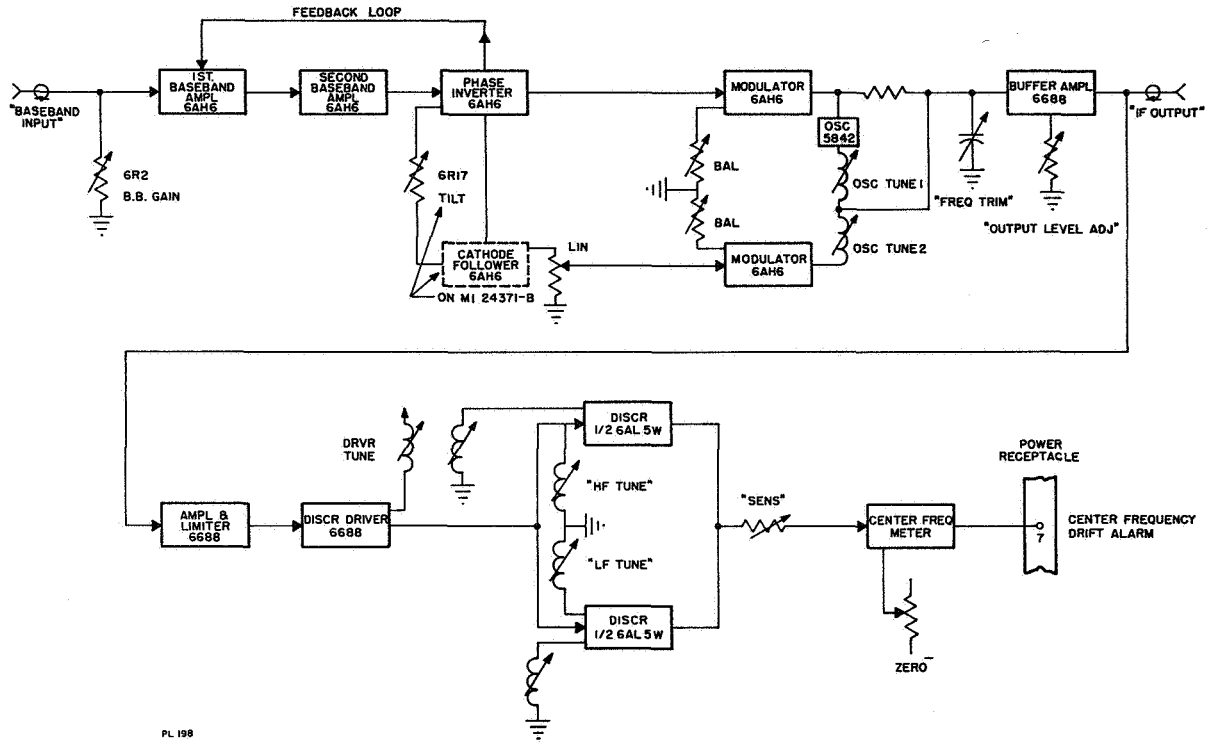


FIGURE 10–5.—Transmitter—modulator section, block diagram.

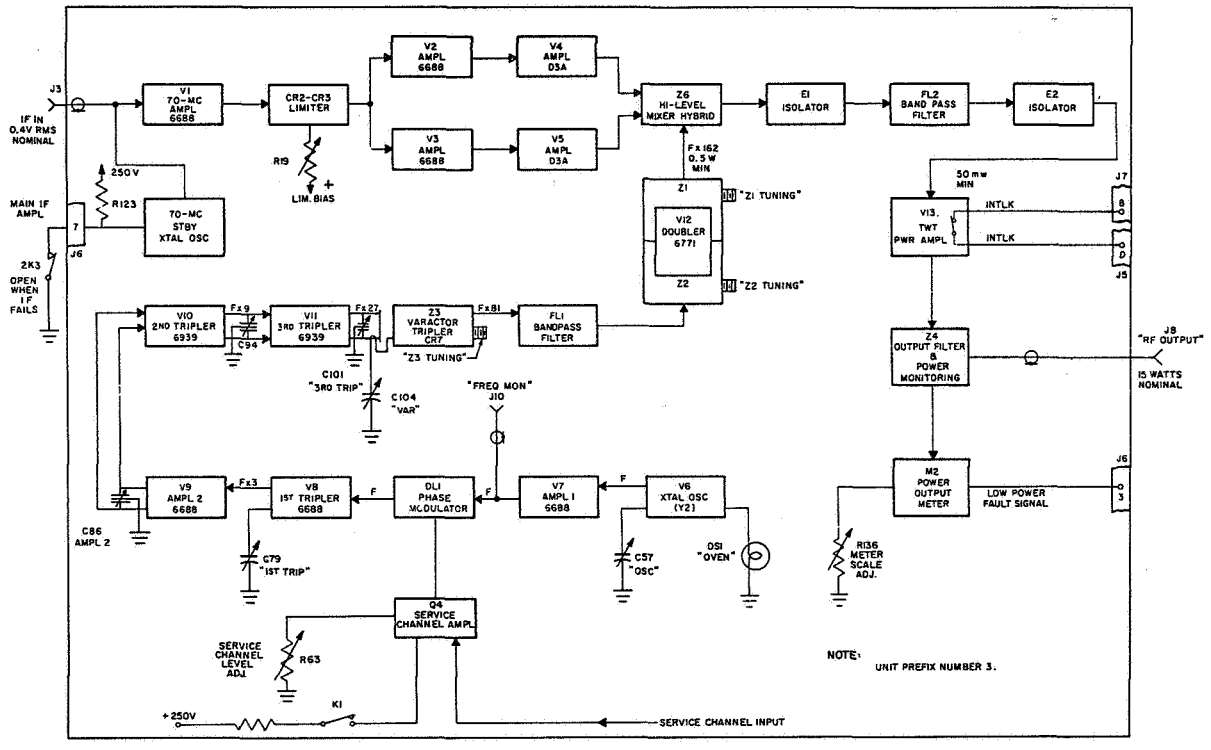


FIGURE 10–6.—Transmitter—RF output section, block diagram.

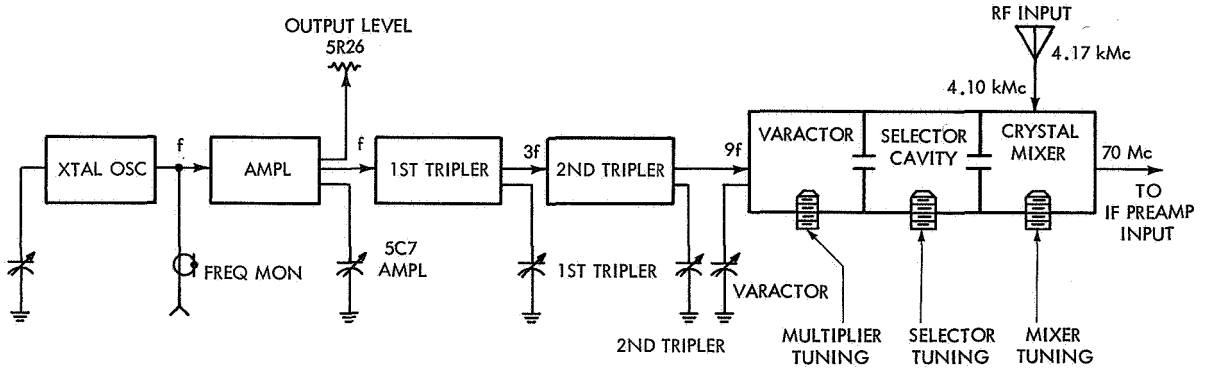


FIGURE 10–7.—Receiver—local oscillator-mixer section, block diagram.

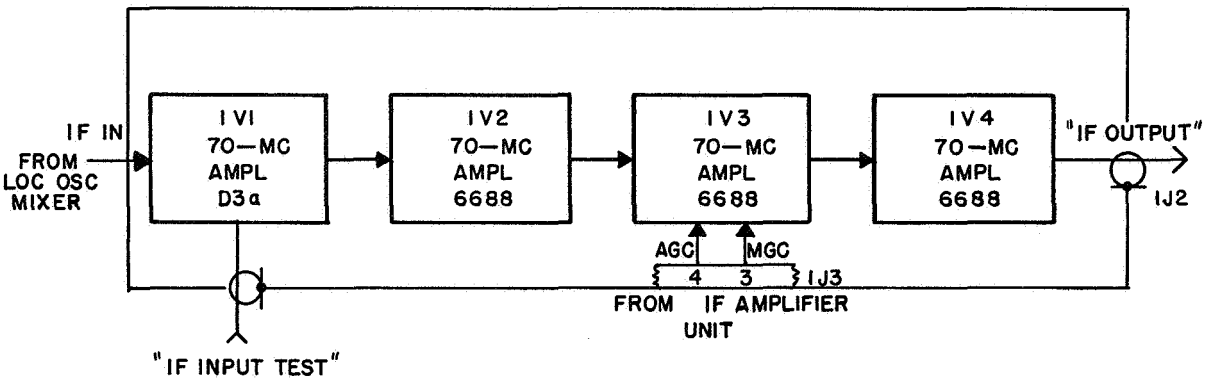


FIGURE 10–8.—Receiver—IF preamplifier section, block diagram.

to-decimal converter; an eight-channel, Sanborn, strip-chart recorder (for the analog word selection); and an HP digital recorder (printer). The last two items are standard laboratory items and will not be discussed further.

An I.T.T. 1735D bar oscilloscope was also part of the installation. It had limited use, but did display all 128 channels (in two 64-word sections). The display frame rate (one per second) was to rapid and made reading too difficult. It did, however, prove useful in displaying the output of the radiation experiment solar cells mounted on the radiation damage panel.

Pulse Synchronizer

The synchronizer was not one of the logic boxes of the decommutation gear but it performed the important task of reconstructing a clean telemetry signal and a true clock pulse, in spite of considerable digital noise. The technique employed was that of integrating a dc restored signal (dc level is automatically adjusted to provide equal positive and negative peaks) for controlled periods obtained from the reconstructed clock. This "smoothing bit detector" effectively proved itself for use with magnetically recorded signals. After integration, the signal was limited and fed to a Schmitt trigger squaring circuit. This reconstructed output was used as the signal for the words sync and recognition unit.

The synchronizer performed an additional function: signals in any acceptable form (NRZ, MNRZ, split phase, or RZ) were converted into the return-to-zero (RZ) format for use by the subsequent decommutator logic.

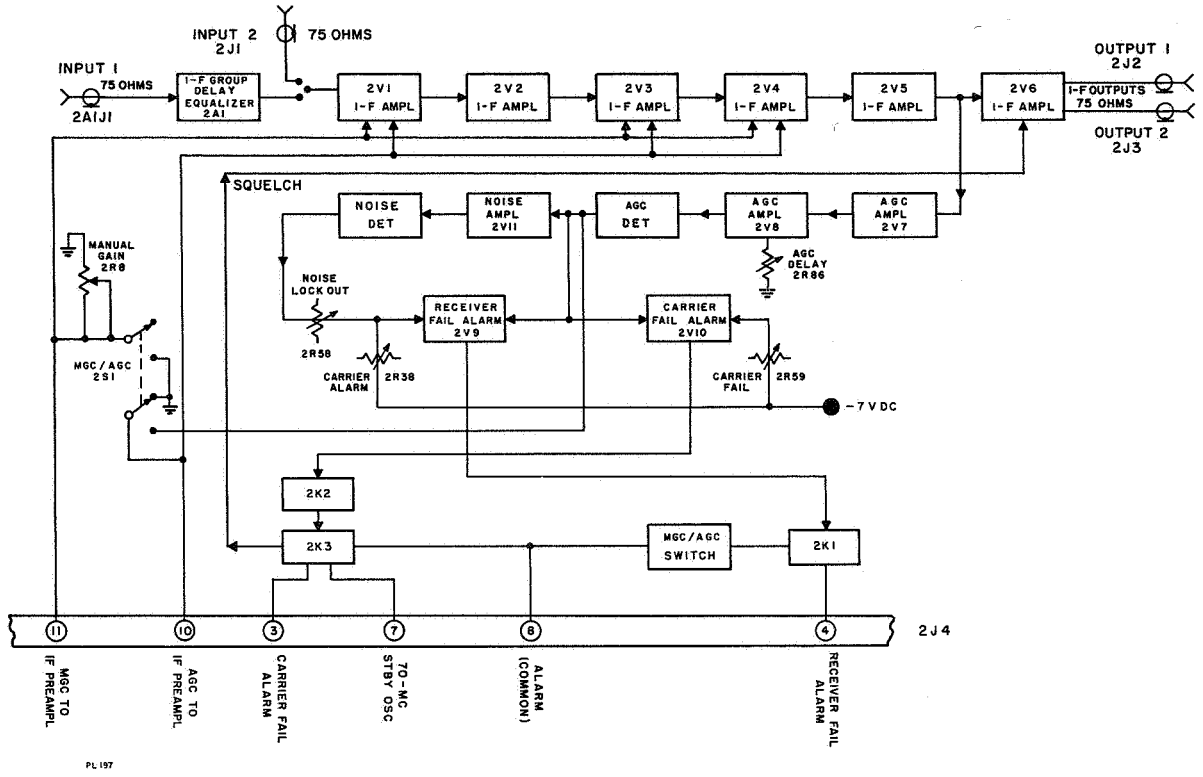


FIGURE 10–9.—Receiver—IF amplifier section, block diagram.

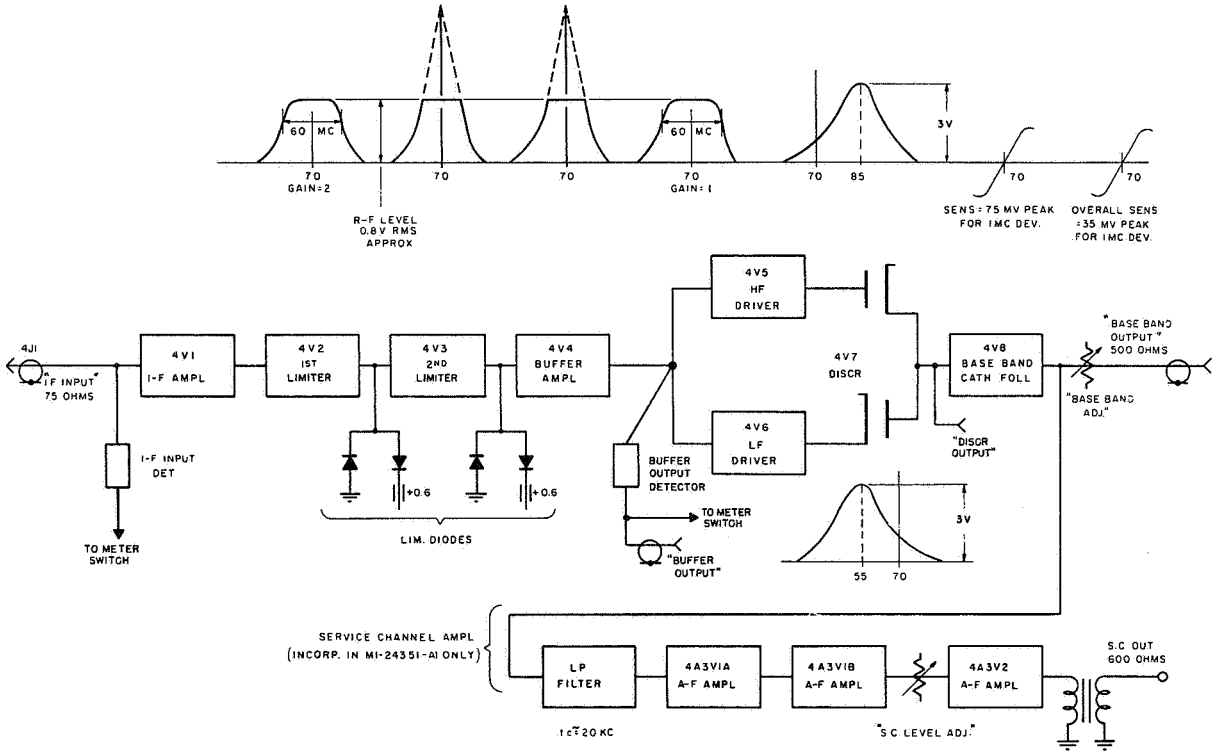


FIGURE 10–10.—Receiver—demodulator section, block diagram.

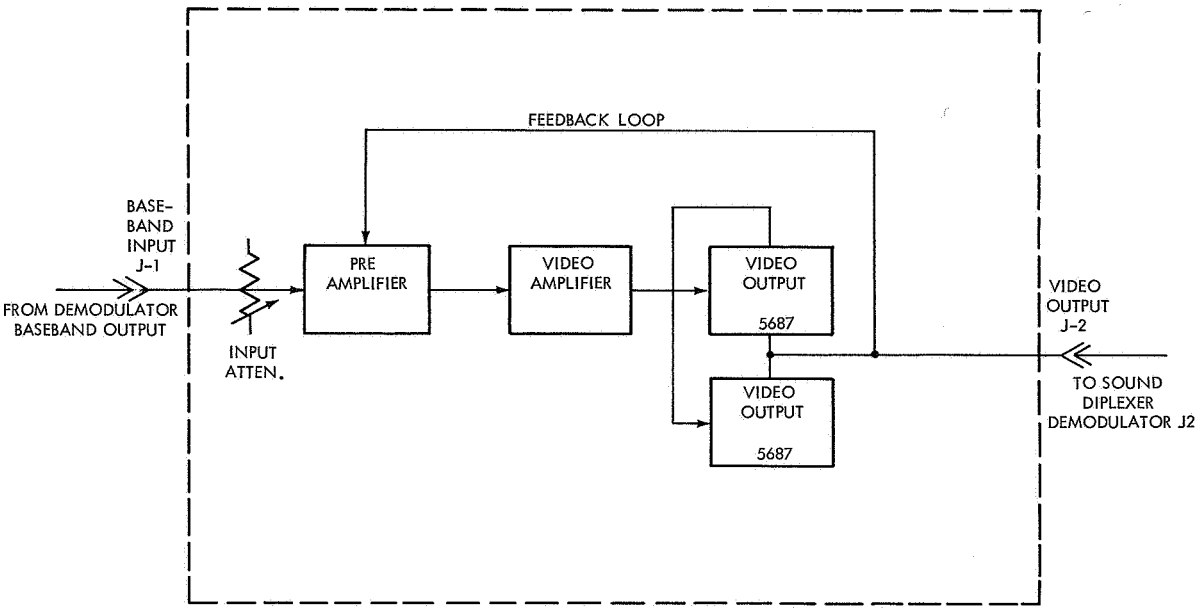


FIGURE 10–11.—Receiver—video amplifier section, block diagram.

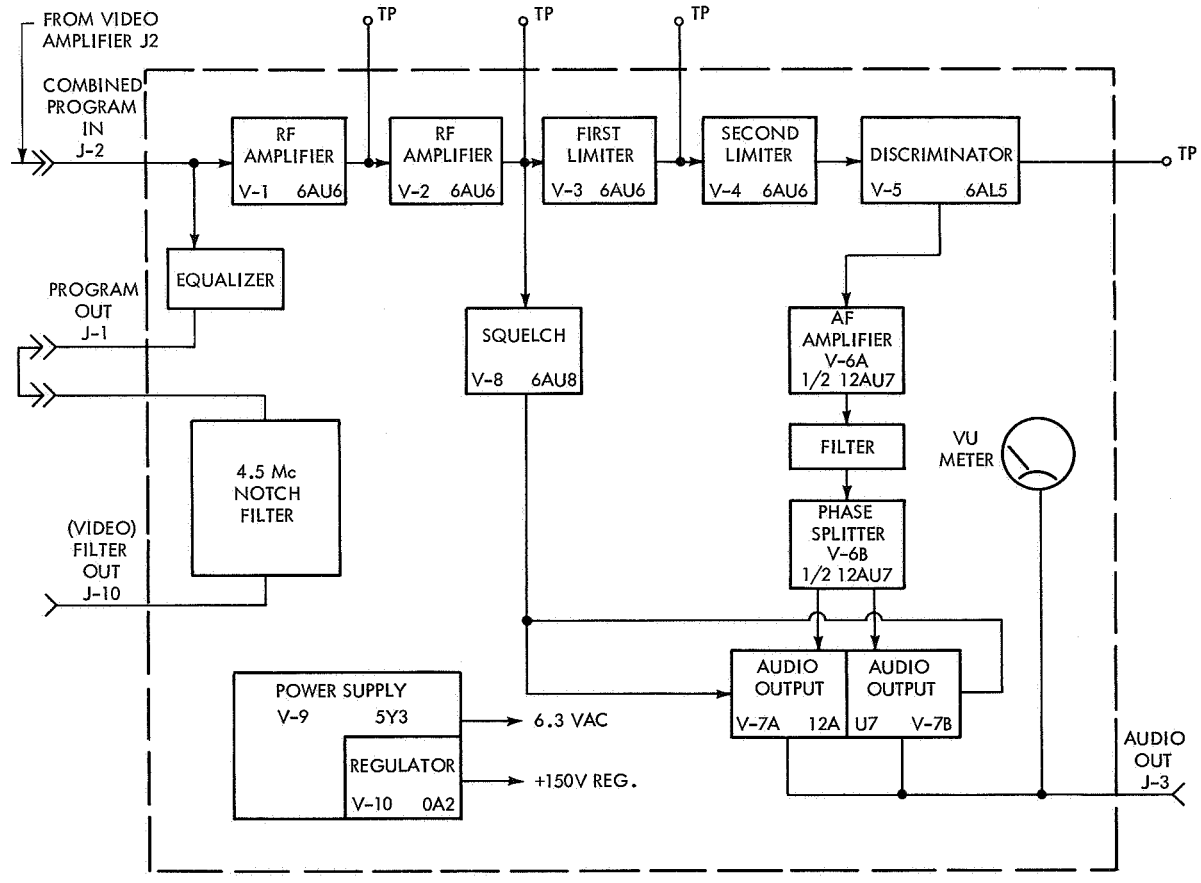


FIGURE 10–12.—Receiver—sound diplexer demodulator section, block diagram.

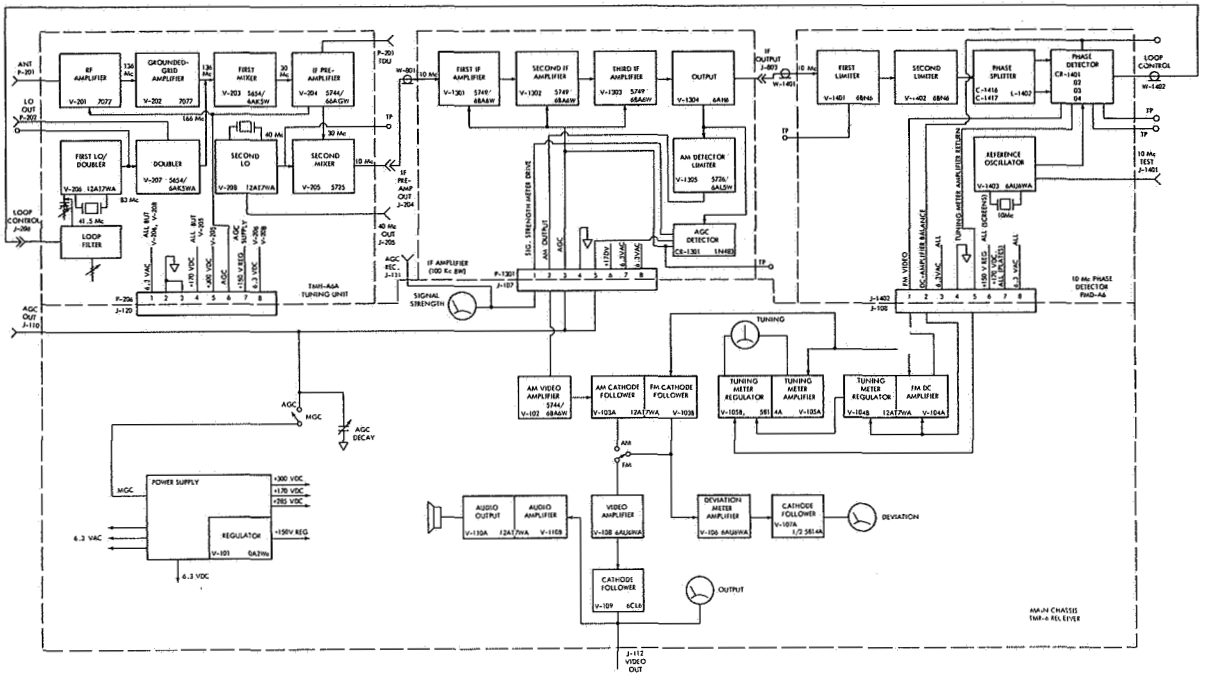


FIGURE 10–13.—Telemetry receiver block diagram.

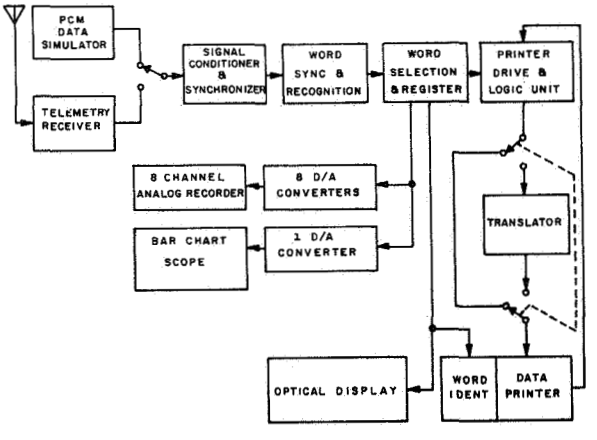


FIGURE 10–14.—Telemetry ground checkout equipment.

Test Generator

The decommutation equipment was relatively complicated and therefore some form of testing, independent of all (possibly faulty) input signals, was necessary. The test generator could provide a substitute signal for direct use with the pulse synchronizer. The latter unit could be bypassed, and the proper signal derived directly from the generator for use with the word recognition unit. Thus, the need for converting the normal word format (split phase) into RZ signals used by the rest of the decommutation equipment is avoided.

The test generator provided signals in four different forms: RZ, NRZ, MNRZ (polarity changes only on the appearance of a one), and split phase. The latter format was used by the satellite encoder. As implied above, however, this type of code was converted by the pulse synchronizer unit into the RZ form for use of the word recognition unit.

A stable, adjustable multivibrator provided the substitute clock pulse (1152 cps nominal bit rate) simulating the encoder.

The clock pulse signal was divided by nine (four flip-flops with feedback) to provide a word rate timing signal. This signal drove a single-shot multivibrator that provided a two-μsec. word pulse. The word rate was divided further by 128, using the last five of a set of seven flip-flops. This provided a frame rate signal with duty cycle of 4/128 to obtain any three chosen words.

The first two flip-flops of the divide-by-128 network were combined in three sets of and-gates to provide three separate signals, all with 25 percent duty cycles, four words wide. Each was shifted ⅓ of the four-word spacing to supply three separate lines (gated by the frame rate pulse) for the first three sync words. A fourth data line provided a data drive of 124 two-μsec word pulses.

Nine sets of or-gates fed the data bits in parallel into a nine-position shift register (driven by the clock). The polarity of each bit could be selected by a panel-mounted toggle switch.

The shift register could be arranged in sequence for each chosen word (including the chosen sync, three-word format) and gated into two serial line outputs by the drive from the clock.

The sync format was arranged by choosing a ground or a hot line for each of three-independently-driven lines for each of the nine or-gates feeding the register. There was no interference between the lines since they were driven sequentially.

The serial output of the register was in MNRZ form. It was combined with the clock signals to provide the split phase format, simulating the satellite signal.

Word Sync and Recognition Unit

It was the function of this unit to recognize the 27-bit sync word format. It counted words and presented a word identification signal to the word selection units and stored the nine-bit word data for use in the later units.

The serial signal from the pulse synchronizer (or the test generator) was fed into a nine-bit shift register for parallel readout. Therefore, the output of this unit was data stored in a 9-bit register, and a means of identifying which telemetry word was in that register.

Analog Word Selector

This unit allowed the operator to select any eight (of the 128) words for presentation as analog signals on the Sanborn strip charts.

Eight sets of thumbwheels constitute eight gates for choosing words identified in the word recognition unit. When this choice was satisfied logically for any word, the stored data in the recognition unit was transferred to one of eight, 9-bit registers in the analog word selector. The data was held and reset during a word sync pulse each frame.

A conventional D/A diode converter converted the outputs of eight flip-flops to dc signals for use by the strip-chart recorder. This unit also supplied the necessary blanking, sync, and deflection signals for the I.T.T. bar scope display.

Digital Word Selector

This unit allowed the operator to select any three of the 128 telemetry words for presentation on the Hewlett Packard printer as in binary format. Alternately, any one word could be printed in decimal form along with any one word in binary.

In a manner similar to that used for the analog word selector, any three words could be stored in registers which were transferred from the word recognition unit for printout purposes, when the selected word code agreed with the word identification presented by the latter unit.

Lamp drivers were fed from the three-word registers to provide a visual signal of the register contents.

The output of the three-word register directly fed the HP printer via appropriate gates.

Binary Decimal Converter

The purpose of this unit was to convert the binary code of the third word, selected in the previously discussed unit, into its decimal equivalent. A word ready signal, from the digital word selector, gated a 50 kc multivibrator into a counter and three conventional binary-to-decimal converters. The counter accumulated a binary code until it matched the stored code transferred from the digital selector's register. A gate word number 3 decimal signal, from the selector, gated the stored decimal code into the printer.

Command Checkout Equipment

Generation and transmission of commands to the spacecraft were accomplished with the following equipment:

1. Command encoder (see Figure 10–15)
2. Command transmitter (COMCO Type 278–6/12 TEF 101)
3. Antenna (Taco Yagi, 136 Mc).

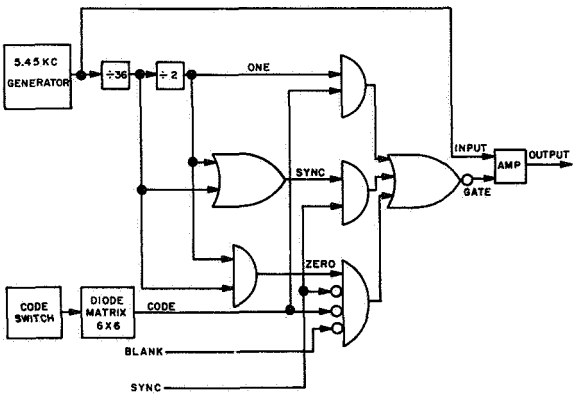


FIGURE 10–15.—Command encoder, logic block diagram.

The especially designed encoder provided a pulse modulated, 5.45-kc subcarrier to the spacecraft's command system. A simple PDM code provided 20 commands, any one of which could be selected from the front panel of the equipment. A panel-mounted key sent a train of five words to the VHF AM command transmitter for radiation to the spacecraft.

The requirements of 18 cycles of tone for a ZERO, 36 cycles for a ONE, and 54 cycles for a SYNC were met by utilizing the tone generator output as the timer for the keying circuit. The logic diagram is shown in Figure 10–15.

The 5.451-kc tone was divided by 36 to yield a square-wave with a 6-millisecond period, and divided again by two to yield a square-wave with a 12-millisecond period (a ONE signal). The logic sum of these signals formed a sync signal, and the logical product formed a ZERO. These three parts of the required code along with a blank were supplied to gates, which in turn were driven by the output of a 6×6 diode code matrix. A code command switch selected any one of the 20 command codes. The output of the code gates were mixed, and their sum was used to gate the output (subcarrier) amplifier. After five words were transmitted, the amplifier was gated off (blanked) until the encoder was keyed again.

General Support Equipment

The following items were required in support of general testing:

1. Oscilloscope (Tektronix model RM 35)
2. Waveform analyzer (HP model 302 AR)
3. Miscellaneous attenuators, detectors, isolators
4. VTVM
5. AC voltmeters (Ballentine 314A).

Solar Simulator

General

Simulation of the sun's effects on the spacecraft required an ultra high intensity light source. However, in order to simulate the sun properly, both the sun's intensity and spectral distribution must be reproduced faithfully.

The solar simulator utilizes carbon arc lamps, and will irradiate a 36-inch diameter circle through a 10-inch diameter port at distances ranging from 80 to 100 inches. It duplicates, within ± 10 percent, the incident solar energy flux as it appears above the earth's atmosphere. Its spectral energy distribution closely approximates that of the sun (see Figure 10–16).

Description

The radiant energy source for the solar simulator was derived from two 13.6 mm high-intensity carbon arc lamps, operated at 77 volts and 160 amperes. These lamps could operate for one hour before the carbon electrodes had to be changed and the change could be made in less than one minute. One lamp could supply sufficient energy to simu-

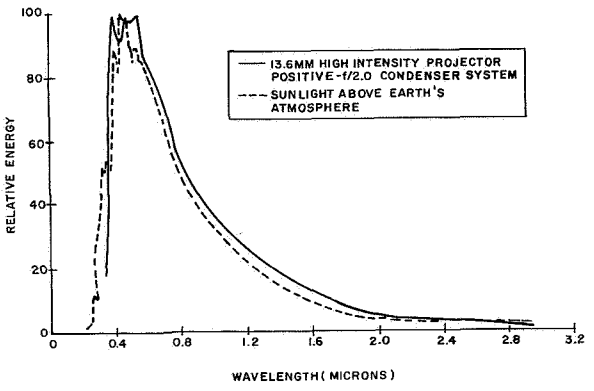


FIGURE 10–16.—Spectral energy distribution of 13.6 mm high intensity carbon arc vs. solar spectrum.

late the sun's intensity as it appears at the earth. However, the optical system to collect this energy and distribute it uniformly over the target area was subject to blocking by a support pedestal of the electrode feed mechanism. This resulted in the shadow of the pedestal being projected onto the target. To eliminate the shadow, two lamps were used. The projected halves were mated on the target to provide a field of uniform incident energy. The solar simulator configuration is shown in Figure 10–17. A removable shield was employed in each lamp-house to block-off energy. Removal of these shields would enable the simulator to supply twice the solar intensity to most of the target area.

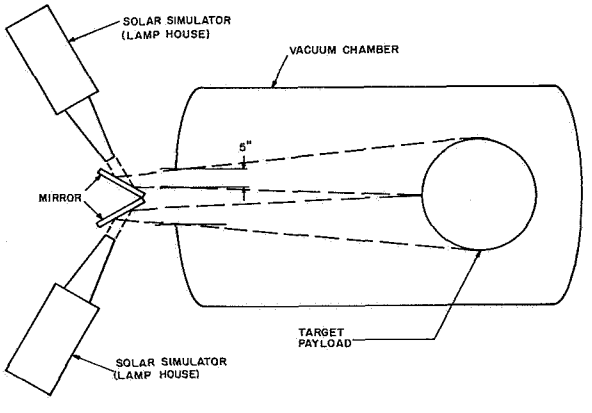


FIGURE 10–17.—Solar simulator configuration.

Rays emanating from the lamp passed through a quartz window and diverged to cover the 36-inch diameter target. This resulted in deviation of the outer rays from the normal to the target plane of 8½ degrees at the outer edge of the target. This deviation resulted in a maximum error of the energy impingement of 1½ percent on a flat surface in the target plane. If the surface were convex, the error could be greater. However, the error due to this deviation decreased at points nearer the center of the target.

The projection system for each lamp was composed of a three-element reflector and a diagonal mirror to fold the light path so as to combine the rays from the two arc lamps. Each element of the reflector focused energy from the carbon arc onto a portion of the target to provide the required uniform distribution of incident energy (see Figures 10–18 and 10–19). All reflectors were vacuum plated with aluminum for high reflection and were overlaid with a coating of silicon monoxide to minimize oxidation and abrasive effects from service.

The arc lamps were mounted on a rigid frame that included all of the operating controls and had retractable casters.

Incident energy flux of the solar simulator's beam at the target was initially controlled by proper adjustment and alignment of the three-element reflector. With use, the energy flux decreased by approximately five percent in 24 hours due to degradation of the reflectors as a result of smoke and sputtering of the arc, and adjustments were made accordingly.

Entry Port

The entry port for the solar radiation simulator was constructed of fused quartz, GE type 105. Figure 10–20 shows the transmission curves of several optical materials, including the type used.

Power Supply

The solar simulators were designed to operate from a three-phase, 60-cycle, 440-volt, 50-ampere power source. Additional utilities

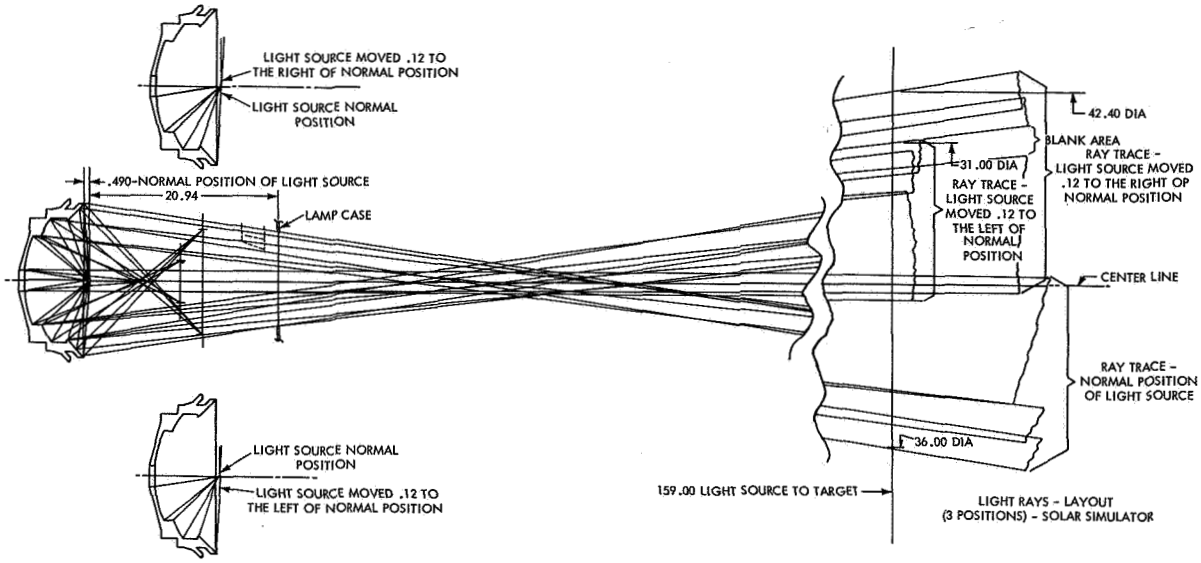


FIGURE 10–18.—Three element reflector ray diagram.

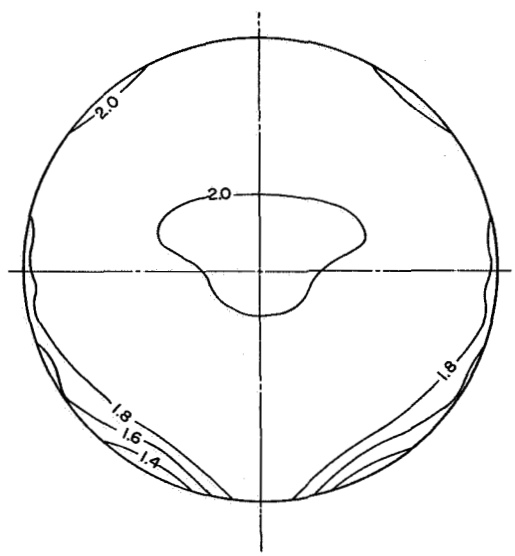


FIGURE 10–19.—Two source energy distribution of solar simulator on a 36-inch target.

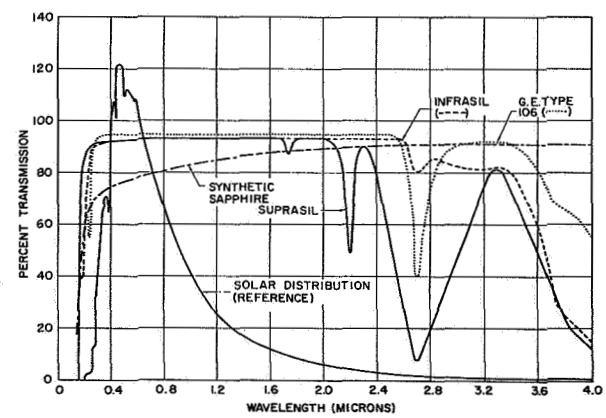


FIGURE 10–20.—Transmission characteristics of optical materials.

required for the solar simulators were: 115-volt single-phase 60-cycle power, water, 90-psi air, and an air exhaust system. The additional utilities are shown in Figure 10–21.

System Layout

The solar simulator assembly was designed to operate in conjunction with a 6-foot diameter × 10-foot long, vacuum chamber. The installation arrangement is shown in Figure 10–22. The operational position of the simulator is drawn in solid lines. The temporary (alignment) position is shown by dotted lines. These two arrangements afford the maximum safety.

Output Measurements

The incident energy output of the solar simulator was measured with a ten-junction pyrheliometer manufactured by Epply Labo-

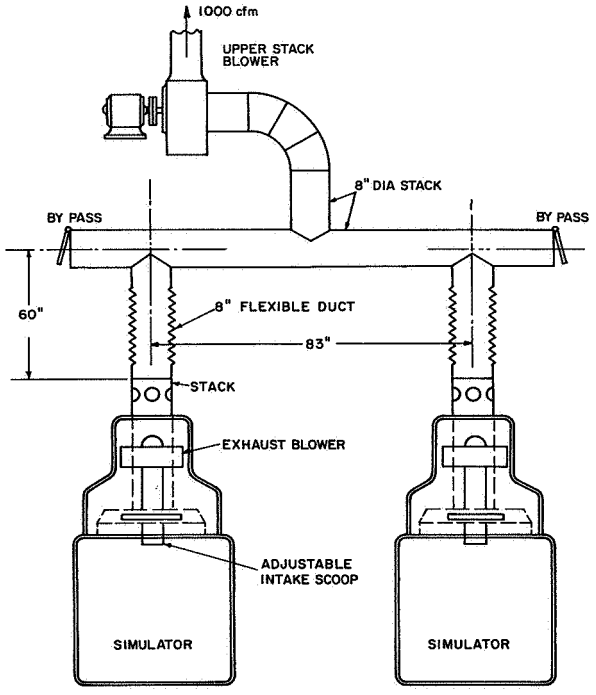


FIGURE 10–21.—Solar simulator cooling and exhaust system.

ratory, Inc. This instrument and a portable millivoltmeter were used for calibrating the solar simulator. They were mounted on a special support fixture in the target area and the fixture was controlled remotely by cables.

The pyrheliometer was mounted on a horizontally and vertically translating slide so that it could be moved to any point in the target plane. The reverse side of the test target was graduated in 2-inch squares. The slide was moved from point to point to position the pyrheliometer in the solar simulator's beam while it was operating. The test target thus protected the operator from exposure to the intense radiation of the solar simulator. The test target also provided a means for accurately recording the solar simulator's light output and facilitates adjustment and calibration.

Design Considerations

A simulator that closely simulated the sun's effects was developed, utilizing existing

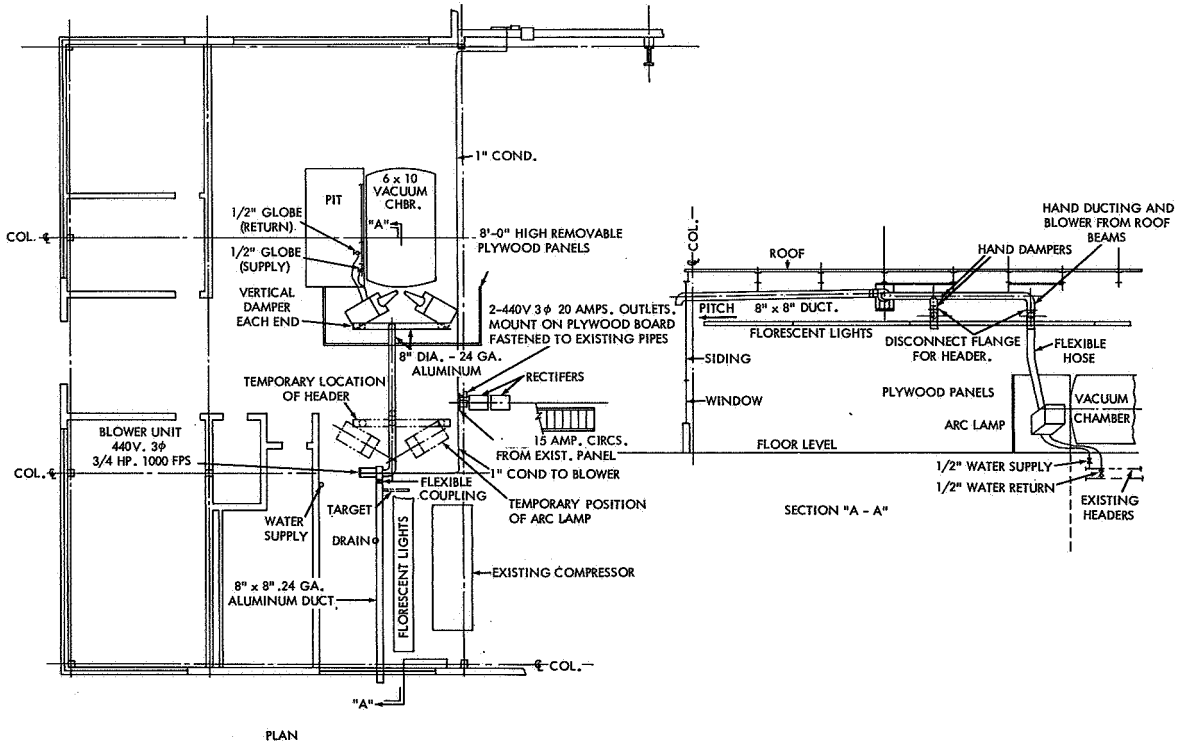


FIGURE 10–22.—Solar simulator test installation.

state-of-the-art concepts because it was felt that this would fulfill requirements with minimum expenditure and delay. General design concepts were studied and a preliminary reflector drawing was made.

Ray traces were drawn to check for possible problems. A wooden mock-up of the 3-element reflector, shown in Figure 10–23, was also constructed to check for interferences within the lamp housing. Figure 10–24 shows the wooden reflector mounted in the lamp housing.

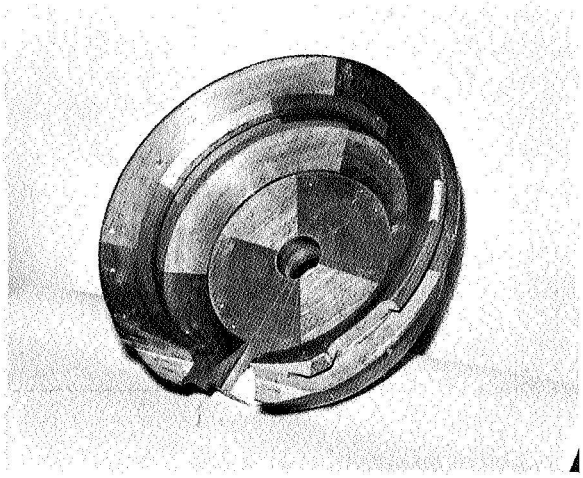


FIGURE 10–23.—Wooden mockup of solar simulator reflector.

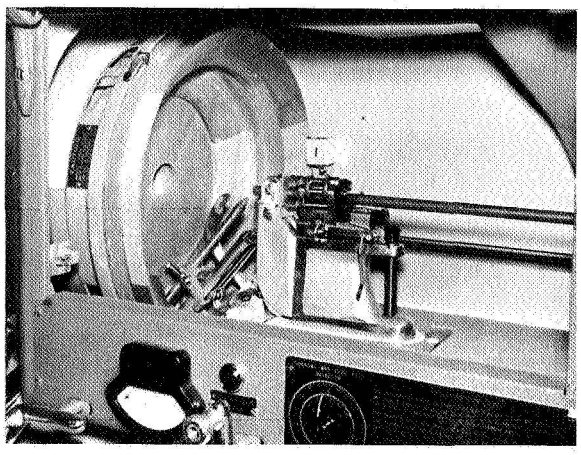


FIGURE 10–24.—Reflector mockup mounted in lamp housing.

The lamp housing ductwork was investigated to evaluate accommodation for ray passage and support of the new reflector. The reflector support inside the lamp housing was redesigned to accept the new three-element reflector shown in Figure 10-25.

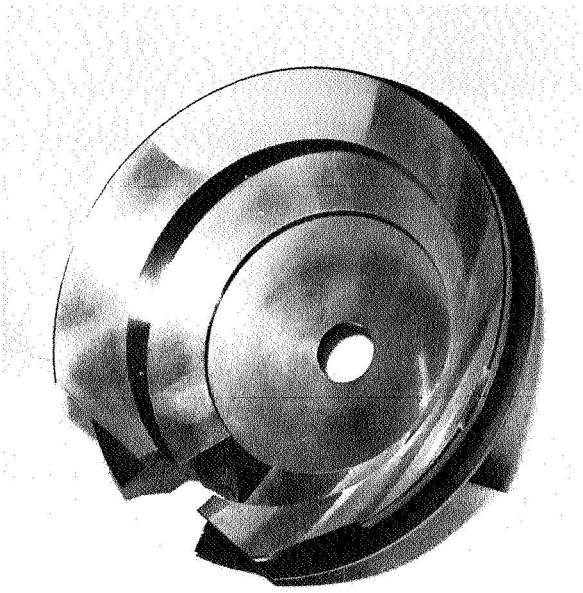


FIGURE 10–25.—Solar simulator reflector.

A test assembly to align the optical system was designed also. The test assembly eliminated the need for striking an arc and then shutting down for slight reflector adjustments. Thus, the field pattern could be adjusted safely by the operator. The schematic description of the alignment assembly is shown in Figure 10–26.

The lamp housing was modified to provide both cooling for the reflector and air washing of the reflection surfaces. The latter was to prevent the formation of carbon deposits on the surface.

In addition, extreme care was taken to provide maximum protection for the operator and others who might be in the area. Operators were required to wear shade No. 14 welders goggles and protective skin cream. Interlocks were provided on all ac-

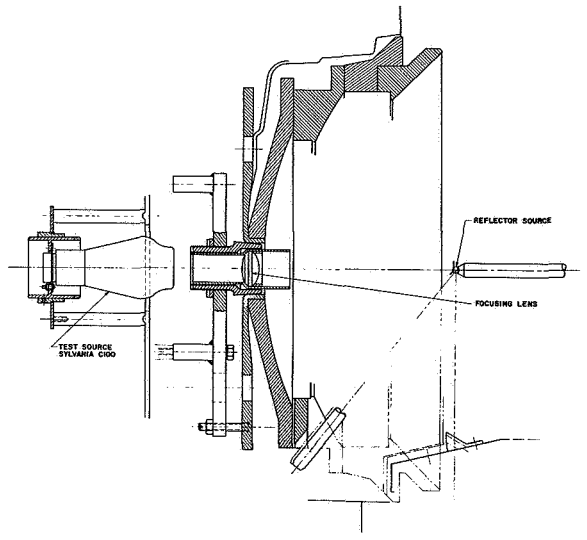


FIGURE 10–26.—Reflector alignment fixture.

cess doors to the lamp house. Baffles were used around the exit light port to minimize stray light reflection. The operating area was enclosed in order to keep unauthorized personnel out of the area.

The lamp housing was a standard projection source supplied by Strong Electric Co. A proper arc was maintained between two carbon rods by means of a drive servo that sensed the arc temperature via a lens system and actuated by a bimetallic thermal relay. In turn the relay actuated the rod drive motors as shown in Figure 10–27. The wiring diagram for the lamp house is shown in Figure 10–28. Power supplies for the source were selenium rectifiers which required 440-volt, 60-cycle, 3-phase input. The schematic diagram for the rectifier is shown in Figure 10–29.

A system control panel was supplied with each lamp. It provided for proper sequencing of switching, and ensured that the housing received proper cooling when in operation. The schematic diagram of the control panel is shown in Figure 10–30.

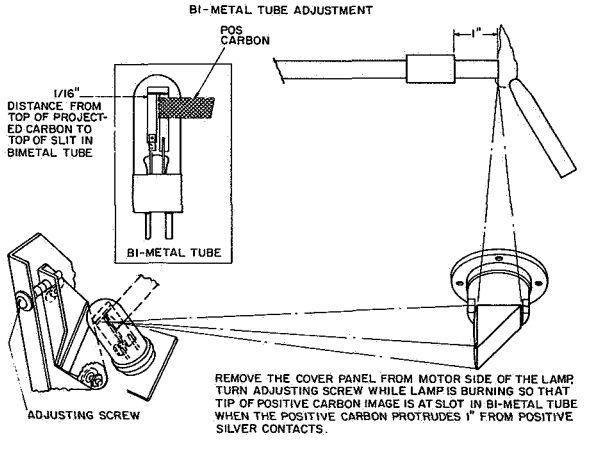


FIGURE 10–27.—Lens servo arc temperature sensing system.

HANDLING PROCEDURES AND FIXTURES

General

The handling procedures and fixtures used on Project Relay were governed not only by the normal considerations for reliability, safety, and ease of implementation, but also by the configuration of the spacecraft whose lifting, holding, or supporting points were limited.

In the flight configuration, the upper and lower ends of the volume enclosed by the solar panels were sealed by segments of the coated mylar thermal enclosure (see Figure

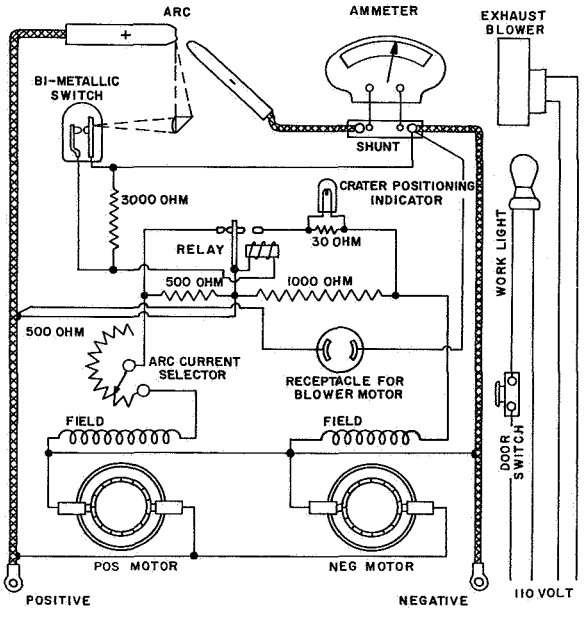


FIGURE 10–28.—Lens servo arc temperature sensing system, schematic diagram.

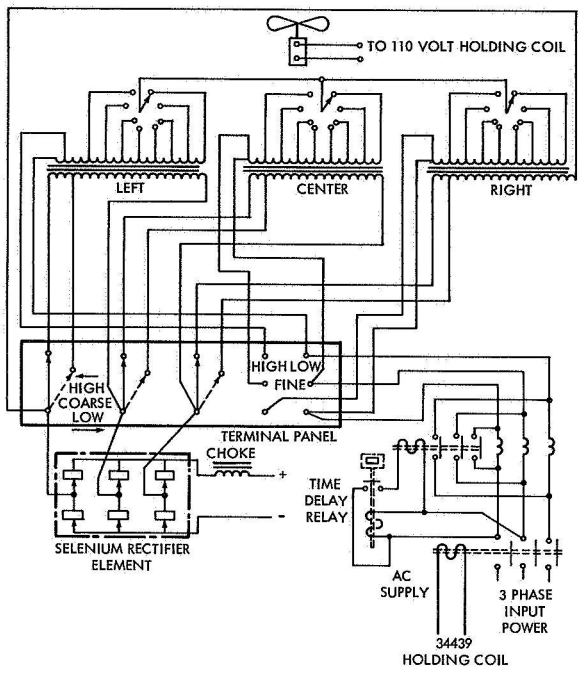


FIGURE 10–29.—Carbon arc power supply schematic diagram.

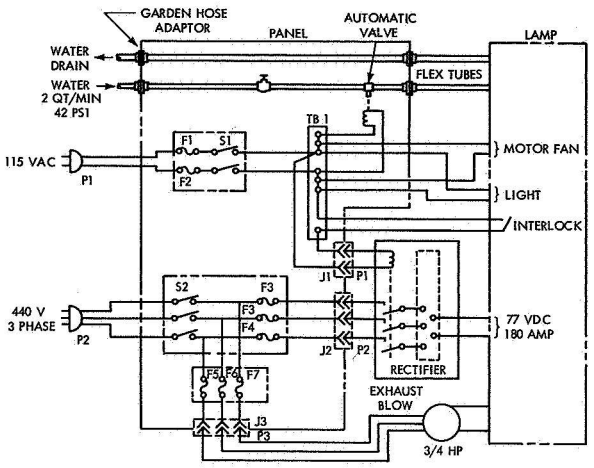


FIGURE 10–30.—Ultra-high intensity lamp system, schematic diagram.

10–31). All that protruded from this main section was the separation ring at the bottom, which mated the third stage of the launch vehicle, and the wideband antenna at the top.

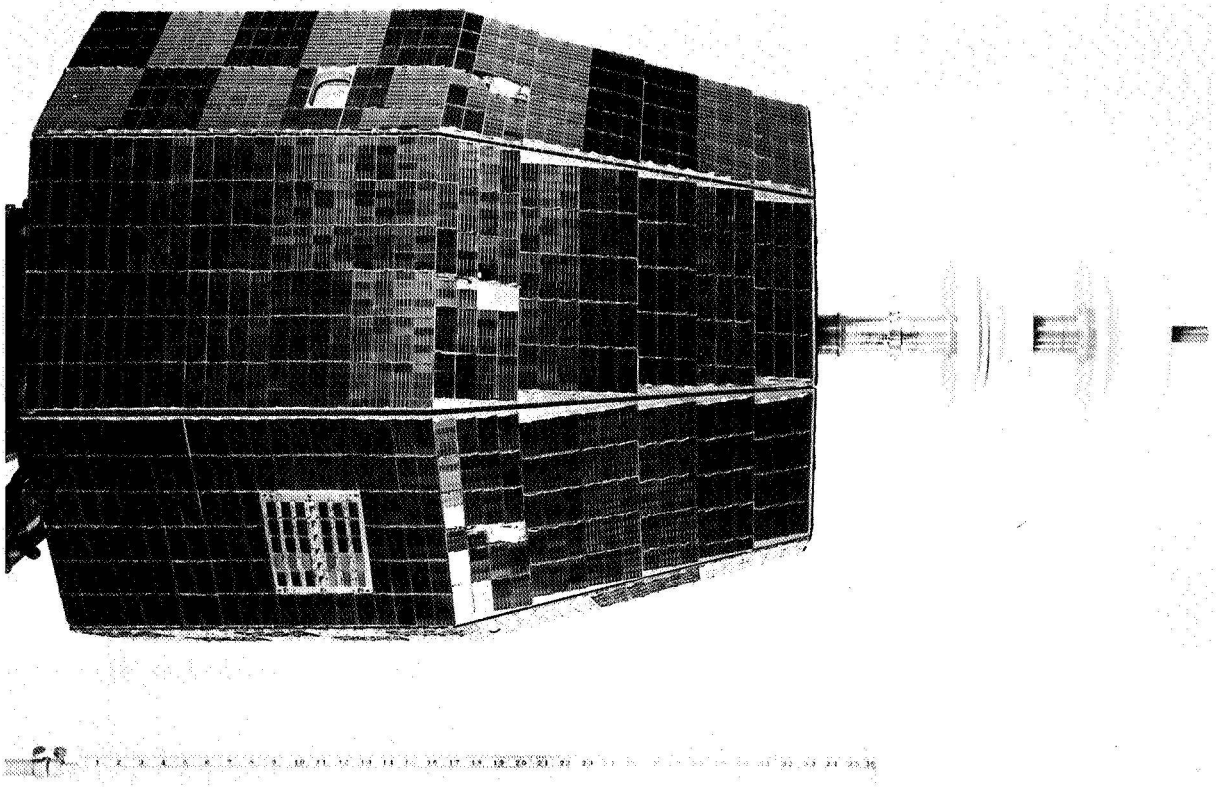


FIGURE 10–31.—Relay spacecraft.

It was decided to provide some attachment point near the top of the spacecraft, to provide stability in handling and also to free the separation ring for use as a rigid clamping surface. Since the tops of the solar panels were almost 9 inches above the top of the structure, providing attachment points from the structure would require brackets to span 9 inches, and would impose an undesirable weight penalty if made permanent. It was decided therefore to incorporate an attachment point on the wideband antenna which took the form of a lip, ⅛ inch wide and ⅛ inch high, machined into the main tubular section of the antenna, above the plane of the top of the panels. The antenna was mounted directly to the main spacecraft structure.

Vertical Lifting Fixture

The mating, vertical lifting fixture (see Figure 10–32) consisted of a clamp, hinged to fit around the antenna, with a machined groove to accept the antenna lip. The clamp was held closed by a self-locking pin. A steel strap, suitably contoured to clear the upper part of the antenna was bolted to and formed part of the clamp assembly, and was fitted with a U-bolt large enough for crane hooks.

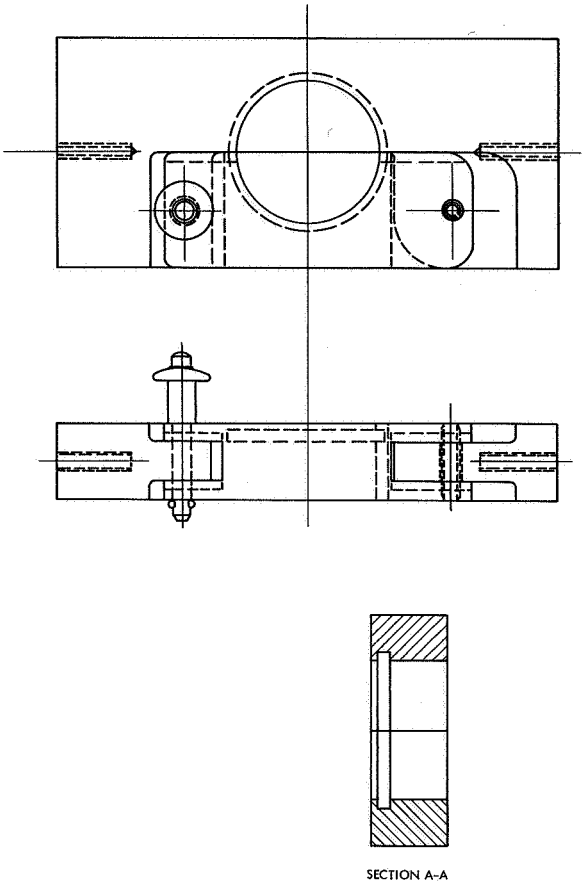


FIGURE 10–32.—Vertical lifting fixture.

Work Stand

The basic fixture for assembly and in-plant transportation was the work stand (see Figure 10–33). This consisted of a welded angle iron tripod, fitted with locking casters and included a hinged mounting plate to allow tilting the spacecraft to 90° from the vertical. A machined ring, simulating the third stage attach fitting, was bolted to this stand. The spacecraft was fastened to the stand by a Marman-type clamp similar to the clamp used on the launch vehicle.

Horizontal Lifting Fixture

The horizontal lifting fixture (see Figure 10–34) was an aluminum channel with extended supports for engaging the separation ring and the antenna when the spacecraft was in horizontal position. To use this fixture; 1) the spacecraft was tilted on the work stand with its spin axis horizontal, 2) the lifting fixture was attached, and all slack was taken up by a portable hydraulic crane, 3) the spacecraft was released from the work stand. This procedure was required for mounting the spacecraft in the horizontal balance machine.

Bird Cage

The bird cage (see Figure 10–35) was a frame consisting of three L-shaped aluminum bars (the short legs of which were fastened to the spacecraft mounting ring through an adapter) and two triangular rings which fastened to and supported the vertical legs. This frame permitted handling the spacecraft while it was fastened only at the separation ring. The spacecraft could be turned

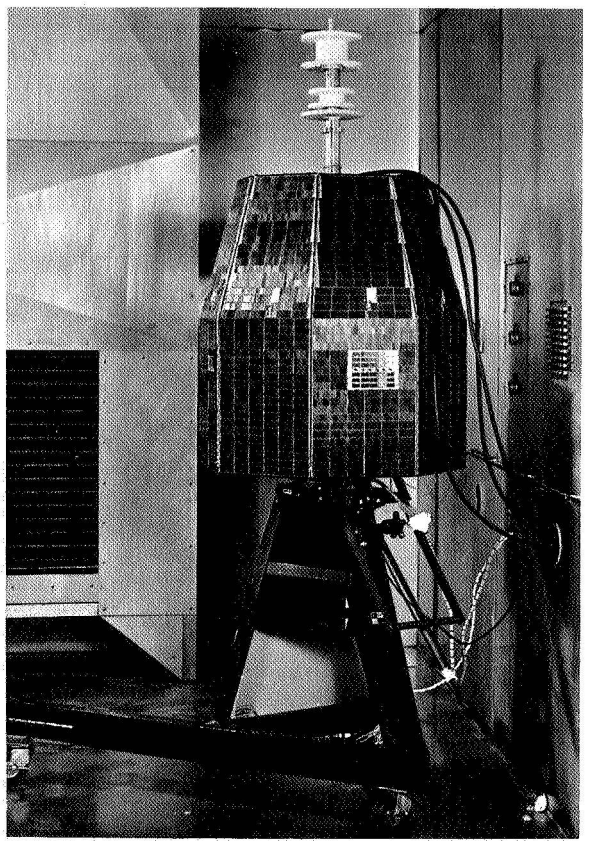


FIGURE 10–33.—Relay spacecraft on work stand.

upside down, as required for the micro-balancing machine; or it could be supported horizontally with access to the bottom of the separation ring, (as used in the moment of inertia measurement); or it could be used as a carrier.

Shipping Container

The design of the shipping container was a departure from the standard type of protective enclosure. Without compromising the basic protective function of the container, it was decided to incorporate some features which would facilitate its use (see Figure 10–36). Thus, the container material selected was aluminum, and standard toggle latches were employed instead of bolt and nut closure of the two sections. Also a split sliding clamp was employed to hold the spacecraft. A ring, designed to mate with the spacecraft separation ring, was bolted to the suspension frame of the container, and the split clamp arranged to hold this ring and the separation ring of the spacecraft together. Toggle latches were used to lock the two halves of the clamp together. A shackle mounted to a T-bar spanning the top of the container provided a lifting point,

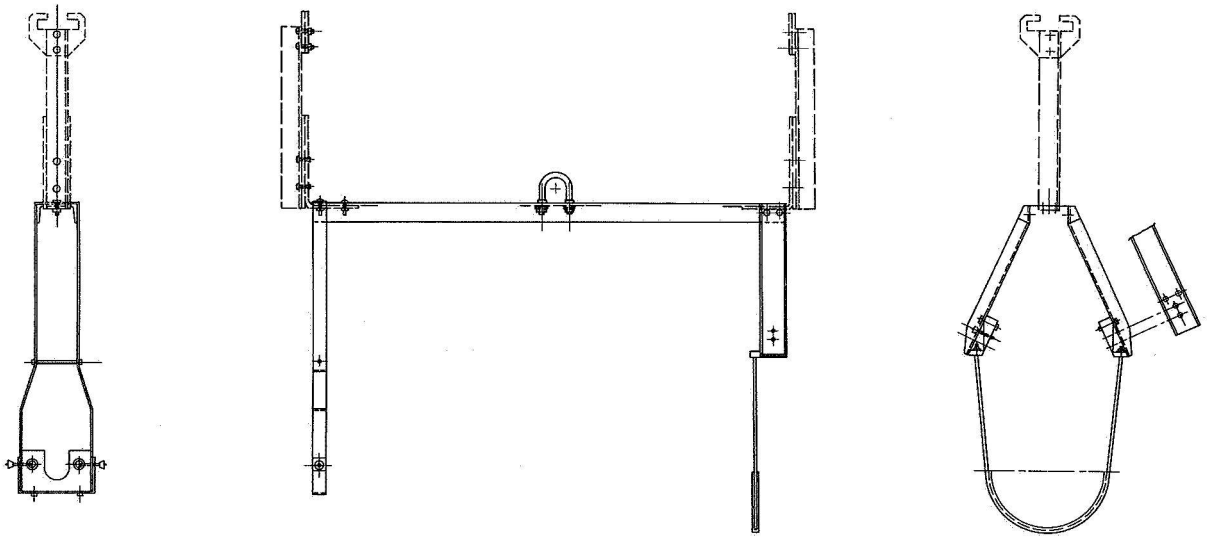


FIGURE 10–34.—Horizontal lifting fixture.

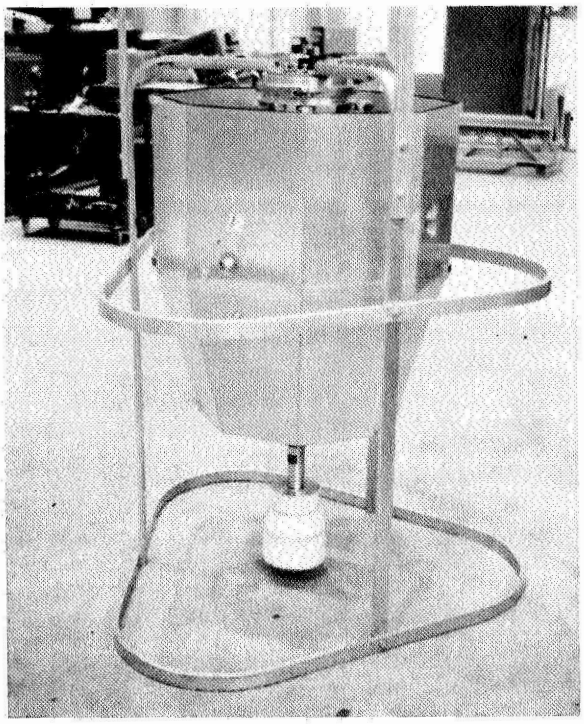


FIGURE 10–35.—Spacecraft model mounted in "bird cage".

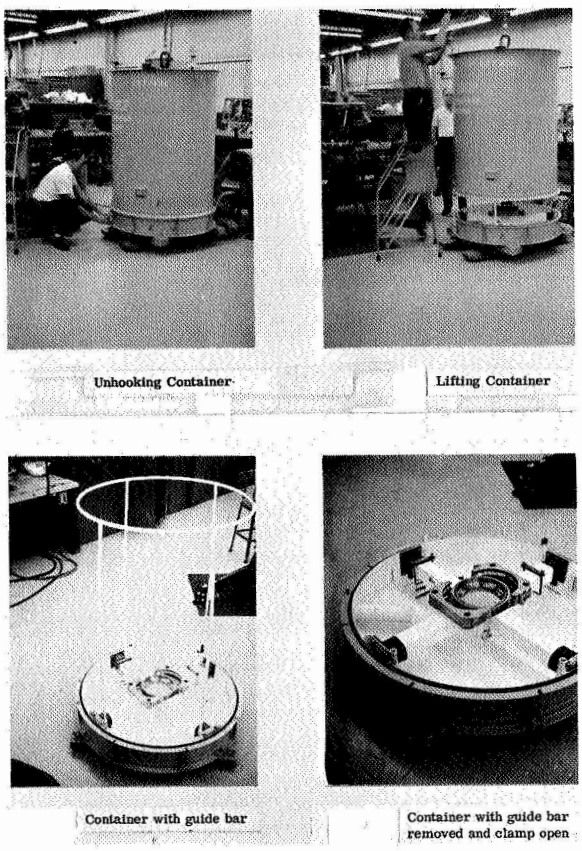


FIGURE 10–36.—Relay spacecraft shipping container.

thus eliminating the need for removable slings and also reducing the headroom required to lift the top section of the container clear of the spacecraft.

The entire shipping container weighed less than 250 lb and it was possible to install or remove the spacecraft, without the use of any tools, in a very short time.

The prototype shipping container was subjected to rough handling tests prior to use. These tests included the edgewise-drop test, the pendulum-impact test, and the inclined-stability test. The container was pressurized before and after the tests and found to be free of leaks. Accelerations measured at the base of the dummy load during the impact and drop tests did not exceed the test criteria of 15 g in the Z-axis direction and 10 g in the X and Y-axes.

AUTHORS. *This chapter was written by* W. SCHREINER, R. NEWMAN, *and* M. GITTLER *of the Radio Corporation of America, Princeton, New Jersey, U.S.A. under contract NAS 5–1272 with NASA/Goddard Space Flight Center.*

N66-10237

Chapter 11

Systems Integration

GENERAL

The systems integration effort consisted of qualification testing of the basic design (using the prototype spacecraft) and acceptance testing of workmanship (using the flight model spacecraft). Both standard electrical test equipment and equipment specially constructed for the tests were used. The test equipment is listed in Table 11–1.

All environmental measurements and recordings were made with instruments conforming to acceptable laboratory standards of accuracy. Instrument calibrations were established prior to testing and were checked periodically to assure accuracy of measurement.

The sequence of environmental tests was determined primarily by the availability of the test facilities. The general electrical test philosophy was to have an electrical performance test before and after each environmental test. When both tests were scheduled concurrently, only the more stringent test was performed.

Before any of the environmental tests were performed, the spacecraft was subjected to the comprehensive operational test under room conditions. A record was made of all data necessary to determine compliance with the applicable spacecraft specifications. These recorded data provided the criteria for checking satisfactory performance of the spacecraft before, during, or after environmental tests.

Test data was entered on data sheets prepared for that specific test whenever possible.

A detailed test log was maintained suitable for reliability review. The log contained all pertinent test information including that entered in the test data sheets.

All electrical performance checks were made in a clean room, having filtered air and controlled temperature and humidity. Standard procedures for clean-room operation were in effect at all times during the electrical performance checks.

ASSEMBLY, QUALIFICATION, AND ACCEPTANCE TESTS

Assembly Tests

Balancing

Specification—

The balancing operation on the Relay Spacecraft was performed in accordance with the requirements of Relay Spacecraft Environmental Qualification Test Specification Number R1–0101. The following were the major requirements:

1. Maximum C.G. offset of spacecraft principal axis from spin axis shall be less than 0.005 in. (amended by waiver to 0.01 in.).

2. Tilt of spacecraft principal axis with respect to spin axis shall not exceed 0.008 radian (amended by waiver to 0.016 radian).

Horizontal Balancing Machine Description—

The horizontal (two-plane) balancing ma-

TABLE 11–1.—*Electrical Test Equipment*

Equipment	Manufacturer and type no.	Equipment	Manufacturer and type no.
FM signal generator	Marconi TF 1066B	Regulated power supply	Alfred 218 BX
Directional coupler	Hewlett Packard 767D	VHF signal generator	HP–608D
Power meter	Hewlett Packard 431A	Multimeter	Simpson 270
Spectrum Analyzer	Panoramic SPA–4A	Test pattern generator	Telechrome 1003 DIA
Microwave transmitting and receiving system.	RCA MM600	Test pattern receiver	Telechrome 1004 B
a. Modulator	MI 24371 B	Pre-emphasis network	RCA laboratory model
b. Demodulator	MI 24351 C	De-emphasis network	RCA laboratory model
c. IF amplifier	MI 24350 C	Noise loading trans	RCA C1–86
d. IF pre-amp	MI 25296 A	Noise loading receiver	RCA C1–87
e. Local osc. and Mixer.	MI 25297 A	Signal generator (2 required)	Hewlett-Packard HP614A
f. Video amplifier	MI 24373, A1 and B1	Signal generator (1 required)	Hewlett-Packard HP618A
g. Transmitter	MI 35270 A	Calorimetric power bridge	Hewlett-Packard 434A
Sweep generator	Alfred GA–408 with 605–102 plug in head.	Power bridge	Hewlett-Packard HP430C
Detector	Hewlett-Packard 420A	Directional coupler	Hewlett-Packard HP 750A
Differential voltmeter	J. Fluke 801	Variable attenuator	Sanders Associates Model 1
Audio oscillator	Hewlett Packard 650 A	Variable attenuator	Hewlett-Packard HP355A
Decade counter	Hewlett Packard 524B with 525A and 525B plug in units.	Fixed attenuator	Polytechnic Research 1100
Transfer oscillator	Hewlett Packard 540–B	Termination load	Bird 81B
Hybrid	Narda 3033	Low-pass filter (5 kMc)	Microlab LA 50T
Oscilloscope	Tektronix 545A	Band-pass filter (tunable)	Waveline 90116–5
Oscilloscope, plug in high gain	Tektronix H	Horizon scanner demodulator	RCA Laboratory Model
Oscilloscope, plug in dual trace	Tektronix CA	Aluminum shroud and windshield for centrifuge	Dwg Nos. 1179665 thru 7, RCA Laboratory Model
High voltage probe	Tektronix, 50 X atten.	Test adapter plugs	3 types
RMS VTVM	Ballantine 320	Solar simulator	RCA laboratory model
Telemetry decommutation and display	Data Control Systems	Heat source (horizon scanner)	RCA laboratory model
Special purpose receiver	Nems-Clarke 1906	Plane mirror (inertia)	RCA laboratory model
Attenuator	50 db, 50 ohms	Encoder	RCA laboratory model
Power supply	HP–721A	Calibrated inertia measurement bar	RCA laboratory model
Power supply, 22.5 v.	Keps SC–32–5	Horizontal (two-plane) balancing machine	RCA laboratory model
0–5A. dc ammeter, ±0.5%	Daystrom Model 931	Vertical balancing machine	Micro Balancing, Inc.
High voltage meter	Sens. res. SEW7	Balancing weights	RCA laboratory model
Filter	Krohnhite Model 330M	Spin rig	RCA laboratory model
0–3 A. ammeter	WE 31347	Dial indicator—.001, 24-inch extension arm.	
0–1 A. ammeter	WE 931	Vertical axis vibration fixture	RCA laboratory model
Variac	GR 17006	Lateral-longitudinal axis vibration fixture	RCA laboratory model
VTVM	RCA–WV 97A	Marman-type vibration clamp	RCA laboratory model
Digital VM	E I DV51–B		
Variable attenuator	Kay Lab Model 30		
Noise figure meter	HP–342A		
UHF noise source	HP–349A		
Carrier frequency voltmeter	Sierra 101C		
Absorption wavemeter	FXR N414A; N410A		
Group-delay transmitter	RCA MI–24365B		
Group-delay receiver	RCA MI–24366A		

chine, designed and fabricated by RCA–AED, consisted of two support bearings to carry the workpiece with the spin axis horizontal. The support bearings were hung by thin steel straps in a flexure suspension which permitted deflection in a horizontal plane in a direction normal to the spin axis. The workpiece was rotated, through a universal joint, by an ac induction motor equipped with a pulley speed reducer, at a speed of 160 rpm.

Each support bearing was attached to the core of a linear, variable, differential transformer, which, in conjunction with an excitation oscillator and phase-sensitive detectors, yielded a voltage proportional to the

bearing displacement. This voltage was read on a calibrated meter. Direction of unbalance was indicated on a reference angle disc mounted on the drive shaft and illuminated by a strobe light synchronized to the bearing deflection voltage. The system was sensitive to 2 inch-ounces in each bearing plane.

Operating Principle—When the workpiece was turned in the support bearings, it tended to rotate about its principal axis of inertia. If any dynamic unbalance existed, the principal axis did not coincide with the geometric axis, and dynamic forces produced by rotation caused displacement of the bearings.

These displacements, measured in magnitude and direction, were indicated by the machine on the calibrated voltmeter and reference angle disc, respectively.

Vertical Balancing Machine Description—

The vertical balancing machine (see Figure 11–1), was a special device designed and built by Micro Balancing, Inc., Garden City Park, Long Island, New York. It consisted of a tripod structure (carrying a rotational, double-pendulum shaft) and a control console (housing indicators and controls). The pendulum shaft was equipped with two universal joints, located at top and bottom. The bottom joint was located just above the workpiece mounting adapter and could be immobilized to form a single pendulum shaft. A clamp was provided to plumb-align the upper shaft.

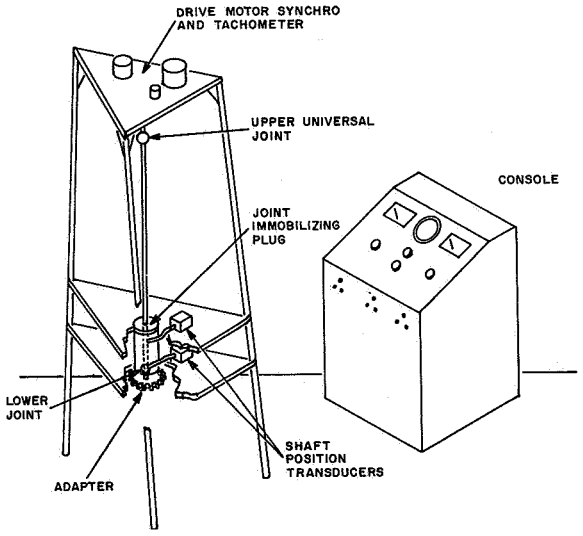


FIGURE 11–1.—Vertical balancing machine.

Transducers, which measured the eccentricity of shaft rotation, were mounted at the lower universal joint and at a point approximately 22 inches above it. A syncro transmitter, rotating with the shaft, provided an angular reference signal for determining the direction of unbalance. Also a tachometer, driven by the shaft, was mounted on the tripod structure.

Performance specifications provided by the builder were as follows:

a. Workpiece weight—50 to 300 pounds
b. Workpiece diameter—20 to 60 inches
c. Balancing speed—120 to 300 rpm
d. Accuracy of static balance—0.002 inch* center of gravity to spin axis (verbal guarantee of 0.001 inch)
e. Accuracy of dynamic balance—0.1 degree* (verbal guarantee of 0.02 degree).

Operating Principle—The static balancing operation was performed with the lower universal joint immobilized. The workpiece tended to rotate about its center of gravity with the pendulum shaft, describing a cone locus (see Figure 11–2). Consequently, the lower transducer output was a sinusoid whose amplitude was proportional to the center of gravity's location from the geometric axis, and whose frequency was proportional to the speed of rotation. The phase of the transducer output (relative to the shaft synchro signal) was determined by the direction of unbalance as measured from a pre-set index point.

Dynamic balancing was performed after static balancing. With the lower joint free, the workpiece tended to rotate about its principal axis of inertia, and the shaft assumed some position to accommodate this condition (see Figure 11–3). As a result,

*Balance accuracy given for workpieces weighing 50 pounds minimum and having a center of gravity 30 inches maximum from the mounting surface.

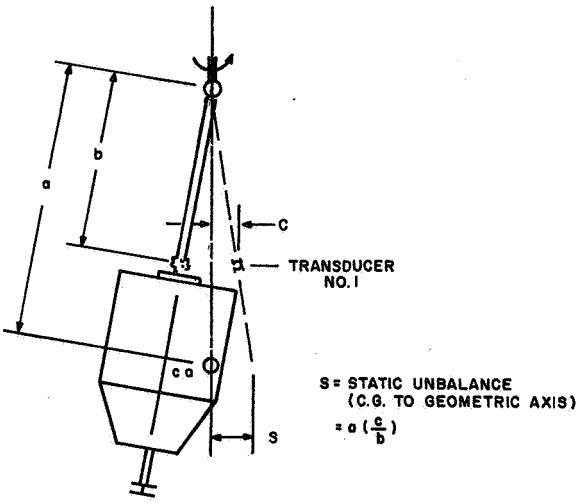


FIGURE 11–2.—Action of static unbalance.

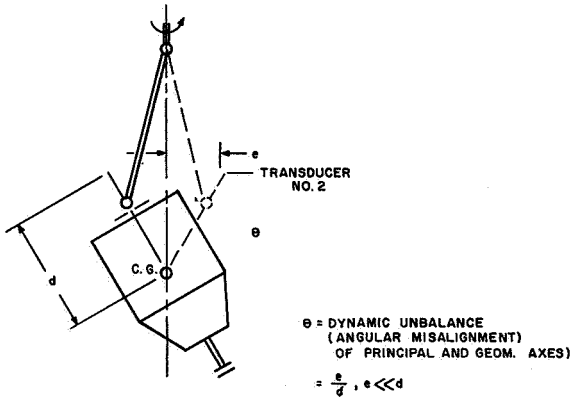


FIGURE 11–3.—Action of dynamic unbalance.

the upper transducer output was proportional to the dynamic unbalance, as defined by the sine of the angle between the principal and geometric axes. Signal frequency was determined as in the static balancing operation. Phase determination, however, was complicated by the fact that operation would occur probably at a speed of rotation not far above the resonant frequency of the lower pendulum. The phase shift, due to this proximity to resonance, had to be determined experimentally, and readings were adjusted to yield the proper direction of unbalance.

Balancing Procedure—

The balancing operation was performed in three stages: First a preliminary rough balance of the spacecraft without solar panels was made on the horizontal balance machine; then, a rough and fine static balance on the vertical balancing machine; and last, the fine balance on the vertical balancing machine was made.

For the horizontal machine, the equivalent of a shaft, locked to the spacecraft and extending beyond it on both sides, was required. An assembly fixture shaft was used for the base end to orient structural members during assembly. Although the wideband antenna was to be used as the extension of this shaft at the other end, possible antenna damage was avoided by replacing the antenna with a steel stub shaft. The solar panels were left off during the rough balance because it was inconvenient to add large weights with the panels in place. Compensating weights were added to the structure to account for the components mounted on two panels. Since the panels themselves were approximately equal in weight, their removal had a minimal effect on spacecraft balance. Thus, the configuration balance was considerably different from the flight model spacecraft; however, it was adequate for the determination and correction of large unbalances.

With the wideband antenna and solar panels removed, the adapter shaft and antenna stub were installed, and the spacecraft transported to the balance machine on the work handling dolly and tilted to the horizontal position. The horizontal lifting fixture was attached, and the load picked up by a portable hydraulic boom, the Tubar crane. The clamp holding the spacecraft to the dolly was removed, and the spacecraft was carefully positioned on the balance machine.

The spacecraft was spun at 160 rpm during the balancing operation. Displacement readings were taken at each shaft bearing support. The upper and lower solar panel support rings were used to mount temporary balancing weights. A trial balance weight

was attached to the upper panel supporting rings, and the bearing displacement readings were taken again. The trial weight was shifted twice, 120° around the ring each time, and displacement readings of both bearings were taken each time. The required balance weight and location was then calculated for the upper plane. The same procedure was followed on the lower ring to determine the balance correction weights required for the lower plane. This procedure was repeated until the residual unbalance was less than 0.050 inch static unbalance, and dynamic unbalance less than 0.08 radian tilt. Using the data taken in the trial runs, *EWx*, *EWy*, *EWxz* and *EWyz* were calculated and, using the equations in paragraph 2 below, the minimum balance weights and their location on the cruciform was determined. The spacecraft was rechecked after the balance weights were poured.

The spacecraft was removed from the horizontal balancing machine, and the panel component compensating weight, assembly shaft, and adapter stub shaft were removed. The solar panels and wideband antenna were installed, and the spacecraft was in the flight configuration.

The fine balance operation was performed on the vertical balancing machine located at Bell Telephone Laboratories, Whippany, N.J.

1. *Repeated Trial Weight Method of Determining Balance*

The trial weight unbalance in the trial weight method of determining balance was represented by T_1 (mass times radius in ounce-inches). The four bearing deflection magnitude readings were represented by:

u = Amount of unbalance without trial weight

r_a = Amount of unbalance with trial weight at 0

r_b = Amount of unbalance with trial weight at 0 + 120°

r_c = Amount of unbalance with trial weight at 0 + 240°.

Referring to Figure 11–4, three lines (*OA*, *OB*, and *OC*) of length μ were drawn to a convenient scale representing the successive angular positions of the test unbalance T_1. From *A*, *B* and *C*, arcs of radius r_a, r_b, and r_c respectively, were drawn to the same scale. The arcs seldom intersected at a point because of experimental error, and the mean position *U* was estimated as shown.

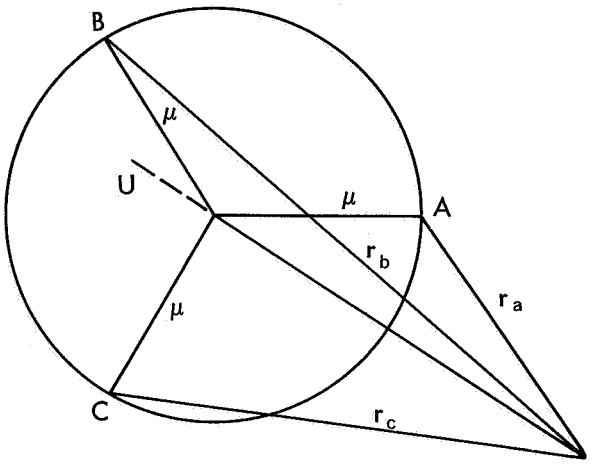


FIGURE 11–4.—Trial weight method for determining balance.

The unbalance requiring correction was then in the direction shown as a broken line. The magnitude of the unbalance was:

$$U = T_1 \left(\frac{\mu}{t}\right)$$

2. *Static and Dynamic Balance Equations*

For complete static and dynamic balance of the spacecraft, the following equations had to be satisfied:

$$\left.\begin{aligned}\textstyle\sum W_x &= 0\\ \textstyle\sum W_y &= 0\end{aligned}\right\} \text{Static}$$

$$\left.\begin{aligned}\textstyle\sum W_{xz} &= 0\\ \textstyle\sum W_{yz} &= 0\end{aligned}\right\} \text{Dynamic}$$

The dynamic and static balances with N number of weights at locations x_i, y_i, and z_i, were determined experimentally (see Figure 11–5).

With the required balancing weights and locations to balance the spacecraft, deter-

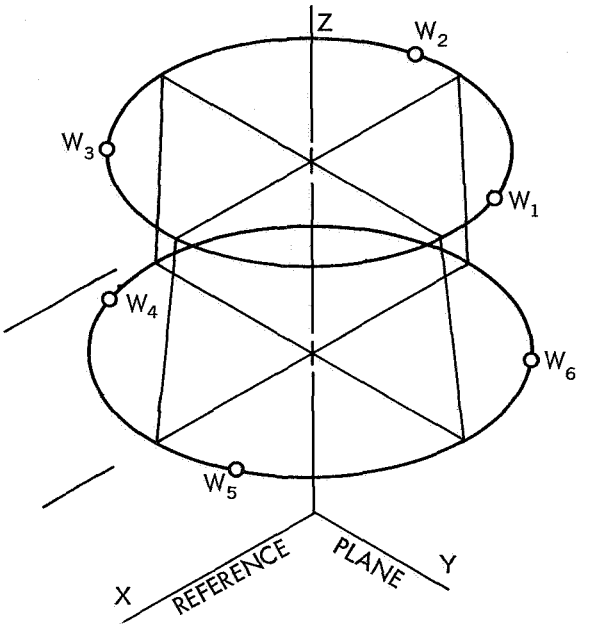


FIGURE 11–5.—Representation of cruciform structure with typical arrangement of weights and orientation of axes.

mined experimentally, the following were calculated:

$$\sum_{i=1}^{n} W_i x_i = N_1$$

$$\sum_{i=1}^{n} W_i y_i = N_2$$

$$\sum_{i=1}^{n} W_i x_i z_i = N_3$$

$$\sum_{i=1}^{n} W_i y_i z_i = N_4$$

The following equations were derived to satisfy N_1, N_2, N_3, and N_4, with minimum weights located on the outer channels of the cruciform rings (see Figure 11–6).

$$[A] \quad W_2 r_2 + w_2 r_1 = N_1 \qquad (11.1)$$

$$[B] \quad w_1 r_1 + W_1 r_2 = N_2 \qquad (11.2)$$

$$[C] \quad W_2 r_2 z_2 + w_2 r_1 z_1 = N_3 \qquad (11.3)$$

$$[D] \quad W_1 Z_1 r_2 + W_1 r_1 z_1 = N_4 \qquad (11.4)$$

Unknowns are W_1, W_2, w_1 and w_2. Solving the above equations:

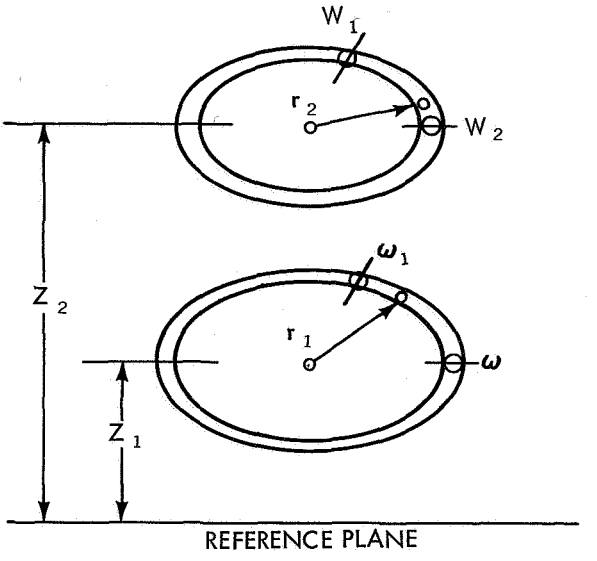


FIGURE 11–6.—Representation of cruciform rings with orientation of minimum weights.

$$[A](z_1)-[C]: W_2 r_2 (z_1 - z_2) = z_1 N_1 - N_3 \qquad (11.5)$$

$$[B](z_1)-[D]: W_1 r_2 (z_1 - z_2) = z_1 N_2 - N_4 \qquad (11.6)$$

Solve for W_2 in equation (11.5) and W_1 in equation (11.6).

$$[A](z_2)-[C]: w_2 r_1 (Z_2 - Z_1) = Z_2 N_1 - N_3 \qquad (11.7)$$

$$[B](z_2)-[D]: w_1 r_1 (Z_2 - Z_1) = Z_2 N_2 - N_4 \qquad (11.8)$$

Proceed as above, solving for w_2 in equation (11.7) and w_1 in equation (11.8).

3. *Balance Weight Design and Installation*

A Cerre de Pasco alloy, Cerrobase, was used for the fabrication of the large (rough) balance weights. This alloy, having a melting point of 225°F, can be poured conveniently into place on the cruciform outer channels. Existing rivet heads, mounting screws, and mounting nuts served to key the poured weight securely. Prior to pouring the Cerrobase, aluminum sheet and Aboseal were used to fabricate the weight form; after solidification, the aluminum and Aboseal were removed. Figure 11–7 shows a typical weight installation.

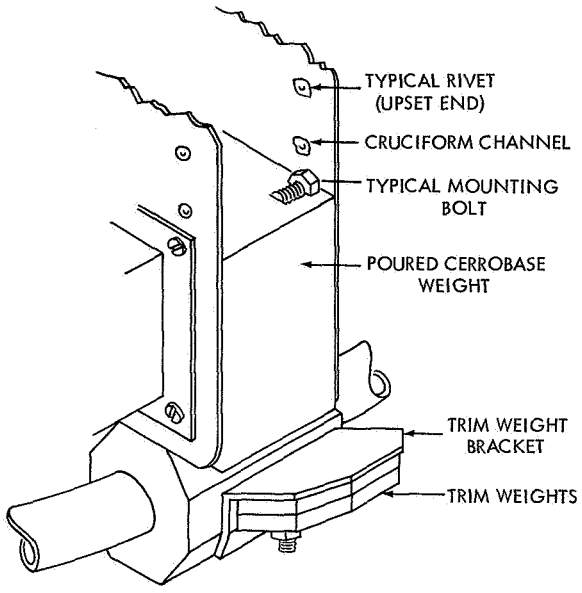


FIGURE 11–7.—Typical weight installation.

Fine Balance—

The spacecraft was mounted in the vertical balancing machine, and physical measurements were taken by dial indicator. As measured on the separation ring, run-out was 0.004 inch T.I.R. and wobble was 0.0025 inch T.I.R. Indicator readings on the balance machine adapter plate showed an eccentricity of 0.002 T.I.R. and a wobble of 0.0025 T.I.R. The vehicle was balanced, as noted in *Operating Principle* above, by first immobilizing the lower joint for static balance and then freeing it, to allow the spacecraft to rotate about its principle axis of inertia, for dynamic balancing. Corrective added weights were made of Aboseal. When balancing was completed, the total number of added weights were vectored into two trim weights for each of the solar panel mounting rings. The permanent trim weights consisted of lead or brass wafers, stacked in multiples, at 90° spacing on the upper and lower solar panel mounting rings. A total of 616 grams of balance weight was added to the spacecraft.

When all weights were permanently installed, a check was made for residual unbalance inherent within the spacecraft. Temporary Aboseal weights were added to the spacecraft to introduce a known static and dynamic unbalance. These weights were spaced at 90 degree intervals, and in each case the sensitivity meter of the machine showed higher unbalance readings with the Aboseal weights in place. This indicated that the spacecraft was already well balanced.

Unbalance Analysis—

1. Residual Static Unbalance — Residual unbalance tests indicate residual static unbalance of:

$$wR = \frac{9.3 \text{ gm} \times 13 \text{ in}}{454 \text{ gm/lb}} + \frac{11.7 \text{ gm} \times 9.5 \text{ in}}{454 \text{ gm/lb}}$$

$$wR = .267 + .245 = .51 \text{ lb-in}$$

where 9.3 and 11.7 gm are Aboseal weights temporarily added.

$$\frac{.51 \text{ lb-in}}{172 \text{ lb}} = .003 \text{ in}$$

Allowing .0015 in for C.G. offset in mounting the vehicle to the Vertical Balancing Machine, maximum static unbalance is .0045 inch C.G. displacement.

2. Residual Dynamic Unbalance—Residual dynamic unbalance tests were made with two Aboseal weights (3.5 and 5 gm) added to top and bottom of the solar panels:

$$wRz = \frac{5 \text{ gm} \times 9.5 \text{ in} \times 15.4 \text{ in}}{28 \text{ gm/oz}} + \frac{3.5 \text{ gm} \times 13.5 \text{ in} \times 16.6 \text{ in}}{28 \text{ gm/oz}}$$

$$wRz = 26.1 + 27.8 = 53.9 \text{ oz in}^2$$

The total runout on the face of the adapter plate was .0025 TIR. This reading was taken at a radius of 5 in. The wobble runout angle was then:

$$\tan \theta_1 = \theta_1 = \frac{.0025}{2 \times 5}$$

$$\theta_1 = .00025 \text{ radians}$$

$$J_{zx} = \theta_2 (I_{\text{spin}} - I_{\text{pitch}})$$

$$\theta_2 = \frac{53.9 \text{ oz in}^2}{(46.44 - 44.29) \text{ lb in sec}^2 \times 386 \text{ in-sec}^2 \times 16 \text{ oz/lb}}$$

$$\theta_2 = .0041 \text{ radians}$$

The maximum dynamic unbalance is therefore .0041 + 0.00025 = 0.0044 radian.

Measurement

Specification — The moment of inertia measurement of the spacecraft was performed in accordance with Project Relay Performance Requirements No. R1–0100. The specification required that the ratio of the null moment of inertia (about the spin axis) to the largest moment of inertia about any axis lying in a plane normal to the spin axis should be no less than 1.05.

Equipment

Bifilar pendulum and universal support bar—This was a two-wire torsional pendulum rigidly anchored and terminating in a support bar designed to accommodate the spacecraft for measurement about pitch or spin axes. (See Figure 11–8).

Instrumentation

1. DC Micro Volt Ammeter
2. Constant current power supply, Video Instr. model SRB200
3. Electronic counter, Hewlett - Packard HP523CR
4. Flip-flop circuit
5. Collimated light source, photocell, and mirror.

The requirement for this instrumentation was that a measurement of the period of uncoupled torsional oscillation be provided, having an accuracy of ±0.0009 seconds. The bifilar pendulum system responded in a coupled torsional-translatory motion when oscillating. It was essential that only the torsional motion should be sensed by the instrumentation. An optical system was used to accomplish this.

A thin collimated band of light was the source. When this light was normal to a mirror mounted on the spacecraft support bar, the light was reflected back to a germanium photo junction cell mounted on the light source housing, which responded to the light pulse by a change in resistance. This in turn triggered the counter.

Procedure — The bifilar pendulum was equipped with strain gages which assured equal loading on each wire. Several calibration checks were carried out, loading each wire equally, using 10-pound load increments between 0 to 100 lb on each wire of the bifilar rig.

A curve was plotted from the average displacement readings of the Micro Volt-Ammeter when the bifilar rig was loaded in increments. This displacement curve was used to assure equal tension on the wires within ½ lb when the satellite was installed on the bifilar rig.

The general formula for measuring Moment of Inertia by means of the bifilar pendulum is:

$$I = \frac{Wt\,R^2\,T^2}{4\pi\,2L}$$

The moment of inertia of the standard test bar weighing 169.59 lb, 4.482 in. diameter, and 37.988 in. long is:

$$I = W[L^2+D^2]$$

$$= \left[\frac{169.59}{385.9}\,\frac{(37.988)^2}{12} + \frac{(4.482)^2}{16}\right]$$

$$I = 53.401 \text{ lb-in-sec}^2$$

The standard test bar was hung onto the universal bar and oscillated approximately 5 degrees about its center of gravity. A mirror attached to the test bar reflected a collimated light beam into the photo cell–flip-flop circuit which in turn was coupled to a counter.

The average time per period (T) was 3.4383 seconds. The length of the bifilar pendulum with 169.59 lb load is 333.25 inches. The weight of the wires was 1.86 lb but only ½ of this weight contributed to the unbalance causing the oscillation. The wires were set 38.280 inches apart by means of a pin gauge.

$$I_{\text{Test Bar}} + I_{\text{Univ. Bar}} = \frac{WR^2T^2}{4\pi 2L}$$

$$\text{where } W = 169.59 + \frac{1.86}{2} + 14.72$$

$$= 185.24 \text{ lb}$$

$$I_{\text{Test Bar}} + I_{\text{Univ. Bar}} = \frac{185.24(19.140)^2(3.484)^2}{4\pi^2 \times 333.25}$$

$$= 60.948 \text{ lb-in-sec}^2$$

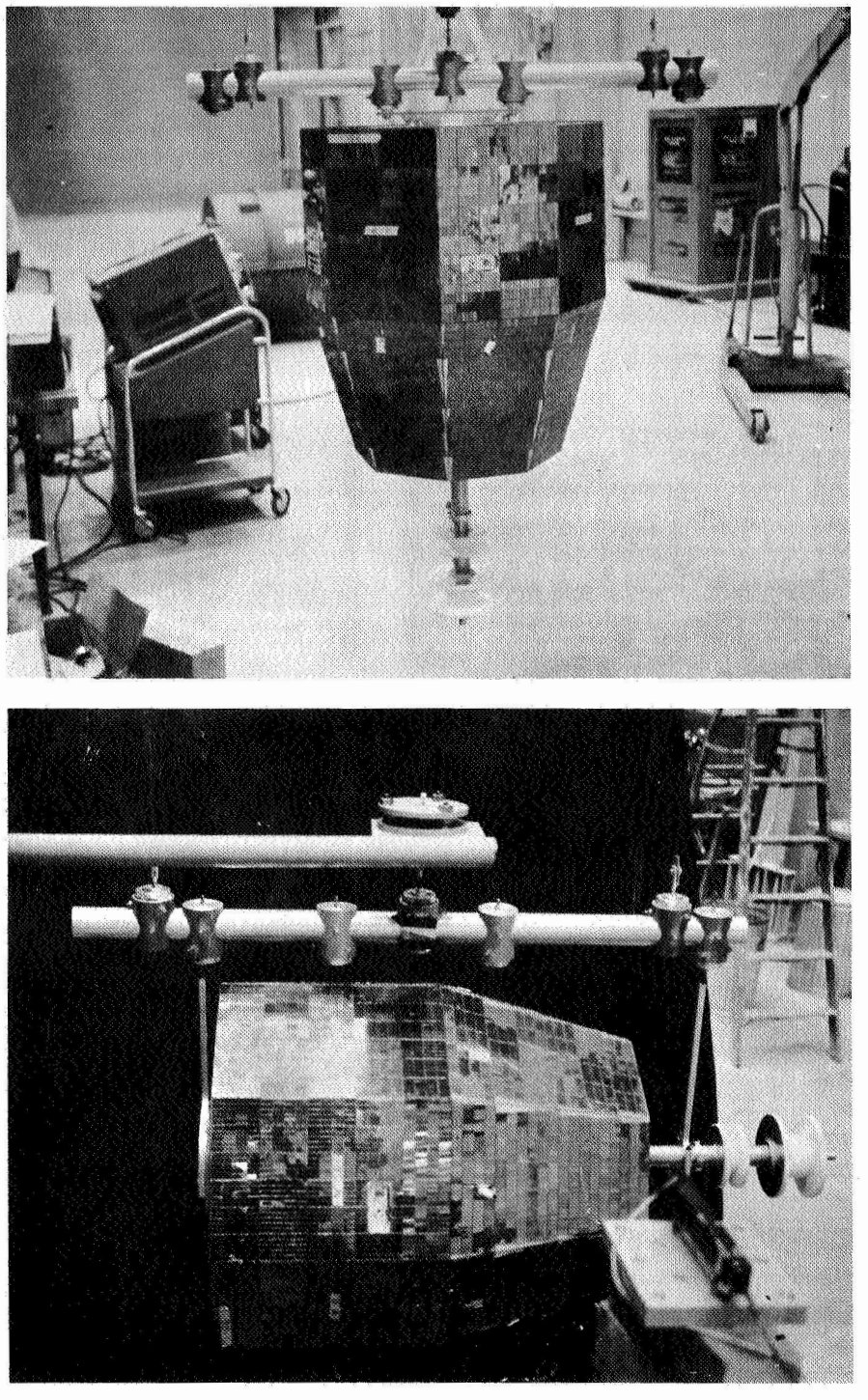


FIGURE 11–8.—Spacecraft mounted on bifilar pendulum for moment of inertia measurement.

The test bar was removed and the period measured of the universal bar and test bar hangers only.

$$\text{Wt.} = 14.72 + \frac{1.86}{2} = 15.65 \text{ lb.}$$

$$I_{\text{Univ. Bar}} = \frac{15.65\,(19.140)^2\,(4.1735)^2}{4\pi^2\,(333.25)}$$

$$= 7.593 \text{ lb-in-sec}^2$$

$$= 60.948 - 7.593$$

$$I_{\text{Test Bar}} = 53.355 \text{ lb-in-sec}^2$$

$$\% \text{ Error} = \frac{53.401 - 53.355}{53.401} \times 100$$

$$= = .086\%$$

The spacecraft was mounted on the bifilar rig for spin axis measurement. The rig was caused to oscillate by displacing the bar 5 degrees and the period was measured. Then the spacecraft was removed and the period of the universal bar alone was measured.

$$I_{\text{Spacecraft + Univ. Bar}} = \frac{(171.94+.93+18.642)\,(19.140)\,(3.1885)}{4\pi^2\,(333.25)}$$

$$= 54.214 \text{ lb-in-sec}^2$$

$$I_{\text{Univ. Bar}} = \frac{(18.642+.93)\,(19.140)^2\,(3.7762)^2}{4\pi^2\,(333.06)}$$

$$= 7.776 \text{ lb-in-sec}^2$$

$$I_{\text{Spacecraft}} = 54.214 - 7.776$$

$$= 46.438 \text{ lb-in-sec}^2$$

The spacecraft was mounted on the bifilar rig for lateral moment of inertia measurements. The rig was caused to oscillate and the period measured. The spacecraft was rotated clockwise (looking from the separation ring) into 45°, 90°, and 135° positions and oscillation periods were obtained for each.

The spacecraft was removed and a similar test conducted with the universal test bar and fixture only. The periods are given below.

Position	Period (seconds)
0°	3.3139
45°	3.2768
90°	3.2308
135°	3.2706
Univ. bar + fixture	4.8947

$$I_{0^\circ} = \frac{(171.94+21.86+.93)\,(19.140)^2\,(3.3139)^2}{4\pi^2\,(333.26)}$$

$$= 59.544 \text{ lb-in-sec}^2$$

$$I_{45^\circ} = 58.218 \text{ lb-in-sec}^2$$

$$I_{90^\circ} = 58.218 \text{ lb-in-sec}^2$$

$$I_{135^\circ} = 57.998 \text{ lb-in-sec}^2$$

$$I_{\text{univ. rig.}} = \frac{(21.86+.93)\,(19.140)\,(4.8974)^2}{4\pi^2\,(333.06)}$$

$$= 15.229 \text{ lb-in-sec}^2$$

Actual Tranverse Moments of Inertia:

$I_{0^\circ} = 59.544 - 15.229 = 44.315$ lb-in-sec^2

$I_{45^\circ} = 58.218 - 15.229 = 42.989$ lb-in-sec^2

$I_{90^\circ} = 56.596 - 15.229 = 41.367$ lb-in-sec^2

$I_{135^\circ} = 57.998 - 15.229 = 42.769$ lb-in-sec^2

The maximum and minimum values were:

$$I_{\max} = 44.362 \text{ at } 2^\circ \text{ CW}$$

$$I_{\min} = 41.327$$

$$\text{Ratio} \frac{I_{\text{trans}}}{I_{\text{spin}}} = \frac{44.362}{46.438} = 0.959$$

Qualification Tests

To qualify the basic design of Relay I, a series of electrical performance tests and simulated - environmental tests were performed on the protoype spacecraft. The sequence of tests was as follows:

1. Electrical performance "D" tests—performed before environmental tests.
2. Temperature survey.
3. Electrical performance "A" test—performed after temperature survey and before spin test.
4. Spin.
5. Electrical performance "B" test—performed after spin test and before vibration test.
6. Vibration.
7. Electrical performance "B" test—performed after vibration and before thermal gradient.
8. Thermal gradient.
9. Electrical performance "A" test—performed after thermal gradient and before humidity test.
10. Humidity.

11. Electrical performance "B" test—performed after humidity and before acceleration.
12. Acceleration.
13. Magnetic dipole moment.
14. Electrical performance "B" test—performed after acceleration and magnetic dipole tests and before WB traffic tests.
15. WB traffic tests (electrical).
16. Electrical performance "B" test—performed before solar simulation.
17. Solar simulation.
18. Electrical performance "B" test—performed after solar simulation.

At the completion of the test sequence, a final calibration was performed on the spacecraft prior to delivery to Cape Canaveral.

Acceptance Tests

To prove the unit workmanship on Relay I, and to insure compliance with the applicable spacecraft specifications, a series of electrical performance tests and simulated environmental tests were performed on the flight model No. 1 spacecraft. The electrical performance tests were identical to those performed on the prototype spacecraft; the environmental conditions were generally less severe than the corresponding tests on the prototype spacecraft. The sequence of tests were as follows:

1. Electrical performance "D" tests—performed before environmental tests.
2. Electrical performance "C" — performed before spin test.
3. Spin.
4. Electrical performance "A" — performed after spin and before temperature survey.
5. Temperature survey.
6. Electrical performance "B" — performed after temperature survey and before vibration.
7. Vibration.
8. Electrical performance "B" — performed after vibration and before solar simulation.
9. Solar simulation.
10. Electrical performance "A" — performed after solar simulation and before magnetic dipole.
11. Magnetic dipole.
12. Electrical performance "D"—after all environmental tests.

At the completion of the test sequence, a final calibration of all telemetry points was performed on the spacecraft prior to delivery to Cape Canaveral.

Electrical Performance Tests

Type "A" Tests

These tests consisted of the following checks on the performance of the various spacecraft subsystems:

1. Power Supply Checkout.
   a. Battery open circuit voltage
   b. Battery charge current
   c. Battery discharge current
   d. Battery trickle charge current and control voltage
   e. Solar bus voltage
   f. Unregulated bus voltage
   g. Regulated voltages
      (1) Radiation experiments regulator
      (2) Wideband No. 1 (WCS–1) regulator
      (3) Wideband No. 2 (WCS–2) regulator
      (4) 9V regulators
   h. Load cutoff operation
   i. Voltage limiter operation
2. Telemetry, Tracking, and Command Subsystem Checkout—Command verification checkout is performed at an input of 4μv at an unregulated bus voltage of 28 vdc.
3. Wideband Communications Subsystem Checkout.
   a. Functional acceptance check (telemetry)
   b. Frequency response

Type "B" Tests

These tests consisted of all of the portions of the "A" tests previously mentioned plus the following checks:

1. Telemetry, Tracking, and Command Subsystem Checkout
   a. Command verification at input level

of 4μv and unregulated bus voltages of 22 and 34 vdc.

b. Command redundancy

c. Telemetry transmitter power output

2. Attitude Control Subsystem Checkout

a. Sun aspect indicator

b. Torque coil

c. Horizon scanner

Type "C" Tests

These tests consisted of those portions of the "A" tests that could be sampled via telemetry, since there were no hard-line connections to the spacecraft other than simulated solar array output. These tests were:

1. Power Supply Checkout

a. Solar bus voltage

b. Battery in-circuit voltage

c. Unregulated bus voltage

d. Solar bus current

e. Total battery current

f. Regulated voltages

(1) Radiation experiments regulator

(2) WB regulators

g. Battery pressure

2. Telemetry, Tracking and Command Subsystem Checkout.—A command verification was performed at an RF level of 4μv as seen by the command receiver.

3. Wideband Communications Subsystem Checkout.

a. Functional Acceptance check (telemetry)

b. Frequency response

Type "D" Tests

These tests consisted of all of the "B" tests previously mentioned and the following additions:

1. Wideband Communications Subsystem Checkout.

a. Functional acceptance check

b. Beyond-horizon switch voltage

c. Output power

d. Frequency

e. Noise figure

f. TV simulation

g. 300-channel noise loading

h. Group delay

i. Two-way crosstalk

j. 24-channel noise loading

2. Radiation experiments.

a. Radiation damage panel

b. Radiation monitors.

Preliminary Test Conditions

1. *Modes of Operation*—

a. Standby mode consisted of the command subsystem and the power supply subsystem in operation, and was the minimum electrical load on the spacecraft.

b. Continuous mode was the simultaneous operation of one unmodulated telemetry transmitter (for tracking purposes) and the standby loads.

c. Radiation mode was the simultaneous operation of the command subsystem, both telemetry transmitters, the telemetry encoder, and all radiation experiments.

d. Wideband mode presented the maximum electrical load to the spacecraft and consisted of the simultaneous operation of one wideband communications subsystem in addition to the radiation mode.

2. *Use of Ground Test Fixture* — The ground test fixture (see Figure 11–9) was connected to the spacecraft with one 25-conductor cable and one 50-conductor cable into the ground test receptacles, 42J1 and 42J2. This box contained appropriate switches and meters to provide for:

a. switching the spacecraft batteries in and out of the circuit, thus providing master switching

b. inserting an ammeter into each battery string to read charge and discharge currents

c. inserting an ammeter into the voltage-limiter circuit to read voltage-limiter current

d. inserting an ammeter into the solar bus to read the input current from the solar-array simulator (external power supply with current limiting)

e. continuous monitoring of the voltages of all three battery strings, the solar bus voltage, and the unregulated bus voltage

f. inserting a low-range ammeter into each battery string for reading trickle-charge current

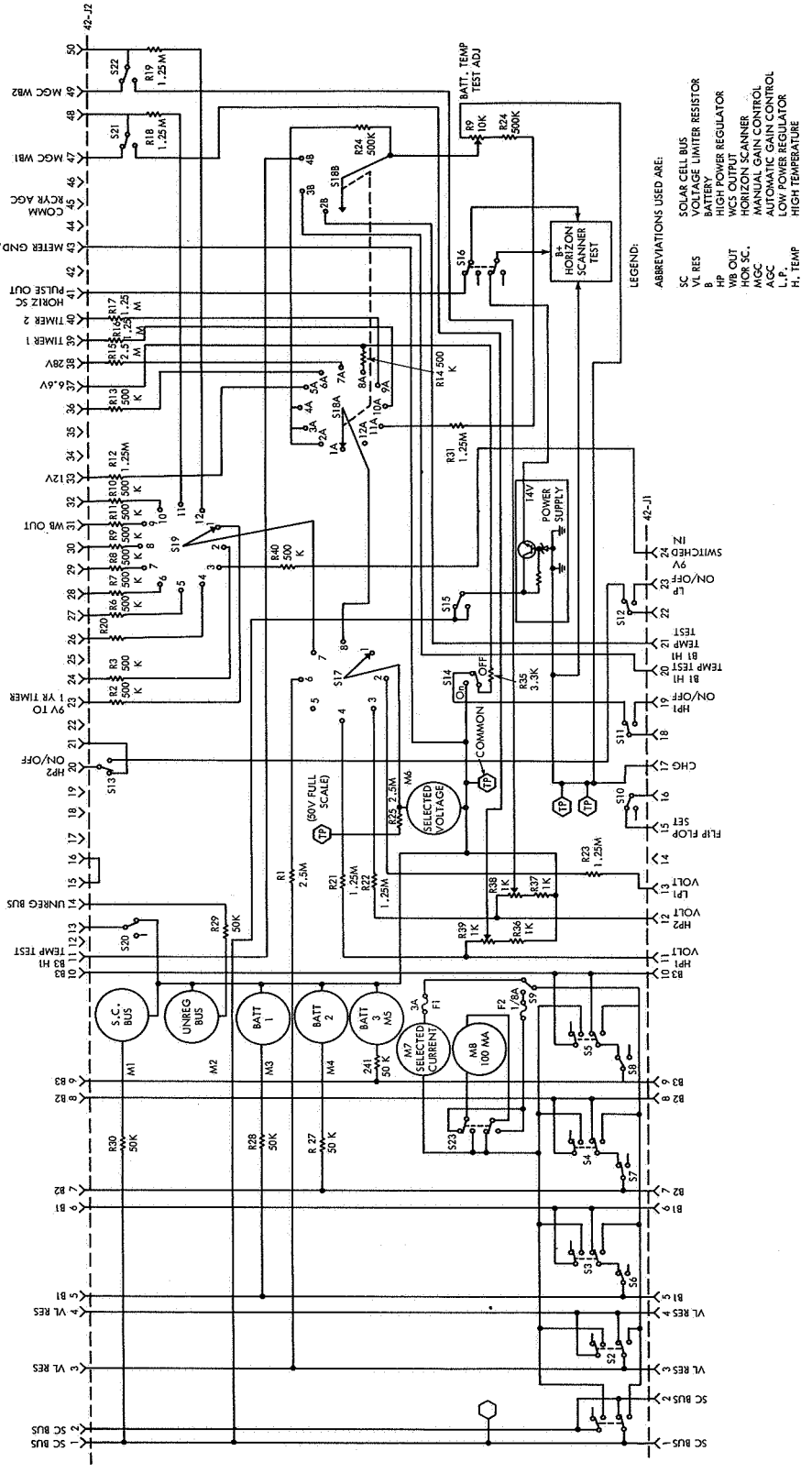


FIGURE 11-9.—Ground test fixture, schematic diagram.

g. monitoring any one of the following selected voltages:

- radiation experiments regulator
- WCS–1 regulator
- WCS–2 regulator
- voltage-limiter transistor collector voltage
- solar bus
- 9–v regulator (timer)
- 9–v regulator (control)
- 9–v regulator (telemetry)
- 6.8v command control box regulator
- 12–v command control regulator
- Unregulated bus at command control box
- WB receiver LO
- WB receiver hi-level mixer
- WB transmitter LO
- transponder AGC
- WB receiver power out
- Beacon oscillator
- timer enable, WCS–1
- timer enable, WCS–2
- VHF modulation switch position
- battery #1 temperature c/o control
- battery #2 temperature c/o control
- battery #3 temperature c/o control
- WCS–1 MGC
- WCS–2 MGC

h. on/off control of the following regulators:

- radiation experiments
- WCS–1
- WCS–2

i. resetting the command control flip-flops to the initial state and enabling the command control box

j. testing the battery hi-temperature cutoff circuitry

k. controlling MGC voltage to each WCS for noise figure measurements

l. reading command receiver AGC

m. simulating the output of the solar array (external power supply).

The ground test fixture was used in all testing except for C tests and those dynamic environmental tests requiring use of shorting plugs.

3. *Use of Shorting Plugs*—Two shorting plugs were used to turn on power to the spacecraft, to provide wire continuity where required, and to set the command control box flip-flops in the initial command states. Inserting either of the plugs turned on the power and completes some of the circuits; inserting the other set up the command control circuitry in the initial state and completes the remainder of the circuits.

The plugs used in testing were identical to the flight plugs except for the 1-year timer bias. The 9–v supply for the timer is disabled during all ground tests to insure that the ultimate turnoff will not be premature due to many hours of extensive testing.

The shorting plugs were used during the electrical performance C tests and the following environmental tests:

a. Spin
b. Acceleration
c. Vibration
d. Magnetic dipole moment.

A special set of shorting plugs was used during solar simulation. In these plugs, the battery straps and the flip-flop set straps were brought out via slip rings for external monitoring and control, while the remaining functions were wired in the normal manner.

Tests with Ground Test Fixture

General—

The spacecraft was normally tested with the solar array removed. The ground test fixture was connected into the ground test receptacles and the external power supply (solar-array simulator) connected into the ground test fixture. Three of the monopole whip antennas were replaced with 50-ohm terminations: the fourth whip was connected to a 20-db attenuator. The spacecraft was commanded by amplitude modulating an HP–608 Signal Generator and hard-lining through a short length of RG–58 cable to the 20-db pad. The command carrier frequency was set to the nominal value, using a decade counter. The telemetry signal from the spacecraft was received on a short monopole antenna near the spacecraft. The TWT

output cables were terminated at all times by the wideband antenna or an external load such as a calorimeter power meter or an 80-watt termination (see Figures 11–10 and 11–11).

Power Supply—

1. *Battery Open-Circuit Voltage*—Battery open-circuit voltage was measured with the digital voltmeter by measuring between each battery test point (42J1–6, 8, 10) and meter ground (42J2–43) on the ground test fixture. The battery master switches (S6, 7, 8) were left open for this measurement. If any battery voltage was less than 24 vdc, the batteries were put on full charge for 30 minutes; the measurement was then repeated.

2. *Battery Charge Current* — Battery charge current was measured by switching (S3, 4, 5) an ammeter into each battery string and recording the current (M7) with

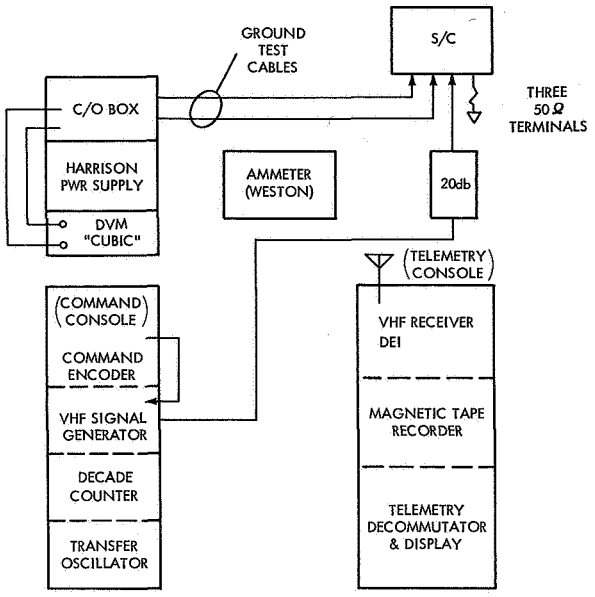


FIGURE 11–10.—Test connections for power supply, command verification, and redundancy tests.

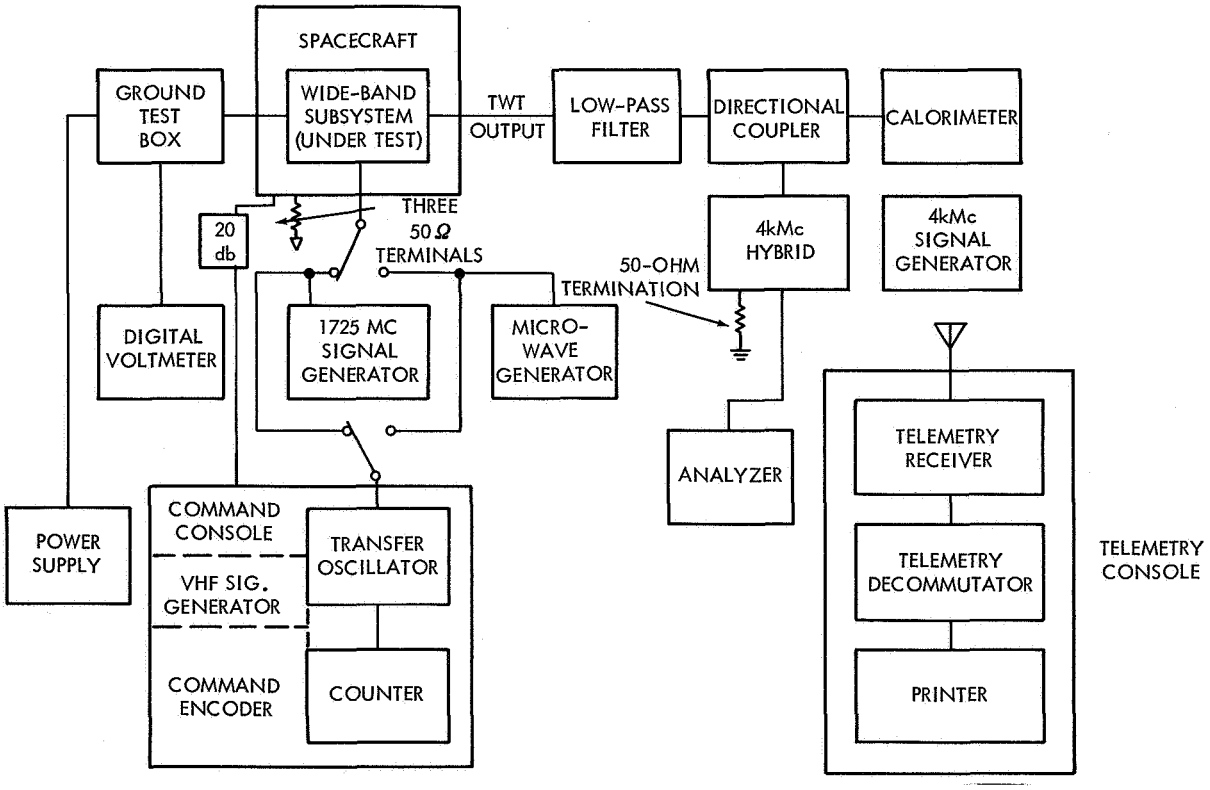


FIGURE 11–11.—Test connections for wideband subsystem functional acceptance test.

the external power supply set to 32 vdc. A reading of 400 to 600 ma on each string was nominal.

3. *Battery Discharge Current* — Battery discharge current was measured as above, but with the external supply turned off (eclipse condition). Each battery should have contributed approximately one-third of the total load. WB–1 was then turned on at the ground test fixture (S11 and S14) and the discharge currents again recorded. Each battery should have contributed approximately one-third of the total load. WB–1 was then turned off and the external charging supply turned on and set at 32 vdc.

4. *Battery Trickle Charge Current and Control Voltage*—Battery trickle charge current and control voltage was measured by switching (S17–8, S15) a variable 0 to 5 vdc test voltage into the cutoff circuit of each battery-string and slowly increasing this voltage (R–9), while observing the charge current mentioned above. When the charge current decreased suddenly to a much lower value, the supply voltage (M6) was recorded, along with the trickle charge current indicated on the low-range ammeter (M8). A momentary contact switch (S9) was provided to switch the low-range ammeter (M8) into the battery string after trickle charge had been established. Removing the test voltage allowed the battery to return to full charge. Readings of 3.3 to 4.1 vdc and 15 to 100 ma were nominal values.

5. *Solar Bus Voltage*—Solar bus voltage was measured with the digital voltmeter between the solar bus test point and meter ground on the test fixture. The solar bus voltage was nominally set to 32 vdc by adjusting the external power supply (solar-array simulator).

6. *Unregulated Bus Voltage*—Unregulated bus voltage was measured with the digital voltmeter by measuring between the unregulated bus test point and meter ground on the ground test fixture. The unregulated bus voltage was nominally 2 volts lower than the solar bus voltage measured in 5 above. When the solar array simulator was turned off, unregulated bus voltage was then nominally greater than 24 vdc. The solar-array simulator was then turned on and set to supply 2.0 amps, current limited.

7. *Regulated voltages*—Radiation experiments regulator output voltage was measured on a DVM between the radiation experiments regulator test point and meter ground. The radiation experiments regulator was turned on at the ground test fixture (S12 and S14) and the DVM reading recorded. A reading between 22.23 and 22.72 vdc was nominal.

WCS–1 regulator output voltage was measured on a DVM between the WCS–1 regulator test point and meter ground. The WCS–1 regulator was turned on at the ground test fixture (S11 and S14) and the DVM reading recorded. A reading between 22.23 and 22.72 vdc was nominal.

WCS–2 regulator output voltage was measured on a DVM between the WCS–2 regulator test point and meter ground. The WCS–2 regulator was turned on at the ground test fixture (S13 and S14) and the DVM reading recorded. A reading between 22.23 and 22.72 vdc was nominal.

8. *Load Cutoff Operation* — Load cutoff operation was checked by monitoring the WCS–1 regulator output voltage (M6 and S17–4) while adjusting the unregulated bus. (For this test, the solar-array simulator was set to 28 vdc and the battery master switches (S6, 7, 8) opened.) The WCS–1 system was commanded on and load cutoff-normal established, using the command console. The unregulated bus voltage was lowered by slowly decreasing the input from the solar-array simulator. At the instant of WCS–1 turnoff, the unregulated bus was nominally 22 $\pm$ 1 vdc. The unregulated bus was then raised to 28 vdc and WCS–1 commanded back on with load cutoff-override, using the command console. The WCS–1 regulator should not turn off when the unregulated bus is lowered to 21 vdc. The unregulated bus was then raised to 28 vdc and the WCS–1 subsystem commanded off. The test was then repeated for WCS–2 using M6 and S17–3. At the conclusion of the check, the battery master

switches (S6, 7, 8) were closed and the solar-array simulator set to deliver 2.0 amps.

9. *Voltage Limiter Operation* — Voltage-limiter operation was checked by monitoring the voltage-limiter collector voltage while raising the solar bus voltage, using the solar-array simulator. (When the solar bus voltage reaches about 32.5 vdc, the voltage-limiter collector voltage starts to decrease with an increase in the solar bus voltage.) The solar bus voltage was raised further until the voltage-limiter collector voltage dropped to 10 vdc; the solar bus voltage was then nominally less than 35 vdc. The solar-array simulator was readjusted to supply 2.0 amps, current limited.

Telemetry, Tracking and Command Subsystem—

1. *Command Verification*—Command verification was performed at unregulated bus voltages of 22, 28, and 32 vdc and at input levels of 4 μv and 50 μv (see Figure 11–10). For the check at 22 vdc, the spacecraft was operated from the solar-array simulator only. The spacecraft was placed in the standby mode by resetting the command control box flip-flops, using the ground test fixture (S10). The command carrier frequency was checked several times during each test, using a decade counter. The PDM level was set to provide 80-percent modulation. The telemetry console was set up to decommutate the output of the DEI telemetry receiver and print-out main commutator channel 21 in decimal for several seconds, and then main commutator channel 16 (subcommutator identification) in binary, and main commutator 28 in decimal, to display high level subcommutator channels 35, 43, and 51. These four channels contain all of the command verification outputs as follows:

Main commutator channel 21
- Load cutoff—normal/override
- WCS–1—on/off
- Mode—TV/Phone

High level subcommutator channel 28/35
- Horizon scanner—on/off
- Modulate—TT#1/TT#2
- Torque coil—positive/off

High level subcommutator channel 28/43
- WCS–2—on/off
- Telemetry transmitter #1—on/off
- Telemetry transmitter #2—on/off

High level subcommutator channel 28/51
- Radiation experiments—on/off
- Telemetry encoder—on/off
- Torque coil—negative/off

The sequence of commands listed in Table 11–2 were next sent to the spacecraft and observations recorded on the data sheet. This sequence was then repeated for each unregulated bus voltage setting and RF level, after first checking the carrier frequency.

TABLE 11–2.—*Command Verification Test Sequence*

Sequence	Command	Function	Observation
A	15	TT1&2 ON	Presence of both carriers (unmodulated) on DEI receiver.
B	7	Encoder ON	Frame sync on decommutator, verification states
C	6	Radiation expts ON	" "
D	8	Horizon scanner ON.	Encoder off, loss of frame sync, presence of 1300 cps squarewave at receiver output.
E	7	Encoder ON	Horizon scanner off, frame sync, verification states.
F	5	Radiation experiments OFF	" "
G	2	WCS–1 ON	" "
H	18	Mode-phone	" "
I	4	WCS–1 OFF	" "
J	3	WCS–2 ON	" "
K	19	Mode–TV	" "
L	4	WCS–2 OFF	" "
M	12	Coil positive	" "
N	11	Coil negative	" "
O	---	Tune DEI to TT–1.	Presence of unmodulated carrier.
P	9	Modulate TT–1	Modulation on carrier, verification states.
Q	13	Coil OFF	" "
R	1	Load cutoff–normal	" "
S	20	Load cutoff–override	" "
T	17	TT–1 OFF	Loss of signal on DEI receiver.
U	10	Modulate TT–2	Retune DEI receiver to TT–2, presence of modulation, verification states.
V	14	Encoder OFF	Loss of frame sync.
W	16	TT–2 OFF	Loss of carrier on DEI receiver.

2. *Command Redundancy*—Command redundancy was checked (see Figure 11–10) by disabling the RF input to one of the command receivers and the opposite command decoder. The decoder is disabled by installing a special Cannon connector in the harness at the decoder. The command verification sequence was then performed at an unregulated voltage of 28 vdc and an RF input of 4 μv. At the completion of this check, the command system was enabled, the opposite receiver and decoder disabled, and the test repeated.

3. *Telemetry Transmitter Power Output*—Telemetry transmitter power output was measured by inserting special 25-inch sections of RG–188/U cable in each antenna feedline and terminating three of the four ports in 25-ohm terminations. At the fourth port, a pad and a 50-ohm load are connected in parallel with an RF power meter connected to the output of the pad. The power output of each transmitter was then measured at unregulated bus voltages at 22, 28, and 32 vdc. The measurements were repeated at each of the other antenna ports. The power was also measured directly out of the transmitter, using a pad in series with the power meter.

Wideband Communications Subsystems—

1. *Functional Acceptance Checks*—Functional acceptance checks (see Figure 11–11) in both TV mode and phone mode were made for each wideband subsystem. This check includes regulator output voltage, current in both warm-up and full power, and timer intervals.

Functional acceptance checks (telemetry) were made, using both TV and phone modes, with RF inputs of –40, –60, and –80 dbm. For those points having a test point on the ground test fixture, a DVM reading was taken for comparison with the telemetry reading.

The input frequency from the UHF generator was checked, using a decade counter and a transfer oscillator. Input levels were measured on an RF power meter and were thus set.

The narrowband (phone mode) carriers were obtained from a special microwave generator using crystal-controlled frequencies. Input level calibrations were made, using a hybrid, a UHF signal generator, and a spectrum analyzer. Input levels to the spacecraft were controlled by attenuators fixed to the output of each generator.

2. *Frequency Response*—Frequency response was checked by applying an input signal from an Alfred sweep generator at levels of –40, –60, and –80 dbm and detecting the output signal with a wideband detector (see Figure 11–12). Photographs were taken of the output in TV mode at input levels of –40 and –60 dbm, and in phone mode at input levels of –40, –60, and –80 dbm. To calibrate the detector, a 1–db pad and two 3–db pads were inserted in front of the crystal detector probe, and multiple-exposure photographs were taken. Frequency limits of the sweep were calibrated, using a hybrid and a decade counter and transfer oscillator.

3. *Output Frequency*—Output frequency was measured using a decade counter and a transfer oscillator. The input signal was set very accurately to 1725.00 Mc and the corresponding output signal from each WB measured in the TV mode. In the phone mode, the input frequency was set accurately to 1723.33 Mc and 1726.67 Mc, and the output frequencies were measured; the beacon frequency was also measured.

4. *Output Power*—Output power was measured after calibrating the output cabling for insertion loss, including a low-pass

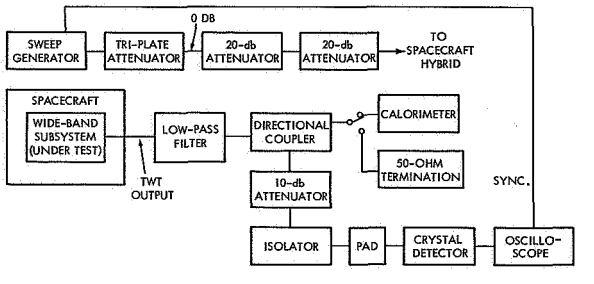


FIGURE 11–12.—Wideband subsystem frequency response test setup.

filter and the directional coupler. Calorimeter readings were taken for input levels from –35 dbm to –90 dbm input in both TV and phone modes. The AGC reading at each input level was also recorded.

In the phone mode, signals of unequal strength were supplied to the input, and the output levels were measured to determine the relative compression.

Beacon power output was measured with respect to the main carrier, using a hybrid, SHF signal generator, and a spectrum analyzer. Beacon power levels were nominally 17 db below the main carrier level.

5. *Receiver Noise Figure*—Receiver noise figure was measured by taking the signal out of the IF strip at 70 Mc. MGC is used to control the gain of the IF amplifier during this measurement.

6. *Television Simulation*—Television simulation was checked (see Figure 11–13) in the wideband mode by modulating the MM600 transmitter with staircase, white window, and multiburst composite video signals. The received signals were photographed for comparison with the back-to-back reference signals to verify the transparency of the spacecraft repeater. In addition, differential gain and differential phase were measured for each system.

7. *300-Channel, Noise-Loading Measurements*—300-channel, noise-loading measurements (see Figure 11–14) were made in wideband mode. A white-noise signal, having a spectral bandwidth from 60 kc to 1300 kc corresponding to 300 full-load telephone channels, was used to modulate the MM–600 transmitter. Because the spacecraft repeater triples the input deviation, the back-to-back reference measurements were made at two extremes. These extremes were:

a. Deviating the modulator by its nominal amount and, therefore, the demodulator by one-third of its nominal amount.

b. Deviating the modulator by three times its nominal amount, with the demodulator now at its nominal deviation.

Both of these measurements showed the contribution of the ground equipment to be negligible in the measurement of the top channel (worst case) distortion.

The intermodulation test set transmitter contains a number of band-rejection filters whose center frequencies (at baseband) and response characteristics are identical to the bandpass filters in the intermodulation test set receiver. A reference reading is obtained by transmitting the full spectrum of noise into the repeater, and measuring the noise present in a given bandpass filter channel. A band-rejection filter is then switched into the transmitter whose center frequency is identical to the receiver band under investi-

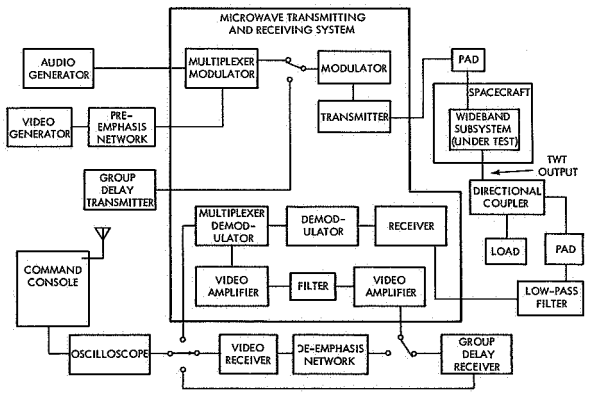


FIGURE 11–13.—Setup for television transmission and and group delay tests.

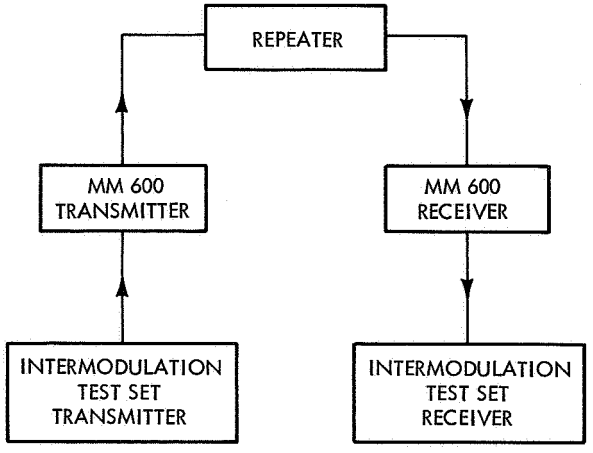


FIGURE 11–14.—300-channel noise loading test setup.

gation. The noise present in the receiver filter is then due to intermodulation distortion in the repeater and thermal noise in the test equipment.

The contribution to the total noise from thermal sources is determined by removing the noise modulation at the transmitter and measuring the noise in the receiver filter channel. The figure of merit, called Noise Power Ratio, is then the difference between the reference reading and the intermodulation distortion and thermal noise, expressed in db.

These measurements were made at filter frequencies of 70 kc, 270 kc, and 1248 kc on both wideband systems, with carrier levels of –40 dbm.

8. *24-Channel Noise-Loading Measurements*—24-channel, noise loading measurements (see Figure 11–15) were made in narrowband mode. The measurement is similar to the 300-channel, noise-loading test described above, with several significant differences. The white-noise spectrum is bandlimited from 60 kc to 108 kc, corresponding to 12 full-load telephone channels per repeater channel. During this test, one microwave carrier is modulated with the noise spectrum while the other carrier is unmodulated. The carrier levels were nominally equal. In the MM–600 receivers, a bandpass filter, tuned to either 65 Mc or 75 Mc, was inserted between the IF pre-amp and the IF amplifier.

The test is performed by modulating one of the repeater channels and listening on the same channel, using the appropriate IF bandpass filter. NPR measurements were made at frequenciees of 70 kc and 105 kc, at a carrier level of –40 dbm, for each repeater channel and for both wideband systems.

9. *Crosstalk Measurements* — Two-way, crosstalk measurements (see Figure 11–15) were made in conjunction with the 24-channel, noise-loading tests.

10. *Group Delay*—Group delay measurements were made in wideband mode, using the Group Delay and Linearity test set. This test set consists of a separate transmitter and receiver for determining the delay distortion

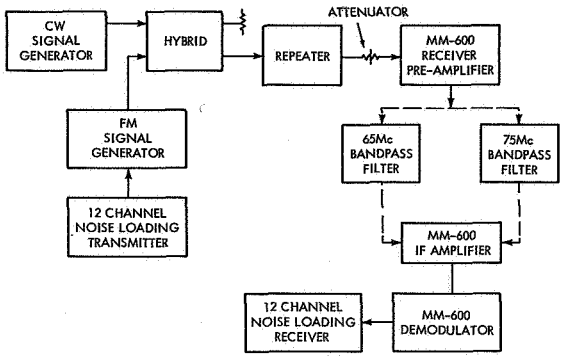


FIGURE 11–15.—24-channel noise loading intermodulation and crosstalk test setup.

caused by the nonlinear phase-vs-frequency characteristic of IF and RF circuits, and for determining the linearity of the transfer characteristic of the modulator/demodulator elements of a microwave radio link. The test set transmitter supplies to the MM600 transmitter a signal swept over the 62– to 78–Mc IF band at a rate of 500 cycles per second. At the same time a tone of 200 kc is superimposed on the signal as low deviation frequency modulation. After passage through the spacecraft repeater and front-end of the MM600 receiver, the IF signal is demodulated and analyzed by the test set receiver for phase-modulation on the detected 200-kc tone. The receiver output is then displayed on an oscilloscope as low frequency voltage whose height is proportional to the delay and whose horizontal position is synchronized with the ± 8 Mc deviation at the rate of 500 cycles per second. A switch on the test set receiver provides a 10-nanosecond-delay display for calibration purposes.

Attitude Control Subsystem—

1. *Sun Aspect Indicator*—Sun aspect indicator operation (see Figures 11–16 and 11–17) was checked using a Sylvania Sun Gun lamp to simulate the sun's rays. The sun aspect indicator was mounted on a solar panel, and since the solar array was not normally mounted on the spacecraft during electrical performance checks, this panel was temporarily mounted. The telemetry subsystem was commanded on, from the command

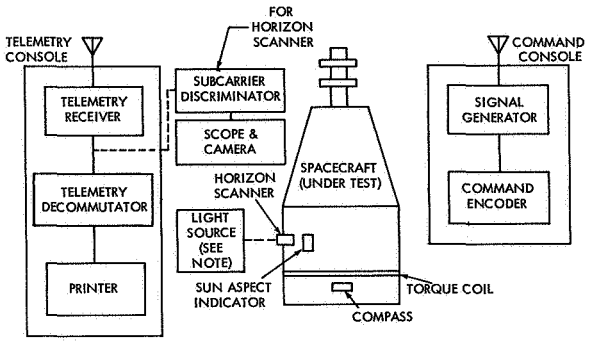


FIGURE 11–16.—Attitude control subsystem test setup.

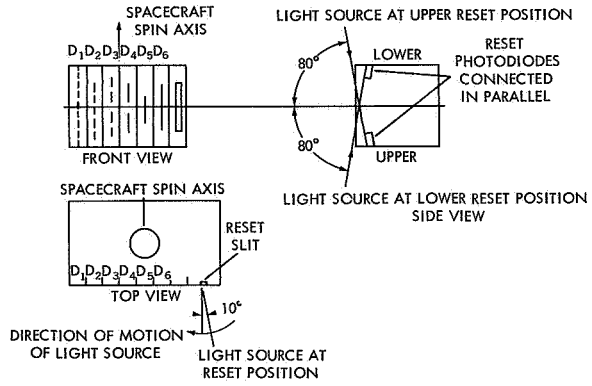


FIGURE 11–17.—Light source positions for sun-aspect-indicator check out.

console; the telemetry decommutator was set to print out in binary the sun aspect indicator channels. The sun gun was turned on, and its lens was positioned to illuminate the surface of the sensor at an angle of about 80° above the equatorial plane; this causes a reset signal to appear on the decommutation display. The illumination was then positioned to an angle of about 25° below the equatorial plane and moved from right to left to simulate the effects of spacecraft spin. The proper response to this excitation was checked. The illumination was then positioned about 25° above the equatorial plane and checked for proper response. The test was completed by illuminating from an angle of −80° (below the equatorial plane), thus covering the appropriate sun aspect indicator angles.

2. *Torque Coil*—Torque coil operation (see Figure 11–16) was verified, using a magnetic compass to sense the magnetic field of the coil while being commanded through its operating states. With the coil in the off state, the compass was positioned slightly below the plane of the coil so that the north-seeking needle pointed tangentially to the coil. Torque coil positive was commanded from the command console; the compass needle pointed inwards towards the spacecraft. Commanding torque coil negative caused the compass needle to point away from the spacecraft. Commanding torque coil off caused the needle to swing to its original position.

3. *Horizon Scanner*—Horizon scanner operation (see Figure 11–16) was checked by exposing the scanner to an infrared source for a short period and photographing the oscilloscope display. A subcarrier discriminator was connected between the video output of the DEI receiver and the oscilloscope. The horizon scanner was commanded on from the command console. The heat source was flashed back and forth in front of the scanner and the resulting signal photographed for record purposes.

Radiation Experiments (See Figure 11–18)—

Radiation Damage Panel—Radiation damage panel performance was checked, using a photo-flood lamp and the telemetry subsystem. The test included checks on thirty solar cells, six thermistors, six diodes, and the two reference voltages of the radiation damage panel. The damage panel was mounted on solar panel 4B, and since the solar array was normally not mounted on the

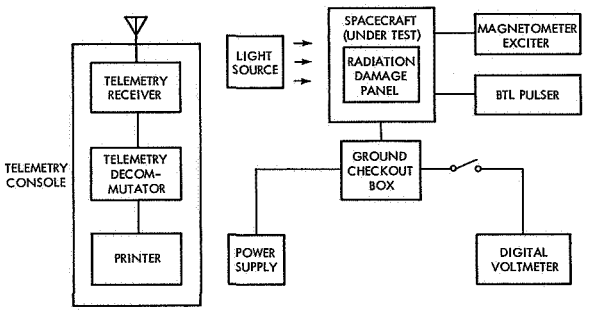


FIGURE 11–18.—Radiation experiments test setup.

spacecraft during electrical performance checks, this panel was temporarily mounted. The telemetry and radiation experiments subsystems were commanded on from the command console; the telemetry decommutator was set to print out in binary those telemetry words which permitted testing of this unit.

Radiation Monitor — Radiation monitor performance was checked, using radioactive sources and/or pulsers and the telemetry subsystem. The electronics elements of the various detectors were checked by injecting the output of a pulse generator into a Microdot connector located on each unit. The proper response for each detector level was checked via the binary output printed from the telemetry decommutator. A special coil and 2.5 cps driver were built to simulate spacecraft spin to check out the spacecraft magnetometer.

Performance of the particle-detector portions of the experiments were checked using radioactive sources of various intensities and emissions (alpha particles for the proton detectors and beta particles for the electron detectors).

Tests with Shorting Plugs

General—

The shorting plugs were used in testing the spacecraft whenever the spacecraft underwent dynamic environmental exposure. This included the electrical performance tests before spin and during spin, acceleration, vibration, and magnetic-dipole tests. A special set of shorting plugs were also used in the solar simulation test. The spacecraft was tested in its flight configuration, including the solar array and the whip antennas. Insertion of the shorting plugs into the ground test receptacles automatically set the spacecraft in the standby mode. Data for the tests were then obtained by commanding on the telemetry subsystem and the particular subsystems under test. As required by the test program, simulated solar-array output was provided via slip rings from the external current-limited power supply.

Power Supply—

1. *Solar-Bus Voltage* — Solar-bus voltage was observed on telemetry main commutator word 18 on the decommutator printer.

2. *Battery-in-Circuit Voltage*—Battery-in-circuit voltage was observed on main commutator words 28–17, 28–25, and 28–33.

3. *Unregulated-Bus Voltage* — Unregulated-bus voltage was observed on main commutator word 19 and was to agree with the solar-bus voltage reading.

4. *Solar-Bus Current* — Solar-bus current was observed on main commutator word 28–41; telemetered reading was generally within 10 percent of the actual simulated solar array input.

5. *Total Battery Current* — Total battery current was observed on main commutator word 20; this reading was normally about 600 ma less than the external input.

6. *Regulator Voltages*—Regulator voltages were observed on main commutator word 28–11 for the radiation experiments regulator and word 28–16 for the wideband regulators. The readings were normally 22.5 $\pm$ 0.25 vdc. The specific wideband regulator examined was identified by observing main words 21 and 28–43 (command verification).

7. *Battery Pressure Monitor Voltage* — Battery pressure monitor voltage was observed on main commutator word 28–3 and was 0.57 $\pm$ 0.1 vdc.

TT&C Subsystem—Command verification was performed by radiating a command carrier to the spacecraft so that the command receiver AGC, observed on main word 28–59, indicated a signal level of approximately 4 μv. The test was performed as described earlier.

Wideband Communications Subsystem—

1. *Functional Acceptance Check* — Functional acceptance check (telemetry) was performed as described earlier before any environmental test.

2. *Frequency Response* — Frequency response was checked as discussed earlier. Multi-path phenomenon was frequently pres-

ent because the spacecraft was not in an RF anechoic environment.

Electrical Tests During Environmental Exposure

Installation Check—Following installation in the test facility, the subsystems of the spacecraft were operated to insure that no malfunction or damage was caused by faulty installation procedure or during handling.

Criteria for Unsatisfactory Performance—Deterioration or change in performance of any subsystem or component which could prevent the spaceraft from meeting functional, operational or design requirement was sufficient reason to consider the spacecraft as having failed to comply with the conditions of the test to which it was subjected and was noted accordingly as a discrepancy.

Evaluation of Equipment — When so directed by the published test procedure, the spacecraft was operated to permit obtaining performance data and was further inspected for evidence of deterioration. The performance data of the spacecraft, under test conditions or upon completion of test, was compared with that obtained in the comprehensive operational check before the start of test. Any observed deterioration that exceeded the published tolerances was considered a discrepancy.

Rejection and Retest — If a discrepancy (i.e., a failure, malfunction, or out-of-tolerance performance) occurred during a test, a review of the details of the test with NASA/GSFC Spacecraft Manager was made prior to further action by the testing group. A written report was made of all discrepancies.

Substition of Equipment—If a unit became unsuitable for further testing during a sequence, a unit with test history acceptable to the NASA/GSFC Spacecraft Manager was substituted on the spacecraft. However, if in the view of the Spacecraft Manager, the substitution substantially affected the significance of results of the test sequence during which the unit failed, the test sequence and any previously completed procedures which could be affected were repeated.

Temperature Survey—The spacecraft temperature was stabilized with the spacecraft in the standby mode. Following stabilization, the spacecraft was operated through one cycle of 36 minutes "on," then 127 minutes "off," for each of the wideband repeaters. The telemetry and radiation experiments subsystems were operated during the entire five-hour test. A check of the power supply subsystem and a command verification were made during the "off" period. The "on" time for the repeaters was utilized to exercise both TV and phone modes, with both CW signals and swept-frequency signals. Sufficient data were obtained to satisfy the requirements of a functional acceptance check (telemetry and a frequency response check). The entire five-hour test was repeated at high temperature.

Spin—The spacecraft, while in an operating condition normal to third-stage powered flight (i.e., radiation mode), was spun-up to 206 rpm (corresponding to 1¼ times the maximum spin rate of the vehicle). The spacecraft was operated for one cycle of 36 minutes "on," then 127 minutes "off," for each of the wideband repeaters. The total test time was approximately five hours, and the subsystem duty cycle was the same as during temperature survey.

Vibration — The spacecraft, while in an operating condition normal for powered flight (i.e., from main engine ignition to injection), was subjected to vibration excitation corresponding to 1.4 times that nominally encountered with the Delta vehicle. In addition to the radiation mode, the wideband communications subsystems were operated with swept-frequency illumination to further check the mechanical design of the subsystem. Duty cycle programming was maintained during each of the three orthogonal directions of vibration.

Thermal Gradient — The spacecraft was operated as if in orbit for six days in this environment. Each repeater was operated for 36 minutes in a 163-minute period (i.e., one earth orbit) with the restriction that there would be no more than 100 minutes

of repeater operation in a given 24-hour period. The radiation experiments and the telemetry subsystems were operated from ten minutes prior to the start of repeater operation until ten minutes after the conclusion of repeater operation. The simulated solar array output from the external power supply was programmed to simulate the effects of sun angle, solar cell conversion efficiency, and eclipse conditions. Command verification runs were made during the continuous mode periods.

Humidity—At the completion of the 24-hour soak in 95 ± 5 percent relative humidity followed by 30-minute drying period, the spacecraft was operated for the equivalent of an "A" test. TWT power output was also measured for both systems.

Acceleration—The spacecraft, while in an operational state normal for powered flight, was subjected to a steady-state acceleration, corresponding to 1½ times that normally encountered with a Delta vehicle. The tests were conducted separately along each of three coordinate axes. The centrifuge was large enough to prevent the "g" gradient along the thrust axis from exceeding +15 percent at the forward end and +10 percent at the aft end, as measured from the spacecraft center-of-gravity. The spacecraft was operated on internal batteries only during this test.

Magnetic Dipole Moment Measurement

The spacecraft was installed in the special Spherical Dipole testing machine and, operating on internal batteries only, was programmed in all of its major modes. The dipole moment was measured for each mode. A permanent magnet was then installed on the spacecraft to null the residual dipole to acceptable values. A recheck was made to establish the remaining values of dipole strength. After compensation, the spacecraft was mounted on a magnetometer test setup and a magnetic survey was made.

1. *Specifications*—The total magnetic moment of the Relay spacecraft was to be reduced to the lowest value consistent with its operation. A value less than 0.1 ampere turns meters squared was a design goal. The spacecraft design minimized the internal magnetic field of the spacecraft and the total external magnetic field. Particular care was to be taken to minimize time-varying magnetic fields where periods were close to, or harmonically related to the spacecraft spin rate.

2. *Equipment*

a. Dipole Testing Apparatus—A spherical aluminum framework, approximately 100 inches in diameter, was constructed in two hemispherical parts (see Figure 11–19). Each part consisted of an equatorial plane ring with half-circle meridianal channels.

Two similar windings of copper wire were installed on the outer surface of each hemisphere. When the spacecraft was mounted in the sphere, the half windings were connected across the equatorial split. Each winding consisted of continuous

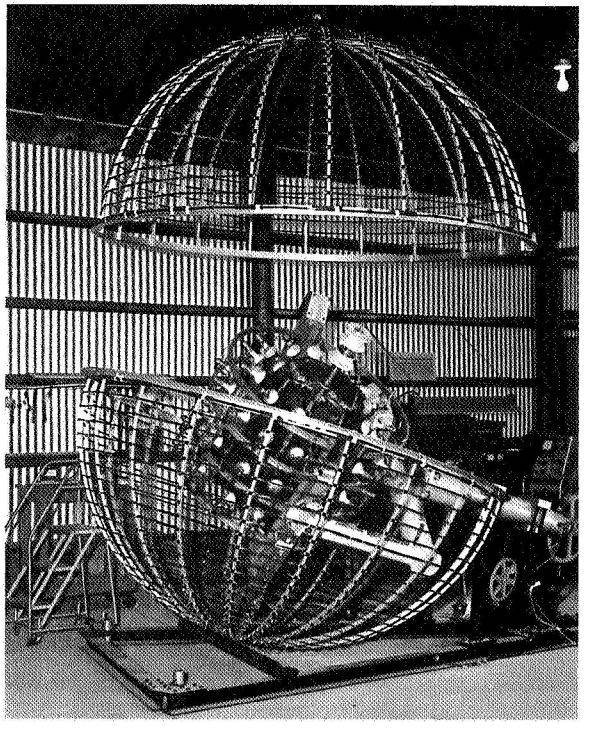


FIGURE 11–19.—Magnetic dipole testing apparatus.

turns parallel to the latitude lines, extending from pole to pole. The density of the winding varied as the sine of the polar angle.

A winding of these specifications on the surface of a sphere had the property of creating a uniform magnetic flux in the sphere when excited by direct current. The flux was parallel to the polar axis.

The sphere was oriented so that the earth's magnetic field vector traversed the sphere, parallel to the polar axis. Current supplied to one of the windings was used to null out the earth's field vector in the interior of the device.

The second winding was used to pick up voltages induced by the rotating spacecraft within the sphere. The signal was proportional to the magnetic strength of the spacecraft and the rate of rotation. A voltage signal in this winding was theoretically independent of position of any dipole or multipole distribution within the sphere. The signal magnitude was proportional to the net dipole present and ignored multiple effects.

Two small test coils were fixed to the framework supporting the spacecraft and rotated with it. These coils were both aligned with and perpendicular to the spacecraft spin axis. Passing measured currents through these coils produced nulling dipole components within the sphere. The magnetic strength of the coils measured the nulling vector magnitudes of the spacecraft.

b. Magnetometer Check Apparatus — This equipment consisted of an aluminum framework designed to support the spacecraft with its spin axis in a horizontal plane, mounted on a turntable to permit angular positioning of the spacecraft. A magnetometer support stand was also provided.

3. *Procedure* — The net machine dipole was established before loading the spacecraft. This was accomplished by setting the current in the component coils to null out the machine residual dipole. The current through the earth's field coil was also set to reduce the second harmonic of rotational frequency to minimum, an indication of cancellation of the earth's field.

The installed spacecraft was operated in all of the major modes, and the dipole moment was measured for each mode. Next a magnet was "cut" to the desired nulling value and installed on the spacecraft. A recheck was made to establish the net remaining values of dipole strength.

The spacecraft was then installed on the magnetometer stand with a magnetometer mounted at a fixed distance from the center of the rotating stand (see Figure 11–20). Magnetometer readings were taken every 20 degrees of spacecraft attitude.

4. *Results*—The data for the magnetic dipole component along the spin axis for each operating mode of Relay Flight No. 1 spacecraft is presented in Table 11–3.

The difference between the dipole level measured in the spherical dipole tester and the level of the magnetometer field test facility was one-tenth of an ampere-turn-meter squared.

Solar Simulation—The electrical programming for this test was very similar to that performed in thermal vacuum testing. The three major exceptions were: 1) the use of a rotating fixture, requiring slip rings for several dc connections (battery master switches and flip-flop reset); 2) antennas for radiating to and from the rotating spacecraft; and 3) the use of a light source to excite the solar array, requiring that the dc power supplied from the external power supply be adjusted to make up the difference between the solar array output and the specified solar bus current. The test was performed for five days, during which the spacecraft was exercised as if it were in orbit.

PRELAUNCH TESTS

General

The prelaunch checkout of the spacecraft encompassed tests both at RCA–AED and at Cape Canaveral. With the exception of

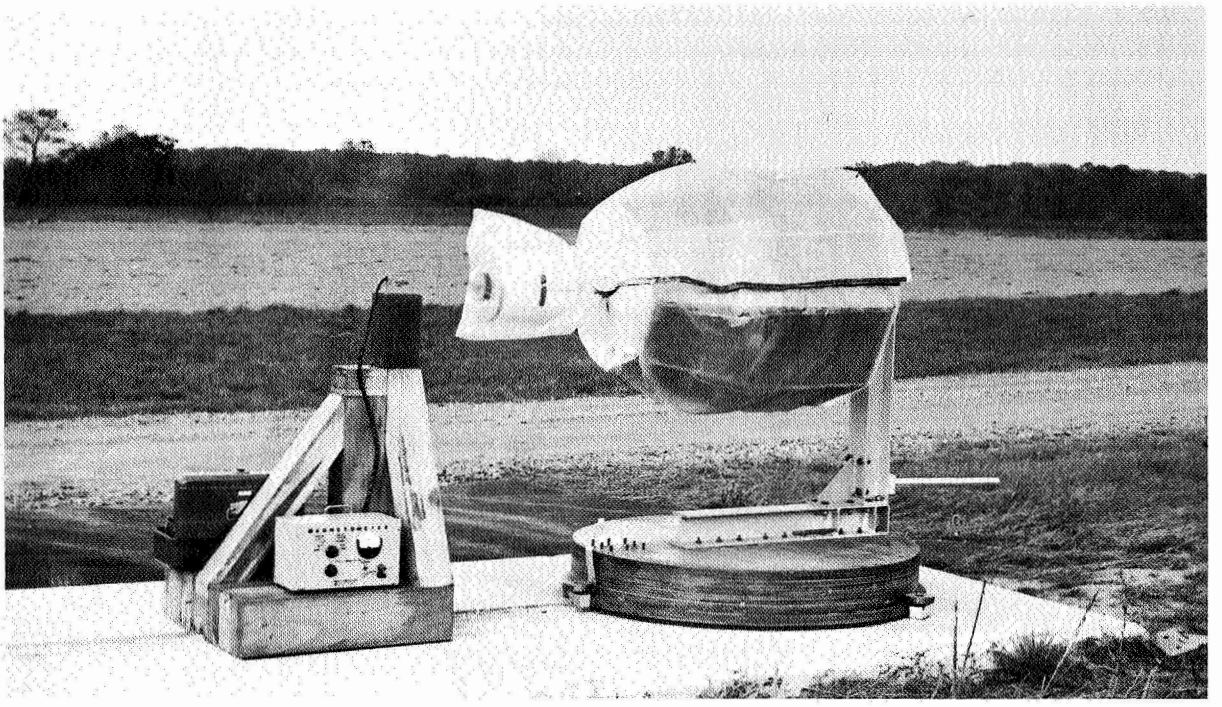


FIGURE 11–20.—Relay I spacecraft mounted on magnetometer stand.

TABLE 11–3.—*Magnetic Dipole Measurements*

Operating mode*	Spin axis dipole**
Uncompensated continuous	−4.43
Compensated continuous	Eclipse +0.17
	Full sun +0.29
Telemetry transmitter #1 or #2 ON	+0.17
Radiation experiment B, C & 1 ON	+0.17
Wideband system #1 ON	+0.28
Traveling wave tube ON	+0.17
Wideband system #2 ON	+0.25
Traveling wave tube #2 ON	+0.25
Horizon scanner ON	+0.15
Attitude coil ON	
Positive	+1.68
Negative	−1.67

*Operation in eclipse as noted.
**Ampere-turn-meter-squared.

checkout following removal of the gantry from the launch pad, an especially constructed payload checkout set was used in conjunction with the Ground Support Equipment checkout Van for all testing. This set differed from the previously described ground test fixture (see Figure 11–9). All switches were hermetically sealed for safe functioning in the explosive atmosphere existing on the ninth level of the gantry (due to the presence of the live third stage rocket). The set was electrically equivalent to the ground test fixture but was constructed in a suitcase configuration and more ruggedly built.

Final Calibration at RCA–AED

Prior to shipment to Cape Canaveral for launch, the completed spacecraft was examined to insure the accuracy of telemetry calibrations. Every telemetry point was sampled and its response compared to the appropriate calibration curve. New curves were generated where required. Following this calibration and final inspection, the prototype and FM–1 spacecraft were shipped by special truck to Cape Canaveral for the subsequent series of prelaunch tests and the mechanical operations involved in mating the spacecraft to the Delta launch vehicle.

At Cape Canaveral the principal test locations for the Relay launch operations were:

1. Launch Complex 17, consisting of two

launch pads, 17A and 17B, and supporting facilities.

2. NASA assembly A/E building where the van was located for the prelaunch checkout. Adjacent to this hanger was the antenna tower, a 50-foot high platform where antennas were mounted to radiate signals and receive signals from the spacecraft at both the spin building and the launch complex. This tower also mounts the satellite-tracking antenna for monitoring telemetry during vehicle ascent and subsequent orbits.

3. Spin Test Building, which was manned by the Douglas Aircraft Company for NASA. Here the Relay spacecraft was mated to the Delta third-stage motor and the combination was spin-balanced prior to installation on the launch vehicle.

Launch Preparations and Facilities

The base location at hangar A/E provided the equipment and handling facilities for checking the spacecraft upon arrival from AED as well as for conducting checks at the other two test locations. The checkout van and the antenna system required in remote testing were located adjacent to hangar A/E.

In the Spin Building, the spacecraft was mated to the third stage of the rocket and the combination was dynamically balanced at the flight programmed spin rate. A special installation there consisted of two corner-reflectors and two four-foot dishes mounted on an external tower and boresighted to the antenna tower at the A/E hangar. Antennas were connected to the spacecraft via coax cables and waveguides.

The third test location was the launch stand, where all testing was done on the 9B level. Signals were radiated directly to and from the spacecraft antennas from the checkout van at hangar A/E.

The prototype spacecraft was made available at Cape Canaveral to check out all the testing and handling procedures at the three locations. It was also used in the radio-frequency compatibility test required by range operations. Two flight models were scheduled for delivery to Cape Canaveral, one as the primary payload and the other as a backup, in case trouble developed in the primary spacecraft.

The first operation of Flight Model 1 (FM–1) spacecraft, after arrival at Cape Canaveral, was the comprehensive initial checkout to verify that all of systems were intact after the trip from RCA–AED. Subsequently, the spacecraft was given a daily routine check while it remained in the assembly hangar, A/E. The backup spacecraft, FM–2, remained at AED for final checkout and was being readied for shipment when FM–1 was launched.

Nine working days before scheduled launch FM–1 was moved from the A/E hangar to the Spin Building for mating to the third stage assembly. This consisted of coupling the spacecraft to the third stage with the explosive-bolt Marman clamp. The combination of spacecraft and rocket third stage was tested for eccentricity before the dynamic spin balancing operation. An electrical checkout, using the payload checkout set, was made from the van at hangar A/E, to insure that the spacecraft had not been damaged.

Following this test, the (spacecraft and third-stage) assembly was moved to the spin test fixture. In the balancing operation, the assembly was rotated at the programmed rate and the imbalance measured with accelerometers. Following the balancing operation, another checkout was performed to verify that no damage occurred during the spin operation.

The assembly was then transported to the launch stand in a special carrying canister four days before launch. After attachment to the second stage of the rocket, the spacecraft and the live third stage were encased in a clear plastic enclosure which was continuously supplied with dust-free, controlled temperature and controlled humidity air.

The spacecraft was tested daily, using the payload checkout set on the 9B level of the gantry. The tests were conducted via RF link from the van at hangar A/E. Flight

shorting plugs were installed just before gantry roll-back, and the final check, immediately preceding the launch, was conducted via RF. External power to the spacecraft was supplied from a power supply in the blockhouse via the first stage umbilical connector. Telemetry monitoring was continued through lift-off until the spacecraft disappeared over the radio horizon.

Satellite Test Facilities at Base Location

Assembly Hangar A/E

The base location for prelaunch operations at Cape Canaveral was in the NASA spacecraft laboratory, hangar A/E. The hangar contained two laboratory areas in addition to a hi-bay loading area. A telemetry receiving complex, an RF laboratory, and the Mission Control Center were also located in that hangar.

Antennas

Antennas at the base location were needed for remote testing by radio coupling to the spacecraft at the Spin Building, for launch stand tests, for terminal/countdown tests, and for the monitoring of telemetry during the ascent trajectory and subsequent orbits.

Commands were transmitted to the other two test locations with a vertically-polarized yagi mounted on top of the 50-foot antenna tower. Boresighting to the test sites was done optically.

Telemetry reception was facilitated by an optically boresighted, horizontally-polarized yagi mounted on the 50-foot tower. Reception of telemetry signals during the terminal countdown, lift-off and ascent trajectory, and subsequent orbits were received on a 9-yagi, cross-polarized, steerable array, mounted on the 50-foot tower. The array was manually steered at acquisition, using computed pointing data and corrected for tracking by scanning both in azimuth and elevation for maximum signal strength.

Microwave (UHF) transmissions to the Spin Building were made via a 4-foot parabolic dish antenna; transmissions to the launch stand were made with a 6-foot parabolic dish. Both were tower-mounted and optically boresighted.

Microwave (SHF) transmissions from the spacecraft while at the Spin Building were received on a small horn antenna. Transmissions from the launch stand were received with a 10-foot parabolic dish. Both were tower-mounted and optically boresighted.

Test Facilities at the Spin Building

At the Spin Building, two 4-foot parabolic dish antennas were mounted on an external tower and optically boresighted to hangar A/E. Waveguides and coaxial cables were used to couple these to the spacecraft microwave systems. Command and telemetry signals were connected to a vertically-polarized corner reflector mounted on the tower. The payload checkout set and a current-limited power supply were installed in the building as far away from the live third stage as the cables would permit.

Spacecraft Facilities on the Launch Stand

Upon completion of spin balancing, the spacecraft-third stage combination was enclosed in a carrying canister for transportation to the launch stand. The carrying canister was lifted up to the ninth level by cranes, where the spacecraft-third stage combination was assembled and mated to the second stage. The spacecraft and third stage of the rocket were each enclosed in clear plastic shrouds continuously supplied with dry, cool air. The working area on the ninth level was also enclosed in a tent.

Spacecraft Testing

Three series of tests were performed on the spacecraft. The first was the initial checkout in A/E hangar, a comprehensive test made just after the spacecraft was received from AED, and included hard-line tests of all subsystems. The second series were daily tests, using hard-lines covering the period from the completion of the initial checkout until delivery of the spacecraft to the spin facility. The third series of tests

were performed via RF link to the spacecraft at the other two test locations.

Initial Checkout

The initial checkout included the following items: physical inspection in detail; power supply checks, command verification checks, command systems redundancy test, VHF power measurements, VHF frequency measurements, wideband functional acceptance checks, swept-response test, wideband frequency measurements, group delay measurements, radiation experiments, sun aspect indicator test, horizon scanner test, and attitude control coil test.

The spacecraft was mounted on the portable pedestal with a Marmon clamp. All solar array panels except 4A were mounted and plugged in (solar panel 4A was off to allow connections to be made to the command receivers). Three of the monopole whips were replaced by 50 Ω terminations; the fourth was replaced on a 20 db pad. This connection made possible precise measurements on the VHF systems without the need to radiate power at the VHF beacon frequency or at the command frequency. The latter consideration is especially important at Cape Canaveral, where all radio-frequency is carefully controlled and frequently prohibited for range safety.

The TWT output cables were removed from the antenna and connected to dummy loads (80 watt terminations or a calorimeter) in order to check out the wideband systems. A diagram of the test setup is shown in Figure 11–21.

Daily Checks

The daily checks were performed under the same conditions as the Initial Checkout. However, the following tests were deleted:

1. VHF power measurements
2. VHF frequency measurements
3. Wideband frequency measurements
4. Command redundancy tests

In addition, an abbreviated check of the radiation experiments was performed.

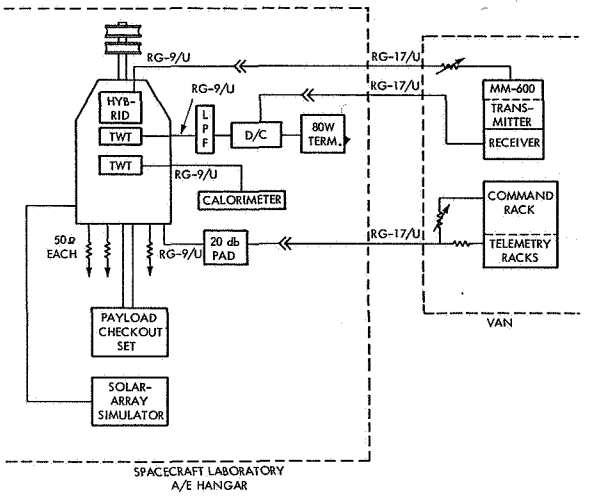


FIGURE 11–21.—Test setup for initial and daily checkouts at A/E hangar at Cape Canaveral.

Tests at the Spin Building

All testing of the spacecraft in the Spin Building was done remotely by RF link from the checkout van at hangar A/E. The payload checkout set was used to monitor certain functions, as a backup for the van. The external power supply was connected to the spacecraft via a test plug. Tests were run on the power supply, command verification, wideband functional check, and swept response.

Tests at the Launch Stand

All testing was performed via RF link to the checkout van. The payload checkout set and the external power supply were connected to the spacecraft but kept far from the spacecraft/third-stage because of the explosive atmosphere. Tests on the various subsystems were similar to those performed at the spin building. In addition, TV simulation and group delay tests were performed. A detailed checkout of the radiation experiments was made by the experimenters using both pulsers and radioactive sources. Horizon scanner, sun aspect indicator, and torque coil were also checked on the gantry. All RF signals at the gantry were handled directly via the spacecraft antenna systems.

Range Operations

Tests on T —11

On the day T —11 ("T minus 11" means eleven working days before launch), the prototype spacecraft was taken from the checkout hangar to the Spin Building where it was mated to a dummy third stage. This event was in preparation for the RF compatibility test on T —10, but it also gave all personnel an opportunity to rehearse procedures before arrival of the flight model at the Spin Building.

Tests on T —10

On T —10, the prototype and dummy third stage were transferred to the launch stand and were attached to the second stage of the Delta vehicle. The RF compatibility test on T —10 showed that all the range radars, the guidance system, the destruction system, vehicle beacons, and the spacecraft systems were mutually compatible.

Tests on T —9

On T —9, the FM–1 spacecraft was transferred to the Spin Building to be mated to the live third stage. Checks were made daily on the spacecraft until T —4 when the spacecraft was transferred to the launch stand.

Tests on T —4

On T —4, the FM–1 spacecraft and live third stage were transferred from the spin building to the launch stand to be mated to the second stage of the Delta vehicle. A check of all spacecraft systems was made via RF from the van.

Tests on T —3

On T —3, an all-systems check was made to verify the readiness of the integrated vehicle and supporting range functions for the launch operation.

Tests on T —2

On T —2, a daily check was made on the spacecraft following a no switching-no radiation period while ordnance installation for first and second stages was accomplished.

Tests on T —1

On T —1, countdown began with a spacecraft checkout of all systems, including a check of the radiation experiments. The overall test time allocated was five hours, 45 minutes. Missile engine checks, missile electrical checks, range readouts, command destruct, and external and internal power checks were made during the time the spacecraft checks were carried out. Following completion of these tests, second stage propellant servicing and pressurization were accomplished.

Tests on T —0

The day T —0 countdown began with a 3½ hour checkout of all spacecraft systems. First stage fueling was also accomplished at this time. A period of no switch-no radiation followed, in which the third stage fairing was installed along with the necessary ordnace items. Another spacecraft test with the flight shorting plugs in place was made following fairing installation. This test was completed in 1¾ hours. During this time, range RF systems and command destruct checks were made. Another no switch-no radiation period was instituted to allow for final installation. Following the completion of the ordnance installation, the gantry tower was moved back to its stowed position. The final spacecraft checkout was made from T —85 minutes to T —35 minutes. Liquid oxygen filling was accomplished during this time. A one-hour, built-in hold was partially used to complete the LOX servicing. Terminal countdown was started at T —35 minutes at 1755 EST. The spacecraft was commanded into the launch condition: i.e., both telemetry transmitters on, encoder on, radiation experiments on, load cutoff normal, TV mode, wideband subsystems off, torque coil off. The external power supply in the blockhouse continued to supply load and battery charging current until T—5 seconds. Ignition and liftoff occurred on schedule at 1830 EST. Main engine cutoff occurred at T + 148 seconds, second stage engine cutoff at T + 316 seconds, third stage spin up at T + 1461 seconds,

third stage engine burnout at T + 1516 seconds, and spacecraft separation at T + 1636 seconds.

Telemetry signals were received from liftoff until the spacecraft dropped below the radio horizon. No changes were observed in the operating mode of the spacecraft during the launch sequence.

LAUNCH VEHICLE AND ORBIT

Description of Delta Vehicle

The Delta vehicle is a three-stage rocket, with ground-guided, liquid-fueled, first and second stages, and a spin-stabilized, solid propellant third stage. A low-drag, fiberglass fairing surrounds the third stage, and the Relay spacecraft was mounted on it in the launch configuration. The overall vehicle was approximately 90 feet high and weighed about 57 tons, fueled and ready for flight.

The first stage is an operational-type Thor missile modified for the Delta use. Its engine uses RP–1 (high grade kerosene) fuel with liquid oxygen (LOX) as the oxidizer and nominally develops 159,200 pounds thrust at liftoff, increasing to 173,700 pounds at steady state. The propellants are injected into the combustion chamber by turbopumps. Vehicle performance is based on the use of at least 99 percent of the propellant, with a burning time to MECO based on LOX-depletion. A flight controller, employing three integrating gyros, three rate gyros, and a programmer is used to provide open loop control until the BTL ground guidance system takes over, about 90 seconds after liftoff. Control is achieved by a combination of hydraulically gimballed main engine nozzle and two small vernier engines.

The second stage propulsion system used unsymmetrical dimethyl hydrazine (UDMH) fuel and inhibited white fuming nitric acid (IWFNA) as the oxidizer. Nominal steady-state thrust developed was 7560 pounds. A gaseous nitrogen retro-system is used on the second stage to provide reverse thrust to get the required separation distance between the second and third stages at third-stage ignition. Second stage in-flight steering control is achieved by hydraulic gimballing of the second stage engine thrust chamber. Roll control is accomplished by discharging helium gas through four roll jets, two of which react in a clockwise direction, and two react in a counter-clockwise direction. Both pitch and yaw control systems respond to commands from the BTL ground guidance system.

During the coast period, starting at second-stage burnout and ending at second/third stage separation, the vehicle was turned to its proper spatial orientation by means of a second-stage coast phase control system. The gyros used to control the second stage during the powered portion of flight supplied the attitude reference used to control the gas jet system during the coast phase. An on-off type of gas jet operation was used.

To provide range safety destruction capability, the Delta vehicle carries command destruction receivers in the first and second stages. The flight termination system in each stage consisted of the receiver and decoder, antenna system, safety and arming mechanism, a detonating cord strand to rupture propellant tanks, and a power supply independent of vehicle power. Prior to first/second-stage separation, either system would destroy both stages.

A large-diameter (approximately 22 inches) ball-bearing mounting, at the forward end of the second stage, supports the spin table, which in turn supports the third stage motor and spacecraft. Prior to third stage ignition, the third stage and spacecraft are spin-stabilized at approximately 165 rpm by small rocket motors attached to the spin table. The third stage propulsion system has a solid propellant motor and a fixed nozzle.

The separation of the spacecraft from the third stage was delayed two minutes after nominal fuel depletion to allow time for afterburning and outgassing of the third stage motor, thus preventing contamination of the satellite. The third stage motor was tumbled, by an asymmetrical weight after separation, to prevent impact with the satellite.

A low-drag fairing was provided to decrease aerodynamic drag and to protect the spacecraft and third-stage motor from aerodynamic heating during flight through the atmosphere. This fairing was jettisoned during second-stage powered flight at an altitude where protection from aerodynamic heating was no longer needed.

Spacecraft/Launch Vehicle Integration

The Delta vehicle for the Relay project placed limits and requirements on the spacecraft to insure compatibility. Dimensions of the standard low-drag fairing established a maximum envelope diameter of 29 inches. A standard Delta payload attachment fitting was incorporated as an integral part of the spacecraft structure to mate with the corresponding fitting on the Delta. The compatibility of the spacecraft design was confirmed at a fit-check mating at Douglas Aircraft Company, Santa Monica, California, when a full-scale accurate mockup of the spacecraft was assembled with the appropriate launch vehicle components.

Orbit Determination and Guidance

The desired Relay orbit resulted from tradeoffs in consideration of Delta capabilities in terms of orbits achievable and spacecraft weight and size. The vehicle performance was very nearly perfect, resulting in the following orbital parameters:

Apogee: 4627 statute miles
Perigee: 818 statute miles
Inclination of orbit to earth's equator: 47.5°
Anomalistic period: 185 minutes

Because of range safety considerations, the launch azimuth may not exceed 108° when a Delta vehicle is launched from Cape Canaveral. This establishes a path which crosses the equator at an angle of about 33°. The orbital inclination will have this value if all three stages are fixed in the initial flight plane, as they would be for maximum energy use. The desired higher inclination of 47.5° was attained by yawing the second and third stages to the south of the initially established ascent trajectory plane when the vehicle had arrived at a point where the range was clear to the south. Since the energy imparted to a spacecraft is reduced by such yawing, the final apogee or perigee or both will be reduced. In developing the ascent trajectory it is necessary to ensure that the command guidance system at the launch site maintains contact with the vehicle during first and second-stage powered flight. The vehicle must stay well above the launch site horizon and be pointed properly so that its antenna will receive guidance signals from the launch site. Several reiterative calculations are required for the determination of the optimum ascent trajectory.

After the second-stage engine cutoff (SECO), the vehicle is allowed to coast upward, losing speed, until finally it reaches the apogee of the ascent trajectory established by the first and second stages. During this coasting period, the second stage was turned to its proper spatial orientation by means of the gas jet system. The third stage was ignited when the vehicle reached the ascent apogee. The third stage axis is maintained in the local horizontal plane at the time of firing, in order that no more energy be wasted, so that the final perigee position will coincide with the ascent trajectory apogee.

The Relay launch vehicle was guided by the BTL command guidance system. The command guidance system consists of a precision tracking ground radar, a digital computer, and a missile-borne system in the second stage of the rocket. This, in turn, consists of a radio guidance receiver, decoder, and transmitter. The ground guidance facility is located about two miles from the launch area, and houses the radar and the computer. In the command guidance system, the launch vehicle position is continuously determined by the precision ground-based automatic tracking radar. The computer analyzes the position data and derives appropriate vehicle velocities. The missile position and velocity data are compared with pre-calculated values, representing the desired trajectory which has been stored in the computer memory prior to flight. Coded steering commands, based on

error signals between the actual and desired values, are transmitted to the vehicle on the radar beam.

An engine cutoff command is sent to the vehicle when the ground-based computer is satisfied that the desired terminal conditions have been met. The high degree of accuracy of the command guidance system results primarily from the combination of reliable communications to the missile, precision radar-tracking, and a unique computation process involving radio inertial guidance principles for determination of velocity.

AUTHORS. *This chapter was written by* W. SCHREINER, R. NEWMAN, *and* M. GITTLER *of the Radio Corporation of America, Princeton, New Jersey, U.S.A. under contract NAS 5–1272 with NASA/Goddard Space Flight Center.*

N66-10238

Chapter 12

Reliability Program

INTRODUCTION

The Relay spacecraft was designed to demonstrate the feasibility of using low-altitude satellites to relay wideband communication signals over great distances. In addition, Relay I obtained extensive information on the effects of the orbital environment on satellites of this type.

To provide and assure the high degree of reliability required for this program a detailed reliability program was formulated. This reliability program was based on:

1. Component part reliability
2. System reliability analyses
3. Conservative design
4. Rigorous testing
5. Quality control.

Component part reliability and redundancy determine the inherent reliability of the spacecraft. Design, testing, and quality control represent the engineering effort required to strive for this maximum inherent reliability.

Because of the effort expended on these areas, Relay I has successfully completed more than one year of operation in space.

PARTS PROGRAM

General

The selection of proper component parts constituted the initial phase of the reliability program.

Component specialists prepared a standard parts list for the control of parts selection. The definition of such parts demanded that the parts possess specific electrical, environmental, and reliability characteristics. The environmental stringencies of outer space precluded use of many parts which were common in ground equipment.

Radiation has a degrading effect on the paper and impregnant used in paper capacitors; non-hermetically sealed wet tantalum and aluminum capacitors lose their electrolyte in vacuum; adjustable components exhibit sensitivity to vibration and other mechanical stress; and many oils, greases, etc., outgas or change physical properties under conditions of high vacuum or radiation. These are examples of factors that had to be considered in the preparation of a standard parts list.

Procedures were also established for utilization of non-standard parts whereby a design engineer submitted application data, requirements, and recommendations to the appropriate component specialist. Analysis and testing, if necessary, resulted in acceptance or rejection of these non-standard parts.

Mission Profile

A mission and environments profile was developed from the requirements specified for system operation. This profile described the maximum conditions the spacecraft was to undergo during its operational life (see Table 12–1).

TABLE 12-1.—*Spacecraft Mission Profile*

Environmental condition	Factory phase	Prelaunch phase	Launch phase	Orbit phase
Radiation intensity				Inner Van Allen Zone proton $E>40$ Mev 2×10^4/cm²sec Electron E>600 kev, 10^8/cm² sec
Electrical interference	MIL–I–26600			
Vacuum			Atmosphere to less than 10^{-4} mm Hg	Less than 10^{-5} mm Hg
Altitude	Sea level to 50,000 feet	Sea level	Sea level to orbit	800 to 2500 miles
Vibration	Non-isolated equipment 3.5 g RMS at 5 to 50 cps 1.5 g RMS at 50 to 300 cps			
Humidity	100%	100%		
Ambient temperature	+160°F unsheltered ground condition −35°F restricted air transport		900°F flash temperature approximately 4 minutes 160°F on inside of nose fairing	Solar radiation 442.4 BTU/hr ft²

Pertinent environmental information was extracted from the profile to dictate subsystem and component requirements necessary for successful operation. The environmental information was then integrated into the parts program to govern the selection of qualified parts.

The most serious of all environmental conditions for spacecraft is radiation in the inner Van Allen zone. The expected integrated radiation levels per year were 10^4 roentgens inside the spacecraft and 10^6 roentgens on the surface. Subsequent scientific experiments disclosed that a more severe radiation problem existed. Since this additional information came too late to be included in the component and design criteria, a special test program was conducted on semi-conductors used in the Relay spacecraft.

Eighty-four power transistors (twelve each of seven types used in the Relay satellite) were irradiated, four at a time, in a 6-Mev LINAC microwave electron accelerator. Performance was followed closely and parameters were plotted after successive doses, corresponding roughly to one day, 10 days, and 100 days in the Relay satellite orbit.

Results were consistent, and indicated that most of the types tested degraded in a predictable manner, with little divergence for any particular component. Degradation was surprisingly rapid for exposed transistors; this indicated that shielding from high en-

ergy electrons was urgently needed.

If additional shielding had not been provided, Beta might have fallen to minimum Beta design value within 5 days for the most sensitive type, the 2N174A, in the high-power, voltage regulators. The generalized Beta degradation curves for the transistors tested, without special shielding, are given in Fibure 12–1. Observed increases in collector-base leakage current were fourfold. Reverse bias on the collector-base junction did not noticeably change the rate of degradation. As a result of this testing, additional shielding was added to protect the 2N665 and 2N1039 transistors in the battery charge controller and the power transistors in the voltage regulators.

Preconditioning

Initial preconditioning plans included a 500-hour, burn-in period for all parts. However, it became apparent in the initial stages of the project that proper implementation and control of the burn-in was not possible because of the short work schedule. An alternate procedure was adopted to be compatible with the work schedule. All parts were baked at elevated temperatures for 168 hours and subjected to electrical testing before and after preconditioning.

The screening process was expected to remove initial failures and potential failures early in the program, thus reducing the required post-fabrication rework and aiding attainment of the reliability specified for the system. Figure 12–2 shows a failure distribution for a typical lot of components. Failure rate is plotted as a function of time. There are two regions of relatively high, non-constant, failure rate. One occurs early in life due to initial defects in manufacture, and the other occurs toward the end of part life and is attributable to wearout. Preconditioning carries the parts beyond the early life, high failure rate, region and into the constant failure rate region. Proper selection of parts prevents reaching the wearout region.

In conjunction with preconditioning, 100-percent incoming-part inspection was employed in lieu of sampling techniques, to assure reliability of each component.

Except for transistors, all components were accepted or rejected on the basis of specification tolerances. In the case of transistors, a 20-percent change in Beta gain or a 100-percent change in leakage current (I_{CBO}) also rendered that part unacceptable.

Inspection after preconditioning resulted in rejection of 8.74 percent of the parts which had already passed earlier inspection. If it can be assumed that the component parts rejected after preconditioning—there were 2090 of them—would have been failures during early test hours, then the value

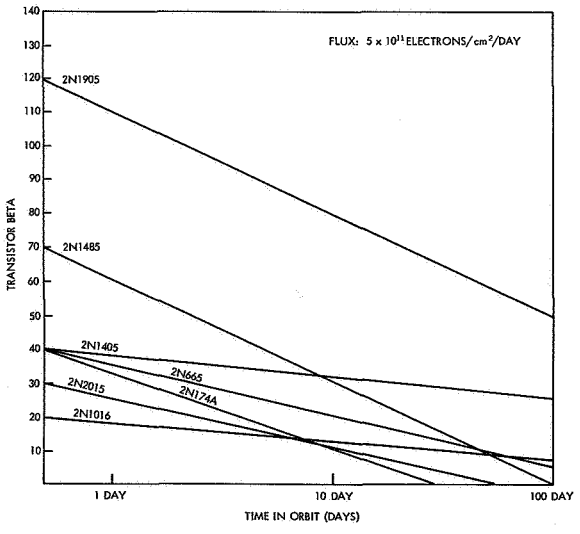


FIGURE 12–1.—Predicted transistor degradation without special shielding.

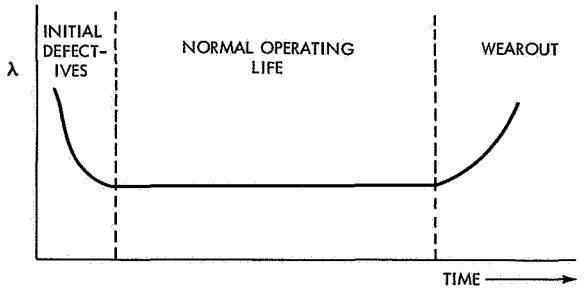


FIGURE 12–2.—Common component part life characteristic.

TABLE 12–2.—*Relay Parts Program, Preconditioning Results*

Equipment	Initial inspection quantity passed	Rejected after burn-in	
		Quantity	Percentage
Capacitors			
Fixed mica dielectric	2736	176	6.43
Glass dielectric, variable	1228	126	10.26
Ceramic dielectric, fixed	1218	142	11.66
Glass dielectric, fixed	2498	284	11.37
Ceramic dielectric, variable	65	5	7.69
CK-types Vitramon	625	53	8.48
Tantalums	224	14	6.25
RCA Drawing No. 8987915	100	7	7.0
Mylar dielectric	10	0	0
Chokes			
RF	733	56	7.64
Crystals			
RCA 8530449	31	0	0
Diodes			
IN251	103	4	3.99
IN256A	15	0	0
IN295A	27	1	4.71
IN486B	20	1	5.0
IN645	390	17	4.35
IN745A	25	0	0
IN746	36	1	2.78
IN750A	22	2	9.10
IN751A	14	0	0
IN753A	14	0	0
IN756A	15	0	0
IN758A	13	0	0
IN759	22	3	13.64
IN831A	60	0	0
IN901	180	12	6.67
IN967B	15	0	0
IN907B	11	0	0
IN1202	30	0	0
IN1508A	27	3	11.12
IN1611AR	14	1	7.15
IN1732	26	0	0
IN1734	15	0	0
IN2979B	10	0	0
IN3018B	15	0	0
RCA 99250–102	81	0	0
PSI PC–116–22A	16	0	0
Filters			
RCA Drawing No. 8950287	60	0	0
Resistors			
Metal film, HT	235	0	0
Carbon composition, fixed	10,880	878	8.07
Wirewound, fixed	16	0	0
Wirewound, variable	66	6	9.1
Transformers			
DO–T–37	11	0	0
Transistors			
DEP–01 (RCA spec. no.)	79	28	35.45
DEP–02	6	3	50.00
DEP–03	30	0	0
DEP–03A	199	1	0.51
DEP–08B	105	12	4.3
2N328A	6	0	0
2N329A	74	3	4.06
2N338	7	0	0
2N384	14	1	7.15
2N498	18	0	0
2N656	55	8	14.55
2N665	48	7	14.59
2N700A	35	4	11.43
2N706A	27	7	25.93
2N718A	219	7	3.20
2N722	170	14	8.24
2N929	25	2	8.00
2N1012	11	3	27.28
2N1016B	25	5	20.00
2N1039	155	14	9.04
2N1132	33	4	12.13
2N1141	61	7	11.48
2N1184B	49	4	8.17
2N1405	255	37	14.51
2N1480	11	3	27.28
2N1485	8	2	25.00
2N1493	128	6	4.69
2N1493X	51	8	15.87
2N1692	48	3	6.25
2N1720	19	3	15.79
2N1905	16	0	0
2N1973	59	1	1.70
2N2015	4	1	25.00
Total	23,902	2,090	(8.74)

of this screening process is obvious. Without preconditioning, the post-fabrication rework would have been excessive. Results of the preconditioning are tabulated in Table 12–2.

De-rating Policy

Component part failure rates increase as the electrical and environmental stresses on the part are increased. To assure conservative design and to keep part failure rates as low as possible, a derating policy was established. Basic provisions of the policy were:

1. The maximum power dissipated by any semiconductor, averaged over a 30-second period, must not exceed 20 percent of the power rating at 25°C. Voltage transients must not exceed 80 percent of the rated breakdown voltage.

2. No mica or ceramic capacitors were operated at voltage levels greater than 10 percent of the rating at 25°C. Tantalum

capacitors were not to operate above 70 percent of the 65°C voltage rating.

3. The power dissipated by any resistor, averaged over a 30-second period, must not exceed 50 percent of the 25°C power rating, nor be subjected to a voltage greater than 80 percent of rated value.

SYSTEM RELIABILITY ANALYSIS

Redundancy

General

The major decision concerning redundancy in the Relay spacecraft system was made during the proposal effort. This decision was based primarily on the following:

1. The calculated reliability of any single system was low without redundancy.

2. The effects of space environment were unknown, especially combined effects of vacuum and radiation.

Redundancy, as applied to the final spacecraft, was integrated at all levels, including piece parts, circuits, *black boxes* and the subsystem level. Applications are discussed briefly below.

Systems Power Supply

Figure 12–3 illustrates the block diagram of the spacecraft power supply. Four areas of redundancy were incorporated in this design: solar cells, battery and charge controllers, high power regulators and the low voltage sensor.

For redundancy in the solar cell area, a series-parallel wiring design allows failures to occur (either short circuits or open circuits), without seriously jeopardizing system power. Figure 12–4 illustrates the interconnection wiring of cells on a section basis. Normally, five series cells make up a shingle; four or six parallel shingles make up a block; fifteen series blocks make up a string; two parallel strings make up a section; two parallel sections make up a panel; and eight parallel panels make up the total array.

The loss of any individual cell can have one of two effects. If the cell shorts, the voltage contribution of that cell is lost. If the cell opens the current contribution of that shingle is lost.

Redundancy was added by increasing the voltage and current capability to offset deg-

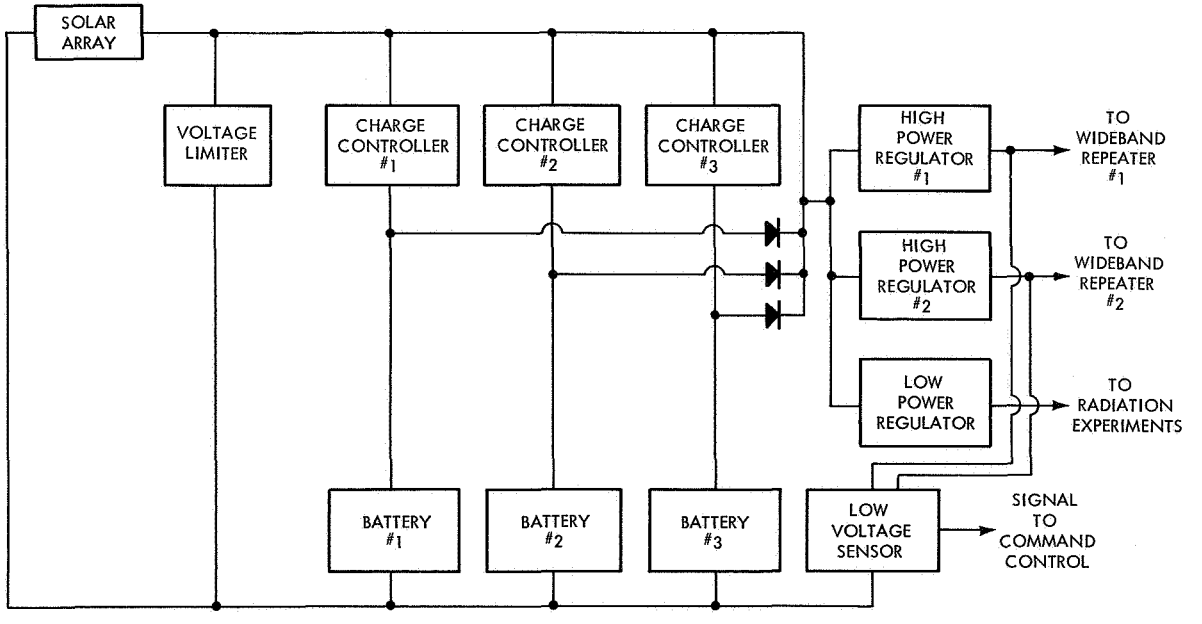


FIGURE 12–3.—System power supply, block diagram.

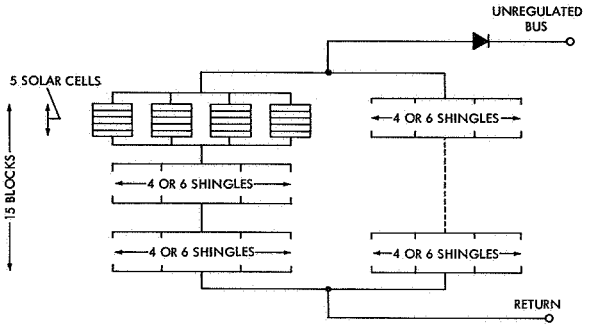


FIGURE 12–4.—Typical section of a solar panel.

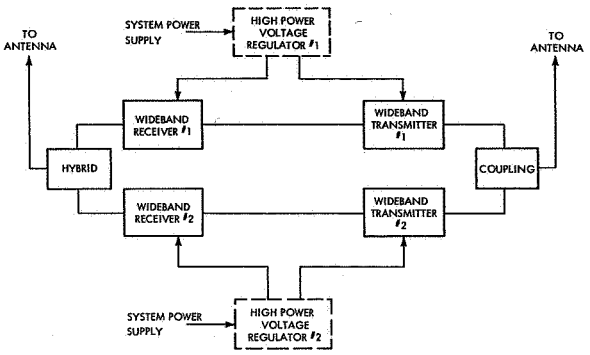


FIGURE 12–5.—Wideband repeater, block diagram.

radation and/or catastrophic failures. With this addition, reliability is dependent not on the simple series function but is more nearly represented by a binomial expression. Reliability is dependent on the amount of additional power designed into the system, over and above the required values.

The second area of redundancy is completely functional. One redundancy is in the battery, battery charge and control circuitry. Here three charging circuits and three batteries have been provided where any two of the three will provide sufficient power for operation, provided the spacecraft is not required to operate extensively during eclipses.

The final point of redundancy in the system power supply consists of two, high power, voltage regulators, one for each of the wideband repeater subsystems. This is not a one-for-one redundancy, but each regulator is a series element in the repeater, where complete subsystems are provided on a one-to-one basis. This is illustrated in Figure 12–5.

Wideband Repeaters

The wideband repeater is a complete subsystem composed of the receiver and the high power transmitter, for handling either TV transmission or for handling two-way voice or telegraphy transmission.

Figure 12–5 shows a system operational block diagram illustrating the complete one-for-one redundancy on a subsystem basis.

Other redundancy aspects are in evidence in the wideband receiver. An IF switch in the receiver allows the unit to process either the one-way TV transmission or two-way voice. The two receivers provide, from the IF switch to the adder circuit, additional reduced modes of operation. The probability of having at least one-way TV or two-way voice transmission is associated with having one-out-of-four of these circuits working, plus the remaining portions of the receiver as series elements. The possibility of having both one-way TV and two-way voice transmission becomes one-out-of-two for each type of circuit, plus the remaining portions of the receiver as series elements.

Command Control Circuitry

The command control is a complete subsystem of project Relay whose function is the reception, demodulation, and decoding of command signals. The subsystem is illustrated in the block diagram shown in Figure 12–6. This diagram is a complete two-redundant configuration of the subsystem utilized in Relay I. The redundancy utilized is standby active. Though the basic reliability gain is less than that with standby inactive, the net gain is greater, since the standby active negates the need for sensing and switching.

This subsystem incorporates redundant receive and demodulate functions and redundant decode functions. Also, each of the ten decoded outputs is channeled through a redundant pair of OR gates. In order to eliminate sensing and switching functions that are generally necessary for redundant con-

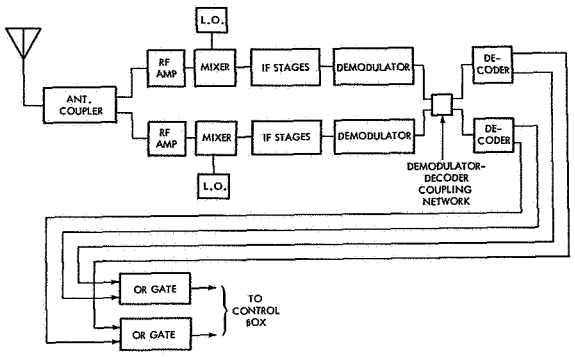


FIGURE 12–6.—Command control system block diagram.

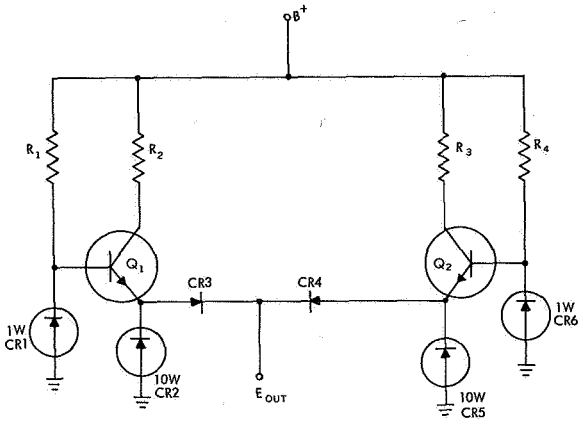


FIGURE 12–7.—Redundant regulator control box.

figuration, an antenna coupler has been utilized to isolate the inputs from each other, yet allows each receiver to be independently operable from a common antenna. The demodulated receiver outputs are fed through appropriate isolation to both decoders resulting in a both-either-or redundancy. Similarly, the decoded outputs are also both-either-or through paired OR-gates. With this arrangement, all functions operate simultaneously, and no requirement exists for sensing or switching. A failure along one channel is not reflected in other parts of the system because of the unidirectional characteristics of signal flow as determined by various forms of isolation.

Outputs from the two decoders are fed to the command control box for performing command functions. The most critical circuits in the control box are the two voltage regulators which are common to each control channel. A failure in either of these can cause the complete loss of spacecraft control. Therefore, complete parallel redundant regulators have been provided as illustrated in Figure 12–7. Review of the circuit illustrates that combinations of particular failure modes are necessary to cause the regulator voltage to exceed its useful range. It will be noted that the most critical failure mode in the regulator is the open circuit. Should a component part open in each regulator circuit, this would cause the loss of the output voltage. However, the open circuit failure is usually a result of overload stress conditions that, in turn, occur as the result of defects in preceding series elements. Overload conditions, however, have been prevented by careful selection of component parts and by monitoring parts application.

Telemetry Circuitry

The telemetry subsystem includes the telemetry data encoder, the horizon scanner and two telemetry transmitters. One of the transmitters has been utilized all the time as a tracking beacon, the other to transmit either the encoder or the horizon scanner data. This set of transmitters was considered a redundant configuration, since if one transmitter survives, the data and tracking function can be time-shared. Time-sharing can be implemented from ground at the discretion of operating personnel.

Reliability Analysis

To determine the value of redundancy and to provide a measure of the inherent reliability of the spacecraft, a reliability analysis was performed. The reliability analysis was based primarily on the application of each part under the specified electrical and thermal conditions. The expected failure rates (λ) associated with each equipment were calculated, along with the associated system survival probability (P_s). The latter was the result of integrating the data on expected

failure rates within the mathematical reliability model.

The failure rate of an equipment is the sum of the failure rates of the involved components and has the following relationship to the unit's probability of survival:

$$P_s = \epsilon^{-\lambda t}$$

where t = duration of operation in hours.

The mathematical model expresses, in concise language, the complex interplay between various equipment, based on the assumption that chance failure of any element is not related to the chance failure of any other element. This relationship is based on application of the general rule of multiplication for the probability of jointly independent events to the probability of successful operation of all equipment. When elements are made redundant, the reliability expression follows the binomial expansion. For 1 out of n redundant functions operating, the survival probability is given by:

$$P_s = 1-(1-P_s)^n$$

Reliability Predictions

Two separate models and a composite of the two were developed to determine the reliability of three modes of transmission.

The results, of the parts program and the system reliability analysis, improved the inherent reliability of the complete communication system to 0.951, the wideband TV and narrow-band transmission subsystem to 0.992, and the telemetry transmission subsystem to 0.959. These values represented gains of 1.5, 11.7, and 2.76, respectively, over the non-redundant counterpart. Table 12–3 is a tabulation of both the non-redundant and redundant areas to illustrate the reliability gain.

TABLE 12–3.—*Summary of Results of Reliability Analysis*

Circuit	Non-redundant	Redundant
System power supply	0.9814	0.9961
Solar panels	0.9997	0.9997
Voltage limiter	0.9972	0.9972
Battery charge & control circuit	0.9854	0.9993
Series diodes to unregulated bus	0.9991	0.9991
Command circuitry	0.9525	0.9978
Command receiver and demod.	0.980	0.9996
Coupling circuit		0.9994
Decoder	0.972	0.9992
Telemetry circuitry	0.9375	0.9570
Encoder	0.9716	0.9716
Horizon scanner & SCO	0.9874	0.9874
Modulator-encoder switching	0.9957	0.9957
Telemetry transmitter	0.9806	0.9806
Wide-band transponder	0.9912	0.9996
Regulator	0.9985	
On-command	0.9998	
Receiver	0.995	
TV-phone switch	0.9999	
2 minute timer	0.9996	
Transmitter	0.9987	
TV-phone drive	0.9998	
Off-command	0.9999	
Communications system	0.9266	0.951

DESIGN, CONSTRUCTION, AND TEST

General

The high reliability parts list, derating policy, and redundancy requirements were integrated into the design. A technical advisory staff, consisting of qualified specialists who were not connected with the design effort, reviewed all designs; skilled technicians in clean-room areas fabricated equipment under the close monitorship of quality control inspectors; and elaborate qualification and acceptance tests were conducted to demonstrate the ability of the spacecraft to deliver the required performance.

Malfunction Reporting and Analysis

In order to provide an effective program for continued reliability control throughout the spacecraft development, all malfunctions, including failures and adjustments necessary to maintain performance, were closely monitored and reported. All malfunctions were analyzed, categorized, and corrective action was instituted.

The purpose of malfunction data collection and analysis was twofold:

1. To determine whether the final product actually possessed the reliability designed into the circuit.

2. To indicate and eliminate problems arising from design, system integration, and testing.

Orbital Malfunction

Despite the careful attention given to all details of spacecraft design, production, and test, one failure mode eluded detection and did not appear until Relay was in orbit. This was the inability to turn off one of the high power regulators and its associated wideband repeater. Rapid analysis indicated that excessive reverse leakage current in the high power regulator series pass transistors was keeping the regulator on, although it was commanded off. Additional analysis and background investigation led us to suspect a dew point problem.

Dew Point

The reverse current of a transistor theoretically should decrease with decreasing junction temperature, over the temperature range of the device. Actually, in most transistors as the temperature decreases from room temperature to −65°C the reverse current goes through a maximum value between room temperature and −65°C. The temperature at which this maximum value of reverse occurs is called the transistor's dew point temperature. Physically, it is a result of moisture (in the sealed atmosphere of a transistor) saturating the atmosphere and precipitating on the active surface of the device at this temperature. The moisture interacts with any contaminant on the surface of the transistor and thereby increases the leakage component of the reverse current.

Verification

Based on the above analyses, a series of tests was organized with the following specific objectives:

1. Determine the magnitude of the dew point currents and the dew point temperatures for sample lots of each of the power transistor types used in the regulators.
2. Obtain a measure of how the leakage values of the transistors used in the satellite compare with those of competing vendors.
3. Determine the effects of high dew-point current on the operation of the regulators.

The I_{CBO} breakpoint between good regulator operation and poor operation at 0 to −30°C temperature was found to be 1 ma. That is, for dew point currents of less than 1 ma, the regulator, in most cases, would turn off properly.

Power transistors were tested from three vendors for the presence of significant dew point effects between 0 and −65°C with the results shown in Table 12–4:

TABLE 12–4.—*Transistor Dew Point Frequency*

Vendor	No. of transistors tested	No. exhibiting dew points	Percent
#1	295	170	57.6
#2	43	2	4.7
#3	200	7	3.5

The sample lot of transistors identical in type (and vendor) to that used as the pass transistor in the high power regulator had a 61 percent occurrence of dew point effects, and 40 percent of these dew point units had a high enough leakage current to prevent regulator turn off.

Once the problem was understood, its solution was apparent: regulator turn-off would occur at a time when the temperature moved away from the dew point region. The redundant regulator was used to complete the mission, once the faulty regulator turned off.

Epilogue

In view of the above conditions, it was apparent that dew point criteria and leakage tests had to be included in all future power transistor procurement specifications, and equipment had to be tested throughout the temperature range, rather than at specific maximum, minimum, and typical temperatures.

QUALITY CONTROL

General

The function of the quality control effort on Project Relay was to ensure the mainte-

nance of design reliability throughout fabrication, testing, and pre-launch activities. To accomplish this, the quality control organization was divided into two functional groups: material quality control and product quality control. MQC (Material Quality Control) had cognizance over all purchased material, preconditioning, and vendor quality control activities. The PQC (Product Quality Control) was charged with responsibility for all fabrication and all activities until spacecraft launching.

Vendor Control

As each vendor was selected, a detailed quality control survey was performed by MQC personnel. Conformance to MIL–Q–9858 was used as a minimum standard for all vendors. When vendors were found to be weak in certain areas, repeat visits were made until the situation improved.

The nature of the Ni-Cd battery manufacture necessitated placement of a full-time, resident, field quality control representative for the duration of the procurement.

The solar cell procurement was also critical. Detailed flow charts were prepared for every stage of panel fabrication. The solar-panel, in-process, manufacturing flow-chart is shown in Figure 12–8.

Because of the encoder complexity (over 5000 separate electronic parts and extreme packing density) special quality control efforts were made by placing a full-time product assurance representative in residence at the vendor's plant.

Preconditioning

All parts were preconditioned by Purchased Material Inspection in accordance with the reliability requirements for Project Relay. These parts were individually identified in such a way as to indicate to both Engineering and Manufacturing that they were suitable for use. If, at any point in the fabrication process, the part identification was missing, a part history inventory file was consulted, which resulted in proper part identification.

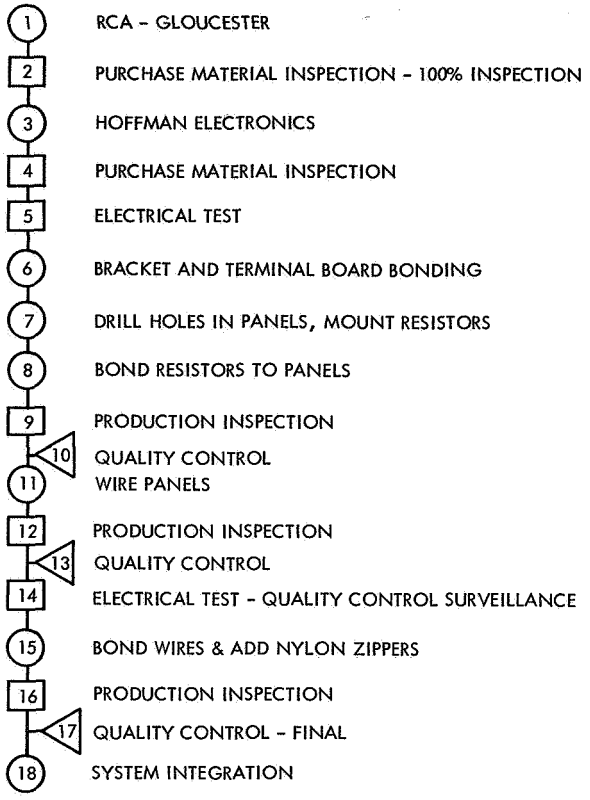


FIGURE 12–8.—Solar panel in-process manufacturing flow chart.

Product Quality Control

A key tool used by the product quality control group was the flow process chart. A typical black-box chart is shown in Figure 12–9. This chart indicates the inspection stations and the specific inspections during assembly, integration, and test. Standards were developed to ensure the application of highest levels of workmanship, commensurate with the fabrication of Military and Space equipment. These standards were compatible with the requirements of Project Relay.

As a general rule, every unit was subjected to an inspection after the completion of each operation in the fabrication process. The basic inspection was performed by production inspectors and rechecked by quality control inspectors. Periodic audits of the competence of inspection and the inspectors

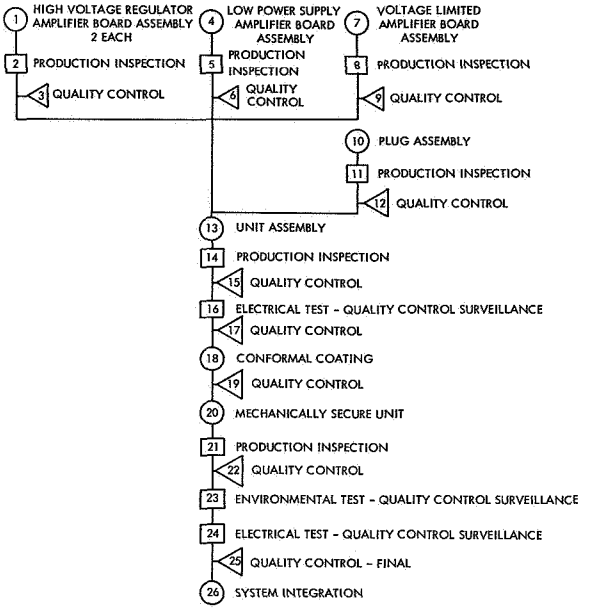


FIGURE 12–9.—Voltage regulator in-process manufacturing flow chart.

were conducted by another group within the quality control organization.

To facilitate auditing, and to prevent the inadvertent omission of any inspection, a travel tag was filled out and accompanied each unit. All subassemblies had travel tags which were removed and integrated with the final unit tag. Before any unit was moved to the next operation, the travel tag had to have a quality control stamp indicating its acceptance at this point in the process.

The product quality control group performed a vital function in monitoring tests. All formal acceptance testing, from component level to spacecraft prelaunch tests, were witnessed: to ensure that the prescribed test procedure was followed; to verify that all anomalies connected with the performance were recorded in the log books and subsequently corrected; and to see that the performance characteristics noted during tests were within the specification limits.

Manufacturing Environment and Handling

To obtain the highest level of quality on the spacecraft, controlled manufacturing environments were employed. All operators were required to wear smocks, and airlocks were used to control entrances to the integration area. All work performed on the spacecraft was monitored by a product quality control representative.

Prior to moving the spacecraft to any environmental test area, a detailed handling procedure was written and had to be approved by the quality control and project office personnel. At least one dry run was made prior to any actual movement of the spacecraft.

Log Books

The use of the log books proved to be of great value in ensuring that highest levels of reliability were obtained in the equipment. The books were of inestimable value in design reviews.

A serialized log book was prepared for each black box, subsystem, and system. The primary responsibility for maintaining the log book was that of the engineer. These books were periodically reviewed by supervisors, by reliability, and product assurance personnel.

All assembly information, test results, and any other anomalies were entered in the log book. Simply stated, the log book was a chronological history of the unit through all of its experience from inception; time and effort spent in compiling these records were well spent.

AUTHORS. *This chapter was written by* H. F. WUERFFEL, R. A. SMITH, L. GOMBERG, *and* D. F. METZ *of the Radio Corporation of America, Princeton, New Jersey, U.S.A. under contract NAS 5–1272 with NASA/ Goddard Space Flight Center.*

PART II

N66-10239

Chapter 1

The Relay Experiment Plan

INTRODUCTION

The success of Project Relay required that the participation of a large number of earth stations be closely coordinated. This dictated an experiment plan which would reflect the experimental capabilities of all the stations and facilitate the scheduling of experiments to be conducted by the various stations on each pass. This was of particular importance during the initial few weeks after launch, in light of the uncertain lifetime of the satellite and the need to collect as much data as possible. The unique characteristics of a satellite relay further imposed rather stringent requirements on the experimental methods. Short visibility periods (in the order of 30 minutes) required that the ground stations be capable of high data-gathering rates and provide means to permanently record data for subsequent analysis. Time variation of many of the other parameters such as range, spacecraft antenna gain (look angle), ground antenna elevation angle, antenna pointing error, and Doppler shift also made it necessary for data to be taken in very rapid sequence.

To aid in the preparation of such a plan, each of the participating stations was asked to submit a detailed experiment plan including test equipment, procedures, and test points, concerning those tests in which that particular station would participate. These detailed plans were necessary to determine the compatibility of the various stations with one another, with respect to levels, test signals, standards, etc. This information was presented in the Relay Experiment Plan in an abbreviated form, giving the general purpose and description of the individual experiments, and the test procedures for each of the stations. It was not the intent of the Experiment Plan to give step by step detailed operating test procedures, but only to present those pertinent test features which would affect operation with other stations or the analysis of the resulting data.

Test and ground stations which participate in communication experiments are listed in Table 1–1 along with their location. The Relay test stations, although principally involved with checking and monitoring the spacecraft performance telemetry and testing of the wideband communication system, also have limited communication experiment capability.

As new stations became operational, the experiment plan was revised to include the capability of these stations. Suggested new experiments and revisions of the original experiments were also incorporated in the plan in the course of its use.

Table 1–2 summarizes the basic participation and frequency capability as to narrowband and wideband modes for each of the stations.

FORMAT

The communications experiments have been divided into three classifications: wideband

TABLE 1–1.—*Stations Participating in Relay Experiments*

Station	Location
Test	
Nutley, New Jersey, USA	40.816° North Latitude 74.167° West Longitude
*Mojave, California, USA	35° 17′ 48″ North Latitude 116° 53′ 57″ West Longitude
Ground	
Andover, Maine, USA	44° 37′ 55″ North Latitude 70° 41′ 54″ West Longitude
Fucino, Italy	41° 58′ North Latitude 13° 36′ East Longitude
Goonhilly, England	50° 2′ 58″ North Latitude 5° 10′ 29″ West Longitude
Pleumeur-Boudou, France	48° 47′ 13″ North Latitude 3° 31′ 30″ West Longitude
Rio de Janeiro, Brazil	22° 57′ 9″ South Latitude 43° 22′ 7″ West Longitude
*Raisting, Germany	47° 54′ 15″ North Latitude 11° 6′ 34″ East Longitude
*Ibaraki Prefecture, Japan	36° 41′ 40″ North Latitude 140° 41′ 43″ East Longitude
*Kashima-machi, Japan	35° 57′ 10″ North Latitude 140° 39′ 58″ East Longitude

*Indicates stations which have been added since the initial launch of Relay.

performance experiments, narrowband performance experiments, and system demonstration experiments. These categories make up all of the regularly planned communication experiments performed by the Relay test and ground stations with the spacecraft in either the wideband or narrowband mode. Tests may be performed in both a loop and straightaway configuration. That is, loop if the station transmits to the satellite and receives the same transponded signal from the satellite; and straightaway if the test is made between two stations. Straightaway tests may be either one-way or two-way. Table 1–3 lists the communication experiments as they appear in the Relay Experiment Plan. Wherever possible the recommendations of CCIR have been followed in keeping with the international character of Project Relay.*

Performance Experiments

System performance experiments—wideband and narrowband — are intended as objective tests to obtain quantitative and statistical data on the electrical parameters of the system by analyzing the response to carefully controlled excitations. From these data we may determine:

1. Compatibility of the selected communications system configuration with the requirements imposed on the system by performance criteria, in an operational environment.
2. The characteristics of observed performance degradation during the communications lifetime of the satellite with particular emphasis on applying failure mode information to future designs.
3. The effects of the unique environment imposed by an orbital system (i.e., Doppler shift, acceleration effects, etc.) on the electrical parameters normally used to define the performance limits of a quality wideband microwave relay system.
4. System design parameters to be recommended for future satellite relay programs.

Performance data are primarily intended to confirm a system capability for quality monochrome television and frequency division multiplex (FDM) telephony. Information has been accumulated in the areas of insertion gain and gain stability, phase characteristics, distortion, intermodulation, interference, and noise.

In order to establish system performance in these areas, a substantial number of tests is required. In addition, data from many of the experiments must be correlated with received signal strength, spacecraft wideband subsystem performance telemetry, spacecraft attitude, ground antenna elevation angle, ground station performance parameters, weather conditions, etc.

Data concerning baseband Doppler shift, absolute delay and tracking were also obtained. While a large number of tests is not required to establish these parameters, they are of utmost importance to the performance of the system.

System Demonstration Tests

The system demonstration experiments emphasize quality television and telephony, but

*Consultative Committee on International Radio (CCIR, Documents of the IXth Plenary Assembly, Los Angeles, 1959, Vol. I, Recommendations), published by the international Telecommunication Union, Geneva, 1960.

TABLE 1–2.—*Summary of Participating Station Capabilities*

Station	Wideband		Narrowband		Multiplex (two-way)		One-way noise loading	
	Transmit (Mc)	Receive (Mc)	Transmit (Mc)	Receive (Mc)	(12–60 kc)	(60–108 kc)	Channel	Channel
Andover, Maine	1725	4169.72	1723.33 1726.66	4164.72 4174.72	X	X	X	X
Fucino, Italy		4169.72		4164.72 4174.72	X	X		
Goonhilly Downs, England.	1725	4169.72	1723.33 1726.66	4164.72 4174.72	X	X	X	X
Nutley, N.J. (Ground Station).			1723.33 1726.66	4164.72 4174.72	X	X		
Pleumeur-Bodou, France.	1725	4164.72	1723.33 1726.66	41.6472 4174.72	X	X	X	X
*Raisting, Germany (COMGEA).					X	X	X	X
Raisting, Germany (COMGEB).			1726.66	4164.72 4174.72	X	X		
Mojave, Calif. (Test Station).	1725	4169.72	*1723.33 *1726.66	*4164.72 *4174.72	*X	*X		
Rio de Janeiro, Brazil.			1726.66	4164.72 4174.72	X			
Ibaraki Prefecture, Japan.		4169.72		*4164.72 *4174.72	X	X	X	
*Kashima-Machi, Japan.	1725	4169.72	1723.33 1726.66	4164.72 4174.72	X	X	X	X
Nutley, N.J. (Test Station).	1725	4169.72						

*Future Capabilities

TABLE 1–3.—*Communication Experiments*

100 SERIES—WIDEBAND PERFORMANCE EXPERIMENTS
- 110 *Received carrier power*
  - 111 Received carrier power—normal
  - 112 Received carrier power—special
- 120 *Insertion gain stability*
  - 121 Audio
  - 122 Composite video
  - 123 Selective fading
- 130 *Noise measurements*
  - 131 Continuous random noise—video
  - 132 Continuous random noise—audio
  - 133 Impulsive noise—video
  - 134 Impulsive noise—audio
  - 135 Periodic noise—video
  - 136 Periodic noise—audio
  - 137 Baseband noise spectrum
  - 138 Satellite noise
  - 139 IF noise and interference
- 140 *Linear distortion*
  - 141 Field-time distortion
  - 142 Line-time distortion
  - 143 Short-time distortion ("2T" and "T" sine-squared pulses)
  - 144 Amplitude-frequency characteristic—baseband
  - 145 Phase-frequency characteristic—baseband
  - 146 Amplitude-frequency characteristic—RF
  - 147 Amplitude-frequency characteristic—audio
- 150 *Nonlinear distortion*
  - 151 Line-time non-linearity (differential gain)
  - 152 Envelope delay distortion (differential time delay)
  - 153 Synchronization non-linearity
  - 154 Audio distortion
  - 155 Intermodulation—harmonic
  - 156 Intermodulation—noise loading
  - 157 Intermodulation—video to audio
- 160 *Interference*
- 170 *Special transmission tests*
  - 171 Baseband doppler shift
  - 172 Absolute delay
  - 173 Tracking
- 180 *Television test patterns*
  - 181 Monochrome
  - 182 Color

200 SERIES—NARROWBAND PERFORMANCE EXPERIMENTS
- 200 *Received carrier power*
  - 211 Received carrier power—normal
- 220 *Insertion gain stability*
  - 221 Selective fading
- 230 *Noise measurements*
  - 231 Continuous random noise
  - 232 Impulsive noise
  - 233 Periodic noise
  - 234 Satellite noise

TABLE 1–3.—*Communication Experiments (Continued)*

240	*Linear distortion*
241	Amplitude-frequency characteristic—baseband
242	Phase-frequency characteristic—baseband
250	*Nonlinear distortion*
251	Envelope delay distortion (differential time delay)
252	Intermodulation—harmonic
253	Intermodulation—noise loading
254	Intelligible crosstalk
260	*Interference*
270	*Special transmission tests*
271	Baseband doppler shift
272	Absolute delay
273	Tracking
274	Clock pulse synchronization
275	Multiple loop
300 SERIES—SYSTEM DEMONSTRATION EXPERIMENTS	
310	*Television*
311	Monochrome
312	Color
313	Narrowband
320	*Telephony*
321	One-way telephony
322	Two-way telephony
330	*Digital data transmission*
331	High data rates
332	Medium data rates
340	*Program material*
341	Music
350	*Comparison of relay and other communication channels*
351	Teletype transmission
352	Facsimile transmission
353	High-rate teletype transmission
360	*Multiple satellite tests*

also include a variety of other data forms such as high bit rate digital data, facsimile, and multichannel teleprinter transmissions. Several of these experiments have been used for public demonstrations of satellite communications. The intent of these experiments is to demonstrate both a system transmission capability for a variety of signals, and provide:

1. A measure of the link quality for monochrome television by investigating a number of picture characteristics including resolution, synch compression, streaking, smearing, set up, ringing, echo, interference, etc.

2. Teletype error rates for a number of channels distributed throughout the available baseband.

3. An evalution of telephony quality for channels distributed over the baseband with particular emphasis on crosstalk, distortion, time delay effects and signal-to-noise ratio.

4. Determination of bit error rate for digital FSK at a variety of signaling rates.

5. An evaluation of facsimile transmission at medium rates checking definition; skew and slippage.

6. A comparative performance analysis for telephone and voice transmission using data available from other channels including land lines, submarine cables, high frequency radio and scatter systems.

As in the case of the performance experiments, these data must also be correlated with the various time-varying parameters of an orbital system.

DESCRIPTION OF EXPERIMENTS

In this section we give brief descriptions of the experiments indicated in Table 1–3. However, since there is a good deal of redundancy in the experiments themselves, e.g., narrowband and wideband, it is more convenient to discuss them in terms of the broader category headings rather than individually. More detailed descriptions of the individual experiments are given in the Relay Experiment Plan.*

Received Carrier Power and Insertion Gain

Received carrier power is of fundamental importance and is measured by all participating stations. This measurement is made by monitoring the ground receiver AGC signal and comparing with a calibration curve. A typical calibration curve (normalized to read received carrier power directly) is shown in Figure 1–1 along with the actual measured carrier power for a particular pass.

Insertion gain measures the effective gain of the entire link. A signal of known level is inserted at the input and the level of the received signal measured at the output. This test establishes a reference level and checks compatibility of the baseband equipment as to signal level at the input and output. Variations of the insertion gain with position in the baseband and with time are also measured to determine selective fading and long-term gain drifts. There should be no significant variations with these parameters. The

*"Relay Communication Experiment Plan," R1–0521A, prepared for Goddard Space Flight Center, Greenbelt, Maryland, 1 December 1963.

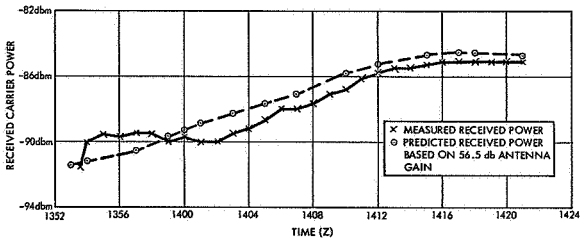


FIGURE 1–1.—Received carrier power (Goonhilly).

CCIR recommendations have been used as performance objectives for Relay. These are:

Insertion gain: 0 db ± 1 db

Short-period (e.g., 1 second) variations: ± 0.3 db

Medium-period (e.g., 1 hour) variations: ± 1.0 db

Noise Measurements

The various noise measurements are designed to determine the signal-to-noise ratio for each mode of operation. Measurements are made for both video and telephone transmission. The principal measurement in both cases is of continuous random noise, periodic and impulsive noise being of secondary importance. In general, the tests are made in accordance with CCIR recommendations.

Two main characteristics are of interest in measuring random noise: the amount of noise and the distribution of the noise over the baseband spectrum. In television, noise is more objectionable at the low-frequency end of the band. Weighting networks are commonly used to account for this effect and make the measurements correspond more closely with the resulting picture quality. Figure 1–2 shows typical weighting curves used in the measurement of noise for television. The sharp peak in the curve for color television is at the color subcarrier frequency which is quite critical. This weighting factor is such that the unweighted signal-to-noise ratio in db is equal to the weighted ratio in db minus the weighting factor, which is also given in db. In this context, signal-to-noise ratio is the ratio of the peak signal power to the RMS noise level. Because of the nature

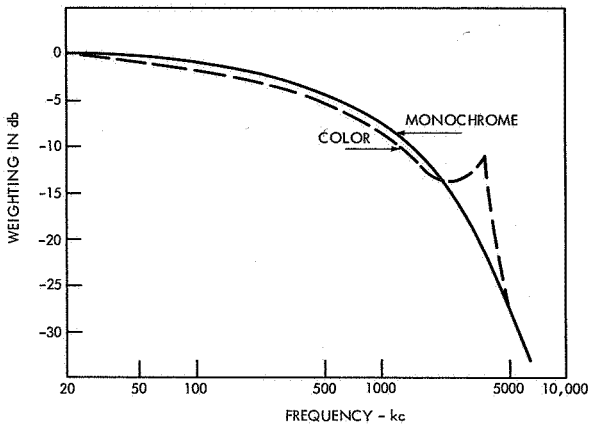
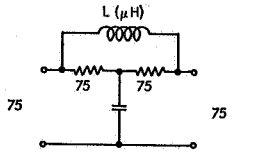


FIGURE 1–2.—Random noise weighting for monochrome and color television.

of the television signal, the signal level is taken from peak white to peak black.

The CCIR recommends a signal-to-noise ratio of 50 db, weighted in accordance with CCIR weighting. For the Relay system, the requirement is 43 db for the smaller stations and 50 db for the larger stations. The weighting factor applied is that shown in Figure 1–3 for the 405- and 525- line systems, namely 12.3 db. Subtracting the weighting factor from the 43-db requirement for the



$L\ (\mu H) = 75\ \tau\ (\mu s);\ C\ (pF) = \frac{\tau\ (\mu s)}{75}\ 10^6$

INSERTION LOSS (db) = $10 \log (1 + \omega^2 \tau^2)$

Number of Lines	f_c (Mc/s)	τ (μs)	$f_c T$	Theoretical Weighting, (db) for: "White" Noise	"Triangular" Noise
405	3	0.33	1.0	6.5	12.3
525	4				
625	5	0.33	1.66	8.5	16.3
625	6	0.33	2.0	9.3	17.8
819	5				
819	10	0.166	1.66	8.5	16.3

Note: f_c is the nominal upper video-frequency limit of the system (Mc/s)

FIGURE 1–3.—Continuous random noise weighting networks.

smaller Relay stations, we obtain an unweighted signal-to-noise ratio of 30.7 db as that required for an acceptable picture. It should be stressed again at this point that the determination of what is an acceptable picture is an empirical one, not based on any theoretical calculations. It is the result of subjective tests, based on viewer reactions. A study was made at STL to arrive at some sort of lower limit of acceptability: in this study, noise was added to the picture in measured quantities to simulate a range of signal-to-noise ratios. It was found that in the judgement of most viewers, a picture quality corresponding to about 30 to 35 db unweighted signal-to-noise ratio was a rough lower limit of acceptability.

The relation of video signal-to-noise ratio to the parameters of the transmission system is given by the equation

$$\left(\frac{S}{N}\right)_{vid} = \frac{3F_{p-p}^2}{\left[N^2\left(\frac{\phi_v}{S_v}\right)+\left(\frac{\phi_g}{S_g}\right)\right]F_m^3}$$

where

F_{p-p} = The peak-to-peak deviation of the signal

F_m = The maximum frequency of the baseband information

$N=3$ = The multiplication in the spacecraft

ϕ_v = The received noise power spectral density in the spacecraft

ϕ_g = The received noise power spectral density at the ground

S_v = The received signal power in the spacecraft

S_g = The received signal power at the ground

The situation for telephony is slightly different. In frequency-division multiplex telephony by a frequency-modulated carrier (FDM/FM) as in Relay, random noise is much more pronounced in the higher channels of the baseband. It is the objective of any such system to achieve equal signal-to-noise performance for all telephone channels across the baseband. To illustrate how this comes about, consider an FM receiver which is to demodulate an FDM/FM signal consisting of

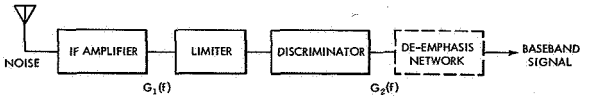


FIGURE 1–4.—Typical FM receiver.

numerous telephone channels. Such a system is shown in Figure 1–4.

The continuous random noise can be considered to originate in the front end of the receiver and to have a spectrum which is flat, as in Figure 1–5. ϕ_i is given by noise temperature or noise figure of the receiver.

If the carrier-to-noise ratio is sufficient for the receiver to operate above threshold, then the noise spectral density is $(\phi_i/S_i)\ f^2$ at the output of the discriminator $G_2\ (f)$. This has the form shown in Figure 1–6.

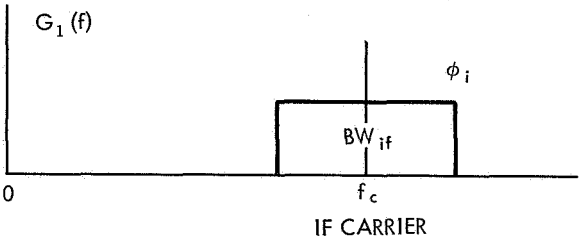


FIGURE 1–5.—Noise spectrum in FM receiver.

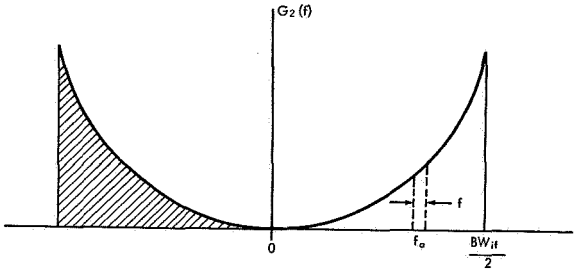


FIGURE 1–6.—Noise spectral density.

An examination of the spectral distribution of the noise at the discriminator output reveals that the thermal noise in the higher channels of the baseband is considerably greater than in the lower channels. A specification of the allowable noise power under

these circumstances must refer to the top channel where the noise is maximum. In order to remedy this, pre-emphasis can be applied at the transmitter followed by de-emphasis in the receiver. With pre-emphasis, the signal-to-noise ratio of the individual telephone channels should be approximately the same throughout. The actual pre-emphasis characteristic being used for Relay I (specified by CCIR) is shown in Figure 1–7.

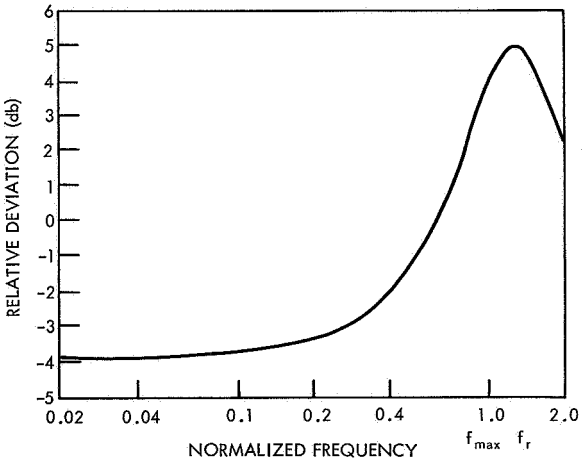


FIGURE 1–7.—CCIR pre-emphasis characteristics for multiplex telephony.

A specification on allowable thermal noise power has been made for the system—for Relay I. It is either 7500 pw or 50,000 pw psophometrically weighted at zero relative level, depending upon the quality of the ground station receiver. A measurement of the actual thermal noise is a check on the system parameters, such as transmitter power — both ground and spacecraft — frequency deviations, and bandwidth.

In the measurement of thermal noise for Relay I a 1-kc tone of 0 dbm0 (1 milliwatt at zero relative level) is intermittently applied to the lowest and highest channels. At the output the signal and noise levels are measured with a true RMS meter.

The purpose of the tone is to establish the reference level at the output for determining the noise power at zero relative level. All channels are checked individually to determine the actual frequency distribution of the thermal noise throughout the baseband.

The technique for measuring noise is normally to pass it through a bandlimiting filter which passes only the frequencies of interest, and then through a weighting network. A power-reading meter is then used to measure the RMS value of the noise. Figure 1–3 shows the CCIR recommendation for a noise weighting network. Actually, these measurements are made both with and without CCIR pre-emphasis/de-emphasis and weighting network. This is necessary to establish the shape of the noise spectrum and determine the effect of these techniques.

Linear Distortion

Two principal methods are used to determine the linear distortion of the wideband signal. The first method employs standard CCIR video test signals* in order to test the frequency response of the system to low, medium and high baseband frequencies. These are the field-time, line-time and short-time distortion experiments respectively. The second method consists of measuring the steady state response or amplitude-frequency and phase-frequency characteristics of the system. This method is also applicable in the narrowband mode.

Measurement of field-time distortion is made by transmitting a square wave at 50 or 60 cps with maximum and minimum amplitude corresponding to the peak white and peak black levels; line-synchronizing pulses also being transmitted at the same time (CCIR Test Signal No. 1). The received square wave is observed on an oscilloscope, and the amplitude across the top of the wave observed. Maximum and minimum amplitudes are established on the basis of qualitative evaluation of the resulting picture.

Line-time distortion is measured using a test signal consisting of a half-line bar with

*Consultative Committee on International Radio (CCIR, Documents of the IXth Plenary Assembly, Los Angeles, 1959, Vol. I, Recommendations), published by the International Telecommunication Union, Geneva, 1960.

sine-squared transitions (CCIR Test Signal No. 2). For short-time measurements, the test waveform has a sine-squared pulse preceding the bar. The pulse is either a "2T" pulse (half-amplitude duration of 0.33 μsec) or "T" pulse (half-amplitude duration of 0.17 μsec) ; the former being useful for evaluating amplitude and phase distortion in the 0.5 to 1.5 Mc region and the latter useful up to about 3.0 Mc. Distortions of the bar portion of the signal indicate response deficiencies up to a few hundred kilocycles. Ringing following the abrupt transitions is indicative of phase distortion. The received signals are generally displayed on an oscilloscope and photographed for later analysis.

Amplitude-frequency characteristics are determined either by inserting discrete tones, or by sweeping a sinewave across the baseband and displaying (or measuring point-by-point) the received signal. The phase-frequency characteristic is determined by sweeping a pair of frequencies (with fixed separation) across the baseband and measuring the phase of the received difference signal. A direct measurement of the modulation delay of a swept subcarrier may also be made, since delay is the derivative of phase with respect to frequency.

Nonlinear Distortion

Nonlinear distortion measurements evaluate the departure from linearity in the system and the attendant signal distortions. In an FM system, these nonlinearities can arise in the baseband, IF and RF equipment. Nonlinearities of the system may be expressed as a power series in the input variable, a percentage of harmonic distortion, or as a differential gain. One type of test signal used for these measurements consists of a low-frequency stairstep, ramp or sinusoid of high amplitude with a superimposed high-frequency, low-level sine wave. The high amplitude signal sweeps over the range of interest (black-to-white in the case of television) and the amplitude and phase variations of the high-frequency signal over this range are a measure of the differential gain and envelope delay respectively.

Differential gain in an FM system is primarily due to baseband equipment. If the nonlinear input-output characteristic is represented by a power series,

$$v_o = a_1 V_i + a_2 V_i^2 + a_3 V_i^3 + \ . \ . \ .$$

the differential gain can be expressed by

$$\text{D. G.} = 1 + 2\frac{a_2}{a_1} V + 3\frac{a_3}{a_1} V^2 + \ . \ . \ .$$

where V is the amplitude of the low-frequency sweep component of the input test signal described above. This expression assumes the system is basically linear and neglects the compression and higher order terms. CCIR recommends that the ratio of the minimum to maximum values of differential gain, over the range of interest, be greater than 0.8.

The identical type of signal is used to measure differential time delay or envelope delay. Envelope delay is proportional to the phase shift of the high-frequency component and it is this phase shift which is actually measured. This may be seen from the following simplified derivation. Figure 1–8 shows a typical test setup. Consider an input signal to the FM deviator of the form

$$V_i(t) = V(t) + v \cos \omega_h t$$

where $V(t)$ = low-frequency, high amplitude sweep signal and $v \cos \omega_h t$ = high-frequency, low-level superimposed signal. The output of the FM modulator is then

$$e_i(t) = E_i \cos [\omega_c t + \theta(t)]$$

where

$$\dot{\theta}(t) = k_1 [V(t) + v \cos \omega_h t] = \omega_i$$

At the output of the transmission link the signal is

$$e_o(t) = E_o \cos [\omega_c t + \theta(t) + \beta(\omega_i)]$$

where $\beta(\omega_i)$ is the phase shift introduced by the link due to the phase-frequency characteristic of the transmission path. The output of the FM demodulator is proportional to the derivative of the incoming phase so that

$$e_D(t) = k_2 [\dot{\theta}(t) + \dot{\beta}(\omega_i)]$$

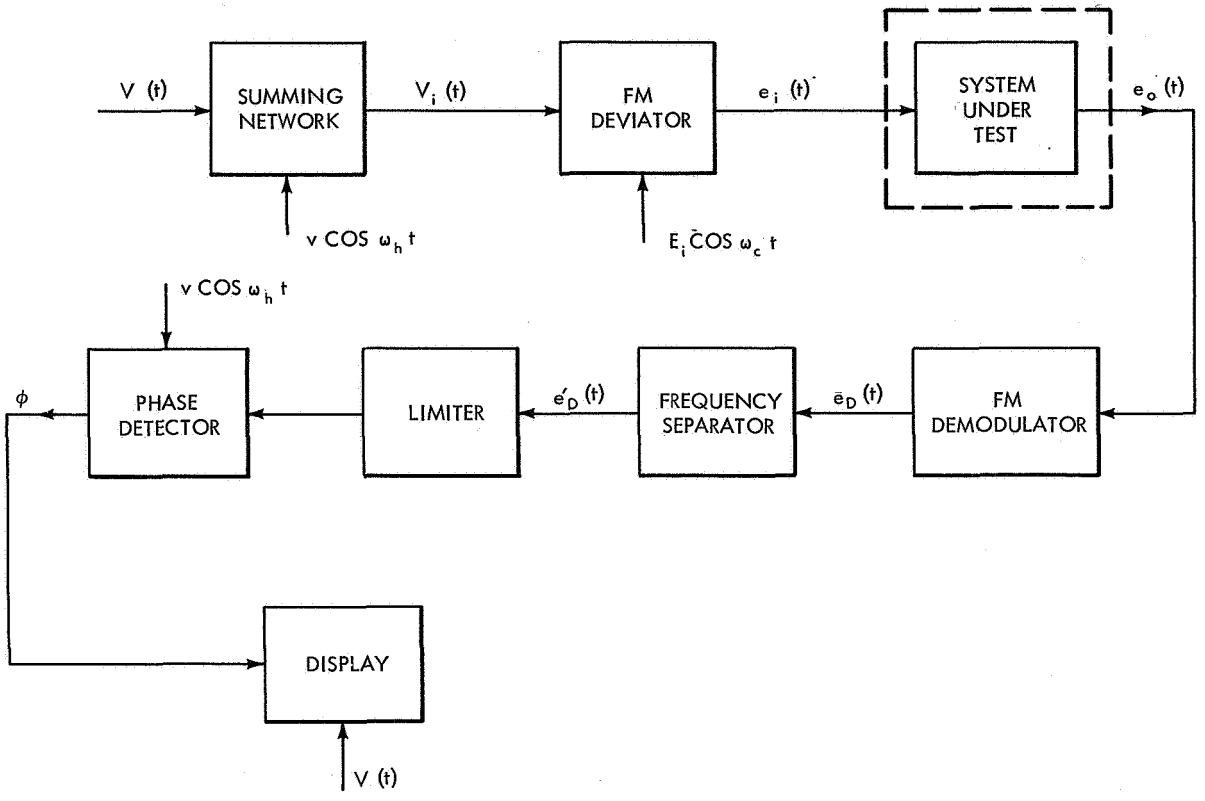


FIGURE 1–8.—Test setup for measurement of differential phase (envelope delay).

Writing

$$\dot{\beta}(\omega_i) = \frac{d\beta}{dt} = \frac{d\beta}{d\omega_i}\frac{d\omega_i}{dt} = \frac{d\beta}{d\omega_i}\ddot{\theta}$$

and substituting in the above expression, the demodulator output becomes

$$e_D(t) = k_1k_2\left[V(t)+v\cos\omega_h t + \frac{d\beta}{d\omega_i}\dot{V}(t)-v\omega_h\frac{d\beta}{d\omega_i}\sin\omega_h t\right]$$

After filtering out the low-frequency terms in $V(t)$ and $\dot{V}(t)$ the high-frequency component of the demodulator output is

$$e'_D = k_1k_2\,v\left[\cos\omega_h t - \omega_h\frac{d\beta}{d\omega_i}\sin\omega_h t\right]$$

$$= A\ (\omega_i)\cos(\omega_h t+\phi)$$

where

$$A(\omega_i) = k_1k_2\,v\left[\ 1+\left(\omega_h\frac{d\beta}{d\omega_i}\right)^2\ \right]^{1/2}$$

$$\phi = \tan^{-1}\omega_h\left(\frac{d\beta}{d\omega_i}\right)$$

Note the coefficient $A(\omega_i)$ is the amplitude of the received high frequency component and the variations of this amplitude with frequency represent the differential gain mentioned previously.

ϕ is seen to be the phase shift of the received high frequency component; differential phase is the variation of this phase shift, over the sweep range of interest, from a constant value. Normally, the phase shift is small and tan ϕ can be replaced by ϕ, so that

$$\tan\phi \approx \phi = \omega_h\frac{d\beta}{d\omega_i}$$

$d\beta/d\omega_i$ is variously known as envelope delay, group delay or differential time delay τ. This is the parameter commonly displayed.

If the phase-frequency characteristic is expressed as a power series, the corresponding

expression for envelope delay is obtained by differentiating with respect to frequency.

$$\beta = b_1\omega_i + b_2\omega_i^2 + b_3\omega_i^3 \ . \ . \ .$$
$$\tau = b_1 + 2b_2\omega_i + 3b_3\omega_i^2 + . \ . \ .$$

Therefore, linear delay corresponds to parabolic or second order phase distortion, parabolic delay to third order phase distortion, etc. The constant delay b_1 corresponds to linear phase and does not cause distortion but merely represents a time delay in the received signal.

For multichannel telephony the most important test is the measurement of intermodulation noise. This is just the noise or distortion of the signal which arises from the system nonlinearities. Again consider a power series representation on the nonlinear input-output characteristic.

$$V_o = a_1V_i + a_2V_i^2 + a_3V_i^3 + . \ . \ . \ .$$

Presumably the system is basically linear so that a_1 is much larger than the higher order coefficients.

Considering only the second term—this is second order amplitude distortion

$$V_2 = a_2\,V_i^2$$

If the input is a tone $V_i = k \cos \omega t$, then

$$V_2 = a_2k^2 \cos^2 \omega t = \frac{a_2k^2}{2} + \frac{a_2k^2}{2}\cos 2\omega t$$

If the input is two tones

$$V_i = k_1 \cos \omega_1 t + k_2 \cos \omega_2 t$$
$$V_2 = a_2(k_1 \cos \omega_1 t + k_2 \cos \omega_2 t)^2$$
$$= \frac{a_2\,(k_1^2+k_2^2)}{2} + \frac{a_2k_1^2}{2}\cos 2\omega_1 t + \frac{a_2k_2^2}{2}\cos 2\omega_2 t + a_2k_1k_2 \cos (\omega_1 + \omega_2)t + a_2k_1k_2 \cos (\omega_1 - \omega_2)t$$

Figure 1–9 illustrates these relationships. If the input is a band of noise of constant spectral density, then the output is a triangular band of noise.

This can be derived by considering the band of noise to be made up of a large number of

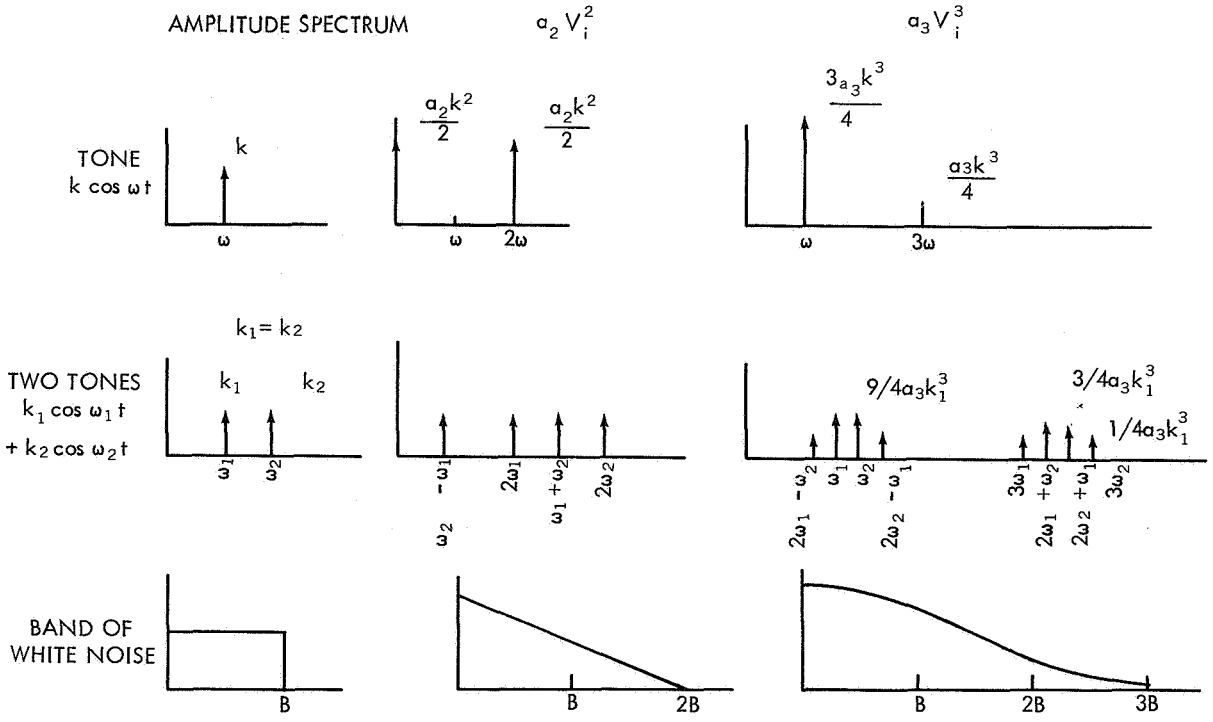


FIGURE 1–9.—Components of noise spectrum.

equal amplitude sine waves. Consideration of the harmonic and cross-product terms resulting from the nonlinearity $a_2V_i^2$ will result in the triangular spectrum with the highest frequency component at 2B.

The third term, or third order amplitude distortion, produces a similar effect. For a single tone input, $V_i = k \cos \omega t$

$$v_3 = a_3V_i^3 = \frac{a_3k^3}{4} \cos 3\omega t + \frac{3a_3k^3}{4} \cos \omega t$$

For a two tone input to the cubic law nonlinearity, $V_i = k_1 \cos \omega_1 t + k_2 \cos \omega_2 t$, the output contains the following frequency components

$$\omega_1, \omega_2, 3\omega_1, 3\omega_2, 2\omega_1 \pm \omega_2, 2\omega_2 \pm \omega_1$$

With a band of noise as the input to the third order nonlinearity the output is as shown in Figure 1–9. The highest frequency component is 3B.

Thus, the output of the nonlinear device consists of harmonics and cross-product terms due to V_i^2, V_i^3, etc., in addition to the frequencies present at the input. If the characteristic is known to be exactly of this form and the coefficients a_2 and a_3 are known, the amount of distortion (harmonic content) can be predicted by inserting a known signal (single tone, pair of tones, or noise). A specification of the allowable harmonic content in turn establishes the linearity requirement (a_2 and a_3) of the device.

Once the signal is converted to FM, we are concerned with the phase-frequency characteristics of the transmission path. This is the principal nonlinearity of an FM system. The phase variations are not of direct concern themselves, but only the frequency deviations caused by them. By a similar procedure the effects of the phase nonlinearities are obtained.

The important system nonlinearities are listed below. Amplitude nonlinearities are mainly due to baseband equipment and phase nonlinearities due to the transmission link.

Baseband Amplitude Nonlinearities

Second order $= a_2 V_i^2$
Third order $= a_3 V_i^3$

RF Phase Nonlinearities

Second order $= b_2 \omega_i^2$; (linear delay)
Third order $= b_3 \omega_i^3$; (parabolic delay)
Sinusoidal $= C \sin (\omega_i/\omega_o)$; (ripple)

Actual measurement of the intermodulation noise is done by means of a noise loading test. This test makes use of the fact that a large number of telephone channels which are frequency division multiplexed can be approximated by a white noise signal having proper frequency limits and power level. The power level of the noise signal is specified by CCIR for equivalent multichannel loading as indicated below where N_c is the number of channels.

$$P_{eq} = -1 + 4 \log_{10}(N_c), \text{ dbm0 } 12 \leq N_c < 240$$
$$P_{eq} = -15 + 10 \log_{10}(N_c), \text{ dbm0 } 240 \leq N_c$$

CCIR specifies the frequency band as the frequency limits of the actual channels.

The particular channel to be measured is cleared of noise at the input and the noise present at the output of this cleared channel is measured. Removal of the noise from a specific channel does not appreciably affect the total input signal since there are a large number of channels (at least 12 for Relay). Figure 1–10 shows a typical test setup for this measurement. Thus, any noise present at the output of the originally cleared channel is due to harmonics and cross-products of the signals (in this case noise) in the other channels. Thermal or random noise is also present of course, but if the signal-to-noise ratio is high, the thermal noise can be neglected. In

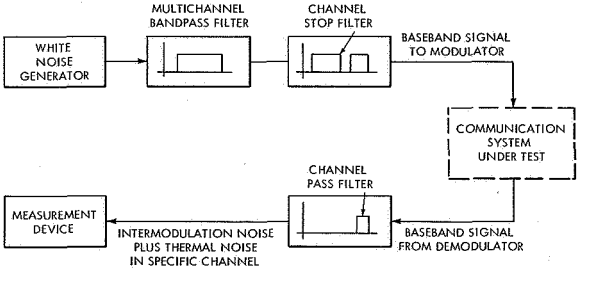


FIGURE 1–10.—Test setup for intermodulation noise measurements.

any case, the amount of thermal noise can be determined by measuring the noise in the channel with the entire input signal removed. This thermal noise value is then subtracted from the total to find the intermodulation noise. The Relay objective for intermodulation noise for the worst channel is 7500 picowatts psophometrically weighted at zero relative level.

Harmonic distortion is measured by inserting two tones at the input and measuring the resulting modulation products at the output. These measured modulation products are also used to predict the nonlinearities of the system (e.g., linear and parabolic delay) and serve as correlation tests for the direct measurements.

Another important nonlinear distortion for telephony is the measurement of intelligible crosstalk. Intelligible crosstalk arises in the narrowband mode with two-way telephone transmission where signals from two different ground stations are simultaneously received at the satellite, separated slightly in frequency, and at different power levels. Both signals pass through the same limiters and amplifiers and, due to the imperfect characteristics of these devices, interact with each other. The effect of this interaction is to transfer the baseband of one carrier onto the baseband of the other carrier at a low level; the result is that a listener hears another telephone message in the background.

If complementary channel operation is used, i.e., each person talks and listens in the same channel, an echo is heard. Since this type of distortion is intelligible, it is more disturbing than thermal or intermodulation noise. Also, it is found that an echo in the background is less annoying than another person's conversation and the system performance may be relaxed if complementary channel operation is used.

The measurement of intelligible crosstalk is accomplished by modulating one of the carriers with a tone and searching the baseband of the other carrier for the presence of this tone. Desirable performance levels for this type of distortion are 31 db signal-to-crosstalk ratio for an echo and 55 db for any other talker.

Special Transmission Tests

These tests include the measurement of Doppler shift at baseband and absolute delay between the transmitted and received signal.

Doppler shift is determined by transmitting a highly stable single tone at the high end of the base band (approximately 3 Mc) and measuring the received frequency with a counter. A second method is to transmit a radio tone in the highest telephone channel and measure the frequency of the received tone in the same channel.

For absolute delay, a short pulse is transmitted at baseband and the delay between the transmitted and received pulse measured.

Television Test Patterns

This experiment provides a basis for subjective evaluation of the system performance for television. The test consists of transmitting various test patterns, displaying the received patterns on a monitor and photographing the patterns for comparison. Test patterns are either taken directly from a pattern generator or generated from test slides scanned by a vidicon camera. The experiment is performed both with and without CCIR pre-emphasis.

System Demonstration Experiments

The system demonstration tests indicate the feasibility of satellite communication for various types of material. These include television, telephony, digital data, teletype and facsimile transmission. Either live or taped material may be transmitted. Subjective evaluation is made of the received transmissions and comparison made with the performance quality predicted from the performance experiments. In addition to subjective judgments, quantitative evaluations are made wherever possible (i.e., error rates, skew, slippage, sync compression, etc.). In general, the experimental procedures are in accordance with the corresponding narrowband or wideband performance experiments —television, telephone, etc.

These system demonstration experiments are also used for public demonstrations. When approved, public demonstrations are scheduled at the request of the participating stations. Many historical and general interest events have been transmitted via Relay.

ACKNOWLEDGMENT

Acknowledgment is given D. W. Butterfield and S. D. McCaskey who prepared the original Relay Experiment Plan under the direction of C. W. Stephens, all of TRW/Space Technology Laboratories.

AUTHOR. *This chapter was written by* R. CAGNON *of TRW/Space Technology Laboratories, Inc., Redondo Beach, California, U.S.A. under contract NAS 5–1302 with NASA/Goddard Space Flight Center.*

N66-10240

Chapter 2

GSFC Relay Communications Satellite Test Station

NASA/GSFC Test Stations are operational at Nutley, N.J. and near Goldstone (Mojave), Calif. as primary control centers for the Relay Communication Satellite. At the direction of the Relay Operations Center, these stations exercise command control, monitor spacecraft telemetry, and conduct communication experiments. The stations are equipped for rapid checkout of the satellite as well as for TV signal transmission and reception. As of June 1964, the Mojave station will be further equipped with two-way 12-channel FDM telephony transmission and reception.

A key design feature is the utilization of a computer to decommutate 49 telemetry items and, within approximately twenty seconds after sampling occurs in the spacecraft, to transmit this data continuously by teletype to the Relay Operations Center. In this manner, near real-time spacecraft status is reviewed, and control is effectively maintained.

THE RELAY COMMUNICATIONS SATELLITE TEST STATIONS

General

As a part of the NASA/GSFC Relay Communications Satellite System, two Test Stations have been constructed. One station is located at Nutley, New Jersey; it became operational in mid-September 1962. The other is located in the Mojave desert near Goldstone, California (150 miles northeast of Los Angeles), and was placed in service at the end of December 1962. The Relay Operations Center at Goddard Space Flight Center is connected by data and phone circuits to both stations and directs the stations in the conduct of command control of the satellite and communication experiments.

In the concept of the Relay satellite system, both stations at Nutley and Mojave were designated as Test Stations and as such have prime responsibility to command the satellite and monitor telemetry. Other stations participating in the program under agreements with NASA are designated as Ground Stations.

A listing of all participating stations and their capabilities is given in Table 2–1.

The Nutley Ground Station and the Nutley Test Station are separate operations, but physically use the same communications antenna. The Test Station, which is manned by STL and owned by NASA, is equipped for wideband transmitting and receiving through the 40-foot antenna. The tracking of the satellite is performed by personnel of International Telephone and Telegraph Corporation (ITT). When telephone testing is involved, ITT provides its transmitter, receiver, and multiplex equipment; test station equipment

TABLE 2–1.—*Summary of Participating Station Capabilities*

	Wideband		Narrowband		Multiplex (two-way)		One-way noise loading	
	Trans	Rec	Trans	Rec	Group A (12–60 kc)	Group B (60–108 kc)	300 Channel	600 Channel
Andover, Maine USA (AT&T)	X	X	X	X	X	X	X	X
Fucino, Italy		X		X	X	X		
Goonhilly, England	X	X	X	X	X	X	X	X
Nutley, N.J. USA (ITT)			X	X	X	X		
Pleumeur-Bodou, France	X	X	X	X	X	X	X	X
Raisting, Germany			X	X	X	X		
*Raisting, Germany					X	X	X	X
Mojave (Goldstone) Calif., USA (NASA)	X	X	X	X	X	X		
Rio de Janeiro, Brazil			X	X	X			
Ibaraki Prefecture, Japan		X		X	X	X	X	
Kashima-machi, Japan	X	X	X	X	X	X	X	X
Nutley, N.J. USA (NASA)	X	X						

*Future capabilities.

is used only for telemetry and command.

Test Station Overall System Description

An examination of Figure 2–1 shows that five major systems are involved in the test station operation. The satellite carries two 136 Mc telemetry transmitters, a command receiver and decoder, a 4080 Mc beacon, and a number of sensors in addition to the microwave repeater. The ground telemetry system receives data from the spacecraft and after computer processing transmits the vital information to the Operations Center at Greenbelt, Md. As a result, telemetry and command verification data can be reviewed by NASA personnel within 20 seconds after encoding occurs in the satellite.

The satellite is controlled by the command system from the selected station in accordance with prearranged schedules, but can be commanded at any time upon instructions from GSFC. The tracking and command antennas are mounted on the same pedestal and are positioned manually (by servo control) in accordance with the orbital data obtained from the Goddard Computer Facility. Since the beamwidth of these antennas is 20 to 30 degrees, no difficulty is encountered with this positioning. Orbital data can also be used to

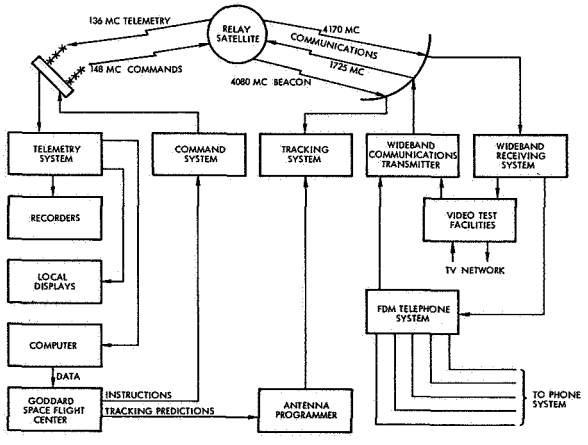


FIGURE 2–1.—Relay communications satellite system.

automatically position the 40-foot communications antenna by means of the Antenna Programmer, so that the satellite appears within the 0.42 degree beam. When the 4080 Mc beacon signal is acquired, it is utilized by the monopulse tracking system to follow the satellite automatically.

The primary communications functions are carried on by means of the wideband microwave transmitter and receiving systems. These are similar in function to standard microwave repeaters except for the 10 kw power output of the transmitter and the approximately 2 db noise figure of the receiving system. RF bandwidths of 25 Mc are employed, and an FM deviation of 16 Mc is used to gain signal-to-noise advantage. Transmission to the satellite is at 1725 Mc and reception from the spacecraft is in the vicinity of 4170 Mc. The 525 line video test facilities and frequency division multiplex equipments are essentially standard.

Test Station Implementation

The differences between the Test Stations at Nutley and Mojave are small so far as system operation is concerned, resulting from the use of different types of communications antennas. The vans at the two stations are similar, except that the monopulse tracking receiver is not installed in the van at Nutley, since this function is provided by ITT. At Nutley, the 10 kw wideband transmitter is mounted in cabinets on the ground and is connected to the antenna through waveguide rotary joints, whereas the transmitter power stage and translator are mounted on the antenna at Mojave, and receive the signal at IF through the cable wrap.

The vans are built with removable sides so that they can be joined together to provide an integrated operations room; the trailers are located adjacent to the 40-foot antennas utilized at both sites. At Mojave, the antenna was built for NASA by Philco Corp., and at Nutley, the antenna is owned by ITT and operated under contract with NASA.

The following sections of this report describe the various systems of the Test Station in detail.

TELEMETRY SYSTEM

General

The Relay Communications Satellite has as its primary function the reception and retransmission of microwave signals used for TV and telephone communications. Since the satellite is essentially an unattended repeater station, a telemetry system is provided to verify command and to permit monitoring of all pertinent system data. A simplified block diagram of the telemetry system is shown in Figure 2–2.

Satellite Telemetry Equipment

Figure 2–3 is a simplified block diagram of the Relay airborne portion of the telemetry system. The submultiplexers, the main multiplexer, and the A/D converter are collectively referred to as the encoder. Encoder output is fed to one of two telemetry transmitters. Selection of the transmitter to be modulated is made by ground command. The transmitters can be turned on or off sepa-

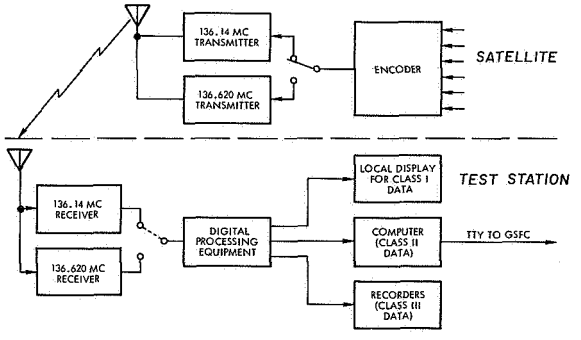


FIGURE 2–2.—Telemetry system.

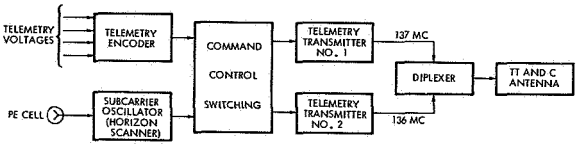


FIGURE 2–3.—Relay airborne telemetry, block diagram.

rately. Since only one transmitter is used at a time for telemetry transmission, the other is normally left on and used as a tracking beacon. Frequencies of both transmitters are 136.620 and 136.140 Mc, with the former planned for tracking, and the latter primarily for telemetry. Both transmitters are connected to a single antenna, which is also used for reception of commands from the ground. Isolation is provided between the received and transmitted signals and between the two telemetry transmitters.

Spacecraft telemetry transmitter output is approximately 250 milliwatts over the range of 24 to 32 volts input. Link calculations indicate that this power should provide a margin in the order of 10 db at elevations greater than 5 degrees above the horizon.

Provision is made in the spacecraft for modulation of the telemetry transmitter output either by the data from the encoder or directly by a horizon scanner. The horizon scanner signal indicates the rotation rate of the spacecraft, and is also used in a more refined analysis in combination with data from the sun aspect indicator, to derive spacecraft attitude. Horizon scanner output, which is in the form of a square wave, frequency modulates a 1300 cps subcarrier oscillator as the horizon scanner crosses the horizon. This signal is then detected by the ground receiver and patched into the horizon scanner discriminator, which feeds a strip chart recorder or can be patched into the magnetic tape recorder.

Telemetry Signal Characteristics

The Relay telemetry signal is PCM/PM, meaning that the bit stream from the encoder is pulse code modulated, and that this bit stream phase modulates the RF carrier radiated by the transmitter. The carrier phase is shifted approximately 140 degrees in one direction or the other by the change of state from "1" to "0" or vice versa. As illustrated in Figure 2–4 the type of coding used is split-phase nonreturn-to-zero. In this type of coding, a bit is identified by a change of voltage in a positive direction if the bit

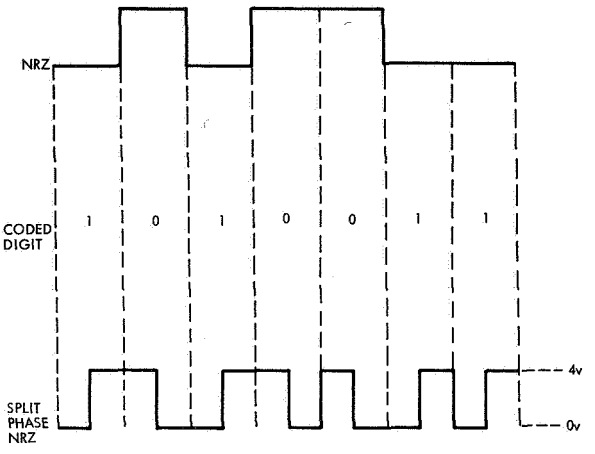


FIGURE 2–4.—Types of NRZ digital coding.

is a "1" and in a negative direction if the bit is a "0." This system permits positive identification of a bit even under poor conditions of reception, since only the direction of the change need be detected.

The bit rate used is 1152 bits per second, a relatively low rate, but adequate for the requirements of the system. Word length is 9 bits, permitting a quantization of 511 levels with a resolution of 10 millivolts, over the 0 to 5 volt range of telemetry voltages.

Figure 2–5 shows the telemetry format. There are 128 words in a complete message, divided as shown, with certain words subcommutated as indicated. The words are "looked at" three at a time in the 27 bit register of the PCM processor so that in some instances, more or less than 9 bits are used for certain information. For example, in word 16 only the first six bits are needed to indicate the frame numbers of subcommutator No. 2, since the maximum number of frames in each cycle is 64.

The main commutator switches through the sequence of main words continuously, but each time it reaches a subcommutated word the subcommutator presents a different measurement by advancing one word each frame. The main commutator completes a cycle in one second; each main word is sampled once per second. Words in subcommutator No. 2, are sampled once every 64 seconds. Those in

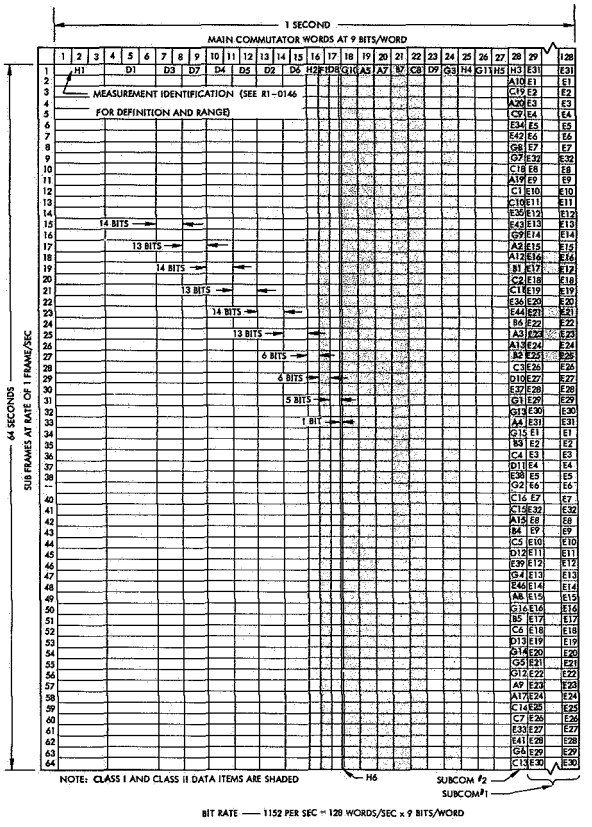


FIGURE 2–5.—Relay telemetry format.

subcommutator No. 1 are sampled at the rate of one sample every 32 seconds.

This unusual format is due to the requirement for measurements of the test panel of solar cells; the telemetry format provides for 100 successive measurements of each solar cell. This series of 100 measurements is required in order that at least one of the readings may record the cell voltage when the cell is on the side of the rotating satellite directly facing the sun. During the data reduction process the one maximum sample is selected and recorded automatically.

Readings E31 and E32 are respectively zero-scale and half-scale calibrations. This inflight calibration is required because of the fact that the solar cell outputs must be amplified before being telemetered, and these can possibly drift in the amplification. Correction will be automatically applied by the computer which performs the data reduction. Table 2–2 shows the Class II telemetry measurement list, with the range of values for each measurement.

A Packard Bell PB250, solid state digital computer is used to perform subroutines to:

1. Pick a maximum signal value for seven selected channels
2. Convert 9-bit binary numbers to measured parameters
3. Convert parameter readings to teletype Baudot code format and punch the teletype tape

In actual operation this data is very close to real-time information. The data punched on teletype tape by the computer is fed directly to a 100 word/minute teletype circuit so that the data is transmitted to GSFC almost as soon as the data is decoded. Not more than 20 seconds elapse for the entire process.

Types of Data

The digital telemetry data is divided into three classes, depending on importance.

Class I data is that data reduced in real time at the Test Station, and may be used for making a GO/NO–GO spacecraft operation decision. There are nine such items of information. A digital limit checker is used which compares the incoming signal values against preset limits. If all critical values are within tolerance, a row of green lights indicates spacecraft conditions. If a signal is out of specification, a red light is indicated and an alarm is sounded. Since the lights are labeled, the operator can tell immediately which parameter is faulty. The Class I data is recorded in analog form on a paper strip recorder.

Class II data consists of 34 items of spacecraft telemetry and is utilized to determine spacecraft condition in more detail than is available from Class I data. Class II data is also reduced in real time, formatted for transmission over a teletype circuit, and is transmitted to GSFC in order that GSFC representatives may observe the detailed status of the spacecraft immediately prior to,

TABLE 2-2.—*Relay Telemetry Measurement List, Class II*

Number	Function	Units	Range	Rate	TM time slot		
					Main com	Sub 1	Sub 2
1	Solar cell bus	Volts	20–40	1/sec	18		
2	Battery No. 1	Volts	20–40	1/64 sec	28		17
3	Battery No. 2	Volts	20–40	1/64 sec	28		25
4	Battery No. 3	Volts	20–40	1/64 sec	28		33
5	Unregulated bus	Volts	20–40	1/sec	19		
6	Battery 1–1 temp	°C	−20 to +66	1/64 sec	28		18
7	Battery 2–1 temp	°C	−20 to +66	1/64 sec	28		34
8	Battery 3–1 temp	°C	−20 to +66	1/64 sec	28		50
9	Total battery current	Amps	+2 to −5	1/sec	20		
10	TM transmitter power output No. 1	MW	0 to 500	1/64 sec	28		19
11	TM transmitter power output No. 2	MW	0 to 500	1/64 sec	28		27
12	Command receiver AGC	Volts	0 to 5	1/64 sec	28		59
13	TWT collector temp	°C	0 to 120	1/64 sec	28		12
14	Lower surface temp	°C	−130 to +5	1/64 sec	28		21
15	Active thermal controller sensor temp	°C	−2 to 40	1/sec	22		
16	AGC—main IF	Volts	0 to 5	1/sec	24		
17	Receiver mixer crystal current	MA	0 to 1	1/64 sec	28		39
18	Transmitter input signal power	MW	0 to 10	1/64 sec	28		55
19	Regulated bus voltage	Volts	0 to 30	1/64 sec	28		16
20	TWT output power	Watts	0 to 12	1/64 sec	28		24
21	Command verification ABC	Volts	0 to 5	1/64 sec	28		35
22	Command verification DEF	Volts	0 to 5	1/64 sec	28		43
23	Command verification GHI	Volts	0 to 5	1/64 sec	28		51
24	Command verification JKL	Volts	0 to 5	1/sec	21		
25	Sun aspect indicator	Mechanical degree		1/sec	16–17 (last 3 bits of 16 first 3 bits of 17)		
26	Solar cell S–1	MV	0 to 170	100/32 sec	29–128	2	
27	Solar cell S–2	MV	0 to 170	100/32 sec	29–128	3	
28	Solar cell S–3	MV	0 to 170	100/32 sec	29–128	4	
29	Solar cell S–7	MV	0 to 170	100/32 sec	29–128	8	
30	Solar cell S–8	MV	0 to 170	100/32 sec	29–128	10	
31	Solar cell S–9	MV	0 to 170	100/32 sec	29–128	11	
32	Thermistor No. 4	°C	−20 to +45	1/64 sec	28		7
33	Radiation monitor A	Counts	0 to 2^{27}	1/sec	4,5,6		
34	Beacon output power	MV	0 to 2	1/64 sec	28		32

during and following utilization of the spacecraft.

Figure 2–6 is an example of Class II data. The first 11-digit number following the *N* is the time that the data was read out of the computer and punched into the teletype tape. The first two digits are the year, the next three are the day of the year, and the last six are the Greenwich Meridian Time in hours, minutes, and seconds. This information is repeated every 16 seconds and is followed by the same six readouts each time.

```
////CFRNC-B////
RR GMRC JSTL
DE GSOC 008A
28/1130Z

THE FOLLOWING IS CLASS II DATA AS OBTAINED FROM RELAY II FROM
GCON ON ORBIT REVOLUTION 0049

  N64028110722 1.79 27.22 2/61 3.67 24/26 2.49
03 86.5 04 26.9 05 26/7 08 3.33
09 4.07 10 14/4 11 .05 13 16/7 16 22/1
  N64028110738 1.80 27.20 2/62 3.66 24/22 2.46
17 27.3 19 .00 20 20/2 21 -4/75 24 1.33
25 27.4 26 29/9 27 1.46 31 3.26 32 1.30
  N64028110754 1.80 27.29 2/63 3.66 24/26 2.47
33 27.4 34 .00 35 .76 40 19/8
41 17/5 42 30/2 43 .73 47 1.28 48 .00
  N64028110810 1.80 27.02 2/60 3.65 24/18 2.46
49 15/6 50 .01 51 1.96 54 1.71 55 .16
59 11/0 63 46/1 64 25/0
170 165 177 162 163  19 1/7

  N64028110826 1.80 27.16 2/62 3.66 24/18 2.47
03 86.5 04 26.8 05 26/6 08 3.35
09 4.05 10 14/8 11 .05 13 16/8 16 22/3
  N64028110842 1.79 27.07 2/63 3.66 24/37 2.45
17 27.3 19 .01 20 20/4 21 -4/53 24 1.33
25 27.3 26 30/2 27 1.47 31 3.28 32 1.32
  N64028110858 1.79 27.07 2/63 3.66 24/15 2.47
33 27.4 34 .01 35 .74 40 20/0
41 17/7 42 30/0 43 .73 47 1.26 48 .01
  N64028110914 1.79 27.00 2/61 3.66 24/15 2.49
49 15/3 50 .02 51 1.97 54 1.70 55 .15
59 11/1 63 46/1 64 24/7
170 165 177 162 163  19 1/7

  N64028110930 1.80 27.09 2/62 3.64 24/07 2.47
03 86.5 04 26.8 05 25/1 08 3.35
09 4.06 10 15/0 11 .05 13 16/8 16 22/4
  N64028110946 1.79 27.00 2/61 3.66 24/15 2.47
17 27.3 19 .02 20 20/4 21 -5/20 24 1.33
25 27.3 26 30/1 27 1.47 31 3.30 32 1.32
  N64028111002 1.80 27.02 2/62 3.65 24/18 2.47
33 27.3 34 .02 35 .75 40 20/1
41 17/9 42 30/2 43 .73 47 1.26 48 .01
  N64028111018 1.79 27.07 2/63 3.66 24/15 2.49
49 15/8 50 .02 51 1.96 54 1.71 55 .14
59 11/5 63 46/3 64 24/8
170 165 177 162 164  19 1/7
```

FIGURE 2–6.—Example of class II data.

These are main frame words 18, 19, 20, 21, 22 and 24. The slant line between certain numbers should be read as a decimal point, but indicates that these readings were taken from a normalized curve by the computer. They can be interpolated to recover the true reading.

The next line shows decommutated words 03, 04, 05, and 08, and their values, from subcommutator No. 2. It is seen that lines 2, 3, 5, 6, 8, 9, 11, and 12 are a continuation of these same words totalling 64 and are repeated in each block, i.e., every 64 seconds.

Line 13 of the format consists of subcommutator No. 1 items 18, 19, 23, 25, and 27, which are solar cell measurements.

Class III data contains all of the Class I and II and radiation experiments telemetry data. Class III data is recorded on magnetic tape for future data reduction. The tape recorder also records digital time for proper time tagging of events. Recording tapes are sent to the data Reduction Center at GSFC.

Test Station Telemetry System

Figure 2–7 is a block diagram of the telemetry system in the Relay Test Stations. Beginning with the telemetry antenna, the

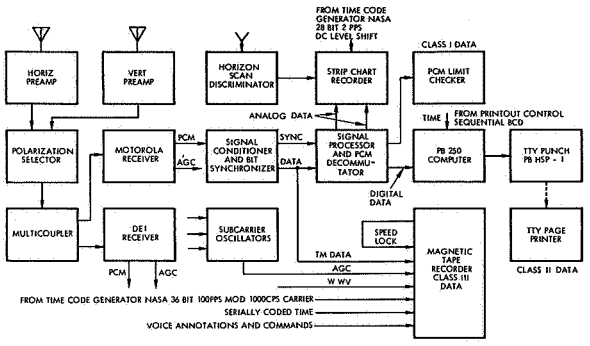


FIGURE 2–7.—Relay ground telemetry system.

signal goes through the polarization selector, which permits selection of circular or linear polarization. Circular polarization may be either right or left-hand, and linear polarization may be either vertical or horizontal. The multicoupler permits the signal to be sent to both phase-lock receivers. Receiver outputs consist of PCM data which is sent to the signal conditioner; AGC information is recorded as an indication of received signal strength. Either receiver may be patched into the digital system.

The signal conditioner and bit synchronizer reconditions the usually noisy bit stream, and provides a synchronizing signal at the bit rate. The signals then go to the signal processor and PCM decommutator. Here certain measurements are selected and converted to analog signals for strip chart recording. The entire bit stream, before reaching the signal processor, is also fed to a magnetic tape recorder. From the signal processor the digital data is fed to a Packard-Bell PB–250 digital computer which selects and reduces certain measurements, producing a punched tape at its output. This tape is then used to drive a teletype page printer for printing out the data in decimal form.

Simultaneously the data is transmitted to the operations office at GSFC. Another digital output from the signal processor operates the PCM limit checker, providing local display of certain critical parameters.

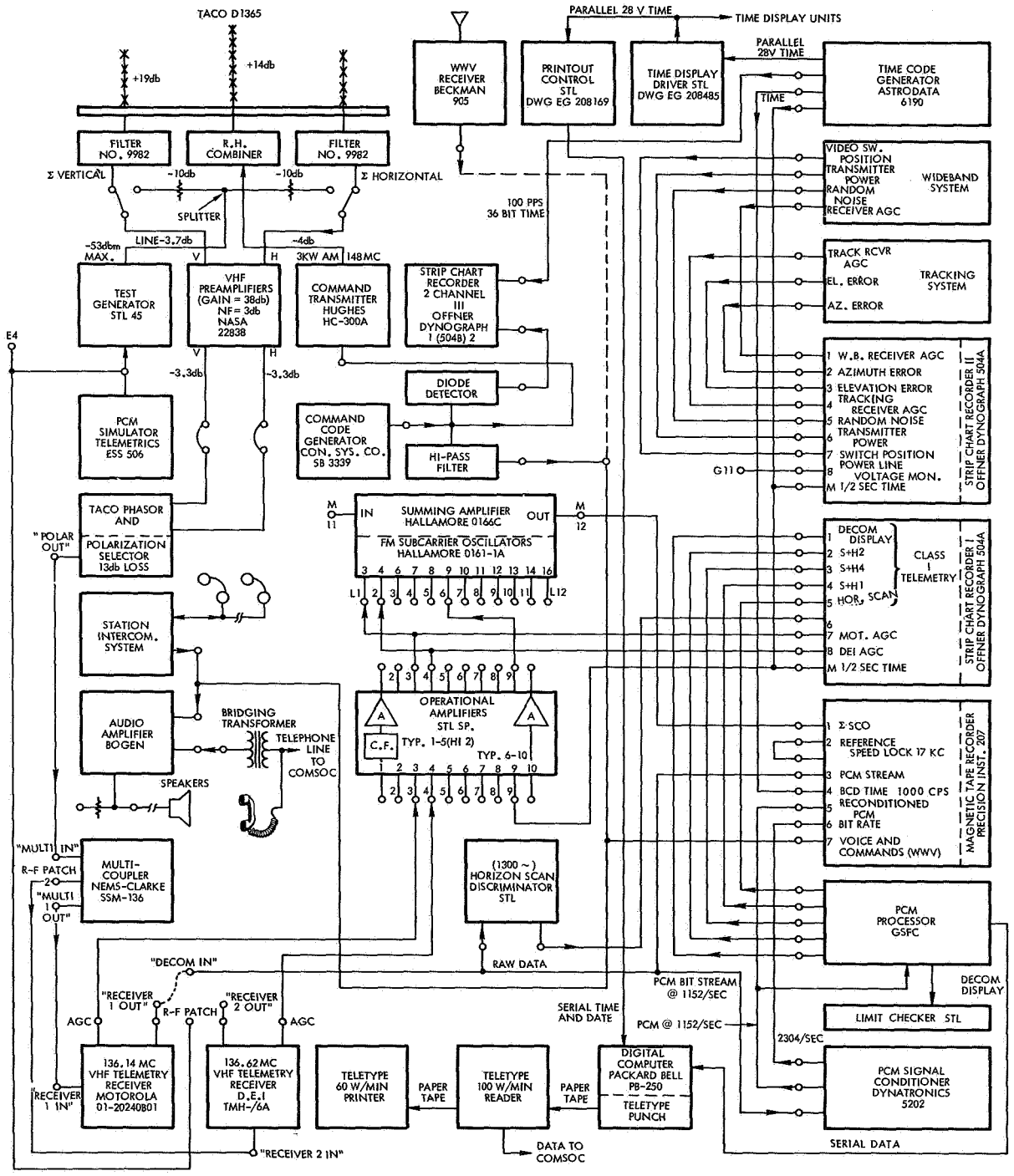


FIGURE 2–8.—Telemetry and command systems.

Detailed Test Station Telemetry System Description*

TACO Antenna

The TACO antenna assembly (Figure 2–9) used at the test stations at Mojave and Nutley includes a command antenna in addition to the telemetry antenna array. The array consists of eight antennas, each a seven-element yagi, dually polarized and cut for a frequency of 136.5 Mc. Outputs of the vertically polarized telemetry elements are connected by coaxial cables to a combiner and then through a filter (to reject the command frequency) to the input of a dual channel preamplifier. Horizontal elements are similarly connected into the other channel of the preamplifier. Preamplifier outputs are routed via cable to the polarization selector where vertical, horizontal left-hand circular or right-hand circular polarization can be chosen. The antenna assembly can be oriented plus or minus 280 degrees in azimuth or plus or minus 80 degrees in elevation by remote control. Telemetry array gain is 20 db, and the beamwidth is roughly 15 degrees in both planes.

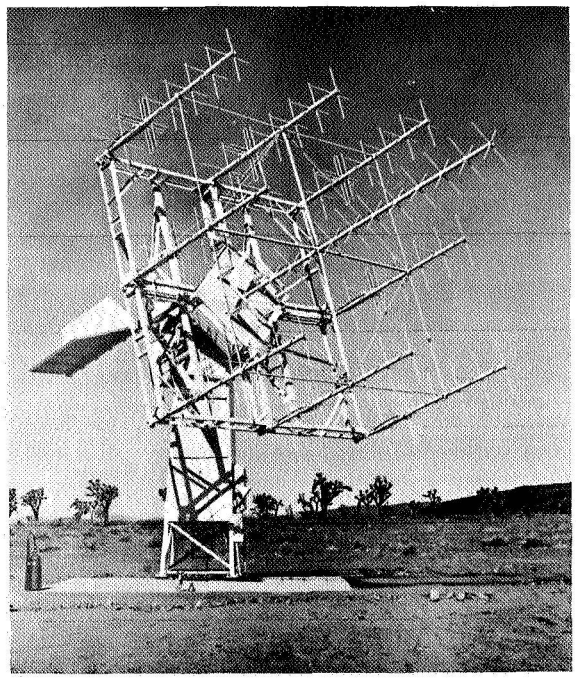


FIGURE 2–9.—TACO telemetry and command antenna.

Receivers

The 136–137 Mc Motorola and DEI receivers were especially designed for NASA for telemetry reception. The Motorola receiver is a phase-lock design capable of receiving amplitude or phase modulated signals in the range from –50 dbm to –157 dbm. Even though the received frequency is off normal by as much as 7 kc because of Doppler shift or transmitter frequency drift, the phase-lock design employing double conversion, will keep the narrowband filter locked to the weak carrier. IF bandwidth is adjustable from 60 kc to 1.5 kc. Loop bandwidth can be switched from 20 to 60 cps. The DEI receiver has characteristics similar to the Motorola receiver, and either can be selected to feed the PCM signal into the signal conditioner.

Data Processing

The signal conditioner and bit rate synchronizer is a Dynatronics Model 5202, also especially built for NASA (see Figure 2–10). It performs the function of regenerating deteriorated PCM serial data and reproducing it free of noise. An output of synchronizing pulses which are phase-locked to the bit rate of the incoming data is also provided. This unit is followed by a PCM data processor which, together with the signal conditioner, forms a realtime telemetry data processing system that is specifically designed to decommutate the Relay satellite telemetry.

The PCM data processor was developed by the Handling and Processing Section, Space Data Control Branch, Space Data Acquisition Division, of the Goddard Space Flight Center. The unit is adjusted to accommodate the word and frame format used by the Relay satellite and provides both digital and analog outputs.

Data Displays

One output of the PCM data processor is serial data sent to the Packard Bell PB–250

*See Figure 2–8.

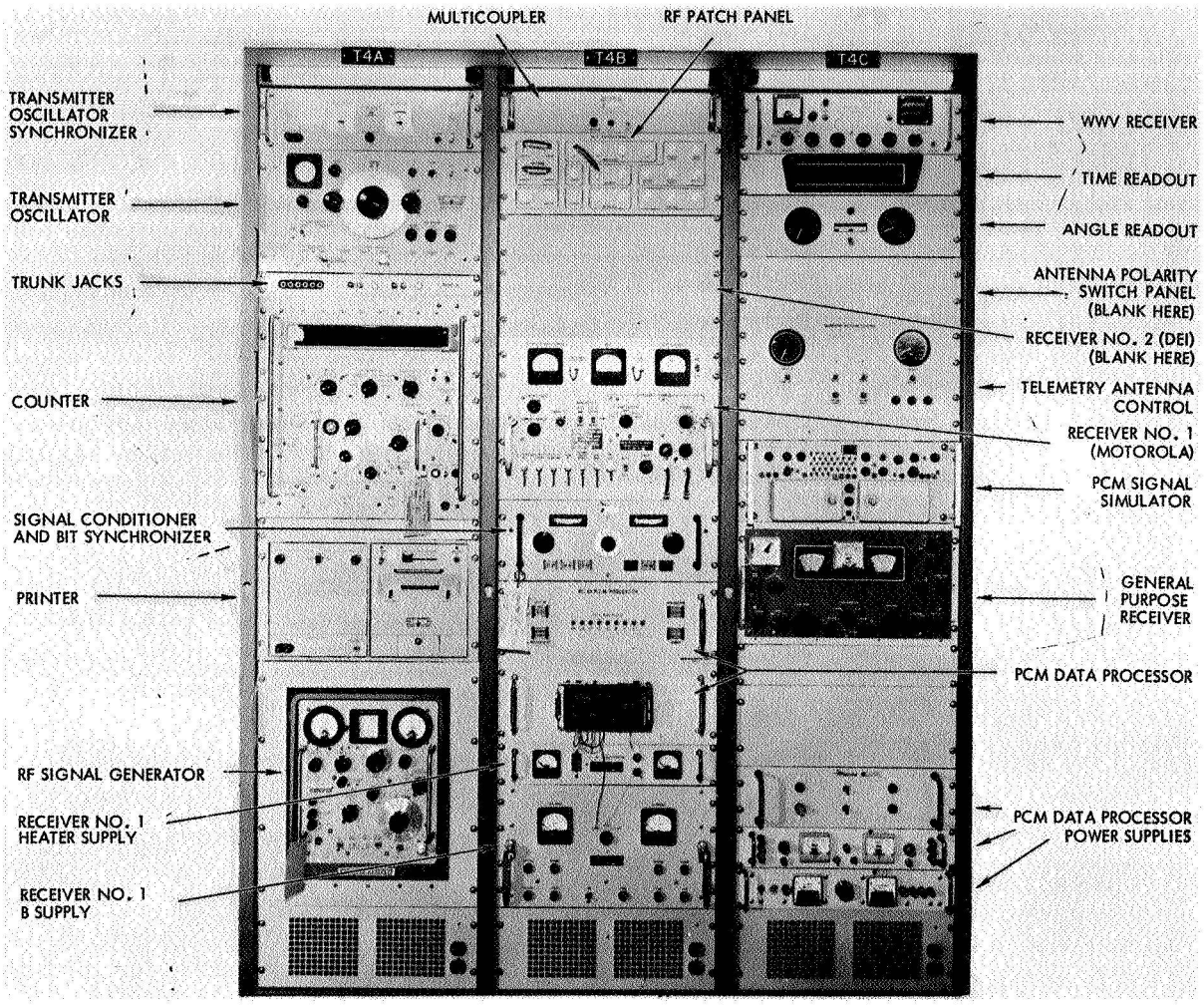


FIGURE 2–10.—Telemetry system.

computer where certain measurements are selected, converted to standard parameters, and punched out in Baudot form for transmission over teletype circuits.

Other digital outputs from the PCM data processor are sent to the PCM limit checker. This unit, designed and built by STL, provides an instantaneous display of red and green lights to indicate the status of the spacecraft. Eight preselected spacecraft functions are continuously examined to ascertain if they are within preset limits. An indication of when the PCM data processor has achieved frame sync is also provided. Analog outputs of the PCM data processor of selected critical measurements are connected to channels of the Offner Dynograph Model 504A strip chart recorder to provide a permanent record.

Verification Equipment

An Astrodata Model 6190 time code generator provides a NASA 28-bit 2-pps time signal to the Offner eight-channel strip recorders and a NASA 100-pps 36-bit time signal to the two-pen recorders.

Outputs from the time display lights of the time code generator (46 wires) are used to

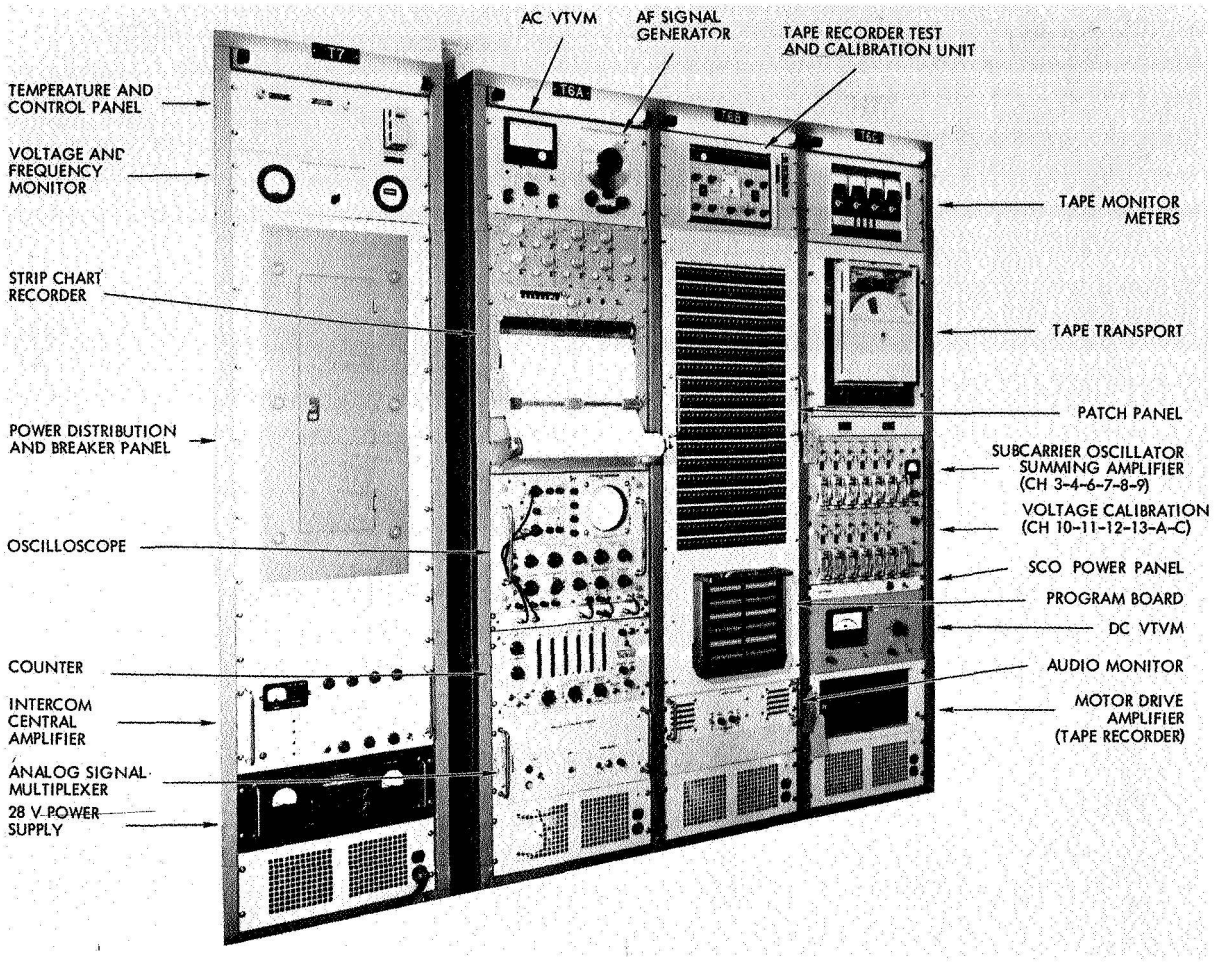


FIGURE 2–11.—Telemetry analog recording equipment.

operate the time display driver which, in turn, operates a number of time displays throughout the vans. These outputs are also used in conjuction with the printout control, to provide time signals to the PB–250 computer for time tagging of the Class II data as it is processed.

Some of the parameters, such as AGC, are fed into subcarrier oscillators and are then combined into a single composite wave train for recording on the Precision Instrument Model 207 seven-track magnetic tape recorder. WWV time signals are recorded as a standard time reference: the NASA 36-bit 100-pps 1000-cps modulated time signals generated by the time code generator are also recorded. A channel is also provided for voice recordings of communications over the station intercom system and for commands transmitted to the spacecraft. Speed lock information is generated within the tape recorder and recorded on the tape in still another channel to enable the playback recorder to maintain the same speed when playing the tape back as during the recording. Another recording is made of demodulated commands sent to the spacecraft; these are recorded along with a time code on a strip chart recorder.

PCM data from the receiver output is recorded on another track. Thus tapes can always be used to recover the data in the event

a failure occurs in the PCM data processing equipment during a satellite pass. Tapes are normally sent to the Goddard Computer Facility for analysis and permanent record keeping.

System Tests

A periodic check of the Test Station telemetry system is made using the Telemetrics Model ESS–506 PCM simulator and STL RF signal generator shown in Figure 2–8. Coaxial relays provide connection into the system at the antennas so that the complete system can be tested. Typical results are shown in Table 2–3.

TABLE 2–3.—*Receiver Error Rate*

Signal level	Receiver No. 1 errors/100,000	Receiver No. 2 errors/100,000
−120 dbm	0	0
−121	0	0
−122	0	2
−123	0	3
−124	0	9
−125	0	2
−126	10	26
−127	56	98
−128	118	239
−129	392	665
−130	911	1265

Since the received signal strengths are in the range of -105 to -115 dbm, data quality has been excellent.

THE COMMAND SYSTEM

General

Because of the variety of experiments available and the redundancy provided in the Relay spacecraft, it is not possible or desirable for all spacecraft systems to be operative simultaneously. The solar array output limits the power available. Thus a command system was provided to permit the orderly conduct of various experiments and to circumvent possible failures of equipment. The basic command system is shown in Figure 2–12.

The command system parameters and the equipment aboard the satellite are discussed

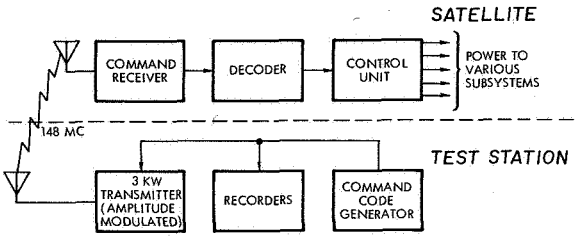


FIGURE 2–12.—The command system.

in detail in a separate report on the command system, but the basic requirements are shown here to facilitate understanding of the test station operation.

Commands are transmitted from the test stations by means of a 3 kw transmitter operating (at about 150 Mc) into a 14 db yagi circularly polarized antenna. Since a 3 to 4 db loss is encountered in the transmission line at either station, the resulting effective radiated power is approximately 33 kw; antenna beamwidth between the half-power points is about 30 degrees. The transmitter is amplitude modulated by a 5.451 kc tone which is pulsed in twenty combinations for the different commands. Command coding format is wholly compatible with the NASA Minitrack network of stations.

Command Code Characteristics

The command encoder used in the Relay test stations produces the standard NASA code, composed of blocks or pulses of 5451 cps tones of various lengths. Pulse duration modulation (PDM) is achieved by keying the tone on or off at about 300 bits per second. Thus, each bit contains 18 cycles of tone. The bits are used in combinations to form pulses which are either one bit long (for "0"s), two bits long (for "1"s), or three bits long for the synchronization pulse. Thus, the "0" is 18 cycles of tone or 3.3 milliseconds (msec) in duration, the "1" is 36 cycles of tone or 6.6 msec in duration, and the sync is 54 cycles of tone or 9.9 msec in duration. A command word is composed of six PDM binary digits preceded by the sync pulse and a readying period. Thus, a word can be thought of as being made up of 8 segments

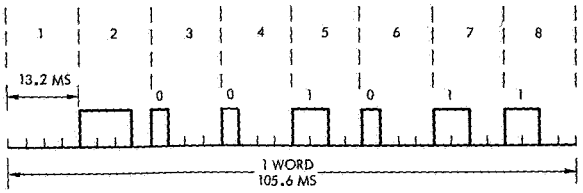


FIGURE 2–13.—Command word format.

as shown in Figure 2–13. The first segment (which carries no information, and must equal or exceed four bits in length) and is followed by the sync pulse (3 bits). Succeeding segments carry the command code. This format also requires combinations of three "0"s and three"1"s in order to be recognized by the spacecraft decoder. Twenty different commands are possible, as shown in Table 2–4. Each word is automatically repeated five times whenever a command is sent, requiring a total time of 528 msec. Provision is made in the spacecraft command control box to prevent simultaneous turn-on of both wideband transponders or of the horizon scanner and encoder.

TABLE 2–4.—*List of Commands*

Channel	Switching function	Code	Decoder line
1	Load cutoff normal	111000	1
2	Transponder No. 1 ON	110100	2
3	Transponder No. 2 ON	101100	3
4	Transponder Nos. 1 and 2 OFF	011100	4
5	Radiation experiment OFF	110010	5
6	Radiation experiment ON	101010	6
7	Telemetry encoder ON/horizon scanner OFF	011010	7
8	Horizon scanner ON/telemetry encoder OFF	100110	8
9	Modulate telemetry transmitter No. 1	010110	9
10	Modulate telemetry transmitter No. 2	001110	10
11	Attitude control current negative	110001	10
12	Attitude control current positive	101001	9
13	Horizon scanner and attitude control OFF	011001	8
14	Telemetry encoder OFF	100101	7
15	Telemetry transmitter Nos. 1 and 2 ON	010101	6
16	Telemetry transmitter No. 2 OFF	001101	5
17	Telemetry transmitter No. 1 OFF	100011	4
18	PHONE ON/TV OFF	010011	3
19	TV ON/PHONE OFF	001011	2
20	Load cutoff override	000111	1

Test Station Configuration

Figure 2–14 shows the units involved in the test station implementation of the command system. It will be seen that the system consists of the command code generator, the transmitter (and antenna), and two different monitoring facilities.

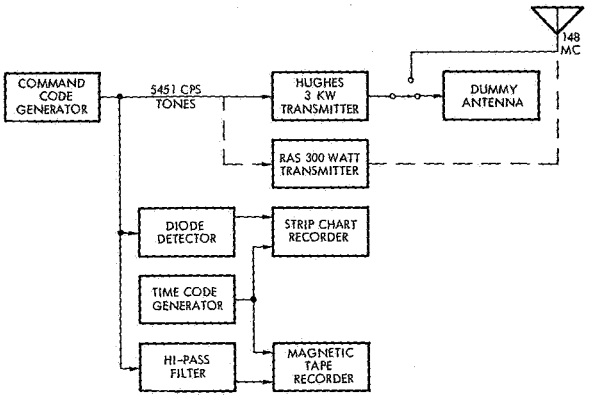


FIGURE 2–14.—Test station command system.

The standby 300 watt transmitter and duplicate monitoring facilities provides a high order of confidence that the commands can be sent and verified.

Command Encoder

The command encoder (see Figure 2–15) was manufactured by Consolidated Systems Corporation for NASA. It is a versatile unit with modular construction capable of generating all commands. As used in the Relay Test Stations, it is equipped with a 5.451 kc tone-generating tuning fork, accurate to 0.005 percent. The output tone signal is used to modulate the transmitter. Contacts to start the strip chart recorder and to key the transmitter automatically are provided.

Command 3 KW Transmitter

The Command Transmitter (see Figure 2–16) is a model HC–300 built by Hughes. It is rated at 3 kw output at 150 Mc, amplitude modulated. The unit is crystal controlled with a temperature stability of 1 part per million per day over the temperature

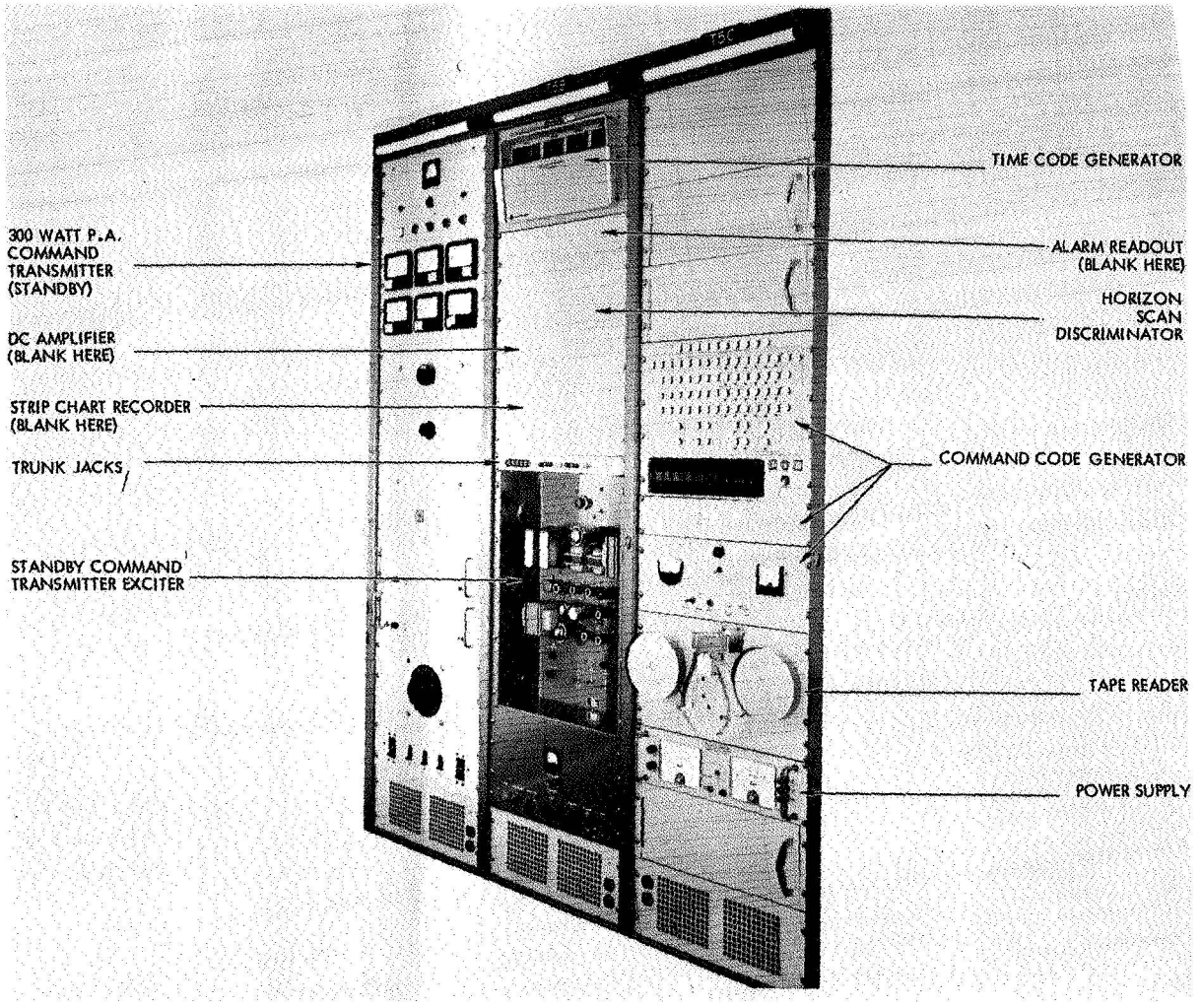


FIGURE 2–15.—Command system equipment racks.

range of 32 to 90°F. A crystal oscillator is followed by a tripler, a doubler, and another tripler to arrive at the final frequency of about 150 Mc. A push-pull driver precedes the single-ended neutralized 4CX300A output state. A four-stage audio amplifier drives the push-pull Class AB 4–100A modulator tubes.

300 Watt Standby Transmitter

The 300 watt transmitter was assembled by Radiation at Stanford (see Figure 2–15). The exciter unit was manufactured by Wilcox Electric and contains the crystal oscillator and multiplier stages. It develops 50 watts for driving the 300 watt power amplifier. This transmitter is used as an emergency unit in case of failure of the 3 kw regular unit.

Command Antenna

The command antenna (see Figure 2–9) is a part of the antenna mount provided by TACO; telemetry antennas are included. It is a circularly polarized yagi with 14.3 ± 1 db gain, designed for 150 Mc operation at 3 kw; antenna beamwidth is 30 degrees at the 3 db points.

Monitoring Facilities

Reference to the command system block diagram (Figure 2–14) shows that all

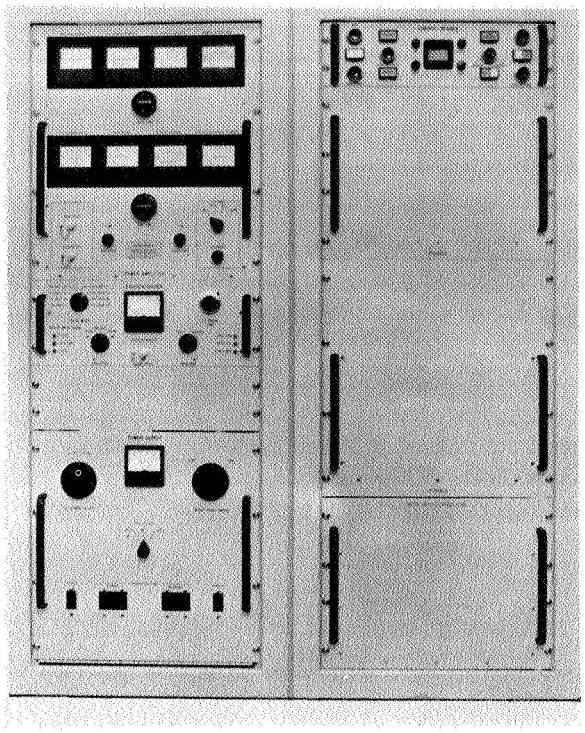


FIGURE 2–16.—Command transmitter.

mand codes are recorded in two ways in order to permit verification of the codes sent. Tones are rectified in one case and are recorded on the strip recorded. In the other case, the pulsed 5451 cps tones are recorded on one track of the magnetic tape recorded.

Operational Experience

As originally operated with a 300 watt transmitter, the command system was able to command the spacecraft correctly except at times when the spacecraft was low on the horizon and at long radio ranges. The maximum radio ranges had increased from the original 5,000 nautical miles to 7,000 nautical miles due to last minute changes made in the planned spacecraft orbit. This change amounts to almost 3 db in received signal level. An STL study indicated that at low elevation angles problems with multipath transmission can reduce drastically the signal received at the spacecraft. Additionally, all things being equal, there were indications that there was a 20 percent probability that at such an angle (below 10 degrees elevation) the satellite spin axis would be oriented in such a position as to cause a 10 db degradation in the received signal. Accordingly, a 3 kw transmitter was installed to raise the signal 10 db above the original level. Command reliability has improved considerably since this change was made. However, at elevation angles above 10 degrees and at radio ranges up to 5,000 nautical miles, 300 watts is adequate.

WIDEBAND COMMUNICATIONS TRANSMITTER SYSTEM

General

The principal task of the Relay satellite is to demonstrate the capability of providing communication functions. A conventional way of accomplishing this is to provide a radio path by which means a "baseband" can be carried. It has become an accepted technique to provide a bandwidth suitable for TV transmission or for frequency division multiplex telephony. The multiplex, in turn can accommodate telephone, teletype, data, or facsimile. Newer techniques permit high speed data over 48 kc channel groups. The Relay satellite system has all these capabilities. A video bandwidth usable to about 5 Mc is available through the complete system of satellite and test stations.

The 10 kw communications transmitter is capable of wideband FM modulation similar to a conventional microwave repeater except that greater FM deviation is used. This results in an improved signal-to-noise ratio, but requires the use of special low threshold techniques in reception such as BTL's feedback or STL's phase-lock demodulators.

Transmission to the satellite is at 1725 Mc, at approximately 5.5 Mc deviation. Deviation is tripled to 16.4 Mc and the frequency is translated to 4170 Mc in the satellite.

10 KW Power Amplifier*

A block diagram of the wideband communications transmitter is shown in Figure 2–19. The power amplifier and heat ex-

*See Figures 2–17 and 2–18.

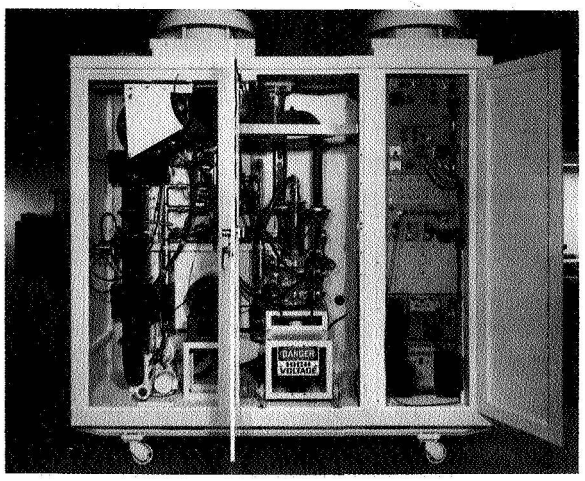


FIGURE 2–17.—10 kw transmitter.

changer were developed by Radiation-at-Stanford. The transmitter uses the Eimac 5 KM70SF high power klystron.

By stagger tuning the klystron (which is inherently a narrowband device), it was possible to achieve a bandwidth of ± 7 Mc flat within 1 db as shown in Figure 2–20. The photograph at the left was taken with the wideband transmitter operating at a level of 10 kw into the dummy load. Reflected energy was less than 100 watts. Sweep width is approximately 14 Mc. The photograph represents the variation of the transmitter output power across the passband. The photograph at the right was taken with the wideband transmitter operating at a level of 10 kw into the antenna.

At the Nutley Station an RCA translator is used to convert from 74 Mc to 1725 Mc; at Mojave a similar function is provided by a Radiation-at-Stanford design. Power level out of the TH deviator is approximately +12 dbm. The output of the RCA translator is between 10 and 15 watts, and is attenuated to approximately 0.5 watts to drive the final stage. An isolator prevents antenna impedance discontinuities from affecting klystron performance. An harmonic filter reduces second and higher order harmonics to a nonobjectionable level. Forward and reverse power level meters permit proper adjustment and, in conjunction with thermometers, flow meters and the dummy load, permits output power to be determined.

The FM Modulator

Generation of the frequency modulated signal, with which the translator and 10 kw power stage are driven, is accomplished by the Western Electric TH deviator. This unit has been adapted to the Relay Satellite System for test station use with minor modifications. Required in the Relay system, 5.5. Mc (peak - to - peak) deviation is obtained by slightly decreasing the feedback in the video amplifier. This results in high-index FM modulation in the downlink, since the deviation is tripled in the spacecraft. (See Figure 2–21.)

The TH deviator receives a baseband signal from a 124-ohm balanced line and delivers a frequency modulated signal to the 10 kw microwave transmitter. The frequency modulated signal is centered about 74.130 Mc. As shown in Figure 2–22, the input signal is amplified in a video amplifier, and is used to modulate a klystron operating at 6174.1 Mc. Output of this klystron and a beating klystron operating at 6100 Mc are combined in a converter from which the difference frequency of 74.1 Mc is obtained. This 74.1 Mc signal is amplified in an IF amplifier to the level required for delivery to the microwave transmitter.

Through a splitting pad and a second IF amplifier, the converter output is also fed to automatic frequency control circuits which compare the beat frequency and the output of a 74.1 Mc reference oscillator at a 30-cycle rate. Correction voltages from a synchronous detector are applied to the beating klystron to keep the IF center frequency within limits. See Table 2–5 for TH deviator performance.

COMMUNICATION RECEIVER SYSTEM*

General

Since the Relay satellite is spin-stabilized,

*For a detailed description of this receiving system, see "GSFC Relay Test Station Wideband Receiving Subsystem" Chapter 3.

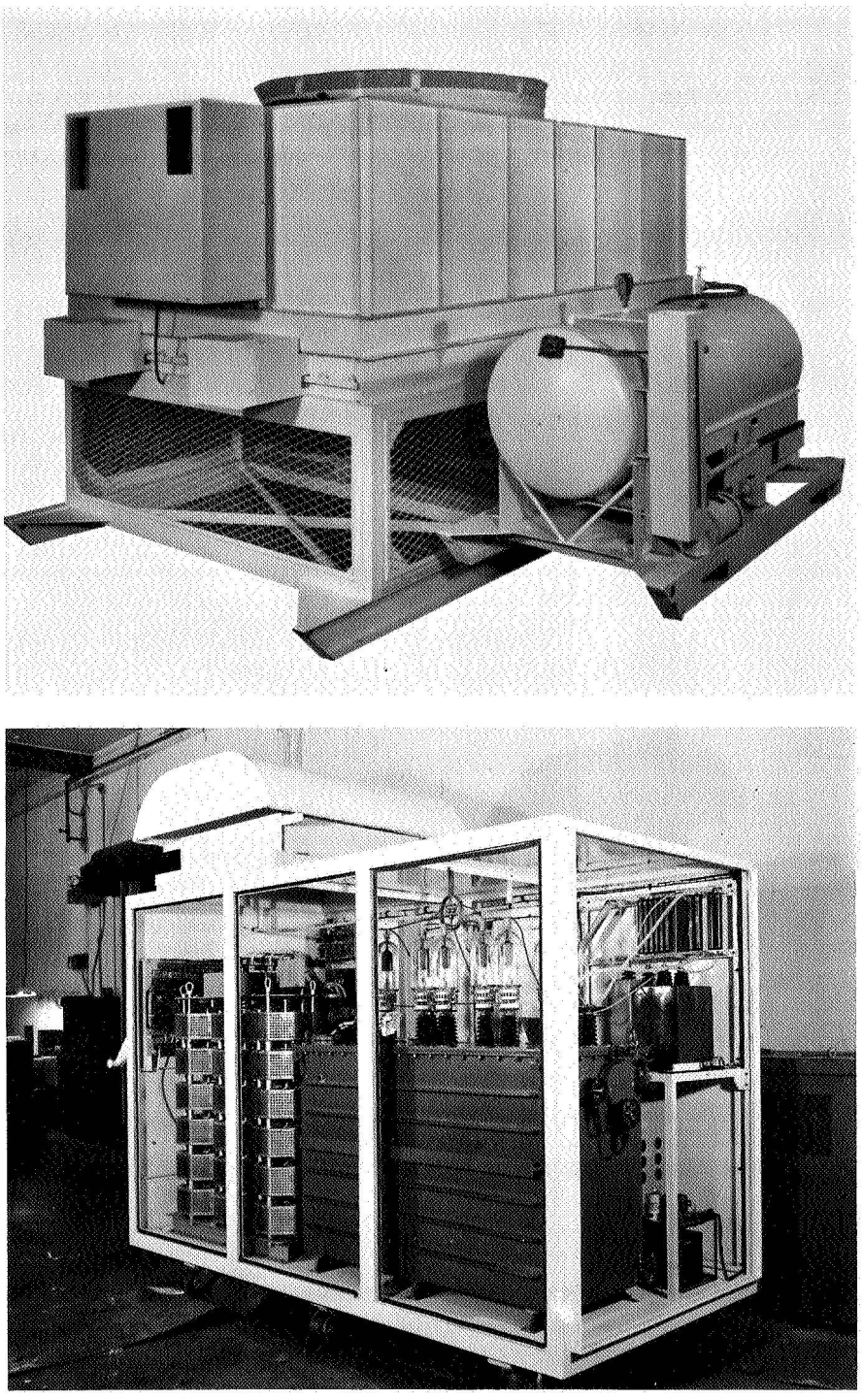


FIGURE 2–18.—10 kw transmitter, heat exchanger, and power supply.

it uses an omnidirectional antenna. Consequently, with the spacecraft transmitter power limited to 10 watts, the signals received at a range of 7000 nautical miles are extremely weak. Because of the wide bandwidth required for television, the system

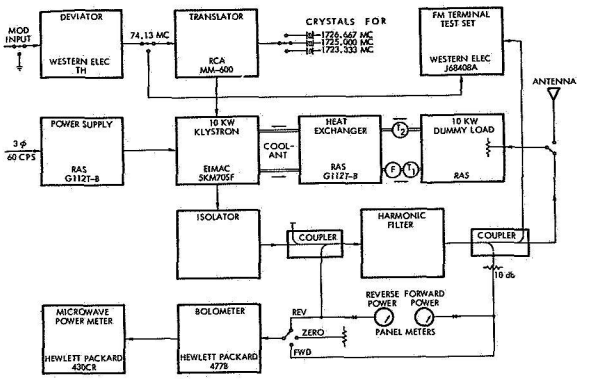


FIGURE 2–19.—10 kw communication transmitter, block diagram.

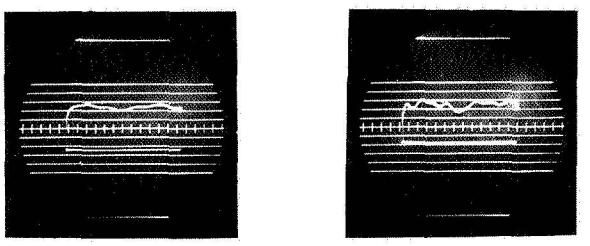


FIGURE 2–20.—10 kw transmitter passband characteristics.

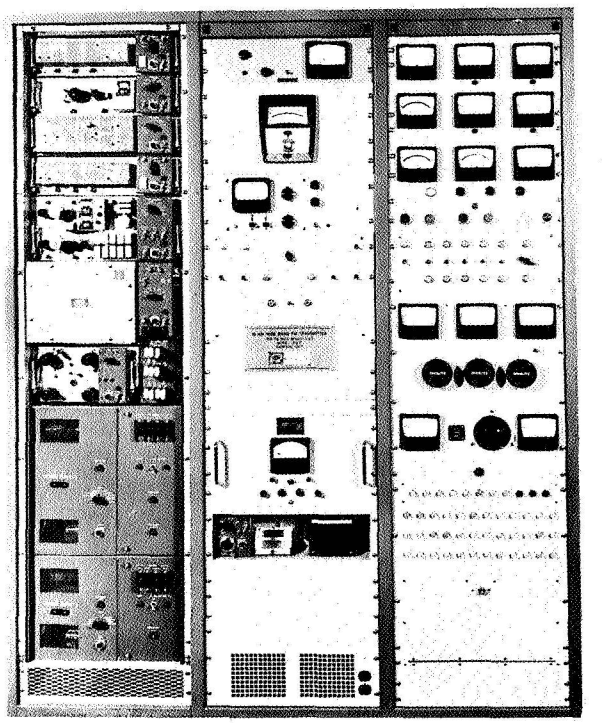


FIGURE 2–21.—Wideband transmitter control racks.

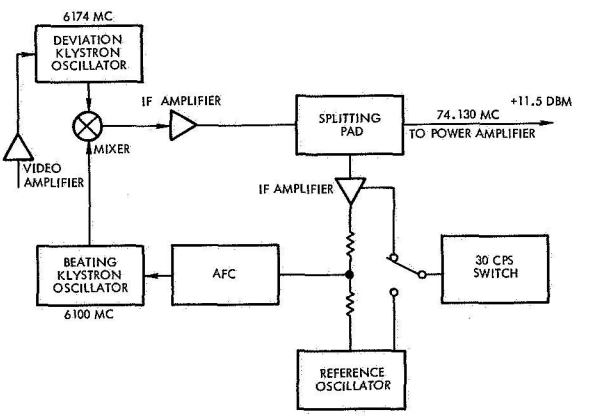


FIGURE 2–22.—Western Electric TH deviator.

noise of a conventional ground receiver would be prohibitively high. Despite the use of large steerable parabolic antennas (40-foot dishes in the case of the test stations), system improvements were still required. Two advanced techniques were used by STL in the design of the test stations to provide performance beyond that obtainable with ordinary microwave receivers.

First, a low noise microwave amplifier was designed utilizing a nitrogen cooled parametric amplifier, followed by a TWT RF stage. Secondly, a threshold lowering phase-locked FM demodulator concept was developed, and used with high modulation index FM. Use of these two devices resulted in a receiver design which produced good TV pictures with receiver carrier power as low as –90 dbm.

The overall system is shown in Figure 2–23.

Parametric Amplifier

The communications receiver uses a non-degenerate varactor diode, cooled parametric amplifier (Figure 2–24). It is typically tuned for a 20 to 25–Mc bandwidth with a gain of 15 to 18 db. Since the parametric amplifier is located on the feed assembly of the 40-foot

TABLE 2–5.—*TH Deviator Performance*

Video frequency characteristics	
Input impedance	124 ohms balanced
Video signal input (synchronizing pulse negative)	0 db
Video amplifier voltage gain (nominal)	15 db (modified)
Video amplifier gain range	10 db
Video amplifier bandwidth at 0.1 db points	A few cycles to 10 Mc
Video amplifier output	5.5 volts peak-to-peak (corresponds to approx 8-Mc deviation)
FM generator characteristics	
Deviation oscillator, nominal frequency	6174 Mc
Beating oscillator, nominal frequency	6100 Mc
Type of modulation	Frequency
Deviation oscillator modulation sensitivity.	Approx 1.45 Mc (modified) per volt
Normal frequency deviation	±4 Mc (modified)
74 Mc characteristics	
Intermediate frequency	74.13 Mc
TRS IF amplifier input	−9 dbm
TRS IF amplifier output	+12.2 dbm
IF output	+11.5 dbm
Bandwidth (0.1 db points)	64 to 84 Mc
AFC characteristics	
AFC IF amplifier input	−15.8 dbm
AFC IF amplifier output	−1 dbm (+2 dbm switched at 30 cycles)
Reference oscillator frequency	74.129 Mc
Reference oscillator output	−1 dbm (+2 dbm switched at 30 cycles)
AFC loop gain	36 db
AFC control	10 Mc shift to within 200 kc
Controlled oscillator	Beating oscillator in FM generator

antenna, it is remotely tuned and controlled. Noise temperature is largely determined by the fact that liquid nitrogen is used to cool the unit.

Traveling Wave Tube

Since the gain of the parametric amplifier is only 15 db, additional noise would be added to the system if low-noise circuitry were not also used following the paramp. A commercial TWT is used as an RF amplifier to provide another 36 db of gain, with bandwidth

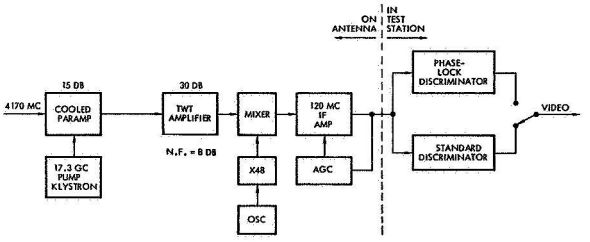
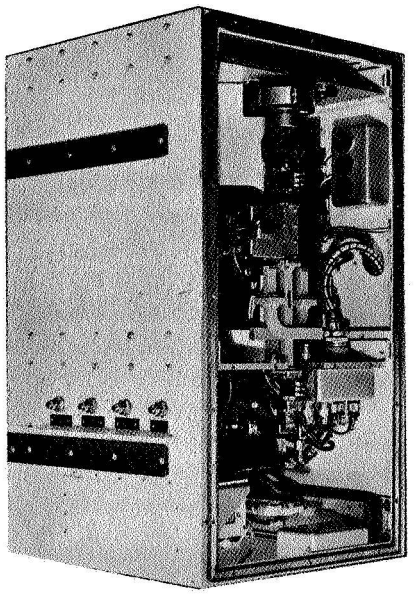


FIGURE 2–23.—Low noise wideband communication receiver system.



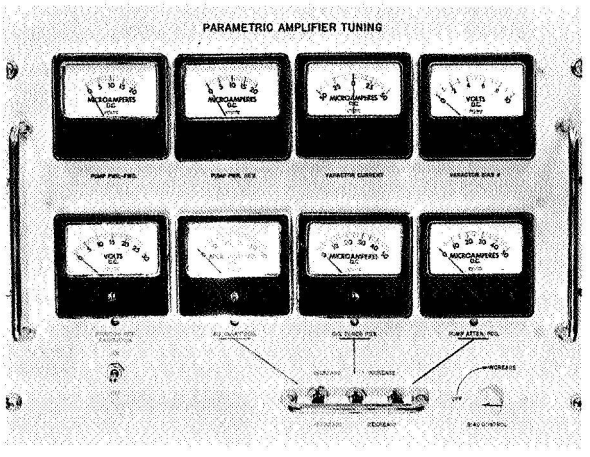


FIGURE 2–24.—Parametric amplifier.

in excess of 60 Mc. Since this tube is selected for low noise and has sufficient gain, the following circuits contribute very little to system noise.

Mixer-Oscillator-IF

The TWT is followed by a mixer-oscillator-IF assembly. The 4170 Mc signal from the TWT is mixed with the crystal controlled local oscillator to produce a 120 Mc intermediate frequency. This is amplified in a multistage stagger-tuned IF circuit. Resulting bandwidth is about 40 Mc (within ± 1 db over 20 Mc), and the signal is increased to approximately —7 dbm level. An AGC circuit holds the signal level to within 2 db.

Phase-Lock Demodulator

The phase-lock FM demodulator used in the Relay satellite system was developed by STL as an extension of techniques used for correlation detection in telemetry and Doppler-measuring systems. It has the capability of demodulating TV video signals and does so with a far better S/N ratio performance than a conventional discriminator. Familiar FM theory (see Figure 2–25) shows that S/N ratio improvement is obtained in FM which increases as the modulation index is raised. This is true as long as the signal is above a critical minimum. Below this point, the FM improvement vanishes rapidly. This threshold S/N ratio is taken as +9 to +12 db with classical limiter-discriminator circuitry. Unfortunately, as the bandwidth is increased the threshold moves up, so that stronger signals are required. With the phase-lock demodulator, the threshold is lowered as shown by the dotted lines in Figure 2–25, and thus the FM improvement can be realized at lower signal levels, or greater deviation can be used to provide a better S/N ratio with the same threshold.

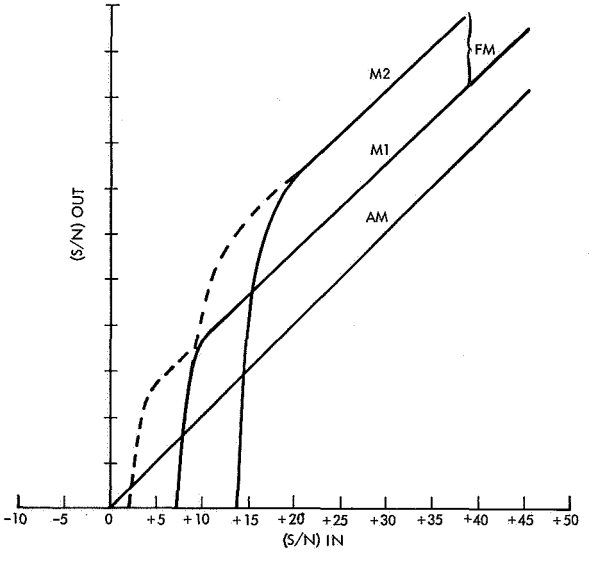


FIGURE 2–25.—FM signal-to-noise threshold effects.

For the television link, the demodulator was designed to meet the Relay system parameters. It was designed to accept a 120 Mc FM signal from the antenna mounted receiver circuits (at —7 dbm) with 16.4 Mc peak-to-peak deviation (video plus sync plus audio subcarrier), and to demodulate this signal into a 1-volt video signal with frequency components up to 3.2 Mc. In addition, the subcarrier frequency of 4.5 Mc (carrying the audio modulation) is also recovered, and is available as an output.

A block diagram of the demodulator unit is shown in Figure 2–26. The input IF amplifier includes a delay equalizer adjusted to correct for the overall system. The phase-lock demodulator section consists of three basic units: VCO, a phase detector which senses the phase error between the incoming signal and the VCO, and a baseband filter-amplifier which drives the VCO into phase synchronism.

Communications Receiver System Performance

The communications receiver system has been found to have the following nominal performance:

RF bandwidth (at 3 db points)	= 25 Mc
Noise bandwidth	= 32 Mc
Receiver noise temperatures	= 120°K
Deviation acceptance	= 16.4 Mc p–p
Video bandwidth (3 db)	= to 3.2 Mc

Video + sync signal level = 1 volt p–p
Audio subcarrier output = 4.5 Mc at 0.65 v

Performance of the phase-lock demodulator is difficult to evaluate precisely, but it has been found in subjective tests that the picture quality is equivalent to that of a conventional discriminator having a 5 db higher S/N ratio.

VIDEO SYSTEM

Each subsystem of the wideband equipment is normally subjected to individual tests, but the only way it can be determined that the entire system design is capable of coping with the potentially changing parameters of the satellite is to conduct overall system performance tests. Since the transmission path losses vary rather rapidly during a satellite orbit and also between passes, it is desirable to perform the tests in rapid sequence. Suitability of the system can therefore be determined almost instantly, and since these tests are repeated routinely, long-term analysis of the data is possible. The wideband receiver and transmitter systems have been designed to transmit TV and these will also satisfy communications requirements for telephone, telegraph, facsimile, or data. Since TV transmission provides a satisfactory overall test of the baseband response, a rapid checkout system was designed to perform a number of video tests.

A semi-automatic test feature is employed. Figure 2–27 shows the Nutley video console with the test selector switch. For each position of the switch, the correct modulating source is connected to the TH deviator, and the correct monitoring equipment is connected to the demodulator. Also, changes in oscilloscope sensitivity and sweep rates are made automatically.

Table 2–6 lists the wideband system performance experiments available at the Nutley test station. With the semiautomatic test feature, a given sequence of experiments can

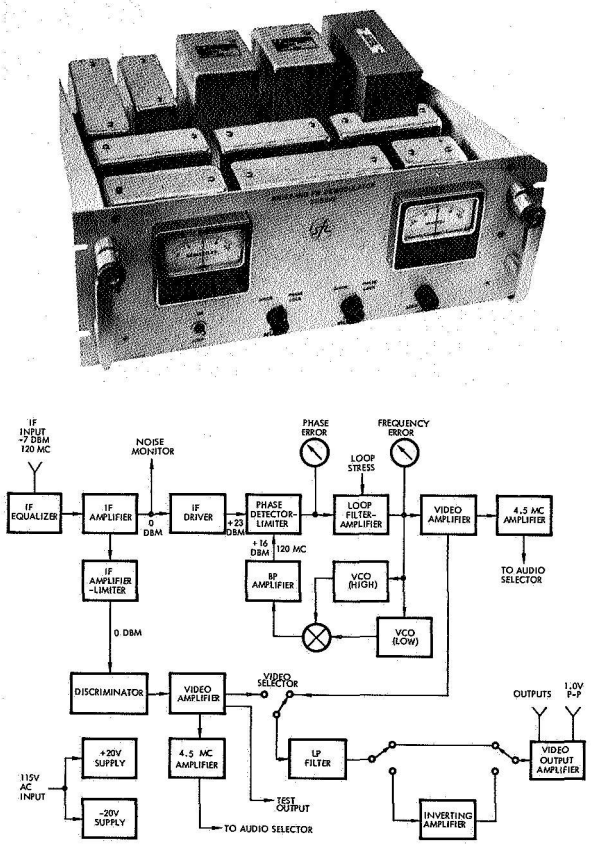


FIGURE 2–26.—STL wideband phase-lock demodulator.

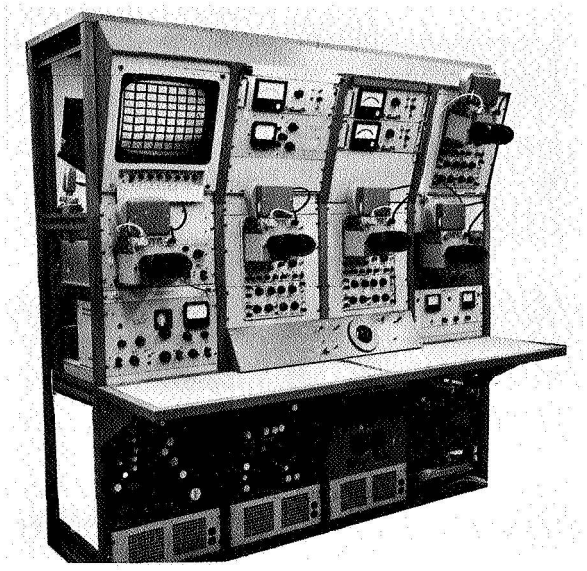


FIGURE 2–27.—Video test console (Nutley).

TABLE 2–6.—*Wideband Experiment List*

Insertion gain stability tests	*Linear waveform distortion tests*
Audio	Field time distortion
Composite video	Line time distortion
	Short time distortion
Noise measurements	
Continuous random noise—video	*Steady state characteristics*
Continuous random noise—audio	Bandpass characteristics
Impulsive noise—video	
Impulsive noise—audio	*Received carrier power*
Periodic noise—video	
Periodic noise—audio	*Television tests*
Fluctuation noise	Test pattern
	Slides
Non-linearity distortion tests	
Line time nonlinearity	
Audio distortion	

be performed in approximately 3 minutes.

Equipment consists of generators to produce the various test patterns, and the oscilloscopes, cameras, spectrum analyzers, RMS or peak reading voltmeters, noise weighting filters, and a video monitor. (See Figure 2–28.)

Operationally, for any given experiment, the test position is selected on the switch. The outgoing signal is photographed on one oscilloscope and the return signal is photographed on another. The two photographs are then compared visually against calibration made earlier.

Ultimate tests, of course, are performed through the satellite, but in order to perform maintenance, and determine limitations of various equipment, it is desirable to "close the loop" in other ways. A spacecraft simulator duplicating the wideband and beacon systems in the satellite is provided at each station. The simulator is either mounted on a boresight tower for a true simulation, or connected into the equipment between waveguide couplers. Other loops are provided to eliminate the need for operation of all high power equipment to isolate problems. It can be seen in Figure 2–29 that a loop, including all video equipment but excluding the wideband transmitter and majority of the receiver, can be activated by operating SW5. The test generator was developed by STL, and uses a linear VCO in which noise in varying amounts can be mixed. A true test of the phase-lock demodulator and video equipment is thereby achieved. This loop also permits evaluation of the audio subcarrier subsystem and video pre-emphasis/de-emphasis networks. Video equipment baseband testing can be performed by operation of SW1, SW2, and SW3 or SW4.

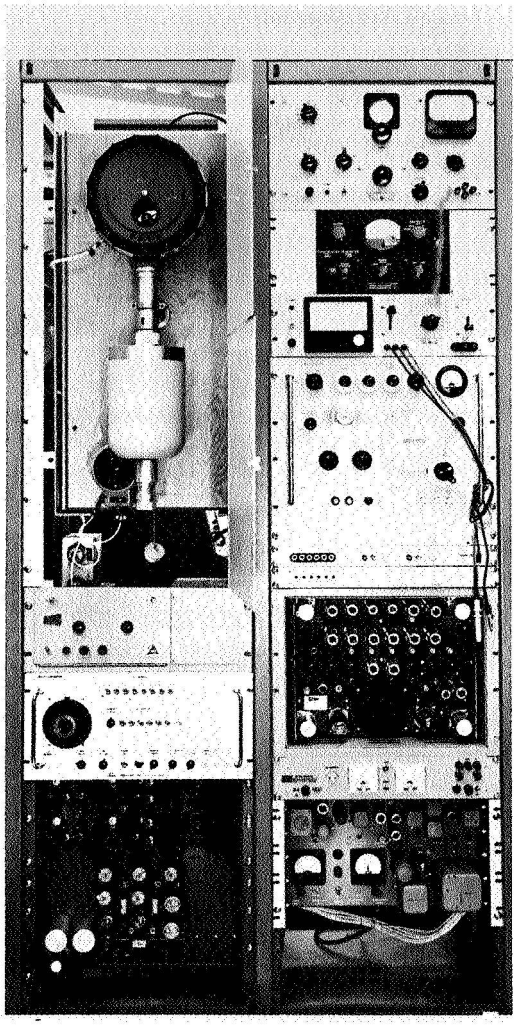


FIGURE 2–28.—Video test equipment.

Television equipment used in the Test Stations is all designed to operate at the American standard of 525 lines, but because of the requirement to transmit the audio subcarrier at 4.5 Mc in the baseband, the video response is limited to 3.2 Mc (3 db

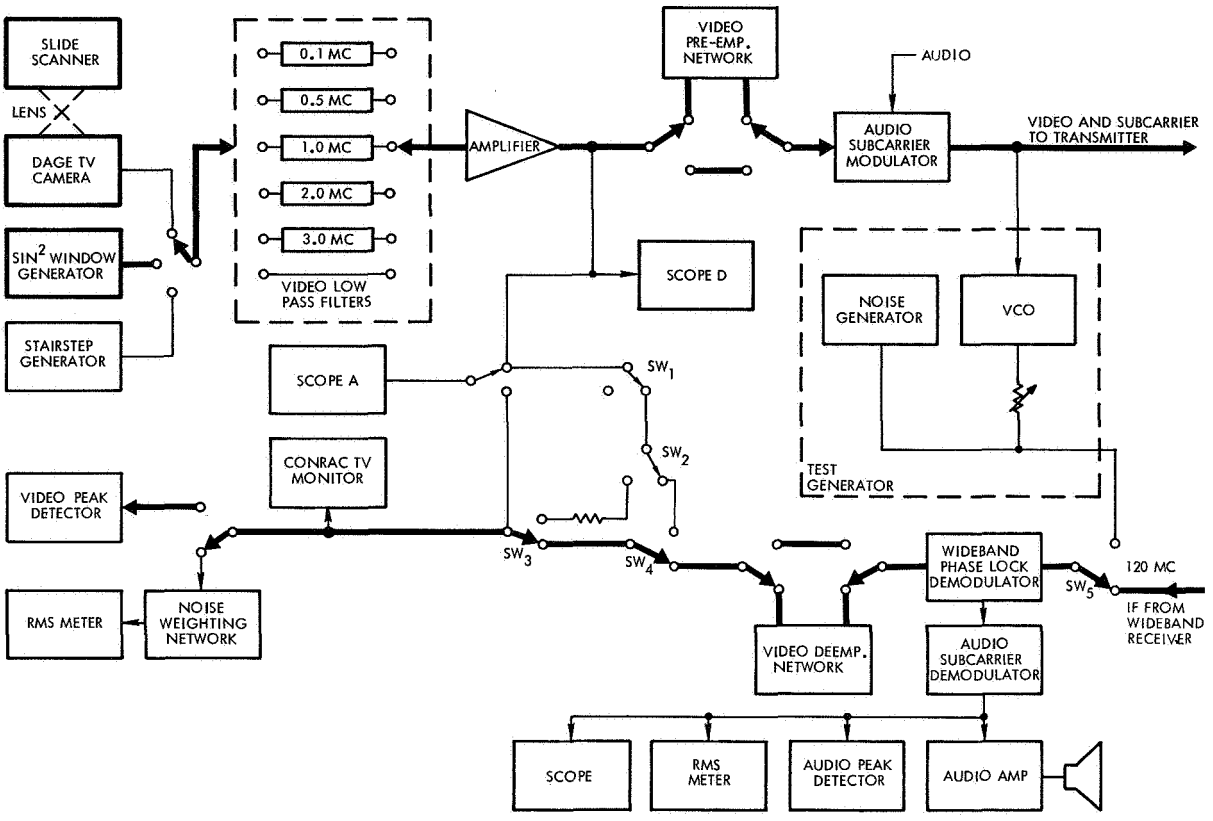


FIGURE 2–29.—Video test console, block diagram.

point) instead of the 4.3 Mc normally transmitted for 525 lines.

When the various tests (shown in Table 2–6) are conducted they may be transmitted through any of four possible transmission loops with relatively minor differences in results, providing that the system is operating properly. Some typical results are shown in the following pages. In order to recognize the different conditions, the loops have been identified as follows:

Loop 1: Baseband-to baseband

Loop 2: Test generator to IF

Loop 3: Through the spacecraft simulator

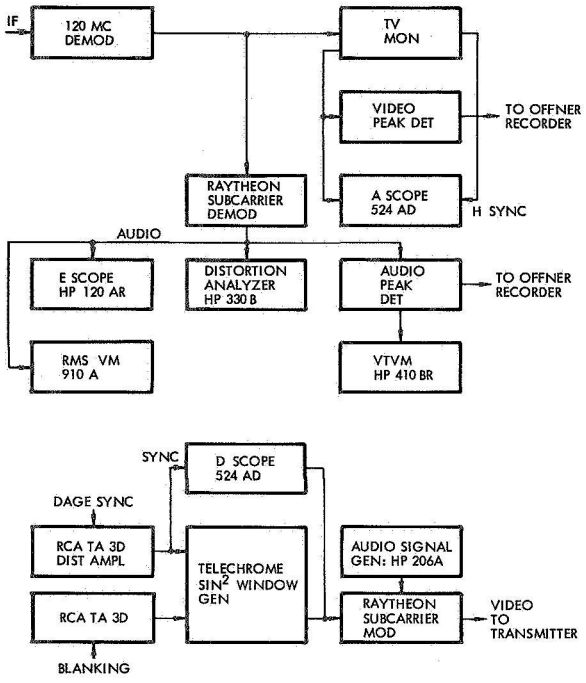
Loop 4: Through the spacecraft itself.

Each test result shown is preceded by a block diagram showing the test equipment configuration as selected by the rotary switch. The positions available are shown in Table 2–7.

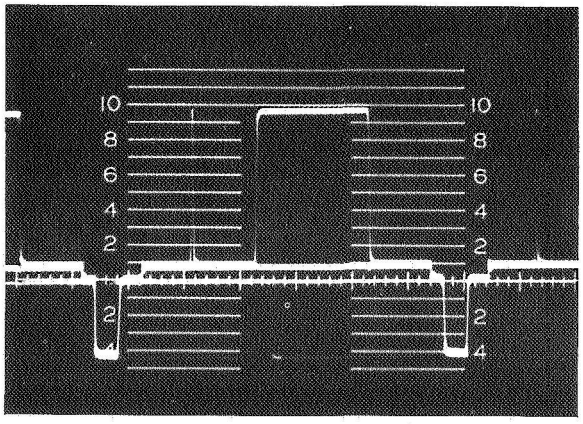
Many of the tests are noise measurements; these and other tests are not listed here, since this report was not intended to provide detailed test results.

TABLE 2–7.—*Test Positions for WBCS*

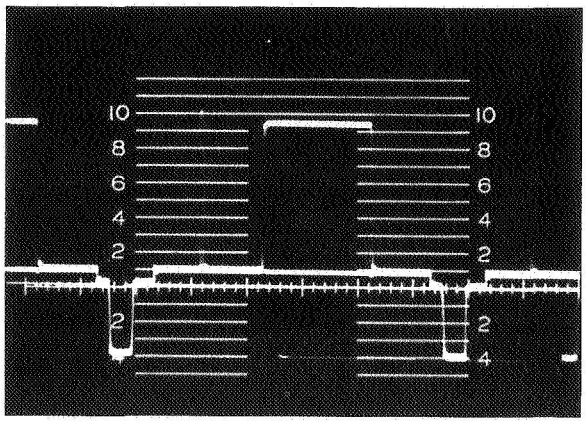
Position	Test
1	Insertion gain—line time nonlinearity 2T
2	T pulse
3	2T
4	Continuous random noise
5	TV test slides
6	½ black, ½ white
7	Line time nonlinearity diff
8	Stair-step
9	Baseband sweep
10	Envelope delay—baseband
11	Sync nonlinearity every 5th line
12	Periodic noise—look with Krohnhite
13	Impulsive noise
14	Baseband segment— 70 kc
15	" " 534 kc
16	" " 1.248 Mc
17	" " 2.938 Mc
18	--------



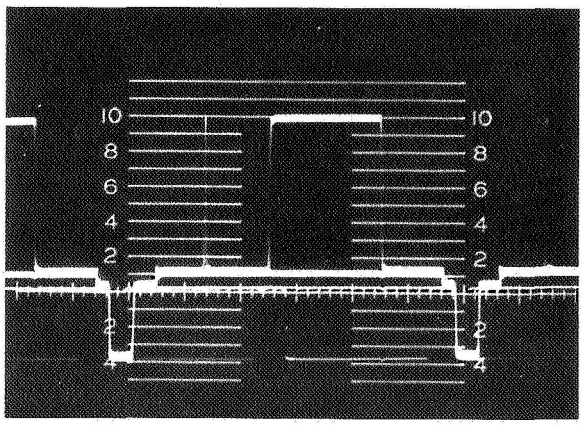
"Video Test Console - Switch Position 1 Interconnections for Insertion Gain-Line Time Distortion"



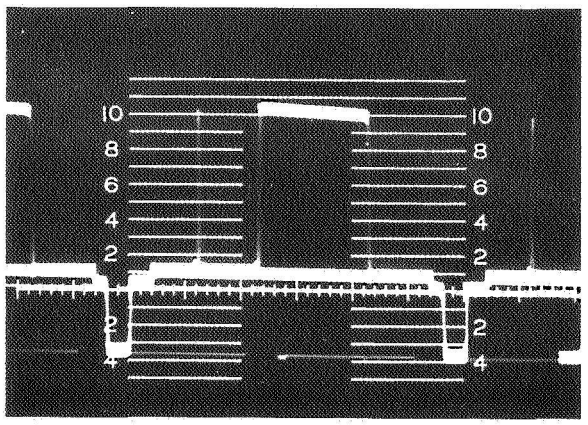
Oscilloscope D
Loop # 1
Position # 1



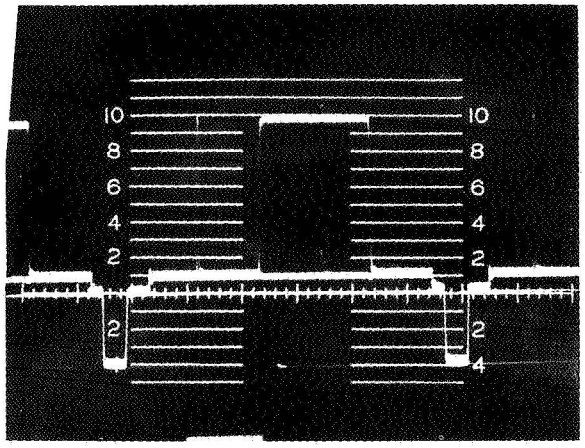
Oscilloscope A
Loop # 1
Position # 1



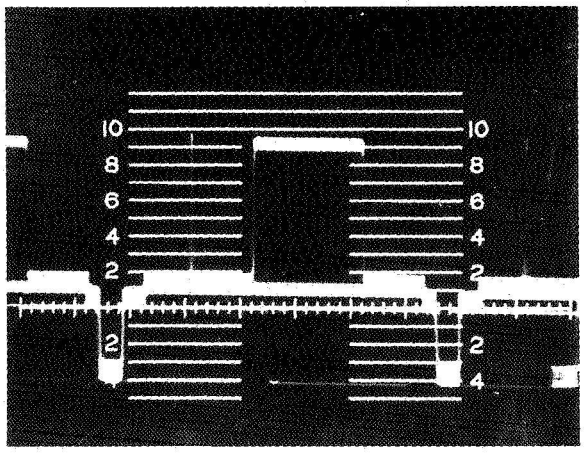
Oscilloscope D
Loop # 2
Position # 1



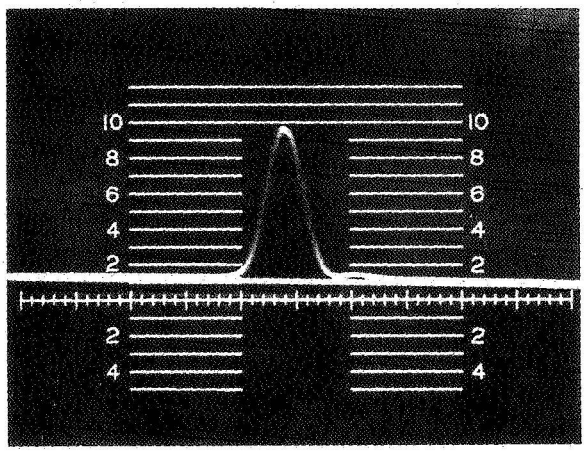
Oscilloscope A
Loop # 2
Position # 1

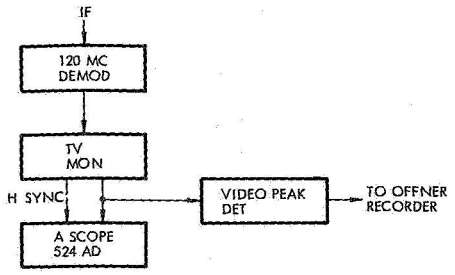


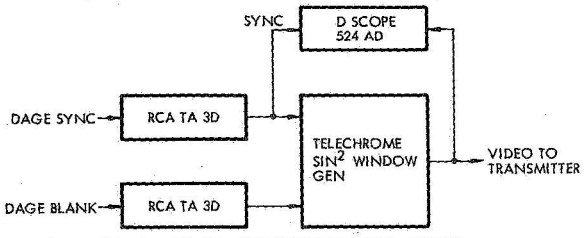
"Oscilloscope D
Loop #3
Position 1"



Oscilloscope A
Loop #3
Position 1

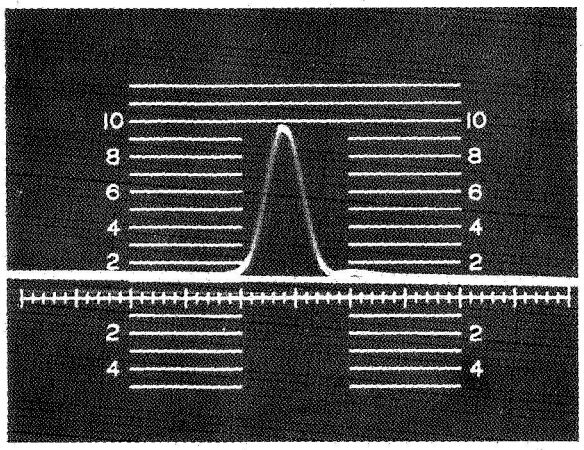




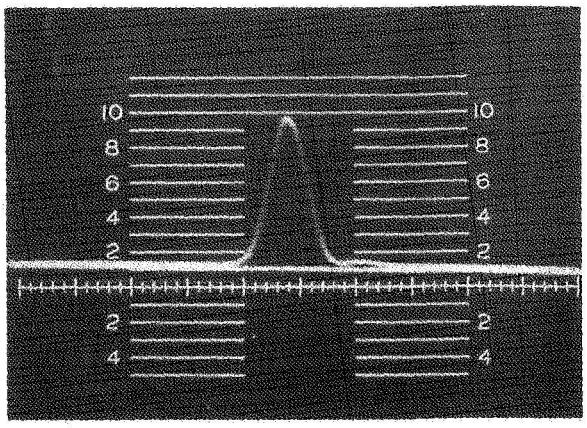


POSITION NO. 2 SHORT TIME DISTORTION - T PULSE
POSITION NO. 3 SHORT TIME DISTORTION - 2T PULSE

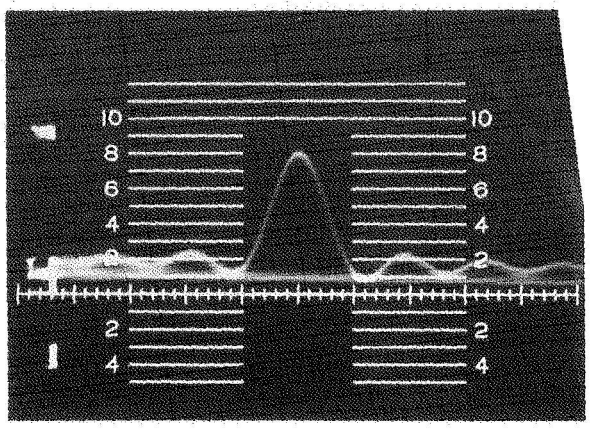
"Video Test Console - Switch Position No. 2, Short Time Distortion (T Pulse) and Position No. 3 - 2T Pulse



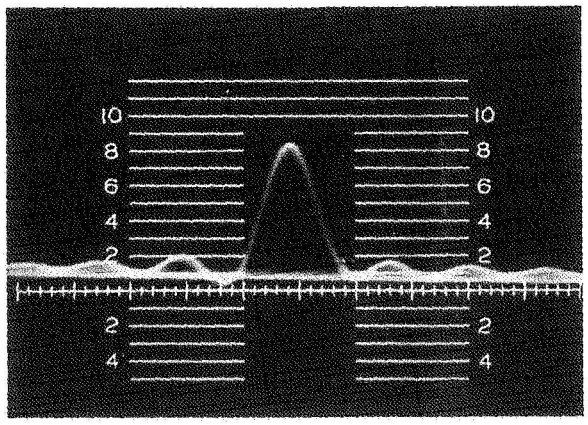
"Oscilloscope A
Loop No. 1
Position 2"



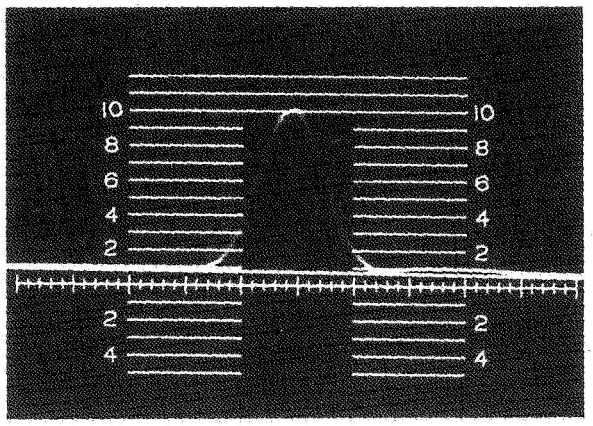
Oscilloscope D
Loop # 2
Position # 2



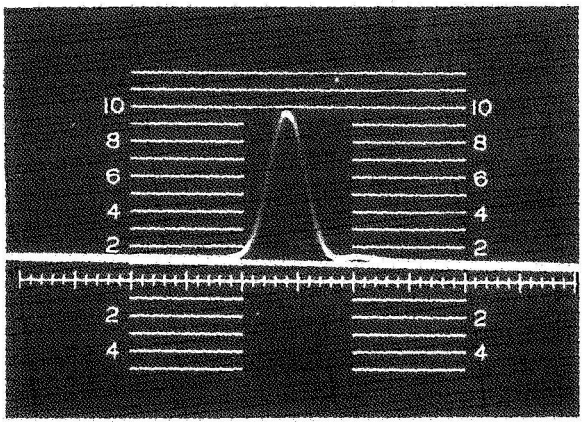
Oscilloscope A
Loop # 3
Position # 2



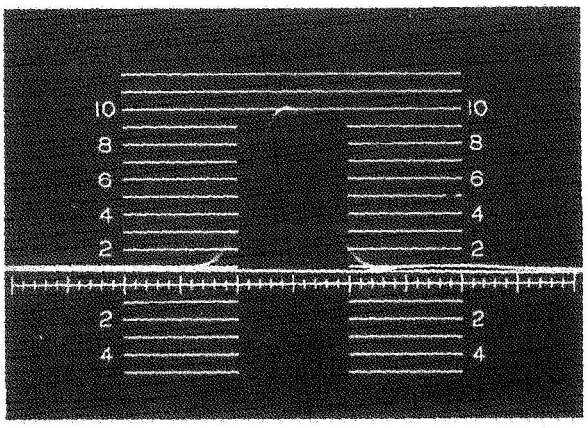
Oscilloscope A
Loop # 2
Position # 2



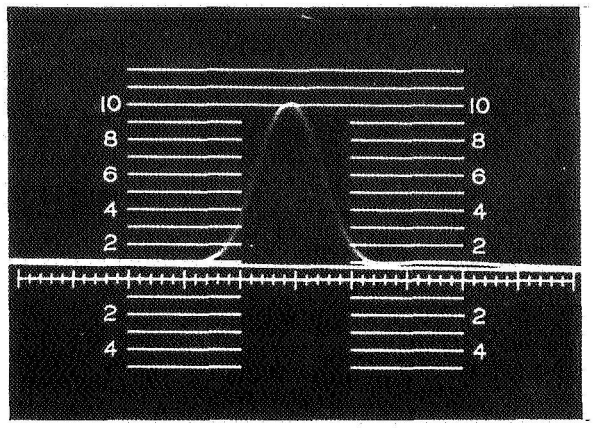
Oscilloscope D
Loop # 1
Position # 3



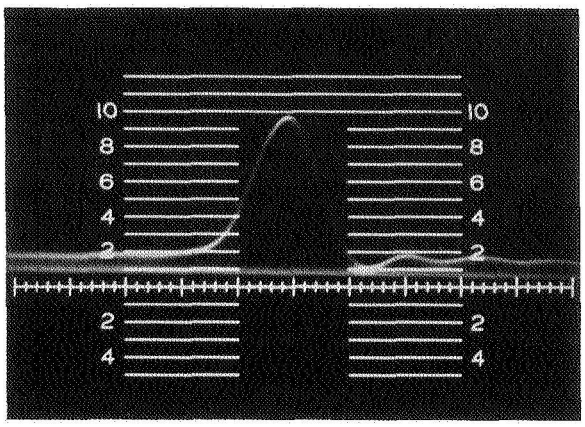
Oscilloscope D
Loop # 3
Position # 2



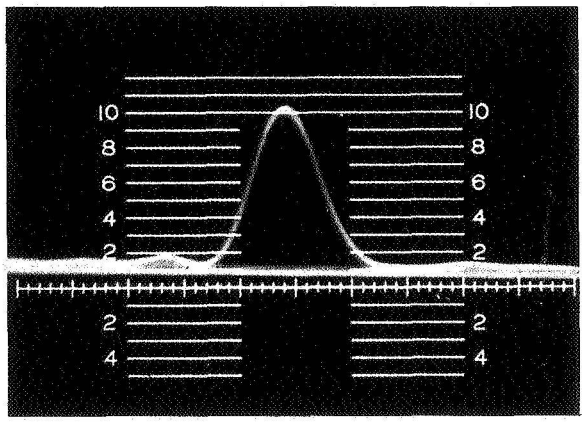
Oscilloscope A
Loop # 1
Position # 3



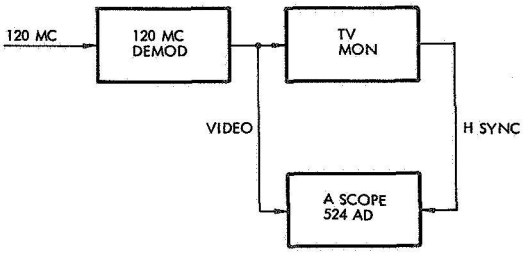
Oscilloscope D
Loop # 2
Position # 3

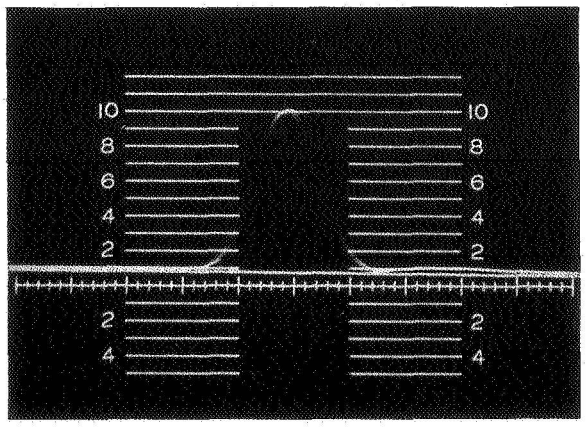


Oscilloscope A
Loop # 3
Position # 3

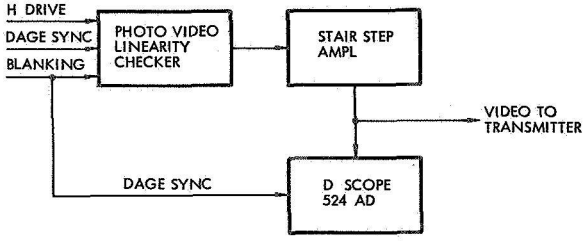


Oscilloscope A
Loop # 2
Position # 3

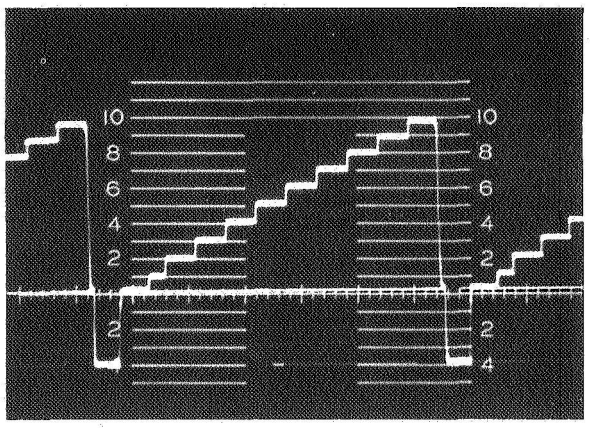




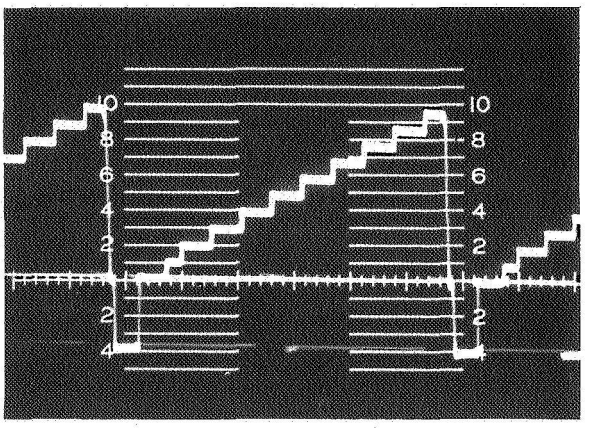
Oscilloscope D
Loop # 3
Position # 3



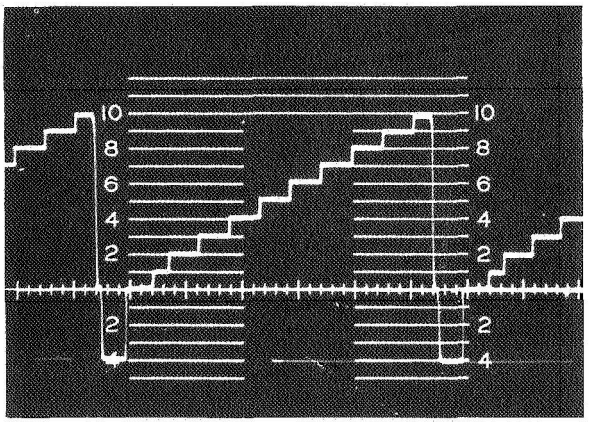
POSITION NO. 8
LINE TIME NONLINEARITY-STAIR STEP



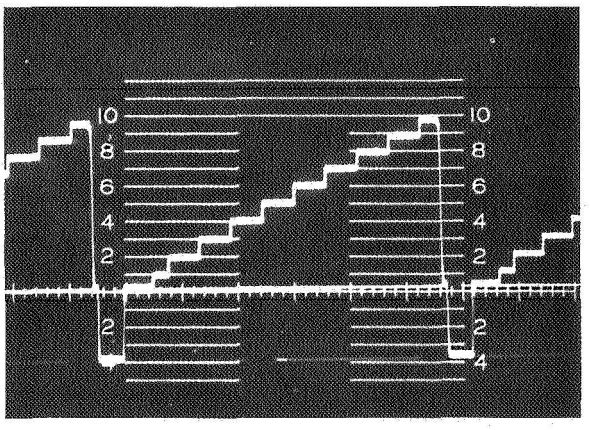
Oscilloscope D
Loop # 1
Position # 8



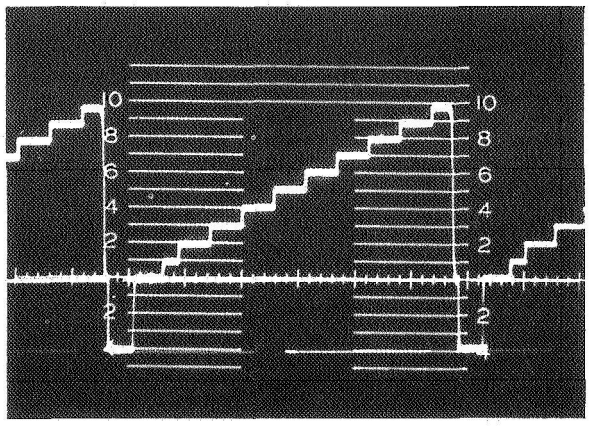
Oscilloscope A
Loop # 2
Position # 8



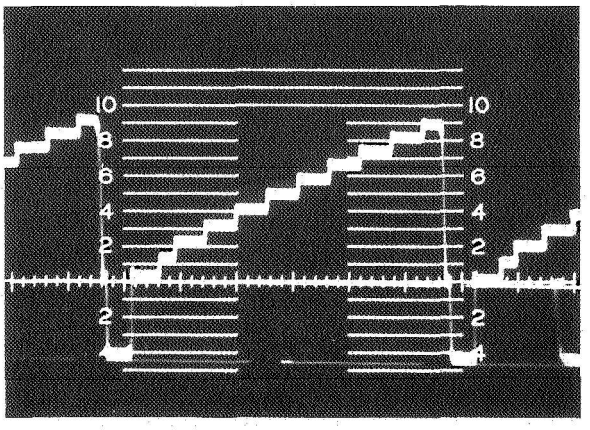
Oscilloscope A
Loop # 1
Position # 8



Oscilloscope D
Loop # 3
Position # 8



Oscilloscope D
Loop # 2
Position # 8



Oscilloscope A
Loop # 3
Position # 8

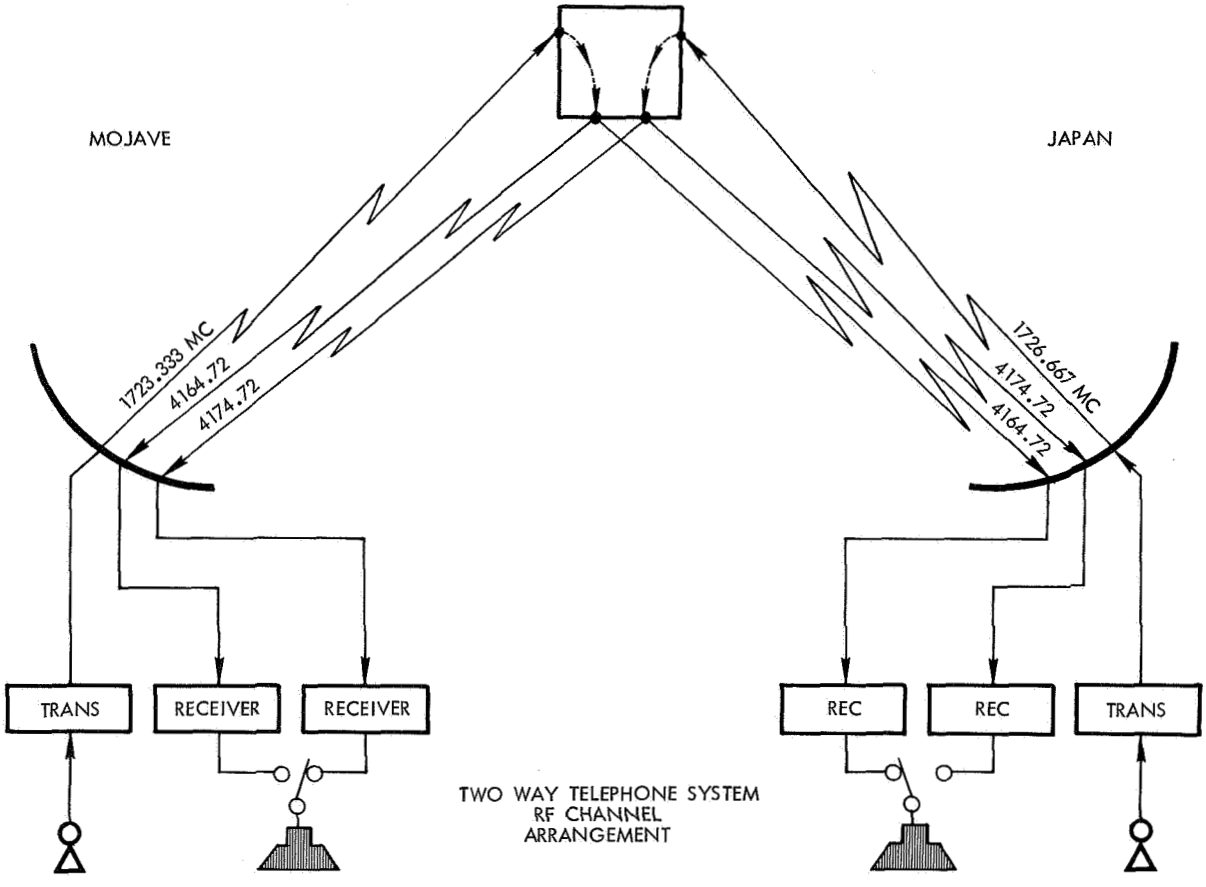


FIGURE 2–30.—Two-way telephone system RF channel arrangement.

FREQUENCY DIVISION MULTIPLEX TELEPHONE SYSTEM

General

The Relay satellite has a narrowband mode as well as a wideband mode, selectable by command. In the narrowband mode, filters are switched in to divide the wideband RF channel into two channels separated by 10 Mc (centered at 4170 Mc). Although these are called narrowband, the name is only proper in comparison to the wideband mode, since each narrowband channel is 2.0 Mc wide between the 3 db points, and can carry 24 or more telephone channels. The purpose of this feature is to provide two-way telephone capability by simultaneously repeating both sides of the conversation in separate RF channels. This is shown in simplified form in Figure 2–30.

The plan was for transmissions from East-to-West to use one RF channel (1723.333 Mc up) and for West-to-East transmissions to use the other one (1726.667 Mc up). Because of the tripling and translation in the spacecraft, this results in reception on the ground of East-to-West signals on 4164.72 Mc and reception of West-to-East transmissions on 4174.72 Mc. The resulting IF frequencies in the Test Station are 115 Mc and 125 Mc and by selecting one or the other, both transmissions can be monitored.

Multiplex

The multiplex equipment used at Mojave

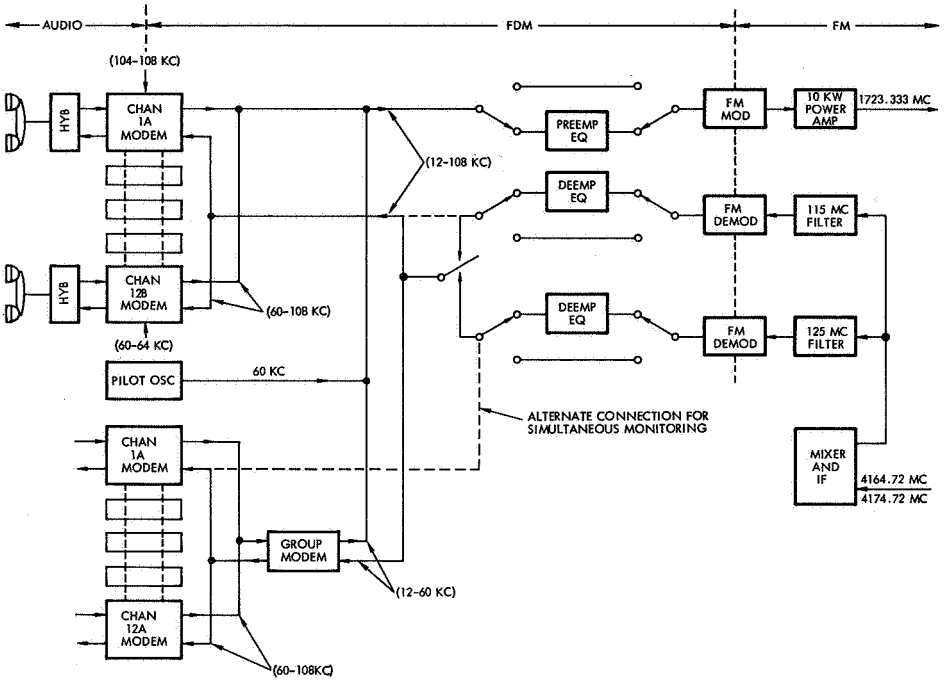


FIGURE 2–31.—Typical telephone multiplex and radio interconnection showing 24 channel connections.

(see Figure 2–31) was supplied by Collins Radio, Dallas Division and is their modified type MX106.

The telephone multiplex equipment is of the frequency division type, and translates the telephone channels in SSB form to the baseband frequency range of 12 to 108 kc. One group of 12 channels (CCIR Group B) occupies the range from 60 to 108 kc; another group of 12 is translated to the 12 to 60 kc region. A pilot frequency for synchronization is transmitted at 60 kc. This baseband then frequency modulates the transmitter carrier on one of the two RF frequencies, as previously explained.

This multiplexing scheme is in accordance with CCIR recommendations for standard microwave systems with the exception that greater FM deviations are used over the radio link. This high index FM is used in conjunction with frequency following FM demodulators to provide improved S/N ratio performance through the satellite repeater in the same fashion as is done for the wideband TV transmissions.

The telephone system parameters are shown in Table 2–8. Deviations and resulting bandwidths have been selected so that minimum FM threshold is achieved and result in a maximum of 50,000 picowatts of thermal noise in any telephone channel with threshold level signals.

Table 2–9 shows the communications link performance for a loop test through the satellite from the Mojave station. This applies for 12 channels of Group A or Group B telephone circuits. Performance on transmissions between Mojave and Japan will be better than that indicated, because the Japanese ground stations have larger antennas.

The multiplex equipment has an associated patch panel permitting rapid changes in configuration so that a variety of different arrangements can be tested. For example, two groups of 12 identical channels can be used on separate RF frequencies, or one whole group can be translated to the Group A baseband frequencies and used simultaneously with the other group to provide 24 channels on one RF channel.

TABLE 2-8.—*Telephone System Parameters*

	Ground-to-space		Space-to-ground	
	Group B	Group A	Group B	Group A
Baseband frequencies			60–108 kc	12–60 kc
Deviation for full load	521 kc p–p	389 kc p–p	1.57 Mc p–p	1.17 Mc p–p
Test tone at "0".	185 kc RMS	137 kc RMS	554 kc RMS	412 kc RMS
Deviation for 1 mw 800 cps at "0" rel lvl.	40 kc RMS	29.6 kc RMS	120 kc RMS	88 kc RMS
Receiver 3 db baseband width.			706 kc	403 kc
Receiver noise bandwidth			2.3 Mc	1.3 Mc
Bandwidth occupied.	737 kc	509 kc	1.79 Mc	1.29 Mc
RF frequencies East to West.	1723.333 Mc		4164.72 Mc IF=114.72	
RF frequencies West to East.	1726.667 Mc		4174.72 Mc IF=124.72	

NOTE: The spacecraft triples the deviation.

Instrumentation and Monitoring Facilities

In order to fulfill the primary purpose of the telephone facilities, test equipment is provided to perform communications experiments in accordance with established plans. These include the following tests:

Insertion gain
Noise measurements
  Random noise
  Impulsive noise
  Periodic noise
Bandpass characteristics
Envelope delay distortion
Intermodulation measurements with noise
Harmonic distortion
Crosstalk

The following test equipment is also included in one trailer.

Test Equipment

Ampex Model 1300 7-track recorder
Siemans Model Rel 3D 32d psophometer H meter
Siemans Model Rel 3D335 frequency selective voltmeter
HP Model 302A wave analyzer
HP Model 650A signal generator
HP Model 130BR oscilloscope
Marconi noise loading test set consisting of:
  TF1225A noise receiver
  TF1226B noise generator
  TM5774 bandstop filter unit
Fluke Model 910A RMS voltmeter

ANTENNA AND TRACKING SYSTEM

General

Both test stations utilize 40-foot, steerable parabolic antennas for transmission and reception of communications signals. Figure 2–32 shows the antenna at the Mojave test station.

The basic requirements for the antenna system at the test stations are:

1. Transmit the 1725 Mc wideband FM signal to the satellite.

2. Receive the 4170 Mc wideband FM signal from the satellite and couple this signal to a cooled parametric amplifier with a loss not to exceed 0.7 db.

3. Point the antenna at the satellite during a satellite pass with an error of less than 0.05 degrees.

Maximum required angular velocity and acceleration are tabulated below:

$$\omega_{max} = 1°/sec$$
$$\dot{\omega}_{max} = 0.2°/sec^2$$

TABLE 2-9.—*Communication Link Performance* Mojave-Mojave*

12 voice channels, CCIR Group A or Group B

Noise performance in any channel referred to zero relative level
Thermal.....50,000 pw (psoph)
Intermodulation... 7,500 pw (psoph)
Total.....57,500 pw (psoph)

	Ground-to-spacecraft	Spacecraft-to-ground	
Frequency	1725 Mc	4170 Mc	
Modulation	FDM/FM	FDM/FM	
Transmitter power	10 kw	4 w	
Diplexer and cable loss	1 db	1 db	
Transmitter antenna gain	44 db	−1 db	
Space loss	179.4 db	187.1 db	
Ellipticity loss	1 db	1 db	
Receiver antenna gain	−1 db	52 db	
Receiver signal power	−68.4 dbm	−102.1 dbm	
Receiver noise density	−101.5 dbm/Mc	−115.8 dbm/Mc	
Group	A or B	A	B
Receiver noise bandwidth	2.3 Mc	1.30 Mc	2.29 Mc
Receiver noise power	−97.9 dbm	−114.7 dbm	−112.2 dbm
Predetection (S/N)	29.5 db	12.6 db	10.1 db
Threshold	12 db	7.4 db	7.4 db
Margin	17.5 db	5.2 db	2.7 db
Full load test tone at zero relative level		13.3 dbm	13.3 dbm
Probability of overload		$<10^{-5}$	$>10^{-5}$
Modulation-feedback receiver noise bandwidth		1.30	2.29 Mc
Modulation-feedback receiver 3 db basebandwidth		403	706 kc

$$K = \left[N^2 \frac{\Phi_s}{S_s} + \frac{\Phi_g}{S_g}\right] = \left[4.36 + 42.6\right] \times 10^{-3} = 47.0 \times 10^{-3} \frac{\text{rad}^2}{\text{Mc}}$$

*At extreme spacecraft range (7000 nmi) and 7.5° elevation angle

The remainder of this section will describe the Mojave antenna system. The Nutley antenna is functionally similar to the Mojave antenna except as noted at the end of this section.

Mojave Antenna System

The antenna consists of:

1. A 40-foot diameter reflector.
2. An X–Y mount for the antenna.
3. A feed support.

The reflecting surface is a paraboloid of revolution of doubly curved solid aluminum sheet panels. The design is such that RMS average deviation from the least square, best-fit paraboloid is intended not to exceed 1/16 inch. Antenna surface is independent of the supporting structure so that it may be separately adjusted. Focal length of the antenna reflector is 16 feet. Antenna mount

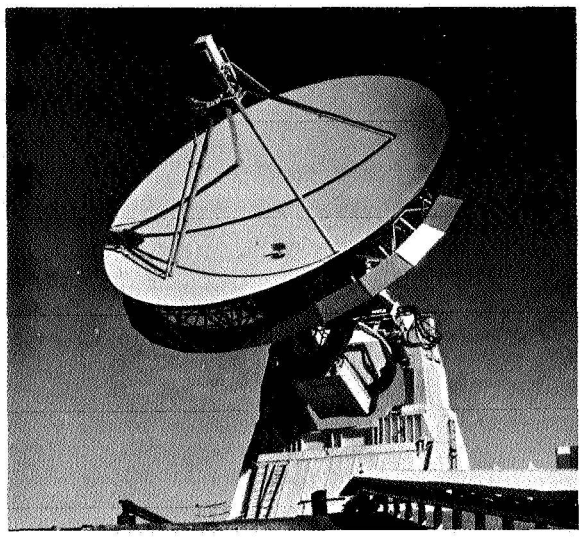


FIGURE 2–32.—Mojave test station antenna.

axes have the following properties:

1. Pointing accuracy is designed to be ± 144 seconds of arc
2. Axes are designed to be capable of tracking at rates from 0 to 1 degree per second with accelerations and decelerations up to 1.5 degrees/sec^2

The feed support is adjustable so that the feed center may be adjusted to be on the axis of the reflector to within ±1/32 inch. This support is intended to hold a weight of 500 pounds, and is not to deflect more than 3/64 inch axially or laterally in any antenna position at maximum antenna accelerations, under the influence of gravity or by wind velocities up to 45 mph.

X–Y Antenna Coordinate System

A brief discussion of the Mojave antenna X–Y coordinate system is in order. The X–Y coordinate system can be envisioned by imagining an azimuth-elevation antenna with the azimuth axis parallel to the earth's horizon (i.e., an azimuth-elevation antenna mount "lying on its side"). The X–Y antenna was conceived by GSFC, so that the antenna would have the capability of tracking a satellite through a zenith or direct overhead pass.

It can be seen intuitively that a near zenith pass over a conventional azimuth-elevation antenna causes the azimuth angular rate to increase sharply and, if automatic tracking is used, usually results in losing lock to the satellite tracking beacon. The GSFC X–Y mount, on the other hand, can track an overhead pass with ease.

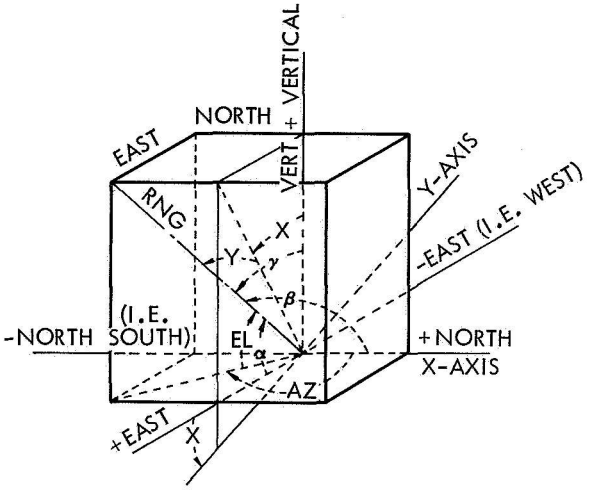


FIGURE 2–33.—*X–Y* coordinate system.

The X–Y coordinate system is illustrated in Figure 2–33. The X axis is oriented north-south and is parallel to the surface of the earth. The X angle is taken to be zero when the east component of range is zero; limits of ±90 degrees are set on the value of this angle. The Y angle is taken to be zero when the North component of range is zero; limits of ±90 degrees are set on the value of the angle.*

Antenna System Operation

Figure 2–34 is a simplified block diagram of the Mojave antenna subsystem.

Tracking is accomplished in either of two modes as selected by switch S1: (1) automatic tracking of the satellite 4080 Mc beacon signal, and (2) programmed steering.

*A. J. Rolinski, D. J. Carlson, and R. J. Coates, "The X–Y Antenna Mount for Data Acquisition from Satellites," *IRE Trans. on Space Electronics and Telemetry*, June 1962.

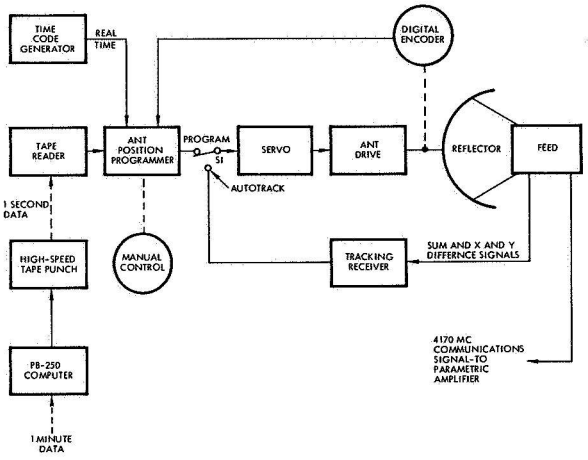


FIGURE 2–34.—Mojave antenna subsystems.

In autotrack, the output of a 4kMc tracking receiver is coupled to the antenna servo input to drive the antenna. The tracking receiver derives the servo error signals from conventional monopulse type sum and difference signals from the antenna feed. This is explained in later paragraphs.

In the programmed steering mode, an antenna position programmed steering mode, an antenna position programmer (APP) (see Figure 2–35) is used to generate analog servo error signals by comparing the predicted antenna angle as read in on punched tape,

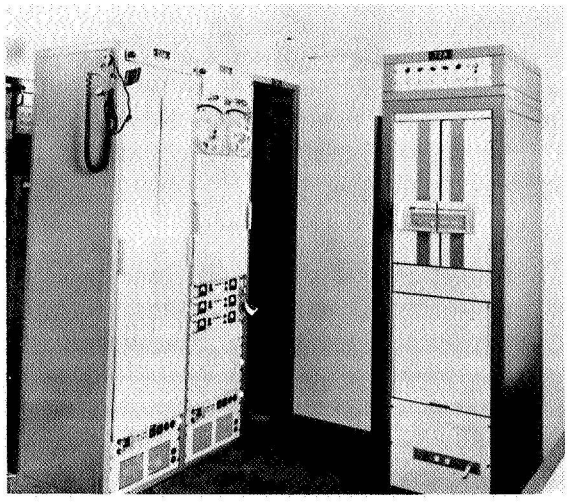


FIGURE 2–35.—Antenna position programmer and PB–250 computer.

with the actual antenna angle measured by an antenna shaft angle digital encoder (encoders are mounted on each antenna axis). The punched tape program is time encoded and the antenna programmer receives a real-time input from the time code generator in order to sample the punched angle information at the correct time. Taped antenna drive information is fed into the programmer by the tape reader. Antenna drive tapes are punched, normally several hours ahead of a satellite pass, by a high speed tape punch driven by a Packard Bell PB–250 computer.

Input to the computer consists of satellite ephemeris data points at one-minute intervals. Computer output, which is punched on a paper tape by the high speed punch, consists of antenna pointing information at one-second intervals in order to drive the APP.

Basic ephemeris information is transmitted to the test station in the form of one minute ephemeris data points over teletype circuits. One-minute data points are transmitted instead of the one-second data points required by the APP because several hours would be required to transmit data in one-second format. GSFC supplied this data at one minute intervals to all Relay ground stations and test stations in GSFC X–Y–Z coordinates (Cartesian coordinate system). As a result, the higher order derivatives of the smoothed data are lower than if the ephemeris were transmitted in, for example, the azimuth-elevation coordinate system used by the Nutley test station. This facilitates the process of curve-fitting which is performed by the PB–250 computer prior to interpolating the ephemeris data at one-second intervals.

Acquisition of the satellite beacon at the beginning of a pass is normally accomplished with the tracking system in the programmed steering mode. The mode is then switched to autotrack (see Figure 2–36 for a view of controls involved).

Programmed steering capability was included in the antenna system not only to facilitate acquisition for autotrack, but also to

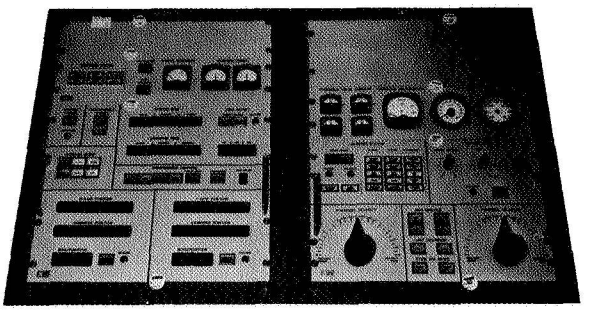


FIGURE 2–36.—Antenna tracking control console.

enable GSFC to experiment with programmed track as a primary means of pointing a communications antenna. It is likely that programmed tracking will be preferred over autotracking for future operations with a commercial communications satellite. This is true because the program track mode does not require the complex autotrack feed and diplexer with attendant RF losses which effectively increase the receiving system noise threshold.

Antenna Feed

The antenna feed consists of:

1. A 1725 Mc transmitting feed.
2. A combined tracking and receiving feed for tracking at 4080 Mc and receiving at 4170 Mc.
3. A comparator network for developing angle tracking information.
4. A diplexer for separating the tracking and wideband communication test signal.
5. Transmission line.

Figure 2–37 is a simplified diagram of the feed. Important feed requirements are listed below:

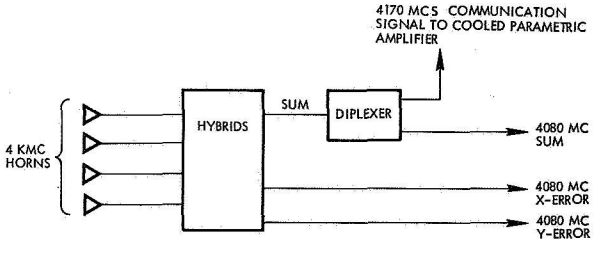


FIGURE 2–37.—Mojave antenna feed.

Transmitting feed	
Input VSWR	1.2:1
Maximum power	10 kw
Frequency	1725 Mc
Illumination taper	12 ± 2 db
Secondary antenna pattern	44 db gain −20 db sidelobes

Tracking and receiving feed	
Frequencies	4080 Mc for tracking signal 4170 for communication receiver
Secondary antenna pattern	51 db gain (sum pattern) 35 db null depth (difference pattern)
Diplexer	23 Mc bandwidth (to 0.1 db points) at 4170 Mc 1 Mc bandwidth to 3 db points at 4080 Mc
Isolation	30 db minimum between 4080 and 4170 Mc
Boresight accuracy	Within ± 1 milliradian to reflector optical axis
Crosstalk	<10 percent between error channels between ± 6 mr off boresight
Contribution to system noise (when installed on a 40-foot reflector).	25° k max due to antenna sidelobes, back lobes and galactic noise
Loss in 4170 Mc channel	0.7 db maximum

Tracking Receiver

The receiver is a three-channel, amplitude comparison, low noise, double conversion, phase-lock receiver which requires conventional sum and difference signals as inputs.

RF input signals are supplied to the receiver by the monopulse type feed. These signals are derived from the feed in such a manner as to furnish a phase and level reference signal and two channels of error information, from the orthogonal X and Y planes. Two channels of error information are processed to provide dc voltages proportional to the magnitudes and polarities of the angle between the line-of-arrival of the received signal and the antenna RF boresight axis.

The receiver exhibits the following performance when operated with loop noise bandwidths indicated below.

$$\zeta = 0.5^*$$
$$\epsilon \text{ max} = 0.35 \text{ rad}$$

Manual search provides coverage of a frequency band of ±250 kc (voltage controlled oscillator tuning range) from the receiver

* ζ is the damping factor assumed for the loop; ϵ max is the maximum loop error.

Noise Bandwidth	Threshold	Maximum tracking rate
10 cps	−148 dbm	5.6 cps/sec
30 cps	−143 dbm	50 cps/sec
100 cps	−138 dbm	560 cps/sec
300 cps	−133 dbm	5000 cps/sec
1000 cps	−128 dbm	56000 cps/sec

center frequency. VCO sweep speed is adjustable between the limits of 1 and 90 seconds per sweep, and upper and lower frequency sweep limits are adjustable over the entire frequency coverage noted above.

AGC tracking loop bandwidth are as follows: 1 cps, 3 cps 10 cps, and 30 cps. The tracking loop bandwith is defined as the 3 db frequency of the AGC low pass filter.

Antenna Position Programmer and Servo

Output of the digital encoders is in gray code. The encoders are optical, 16-bit encoders.

The antenna servo loop in program mode is a sampled data control loop; the programmer samples the encoders at a sampling frequency of 10 per second.

The servo is a type 2 servo and as such can follow a ramp input with essentially zero error. Analytical studies conducted during the design of the programmer in the servo loop indicated that overshoot is such that the error is forced below 0.04 degrees in about 0.6 seconds following application of a ramp input.

Nutley Antenna System

The Nutley antenna differs from the Mojave antenna as noted:

	Mojave	Nutley
Feed	Focal point	Cassegranian
Drive	Hydraulic	Electric
Mount coordinates	*X–Y*	Azimuth-elevation
Surface accuracy	1/16 inch RMS	Approx. 1/4 inch RMS

TEST STATION CONSTRUCTIONAL FEATURES

General

The volume of equipment required in the test station and the need for flexibility of movement of the station invited a new conceptual design to be used for housing the equipment. Consequently, special trailers were designed for this purpose (Figure 2–38). The Gerstenslager Company of Wooster, Ohio produced a mechanical design to comply with Project Relay specifications. One

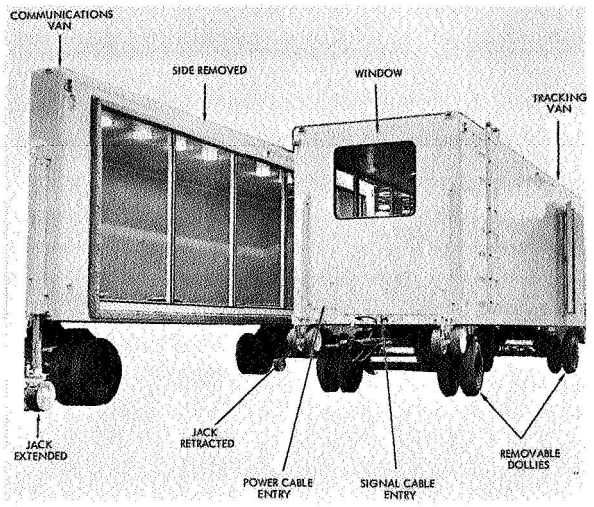


FIGURE 2–38.—Test station vans with sides removed for joining.

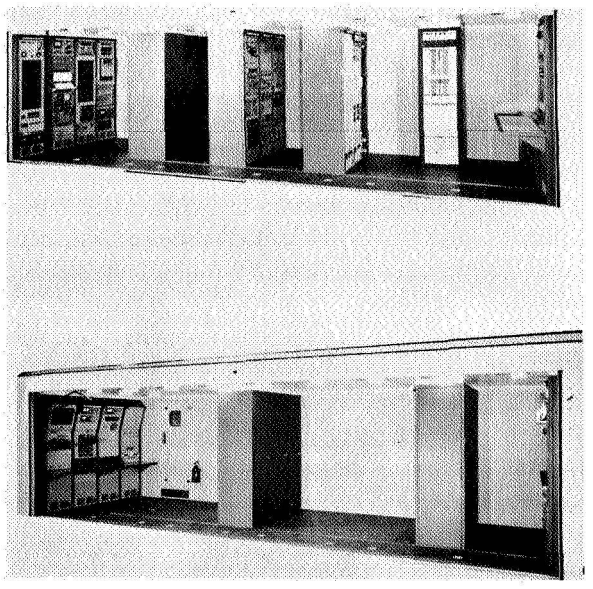


FIGURE 2–39.—Inside view of trailers with sides removed.

side of each trailer is fitted with removable panels. These panels are used only during shipment. Panels are removed at the site, and the two trailers are mated with the open sides facing each other to form a single large operations area. A gasket and a narrow roof at the junction of the two trailers are used to prevent the entry of rain. Removable trailer sides make it easy to install equipment in the trailers, since fully assembled racks of equipment can be placed in position without the need to fit them through doorways and down long aisles (see Figure 2–39). It is worthy of mention that future expansion of the station can be accomplished quite simply by the addition of a third van. This van would have both sides removable for placement between the existing vans. If necessary, 18 additional racks of equipment could be added in this manner.

Trailers are air conditioned by means of portable 7½-ton capacity air conditioners, connected by flexible pipe to a false ceiling. The false ceiling is divided into two longitudinal sections; a ceiling portion over the racks is the cold air inlet, and the portion over the aisle is the cold air exhaust. Cool air is directed downward through each rack of equipment and exhausted into the room at the bottom of the racks.

The trailers are quite complete but do not contain some major equipment items, such as

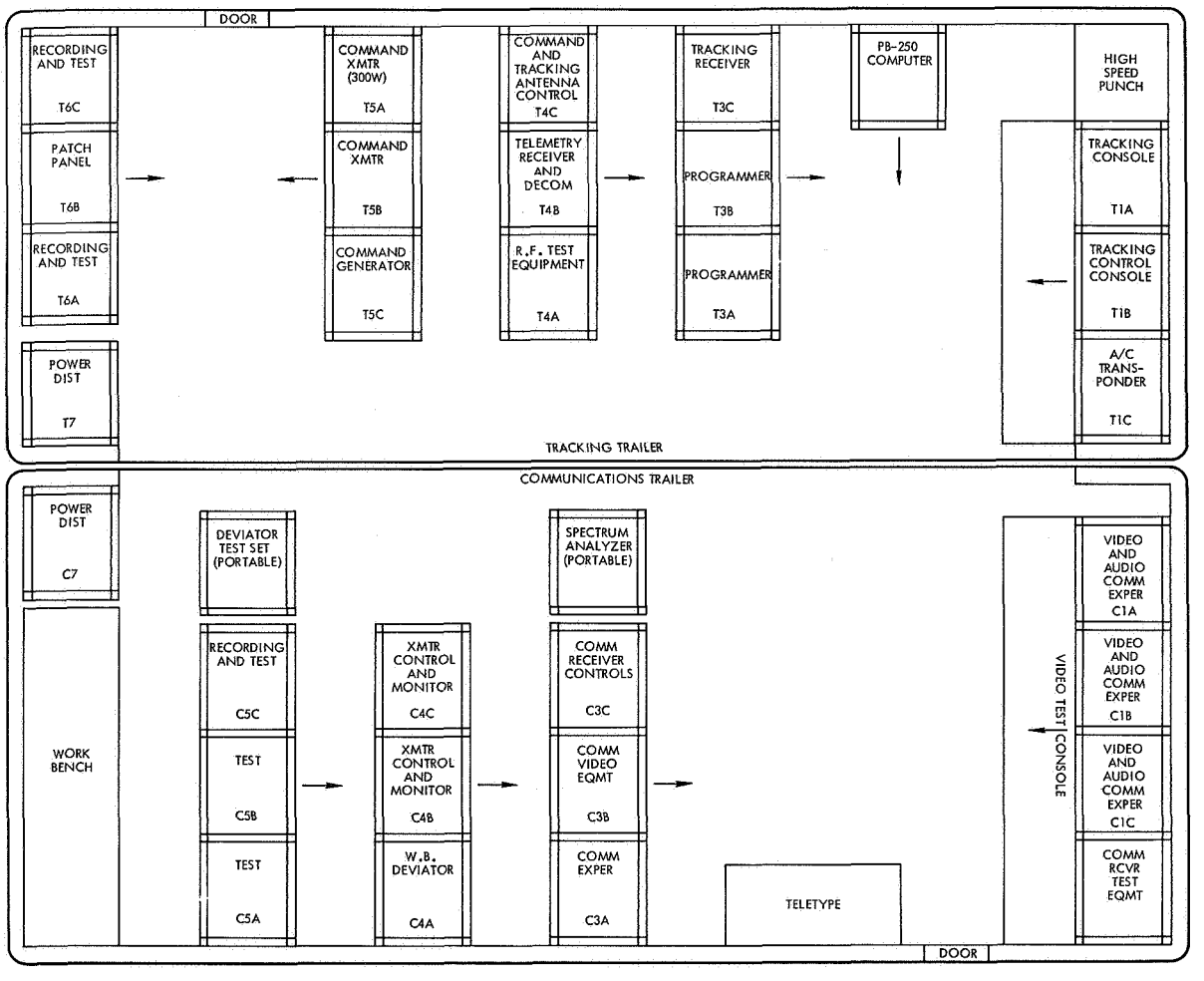


FIGURE 2–40.—Test station equipment layout diagram.

the 10 kw communication transmitter and power supply; these are located outside. The parametric amplifier and converter-IF are installed on the antenna. Both of these items, however, are controlled from the van.

FDM telephone equipment is located in a third trailer at Mojave, which is located adjacent to the main trailers.

Equipment Layouts

From Figure 2–40 the plan view for the assembled trailer room may be seen. The upper trailer in the illustration is the tracking trailer, and the lower one is the communications trailer. The tracking trailer contains all command, telemetry, and tracking equipment.

The communications trailer contains the equipment necessary for the generation, transmission, and reception of wideband video test signals.

The following drawings show how the equipment is installed in the racks.

Antenna tracking console (Figure 2–41)

Command transmitter and Encoder (Figure 2–42)

Telemetry reception (Figure 2–43)

Telemetry analog recording (Figure 2–44)

Video test console (Figure 2–45)

Video signal generators and receiver controls (Figure 2–46)

Wideband transmitter (Figure 2–47)

In addition, space has been provided for work bench facilities and the storage of general purpose test equipment.

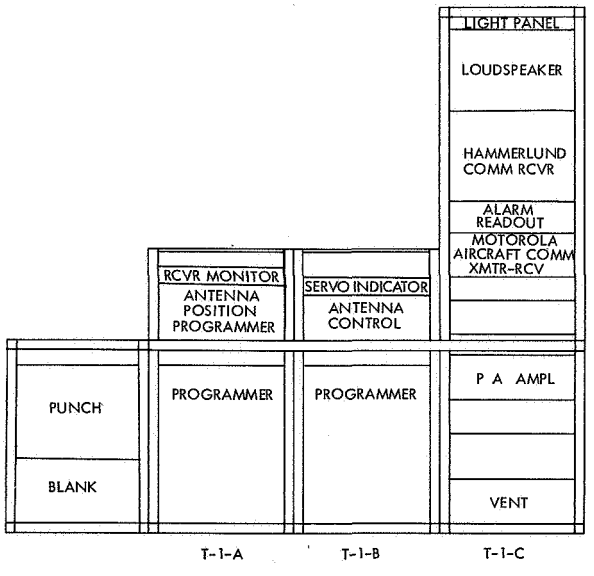


FIGURE 2–41.—Antenna console.

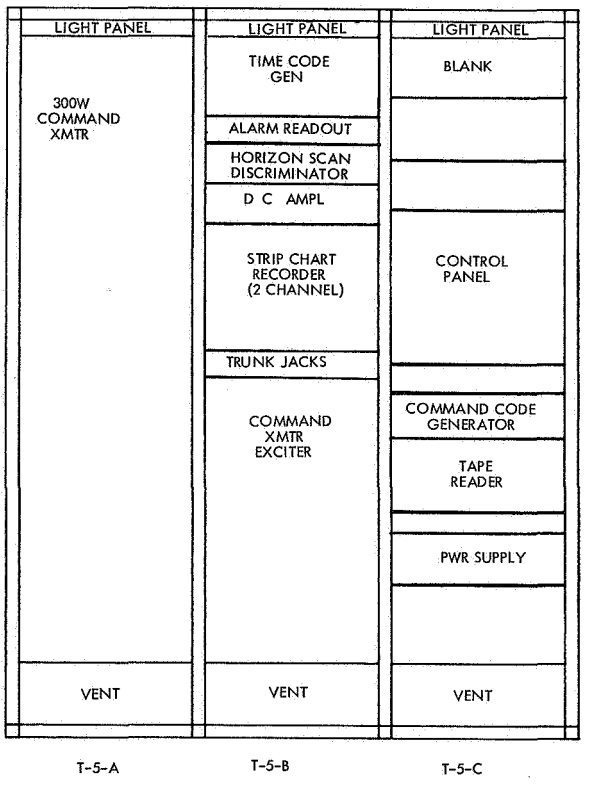


FIGURE 2–42.—Command transmitter rack.

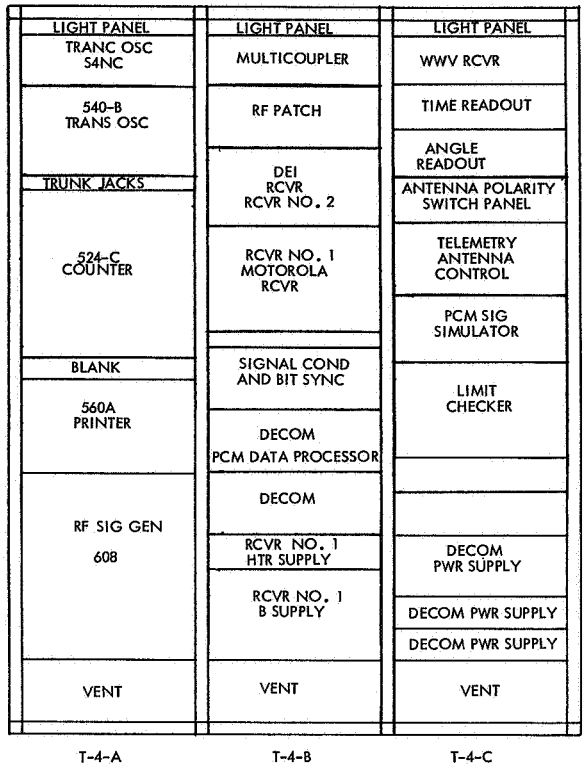


FIGURE 2–43.—Telemetry equipment rack.

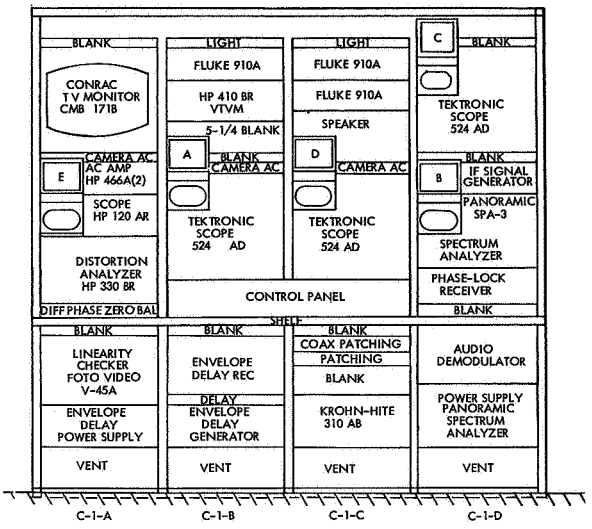


FIGURE 2–45.—Video test console.

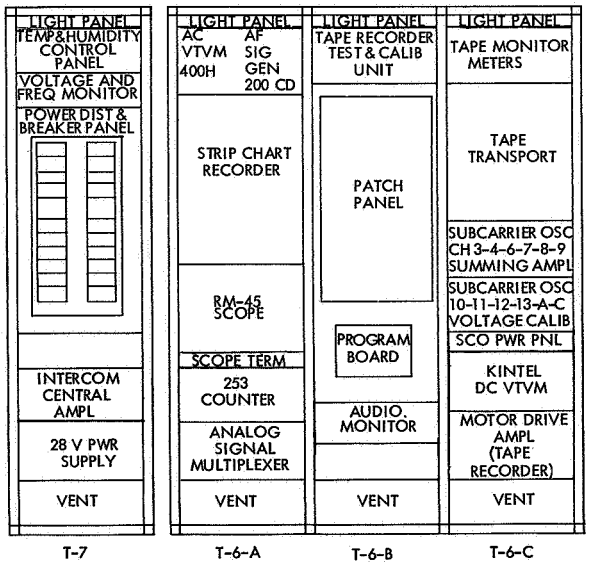


FIGURE 2–44.—Telemetry analog recording equipment.

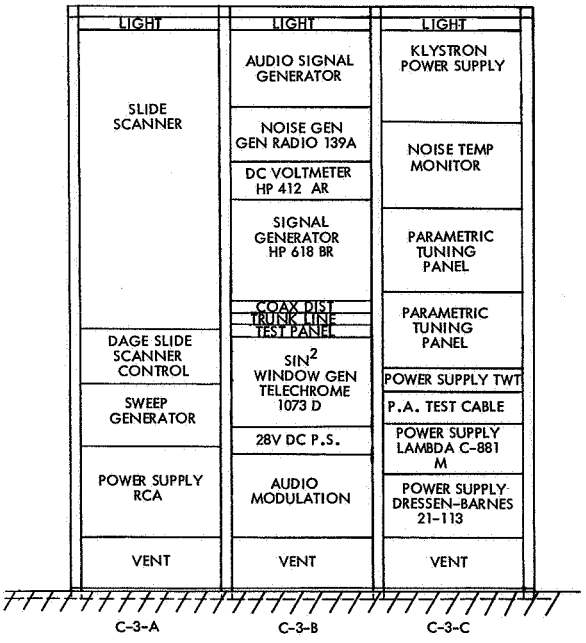


FIGURE 2–46.—Video signal generators and wideband receiver control.

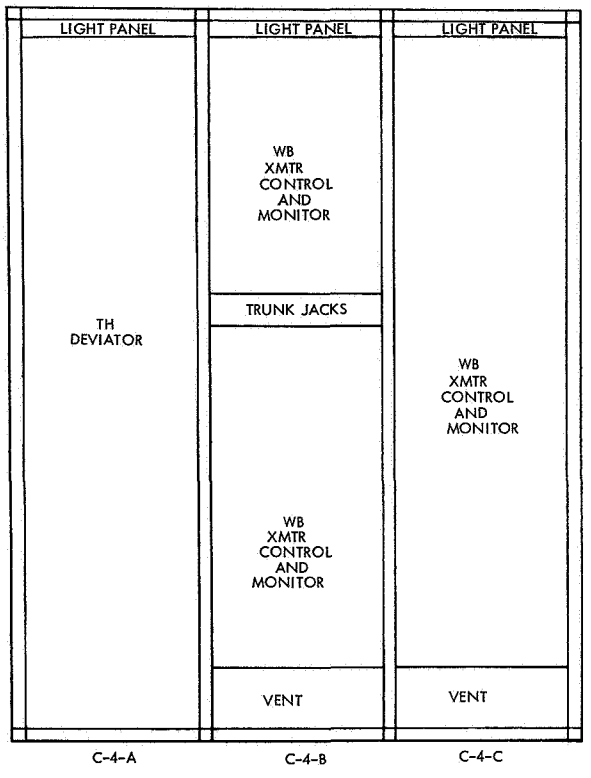


FIGURE 2–47.—Wideband transmitter control equipment.

AUTHORS. *This chapter was written by* T. H. GUERIN, R. G. SLAUGHTER, *and* W. C. WRAY *of Space Technology Laboratories, Inc., Redondo Beach, California, U.S.A. under contract NAS 5–1302 with NASA/Goddard Space Flight Center.*

N66-10241

Chapter 3

The Relay Test Station Low Noise Receiving and Demodulation Systems

10241

The wideband FM receiving subsystems in use at the NASA Goddard Relay Test Stations are similar in design except for the antennas. Descriptions are presented of the equipment, with special attention directed to the theory of operation and performance data of the 4 Gc, liquid nitrogen cooled, parametric amplifier and wideband phase-lock demodulator. System noise temperatures of 100°–125° K have been measured in accordance with performance objectives. Threshold improvement of 5 db over that of a conventional discriminator has been demonstrated by the use of the phase-lock demodulator.

Author

INTRODUCTION

As a part of the Relay satellite system test stations, the wideband low noise receiver was perhaps the most challenging development required. The STL engineers under contract to NASA found it necessary to stretch the state-of-the-art in several ways in order to achieve the performance goals set by previous system studies. Fundamentally, the first problem obvious was the selection and development of a low noise input amplifier to provide the best possible signal-to-noise performance. Even with this, however, the system performance calculations showed the link to be marginal, and additional improvement was required. Because of previous experience in low level signal telemetry, the STL engineers conceived a method of phase-lock demodulation which resulted in a threshold which was appreciably lower than that of a conventional FM discriminator-type demodulator. System studies had shown that frequency modulation was the preferred modulation technique, and by means of the threshold lowering demodulator, greater advantage of the FM improvement factor was possible. Consequently, the final receiving system uses, in addition to the low noise circuitry, an unusually wide bandwidth in order to accommodate the high modulation index FM.

High quality of the many relayed television demonstrations has amply proved the suitability of receiving and demodulation system design. These designs, and the manner in which they were derived, are presented in the following pages. A division is made into two main sections: a) the low noise receiving system which includes the parametric amplifier, the traveling wave tube, 120-Mc amplifier, control and monitoring circuitry, and b) the demodulation system.

LOW NOISE RECEIVER SYSTEM

Development of the Low Noise Receiver System

In the early stages of the Relay program,

the antenna to be employed by NASA was not specifically defined. The low noise receiver system, therefore, was designed to mount on any of the proposed low noise antenna configurations. These were 40, 60, and 85 foot parabolic reflectors on X–Y or azimuth-elevation mounts, with provisions for mounting the receiver system close to the antenna feed. Additional considerations were: a) bandpass characteristics to be compatible with the wideband video signals to be received at 4.170 Gc, b) a 175 degree Kelvin system noise temperature including the noise contributions of the antenna, feed and diplexer loss; and c) receiver system. The receiving system noise temperature specification ($T_R \leq 125°K$) satisfied the system requirement for expected antenna noise contributions.

Figure 3–1 shows the state of the art in low noise amplifiers at the time the Relay system became operational. It is obvious that only the maser and the cooled parametric amplifiers would meet the above noise temperature specifications. The maser is an extremely low noise amplifier, but, it is more difficult to maintain, more expensive, and more complex than the cooled parametric amplifier. Accordingly, the cooled parametric amplifier was chosen for the first stage microwave amplifier. A low noise traveling wave tube, being compact, stable, reliable, and economical, was selected for the second stage RF amplifier.

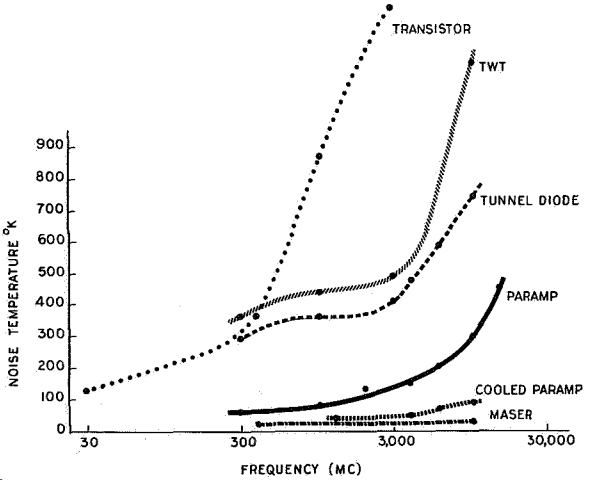


FIGURE 3–1.—State-of-the-art of low noise amplifier.

STL was selected to design and develop the liquid nitrogen cooled parametric amplifier, and to purchase, integrate, and package the TWT, the remainder of the microwave low noise receiver, and the control and monitoring circuitry. Within 10 months after this selection, the first low noise receiving system was delivered to Nutley, New Jersey, for installation on the 40-foot Cassegrain feed-type antenna.

System Description

Broadband low noise receiving systems were installed at both the Nutley, New Jersey, and Mojave, California sites. The systems are nearly identical, packaging being the main difference. The cooled parametric amplifiers themselves were made alike; each slides on rails into a receiver box. This facilitates maintenance, since the parametric amplifiers can be removed without disturbing the receiver box which is fastened to the antenna. Also, the Mojave paramp can be used as a backup for the Nutley paramp in the event of catastrophic paramp failure.

Remote monitoring and control chassis are located in the communications van located approximately within 250 feet from the base of the antenna.

The following is a discussion of the receiving system block diagrams of the Nutley and Mojave sites.

Nutley Receiving System

The wideband receiver is rack mounted in the equipment enclosure on the 40-foot diameter paraboloid of the Cassegrain feed-type antenna. The 120-Mc receiver and the low noise receiving system chassis are controlled and monitored from the Communications van. The system layout is shown in Figure 3–2; a block diagram of the receiver is shown in Figure 3–3.

The coaxial input to the low noise receiver is connected to the waveguide switch by means of a 9-inch length of coaxial cable and

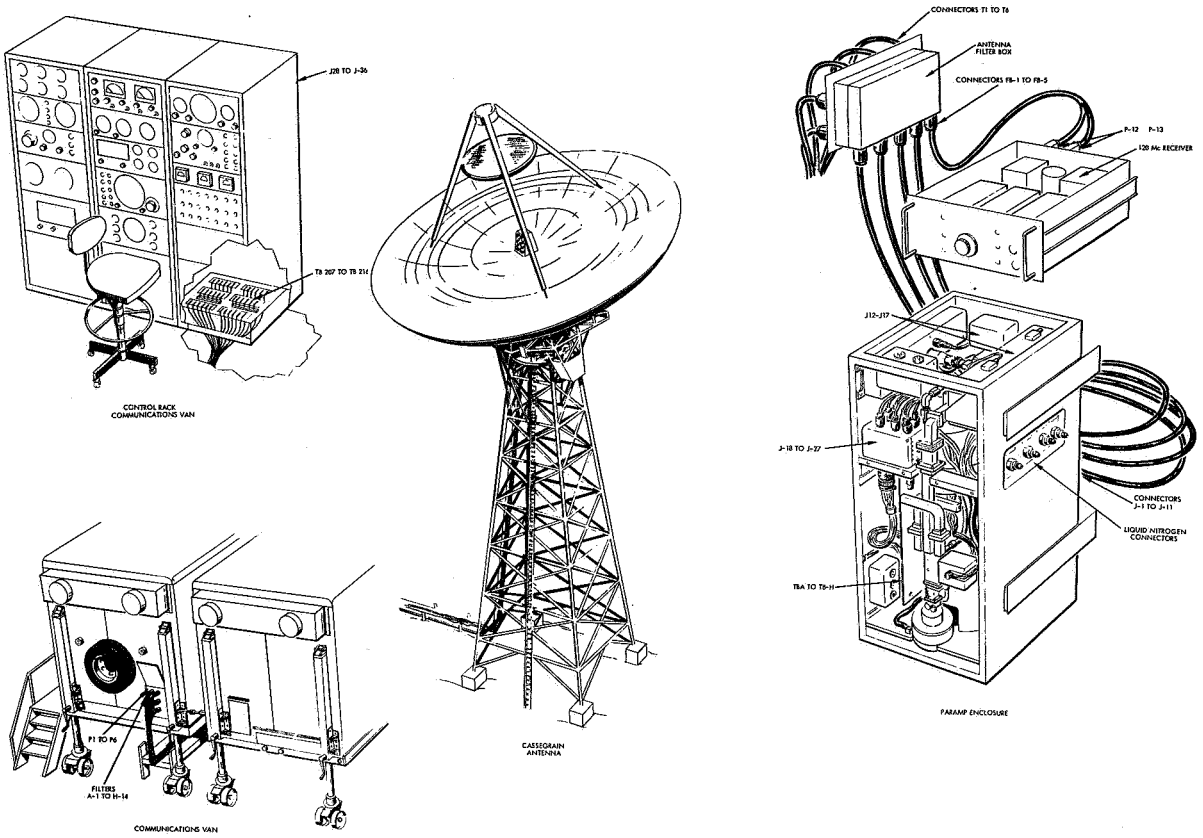


FIGURE 3–2.—Nutley receiving system layout.

waveguide-to-coax adapter. A four-pole waveguide switch permits the input to the cooled paramp to be connected to the antenna for receiving, or to a termination for tuning and calibration. System noise temperature is monitored at the input to the low noise receiver chassis by coupling the noise tube into the system with an 18-db directional coupler. The cooled paramp is operated at 15 db gain and greater than 20 Mc bandwidth. Paramp bias supply and motorized tuning controls are located in the Communications van. Signal power at 4170 Mc is split and fed through isolators to the IT&T facility and to the 120-Mc receiver. Power out of the 120-Mc receiver is nominally +3 dbm and is fed to the demodulator by a length of RG14 coaxial cable. Liquid nitrogen is fed to the antenna mounted equipment under pressure through an insulated line from the base of the antenna (Figure 3–4). The insulated line is disconnected at the azimuth table to permit antenna movement after the Dewar is filled with liquid nitrogen.

Figure 3–5 shows the front and top views of the low noise receiver chassis with slides on the side for mounting in the antenna equipment enclosure. Vent and fill ports for liquid nitrogen are shown on the side of the enclosure.

A computer program was used to calculate thermal conditions expected in the enclosure for system operating during a hot day, when the rays of the sun beat directly on the receiver enclosure. Maximum average air temperature inside the enclosure was computed to be 58°C.

Mojave Receiving System

Shown in Figure 3–6 is the Mojave receiving system block diagram. This system is basically the same as the Nutley system ex-

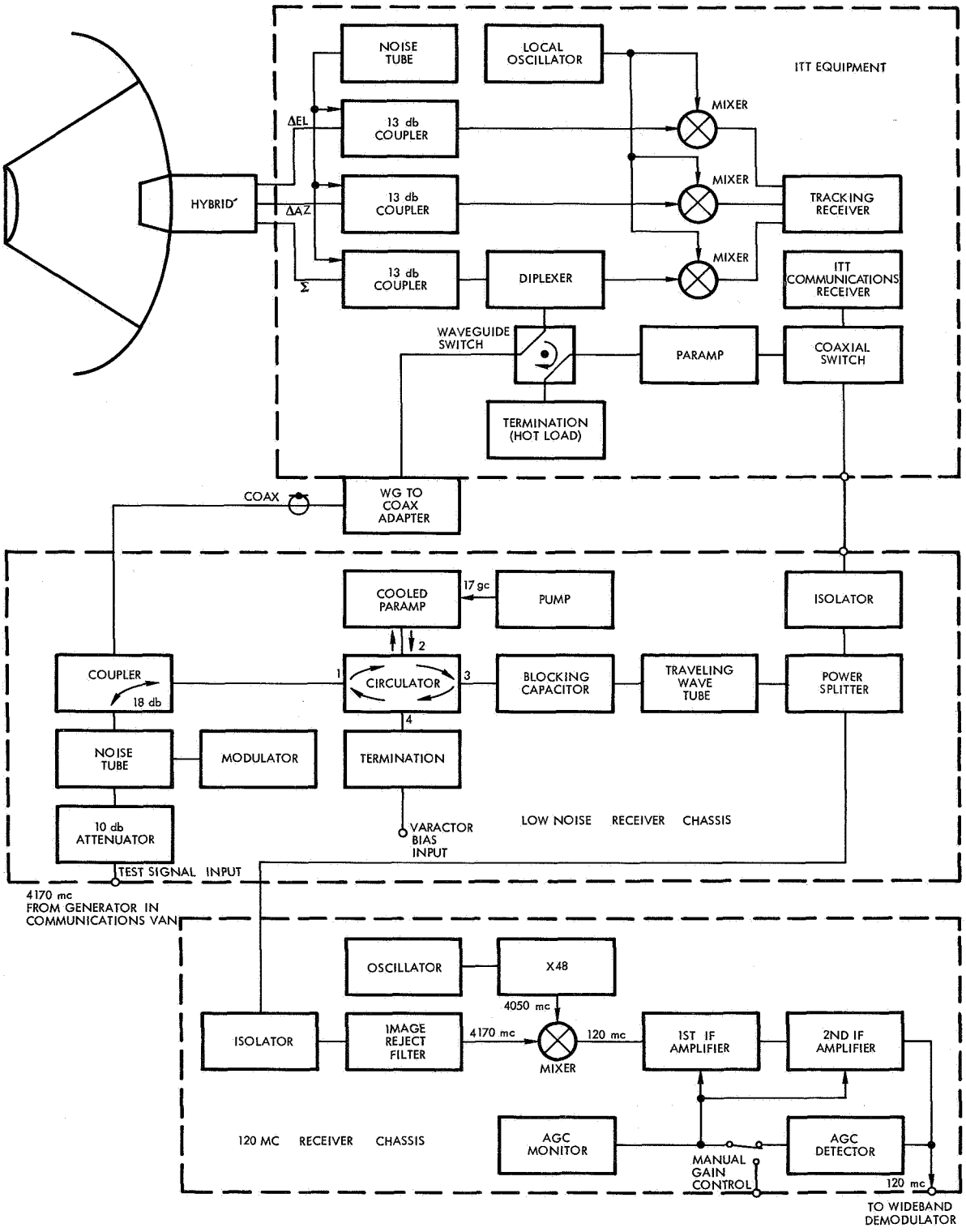


FIGURE 3–3.—Nutley receiving system, block diagram.

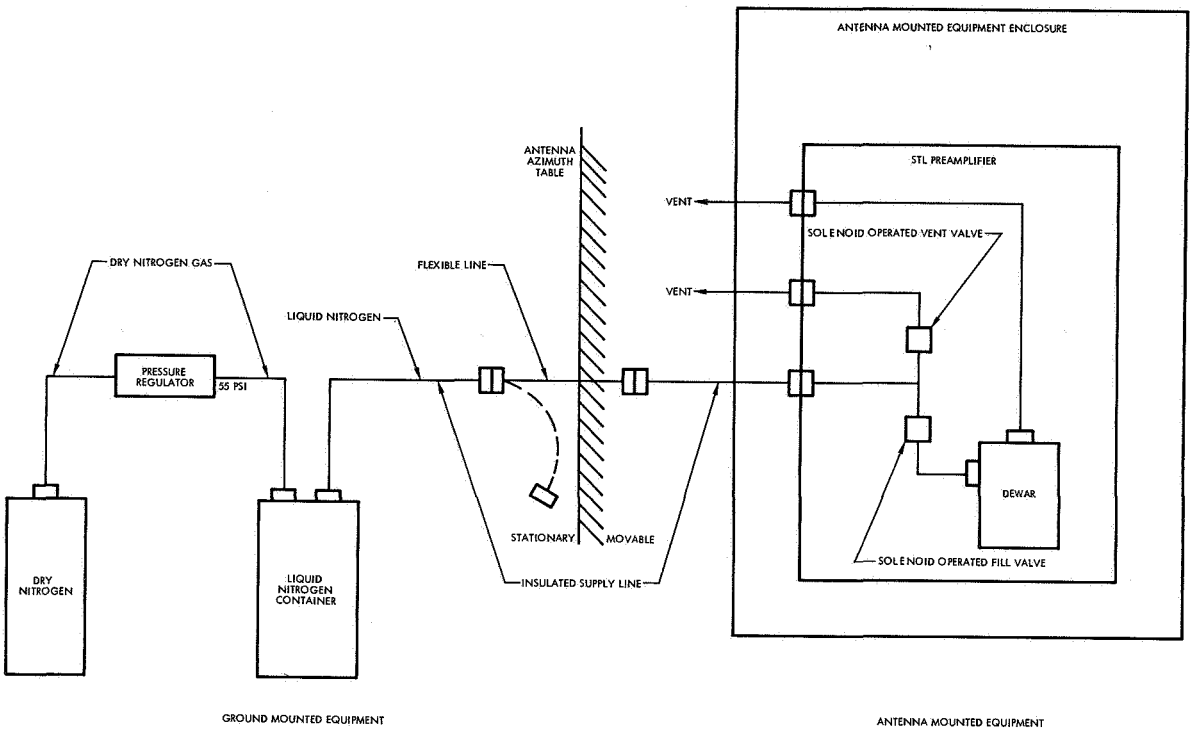


FIGURE 3–4.—Liquid nitrogen circulation system.

cept that the output of the TWT is not split. Packaging is entirely different, however. The receiver at Mojave is mounted beyond the apex of the quadrapod holding the feed in front of the paraboloid as shown in Figure 3–7. Figure 3–8 illustrates the component placement in the receiver enclosure; the cooled parametric amplifier has been removed. For filtering all incoming lines and outgoing monitoring and control signals, a filter box is mounted on the side of the enclosure. Directly below the filter box are the liquid nitrogen venting and filling ports.

The 120-Mc receiver is mounted in the top rear of the enclosure by four bolts. Care was taken to insure that the weight and center of gravity of the enclosure was precisely as predicted; this data was supplied to the antenna designers early in the development stage.

System Design and Performance

This section discusses design and performance of the liquid nitrogen cooled-parametric amplifier, the TWT and 120-Mc receiver, and the control and monitoring circuitry. System design specifications were as follows:

- Antenna mounted (on almost any style of antenna).
- Remotely controlled.
- Frequency—4170 Mc.
- Gain (paramp)—15 db.
- Bandwidth (3 db) design goal—60 Mc.
- Overall receiver noise temperature — $<125°K$ (at input to circulator).
- Antenna ambient temperatures as located on East and West Coasts of the U.S.
- The receiving system may consist of a cooled parametric amplifier for the first RF amplifier and a low noise TWT for the second RF amplifier.
- Bandwidth of the RF amplifiers must be such that no degradation is noticeable on wideband video signals.
- Gain of the parametric amplifier must reduce the second stage system noise contribution.

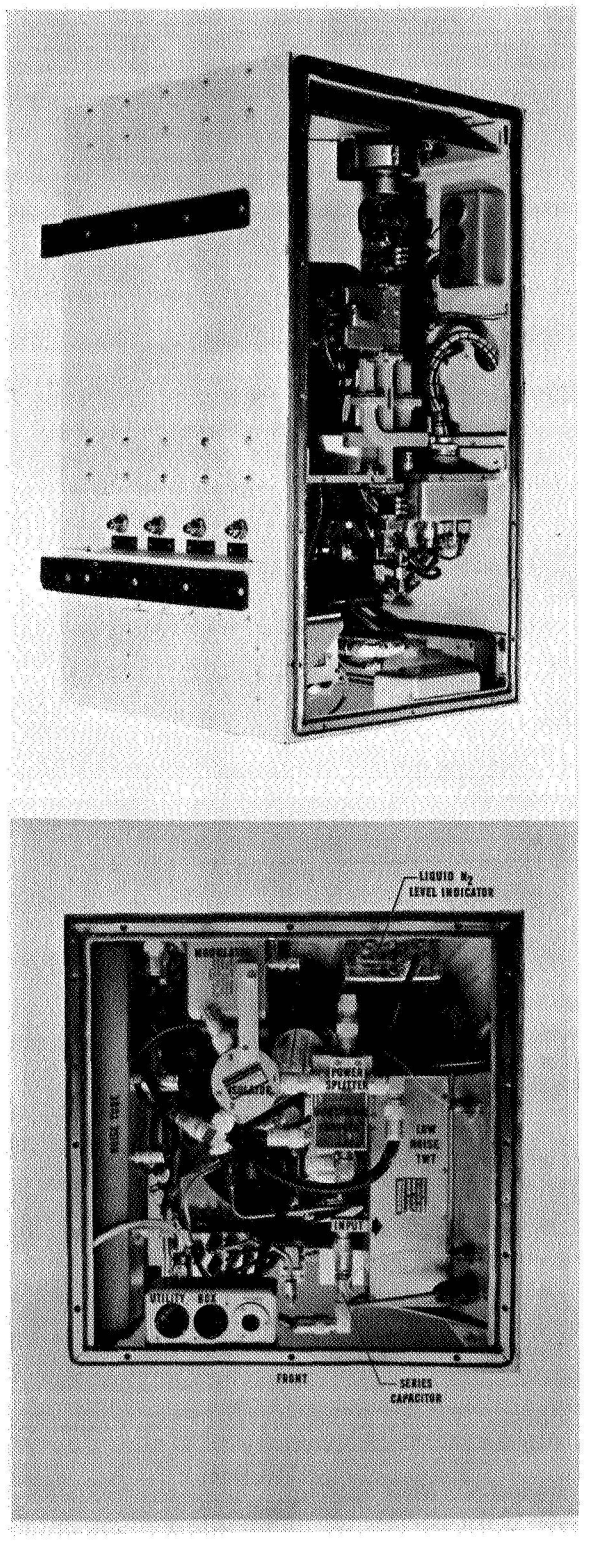


FIGURE 3–5.—Nutley low noise receiver chassis.

Cooled Parametric Amplifier

Varactor Design

Parametric amplification is the process by which energy is transferred from a "pump" through a nonlinear or time-varying element to the signal to be amplified. The Relay amplifier utilizes a variable capacitance (varactor) diode as the nonlinear element. Capacitance is made to vary with the application of a pump voltage across the varactor. When a signal interacts with the reactive element varying at the pump frequency, other frequency components are generated. If the idler frequency (pump minus the signal frequency) is allowed to flow, a negative resistance is generated yielding the possibility of high gain or undesired oscillation.

Figure 3–9 shows the reactance variation of two varactors tested in the paramp. A dc bias is selected for the varactor such that an equal reactance change occurs as pump voltage is applied on the dc bias. The varactor is not pumped hard enough to draw current in either forward or reverse directions. Therefore, the main source of noise in the amplifier is thermal noise of the circuit losses and that caused by varactor spreading resistance. To minimize this noise the varactor must be cooled.

At the time of amplifier design, very little specific data was available on the effects of cooling varactors. The paramp was accordingly designed to accept most commercially available varactor types (Figure 3–10), and also to operate at both ambient and liquid nitrogen temperatures. This necessitated provision of a remote tuning mechanism so that the paramp could be operated on the antenna in either the uncooled or, more sensitive, cooled mode of operation.

Figure 3–11 is a cutaway of the paramp designed to meet these requirements. Figure 3–12 is the block diagram of the paramp and pump circuit. Actual development was based on theoretical considerations given in this paper and the experience experimentally gained in building and testing parametric amplifiers.

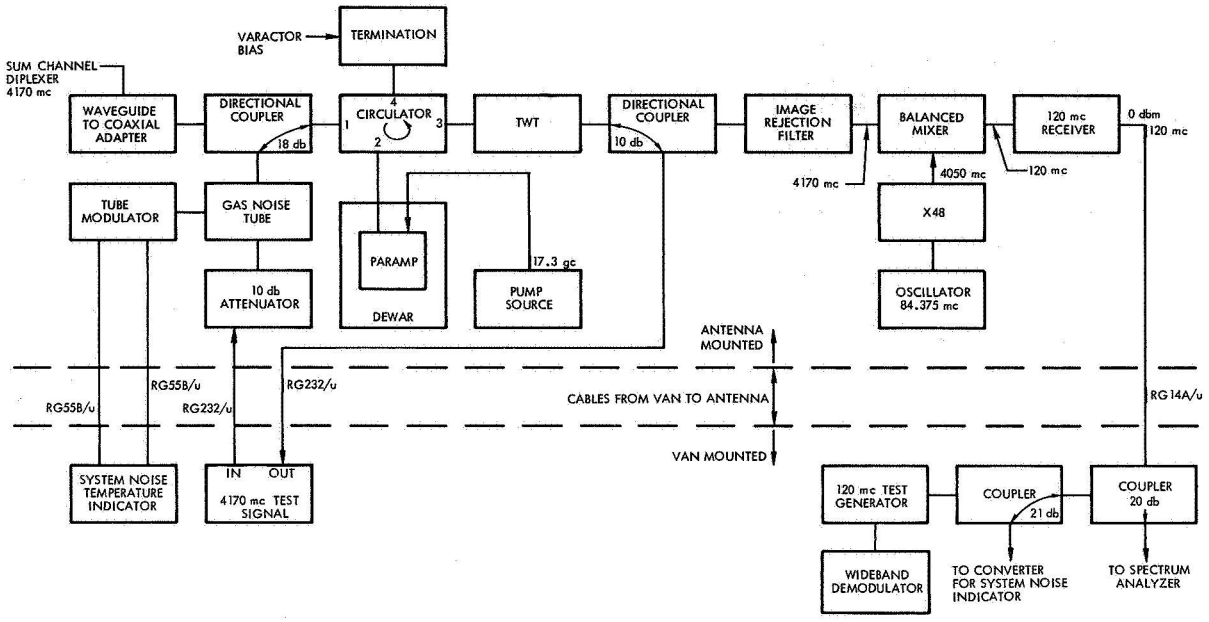


FIGURE 3–6.—Mojave receiving system, block diagram.

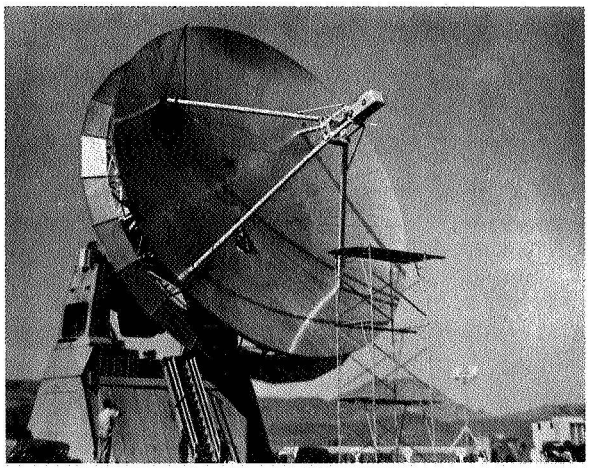


FIGURE 3–7.—Receiver mounting on the Mojave antenna.

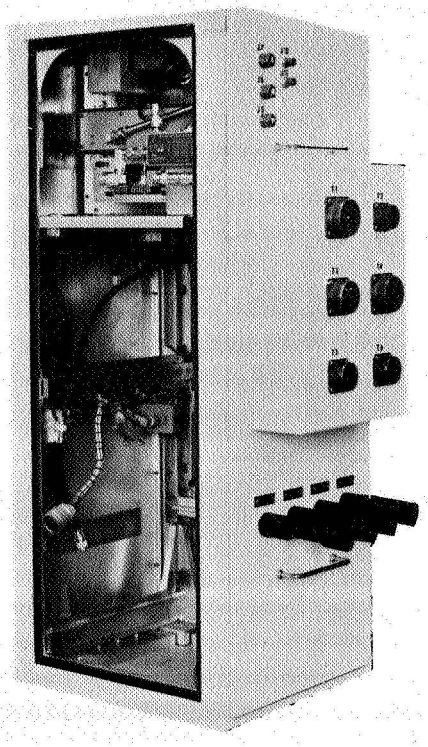
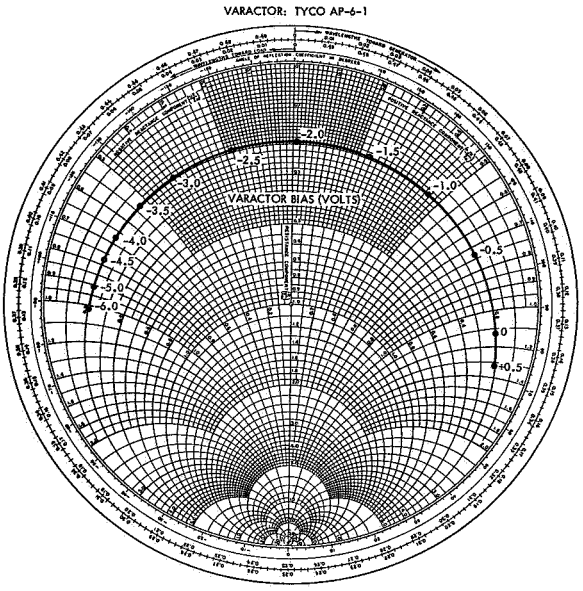


FIGURE 3–8.—Mojave receiver enclosure.

Theoretical Considerations

Theoretical analyses were performed to determine the minimum noise temperature achievable for a 4.2 Gc signal frequency and for selection of the best varactor diodes commercially available. The analysis of Kuro-



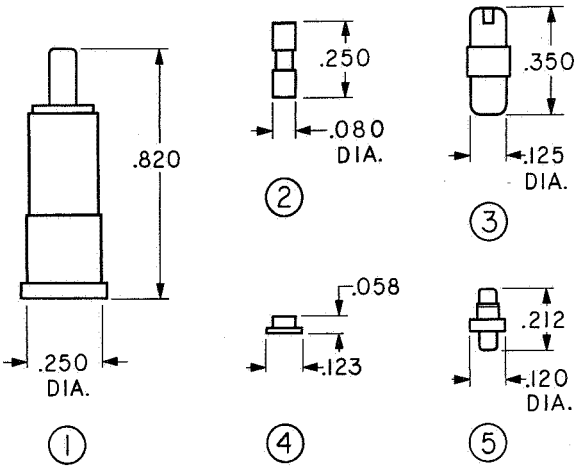


FIGURE 3–10.—Commercially available varactor packages.

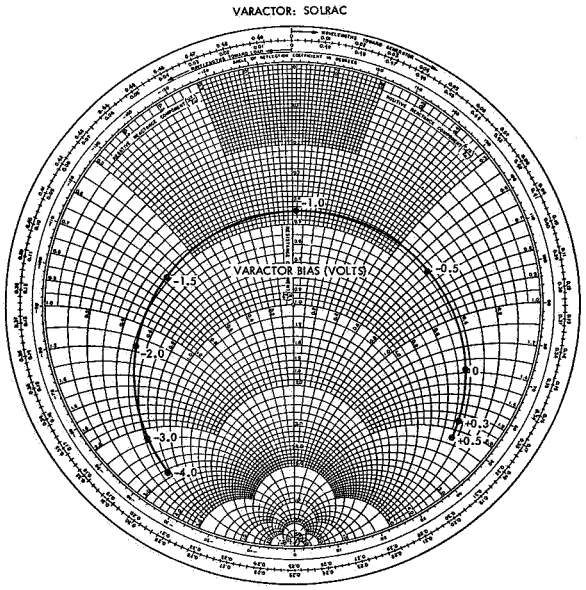


FIGURE 3–9.—Varactor reactance variations.

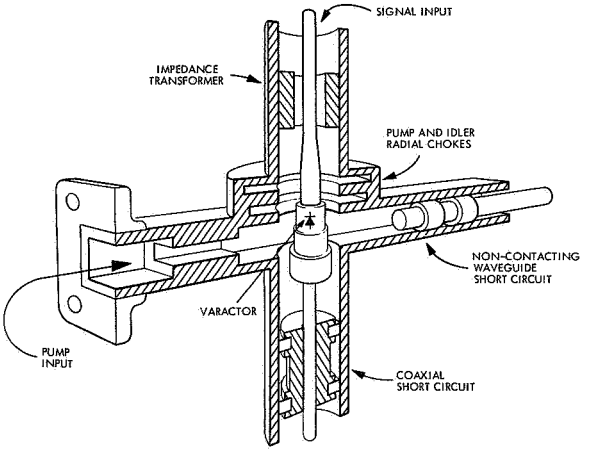


FIGURE 3–11.—Paramp cutaway.

kawa and Uenohara on varactors was expanded for the Relay paramp. Figure 3–13 shows the minimum noise temperature of the amplifier for a given diode and pump frequency. Equations involved in the plot are:

$$T_e(\min) = \frac{T_s\left[1+\tilde{Q}_1^2\left(\frac{\omega_1}{\omega_2}\right)^2\right]}{\frac{\omega_1}{\omega_2}\tilde{Q}_1^2 - 1}$$

$$\tilde{Q}_1 = Q_1 \frac{1}{\frac{2}{\gamma}\quad\frac{\gamma}{2}} \qquad \gamma = \frac{C_1}{C_o}$$

$$Q_1 = \frac{1}{\omega_1 C_o R_s}$$

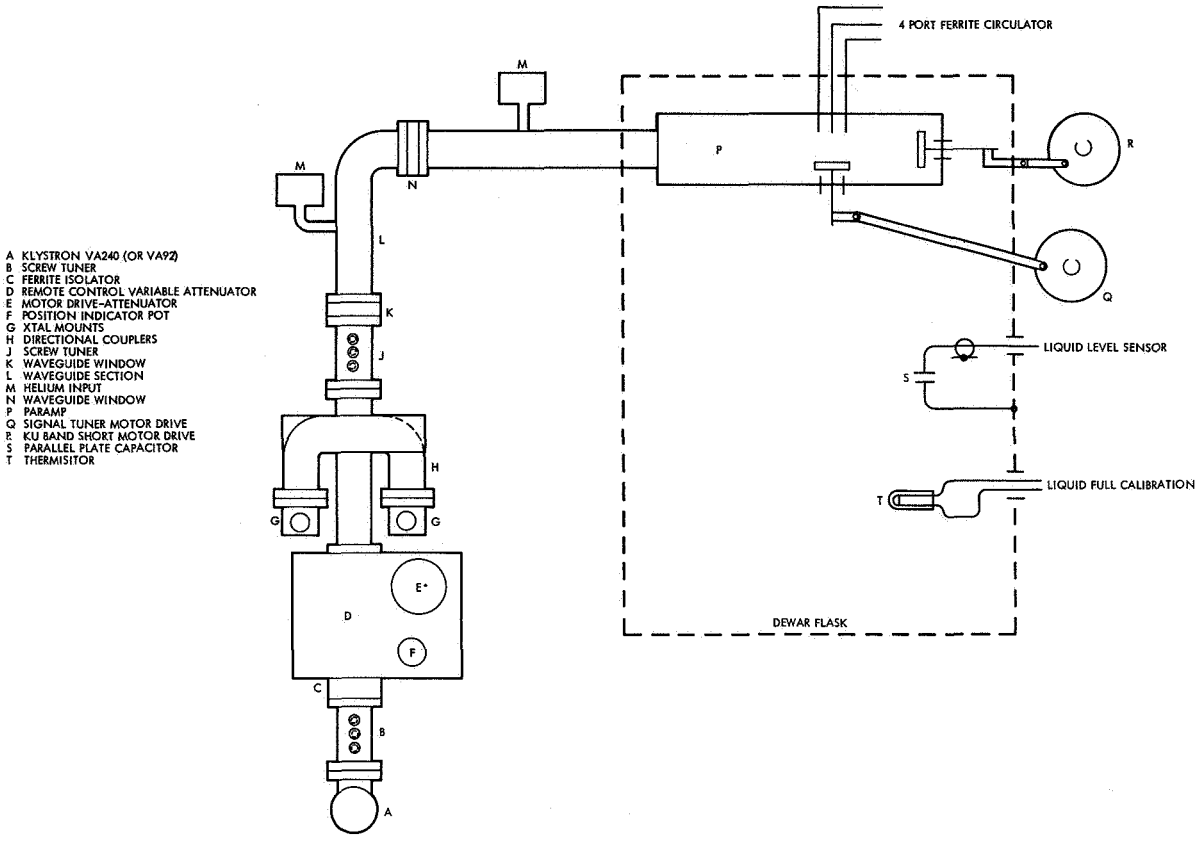


FIGURE 3–12.—Paramp and pump circuit block diagram.

C_o = Capacitance of varactor at bias point

C_1 = maximum capacitance change from C_o due to pumping the varactor

Q_1 = Q of the varactor at C_o and the signal frequency

$\tilde{Q}_1$ = dynamic Q of the pumped varactor

R_s = series resistance of the varactor

T_e = minimum equivalent noise temperature of the amplifier

T_s = temperature of the diode resistance

$\frac{\omega_1}{2\pi} = f_1$ = signal frequency

$\frac{\omega_2}{2\pi} = f_2$ = idler frequency

$\frac{\omega_1+\omega_2}{2\pi} = f_3$ = pump frequency

Assumed values are:

$T_s = 90°K$

$\gamma = 0.5$

$f_1 = 4.2$ Gc

$Q_1 = 22.5$ at zero bias

$= 34.3$ at -2 volts bias

Figure 3–13 assumes that all impedances are adjusted for a minimum noise figure. Using these assumed values, the minimum amplifier noise temperature versus pump frequency can be obtained. It may be noted that there is an optimum pump frequency for minimum noise temperature, and also that the slope of the curves for high Q diodes is very small for a large range of pump frequencies.

For the zero-biased diodes with a realistic Q of 22.5, minimum noise temperature is

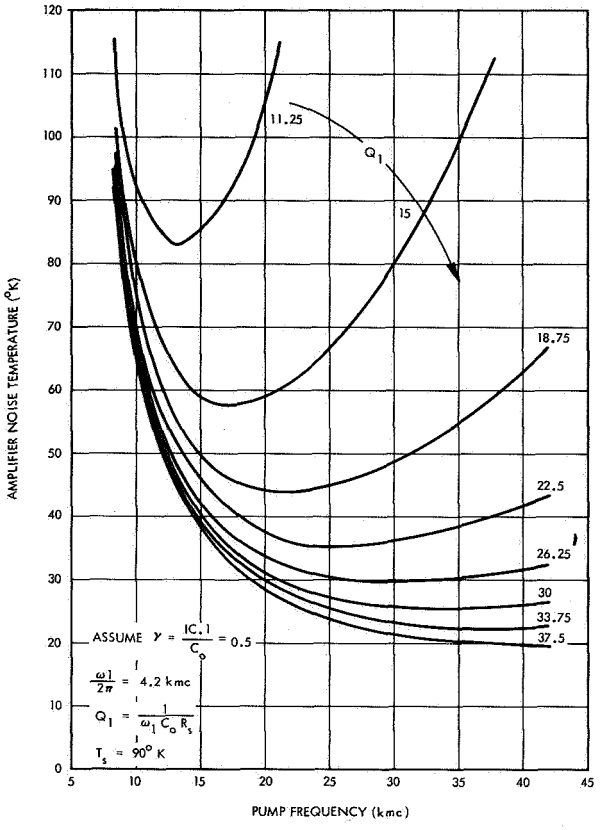


FIGURE 3–13.—Paramp noise temperature achievable.

35.4°K for the optimum pump frequency of 25 Gc., and 40.4°K for a pump frequency of 18 Gc For a lower Q diode, the optimum pump frequency approaches 18 Gc.

Pump frequency was chosen as 18 Gc and was to be generated by a 9 Gc klystron followed by a varactor frequency doubler. This decision was based on factors such as available diodes, high cost and low power of high frequency klystrons, and longer life, superior stability, higher power, lower cost, and shorter delivery time for tubes at 9 Gc compared to those available at much higher frequencies. Also, the pump circuit mechanical tolerances are less critical at 18 Gc than at 25 Gc.

A varactor doubler was designed and built with the following performance characteristics:

Input frequency: 9 Gc
Output frequency: 18 Gc
Input power: 500 mw
Output power: 120 mw
Varactor
Microstate
Equivalent to No. MS2545
Capacitance 1 pf at 0 volts

A plan to use the varactor doubler was dropped, however, due to a tight schedule for packaging and refining the design, and because a low cost 18-Gc klystron tube suitable for this application became available. This tube was employed with excellent results.

At 17.3 Gc., the klystron power into an optimum load, provided by screw tuners is 255 milliwatts; power is remotely controlled by a cam-driven resistive vane attenuator. Directional couplers and crystal detectors are used to monitor pump power. Parametric amplifier stability is predominantly determined by klystron power and frequency stability; Figure 3–14 shows dependence of the parametric amplifier gain upon pump power. A change in pump frequency shifts the signal passband characteristics of the amplifier but can cause instability. Klystron frequency stability is high when the tube temperature remains below 150°C. Thermal data of the receiving system and enclosure were fed into a computer. The receiver enclosure maximum ambient air temperature of 58°C and the blower requirements to keep the klystron

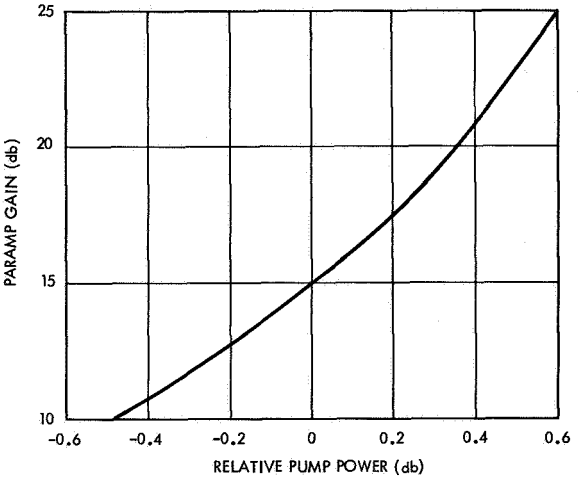


FIGURE 3–14.—Paramp gain vs. pump power.

temperature at less than 150°C were computed.

For 50 cfm of ambient air (58°C) in a 4 square-inch duct flowing on the tube, the maximum klystron temperature was 125°C. Without the blower, the maximum tube temperature was 300°C. Experimentally, it was found that for an ambient temperature of 23°C and a blower capacity of 100 cfm in a 9 square-inch duct, the maximum tube temperature with filaments on is 36°C, and when operating is 70°C. Therefore, a blower was required to keep the tube below 150°C for best klystron stability.

Circulator Design

In order to effectively use a low noise amplifier, the losses prior to the amplifier must be minimized. Melabs designed a low loss 4-port ferrite circulator for coupling the signal into and out of the parametric amplifier. The circulator isolation characteristic versus temperature is shown in Figure 3–15. The insertion loss remains less than 0.15 db at 4170 Mc from the antenna port to the paramp port. For all expected temperatures the circulator maintains $>$ 29 db isolation. This is required for gain stability. The varactor bias is applied through the termination on the 4th port of the circulator. The termination consists of a deposited film resistor on the center conductor with a slug inserted behind the resistance which gradually tapers from the outer conductor to the inner conductor. Manufacturing tolerances on the slug are such that a 1 mil thick polyester film electrical tape may be wrapped about the slug, keeping the center conductor and outer conductor from shorting without affecting the operation of the termination at microwave frequencies.

Cryogenic Circuit Design

The cryogenic circuitry was a major design effort. One method which was studied was the possibility of cooling the paramp thermoelectrically to 200°K. It was found, however, to be simpler and less expensive to design a liquid nitrogen system providing cooling to 77°K. In addition to simplicity and lower cost, there is a noise figure improvement in

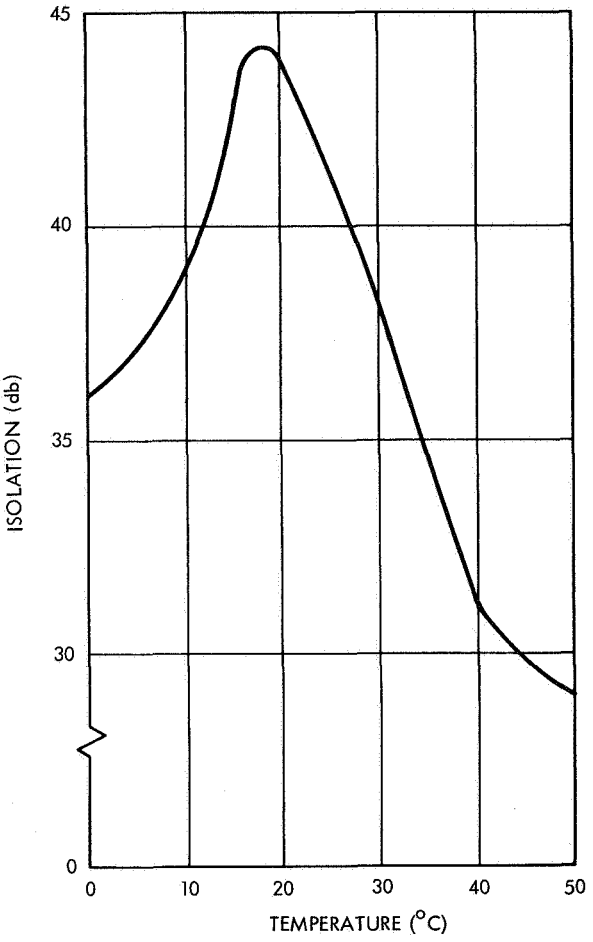


FIGURE 3–15.—Circulator isolation characteristic vs. temperature.

cooling from 200°K to 77°K, although not as much as the initial cooling to 200°K.

Once the decision to cool with liquid nitrogen was made, a choice of open cycle or closed cycle was necessary. For the purposes of Relay, the open cycle system was the most economical, and at the time, the simplest to design and maintain in the field.

The delivery schedule precluded extensive custom Dewar construction, so a Hoffman Laboratory stainless steel Dewar was selected. Stainless steel construction rather than glass was chosen to permit rough handling during transportion, installation, and removal. The 8¼ inch inside diameter accepted the existing uncooled breadboard par-

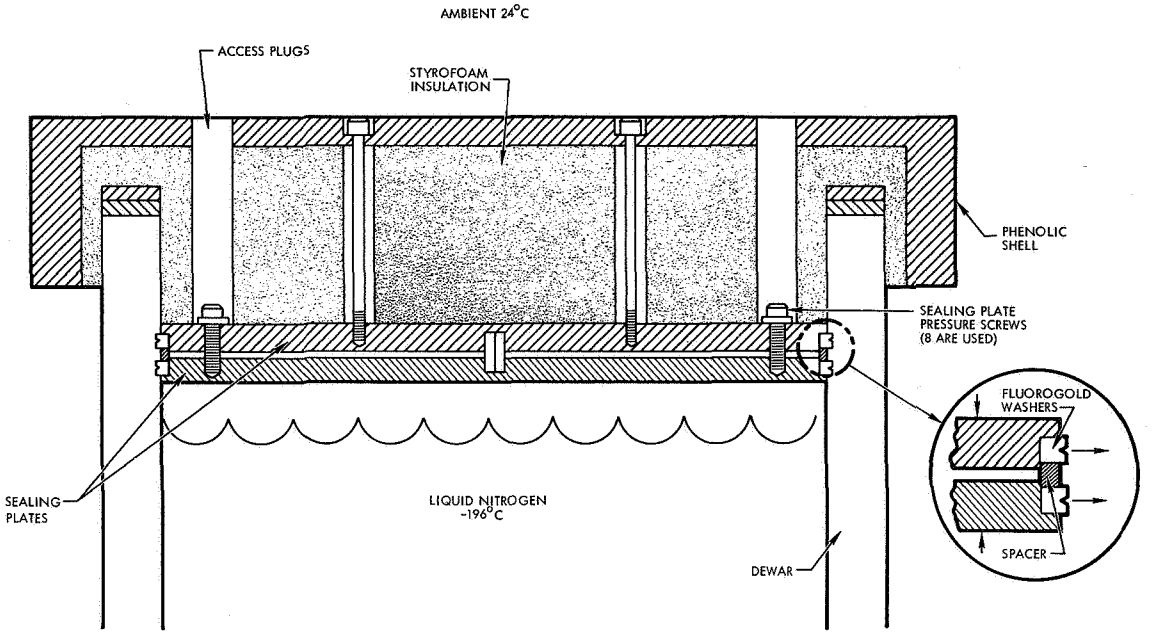


FIGURE 3–16.—Dewar cap and sealing mechanism.

amp with a minimum of alteration, and 13.6 liter capacity was considered sufficient for a reasonably long life system.

Since the Relay paramp was antenna mounted, it was necessary to design a suitable Dewar cap to permit tipping the paramp assembly without leaking, or causing excessive evaporation of the liquid nitrogen. Due to the extremely low temperature (77°K) and low viscosity of liquid nitrogen (0.15 vs. water at 1.0), design of a rather unique cap and sealing mechanism was necessary (see Figure 3–16). The cap consisted of a phenolic shell, filled with a 3-inch thick piece of styrofoam fitting on top of the sealing mechanism. Styrofoam proved to be a very effective insulator in this application.

The sealing mechanism consists of two large diameter stainless steel plates, arranged so that they can be drawn mechanically toward one another after installation in the Dewar. Sufficiently high force is generated when the plates are forced together to cause the teflon washers separating them to "cold flow" radially and thus tightly hug the inside of the Dewar, filling all imperfections in the Dewar itself. When properly installed this form of gasket proved to be a very effective seal for liquid nitrogen.

Evaporation rates of the Dewar with and without cap and at different attitudes is given in Figure 3–17. Eight to twelve hours between necessary filling operations is considered reasonable.

Figure 3–18 is a photograph of the Relay parametric amplifier body. The coaxial input is located on the top of the Dewar lid; a thin walled stainless steel coaxial waveguide goes through the Dewar lid to the varactor housing. The coaxial and rectangular waveguides extending through the Dewar cap are constructed of thin wall stainless steel to minimize the loss of heat. Figure 3–19 shows the parametric amplifier body mounted on the underside of the Dewar cap sealing plate. The signal tuner drive used to resonate the signal circuit and the K_u tuner drive mechanisms used to resonate the idler circuit are also shown. The complete paramp assembly with the Dewar in place is shown in Figure 3–20.

The paramp is cooled by both conduction and convection. To prevent any liquid nitro-

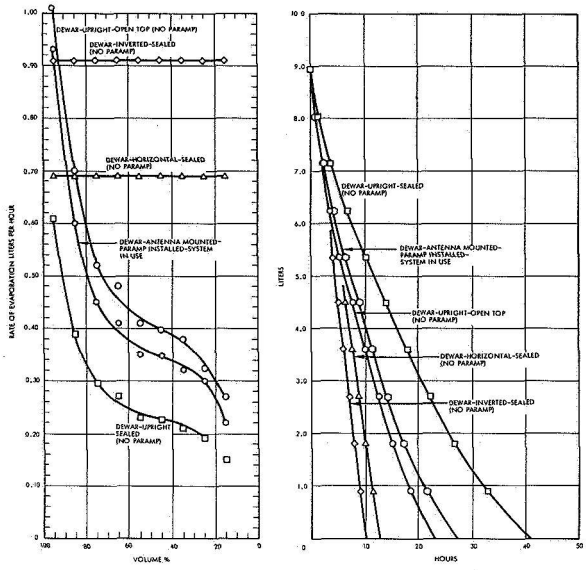


FIGURE 3–17.—Dewar evaporation rates.

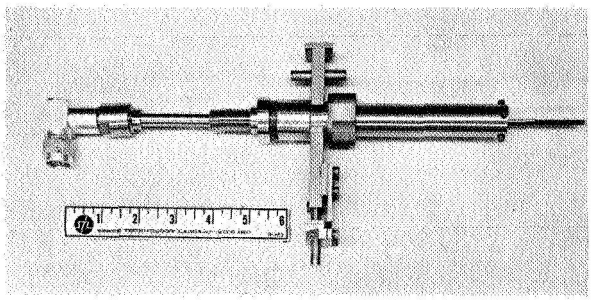


FIGURE 3–18.—Paramp body.

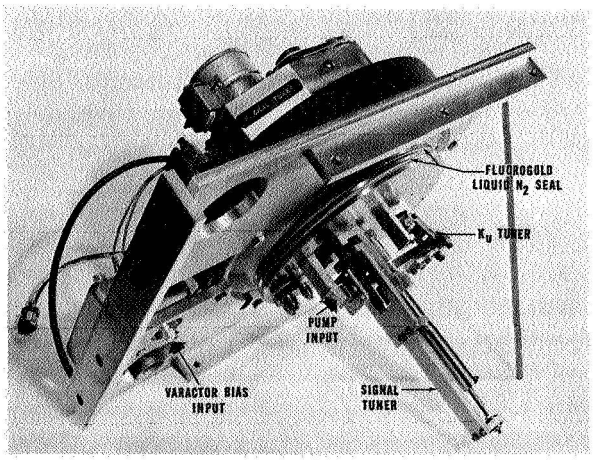


FIGURE 3–19.—Paramp mounted on Dewar cap.

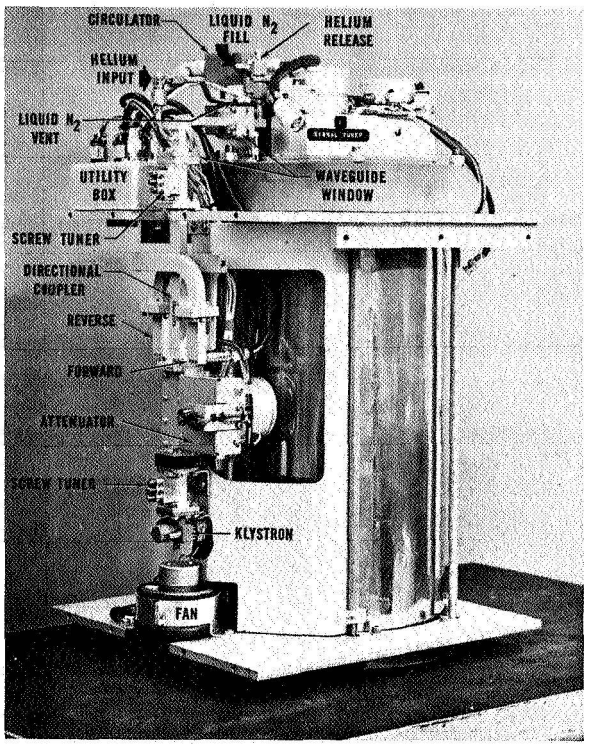


FIGURE 3–20.—Complete paramp assembly.

gen from leaking into the RF circuitry paramp body is pressurized with dry helium gas. Dry helium is pre-cooled through a copper tube coiled in the Dewar prior to entering the paramp cover.

Since the sealing of waveguide joints and tuning mechanisms are difficult, a cover is provided to slip over the paramp and tuning mechanisms. Helium is vented at the top of the Dewar cap on the pump waveguide for purging the system of moisture prior to cooling the paramp.

The liquid nitrogen level is monitored remotely in the test station van. Since the receiver had a requirement for operating on various antenna mounts, a level detecting system had to be capable of providing indication even when the receiver was rotated or tipped to the horizon in any direction. A cylindrical parallel plate capacitor was chosen since the Dewar was cylindrical. The capacitance is varied by the change in dielectric constant of the liquid between the plates.

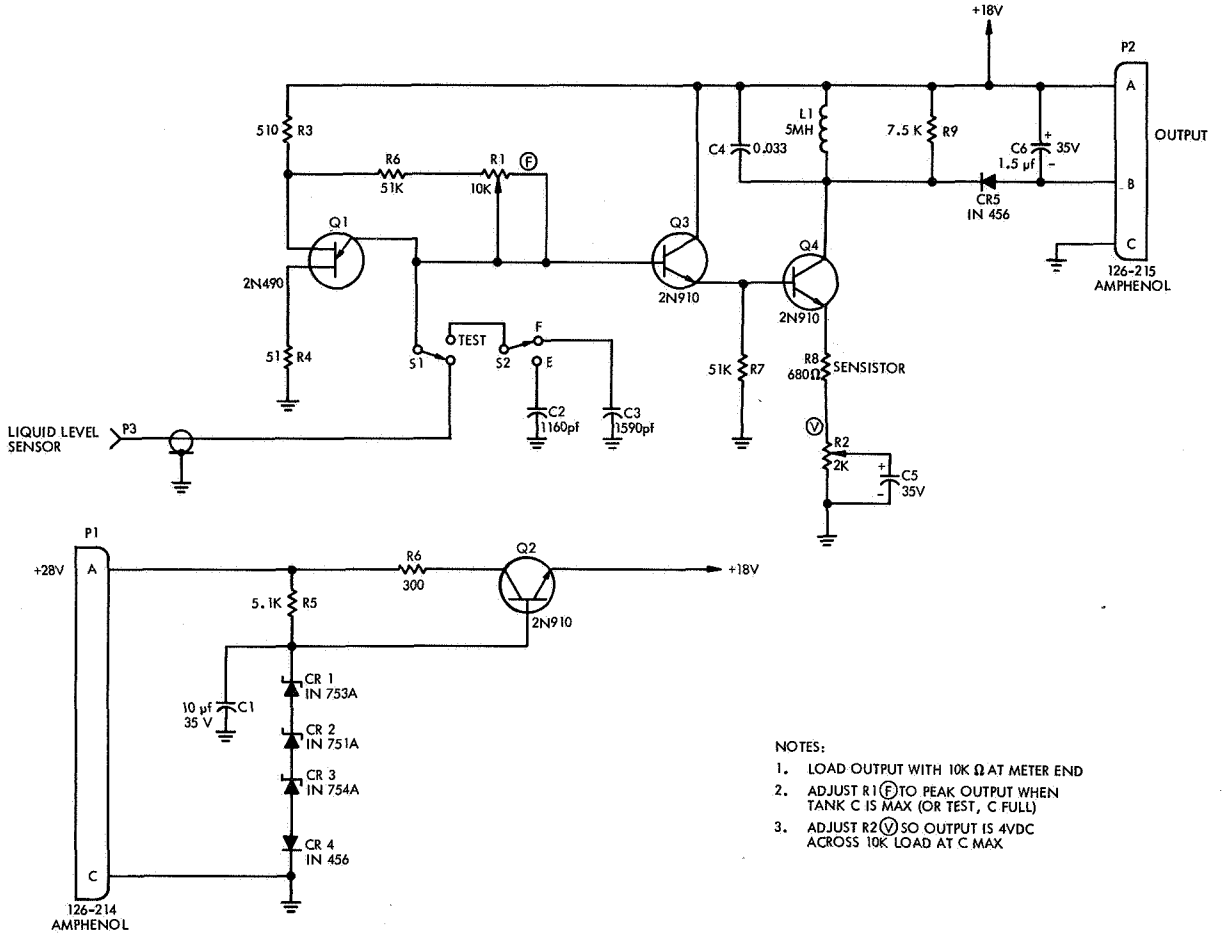


FIGURE 3–21.—Liquid nitrogen level detector schematic.

Most commercial liquid level detector units have small diameters and would not record liquid level for all attitudes of the Dewar.

The outside diameter of the parallel plate capacitor was thus constructed to be slightly smaller than the inner Dewar diameter. Capacitance of the liquid level capacitor was 1160 pf when empty, and 1590 pf when the Dewar is full of liquid nitrogen. This capacity controls the frequency of a unijunction oscillator which is then discriminated, and converted to dc level proportional to the liquid level in the parallel plate capacitor. Figure 3–21 is the schematic of this liquid nitrogen level detector.

Since it is inconvenient to extend the capacitor plates to the top of the Dewar, a thermistor is used in a self-heating mode to indicate that the liquid level is at the top. The self-heating mode of operation depends on the change in thermal conductivity of the medium surrounding the thermistor. The thermistor is biased such that a stable thermistor temperature is established when it is immersed in the liquid nitrogen but not when surrounded by cold nitrogen gas, since the thermal conductivity of the cold gas is less than the liquid. Figure 3–22 shows the circuit used to light the system monitor lamp, when the liquid level has reached the thermistor. When the lamp is lit, the liquid level indicator can be calibrated.

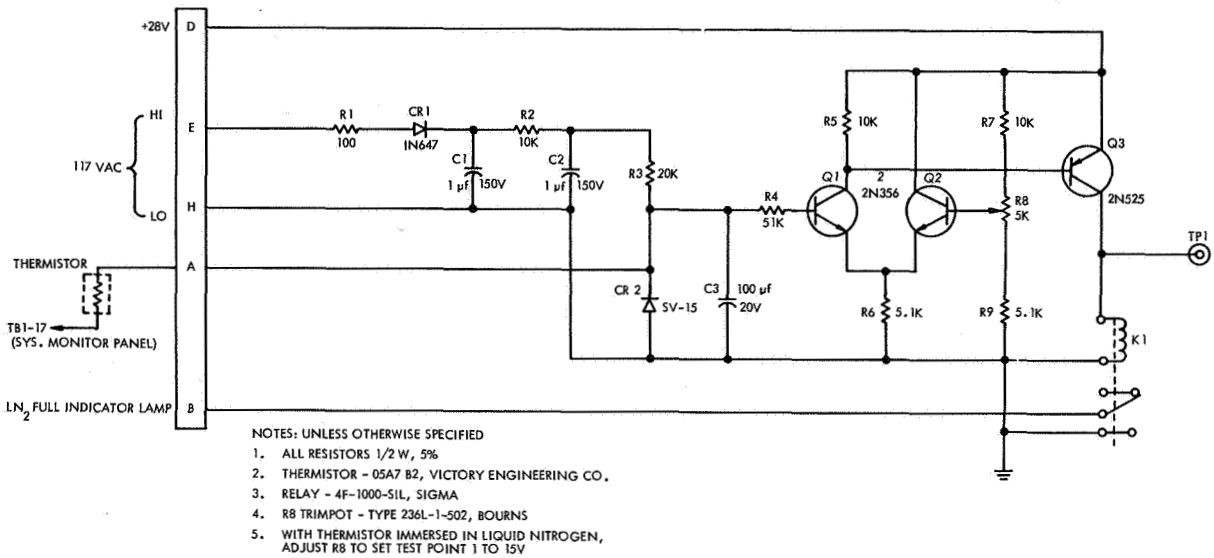


FIGURE 3-22.—Monitor panel light circuit.

Tuning Mechanism

Tuning of the signal and K_u band short are accomplished remotely by motor and gear box drives mounted on the outside of the Dewar cap. The activator which moves the K_u short is itself mounted within the Dewar in the cryogenic environment. Power is transmitted between the gear box and the activator by a slender stainless steel rod, thus minimizing heat loss. The activator consists of a lead screw, a bushing supported both top and bottom, with a nut mounted on the screw threads. The nut is restrained from rotating, so that it moves up and down the length of the lead screw as the screw rotates. This movement of the nut is used to actuate suitable levers which moves the shorting piece.

The lead screw consists of approximately one inch of 10–32 threads, with a 3/32 inch bearing surface turned on the shaft above the threads. Backlash in the system is minimized by selection and fitting of the bearing diameters and the nut and thread combination. The lead screw rotates at 1 rpm when tuning.

The lead screw bearing surfaces are mounted in Teflon bearings. Stainless steel was originally used, in order to maintain uniform coefficients of thermal expansion of all parts over the extreme temperature range encountered by the device (approximately 220°C), but the support bearings were changed to Teflon when galling was encountered with the stainless steel units. For the same reason, the nut mounted on the lead screw was changed from stainless steel to brass; the lead screw is lubricated with dri-film lubricant.

An identical parametric amplifier has been in use for the same period of time at another site. Here the activators are all stainless steel and have operated satisfactorily at ambient temperature (24°C) for a period of 58 weeks without difficulty.

The parametric amplifier performance measured at Nutley after nine months' service in the field is tabulated below.

	Equivalent noise Temp (°K)	*Gain (db)*
Paramp	75 to 89	18

Bandwidth (Mc)

24 with gallium arsenide and silicon varactors

TWT and 120-Mc Receiver

The noise figure of a low noise receiver is determined predominantly by the first stage

of amplification. Second stage noise figure contribution to the receiver noise is reduced by the gain of the first stage. The Relay receiver design allowed the second stage noise figure to be less than 5.5 db.

TWT

A traveling wave tube was selected as a second stage amplifier because of its reliability, low cost, and availability. A General Electric ZM–3113 traveling wave tube was ordered with the following specifications:

Frequency range: 4.10 to 4.25 Gc
Noise figure: <5.5 db
Gain: >30 db

Manufacturer's test data showed that the tubes exceeded the above specifications. Tests agreed on all measurements except the noise figure; gain was typically 36 db. Figure 3–23 shows a gain versus frequency plot for one of the tubes. The noise figure was measured at 4.17 Gc with a noise tube and a 120-Mc IF strip. The noise figure measured 6.6 db to 6.8 db. A hot-cold load was also used, and a 6.7 db noise figure was obtained. An image rejection filter was mounted after the traveling wave tube to prevent image noise from entering the mixer, and the same noise figures were measured. System threshold measurements also indicated the traveling wave tube noise figure was 6.5 to 7.0 db. This was the only "cut of specification" measurement finally accepted.

120-Mc Receiver

The 120-Mc receiver included a varactor multiplier chain for the local oscillator source to convert 4.17 Gc to 120 Mc. Approximately 80 db of gain is available at 120 Mc. Output of the 120 Mc receiver with AGC is approximately +3 dbm. Receiver gain is flat within ± 1 db over a 40-Mc bandwidth (100 to 140 Mc).

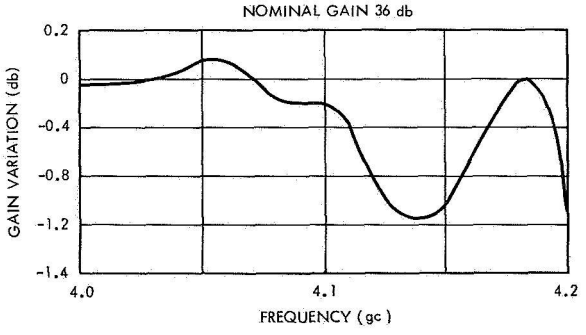


FIGURE 3–23.—TWT gain vs. frequency plot.

Control and Monitoring Circuitry

The control and monitoring circuitry units are rack mounted in the Communications van racks, as shown in Figure 3–24; the system monitor panel is shown in Figure 3–25.

Liquid nitrogen filling of the Dewar is accomplished by throwing the liquid nitrogen feed control switch to the VENT position. Then the switch is thrown to FILL, and the liquid flows into the Dewar (see Figure 3–4). The lamp marked FULL is activated by a thermistor sensor at the top of the Dewar, as previously described. The balanced crystal mixer currents are monitored as well as the AGC voltage in the 120-Mc receiver. A noise

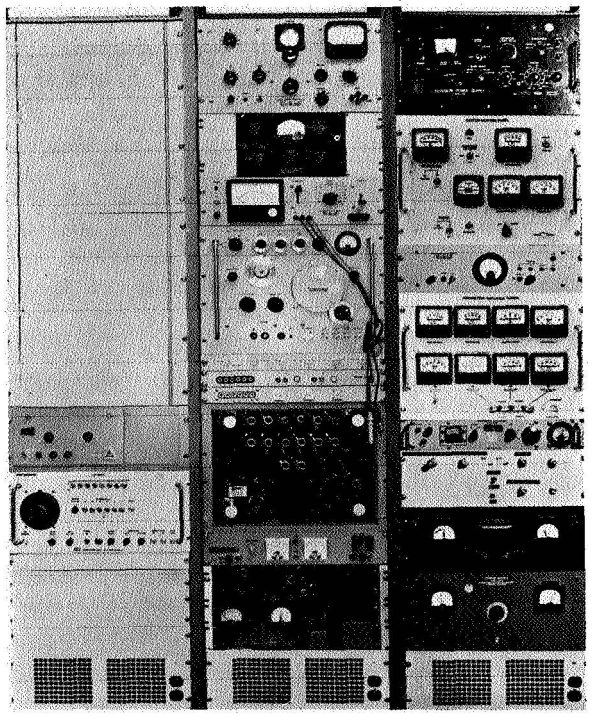


FIGURE 3–24.—Paramp control circuitry and power supply equipment rack.

mixer converts the 120 Mc IF frequency to 30 Mc for the Hewlett Packard system noise temperature monitor; the parametric amplifier tuning panel is shown in Figure 3–26. The PUMP ATTENUATOR switch varies the pump power while the SIGNAL TUNER control resonates the signal circuit of the paramp. The K_u SHORT switch tunes the idler circuit. The SHF signal generator is used for calibration purposes, and a spectrum analyzer displays the received spectrum. A switch is provided on the receiver monitor panel to actuate the waveguide switch at the input to the low noise receiver. A quick relative system noise performance check is made by switching the antenna and a termination at ambient temperature to the receiver input and observing the change in output noise power with a field intensity meter.

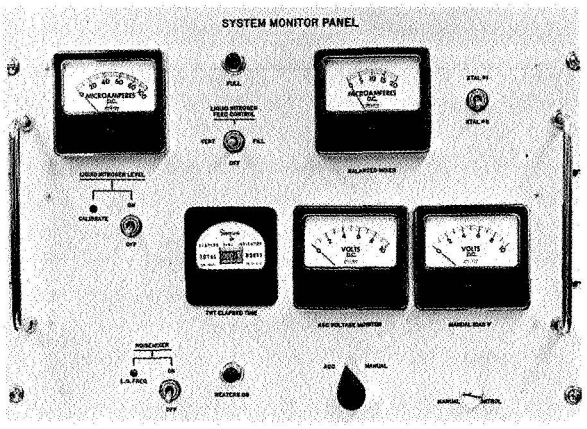


FIGURE 3–25.—Paramp system monitor panel.

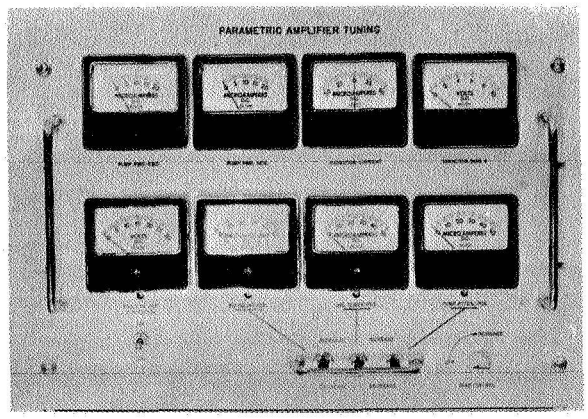


FIGURE 3–26.—Paramp tuning panel.

Low Noise Receiver System Performance

(System performance as measured at Nutley after nine months service in the field)

	Noise Figure (db)	Equivalent noise temp (°K)	Gain (db)	Bandwidth (Mc)	
Low noise receiving system	2.4	214	15	26	Paramp uncooled
	1.36	107	18	20	Paramp cooled

DEMODULATION SYSTEM

Development of the Wideband Phase-Lock Demodulator

The phase-lock FM demodulator for Relay television reception is an extension to ultra-wide-bandwidth techniques previously in use for improving synchronization,* telemetry,** and Doppler-measuring systems. Where varying signal strengths are encountered, such as in satellite transmission links with limited transmitter power, operation at low carrier levels, i.e., below the threshold of the conventional discriminators it is desirable to extend the visibility period during which the demodulated signal is of useful quality.

A familiar property of frequency modulation is the exchange of bandwidth for increased output signal-to-noise ratio. For wide deviations, this "FM improvement" over an amplitude modulation system of the same transmitted power is proportional to the square of the modulation index. However, this improvement is only available above a minimum carrier-to-noise C/N level. Below this minimum threshold which depends on the particular detection circuit used, the FM improvement vanishes rapidly.

*An early analysis is by Edouard Labin, "Theorie de la Synchronisation par Controle de Phase," *Philips Research Reports*, August 1949, pp. 291–315.

**Wolf J. Gruen, "Theory of AFC Synchronization," *Proc. IRE*, August 1953, pp. 1043–1048.

Bandwidth occupied by the transmitted FM spectrum is approximately 2 $(\Delta F + f_m)$, where ΔF is the peak deviation, and f_m is the maximum modulation frequency. Since the predetection bandwidth in the receiver must be sufficiently wide to pass this spectrum without distortion, a considerable portion of the receiver front-end noise will be present in the detector nonlinear characteristic, leading to interaction between the signal and noise. The region of input C/N ratios where interaction becomes important is at the threshold of the detection system.

Lowering of threshold is the target of feedback detection techniques, such as the phase-lock demodulator and the frequency-feedback demodulator.

Comparison of Phase-Lock and Frequency-Feedback Demodulators

The phase-lock demodulator feedback loop causes a local voltage-controlled oscillator (VCO) to track the instantaneous phase of the incoming signal; the voltage controlling the VCO is then proportional to the instantaneous frequency and is therefore the desired output. The loop maintains phase tracking at a C/N in a noise bandwidth which is lower than the threshold C/N of a limiter-discriminator. The difference between these C/N levels is the threshold improvement available from phaselock demodulation. Frequency-following demodulators cause the VCO to follow the instantaneous frequency of the signal, producing a compressed spectrum of the modulated carrier which may further be filtered in a narrower loop IF. This raises the C/N above the threshold of the loop discriminator.

Analyses have been made showing that for optimally-designed phase-lock and frequency-feedback demodulators, threshold improvements available are comparable. The phase-lock system was chosen for development at STL because of the inherently simpler nature of the units which make up the phase-lock loop.

The phase-lock loop consists of only three units: a VCO, a phase detector, which senses the phase error between the incoming signal and the VCO, and a baseband filter-amplifier which drives the VCO into phase synchronism and controls the loop transient response. The task of reducing the phase-lock principle to practice for the extremely wide television bandwidths is thus greatly simplified. Development of the phase-lock type demodulator began in August 1961 and was complete in mid-1962.

Summary of Phase-Lock Principles

A block diagram of the basic phase-lock demodulator is given in Figure 3–27.

Input to the FM system is a carrier at a frequency ω_c with phase angle modulation

$$\theta_i(s) = \frac{\Delta\omega(s)}{s} \tag{3.1}$$

The VCO rest frequency is also at ω_c; its phase transfer function is K_v/s where K_v is the control voltage slope in radians/second/volt. Phase error is generated in the phase detector, whose transfer function is $K\phi$ sin $(\theta_i - \theta_o)$ volts. The slope $K\phi$ is a function of input and local oscillator levels. Phase error voltage drives the filter-amplifier, with dc gain K_F and frequency response $F(s)$. Other frequency responses inherent in practical implementations of the loop may also be lumped in $F(s)$.

The loop equation is then:

$$\theta_o(s) = K\phi \sin(\theta_i - \theta_o) \cdot K_F F(s) \cdot \frac{K_v}{s}$$

$$= \frac{KF(s)}{s} \sin(\theta_i - \theta_o) \tag{3.2}$$

For a frequency difference between the input

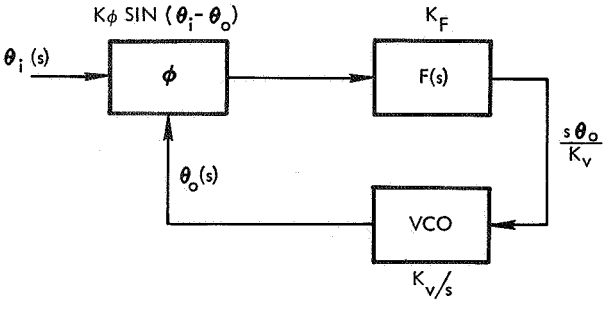


FIGURE 3–27.—Basic phase-lock loop.

and rest frequency of the VCO, $\theta_o(s)$ may be written as $\Delta\omega/s$, for which

$$|\sin\Delta\theta| = \frac{\Delta\omega}{KF(s)} \leq 1 \qquad (3.3)$$

Thus, for a steady frequency difference, and where $F(s=0)=1$,

$$|\Delta\omega|_{max} = K \qquad (3.4)$$

which is the hold-in range of the loop. Clearly K should be large to minimize phase error caused by steady frequency errors. The parameters K, which is the total gain, has the dimensions of radians/second.

An additional term affecting K is due to a limiter which drives the loop. Since the output power of a bandpass limiter is constant, constant signal level will be fed to the loop at high C/N ratio conditions, resulting in constant loop gain. At C/N ratio levels below + 10 db, the signal component of the limiter output drops with respect to its maximum value according to the relation:

$$\frac{e_s}{e_o} = K_a = \sqrt{\frac{1}{1+a\left(\frac{N}{C}\right)_i}} \qquad (3.5)$$

where a varies from ½ at high (C/N) ratios, to $4/\pi$ at low (C/N) ratios. The factor K_a is the limiter suppression.

The nonlinearity, $\sin(\theta_i - \theta_o)$, which limits the maximum instantaneous phase error to $\pi/2$ for tracking, is the cause of loop thresholding. To analyze the loop above its threshold, phase error is assumed to be small enough to use the approximation

$$\sin(\theta_i - \theta_o) \cong \theta_i - \theta_o = \Delta\theta \qquad (3.6)$$

The resulting closed-loop transfer function is:

$$\frac{\theta_o}{\theta_i} = \frac{KF(s)}{S+KF(s)} = G(s) \qquad (3.7)$$

The functon $F(s)$ is chosen to minimize total tracking error $\epsilon(s)$, which is the difference between the desired signal and the loop output, given an input θ_i. Where θ_i consists of the modulation $m(s)$ plus receiver noise $n(s)$, the tracking error is

$$\begin{aligned}\epsilon(s) &= m(s) - \theta_o \\ &= m(s) - \theta_i G(s) \\ &= m(s)[1-G(s)] - n(s)G(s) \\ &= \epsilon_m(s) - \epsilon_n(s) \qquad (3.8)\end{aligned}$$

Since signal and noise are usually uncorrelated, each term on the right of Equation (3–8) must be minimized separately by proper choice of $G(s)$.

Optimization studies* have resulted in several filter characteristics depending on the assumptions made for $m(s)$ and $n(s)$, and on the minimization criteria, such as magnitude of $\epsilon_n(s)$, mean square value. For the case of television, $m(s)$ is the result of modulation frequency ramps produced by video transients, $n(s)$ is band limited gaussian noise modified by wideband limiting, and the error is minimized on the basis.

$$\epsilon(t) = |\epsilon_m + \sigma\epsilon_n| < \pi/2 \qquad (3.9)$$

where ϵ_m is the peak error due to modulation, ϵ_n is the RMS noise error, and σ the peak factor for the noise, which is typically 3 for gaussian noise. In our case, the noise is not gaussian, because of the wide loop bandwidth after the phase detector nonlinearity is introduced. An arbitrary choice for σ is made in the design to be described.

Phase-Lock Loop Application to Television Signal Demodulation

The loop response $G(s)$, given in Equation (3–7), which is the baseband response when the output is the VCO control signal, and the input is frequency-modulation by the video

*R. Jaffe and E. Rechtin, "Design and Performance of Phase-Lock Circuits, etc.," *IRE Trans. on Information Theory*, March 1955, pp. 66–76.

C. E. Gilchriest, "Application of the Phase-Locked Loop to Telemetry as a Discriminator or Tracking Filter," *IRE Trans. on Telemetry and Remote Control*, June 1958, pp. 20–35.

A. J. Viterbi, "Acquisition and Tracking Behavior of Phase-Locked Loops," *Proc. Symposium on Active Networks and Feedback Systems*, Polytechnic Institute of Brooklyn, April 1960.

C. R. Cahn, "Comparison of Optimized Phase-Lock and Frequency Feedback FM Demodulators," presented at IEEE 6th Region Technical Conference, 23 April 1963.

signal, is obtained in the practical case by using a loop filter $F(s)$, where:

$$F(s) = \frac{1 + \tau_2 s}{1 + \tau_1 s} \qquad (3.10)$$

This is an approximation to an ideal integrator;* a filter of the form of Figure 3–28. In this basic form,

$$\tau_1 = (R_1 + R_2)\, C$$

and

$$\tau_2 = R_2\, C$$

The filter used in the STL demodulator lumps the forward gain K_F with the frequency response $F(s)$ as in Figure 3–29.

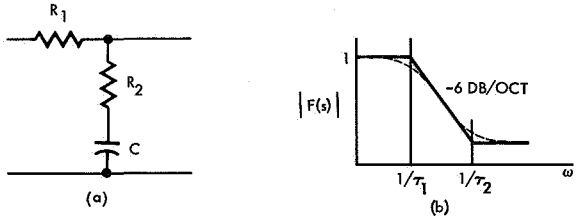


FIGURE 3–28.—Loop filter and response.

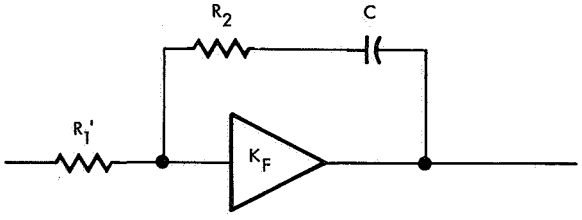


FIGURE 3–29.—Loop filter with gain.

For this case,

$$\tau_1 = K_F R'_1\, C$$

and

$$\tau_2 = R_2\, C \qquad (3.12)$$

The closed loop response is then

$$G(s) = \frac{1 + \tau_2 s}{1 + s\left(\tau_2 + \frac{1}{K}\right) + \frac{\tau_1}{K} s^2} \qquad (3.13)$$

Since K is usually much greater than $1/\tau_2$, the approximation

$$G(s) \cong \frac{1 + \tau_2 s}{1 + \tau_2 s + \frac{\tau_1}{K} s^2} \qquad (3.14)$$

can be made. This second-order response is a familiar one in servo system analysis. Substituting for τ_1 and τ_2 as follows:

$$\frac{\tau_1}{K} = \frac{1}{\omega_n^2} \text{ and } \tau_2 = \frac{2\zeta}{\omega_n} \qquad (3.15)$$

then

$$G(s) = \frac{1 + \frac{2\zeta}{\omega_n} s}{1 + \frac{2}{\omega_n} s + \frac{s^2}{\omega_n^2}} \qquad (3.16)$$

The quantity ω_n is the loop undamped natural resonant frequency in radians/second, and ζ is the ratio of the loop damping to critical damping. The magnitude of $G(s)$ for $s = j\omega$ is

$$|G(j\omega)| = \left[\frac{1 + 4\zeta^2 \frac{\omega^2}{\omega_n^2}}{1 + (4\zeta^2 - 2)\frac{\omega^2}{\omega_n^2} + \frac{\omega^4}{\omega_n^4}}\right]^{1/2} \qquad (3.17)$$

which is the low pass response plotted in Figure 3–30 for various ζ as a function of

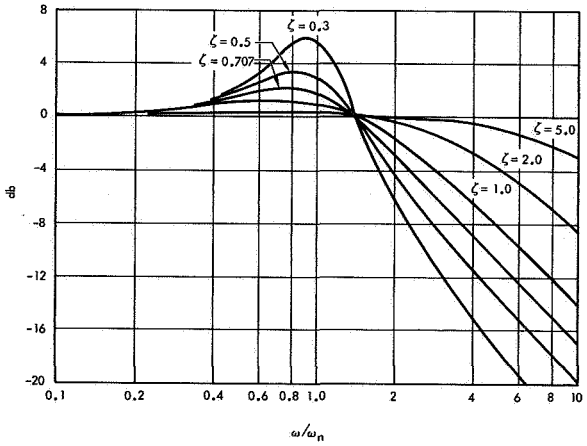


FIGURE 3–30.—Loop baseband response for various damping ratios.

*A useful reference containing design equations and graphs applicable to the linear model is by L. A. Hoffman, "Receiver Design and the Phase-Lock Loop," prepared for the IEEE Electronics and Space Exploration Technical Lecture Series, Spring 1963.

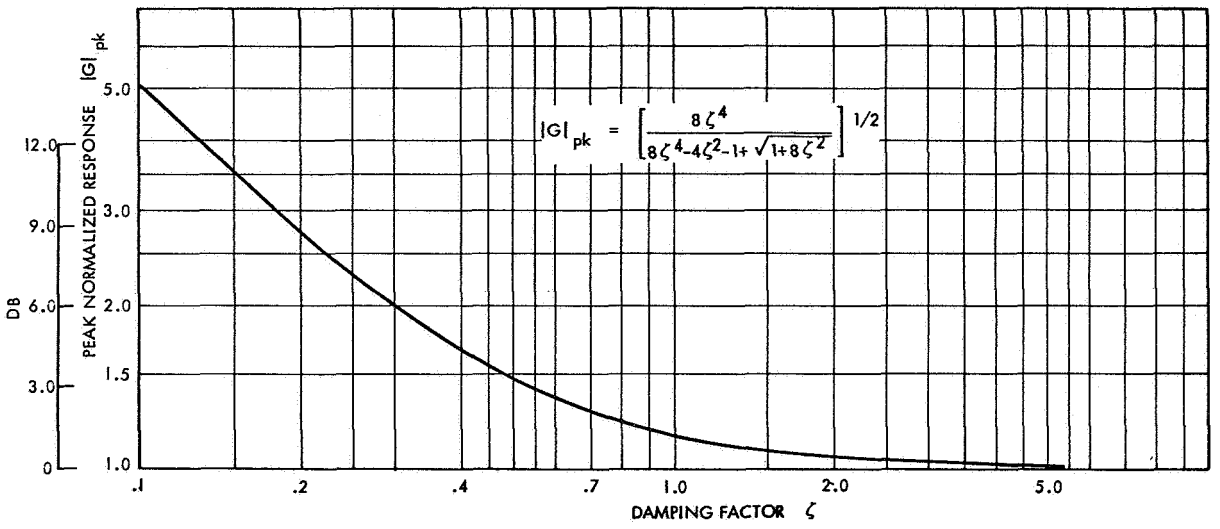


FIGURE 3–31.—Frequency of response peak vs. damping factor.

the normalized frequency variable ω/ω_n.

The frequency at which the response peak occurs is plotted in Figure 3–31, and the magnitude of the peak in Figure 3–32, both as a function of damping factor ζ. The error function $1 - G(s)$ which is due to modulation is obtained from Equation (3.16).

$$1 - G(s) = H(s) = \frac{\frac{s^2}{\omega_n^2}}{1 + \frac{2\zeta}{\omega_n}s + \frac{s^2}{\omega_n^2}} \quad (3.18)$$

which is valid for $\omega << K$.

In the television case, response to frequency ramps is of most interest, and therefore

$$\theta_i(s) = \frac{\dot{\omega}}{s^3} \quad (3.19)$$

where $\dot{\omega}$ is the maximum rate of change of frequency. The resulting time function may be shown to be, for $\zeta < 1$ and large K,

$$\epsilon_m(t) = \frac{\dot{\omega}}{\omega_n^2}\left[1 - e^{-\zeta\omega_n t}\left(\cos\sqrt{1-\zeta^2}\,\omega_n t + \frac{\zeta}{\sqrt{1-\zeta^2}}\sin\sqrt{1-\zeta^2}\,\omega_n t\right)\right] \quad (3.20)$$

Plotting the term in brackets as a function of $\omega_n t$ (Figure 3–33), it is clear that a damping ratio ζ of about $\sqrt{2}/2$ results in rapid decay of the transient term with small overshoot. The maximum for this phase error is then (for $\zeta = \sqrt{2}/2$)

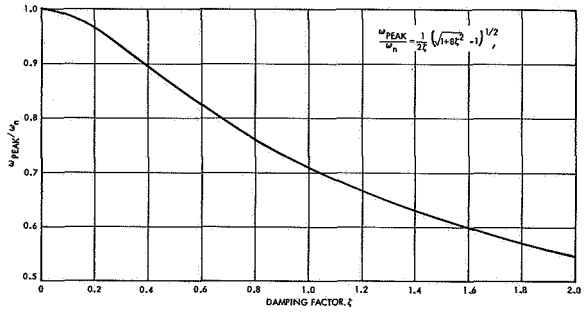


FIGURE 3–32.—Peak response of loop normalized to zero—frequency gain vs. damping factor.

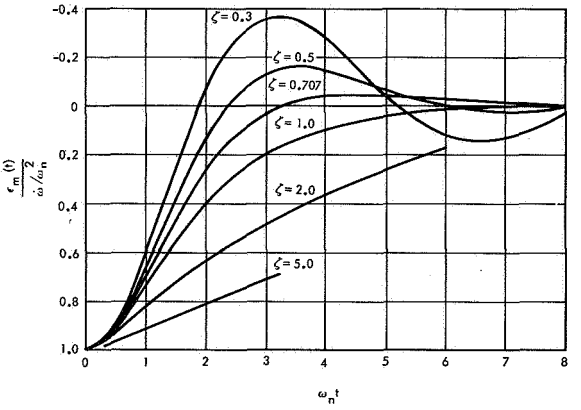


FIGURE 3–33.—Transient phase-error for frequency ramp.

$$\epsilon_m(\max) = 1.043\frac{\dot{\omega}}{\omega_n^2} \qquad (3.21)$$

For modulation which includes a subcarrier at frequency ω_{ms} with peak deviation $\Delta\omega_{cs}$, the maximum phase error may be computed from

$$\epsilon_{ms}(\max) = \frac{\Delta\omega_{cs}}{\omega_{ms}\sqrt{1+\left(\frac{\omega_n}{\omega_{ms}}\right)^4}} \qquad (3.22)$$

The square of the noise component ϵ_n in Equation (3.8) for white input noise of large bandwidth is the N/C ratio in the loop:

$$\epsilon_n^2 = \frac{\Phi}{C}\int_{-\infty}^{\infty} |G(j\omega)|^2 \frac{d\omega}{2\pi} \qquad (3.23)$$

where C is the input carrier power in watts, Φ is the noise density in watts/cps, and the integral is the two-sided loop noise bandwidth B_N in cps. This is

$$B_N = \omega_n\left(\frac{1+4\zeta^2}{4\zeta}\right) \qquad (3.24)$$

where ω_n is in radians/sec. To minimize ϵ_n, damping ratio ζ should be ½ for which $B_N = \omega_n$; however, since ζ equal to $\sqrt{2}/2$ was chosen for good transient response, we find that B_N is now $(3/2\sqrt{2})\cdot\omega_n = 1.06\,\omega_n$.

The maximum error for a frequency ramp may be obtained from Equation (3.20), and is approximately*

$$|\epsilon_m|(\max) = \frac{\dot{\omega}}{\omega_n^2}\left(1+e^{\zeta\pi/\sqrt{1-\zeta^2}}\right) \qquad (3.25)$$

This is plotted in Figure 3–34.

It may be shown from the equations above that for the following normal conditions

$$1 < M < 5,\ 0.1 < |\epsilon_m| < 1, \text{ and } 0.1 < \zeta < 2 \qquad (3.26)$$

for modulation index, phase error, and damping ratio, respectively, the required loop noise bandwidth will be larger than the minimum IF bandwidth $2f_m(M+1)$. This means that loop noise error is independent of ω_n. For this case, natural resonance ω_n should be made as large as possible, with damping ζ in the range of Equation (3.26) above, in order to reduce the modulation phase error to a negligible portion of the total loop error.

This consideration is important in the case of practical designs, where large ω_n is accompanied by decreasing ζ due to time delays

*J. P. Frazier and J. Page, "Phase-Lock Loop Frequency Acquisition Study," *IRE Trans. on Space Electronics and Telemetry*, September 1962, p. 224.

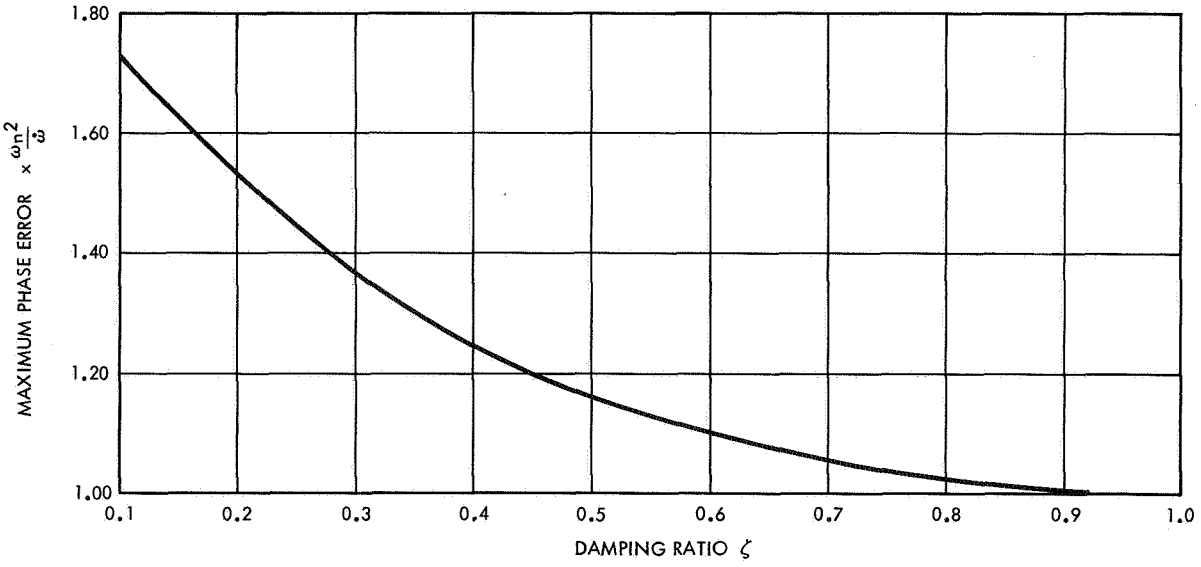


FIGURE 3–34.—Maximum phase error for frequency ramp vs. ζ.

and high frequency poles inherent in the physical realizations of the elements of the loop.*

It is apparent, therefore, that if large ω_n is available from a given loop circuit design, with sufficiently large ζ (greater than 0.1), that maximum modulation phase error may be smaller for a highly-underdamped, very wideband loop, than for the optimally-damped narrowband loop. Further study of improvement achievable by this means seems justified.

Description of Demodulator Design

Figure 3–35 is the block diagram of the overall demodulator, which consists of equalizer, IF amplifiers, phase-lock loop, discriminator, video filter and amplifiers, and metering and control circuits.

Equalizer

The input, at a nominal carrier power level of —7 dbm, is fed to an equalizing filter circuit whose function is to correct phase distortion produced in the receiver section ahead of the demodulator.

Figure 3–36 is a simplified schematic of the equalizer, which consists of four cascaded bridged-*T* sections, with input and output grounded base amplifier stages. Overall gain is 0 db.

IF Amplifier

Output of the equalizer is amplified by a wideband IF grounded-base stage which drives a hybrid splitter. The two split signals

*R. C. Booton, Jr., "Demodulation of Wideband Frequency Modulation Utilizing Phase-Lock Technique," *Proc. National Telemetering Conference*, May 1962, Session 6.

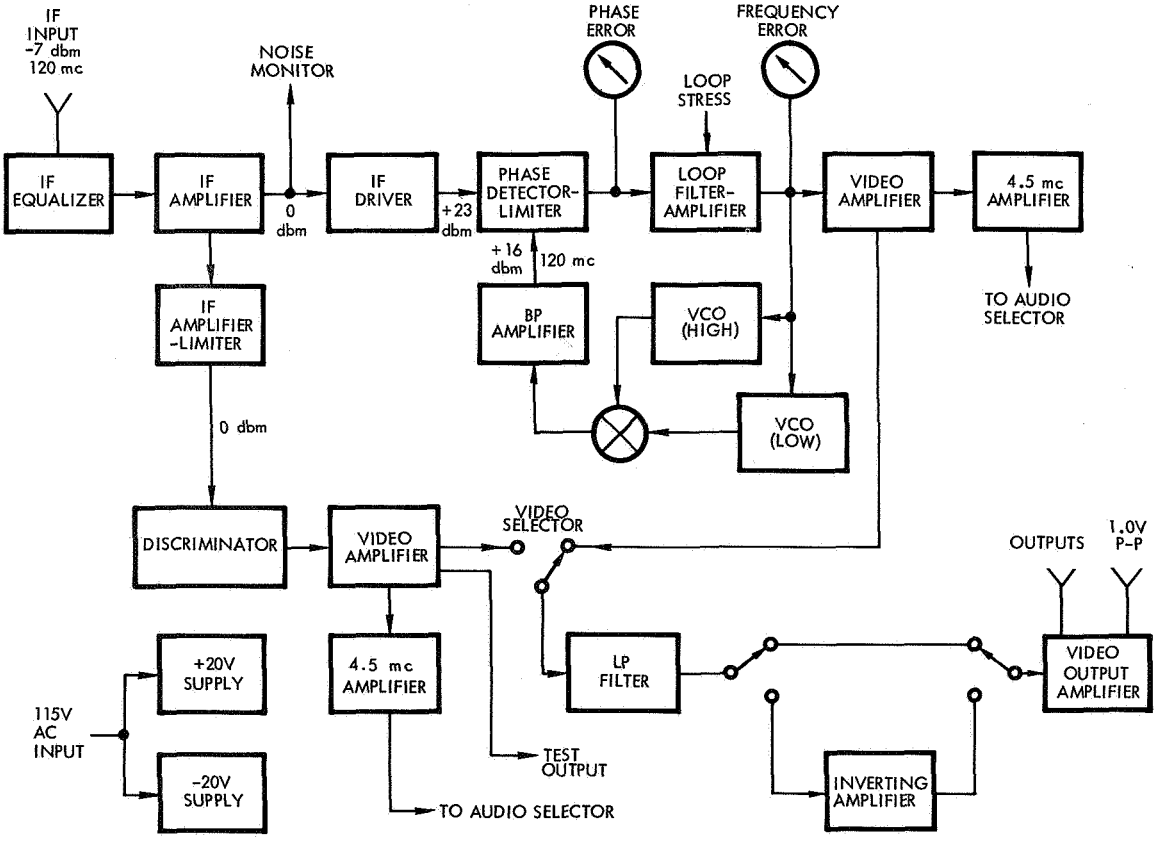


FIGURE 3–35.—Block diagram of STL wideband demodulator.

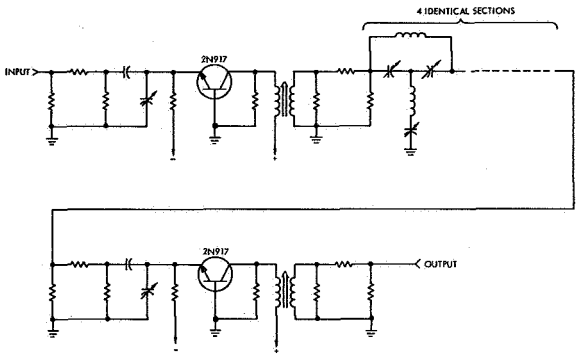


FIGURE 3–36.—IF equalizer.

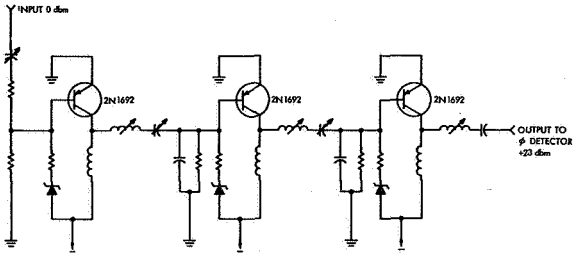


FIGURE 3–38.—IF driver amplifier.

are amplified, respectively, in a linear stage to 7 db above the input for the phase-lock section, and in a limiting stage to 0 dbm for the discriminator. Bandwidths of these stages exceed 40 Mc between 1 db points. Figure 3–37 is an abbreviated schematic of this IF amplifier module.

IF Driver Amplifier

To obtain high loop gain, power levels into the phase detector must be large. Nominal output of the IF amplifier, at 0 dbm, is raised to + 23 dbm by a driver module consisting of three grounded-emitter stages. Overall bandwidth is at least 60 Mc between 1 db points. Figure 3–38 shows a schematic of this circuit. The driver output saturates at about + 26 dbm.

Phase Detector

Limiting action is automatically achieved in the phase detector by increasing the signal power to a level 7 db greater than the VCO power. The resulting phase detector slope and maximum output is proportional only to the VCO power, constant over a 20 Mc band about the VCO rest frequency.

The phase detector (Figure 3–39) is a four-diode bridge, transformer-driven by the signal and VCO voltages. Close coupling is obtained by toroidal cores and bifilar windings. Variable capacitors are used for noise-balancing. For reasonable efficiency at the relatively high carrier frequency at 120 Mc, diode switching must occur within a small fraction of one period (8.25 nsec), and diode forward conduction must be large. The diodes chosen (CR 1–4) are Microstate gallium arsenide types, with 0.5 nsec recovery time and 5-ohm dynamic resistance. The resulting phase detector output is 1.5 volts peak.

Loop Filter-Amplifier

Design of the loop filter-amplifier follows the method described in a previous paragraph, with additional clipping circuits as shown in Figure 3–39. Resistors R1 and R2 are variable to allow trimming of the closed-loop response for desired resonance and

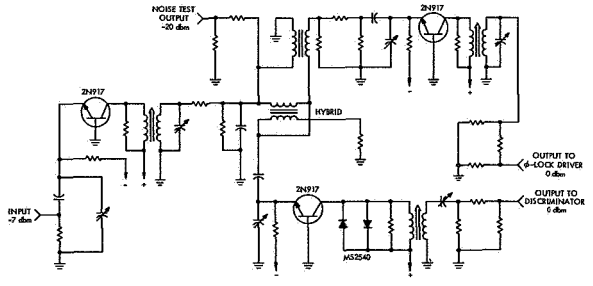


FIGURE 3–37.—IF amplifier.

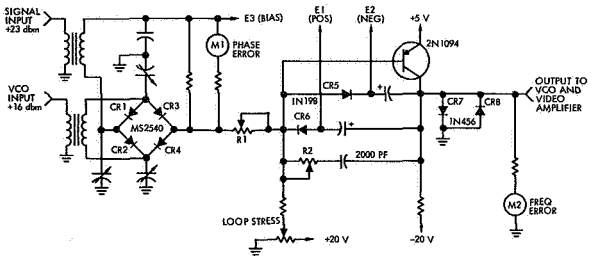


FIGURE 3–39.—Phase detector and loop filter amplifier.

damping; nominal dc gain of the amplifier is 20.

Diodes CR5 and CR6 are germanium, biased by voltages E_1 and E_2 to conduct when the VCO control voltage exceeds predetermined levels, due to noise peaks. Conduction of either diode momentarily reduces the amplifier gain by increasing the feedback from the transistor collector to the base. In addition, diodes CR7 and CR8 limit the maximum peak-to-peak swing to the VCO to about one volt. The effect of this multiple clipping is to reduce the time required for the loop to reacquire lock once it is lost because of noise peaks, and thus reduce the length of black or white streaks visible on the TV display. Voltages E_1 and E_2 are adjustable for optimum streak reduction.

The meters M_1 and M_2 shown in Figure 3–39 measure average phase and frequency errors, respectively, for use in initial acquisition and loop monitoring. The phase error measured is the dc component of the phase detector output, and the frequency error is the dc component of the VCO control voltage. Figure 3–40 is a simplified schematic of the bias sources for E_1 and E_2, as well as the base current source (E3) for the germanium transistor. Diodes CR9 and CR10 furnish temperature compensation for these bias sources.

A loop stress voltage is obtained from a potentiometer control mounted on the front panel. This control produces a plus-or-minus voltage at the VCO control line for initial locking to the input signal.

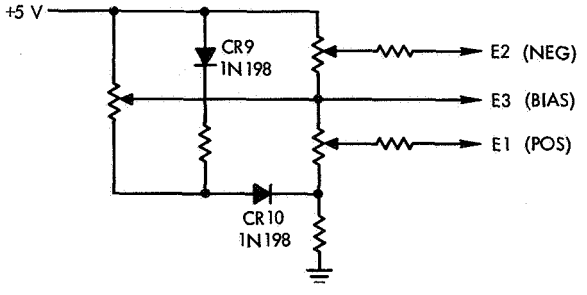


FIGURE 3–40.—Clipping and base bias voltages network.

Video Amplifier

The demodulated baseband signal, which is also the VCO control, is fed to a video amplifier with adjustable gain of about 1.4. Frequency response of this amplifier is flat beyond the maximum modulation frequency, since the post-detection bandwidth is later defined by the sharp cutoff lowpass video filter shown in the schematic of Figure 3–41.

The video amplifier module includes a bandpass circuit (L1 and C1) 1 Mc wide at —3 db points, centered at 4.5 Mc, to extract the aural subcarrier for demodulation by an auxiliary discriminator.

VCO

The VCO is designed to furnish a relatively high, constant power (40 milliwatts), with frequency a linear function of a control input voltage. A basic requirement is low input capacitance and circuit delay, in order not to seriously affect the effective loop filter time constants.

This design (Figure 3–42) uses two isolated grounded-base oscillators with varactor diodes VC1 and VC2 in the collector resonant circuits. Frequencies of the oscillators (425 Mc and 305 Mc) are 120 Mc apart and have been chosen to minimize spurious products in the balanced mixer diodes CR1 through CR4, which generate the desired difference frequency. Biasing and varactor diode polarities in the respective oscillators are such as to give differential frequency control. The result of differential action is first-order cancellation of the inherent nonlinear frequency control characteristic of the varactor as used in these circuits, as well as doubling of the slope of frequency change.

The balanced mixer is followed by two stages of wideband amplification in grounded-

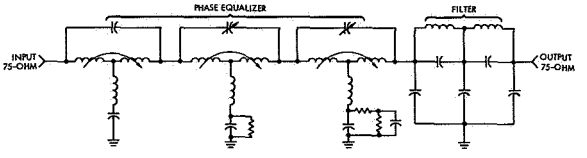


FIGURE 3–41.—Video low pass filter.

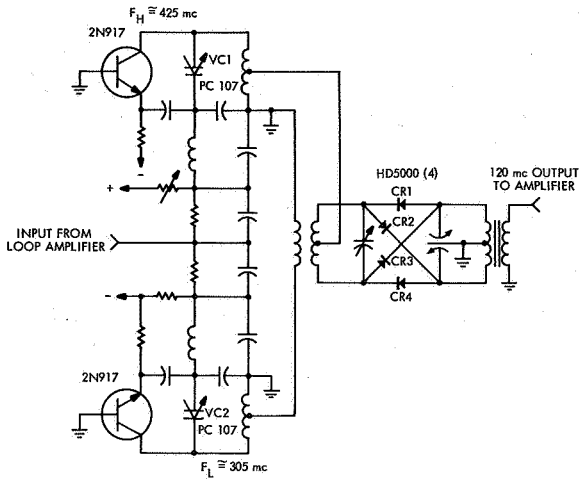


FIGURE 3–42.—VCO and balanced mixer.

base circuits. Power level is constant within 0.2 db over a frequency excursion ± 10 Mc from the nominal rest frequency; slope is 20 Mc/volt and nonlinearity is less than 0.5 percent.

Baseband Circuits

Output of the video amplifier is selected by a front-panel switch and fed to the low-pass filter mentioned above. This is followed by a video output amplifier which has two functions: selectable inversion of the video polarity and impedance-matching to the output cables.

The inverting amplifier, which may be bypassed by means of a switch on the module, has an insertion gain of unity, and consists of a grounded-emitter stage followed by an emitter-follower. Negative and positive feedback paths shape the response for adequate high-frequency output together with low tilt for the square waves.

The line-driving amplifier consists of two grounded-emitter stages feeding a grounded-emitter complementary-pair output stage. Five feedback paths control the square-wave response. Figure 3–43 presents a schematic of these amplifiers, which is included to show the multiple-feedback since a few words are not adequate to describe the circuits.

A variable resistor is used to adjust the positive feedback at low frequencies for zero tilt. Two 70-ohm output loads may be driven simultaneously.

Discriminator Section

The passive discriminator circuit driven by the limiting stage of the IF amplifier is included for two purposes: backup where the threshold improvement of the phase-lock loop is not required, or where there is malfunction of the loop, and for simultaneous comparison of the respective methods of detection.

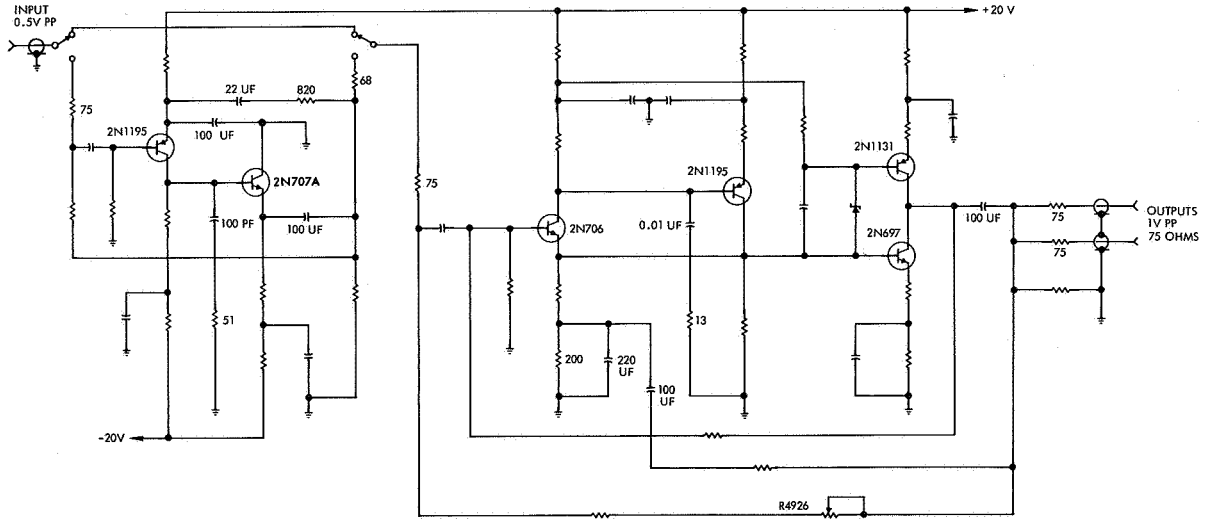


FIGURE 3–43.—Video output amplifier schematic diagram.

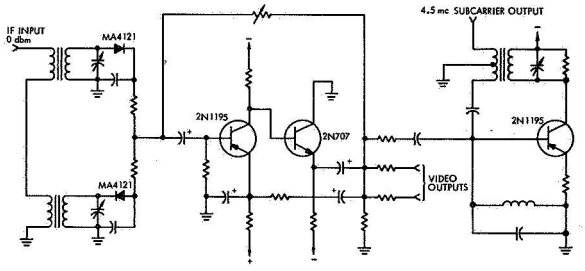


FIGURE 3–44.—Discriminator and amplifier.

The discriminator (Figure 3–44) consists of two envelope detectors, each driven by a tuned circuit of bandwidth and center frequency required for optimum linear response over at least a ± 10 Mc band. The detector outputs are differenced, and this difference is fed to a two-stage video amplifier consisting of a grounded-emitter transistor and an emitter-follower. A variable negative feedback path adjusts the video gain, and a feedback path controls square-wave tilt.

A bandpass circuit, similar to that in the phase-lock video amplifier, extracts the 4.5 Mc subcarrier.

Both baseband and subcarrier signals from the discriminator circuitry may be selected to drive the output lines of the demodulator by means of two switches on the front panel.

Physical Description

The photograph of Figure 3–45 and Figure

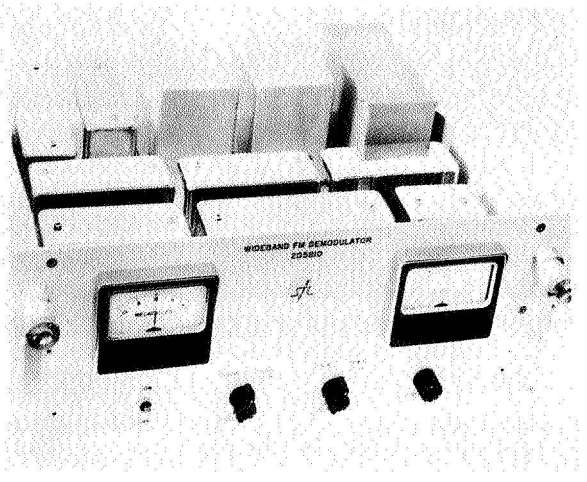


FIGURE 3–45.—Complete demodulator.

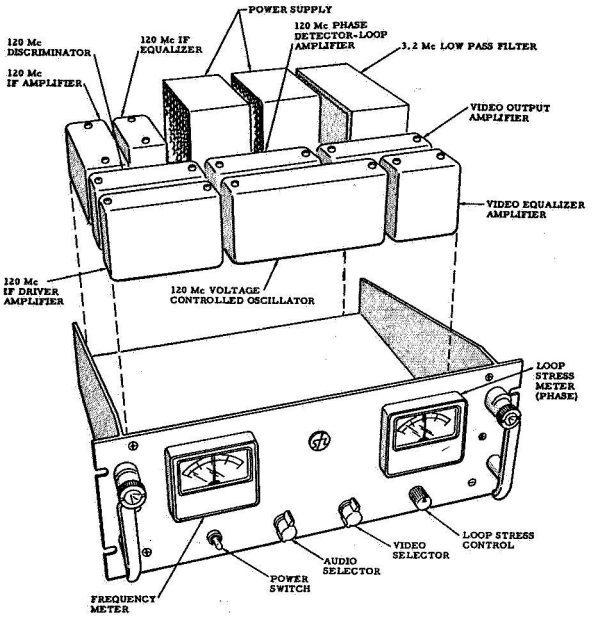


FIGURE 3–46.—Relay demodulator chassis layout.

3–46 show the top view of the complete demodulator. Circuits are separated on a functional basis in a number of chassis-mounted modules, interconnected below the chassis by coaxial cables. Quick access and removal for maintenance is thus achieved.

The large twin modules in the figures are commercial power supplies (+ and — 20 volts). The demodulator is therefore self-contained: only ac line power and signal are required. Power drain is about 35 watts at 115 volts, 60 to 400 cps.

Dimensions of the unit are: front panel, 19″ wide by 7″ high; chassis, 17″ wide and 15″ deep. Weight is 32 pounds.

TV Reception

The design of the STL demodulator for Relay is capable of resonant frequency ω_n of approximately 25×10^6 radians/second (i.e., 4.0 Mc), with a damping ratio ζ of $\sqrt{2}/2$. For these parameters, loop noise bandwidth B_N is 26 Mc, which is approximately equal to the IF bandwidth. Nominal gain of the components within the loop at strong signals is 3.8×10^9 radians/second. Adjustment of the parameters is such that damping and resonant frequency at + 2 db C/N are as stated.

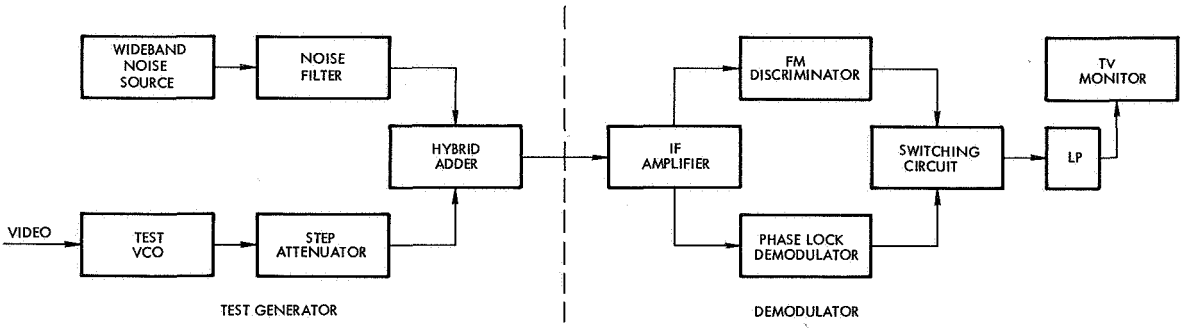


FIGURE 3–47.—Experiment to measure TV threshold improvement.

Input characteristics are: maximum video frequency (including synchronization pulses) of 3.2 Mc, deviating the carrier 13.7 Mc peak-to-peak; aural subcarrier at 4.5 Mc with deviation of 2.7 Mc peak-to-peak.

The available threshold improvement is in the case of television somewhat qualitative depending on visual criteria. To obtain a measure of the improvement, the experiment described in the diagram of Figure 3–47 was performed.

The white noise source is fed to a filter of approximately square response, with a noise bandwidth of 32 Mc. This is equal to the noise bandwidth of the Relay receiver parametric amplifier front end. The VCO is modulated by standard TV video material obtained from commercial television. Relative power levels of signal and noise are measured following addition in a linear hybrid circuit.

This noisy signal is fed to the wideband demodulator input. Outputs of the respective detectors, phase-lock and discriminator-limiter, are alternately sampled and displayed on a studio TV monitor. The results of this experiment, as shown in the photographs of Figure 3–48, indicate that the phase-lock output is roughly equivalent, at 0 db input C/N, to that from the discriminator at + 5 db, yielding a 5 db improvement.

Baseband Noise Measurements

Comparison of the baseband output noise of the phase-lock and discriminator demodulators, with various input C/N levels, yields information on the effective threshold of each device.

Noise power spectrum over the baseband range of 50 kc to 3 Mc was measured using an analyzer of 4 kc bandwidth.* The input consisted of an unmodulated carrier plus bandlimited noise. The results are plotted in Figure 3–49. At the point of measurement, 0 dbm corresponds to 11.0 Mc Peak-to-peak deviation.

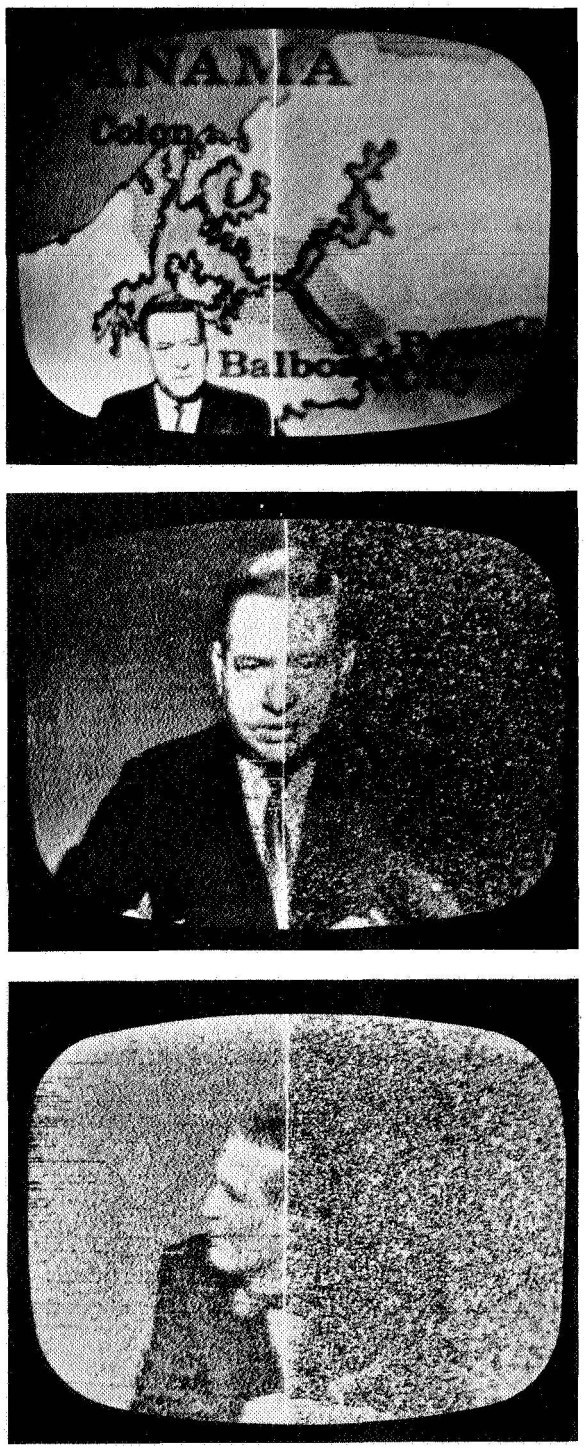
For $C/N$of +20 db, the output noise levels of both demodulators are comparable; the discriminator noise is 5 db higher at 50 kc due to masking by $1/f$ noise of the video amplifier following the discriminator circuit. At frequencies above 1 Mc, phase-lock noise increases faster due to a rise in loop response near natural resonance, which is not corrected in these measurements.

For the discriminator $C/N = +10$ db, noise output is nearly equal to that of the phase-lock circuit at $C/N = +5$ db. At lower C/N inputs, the threshold improvement is maintained: both demodulators exhibit approximately flat noise spectrum as predicted by S. O. Rice.** It is postulated that loss of lock in the loop, characterized by 2π radian phase steps, contributes to generation of noise with flat frequency spectrum to fill in the normally triangular characteristic of FM noise.

For the case of a sine-wave modulated car-

*These measurements were made at Bell Telephone Laboratories, Murray Hill, N. J., by J. G. Chaffee and A. J. Giger.

**S. O. Rice, "Statistical Properties of Sine Wave Plus Random Noise," *Bell System Technical Journal*, January 1948, pp. 109–157.



PHASE LOCK DISCRIMINATOR

FIGURE 3–48.—Comparison of TV quality at various IF C/N ratios (top, +5 db C/N; center, +0.5 db C/N; lower, −3.5 db C/N)

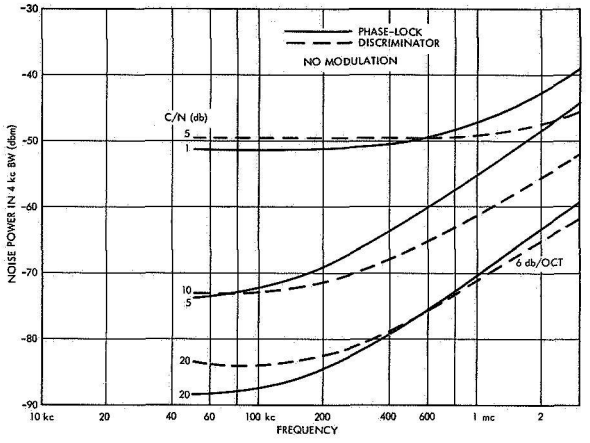


FIGURE 3–49.—Baseband noise spectra comparison.

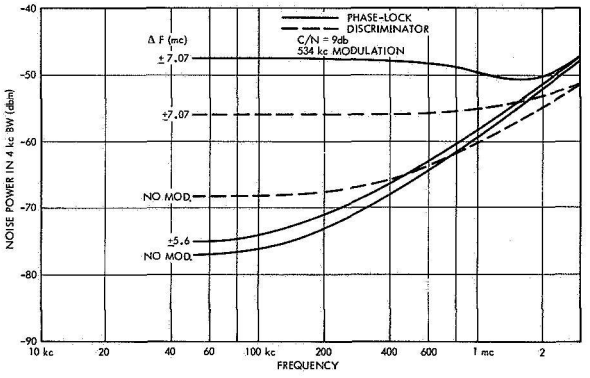


FIGURE 3–50.—Noise enhancement by modulation.

rier, with $C/N = +9$ db, enhancement of the noise output, (as noted by Giger and Chaffee for the frequency-following demodulators)* is apparent from Figure 3–50. This enhancement is severe for wide deviations by high frequency modulation, where loss of lock is increased by modulation phase error. For the discriminator, noise enhancement is not a function of the frequency of the modulation, whereas phase-lock loop noise is little affected by a 100 kc signal at ±10 Mc deviation.

Pre-emphasis of high frequencies in the signal does not, therefore, improve a band-

*A. J. Giger and J. G. Chaffee, "The FM Demodulator with Negative Feedback," *Bell System Technical Journal*, July 1963, p. 1127.

width-limited phase-lock demodulation link. The effect of this modulation noise enhancement is to generate additional lower-frequency noise which tends to subtract from the threshold improvement available for the unmodulated carrier.

AUTHORS. *This chapter was written by* R. S. EASTMAN *and* R. A. MILLER, JR., *of TRW/Space Technology Laboratories, Inc., Redondo Beach, California, U.S.A. under contract NAS 5–1302 with NASA/Goddard Space Flight Center.*

N66-10242

Chapter 4

Relay System Operations

10242

This paper discusses the operational aspects of Relay with respect to the techniques used in operating the spacecraft in orbit and the experience acquired during the extended period of successful in-orbit operation.

A description is given of the Relay Operations Center and its functions, including the support communications network of telephone, teletype, and video monitor links that were required for effective control of the satellite and coordination of operations.

The requirements for satellite command and for real-time telemetry data reduction and evaluation are outlined, and a description is given of the system used to meet these requirements. Examples are given of how the system was applied to specific operational situations.

The operation of the satellite involved the issuance of operational plans that provided for scheduling of communication experiments and of station participation. A discussion is given of the basis for such scheduling, such as selection of specific orbit revolutions for specific stations and experiments on the basis of mutual visibilities, slant ranges, spacecraft look angles, ground antenna elevation angles, eclipses, and spacecraft duty cycle. The effect of precession of the orbit on mutual visibilities is also discussed.

INTRODUCTION

The problems connected with the operation of a system employing earth satellites are complicated by the inherent short lifetime of such satellites and their inaccessibility for adjustments or repair once in orbit. Successful conduct of operations required not only well-defined experiment plans, but strict operational procedures which provided for maximum utilization of the satellite lifetime and guarded against its misuse.

Operational practices employed on Relay took into account the capabilites of the entire system, including the spacecraft, the participating communication stations, the GSFC Test Stations, the support communications network, and specialized NASA facilities such as the GSFC Data Processing Branch and the Minitrack Network.

The objective of Relay was to demonstrate the feasibility of one-way wideband and/or two-way narrowband transmission between distant areas (such as the United States and Europe) by means of a low-altitude, active-repeater satellite. This objective was accomplished. Relay also carried a radiation experiment package which gathered data on the radiation environment encountered and its effect on solid-state devices such as solar cells.

SYSTEM DESCRIPTION

The Relay system consisted of the orbiting satellite, the complex of participating ground and test stations, Operations Center, and GSFC supporting activities (see Figure 4–1).

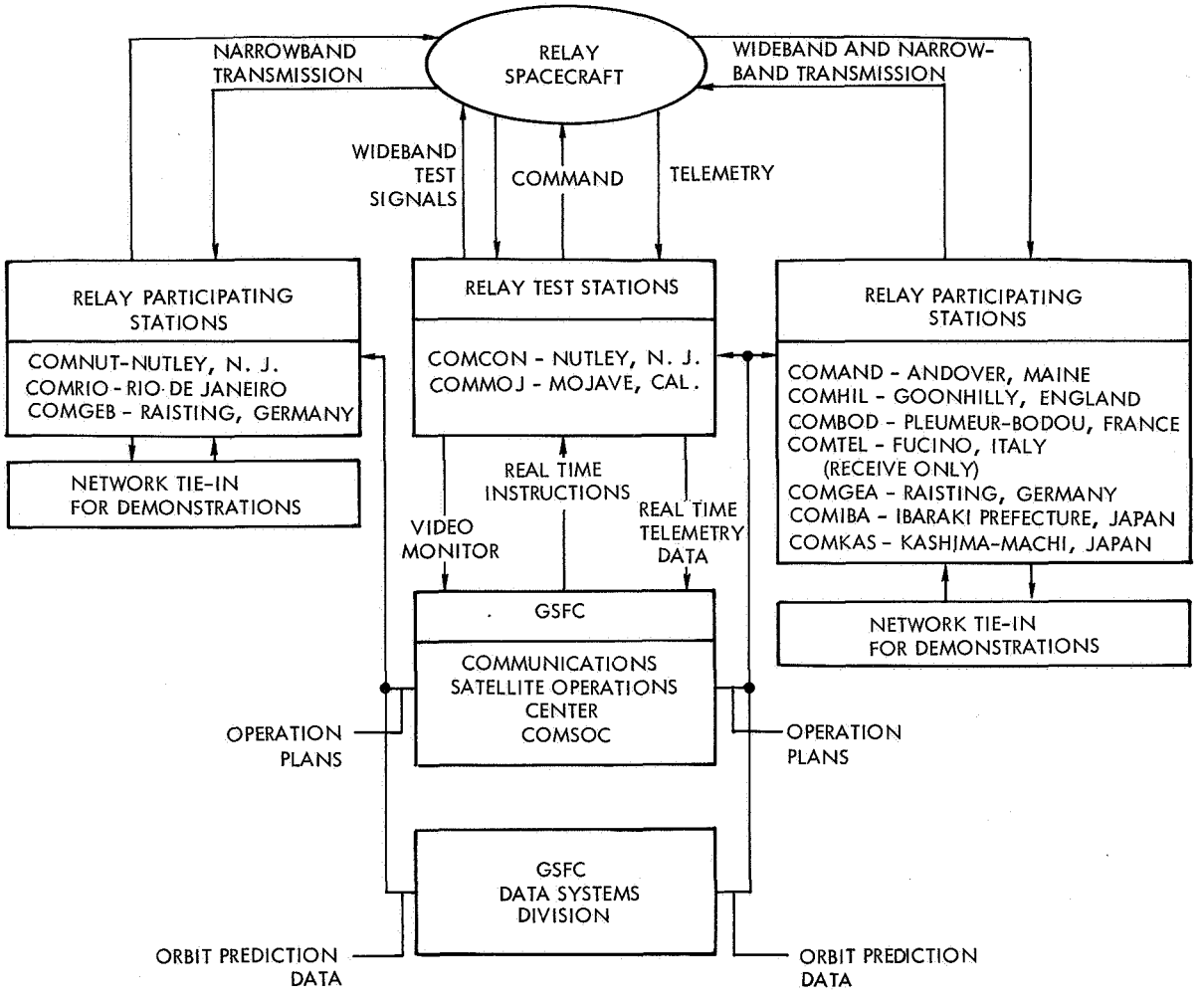


FIGURE 4–1.—Relay system.

The Relay satellite was basically a microwave repeater which received communication signals on a nominal frequency of 1725 Mc and retransmitted on 4170 Mc. The repeater could transmit a one-way television signal or twelve simultaneous two-way telephone conversations. Communications satellites such as Relay differ considerably from the scientific variety in that almost all the experiment data is gathered on the ground by communication stations. Each participating station performed experiments; the performance of the spacecraft transponder was considered a known quantity based on prelaunch laboratory measurements. The communication experiment data were unique to each ground station. Additional data on the spacecraft components were telemetered to measure their performance characteristics and to determine the current status or long-term degradation of the satellite.

In addition to a redundant wideband communication system, the spacecraft had a radiation experiment package, electrical power system, command and telemetry system, and supporting structure. The spacecraft contained earth horizon and sun sensing devices, an attitude control system, a precession damper and an active thermal controller. The spacecraft was designed to provide 100 minues total wideband operation per day over three or four consecutive orbit passes and

approximately eight hours of radiation experiment data per day.

The participating stations consisted of the American Telephone and Telegraph station at Andover, Maine (COMAND); the International Telephone and Telegraph station at Nutley, New Jersey (COMNUT); the British Post Office station, Goonhilly Downs, Cornwall, England (COMHIL); the National Center of Telecommunications Studies (CNET) station, Pleumeur-Bodou, France (COMBOD); Telespazio station at Fucino, Italy (COMTEL); two Deutsche Bundepost stations at Raisting, Germany (COMGEA and COMGEB); Radio Nationale, Rio de Janeiro, Brazil (COMRIO); Kikusai Densin Denwa Co., Ltd., Ibaraki Prefecture, Japan (COMIBA); and Radio Research Laboratories of the Japanese Post Office located at Kashima-Machi, Japan (COMKAS). Table 4–1 lists the basic characteristics of each station.

The two GSFC control and test stations used as primary command posts are located at Nutley, New Jersey (COMCON) and Mojave, California (COMMOJ). Each test station was contained in two mobile trailers joined to form a single unit. In addition to its command and telemetry capability, each site had a wideband test capability. This provided a continuous capability for periodic examination of the communication link performance of the satellite to detect degradation of the system.

All experimental scheduling, spacecraft command and control, and real-time evaluation of spacecraft status was carried out at an operations center located at GSFC. The functions of this center are detailed in a subsequent section of this volume.

The remainder of the Relay system consisted of GSFC support activities providing orbital prediction data, telemetry data processing, and satellite tracking information. The operational support communications network, which was used for all operational traffic, was supplied by GSFC. The NASA STADAN stations, a network of fixed ground stations throughout the world, provided precision tracking, command and telemetry for the satellites. These stations were used with Relay to gather telemetry data and to provide tracking information for orbital computation.

RELAY OPERATIONS CENTER

In order to assure that experiment scheduling, daily operations planning and data processing were handled in an efficient manner, a center was established for this purpose. This center, referred to as the Communications Satellite Operations Center (COMSOC), also provided a centralized command post to exercise control over the satellite.

The primary function of the center was to coordinate communication experiments among all participating stations and agencies to insure that experiments were performed in accordance with participant requirements. This coordination eventually resulted in the generation of a specific operation plan which was issued daily and was considered the controlling document.

Both GSFC test stations processed telemetry data which were printed out in the operations center on a real-time basis. During each scheduled pass the test station assigned command responsibility was in telephone conference with the operations center. All commands sent to the spacecraft were listed in the Daily Operations Plan and transmitted by the assigned test station at the specific times listed, after verbal acknowledgment by the operations center. This allowed COMSOC to assure that the proper commands were being transmitted in the proper sequence. COMSOC could also change any commands or instruct that other commands be sent to the spacecraft at any time during an operation. The final responsibility for spacecraft commands always rested with the operations center. The telemetry data were evaluated in real-time during the operation, and spacecraft commands could be required at any time when the data indicated that systems must be turned on or off.

Spacecraft telemetry evaluation was performed at the operations center in real time

TABLE 4–1.—*Relay Ground Station and Test Station Design Characteristics*

Station	Transmit and receive capability	Antenna	Gain		Receiver	Total system noise temp at 7.5° elev	1725-Mc transmitter output
			1725 Mc	4170 Mc			
Andover, Maine ground station.	One-way television and 300-channel telephony; two-way, 12-channel telephony.	3600-ft² aperture horn, AZ–EL mount, under radome.	50.2 db	57.6 db	4°K Maser	50.8°K	10 kw
Fucino, Italy ground station.	Receive 12-channel telephony.	30-ft-diam Cassegrain parabola, AZ–EL mount.	Not applicable	48.6 db	Cooled parametric amplifier	220–250°K	Not planned
Goonhilly Downs, England ground station.	One-way television and 300-channel telephony; two-way, 12-channel telephony.	85-ft-diam parabola, AZ–EL mount.	50.7 db	58.4 db	Maser	100°K	10 kw
Mojave, California test station.	Wideband test signals	40-ft-diam parabola, X–Y mount.	44 db	52 db	120°K cooled parametric amplifier	200°K	10 kw
Nutley, New Jersey test station.	Wideband test signals	Same as Nutley ground station.	42.9 db	51.1 db	120°K cooled parametric amplifier	200°K	10 kw
Nutley, New Jersey ground station.	Two-way, 12-channel telephony.	40-ft-diam Cassegrain parabola, AZ–EL mount.	42.9 db	51.1 db	290°K parametric amplifier	420°K	10 kw
Pleumeur-Bodou France ground station.	One-way television & 300-channel telephony; two-way, 12-channel telephony.	3600-ft² aperture horn, AZ-EL mount, under radome.	50.2 db	57.6 db	4°K Maser	50.8°K	10 kw
Raisting, Germany ground station.	One-way television and 300-channel telephony; two-way, 12-channel telephony.	85-ft-diam Cassegrain parabola, AZ–EL mount, under radome.			Maser		Not planned
Rio de Janeiro, Brazil ground station.	Two-way, 12-channel telephony.	35-ft-diam Cassegrain parabola, AZ–EL mount.	40.2 db	48.2 db	290°K parametric amplifier	420°K	10 kw

during the pass for its effect on the planned operation. Long-term evaluation of this data was also performed as an aid in determining spacecraft duty cycle and general degradation.

The participating communication station was often contacted by telephone or teletype facilities immediately prior to the intended pass, so that a readiness report could be obtained prior to the planned operation. During some critical passes where more than two stations were involved or where precise switching or cueing was required, the stations were placed in telephone conference.

SUPPORT COMMUNICATIONS

To achieve the objectives of Relay, it was necessary that a great amount of data be handled in a smooth and expeditious manner. This was accomplished by use of a teletype network as the primary communications medium. Orbit prediction and pointing data, monthly and daily operations plans, station operations reports and operation summary reports were transmitted via this system. Real time telemetry data, which was reduced at the test stations, was printed out in real time at COMSOC by a 100 word-per-minute simplex teletype.

The teletypewriter communications were provided between COMSOC and all participants on a 24-hour-per-day basis. End equipments were not necessarily manned 24 hours per day but were capable of receiving teletype traffic while unattended. Tape reperforators were provided at all stations so that punched paper tape could be used for reading GSFC topocentric coordinate satellite predictions into the station computers. Full-period telephone service was also provided between COMSOC and the participating stations so that real-time voice instructions and data could be handled. The Rio de Janeiro station and the two Japanese stations were serviced by telex and toll telephone. Figure 4–2 gives a simplified block diagram of the operational support communications network for Relay. There was an occasional need for a conference arrangement of all stations on the teletype set. This was

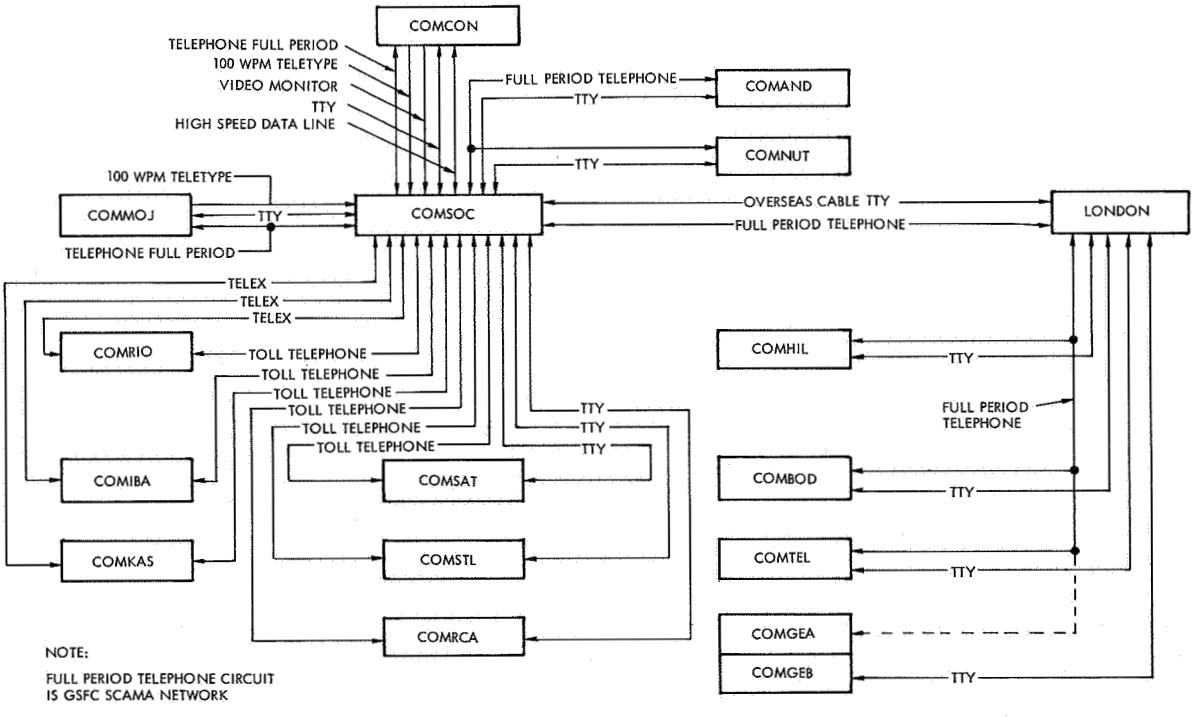


FIGURE 4–2.—Relay ground communications.

sometimes required when specific instructions were needed at more than one station simultaneously, although voice communication via the full-period telephone circuits was the primary means of issuing commands to the test stations and instructions to participants. All teletype traffic handling was accomplished in accordance with established GSFC procedures for a torn tape relay. This network has since been computerized, providing complete automatic switching capability.

STL (COMSTL), RCA (COMRCA), and GSFC Relay project office (COMSAT) were also in the communications network, to provide liaison as required.

TELEMETRY REQUIREMENTS

The spacecraft telemetry system consisted of two redundant transmitters and a single encoder. Either transmitter could be modulated by the encoder or by the output of a horizon scanner. The transmitter operated at frequencies of 136.620 and 136.140 Mc. The system was Pulse-Code-Modulated at a rate of 1152 bits per second. Each telemetry word consisted of nine bits, making a total of 128 telemetry words. Words 4 through 17 and 29 through 128 were used for the transmission of data from the radiation experiments. Of the remaining telemetry words, 1, 2 and 3 were used for a 27-bit frame sync. Thus only 10 main telemetry words remained available to monitor spacecraft performance. One of these telemetry words (No. 28) was submultiplexed into 64 channels, so that there were 73 channels available for monitoring spacecraft performance. Figure 4–3 indicates the telemetry word assignment.

Telemetry data from Relay could be received by all STADAN stations and by the two test stations. Only the two test stations had the capability of processing the telemetry data in real time to make it available for use during actual transponder operations. Figure 4–4 shows the station telemetry system.

The telemetry data was arbitrarily separated into three classes. The first, Class I, was processed in real time at the two test stations and displayed by means of a strip chart recorder and a limit checker to give GO/NO–GO indications. These items were considered the most critical parameters and served as a backup when the more refined real-time Class II data were not available. Class II data was likewise processed at the test stations; it was reduced by a small service computer (Packard Bell 250), transmitted to the Operations Center via the 100-word teletype circuit, and printed out in real time. This data indicated spacecraft performance and was used in real time as an aid during the conduct of operations. All received telemetry data were recorded on magnetic tape for subsequent mailing to GSFC for processing. Telemetry data in this form are referred to as Class III. A separate classification was required for horizon-scanner data, which could be telemetered only when the encoder was off. The horizon scanner data were likewise recorded on magnetic tape and mailed to GSFC for processing. Under normal circumstances there were no critical time requirements on Class III data. The radiation experiment data were in this latter category. Processing was accomplished at GSFC for subsequent transmittal to the GSFC, SUI, and BTL radiation experimenters.

Class I data, as indicated, were reduced and displayed in real time at the test stations to provide a basis for a GO/NO–GO decision regarding the planned wideband communication experiment for the given pass. The Class I telemetry items are listed in Table 4–2 and represent the most critical parameters that affected the gross performance. In addition, the command verification channels are included as part of the Class I items. Items processed by means of a PCM limit checker gave red or green light indications when the parameter was within acceptable limits. Some of these verified the occurrence of certain events in a normal operation. The transponder regulated bus voltage indication went from red to green

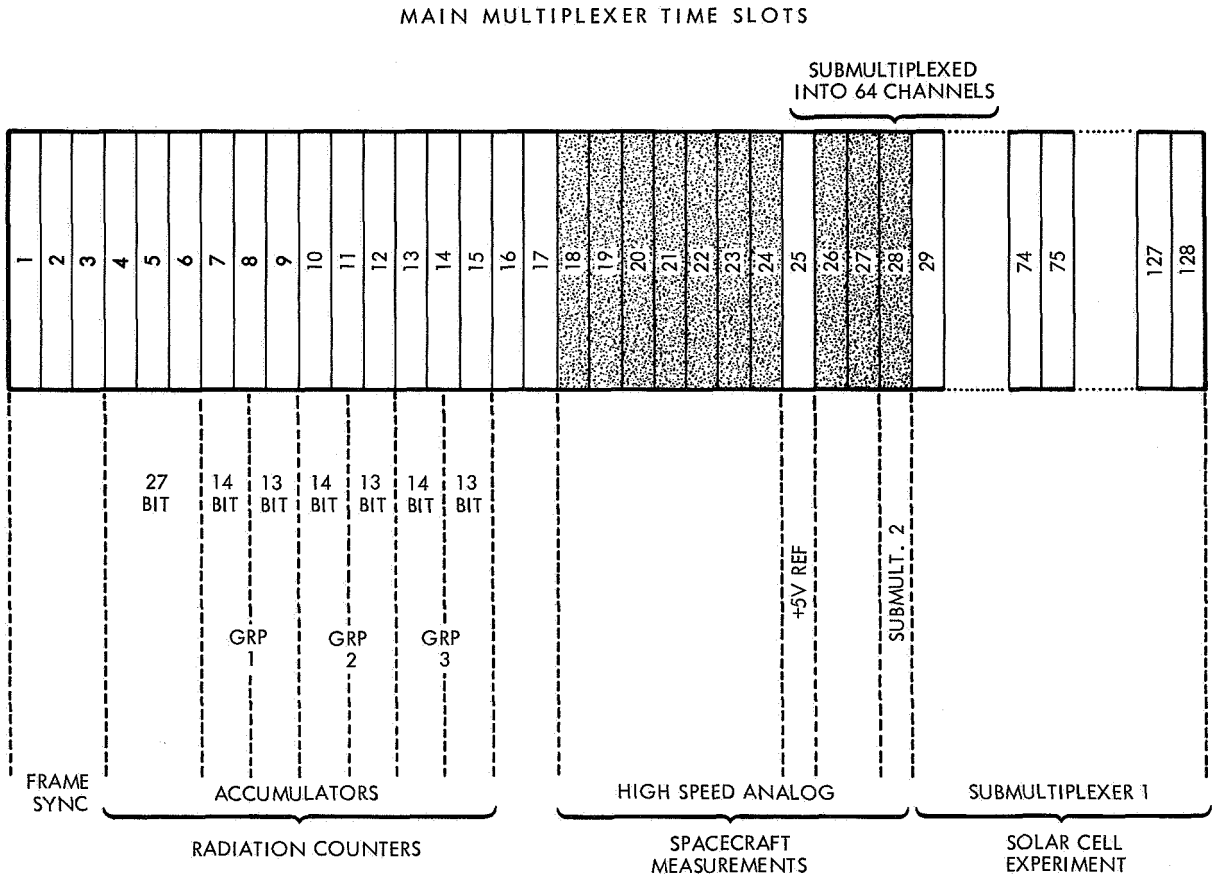


FIGURE 4–3.—Telemetry main frame word assignment.

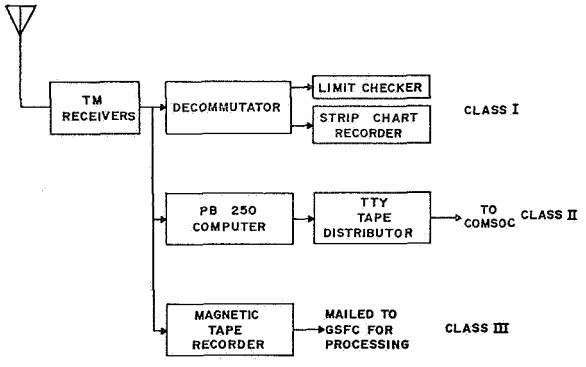


FIGURE 4–4.—Telemetry flow diagram at test station.

when the transponder was commanded on, the Main IF AGC voltage indication went from red to green when a transmitting ground station was illuminating the spacecraft with a wideband carrier, and the TWT power output and TWT beam current indications went from red to green when the transponder high power came on. A green light indication was also given when the radiation experiment was turned on.

On the seven items processed through the limit checker, the battery voltage and the battery temperature were considered the two most critical. Battery voltage indication was red when it was below 22.5 volts. The battery temperature indication was red when it was above 32.5°C. Both of these conditions were considered critical, and operations with the transponder were not attempted unless both indications were green.

All the Class I items were displayed on a strip-chart recorder showing analog measurements of telemetry voltages. This per-

TABLE 4–2.—*Class I Telemetry and Limit Checker Items*

Telemetry items		Item	Approximate values		Sample rate
Main word	Sub com		**Limit checker A range red	TLM volts B range green	
*18	--	TWT power output	0–1.0	1.0–5.0	1/sec
19	--	Unregulated bus voltage			1/sec
20	--	total battery current			1/sec
*24	--	Main IF AGC voltage	0–1.5	1.5–5.0	1/sec
28	09	TWT helix voltage			1/64 sec
*28	11	Rad. exp. regulated bus voltage	0–3.5	3.5–5.0	1 64 sec
*28	16	Transponder regulated bus voltage	0–1.5	1.5–5.0	1/64 sec
*28	17	Battery No. 1 voltage	0–3.0	3.0–3.0	1/64 sec
28	24	Command verification, JKL			1/64 sec
*28	26	Battery No. 3 temperature	3.6–5.0	0–3.6	1/64 sec
28	35	Command verification, ABC			1/64 sec
28	43	Command verification DEF			1 64 sec
28	51	Command verification, GHI			1/64 sec
*28	63	TWT beam current	0–3.0	3.0–5.0	1/64 sec

*Item further processed through a limit checker to provide red-green light indication.
**The normal indication provided by the limit checker is a red light when the telemetered voltage is in the "A" range and a green light for the "B" range.

mitted interpretation of the data with fair accuracy by use of the calibration curves. As previously indicated, the primary use of Class I data was to provide a backup capability in the more elaborate Class II data system. Class I data was not normally considered sufficient information for operation of the wideband transponder except in special circumstances. Some operations were started using Class I data when difficulties were encountered in the Class II until that system was operating. Likewise, some passes were started on Class II data and finished on Class I when difficulties were encountered.

Class II data consisted of 40 spacecraft system items plus 5 test solar cell measurements. These were selected from the total bit stream and processed to provide a printout of data in engineering units. These items were selected by considering the most critical priorities and limiting the total amount of data so that the resultant printout would be compatible with a 100 word-per-minute teletype circuit. These data, when processed and transmitted via the teletype circuit, provided data printout in real time. In the actual system there was a delay of only a few seconds from the time the telemetered item was monitored in the spacecraft until it was printed out in the operations center. Figure 4–5 gives a printout of a typical block of Class II data as received at the operations center.

Main telemetry word 28 was submulti-

plexed into 64 channels, so that 64 seconds were required to monitor all telemetry points in the spacecraft. Each block of Class II data required 64 seconds to print out and covered a time span of the same duration. Main frame words monitored as part of Class II were sampled once per second, but were only printed out every 16 seconds. These items were printed out frequently enough to determine performance and yet conserve the available time-spacing provided by the computer-teletype system employed.

The first line of the example given in Figure 4–5 consists of the station designator, date-time group and the main telemetry items; these were printed out every 16 seconds. The letter "N" designates the Nutley Test Station, 64 is the year, 085 is the day of the year, 05 is the hour, 39 is the minute of the hour and 47 is the second within the minute. The telemetry word immediately following the date-time group is the TWT output power in telemetry volts followed by the unregulated bus voltage in volts, the total battery current in amps, the command receiver AGC in telemetry volts, the active thermal sensor temperature in degrees C and the Main IF AGC voltage in telemetry volts. These items are main telemetry words 18, 19, 20, 21, 22, and 24. Immediately following each date-time group and main telemerty printout lines are two lines of items from subcommutator No. 2. Each printout was preceded by the subcom channel designator; it can be seen from the example that channels 03, 04, 05, and 08 were printed out immediately following the first date-time group line. Table 4–3 gives a complete listing of all Class II items.

```
  N64085053947 1.70 26.08 2/92 3.29 2/91 2.24
03 -19.5 04 25.8 05 11/1 08 3.35
09 4.04 11 .10 12 10/1 13 2/02 16 22.3
  N64085054003 1.71 26.08 2/92 3.29 30/98 2.27
17 26.4 19 3.80 20 3/57 21 -35/1 24 1.95
25 26.5 26 3/69 27 .02 31 3.23 32 1.32
  N64085054019 1.71 26.15 2/92 3.27 2/80 2.24
33 26.4 34 3.08 35 2.00 40 4/41
41 4/56 42 2/11 43 1.30 47 1.27 48 .01
  N6085054035 1.71 26.08 2/91 3.29 2/91 2.24
49 -28/0 50 1.04 51 1.95 54 2.07 55 .11 56 2.98
59 -2/56 63 46/0 64 4/95
142 138 154 127 149  11 1/33
```

FIGURE 4–5.—Typical block of class II data.

Additional items are given at the end of the Class II printout. The first five (see line 13 of the format) are five solar cell measurements of the radiation damage experiment to provide the GSFC project scientists with quick-look data on these particular cells. The next item is the sun aspect indicator output, which must be converted by use of a calibration chart to sun look angle. The last item of the format is the solar array bus current in amps. The computer provided a double line feed printout at the end of each Class II data block to allow a space between each 64 seconds of data.

The computer output was in the form of a punched plastic tape, compatible with standard teletype equipment; this tape was fed immediately into the 100-wpm teletype tape distributor. This was physically mounted so that the tape loop between the computer and the tape distributor was only a few inches.

The operations center received this data in the form of standard teletype page print and teletype reperforated tape, so that if necessary the data could be retransmitted to other locations. This data was provided to RCA on a routine basis for their information and to STL on a routine basis whenever a detailed examination was required.

One key to the successful use of the PB 250 computer at the test stations was the simplified method of telemetry calibration. Most spacecraft telemetry sensors have a nearly linear calibration characteristic. For this reason all items of Class II telemetry were linearized where a good fit could be made over the expected operating range of the parameter in question. Those telemetry calibrations which could not be fitted, to a reasonable degree, with a straight line were printed out in the Class II data as actual telemetry voltage. The result was that most items were printed out in engineering units and the remaining items were printed out in telemetry volts. A number of signal presence measurements having no meaningful

TABLE 4–3.—*Class II Data Items*

Telemetry word	Item	Telemetry word	Item
18	TWT power output	28/33	Battery No. 3 voltage
19	Unregulated bus voltage	28/34	Narrowband signal presence channel 1
20	Total battery current	28/35	Command verification AGC
21	Command receiver AGC	28/40	Current transducer temp.
22	Thermal controller sensor temp.	28/41	Wideband baseplate temp.
24	Main IF AGC voltage	28/42	Battery temp. 2–2
28/3	Thermal controller position	28/43	Command verification DEF
28/4	Voltage limiter current	28/47	Wideband trans. L.O. output
28/5	TWT power supply No. 1 temp.	28/48	Thermistor No. 8 temp.
28/8	TWT collector voltage	28/49	Solar panel temp. 3B–1
28/9	TWT helix voltage	28/50	Narrowband signal presence channel 2
28/11	Radiation experiment regulated bus	28/51	Command verification GHI
28/12	TWT collector temp.	28/54	Wideband H. level mixer drive
28/13	TWT power supply No. 2 temp.	28/55	TWT power input
28/16	Wideband regulated bus voltage	28/56	WB beacon L.O. output
28/17	Battery No. 1 Voltage	28/59	Collar assembly temp. No. 1
28/19	Tlm. trans. No. 1 power output	28/63	TWT beam current
28/20	Encoder temperature	28/64	Collar temp. No. 3
28/21	Lower surface temp.	29–128/18	Solar cell 16 NP/ 60
28/24	Command verification JKL	29–128/19	Solar cell 17 N/P 60
28/25	Battery No. 2 voltage	29–128/23	Solar cell 21 GA 3
28/26	Battery temp. 1–2	29–128/25	Solar cell 23 GA 12
28/27	Tlm. trans. No. 2 power output	29–128/27	Solar cell 25 GA 60
28/31	Wideband receiver L.O. output	16–17	Sun aspect indicator
28/32	Wideband beacon output	26	Solar cell bus current

calibration other than giving gross ON or OFF indications were also printed out as telemetry volts.

Figure 4–6 indicates a typical calibration curve for a spacecraft measurement and also shows the linearized approximation which is used in the PB 250 computer. Figure 4–7 is the telemetry calibration for the wideband received signal strength; it is obvious that a complex curve like this cannot be reasonably approximated by a straight line. This type of item is therefore printed out in telemetry volts. Items which are not accurately linearized (linear approximation does not fit curve precisely) are flagged in the Class II format by the use of the slant symbol for a decimal point. This can be seen in the sample format given in Figure 4–5, where the symbol indicates that the data should not be used for accurate evaluation without consulting the calibration curve. All items which are printed out as telemetry volts are given to two decimal places. Most other items are given to only one significant decimal place.

Figure 4–8 gives five typical blocks of Class II data which were taken from an operational pass. Each block given in the example is annotated for each area of concern in the spacecraft system to illustrate the relative distribution of items for each subsystem. This example is intended to illustrate the ease with which the data can be interpreted after one becomes familiar with the items listed. One other aspect of the utilization of a compatible teletype system is that the page print of the data provides a permanent copy of reduced telemetry information easily stored for future reference.

The immediate use for Class II data was at the operations center to verify the command status of the spacecraft and to determine spacecraft condition prior to any planned operations. During normal routine

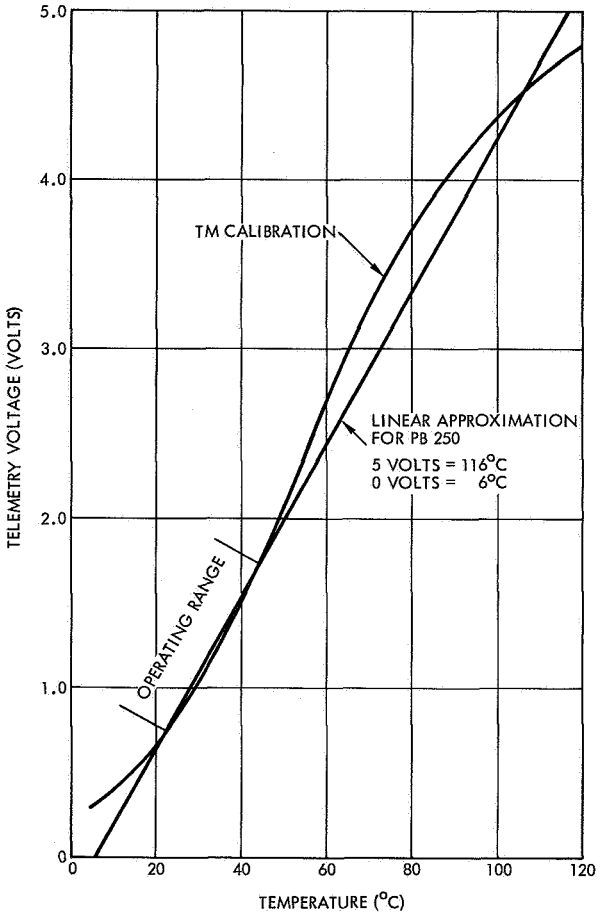


FIGURE 4-6.—TWT collector temperature TM calibration.

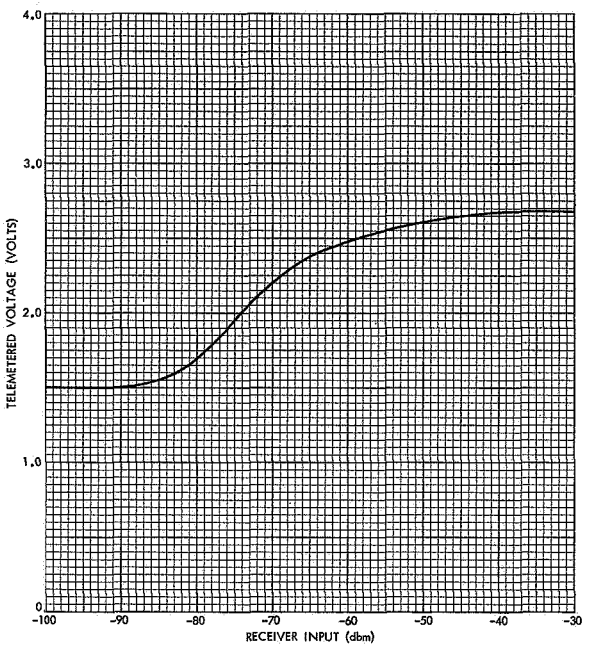


FIGURE 4-7.—WBCS No. 2 receiver input TM calibration (main IF AGC voltage).

operations, only one minute was required for complete examination, although five minutes of Class II data were usually taken prior to the operation of the transponder. The data were then continuously reduced and printed out during the entire operation, plus two or three minutes of data taken after the transponder had been turned off. The data at the end of the pass were used to insure that all systems turned off as commanded and for a final check of the spacecraft.

A selected number of Class II data items were plotted on a routine basis after each operational pass. These were retained in the operations center to provide a record of performance. Some of these items, such as battery dischage characteristics, were used in determining the available duty cycle of the spacecraft. Solar array output characteristics and spacecraft temperature histories were likewise provided for use in detailed analyses. Performance characteristics of the wideband system were also plotted and recorded so that long-term degradation could be observed.

All telemetry data received by either the test stations or the STADAN stations were recorded on magnetic tape; as noted above, this constituted Class III data. The NASA STADAN stations were scheduled to turn on the radiation experiment and record Class III data during periods when visibility did not exist at the test stations. This data was mailed to GSFC from all receiving sites for processing and subsequent transmittal to the GSFC, SUI, and BTL radiation experimenters.

A computer routine is available at GSFC for processing of spacecraft performance data as well as radiation experiment data. Whenever anomalous performance was indicated in the Class II data, the revolution

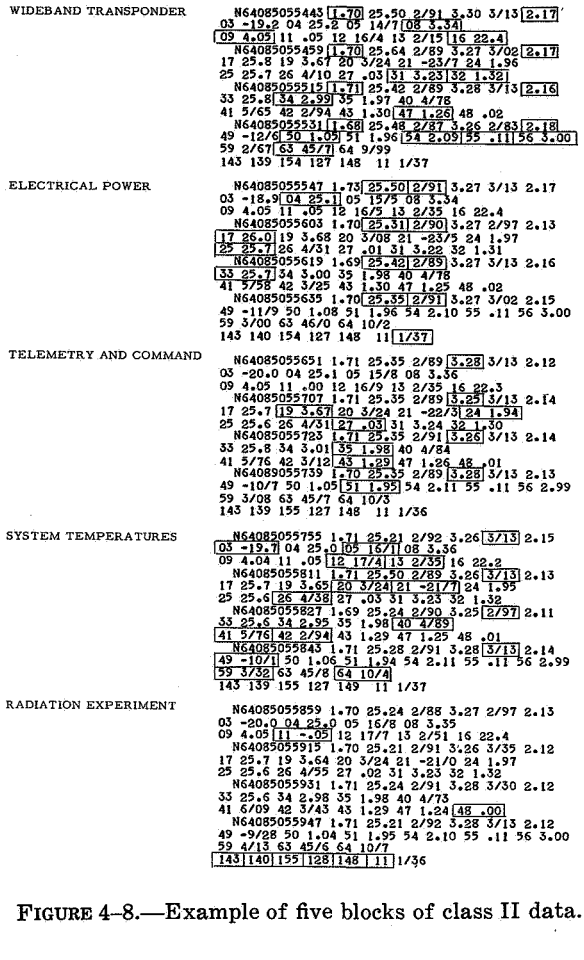


FIGURE 4–8.—Example of five blocks of class II data.

number was noted. After the magnetic tape for the pass in question had been received at GSFC, the data were processed in the Class III data format. This print-out permitted detailed examination of all spacecraft performance items.

EXPERIMENT SCHEDULING

In order to make the most effective use of the entire Relay system, which includes the complex of participating stations as well as the satellite, it was necessary to schedule the communications experiments with some care. These experiments are the basic purpose of the entire project, and had to be carefully planned to make maximum use of the limited time available for wideband transponder operation. This planning, which had to take into account several factors simultaneously, was carried out at the operations control center in coordination with the participating stations.

Experiment schedules were initially planned over a one-month period. It was found useful early in the program to assign operational days during each week to designated stations, with the days assigned arbitrarily. Examination of orbital data would then indicate which passes on each day were usable for the station designated for that day. A one-month schedule was developed in this way and transmitted to the participating stations. This initial schedule was refined in the light of then current conditions to provide a daily operations plan for each day. This plan, which was sent by teletype to all stations, governed all operations with the satellite.

The selection of one or more orbit passes for wideband operations with the station designated for the day in question was accomplished in the following manner. First the orbital data for the given station (MUSTAP program) was examined to determine the useful period of visibility for that station. This period then had to be further constrained to the time of mutual visibility of the satellite by both the participating station and one of the two GSFC test stations. One of these stations had to be able to receive and process telemetry data and to transmit commands to the satellite during wideband operations, and a short period was required before and after wideband transponder operation for the acquisition of telemetry data by the test station.

Once the period of useful visibility had been established, it was necessary to determine whether the spacecraft look angles for the station (or station pairs) scheduled to use the satellite were suitable for wideband communications; as Figure 4–9 indicates, the spacecraft antenna gain falls off sharply at large angles from the perpendicular. It is apparent that angles near 0 or 180 degrees would be extremely unfavorable, and in practice it has been found best to restrict the look angle for a participating station to the

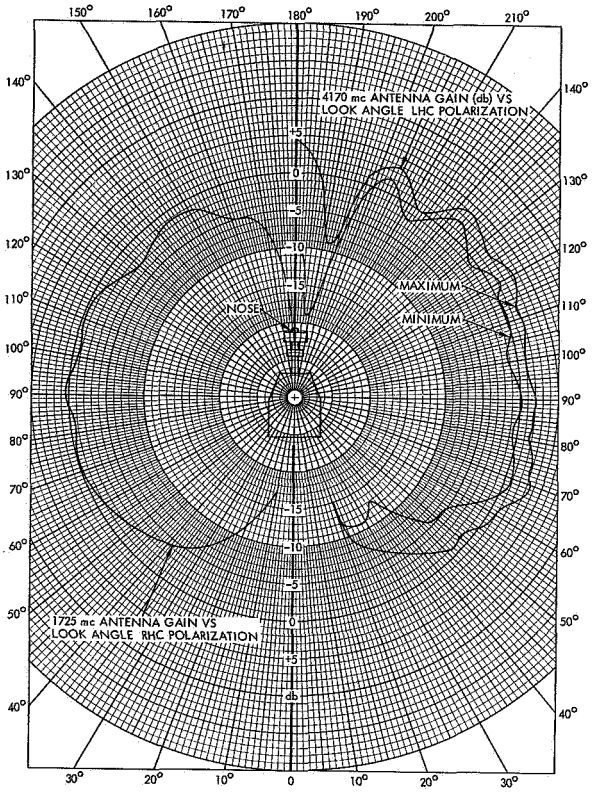


FIGURE 4–9.—Spacecraft transmitter and receiver antenna gain vs. look angle.

range between 65 and 140 degrees. A few experiments were scheduled to measure results over a greater range of look angles, but it was found that no useful results were obtained for look angles greater than 160 degrees.

The next consideration was that of the slant range of the spacecraft from the given station. It was necessary to determine that the slant range combined with the look angle did not result in a link having power levels below the performance margin of the station or stations scheduled to participate. On the basis of these considerations it was desirable to select passes with minimum range for stations such as Rio or Fucino which had 30-foot diameter antennas.

Once the link parameters had been considered, it was necessary to determine whether the electrical power available in the spacecraft would support wideband transponder operation for the period planned. This information was derived from a continuous evaluation of the spacecraft electrical power system, based on the complete history of its performance maintained at the operations center. The factors of most importance are the condition of the batteries, the output of the solar array, and the prevailing eclipse conditions. The wideband transponder was never operated while the spacecraft was in eclipse, since such operation would have placed an excessive drain on the batteries. For the same reason, no extended transponder operation was scheduled immediately prior to the beginning of an eclipse; the batteries would not have been recharged from the heavy transponder load, and the normal housekeeping loads would have depleted them still further, entailing a risk of anomalous command states associated with low battery voltages.

On the basis of these considerations, the duration of the planned operation was determined and specific on/off times were established for the telemetry encoder and the wideband transponder. Commands were also scheduled, where appropriate, to switch the transponder from wideband to narrowband operation or the reverse.

Another factor which had to be taken into account in planning operations was the antenna elevation angle for the participating stations. Those stations having Ax–El mounts for the antenna could not track the satellite through zenith, and allowance had to be made for this constraint. It was also necessary to check the azimuth profile for the station concerned to determine that no ground hazard was created or that no obstructions (such as hills, mountains, or structures) existed at the planned azimuths and elevations. Ordinarily communications experiments were not scheduled for antenna elevations below 5 degrees. For some special tracking tests, the transponder was turned on below the horizon of the designated station so that the tracking beacon could be acquired at extremely low elevation angles. Where there were no obstructions, the larger

stations could perform wideband experiments at elevations as low as 3 degrees.

The specific experiment to be performed on each operational pass was normally indicated in the daily operations plan issued by the operations center. The experiment was selected primarily on the basis of the recommendation of the station scheduled to operate with the satellite, although if the station had expressed no preference the operations center could have selected the experiment itself. In general, it was desired to cover as completely as possible the entire experimental program given in the Communication Experiment Plan, with as many of the stations as possible. The operations center maintained complete records of all experiments performed, and was able on the basis of these records to recommend desirable experiments to the various stations.

The selection of experiments was carried out in close coordination with the participating stations. Each station supplied the operations center with its desired priorities for experiments, and the results of earlier experiments were known to the center so that it was aware of those areas requiring additional data. The experiments listed in the Experiment Plan were not all of equal importance, and some required much more frequent repetition than others. A weighting factor was applied in planning experiments to assure that the entire program was properly balanced.

Experiment scheduling also had to reflect, in some cases, the link requirements for the experiment planned. Some experiments require a high-quality link with favorable look angles and very short ranges, while others could be performed over the entire spectrum of ranges and look angles.

In addition to the wideband communication experiments, the operations center was also required to schedule the operation of the radiation experiment carried on the satellite. The radiation experiment did not constitute a heavy electrical load, and was operated for several hours at a time. Additional flexibility was afforded by the fact that the STADAN stations could receive and record radiation experiment data; their participation was scheduled through the STADAN net controller of GSFC. In general, they could take radiation data from the Relay satellite whenever the radiation experiment and telemetry encoder were on and when they were not required to acquire higher-priority data from another satellite.

The final result of the scheduling operation was, as indicated previously, a Daily Operations Plan which was generated at the Operations Center and transmitted by teletype to all participants. Figure 4–10 is a reproduction of a typical daily plan. It lists the orbit revolutions during which operations are to be performed, lists the commands to be sent to the spacecraft together with the time for each command, indicates the times when ground station equipment is to be turned on, and lists the experiments to be performed with their beginning and end times. The Daily Operations Plan does not list radiation experiment operations unless the experiment is to be turned on or off by command from one of the two GSFC test stations, but those passes scheduled for telemetry or horizon scanner data only are listed.

The Daily Operations Plan was transmitted to the participating stations at least 24 hours in advance of the period covered by the plan. This permitted the ground and test stations to make appropriate preparations for turning on equipment, taking telemetry, or sending commands on the schedule indicated. In general, no operations other than those specifically shown in the plan were performed. It was possible, however, for the operations center to modify the planned operation at any time; changes were made by notifying the appropriate test station via the full-period telephone circuits maintained with both stations. At no time during the operation were commands transmitted to the satellite without specific acknowledgement from the control center.

In the case of public demonstrations with the Relay satellite, the scheduling procedure

NOTE: Proper teletype heading was left off to just illustrate text of a typical Daily Operations Plan.

```
BT
DAILY OPERATIONS PLAN 5/10/64 RELAY 1B
REV 814
1115 COMCON-REPORT READINESS
1125 COMCON-COMMAND ENCODER ON-TAKE CLASS II DATA
1130 COMCON-COMMAND ENCODER OFF

REV 815
1402 COMCON, COMBOD-REPORT READINESS
1412 COMCON-COMMAND ENCODER ON-TAKE CLASS II DATA
1415 COMCON-COMMAND TV ON/PHONE OFF
1417 COMCON-COMMAND TRANSPONDER NO. 2 ON
1418 COMBOD-TURN ON 1725 MC XMTR
1420 COMBOD-REPORT PRESENCE OF 4 KMC BEACON
1420-1442 COMBOD-CONDUCT THE FOLLOWING EXPERIMENTS
1420-1430 151 CONTINUOUS RANDOM NOISE
1430-1442 135 PERIODIC NOISE - VIDEO
1442 COMCON-COMMAND TRANSPONDER OFF
1442 COMBOD-REPORT LOSS OF BEACON
1442:15 COMBOD-TURN OFF 1725 MC XMTR
1447 COMCON-COMMAND ENCODER OFF

REV 816
1642 COMMOJ, COMAND, COMIBA-REPORT READINESS
1652 COMMOJ-COMMAND ENCODER ON-TAKE CLASS II DATA
1657 COMMOJ-COMMAND TRANSPONDER NO. 2 ON
1659 COMAND-TURN ON 1725 MC XMTR
1700 COMAND, COMIBA-REPORT PRESENCE OF 4 KMC BEACON
1700-1712 COMAND, COMIBA-CONDUCT THE FOLLOWING EXPERIMENTS
1700-1706 151 LINE TIME NON-LINEARITY (WITH 1 MC SUPERIMPOSED)
1706-1712 153 SYNCHRONIZED NON-LINEARITY
1712 COMMOJ-COMMAND TRANSPONDER OFF
1712 COMAND, COMIBA-REPORT LOSS OF BEACON
1712:15 COMAND-TURN OFF 1725 MC XMTR
1717 COMMOJ-COMMAND ENCODER OFF

REV 817
2045 COMCON-REPORT READINESS
2055 COMCON-COMMAND ENCODER ON-TAKE CLASS II DATA
2058 COMCON-COMMAND RADIATION EXPERIMENT ON
2100 COMCON-STOP TAKING CLASS II DATA-CONTINUE TAKING CLASS I
AND III DATA

REV 818
2342 COMMOJ-REPORT READINESS
2352 COMMOJ-TAKE CLASS II DATA
2355 COMMOJ-COMMAND RADIATION EXPERIMENT OFF
2357 COMMOJ-COMMAND ENCODER OFF
BT
```

Day covered by plan (5-month of May, 10-tenth day, 64-1964); time interval of the plan is 0000 - 2400 (hours and minutes) of this day, all times are GMT.

Revolution (pass) in orbit starting from injection. REV 000 starts at orbit injection and ends at the first ascending node (orbit and equatorial plane intersections). REV 001 starts at the first ascending node and ends at the second ascending node.

Passes used to take Class II data only to examine condition of spacecraft.

Stations listed are those that are scheduled to participate in communication experiments.

Experiments to be conducted during the pass at the times indicated. Please note that experiment designations are those as listed in the GSFC RELAY Communication Experiment Plan, R1-0521A revised 1 December 1963.

Orbit passes that are used for acquiring radiation experiment data only. COMCON commands on telemetry system and radiation experiment subsystem.

COMCON commands radiation experiment and telemetry off at the end of a complete orbit. NOTE: Instructions to Minitrack Stations to acquire radiation experiment data are issued by the Net Controller and will not be included in the RELAY Daily Operations Plan.

FIGURE 4–10.—Typical daily operations plan.

was somewhat different from that described for technical tests. The specific pass was selected in the same way, and the details of the operation were given in the Daily Operations Plan as for other operations. The chief difference was in the scheduling of the specific time for the demonstration.

A station outside of the United States wishing to perform a public demonstration made the request directly to the operations center. If the station had already been scheduled to operate on the pass requested, no special coordination of the time was required. If other operations were planned for the pass requested, it was necessary to coordinate the request with the participating stations. In either case, the agency requesting the demonstration arranged for the material content and for routing of the received transmission.

Requests for demonstrations originating in the United States were directed to the Program Developing office of NASA Headquarters. Approved requests were forwarded to the Relay Project Coordinator at GSFC, who determined compatibility of the request with scheduled operations. In general, requests for public demonstrations were made several days in advance of the desired date in order to permit adequate coordination, but such advance notice was not always possible.

COMMUNICATION EXPERIMENT DATA

The primary object of Relay was to gather communication experiment data in addition to the radiation experiment data. The communication experiments comprised all tests performed by the Relay participating ground and test stations in conjunction with the spacecraft wideband system. These tests were performed either in a wideband or narrowband mode. Most of the experiments were performed in loop configuration; that is, one station transmitting and receiving its own signals. However, all tests could be performed either in a loop or straightaway configuration. Straightaway means that one station transmits wideband signals and a second station receives them. Most narrowband experiments were conducted in a two-way configuration with both stations transmitting and receiving simultaneously. Communications experiments are detailed in GSFC Document R1–0521A entitled *Relay Wideband Communication Experiment Plan*, revised December 1, 1963.

The communication experiments are broadly categorized as performance tests and system demonstration tests. The performance experiments are objective tests used to obtain quantitative and statistical data on the electrical parameters of the system. The performance data are primarily intended to confirm a system capability for quality monochrome television and frequency division multiplex (FDM) telephony. Data were gathered on the gain stability phase characteristics, distortion, intermodulation, interference and noise of the complete communication link including ground station, baseband equipment and satellite.

The system demonstration experiments were designed to emphasize quality wideband television or telephony, some of which were used for public consumption. These experiments also include high bit rate digital data transmission, telephoto and facsimile data and multiple channel teleprinter transmission.

Each participating station was responsible for the acquisition of experiment data for the satellite operations in which it participated. These data were used in the evaluation of each station by its responsible agency. Most data is in the nature of ground station received and transmitted characteristics. Those items of information concerning the performance of the satellite wideband system, such as received signal strength and transmitted power, were transmitted to each participating station by the operations center in the form of an operational summary for each scheduled pass.

Each station also sent a quick-look report to the operations center soon after each pass in which it participated. These operations reports listed all significant events with their times of occurrence. Times of wideband signal acquisition, end of communication experiment, and change of tracking mode were typical items given in the operations report. The test stations likewise submitted an operations report approximately one hour after each scheduled pass, listing all commands transmitted to the spacecraft along with other pertinent data. The experiments performed by each station for that particular pass were also listed and a qualitative assessment of the results given. These indicated the degree of success of the experiment and noted any malfunction, out-of-tolerance performance, or loss of signal. Any interference noted during the tests was usually also listed. Figure 4–11 illustrates a typical station operations report. These quick-look reports were used at the operations center to determine the success of the scheduled operations as applied to the scheduling of future experiments. A complete history of all experiments performed by each station was maintained and updated from the operations report as a guide in recommending additional experiments by some stations.

Each participating station performed a detailed analysis of its own communications experiments. Copies of these were supplied to GSFC either individually or in complete documentation form. This data was then used to perform an overall system evaluation of Relay.

```
JTL002A
RR GSOC JSTL GMSA
DE GNUT 001
30/1434Z
INFO JSTL GMSA

OPS REPORT     REV 486      RELAY II      MARCH 27, 1964
1337           COMNUT TURNED ON 1.7 KMC XMTR    10 KW
1340           4 KMC BEACON ACQUIRED
               BEACON LEVEL -112 DBM AVG
               MONITOR LEVEL -103.3 DBM AVG
               COM LEVEL -103.9 DBM AVG
               COMMUNICATIONS CHANNEL NOISE TEMPERATURE 399 DEGREES K
               MONITOR CHANNEL NOISE TEMPERATURE  399 DEGREES K
               COMNUT AND COMMOJ PERFORMED THE FOLLOWING EXPERIMENTS:
1340-1342      CHANNEL 5 CONTINUOUS RANDOM NOISE.  COMMOJ TRANSMITTED
               A 1 KC TONE IN CHANNEL 5.  COMNUT MEASURED THE
               RECEIVED SIGNAL LEVEL AND THE NOISE LEVEL.
               SIGNAL LEVEL       -        0.87 V
               NOISE LEVEL        -        7.8 MV
               COMNUT TRANSMITTED A 1 KC TONE AT -14 DBM IN
               CHANNEL 5 AND COMMOJ MEASURED RECEIVED SIGNAL AND
               NOISE.  THE DEVIATION WAS 29.6 KC RMS PER CHANNEL.
1342-1345      CHANNEL 5 FREQUENCY RESPONSE.
               COMMOJ VARIED THE INPUT SIGNAL FREQUENCY FROM 500 CPS
               TO 3000 CPS AND COMNUT MEASURED THE RECEIVED SIGNAL
               LEVEL.
               FREQUENCY                SIGNAL LEVEL
                 (CPS)                    (CPS)
               ---------                ------------
                 500                        .88
                1000                        .87
                1500                        .88
                2000                        .82
                2500                        .87
                3000                        .81
               COMNUT VARIED THE INPUT SIGNAL FREQUENCY FROM 500 CPS
               TO 3000 CPS AND COMMOJ MEASURED THE RECEIVED SIGNAL
               LEVEL.  THE INPUT SIGNAL LEVEL AT COMNUT WAS -14 DBM
               AND THE DEVIATION WAS 29.6 KC RMS PER CHANNEL.
1345-1403      TWO WAY TELEPHONY BETWEEN MR. YUDD AT COMMOJ AND
               MR. SUNDERLIN AT COMSOC.
1403           4 KMC BEACON TURNED OFF
               BEACON LEVEL    -107 DBM AVG
               MONITOR LEVEL   -100.5 DBM AVG
               COM LEVEL       -100.3 DBM AVG
               COMMUNICATIONS CHANNEL NOISE TEMPERATURE 364 DEGREES K
               MONITOR CHANNEL NOISE TEMPERATURE   382 DEGREES K
1403:15        1.7 KMC XMTR OFF
WEATHER:       TEMPERATURE       36 DEGREES F
               HUMIDITY          58 PER CENT
               BAROMETER         29.97 IN RISING
               WIND              10-25 MPH
               PRECIPITATION     0
COMMENTS:      A DELAY OF APPROXIMATELY 3 MINUTES IN COMPLETING THE
               TELEPHONE CALL WAS DUE TO A BAD PATCH COARD.  AFTER
               THIS CORD WAS LOCATED AND REPLACED THE CALL WAS
               SUCCESSFULLY COMPLETED.

30/1456Z MAR GNUT
```

FIGURE 4–11.—Typical station operations report.

ORBITAL DATA

Precise orbital data is essential to the operation of a communication satellite system. The provisions made by GSFC to supply participants with accurate antenna pointing data have been a major element in the smooth operation of the system.

The origin of all orbital data used in connection with Project Relay is the tracking data supplied by the STADAN (formerly Minitrack) network. This worldwide complex of tracking stations operated by NASA makes use of interferometric techniques to track satellites. In the case of the Relay satellite, the stations track the unmodulated 136-Mc carrier from one of the two telemetry transmitters. One transmitter is left on continuously for tracking puposes.

The tracking data acquired by the STADAN network is transmitted to the GSFC Data Systems Division by teletype in the form of direction cosines. The Data Systems Division has available a number of computer routines which can generate from this tracking data a variety of outputs to meet the needs of Project Relay. These outputs are as follows:

1. *Orbital Elements*—Figure 4–12 is an example of the computer output giving the elements of the Relay orbit. This information was updated at weekly intervals and transmitted to all participating stations.

```
THE FOLLOWING ARE THE ORBITAL ELEMENTS FOR SATELLITE 1962 B-UPSILON
ONE RELAY COMPUTED FRM MINITRACK OBSERVATIONS AT THE NASA COMPUTING
CENTER AND ISSUED ON 03 APR 1964 BY THE GODDARD SPACE FLIGHT CENTER
EPOCH  64 Y 03 M 27 D AT 23 HOURS 50.00 MIN. UT
SEMI-MAJOR AXIS       010758.64   KILOMETERS
ECCENTRICITY          0.28505
INCLINATION           047.522     DEGREES
MEAN ANOMALY          015.102     DEGREES
ARGUMENT OF PERIGEE   027.421     DEGREES
     MOTION PLUS      01.2124     DEG. PER DAY
R.A. OF ASCEND.NODE   337.359     DEGREES
     MOTION MINUS     01.2791     DEG. PER DAY
ANOMALISTIC PERIOD    0185.08928  MINUTES
     MOTION PLUS      0.00000     MIN. PER DAY
HEIGHT OF PERIGEE     001313.55   KILOMETERS
HEIGHT OF APOGEE      007446.95   KILOMETERS
VELOCITY AT PERIGEE   029378      KM. PER HR
VELOCITY AT APOGEE    016345      KM. PER HR
GEOC.LAT.OF PERIGEE   19.856      DEGREES
```

FIGURE 4–12.—Orbital elements.

2. *MUSTAP World Map Printout* — One computer routine provides a printout of Mutual Station Predictions (MUSTAP) as illustrated in Figure 4–13. In addition to the range, azimuth, elevation, and antenna look angle data for all stations to which the satellite is visible at a given time, it gives the location of the sub-satellite point in longitude and latitude and the height of the satellite above the sub-satellite point. All data is given at two-minute intervals. The "S" printed at the end of each line indicates that the satellite is in sunlight at that time, and the percentage of sunlight for the entire orbit revolution is printed out at the end of the data list for the period. This printout was supplied only to the operations center and to the Project Office for planning purposes.

3. *MUSTAP Mutual Visibility Printout*— Another routine for the MUSTAP program generates an output to indicate which stations are able to see the satellite at a given time. A sample page of this document is

YYMMDD HHMM	STAT.	RANGE (KM)	AZI.	ELEV.	S/C LOOK	LAT.	LONG.	HEIGHT (KM)
			----------DEGREES----------					
64 123 1843	COMNUT	4102.9	90.4	39.4	124.2	37.9	-49.2	3147.7 S
	COMAND	3934.5	105.1	43.6	123.7			
	COMBOD	5582.2	269.1	15.4	129.6			
	COMHIL	5473.0	265.9	16.8	128.9			
	COMTEL	6999.4	287.1	0.7	131.4			
	COMGEB	6651.8	280.2	4.0	128.3			
64 123 1845	COMNUT	4385.2	93.4	29.9	114.2	35.4	-44.4	2990.5 S
	COMAND	4206.4	105.6	33.2	113.5			
	COMBOD	5277.9	261.3	16.6	125.5			
	COMHIL	5189.5	257.8	17.7	124.6			
	COMTEL	6619.3	281.6	2.3	128.8			
	COMGEB	6334.8	273.9	5.0	125.0			
64 123 1847	COMNUT	4740.7	95.7	21.2	105.2	32.5	-39.7	2841.1 S
	COMAND	4557.3	106.0	23.9	104.2			
	COMBOD	5038.5	252.5	17.1	120.0			
	COMHIL	4974.8	248.7	18.0	118.8			
	COMTEL	6275.6	275.3	3.6	125.0			
	COMGEB	6064.9	267.0	5.6	120.6			
64 123 1849	COMNUT	5156.0	97.4	13.3	97.0	29.4	-35.2	2701.1 S
	COMAND	4972.6	106.4	15.6	95.9			
	COMBOD	4878.4	242.9	16.8	113.2			
	COMHIL	4842.8	239.0	17.2	111.8			
	COMTEL	5979.1	268.4	4.5	120.2			
	COMGEB	5852.7	259.5	5.8	115.2			
64 123 1851	COMNUT	5618.4	98.9	6.3	89.6	25.9	-30.9	2571.9 S
	COMAND	5438.3	106.8	8.2	88.4			
	COMBOD	4810.0	233.0	15.4	105.4			
	COMHIL	4804.5	229.0	15.5	103.9			
	COMTEL	5741.7	260.7	5.1	114.3			
	COMGEB	5708.7	251.5	5.4	108.9			
64 123 1853	COMAND	5942.5	107.1	1.5	81.7	22.2	-26.7	2455.2 S
	COMBOD	4840.6	223.1	13.0	96.9			
	COMHIL	4865.6	219.3	12.7	95.4			
	COMTEL	5574.8	252.4	5.1	107.4			
	COMGEB	5641.2	243.1	4.4	101.8			

FIGURE 4–13.—Sample printout.

shown in Figure 4–14. This document is of great value in planning operations, since it indicates not only those stations to which the satellite is visible at each two-minute interval of time, but also look angle for each station (the figures printed under the headings for the various stations), antenna elevation (the code following the look angle indicates whether the antenna elevation is below 5 degrees, between 5 and 9 degrees, or above 10 degrees), and range (a "T" is printed with the antenna elevation code if the range is greater than 5000 nautical miles). This single printout thus provides all the information necessary to determine whether a satisfactory link can be established between any given pair of stations. It was provided to all stations on a monthly basis, with each document containing the data for one calendar month.

4. *Equator Crossings*—Each numbered orbit revolution begins as the subsatellite point crosses the equator in a northbound direction. The numbering of revolutions and the time interval covered by each revolution are thus defined by these equator crossings. A separate printout, supplied to all stations, indicates the times of all northbound equator crossings.

5. *Antenna Pointing Data*—The basic information required by all stations is the data required to point their antennas correctly in order to acquire and track the satellite. These data are supplied in two forms, depending on the tracking method used by the given station. Those stations not having programmed tracking capability were provided with azimuth and elevation coordinates, together with range data, for each one-minute interval of the period during which the satellite is visible to the station. These data were sent by teletype over the Support Communications Network well in advance of the pass to which the data ap-

ORBIT NUMBER 3929
MUTUAL VISIBILITY OF 62681 FOR FOLLOWING STATIONS

YYMMDD HHMM	S/C NUT	S/C MOJ	S/C AND	S/C BOD	S/C HIL	S/C TEL	S/C RIO	S/C GEB	S/C IBA	S/C SCA	S/C KAS	S/C AIN
64 5 1 1618		0922 5										
64 5 1 1620		0981 9										
64 5 1 1622		1059 A										
64 5 1 1624		1170 A										
64 5 1 1626		1343 A										
64 5 1 1628		1602 A										
64 5 1 1630	1228 5	1603 A	1176 5									
64 5 1 1632	1315 A	1369 A	1244 A									
64 5 1 1634	1434 A	1215 A	1333 A									
64 5 1 1636	1588 A	1113 A	1439 A									
64 5 1 1638	1579 A	1041 5	1470 A									
64 5 1 1640	1346 A		1295 A									
64 5 1 1642	1148 A		1099 A	1052 5	1041 5							1109 5
64 5 1 1644	1006 A		0964 A	1009 9	0997 9			0954 5		0866 5		1063 A
64 5 1 1646	0914 A		0874 A	0955 A	0940 A							
64 5 1 1648	0846 A		0809 A	0890 A	0874 A	0960 5		0902 5		0814 5		1004 A
64 5 1 1650	0794 A		0759 A	0822 A	0805 A	0906 9		0846 9		0762 5		0933 A
64 5 1 1652	0751 9		0718 9	0754 A	0738 A	0849 9		0788 9		0711 5		0856 A
64 5 1 1654	0714 5		0684 9	0691 A	0677 A	0790 A		0731 A		0663 5		0780 A
64 5 1 1656			0654 5	0634 A	0622 A	0732 A		0677 A		0619 5		0709 A
64 5 1 1658				0584 A	0574 A	0677 A	1244 5	0626 A		0578 5		0645 A
64 5 1 17 0				0541 A	0533 A	0625 A	1188 5	0580 A		0541 5		0589 A
64 5 1 17 2				0503 A	0496 A	0577 A	1133 9	0538 A		0507 5		0541 A
64 5 1 17 4				0469 A	0464 A	0534 A	1082 9	0500 9		0476 5		0499 A
64 5 1 17 6				0440 A	0436 9	0494 A	1033 9	0466 9				0463 A
64 5 1 17 8				0413 9	0411 9	0458 A	0987 9	0435 9				0431 A
64 5 1 1710				0390 9	0389 9	0426 A	0944 A	0407 9				0404 A
64 5 1 1712				0369 5	0368 5	0396 9	0904 A	0381 5				0379 A
64 5 1 1714				0350 5	0350 5	0369 9	0867 A	0358 5				0358 A
64 5 1 1716				0333 T5		0345 9	0833 A	0336 T5				0339 9
64 5 1 1718						0323 T5	0802 A					0322 9
64 5 1 1720						0302 T5	0773 A					0307 T9
64 5 1 1722						0284 T5	0747 A					0294 T5
64 5 1 1724						0268 T5	0723 TA					0283 T5
64 5 1 1726							0701 TA					
64 5 1 1728							0681 T9					
64 5 1 1730							0663 T9					
64 5 1 1732							0647 T9					
64 5 1 1734							0633 T9					
64 5 1 1736							0621 T9					
64 5 1 1738							0610 T9					
64 5 1 1740							0601 T5					
64 5 1 1742							0593 T5					
64 5 1 1744							0587 T5					
64 5 1 1746							0582 T5					
64 5 1 1748							0579 T5					

FIGURE 4–14.—Mutual visibility printout.

plies. A sample of this type of data is shown in Figure 4–15.

For those stations having a capability for programmed tracking, the pointing data was supplied in the form of topocentric *XYZ* coordinates as shown in Figure 4–16. These data were teletyped to the station for one-minute intervals over the period of visibility of the satellite to the station. The punched tape was then fed to a computer at the station, which interpolated between the given data points to generate intermediate points giving a best-fit curve through the points provided. Interpolation of about the sixth order is usually sufficient to maintain the accuracy of the original points. The computer then generated a punched tape carrying the smoothed data, and this tape was fed to the antenna programmer to steer the antenna.

The orbital data operation for Project Relay was excellent from the beginning of operations. The pointing data supplied to the stations was extremely accurate and has

Y	M	D	H	M	S	R KM	AZ	EL
64	03	24	13	52	40	012232	30699	0002
64	03	24	13	53	40	012120	30668	0097
64	03	24	13	54	40	012007	30635	0192
64	03	24	13	55	40	011892	30600	0288
64	03	24	13	56	40	011776	30564	0384
64	03	24	13	57	40	011659	30527	0480
64	03	24	13	58	40	011540	30487	0576
64	03	24	13	59	40	011421	30446	0673
64	03	24	14	00	40	011299	30403	0770
64	03	24	14	01	40	011177	30359	0867

FIGURE 4–15.—Example of AZ–EL orbital prediction printout.

Y	M	D	H	M	S	E. .01KM	N. .01KM	V. .01KM
64	03	24	13	52	00	-00980145	00743948	-00013047
64	03	24	13	53	00	-00975313	00732039	00007217
64	03	24	13	54	00	-00970162	00719685	00027185
64	03	24	13	55	00	-00964705	00706920	00046805
64	03	24	13	56	00	-00958934	00693720	00066105
64	03	24	13	57	00	-00952862	00680118	00085039
64	03	24	13	58	00	-00946484	00646484	00103622
64	03	24	13	59	00	-00939798	00651667	00121850
64	03	24	14	00	00	-00932815	00636841	00139692
64	03	24	14	01	00	-00925528	00621609	00157159

FIGURE 4–16.—Example of *XYZ* topocentric coordinate printout.

resulted in completely satisfactory tracking of the satellite.

EFFECT OF ORBITAL MOTION ON OPERATIONS

Table 4–4 lists the initial characteristics of the Relay I orbit as compared with the prelaunch nominal values. Figure 4–17 is provided to give indication of the relationships of the orbit, the earth, and the sun. There are two types of orbital motion which have a direct effect on operations.

TABLE 4–4.—*Relay I Orbit Characteristics*

Item	Nominal	Actual
Height of apogee, nm	3999.48	4020.70
Height of perigee, nm	699.92	712.13
Period, min	184.36	185.09
Eccentricity	0.28475	0.28462
Inclination, deg	47.766	47.496
Right ascension of ascending node, (injection), deg	217.22	218.74
Argument of perigee, (injection), deg	176.426	177.5
Nodal rate, deg/day	−1.2845	−1.2779
Perigee rate, deg/day	1.2030	1.2123

The first of these is the rotation of the line of apsides (the line joining the apogee and the perigee) in the orbit plane. This motion, which is slightly greater than one degree per day, causes the apogee (and thus of course the perigee) to describe a complete circle in the orbit plane in approximately one year. As can be seen from the figure, the most favorable position of the apogee for operations with the present Relay network occurs when the subsatellite point at apogee is at the most northerly latitude. The extreme limits of this latitude, both north and south, are equal to the orbital inclination of 47 degrees. Between these limits the latitude of the apogee subsatellite point varies in a nearly sinusoidal fashion in the course of its approximately one-year cycle, as shown in Figure 4–18, as the line of apsides rotates through a complete revolution.

When the apogee is in the southern hemisphere the maximum mutual (Europe-US) visibility on any single pass, also plotted in Figure 4–18, decreases sharply and, in fact, vanishes entirely for a short period at maximum southern latitude of apogee. The position of the line of apsides in its cycle is thus of considerable importance in the planning of operations, since it determines the maximum period of mutual visibility during any one pass of a given day. The relationship of the period of the satellite and the rotation of the earth is such that normally four or five successive passes out of the approximately eight per day have comparable mutual visibility characteristics. When the single-pass mutual visibility is at its highest (68 minutes), the total mutual visibility time for that day may reach 140 minutes.

The second type of orbital motion which directly affects operations is the orientation of the orbit plane with respect to the line joining the earth and the sun. Since the satellite derives its electrical power from sunlight, the amount of time it is in sunlight strongly affects the length of time the wideband transponder can be operated. The transponder draws considerably more current than the solar array provides, so that its operation time is determined to a large extent by the state of charge of the batteries. The batteries in turn are charged only when the satellite is in sunlight.

It is clear that when the plane of the orbit is facing the sun, the satellite will remain in sunlight at all times. This full sunlight condition is the most advantageous for opations, since it provides maximum time for battery charging. The orbit plane, however, rotates in inertial space. Therefore, as the earth moves about the sun the orbit plane enters the earth's shadow similar to that shown in Figure 4–19, reducing the amount of time in sunlight and consequently the charging time for the batteries. These eclipse seasons have a second effect on the spacecraft power system in that the satellite temperature is lower, reducing the output of the solar array and the capacity of the batteries.

The actual pattern of eclipses is not as

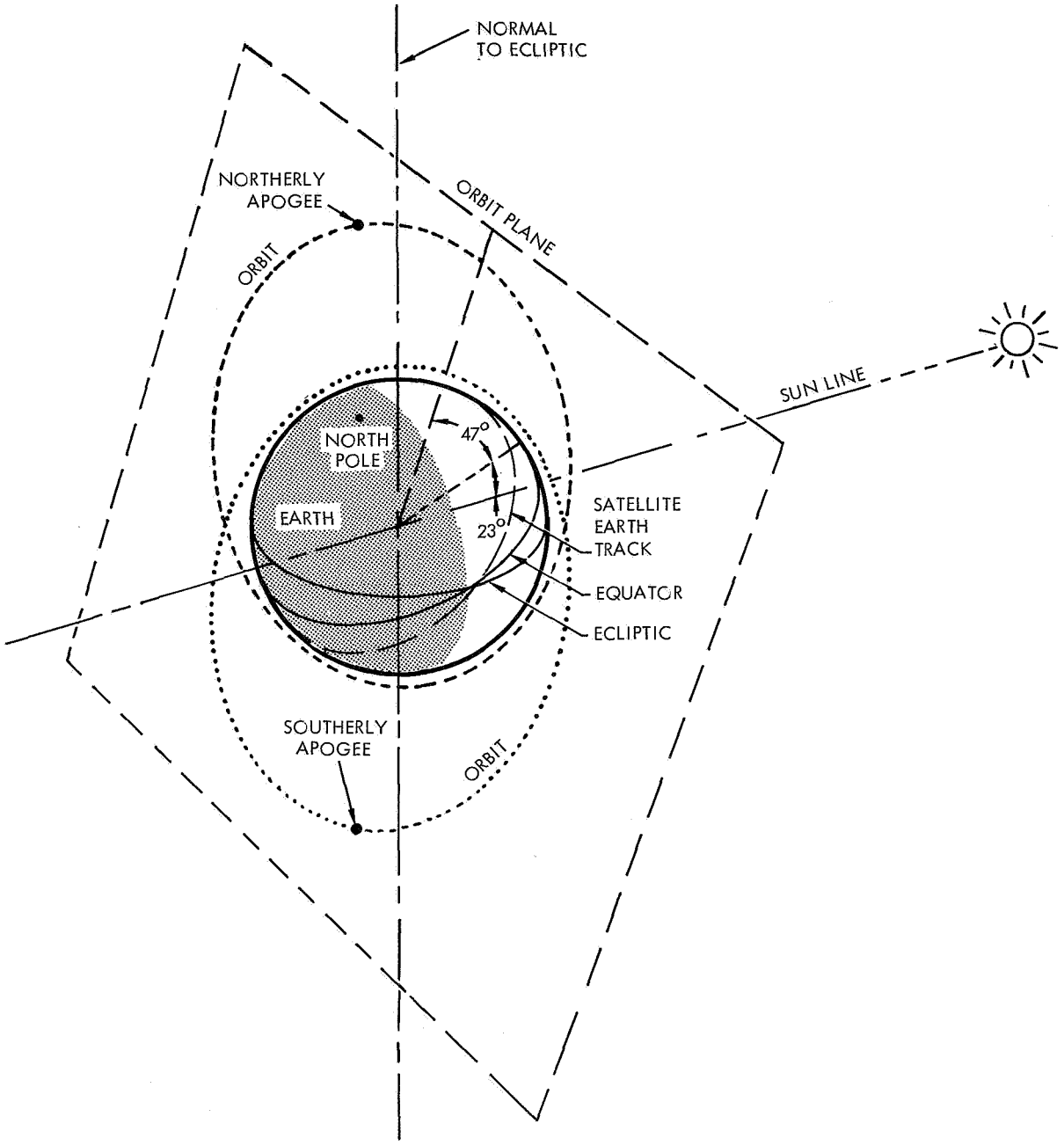


FIGURE 4–17.—Relation of Earth, apsidal rotation, and Sun.

simple as is indicated in Figure 4–19, but is quite irregular because of rotation of the line of apsides and other factors including a rotation of the Relay plane greater than 360° per year. Figure 4–20 shows the eclipse pattern in terms of percentage of time the satellite is in sunlight, together with the accumulated operating time of the wideband transponder. It can readily be seen that operating time accumulates at a much more rapid rate during the periods of 100 percent sunlight, when there is adequate electrical

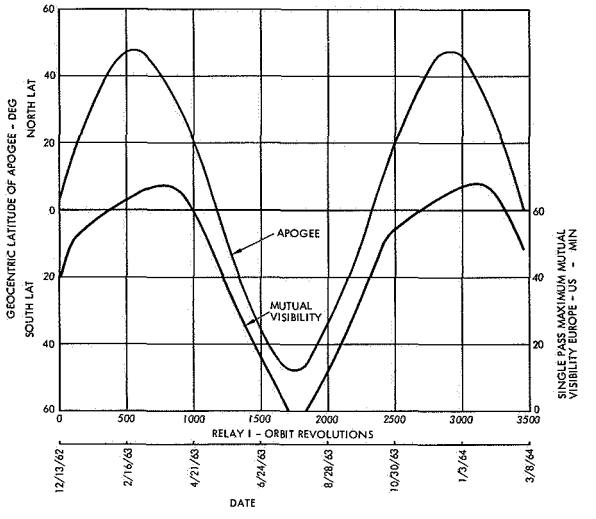


FIGURE 4–18.—*Geocentric latitude of Apogee and* Europe-US mutual visibility vs. orbit rev and date for Relay I.

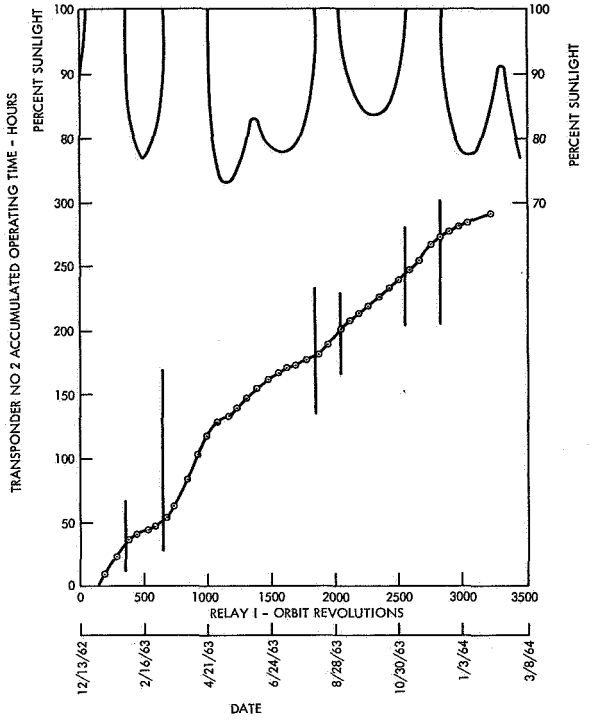


FIGURE 4–20.—Accumulated transponder No. 2 operating time vs. eclipse history.

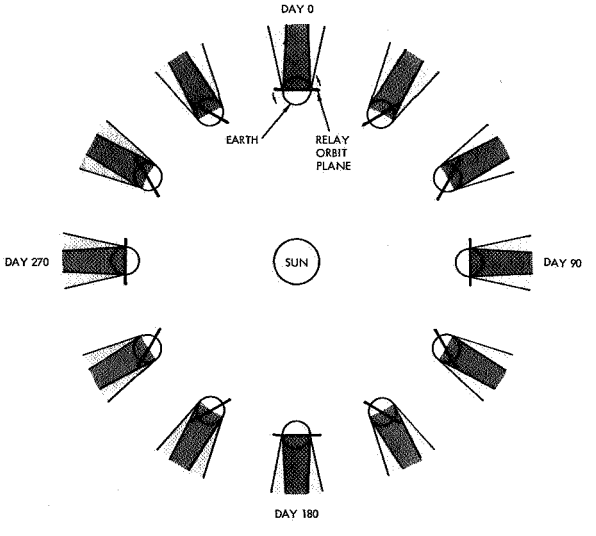


FIGURE 4–19.—Relative motion of orbit plane and Earth shadow.

power available for operation during all mutual visibility periods.

ATTITUDE DETERMINATION

From the standpoint of operations, the attitude of the spacecraft (i.e., the orientation of the spin axis in inertial space) was important only in that it affected the spacecraft antenna look angles. The initial orientation of the spin axis at injection was selected to provide optimum look angles for the stations in the Relay network. Since the satellite is spinning, this orientation should nominally remain constant for the life of the satellite.

There are, however, certain factors which tend to perturb the orientation of the spin axis, causing it to precess about its nominal position. Provision was made in the design of the spacecraft for sensors to determine the attitude and for a mechanism to modify the attitude if it should prove desirable to do so. The sensors are a sun aspect indicator which provides an input to the telemetry

data indicating the angle between the satellite axis and the line to the sun, and a horizon scanner which provides a signal each time the rotation of the satellite causes the instrument to sense the change from the cold of space to the relatively warm surface of the earth, or vice versa. These two indications in combination provide sufficient data to permit computation of the inertial orientation of the satellite spin axis.

The attitude of the spacecraft can be modified, to a limited extent and at a relatively slow rate, by the operation of the attitude control coil incorporated in the satellite. This is a coil of wire to which current can be supplied in either a positive or a negative direction. When the coil is energized, its magnetic field interacts with the earth's magnetic field to impart a precessional motion to the spacecraft spin axis, with the direction of motion determined by the direction of the current supplied to the coil. Since it was expected that any deviations of the spin axis from its nominal attitude would be small, this simple attitude-control system was sufficient for the requirements of the program.

One aspect of spacecraft operation, then, was to monitor the spin axis orientation by means of the horizon scanner and sun aspect indicator data, and to determine whether any attitude corrections should be carried out. Monitoring of the attitude in the planned manner, however, was not possible because of the apparent failure of the horizon scanner to provide usable data. It was originally planned to operate the horizon scanner on a regular schedule, perhaps once per month, and from the resulting data combined with the sun aspect indication to determine the spin axis orientation. The horizon scanner operates only on command, and its output is used to modulate directly the carrier from one of the two telemetry transmitters; it is not included in the routine telemetry data.

One operation of the horizon scanner early in the program (Rev 155), did provide useful data which indicated that the spin axis attitude was 2.5 degrees from nominal; this is a sufficiently small deviation so that no correction was indicated.

The sun aspect indicator operated satisfactorily, providing a check on spin-axis orientation in one plane at least. Figure 4–21 is a plot of the sun aspect as determined from telemetry compared to the theoretical values computed from the nominal orbit. It can be seen that the deviations are

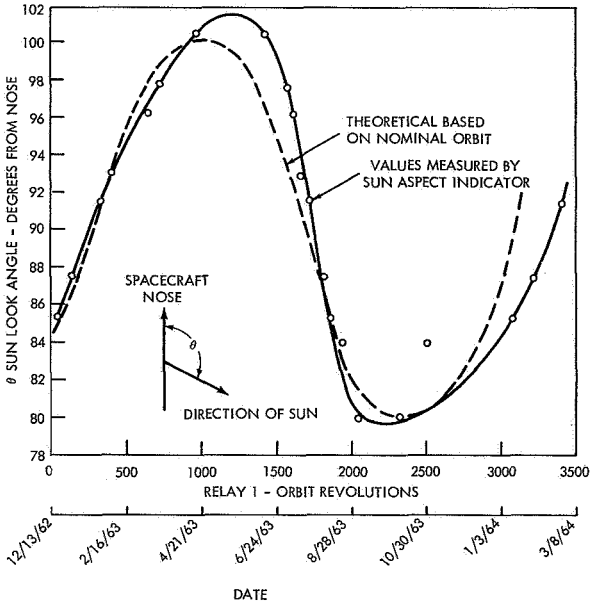


FIGURE 4–21.—Relay I sun aspect history.

relatively small, indicating that the attitude of the spacecraft has probably remained very near its nominal value.

A further indication is provided by the fact that the received signal levels at the various ground stations have been close to the values which would be expected with the nominal look angles. This is only a rough indication, but it can be concluded that there have been no gross deviations from the nominal.

Since there has apparently been no need for attitude corrections, the attitude-control

coil on the satellite has never been deliberately operated. It was occasionally turned on as a result of command anomalies, but its operation was so slow that these short periods of operation had no perceptible effect on spacecraft attitude.

AUTHORS. *This chapter was contributed jointly by* D. E. KENDALL, *Space Technology Laboratories, Inc., Redondo Beach, California, U.S.A. and* W. S. SUNDERLIN, *NASA/ Goddard Space Flight Center, Greenbelt, Maryland, U.S.A.*

N66-10243

Chapter 5

Spurious Signals In Satellite Command Systems

INTRODUCTION

The problem of providing secure command systems for satellites has become more prominent as an increasing number of operational satellites orbit the earth. As this problem becomes greater, systems engineers must learn about the systems which are in use today in order to avoid the pitfalls that exist. This report describes a command system used today by the Relay I active communication satellite, but the scope of this work is beyond that of a single system.

The author feels strongly that the problems discussed here are not unique; rather, some of them appear in nearly all remote control systems, although they may take slightly different form. Perhaps the greatest mistake one can make is to look at the shortcomings of one system and deny the possibility of similar deficiencies in another system. For this reason the author feels justified in generalizing on the subject of satellite command control by using the problems encountered in the operation of the Relay I command system as a basis for discussion.

It is unfortunate that greater emphasis is not placed on RFI when a system design emerges. So often RFI (Radio Frequency Interference) problems are set aside, due to difficulty in defining precise limits of acceptability. In the specific case of a command system, the problem of providing a realistic RFI level (in which the system may be tested) is very great. This being the case, it is important for the system designer to take advantage of past experience in his field, and for this reason it is felt that a thesis of this nature is justified.

DESCRIPTION AND ANALYSIS OF THE RELAY I COMMAND SYSTEM

The purpose of the Relay command system was to provide ground control of the satellite with extremely high reliability, and simplicity of satellite command equipment. Extremely high reliability was accomplished by using an error-detecting communication code and redundant spacecraft equipment to effect the commands. Simplicity of operation was attained with consoles that produce proper commands by push-button and one-way command link only. No satellite verification that the proper command has been received is required for execution of the command. A block diagram of the command system is given in Figure 5–1.

A six-bit, error-detecting, binary code was chosen for the Relay system. The code consists of three ones and three zeros; this provides a total of twenty combinations of three ones, and three zeros, or twenty, six-bit, command words. In practice, a command word consists of six bits and a sync pulse that clears the command decoder of all previous information. Figure 5–2 illustrates a typical PDM code waveform. A command

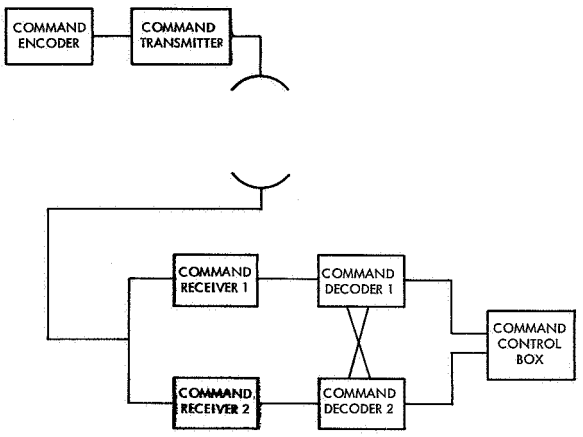


FIGURE 5–1.—Relay command system, block diagram.

word is 105.6 milliseconds (msec) long and consists of eight time-slots, each 13.2 msec long. The first time-slot contains no information and contains no signal at all. The second time-slot contains the sync pulse, which in PDM form is 9.9 msec long, followed by a 3.3 msec period of no signal. The last six time-slots contain the command code (a one is a 6.6 msec pulse, and a zero is a 3.3 msec pulse). This PDM code amplitude modulates a 5.451 kc subcarrier tone 100 percent. These PDM tone bursts are the output of the command encoder, which is used to amplitude modulate the 148 Mc RF carrier. The command encoder generates the command and repeats the command five times. The RF carrier is turned on one second prior to transmission of the five-command sequence. This is done to "quiet" the command receiver in the spacecraft.

The command receivers receive the AM signal, demodulate it, and present the decoder with the 5451 cps tone bursts which make up the desired commands. The decoder actually performs two functions: First, the decoder demodulates the 5451 cps subcarrier and reconstructs the PDM waveform; secondly, the PDM waveform is decoded and the corresponding code is indicated by a positive or negative pulse on one of ten output lines. This pulse is then used to effect the proper changes in flip-flop memories contained in the command control box. These memories, in turn, control various power switches in the control box that supply different satellite systems with proper on-off signals.

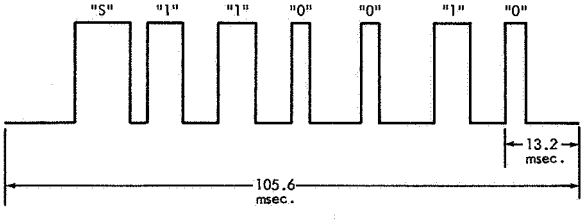


FIGURE 5–2.—Typical code waveform.

As indicated in Figure 5–1, the command system components are completely redundant in the case of the command receiver and decoder. The reconstructed PDM output of each decoder is cross-coupled to the other decoder to provide increased system reliability.

For sake of completeness, and also because it will aid in the error-analysis which follows, a more detailed description of the satellite equipment is deemed necessary.

Command Receiver

The command receiver was equipped to receive ordinary DSB–AM, and is completely compatible with the ground transmitter. Pertinent characteristics are itemized in Table 5–1. The unit is a single conversion receiver with a crystal-controlled, local oscillator and a 40 kc wide (6 db) crystal filter at the input to the IF amplifier; the IF frequency is 20 Mc and the IF amplifier is 700 kc wide so that the overall bandpass characteristic is determined by the crystal filter. This same receiver has enjoyed excellent success in several current space programs.

Command Decoder

Figure 5–3 illustrates the block diagram of the command decoder. The input from the receiver is filtered, amplified, and then applied to the slicer amplifier circuit. The slicer amplifier samples the signal at approximately the 50-percent level. This signal is

TABLE 5–1.—*Parameters for the Relay Command Receiver*

Input frequency band	148 Mc
Modulation	AM
Noise figure	Typical, 7 db; maximum 10 db
IF frequency	20 Mc
IF selectivity	40 kc bandwidth, 6 db down
	100 kc bandwidth, 60 db down
Spurious rejection	Down 50 db, or more
Input impedance	50 ohms
Audio output impedance	2000 ohms
Voltage gain	120 db ±3 db over temperature range from −10°C to +60°C
Audio output voltage for 90% modulation at 1 KC	1 volt, RMS
Oscillator stability (−10°C to +60°C)	±0.005%
AGC dynamic range	Audio output constant to ±1.5 db for input signal between 2.0 and 10,000 microvolts
Overload level	50,000 microvolts
Power supply	15 milliamperes at 24 volts, dc
Power-supply regulation	Receiver has internal regulator to permit operation from 20 to 35 volts
Operating temperature range	−15°C to +60°C
Weight	2 pounds (two receivers)

then demodulated, filtered again, and used to activate the Schmitt trigger circuit. The Schmitt trigger output is amplified and then gates a multivibrator. The output of this multivibrator is a series of pulses, the number depending on the length of the input pulse. The multivibrator output is combined with the Schmitt gate by an AND gate and applied to a counter. Depending upon the number of pulses, either one, two, or three, the counter output is a ZERO, a ONE, or a SYNC pulse, respectively. The counter is reset by the leading edge of the Schmitt trigger output.

The ONE's from the first counter are used to trigger the information driver which inserts ONE's into the shift register. The ONE's output is also fed to a 3-counter and to a delay circuit. The delay circuit output triggers information stored in the low line of the shift register into the upper line of cores. The 3-counter counts the number of ONE's in each message to determine that there are three. The ZERO's are fed to the same delay circuit and to a separate 3-counter which determines that the message contains three ZERO's. The SYNC pulse output of the first counter is used to reset both 3-counters and to initiate delay circuit A. The output of delay circuit A triggers a

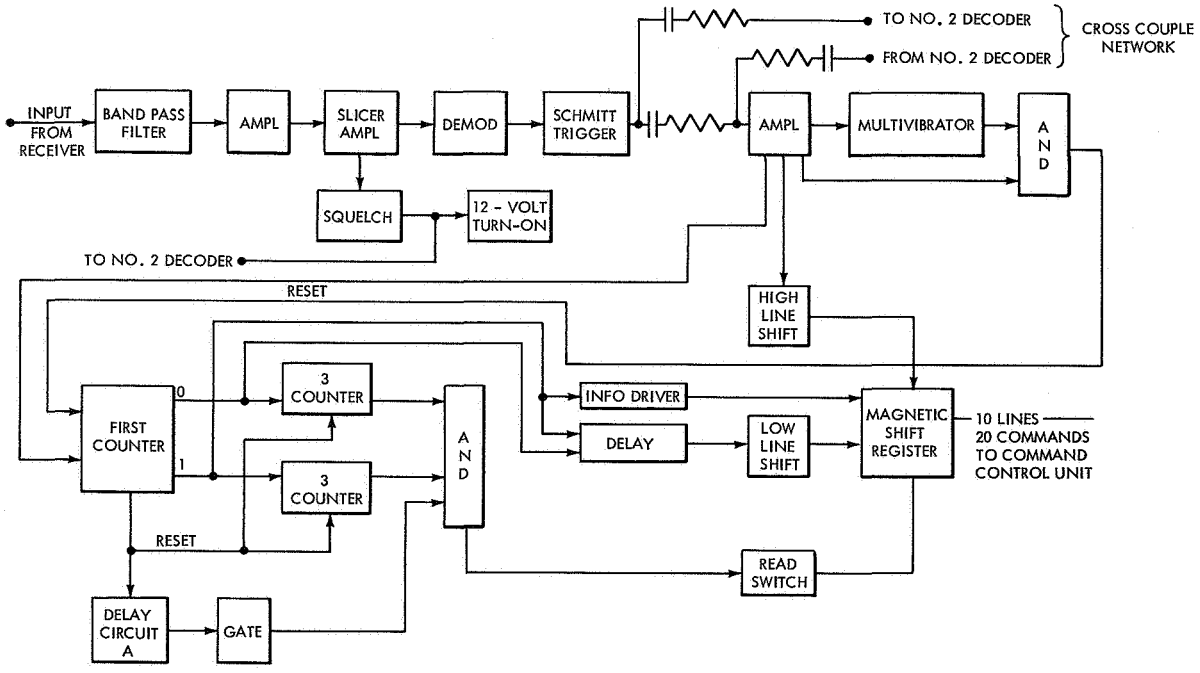


FIGURE 5–3.—Decoder block diagram.

gate circuit, whose output is applied to an AND circuit along with the output of both 3-counters. The AND gate output drives a read switch circuit that enables the magnetic shift register to read out stored information.

Six cores, which have information stored corresponding to each of the six bits, have ten lines wound about them in such manner that when the cores are read out, the flux induces a positive or negative pulse on only one of the ten lines.

Command Control Box

The function of the command control circuit is to accept the decoded commands and enable the command function to be performed. This is accomplished by storing the decoded commands in bistable memories and operating transistor power switches, according to the state of the memories. In most cases the on-off function is accomplished by directly switching the power to the desired subsystem; however, in the case of the wideband system, the radiation experiments, and the telemetry encoder, only an on-off signal is supplied by the command control circuit.

In addition to the switching functions performed in the control circuit, several other outputs are provided:

1. *Command verification* — This circuit provides four telemetry voltages to indicate the state of the command control memory.

2. *Third stage separation indication*—This is a telemetry voltage which indicates separation of the third stage.

3. *Command Receiver AGC*—The AGC voltage from the command receiver is amplified in the command control circuit and presented as a telemetry voltage.

In addition to these items and on-off switching, certain logic is incorporated within the control circuit to perform the following functions for the wideband system:

a. *Low Voltage*—Shutdown occurs when the unregulated bus falls below some nominal pre-set level. Shutdown may be inhibited by command.

b. *Low Signal Received*—Shutdown occurs when signal strength in the receiver falls below some nominal level for a period of more than two minutes. The timers which provide the shutdown signal may be reset by repeating the *on* command to the respective wideband system.

c. Pulse steering logic assures that only one wideband system can be on at one time, and that the telemetry transmitter is modulated by only one signal.

The functional listing of commands given in Table 5–2 is helpful in understanding the various Relay systems.

TABLE 5–2.—*List of Commands Used to Control the Relay I Satellite*

Command No.	Digital Code	Function
1	111000	Load cutoff normal
2	110100	Transponder No. 1 ON
3	101100	Transponder No. 2 ON
4	011100	Transponders OFF
5	110010	Radiation experiments OFF
6	101010	Radiation experiments ON
7	011010	Telemetry encoder ON
8	100110	Horizon scanner ON
9	010110	Modulate telemetry transmitter #1
10	001110	Modulate telemetry transmitter #2
11	110001	Attitude control negative
12	101001	Attitude control positive
13	011001	Attitude control and horizon scanner OFF
14	100101	Telemetry encoder OFF
15	010101	Telemetry transmitters 1 and 2 ON
16	001101	Telemetry transmitter No. 2 OFF
17	100011	Telemetry transmitter No. 1 OFF
18	010011	Wideband mode
19	001011	Narrowband mode
20	000111	Load cutoff override

A brief glossary of terms will clarify the command functions in Table 5–2.

The load cutoff normal and override commands control the circuit that senses satellite bus voltage and shuts off heavy power loads, if load cutoff normal is commanded and the bus voltage falls below the pre-set value.

Transponder refers to the communications system in the satellite; wideband and narrow band modes refer to the type of operation desired with the transponder. A TV transmission would require a wideband mode command, whereas two-way voice transmis-

sion would require a narrowband mode command.

Telemetry encoder-on or horizon scanner-on commands refer to the type of telemetry information required. An encoder-on command automatically turns off the horizon scanner, and vice-versa. This prevents simultaneous modulation of a telemetry transmitter by both the encoder and horizon scanner. Attitude control, positive or negative, refers to the direction in which current is commanded to flow in a large coil which encircles the satellite. This coil develops a magnetic field which reacts with the earth's magnetic field and develops a torque to correct any small attitude errors. As in the case of the encoder and horizon scanner, attitude positive and negative commands cannot be effected simultaneously.

Errors of the Command System

The measure of any command system is the ability of that system to effect the desired command without error. Two basic types of error may occur in a command system such as Relay has. The first type is failure of the command system to effect a desired command, and this type is the least serious, since it can be commanded again. The second type is the occurrence of a spurious command, i.e., a command that is not transmitted. In any digital system, there is (for each word) a probability-of-error which is a function of the signal-to-noise ratio of that word. The calculation of this probability provides a performance index or comparison between systems.

Thus, the following section will calculate two error probabilities. The first is the probability that the command system will fail to respond to a desired command and the second is the probability that a spurious command will occur. It should be emphasized that these probabilities are theoretical values, and should be compared with the results given on page 394 of this chapter which describes the performance of the Relay command system. The analysis which follows is based on the following three assumptions:

1. The noise output of the command receiver is gaussian and white over the receiver output spectrum. This is a standard and reasonable assumption for a calculation of this nature.
2. Receiver noise is considered to be thermal noise only. No external signals are considered present other than the desired command. This is a simplification of the problem rather than a justifiable assumption.
3. Ideal decoder performance is assumed, to the extent that filters are assumed to have flat response over the band and linear phase characteristics. Wherever possible, actual decoder characteristics are taken at face value, when the circuit operation figures directly into the error analysis. An example of direct contribution of decoder design to error probability would be the circuit that distinguishes between a SYNC, ZERO, and ONE in the incoming code. This circuit consists of a multivibrator which is gated on for one, two, or three pulses. If a single pulse is missed by the counter, the signal is incorrectly recognized, and an error has occurred. By sampling the waveform at a rate consistent with the filter bandwidth in the decoder, this circuit could detect the filter bandwidth in the decoder, and also notches in the PDM waveform that caused the improper signal recognition. Thus a multivibrator rate which is five times as fast would produce five pulses for a ZERO, ten pulses for a ONE, and fifteen pulses for a SYNC. This, however, would make it harder to effect the proper command and would require increased circuitry, and is not really worth the added weight, power, and space.

DETERMINATION OF THE PROBABILITY OF ERROR

Two probabilities were required to calculate the over-all probability of error in the Relay system: the probability that a ZERO would be changed to a ONE and probability that a ONE would be changed to a ZERO. These two probabilities, P_{01} and P_{10}, are not equal, as will be shown in the following analysis. In determining the error prob-

ability in a PDM system, the envelope of signal-plus-noise is examined at the output of the bandpass filter. The knowledge of the filter bandwidth allows the examination of the envelope at discrete time intervals $\frac{1}{2B_f}$ apart, as it is known that the envelope cannot assume a new value in an interval of less than $\frac{1}{2B_f}$.

A ONE in the Relay system is defined as the presence of a 5.451 kc subcarrier, whose envelope is 0.7 volts (or greater) for a continuous period of 6.6 milliseconds, and a 6.6 msec period of no signal in the 13.2 ms time slot given to each bit. A ZERO is defined as the presence of the same amplitude and frequency subcarrier for a continuous 3.3 msec period and a 9.9 msec period of no signal, during the basic 13.2 msec time slot for a digit. Thus for a ONE to be changed to a ZERO, the noise must add to the signal in such a way that the envelope of signal-plus-noise is below 0.7 volts, at the instant the multivibrator in the decoder is sampling the waveform. In determining whether the one is changed to a zero, the envelope of signal-plus-noise is sampled at the rate of one sample per 3.3 msec (since the multivibrator period is 3.3 msec) and the question is asked at each sample point: "Is the envelope greater than 0.7 volts?" At each of these sample points, there is a finite probability that the envelope will be below 0.7 volts. The probability that at one of the two samples the envelope will be below 0.7 volts is $(P_b P_a)$ where

P_b = Prob. envelope is $<$ 0.7 volts

P_a = Prob. envelope is $>$ 0.7 volts

$P_a = 1 - P_b$

There are two ways in which the envelope can be distorted so that the envelope of signal-plus-noise is below 0.7 volts, at one of the two samples:

The envelope may be below 0.7 volts at the first sample and above 0.7 volts at the second sample, or above 0.7 volts at the first sample and below 0.7 volts at the second sample.

Thus the total probability that a one is changed to a zero is

$$P_{10} = 2P_a P_b \qquad (5.1)$$

It is then reasonably easy to obtain an expression for the P_{10} and P_{01} as a function of signal-to-noise ratio, a. First values for P_a and P_b (as previously defined) are tabulated as functions of a with the value of v fixed. Several curves may be obtained as v is varied. Rice* has already plotted several curves for value of $a = 0$, 1, 2, 3, 5, and infinity. These curves, and some additional curves which were plotted by the author for values of a which are of specific interest, were used to obtain values of P_a, P_b, and P_A.

When values of P_a, P_b, P_A were tabulated, these values were used directly with Equation (5.1) to obtain curves for P_{10} vs a and with equation (5.2) to obtain curves for P_{01} vs a.

These functions are plotted in Figures 5–4 and 5–5. The value of S/N used in the calculation is the value of S/N following the 5.451 kc filter. This filter provides signal-to-noise improvement of 13 db over the signal-to-noise ratio out of the command receiver, i.e., the improvement gained in going from a 20 kc bandwidth to a 1 kc bandwidth. The curves shown are plotted with respect to the signal-to-noise ratio at the output of the command receiver. A similar analysis for the calculation of P_{01} may be made. In this case, the noise must add to the signal so that the envelope of signal and noise is above 0.7 volts for two samples by the multivibrator. Since the subcarrier signal is present for only one sample, this means that the envelope of noise alone must be greater than 0.7 volts for the second sample. Thus, the probability that the envelope will exceed 0.7 volts for two counts is $(P_a P_A)$.

P_a = probability that the envelope of signal-plus-noise is greater than 0.7 volts.

P_A = probability that the envelope of noise alone is greater than 0.7 volts.*

*Rice, S. O., "The Mathematical Analysis of Random Noise," Bell System Technical Journal, Vols. 23 and 24.

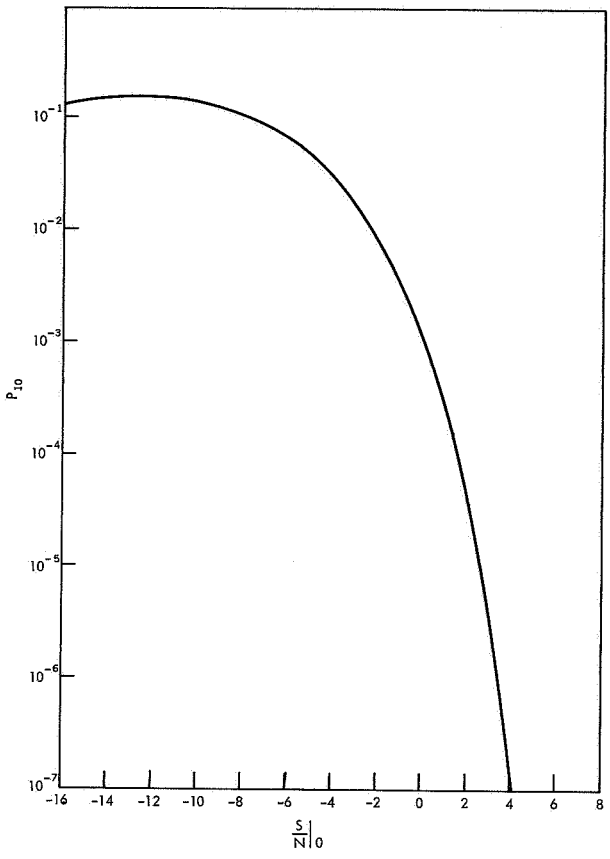


FIGURE 5–4.—P_{10} vs. the S/N ratio at the receiver output.

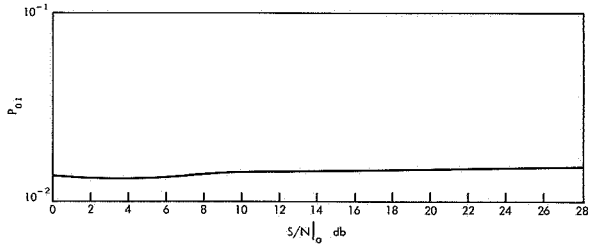


FIGURE 5–5.—P_{01} vs. the S/N ratio at the receiver output.

This event may occur in two ways, i.e., first when noise alone is sampled above 0.7 volts, followed by signal-to-noise sampled above 0.7 volts, and the other when the sampling order is reversed.

Thus the probability that a zero is changed to a one is given by the expression

$$P_{01} = 2P_a P_A \qquad (5.2)$$

It should also be noted that for a given signal-to-noise ratio,

$$P_{01} = P_{10}$$

Once values of P_a, P_b, and P_A are calcu-

$$*P_A = \int_{0.7}^{\infty} \frac{R}{0.05}\, \epsilon^{-\frac{R^2}{0.1}}\, dR = -\epsilon^{-\frac{R^2}{0.1}}\Big|_{0.7}^{\infty} = 7.4 \times 10^{-3}$$

lated, the corresponding values of P_{10} and P_{01} may be obtained by direct substitution into Equations (5.1) and (5.2).

In Rice's paper*, an analysis is given for the distribution of noise-plus-sine-wave. For the sake of completeness, the part of Rice's analysis which deals with the envelope of noise-plus-sine-wave will be repeated here. It will be seen that the probability density function for the envelope distribution may be used directly in the calculations of P_a, P_b, and P_A. If

$$V(t) = P \cos pt + V_n \qquad (5.3)$$

The envelope distribution of $V(t)$ is the case of interest.

The envelope of $V(t)$ is defined as $R(t)$ where

$$R^2(t) = (P + V_c)^2 + V_s^2 \qquad (5.4)$$

where V_c is the component of V_n in phase with cos pt and V_s is the component of V_n in phase with sin pt:

$$V_c = \sum c_n \sin [(\omega_n - p)t - \phi_n]$$
$$V_s = \sum c_n \cos [(\omega_n - p)t - \phi_n]$$
$$V_n = V_c \cos pt - V_s \sin pt$$
$$\overline{V_n^2} = \overline{V_c^2} = \overline{V_s^2} = \Psi_o$$

Since the values of P_{01} and P_{10} are now available, it is possible to obtain an expression for

P_S = probability of obtaining a spurious command

P_E = probability that there is an error of any type in a command word. Since the

*Rice, S. O., "The Mathematical Analysis of Random Noise", by Bell System Technical Journal, Vols. 23 and 24.

code is an error-correcting code, one would intuitively expect that

$$P_E > P_S$$

and such is the case, as will be shown.

The probability of obtaining a spurious command is simply the sum of the probabilities of all events which are considered spurious commands. Since there are 20 possible commands, one command is correct, and 19 commands are considered to be spurious, if any one of these should occur. Assume any given command has been sent, say

$$1_1\ 1_2\ 1_3\ 0_1\ 0_2\ 0_3$$

where

1_1 is the first ONE
1_3 is the third ONE
0_2 is the second ZERO, etc.

This allows examination of the code, with no loss of generality.

If there is an error in 1_i, $i = 1, 2,$ or 3, there must be a corresponding error in 0_j, $j = 1, 2,$ or 3 to produce a spurious command; and

$$P_e(1_i) = P_{10},\ P_e(0_j) = P_{01}$$

The probability of obtaining a spurious signal with an error in only one one and one zero becomes

$$P_e(1_i)\,P_e(0_j)\,[C_1^3]^2 = 9\,P_{10}\,P_{01}$$

If there is an error in 1_i and 1_j, $i \neq j$, $i, j =$ 1, 2, or 3, there must be corresponding errors in 0_k and 0_j $k \neq j$, $k, j = 1, 2,$ or 3 and

$$P_e(1_i\,1_j) = P_{10}^2$$
$$P_e(0_k\,0_j) = P_{01}^2$$

The probability of obtaining an error in two ones and two zeros becomes

$$P_e(1_i\,1_j)\,P_e(0_k\,0_j)\,(C_2^3)^2 = 9\,P_{10}^2\,P_{01}^2$$

Finally, the probability of obtaining an error in all three ones and all three zeros is

$$P_e(1_1\,1_2\,1_3)\,P_e(0_1\,0_2\,0_3)\,(C_3^3)^2 = P_{10}^3\,P_{01}^3.$$

Since the events are mutually exclusive, the probability that any one event occurs is the sum of the probabilities of all the events, and

$$P_s = 9\,P_{10}\,P_{01} + 9\,P_{10}^2\,P_{01}^2 + P_{10}^3\,P_{01}^3. \quad (5.5)$$

The probability that an error of any type occurs is where

$$P_E = 1 - P_{E^1} \quad (5.6)$$

P_{E^1} = probability that no error occurs. It is not difficult to see that

$$P_{E^1} = (1-P_{10})^3(1-P_{01})^3$$

Since the probability that any given bit in the command is correct is independent of the probability that any other bit is correct, by direct substitution into (5.6),

$$P_E = 1-(1-P_{10})^3(1-P_{01})^3 \quad (5.7)$$

Curves of P_S and P_E vs. the signal-to-noise ratios on the output of the command receiver are shown in Figures 5–6 and 5–7. These

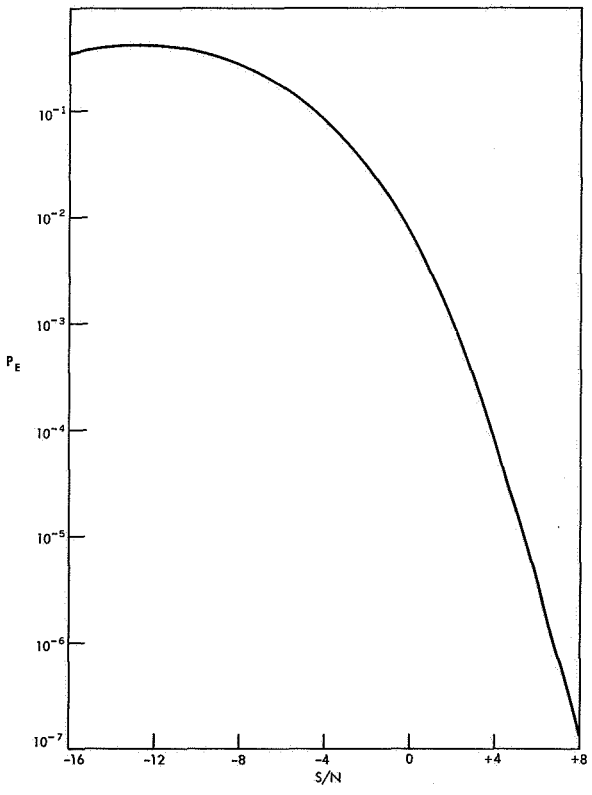


FIGURE 5–6.—P_E vs. the S/N ratio at the receiver output.

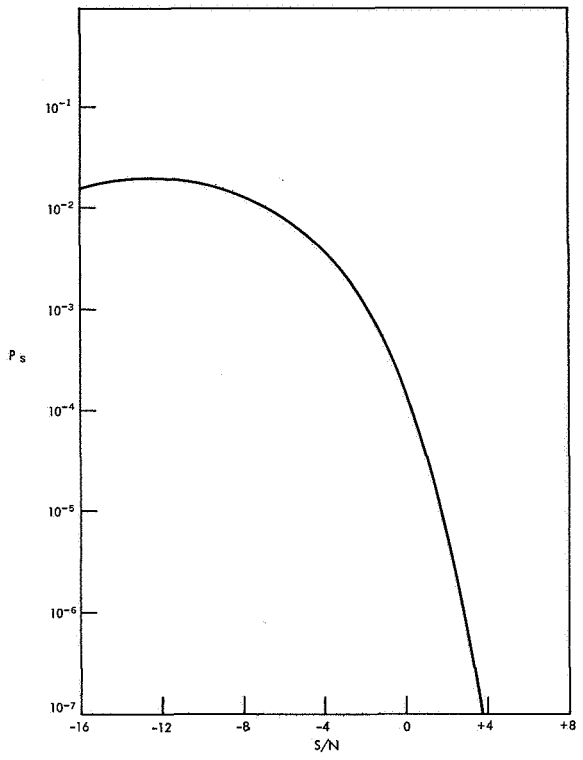


FIGURE 5–7.—P_s vs. the S/N ratio at the receiver output.

values were obtained with the aid of the curves shown in Figures 5–4 and 5–5 and Equations (5.7) and (5.5).

Since V_c and V_s are normally distributed about zero with a variance of Ψ_o, the probability densities of the variables

$$x = P + V_c$$
$$y = V_s$$

are

$$\frac{1}{\sqrt{2\pi\,\Psi_o}} \exp\left[-\frac{(x-P)^2}{2\,\Psi_o}\right]$$
$$\frac{1}{\sqrt{2\pi\,\Psi_o}} \exp\left[-\frac{y^2}{2\,\Psi_o}\right]$$

respectively. Setting

$$x = R\cos\theta$$
$$y = R\sin\theta$$

and using these distributions shows that the probability of a point (x, y) lying in the ring R, $R + dR$ is

$$\frac{RdR}{2\pi\,\Psi_o}\int_0^{2\pi} \exp\left[-\frac{1}{2\Psi_o}\,(R^2 + P^2 - RP\cos\theta\,\right] d\,\theta$$

$$= \frac{RdR}{2\pi\,\Psi_o}\,\exp\left[-\frac{R^2+P^2}{2\Psi_o}\right] I_o\left(\frac{RP}{\Psi_o}\right) \qquad (5.8)$$

where I_o is the Bessel function with imaginary argument

$$I_o(z) = \sum_{n=0}^{\infty} \frac{x^{2n}}{z^{2n}\,n!\,n!}$$

which is a tabulated function.

Employing a useful change of variables let

$$\mathrm{v} = \frac{R}{\Psi_o^{1/2}}\,,\ dv = \frac{dR}{\Psi_o^{1/2}}\,,\ a = \frac{P}{\Psi_o^{1/2}} \qquad (5.9)^*$$

a may be recognized as the voltage S/N ratio defined as peak signal/RMS noise.

The random variable is now changed from R to v, whose probability density is

$$P(v) = v\exp\left[\frac{v^2+a^2}{2}\right] I_o(av) \qquad (5.10)^*$$

The probability that v is less than some stated amount, as distribution curves for v may be obtained by integrating

$$\int_0^{v_1} P(v)\,dv = P_r(v < v_1)$$

$$P_r(v < v_1) = 1 - P_r(v < v_1)$$

Unfortunately this integral requires numerical integration. Rice provides a useful expression for this purpose from W. R. Bennett in an unpublished work. This expression is

$$P_r(v<v_1) = \exp\left[\frac{v^2+a^2}{z}\right]\sum_{n=1}^{\infty}\left(\frac{v_1}{a}\right)^n I_n(av_1) \qquad (5.11)^*$$

THEORETICAL EXPECTATIONS OF THE COMMAND SYSTEM

Before describing the experimental results obtained during Relay I operation, it would be worthwhile to present a theoretical esti-

*Ibid., Section 3–10.

mate of the command system performance. As was previously stated, the performance could be measured by the ability of the command system to execute the desired commands without error. Two types of errors were mentioned: spurious commands as discussed before, and the failure of the command system to execute the desired commands.

The probability of spurious commands is given by equation (5.5) and Figure 5–7. The latter type of error should be almost nonoccurent since commands are repeated five times and

P_M = probability of command system failing to execute the desired command

$$P_M = (P_E)^5 \qquad (5.12)$$

To obtain a quantitative estimate of P_S and P_M, Table 5–3 presents a calculation of the signal-to-noise ratio out of the command receiver. Calculations are based on the Relay system parameters. The expected signal-to-noise ratio out of the command receiver is +9 db. This signal-to-noise ratio is so high that it does not have a corresponding value for P_S or P_E in Figures 5–6 and 5–7. P_S has a value of approximately 1×10^{-7} and $S/N_o = +4$ db and the curve is falling off at the rate of approximately one order of magnitude per db. Extrapolating the curve with this approximation results in a value for P_s of 1×10^{-12} which is extremely low, and this result indicates that spurious commands would be almost unheard of.

In a similar manner, P_E may be evaluated. At +9 db, P_E has an approximate value of 1×10^{-7}. This corresponds to a P_M of 1×10^{-35}, in other words, a missed command would never occur.

TABLE 5–3.—*Relay System Parameters*

Assumed system parameters

Carrier frequency	150 Mc
Nominal range	7000 nautical miles
Polarization	Circular (ground), Linear (spacecraft)
Elevation	10°
Transmitter power	300 watts
Modulation	80% AM

Calculation of received signal power

Item	Gain (db)	Loss (db)	Net power level
Transmitter power			54.8 dbm
Ground station losses		3.5	
Antenna gain	13.5		
Tracking loss		0.3	
Net radiated power			64.5 dbm
Free space loss		158.2	
Atmospheric attenuation		0.5	
Fading margin		5.0	
Spacecraft antenna gain	2.0		
Line and diplexer loss		1.5	
Receiver power split		3.0	
Polarization loss		3.0	
Net propagation and spacecraft losses		173.2 db	
Received power			−108.7 dbm

Calculation of the signal-to-noise ratio at the receiver output

Received power (see above)	−108.7 dbm
Noise power at receiver input (see below)	−117.7 dbm
Signal-to-noise ratio at the command receiver output	+9 db

A CALCULATION OF RECEIVER NOISE DENSITY AND RECEIVER NOISE POWER

The receiver noise density is given by the following expression:

$$\sigma_{\text{rec}} = Kt_s$$

where K = Boltzmann's constant and T_s = system noise temperature.

$$T_s = \frac{1}{L_1 L_2}\left[T_A + T_1(L_1 - 1)\, T_2(L_2 - 1)L_1\right] + (F-1)\,T_o \qquad (5.13)$$

T_A = Antenna noise temperature

T_o = Temperature of spacecraft receiver (290°K)

T_1 = Temperature of spacecraft diplexer (290°K)

T_2 = Temperature of spacecraft power splitter (290°K)

F = Receiver noise figure (10 db)

L_1 = Line and diplexer loss (1.5 db or $\sqrt{2}$)

L_2 = Receiver power splitter loss (3.0 db or 2)

$$T_A = T_E k + T_C (1 - k) \qquad (5.14)$$

k = Total fraction of galactic sphere intercepted by earth for an isotropic antenna at 5000 nautical miles from earth

T_E = Temperature of earth (290°K)

T_G = Integrated galactic noise temperature

$$k = (T_G \approx 290\,\lambda^2)^* \cdot \tfrac{3}{16}\left(\frac{r_E^2}{(5000 + r_E)^2}\right) \quad (5.15)$$

r_E = Radius of the earth in nautical miles
= 3390 nautical miles

k = 0.03

T_A = 290 (0.03) + 1160 (0.97) = 1130°K

Substitution of this value in the first equation results in the following expression:

$$T_s = \frac{1}{2\sqrt{2}}\left[1130 + 290(\sqrt{2-1}) + 290(2-1)\sqrt{\sqrt{2}} + (10-1)\,290\right]$$
$$= 3200°\text{K}$$

Receiver Noise Density

$$\sigma_{rec} = KT_s \text{ or } -163.7 \text{ dbm/cps}$$
$$P_{noise} = \sigma_{rec} B_{if}$$

where

P_{noise} = Noise power at receiver input

B_{if} = IF bandwidth of command receiver
= 40 kc

P_{noise} = −117.7 dbm

PERFORMANCE ANALYSIS OF THE ORBITING RELAY I COMMAND SYSTEM

Following the launch of Relay I spurious commands became a serious problem which required special investigation.

The previous pages predicted the performance of the command system and gave an estimate of the number of spurious commands which might be expected. But actual spurious commands were occurring at a much greater rate than expected.

Generally speaking, the orbiting spacecraft exhibited several anomalous performance patterns. These patterns fell into the following groups:

1. *Spurious Commands Occurring Spontaneously*

These occurred both when the satellite was in view and out of view. It was felt that these spurious commands were not related to operational procedure, since the number occurring during operation of the spacecraft was roughly proportional to the length of the operational cycle. For example, if the satellite were monitored 15 percent of the time, approximately 15 percent of the spurious responses occurred while the satellite was monitored. This was most puzzling, since spurious commands were expected to occur only upon transmission of a command. All commands in this category occurred when commands were not being transmitted.

2. *Spurious Commands Generated on Transmission of a Command*

In this phenomenon, there appeared to be no relationship between the code of the command sent and the code of the spurious command received. This phenomenon disappeared when the command transmitter power was increased to 3 kw. There were few spurious commands in this category and they were the type that were expected.

3. *Command System Failing to Respond to Commands*

This was totally unexpected, since the system calculations (Table 5–3) indicated that there should be more than enough margin in the system. This phenomenon also disappeared when the transmitter power was increased to 3000 watts.

4. *High AGC Voltage in the Command Receiver*

Telemetry indicated signal presence in the command receiver. The AGC voltage was telemetered for indication of signal presence, and since the command transmitter was off except during command transmission, this result was surprising.

A systematic study was undertaken to determine the possible cause of the anomalous command system behavior.

The first effort was by a data reduction team which reduced telemetry data, making

*From "The Effective Noise Temperature of the Sky," by Hogg and Mumford, *Microwave Journal*, March 1960.

note of unusual command system performance. Command receiver AGC was plotted as a function of time and spacecraft location. These results were correlated with NASA information on anomalous command system behavior and studied for possible relationships between spacecraft system performance and the spurious commands.

The second effort consisted of a very thorough laboratory study of the command subsystem. Tests (prior to launch) to determine the susceptibility of the spacecraft to spurious commands proved to have been too narrow in scope, as they considered only those interfering signals whose center frequencies were exactly on the frequency of the command receiver. Nevertheless, confidence in the Relay I command system was borne out in Relay prototype and Relay I system tests, during which the spacecraft never exhibited the anomalous command system performance observed following launch. The tests in the laboratory following launch were considered to be as thorough as possible, and these tests revealed that several combinations of events would lead to spurious commands through the RF command link. Attempts were made to locate ground transmitters at or near the Relay command frequency, and the effects of their signals were considered with respect to the results of the laboratory experiments.

The third part of the study consisted of an investigation of circuit changes, in the command decoder, to eliminate the spurious commands observed during Relay I testing.

Telemetry Data Reduction

Analysis of data obtained from telemetry, and subsequent analysis of operations reports obtained from NASA, yielded some rather interesting results. The four basic modes in which the anomalous performance patterns may be classified have previously been described.

The first and fourth items were the predominant modes of anomalous performance, and since the other anomalies disappeared when command transmitter power was increased, the major effort concentrated on explaining these predominate modes.

The spurious commands seemed to occur at random, both with respect to time and to the specific spurious command. Table 5–4 gives a listing of the commands and the frequency of their occurrence. It should be noted that certain commands could have occurred spuriously and gone unnoticed. For example, a Wideband Systems #1 and #2 OFF command would not be noticed if the wideband systems were off. Since the wideband systems shut themselves off after two minutes if no carrier is present in the wideband receiver, a Wideband ON spurious command would go unnoticed unless the spacecraft was in view. Some evidence has been found that the Wideband Systems had come on spuriously and shut themselves off. This evidence lies in the fact that the spacecraft temperature in the vicinity of the TWT was higher than anticipated when telemetry data was taken, indicating that the TWT had probably been on sometime during the orbit.

TABLE 5–4.—*Spurious Commands as a Function of Command Number During January 1963*

NASA command number	Command	Number of times appeared spuriously
1	Load cutoff normal	1—Normal state
2	Transponder No. 1 ON	3
3	Transponder No. 2 ON	-------
4	Transponder No. 1 & 2 OFF	0—Normal state
5	Radiation experiments OFF	1—Normal state
6	Radiation experiments ON	9
7	Telemetry encoder ON (horizon scanner OFF)	2
8	Horizon scanner ON (telemetry encoder OFF)	4
9	Modulate telemetry trans. No. 1	8
10	Modulate telemetry trans. No. 2	0—Normal state
11	Attitude control negative	3
12	Attitude control positive	6
13	Horizon scanner and attitude control OFF	2—Normal state
14	Encoder OFF	2—Normal state
15	Telemetry transmitters No. 1 & No. 2 ON	9
16	Telemetry transmitter No. 2 OFF	9
17	Telemetry transmitter No. 1 OFF	5—Normal state
18	Phone ON—TV OFF	1
19	TV ON—phone OFF	2
20	Load cutoff override	7

Another anomaly which became apparent during a study of the spurious commands was the occasional inversion of telemetry modulating signals. Inversion of telemetry modulating signals means that the encoder signal is suddenly replaced by the horizon scanner signal (or vice versa). This is consistent with the circuit logic employed in the Command Control Box to ensure that the two telemetry modulating signals are not commanded on simultaneously. Occasionally, when the satellite went out of view (of the Nutley, New Jersey tracking station) with the horizon scanner signal modulating the transmitter, it came back into view on the next orbit with the encoder modulating the transmitter. This seems to point to spurious commands being generated through the RF command link (rather than from transitions in command control box flip-flop memories) since it would require two transistions in the flip-flops to give the telemetry modulating reversal described above. The random occurrence of commands indicated by Table 5–4 seems to indicate that no particular command decoder output, or command control input, is more sensitive to spurious signals than another.

Varying command receiver AGC of levels much higher than anticipated also proved to be a cause of major concern. The pattern evolved that the AGC in the command receiver could be as high as six microvolts when the wideband system was on, or when both telemetry transmitters were on. As will be explained later, tests conducted on the prototype spacecraft revealed that the second harmonic of the wideband receiver IF Amplifier interfered with the command system. While this explained some of the high AGC readings, there were still numerous cases where the wideband system was off, and telemetry indicated signal presence in the receiver.

There did seem to be a relationship between high AGC and spurious commands although the correlation sample available was too small to arrive at any solid conclusions. It is mentioned at this time, since this phenomenon was observed and the results of laboratory work bear this theory out. Generally speaking, it may be said that spurious commands implied high command receiver AGC, but the converse was not true.

The occasional spurious command generated when a command was transmitted, and the failure of the command system to respond to a command occurred when the AGC of the receiver was unusually high. It is believed that these phenomena were caused by other signals blocking the command receiver, since they disappeared when the command transmitter power was increased. Laboratory experiments described in the following pages have shown that if two signals are present in the receiver, the signal which is 3 db stronger will capture the system; if the signals are of comparable signal strength and one signal is quite noisy, the command information carried by the other signal may be distorted enough to give a spurious command. This is the type of spurious command which has been analyzed in the first section.

Laboratory Investigation

Using results obtained from the analysis of Relay I performance, a careful laboratory investigation was begun to study the effects of interfering signals on the command system. Extensive tests were run and a description of the tests and their results are tabulated in Table 5–5. As would be expected, the key to generation of spurious commands was in opening the squelch circuit in the decoder. The squelch circuit inhibits generation of any command, unless it is opened with a 5.4 kc subcarrier tone for an appropriate length of time. But once the squelch is opened, the door is opened to spurious commands, as evidenced by the Table 5–4.

One surprising result was the effect of AM and FM signals, the carriers of which were located on the skirt of the command receiver response curve. Since the skirt of the receiver response curve acted like an FM discriminator, audio outputs were obtained

TABLE 5–5.—*Laboratory Tests on the Relay Command Subsystem*

Test description	Command decoder squelch	Results
Modulating carrier with random noise (0–20 kc)	Squelch would not open	No false commands
Modulating carrier 100% with audio tone swept from 10 cps to 20 kc. Slow and rapid scan.	Squelch opens in vicinity of 5.4 kc	No false commands
Two carriers—one CW, one modulated with commands	Squelch opened for commands	No false commands. Signal 3 db stronger captured system
Two carriers—one modulated 80% with proper codes, one modulated 20–80% by 2.5 kc keyed 2–100 cps	Squelch opened only for proper commands	No false commands; 2.5 kc would not open squelch
No input; maximum receiver noise output. (600 mv. RMS)	Squelch manually held open	No false commands
Subcarrier frequency varied from 2.5–8 kc. Proper commands modulating subcarrier. 80% RF modulation	Squelch manually held open	No false commands; commands would activate from 4.5–6 kc
Correct commands with 2.5 kc subcarrier overmodulating the carrier	Squelch manually held open	Command system responded
Using an electric drill to produce noise, varying speed and level	Squelch manually held open	No false commands. Command receiver AGC read as high as 80 μvolts
Tested decoder to see if temperature difference would open the squelch	Squelch would not open for temperature difference of 10°C	
No input; maximum receiver noise output. (600 mv. RMS). Decoder one shot read window held open	Squelch manually held open	False commands occurred at the rate of 1 per minute
Two low level carriers (0.5 v.) applied to system 5.4 kc apart	Squelch opened	Sporadic false commands
Carrier at 148.260 Mc—15 kc frequency modulated with an audio frequency signal	Squelch opened sporadically	Occasional false commands

which generated spurious commands in the command system. The mechanism which generated the spurious commands was the AGC system which saw a lower average power than it did with an on-center frequency signal, due to the characteristics of the 20 Mc crystal filters.

The gain of the receiver was then greater than normal for side bands of the signal closer to center frequency. In this way, audio output voltages greater than could be obtained by on-center frequency signal were observed. These higher audio outputs were capable of opening the squelch circuit and generating spurious commands. Another contributing factor lay in the fact that the spectrum of interfering signals might be narrower than the 20 kc spectrum which the receiver was capable of handling. The spectrum on the interfering signal might contain

components close to the subcarrier frequency and hence the theoretical 13 db improvement provided by the bandpass filter in the command decoder could not be expected.

Broadcast material such as rock and roll music was recorded and played into the command system by means of an FM signal generator whose carrier frequency was 15 kc below the Relay command frequency of 148.260 Mc. With a signal strength of 3 microvolts, spurious commands were generated at the rate of several per minute. The corrective approach would be to modify the command decoder to discriminate against noise signals. This is discussed more fully in the section on the decoder modifications.

On the basis of these experiments, a theory arose that ground-based stations near the Relay command frequency could be causing spurious commands. An attempt to pinpoint ground stations was made by plotting the satellite orbit and recording AGC voltage along with the orbit in the correct position. The idea was to see if the transition between high AGC and low AGC was gradual or abrupt. In several cases abrupt changes were evident. This would correspond to the satellite dropping out of view of a transmitting station. By making note of the points at which these transitions occurred, the station could be pinpointed on the map. Figure 5–8 indicates the geometry involved. The perpendicular bisectors of the chords between three transition points intersect at the location of the transmitting station. Figure 5–9 shows orbit data plotted for three orbits which revealed sharp transitions in the AGC. Straight lines connect the transition points. Perpendicular bisectors intersect at a point in the lower half of South America. The results do, however, point to the fact that signals near the Relay frequency are being radiated from South America. A check on international communications frequency assignment did reveal an Argentine station AYY627 at 148.255 Mc. It is rated at 250 watts and emission 36F3. At minimum range which is in the Southern hemisphere, 50 watts would produce a signal level of about 3 microvolts. This would be sufficient to produce spurious commands.

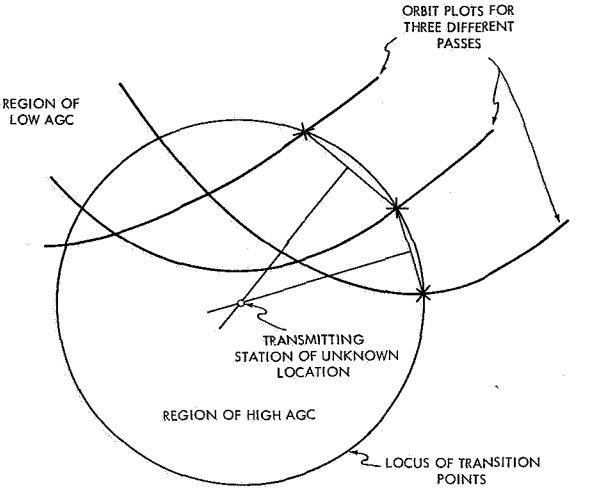


FIGURE 5–8.—Geometry involved in the location of a transmitter.

The investigation of ground stations radiating at or near the command frequency of 148.260 Mc brought up several interesting points. As mentioned above, ground stations do exist which either share or infringe on the Relay command frequency. FM stations in Canada and the United States also have sufficient power to interfere with the command receiver. European stations are believed to exist in this band (148.26 Mc $\pm$ 40 kc) radiating as much as 1 kw.

In the United States alone there are several satellites which share the Relay command frequency; Injun and Syncom both had active ground stations during the period in which high AGC levels and spurious commands were received. The effect of the Injun command system has been shown in the laboratory to have little probability of generating a suprious command in the Relay spacecraft. RCA personnel visited the Syncom ground station at Lakehurst, New Jersey. Tests there revealed no spurious commands, however, the decoder squelch circuit would open with certain modulating signals used during Syncom operation. This is mentioned since the opening of the squelch

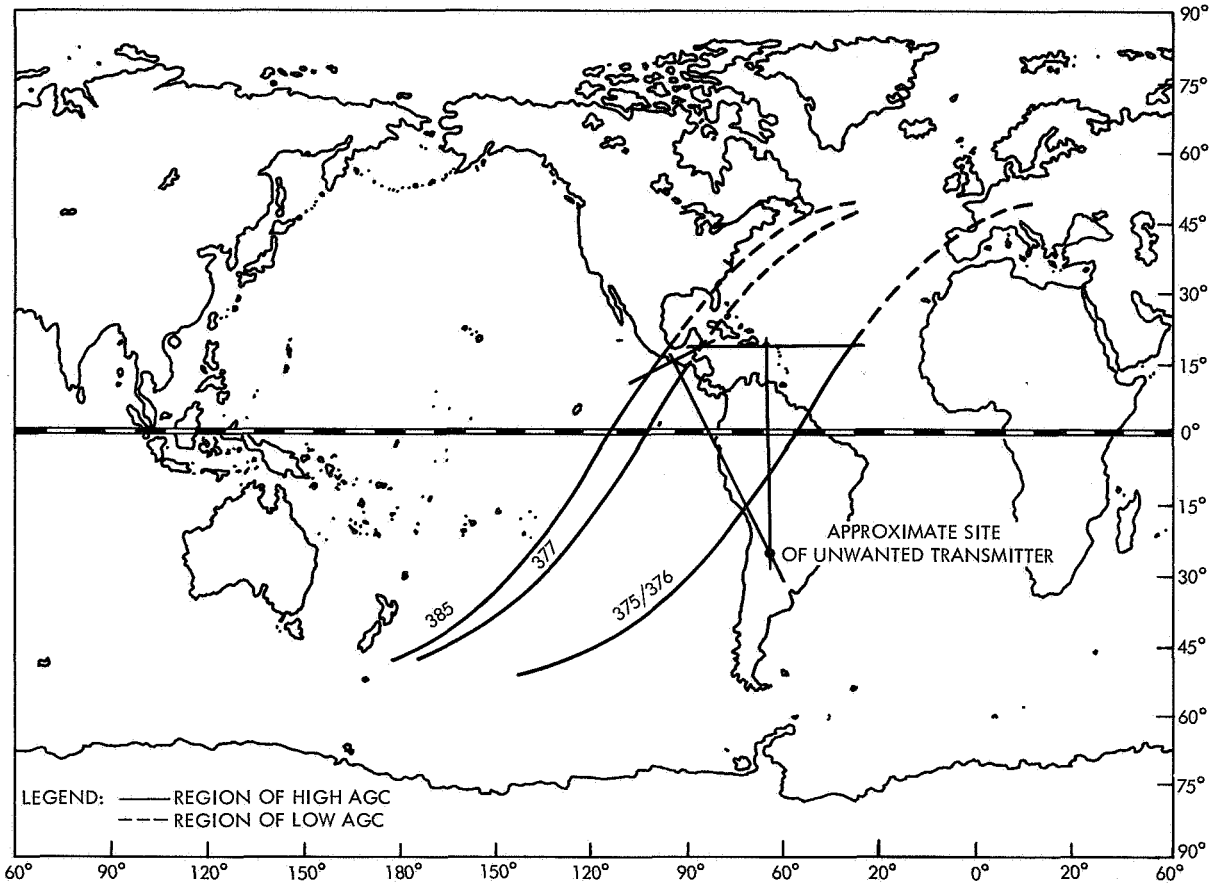


FIGURE 5–9.—Orbit data from three passes which showed abrupt changes in telemetered AGC voltage.

is the key to spurious commands. The OAO Project, Project SERT, and a military satellite, all share the Relay command frequency. The military satellite is the only operational satellite, other than Relay and Injun, and while little information is available on the military satellite, it is known that this satellite is also experiencing spurious commands.

The possibility that spurious commands could be caused by internally radiated RF (such as from the wideband system or the telemetry transmitters) was also thoroughly investigated. Extensive testing of the prototype following launch of flight model I revealed the following:

1. Radiation from the wideband system does exist. The high signal level present when the wideband system was turned on could be explained by the fact that the IF frequency of the wideband repeater is 70 Mc and is 25 Mc wide. The IF output is limited and then tripled. In the tripling process, a considerable second harmonic is also produced. The second harmonic of 74 Mc is 148 Mc, and thus it is reasonable to expect that this is probably the source of the wideband interference noted during Relay I operation. This interference is not the type which could cause spurious commands in itself, since the interference is in effect a white noise spectrum across the receiver band. Tests on the command system have shown that pure random noise alone is not sufficient to cause spurious commands, unless it is of a level greater than the com-

mand receiver can supply. It is desirable to reduce this interference, however, since it serves to de-sensitize the command receiver.

It was found also that interference was being radiated from power leads to the wideband system. These leads were long enough to become antennas at the command frequency. The effect of these leads as radiators could be decreased with a combination of shielding and addition of ferrite co-axial filters on the leads. This made radiation from the power leads at the command frequency virtually impossible.

2. Interference from the telemetry transmitters could occur only when there was an unbalance in the diplexers, such as a broken antenna whip. Such an unbalance does not cause spurious commands, however; the unbalance produces a blocking effect on the command receiver, and the command system fails to respond to command.

Command Decoder Investigation

Following experiments performed in the laboratory to determine mechanisms for spurious commands, the command decoder circuit was re-evaluated to see if any of these mechanisms might be avoided in the future. One improvement was immediately apparent. Spurious commands occurred when the energy in the subcarrier band was irregular, as might be expected with an interfering signal. The squelch circuit in the decoder was thus keyed on and off and the voltage regulator for the counters in the decoders was keyed on and off as well. Greater stability could be maintained in the counters if the regulated voltage was on constantly and the squelch signal used to inhibit the output of the Schmitt trigger, rather than using the squelch signal to turn on the regulator.

Another possibility for improvement of the decoder could be realized if the signals of low signal-to-noise ratio could be rejected. A careful study of the code waveform at various points in the decoder was made. Recognition and rejection of the noisy signals could be made, following the slicer amplifier and demodulator circuit, by integrating the signal at this point. Integration provides a measure of the energy in the signal, and since the energy in any code waveform is less than the energy of a code waveform plus noise, this fact may be used to discriminate between a code signal with a small amount of noise and a code signal with a great deal of noise. Such a circuit was designed and incorporated into a decoder. The period of integration was 100 milliseconds or approximately the period of one command word.

A threshold device sensed the output of the integrating network and provided a signal if the integrated value exceeded a preset level. This signal was provided as an additional input to the squelch circuit so that now either of two events could squelch the decoders: the absence of signals in the subcarrier band, and the presence of too much energy in the subcarrier band (as would correspond to a signal distorted greatly by noise).

The squelch circuit was changed so that this signal no longer was used to turn on and off the regulated supply to the counters. Instead, the squelch action was applied to the output of the Schmitt trigger circuit.

This modified decoder was then used in a test which had produced spurious commands with the original decoder. This modified decoder proved to be free of spurious commands. It was recommended that these modifications be incorporated in all future Relay decoders.

While this modification proved to be quite effective, testing was continued to see if any weak links still existed which might cause problems in the operational Relay system. Extensive laboratory tests revealed one very restrictive set of circumstances which would result in spurious commands. When commanding at the threshold of the command system, i.e., at that RF level which was barely adequate to effect a command, spurious commands at threshold often follows very closely. The frequency of spurious commands at threshold follows very closely the value predicted by Equation (5.5) for the

signal-to-noise ratio expected at threshold. The value of signal-to-noise at threshold may be shown to be

$$a = \frac{A}{\Psi_o^{1/2}}$$

A = Zero to peak amplitude of the signal at threshold
$\Psi_o^{1/2}$ = RMS value of the noise at threshold
R_o = RMS value of the receiver output

$A_o = 1$ volt RMS,
$A = 0.7$ volts at threshold

$$\frac{A^2}{2} + \Psi_o = R_o^2$$

$$\Psi_o = 0.75 \frac{A^2}{\Psi_o} = a^2$$

$$= 0.66 \text{ or } S/N \mid \text{db} = -1.75 \text{ db}$$

Since the filter provides 13 db improvement, the S/N after the bandpass filter is 11.25 db. This corresponds to a probability of spurious command (from Figure 5–7) of 1×10^{-3}. The obvious solution to the greater susceptibility of the decoder to spurious signals at threshold is to assure that commanding is done well in excess of threshold.

CONCLUSIONS AND GENERAL REMARKS

The preceding analyses and discussion centered around a specific example of a satellite command system. The following discussion is included to broaden the scope of this thesis, since spurious signals in any satellite command system create problems for the design engineer which should not be ignored. Usually, when a command system is designed, its operation is successful only within the framework established by the system designer. Theoretical performance calculations are only valid within this framework, and too often real situations are ignored or forgotten in establishing the framework. The result is in the emergence of a system in which the actual performance differs considerably from the performance predicted by theory. The solution to this problem is not clear-cut. On one hand the system designer may attempt to expand the framework of his design in arriving at theoretical performance predictions. On the other hand the designer may require an operational procedure in commanding which assures that the system is operating within the framework of the original design. Both solutions require working knowledge of the problems encountered by various systems, such as Relay I, and it is felt that some of the problems discussed here are common to all satellite programs. It is unfortunate that little documentation is available on systems other than Relay, and this paper provides the only documentation available on that program.

The fundamental concept in the analysis of the orbiting Relay I system was the realization that interfering signals had a profound effect on operation of the satellite. These interfering signals should be considered as a basic problem which any command system will encounter, i.e., they should be included within the framework of the system design, and necessary precautions taken to minimize their effect on the system. It is common practice today to estimate the performance of a system with the aid of a mathematical model in which interference is neglected and gaussian noise is the only variable against which system performance is measured. The value of analyses such as these lies in the mathematical convenience of the gaussian model since results are often obtained in closed form. These analyses also provide expressions with which a comparative analysis of different systems may be made. It is here that their value ends, however, since the gaussian noise interference would actually be only a second order effect in the presence of intense interference.

There are two basic effects which result from the presence of interfering signals. The first effect is the so-called capture effect. The interfering signal is thus stronger than the proper command signal and the command message is not received by the satellite. The second effect is the concentration of the interfering signal spectrum in a band much narrower than the video bandwidth of the command receiver. This effect results in

signal-to-noise ratios much lower than expected when bandwidth reduction techniques are used to provide signal-to-noise improvement in the system. The lower signal-to-noise ratios obtained result in system performance which is much worse than the performance predicted by theory.

The solution to this system designer's dilemma lies in the acknowledgement that spurious signals are indeed a problem, and then attacking the problem from several angles which will be discussed below. In general, however, it may be stated that any system design should be considered incomplete unless major consideration is given to the effect of spurious signals. This may be done in several ways and a discussion of each technique follows.

The Inclusion of Spurious Signals in the Performance Analysis

Needless to say, this would be a valuable tool in estimating any system's performance were it not for the fact that the mathematical complexity which occurs may obscure the desired results. This has been encountered in the development of expressions for error probability as functions of the signal-to-noise ratio. This is so because in practice there are no systems whose probability of error is a function of the signal-to-noise ratio alone. Another important factor in any error analysis is the effect of the receiver AGC on the output signal-to-noise ratio. This is especially important when the effect of interfering signals is considered. A second factor would be the nature of the interfering signals, i.e., an analysis which considered white noise interference would produce results which may differ considerably from the results obtained with an analysis which considered CW-type interference.

Generally speaking, it is extremely difficult to include interfering signals in any mathematical model of a command system, and only that type of interference which would seriously degrade the performance is worth considering at all.

Recently some systems have evolved which tend to decrease the effect of interfering signals. These systems employ spectrum spreading such as would be obtained with modulation index FM or large modulation bandwidths as would be obtained with the so-called random-access, discrete-address, class of systems. Systems such as these have been proposed for various secure communications networks. They unfortunately require a large portion of the spectrum and corresponding increases in equipment complexity. Systems such as these may be more immune to interference but the cost in terms of bandwidth, weight, and circuit complexity makes them unfeasible for command control systems.

Secure Command Systems Through Increased Complexity in Operational Procedures

This technique is being employed today in several satellite command systems, and results indicate a practical solution to the problem of spurious commands. Basically there are two procedures employed.

One procedure involves transmission of the command, decoding the command in the satellite, tranmission of the command verification from satellite to earth, and transmission of a command-execute signal to the satellite. Such a technique requires a two-way communication but this usually is not a problem since such verification may be easily provided through the telemetry link.

The second procedure requires transmission of the command a second time and a bit-for-bit comparison is made in the satellite. Naturally, this type applies only to digital command systems.

The techniques described here practically eliminate spurious commands, although they certainly don't solve the problem of intense interference capturing the command system. The only solution to that problem is to provide command signal levels at the satellite well in excess of the calculated system threshold.

Command System Squelching with Improper Signal Recognition

This, essentially, is the technique employed in the modification program performed on the decoders for use in the Relay II program. This technique examined the command signal for characteristics to distinguish the command signal from a spurious signal in the receiver. In the Relay system, the integrated command signal level was less than the integrated signal of random noise, voice, or any waveform whose duty cycle in a given period was 100 percent. As described earlier, this integrated signal level was passed through a threshold device and the output used to squelch or unsquelch the decoder, depending on whether the proper command signal or a spurious signal was present. An identical technique could be used in almost any digital command system. Results from the operation of the Relay II satellite indicate proper command system performance, i.e., no spurious commands since the launch, and the problem of spurious commands occurring spontaneously has been virtually eliminated.

The three techniques described above should be considered practical answers to the problem of spurious signals in satellite command control systems. Radio frequency interference has always been a practical problem in communication systems and the elimination of the problem is impossible unless systems are designed with RFI in mind. This paper has concerned itself with interference in satellite command systems because so little information is available for review by systems designers. There is some feeling today that spurious commands which occur in satellite programs should not be publicized as they might reflect design deficiencies and prove to be a source of embarrassment. Such a philosophy not only is unwarranted but also contributes to the designer's dilemma. The designer is left to learn by bitter experience or word-of-mouth of the problems encountered by others in this field.

AUTHOR. *This chapter was written by* J. C. BLAIR *of the Radio Corporation of America, Princeton, New Jersey, U.S.A. under contract NAS 5–1272 with NASA/Goddard Space Flight Center.*

N66-10244

Chapter 6

The Energetic Particle Environment of Relay I

10244

Two semiconductor p-n junction particle detectors have been supplied by Bell Telephone Laboratories for the Relay I payload in order to evaluate portions of the energetic particle environment encountered by the spacecraft and to add to the over-all understanding of the trapped radiation belts. One of these detectors measures electrons with energies above approximately 1 Mev, and the other measures protons in several energy ranges with principle sensitivity in the 2.5 to 8 Mev region. Analysis of the first seven months of data shows the electron measurements to be in good agreement with those made on Explorer XV, and to be characterized by a stable high intensity inner belt with a maximum on a magnetic field line with $L \approx 1.3$ earth radii, a relatively unstable outer belt with a maximum on a magnetic field line approximately 4.5 earth radii, and a deep minimum between 2 and 3.5 earth radii. The flux of low energy protons reaches a single maximum at an equatorial value of L of about 1.9 earth radii for protons of about 5 Mev and 2.1 earth radii for protons of about 2.5 Mev. It is these low energy protons with their extremely high damage rate per particle in semiconductor materials that are responsible for most of the damage sustained in radiation damage experiments with unshielded solar cells on Relay I. The observed maxima in the damage rate coincide with periods during which the satellite is spending a large amount of time in or near the maximum in the proton distribution.

INTRODUCTION

The electrons and protons distributed in the Van Allen belts present a number of unresolved geophysical questions concerning their origin and their interaction with the fluctuating magnetic field of the earth and the electromagnetic and hydomagnetic waves which propagate in the trapped particle space. These particles also present a variety of technological problems since they constitute a radiation environment which is damaging to electronic components in satellites. The radiation experiments on Relay I were designed to help answer both the scientific and technological questions. This report describes the parts of the radiation experiment provided by Bell Telephone Laboratories and discusses some of the results that have been obtained from analysis of the first seven months of data. It concludes with consideration of the radiation damage effects that the environment can be expected to produce.

DESCRIPTION OF THE EXPERIMENTS

The Particle Detectors

The experiments include two detectors which are designed to measure electrons and low energy protons throughout the inner Van Allen belt and a part of the outer belt.

Both of the detectors are phosphorous diffused silicon p–n junction diodes. A cross section view of the detector construction is shown in Figure 6–1. The active device is

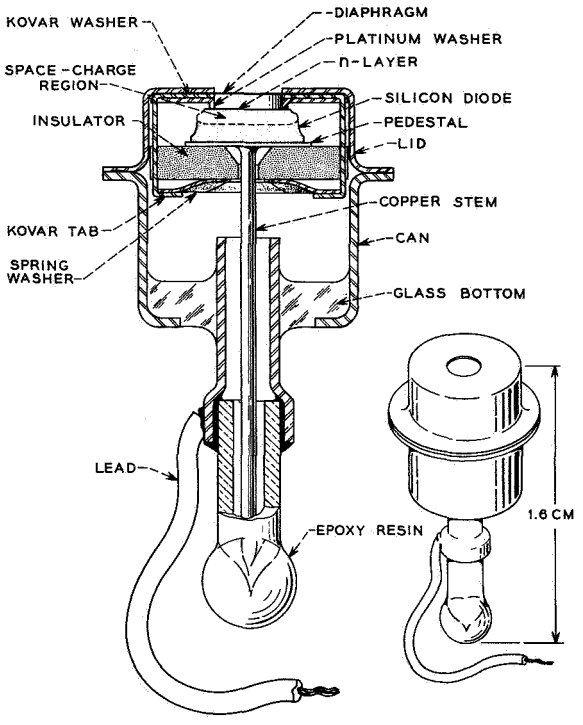


FIGURE 6–1.—Cutaway view of the particle detector.

encapsulated in a transistor-like can to provide high reliability under varying ambient atmospheric conditions. The entrance aperture in the lid of the can is 2 millimeters in diameter. The vacuum tight encapsulation is completed over this aperture with a thin Kovar diaphragm of approximately 6.5 mg/cm^2 surface density. This packaging has provided long term stability to the device characteristics, which are extremely sensitive to changes in the chemistry at the surface of the device.

The diode is operated under reverse bias as a small solid state ionization chamber. Figure 6–2 shows schematically its mode of operation. There is a space charge region or depletion layer adjacent to the extremely thin (approximately 4 microns) heavily doped phosphorous diffused surface layer.

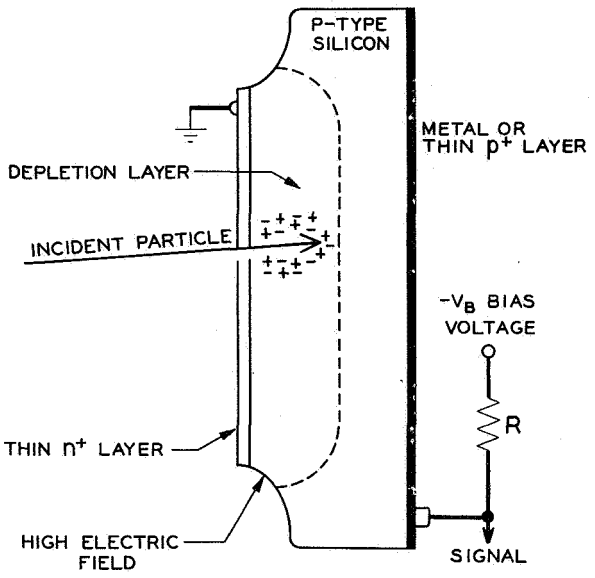


FIGURE 6–2.—Schematic of detector operation.

The thickness of the space charge region depends upon the reverse bias applied to the diode, and at 120 volts, the maximum used in the experiments, is about .3 to .4 millimeters. This region thus contains an electric field of several hundred volts per centimeter. An incident charged particle creates holes and electrons as it passes into or through this region, in a number which is proportional to the energy that the particle loses in its passage. These electrical carriers are swept across the space charge region by the electric field and constitute a current in the output circuit. The integral of this current, the total charge in a pulse produced by a single particle, is then proportional to the energy lost in the space charge region by the incident particle. By pulse height analysis of the charge pulses it is possible to distinguish particles of different energy. Because the penetration properties of electrons and protons are very different at the same energy it is possible to distinguish these from one another in many cases.

The silicon diodes are capable of counting at high rates, the collection time for holes and electrons being the order of 0.1 μ sec. The speed of the diodes combined with their

small size makes it possible to carry out experiments on relatively low energy particles with their very high fluxes in the Van Allen belt.

The Proton Detector (E), Protons > 2.5 Mev

Figure 6–3 shows a cross section of the proton detector mount containing one of the encapsulated devices described above. Particles reach the device through an entrance cone of 25 degrees half angle and through an aperture 2 millimeters in diameter, matching the entrance aperture of the detector encapsulation. The geometrical factor of the detector is 1.9×10^{-2} cm² steradians. Outside the acceptance cone the shielding of the detector is sufficiently heavy to exclude protons of <80 Mev and electrons of <10 Mev. There is a magnet surrounding the entrance cone which partially excludes electrons with energies of 300 kev and excludes lower energy electrons with increasing efficiency. At the time the detector was designed it was thought there might be a sufficiently high flux of such particles in space that pileup of small pulses might be confused with protons. Although the electron flux is very high in the peak of the inner Van Allen belt, particularly since the high altitude explosion of July 1962, there is no direct evidence for an immense flux of electrons of about 100 kev energy.

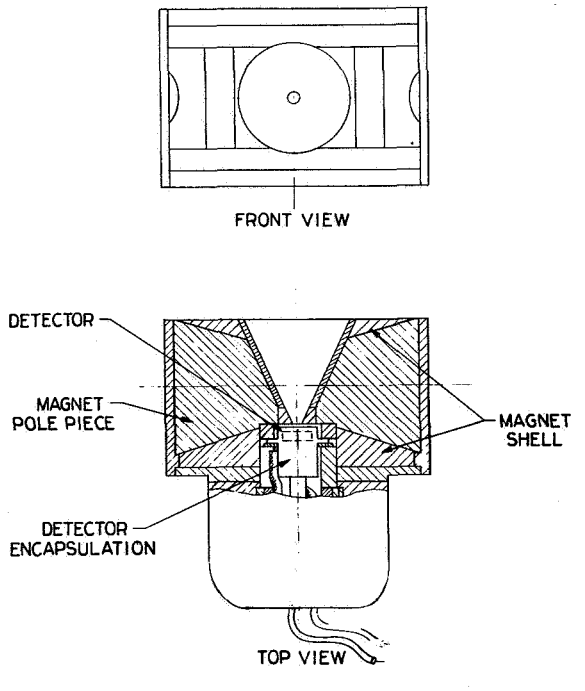


FIGURE 6–3.—Cross-section of the E detector mount.

The output pulse response of the proton detector to protons of different energies is shown in Figure 6–4. The pulse size is the

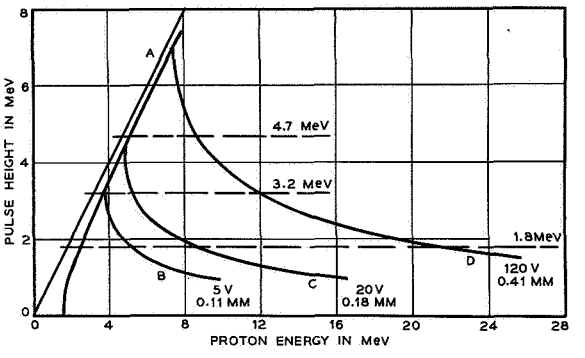


FIGURE 6–4.—Pulse response of detector E for protons at three bias levels.

charge collected in a single pulse indicated on an energy scale corresponding to 3.6 ev for a hole-electron pair. Line A of the figure is a limiting line for which the output pulse is just equal to the total proton energy. Curves B, C, and D have been obtained from measurements of the detector under three different conditions of bias using protons of up to 17 Mev from the Princeton cyclotron. Such measurements permit determination of the active thickness of the device as shown on the curves. The active thickness is actually a little greater than the space charge thickness because electrons created just beyond the space charge region can diffuse to the region and be swept up by the field. For this reason the active thickness does not quite increase as the square root of the bias. From a knowledge of this thickness the response can be computed at higher energies than those for which it has been measured and at energies lower than 3 Mev where the energy of the cyclotron protons, degraded by absorbers, is poorly known.

The response at a single bias such as curve D is double valued in proton energy because higher energy particles pass through the active thickness of the detector and leave less energy than lower energy particles whose range is nearly equal to this thickness. Using differential pulse height analysis between the levels indicated by dashed lines in Figure 6–4, observed pulses might be produced by protons in either a low or a high range of energies. By changing the detector bias, however, the double valued energy bands shift and the ambiguity can be removed. These bands are illustrated in Figure 6–5.

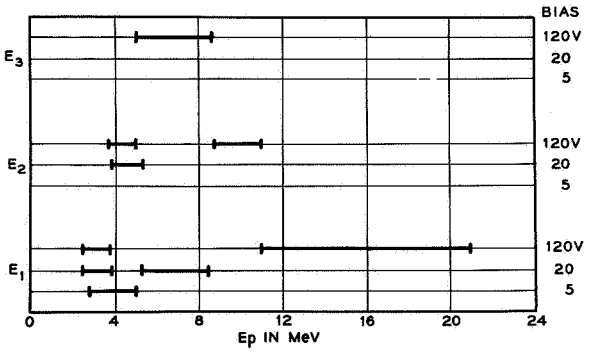


FIGURE 6–5.—Energy bands of detector E response at three biases.

With three detector biases and three discriminator levels a total of nine observations can be made. Curves B, C and D of Figure 6–4 at energies below their peaks differ from Curve A because of the 6.5 mg/cm² Kovar absorber and the 1 mg/cm² phosphorous-rich n-layer at the front of the detector. In addition there is a small loss in charge due to the finite rise time of the detector pulses and the pulse shaping of the amplifier and there are small losses due to incomplete collection of the hole-electron pairs produced by protons because of trapping of the mobile carriers in transit across the space charge region.

The lowest discriminator level of the detector is set at 1.8 Mev. The probability that an electron of this or higher energy will give a 1.8 Mev pulse is less than one in 10^3 because of the long range of such energetic electrons compared with the .41 millimeter space charge thickness of the detector even at 110 volts bias. Electrons of about .5 Mev, however, are stopped with relatively high probability so that electron pulses at multiplicities of four or more cannot be ignored.

The Electron Detector (F), Electrons > 1 Mev

Figure 6–6 shows a cross section of the electron detector mount. Electrons are admitted through a cone of 10° half angle with an aperture 2 millimeters in diameter at its apex. The effective geometrical factor of the

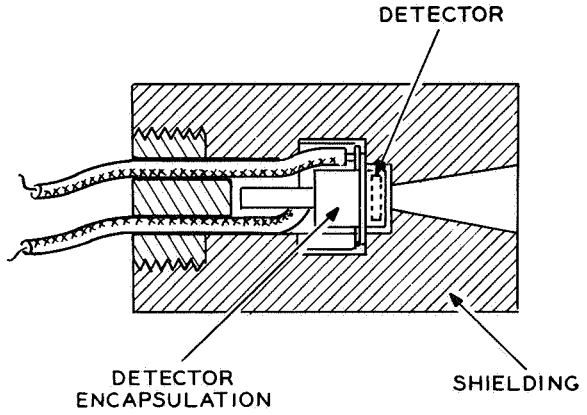


FIGURE 6–6.—Cross-section of the F detector mount.

detector is 1.5×10^{-3} cm² steradians. Outside of the acceptance cone protons of <60 Mev and electrons <6 Mev are effectively excluded. Near the cone apex is an absorber of 425 mg/cm² aluminum. This absorber was added to the original experiment after Injun I, Telstar I, and Explorer XV had measured very high densities of high energy electrons following the nuclear explosions of the summer and fall of 1962. Many fewer particles and a much less energetic spectrum had been expected before that time. The absorber pushes the energy response of the detector upward and allows direct observation to be made of electrons having much more damaging consequences for satellite components. Because of the nature of the energy loss processes of electrons in solids, however, the absorbers broaden an initial spectrum and

as a result pulse height analysis of the detector output does not permit sharp definition of the incident energy. This is apparent in Figure 6–7 which shows the efficiency for

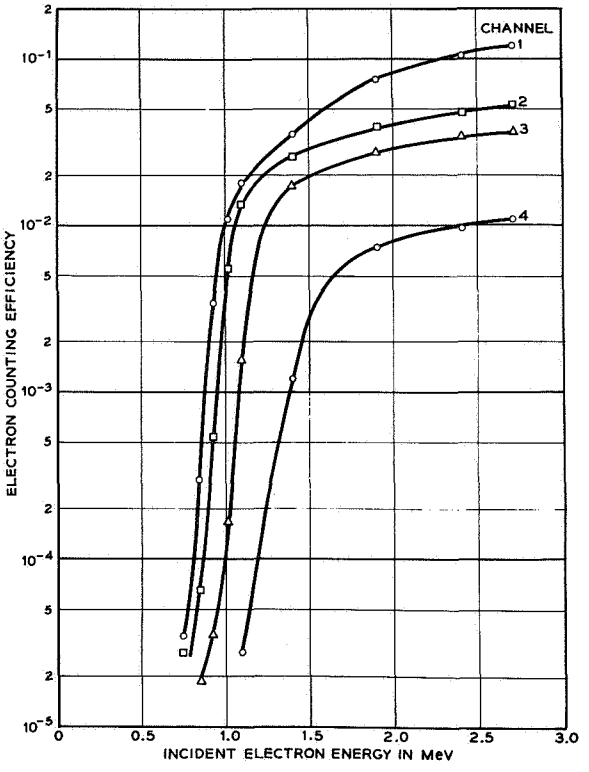


FIGURE 6–7.—Efficiency of detector F for electrons.

electron counting into four pulse height channels in response to monoenergetic electrons up to 2.7 Mev. Pulse height channels 1 to 4 correspond respectively to .2 to .35, .35 to .55, .55 to .75 and .75 to 1.0 Mev pulses in the detector. At the highest energy in the figure most of the electrons penetrate the absorber and the difference in counting efficiency is due primarily to the relative probability with which a high energy electron deposits a small or major part of its energy in the space charge region of the detector.

The Detector Circuitry

The Block Diagram

A block diagram of the detectors and their associated circuits is shown in Figure 6–8.

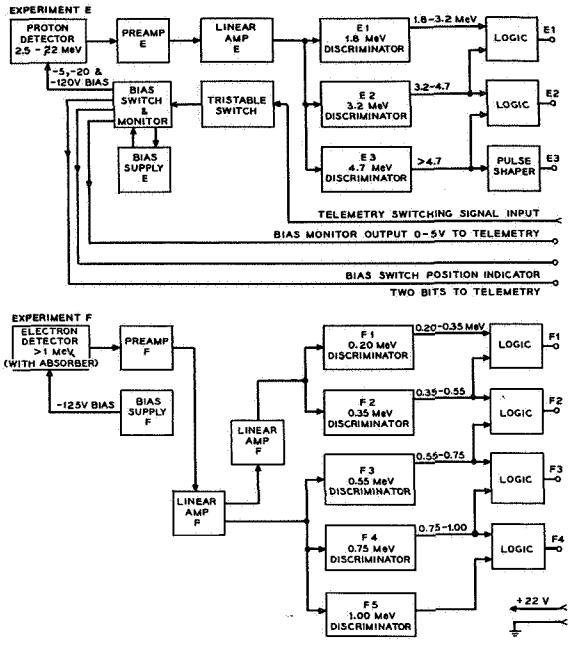


FIGURE 6–8.—Block diagram of Relay experiments E and F.

Each of the detectors delivers pulses to a low noise charge sensitive preamplifier which gives an output voltage proportional to the charge produced by a particle in the active thickness of the detector. A linear amplifier follows the preamplifier. In the electron experiment, designated F in the complement of Relay radiation experiments, a second amplifier provides extra gain for the most sensitive electron channels. An array of discriminators is supplied from each linear amplifier. These in turn control logic units whose function it is to determine the highest discriminator that has fired in response to a single input pulse. In the electron experiment five discriminators determine the edges of four differential pulse height channels. A high degree of selectivity is provided against protons in this way since protons can give much larger pulses than electrons and only a very narrow range of proton energies can give the small pulses that the discriminator-logic chain of experiment F will accept. In the proton experiment, experiment E, three discriminators determine the edges of two differential channels and one integral chan-

nel. The outputs of the four electron channels and the three proton channels are fed to the State University of Iowa/University of California, SUI/UCAL, commutator box where they are multiplexed into storage registers in the telemetry.

The remainder of the block diagram indicates the detector bias supplies and the various switching and monitoring lines. The proton detector bias supply provides 120, 20, and 5 volts to the detector in sequence. The electron detector is fixed at a single bias of 125 volts. The proton detector supply is monitored by the telemetry.

Linear Signal Shaping

To eliminate changes in the effective discriminator level from base line shifts due to changes in pulse repetition rate, the pulses are double RC differentiated. The signal as it appears at the linear amplifier output is shown in Figure 6–9. The peak of the pulse

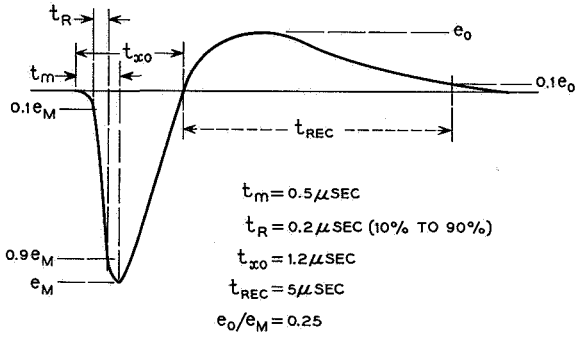


FIGURE 6–9.—Linear amplifier output pulse shape.

is reached approximately 0.5 μ sec after its start, the 10 to 90 percent rise time being 0.2 μ sec. The crossover time is 1.2 μ sec and the over-all recovery of the double clipped pulse is approximately 6 μ sec.

Discriminators

The discriminator circuit is based on an emitter-coupled monostable multivibrator to take advantage of the inherent compensation of base-emitter voltage change with temperature. All but one other voltage drop that would affect threshold sensitivity are eliminated. That one adjusts the discriminator threshold and is derived from a zero temperature coefficient reference element. The measured discriminator threshold is stable within $\pm$ 1 percent over the range from $-50°$ to $+50°$C.

The Logic Units

As indicated in the previous section, logic units make the decision as to which is the highest of several discriminators that have fired from a single input pulse. A typical arrangement is shown schematically in Figure 6–10. Each discriminator's output is

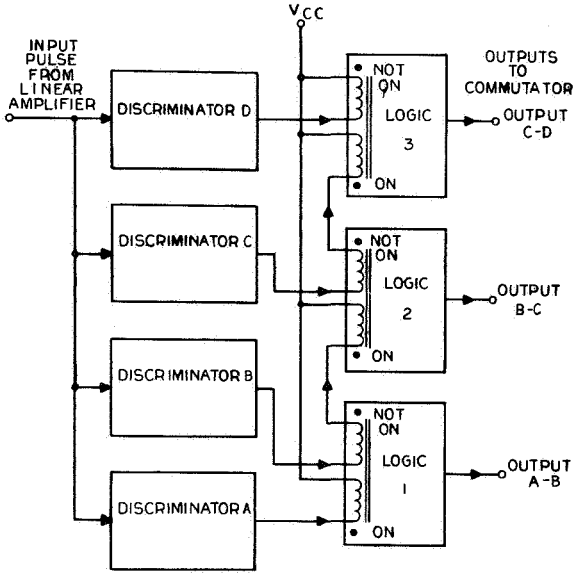


FIGURE 6–10.—Diagram of the operation of the logic units.

trying to turn a logic unit on while at the same time keeping the one below it from turning on. This is accomplished by making use of opposing input windings on the logic transformer. Two additional windings on this transformer (not shown in Figure 6–10) are a part of a modified blocking oscillator that produces the output pulse. The total time from input pulse to complete recovery of the blocking oscillator is about 10 μ sec.

Packaging

The detectors and their associated circuitry shown in block diagram in Figure 6–8 are packaged together in a single box. The circuit blocks are constructed in a conventional manner on circuit boards with swaged feed-through terminals providing component and wiring tie points on both sides of the boards. In the final assembly, circuit boards are stacked as close together as components will permit, with strips interlocking their corners to form a rigid "egg crate" type of structure. The detectors are rigidly mounted in the front of the box, behind holes in the front face. The proton and electron experiments occupy separate compartments within the box for electrical isolation. As a final operation, the box is filled with polyurethane foam for vibration damping. The whole box assembly is mounted to the spacecraft frame with the detector axes perpendicular to the spin axis of the satellite. The detectors look out through a clearance hole in one of the honeycomb panels comprising the satellite skin.

The Sequence of Measurements

There are seven storage registers in the telemetry into which various outputs of the BTL and SUI/UCAL experiments are fed on a time-sharing basis. The multiplexing is carried out in the SUI/UCAL commutator box, Figure 6–11. In a scheme proposed by McIlwain, rather than feeding pulses from a detector to a register continually for several seconds while the satellite spins, the detector pulses are interrupted by a gate controlled by a magnetometer. Pulses are stored only while the axis of the detector is pointing within approximately $\pm 10°$ of the normal to the local magnetic field. The angular spread is measured in the plane of rotation

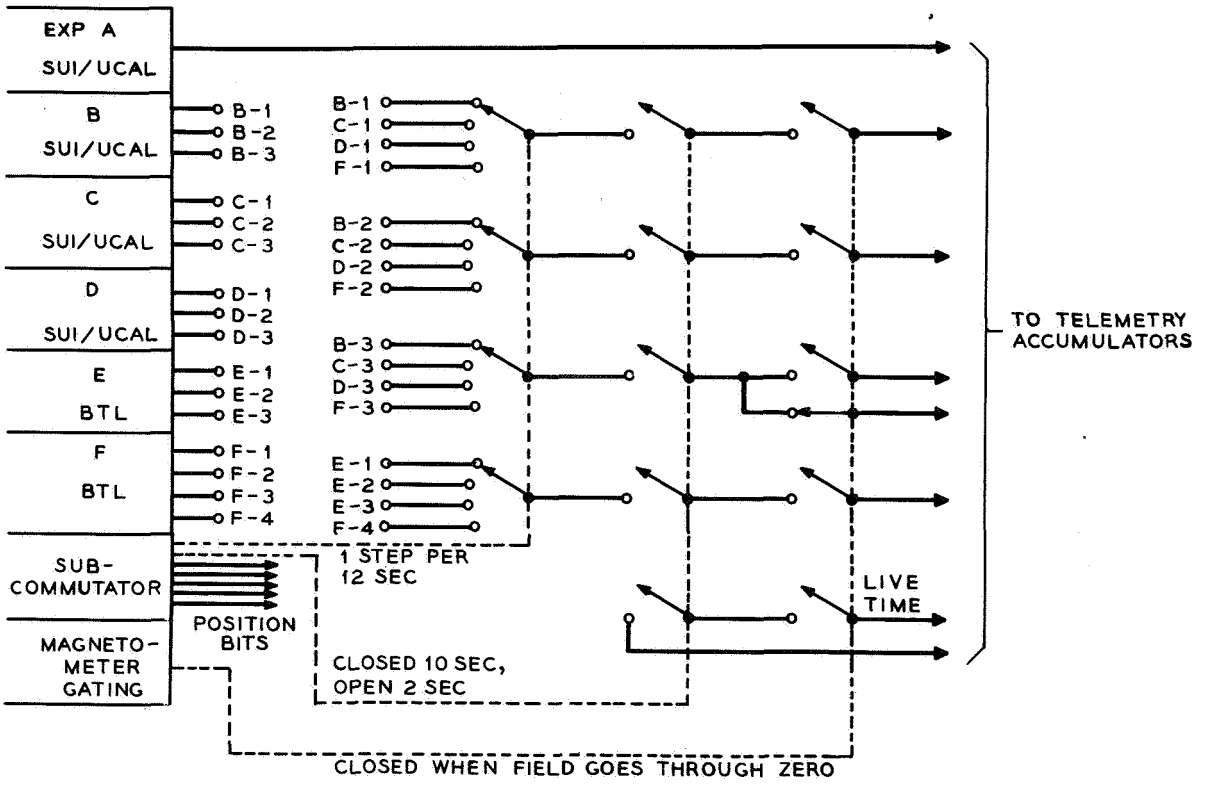


FIGURE 6–11.—Commutation of the Relay radiation experiments by D. Enemark, SUI.

of the detectors, Figure 6–12. In this way an approximate measurement of directional intensity of the particle flux normal to the magnetic field line is obtained. This measurement depends slightly on the angle γ between the spin axis of the satellite and the

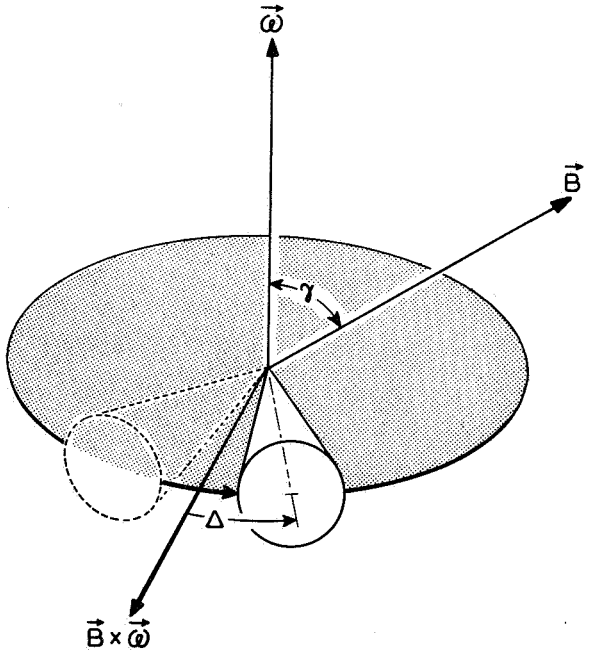


FIGURE 6–12.—Angular orientation of a gated detector. Measurements are made during rotation through $\pm \Delta$.

magnetic field direction because of differences in the relative particle directions that are seen in a $\pm$ 10° interval measured in the rotational plane of the satellite.

The time sequence of the Bell Laboratories measurements is as follows. During 12 seconds of a 48-second period, each of the four electron channels occupies a single telemetry register, accumulating pulses in that register for an elapsed time of 10 seconds with approximately a 10 percent duty cycle provided by the magnetometer gating. The register is read each second and finally with no pulses flowing into the register it is read twice redundantly at one second intervals for the final count. During this same twelve second time, one of the four electron channels (F_3) feeds into a fifth register during the 90 percent of the time when the magnetometer gate is blocking the flow of pulses to the first four. The same final redundant readout is provided in this case. The three proton channels at one detector bias occupy a single register for three successive 12 second intervals in the 48 second period. Each 48 seconds the bias is changed during the remaining 12 second interval, so that a complete sequence of proton measurements occurs every 144 seconds. The magnetometer gating and register readout are the same as for the electron channels.

DATA PROCESSING

The Coordinate System

The energetic particles that make up the Van Allen belts are trapped in the magnetic field of the earth and have trajectories which are controlled by the distorted dipole shape of that field. It is essential to organize the information concerning the trapped particles in a coordinate system that takes account of the properties of the field which are constants of the motions of the particles. Such a system, devised by McIlwain and now quite generally adopted, is illustrated in Figure 6–13. A charged particle can be identified in terms of the magnetic field line L around which it spirals and the magnetic field intensity B at which the pitch of the spiral reaches 90 degrees and the particle mirrors (labeled in Figure 6–13 as B_M), McIlwain has essentially mapped the irregular magnetic field of the earth onto a dipole magnetic field which has the same first moment. In this representation a field line is labeled by L when it crosses the magnetic equator at a distance L from the center of the dipole. In the dipole field it is often convenient to utilize another pair of coordinates R and λ which are dipole radial distance and dipole latitude, simply related to B and L. In this B, L, $-R$, λ space the earth is not a sphere and the atmosphere does not have a uniform density at a fixed R, a complication which has to be dealt with in considering atmospheric loss of parti-

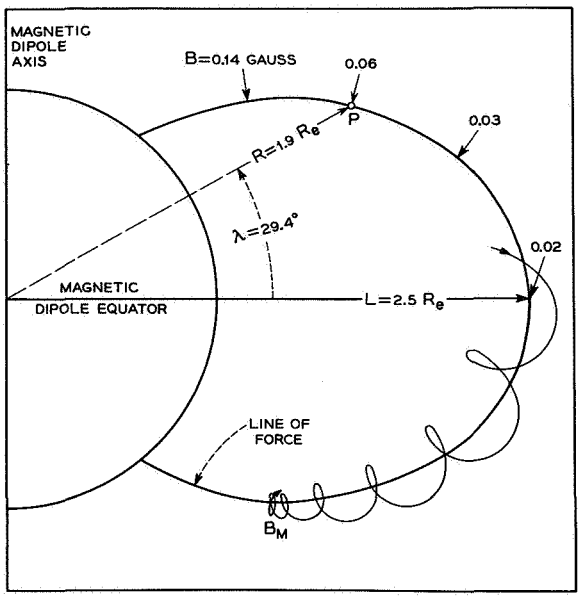


FIGURE 6–13.—The B, L–R, λ coordinate system.

cles, for example. However, in the B, L—R, λ space the motion of the energetic charged particles is directly described, and measurements made at different places in the geographic space about the earth can be properly associated. The symmetry of the dipole field allows the entire three-dimensional space to be collapsed into half a meridian plane, the coordinate of longitude having disappeared and north and south latitudes being identical. In the analysis of the Relay data this coordinate system has been used in a variety of different ways.

Orbit Plots

The region in which the satellite has acquired data on a particular pass or day is conveniently represented in a trace in B, L space, such as that shown in Figure 6–14. In this log-log plot the equator, $\lambda = 0$ is a

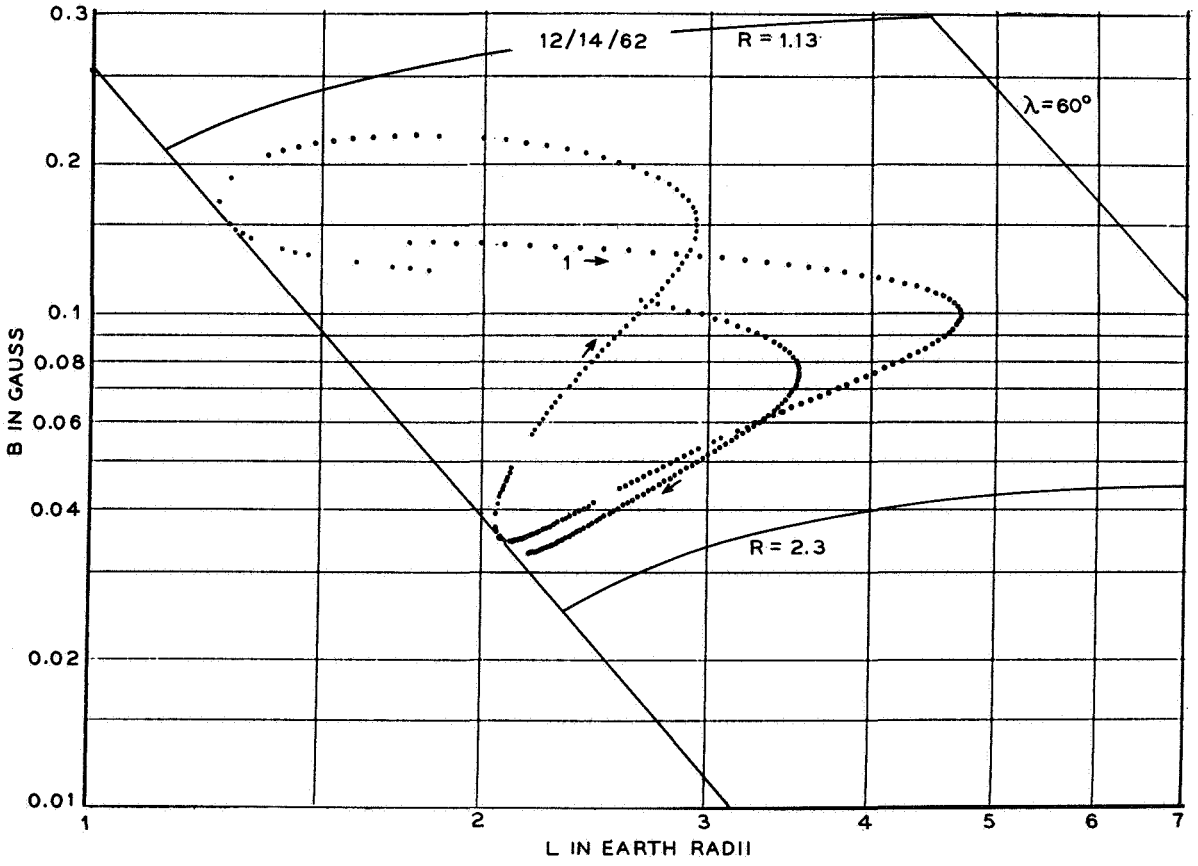


FIGURE 6–14.—A B, L plot of the points at which data were received on December 14, 1962.

straight line and all other dipole latitudes are straight lines parallel to it. Lines of constant dipole radial distance all have the same shape and join the equator by definition at $R = L$. The points in the figure are points at which data was acquired on December 14, 1962 immediately following the launch of Relay I. The arrow indicates the direction of satellite motion and the point spacing, except where there are obvious breaks in the line, are at 48 second intervals, corresponding to the time base on which the multiplexing of the data takes place. A crossing of the magnetic equator is a point at which the orbit touches the $\lambda = 0$ line in this collapsed coordinate space. The region to the left of $\lambda = 0$ is forbidden. The point spacing becomes very small as the satellite approaches apogee since most of its velocity is in geographic longitude, a coordinate degenerate to first order in the B, L space. As indicated in Figure 6–14, there were data during the first complete orbit and approximately half of the second orbit. The irregularity of the magnetic field shows up directly in the difference between these two orbits which geographically differ by approximately a 45 degree rotation of the earth under the satellite. The lines at $\lambda = 60$ degrees and $R = 1.13$ and 2.3 earth radii represent approximate extremes of the Relay orbit in the B, L space. During the period of precession of the latitude of apogee this space is essentially completely covered by the satellite. Figure 6–15 and 6–16 show quite different orbital traces for which data were obtained on January 27 and April 22. Apogee has precessed from —2 degrees on

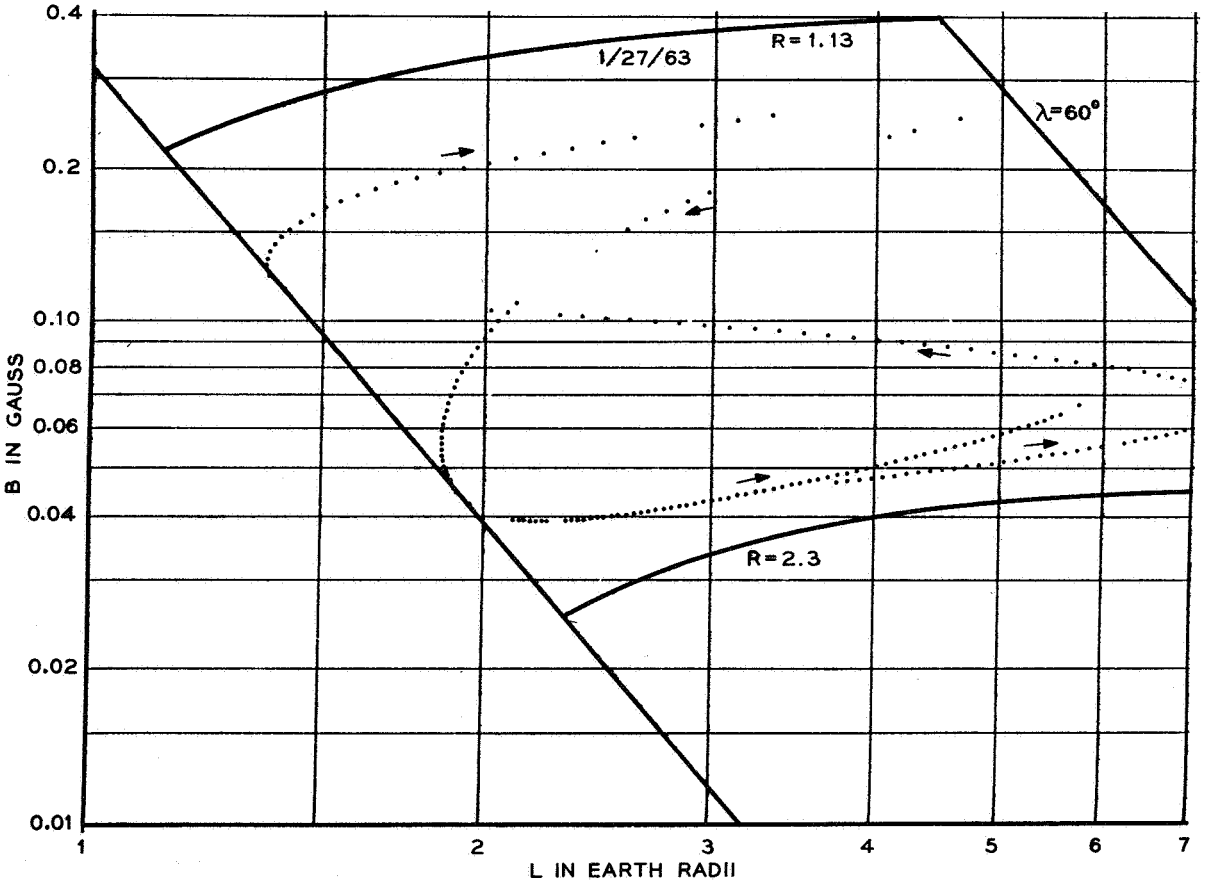


FIGURE 6–15.—A B, L plot of the points at which data were received on January 27, 1963.

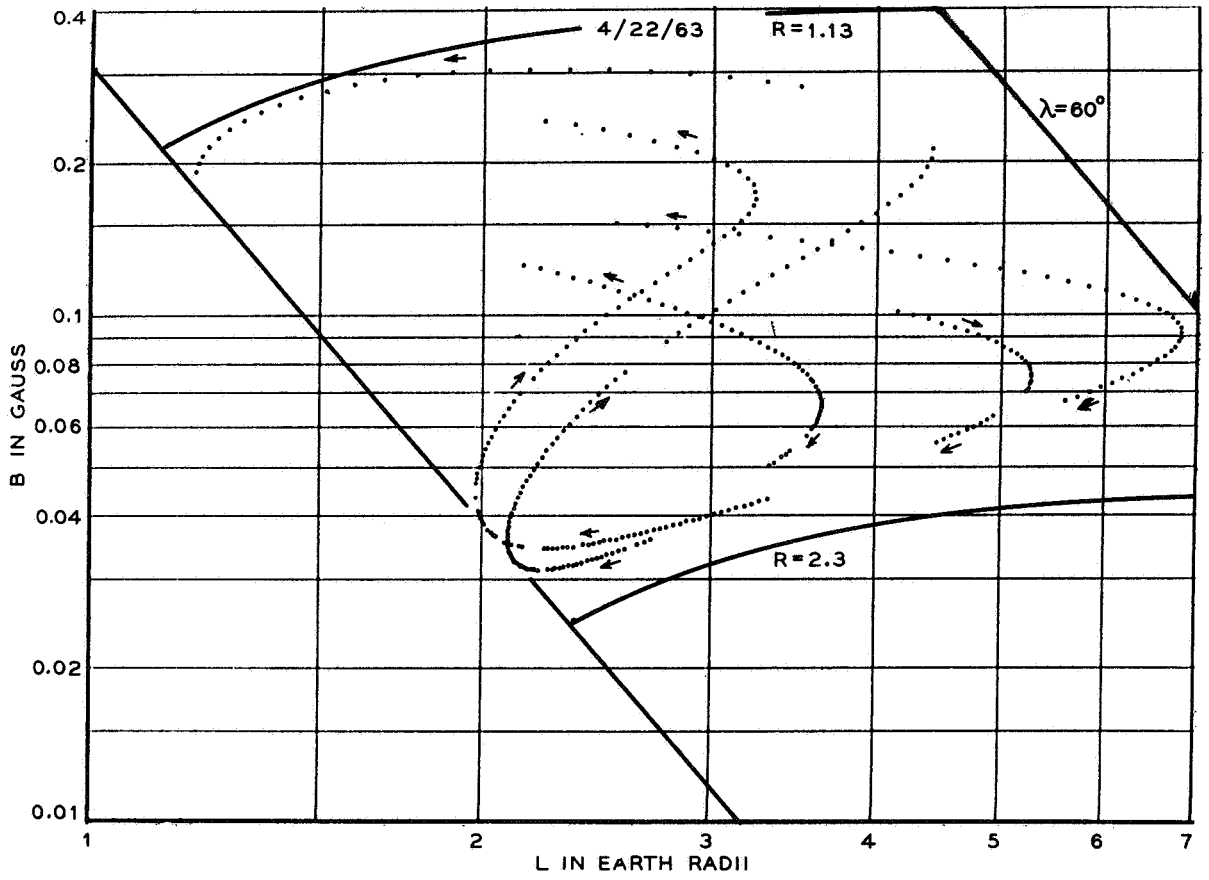


FIGURE 6–16.—A B, L plot of the points at which data were received on April 22, 1963.

December 14 to +35 degrees on January 27 and to +19 degrees on April 22. Only 5 percent of the data which have been taken from December 1962 through August 1963 exists at values of $L < 1.9$. The high energy electrons of the inner belt are strongly concentrated at L values between 1.2 and 1.7, so that a rather sketchy coverage of the inner belt has been made.

ϕ, L Plots

In association with the B, L plots of the previous section, it has been extremely convenient to produce plots of the flux (ϕ) in each of the detector output channels as a function of L. Figure 6–17 shows such a plot for the second orbit on December 14 (Figure 6–14) as the satellite moves toward $\lambda = 0$ at $L \approx 2.2$. The data are for the three

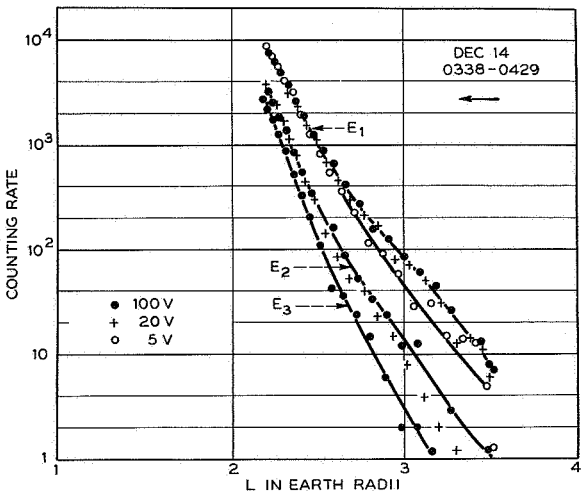


FIGURE 6–17.—ϕ, L plot of detector E on December 14, 1962.

proton detector channels (experiment E) at different detector biases. This figure will be discussed in more detail. The data reduction program which processes the data from the original data tape supplied by Goddard Space Flight Center provides checks on the consistency of the data during the consecutive readouts over the 10 second accumulation period and during the final pair of redundant readings of the accumulated total. In the process, it examines the possibility of overflow of the storage registers and makes appropriate corrections if necessary. The program also checks on the consistency of the time sequence of bias switching in the E detector and on the absolute bias level at each point.

Visual inspection of the results of the data reduction displayed in computer plots such as Figure 6–17 allows rapid evaluation of the quality of the result. These plots also provide a direct means for interpolating to obtain counting rates at specific values of L, or L coordinates for specific counting rates. At times when the satellite is moving through L rapidly, as in places where the points are far apart in Figure 6–14, interpolation is more difficult than in Figure 6–17 where the points are closely spaced.

In the region between $L = 3.5$ and $L = 2$ covered in Figure 6–17 the electron flux is very low. This is the region of the "slot" between the inner and outer electron belts. Several passes during July 1963 produced particularly nice illustrations of the divided electron belts. One of these is shown in Figure 6–18 for a pass on July 3. The data are for channels F_1 and F_4 for the inbound pass shown in the B, L orbit trace in Figure 6–19.

ϕ, B Plots

Because the data is sparse in many parts of B, L space, another procedure has been adopted to utilize all the data that exists in devising flux distributions. This involves collecting all the data in a particular small range of L over a period of as much as a month or even longer and carrying out a least-square fit to determine the time dependence and the B and L dependence of that data. The time and L dependence can then be removed and the data displayed as flux vs. B for a particular value of L, usually one of the limiting edges of the originally chosen L range. A typical result of this kind is shown in Figure 6–20 for electrons of channel F_4 for the L range between 1.5 and 1.6 for the month of July. The left-hand part of the figure shows the data as collected before carrying out the functional fit. The right-hand part of the figure shows the same data but now with all points functionally transferred to $L = 1.6$ at the beginning of the month. The principal reason for the scatter in the original display is the strong

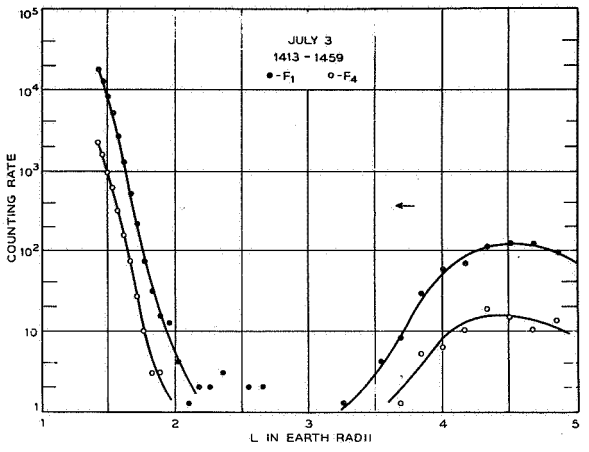


FIGURE 6–18.—ϕ, L plot of detector F on July 3, 1963.

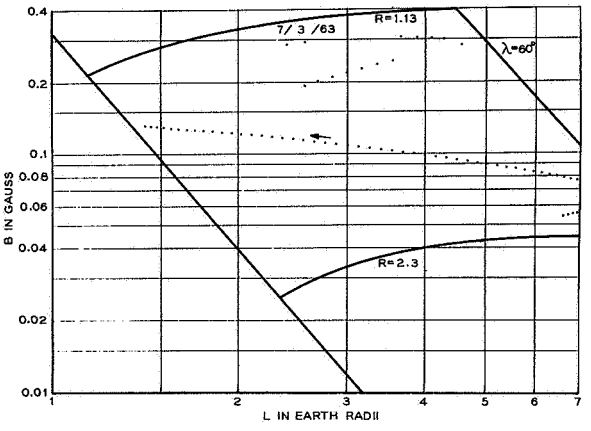


FIGURE 6–19.—B, L plot of data points, July 3, 1963.

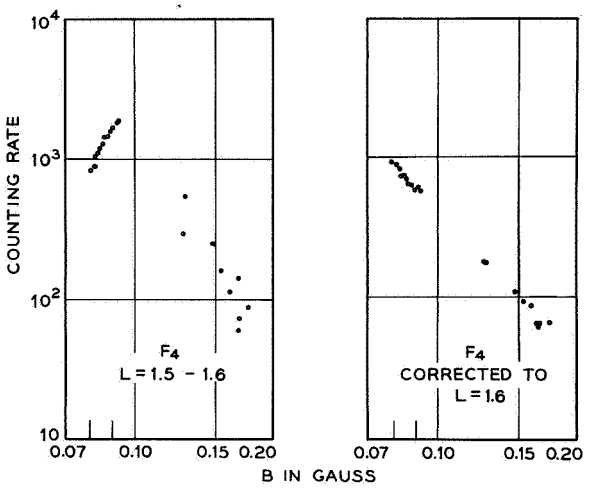


FIGURE 6–20.—ϕ, B plot with functional interpolation.

L dependence of the electron flux in this region of space. All of the points result from just five passes through part or all of the L range during July. The corrected points show no flux maximum except close to the equator which at $L = 1.6$ occurs at $B = .076$ gauss. The flux variation with B is well represented in this case by a simple power law; a straight line on this plot with slope of −3.5. This procedure for producing ϕ, B plots is a reliable one for small ranges of L. However, the variation of the ϕ, B slope with L is itself often substantial, and functionally fitting a wide L range must be done with care.

The Measured, Directional, and Omnidirectional Flux

As described previously, the counting rates that are measured are approximately those due to particles with velocities perpendicular to the local magnetic field, and thus particles that are mirroring at the B of the satellite. This is only approximately true because of the finite acceptance angle of a particle detector and because of the finite angle through which the detector rotates during the time of measurement. The maximum in ϕ vs. B usually occurs at the equator, as for example in Figure 6–19, and only occurs off the equator for a short time after some anomalous injection of new particles such as those added by a high altitude nuclear explosion. The normal condition leads to an angular distribution of particles at any B which is peaked at a particle pitch angle $\alpha = \pi/2$. That is, the maximum particle flux is perpendicular to the field line at all points along the field line. In this case the finite detector aperture and the finite rotation during measurement always produce a measured flux less than the flux perpendicular to the field line. The more sharply peaked the angular distribution of the particles is around $\alpha = \pi/2$, the larger is the reduction in measured flux, ϕ_m, compared with the flux at $\alpha = \pi/2$, $\phi(\pi/2) = \phi_\perp$.

The relationship between ϕ_m and $\phi_\perp$ has been computed for the two detectors of the BTL experiment and is shown in Figure 6–21. The angular distribution of the particles has been assumed to be $\sin^n\alpha$ where n takes values between 1 and 64. The abscissa in the figure is gamma, the angle between the spin axis of the satellite and the local magnetic field (Figure 6–12). As expected, for large values of n, $\phi_m/\phi_\perp$ decreases, and most severely for the larger detector aperture. The gamma dependence is quite small for $\beta_{1/2} = 25°$ (because the rotation during

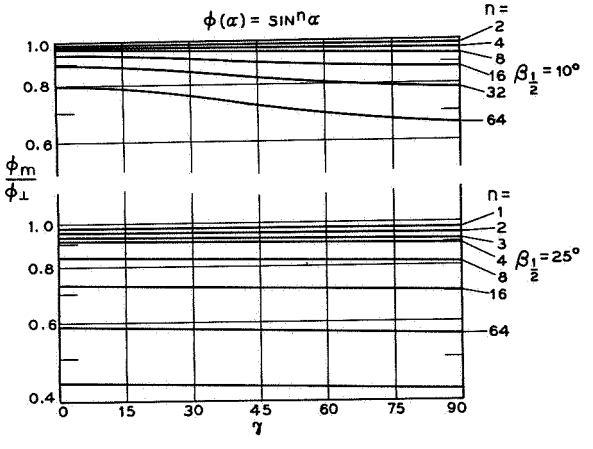


FIGURE 6–21.—The ratio $\phi_m/\phi_\perp$ for the two detector angles.

measurement is small compared to the detector angle) and only amounts to 20 percent between $\gamma = \pi/2$ and $\gamma = 0$ for $n = 64$, a very sharply peaked distribution.

The omnidirectional flux at a given B is related to $\phi_\perp$ by the integral

$$\phi_{\text{omni}}(B) = 2\pi B \int_B^{B_{\max}} \frac{\phi_1(B_1)\, dB_1}{B_1^2 \sqrt{1 - B/B_1}} \quad B_1 \geqq B \tag{6.1}$$

where the upper limit is the maximum field at which ϕ has a nonzero value. If $\phi_\perp$ is a power law in B_0/B, where B_0 is the equatorial value of B.

$$\phi_\perp(B) = A \left(\frac{B_0}{B}\right)^m$$

then

$$\phi_{\text{omni}}(B) = 2\pi \phi_\perp(B) \int_{B/B_{\max}}^1 \frac{y^m\, dy}{\sqrt{1-y}} \tag{6.2}$$

where the substitution $y = B/B_1$ has been made. As long as $B/B_{\max}$ is small, the omnidirectional flux will have the same B dependence as $\phi_\perp$. Assuming that the lower limit is zero, the integral is dependent on n, but independent of B. The assumption only appreciably affects ϕ_{omni} at low values of flux. Combining this integral with the correction factors of Figure 6–21 which gives the $\phi_\perp$ flux from ϕ_m, the measured flux, one can deduce the omnidirectional flux in terms of ϕ_m. The calculated relationship is shown in Figure 6–22 for the two detector angles, for the extremes in gamma, and as a function of n, where $\phi_\perp(B) \sim 1/B^{n/2}$ corresponding to the local directional flux $\phi(a, B) \sim \sin^n a$. In a uniform angular distribution of particles $n = 0$ and the ordinate of the figure equals 1, the measured directional flux being just $1/4\pi$ as large as the omnidirectional flux. For values of n from approximately 3 to 10 the measured flux needs to be multiplied by approximately 2π to obtain ϕ_{omni}. These corrections, or similar corrections devised from the integrals without the $\sin^n a$ assumption, can in principle be applied directly by the computer to the measured results to obtain an omnidirectional flux or to compute $\phi_\perp$. This step can be done rigorously if the measured flux is known over a sufficiently wide range of B. It can be done approximately if more limited measurements exist. The computer program for this transformation is not yet complete.

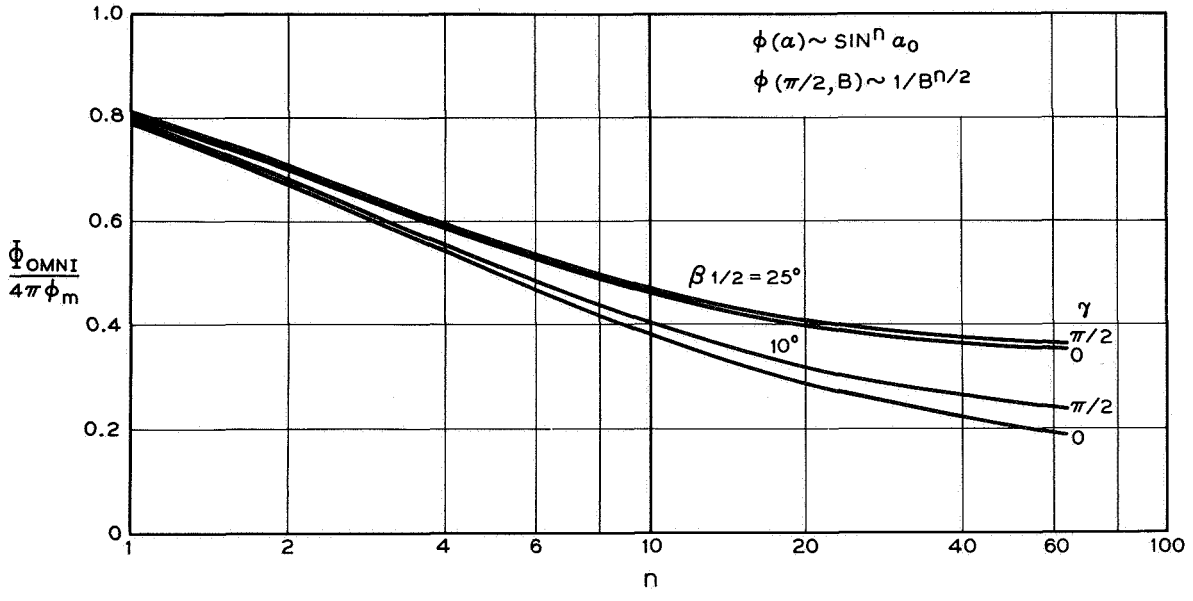


FIGURE 6–22.—The ratio $\phi_{\text{omni}}/4\pi\phi_m$ for the two detectors.

RESULTS

Protons

A number of observations concerning the proton spectrum can be made by inspection of curves such as those of Figure 6–17 in conjunction with the energy bands of detector response in Figure 6–5. First, there is very little difference between E_1 at 5, 20, and 120 volts bias, particularly at L values below 1.5. The same is true of E_2 between 20 and 120 volts. Since the higher energy segment of the E_1 response (Figure 6–5) is very strongly modified by bias, one concludes that protons below 4 Mev are dominating the the E_1 counting rate, and protons below 5 Mev are dominating the E_2 counting rate. Second, E_1 exceeds E_2 and E_2 exceeds E_3. This again argues for a spectrum heavily weighted at low energies because the size of the energy interval of measurement in E_3 at 120 volts exceeds the low energy interval in E_2 and E_1. Third, at the large values of L, E_2 and E_3 decrease more rapidly than E_1. Thus the spectrum is getting progressively richer in low energy protons. In spite of the fact that the low energy portion of the E_1 response is dominating, there is an increase in the E_1 counting rate with increasing bias in the region between $L = 2.7$ and 3.5. This can only be due to an increase in the efficiency of collection of hole-electron pairs produced by low energy protons in the increased electric field of the junction at higher biases. This emphasizes the importance of the lowest energy end of the sensitive energy region because of the increasing dominance of very low energy protons at larger L values. This effect is indicated in a slightly smaller low energy edge to E_1 at 20 and 120 than at 5 volts bias. A similar effect to a lesser extent is apparent in E_2 at 20 and 120 volts.

Flux maps of protons have been constructed by interpolation in the ϕ, L plots for December and January as discussed in another section. Two of these plots of ϕ_m for E_1 and E_3 are shown in Figures 6–23 and 6–24. In all cases in these contours the particle flux decreases with increasing B along any L line, consistent with the assumptions as described in the previous section. These plots can thus be corrected to $\phi_\perp$ using the results of Figure 6–21, with corrections which are at most 20 percent. There are no data points plotted for E_1 below $L = 1.4$ because electron pile-up dominates the protons in this region. This is clearly evident as a very rapid rise in the E_1 counting rate as the maximum of the inner belt electron distribution is approached. A similar effect does not occur for E_3. The contours consequently are much better determined at their low altitude equatorial crossing for E_3 than for E_1.

The maximum in intensity of the two proton groups occurs at different equatorial L values, the highest energy group (5 to 8.6 Mev) at about $L = 1.95$ and the lower (2.5 to 3.8 Mev) at about 2.07. This agrees with the general trend of the proton maximum for much lower and much higher energy particles. At L values >2.1 the low energy particles always dominate. At lower L values the opposite is true.

The data for E_1 starting in February and March show very significant changes from December. There is a drop in the E_1 5 volt counting rate which in April is as much as a factor of 6 in the region around $L = 2.2$. The drop in E_1 120 volts is only about a factor of 2 in the same time. The detector is suffering from radiation damage produced by low energy protons. The very large number of particles to which the detector was exposed in the energy range of E_1 and the very high damage rate per particle at these low energies makes E_1 the most susceptible to this damage effect. Hole-electron pairs are produced as before by incident particles. However, many of these mobile carriers are trapped at structural damage defects as they are being swept across the space charge region. Ultimately they complete their transit, but at a time much longer than the pulse shaping times of the detector circuits. Effectively the collected charge pulse is smaller and does not meet the discriminator requirements of channel E_1. The smaller effect in

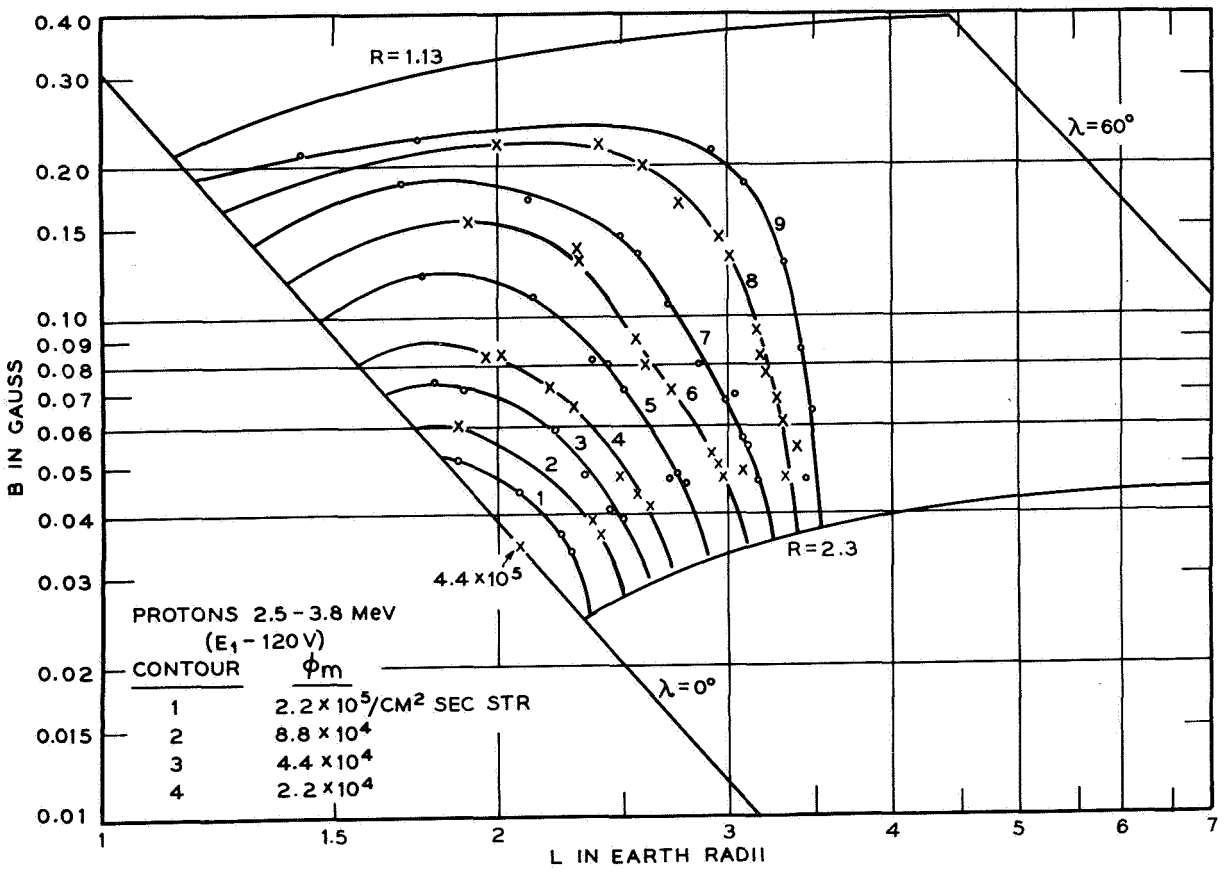


FIGURE 6–23.—*B*, *L* flux map for 2.5–3.8 Mev protons, December 1962 to January, 1963.

E_1 120 volts is due simply to the higher electric field which sweeps the carriers through the region of severe damage more rapidly and thus with less trapping loss. E_3 shows very little change over the seven months from December through July. The particles which it detects penetrate much more deeply into the detector and create hole-electron pairs out of the region of severe damage. Thus the collection loss suffered is much smaller.

A calculation is in progress to evaluate the details of the damage effect from the particle exposure of the detector, the energy dependence of damage in silicon, and the electric field distribution in the detector. Qualitatively the results are in agreement with this simple model of the process. It is unfortunate that the available data during December and January is too little to permit more detailed observations of the lowest energy protons before the detector damage was substantial. It is planned to acquire data from Relay II concurrently with that for Relay I. Hopefully, this will permit recalibration of the Relay I detectors and help provide an understanding of events during the intervening months.

Figure 6–25 is a flux map made by interpolation in data of June and July organized in ϕ, L and ϕ, B form. This map differs appreciably from that of Figure 6–24 made from December and January data, particularly at higher L values. There are apparently more particles at the later date. The detector is an obvious possibility, but the sign of the change is puzzling for it. The effect can be described by a downward shift

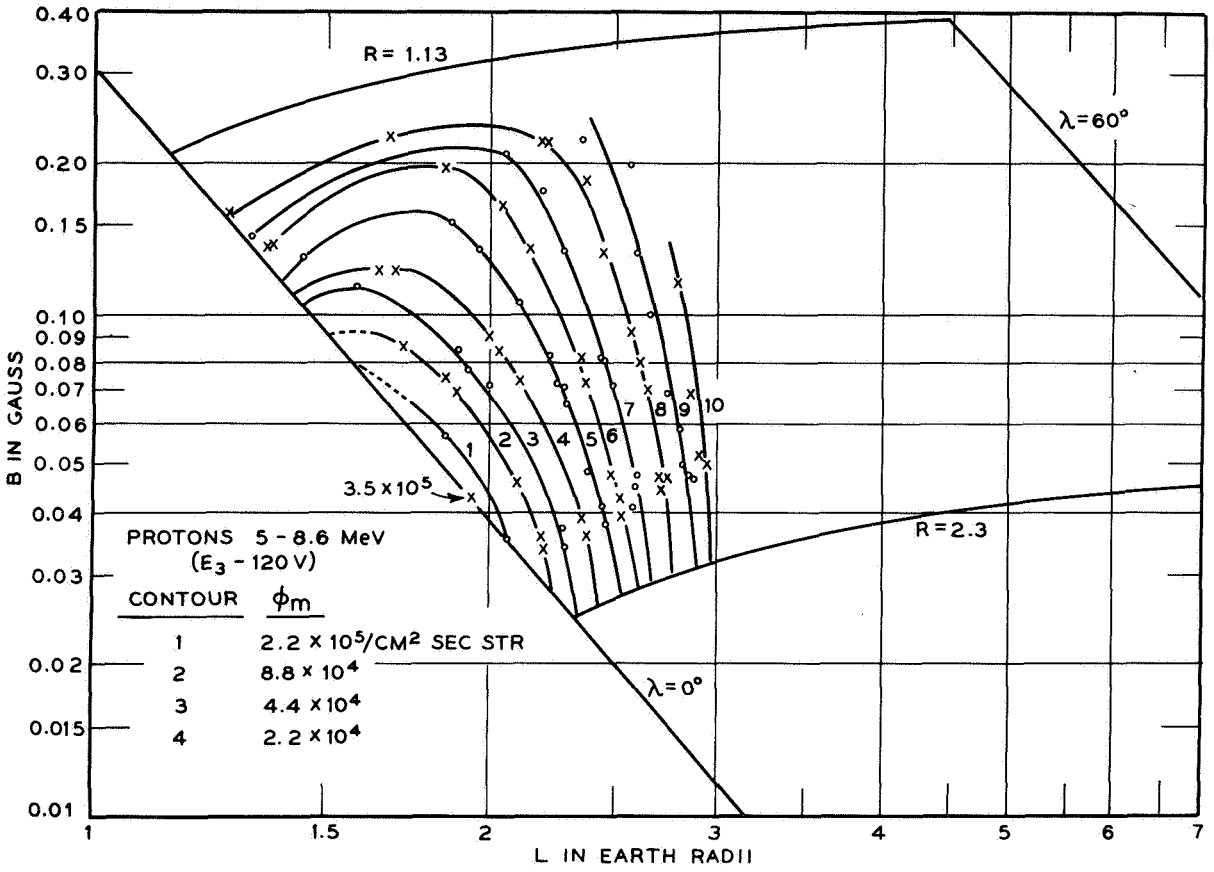


FIGURE 6–24.—*B*, *L* flux map 5.0–8.6 Mev protons, December 1962 and January 1963.

of the third discriminator level so that E_3 includes lower energy protons. Such a downward shift requires an effective increase of gain in the system which is certainly unexpected. The change in proton flux may be real, but such a conclusion will certainly require substantiation by other observations.

The energy spectrum of protons varies in a complex way with *L* and *B* and is still under investigation. Some preliminary results for the region $L \geqq 2.2$ are shown in Figure 6–26. Choosing differential energy spectra of exponential or power law form, the relative counting rates in different channels permit a choice of the e-folding energy or the power of the power law. Nature, of course, is not constrained to these particular mathematical forms, but they provide a useful scale for expressing the approximate energy distribution.

Exponential spectra seem to be more consistent with the limited data which have been examined than power law spectra. Figure 6–26 indicates the e-folding energy, ϵ_0, obtained for different ratios among detector channels at different *B* and *L* values. The ϵ_0 values from one detector ratio at one *B* and *L* value are determined from statistics. That is, at each point the observed counting rate ratio is modified to high and low extremes on the basis of one standard deviation in the actually observed counts in the two channels. In general the determination from the various ratios are reasonably consistent although they do not always overlap. The ϵ_0 values clearly increase as *L* decreases (the spectrum gets harder) and increase as *B* increases on a given *L* line. A representa-

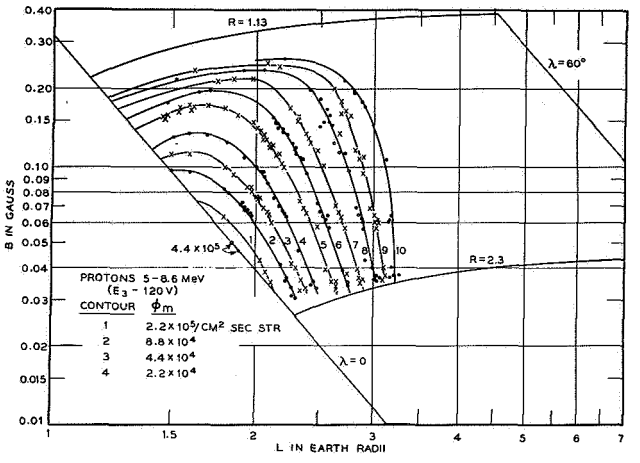


FIGURE 6–25.—B, L flux map 5.0–8.6 Mev protons, June and July, 1963.

tive value is the order of 1 Mev. The increase with L is immediately evident in Figure 6–17. The increase with B is evident in examining the flux maps of Figures 6–23 and 6–24. The magnitude of ϵ_0 joins quite well with the values obtained by Davis for still lower energy particles.

Electrons

Figure 6–27 is a flux map for electrons from Channel F_1. The contours are of equal counting rate, Cm. The inner belt has been constructed combining the available data from December through July. The data are quite consistent over this time. If there have been changes in the region $L = 1.7$ and below, they are not larger than 30 percent. The outer belt on the other hand is highly variable and the data used in drawing it are from the middle of July. Figure 6–28 shows the time variations observed from December through July at an L of approximately 4.5 for $B < .1$ gauss. The variation of ϕ_m with B is small in this range as shown in Figure 6–27, and no attempt has been made to correct it. The maximum intensity from the outer belt over the period is $<3 \times 10^4$ counts/cm² sec steradian. As is evident in Figure 6–28 there have been many rather long periods in which no data have been taken, so that larger excursions of the outer belt could have occurred and been unnoticed. The "slot" between the inner and outer belts has been very deep (Figure 6–27). The particles introduced into it in July and October 1962 had largely disappeared by the time of the Relay I launch.

The electron spectrum and the absolute electron flux are closely connected through Figure 6–7. From observations like those of Figure 6–18, comparing the lowest and highest electron channels with one another in both the inner and outer belt, it is clear that there is no dramatic change in the spectrum involving electrons of 1.0 to 1.5 Mev. It is in this energy region that the detector is capable of distinguishing different spectra. If a large part of all the electrons above 1 Mev are below 1.5 Mev, then the ratio of the counting rates of F_1 and F_4 will be very large. The data show this is not the case. The ratio is between 8 and 10, approximately the value to be expected in a fission-like electron spectrum. It can be concluded that in the 1 to 1.5 Mev energy range the spectrum is as hard as a fission spectrum.

The absolute efficiency for channel F_1 for a fission-like spectrum is .032 for all electrons above zero energy. Applying this factor to the counting rate of the maximum contour in Figure 6–27 (6×10^6 counts/cm² sec ster) the flux ϕ_m is found to be 1.8×10^8 electrons/cm² sec ster. In the region of the maximum contour the ϕ, B slope is approximately —8. Using the appropriate factor read from Figure 6–22 (at $n = 16$) the omnidirectional flux of the maximum contour

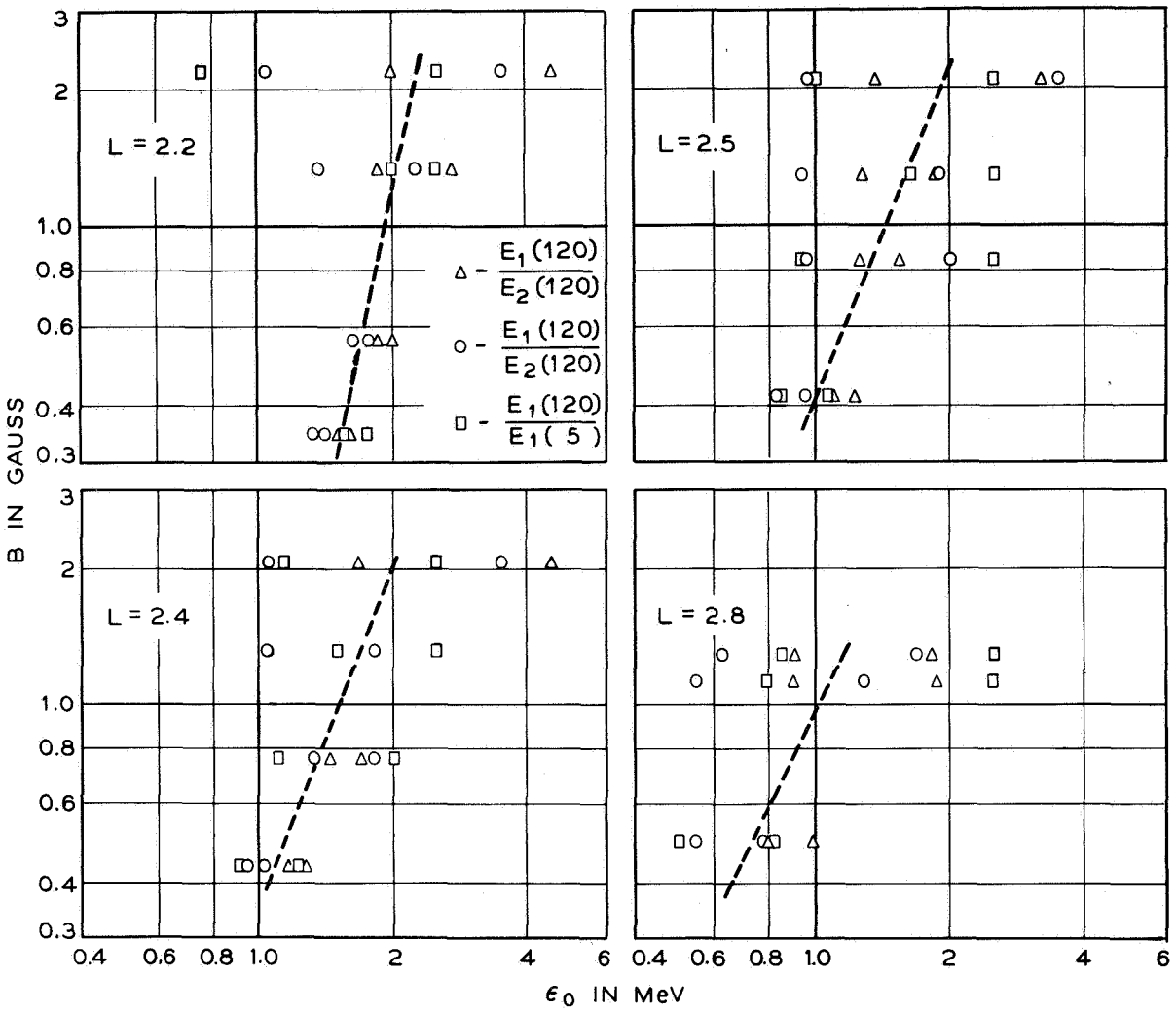


FIGURE 6–26.—Proton energy spectra.

is determined to be 7.2×10^8 electrons/cm^2 sec in quite close agreement with previously measured values. To specify a flux above 1 Mev (rather than zero) the counting rate of F_1 is to be multiplied by 14.

R, λ Flux Maps

Because the *R*, λ space is more easily visualized, the *B*, *L* flux maps of Figures 6–23, 6–25, and 6–27 have been transformed into *R*, λ space in Figures 6–29, 6–30, and 6–31. They are contours of directional flux. The omnidirectional flux can be derived for them to a good approximation for the higher contours by applying factors of 6.5 for the protons and 4 for the electrons. The electron map is now shown in flux rather than counting rate, using the efficiency discussed in the previous section.

IMPLICATIONS FOR RADIATION DAMAGE TO SOLAR CELLS

Damage Equivalence

It has been convenient to measure radiation damage in solar cells in terms of an equivalent flux. This flux is the flux of 1 Mev electrons normally incident on a given type of bare solar cell which will produce in that type of cell the same degree of damage as some other particle or spectrum of

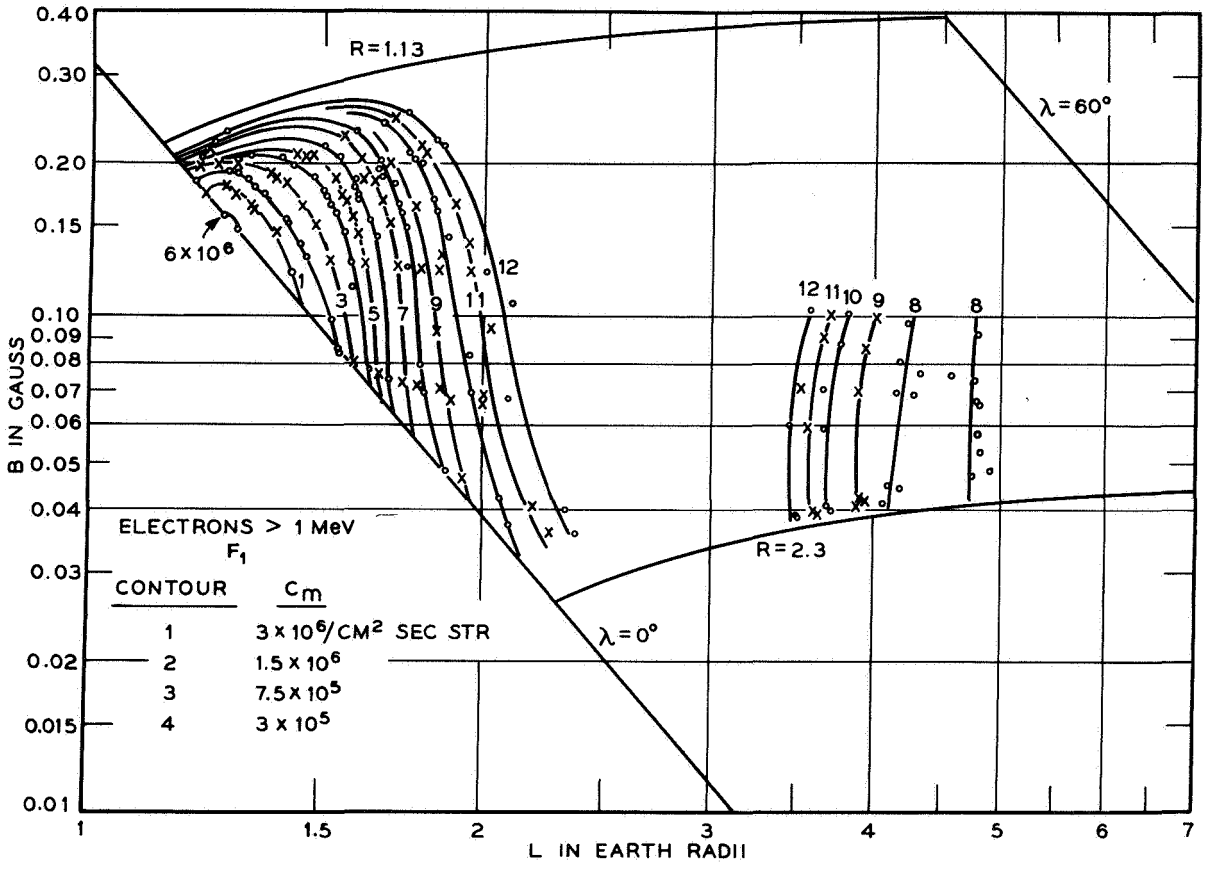


FIGURE 6–27.—*B*, *L* flux map for electrons, December 1962 through July 1963. The contours are of equal counting rate.

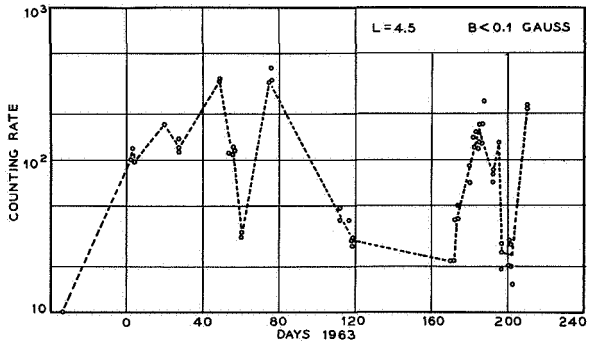


FIGURE 6–28.—Flux vs. time at $L = 4.5$, $B < .1$ gauss, December 1962 through July 1963.

particles incident in some specified orientation with some specified shielding. Figure 6–32 illustrates the damage equivalance of different monoenergetic protons arriving in a uniform omnidirectional flux on a heavily back-shielded n-on-p solar cell. The curves show the no-front-shield case and various typical shields. It is apparent that the damage effectiveness at low energies rises steeply. Particles below 5 Mev can be removed by relatively thin shielding, but for unshielded solar cells the high density of low energy particles in space provides a severely damaging environment.

Low Energy Proton Damage

Figure 6–33 shows the integral of the 2.5–3.6 Mev proton flux encountered by Relay in the first few days in orbit. The first orbits have been integrated in detail and show a step structure associated with passage of the satellite through the maximum of the low energy proton distribution on each orbit. These steps correspond in time with the rapid changes in solar cell output

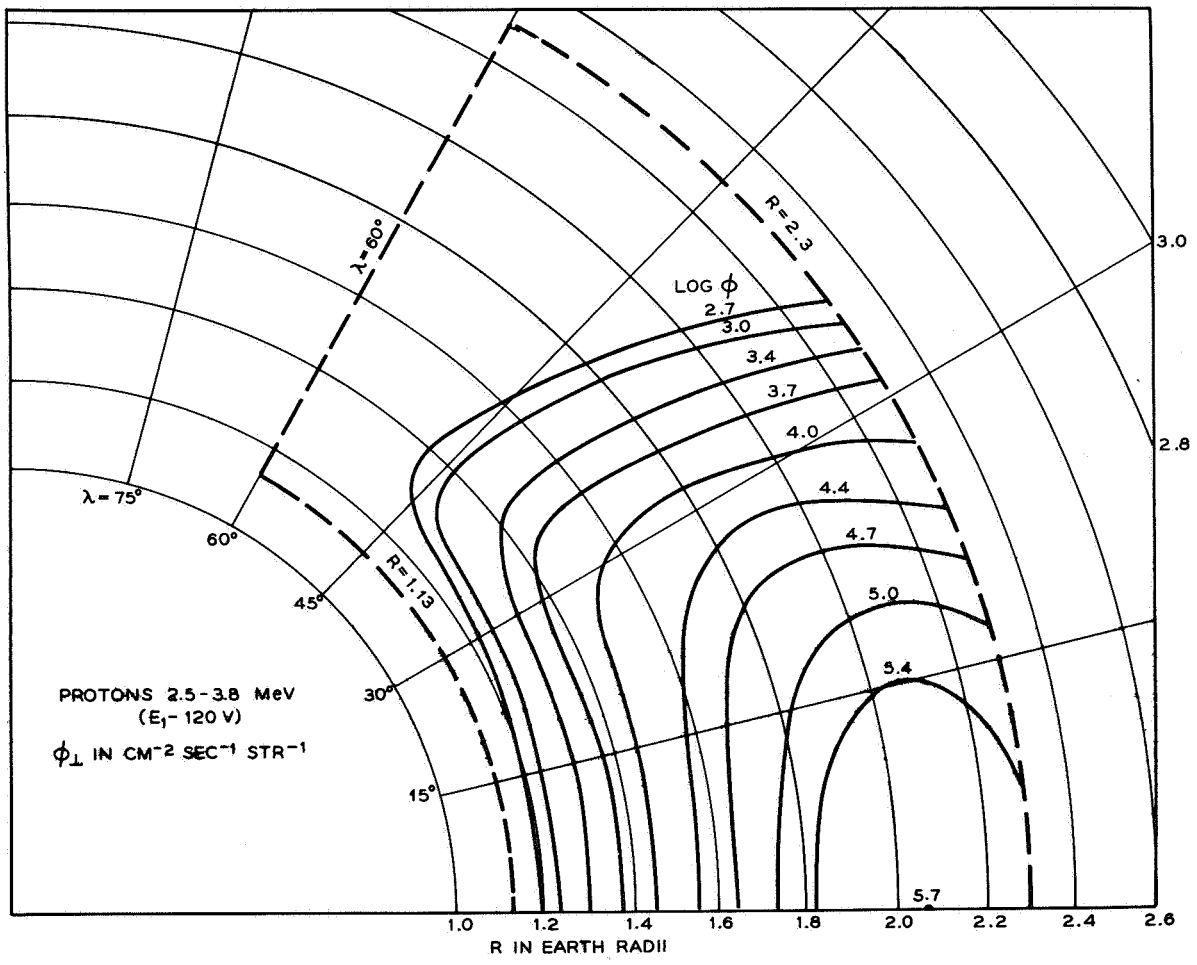


FIGURE 6–29.—R, λ flux map for 2.5–3.8 Mev protons, December 1962 and January 1963.

observed by R. C. Waddel* of Goddard Space Flight Center on unshielded devices. The position of the satellite in R–λ space during the first orbits is shown in Figure 6–34. Comparing this figure with the R–λ flux map of Figure 6–29, the grossly varying flux exposure is evident. Beyond the first day in orbit the steps on a logarithmic scale become too small to distinguish and the daily accumulated total is plotted.

Figure 6–35 shows the exposure per day over a much longer time. As apogee precesses from being nearly at the equator at launch to its northern extreme, the satellite spends less and less time in the maximum of the proton distribution and the incident flux decreases by a factor of about 5. The pattern is repeated as the latitude of apogee returns to the equator and goes to the southern extreme. The two extremes are different because of the assymetry of the earth's magnetic field.

An omnidirectional flux of protons in this low energy range has a damage equivalence of about 6×10^3 1 Mev electrons for n-on-p solar cells (Figure 6-32). Thus at the end of 1 day the exposure of Figure 6–34 amounts to approximately 2.4×10^{14} equivalent 1 Mev electrons/cm^2. This is considerably smaller than Waddel's observed damage rate, but still lower energy protons need to be included. By extrapolating the proton

*See Chapter 8, this report.

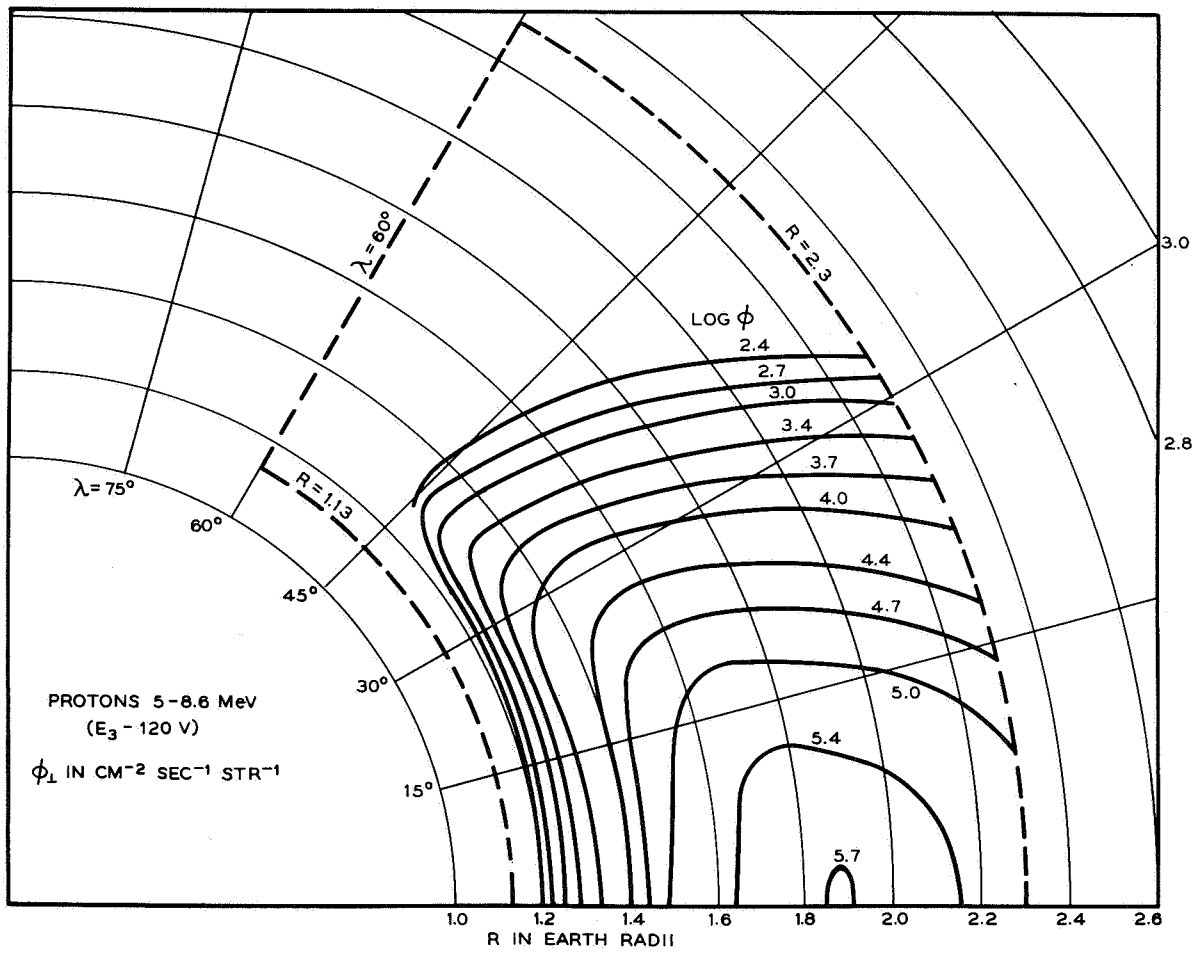


FIGURE 6–30.—R, λ flux map for 5.0–8.6 Mev protons, June and July 1963.

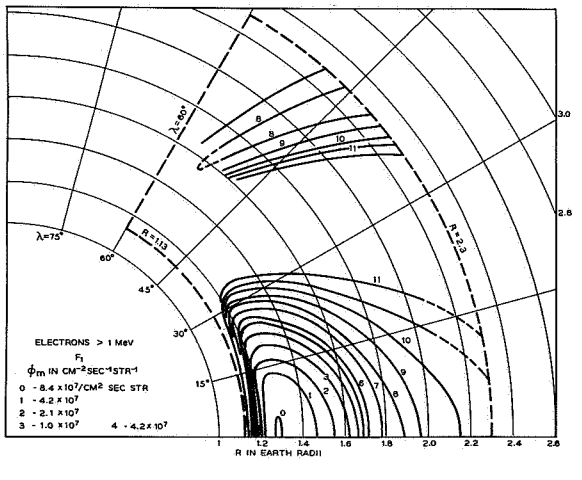


FIGURE 6–31.—R, λ flux map for > 1 Mev electrons.

spectra of Figure 6–26 downward in energy and only including protons of 1 Mev and above, the equivalent damaging flux is increased by about a factor of 10.

Electron Damage

The low energy protons do not matter for damage in the main power plant of Relay I or in any but the unshielded damage measuring cells. In the 30 and 60 mil glass shielded devices electrons and higher energy protons are contributing the damage. Figure 6–36 is a daily exposure plot for electrons >1 Mev. The phase of the maxima and minima are interchanged with respect to those of Figure 6–35. The satellite spends

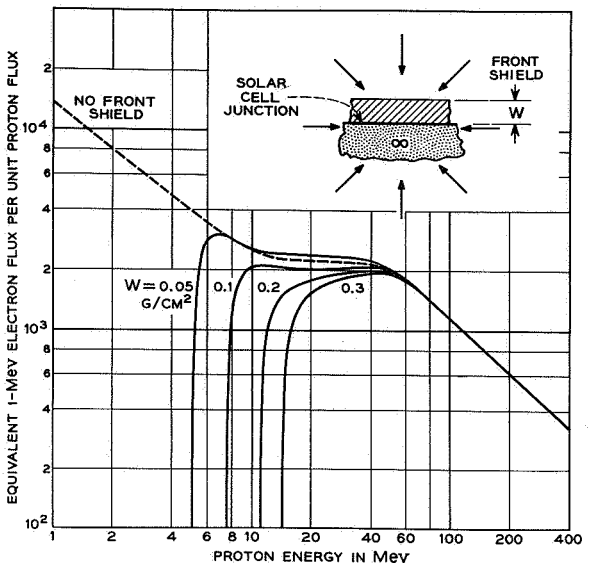


FIGURE 6–32.—Damage equivalence of protons on n-on-p solar cells.

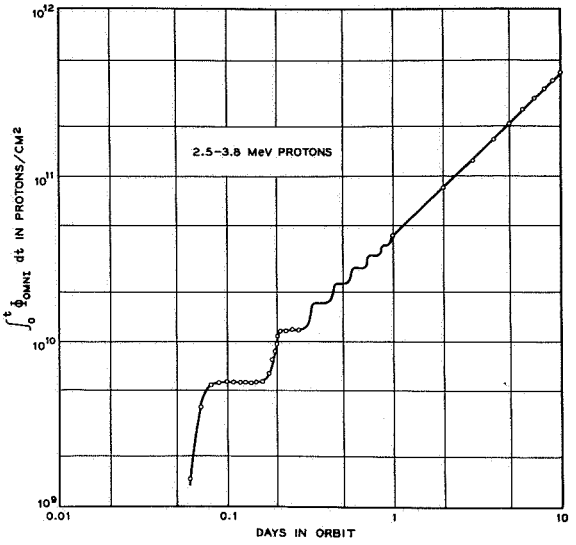


FIGURE 6–33.—The integral exposure of the satellite to 2.5–3.6 Mev protons during the first few days in orbit.

the greatest amount of time in the region of the high intensity of the inner belt (and the outer belt) when apogee is near an extreme of latitude. When apogee is on the equator the satellite almost skirts the inner belt. The average exposure of the satellite to electrons >1 Mev over a period of months is approximately $8 \times 10^{11}/cm^2$ day. The damage equivalence of fission-spectrum electrons for 60 mil glass shielded n-on-p solar cells is approximately 0.8. Thus the electrons are contributing the equivalent of about 6×10^{11} 1 Mev e/cm² day, somewhat less than half the total damage observed by Waddel. Presumably protons in the vicinity of 20 Mev are responsible for the remainder. The maxima of the electron exposure have a period of about 145 days (half the period of precession of apogee) and there is a small second harmonic contribution as well, apparent in the dip at the northern apogee extreme.

ACKNOWLEDGMENTS

We are deeply indebted to a large number of people who have contributed to these experiments: to T. M. Buck, G. H. Wheatley and J. W. Rodgers who fabricated and meticulously tested the particle detectors; to E. W. Thomas and G. L. Miller who played major roles in the circuit development; to G. Skewis under whose energetic direction Branch Shop 3 carried out the mechanical construction; to Mrs. W. L. Mammel and J. D. Gabbe who have been heavily consulted in the reduction of the data; to B. M. Berry who is studying the radiation damage problem; to W. M. Augustyniak, and to A. Eman of Princeton University, and K. A. Wright of M.I.T., who carried out the detector calibrations; to C. E. McIlwain of the University of California and D. Enemark of the State University of Iowa whose concept and execution of the logic of the experiment has been invaluable; to D. M. Brown of Goddard Space Flight Center whose efforts as project coordinator kept the project moving; and to W. Rosenzweig whose work in radiation damage of silicon solar cells has been used in drawing the implications for Relay radiation damage.

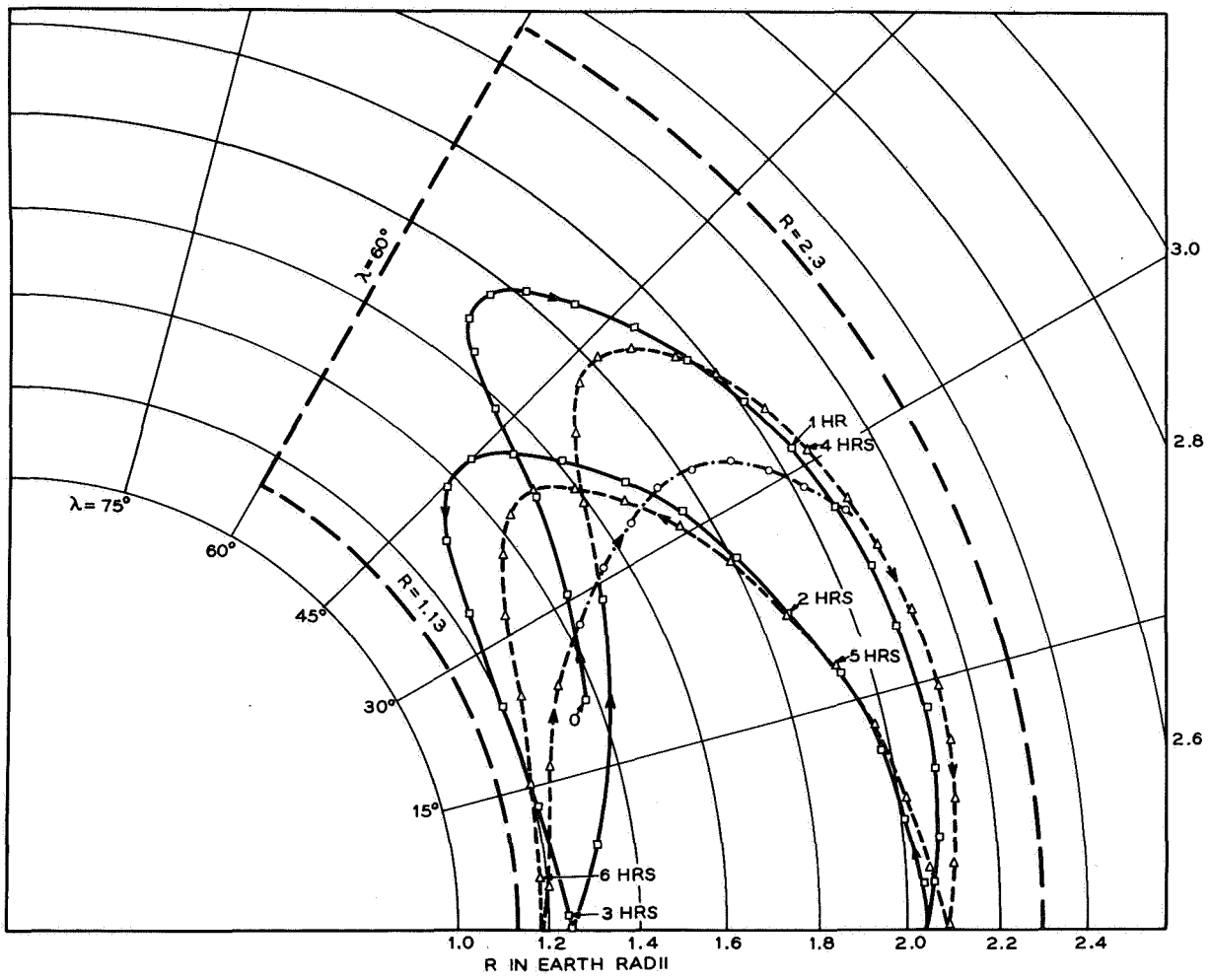


FIGURE 6-34.—The satellite position in R–λ space during the first few orbits. The points are 5 minutes apart.

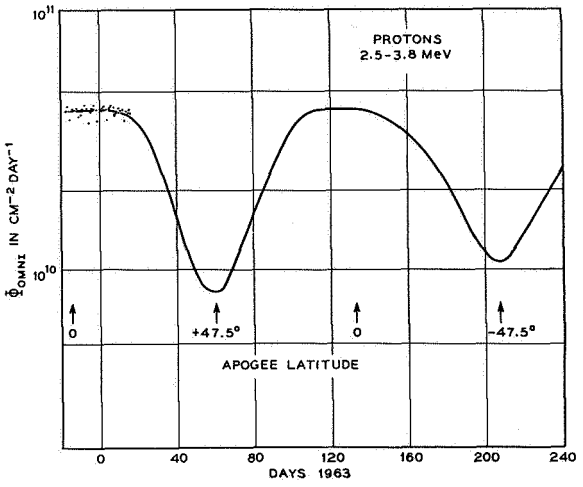


FIGURE 6-35.—Daily exposure of Relay I to 2.5–3.6 Mev protons from launch through the first 8 months of 1963.

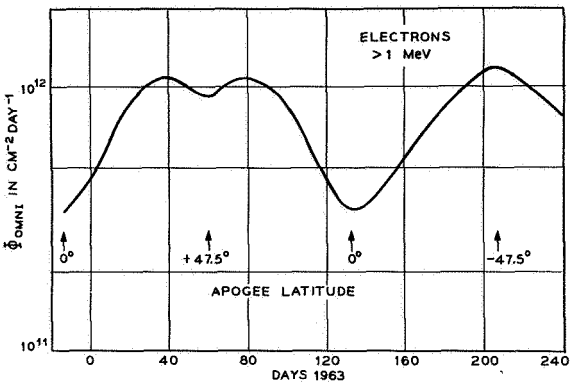


FIGURE 6-36.—Daily exposure of Relay I to >1 Mev electrons from launch through the first 8 months of 1963.

AUTHORS. *This chapter was written by* W. L. BROWN, L. W. DAVIDSON, *and* L. V. MEDFORD *of the Bell Telephone Laboratories, Inc., Murray Hill, New Jersey, U.S.A. under Western Electric Corporation contract NAS 5-1678 with NASA/Goddard Space Flight Center.*

N66-10245

Chapter 7

Relay I Trapped Radiation Measurements

10245

The spatial dependence of the intensities of geomagnetically trapped electrons with energies greater than 0.45 Mev and of protons in four energy ranges have been measured in the region within radial distances of 1.2 and 2.3 earth radii.

Author

INTRODUCTION

A set of four particle radiation detectors was designed and constructed at the State University of Iowa* for flight aboard the Relay satellite. As was originally planned, the reduction and analysis of the data resulting from the successful launchings of the Relay I and Relay II satellites are now being performed at the University of California at San Diego. This paper is based upon a partial analysis of the data obtained by Relay I during its first year in orbit.

The principal objective of obtaining a description of that part of the particle radiation environment which can produce radiation damage has been met despite the fact that some of the detectors were themselves damaged by the particles which they were measuring.

RADIATION DETECTOR SYSTEM

The identification of particles as protons or electrons is accomplished with a high degree of success within the detectors themselves by judicious choices of sensor (size and type), detector shielding, and proper choice of electron discrimination levels. Once particle type is determined, the particle incident energy should be classified according to magnitude.

All the detectors produce a quantity of charge related to the energy lost by the incident particle in the sensor. Two of the sensors are of the solid state type and two are scintillation crystals mounted on photomultiplier tubes. In the solid state detectors, designated here as B and C, the charge produced at the output is linearly related to the energy lost by the particle in the sensor. The charge output of the scintillation crystals, here designated as A and D, is also related to the particle energy lost in the sensor but not always linearly.

To avoid difficulties due to variations in the capacitance at the sensor output, the input amplifier was designed to respond to the charge generated by the sensors rather than the voltage. At the output of these amplifiers a voltage pulse is present related to the energy loss in the sensors. Since the energy loss as a function of the energy of the incident particles can be both measured and calculated, the energy spectrum analysis is reduced to a voltage pulse height analysis.

Other electronic blocks common to each

*Fillius, R. W., Satellite instruments using solid state detectors, SUI 63-26 (State University of Iowa Master's Thesis, 1963). Enemark, D. C., Electrical design of the radiation effects experiment for the satellite Relay SUI 62-16 (State University of Iowa Master's Thesis, 1962).

detector are: a delay line inter-stage network to clip the pulses to a length of .25 μsec, a voltage post amplifier and voltage amplitude discriminators. The amplitude discriminators form the input circuits to pulse height analyzers for each detector. Since analyzers for each detector are somewhat different they will be described individually. Photographs of Detector A and the B-C-D detector complex are shown in Figures 7–1 and 7–2.

The B, C, and D detectors are directionally sensitive with the consequent need for the knowledge of magnetic field orientation for good intensity measurements. Detector A however is an omnidirectional detector whose response is independent of the field orientation.

The systems design is governed by the dynamics of trapped particles in the earth's magnetic field. The particles are constrained to travel in approximately helical paths about the lines of force. The angle a which the particle velocity makes with respect to the field line varies with the magnitude of the magnetic field B along the field line according to the equation $\sin^2 a = B/B_m$ where B_m refers to the point $a = 90°$. The angular distribution about the field line is almost always such that the peak intensity occurs in the plane perpendicular to the field line, i.e., at $a = 90°$. The magnetometer gating is arranged so that counts are accumulated only when the detectors are pointing perpendicular to the field line. The complete angular distribution at any point can be obtained by obtaining the dependence of the intensity at $a = 90°$ upon B_m and using the equation $\sin^2 a = B/B_m$ to transform this dependence upon B_m into the a dependence at the desired value of B.

Since the peak intensity occurs normal to the magnetic field lines it is only necessary to determine when the field component along the detector axis is zero and arrange to turn on the detectors for an interval during which the rate is relatively constant. Previous measurements at 920 km have shown the angular distribution to be symmetrical about the normal plane and the intensity to vary less than 10 percent over 10 degrees on either

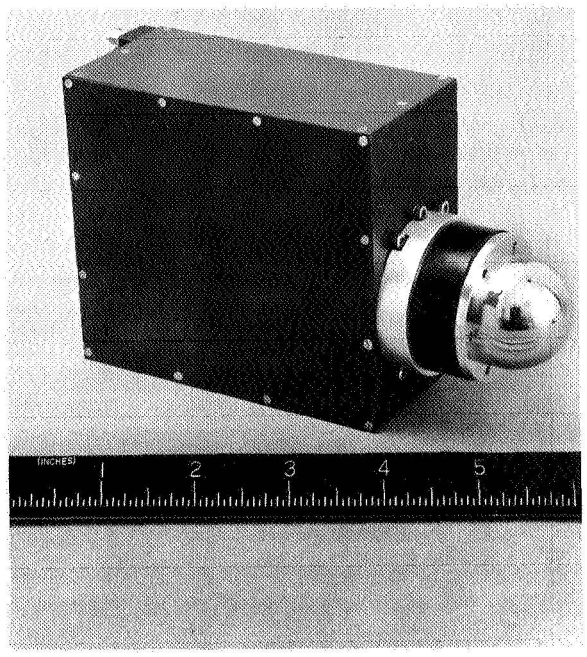


FIGURE 7–1.—Relay I omnidirectional detector A.

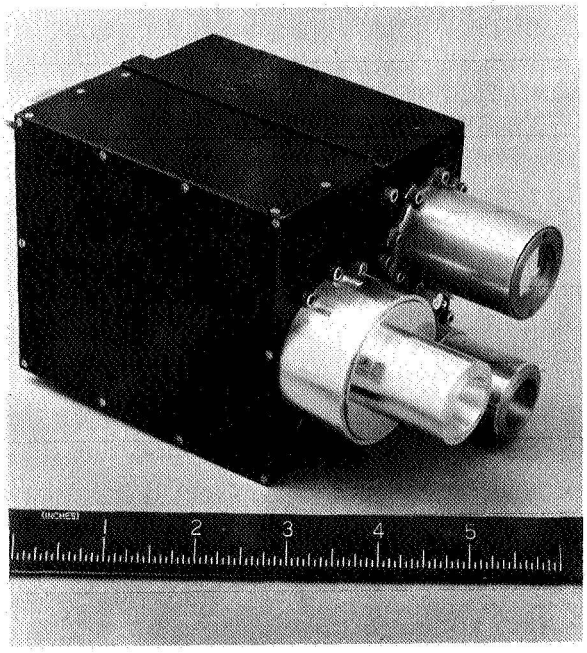


FIGURE 7–2.—Relay I B-C-D directional detector complex.

side of the peak. At Relay I altitudes the variation is expected to be even less. From this then it is seen that if the detectors are turned on about 10 degrees ahead of the zero crossing of the field and turned off about 10 degrees after zero crossing, a good measure of the peak intensity can be made.

Relay I spins at approximately 2.7 rps in a known sense. The detector gating was achieved by placing an ac coupled flux gate magnetometer about 13 degrees ahead of the detector axis in rotation. At zero ac field crossing along the magnetometer axis, a turn on signal is generated which allows the detectors to accumulate counts for the fixed interval of exactly 24 satellite clock pulses, after which the detectors are gated off. With the satellite clock rate of 1152 pulses per second, the on time is 0.021 seconds or about 19 degrees of revolution. The number of clock pulses during each active interval is counted to provide an accurate measure of the total time of data accumulation.

When the spin axis of the satellite happens to be aligned with the field line and the detectors are always in the normal plane, no ac field variation is seen by the magnetometer. Whenever the ac field variation has not gone through zero for one second, a free runnning multivibrator (at the nominal spin rate) is started to operate the magnetometer gating circuitry and produce an identification bit for transmission to indicate that it is in the special mode. The conditions necessary for this special mode have been met in flight but it is a rare occurrence.

In addition to the magnetometer gating scheme a large amount of sub-commutation is needed for the radiation experiments because only seven accumulators are available for all the outputs. Whenever possible all of the outputs of a particular detector are examined at once to allow a direct measure of the particle intensity in each energy increment during the same time interval. The accumulators and data conditioning system are both in the encoder and are not an integral part of the radiation experiment. It can be seen from the overall block diagram (Figure 7–3) that the basic clock frequency (1152 cps) of the encoder and a sub-commutator advance signal are provided by the encoder. The clock signal is gated on (not shown explicitly in Figure 7–3) at the same

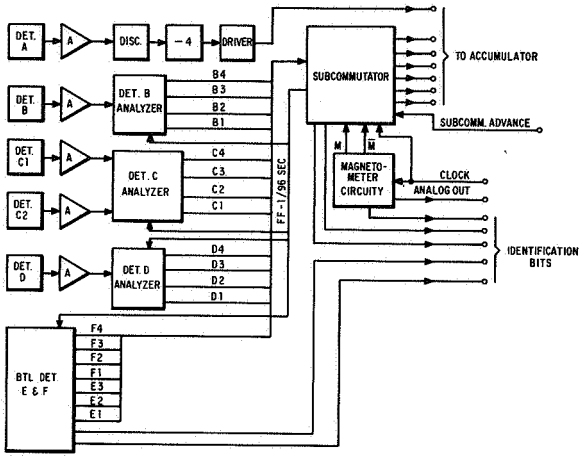


FIGURE 7–3.—Radiation detector system block diagram.

time the detector outputs are sampled and fed to an accumulator in the encoder to provide a direct measure of detector live time. Detectors E and F shown, which are channeled through the same subcommutator, are from a separate experiment performed by Bell Telephone Laboratories. They will not be discussed here.

The subcommutator advance signal from the encoder has a period of twelve seconds, two seconds in one state and ten seconds in the other. In the ten second state the accumulators are free to register counts each time the detector outputs are gated on by the magnetometer signal; in the two second state the accumulators are read out. Signal M is the gate from the magnetometer circuitry. It is in one state for 24 clock pulses (about 0.021 sec) and in its complement state $\overline{M}$ for the rest of the period (about 0.179 sec) when it is used for a background measurement on B3, C3, D3, B4, C4, and D4 each at different subcommutator cycles. The

term "background" is used to designate the counts accumulated when the detectors are not looking at the peak intensity.

It should be noted that with the exception of detector A, all detector analyzer outputs are fed to the sub-commutator where they are switched to the accumulators one detector at a time. These accumulators are read out once a second while counting for ten seconds, then inhibited and read twice, then reset for the next detector. By rejecting the data in which the two final readouts do not agree, the probability of an erroneous reading produced by transmission noise is reduced to a very small value (in practice, very few errors in over 10^5 readings have been discovered). Detector A is permanently connected through its driver to an accumulator which is read out every second but is never reset. Accumulator overflow is detected during data reduction. The remaining lines shown are information signals for transmission; vis.,

1. Two identification bits to indicate subcommutator position.
2. One identification bit for magnetometer gating circuit mode.
3. One analog channel, sampled once a second, which time shares on equal basis between the sine wave output of the magnetometer and on an identification bit to indicate which of the alternate outputs of the analyzers is in use.
4. Two identification bits from the Bell Telephone Laboratories experiment.

In the detailed discussion of the detector parameters which follows, it will be convenient to consider them in the order of increasing complexity associated with their energy analyzing system.

The measurements of the magnetometer signal can be compared with the computed magnetic vector to derive the orientation of the satellite spin vector. Shortly after the launch of Relay I, the spin vector was ascertained in this manner to be within 4 degrees of a declination equal to —69 degrees and a right ascension of 125 degrees on the celestial sphere.

Detector A Characteristics

Detector A is primarily an omnidirectional 35 to 300 Mev proton detector but with some sensitivity to high energy electrons. The sensor is a 0.932 cm diameter sphere of National Radiac Sintilon plastic scintillator optically coupled to the phototube through a conical light pipe (see Figure 7–4). The

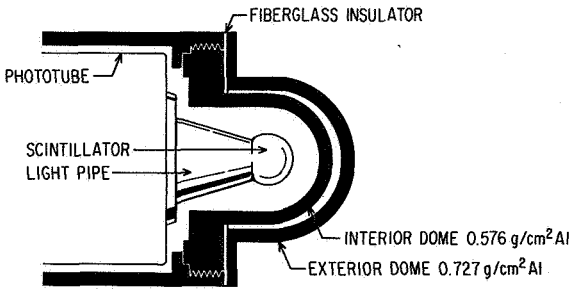


FIGURE 7–4.—Detector A scintillator mount and shielding.

height of the light pipe is chosen to place the center of the sphere at the center of the two concentric hemispherical aluminum domes so that particles entering from the front and sides will see the same amount of shielding; viz., 1.30 g/cm². This shielding thickness stops all protons of energy less than 34 Mev and electrons less than 2.7 Mev.

One amplitude discriminator is placed at the amplifier output with pulse height setting corresponding to the integral energy spectrum end point of Co^{60}. For the scintillator's size and type this setting represents an energy loss in the crystal of approximately 1.0 Mev since the most important photon physical process at this energy is Compton scattering. Consequently, the detector proton and electron thresholds are 34 Mev and 3.7 Mev. In the proton case it is evident that the shielding thickness is the dominant parameter for setting the energy threshold. For the electron threshold the electronic discriminator level must be known accurately also.

An experimental measurement of the proton energy threshold was performed on the

University of Minnesota linear accelerator and was found to be 35 Mev to an accuracy better than 3 percent. Direct electron threshold measurements could not be performed because of the lack of a monoenergetic high energy electron source.

Detector D Characteristics

Detector D is primarily a directional electron detector with some sensitivity to protons. The sensor is a cylinder of Scintillon 0.254 cm diameter and 0.254 cm in height. It is optically coupled to the phototube through a glass disc (see Figure 7–5) to

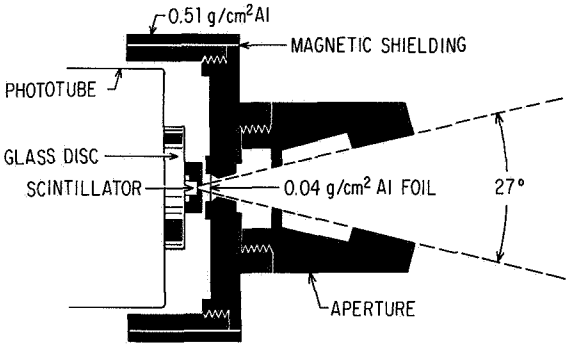


FIGURE 7–5.—Detector D scintillator mount, shielding and aperture.

provide an additional 0.81 g/cm² of shielding in the backward direction. A minimum of 1.07 g/mc² of platinum shields the crystal from the forward direction except for a circular entrance area of 1.37×10^{-2} cm². Particles entering the scintillator from the forward direction must penetrate 0.048 g/cm² of aluminum foil after passing through a 27 degree conical acceptance aperture. From the parameters of shielding and entrance area, solid-angle product along with the geometric factors, G, are listed (see Table 7–1).

Several features of the above list should be explained. The transition between the two values for geometric factor occurs when the range of incident particles exceeds the 1.07 g/cm² of platinum. For particles greater than this range the sensitive entrance area

TABLE 7–1

G	Electrons	Protons
2.38×10^{-3} cm²-ster	0.20 to 3.0 Mev	5.0 to 20 Mev
8.80×10^{-3} cm²-ster	greater than 3.0 Mev	greater than 20 Mev

expands to the full diameter of the cylindrical scintillator. Fortunately, both electron and protons intensities fall rapidly with increasing energy in the trapped radiation allowing the use of $G = 2.38 \times 10^{-3}$ cm²-ster alone to a high degree of accuracy.

Four amplitude discriminators are placed at the amplifier output, each providing a point on an integral pulse height spectrum of the detected particles. In view of the previous discussion about the geometric factor, it is seen that to high accuracy the shielding serves to solely determine a lower energy cutoff for electrons and protons. The energy equivalent of the electronic discrimination level settings will just add to this low energy cutoff to provide integral energy channels labelled D1, D2, D3, and D4 (see Table 7–2). When the counting due to pro-

TABLE 7–2

	Energy loss required	Electrons	Efficiency	Protons	Efficiency
D1	.13	<0.30 Mev	.7	<5.1 Mev	1.0
D2	.28	<0.45 Mev	.6	<5.1 Mev	1.0
D3	.43	<0.62 Mev	.45	<5.2 Mev	1.0
D4	.64	<0.82 Mev	.13	<5.2 Mev	1.0

tons is important, the differences in the efficiencies for protons and electrons in the different channels can be used to separately determine the electron and proton fluxes.

The discrimination levels can be reproducibly set with a laboratory Sr^{90} electron source by noting the number of counts at each output and the count ratios of neighboring levels. Basic calibration of the energy thresholds and efficiences were obtained using the Bell Telephone Laboratories 1 Mev accelerator. A graph of the efficiency vs. energy

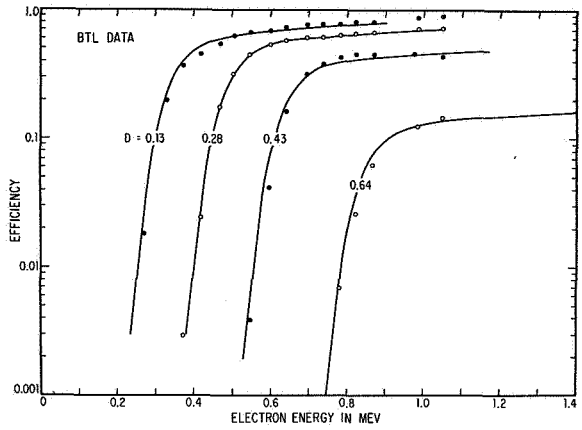


FIGURE 7–6.—Relative efficiency vs. energy curves for detector D outputs.

shown in Figure 7–6 serves to illustrate the manner in which the stated integral energy levels were chosen. Further calibrations were made with a fission beta spectrum at Los Alamos with the following results for the product, the efficiency (ϵ), and geometric factor (see table 7–3).

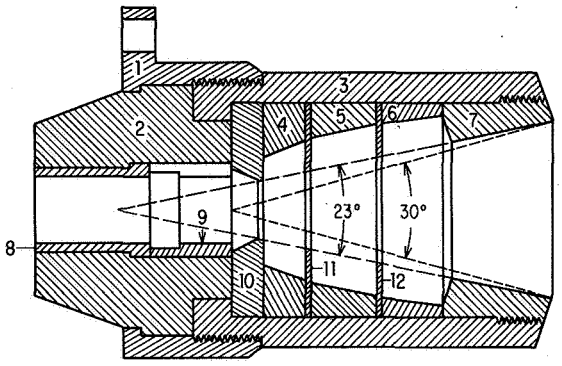
TABLE 7–3

Channel	(ϵG) fission
D1	1.46×10^{-3} cm^2-ster
D2	1.16×10^{-1}
D3	5.92×10^{-3}
D4	1.18×10^{-4}

Detector B Characteristics

Detector B is a single p–n junction diode (Ortec surface barrier detector) designed to detect protons with nominal energy for 1 to 4.5 Mev with a high discrimination against the ambient electron flux. Insensitivity to electrons is achieved through

1. Use of a thin sensor so that entering electrons cannot deposit much energy in it.
2. Discrimination levels that are set much higher than the pulse amplitude typically produced by electron energy loss in the sensor.
3. The previously mentioned 0.25 μ sec pulse clipping to decrease the probability of pulse pile-up of many low energy events. Brass shielding about the sensor confines the entrance aperture, for protons less than 85 Mev, to a 15 degree conical half-angle. Details of aperature construction are shown in Figure 7–7. Two thin annular discs serve



DETECTOR "B" APERTURE

1. MOUNTING RING
2. REAR SHIELD
3. MAIN HOUSING
4. REAR SPACER
5. SECOND SPACER
6. UPPER SPACER
7. APERTURE DEFINING
8. CONNECTOR INSULATOR
9. DETECTOR HOLDER
10. SOURCE MOUNT
11. ELECTRON BAFFLE
12. ELECTRON BAFFLE

FIGURE 7–7.—Detector B aperture.

as electron baffles to limit electron scattering into the detector. A nickel foil 1.2 mg/cm^2 thick is mounted on the inner baffle to shield the detector from light. The 6.5 mm^2 sensor area results in a geometric factor of 0.015 cm^2-steradians for the detector.

The detector B electronic discrimination levels (B_α, B_ρ, B_γ, B_δ) are set at 0.98 Mev, 2.10 Mev and 3.84 Mev respectively. But because of the small depletion depth (100 microns) of the detector a given discrimination level may be triggered both by a proton which stops in the active depth and a higher energy proton which penetrates it. Penetrating protons of still higher energy cannot deposit sufficient energy in the active depth to trigger the discrimination level. Therefore the proton energies associated with a given pulse hieght are double valued. This characteristic of detector B is displayed in Figure 7–8 with the discrimination levels marked. Here it is clearly shown that although the output of the discriminators are

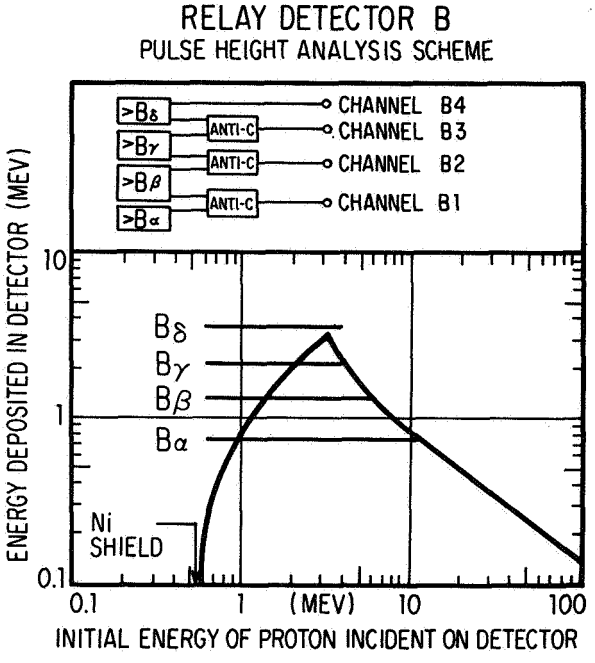


FIGURE 7–8.—Typical detector B energy response characteristics with discriminator settings indicated.

integral in pulse height they represent redundant differential proton energy intervals. Further, level B_δ is set higher than any possible pulse height obtainable from protons received through the entrance aperture. It can be triggered only by heavier particles, such as α-particles, or protons (greater than 85 Mev) penetrating the side of the shield and traversing the detector sideways. Level B4 yields a crude measure of the omnidirectional background flux which penetrates the shield.

Adjacent discrimination levels are placed in anti-coincidence (top of Figure 7–8) to yield four output channels labelled as B1, B2, B3, B4 with proton energy ranges

B1: 1.1 to 1.6 Mev and 7.1 to 14 Mev

B2: 1.6 to 2.25 Mev and 4.75 to 7.1 Mev

B3: 2.25 to 4.74 Mev

B4: greater than 85 Mev background channel.

It can be seen that the overlapping energy intervals have been eliminated but an unambiguous identification of an energy spectrum still depends upon some prior knowledge of spectral shape. Calibrations of these ranges are based partly upon protons generated by the $d(He^3,p)He^4$ reaction on the Cockcroft-Walton accelerator at the State University of Iowa, shielding calculations, and the use of an accurately calibrated electronic pulser. Reaction produced protons are used to determine the detector bias voltage required for the desired depletion depth and to find the upper cutoff energy for penetrating protons in each channel. Lower cutoff energies for non-penetrating protons are based upon the discrimination levels set by a calibrated pulser with allowance for the proton energy loss in the light-tight foil.

Detector C Characteristics

Detector C is a two element proton telescope which classifies proton energies in three bands from 18.2 to 63 Mev. Directionality and solid angle are defined by two 1 cm^2 Li-drift detectors separated a distance of 2 cm with their faces parallel and their sides rotated at 45 degrees with respect to each other. The resulting geometric factor is 0.216 cm^2-steradian.

High energy protons coming from the right direction penetrate both detectors producing time coincident pulses. The rear detector, designated C2, performs the pulse height analysis on the penetrating part of the characteristic while the front detector serves to resolve the ambiguity in the double values characteristic of the rear detector. Characteristics for detectors C1 and C2 are given in Figure 7–9 with the placing of electronic discrimination levels shown. The block diagram at the top of the figure indicates the logical sorting of discriminator levels which combine to form analyzer outputs C1, C2, C3, and C4. Output C4 is different from the other outputs in that it represents the singles rate of pulse amplitudes between $C2_\alpha$ and $C2_\beta$ rather than time coincident pulses in the two detectors. Channel C4 is used as a background monitor to allow an estimate of the random coincidence

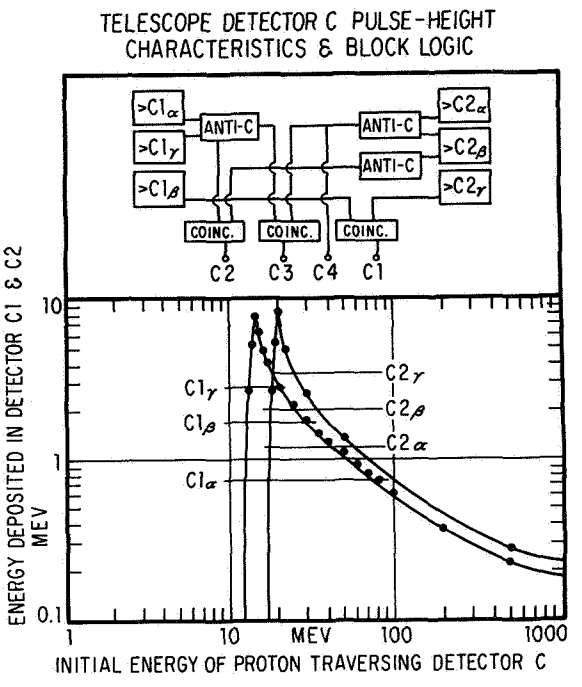


FIGURE 7–9.—Typical detector C energy response characteristics with discriminator settings indicated.

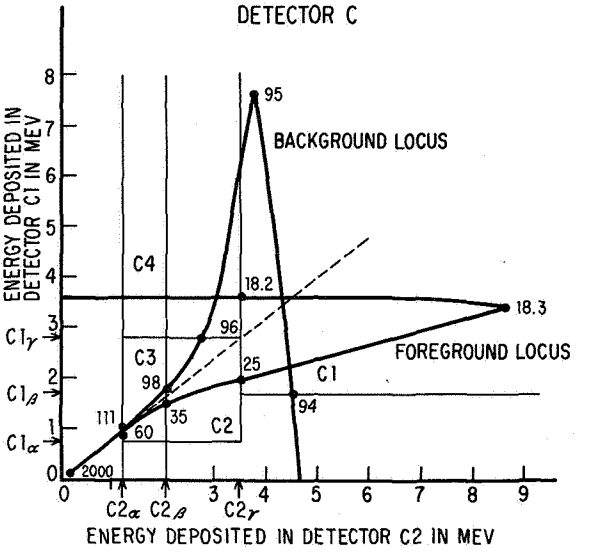


FIGURE 7–10.—Detector C telescope proton analysis.

rate. Resultant differential energy proton channels are

C1: 18.2 to 25 Mev

C2: 25 to 35 Mev

C3: 35 to 63 Mev

C4: background

These results are shown succinctly by Figure 7–10 where the foreground locus represents the energies recorded by the output channels when a proton traverses C1 first and the background locus when C2 is traversed first.

Once again protons from the d(He^3, p)He^4 reactions were used to determine the front and back dead layers and the depletion depth for the two component sensors. Typical values were found to be 4.7 Mev, 13 Mev, and 7.25 Mev respectively. A final check of lower energy cutoffs for two of the output channels was performed with the 40 Mev linear accelerator at the University of Minnesota. Counting rates from the three channels as a function of incident proton energy compared favorably with the expected values calculated from the measured detector parameters and discrimination levels.

DETECTOR RADIATION DAMAGE

A comparison of the detector A and D measurements with results from similar detectors aboard Explorer XV indicates that the effective amplification of the Relay I scintillation detectors decreased by about a factor of 1.3 during the first month in flight. The data also indicates that smaller decreases occurred during the next two months. All of the data taken since May 1, 1963, however, is consistent with the assumption that the effective detector gains remained stable to within 10 percent. The absolute discrimination levels used in this paper are probably not in error by more than 15 percent but comparison with the data from Relay II will provide a more accurate and trustworthy determination of the characteristics assumed by the Relay I detectors after May 1, 1963.

In the case of detector D, the change in characteristics can be directly attributed to radiation damage in that the glass disc upon which the scintillator is mounted can be darkened by a particle radiation dose comparable to that received in flight. This source of difficulty has been corrected in the detec-

tor D units to be flown in the future by replacing the glass with sapphire.

Two effects of radiation damage were observed on the B detector. First, the resistivity of the silicon increased so that the depletion depth increased. Knowing that this change occurred (by the appearance of large pulses) the necessary minor modifications in the interpretation of the data can be made with confidence. The second effect was that after 120 days in orbit, the size of the pulses began to decrease so that after 160 days in orbit, the counting rates from the B detector approached zero. The total number of protons reaching the sensitive element of the detector by this time was about $10^{12}/cm^2$ corresponding to a radiation dose of about 10^6 rads. The solid angle subtended by the detector B aperture was reduced by a factor of 2.2 on the unit Relay II so that a somewhat extended detector life is anticipated.

After one year in orbit the counting rates due to protons in detector C remain the same as on the day of launch. This indicates that the radiation damage to the two sensors in this detector has not been important.

ELECTRON DISTRIBUTIONS

The usual magnetic coordinates B and L^* are used throughout this paper to organize the data received from different locations in space. The L value for a point in space is approximately equal to the maximum radial distance reached by the line of force going through the point and is given in units of earth radii. B is the scalar magnitude of the magnetic field at that location in units of gauss.

After the initial reduction of the telemetered information, the counting rates from all 19 channels of data are interpolated to a particular set of L values: 1.1, 1.15, 1.2, etc.

On July 9, 1962 a high altitude nuclear explosion injected large numbers of energetic electrons into trapped orbits in the earth's magnetic field. Subsequent measurements** have shown that at least until February 1963 these electrons constituted an important radiation hazard to spacecraft traversing certain regions of space. The Relay I data presented here show that this situation persisted throughout the year of 1963.

The flux of electrons with energies greater than 0.45 Mev can be uniquely obtained by subtracting the D4 channel (Detector D, fourth discrimination level) from the D2 channel to remove the proton contribution to the D1 counting rate. The unidirectional

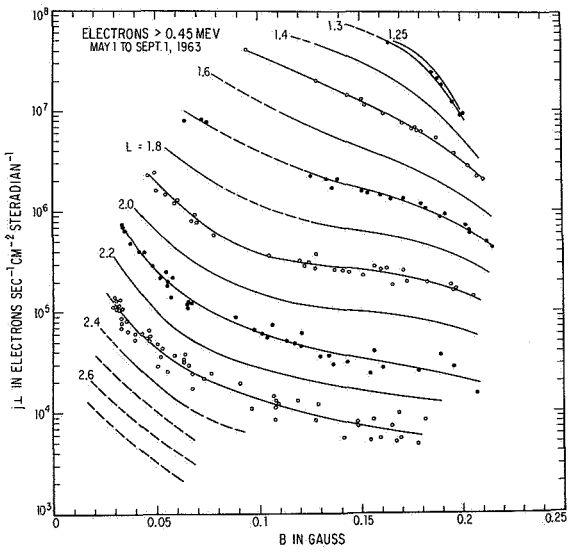


FIGURE 7–11.—Electron intensity normal to the magnetic field as a function of B for various values of L.

intensity perpendicular to the line of force of electrons greater than 0.45 Mev obtained in this manner is shown in Figure 7–11 as a function of B for a set of lines of force with L values between 1.25 and 2.7 earth radii. The actual data points are shown for some of these lines of force to illustrate the distribution and scatter of the data points.

In the future, as more data is received, analytic fits to these data points will be made

*McIlwain, C. E., Coordinates for mapping the distribution of magnetically trapped particles, J. Geophys. Res. *66*, 3681–3691, 1961.

**McIlwain, C. E., The radiation belts, natural and artificial, Science, *142*, 355–361, 1963.

as a function of B and time for each line of force. This will make possible a normalization of the intensities to a reference time which will considerably reduce the scatter in the data. Analytic fits will also simplify the integration of the unidirectional intensities to obtain the angular distributions and the omnidirectional intensities. In lieu of actual integration, it is a useful fact that the omnidirectional intensity is almost always within a factor of 1.5 of six times the unidirectional intensity perpendicular to the line of force.

The plot of contours of constant intensity in B–L space shown in Figure 7–12 were derived from the same data shown in Figure 7–11. The ratio of intensities between adjacent contours is $10^{0.25} = 1.778$.

Comparing these results with the Explorer XV data, which were obtained between November 1, 1962 and February 1, 1963, it is found that the relative spatial distributions given by the two sets of data are identical to within 30 percent in the region $L = 1.3$ to 1.6. The absolute intensities obtained from the Relay I measurements in this region may be as much as a factor two lower than the earlier Explorer XV results. Determination of the true time dependence must await comparison with the Relay II results but the present results indicate that the time constant for decrease in the intensities in this region is greater than one year. Since few reliable measurements of electrons greater than 0.5 Mev were made previous to the "Starfish" event, it is not yet possible to determine what part of the intensities are due to naturally occurring electrons.

The Relay I omnidirectional detector (detector A) is sensitive to electrons with energies greater than 3.5 Mev and protons with energies greater than 34 Mev. As mentioned previously, the effective gain suffered an initial decrease. By May 1, 1963 the gain reached a stable value approximately a factor of 1.5 lower than before launch. This caused the discrimination level to approach the largest pulse size which can be

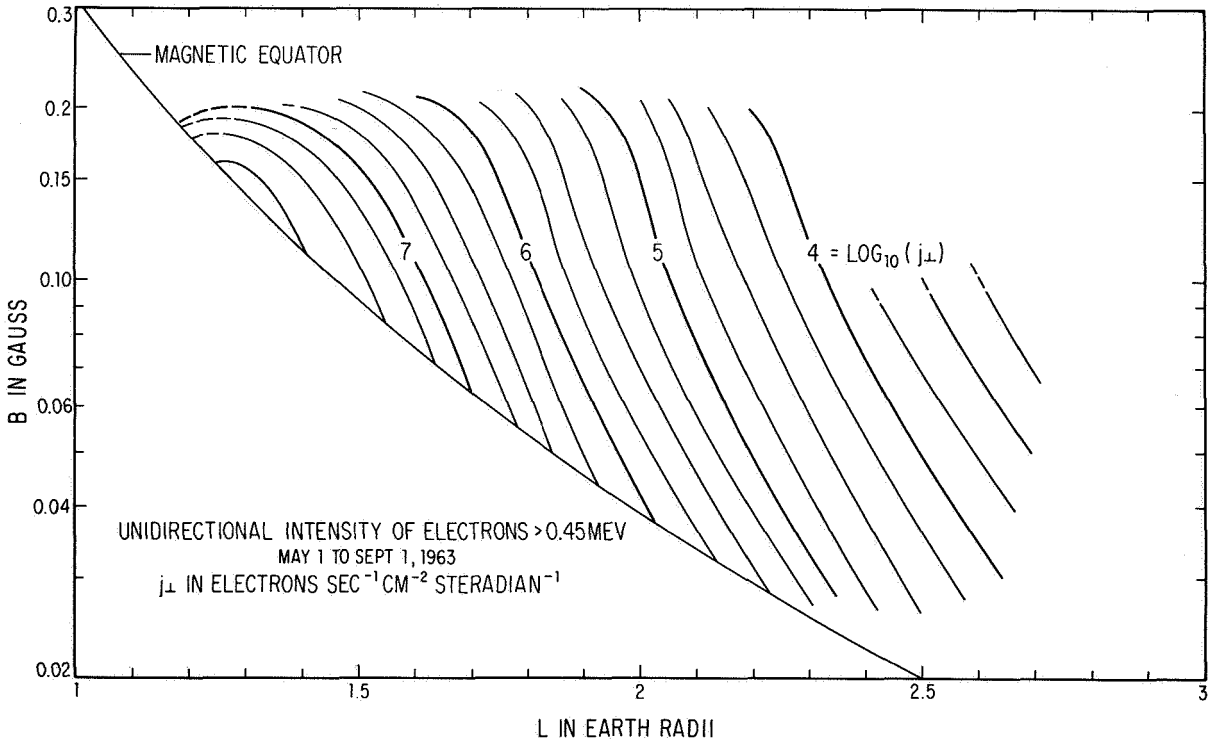


FIGURE 7–12.—Contours of constant intensity.

produced by an electron thereby reducing the efficiency for electrons to about one tenth of the initial value. Since there were no independent measurements of high energy electrons made between February 1 and May 1, 1963, it is possible that the measured decrease of a factor 10 in the electron counting rates may include a factor due to the change in the trapped electron intensities. The Relay II results, when available, can be used to recalibrate the Relay I detector and will therefore remove most of the present uncertainty.

It should be noted that most of the pulses produced by protons in the Relay I detector A remained far larger than the discrimination level. The efficiency for protons can therefore be accurately computed.

At L values greater than 3.0 earth radii, the counting rate due to protons is very small, thereby permitting good measurements of the high energy electrons in the outer zone. The analysis of the complex time and spatial dependences of the outer zone is not yet complete and will therefore be presented in a later paper.

At L values of less than 1.45, over 80 percent of the detector A counting rate is due to electrons. The observed counting rates along several lines of force in this region are shown in the upper part of Figure 7–13. The corresponding contours of constant counting rate in B–L space are shown in the left side of Figure 7–14. For comparison, the contours of constant intensity of electrons with energies greater than 5 Mev as measured by Explorer XV are shown in Figure 7–15. As expected, the contours are very similar in the region $L = 1.25$ to 1.5. In the region $L < 1.25$, there probably has been an appreciable decrease in the high energy electron intensities, but no Relay I data taken in this region after May 1, 1963 is available, so that the reality of this decrease cannot be demonstrated.

PROTON DISTRIBUTIONS

During the period May 1 to September 22 of 1963, over 80 percent of the detector A

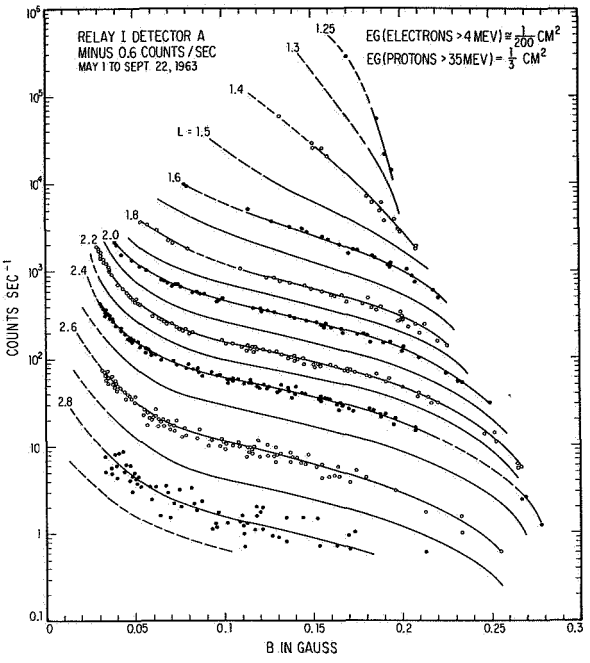


FIGURE 7–13.—Counting rate of the omni-directional detector.

counting rates in the region $L = 1.8$ to 2.8 earth radii were probably due to protons. The efficiency for protons rises rapidly from near zero at 34 Mev and remains constant within a factor of 1.5 between 35 and 300 Mev. Since the flux of protons with energies greater than 300 Mev is relatively small in the region being considered, the detector A counting rates correspond to the total flux of protons with energies greater than 35 Mev. The weighted average value of the efficiency times the geometrical factor is calculated to be 1/3 cm² with a probable error of less than 30 percent. The counting rates along lines of force in this region are shown in the lower part of Figure 7–13. The cosmic ray contribution has been removed by subtracting 0.6 counts per second. The corresponding contours of constant counting rates are shown in the right-hand part of Figure 7–14. These contours are very similar to the contours of 40 to 110 Mev protons measured by Explorer XV*. The differences are well explained by the spatial dependence of the

*McIlwain, C. E., The radiation belts, natural and artificial, Science, *142*, 355–361, 1963.

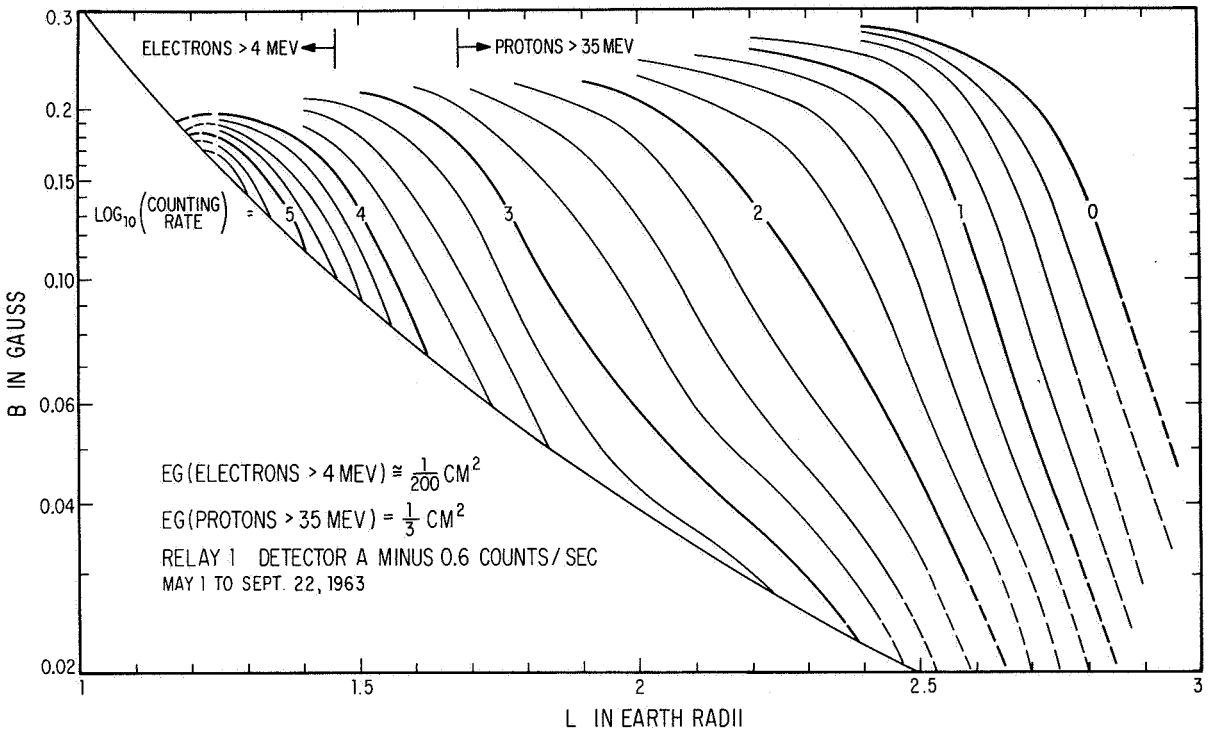


FIGURE 7–14.—Contours of constant counting rate.

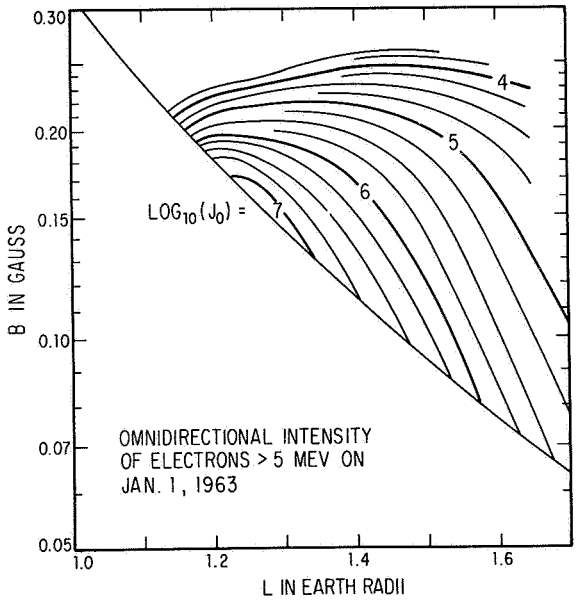


FIGURE 7–15.—Contours of constant omnidirectional intensity of electrons.

proton energy spectrum as measured by the Relay I detector C.

Detector C measures the unidirectional flux of protons in three energy ranges between 18.2 and 63 Mev. The lower two channels C1 and C2 have electron efficiencies of very near zero. The third channel, C3, has a small ($\sim .001$) efficiency for electrons with energies greater than 3 Mev as well as an efficiency of near unity for protons with energies between 35 and 63 Mev. The flux of electrons with energies greater than 3 Mev in the region below $L = 1.5$ are as much as ten thousand times the flux of 35 to 63 Mev protons, therefore the C3 channel does not yield reliable measurements of protons in this region. In the region of $L = 1.5$ to 3.0 earth radii, however, there is little if any interference due to electrons.

The contours of constant intensity of protons with energies between 18.2 and 35 Mev along lines of force as measured by channels

C1 and C2 are shown in Figure 7–16. The radiation damage to solar cells shielded by .4 g/cm² of material on satellites which traverse the region between 1.5 and 2.5 earth radii is primarily due to protons in this energy range.

The electron counting rates in the D4 channel after May 1, 1963 were only about 5 percent of the electron counting rates in the D2 channel. Since the efficiency for protons in the two channels is very nearly the same, the difference between the D2 and D4 channels can be used to estimate the fraction of the D4 counting rate which is due to electrons. Along lines of force between $L = 1.8$ and 2.6 this fraction is observed to be less than 20 percent, so that the counting rate due to protons can be computed with a probable error of less than 10 percent. The unidirectional intensities of protons with energies greater than 5.2 Mev derived in this fashion are shown in Figures 7–17 and 7–18.

The sum of the B1, B2 and B3 channels yields the flux of protons with energies between 1.1 and 14 Mev with little if any unwanted effects due to electrons. The contours of constant unidirectional intensities of these protons are shown in Figure 7–19. Data coverage was rather poor during the time period in which detector B was operating properly, therefore the intensities given in some parts of this figure may be in error by as much as a factor of two. It is expected that a more complete analysis of the available data will reduce the probable error to less than 20 percent. Radiation damage to unshielded solar cells on satellites which traverse the region around 2 earth radii is primarily due to these low energy protons.

A comparison of Figures 7–14, 7–16, 7–18, and 7–19 reveals that the spatial distributions of protons are quite different in the different energy ranges.

The proton energy spectrum is a strong function of L and on some lines of force the

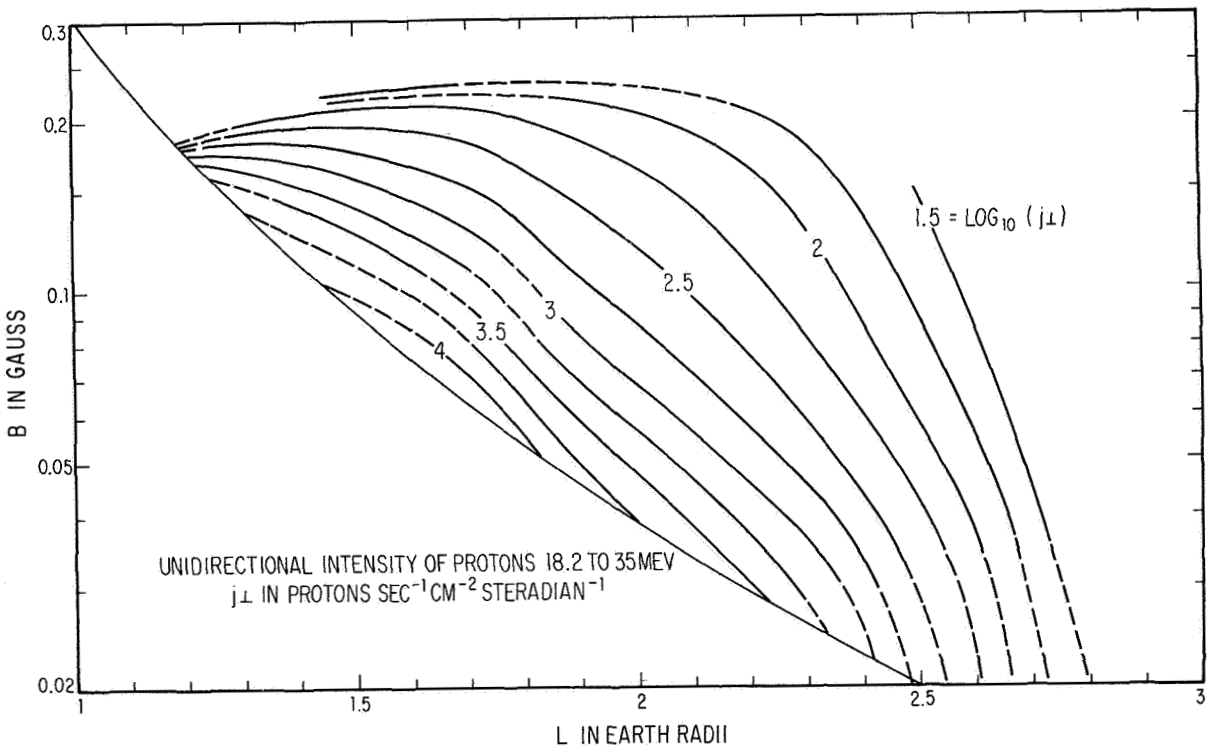


FIGURE 7–16.—Contours of constant unidirectional intensity of protons.

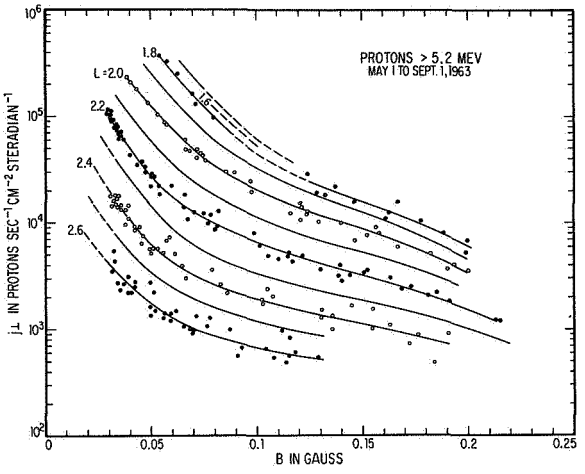


FIGURE 7–17.—Unidirectional intensity of protons.

spectrum varies importantly with B. For all energies along all lines of force, the maximum intensity occurs at the magnetic equator. These maximum intensities for four different energy ranges are shown as a function of L in Figure 7–20. The intensities in the 40 to 110 Mev energy range are derived from the Explorer XV data. Unfortunately, the proton energy spectrum over the full range of 1.1 to 110 Mev cannot be adequately represented by any simple spectral form like a power low or exponential dependence on energy. No one parameter, such as the E_0 previously suggested* has been found with which the spatial dependence of the spectrum can be easily characterized.

Detailed energy spectra can be obtained by using all eight of the channels producing proton data (channels B1, B2, B3, D4, C1, C2, C3, and A). This analysis is not yet complete and will be presented in a future paper.

MAGNETIC STORM EFFECTS

Between 2100 hours UT on September 22 and 0300 hours UT on September 23, the largest fluctuations in the earth's magnetic

*McIlwain, C. E. and G. Pizzella, On the energy spectrum of protons trapped in the earth's inner Van Allen zone, J. Geophys. Res. *68*, 1811–1823, 1963.

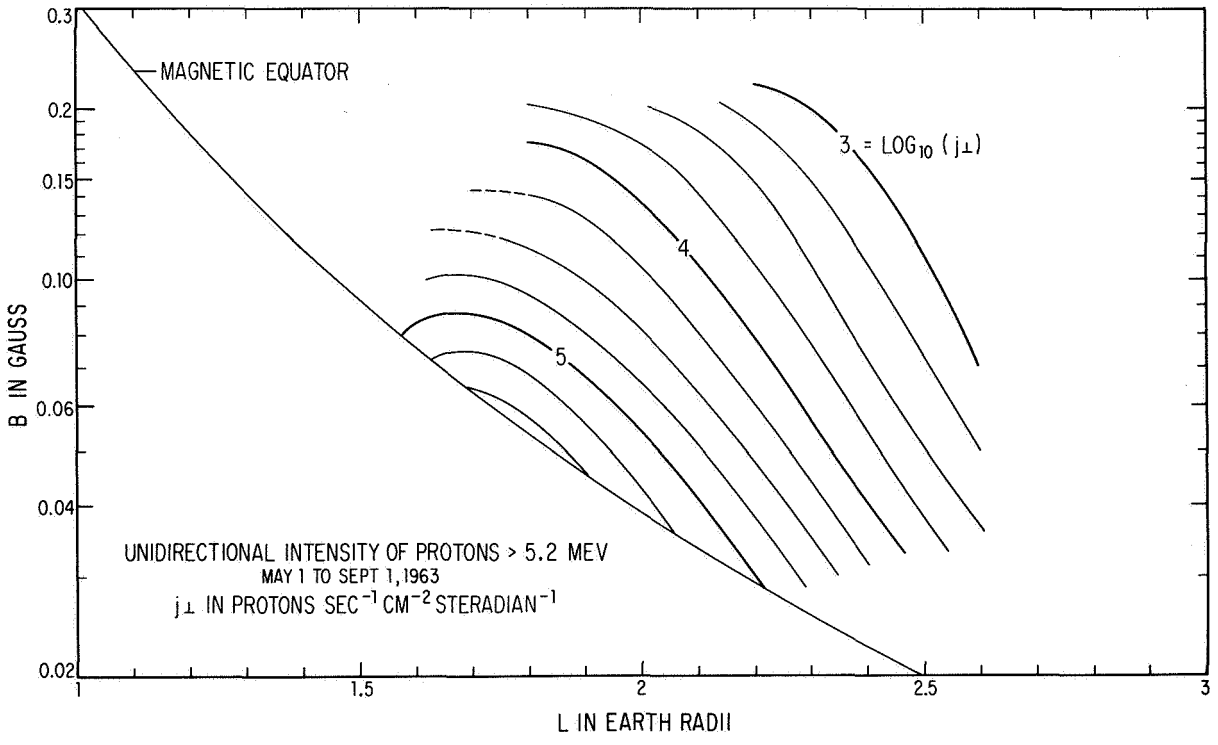


FIGURE 7–18.—Contours of constant intensity.

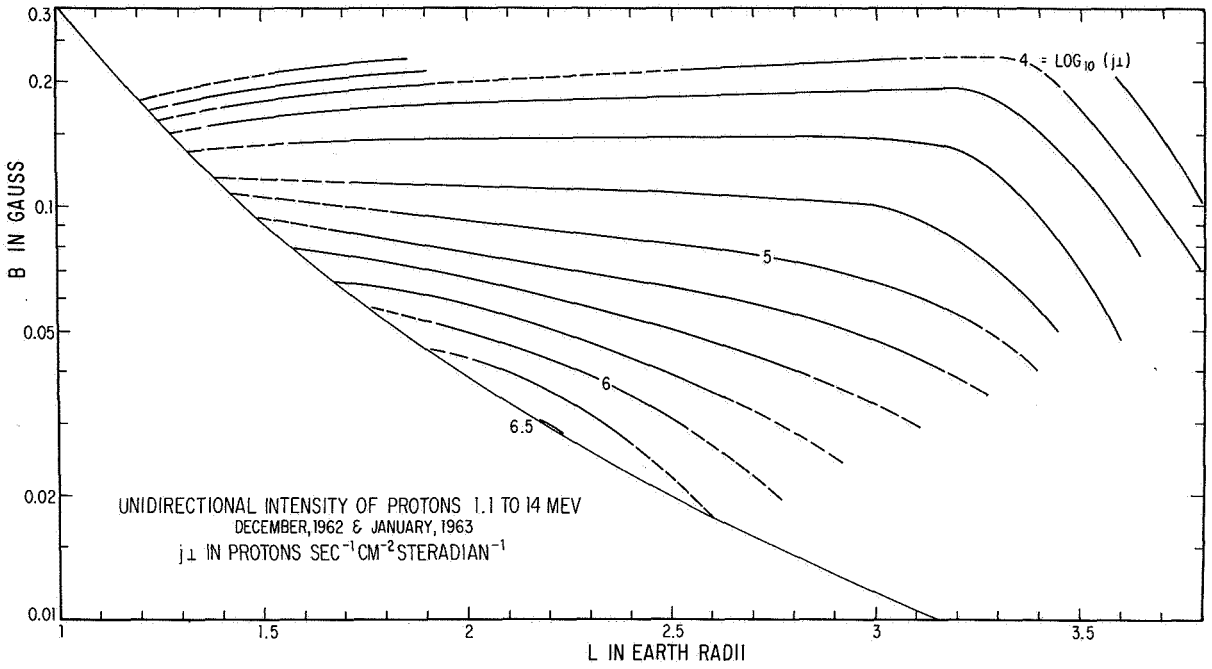


FIGURE 7–19.—Contours of constant unidirectional intensity.

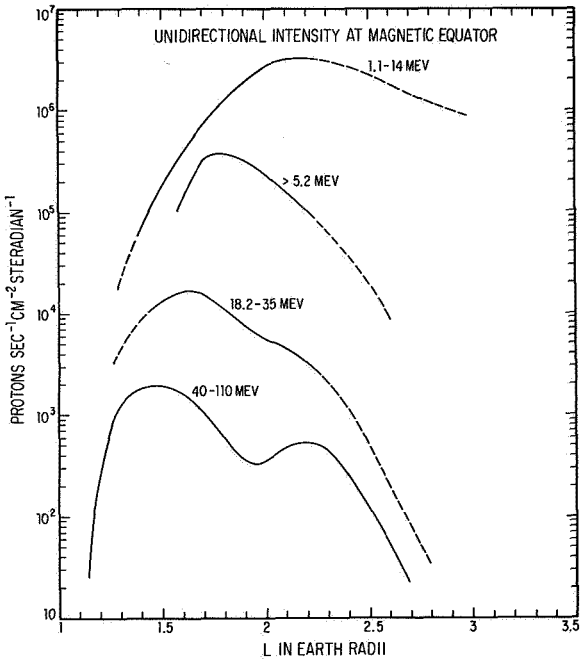


FIGURE 7–20.—Unidirectional intensities perpendicular to the magnetic field as a function of L along the magnetic equator.

field during the year of 1963 occurred. Within almost the same short period of time, the proton distribution measured by detector A underwent a radical change. The new distribution of protons with energies greater than 35 Mev is shown in the right side of Figure 7–21. For comparison, the earlier distribution is shown on the left side. At L values of less than 2.0 no change larger than 10 percent was observed, while outside $L = 2.5$ the intensities typically decreased by over a factor of ten. The earlier distribution had remained stable for many months. Similarily, the new distribution has remained unchanged as of the latest observations which were made late in December 1963.

It seems quite possible that a thorough analysis of this event will reveal the true character of the mechanisms which control the behavior of trapped protons.

Simultaneous with the proton changes, an intense new outer zone of electrons began to form with a peak intensity at $L = 3.2$ earth radii. In addition to the relatively energetic electrons in the outer zone, a high intensity of low energy (less than 0.7 Mev) electrons appeared in a wide region of space. Immediately after the event, the unidirectional intensity of electrons with energies greater than 0.45 Mev at a radial distance of 2.0 earth radii was greater than 3×10^6 sec^{-1} cm^{-2} $steradian^{-1}$ from $L = 4.0$ down to at least $L = 2.0$. Referring to Figure 7–12, the contour corresponding to $\log_{10}(j_\perp) = 6.5$ apparently moved outward by over two earth radii. Unfortunately very little data was taken from the Relay I radiation detectors after this event (except from detector A, which is on continuously) until December by which time the anomalous low energy electron intensities had undergone considerable decreases.

INTEGRATED FLUXES

The Explorer XV data has been used to construct a computer program* which can be used to determine the omnidirectional fluxes of three categories of particles which were present at arbitrary locations in space on January 1, 1963. This program has been used to obtain the total flux of these particles striking the Relay I satellite over 8 complete revolutions (1.02 days) for 40 different days

*McIlwain, C. E., The radiation belts, natural and artificial, Science, *142*, 355–361, 1963.

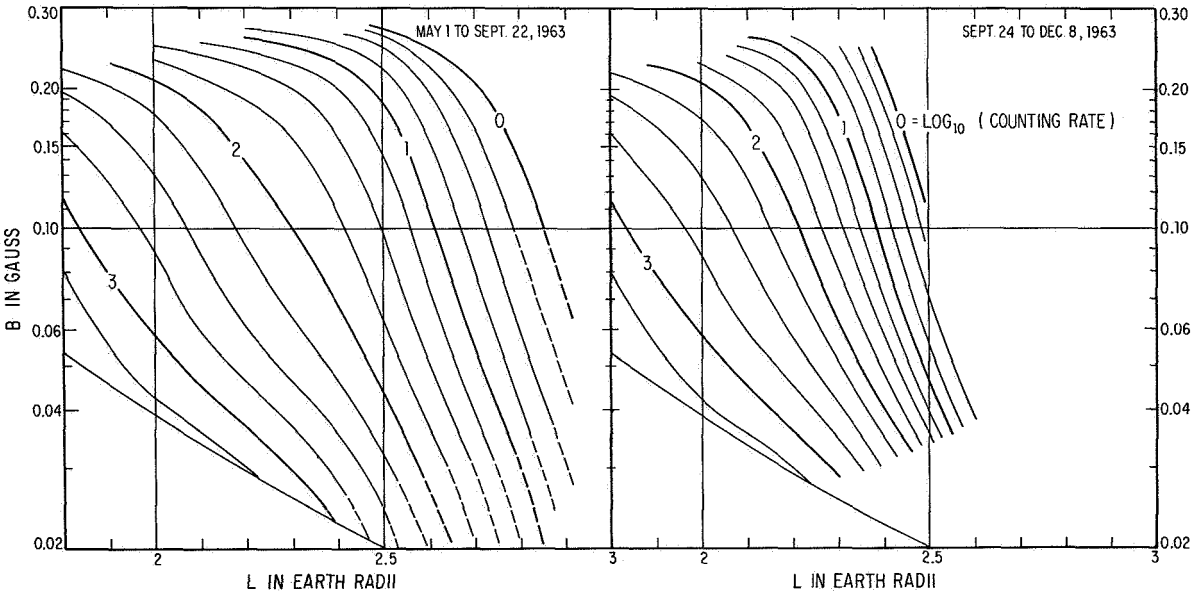


FIGURE 7–21.—Contours of constant counting rates.

listributed throughout 1963. An examination of these results reveals two important facts: (1) the total flux per day varies smoothly from day to day, (2) the total flux per day for each category of particles is a unique function of the latitude of perigee (assuming no changes of particle intensities with time). The dependence of the daily fluxes of particles upon the latitude of perigee, shown in Figure 7–22, can therefore be used (along with the known variation of the latitude of perigee with time) to determine the daily fluxes as a function of time as is shown in Figure 7–23. The relative differences in the curves are of course due to the different spatial distributions of the particles. It is interesting to note that the daily fluxes of protons with energies greater than 1.1 Mev would be peaked at the times that the daily fluxes 40 to 110 Mev protons are a minimum.

Data from a detector on the INJUN 3* indicates that the flux of 40 to 110 Mev protons did not vary importantly during the first eight months of 1963 and the Relay I data indicates that the daily fluxes of electrons were no more than a factor of three

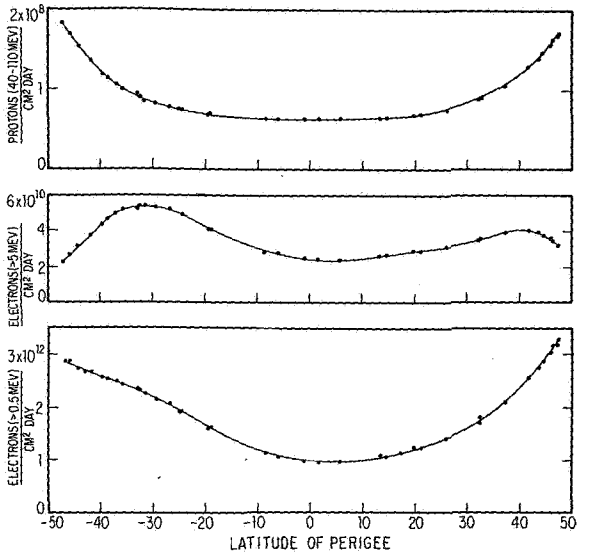


FIGURE 7–22.—Total omnidirectional fluxes of several categories of trapped radiation.

*Valerio, John, Protons from 40 to 110 Mev observed on Injun 3, J. Geophys. Research *69*, No. 23, 4949–4958.

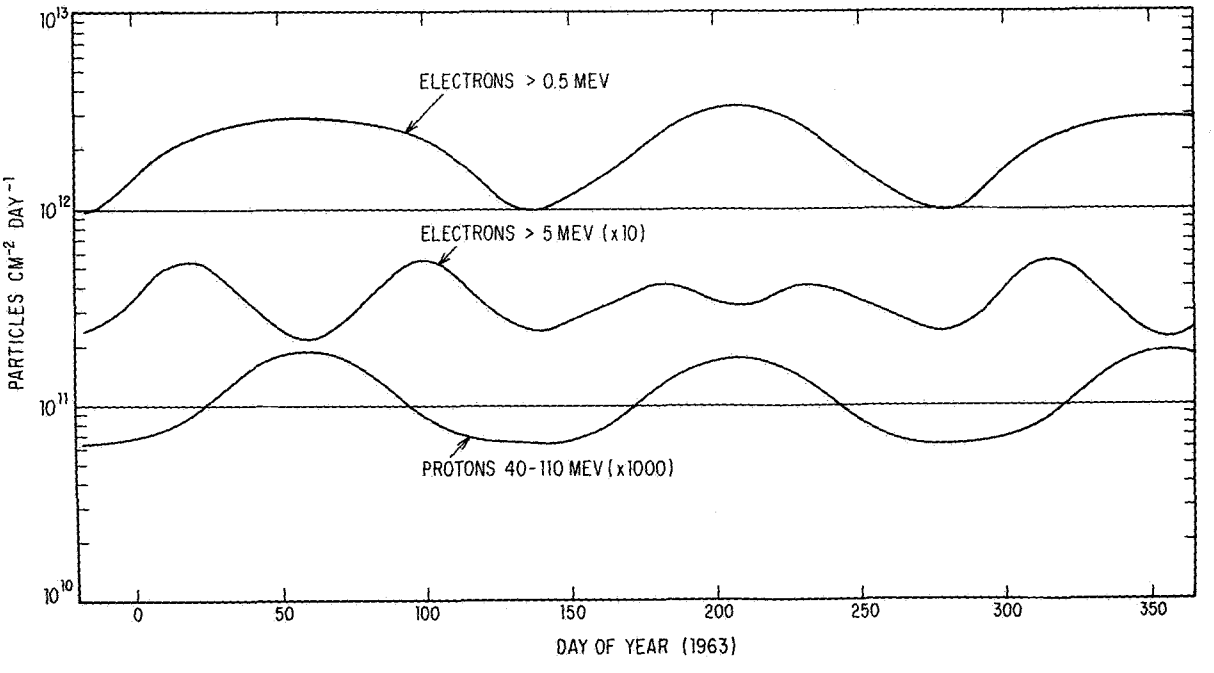


FIGURE 7–23.—Daily average omnidirectional intensities vs. time.

lower at the end of 1963 than at the time of the Explorer XV measurements.

The curves in Figure 7–23 have been integrated over the first year after the launch of Relay I. The resulting average fluxes per day were found to be:

(1) $(2.1^{+.3}_{-.8}) \times 10^{12}$ electrons ($E > 0.5$ Mev) $cm^{-2}\,day^{-1}$

(2) $(3.6^{+.4}_{-1.7}) \times 10^{10}$ electrons ($E > 5$ Mev) $cm^{-2}\,day^{-1}$

(3) $(1.07 \pm .15) \times 10^{8}$ protons ($E = 40$ to 110 Mev) $cm^{-2}\,day^{-1}$

where the error limits correspond to the sum of all possible errors and the maximum possible changes in the particle intensities allowed by the Relay I measurements.

Since the solar cells making up the Relay I power plant were shielded by about 0.4 g/cm² of quartz, which can be penetrated by protons with energies greater than about 17 Mev, it is of interest to anticipate the result of a proper integration of the data obtained by detector C. A comparison of the bottom two curves of Figure 7–20 and similar curves for other latitudes leads to the estimate that the average flux of proton with energies greater than 18.2 Mev is a factor of 10 ± 2.5 larger than the average flux of 40 to 110 Mev protons. This flux of $(1.1 \pm .3) \times 10^{9}$ protons ($E > 18.2$ Mev) $cm^{-2}day^{-1}$ appears to be adequate to produce the observed solar cell radiation damage (Waddel, private communication). For n on-p solar cells this average omnidirectiona flux of protons produces radiation damag equivalent* to a beam of one Mev electron at normal incidence with a flux of $(2.0 \pm .6) \times 10^{12}$ $cm^{-2}day^{-1}$. By comparison, the average electron spectrum implied by the data above, when weighted by the energy dependence of the electron damage to n-on-p type solar cells under 0.4 g/cm² of quartz* indicates that the average damage due to electrons was equivalent to a beam of only $(0.6 \pm .4) \times 10^{12}$ one Mev electrons cm^{-2}-day^{-1}. These calculations therefore indicate that three quarters (.77 ± .17) of the damage to the solar cells protected by 0.4 g/cm² of quartz was probably produced by protons. The measured energy spectra of electrons and protons are such that as the shielding is reduced below 0.4 g/cm² the fraction of the damage produced by protons rapidly approaches unity.

Detector A is connected to a large register which is not reset after each reading and which accumulates $2^{29} = 5.37 \times 10^{8}$ counts before overflowing. The counts in this register can therefore be used to determine the total number of detector A counts per day. Some 300 measurements of this kind are show in Figure 7–24. Since the detector was

*Brown, W. L., J. D. Gabbe, and W. Rosenzweig, Results of the Telstar radiation experiments, Bell Syst. Tech. J., *92*, Nov. 4, part 2, 1505–1957, 1963.

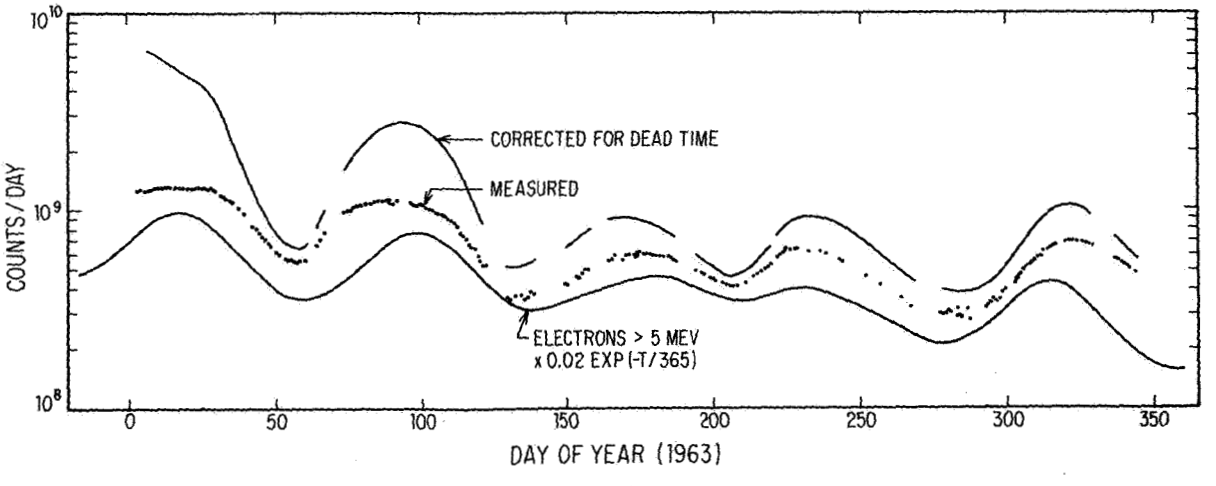


FIGURE 7–24.—Total counts per day registered by detector A.

not designed to properly measure the high intensities of artificially injected electrons, the dead time corrections necessary are relatively large. The average correction factor for a day's accumulation of counts depends upon how the counts were obtained. For example, a given number of counts obtained in a short time requires a larger correction factor than the same number of counts obtained in a longer period of time. The detailed rates of accumulation as predicted by the Explorer XV data has been used to calculate the desired average correction factor in a manner which is relatively independent of the variations in the detector A efficiency with time. The resulting calculated values for the true number of counts per day is shown in the upper curve of Figure 7–24. Except for the times where the number of counts per day exceeds 1.5×10^9, this curve is probably accurate to within 15 percent. For comparison, the computed intensity of electrons greater than 5 Mev (see Figure 7–23) multiplied by $0.02 \times \exp$ (—day of year/365) is shown in the bottom curve. After day 121 (May 1) it can be seen that the number of true counts per day was slowly decreasing but with a time constant of greater than one year. Since these daily counting rates are largely due to electrons it must be remembered that after May 1, the effective discrimination level was in a region of the electron pulse height distribution where a 2 percent change in discrimination level would produce a change in counting rate of at least 10 percent and probably about 20 percent. The apparent decrease in the daily number of counts can therefore be used only to indicate that there was no large change (i.e., larger than a factor of two) in the high energy electron fluxes between May 1 and December 10, 1963 and to indicate that the effective gain of the detector has been relatively stable since May 1, 1963.

SUMMARY

The highest electron intensities are found around the magnetic equator at radial distances between 1.2 and 1.6 earth radii. The Relay I data shows that intensities measured earlier in this region by Explorer XV persisted throughout the year of 1963 and did not decay by more than a factor of three.

The spatial distribution of protons in four different energy ranges has been determined and found to depend strongly upon energy. The proton intensities at L values greater than 2.0 earth radii were observed to decrease during a large magnetic storm. At all other times the proton fluxes exhibited no important changes with time.

The integrated fluxes of various particle types along the Relay I orbit have been computed and are found to be adequate to explain the observed degradation of solar cells.

AUTHORS. *This chapter was written by* C. E. MCILWAIN, R. W. FILLIUS, J. VALERIO, *and* A. DAVE *of the University of California (San Diego), LaJolla, California, U.S.A. under contract NASr–116 from NASA Headquarters.*

N66-10246

Chapter 8

The Relay I Radiation Effects Experiment

10246

Solar cells on Relay I were monitored for radiation damage by measurement of short circuit current. The orbit was 1321 km perigee, 7439 km apogee, 47.5 degrees inclination. Unshielded N/P, P/N, and gallium arsenide cells degraded in 10 days to 52%, 28%, and 18%, respectively. This damage is ascribed to low energy protons. At 300 days silicon N/P and P/N cells, shielded with 30 mils of fused silica, had degraded to 73% and 53%, respectively. At 300 days silicon N/P and P/N cells, shielded with 60 mils of fused silica, had degraded to 80% and 61%, respectively. Available space flux maps predicted somewhat greater damage to the heavily shielded cells, from either electrons or high energy protons, than that observed. The minority carrier lifetime of some 1N645 silicon diodes declined to 50% in about 45 days.

INTRODUCTION

Objectives

Numerous experiments have shown the presence of energetic electrons and protons trapped by the earth's magnetic field at high altitudes. The center of the "inner belt" of such particles is at an altitude of about 0.5 earth radii, over the magnetic equator. These electrons and protons damage semiconductor devices directly, and through the x-rays generated when the electrons are decelerated. Solar cells, widely used on spacecraft to convert sunlight to electric power, are particularly vulnerable. To function they must be situated in exposed positions and they can be shielded by only moderate amounts of transparent materials.

It is, therefore, of considerable interest to observe the radiation damage sustained by various types of solar cells with various shields, on an orbiting body. Such experiments provide direct empirical engineering information, useful in the design of solar power supplies for satellites with similar orbits. Further, they allow a test of the state-of-the-art through comparison of observed damage and that predicted from laboratory damage studies and a knowledge of the character of the trapped particles.

It is the purpose of this report to describe such a satellite radiation damage experiment, to compare the results with predictions based on various information sources and with other satellite damage experiments.

Orbit Parameters

The Relay satellite was launched from Cape Kennedy on 1962^{y}, 347^{d}, 23^{h}, 30^{m}, 01^{s} GMT. It carried wideband relay communications equipment, radiation measuring devices, and the radiation effects experiment

herein reported. Final stage burnout and nominal injection in orbit occurred on 1962^{y}, 347^{d}, 23^{h}, 49^{m}, 06^{s} GMT. For convenience in this report the zero for "time in orbit" has been taken as 1962^{y}, 348^{d}, 00^{h}, 00^{m}, 00^{s}. It is believed that no significant radiation damage effects occured before this time.

Table 8–1 shows some of the orbit characteristics. It is seen that perigee and apogee are such that the spacecraft is subjected to the radiations of the "inner belt."

TABLE 8–1.—*Orbit Parameters of Relay I*

Apogee	=7439 KM
	=4001 NM
	=1.17 R_e
Perigee	=1321 KM
	=713 NM
	=0.21 R_e
Inclination	=47.5 degrees
Period	=185.1 minutes
	=3.085 hours
Eccentricity	=0.285
Maximum latitude	=47.62 degrees

APPARATUS

The satellite devices concerned with the radiation effects experiment are the radiation damage panel, the radiation effects circuitry box, and the solar aspect indicator.

Radiation Damage Panel

The devices subjected to radiation damage are listed in Table 8–2. They were mounted on the surface of a "damage panel" attached to the skin of the satellite. The panel "looked" perpendicularly to the spin axis.

TABLE 8–2.—*Radiation Damage Sensors*

Device	No.	Type	Shield, mils
Solar Cell	3	P/N	0
" "	3	P/N	30
" "	3	P/N	60
" "	3	N/P	0
" "	3	N/P	30
" "	3	N/P	60
" "	3	REV	0
" "	3	REV	30
" "	3	REV	60
" "	3	GaAs	0
Diode	6	1N645	0

Four types of solar cells bearing shields of three thicknesses were used. Also, measurements were made in triplicate.

The diodes used were IN645 silicon diodes, manufactured by the Texas Instrument Company. They were diffused power rectifiers with a peak inverse rating of 225 volts and an average forward current of 400 ma. The glass envelope constitutes a shield of about 20 mils thickness. This diode type has been widely used in exposed positions on solar panels as a reverse current blocking device. It also happens to have a relatively long minority carrier lifetime, which simplified the associated circuitry. The diodes used were selected for long carrier lifetime, which, initially ranged from 11.5 to 16.5 microseconds.

As shown in Figure 8–1, the solar cells and diodes were mounted on a 4.0 inch by 5.3 inch by 1/8 inch aluminum panel, for temperature uniformity. Eight thermistors were imbedded in the panel for temperature determination, since both solar cell and diode responses were temperature sensitive. An enclosure attached to the back of the panel carried the solar cell load resistors and circuitry for energizing the thermistors and for providing a mid-scale calibration signal of 100 mv.

The solar cells were insulated from the panel. The shields were of Corning Type 7940 clear fused silica, of density 2.20 grams per cm^2. This shield material, and the proprietary transparent adhesive, are very resistant to darkening under irradiation.

Silicon solar cells of the P/N (P on N) and N/P types carried on the damage panel have been widely used in satellite solar power supplies. The gallium arsenide cells are not considered commercially available yet but, on a theoretical basis, have shown promise of high efficiency and high radiation damage resistance.

The "REV" (for "reversed") cells of Table 8–2 were devised and included in order to have some cells on board that were particularly susceptible to radiation damage, since an uncertainty of several orders of

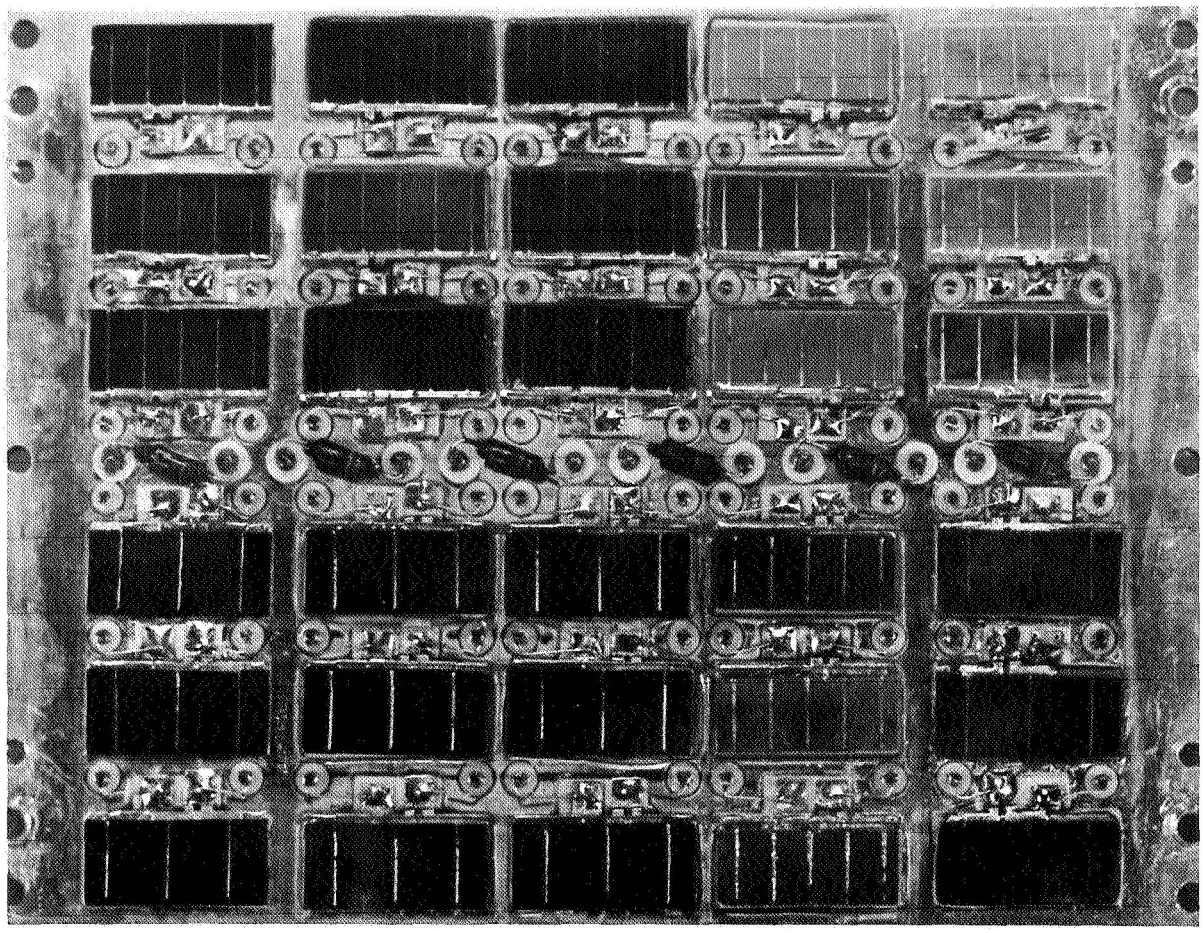


FIGURE 8–1.—Radiation damage panel, front.

magnitude existed in the damage effects to be expected in orbit. These cells were of silicon, with a front (illuminated) layer about one diffusion length thick. On theoretical grounds, such a cell, while of low efficiency, should be susceptible to damage. This is because radiation damage shortens minority carrier lifetime and diffusion length, leaving carrier pairs generated near the surface (by photon absorption) at a distance from the junction greater than a diffusion length, and therefore unavailable externally.

In order that cells of a given type be uniform in characteristics, they were cut from the same crystal ingot and processed together. They were then further selected for uniformity on a basis of spectral response and efficiency. It is believed that the silicon P/N and N/P cells used are representative of the central part of the distribution of commercial cells of these types. Both were of nominal 1 ohm-cm base resistivity.

The condition of the solar cells was judged by noting the currents furnished to low resistance loads. The use of short circuit current in evaluating radiation damage is common. However, some laboratory damage experiments have shown that such a measurement does not always accurately reflect the power generating capability of some types of cells after damage by low energy radiations.

The load resistors were individually adjusted for each cell to give an expected output of 160 mv under normal space illumination.

The damage panel weighed 1.02 pounds, occupied 15.7 cubic inches, and required 0.54 watts.

Radiation Effects Circuitry

Figure 8–2 shows a block diagram of the circuitry used in determining the minority carrier lifetime of IN645 diodes by the "injection-extraction" method.* Radiation damage to a semi-conductor diode reduces

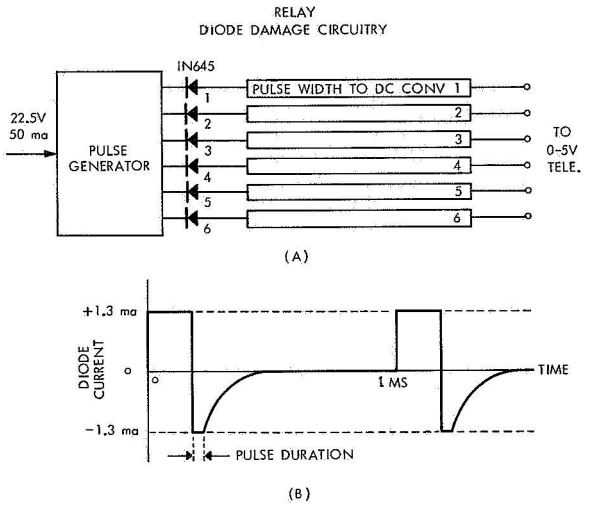


FIGURE 8–2.—Radiation effects circuitry.

this lifetime and causes an associated deterioration in both forward and reverse conduction characteristics. As indicated by the waveform in Figure 8–2, the circuitry periodically establishes forward conduction at 1.3 ma in the diodes. This is followed by the application of a reverse voltage of such value and at such impedance level that the characteristic flat-topped reverse current transient is also 1.3 ma. The duration of the flat-topped pulse is proportional to minority carrier lifetime. When forward and reverse currents are equal the lifetime is very nearly four times the pulse duration. As indicated by Figure 8–2, the diode circuitry, after supplying the forward and reverse conduction conditions, provides an analog telemetry signal proportional to the pulse duration. This circuitry weighed 1.4 pounds, occupied 67.5 cubic inches, and required 1.15 watts.

Solar Aspect Indicator

The condition of the experimental solar cells is judged by measuring their short circuit current under some standard environmental condition. The standard illumination source here is the sun, at normal incidence and at its mean distance from the Earth. The actual angle of incidence is measured by a solar aspect indicator, whose readings are later used to correct the outputs from the solar cells to normal illumination, using correction data determined in the laboratory. In obtaining this aspect calibration information, the sun was used as a source, sky-light being excluded by a 6-foot collimator.

A photograph of the aspect sensor is shown as Figure 8–3. In principle, it consisted of an arrangement of narrow slits and

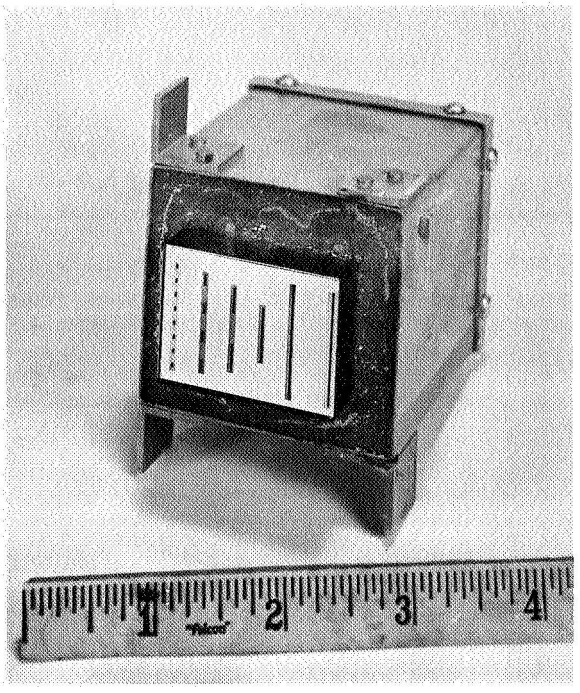


FIGURE 8–3.—Solar aspect indicator.

*Lax, Benjamin, and Neustadter, S. F., "Transient Response of a p–n Junction," J. Applied Physics 25 (9): 1148–1154, September, 1954.

associated light sensitive photo-resistors. At a given angle of illumination a unique combination of photo-resistors was energized.* These controlled six flip-flops whose states indicated, through a six bit binary word in the Gray code, the solar aspect angle. The angular resolution was about 3 degrees, and the range was from plus 80 to minus 80 degrees. The weight was 0.52 pounds, the volume was 16.8 cubic inches, and the power requirement was 0.075 watts.

RESULTS

Telemetry and Data Processing

The data concerning the radiation effects apparatus and other satellite-bourne devices was transmitted to ground by a 9 bit word PCM telemetry system that would accept digital inputs (as from the aspect sensor), zero to 5 volt analog signals (as from the thermistors), and zero to 200 millivolt analog signals (as from the solar cells). The word rate was 128 per second. This allowed 100 successive samplings of a given solar cell in 100/128 second. Because of the satellite spin rate at least two maxima in the solar cell output were observable in this interval. These maxima, when corrected to zero solar aspect angle, to mean solar distance, and to 25°C, indicated the condition of the solar cell.

The aspect angle variations are shown in Figure 8–4. This angle never exceeded 11 degrees. The associated solar cell corrections were not greater than 2 percent. Temperatures at times when data was taken ranged from 2°C to 28°C. The maximum associated cell correction was less than 3 percent for most of the cells. The maximum correction for solar distance was about 3.5 percent.

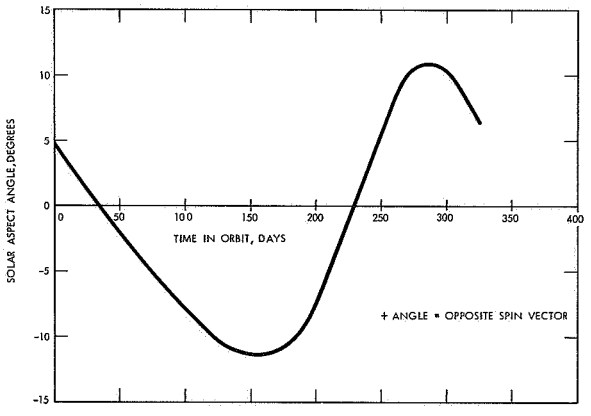


FIGURE 8–4.—Relay I solar aspect vs. time.

A suitable computer program selected the maximum value (during spacecraft spin) of a cell output from the telemetry recording and corrected it for telemetry zero shift, telemetry gain change, cell temperature, aspect angle, and solar distance. Six such responses of a given cell were read from the printed record, normalized with respect to the initial undamaged value, averaged, and then averaged with the results from the other two cells of the same type and shield. Thus, each final data point for a given cell type at a given time represents 18 observations.

The telemetered voltage signals from the six diodes on the damage panel were corrected for telemetry and temperature effects, converted to pulse length through a somewhat non-linear calibration function, and normalized with respect to initial undamaged values.

Solar Cell Damage

Tables 8–3, 8–4, and 8–5 show relatively raw data from some of the solar cells to indicate the consistency of the results. It is evident that the three cells of a given type and shield deteriorated, in general, in a similar way. Exceptions are the N/P, 60 (N on P, 60 mils shield) cell 17 which suffered a catastrophic drop in output, between 45 and 49 days in orbit. The data from this cell was not used in computing the average behavior of the N/P, 60 cells after this sudden change in characteristics. The gallium arsenide cell 29 had a low initial output but degraded in a regular manner.

Figure 8–5 shows the normalized, corrected short circuit current signals from the

*Albus, J. S., and Schaefer, D. H., "Satellite Attitude Determination: Digital Sensing and On-Board Processing," NASA–GSFC Document X–631–63–133, July, 1963.

TABLE 8–3.—*P/N Silicon Solar Cell Load Voltages for Various Times*

Orbit time (days)	Cell 1 P/N, 0 (mv)	Cell 2 P/N, 0 (mv)	Cell 3 P/N, 0 (mv)	Cell 7 P/N, 0 (mv)	Cell 8 P/N, 0 (mv)	Cell 9 P/N, 0 (mv)
0.020	164	158	157	161	160	159
0.083	107	103	103	159	158	158
0.185	94	89	90	157	157	157
0.448	72	72	72	160	161	161
0.860	68	65	65	159	159	159
12.8	43	41	42	133	136	136
45.5	39	37	38	117	122	121
93.0	36	34	34	106	111	109
148.	33	31	31	101	104	103
312.	26	24	25	93	98	96

TABLE 8–4.—*N/P Silicon Solar Cell Load Voltages for Various Times*

Orbit time (days)	Cell 10 N/P, 0 (mv)	Cell 11 N/P, 0 (mv)	Cell 12 N/P, 0 (mv)	Cell 16 N/P, 60 (mv)	Cell 17 N/P, 60 (mv)	Cell 18 N/P, 60 (mv)
0.020	160	163	174	166	163	169
0.083	148	146	157	165	161	167
0.185	142	140	150	164	161	166
0.448	117	115	124	162	160	164
0.860	106	103	111	161	156	163
12.8	85	80	88	158	155	161
45.5	59	62	65	152	149	153
93.	42	46	47	143	8	145
148.	25	28	27	139	7	140
312.	13	15	17	131	3	134

TABLE 8–5.—*Gallium Arsenide Solar Cell Load Voltages for Various Times*

Orbit time (days)	Cell 28 GaAs, 0 (mv)	Cell 29 GaAs, 0 (mv)	Cell 30 GaAs, 0 (mv)
0.020	160	95	159
0.083	144	87	137
0.185	130	82	121
0.448	111	73	102
0.860	85	63	71
12.8	22	26	20
45.5	25	24	21
93.	22	18	16
148.	16	13	12
312.	2	2	2

silicon and gallium arsenide cells as a function of time in the log-linear coordinates often used in this field. The uncertainty bars are plus and minus one percent of full scale in length, and the curves, in general, can be passed through the bars without effort. Certain features invite comment.

The damage plateaus shown by the shielded cells from about 70 to 100 days are very probably real. The steep drop in the N/P, 0 cells around 135 days was present in all three cells of this type, and must be real. The early data for the unshielded cells show that they suffered large damage during the first orbit (an orbit is about 0.13 days). Gaps in the data are due to the satellite being out of range of the ground stations, or the experiment not being commanded ON. The gap between 1 and 12 days is due to satellite malfunction. Lacking data, the curves be-

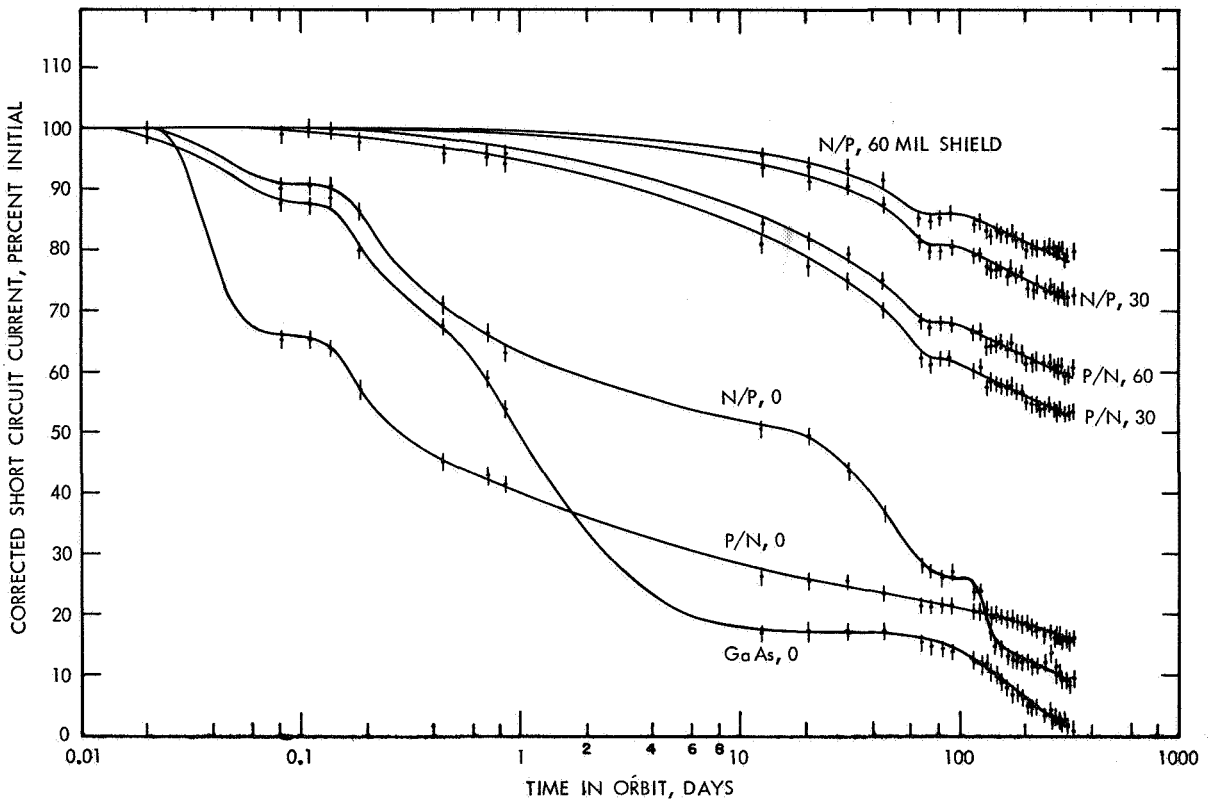


FIGURE 8–5.—Response of silicon and gallium arsenide cells vs. log time.

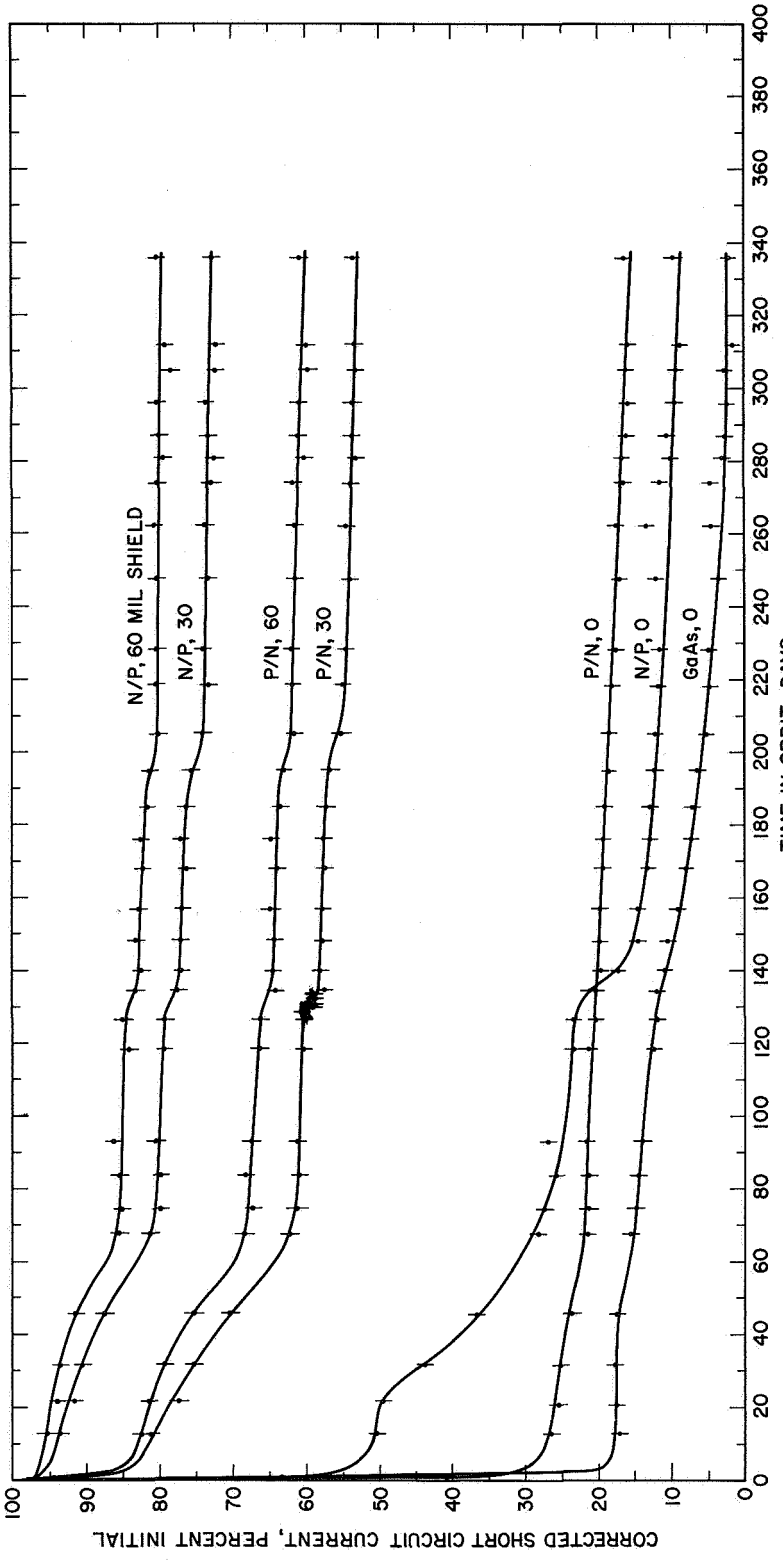


FIGURE 8-6.—Response of silicon and gallium arsenide cells vs. time.

tween 0.02 and 0.8 days, and between 0.9 days and 13 days are simply drawn in a smooth, but arbitrary, manner.

Figure 8–6 shows the same information as Figure 8–5 but on a linear time scale. The curves of this Figure are drawn closer to the data points than they were in Figure 8–5. There is a strong suggestion of damage steps for the shielded cells near 130 days, confirmed by the additional data for the P/N, 30 cells near this time. Another apparent step occurs near 200 days. A non-uniform irradiation rate is indicated.

Table 8–6 shows numerical values of the relative responses from the silicon and gallium arsenide cells at various times. Some interpolation and extrapolation is here necessary. Values less certain are in parentheses.

Table 8–7 shows the orbit times at which various types of cells fell to given response levels. Again parentheses indicate less certain values. The 75 percent level is of particular interest, since the associated particle fluxes or orbit times have been widely used in comparing solar cells. In any event, the non-uniform irradiation rates make time only an approximate measure of total irradiation, especially for the bare cells during the first day. However, all cells were subjected to the same flux with a high degree of uniformity, so that cells can be compared at given times with considerable confidence, especially if the observation is made at or near a data-taking time.

Figure 8–7 shows the results obtained from the "reversed," presumably highly susceptible solar cells. Their behavior is obviously anomalous. They show initial increases in relative response before they eventually fall. The responses suggest that there is an "annealing" action by some

TABLE 8–6.—*Percent Initial Short Circuit Current for Various Solar Cells at Given Times*

Orbit time (days)	P/N, 0 (%)	P/N, 30 (%)	P/N, 60 (%)	N/P, 0 (%)	NP/, 30 (%)	N/P, 60 (%)	GaAs, 0 (%)
0.01	100	100	100	100	100	100	100
0.03	95	100	100	98	100	100	96
0.1	66	100	100	91	100	100	98
0.3	(49)	98	99	(76)	100	100	(72)
1.	40	95	96	63	99	99	50
3.	(34)	(90)	(93)	(57)	(97)	(98)	(27)
10.	28	84	87	52	95	96	18
30.	25	76	79	45	91	94	18
100.	21	61	67	25	80	85	15
300.	16	53	61	9	73	70	2
1000.	(9)	(45)	(51)	(0)	(66)	(70)	(0)

TABLE 8–7.—*Times in Orbit at Which Various Solar Cells Fell to Given Percent Initial Values*

Output (%)	P/N, 0 (days)	P/N, 30 (days)	P/N, 60 (days)	N/P, 0 (days)	N/P, 30 (days)	N/P, 60 (days)	GaAs, 0 (days)
90	(0.033)	(3.2)	(5.7)	0.14	34	50	(0.06
75	(0.044)	32	47	0.33	197	(480)	0.25
60	0.17	128	300	(1.6)	(1800)	(4000)	0.66
50	(0.28)	(470)	(1200)	17	(7200)	(18000)	1

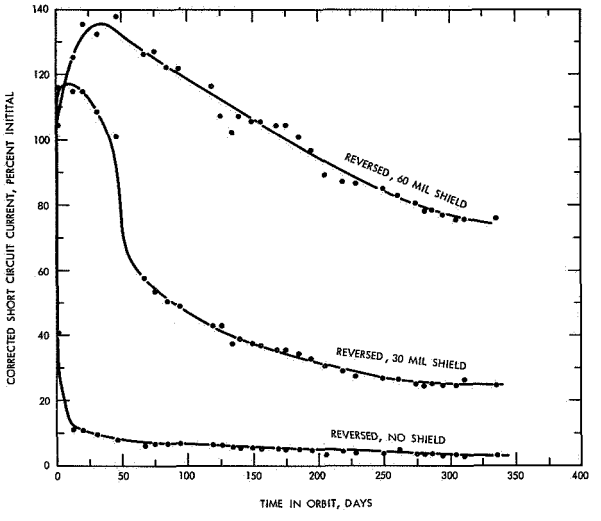


FIGURE 8–7.—Response of reversed cells vs. time.

aspect of the environment which is finally overpowered by a damage mechanism which is retarded, as shown, by the shields of increasing thickness. In any event, these cells hardly served their intended purpose.

Diodes

The normalized diode pulse length (or minority carrier lifetime) versus time is shown in Figure 8–8 for several of the diodes, together with the responses from the P/N, 0 and P/N, 60 solar cells. Curves for several of the diodes are not shown because they are practically identical with those given in Figure 8–8. While the diode data is limited in amount and in dynamic range, an initial steep damage rate, intermediate between the P/N, 0 and P/N, 60 solar cells, is evident.

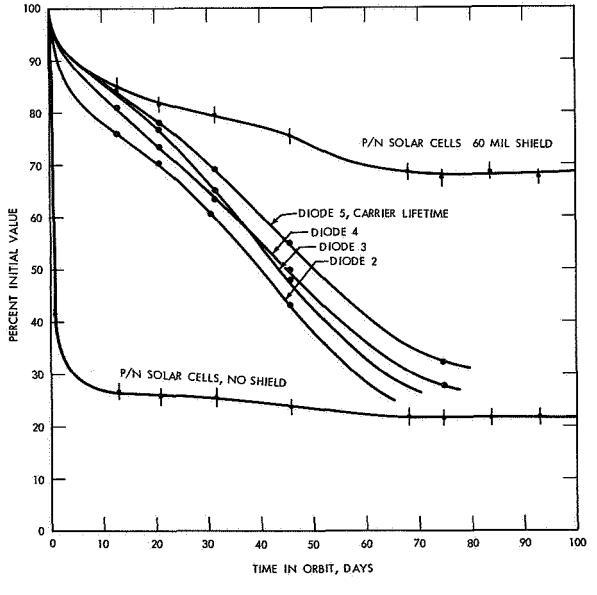


FIGURE 8–8.—Diode carrier lifetime vs. time.

DISCUSSION

Merits of Various Cell Types

Figure 8–5 and 8–6 indicate that the order of merit of the shielded cells is N/P, higher, and P/N, lower. The unshielded cells, judged while their relative responses are above 50 percent, have the order N/P, GaAs, and P/N. It must be remembered that this comparison, and others to follow, is influenced by the character of the radiations present in the Relay orbit.

It may be determined from Figures 8–5 and 8–6 that the N/P, 60 cells last 10 times longer than the P/N, 60 cells, when judged at the 75 percent level. Further, the N/P, 30 cells last 5.9 times longer than the P/N, 30 cells. The degradation of the bare cells is so rapid and the early irradiation rate is so non-uniform that making numerical comparisons among them is scarcely meaningful. It is apparent that the N/P, 0 and the GaAs, 0 cells behave quite similarly down to the 70 percent level, with several odd changes in order of merit among the bare cells at large degradations. The GaAs cells do not show the expected superiority over silicon cells under the conditions of this experiment, using bare cells and short circuit current as a measure of merit.

Merits of Shields

Figures 8–5 and 8–6 show, at the 75 percent response level, that the N/P, 60 cells last about 2.3 times longer than the N/P, 30 cells. The P/N, 60 cells last about 1.4 times longer than the P/N, 30. Thus, for both types, doubling the weight of shield material (which contributes materially to the total spacecraft weight) only extends life (at the

75 percent level) by about 2 times. This same life extension could be attained by using an additional 5 percent of the less heavily shielded cells.

The useful lifetime of the unshielded cells its so short as to prohibit their use in spacecraft in this type of orbit. It is apparent that even a 30 mil shield increases the useful lifetime of the bare silicon cells by a factor of about 600.

Solar Cell Damage Predictions

Prediction Methods

Damage to solar cells by trapped radiations may be predicted by various methods. The empirical approach is to examine the literature to find a spacecraft whose orbit is similar to the one of interest and to determine the radiation damage it sustained, either in its main solar cell power supply or in some damage experiment like that reported here. This method is necessarily approximate.

Another approach that might be attempted would be to fully determine the character of the semiconductor materials of the type of solar cell of interest, the nature of any shield, and the character of the radiations to be encountered in orbit. The damage contributed by each component of the radiation would then be calculated from fundamental physical principles and the power output at, say, the end of a given time in orbit would be determined.

This method would require a detailed space map of particle type, intensity, energy distribution, and angular distribution, with allowance for possible variations with time. Such maps are being built up, but the accuracy claims are still very modest. Also required would be a method of calculating how the shield material alters the radiation in intensity, energy, and angular distribution. These matters cannot yet be calculated easily or accurately.

The composition and structure of the solar cell must be known, and the number and nature of the lattice defects caused by the various components of incident radiation calculated, together with their influence on the efficiency of the cell. These matters involve the frontiers of solid state physics.

The above academic approach, while desirable, is not yet practicable.

Of several approaches, intermediate between the extremes noted above, the following was chosen.

Bare silicon cells similar to the ones used in this experiment have been subjected to well controlled radiation damage using 1 Mev electrons and 4.6 Mev protons from accelerators by W. R. Cherry and L. W. Slifer.* The short circuit current was monitored, with the cells illuminated by a 2800°K tungsten source, filtered by 3 cm. of distilled water. The intensity was comparable with sunlight.

The above information on damage susceptibility will be combined with the available knowledge of the electron and proton intensity (and, to some extent, energy) distribution in space. This information will come from several sources, but will not include data obtained by the radiation measuring instruments on Relay. A suitable computer program will, in effect, carry the experiment through the trapped particles, computing the accumulated doses for a number of Relay orbits. This radiation information will be modified to account for the effect of the shielding. The result of combining the laboratory determined damage susceptibilities with the radiation information will permit prediction of cell damage.

This approach has its weaknesses. The cells measured in the laboratory are similar to, but not identical with those used in orbit. The light source used to evaluate the laboratory damage is different in spectral energy distribution from sunlight. This causes apparent damage different from that obtained in orbit. This effect depends on cell type, and nature and energy of the particle that did the damage. It is being investigated

*Cherry, W. R., and Slifer, W. W., "Solar Cell Radiation Damage Studies with 1 Mev Electrons and 4.6 Mev Protons," NASA–GSFC Document X–636–63–110, May 27, 1963.

further. The laboratory damage studies directed beams of particles perpendicularly to the cell surface and the effect of oblique irradiation, which occurs in space, can only be estimated. Interpolation and extrapolation of the laboratory damage data will be required.

Concerning the space maps of particle distribution, these are being assembled and modified as more information becomes available. Data on energy distribution is incomplete. Finally, the maps are subject to change with time as a result of natural and man-made disturbances. In view of the above, approximate prediction of damage is all that can be expected.

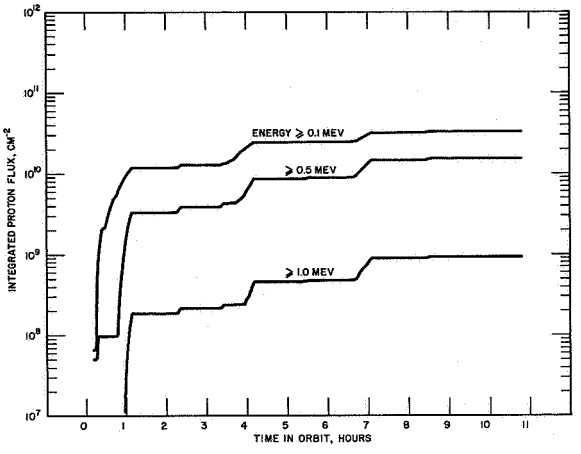


FIGURE 8–9.—Low energy proton flex vs. time.

Unshielded Silicon Cells

It has been shown that bare silicon solar cells are damaged by either electrons or protons whose energy exceeds a few hundred kev. A cursory review of approximate doses of the particle fluxes along the Relay orbit indicated that low energy protons would probably be the predominant cause of damage to bare silicon cells. Davis and Williamson have reported a large flux of protons of energies above 100 kev centering about an equatorial altitude of about 2.5 earth radii.* The measurements were made on Explorer XII. The Relay orbit penetrates high latitude parts of this distribution.

Davis has organized this data into a space map of protons of energies above 100 kev, 500 kev, and 1000 kev, and integrated the fluxes over the first eleven hours of the Relay path, using 1 minute steps. The resulting plots are shown in Figure 8–9. Major damage steps at about three hour (one orbit) intervals are evident. An accuracy of plus or minus fifty percent is quoted.

The susceptibility of silicon solar cells to proton damage is known to be relatively small at both very high and very low energies. Baicker, Faughnan, and Wysocki have shown that the susceptibility is a maximum around 1 Mev, falling rapidly below 0.2 Mev and slowly above 1 Mev, when judged by maximum power output under sunlight illumination.** It will be assumed here that the damage susceptibility to protons is zero up to 0.5 Mev, where it has a maximum value, and above which it falls inversely with energy. The latter characteristic is indicated by both theory and experiment, for energies up to about 100 Mev. Thus, the Figure 8–9 curve for proton energies equal to or greater than 0.5 Mev is of interest. The figure indicates that the proton population falls rapidly with energy. It is estimated that the "energy center" of the protons whose energy is above 0.5 Mev is at 0.7 Mev. Using the assumption that the damage susceptibility is inverse with energy, we then multiply the ordinates of the 0.5 Mev curve of Figure 8–9 by 4.6/0.7 to obtain the number of equivalent 4.6 Mev protons per cm² as a function of time. We then use the Cherry and Slifer 4.6 Mev proton damage data of Figure 8–10 to convert the above predicted equivalent 4.6 Mev orbital proton fluxes to solar cell damage values. The result, for silicon P/N cells, is shown in Figure 8–11, together with data obtained from the Relay radiation damage experiment.

It is evident that the predicted values of

*Davis, Leo R. and Williamson, James M., "Low Energy Trapped Protons," NASA–GSFC Document X–611–62–89, May, 1962.

**Baicker, J. A., Faughnan, B. W., and Wysocki, J. J., "Radiation Damage to Silicon," Third Semi-Annual Report on Contract NAS 5–457, April 15, 1962.

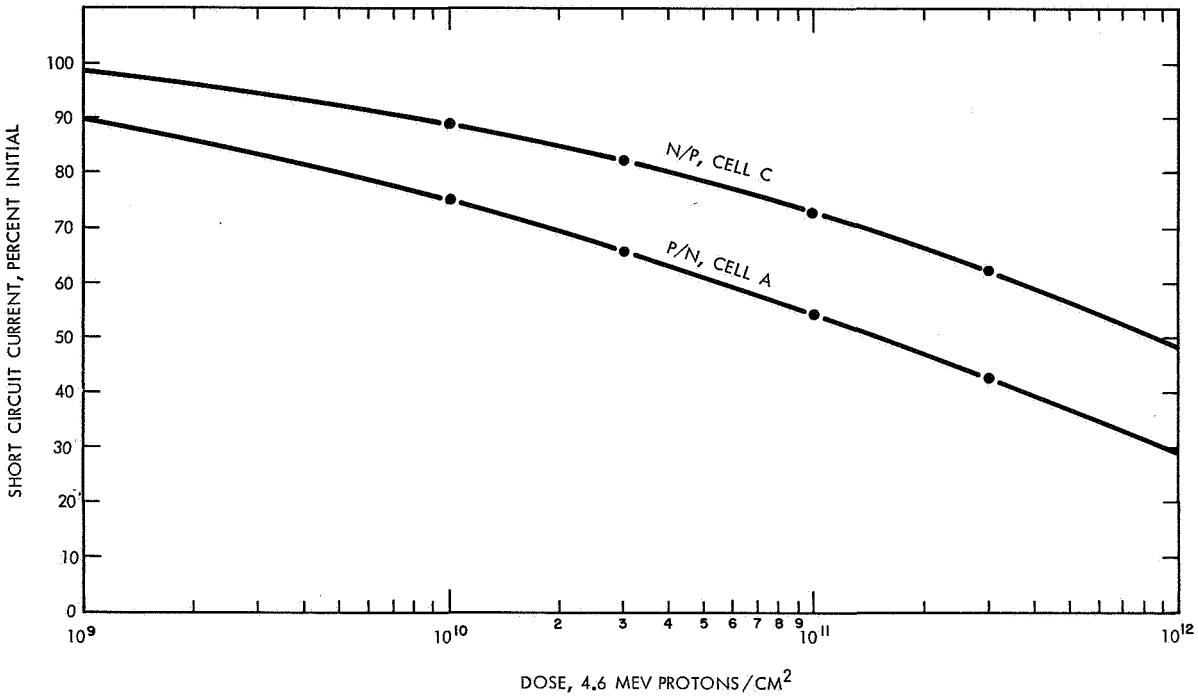


FIGURE 8–10.—Response of silicon solar cells vs. flux of protons.

short circuit current are in fair agreement with the observed values, most of which fall within the error limits associated with the 50 percent uncertainty in orbital fluxes. The predicted values are systematically higher than the observed ones.

The time structure of the observed damage is correctly predicted, with the indication that a damage step probably occurred near seven hours, but was not observed. It may be mentioned that damage predictions based on high energy protons and on electrons failed to account for the magnitude of the damage to these unshielded cells and the predicted damage steps occurred at the wrong times.

Figure 8–12 shows a plot of the first six hours of orbit in the B, L coordinates described in Chapter 7. The predicted damage steps centering at 0.8, 3.9, and 6.9 hours in Figure 8–11 have B, L coordinates of (0.064, 3.46), (0.053, 3.04), and (0.049, 2.67), respectively. These all lie at about 30 degrees south latitude, at an altitude of about 6,100 km.

The result of the above damage prediction procedure when applied to the N/P silicon solar cells is shown in Figure 8–13. The Cherry and Slifer laboratory damage data of Figure 8–10, were again employed. The observed damage points in Figure 8–13 fall near the upper error limits of the predicted values, a systematic difference of sign opposite to that of Figure 8–11 being evident. The predicted time variation is in agreement with that observed. The desirability of more frequent and complete data in observing orbital damage is obvious.

Since laboratory proton damage studies on gallium arsenide equivalent to those of Figures 8–10 and 8–14 are not available, the above type of prediction of gallium arsenide damage cannot be attempted. Baicker et. al.* have considered the unexpectedly rapid deterioration of the gallium arsenide cells on Relay and attribute it to a relatively high

*Baicker, J. A., Faughnan, B. W., and Wysocki, J. J., "Radiation Damage to Silicon," Third Semi-Annual Report on Contract NAS 5–457, April 15, 1962.

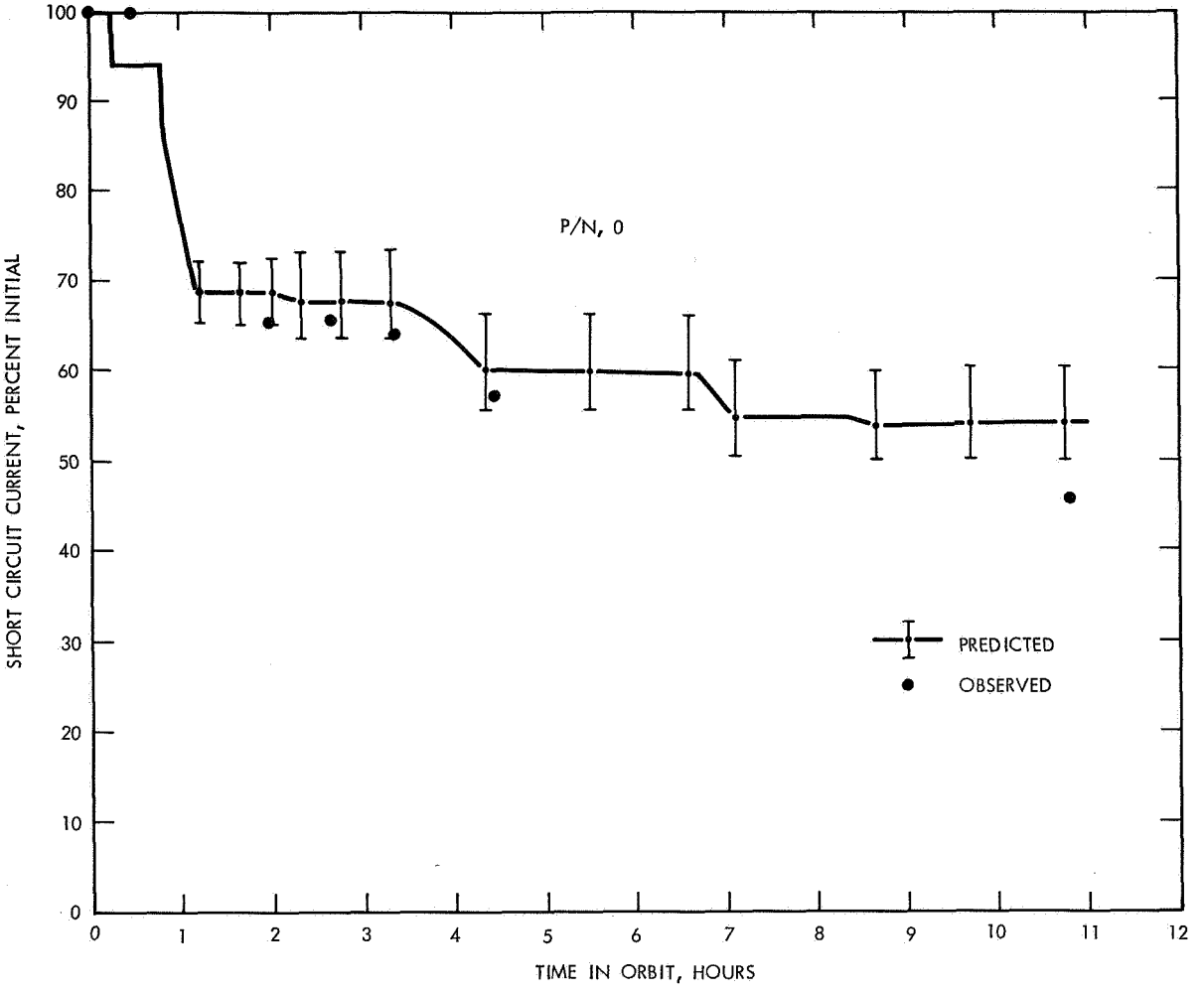


FIGURE 8–11.—Predicted and observed damage to *P/N* cells.

damage susceptibility to protons of energies below a few hundred kev. This is related to the fact that the useful volume of a gallium arsenide solar cell is located in a much thinner front layer than is the case for silicon. A shield of even 1 mil of fused silica would stop all low energy protons up to 1.5 mev, and presumably allow the gallium arsenide cells to exhibit the high radiation damage resistance indicated by theory and by laboratory damage studies when protons above about 2 Mev are used.

Proton Damage to Shielded Cells

We will here attempt to predict the damage suffered by silicon P/N and N/P cells, shielded by 60 mils (0.336 grams per cm^2) of clear fused silica (Corning 7940). Since the damage per orbit was too small to be resolved, only long time damage effects will be considered.

A fused silica shield of 60 mils thickness will, nominally, stop a 16.5 Mev proton and a 0.90 Mev electron. The large flux of low energy protons which evidently damaged the unshielded cells are therefore excluded.

The Mathematics and Computing Branch of the Theortical Division of GSFC kindly calculated fluxes of high energy protons and electrons over intervals of Relay flight. These predictions covered five two day intervals. Fourteen second steps were used. The cumu-

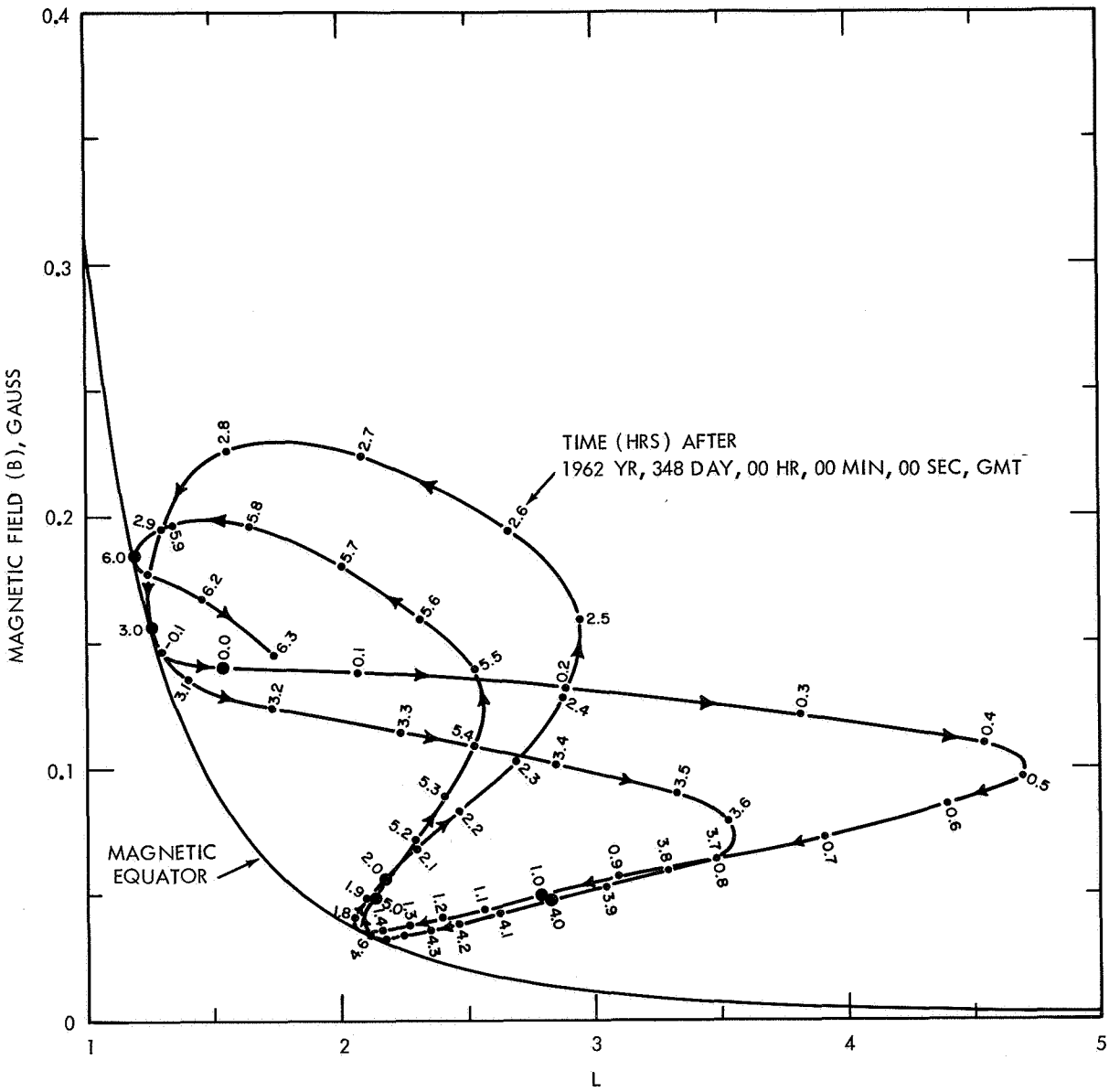


FIGURE 8–12.—Orbit plot in B vs. L coordinates.

lative flux of protons of energy above 30 Mev involved use of the P_1 proton grid, or space particle distribution map. Electron fluxes were made with the E8U and E8L electron grids, giving upper and lower limits. This information is summarized in Table 8–8. The fluxes are omni-directional.

The mean proton flux of Table 8–8 refers to protons of energy above 30 Mev. It is necessary to move the cut-off energy downward from 30 Mev to 16.5 Mev. According to McIlwain and Pizella* the ratio of the proton fluxes Q_1 and Q_2 having energy cut-offs at E_1 and E_2, respectively, is given by

*McIlwain, C. E., and Pizzella, G., "On the Energy Spectrum of Protons Trapped in the Earth's Inner Van Allen Zone," J. Geophysical Research 68 (7), 1811–23, April 1, 1963.

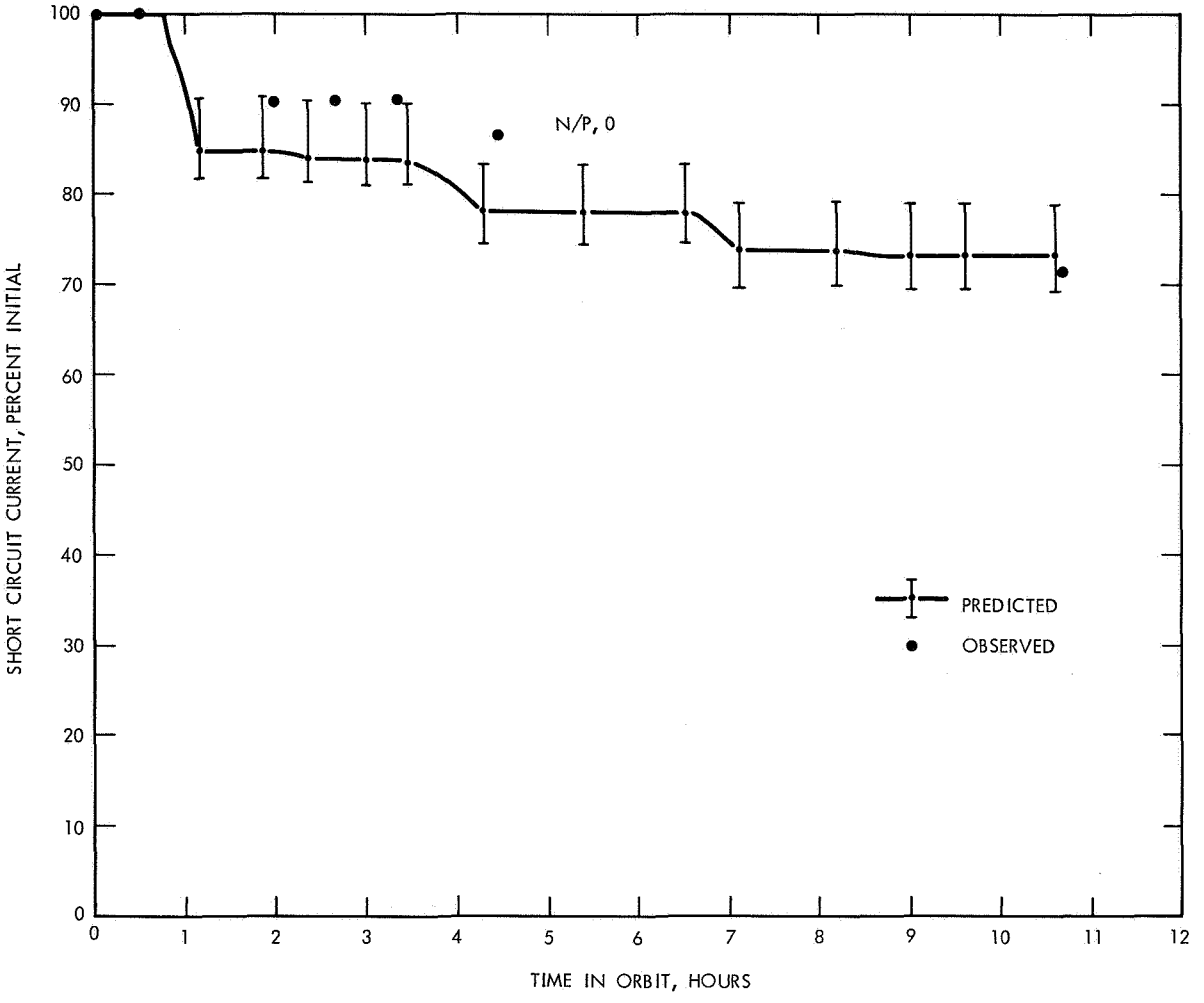


FIGURE 8–13.—Predicted and observed damage to N/P cells.

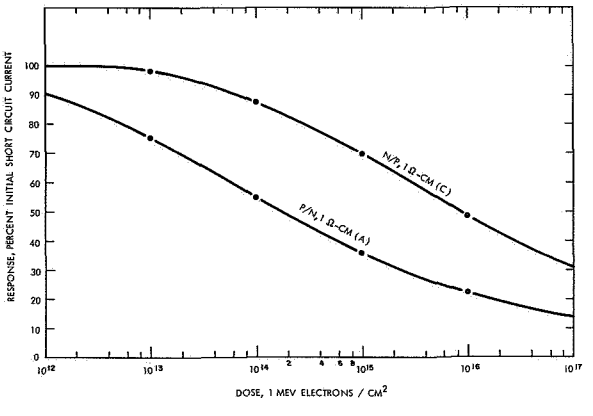


FIGURE 8–14.—Response to silicon solar cells vs flux of electrons.

$$\frac{Q_1}{Q_2} = \exp \frac{E_2 - E_1}{E_0} \qquad (8.1)$$

where

$$E_0 = 306\, L^{-5.2} \qquad (8.2)$$

Assuming that the major cell damage occurred near equatorial crossings an average equatorial L value of 1.7 was determined from orbit predictions. This, with Equation 8.2, gives a value of E_0 of 19.45 Mev. When this is entered in Equation 8.1, together with the energy cut-off values of 30 and 16.5 Mev, the flux extension factor is found to be 2.0. Other factors to be applied to the mean proton flux value of 8.79×10^8 protons/cm^2 –day are estimated as: 1/2 (for infinite rear

TABLE 8–8.—*Predicted Omnidirectional Proton and Electron Fluxes*

Days in orbit	Protons/cm²-day	Electrons/cm²-day, upper	Electrons/cm²-day, lower
0 to 2	0.254 (9)	2.87 (12)	1.58 (12)
14 to 16	0.305 (9)	3.74 (12)	1.85 (12)
45 to 47	10.5 (9)	8.72 (12)	5.78 (12)
83 to 85	17.4 (9)	14.1 (12)	6.92 (12)
194 to 196	10.5 (9)	8.17 (12)	4.58 (12)
	Mean = 8.79 (8)	Mean = 7.52 (12)	Mean = 4.14 (12)
		Mean = 5.83 (12) ± 30% electrons/cm²-day	

Proton energies are equal to or greater than 30 Mev.
Electron energies are equal to or greater than 0.5 Mev.

shielding), 1/3 (for oblique incidence) and 1 (to get 4.6 Mev equivalence). The latter is roughly estimated as follows: the steeply falling incident integral proton spectrum is considered cut off below 16.5 Mev. Increasing numbers of protons of initial energies greater than this value penetrate the shield, with exit energies rising from zero. The rise is estimated to terminate in a few Mev, after which a fall dictated by the shape of the initial spectrum occurs. The maximum is probably at a few Mev. Since laboratory damage information on these types of cells was available at 4.6 Mev, this same energy equivalent of the protons penetrating the shield is assumed, lacking a more precise determination. The straggling of protons in shields is very severe.

The overall factor deduced above is 1/3, giving a predicted 4.6 Mev normal incidence proton flux of $1/3 \times 8.79 \times 10^8$ or 2.93×10^8 protons/cm² –day, or 8.8×10^{10} protons/cm² over 300 days. Using this value with the damage curves of Figure 8–10 gives cell responses of 56 percent for the P/N, 60 cells and 75 percent for the N/P, 60 cells. These are to be compared with the observed values of 60 and 79 percent. The agreement is fair.

Electron Damage to Shielded Cells

Table 8–8 indicates a predicted average omni-directional electron flux of 5.83×10^{12} electrons/cm²–day. We will assume they have a fission spectrum and utilize a function* to convert this value to equivalent normal incidence 1 Mev electrons after passage through shielding material. The result is, for the P/N 60 cells, a factor of 0.14, and, for the N/P, 60, a factor of 0.31. Thus the predicted equivalent 1 Mev electron flux per cm² –day becomes 8.16×10^{11} electrons/cm² –day or 2.45×10^{14} electrons/cm² over 300 days, for the P/N, 60 cells. Using the appropriate damage curve of Figure 8–14 we obtain a predicted cell response of 47 percent. This is considerably smaller than the observed value of 59.8 percent. Similarly, for N/P, 60 cells the predicted flux per cm² over 300 days is 5.4×10^{14} equivalent 1 Mev electrons, giving a predicted response of 75 percent, versus an observed 79 percent, which is fair agreement.

Thus, the predicted damage by both electrons and protons on heavily shielded silicon cells exceeds that observed. This nature of disagreement can be partly attributed to the use of tungsten light in evaluating the laboratory damage curves of Figure 8–10 and 8–14. This tends to exaggerate damage, as

*Rosenzweig, W., "Radiation Damage Studies," IEEE Photovoltaic Specialists Conference, Washington, D. C., April 10–11, 1963. See also Fig. 6–32, this report.

TABLE 8–9.—*Orbital Radiation Damage Experiments*

No.	Satellite	Perigee (km)	Apogee (km)	Incl. (deg.)	Launched	Cell type	Mils, shield	$T_{0.75}$ (days)
1	Explorer XI	491	1799	28.8	4/27/61	N/P	0	70
2	Midas III	3450	3510	91.2	7/12/61	P/N	40, silica	100
						P/N	80, silica	250
						N/P	60, silica	1000
3	Explorer XII	304	77000	33.	8/16/61	P/N	3, glass	1000
						P/N	0	1 orbit
4	Midas IV	3530	3760	95.9	10/21/61	P/N	40, silica	53
						P/N	80, silica	110
5	Telstar I	952	5660	45.	7/26/62	N/P	30, sapp.	400
6	Alouette	1004	1029	90.	9/29/62	P/N	12, glass	30
7	Explorer XIV	278	99000	33.	10/21/62	P/N	0	1 orbit
8	1962–BK	191	5550	71.	10/26/62	P/N	6, glass	4
						P/N	60, glass	100
						N/P	6, glass	50
9	ANNA 1B	1090	1180	50.	10/31/62	P/N	6, glass	40
						P/N	20, silica	90
						P/N	30, sapp.	400
						N/P	30, sapp.	1400
10	Relay 1	1321	7439	47.5	12/13/62	P/N	0	1 orbit
						P/N	30, silica	32
						P/N	60, silica	47
						N/P	0	0.33
						N/P	30, silica	197
						N/P	60, silica	480
						GaAs	0	0.06

compared with that demonstrated in orbit with sunlight illumination. The electron damage prediction also neglected a decrease in electron intensities which is known to have occurred during the experiment.

Comparison with Other Orbital Damage Experiments

Table 8–9 shows the orbit parameters of some other satellites which have carried radiation damage experiments, together with cells, shields, and times estimated for cell responses to fall to 75 percent of their original values. This data is largely taken from Cooley et al.*

Some comparison may be made. Midas III has a circular polar orbit at about the same mean altitudes as Telstar I and Relay I. They all carry N/P cells with about the same effective shields. Their "lifetimes" in orbit are 1000, 400, and 480 days, respectively. The fact that Midas III was at the altitude of the "inner belt" is evidently compensated by the fact that it spends a large part of its time in low damage regions near the poles.

The Explorer XII and Explorer XIV P/N, 0 cells and the Relay I P/N, 0 cells, although in greatly different orbits, agree in that they were all very severely damaged in one orbit. The fact that the Explorer XII (P/N, 3 glass) cells had such a long lifetime compared to the unshielded cells strongly indicates damage by low energy protons, to which the damage to the unshielded cells on Relay has been quantitatively ascribed.

The (P/N, 60 glass) cells on 1962 BK and the (P/N, 60 silica) cells on Relay had roughly the same mean altitudes and their critical times of 100 and 47 days, respectively, are comparable.

*Cooley, William C., Janda, Robert J., and Shivanandan, Kandiah, "Handbook on Space Radiation Effects to Solar Cell Power Systems," prepared for NASA under contract NASw–598, July 22, 1963.

Although not shown in Table 8–9 ANNA 1B carried a gallium arsenide cell with a 6 mil glass shield. This appeared more damage resistant than any of the much more heavily shielded silicon cells up to 80 days in orbit, when it apparently began to degrade rapidly. Although its orbit is quite different from that of Relay, the long lifetime compared to the unshielded gallium arsenide cells on the latter spacecraft (0.06 days) suggests again that low energy protons were the damaging agent.

A review of Table 8–9 strongly indicates that N/P silicon solar cells, shielded with the equivalent of 60 mils of Corning Type 7940 transparent fused silica would probably have a lifetime (75 percent point) of about one year if in the most damaging orbit. This presumably would be an equatorial one at an altitude of about 300 km.

In view of the approximations now required in the prediction of the lifetime of solar cell power supplies in orbit it is obviously prudent to check such predictions against empirical information of the kind indicated in Table 8–9.

CONCLUSIONS

The radiation effects experiment carried on Relay has shown, by virtue of observations taken over about one year, that silicon N/P solar cells shielded with 60 mils of Type 7940 silica last about 10 times longer than similarly shielded P/N cells, when judged by short circuit current at the 75 percent initial value level.

Silicon N/P cells with 30 mil shields last about six times longer than similar P/N cells.

Silicon N/P cells with 60 mil shields last about 480 days; silicon N/P cells with 30 mil shields last 197 days, all at the 75 percent level.

Unshielded silicon N/P, P/N, and gallium arsenide cells all last less than one day.

The use of 60 mil shields approximately doubles the life of a silicon cell, as compared to one using a 30 mil shield.

Fluctuations in the degradation rates were apparent. Early effects were attributable to successive passes through highly damaging regions of space.

Early damage to unshielded P/N and N/P cells was approximately accounted for, in magnitude and in time, by predictions based on a space map of low energy protons, to which unshielded cells, particularly those of gallium arsenide, are very sensitive.

The long term degradation of the shielded silicon cells was predicted, approximately, by consideration of the effects of protons of energy greater than 16.5 Mev, using the GSFC P1 proton grid.

However, a consideration of the damage causd by electrons of energy greater than 0.5 Mev, using the GSFC E8 grid, also approximately predicted the observed damage. This prediction ignored a decrease in electron intensities which is known to have occurred during this flight.

It thus appears that protons were the principal cause of damage to the heavily shielded cells. Also, the particle information, the data on laboratory radiation damage, or approximations in the calculations have tended to an over-prediction of damage to shielded cells.

The radiation damage observed on Relay is similar to damage occurring on Midas III and Telstar I. This is reasonable when the orbits are considered. The empirical information indicates that for a solar cell powered spacecraft to last one year in an equatorial orbit of about 3000 km altitude, N/P silicon cells shielded with at least 60 mils of fused silica would be required if the performance were not to fall below the 75 percent initial value.

It would be of great value if future satellite solar cell damage experiments were such that the maximum power from the cells were measured, instead of short circuit current, which is known to be only a poor measure of power under some conditions. The use of gallium arsenide cells with a variety of shields may allow this material to demonstrate its potential. More complete and ac-

curate space maps of the trapped radiations are highly desirable, together with improved laboratory damage studies on solar cells. Damage studies using high energy electrons and protons on shielded cells would remove some of the uncertainties now involved in calculating shielding effects, particularly if the damage were evaluated in sunlight.

ACKNOWLEDGMENT

The invaluable assistance of Luther Slifer in supervising the procurement of the radiation damage panel and in calibrating it for aspect angle is acknowledged. James Albus designed and provided the solar aspect indicator. Justin Schaffert designed the diode circuitry. Daniel Brown provided liaison with the Communications' group. Joseph Bourne gave valuable aid in processing the data of this experiment.

AUTHOR. *This chapter was contributed by* R. C. WADDEL, *NASA/Goddard Space Flight Center, Greenbelt, Maryland, U.S.A.*

Chapter 9

N66-10247

The Andover Ground Station

INTRODUCTION

The Andover ground station was designed to provide means for transmitting to and receiving from communications satellites similar to Relay. The station includes the communication antenna, transmitting and receiving equipment, coupling circuitry, satellite tracking equipment and means for programming the antenna to track the visible portion of a satellite's orbit. In addition, VHF command transmission and telemetry reception facilities appropriate to Relay satellites are provided. The station has been used for evaluation tests of and successful demonstrations via Telstar I and II, Relay I and II, and Syncom II.

SITE SELECTION

In selecting a site suitable for a ground station, several factors were taken into account. These included freedom from interference, suitability for commercial operation, proximity to Europe and climatic conditions. The major sources of interference were considered to be TD–2 and TH microwave systems, airplane routes, major highways and large cities. Consideration was given not only to existing sources of interference but to any that might obtain in the foreseeable future. Suitability for commercial operation dictated that the site be large enough to house several antennas and be close enough to existing radio relay telephone and television routes for economical interconnection. A location in the northeastern United States was required to fulfill the criterion that the station be near Europe.

Several possible areas were selected in the northeastern states. Of these, Maine was chosen as the most promising. Exploration of this area by a siting team resulted in the selection of the site at Andover, Maine. Conclusions based on detailed studies of this site indicated that it was satisfactory. These conclusions have been validated by subsequent performance of the station.

The location of the station is shown in Figure 9–1. It is in southwestern Maine close to the New Hampshire border, latitude 44.6355406°N, longitude 70.694033°W. Interconnection with existing radio relay systems was obtained via a four hop system, two sections of which are TD–2 and two sections of TJ (11 Gc). The use of TJ for the sections closest to the site, and utilizing frequencies at the low end of the TD–2 band avoided interference from the entrance link to the ground receiver.

The station is situated on a low, rounded hill at an elevation of 900 feet in a tract of about 1100 acres. The 1100 acre tract is in turn, in a wide, shallow valley about 10 miles in diameter. The surrounding hills provide additional shielding against interference in almost all directions without significantly interfering with satellite visibility. Figure 9–2 is a general aerial view of the Andover

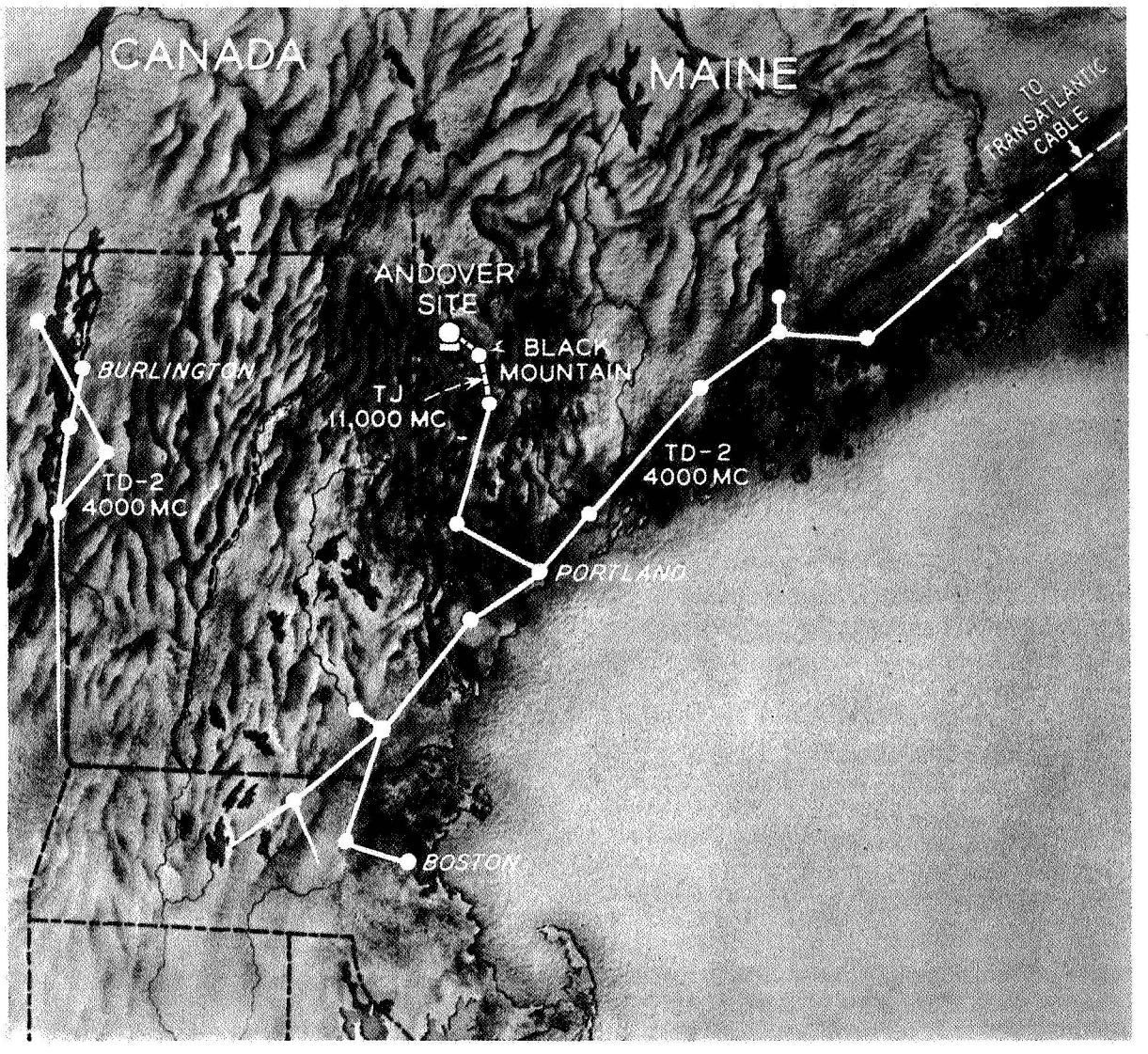


FIGURE 9–1.—Andover site-map.

site. Figure 9–3 is a close-up aerial view of the site. In this view the air-supported radome is the most prominent feature of the station. Figure 9–4 presents the profile of the optical horizon from the site of the antenna.

Communications Antenna

The communications antenna at Andover is a much enlarged version of similar antennas widely used on Bell System microwave relay routes. Figure 9–5 shows a model of the Andover antenna. For structural reasons, the horn at Andover is conical rather than pyramidal, as was the case in the smaller versions. The antenna rotates in azimuth on two concentric rails and in elevation about the axis of the conical feed horn on a large bearing at the rear and a truck and rail combination at the forward

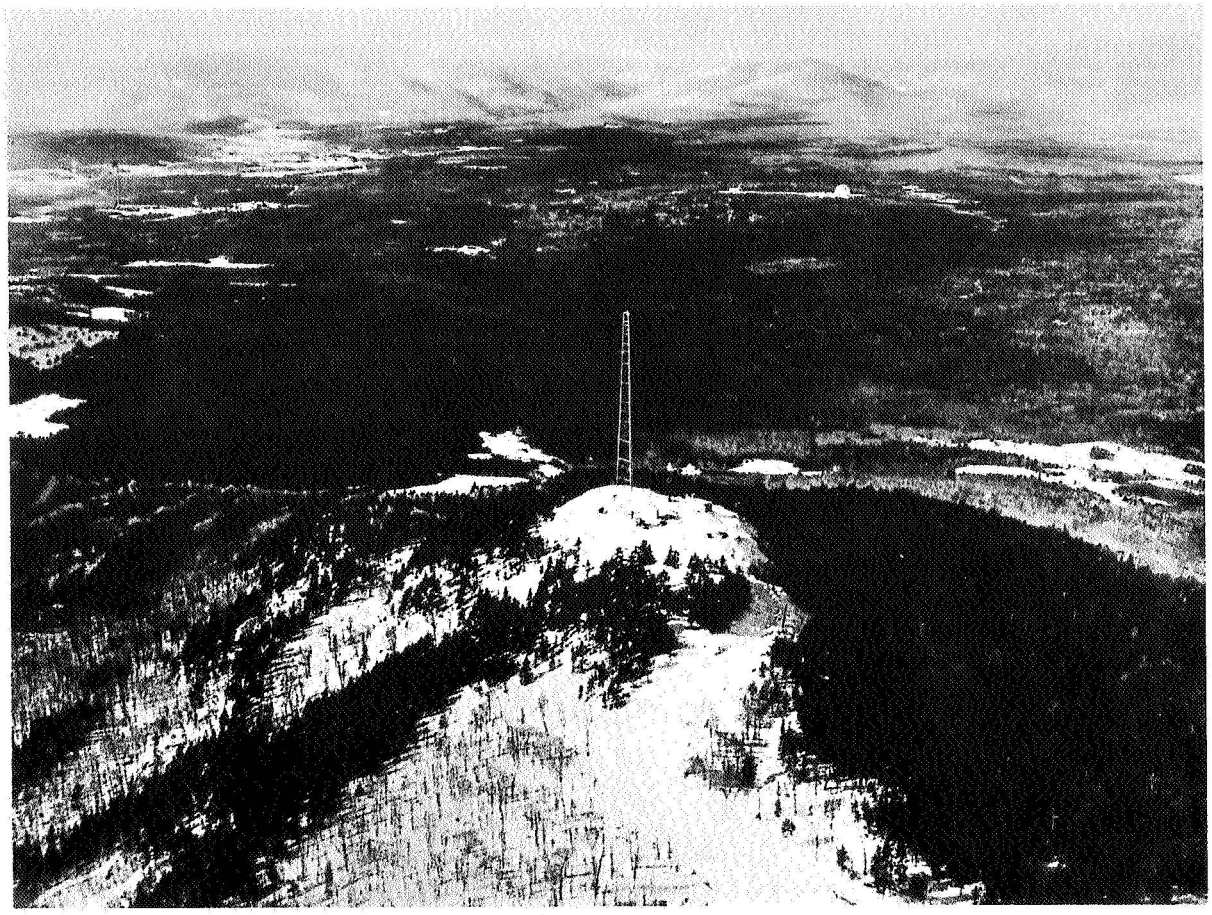


FIGURE 9–2.—Andover site—aerial view.

end. Two equipment rooms are carried on the structure.

This configuration has several advantages over other possible forms. It is extremely broadband, presents an excellent impedance to the transmitter, and the parabolic surface is efficiently illuminated. The antenna also has very low sides and back lobes. The provision of equipment rooms on the structure permits connections to the receiver with short, low loss connections, resulting in low system noise temperature.

Table 9–1 gives the principal physical and performance characteristics of the Andover horn.

Pointing calibration was made by tracking radio stars. Accurate corrections to accom-

TABLE 9–1.—*Horn Reflector Antenna*

Structural characteristics		
Aperture	3600 square feet	
Length	177 feet	
Weight	380 tons	
Reflector accuracy	0.060 inch (1 Sigma)	
Tracking and slewing	**Azimuth**	**Elevation**
Maximum tracking velocity	1.5 deg/sec	1.5 deg/sec
Maximum slewing velocity	1.5 deg/sec	1.5 deg/sec
Maximum acceleration	1.3 deg/sec^2	3.0 deg/sec^2
Error during acceleration	0.26° pre deg per sec^2	
Performance	**4170 mc**	**6390 mc**
Gain	58 db	61 db
Beamwidth (3-db points)	0.23 degree	0.16 degree

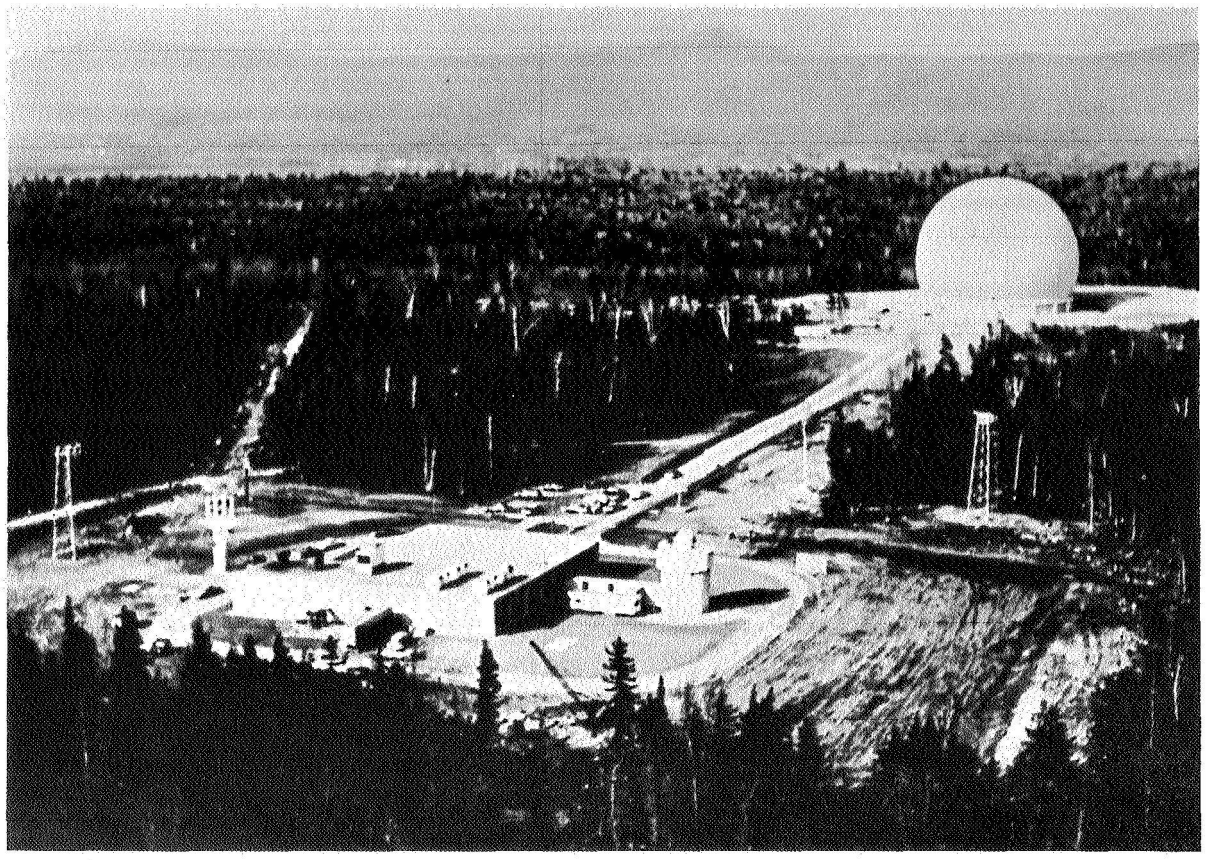


FIGURE 9–3.—Andover site—closeup aerial view.

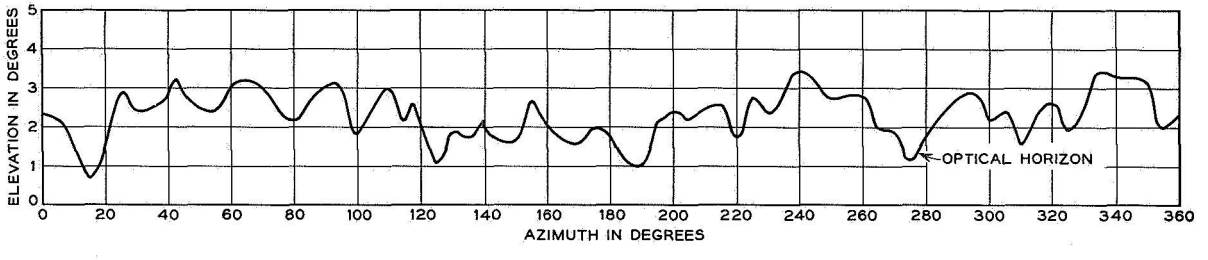


FIGURE 9–4.—Andover optical horizon.

modate the structural distortions indicated by these calibrations are known. These are included in computations so that with good ephemerides data the antenna beam may be pointed at the satellite within a fraction of a beam width.

All connections to the antenna are made through slip rings located around a pintle bearing at the azimuth axis. This permits free rotation of the antenna. Cooling water, power and control leads are also carried through rotating joints and slip rings at the

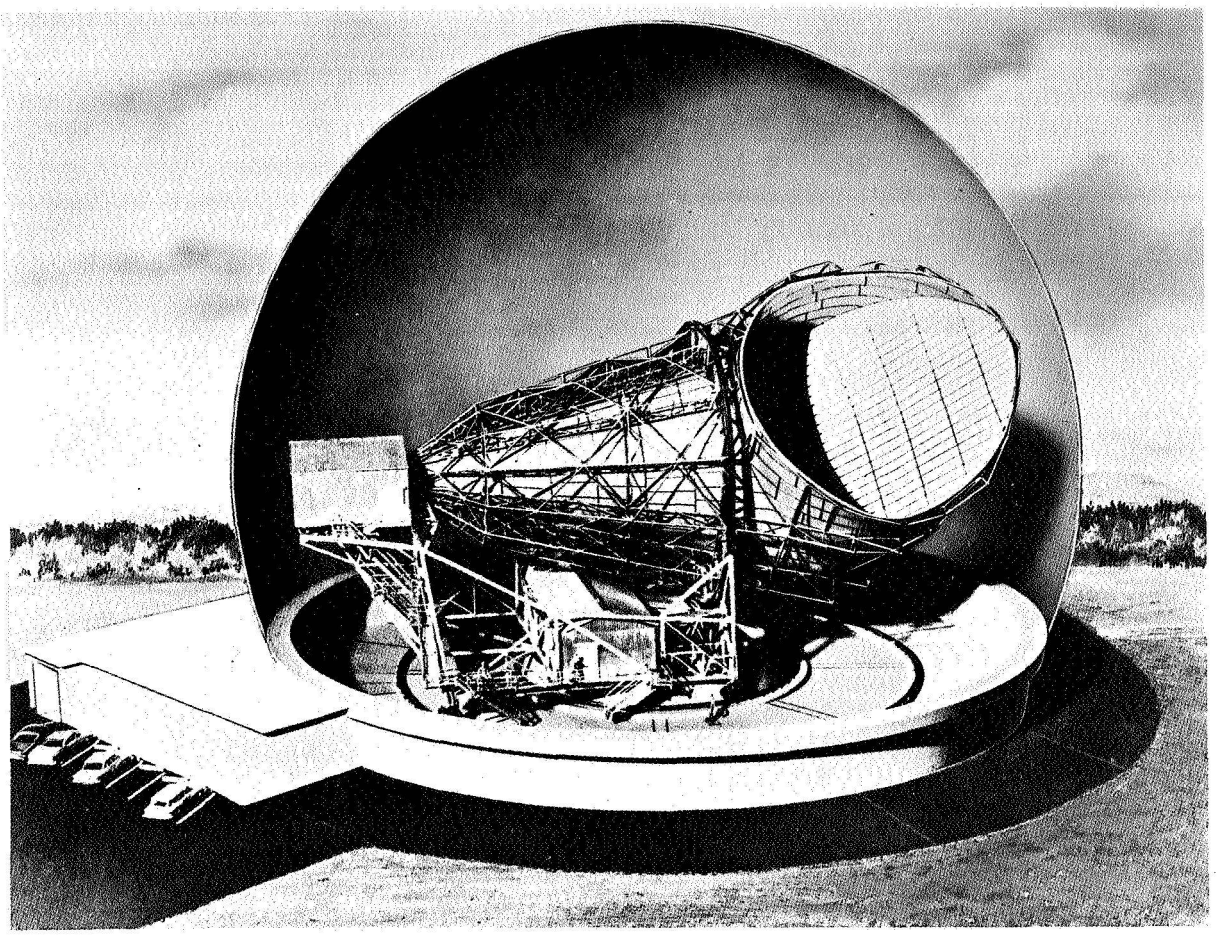


FIGURE 9–5.—Andover antenna—model.

pintle bearing.

The entire antenna is housed in the previously mentioned radome. This structure is made of rubberized dacron. It is 210 feet in diameter and 165 feet high.

Transmitters

There are two ground transmitters associated with the horn antenna. One is used when tests or demonstrations are to be conducted using Telstar. The second transmitter is used when Relay is the satellite of interest.

The Telstar transmitter, shown in Figure 9–6, provides an FM signal of 3000 watts maximum with a peak deviation of ±10 Mc. The FM deviator and modulator amplifier stages are modified versions of TH radio transmitting equipment. The output stage is a power amplifier using a high-power traveling wave tube. The center frequency is 6.390 Gc when the transmitter is used for

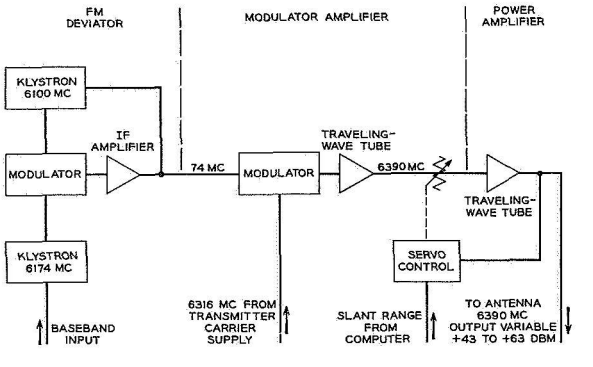


FIGURE 9–6.—Ground transmitter block diagram.

television or other straight-away tests. It can be shifted ±5 Mc for two-way message experiments. The servo control shown can be used to vary the output power to maintain a prescribed received power at the satellite. This is used in two-way telephone tests, where approximately equal carrier levels at the satellite are desired.

The Relay transmitter provides an FM signal of 10,000 watts maximum with a peak deviation of ±7 Mc. The output stage embodies a power klystron.

The center frequency is 1.725 Gc when the transmitter is used for television or straight-away tests. It can be shifted ±5/3 Mc for two-way message experiments.

Receivers

The station is equipped with two receivers. A standard FM receiver operating at 74 Mc similar to those used in the TH radio relay systems and an FM feedback receiver. The FM feedback receiver reduces the effective noise bandwidth of the receiver to give a 4 to 5 db advantage in threshold when compared to a conventional receiver.

A block diagram of the receiving system is shown in Figure 9–7. This diagram shows the FM feedback receiver. Signals received through the antenna are amplified 40 db by a ruby maser. They are then converted to a 74 Mc IF frequency where the major portion of the receiver gain is obtained. Then they are shifted to the 6 Gc band for demodulation in a frequency compression detector. This detector permits the baseband signal to noise advantage of wide deviation FM to be realized without the loss in threshold level that would obtain in a conventional detector of the same bandwidth. Compression of the noise band is achieved by feeding back part of the baseband output to a voltage controlled local oscillator. Thus, the local oscillator follows the deviations of the incoming signal. In this way, the IF frequency deviations applied to the discriminator are reduced by the feedback factor.

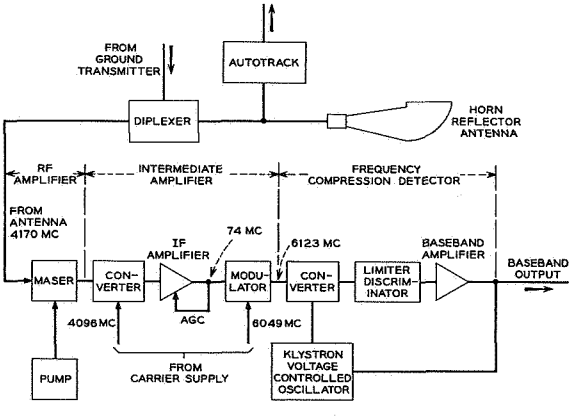


FIGURE 9–7.—Ground Receiver block diagram.

The center frequency when receiving television or during straight-away tests is 4.170 Gc. This is shifted ±5 Mc for two-way telephone tests.

The overall receiver noise temperature of the system is 42 degrees K when the antenna is at 7.5° elevation angle and 32 degrees K when pointed at zenith.

Coupling Circuitry

The coupling circuitry needed to permit the connection of the 6 Gc, the 1.725 Gc transmitters and the 4 Gc receiver to the horn antenna is shown in Figure 9–8. The signal from the 6 Gc transmitter comes from the left of the diagram via a rectangular waveguide with horizontal polarization. The signal travels essentially unchanged over a waveguide transition and through the polarization coupler. The polarizer transforms the linearly polarized signal into circular polarization for transmission by the antenna.

The 4 Gc signal from the antenna, after going through the polarizer, appears as a vertically polarized wave which is guided through the polarization coupler into the rectangular waveguide leading to the maser.

The 6 Gc into the maser is kept within tolerable bounds by means of the two mode suppressors, I and II, and the low pass filter in the waveguide leading to the maser.

The 1.725 Gc transmitting signal used in conjunction with Relay is coupled to the antenna in the conical section directly behind the apex taper. Two 1.725 Gc signals of equal amplitude and 90° phase difference are

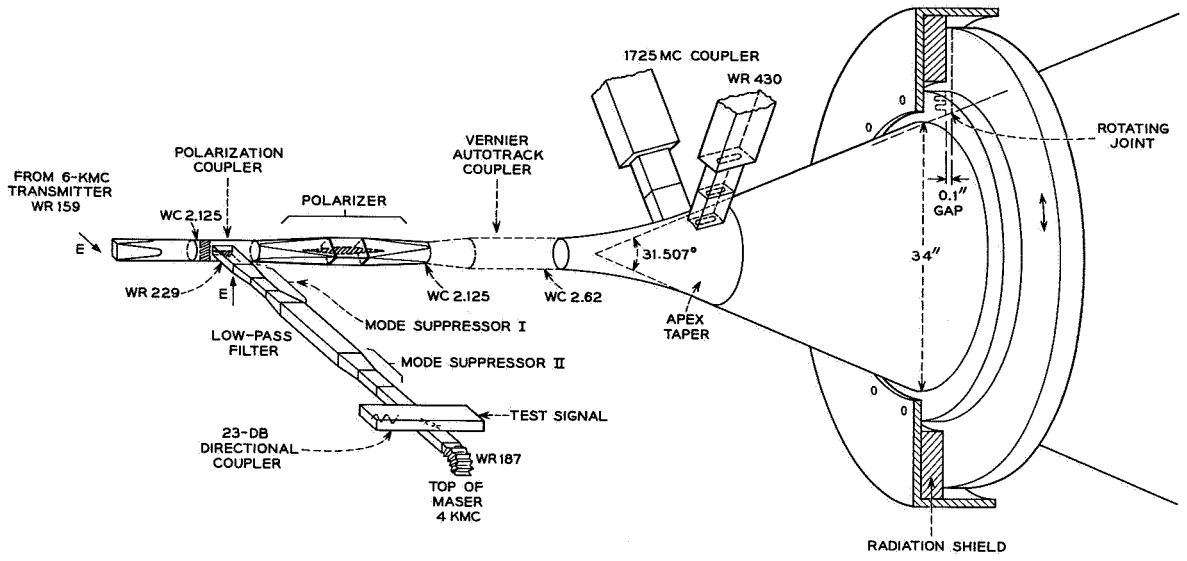


FIGURE 9–8.—Diplexer and associated waveguide circuits.

coupled at right angles into the horn. A hybrid is used to obtain two signals. The phase difference is such as to give a signal right-hand circularly polarized in space. The coupling slots are longitudinal and are located at a point where the circumferential wall current at 1.725 Gc has the first maximum. This maximizes the coupling for the TE_{11} mode and keeps excitation of the TM_{01} mode at a low level. The coupling slots are backed by two-cavity bandpass filters giving a maximally flat transmission with a 60 Mc bandwidth. The filters are built in small-sized waveguide (4.0 by 0.9 inch) to reduce the number of undesired modes which might be excited at 4 and 6 Gc.

Insertion loss of the filters at 1.725 Gc is less than 0.1 db. The filters also act as transformers between the conical section of the antenna and the large waveguide (WR430) which is used for the rest of the installation. The coupler has no measurable effect on the 6.390 or the 4.170 Gc signals. The noise contribution to the system by the coupler at 4 Gc was held to less than 1°K by careful mechanical design of the iris located in the apex taper.

The rotating joint shown in Figure 9–8 is located at a cone diameter of 34 inches. This rather large diameter and a gap width of 0.1 inch simplify the electrical design of a joint required to work at 6.390, 4.170, and 1.725 Gc. A double choke is used and optimized at 4.170 Gc. Measurements have indicated that for gap widths of up to 0.5 inch and with absorbing material covering the outside of the joint, the 4 Gc noise contribution was still below 1°K. The radiation shield was required to keep the radiated energy at 6.390 and 1.725 Gc below the Bell System safety limit for continuous exposure of 1 milliwatt per cm^2.

Satellite Tracking Equipment

The tracking equipment at Andover consists of four subsystems. These are (1) the command tracker including its control, (2) the precision tracker and its control, (3) the communications (horn reflector) antenna and its control and (4) the computers. A commercial system would not require as complex or elaborate a system as this. However, this system provides the flexibility necessary for evaluating the optimum sys-

tem for a commercial station. Figure 9–9 shows the four parts of the system and their interrelation.

The computer (IBM 1620) is programmed to produce drive tapes from any one of three different sources of information, (1) ephemeris data, (2) orbital elements and (3) X–Y–Z topocentric coordinates obtained from NASA. The drive tapes may be used to point all three antennas to the predicted position of the satellite. A different mode of operation which does not depend on accurate drive tapes is as follows:

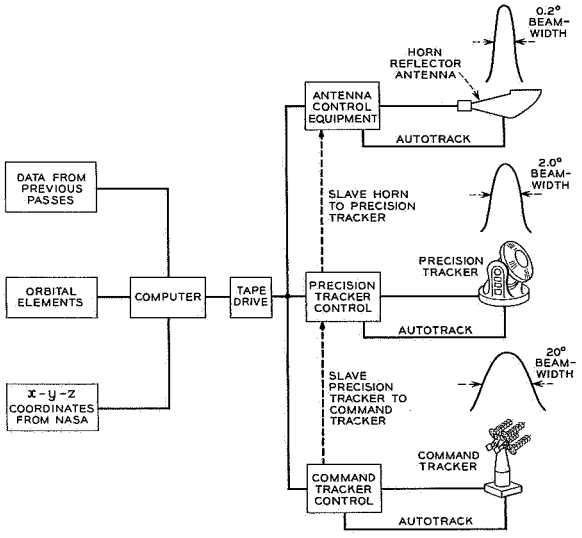


FIGURE 9–9.—Tracking system, block diagram.

The command tracker, with its beam of 20°, picks up the 136 Mc beacon as the satellite rises above the horizon. When autotrack has been obtained with this antenna, the satellite is located within 1°. Then prescribed procedures are followed to energize the repeater in the satellite. At this time the satellite transmits the 4.080 Gc beacon. The precision tracker, slaved to the command tracker, can now acquire the microwave beacon with its 2° beam. When autotrack is obtained, the satellite is located to within 0.02°. The horn antenna, slaved to the precision tracker, can then acquire the microwave beacon with its 0.2° beam and autotrack. Once this is accomplished, the horn can continue to track the satellite without further aid.

The procedure outlined above is one of many possible modes of operation. If good pointing information is available the communication antenna can be directed to acquire and then autotrack the satellite without going through the step by step procedure outlined above. This has been done on many occasions at Andover and a commercial system would probably be operated on this basis.

AUTHOR. *This chapter was written by* W. A. KLUTE *of the Bell Telephone Laboratories, Inc., Murray Hill, New Jersey, U.S.A. under Western Electric Corporation contract NAS 5–1987 with NASA/Goddard Space Flight Center.*

N66-10248

Chapter 10

Communications Experiments Conducted at Andover, Maine

INTRODUCTION

This is a final report of data taken at the AT&T Co. earth station at Andover, Maine during communications tests conducted on the Relay I satellite since its launch on December 13, 1962. The data presented in this and previous reports are in good agreement with theoretical values. In addition, Andover station reports which presented applicable raw data, have been furnished for each pass operated.

Andover has also participated in numerous successful monochrome television and two-way telephony transmissions to demonstrate the feasibility of satellites as a communications media. A monthly tabulation of the passes worked for either technical tests or demonstrations is presented below.

Month	Technical tests	Demonstrations
January	22	8
February	4	2
March	10	6
April	14	6
May	2	11
June	20	16
July	4	1
August	11	0
September	5	2
October	10	6
November	30	8
December	14	6

Stations participating with Andover in tests and demonstrations are listed below:

COMHIL: Goonhilly Downs, England
COMBOD: Pleumeur-Bodou, France
COMNUT: Nutley, New Jersey
COMRIO: Rio de Janeiro, Brazil
COMGEB: Raisting, Germany
COMTEL: Fucino, Italy
COMIBA: Ibaraki, Prefecture, Japan
COMMOJ: Mojave, Goldstone, California

Many of the tests were conducted on a loop basis (that is from Andover to the satellite and back to Andover).

GROUND STATION COMMUNICATIONS SYSTEM

The Andover communications system is shown in block diagram form in Figure 10–1. As can be seen from this figure the communications equipment is divided between two locations: the control building, which houses the major part of the test and control equipment, and the radome, which houses a large part of the communications equipment, including the ground transmitter and ground receiver. These areas are connected by means of a video transmission system and 1600 feet of cable. The Andover station is connected to Boston via a microwave radio relay system which terminates in the test area. From Boston the Andover station may be connected to any other part of the country by the Bell System communications network.

Four types of loop tests were conducted to facilitate evaluation of satellite performance as indicated in Figure 10–1. They are

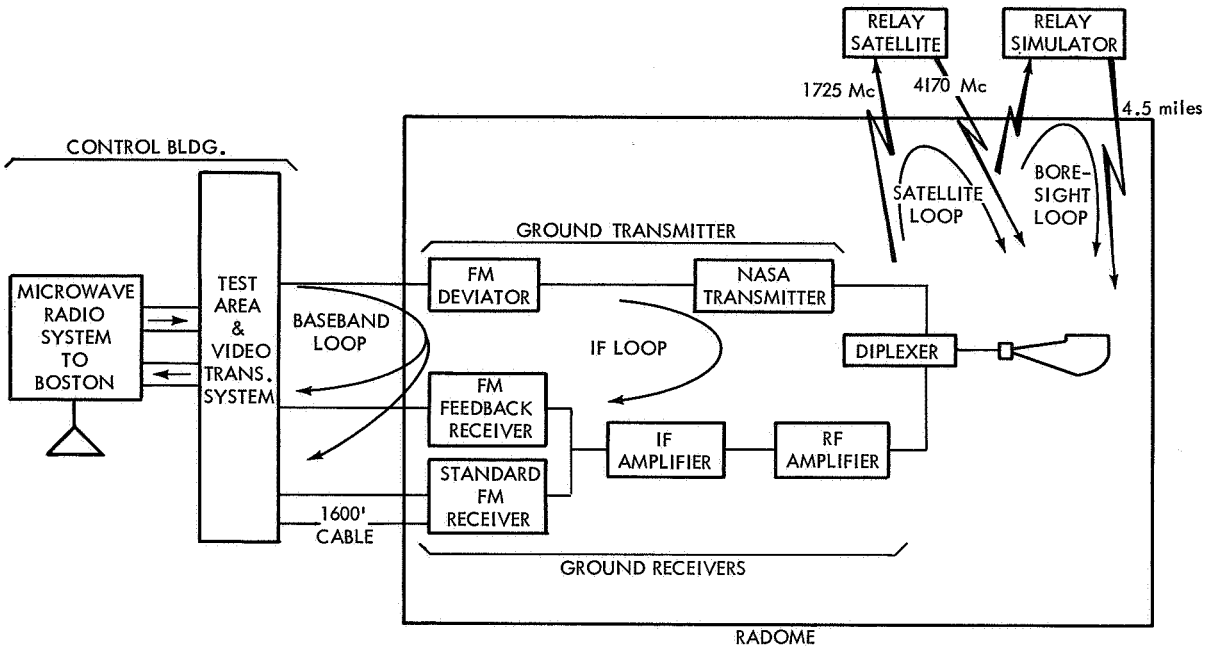


FIGURE 10–1.—Andover communications system.

as follows (1) the baseband loop which includes the video transmission system from the test area to the FM deviator and back to the test area; (2) the IF loop which includes the FM deviator, IF amplifier and the standard or FM feedback receiver in addition to the equipment required for the baseband loop; (3) the boresight loop includes all the ground station equipment including the ground station transmitter, receiver, diplexer, antenna and a repeater similar to the satellite; (4) the satellite loop is identical with the boresight loop except that the actual satellite is used rather than the repeater at the boresight tower. The majority of tests discussed in this report are satellite loop tests. Two types of FM receivers were used at Andover; a standard FM receiver and an FM feedback receiver. The FM feedback receiver provides some additional margin against breaking but has a somewhat restricted bandwidth compared to the standard FM receiver. In general, using the standard FM receiver without band-limiting filters results in a transmission characteristic flat to beyond 5 Mc while using the FM feedback receiver without band-limiting filters results in a transmission characteristic flat to about 4 Mc.

Many of the tests conducted use the multiplex equipment shown in Figure 10–2. This figure shows in block diagram form the optional arrangements for television and two-way telephony transmission. For television transmission, the audio signal is applied to the transmitting diplexer, which frequency modulates the audio signal on a 4.5 Mc subcarrier. The video signal is band-limited by a 3.5 Mc linear phase filter and combined with the 4.5 Mc aural subcarrier. The combined signal is then transmitted via the video transmission system to the ground transmitter. At the receiving end of the system the combined signal is received at the ground receiver, transmitted via the video transmission system to the control building. After amplification, the 4.5 Mc aural subcarrier is separated from the video signal and demodulated by a discriminator centered at 4.5 Mc. Two outputs are provided from the diplexer; one for video, the other for audio.

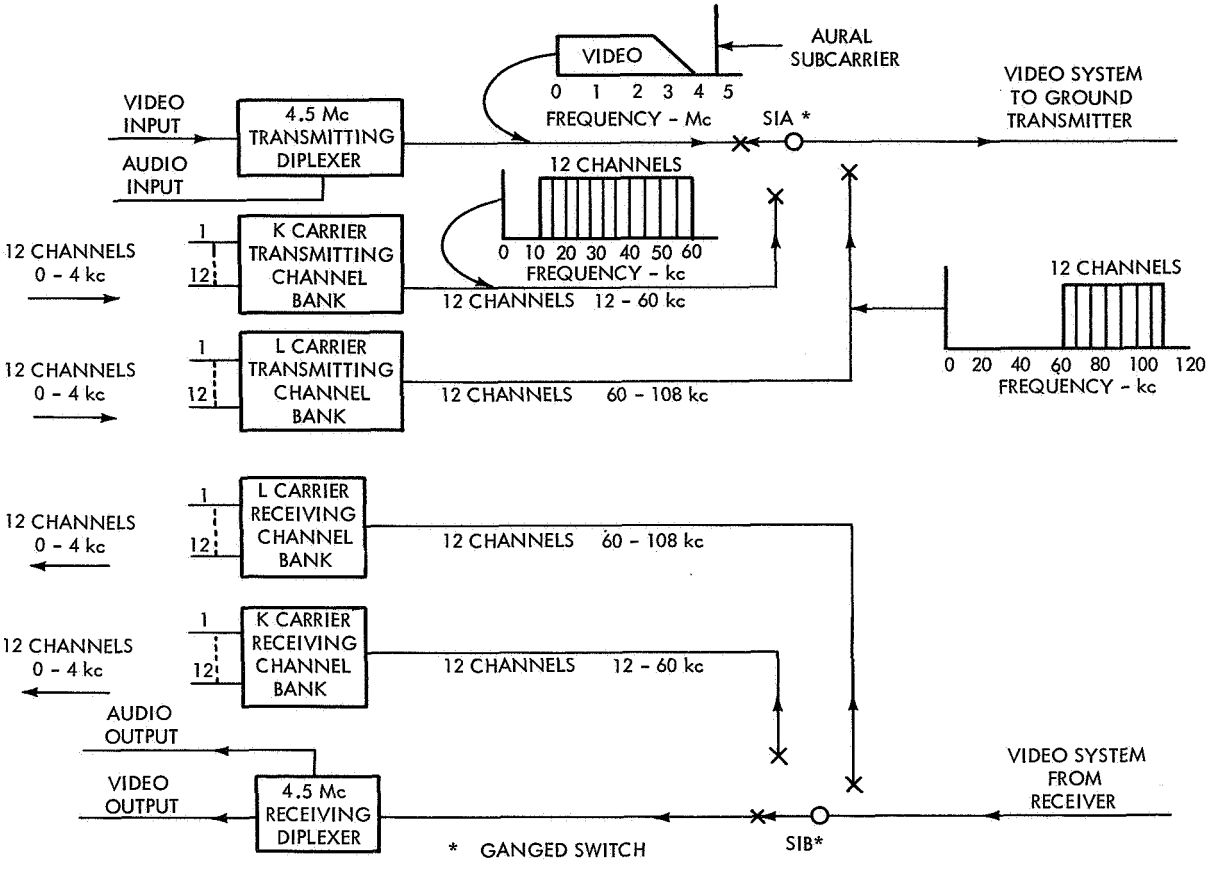


FIGURE 10–2.—Andover multiplex system.

Two-way telephone transmission is accomplished using standard "L" or "K" carrier multiplex equipment. Using "L" carrier multiplex equipment, 12 individual (0 to 4 kc) channels are translated in frequency to the 60 to 108 kc band. Using the "K" carrier multiplex equipment, 12 individual (0 to 4 kc) channels are translated in frequency to the 12 to 60 kc band. After multiplexing, the combined signal is transmitted to the ground transmitter via the video transmission system. Table 10–1 lists the frequencies used for one and two-way transmission through the satellite.

This table indicates that for two-way transmission the ground transmitter frequency is offset by 1.667 Mc and the ground receiver is offset by 5.000 Mc from that normally used (1725 and 4169.72 Mc). This permits the splitting of the RF bandwidth for simultaneous transmission in both directions by two ground stations. Narrow bandpass filters 3 Mc wide are inserted at IF at the ground station to select the desired IF signal. The undesired signal is also amplified and the two signals are compared to permit equalizing the carriers if this is required for optimum results.

TABLE 10–1

One-way transmission
1725 Mc from ground to satellite
4169.72 Mc from satellite to ground
Two-way transmission
Station A
1723.333 Mc from ground to satellite
4174.72 Mc from satellite to ground
Station B
1726.667 Mc from ground to satellite
4164.72 Mc from satellite to ground

The normal frequency deviations used for two-way telephone transmission are presented in Table 10–2.

TABLE 10–2.—*Frequency Deviations for Two-Way Telephone Transmission*

Type	No. of channels	RMS deviation per channel (for a 1000 tone at 0 toll level)	
		Ground to satellite	Satellite to ground
"K" Carrier (12–60 kc)	12	29.6 kc	88.8 kc
"L" Carrier (60–108 kc)	12	105.0 kc	315.0 kc

The normal frequency deviations for television are given in Table 10–3.

TABLE 10–3.—*Frequency Deviations for Television*

Video peak to peak	13.7 Mc
Aural subcarrier peak to peak	2.7 Mc
Audio deviation of aural subcarrier peak to peak	100.0 kc

RECEIVED CARRIER POWER

In light of the importance of received carrier power data in the analysis of satellite performance and because of the many variables involved, repeated measurements were made to insure valid data.

The received carrier power in the communications channel was measured continuously during tests at the ground receiver by monitoring the voltage in the main IF amplifier's automatic gain control circuit. Measurements of received carrier power at the satellite were obtained from NASA. This data reported the received carrier power at the satellite at 1-minute intervals during the tests.

Measurements are estimated to be accurate ±0.5 db at the ground receiver. In general, when range, spin angle and measurement accuracies are considered, the measured values of received carrier powers at the satellite agree with the predicted values. The measured values of received carrier powers at the ground are higher than those computed from published data of effective radiated power by approximately 2 db.

Received Carrier Power vs. Range

Figure 10–3 is a plot of the ground received carrier power vs. range measured at

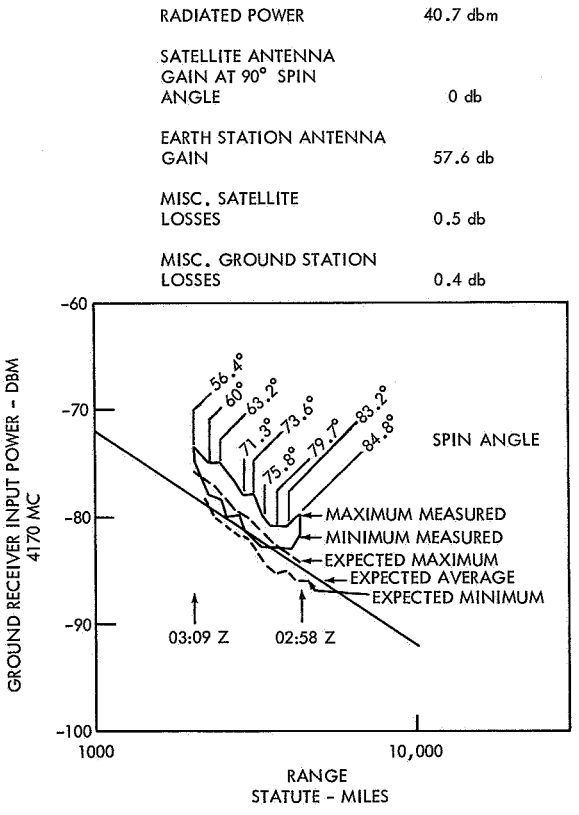


FIGURE 10–3.—Ground receiver input power—4170 Mc.

Andover during pass 1963. The expected value of received carrier power is also plotted along with the anticipated variation due to spin modulation. The assumptions used in the calculations are given in Table 10–4.

As can be seen from Figure 10–3 two effects are outstanding: (1) the effect of spin modulation varied from 1 through 4 db during the pass, and (2) as mentioned above,

the average received carrier power measured was some 2 db higher than anticipated, indicating an effective radiated power 2 db higher than assumed in the computations.

TABLE 10–4.—*System Constants*

	1725 Mc	4170 Mc
Radiated power	+70 dbm	40.7 dbm
Satellite antenna gain at 90° spin angle	0.0 db	0 db
Earth station antenna gain	+49.9 db	57.6 db
Misc. satellite losses	0.5 db	0.5 db
Misc. ground station losses	2.3 db	0.4 db

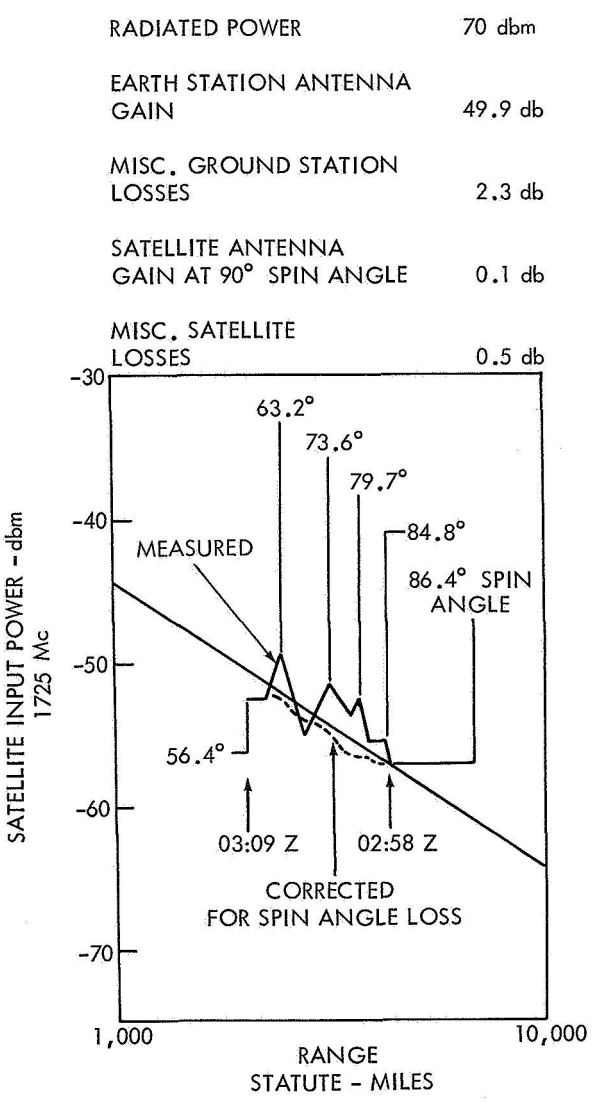


FIGURE 10–4.—Satellite input power—1725 Mc.

Figure 10–4 is a plot of the satellite input power vs. range during pass 1963. The expected value of received carrier power at the satellite, based on the assumptions given in Table 10–4, is also plotted in the same figure as a straight line (the loss due to variations in the spin angle is shown as a dashed line). In general, the average value measured agreed with the anticipated average.

BASEBAND TRANSMISSION

Although only typical results are presented in this section many baseband transmission measurements were made: (1) because the nature of the test program required this data as an auxiliary to other data being gathered, and (2) because the experimental nature of the station required that many different circuit configurations be used.

The baseband gain vs. frequency characteristics for various loops are shown in Figure 10–5 through 10–17. Figures 10–5 through 10–8 show the bandpass characteristic for the test trunks, baseband loop, IF loop, and boresight loop, respectively. Figure 10–9 and 10–10 show bandpass characteristics on the satellite loop taken at different times during pass 1633. These figures were taken when the circuit included the standard FM receiver and its associated circuitry without

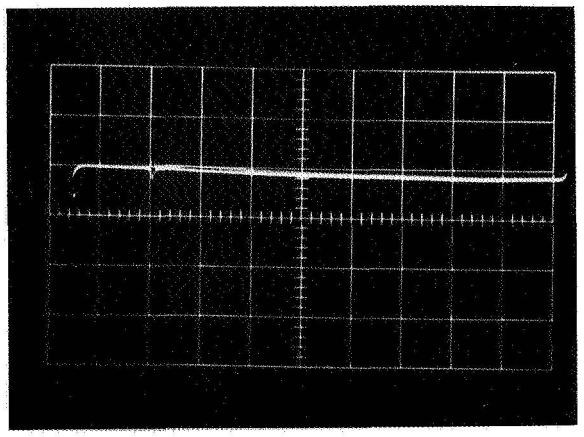


FIGURE 10–5.—Bandpass characteristic—transmitting test trunk #1 to receiving test trunk #2. Pass 1633—7/11/63.

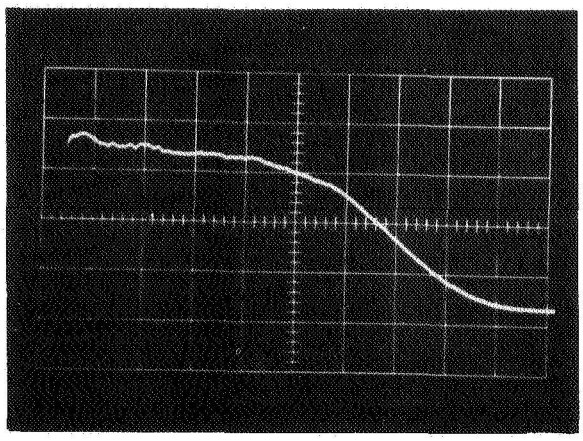


FIGURE 10–6.—Bandpass characteristic — standard receiver baseband loop—no filters, diplexers or clampers.

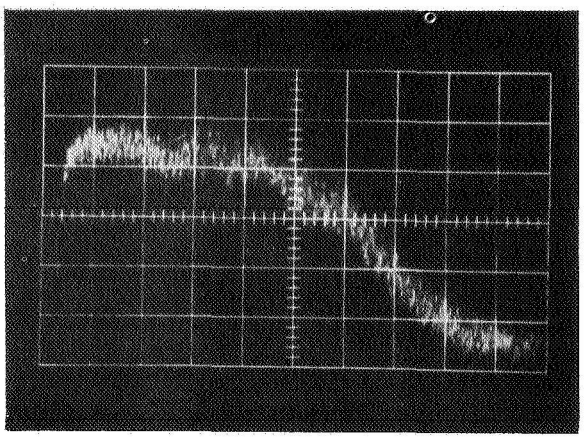


FIGURE 10–8.—Bandpass characteristic — standard receiver boresight loop—no filters, diplexers or clampers.

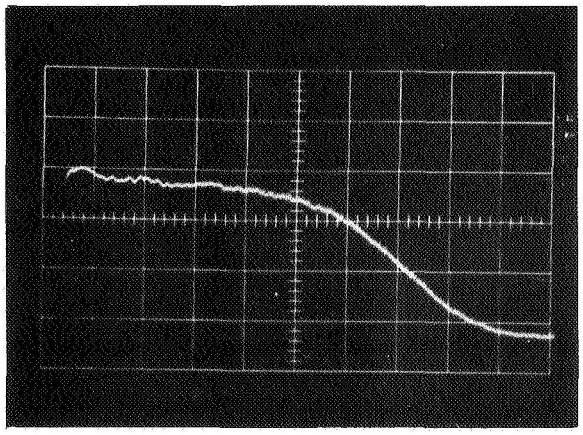


FIGURE 10–7.—Bandpass characteristic — standard receiver IF loop—no filters, diplexers or clampers.

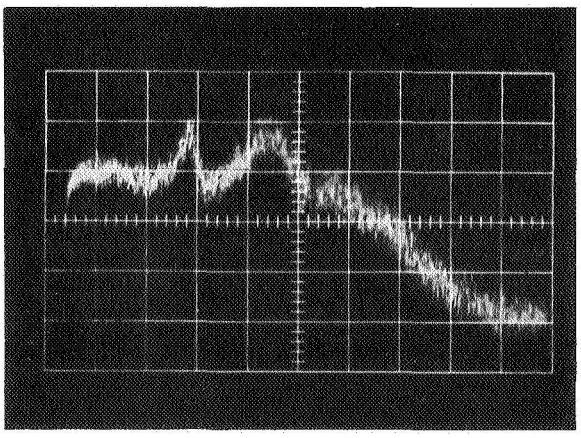


FIGURE 10–9.—Bandpass characteristic — standard receiver satellite loop — no filters, diplexers or clampers. Pass 1633—1800Z time.

clampers, diplexers or band-limiting filters. Figures 10–9 and 10–10 taken at different times during the pass show pronounced peaks ($\cong$ 1 db) centered at 2.9 and 4.5 Mc. Comparing these figures with Figure 10–7 shows these gain deviations are attributable to the Relay satellite. In general, the satellite loop is flat to within 1.5 db out to 6.0 Mc.

Figures 10–11 through 10–15 show the bandpass characteristics for the baseband, IF boresight and satellite loops, respectively when using the FM feedback receiver and its associated circuitry without clampers, diplexers and band-limiting filters. As can be seen from Figure 10–11 the baseband loop is similar to that used with the standard FM receiver. Figure 10–14 and 10–15 show the bandpass characteristic of the

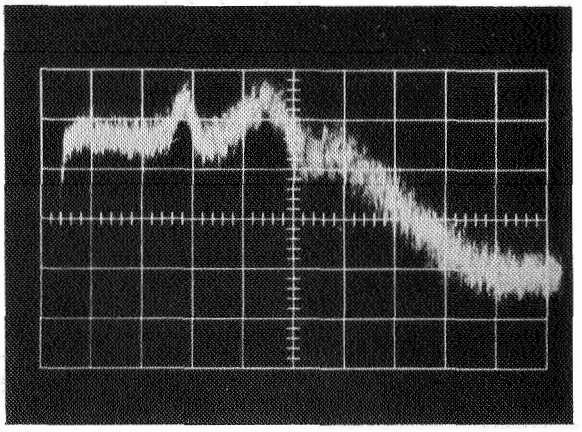


FIGURE 10–10.—Bandpass characteristic — standard receiver satellite loop — no filters, diplexers or clampers, pass 1633—1806Z time.

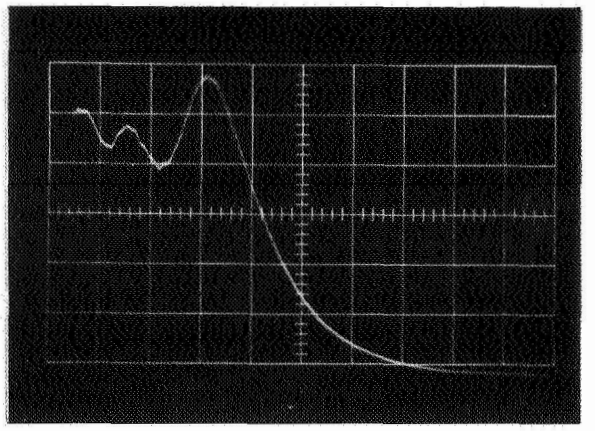


FIGURE 10–12.—Baseband characteristics—FM receiver IF loop—no filters, diplexers or clampers.

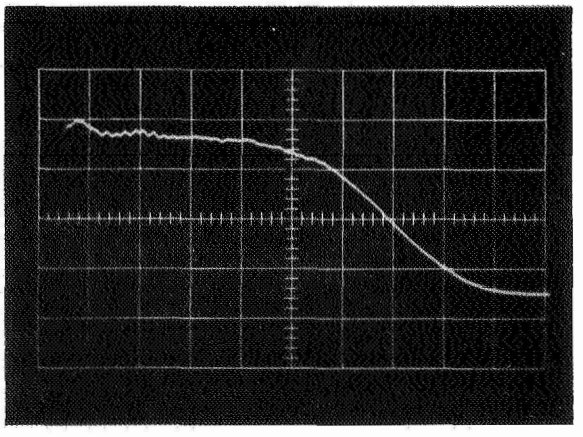


FIGURE 10–11.—Bandpass characteristic—FM feedback receiver baseband loop—no filters, diplexers or clampers.

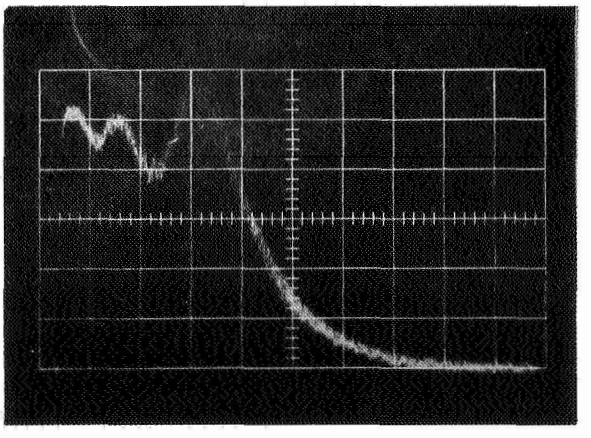


FIGURE 10–13.—Baseband characteristics — FM receiver boresight loop — no filters, diplexers or clampers.

satellite to be similar to that of the IF loop which is controlling.

Figures 10–16 and 10–17 show the bandpass characteristic obtained with the standard and FM feedback receiver circuit on a baseband loop when the circuit includes the diplexers and 3.5 Mc linear phase filters. As can be seen from these figures the 3 db bandwidth is limited to about 3.5 Mc when sound is added to the picture.

The Western Electric Video Visual Test Set was used to make the loop measurements. The set operates as follows: A low level signal (approximately —20 dbm) is swept through the video band and the return signal is measured for gain and displayed on a scope as a function of frequency. The result is then photographed.

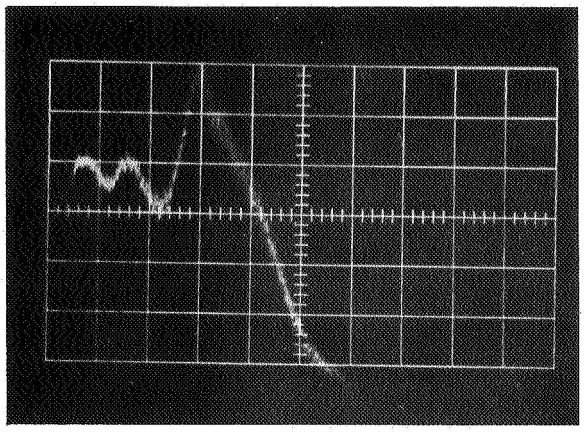


FIGURE 10–14.—Baseband characteristics—FM feedback receiver satellite loop, pass 1633, 1802Z time —no filters, diplexers or clampers.

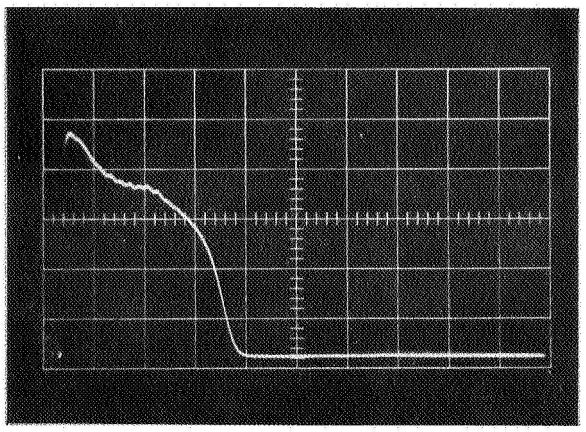


FIGURE 10–16.—Baseband characteristic FM feedback receiver baseband loop, diplexers and 3.5 Mc linear phase filters included in the circuit.

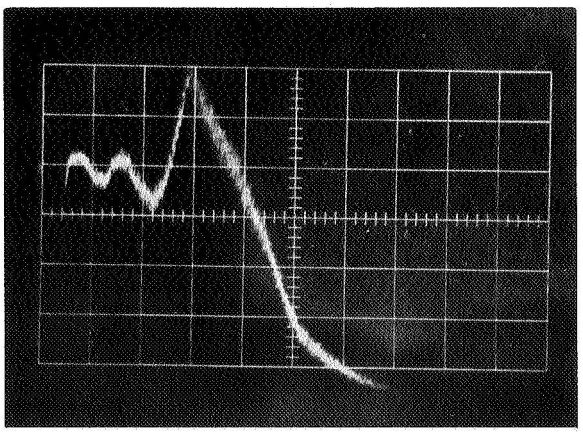


FIGURE 10-15.—Bandpass characteristic—FM feedback receiver satellite loop, pass 1633, 1803Z time—no filters, diplexers or clampers.

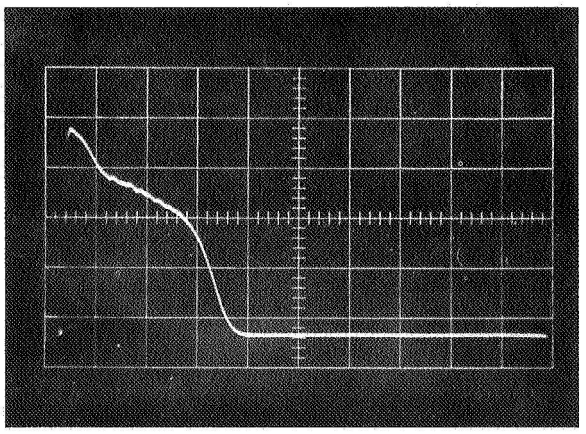


FIGURE 10–17.—Bandpass characteristic — standard receiver baseband loop—diplexers and 3.5 Mc linear phase filters included in the circuit.

NOISE

In view of the many parameters affecting the system baseband noise (e.g., satellite slant range, spin angle, satellite input power, ground receiver input power, noise temperature, etc.) repeated measurements were made to insure valid data.

Baseband Noise Spectrum

Typical measurements made from the test area are shown in Figure 10–18. These measurements were made using the FM feedback receiver in the circuit without clampers, diplexers or band-limiting filters. Curves 1, 2, and 3 represent the noise measured on the satellite loop. Curves 4 and 5 represent the noise measured on the IF and baseband loops, respectively. All curves have been corrected for the transmission characteristic measured. Curves 1, 2, and 3 were measured at separate times and at different slant ranges indicating the increase of noise with range. These curves in conjunstion with Curves 4 and 5 show the contribution of the baseband and FM terminals to the noise below 500 kc.

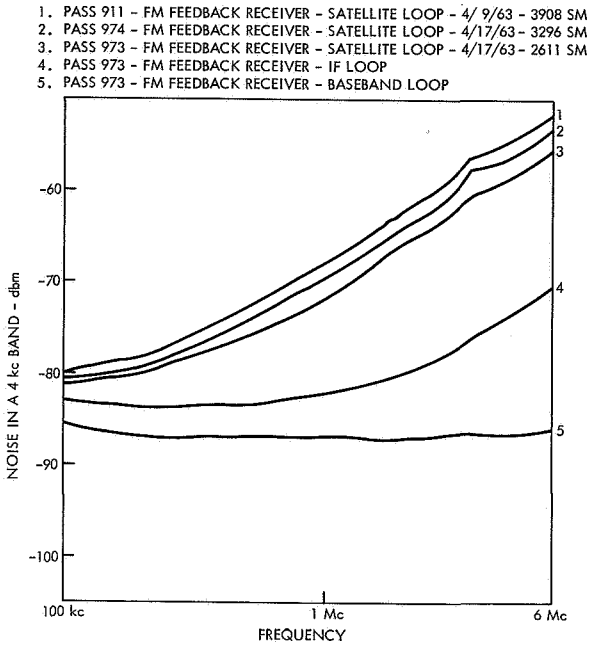


FIGURE 10–18.—Baseband noise spectrum FM feedback receiver.

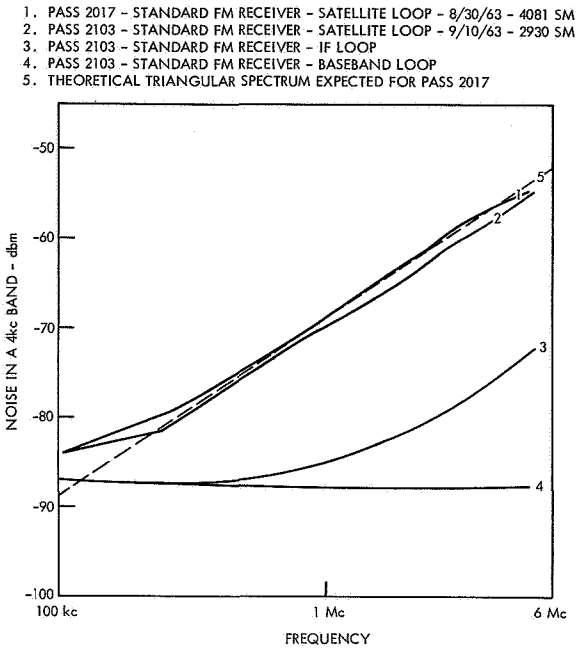


FIGURE 10–19.—Baseband noise spectrum standard FM receiver.

Other measurements were made using the standard FM receiver in the circuit without clampers, diplexers or band-limiting filters. The results of these measurements made from the test area are shown in Figure 10–19. Curves 1 and 2 represent the noise measured on the satellite loop at different times and different ranges and Curves 3 and 4 represent the noise measured on the baseband and IF loops, respectively. Curves 1 and 2 show the effect of increasing noise with increased range. These curves in conjuction with Curves 3 and 4 indicate the noise contribution of the video circuits and FM terminals. Comparing the two figures (10–18 and 10–19) it can be seen that the baseband noise is about the same in both cases but that the IF noise measured with the FM feedback receiver is about 2.5 to 3.5 db higher throughout the band.

Curve 1 of Figure 10–19 is a plot of the noise measured at 01:27Z time on August 30, 1963 on pass 2017. It is representative of the noise spectrum measured at about 2-minute intervals during the pass. At that time the ground receiver and satellite input powers measured -84 ± 1 dbm and -55.9 dbm, respectively. The corresponding calculated values based on the constants of the system noted previously in Table 10–4 and including a correction to take into account the loss due to the effect of an 83.2° spin angle were -84.4 ± 1.5 dbm and -56.1 dbm, respectively. Using the calculated values of received carrier powers, assuming a 14 db noise figure for the satellite, and a ground receiver noise temperature of 36.5° Kelvin, the computed value of the noise at the output of the received was -54 dbm in a 4 kc band centered at 10 Mc. From FM theory the noise should decrease by 20 db per decade resulting in a noise level of -74 dbm in a 4 kc band centered at 1 Mc. This corresponds to -68.8 dbm when measured at the test area rather than at the receiver output. The measured value at the test point was -68.8 dbm. The computed noise has been plotted as a dashed line Curve 5 on Figure 10–19. Curves 1 and 5 show the anticipated deviation from the triangular

spectrum since in practice the baseband noise is increased at low frequencies by the contribution of the baseband video and FM terminal circuits and the noise due to the satellite carrier supplies. A slight peak is also noticeable at about 3 mc. This corresponds to the peak in the transmission characteristic of the satellite noted earlier.

Telephone Noise

The thermal noise in the channels of a 600 channel telephone system can be calculated from the baseband spectrum. In the calculations made, the constants in Table 10–5 were assumed. Since the transmission level

TABLE 10–5

Average talker power at 0 TL	−11 dbm
Activity factor for multichannel telephony	0.25
Average power in a 600 channel load at 0 TL	+10.8 dbm
Peak factor for 600 channel load	12 db
Full load test tone at 0 TL	+22.8 dbm
Full load test tone in test area	− 5.2 dbm
Transmission level in test area	−17.6 db TL
0 dbm of white noise in a 3 kc band	88 dbrn C

(TL) at the test area is −17.6 db, the noise measured at that point is 17.6 db lower than that same noise measured at 0 TL. Further, since the noise was measured with the 37B Transmission Measuring Set having a 4 kc bandwidth, the level must be reduced by 1.2 db to obtain the equivalent noise in a 3.0 kc band (the assumed bandwidth of the actual telephone channel). Making the above correction and converting from dbm to dbrn "C" message weighted, the thermal noise expected in any channel may be determined from the baseband noise spectrum. This was done for eleven different channels using the CCITT frequency allocation for a 600 channel system and for the conditions that prevailed during pass 2017 as noted above and shown by Curve 1 of Figure 10–19.

The results are shown in Table 10–6.

Television Noise

Video Noise

The noise in the video channel was determined from the baseband noise spectrum by integration. This was done graphically using

TABLE 10–6.—*Telephone Channel Noise at O TL*

Channel #	Group #	Super group #	Frequency kc	Noise dbrn "C" mess. wt.
3	5	1	96–100	20.3
1	1	1	296–300	26.0
12	5	2	548–552	30.7
1	1	3	800–804	33.6
1	1	4	1048–1052	36.0
1	1	5	1296–1300	37.9
1	1	6	1544–1548	39.3
1	1	7	1792–1796	40.6
1	1	8	2040–2044	41.8
1	1	9	2288–2292	42.9
1	1	10	2536–2540	44.0

the baseband noise spectrum plotted as Curve 1 of Figure 10–19. The unweighted peak-to-peak signal to RMS noise determined was 42.2 db. The applicable curve of the latest Bell System weighting network was used and the weighted peak-to-peak signal (1 volt peak-to-peak) to RMS noise was calculated to be 52.2 db. The data for the baseband noise spectrum was taken on pass 2017 at 01:27Z time on August 30, 1963. At that time the ground receiver and satellite input powers calculated, as mentioned previously, were −84.4 ±1.5 dbm and −56.1 dbm, respectively, and the noise temperature was 36.5°K at the input to the ground receiver. Using these values and a satellite noise figure of 14 db in the following expression:

$$\frac{S}{N} = \frac{3 f_{p\text{-}p}^{\,2}}{\left[n^2\left(\frac{\phi_v}{S_v} + \frac{\phi_g}{S_g}\right)\right] f_m^{\,3}}$$

where

$f_{p\text{-}p}$ = peak-to-peak satellite to ground signal frequency deviation, cps
n = the deviation multiplication factor of the satellite
ϕ_r = satellite receiver noise density, watts/cps
ϕ_g = ground receiver noise density, watts/cps
S_v = satellite received power, watts
S_g = ground received signal power, watts

The unweighted peak-to-peak signal to noise calculated was 41.9 db and the corresponding weighted peak-to-peak signal to

noise calculated was 51.9 db. This compares with the measured values of 42.2 and 52.2 db, respectively.

The weighted peak-to-peak signal to RMS noise was measured directly on many passes during the period of the tests. Typical measurements are given in Table 10–7.

TABLE 10–7.—*Video Noise*

Pass.	Rec.	Time Z	Range statute miles	Weighted Peak-to-peak signal / RMS NOISE
231	STD	15:15–15:37	4650–3059	52.8–54.4 db
323	STD	10:32–10:56	4863–4440	51.0–52.0 db
502	STD	10:47–11:08	4845–4192	50.8–52.0 db

These measurements are also plotted against the expected theoretical value in Figure 10–20.

Audio Noise

The noise in the audio channel associated with television transmission was measured using the Bell System 8 kc program noise-weighting network in the 3A noise measuring set. As noted earlier, in the Relay system, the audio portion of the television material is multiplexed on the baseband video signal and the composite signal is used to frequency modulate the carrier. The quality of the audio is determined in part by the thermal noise present in the channel.

The peak signal to RMS noise ratio measured for passes 642 and 880 is plotted in Figure 10–21 as a function of range. Also plotted in the figure is the expected value of peak signal to RMS noise determined as follows:

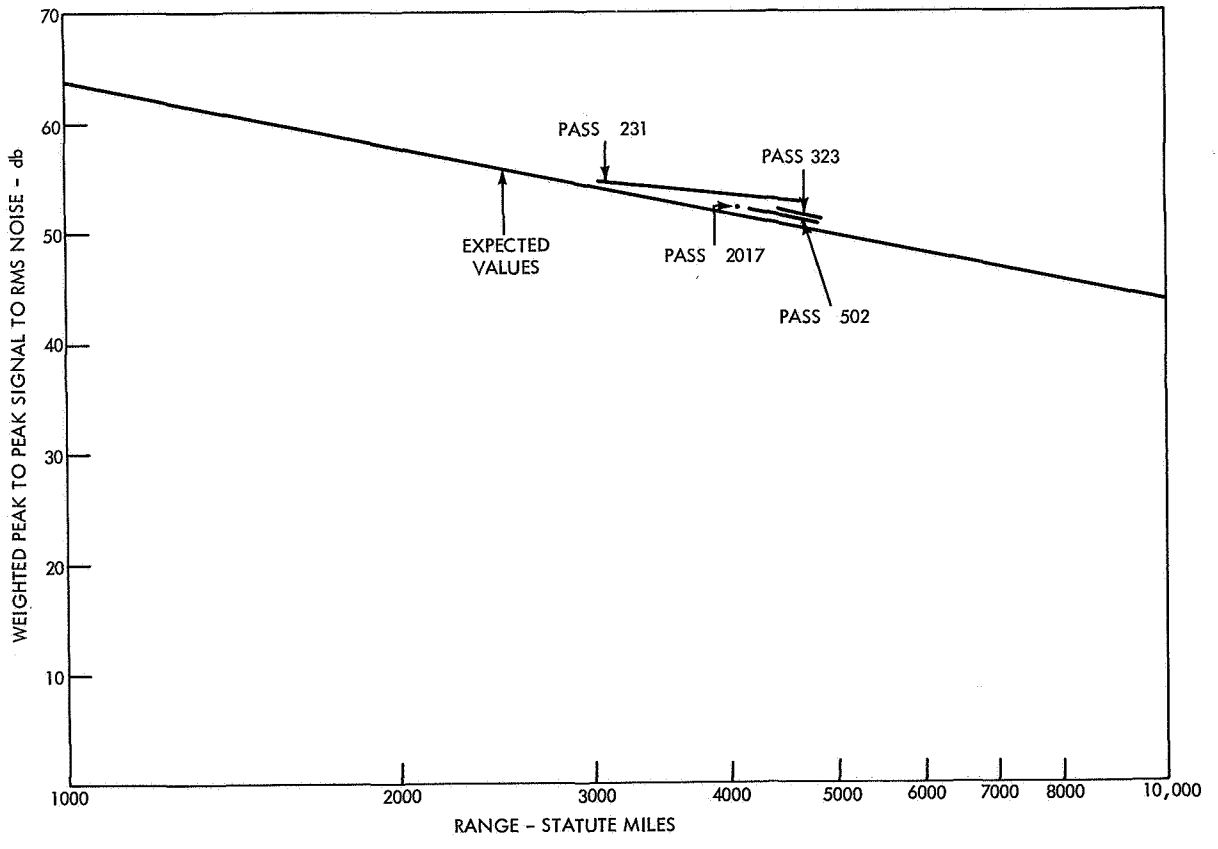


FIGURE 10–20.—Video signal-to-noise.

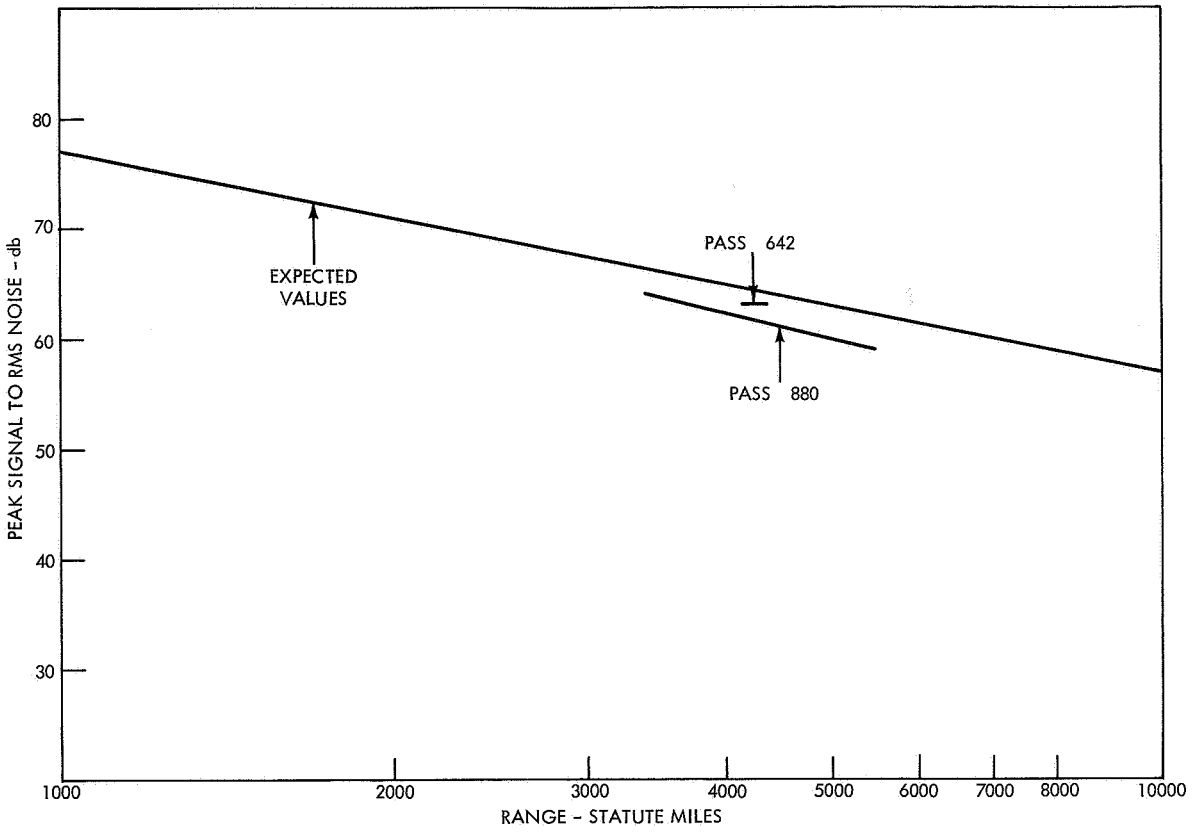


FIGURE 10–21.—Audio peak signal/RMS noise.

The unweighted peak to RMS noise ratio for an FM–FM subcarrier system is:

$$\frac{S}{N} = \frac{3\,\phi_{sc}^2\, f_{pa}}{2\left[\, n^2\left(\frac{\phi_s}{S_s} + \frac{\phi_g}{S_g}\right)\right] f_a{}^3}$$

where

ϕ_{sc} = the modulation index of the audio subcarrier on the carrier from satellite to ground, radians

f_{pa} = peak deviation of the audio subcarrier, cps

f_a = highest audio frequency, cps

$n, \phi_s, S_s, \phi_g, S_g$ = have been defined on page 486.

The unweighted peak signal to RMS noise ratio is decreased by some 4.8 db when program weighting is used and is increased by a factor of 8.7 db because of the effect of pre-emphasis and de-emphasis as computed from the following expression.*

$$D = \frac{f_a{}^3}{3\,f_1{}^3\left[\frac{f_a}{f_1} - \tan^{-1}\frac{f_a}{f_1}\right]}$$

where

f_1 = first breakpoint of the de-emphasis network = 2.1 kc

f_a = highest audio frequency, cps

The measurements on pass 642 were made with the standard FM receiver in the circuit while those on pass 880 were made with the FM feedback receiver in the circuit. All measurements were made without a video signal present. This precludes video to audio cross modulation which adds to the noise in the channel as discussed later in this chapter.

*Mischa Schwartz, Information Transmission, Modulation and Noise, McGraw-Hill, 1959, p. 309.

NONLINEARITY

Repeated measurements were made of the various causes of distortion in the FM systems to insure that the constants of the system remained stable. Typical results are presented.

Envelope Delay Distortion

The envelope delay distortion discussed here is generated in the IF and RF circuitry of the system and causes cross modulation in FM systems. Envelope delay distortion was measured by the two frequency sweep method, using the standard test set used on TD–2 and TH radio systems. In this method the carrier is swept approximately ±4 Mc with a 100 cps sine wave applied to the BO klystron of the FM deviator so that the output of the IF is swept from 70 to 78 Mc. Simultaneously a 278 kc sine wave is applied at the video input to the FM deviator to provide a peak deviation of about 80 kc. The 100 cps and 278 kc signals are recovered and separated at the FM receiver video output. (Because of the tripling action of the satellite, the IF sweep on the down path is from 62 to 86 Mc.) The 100 cps sine wave is used for horizontal scope deflection. The 278 kc tone which has been phase modulated by the transmission delay distortion of the system is compared in phase with a 278 kc crystal controlled oscillator located in the delay set reciever. The crystal controlled oscillator is phase locked to the long-term average phase of the received 278 kc tone. The phase variations are used for vertical scope deflection with a sensitivity of 5 nanoseconds (nsec.) per small division. (At 278 kc, 1 degree is equivalent to 10 nsec.)

Each of the elements shown in Figure 10–1 contributes to the total envelope delay distortion (EDD) of the system. The EDD is mostly parabolic and is inherent in the bandpass characteristic of the system. Using delay equalizers with the inverse characteristic improves the cross modulation performance of the system for telephone operation and differential phase for TV operation. Delay equalizers have been provided for the IF loop. The loop included the deviator, FM receivers and the ground receiver IF amplifier combination. Figure 10–22 shows that the EDD measured on the IF loops is negligible. Figure 10–23 shows the envelope delay distortion measured on a satellite loop on pass 200, January 8, 1963. This is typical of several measurements made during the testing period. In this case, the shape of the EDD is made up principally of about 45 nsec slope and 30 nsec of parabola across the 24 Mc band. In addition, a ripple of 5 to 6 Mc period and about 10 nsec duration peak to peak appears superimposed on the curve. No delay equalization has been provided for the RF portion of the system which includes the ground transmitter, the satellite and the RF portion of the ground receiver.

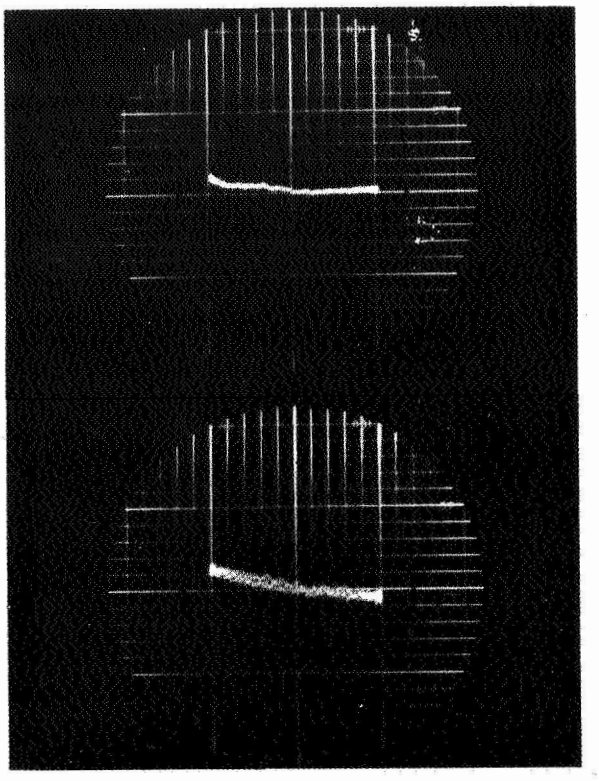


FIGURE 10–22.—Envelope delay distortion of IF loop.

Differential Phase and Gain

Differential phase is a measure of the phase nonlinearity of a system over the RF

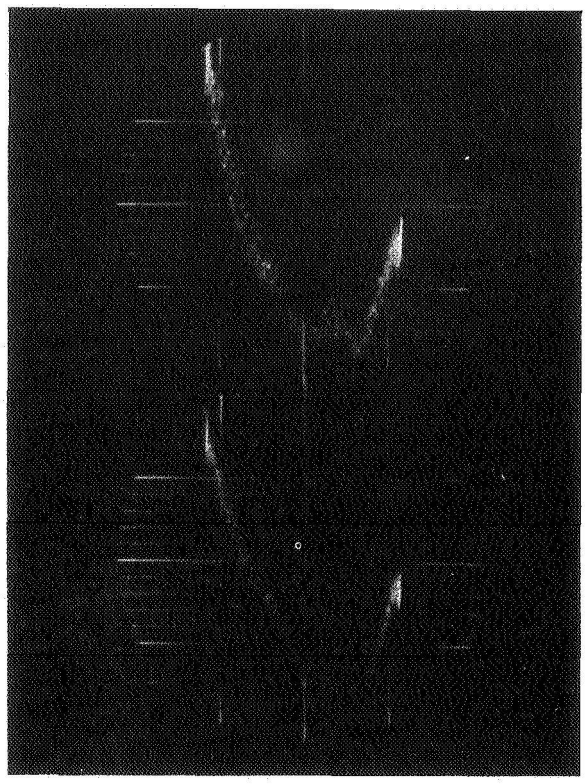


FIGURE 10–23.—Envelope delay distortion of satellite loop.

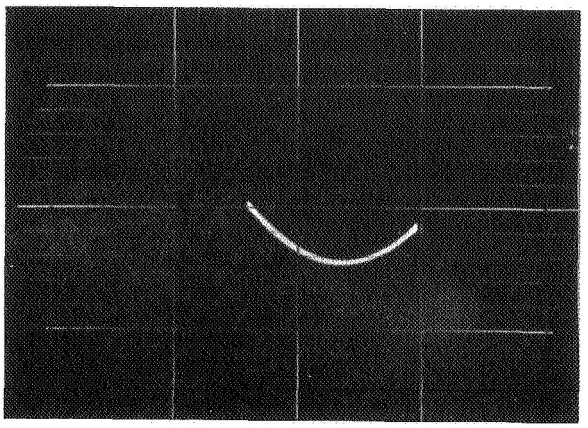


FIGURE 10–24.—Baseband loop differential gain, standard FM receiver.

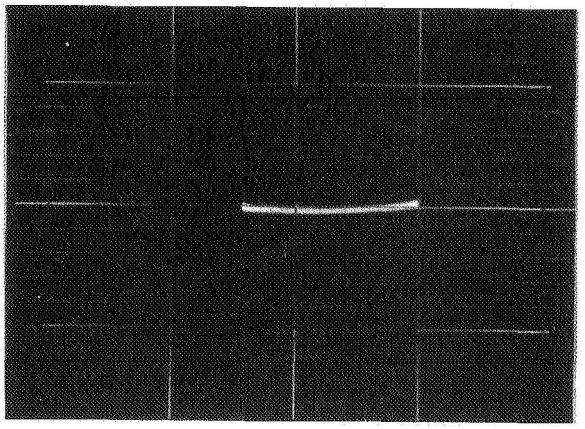


FIGURE 10–25.—Baseband loop differential phase, standard FM receiver.

bandwidth corresponding to the frequency deviation of the picture portion of the video signal. Differential gain is a measure of the amplitude nonlinearity of the system and is due primarily to the baseband nonlinearity.

The measurements were made by transmitting two test signals, one at a low frequency (15.75 kc) adjusted to sweep ±7 Mc at 74 Mc. The other, a fixed frequency at 3.58 Mc applied at a power level 14 db below that of the low frequency signal. The test signals were applied to the video lines in the test area. At the receiving end of the system, the 15.75 kc tone drove the horizontal sweep and either the gain or phase variations of the 3.58 Mc tone may be selected to drive the vertical sweep.

Figures 10–24 and 10–25 show the differ-

ential gain and phase measured on the baseband loop. Figures 10–26 and 10–27 show the differential gain and phase measured on the satellite loop. These are typical of other measurements made during the testing period. As can be seen from Figure 10–27 the differential phase was high, in the order of 45°. However, the system was not delay equalized at RF and since the differential phase and EDD are related, delay equalization would reduce the amount of differential phase in the system.

Noise Loading

The performance of a 600 channel multiplex telephony system can be approximated by a noise loading test. For this test a broad band of noise from 60 to 2660 kc was transmitted from the test area at power levels varying from —7 to —51 db. Three narrow band stop filters centered at 70 kc, 1248 kc and 2438 kc prevent the signal from being transmitted in these bands. At the receiving end of the circuit, the noise in a 3.1 kc band centered at 70 kc, 1248 kc and 2438 kc was measured as a function of the transmitted power level. Noise (cross modulation + thermal noise) was then plotted as a function of the RMS deviation of a 0 dbm test tone at 0 toll level. The constants noted in Table 10–5 are applicable to the calculations.

Figures 10–28, 10–29, and 10–30 show the results of measurements made with the standard FM receiver without pre-emphasis on the baseband, IF, and satellite loops. The data used to obtain Figure 10–30 were taken from 02:56:44 through 03:07:45Z time on

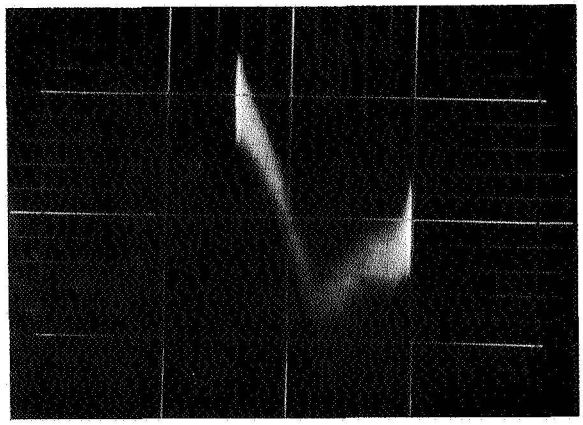


FIGURE 10–26.—Satellite loop—differential gain pass 339, 1/26/63—standard FM receiver.

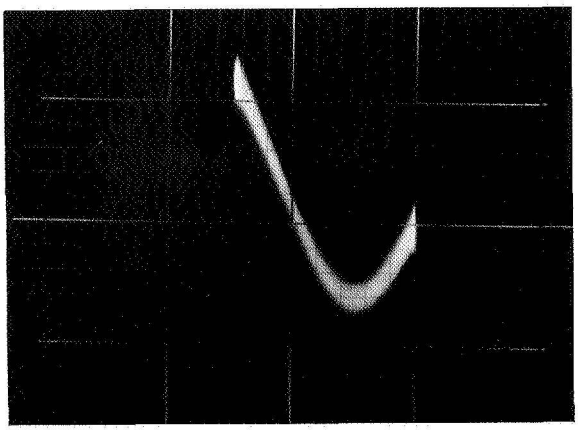


FIGURE 10–27.—Satellite loop—differential phase, pass 339—1/26/63. Standard FM receiver.

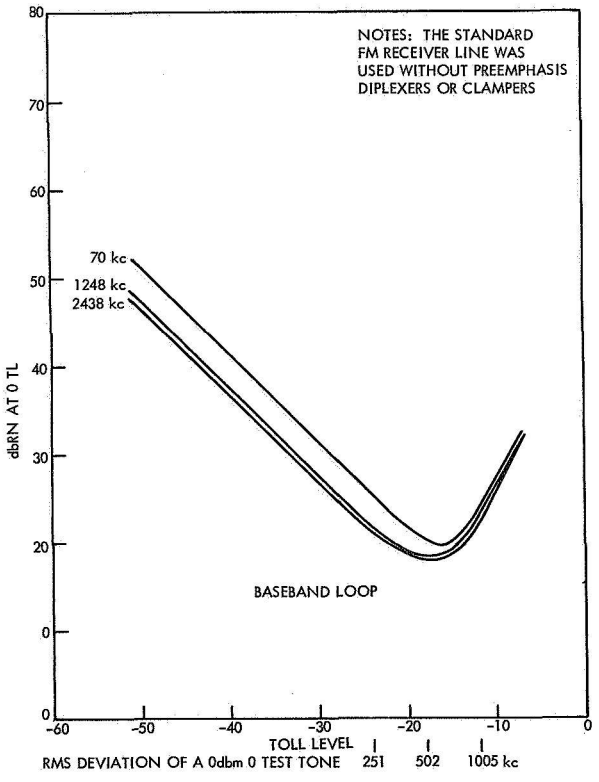


FIGURE 10–28.—Relay pass 1963—600 channel noise loading—baseband loop.

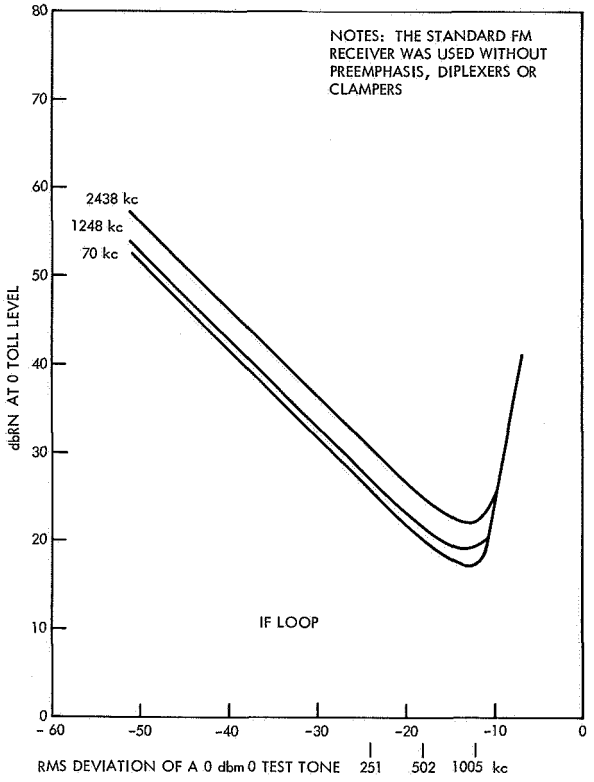


FIGURE 10–29.—Relay pass 1963—600 channel noise loading—IF loop.

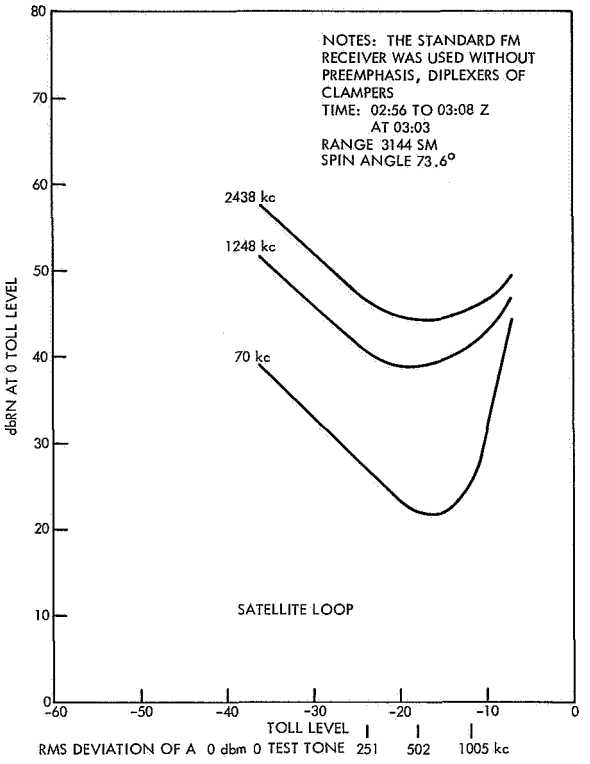


FIGURE 10–30.—Relay pass 1963—600 channel noise loading—satellite loop.

pass 1963. At 03:03Z time the range was 3144 statute miles and the spin angle was 73.6°. The ground receiver and satellite input powers calculated using the constants given in Table 10–4 were —82 and —54.6 dbm, respectively.

The thermal noise calculated for a test tone deviation of 502 kc was 35.8 dbRN "C" message weighted, at 0 TL at the center frequency of 1248 kc. The measured value of the thermal noise from Figure 10–30 was 35 dbRN "C" message weighted. The total noise measured (cross modulation plus thermal) was 38.8 dbRN "C" message weighted. The difference on a power basis represents the cross modulation noise. In this case the cross modulation noise was 36.5 dbRN "C" message weighted.

Noise loading tests using the FM feedback receiver were conducted on pass 858. The results of these measurements are shown in Figures 10–31, 10–32 and 10–33 representing measurements made on the baseband, IF, and satellite loops without pre-emphasis. The data taken for Figure 10–33 were taken at about 04:11Z time. At that time the range was 4006 statute miles. The ground receiver and satellite input powers calculated using the constants given in Table 10–4 were —84 and —56.6 dbm, respectively. The thermal noise calculated for a test tone deviation of 502 kc was 38.3 dbRN "C" message weighted at 0 TL at the center frequency of 1248 kc. The measured value of the thermal noise from Figure 10–33 was 40.5 dbRN "C" message weighted. The total noise measured (cross modulation plus thermal) was 42.5 dbRN "C" message weighted. The difference on a power basis represents the cross modulation noise. In this case, the cross modu-

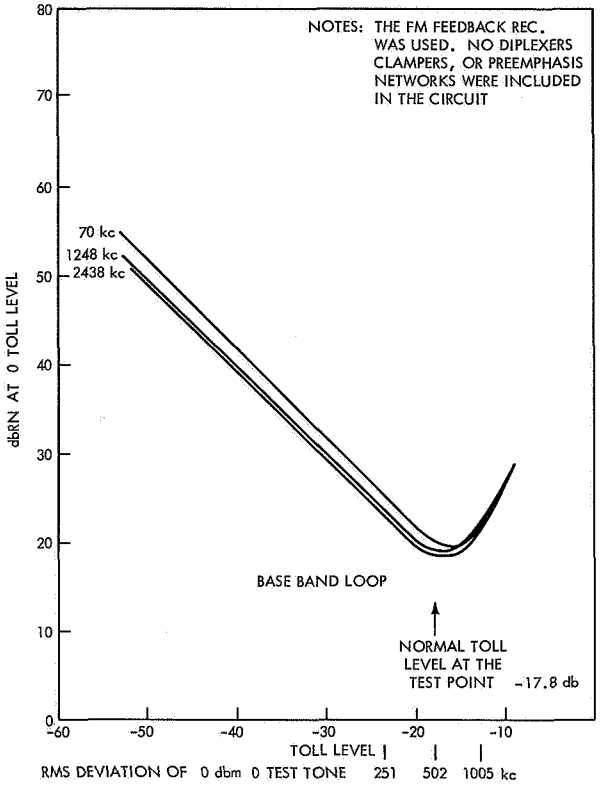


FIGURE 10–31.—Relay pass 858—600 channel noise loading—baseband loop.

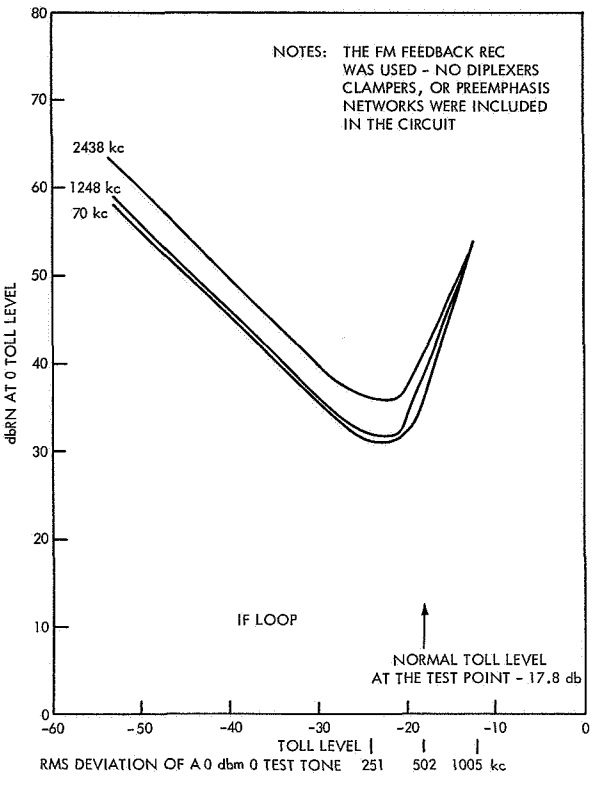


FIGURE 10–32.—Relay pass 858—600 channel noise loading—IF loop.

lation noise is 38.2 dbRN "C" message weighted.

Video to Audio Intermodulation

Audio noise measurements were previously discussed for the condition where no video signal was being received. When video material is present, the audio noise increases due to cross modulation resulting from the nonlinearity of the overall system. The data taken for the two passes previously used to discuss audio noise is given in Table 10–8. As can be seen from the data, considerable degradation in the audio S/N ratio can be attributed to the presence of the video signal.

TABLE 10–8.—*Video-to-Audio Cross Modulation*

Video signal	Pass 642 Stanbard receiver $\frac{\text{Peak signal}}{\text{RMS noise}}$ db Program weighted	Pass 880 FM feedback receiver $\frac{\text{Peak signal}}{\text{RMS noise}}$ db Program weighted
None	63.0	59.0–64.0
Monoscope	58.0	54.0
Stairstep	58.5	57.0
$\sin^2$ pulse and window	57.0	52.0
Multiburst	59.0	53.0

TELEVISION TEST PATTERNS

Typical photographs of test patterns transmitted through the Relay I satellite, selected from the many taken on various passes, are presented in this section. Such photographs afford a means of rapidly evaluating satellite performance.

FM Feedback Receiver

Television test patterns are used to evaluate the over-all transmission characteristics of a satellite system. Relay pass 880 was used to photograph the multiburst, sine-

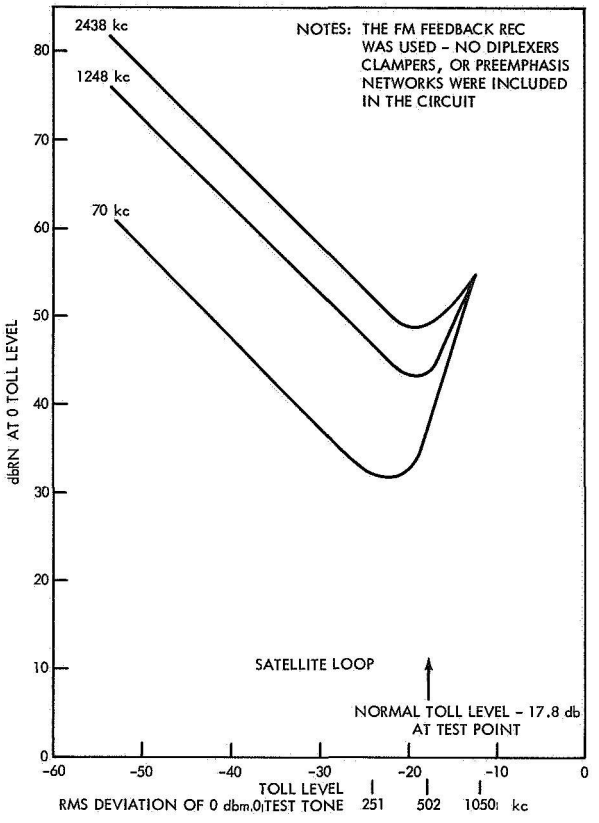


FIGURE 10–33.—Relay pass 858—600 channel noise loading—satellite loop.

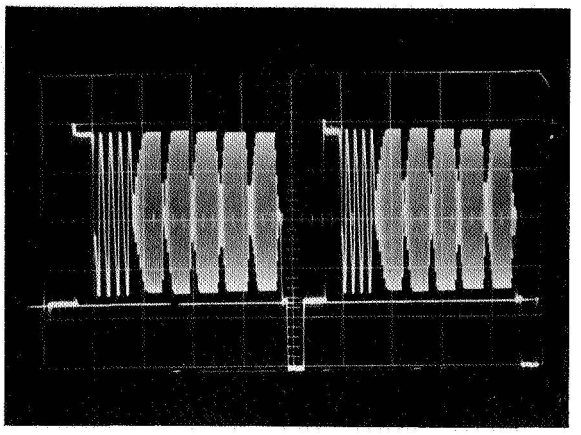


FIGURE 10–34.—Oscilloscope presentation of multiburst test pattern, Andover satellite up path.

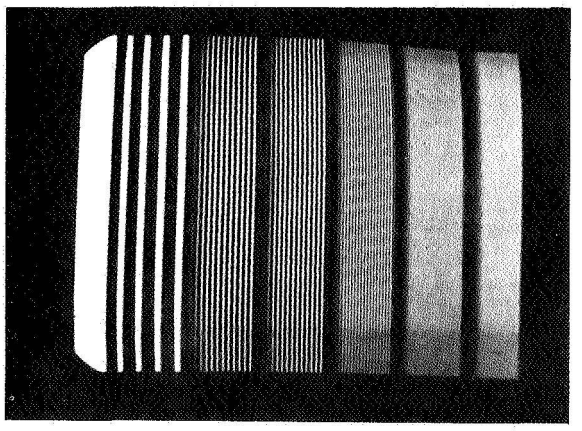


Figure 10–35.—Monitor presentation of multiburst test pattern, Andover satellite up path.

squared pulse, stairstep, window and monoscope test patterns on the baseband, IF and satellite loops. The FM feedback circuit used included video clampers and audio diplexing equipment. No video pre-emphasis or band-limiting filters were included in the circuit. Table 10–9 is an index of (Figures 10–34 thru 10–77). This table lists for each photograph the type of signal, the loop used, the receiver used and the type of presentation and sweep rate where necessary. It can be seen from the photographs that no appreciable degradation of the signal can be attributed to the satellite except for the expected noticeable increase in noise. The band limiting shown by the multiburst is due primarily to the audio diplexing equipment used. Included for direct comparison are photographs of the test patterns before transmission. Both oscilloscope and monitor photographs are included.

TABLE 10–9.—*Photographic Index*
[*Relay Pass 880—April 5, 1963*]

Figure No.	Type of signal	Circuit	Receiver	Monitor	Oscilloscope	Oscilloscope sweep
10–34	Multiburst	Up path	----------		√	
10–35	"	Up path	----------	√		
10–36	"	BB loop	----------		√	
10–37	"	BB loop	----------	√		
10–38	"	IF loop	FMFB		√	
10–39	"	IF loop	FMFB	√		
10–40	"	SAT loop	FMFB		√	
10–41	"	SAT loop	FMFB	√		
10–42	Sin^2	Up path	----------		√	
10–43	"	Up path	----------	√		
10–44	"	BB loop	----------		√	
10–45	"	BB loop	----------	√		
10–46	"	IF loop	FMFB		√	
10–47	"	IF loop	FMFB	√		
10–48	"	SAT loop	FMFB		√	
10–49	"	SAT loop	FMFB	√		
10–50	Stairstep	Up path	----------		√	
10–51	"	Up path	----------	√		
10–52	"	BB loop	----------		√	
10–53	"	BB loop	----------	√		
10–54	"	IF loop	FMFB		√	
10–55	"	IF loop	FMFB	√		
10–56	"	SAT loop	FMFB		√	
10–57	"	SAT loop	FMFB	√		
10–58	Window	Up path	----------		√	Line
10–59	"	Up path	----------		√	Field
10–60	"	Up path	FMFB	√		
10–61	"	BB loop	----------		√	Line
10–62	"	BB loop	----------		√	Field
10–63	"	BB loop	----------	√		
10–64	"	IF loop	FMFB		√	Line
10–65	"	IF loop	FMFB		√	Field
10–66	"	IF loop	FMFB	√		
10–67	"	SAT loop	FMFB		√	Line
10–68	"	SAT loop	----------		√	Field
10–69	"	SAT loop	FMFB	√		
10–70	Monoscope	Up path	FMFB		√	
10–71	"	Up path	FMFB	√		
10–72	"	BB loop	FMFB		√	
10–73	"	BB loop	FMFB	√		
10–74	"	IF loop	FMFB		√	
10–75	"	IF loop	FMFB	√		
10–76	"	SAT loop	FMFB		√	
10–77	"	SAT loop	FMFB	√		

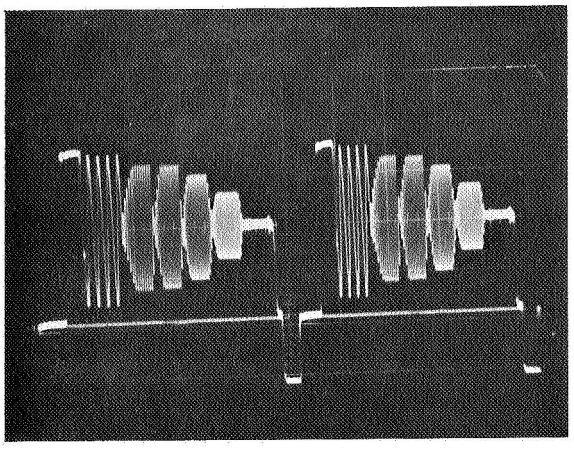


FIGURE 10–36.—Oscilloscope presentation of multiburst test pattern, Andover baseband loop satellite down path.

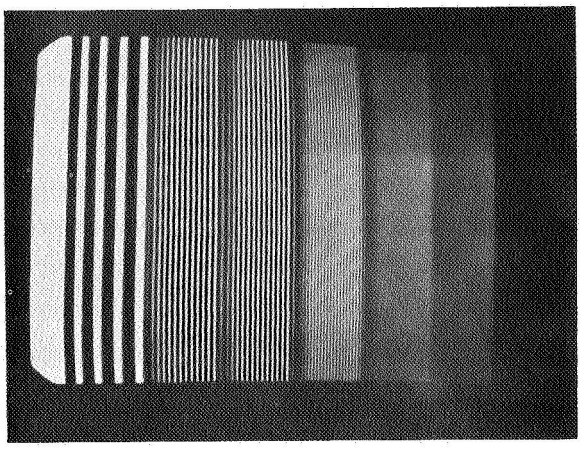


FIGURE 10–37.—Monitor presentation of a multiburst test pattern, Andover baseband loop satellite down path.

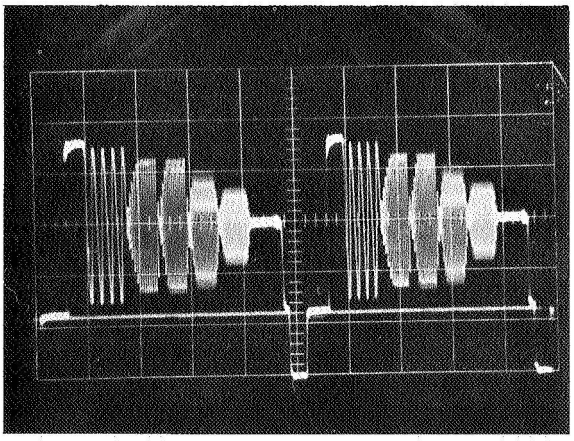


FIGURE 10–38.—Oscilloscope presentation of multiburst test pattern, Andover IF FMFB loop satellite down path.

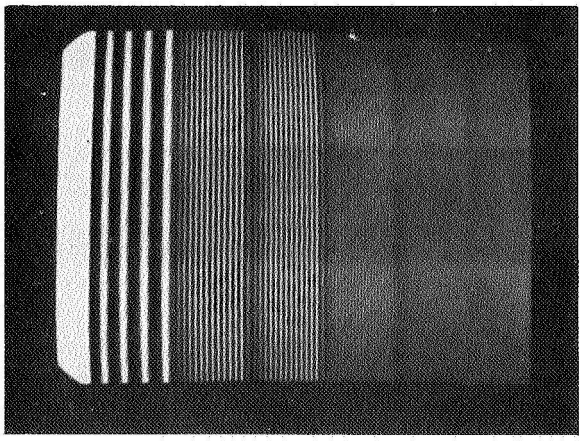


FIGURE 10–39.—Monitor presentation of multiburst test pattern, Andover IF FMFB loop satellite down path.

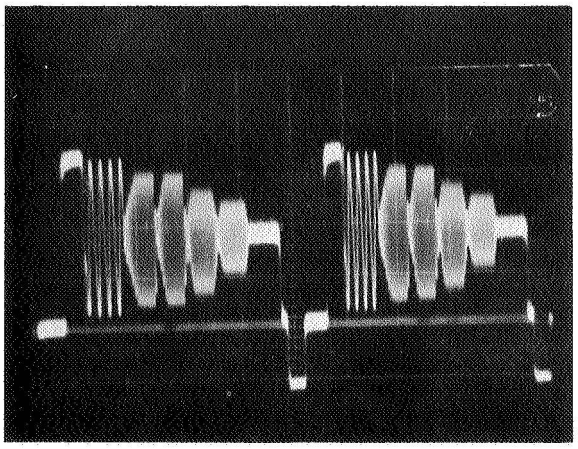


FIGURE 10–40.—Oscilloscope presentation of a multiburst test pattern, Andover satellite loop satellite down path.

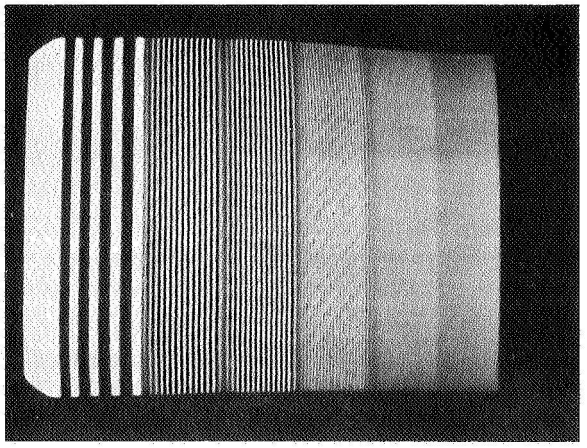


FIGURE 10–41.—Monitor presentation of multiburst test pattern, Andover satellite loop satellite down path.

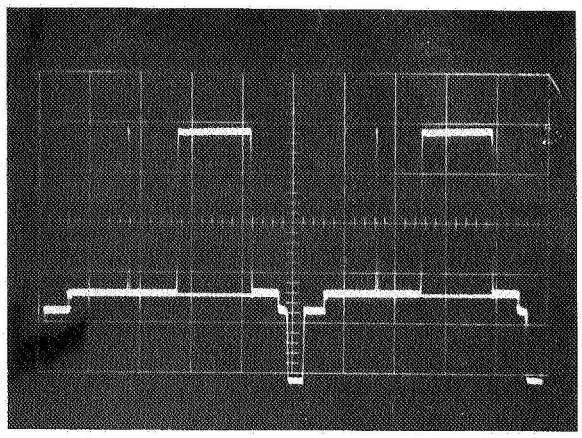


FIGURE 10–42.—Oscilloscope presentation of sine squared test pattern, Andover satellite up path.

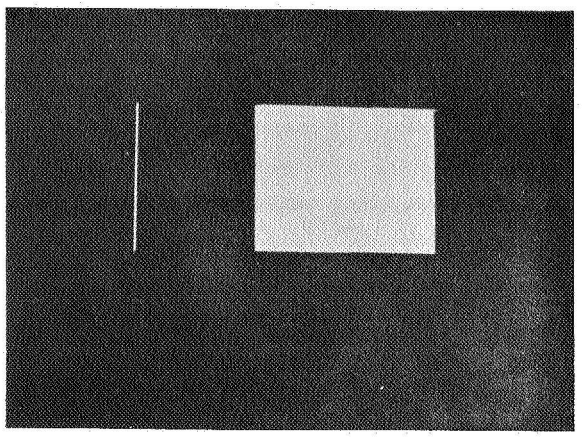


FIGURE 10–43.—Monitor presentation of sine squared test pattern, Andover satellite up path.

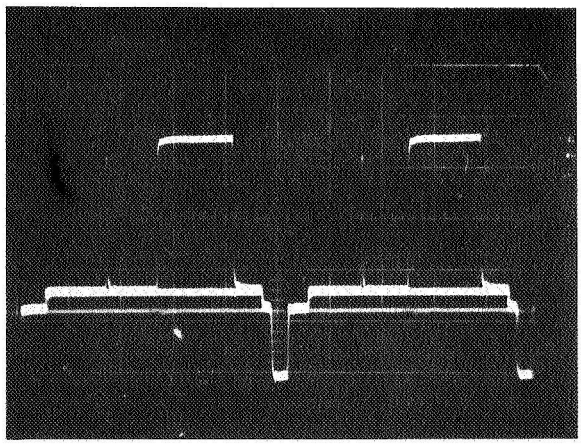


FIGURE 10–44.—Oscilloscope presentation of sine squared test pattern, Andover baseband loop satellite down path.

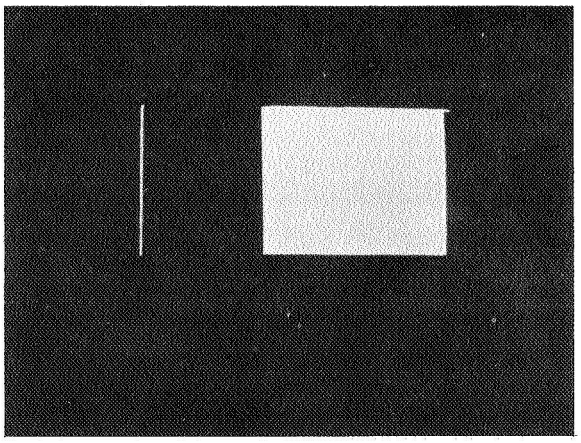


FIGURE 10–45.—Monitor presentation of sine squared test pattern, Andover baseband loop satellite down path.

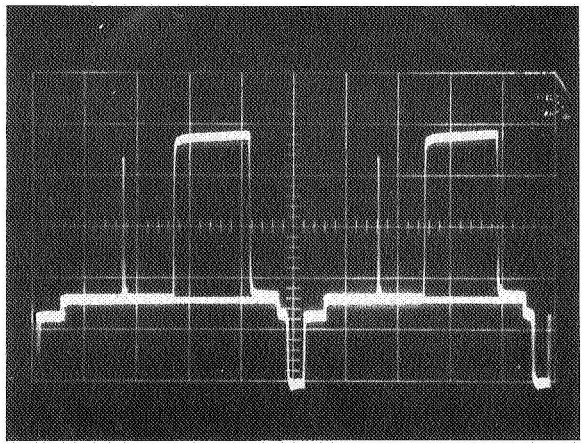


FIGURE 10–46.—Oscilloscope presentation of sine squared test pattern, Andover IF FMFB loop satellite down path.

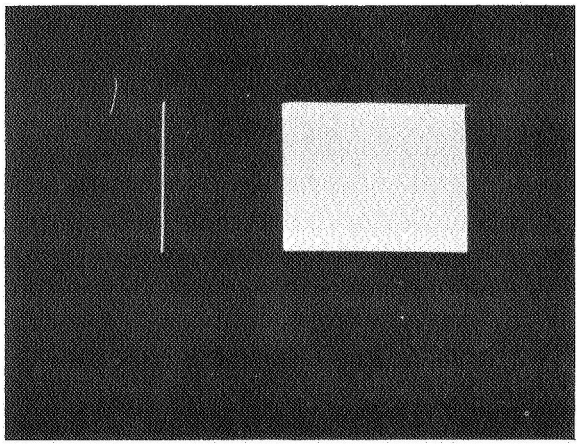


FIGURE 10–47.—Monitor presentation of sine squared test pattern, Andover IF FMFB loop satellite down path.

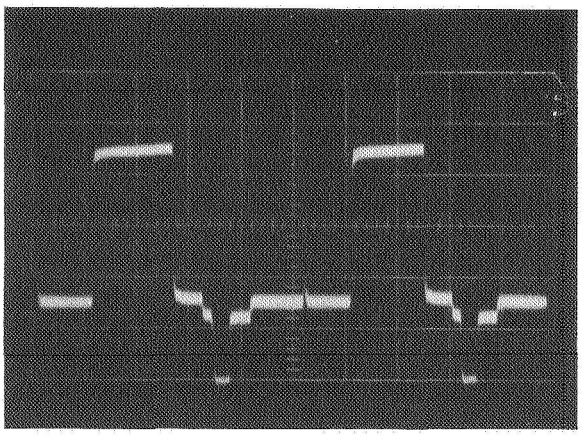


FIGURE 10–48.—Oscilloscope presentation of sine squared test pattern, Andover satellite loop satellite down path.

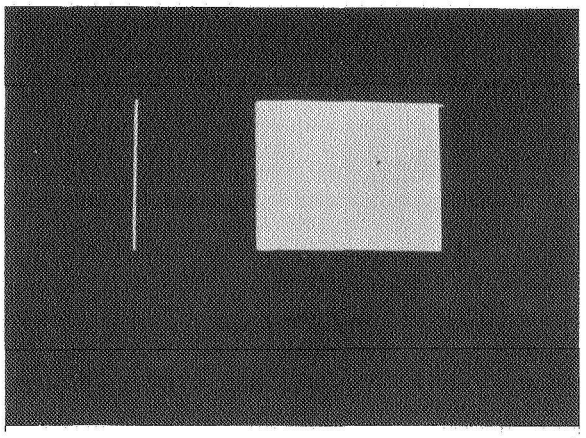


FIGURE 10–49.—Monitor presentation of sine squared test pattern, Andover satellite loop satellite down path.

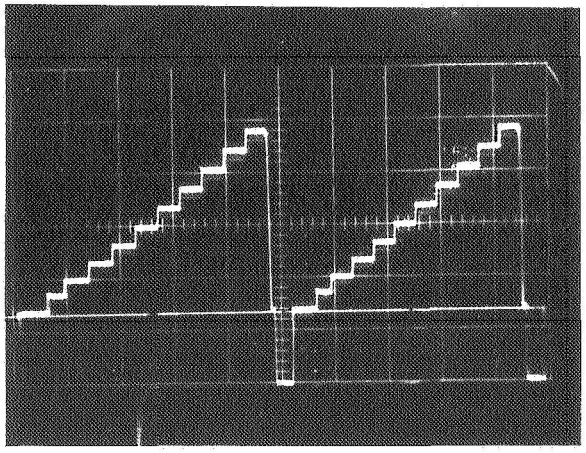


FIGURE 10–50.—Oscilloscope presentation of stair step test pattern, Andover satellite up path.

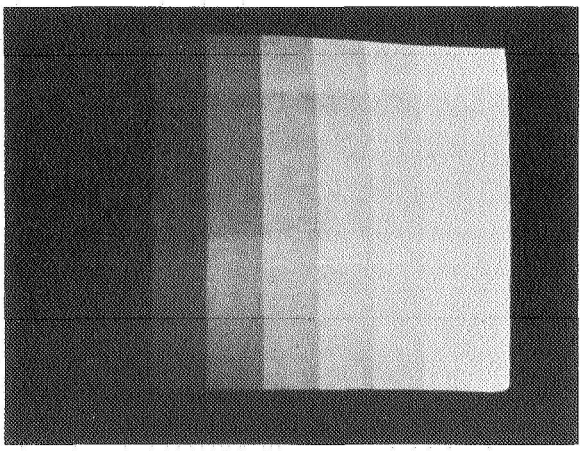


FIGURE 10–51.—Monitor presentation of stair step test pattern, Andover satellite up path.

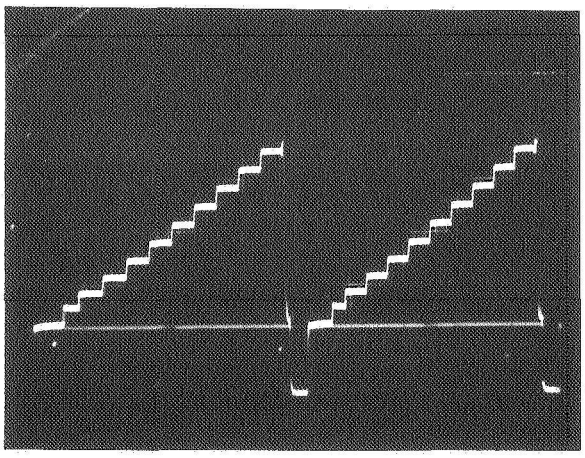


FIGURE 10–52.—Oscilloscope presentation of stair step test pattern, Andover baseband loop satellite down path.

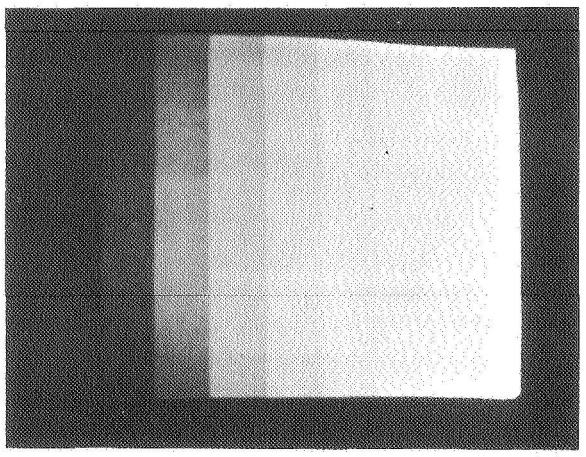


FIGURE 10–53.—Monitor presentation of stair step test pattern, Andover baseband loop satellite down path.

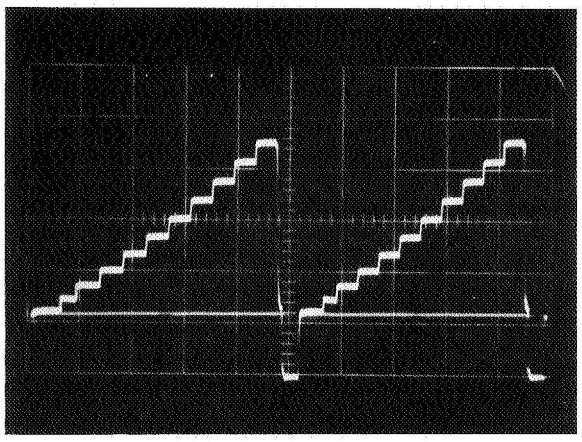


FIGURE 10–54.—Oscilloscope presentation of stair step test pattern, Andover IF FMFB loop satellite down path.

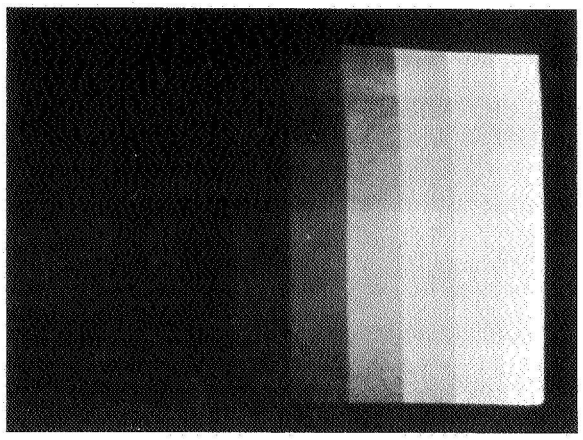


FIGURE 10–55.—Monitor presentation of stair step test pattern, Andover IF FMFB loop satellite down path.

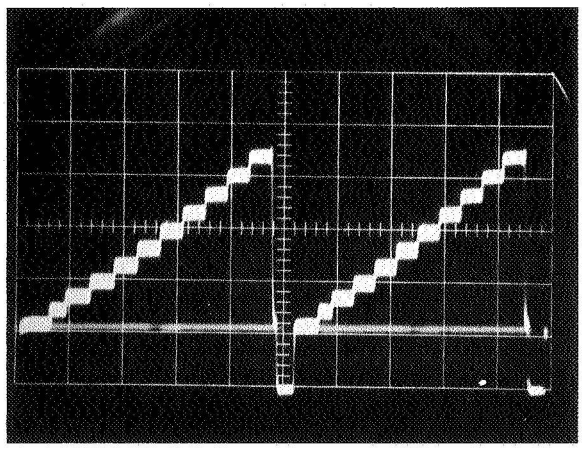


FIGURE 10–56.—Oscilloscope presentation of the stair step test pattern, Andover satellite loop satellite down path.

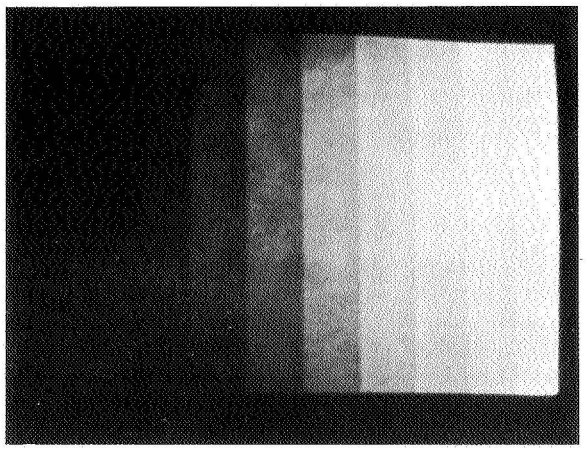


FIGURE 10–57.—Monitor presentation of stair step test pattern, Andover satellite loop satellite down path.

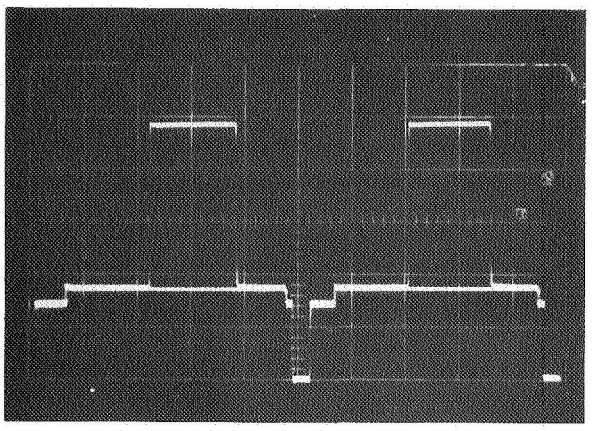


FIGURE 10–58.—Oscilloscope presentation of window test pattern, Andover satellite up path.

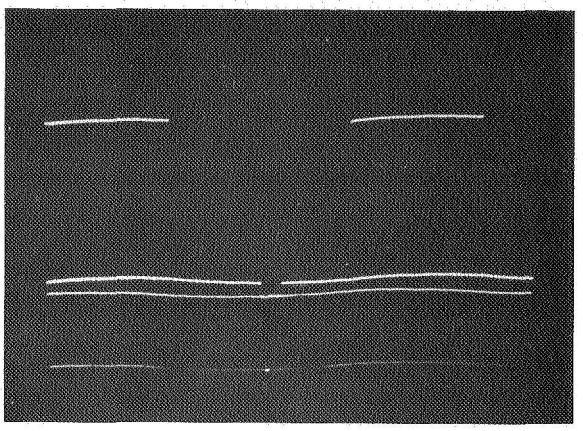


FIGURE 10–59.—Oscilloscope presentation of window test pattern, Andover satellite up path.

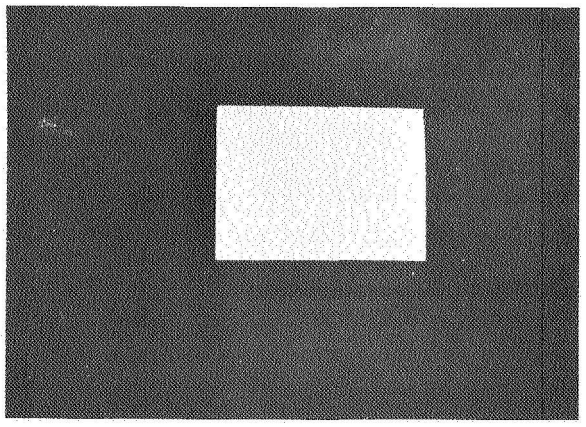


FIGURE 10–60.—Monitor presentation of window test pattern, Andover satellite up path.

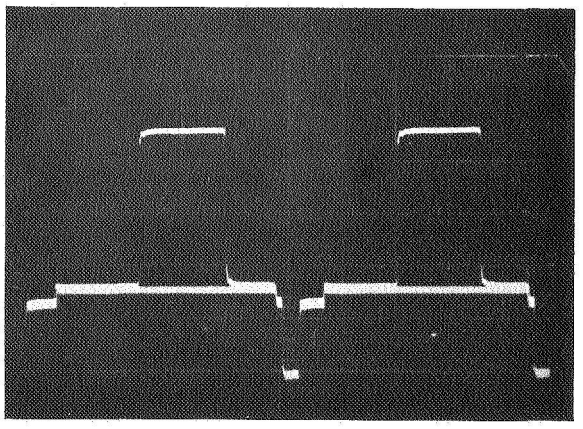


FIGURE 10–61.—Oscilloscope presentation of window test pattern, Andover baseband loop satellite down path.

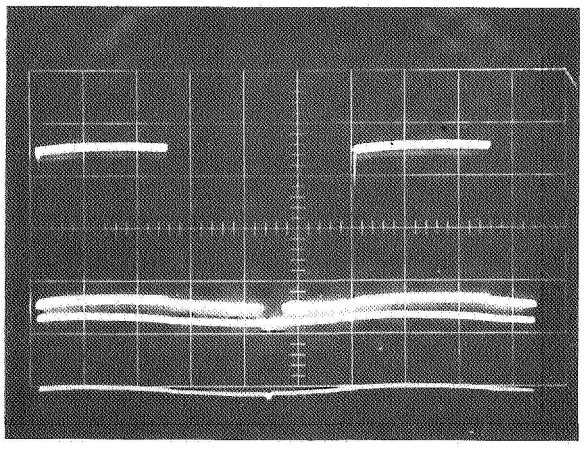


FIGURE 10–62.—Oscilloscope presentation of window test pattern, Andover baseband loop satellite down path.

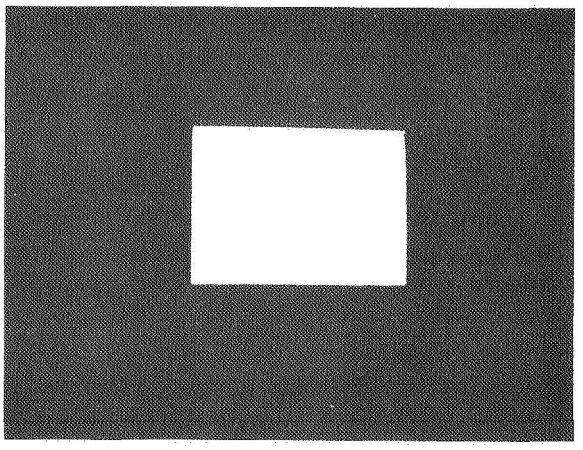


FIGURE 10–63.—Monitor presentation of window test pattern, Andover baseband loop satellite down path.

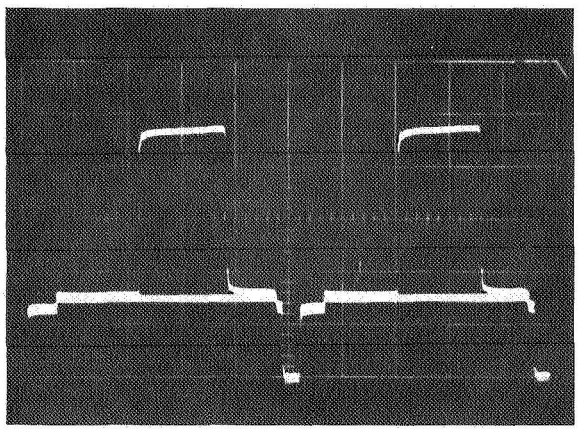


FIGURE 10–64.—Oscilloscope presentation of window test pattern, Andover IF FMFB loop satellite down path.

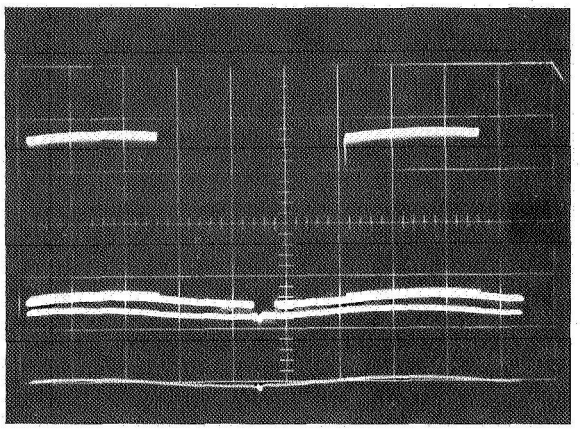


FIGURE 10–65.—Oscilloscope presentation of window test pattern, Andover IF FMFB loop satellite down path.

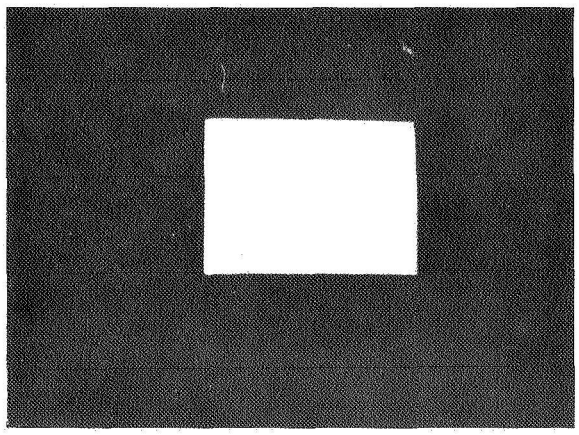


FIGURE 10–66.—Monitor presentation of window test pattern, Andover IF FMFB loop satellite down path.

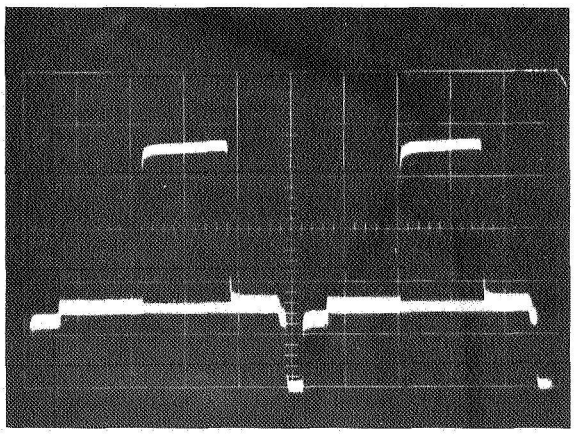


FIGURE 10–67.—Oscilloscope presentation of window test pattern, Andover satellite loop satellite down path.

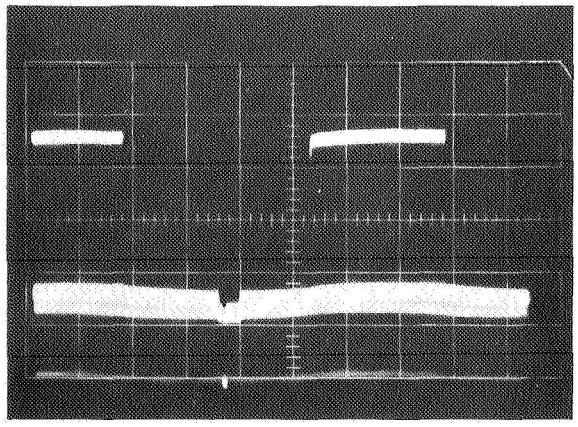


FIGURE 10–68.—Oscilloscope presentation of window test pattern, Andover satellite loop satellite down path.

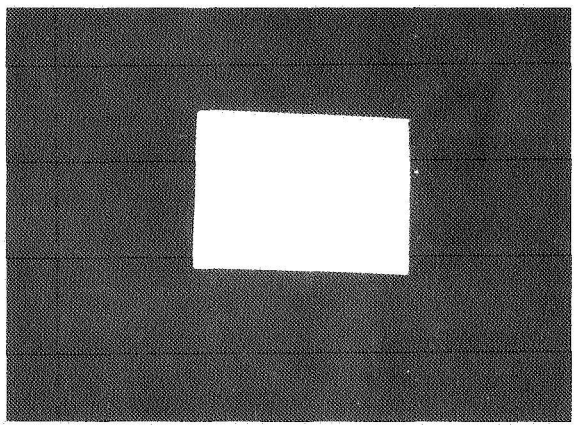


FIGURE 10–69.—Monitor presentation of window test pattern, Andover satellite loop satellite down path.

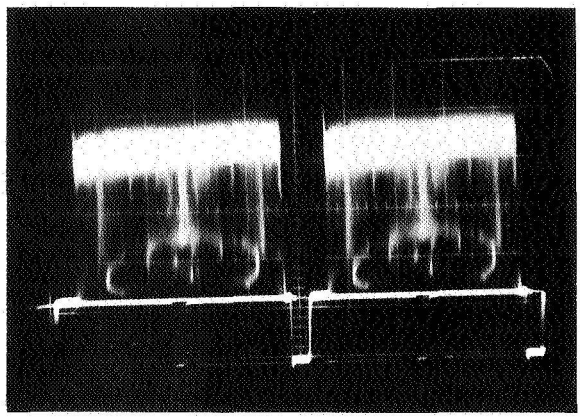


FIGURE 10–70.—Oscilloscope presentation of monoscope test pattern, Andover satellite up path.

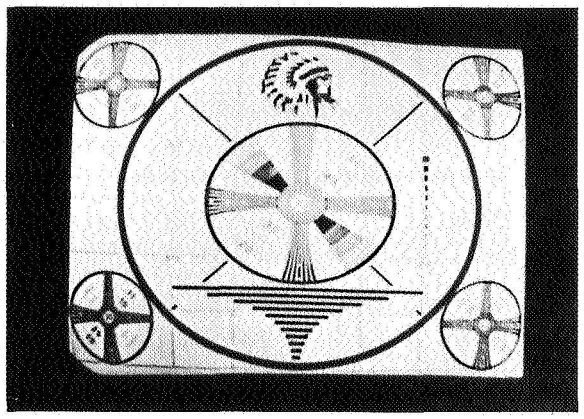


FIGURE 10–71.—Monitor presentation of monoscope test pattern, Andover satellite up path.

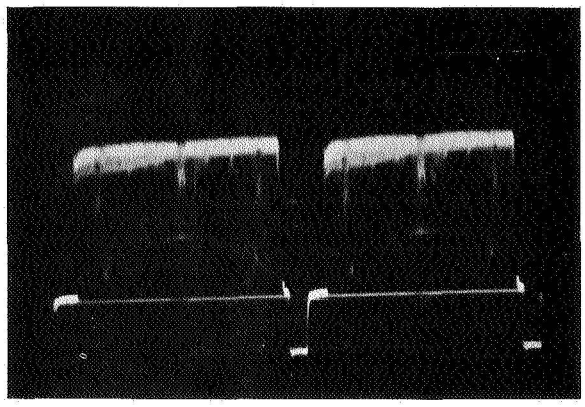


FIGURE 10–72.—Oscilloscope presentation of monoscope test pattern, Andover baseband loop satellite down path.

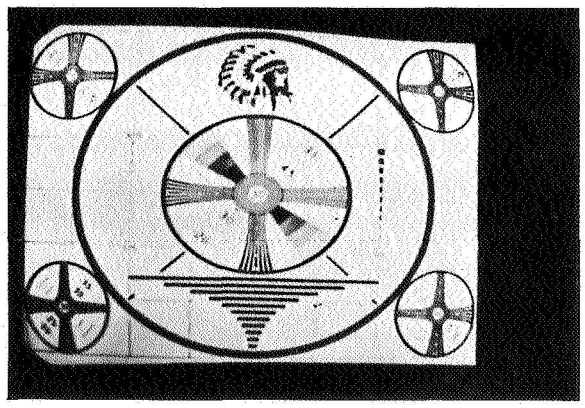


FIGURE 10–73.—Monitor presentation of monoscope test pattern, Andover baseband loop satellite down path.

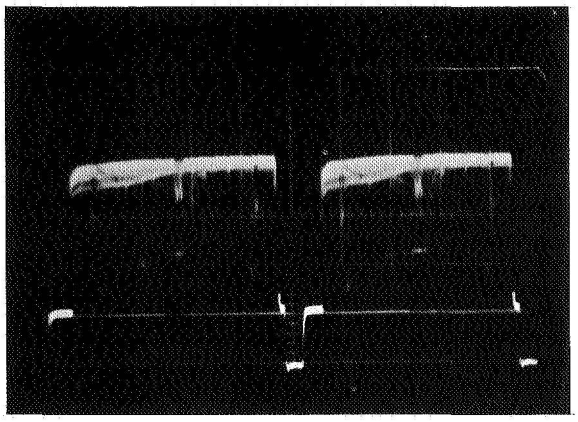


FIGURE 10–74.—Oscilloscope presentation of monoscope test pattern, Andover IF FMFB loop satellite down path.

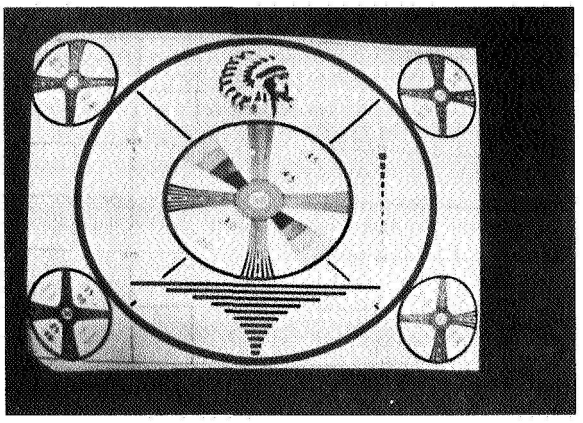


FIGURE 10–75.—Monitor presentation of monoscope test pattern, Andover IF FMFB loop satellite down path.

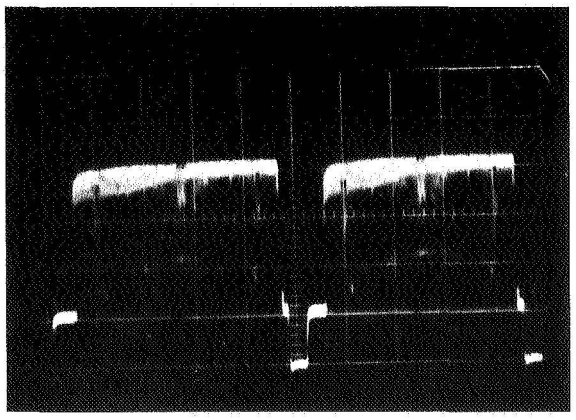


FIGURE 10–76.—Oscilloscope presentation of monoscope test pattern, Andover satellite loop satellite down path.

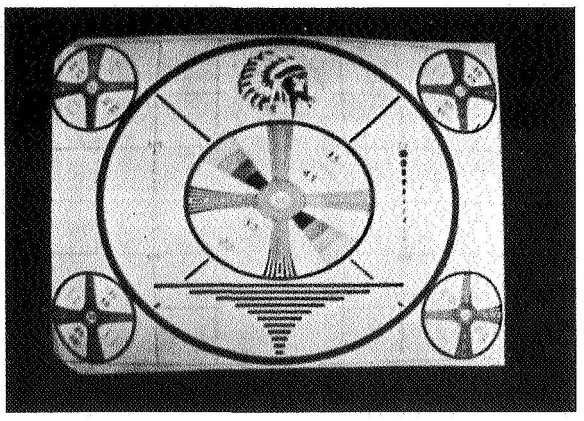


FIGURE 10–77.—Monitor presentation of monoscope test pattern, Andover satellite loop satellite down path.

Standard FM Receiver

Photographs of television test patterns were taken on pass 2070. The circuit used in this case included the standard FM receiver, video clampers and audio diplexing equipment. No video pre-emphasis or band-limiting filters were included in the circuit. Table 10–10 is an index of Figures 10–78 thru 10–109. This lists the figure number, the type of signal, the circuit (the baseband, IF, boresight or satellite loop), the receiver and the type of presentation. Again it can be said that no appreciable degradation can be attributed to the satellite and that the band limiting shown by the multiburst is due primarily to the audio diplexing equipment used.

TABLE 10–10.—*Photographic Index*
Relay Pass 2070—Test Patterns

Figure No.	Type of signal	Receiver	Type of circuit	Monitor	Oscilloscope
10–78	Monoscope	Standard	Baseband loop		√
10–79	"	"	"	√	
10–80	Multiburst	"	"		√
10–81	"	"	"	√	
10–82	Window	"	"		√
10–83	"	"	"	√	
10–84	Stairstep	"	"		√
10–85	"	"	"	√	
10–86	Monoscope	"	IF loop		√
10–87	"	"	"	√	
10–88	Multiburst	"	"		√
10–89	"	"	"	√	
10–90	Window	"	"		√
10–91	"	"	"	√	
10–92	Stairstep	"	"		√
10–93	"	"	"	√	
10–94	Monoscope	"	Boresight loop		√
10–95	"	"	"	√	
10–96	Multiburst	"	"		√
10–97	"	"	"	√	
10–98	Window	"	"		√
10–99	"	"	"	√	
10–100	Stairstep	"	"		√
10–101	"	"	"	√	
10–102	Monoscope	"	Satellite loop		√
10–103	"	"	"	√	
10–104	Multiburst	"	"		√
10–105	"	"	"	√	
10–106	Window	"	"		√
10–107	"	"	"	√	
10–108	Stairstep	"	"		√
10–109	"	"	"	√	

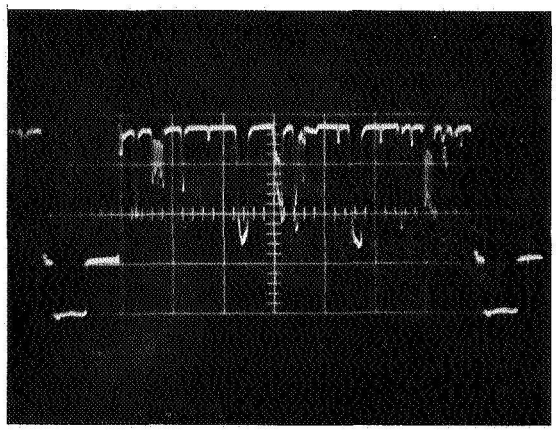


FIGURE 10–78.—Monoscope pattern—standard receiver—baseband loop.

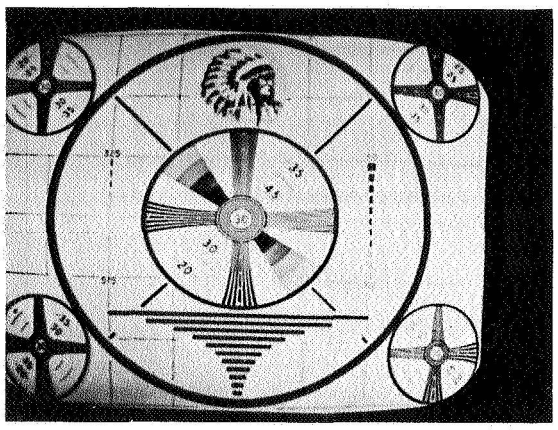


FIGURE 10–79.—Monoscope pattern—standard receiver—baseband loop.

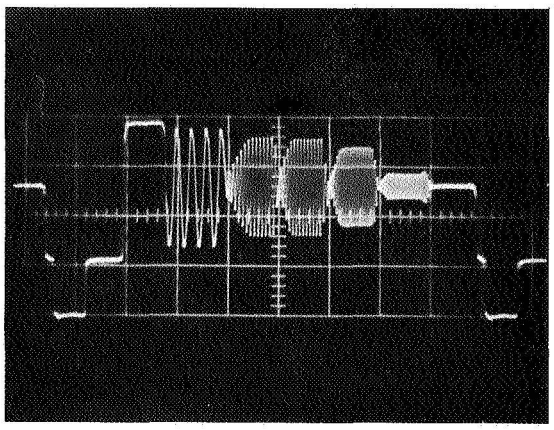


FIGURE 10–80.—Multiburst pattern—standard receiver—baseband loop.

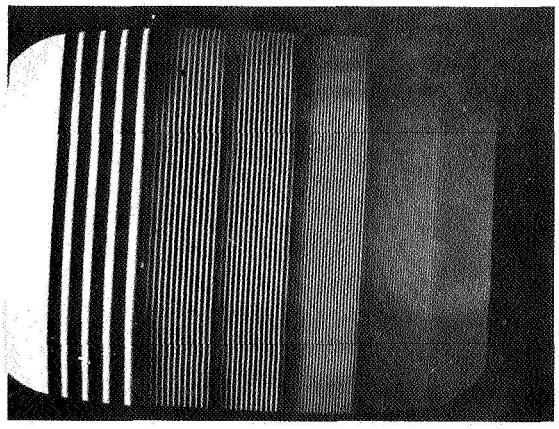


FIGURE 10–81.—Multiburst pattern—standard receiver—baseband loop.

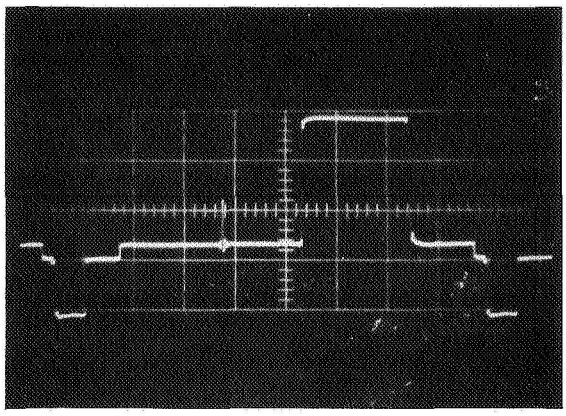


FIGURE 10–82.—Window pattern—standard receiver—baseband loop.

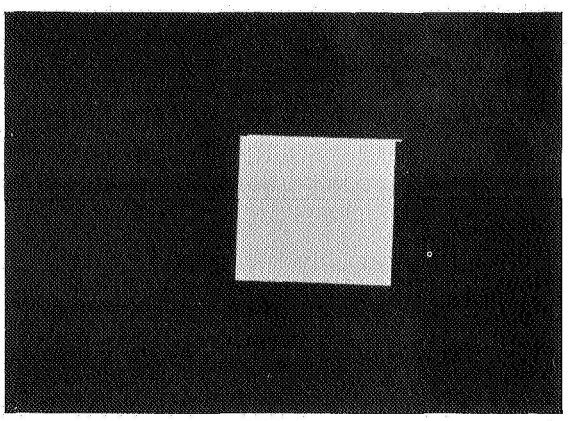


FIGURE 10–83.—Window pattern—standard receiver—baseband loop.

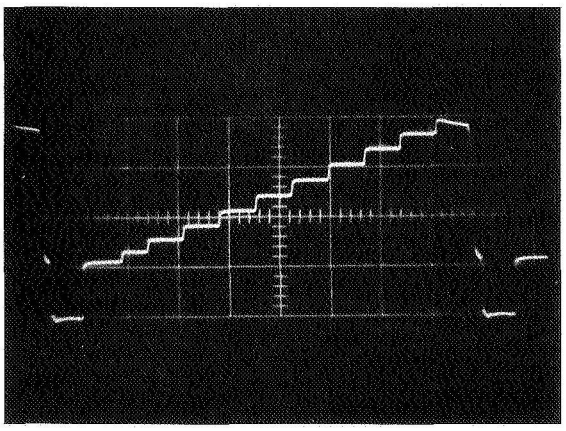


FIGURE 10–84.—Stairstep pattern—standard receiver—baseband loop.

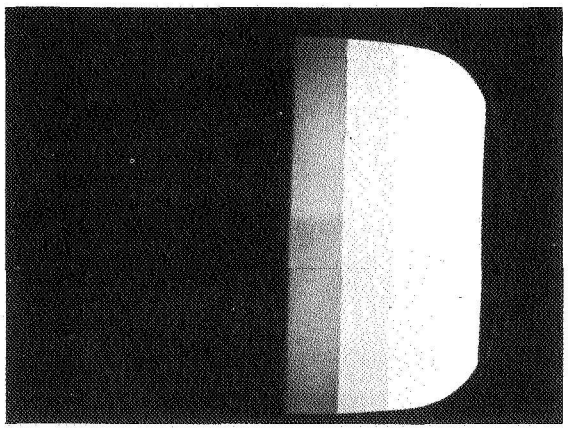


FIGURE 10–85.—Stairstep pattern—standard receiver—baseband loop.

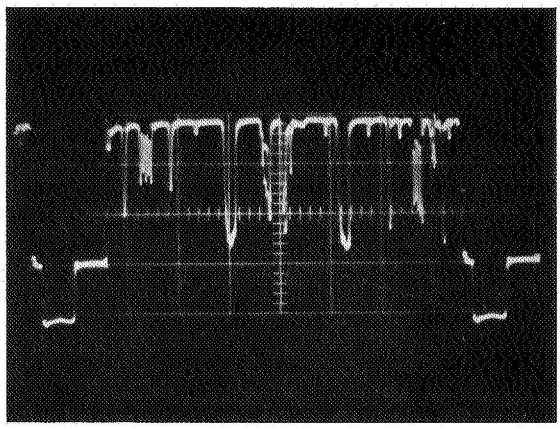


FIGURE 10–86.—Monoscope pattern—standard receiver—IF loop.

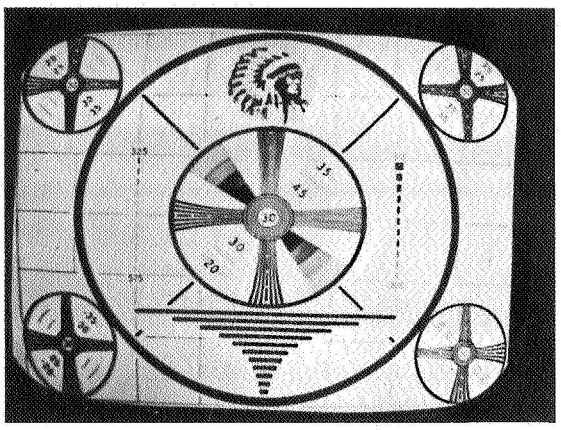


FIGURE 10–87.—Monoscope pattern—standard receiver—IF loop.

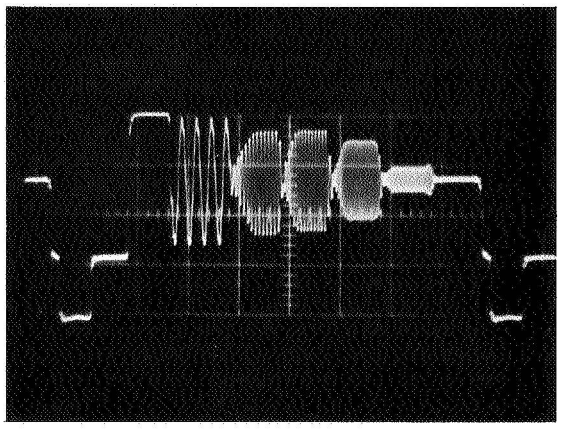


FIGURE 10–88.—Multiburst pattern—standard receiver—IF loop.

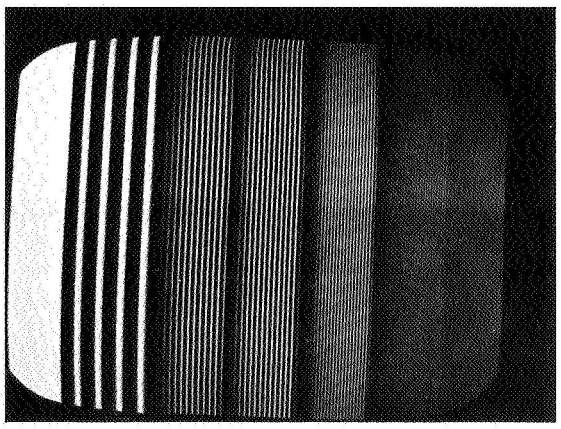


FIGURE 10–89.—Multiburst pattern—standard receiver—IF loop.

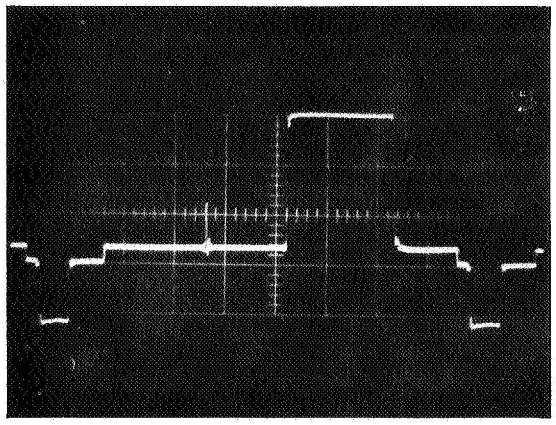


FIGURE 10–90.—Window pattern—standard receiver—IF loop.

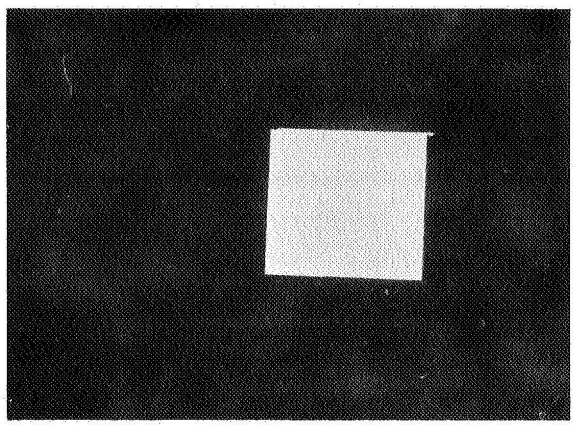


FIGURE 10–91.—Window pattern—standard receiver—IF loop.

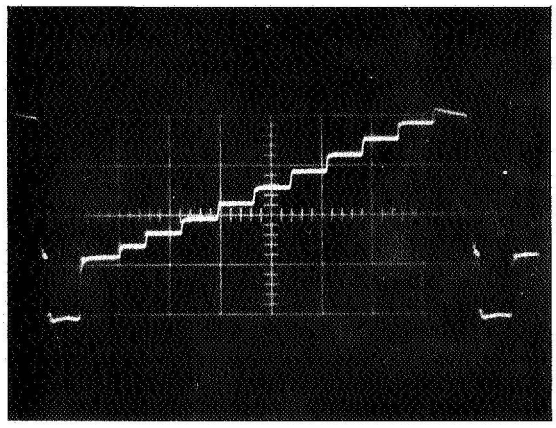


FIGURE 10–92.—Stairstep pattern—standard receiver—IF loop.

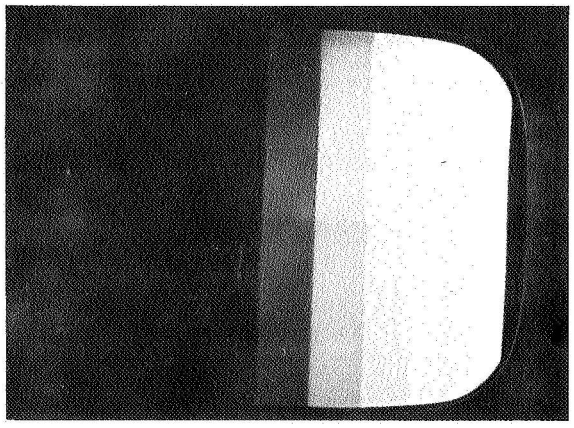


FIGURE 10–93.—Stairstep pattern—standard receiver—IF loop.

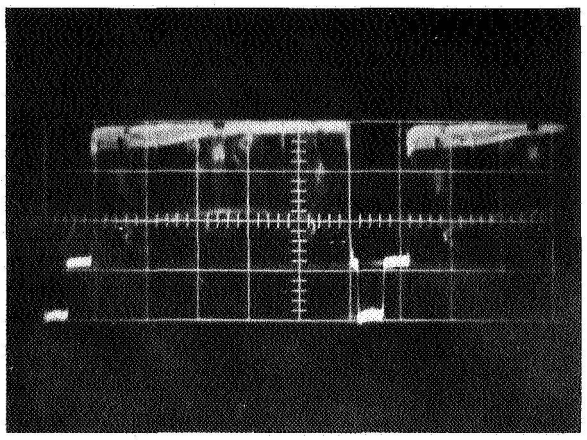


FIGURE 10–94.—Monoscope pattern—standard receiver—boresight loop.

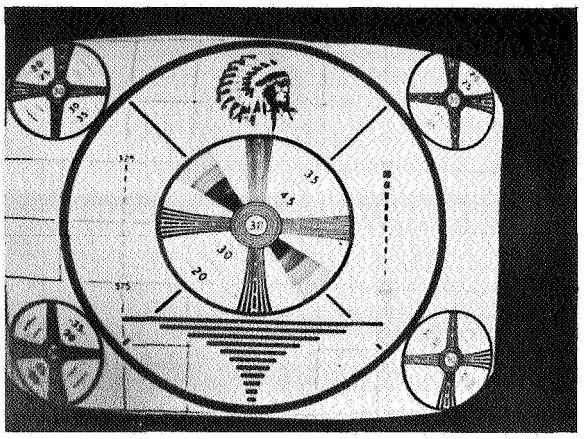


FIGURE 10–95.—Monoscope pattern—standard receiver—boresight loop.

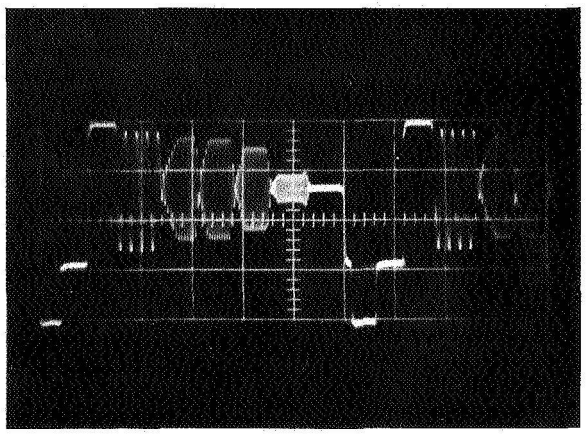


FIGURE 10–96.—Multiburst pattern—standard receiver—boresight loop.

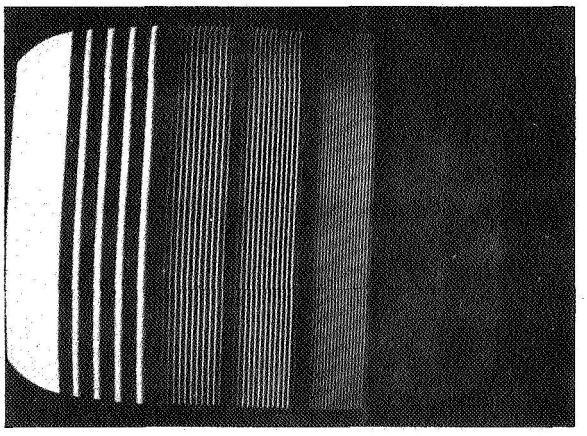


FIGURE 10–97.—Multiburst pattern—standard receiver—boresight loop.

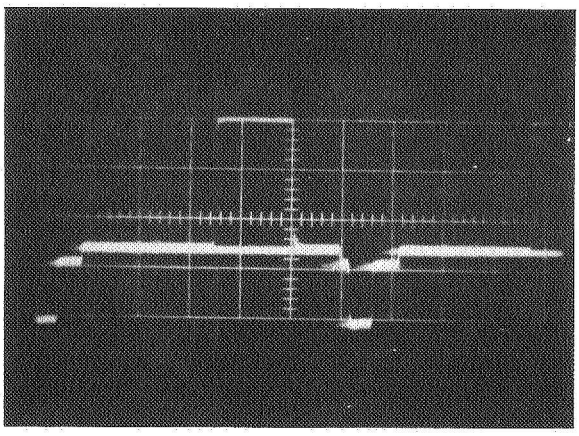


FIGURE 10–98.—Window pattern—standard receiver—boresight loop.

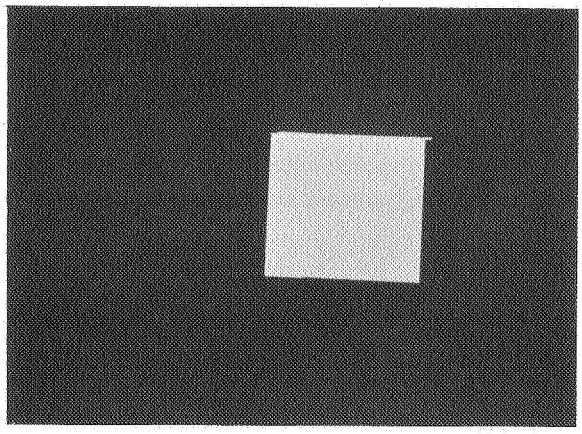


FIGURE 10–99.—Window pattern—standard receiver—boresight loop.

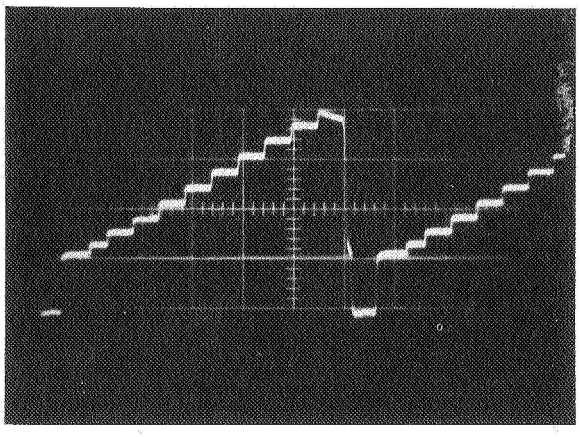


FIGURE 10–100.—Stairstep pattern—standard receiver—boresight loop.

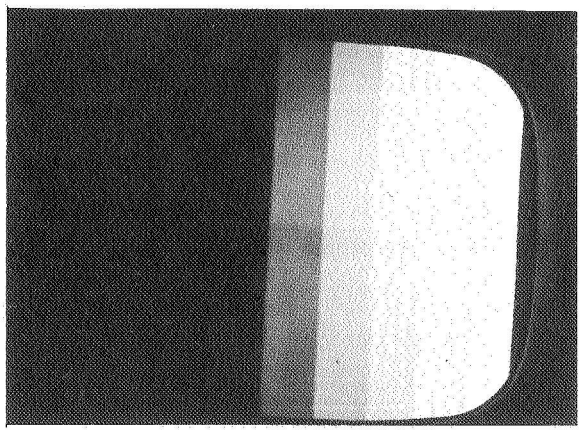


FIGURE 10–101.—Stairstep pattern—standard receiver—boresight loop.

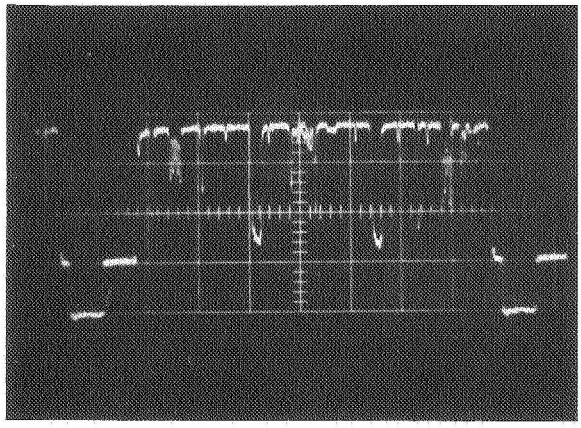


FIGURE 10–102.—Monoscope pattern—standard receiver—satellite loop.

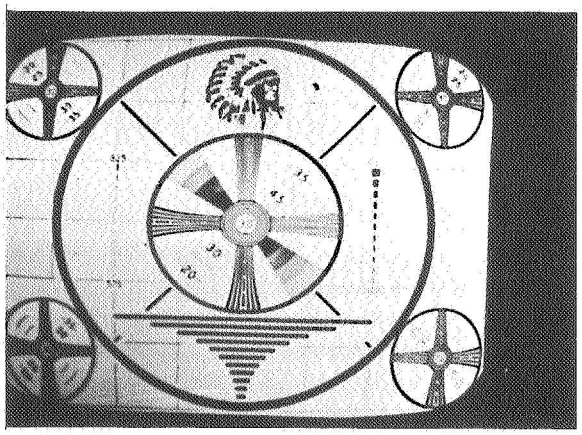


FIGURE 10–103.—Monoscope pattern—standard receiver—satellite loop.

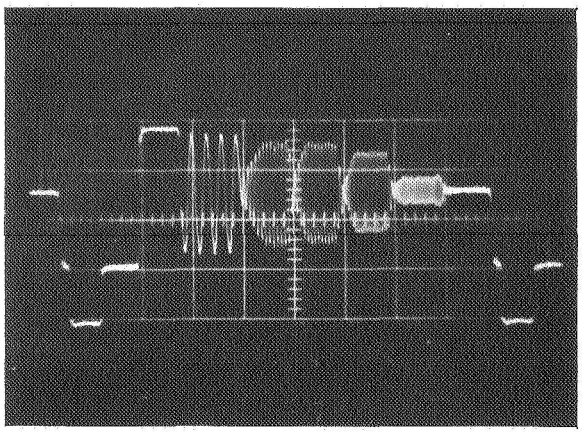


FIGURE 10–104.—Multiburst pattern—standard receiver—satellite loop.

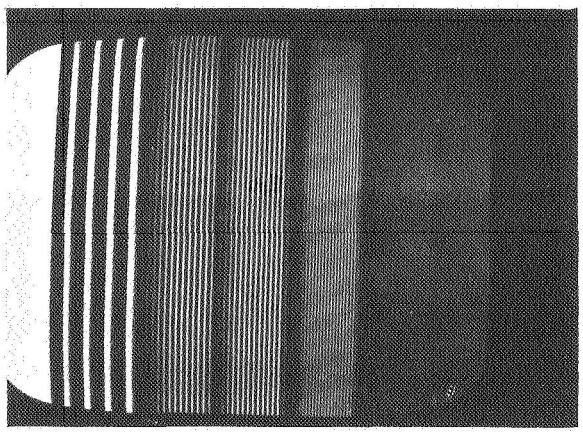


FIGURE 10–105.—Multiburst pattern—standard receiver—satellite loop.

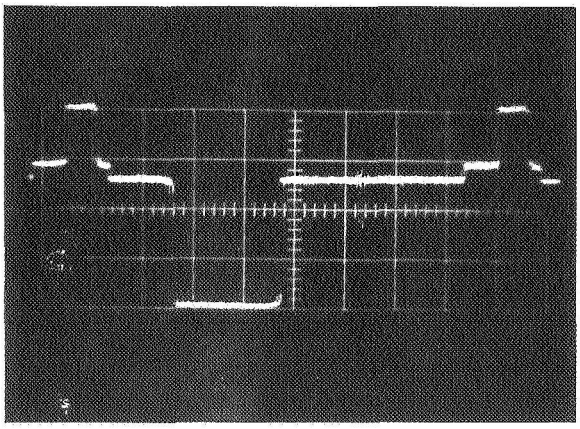


FIGURE 10–106.—Window pattern—standard receiver—satellite loop.

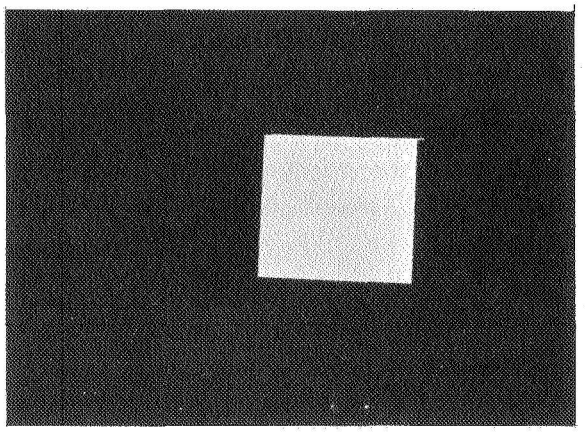


FIGURE 10–107.—Window pattern—standard receiver—satellite loop.

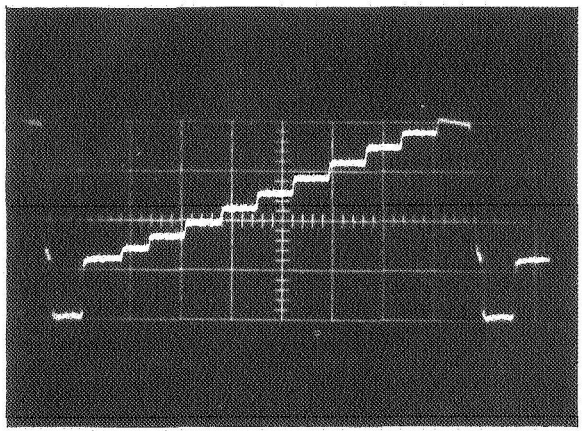


FIGURE 10–108.—Stairstep pattern—standard receiver—satellite loop.

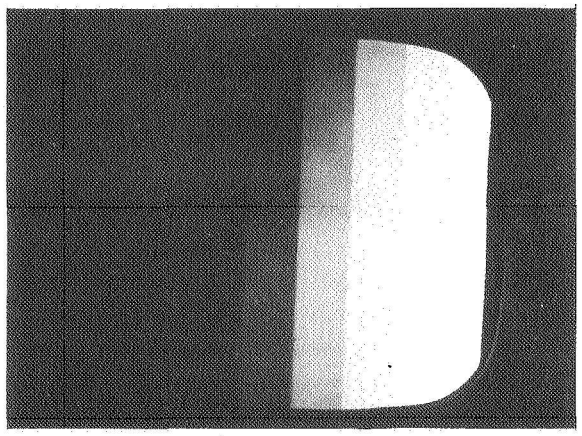


FIGURE 10–109.—Stairstep pattern—standard receiver—satellite loop.

TWO-WAY TELEPHONY

Tests to evaluate two-way telephony performance require coordination of many measurements at widely separated stations. To insure valid data, many two-way telephony tests were conducted with Pleumeur-Bodou, France, and Goonhilly Downs, England during the months of November and December of 1963. Typical results are presented in Table 10–11.

Insertion Gain

Insertion gain measurements are tabulated in Table 10–11. The transmitting station, pass, and the date are also listed. The data indicates that minor adjustments at the channel banks can easily correct for the minor deviations from nominal level.

Channel Noise

Channel noise was measured during the two-way telephony tests conducted with Pleumeur-Bodou, France and Goonhilly Downs, England. For these tests, the "L" carrier multiplex equipment was used (60 to 108 kc). The station transmitting frequencies and the deviations used are listed in Tables 10–1 and 10–2, respectively. Typical noise measurements made on the baseband loop are tabulated in Table 10–12. Noise measurements made during the pass are tabulated in Table 10–13. Also included in Table 10–13 is the date, time of measurement, cooperating station, range, spin angle, noise temperature, etc. Using these constants the expected noise channel 1 was calculated for each pass and is presented in Table 10–13. The average increase in noise measured over that which could be expected with an ideal triangular spectrum was 5.7 db. This is in agreement with the 5.0 difference indicated in Figure 10–19.

Intelligible Crosstalk

The simultaneous amplification of two FM signals in a single satellite repeater will re-

TABLE 10–11.—*Insertion Gain—db*

Pass	2613	2621	2644	2652	2761	2768	2776	2784
Channel 1	+0.5	+0.0	+0.5	+0.2	+0.2	+0.0	+0.4	+0.1
3	+0.5	+0.0	----------	+0.0	+0.1	−0.1	+0.2	+0.0
5	+0.1	+0.0	----------	+0.0	+0.2	−0.5	+0.2	−0.4
7	+0.8	−0.2	----------	−0.5	+0.0	+0.3	−0.1	+0.3
9	+0.5	+0.6	----------	+0.4	+0.6	+0.0	+0.7	+0.1
11	+0.5	−0.2	----------	−0.5	+0.0	+0.0	+0.0	+0.0
Station	COMBOD	COMHIL	COMBOD	COMHIL	COMHIL	COMBOD	COMHIL	COMBOD
Date	11–14–63	11–15–63	11–18–63	11–19–63	12–3–63	12–4–63	12–5–63	12–6–63

TABLE 10–12.—*Baseband Loop Noise DBRN* at 0 Toll Level*

Pass	2613	2621	2644	2652	2761	2768	2776	2784
Channel 1	27.5	24.0	25.0	24.0	24.0	25.0	24.0	24.5
3	27.5	24.5	25.0	25.0	25.0	25.0	24.0	24.0
5	29.5	25.0	25.5	25.5	26.0	26.0	25.0	25.5
7	28.5	25.0	25.0	25.5	26.0	28.0	26.0	26.0
9	30.0	25.0	25.0	25.0	26.0	27.0	26.0	26.0
11	29.5	24.5	25.0	25.0	25.5	29.0	25.0	25.5

*"C'Message Weighted.

TABLE 10–13.—*Satellite Noise—Andover*
[*Dbrn* at O toll level*]

Pass	2613	2621	2644	2652	2761	2768	2776	2784
Channel 1	30.0	30.0	32.0	29.0	33.0	31.0	30.5	30.5
3	30.0	29.5	30.0	28.5	32.0	31.0	30.5	30.5
5	30.0	29.0	33.0	28.5	32.0	31.0	30.0	30.0
7	30.5	29.0	30.5	28.5	32.0	30.0	29.0	30.0
9	31.5	28.0	32.5	27.5	31.0	31.0	28.0	31.0
11	32.0	28.0	30.5	27.0	31.5	31.0	27.5	30.5
Date	11–14–63	11–15–63	11–18–63	11–19–63	12–3–63	12–4–63	12–5–63	12–6–63
Time Z	15:17	15:54	14:52	15:33	15:53	13:14	14:01	14:50
Cooperating station	COMBOD	COMHIL	COMBOD	COMHIL	COMHIL	COMBOD	COMHIL	COMBOD
COMBOD or COMHIL:								
Range-statute mi.	6040	6690	6050	6360	6040	5950	5760	5580
Spin angle	79.4°	73.8°	68.8°	69.9°	64.5°	65.7°	63.4°	62.4°
ANDOVER:								
Range-statute mi.	4268	4485	4330	4361	4096	4516	4359	4089
Spin angle	46.0°	54.1°	45.2°	47.4°	40.1°	41.7°	38.3°	37.5°
Noise temp.—°K	31.5°	37.0°	34.0°	36.0°	91.0°	52.0°	33.5°	31.0°
SATELLITE:								
Trans. power	33.7 dbm							
Noise figure	14.0 db							
Channel 1 noise calculated assuming a triangular spectrum	24.9	25.2	24.9	25.3	25.8	25.5	23.9	24.9

*"C" Message Weighted.

sult in crosstalk from one carrier to another. The mechanism is such that with reduced circuit noise, intelligible crosstalk will occur from a particular telephone channel on one carrier to the corresponding channel on the other carrier. No difficulty was actually encountered in the two-way telephony tests conducted to determine the crosstalk loss. One such test was conducted on Relay pass 819. The tests were run from 03:51 through 04:14Z time on March 28, 1963.

The data taken, along with the results obtained, are given in Table 10–14. The conditions under which measurements were made are also tabulated. The signal to crosstalk level is tabulated along with the signal to noise level. The data indicate that the crosstalk level is not a function of the deviation but that it is a function of frequency. The crosstalk increases at about 6 db per octave of frequency regardless of the deviation used. The signal to crosstalk level is minimum at 400 kc and was measured at 33.6 db.

TABLE 10–14.—*Relay Pass 819—Intelligible Crosstalk*

Time Z	And trans	Bod trans	p–p dev	And trans freq	And rec	And rec freq	37B TMS		Signal to crosstalk level	Signal to noise level
							Freq kc	Level dbm		
03:51	100 kc	CC	1 Mc	1726.67	69 Mc	1723.33	100 kc	−64.8	44.8	
52	100 kc	"	"	"	79 Mc	"	"	−20.0		
53	CC*	"	"	"	69 Mc	"	"	−75.4		55.4
54	CC	"	"	"	79 Mc	"	"	−75.4		
55	200 kc	"	"	"	69 Mc	"	200 kc	−59.0	39.1	
56	200 kc	"	"	"	79 Mc	"	"	−20.1		
57	CC	"	"	"	69 Mc	"	"	−76.5		56.4
58	CC	"	"	"	79 Mc	"	"	−75.2		
59	400 kc	"	"	"	69 Mc	"	400 kc	−54.2	33.6	
04:00	400 kc	"	"	"	79 Mc	"	"	−20.6		
01	CC	"	"	"	69 Mc	"	"	−72.0		51.4
02	CC	"	"	"	79 Mc	"	"	−70.6		
03	100 kc	"	500 kc	"	69 Mc	"	100 kc	−71.2	45.2	
04	100 kc	"	"	"	79 Mc	"	"	−26.0		
05	CC	"	"	"	69 Mc	"	"	−78.3		52.3
06	CC	"	"	"	79 Mc	"	"	−76.3		
07	200 kc	"	"	"	69 Mc	"	200 kc	−65.5	39.2	
08	200 kc	"	"	"	79 Mc	"	"	−26.3		
09	CC	"	"	"	69 Mc	"	"	−75.6		49.3
10	CC	"	"	"	79 Mc	"	"	−74.4		
11	400 kc	"	"	"	69 Mc	"	400 kc	−61.0	35.2	
12	400 kc	"	"	"	79 Mc	"	"	−26.8		
13	CC	"	"	"	69 Mc	"	"	−71.9		45.1
14	CC	"	"	"	79 Mc	"	400 kc	−70.1		

*CC = Complementary Channel.

AUTHOR. *This chapter was written by* R. E. BLATZ *of the Bell Telephone Laboratories, Inc., Murray Hill, New Jersey, U.S.A. under Western Electric Corporation contract NAS 5–1987 with NASA/Goddard Space Flight Center.*

N66-10249

Chapter 11

The Nutley Ground Station

INTRODUCTION

In 1960, a Space Communications Station was placed in service on the grounds of the ITT Federal Laboratories in Nutley, New Jersey. This station was a company-funded research facility intended to evaluate the feasibility of using Moon-echo and repeater-satellite relays as a means of establishing intercontinental communications on a commercial basis.

Communication and analytical tests were the two broad classes of experiments considered in establishing basic station requirements. For the analytical tests, the station was equipped to measure and record frequency, power, and modulation.

For the communication tests, transmitters, receivers, and traffic terminal equipment were installed. These were compatible with several existing and planned satellites, including the moon. As indicated in Figure 11–1, the transmitter power required for active satellites is normal, ranging from 0.1 to 10 watts per voice channel. However, to accommodate passive satellites such as the moon for store and forward teleprinter transmission, considerably higher powers are required. Further, economical antenna size requires transmitters of higher power than indicated by the active-satellite analysis. For these reasons, a 10-kilowatt transmitter and a 40-foot (12.2-meter) antenna were selected.

PARTICIPATION IN PROJECT RELAY

Early in 1961, ITTFL was invited by NASA to participate in the Project Relay communication satellite program. To accept this invitation, modifications were required to make the station compatible with the

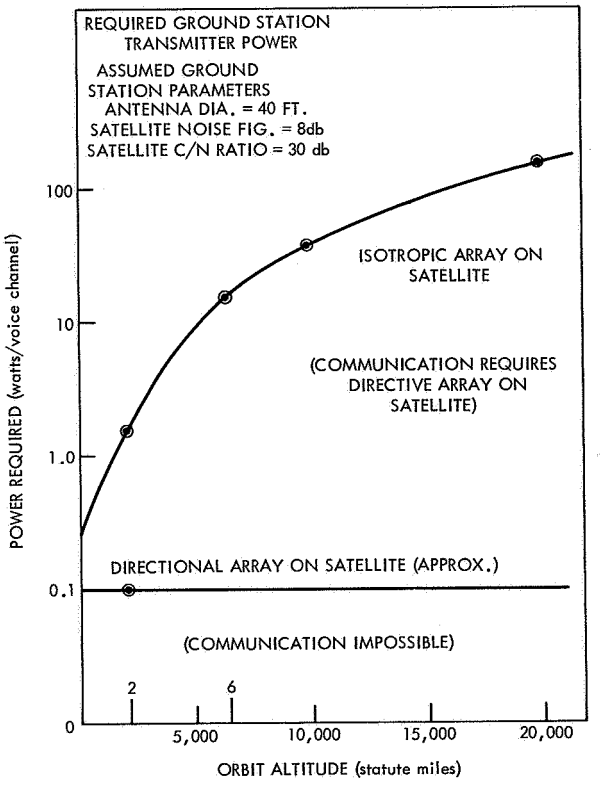


FIGURE 11–1.—Transmitter power vs. orbit attitude.

Relay system requirments as detailed in the NASA "Relay Ground Station Requirements R1–0240."

The following sections contain a description of the ITTFL Space Communications Research Station as modified for Project Relay.

STATION DESCRIPTION

There are 6 major equipment categories in the ground station: transmiter, communication receiver, terminal equipment, antenna and tracking system, coordinating facilities, and special test equipment.

Transmitter

The transmitting system includes the local oscillator, frequency modulator, and 10-kilowatt power amplifier. The local oscillator and frequency modulator are part of an ultra-high-frequency exciter similar to the one used in the Courier satellite program. The local oscillator uses a vacuum-tube multiplier chain to generate a frequency 70 Mc above the required carrier frequency from an oven-controlled crystal accurate to 5 parts in 10^6. The frequency modulator generates a 70 Mc carrier with a peak-to-peak deviation of up to 2 Mc. A 12-channel pre-emphasis network that meets the requirments of the International Consulting Committee on Radio (CCIR) is included in the modulator input circuit.

The exciter is also used at 2300 Mc for moon reflection experiments with the substitution of an appropriate oven-controlled crystal.

The power amplifier uses a Varian type-800E klystron to generate a continuous-wave output of 10 kilowatts from the 50-milliwatt carrier input. To minimize local interference and satisfy the Relay system requirement for harmonic content of the transmitter output, a 3-Gc low-pass filter was inserted in the waveguide. The output frequency of the power amplifier is 1723.33 Mc for Relay experiments. The klystron is connected to the antenna by WR–430 waveguide through wideband rotary joints and operates within the band from 1720 to 2400 Mc. The waveguide system is pressure dehydrated at 0.5-pound per square inch gauge. Power is radiated with right-hand circular polarization for Relay and linear or circular polarization for moon reflection experiments.

The transmitter output can be switched to water-cooled dummy load for testing and for standing by. The power amplifier is designed to turn on semi-automatically and has fully automatic fault detection and protective action.

Communication Receiver

Performance characteristics for the Relay communication receiver are given in Table 11–1.

TABLE 11–1.—*Communication Receiver Performance*

Relay experiment frequencies in Mc	4165 and 4175
System noise temperature in degrees Kelvin	360
Intermediate frequencies in Mc	60 and 70
Carrier-to-noise ratio at threshold in db	7.2
Intermediate-frequency peak-to-peak deviation in Mc	1.2
Acquisition range in Kc	±800
Baseband width in Kc	0.3 to 400
Intermodulation noise-power ratio in db (12 channels)	50

The equipment used with Relay includes a parametric amplifier and a dual communication receiver. The parametric amplifier with its associated mixer-preamplifier and local oscillator is mounted in an air-conditioned enclosure close to the apex of the 40-foot paraboloidal reflector. This minimizes the length of waveguide between feed and amplifier and eliminates loss rotary joints. As a result, the system noise temperature is 360 degrees Kelvin. The parametric amplifier and its mixer-preamplifier have a combined 1-decibel-down bandwidth of 14 Mc, centered at 4170 Mc. Thus both carriers, one at 4165 and the other at 4175 Mc, can be accommodated without band switching. The local-oscillator frequency is 4105 Mc, giving intermediate frequencies of 60 and 70 Mc after conversion. These are supplied to the dual communication receiver where they are separated and then amplified.

Demodulation takes place in a phase-locked loop and a wideband limiter-discriminator.

Terminal Equipment

The terminal equipment (Figure 11–2) includes multiplex, recorders, signal generators, meters, and patching facilities.

The multiplex equipment is a 24-channel unit. Presently, only the 12-channel group from 12 to 60 Kc is in use for Project Relay.

A 7-track Ampex recorder will respond directly to frequencies as high as 50 Kc. Using a frequency modulation subcarrier, it will record signal frequencies as high as 4 Kc. The Ampex was used to record experimental data for later analysis.

An 8-channel Sanborn recorder registers antenna pointing errors, received signal strengths, and other pertinent data.

For teleprinter experiments, 3 audio-frequency-tone keyers with matching demodulators are used. The keyers can be operated from a keybord or a punched-tape reader. The demodulators can supply either of two page printers or a tape punch.

To handle telephone conversations via the satellite, eight 2-wire telephone lines are connected to the multiplex equipment through 4-wire terminations.

A 4-wire data line connects the station at Nutley to American Cable and Radio Corporation in New York City. This link is used for high-speed data-transmission experiments and multichannel teleprinter experiments with the satellite.

Antenna and Tracking System

The antenna and tracking system may be divided into the following:

- Antenna structure
- Servo control system
- Automatic-tracking receiver

The antenna uses a 40-foot (12.2-meter) paraboloidal reflector with a Cassegrainian feed system. The horns are located at the apex of the reflector and can be replaced or supplemented for transmission at either 6 or 8 Gc. A hyperboloidal secondary reflector provides a virtual focus near the apex. An air-conditioned microwave-electronics package is mounted close to the horn structure and moves with the antenna. Table 11–2 summarizes the performance of the antenna and tracking system.

The tracking-receiver and communication-receiver front ends are mounted in the microwave-electronics package. All receiver frequencies are converted to an intermediate frequency of 60 or 70 Mc before they leave the microwave-electronics package. In addition, there is space for a 10-kilowatt power amplifier covering the 6-Gc band.

Two feed systems are presently in use. One is the 2-horn transmitting feed. The other is a 4-horn monopulse receiving system with three outputs. Of the three outputs, one is the sum of the outputs from all 4 horns and the other two are the algebraically derived evaluation and azimuth difference outputs, which are used in a simultaneous amplitude-comparison technique to generate antenna pointing-error information. The sum output, at 4165 and 4175 Mc, goes to the communication-receiver parametric amplifier through one arm of a diplexing filter and, at 4080 Mc, to the tracking-receiver sumchannel mixer through the second arm of the filter The two difference outputs, at 4080 Mc, go directly to their respective difference-channel mixers with no preamplification. The noise figure of the mixer and intermediate-frequency preamplifier is 8 decibels.

To obtain an acquisition sensitivity at 4080 Mc of −128 decibels referred to 1 milliwatt, the sum or reference signal is detected in a narrowband phase-locked loop centered at 9.8 Mc. A quadrature phase detector provides automatic gain control.

The phase-locked oscillator in the sum channel acts as the local oscillator for all three channels of the tracking receiver, thereby reducing frequency-modulation noise in the difference channels. Coherent detection with post-detection filtering to 10 cps is used in the difference channels to achieve a low-noise tracking error signal.

The antenna is driven along each axis of its mount by a pair of contrarotating con-

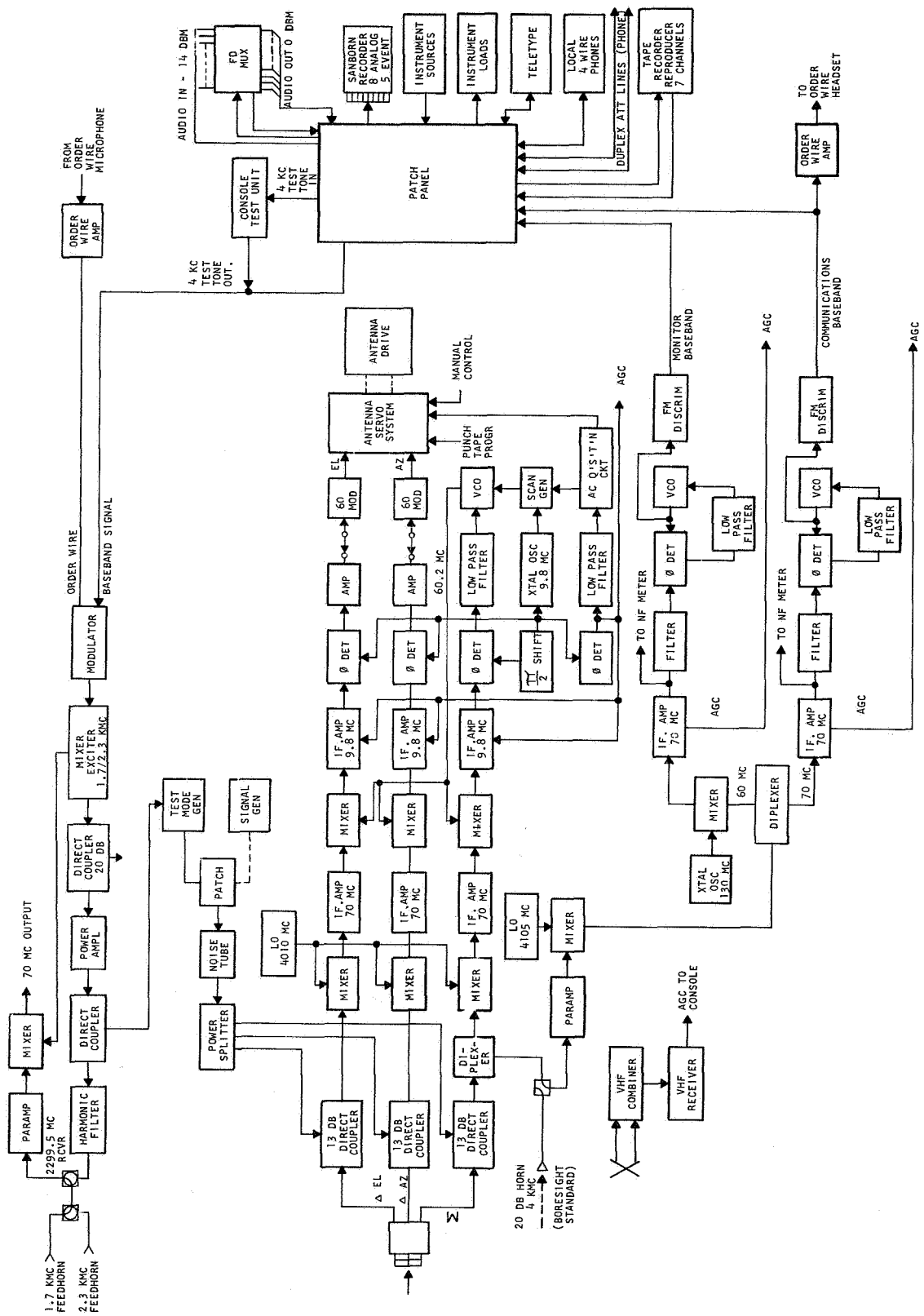


FIGURE 11–2.—Station block diagram.

TABLE 11–2.—*Antenna and Tracking System Performance*

Tracking system	
Operational modes	Automatic (normal or rate memory) and manual tracking
Maximum rates along each axis in degrees per second	10
Maximum accelerations along each axis in degrees per second per second	6
Maximum operational wind speed in miles per hour	35 (with gust factor of 1.25)
Tracking accuracy along each axis in degrees:	
Automatic tracking	0.10
Programmed tracking	0.10
Angle-tracking receiver:	
Signal frequency in megacycles per second	4080
Local-oscillator frequency in megacycles per second	4010
Intermediate frequency in megacycles per second	70
Mixer type	Crystal, nonlinear resistance
Conversion loss in decibels	10
Noise figure in decibels	8
Average signal level in decibels referred to 1 milliwatt	−120
Local-oscillator signal level in milliwatts	1
Bandwidth in megacycles per second	2
Impedance level in ohms	50
Minimum isolation in decibels between signal and local oscillator circuits	30
Spurious output in decibels	−60
Frequency search modes	Open loop, manual; closed loop, manual; closed loop, automatic
Frequency search characteristics:	
Maximum excursion in kilocycles per second	150 manual; 200 automatic
Maximum rate in megacycles per second per second	1.5 (automatic)

Antenna characteristics	
Communications antenna:	
Reflector diameter in feet (meters)	40 (12.2)
Type	Cassegrainian
Mount	Elevation over azimuth
Frequency range in megacycles per second:	
Transmit	1710 to 2300
Receive	4000 to 4200

Antenna characteristics (continued)	
Gain in decibels:	
Transmit (1725 Mc)	38.4 ± 1.0
Receive (4080 Mc)	49.1 ± 0.8
Beamwidth at 3-decibel-down points in degrees:	
Transmit	1
Receive	0.45
Side lobes in decibels:	
First-order	−15 or lower
High-order (beyond 4th)	−30 or lower
Polarization	Circular (right-hand or left-hand or linear)
Transmitter power in kilowatts	10
Antenna control:	
Boresight collimation in degrees	0.05
Tracking accuracy in degrees	0.1 (3_σ error)
Static pointing accuracy in degrees	0.2 (3_σ error)
Maximum tracking speed in degrees per second	10
Maximum angular acceleration in degrees per second per second	6
Minimum tracking speed in degrees per second	0.01
Maximum operational wind speed in miles per hour	35
Operation modes	Manual Beacon automatic tracking with acquisition scan Programmed tracking Rate memory and reacquisition

VHF beacon receiving system	
Very-high-frequency receiver:	
Operating frequency in megacycles per second	55 to 260
Noise figure in decibels	6
Intermediate-frequency-bandwidth in kilocycles per second	50
Image rejection in decibels	45
Dynamic range in decibels	60
Very-high-frequency antenna:	
Frequency range in megacycles per second	135 to 138 (receive only)
Gain in decibels (at 136 megacycles per second)	+16
Bandwidth in degrees (at 136 megacycles per second)	20
Side lobes in decibels:	
First-order	−15 or lower
Higher-order (beyond 4th)	−30 or lower
Polarization	Circular (right-hand or left-hand or linear)

stant-speed alternating-current motors with eddy-current clutches on their output shafts. A 2-speed synchro system provides high-accuracy position feedback with a static pointing accuracy of ±4 minutes of arc.

A very-high-frequency receiver is available to acquire a 136-Mc beacon signal from a satellite before line-of-sight acquisition is achieved. Orbit prediction accuracy has made the receiver superfluous at Nutley since very reliable acquistion has been possible at the 4 kMc beacon frequency. However, the

very-high frequency technique is being studied for application to mobile and transportable stations in uncharted areas.

The very-high-frequency antenna is a crossed dipole mounted in front of the 6-foot (1.8 meter) secondary reflector. This proximity to the primary focus of the 40-foot (12.2 meter) paraboloid yields a gain of 16 decibels at the beacon frequency.

Coordinating Facilities

Coordinating facilities are used mainly during satellite passes to regulate operations with other stations and National Aeronautics and Space Administration headquarters. These include the following:

1. The communication control console, which allows its operator to turn the exciter on and off, to insert test signals into the system before a pass, to monitor received signal strength and receiver phase lock, and to turn the paper recorder on and off. It also has a 24-hour digital clock indicating universal time.
2. An intercommunication and public-address system.
3. A tape recorder for the intercommunication system.
4. A telephone handset connected to one of the multiplex channels during a pass to coordinate experiments with the remote station.
5. A direct telephone link to NASA/GSFC for real-time test coordination.

Special Test Equipment

A test mode generator provides a signal at 4080 Mc to check tracking-receiver operation. Also, when supplied with a 1723-Mc communication signal, it produces an output at either 4165 or 4175 Mc having three times the frequency-modulation deviation of the input signal, for testing the dual communication receiver. These signals are coupled directly to the three antenna outputs by directional couplers to simulate received signals in the presence of antenna noise.

A replica of the equipment in the Relay satellite is mounted on the 88th floor of the Empire State Building in New York City with receiving and transmitting antennas oriented toward Nutley. This enables a complete system check, including performance of the dynamic tracking system, receiver system, and modulator-transmitter.

STATION APPLICATIONS

Initially, the ground station (Figure 11–3) was used in tracking and acquisition experiments, and in communication experiments using the moon as a passive reflector. At present, under contract to the National Aeronautics and Space Administration, the station operates as a medium capacity experimental communication terminal with the Relay satellite. To meet the requirements of this program, the station has been modified and expanded. Frequencies have been changed and telemetry, command, and control added (the latter government supplied). The expanded station is shown in Figure 11–4.

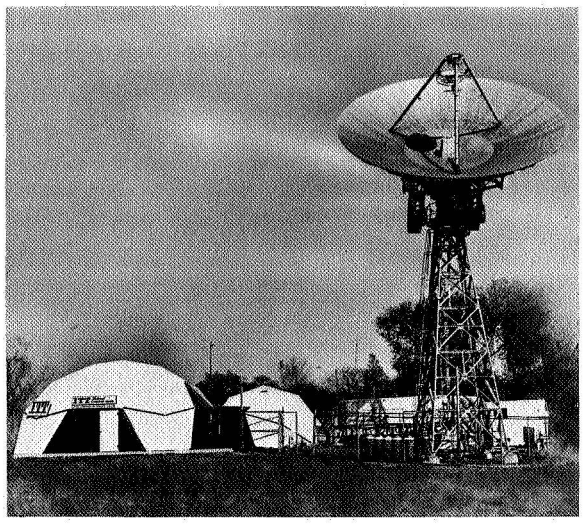


FIGURE 11–3.—Basic medium capacity facilities.

Station Facilities and Equipment

The equipment available at the Nutley station for performing experiments and carrying out demonstrations includes internal test equipment, outside telephone lines, and equip-

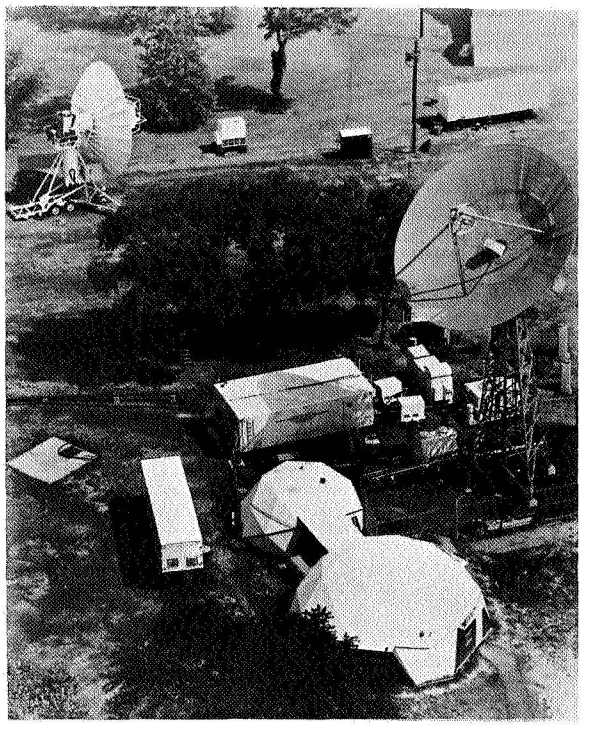


FIGURE 11–4.—Project Relay communication terminal.

ment located at American Cable and Radio in New York City, available for multichannel teletype and high speed digital data experiments.

Interconnections

All interconnections for testing are handled by a central patching facility. This facility uses 75-ohm video jacks for connections to transmitter, receiver, tape recorder, signal generators, and metering facilities. Phone jacks are used for connections to the multiplex equipment, external telephone lines, teletype equipment, and auxiliary amplifiers. The patchboard was designed for maximum flexibility and for shortest possible point-to-point connections.

Internal Test Equipment

This category includes equipment that is phsysically located within the station. Included are several types of voltmeters and signal generators, test sets for measuring intermodulation with white noise and for measuring delay distortion, teletype tone keyers and demods, a 12-channel telephone multiplex, and three recorders.

The equipment satisfies experimental and operational requirements for the Relay program and provides maximum flexibility for future programs.

A list of this equipment with major specifications follows:

1. Test Indicators
   a. Hewlett Packard Type 400H Vacuum Tube Voltmeter
      Amplitude range — 0.003v to 300v RMS
      Frequency limits—10 cycles to 4 Mc
      Accuracy—±2% to 1 Mc
      —±5% to 4 Mc
      Z input —10 megohms
   b. Wandel and Golterman Selective Voltmeter Type TFPM–76
      Frequency range—2 kc to 1.5 Mc
   c. Ballantine Model 320 True RMS VTVM
      Frequency characteristic—5 cps to 500 kc
      Amplitude accuracy—±3%, 15 cps to 150 kc
      —±5%, 5 cps to 15 cps
      —±5%, 150 kc to 500 kc
      Amplitude range — —80 to +50 dbv
      Z_{in}—10 megohms
   d. Tektronix Type 512 Oscilloscope
      Vertical amp. passband—dc to 1 Mc
      Vertical sensitivity — .005v/cm to 50v/cm
      Horizontal sensitivity—1.5v/cm
   e. Hewlett Packard Type 522B — Electronic Counter
      Frequency response—10 cps to 120 kc
      Frequency accuracy— ±1 count ± time base accuracy
      Frequency stability—10 pp million
      Minimum input amplitude — 0.2v RMS

f. Sanborn Model 850 Paper Recorder
8 analog channels
6 event marked channels
8 writing channels:
Frequency characteristic — 125 cps max.
Sensitivity—0.005v/div on 50 division 4-cm wide paper
Z input—5 megohms
6 event markers
Sensitivity—1.5v at 1 ma for deflection

2. Signal Generators
a. Gruen Model PSG–1 Pulse and Square Wave Generator
Frequency range—1 cps to 1 Mc
Accuracy—±2%
Pulse width—0.3 μsec to 0.3 sec
Accuracy—±2%
Output amplitude—9v into 100 ohms peak-to-peak
—45v into 500 ohms peak-to-peak

b. Hewlett Packard Type 650A Test Oscillator (2 units)
Frequency range—10 cps to 10 Mc
Frequency accuracy—±2% 10 cps to 100 kc
±3% 100 kc to 10 Mc
Amplitude—3v max. into 600 ohms
Accuracy—±1 db ±5% of full scale

3. Test Sets
a. Marconi Noise Measuring Set
Consists of:
(1) 1225A Noise Receiver
Receiving frequencies 14 kc, 34 kc and 56 kc
Bandwidth (effective)—1200 cps
Amplitude — noise power ratios from 0–100 db in 1 db steps
N.F.—13 db
$Z_{in} = 75$ ohms
(2) TM 5774 Band Stop Filter Unit
Stop frequencies — 14 kc, 34 kc and 56 kc
Bandwidth—3 kc
Rejection—80 db
(3) 1225B Noise Generator
Noise band—12 kc to 60 kc
Noise amplitude—minus 2 dbm to +4.9dbm
—plus 4.9 dbm to +17.0 dbm
Z_{out}—75 ohms

b. Western Electric Delay Measuring Set (J68347)
Consists of:
(1) Delay Exciter (generator)
Output frequencies—100 cps
—277.778 cps
Output amplitudes—100 cps > 8v into open circuit
—277.778 kc > 0.3v into 75 ohms
(2) Delay Detector
Delay = $d\phi/df$—0 to 300 nsec
Accuracy—±2 nsec at < 75 nsec
—+2% at > 75 nsec
Input amplitude—100 cps, 0.5v rms
—277.778 kc, 0.005 v RMS
Delay output—10 nsec/degree phase
—25 nsec/inch Y deflection

4. Telephone Multiplex
Standard Telephone and Cables No. 8041
12 channel multiplex system
Audio characteristic — 250 to 3300 cps
Audio level input—14 dbm, 600 ohms
Audio level output—0 dbm, 600 ohms
Audio Z input—600 ohms
Audio Z output—600 ohms
Baseband characteristics — 12 kc to 60 kc
B.B. transmit level—0.027 volts (minus 20 dbm) 75 ohms
B.B. receive level—0.019 volts (minus 23 dbm) 75 ohms

5. Teletype Keyers and Demod
   a. Mackay Radio CNY 2130 and CNY 2131
      (1) Tone Keyer CNY 2130
      Frequencies—Mark 1155 cps
      —Space 1055
      Output level—14 dbm, 600 ohms
      (2) Tone Demod
      Frequencies—as above
      Input level—0 dbm, 600 ohms
   b. Northern Radio (1 channel, dual diversity)
      Keyer type 153
      Frequencies cps—Mark 467.56 and 2167.5
      —Space 382.5 and 2082.5
      Output level—14 dbm into 600 ohms
      Demod type 174
      Frequencies—as above
      Input level — 0 dbm 0.788v at 600 ohms
6. Miscellaneous
   a. Tape Recorder-Ampex FR100 B–7 channel
      Frequency response
      —channels 1, 3 and 7, dc to 6 kc (fm—27 kc subcarrier)
      —channels 5—50 cycle servo
      —channels 2, 4, and 6 — 200 cps to 50 kc at 30 ips
      — 200 cps to 100 kc at 60 ips
      Tape Speed—30 ips and 60 ips
      Input level — .788v (high impedance)
      Output level—1 volt RMS nominal
   b. Auxiliary transistorized amplifiers (6 units)
      Frequency response — 200 cps to 200 kc
      Gain—variable from 0 to 20 db into 600 ohms
      Input and output are floating
   c. Teletype Corporation Model 28 ASR
      Accessories include: keyboard-operated tape punch reperforator transmitter distributor
      Operating speed—50 bauds
   d. Teletype Corporation Model 28 R/O (Page printer only)
      Operating speed—50 bauds

Outside Telephone Lines

There are eight 2-wire lines conected to the company PBX which can be connected with the Nutley central office by dialing a code number. These lines are terminated in a standard headset. They may be terminated in a hybrid by throwing a switch. The 4-wire side of the hybrid is available at the patch bay. An earphone is provided for monitoring the line when it is terminated in the hybrid. These lines are not equalized.

A high quality 4-wire telephone line (class IV) connects the station with American Cable and Radio, Inc., in New York City. The line has a frequency characteristic equalized to within ±2 db of flatness from 300 to 3300 cycles and has an insertion loss of 9 db. American Cable and Radio has 4-wire telephone lines connecting with the wire press services in New York City. By patching between the Nutley 4-wire lines and the wire services lines, the inputs to those services and their outputs become available at the Nutley station patchboard.

In addition to these lines, there is a 2-wire dc line installed between the station and the Empire State Building in New York City for remote control of the spacecraft simulator.

MULTICHANNEL TELETYPE, DATA, AND FACSIMILE FACILITIES

Multichannel teletype, low-speed digital data, and facsimile terminal equipment are available to the Nutley station. This equipment is located at American Cable and Radio, Inc. in New York City and is accessible through the equalized 4-wire line described previously.

The data equipment is capable of transmitting and receiving a data stream of up to 3600 bits per second and counting errors in the received signal.

A list of the equipment available follows:

1. Teletype Equipment
   a. 24 Channel BTM–FMVFT Bay —

frequency shift modulator and demodulator, 50 bauds.
   b. Siemens and Halske Elmux — 4-channel time division multiplex, 192 bauds.
   c. Mackay Tone Keyer and Demod. (1105 cps) CNY02130/2131 frequency shift ±50 cps.
2. Data Equipment
   a. Rixon Data Modem DD model—Vestigial Sideband — 1200 to 3600 bps 2400 cycle carrier.
   b. Standard Radio and Telegraph — TIJB Data Modem 1200 baud frequency shift keying ±400 cps.
   c. Rixon Word Analyzer and Generator Models 1032 and 132.
3. Facsimile Equipment
   a. Alden Facsimile Flat Copy Scanner Model 919–9165 120—60 rpm
   b. Alden Helix Recorder Model 319EA 120—60 rpm
   c. Rixon Adfax (Facsimile/Data Converters)
   d. Crosby AM to FM Converter (Facsimile Transmitter) mean frequency 1900 cps, frequency shift ±400 cps
   e. Crosby FM to AM Converter (Facsimile Receiver).

SUMMARY

Design studies during 1960 and 1961 used a fixed ground station to conduct narrow-band experiments using the moon as a reflector. These and later experiments with active satellites provided useful data on such parameters as terrestrial interference, atmospheric absorption, and satellite transmission characteristics.

A practical medium-capacity ground station includes a 10-kilowatt transmitter, a 40-foot (12.2 meter) paraboloidal antenna with Cassegrainian feed system, and a radio-frequency equipment pod located near the apex of the primary reflector.

Voice and teleprinter communication via satellites have been demonstrated repeatedly. The ground station can be adapted to communicate with all present satellites, this flexibility being achieved primarily through the use of a universal transmitting and receiving system with interchangeable front ends and antenna feed systems.

The space-research ground station has provided information on terrestrial interference, moon-communication parameters, and general propagation parameters between 1 and 10 Gc. In addition, it has served as a proving ground for space-communication techniques and equipment.

A medium-capacity satellite communication system has been tested as part of Project Relay, a National Aeronautics and Space Administration program. The data provide valuable information with which to plan systems. Acquisition and tracking requirements, noise and distortion characteristics, experimental techniques, and the type of data to be taken are a few of the areas under study.

The research operation has resulted in a number of new equipment designs, which have been combined in a transportable ground station capable of supporting the medium-capacity satellite system.

With this research facility, we continue to evaluate operational techniques and ground-equipment designs to improve our capabilities in the field of space communications.

AUTHORS. *This chapter was written by* B. COOPER *and* R. MCCLURE *of International Telephone and Telegraph Federal Laboratories, Nutley, New Jersey, U.S.A. under contract NAS 5–2056 with NASA/Goddard Space Flight Center.*

N66-10250

Chapter 12

Results of Relay I Narrowband Experiments

INTRODUCTION

The ITT Federal Laboratories Space Communications Research Station has been operating as a participant in Project Relay since January 5, 1963. This participation has involved the performance of communication experiments, demonstrations, and operational support of the NASA Test Station.

The station (see Figure 11–3) consists of a 40-foot Cassegrainian antenna and two geodesic domes containing the radio frequency equipment and the master control and terminal center. Subsequent addition of the East Coast Test Station equipment (see Figure 11–4) has expanded the facility. The official address and identification of the ITT Space Communications Stations is "COMNUT." The official identification of the NASA East Coast Test Station is "COMCON."

The purpose of this program is to determine the feasibility of a low-altitude active-satellite communication system. The primary function of the Nutley station is the performance of communications experiments and analysis of data obtained during these experiments. An additional function is the acquisition of operational experience using communications satellite systems. Particular emphasis is placed on UHF tracking performance.

The purpose of the experiments is to determine the extent to which a communications system designed on paper can be implemented to meet a specific group of performance requirements and to determine what additional requirements are needed to completely specify the system. The data obtained from experiments performed to date has provided considerable information on the performance of a system consisting of ground stations communicating via an orbiting spacecraft. A table of experiments, showing their frequency of performance, is given in Table 12–1.

TABLE 12–1.—*Frequency of Performance of Communications [Experiments with Relay I for January-December 1963]*

Experiment	Number of times performed
IIIA1—Insertion gain	70
IIIB1—Continuous random noise	141
IIIB2—Peak noise	53
IIIB3—Periodic noise	22
IIIC—Bandpass characteristics	36
IIID—Envelope delay	25
IIIE—Received carrier power	645
IIIF1—Harmonic performance	116
IIIF2—Noise intermodulation	82
IIIG—Loop delay	10
IIIH—Intereference	2
IIII—Intelligible crosstalk	6

Overall specifications for the Relay system have resulted in subsystem specifications defined for the ground stations and the orbiting spacecraft. To date, a number of ground subsystem performance requirements and capabilities have been verified.

These include the following:

1. The extent of the FM threshold improvement that could be obtained practically in the space-to-ground link.
2. Operational performance requirements of a spacecraft acquisition and tracking system.
3. Distribution of intermodulation sources among the various parts of the ground-space-ground communications link.
4. Satellite performance after extended exposure to outer space environment.

The sections that follow present detailed analyses of the results of several of the selected experiments performed with Relay I. For each experiment, the performance of the ground station is considered separately in order to isolate its effect on the link. Conclusions are drawn about both link and satellite.

INTERMODULATION DISTORTION TESTS

In this section, results of three different types of intermodulation distortion measurements will be presented, and compared with values calculated from theoretical considerations. The most significant measurement of the three types is the "two-tone" test, where two sinewave tones are applied to the baseband, and the 2nd and 3rd order intermodulation products are measured. From these measurements, a set of power series coefficients can be calcuated. This calculation is based on the approximation of the system amplitude and phase response by a truncated power series.* Using these coefficients, and assuming a white gaussian noise input, the individual intermodulation products resulting from phase and amplitude distortion are determined. In addition, linear envelope delay and parabolic envelope delay are calculated.

Envelope Delay

Envelope delay is related to the slope of the system phase vs. frequency characteristic. In general, the phase characteristic is a nonlinear function of frequency, and therefore, the envelope delay will be a function of frequency. The effect of this frequency dependence is to create intermodulation products in the FM detection process. These products contribute to the total intermodulation power. The remainder of the intermodulation power is the result of amplitude nonlinearities.

The delay test set measures delay by sweeping a 278-kc signal across the system passband at 800 cps and comparing the phase of the received 278 kc to a locally generated 278-kc signal whose phase is the average 278-kc phase over the sweep. The phase of the received 278-kc signal will vary as it sweeps across the passband. A phase discriminator in the delay set compares the two 278-kc signals and produces an output voltage which is instantaneously proportional to their phase difference. This phase difference is proportional to the envelope time delay by the factor 1/278 kc; i.e., delay = phase change $\div$ 278 $\times$ 10^3 sec. Therefore, the discriminator output is proportional to the instantaneous envelope delay. This voltage is displayed on the Y-axis of an oscilloscope. The 800 cps used for sweeping the 278-kc signal across the passband is proportional to the received carrier deviation and is displayed on the oscilloscope X-axis. Thus the curve displayed on the oscilloscope is envelope delay as a function of frequency.

Since the modulation index of the 278 kc signal is low, the process of sweeping the 278-kc signal can be considered as sweeping a carrier f_c with two significant sidebands across the passband at an 800 cps rate. One sideband is at f_c + 278 kc and the other is at f_c — 278 kc. The delay test set measures the average phase shift of these two sidebands divided by their frequency separation. Therefore, the delay indicated is the slope of the chord joining the coordinates of the phase at f_c + 278 kc and the coordinates of the phase of f_c — 278 kc. If this carrier and the sidebands are now moved to various positions in the passband and the slopes of

*D. P. Sullivan, "Intermodulation Distortion Study for FM Communication Satellite Systems," 15 June 1962, prepared for NASA by Space Technology Laboratories, Inc., Redondo Beach, California.

the chords joining the sideband coordinates are measured and plotted, the resultant curve is the delay vs. frequency curve that is displayed by the delay test set. Because of the manner in which this display is generated (by averaging over 2×278 kc), an average slope is displayed, and some fine grain detail is lost.

At first it appears that another way to measure the actual delay would be to reduce the sweep frequency by, say, a factor of 0.1 giving a subcarrier frequency of 27.8 kc. This would allow the actual delay to be measured more accurately because the slope of the line joining the sideband phase coordinates would be an approximation closer to the actual slope. However, the sensitivity of the measurement to noise is correspondingly increased by a factor of 10, and would make almost all passes unusable for this test.

Noise Power Ratio Test

Noise Power Ratio is an overall measure of the linearity of a transmission system. For a multichannel link, the noise level existing in a given channel when all remaining channels are loaded with white noise is compared with the level in that channel when it, too, is noise loaded. The resulting ratio (NPR) is a measure of the level of intermodulation products as compared to normal channel level. Both phase and amplitude non-linearities may contribute to the intermodulation noise.

A special test set, consisting of a noise transmitter, a filter unit, and a noise receiver, is used to make this measurement. The output of the noise transmitter is Gaussian noise uniformly distributed over the 12 to 60 kc baseband frequency range. This band-limited white noise is then fed to the filter unit which consists of three 4 kc wide band-stop filters, one each centered about 14, 34, and 56 kc. The output of the filter unit goes to the modulator input. The noise receiver, connected to the receiver output, is actually a power meter which can be tuned to 14, 34, or 56 kc. The noise receiver is 1200 cps wide. The measure the NPR in, say, the 56 kc channel, the noise receiver is tuned to this frequency. The noise power is measured first with flat noise over the entire baseband and second with the 56-kc bandstop filter inserted following the transmitter. With the filter in, the noise receiver measured no direct noise power; only intermodulation noise power.

Two-Tone Harmonic Performance Test

The two-tone harmonic performance test is one of several methods of measuring system nonlinearity. It has the decided advantage that the results of its measurements may be used to predict envelope delay and Noise Power Ratio and also to give a qualitative idea of the source of the nonlinearity.

To perform the test, two sine-wave tones of different frequency are applied directly to the baseband input to the modulator. At the receiver baseband output, the second and third-order intermodulation products and harmonics are measured with a selective voltmeter. From the levels of these products, coefficients may be derived for nonlinear amplitude and phase terms in a truncated power series that represents an approximation to the system input-output function.

Equations Used to Calculate Intermodulation Noise and Envelope Delay

It is assumed that the system transfer characteristic can be represented by:

$$\frac{V_o}{A} = V_i + m_2 V_i^2 + m_3 V_i^3 + m_4 \frac{d}{dt}(V_i^2) + m_5 \frac{d}{dt}(V_i^3) \qquad (12.1)$$

where

V_o = output time-varying voltage
A = system gain, input to output
V_i = input time varying voltage
m_2, m_3 = constants determined empirically from the two-tone tests which are related to the amplitude characteristics of the system.
m_4, m_5 = constants determined empirically from the two-tone tests which are related to the phase characteristics of the system.

For the two-tone test, $V_i = g\ (\sin \omega_1 t + \sin \omega_2 t)$, where g is the peak input amplitude and ω_1 and ω_2 are the two input angular frequencies. Performing the indicated operations on V_i and summing terms of like frequency, the following expression for the $\omega_1 \pm \omega_2$ and $\omega_1 \pm 2\ \omega_2$ terms results (see Appendix A):

$$V\ (\omega_1 \pm \omega_2) = Ag^2 \left[m_2^2 + m_4^2 (\omega_1 \pm \omega_2)^2 \right]^{1/2}$$

$$V\ (\omega_1 \pm 2\omega_2) = \frac{3Ag^3}{4} \left[m_3^2 + m_5^2 (\omega_1 \pm 2\,\omega_2)^2 \right]^{1/2}$$

where $V\ \omega_1 \pm \omega_2$ is the peak voltage at $\omega_1 \pm \omega_2$; $V\ \omega_1 \pm 2\,\omega_2$ is the voltage at $\omega_1 \pm 2\,\omega_2$.

Each of these expressions is actually two equations in two unknowns: one equation for the sum frequency term and another for the difference frequency term. These are then solved for m_2, m_3, m_4 and m_5 in terms of V and

$$m_2^2 = \frac{1}{16 V^4 \omega_1} \left[V^2 (\omega_1 - \omega_2)\ \mathrm{RMS} \frac{(f_1 + f_2)^2}{f_1 f_2} - V^2 (\omega_1 + \omega_2)\, \mathrm{RMS} \frac{(f_1 - f_2)^2}{f_1 f_2} \right] \quad (12.2)$$

$$m_3^2 = \frac{1}{72 V^6 \omega_1} \left[V^2 (2\,\omega_2 + \omega_1)\ \mathrm{RMS} \frac{(2f_2 + f_1)^2}{f_2 f_1} - V^2 (2\omega_2 - \omega_1)\, \mathrm{RMS} \frac{(2f_2 - f_1)^2}{f_2 f_1} \right] \quad (12.3)$$

$$m_4^2 = \frac{1}{16 V^4 \omega_1\ \ \omega_1 \omega_2} \left[V^2 (\omega_1 + \omega_2)\, \mathrm{RMS} - V^2 (\omega_1 - \omega_2)\, \mathrm{RMS} \right] \quad (12.4)$$

$$m_5^2 = \frac{1}{72 V^6 \omega_1\ \ \omega_1 \omega_2} \left[V^2 (2\omega_2 + \omega_1)\, \mathrm{RMS} - V^2 (2\omega_2 - \omega_1)\, \mathrm{RMS} \right] \quad (12.5)$$

From consideration of the spectral densities of the signal and intermodulation products when the signal is white gaussian noise, expressions may be written which yield the intermodulation noise contribution in the top channel due to each type of nonlinearity. In the following equations, N_{pw_k} is the contribution in picowatts (psophometrically weighted) of intermodulation noise due to the k^{th} term in the series, Equation (12.1):

$$N_{pw_2} = \frac{(2\pi F_d\, Peq)}{a_1} \frac{3.1 \times 10^{12}}{10^{0.25}\,(F_2 - F_1)} m_2^2 \quad (12.6)$$

$$N_{pw_3} = \frac{[(2\pi)^2 F_d^2\, Peq^{3/2}]^2}{(a_1)^2} \frac{3\ (3.1 \times 10^{12})}{10^{0.25}\,(f_2 - f_1)} m_3^2 \quad (12.7)$$

$$N_{pw_4} = \frac{[(2\pi)^2 F_d\, Peq\, f_2]^2}{(a_1)} \frac{3.1 \times 10^{12}}{10^{0.25}\,(f_2 - f_1)} m_4^2 \quad (12.8)$$

$$N_{pw_5} = \frac{[(2\pi)^3 F_d^2\, Peq^{3/2} f_2]^2}{(a_1^2)} \frac{3\ (3.1 \times 10^{12})}{10^{0.25}\,(f_2 - f_1)} m_5^2 \quad (12.9)$$

where

F_d = RMS per-channel deviation of the up-link = 29.6 kc

a_1 = modulation constant = 6.789×10^6 sec/volt

Peq = equivalent white gaussian noise power extending from f_1 to f_2 which the CCIR recommends to represent the multiplex of telephone channels at zero relative level, referenced to a single channel = 2.7 mw

f_1 = frequency of the lower edge of the bottom multiplex channel = 12 kc

f_2 = frequency of the upper edge of the highest multiplex channel = 60 kc

Similarly, the values of linear and parabolic envelope delay may be calculated knowing coefficients m_4 and m_5:

$$T_{dl_{pp}} = \frac{4\pi B_{rf} m_4}{3 a_1} \quad (12.10)$$

$$T_{dp_{pp}} = \frac{3\pi^2 B_{rf} m_5}{(3a_1)^2}$$

where

$T_{dl_{pp}}$ = peak-to-peak linear envelope delay component

$T_{dp_{pp}}$ = peak-to-peak parabolic envelope delay component

B_{rf} = RF bandwidth being swept = 1.17 Mc

a_1 = modulation constant = 6.784×10^6 sec/volt

(Note that a factor of 3 has been inserted in front of a_1 to reference the measurement to the down link).

Results of Tests Run with High C/N and with Controlled High Delay Distortion

A series of tests was run for the purpose of comparing calculated and measured values of envelope delay and white noise intermodulation. The tests were set up as an RF loop through the station equipment. The RF carrier-to-noise ratio was set at 35 db and the parabolic envelope delay was increased above the usual level to 90 nanoseconds *p–p*. The purpose of these adjustments is, first, to reduce the thermal noise so that it will affect the measurements as little as possible and, second, to increase the delay distortion to the point where it will have a marked effect on the third order intermodulation products, thereby making the calculation of parabolic envelope delay less subject to error. While this value of envelope delay is not representative of normal station performance, it was introduced in order to improve the correlation between measured and calculated values. The results of the tests are given in Table 12–2. Substitution of the proper signal voltages from the 2-tone test into Equations 12.5, 12.6, 12.7, and 12.8 give the following values for m_2, m_3, m_4, and m_5:

$$m_2 = 8.47 \times 10^{-2} \text{ volts}^{-1}$$
$$m_3 = 0.0825 \text{ volts}^{-2}$$
$$m_4 = 1.00 \times 10^{-7} \text{ sec/volt}$$
$$m_5 = 1.19 \times 10^{-6} \text{ sec/volt}^2$$

Substitution of these values for the m_k into the equations for N_{pw_k} gives the following results:

$$N_{pw_2} = 1425\ pw$$
$$N_{pw_3} = 820\ pw$$
$$N_{pw_4} = 280\ pw$$
$$N_{pw_5} = 245\ pw$$

It is assumed that the various contributions to the total inter-modulation noise are statiscally independent so that the total is the sum of the four contributions. Thus $N_{pw_{tot}} = 2770\ pw$. This is the calculated value of the psophometrically weighted intermodulation noise power in the top channel. This corresponds to a noise power ratio (NPR) of 44.1 db in the top channel. The noise-loading tests performed at the same time as the 2-tone tests showed a top-channel NPR (after correcting for residual thermal noise) of 44.5 db which is equivalent to an N_{pw} of 2,600 picowatts. The difference between the measured and calculated values (0.4 db) is within measurement error.

TABLE 12–2.—*Results of Intermodulation Tests*

1. Two-tone test 0 db—44 mv			*2. Noise intermodulation*		
Component	Freq. (kc)	Sig. level (db)	Channel freq.	NPR (db)	Thermal noise(db)
f_1	22	0	14 kc	34.5	−34.5
f_2	37	−0.5	34 kc	43.5	−45.0
$2f_1$-f_2	7	———	56 kc	40.0	−42.0
f_2-f_1	15	−42.5			
$2f_1$	44	−49.5	*3. Envelope delay test*		
$2f_2$-f_1	52	−52.5	Linear delay = 5 nanoseconds (pp)		
f_2+f_1	59	−41.8	Parabolic delay = 90 nanoseconds (pp)		
$3f_1$	66	———			
$2f_2$	74	−52.5			
$2f_1$+f_2	81	−48.5			
$2f_2$+f_1	96	−47.5			
$3f_2$	111	−53.5			

Calculation of linear and parabolic envelope delay gives values of 72 and 116 nanoseconds, respectively, for the linear and parabolic components. There is good agreement between values of measured and calculated parabolic envelope delay. The measured value is 90 nanoseconds which differs by about 20 percent from the calculated value of 116 nanoseconds.

The majority of the error is attributed to the fact that the passband phase variations are averaged over $2 \times 278 = 556$ kc. This has the effect of smoothing the ripple component and reducing the measured parabolic component.

There is a large discrepancy between the measured and calculated values of linear envelope delay, which are 5 and 72 nanoseconds, respectively. The calculated value of linear envelope delay is a function of m_4, which depends on the difference of the squares of the two 2nd order product voltages. These two voltages differ by only 0.7 db. An error of 0.3 db in both of these voltages could change the calculated value of linear envelope delay from 72 to 15 nanoseconds. Since there is at least a 0.3 db variation in the meter reading due to additive noise, the calculated value of linear envelope delay will be highly subject to error.

Conclusions

The usefulness of the two-tone test lies in its ability to separately evaluate the various contributions to the total intermodulation noise in an FM–FDM system. As such, this technique is very useful in subsystem evaluation to quickly determine the major contributors to intermodulation distortion.

With the exception of the prediction of linear envelope delay, the results show good agreement between measured and calculated values. This indicates that the equation used to describe the system is, in fact, a good approximation.

The technique for measuring 2nd and 3rd order intermodulation products is presently being studied and will be refined to increase its accuracy. If this can be successfully accomplished, the prediction of envelope delay will become more accurate.

For comparison, a harmonic performance test performed through the satellite will typically show that the third-order product voltages are below thermal noise, and thus not measureable. A typical value of thermal noise is 62 db below the 44 mv amplitude of the fundamental frequencies. In other words, typical third-order products are at least 10–15 db below the levels shown in Table 12–2 which are the results of deliberately inducing a high value of envelope delay in order to prove empirical and theoretical agreement. Since the magnitude of parabolic envelope delay is dependent on the difference of the squares of these voltages, the calculated delay will drop rapidly as the voltages decrease, even though their ratio may remain the same.

SYSTEM THRESHOLD WITH AND WITHOUT EXTENSION

One of the most fundamental performance measurements on an FM system is the determination of the threshold point or, more generally, the variation of the signal-to-noise ratio (S/N) as a function of carrier-to-noise ratio (C/N). This S/N versus C/N curve is made up of three regions. The first region is the one in which the carrier voltage vector is significantly larger than the noise voltage vector. In this case, S/N is proportional to C/N; i.e., a 1-db increase in C/N produces a 1-db increase in S/N. In the second region, the C/N ratio varies from 10 db to 0 db and S/N is approximately proportional to $(C/N)^3$. The intersection of these two lines is the threshold point. It is usually specified in terms of C/N ratio; i.e., for a system in which these two portions of the curve intersect at 6 db C/N, the system threshold is 6 db. In the third region, the carrier voltage vector is much smaller than the noise voltage vector and S/N is proportional to $(C/N)^2$.

The theoretical S/N ratio above the threshold point may be calculated. The formula holds for the worst channel (usually the top channel) in an FDM–FM system when a 1-kc

reference test tone is applied to that channel at zero-relative level.

$$S/N = C/N + 20 \log\left(\frac{\Delta F}{f}\right) = 10 \log\frac{B}{2b} - MCLF + PDI$$

where:

C/N = pre-detection carrier-to-noise ratio
ΔF = peak frequency deviation
f = highest modulating frequency
B = pre-detection noise bandwidth
b = post-detection channel bandwidth
$MCLF$ = multichannel loading factor (16 db for 12 channels for limiting)*
PDI = Pre-emphasis de-emphasis improvement (4 db)**

Substituting:

$$S/N = 11 + 20 \log\frac{585}{60} + 10 \log\frac{2 \text{ Mc}}{6 \text{ kc}} - 16 + 0 + 4 = 11 + 19.8$$

$$+ 25.3 - 16 + 4 = 44.1 \text{ db}$$

The measured S/N ratio at 11 db C/N in the top channel with the discriminator demodulator is 44.5 db.

Station Loop Test Mode Generator Results with Threshold Extension

Figures 12–1 through 12–6 show S/N as a function of C/N as measured using a 1-kc tone in multiplex channels 1, 6, and 12. A general characteristic of all these curves is that they threshold at from 5 to 7 db C/N and 40 to 45 db S/N (noise referenced to 1.3 Mc band). Because of the high S/N ratio at which the system thresholds, the portion of the curve above the breakpoint does not follow the classic 45-degree line (1 db change in C/N equals 1 db change in S/N). Instead, the curves flatten out somewhat at higher C/N indicating that S/N is limited by resid-

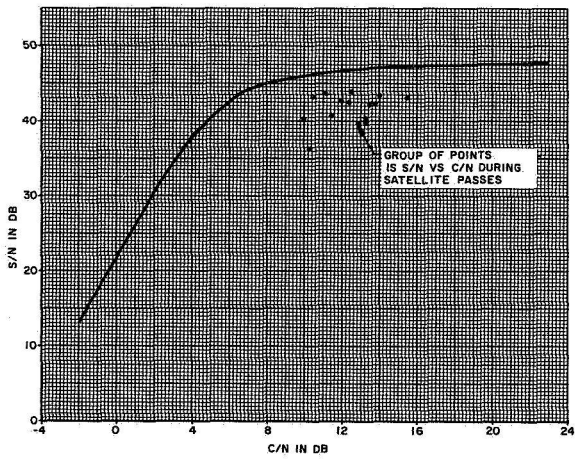


FIGURE 12–1.—S/N vs. C/N, channel 1, monitor receiver.

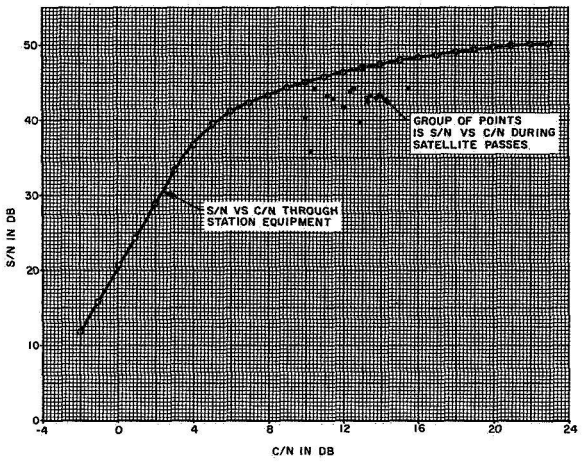


FIGURE 12–2.—S/N vs. C/N, channel 6, monitor receiver.

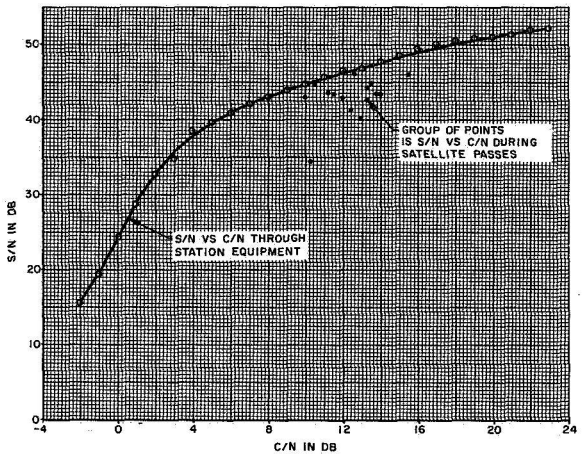


FIGURE 12–3.—S/N vs. C/N, channel 12, monitor receiver.

*B. D. Holbrook and J. T. Dixon, "Load Rating Theory for Multichannel Amplifiers," B. S. T. J., XVIII (October, 1939).

**Recommendation No. 275 of C. C. I. R.

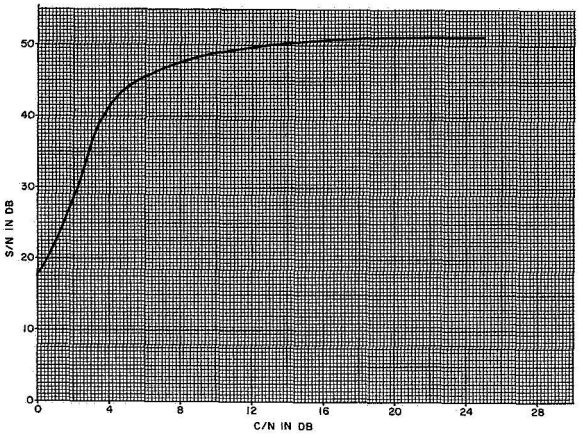


FIGURE 12–4.—S/N vs. C/N, channel 1, communications receiver.

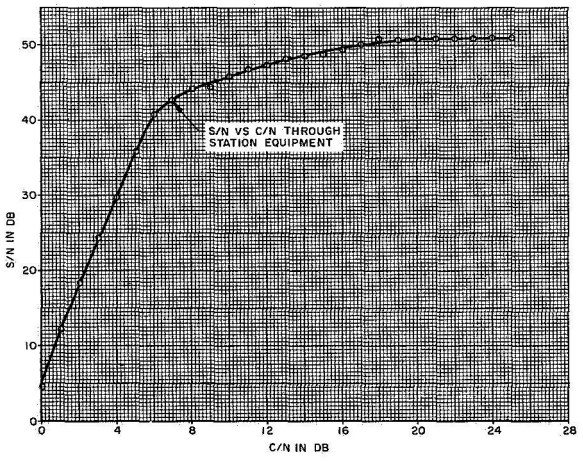


FIGURE 12–5.—S/N vs. C/N, channel 6, communications receiver.

ual noise including residual FM and thermal noise in the receiver baseband amplifier. Depending on the receiver under test and the channel being checked, the limiting thermal noise is between —50 and —55 db with respect to full channel output.

Over the range of C/N from 6 db to 14 db, the S/N in the lowest, middle, and highest frequency channels are within 1 db of each other. This indicates that the pre-emphasis characteristic is properly matched to the system noise characteristic over this range.

The measurements shown on Figure 12–6 (S/N in channel 12 through the communications receiver) were taken both with the phase-locked loop and without it. The phase-locked loop thresholds at a C/N about 4 db lower than that of the discriminator. All curves are referenced to a noise power of —111 dbm in a 1.3 Mc bandwidth.

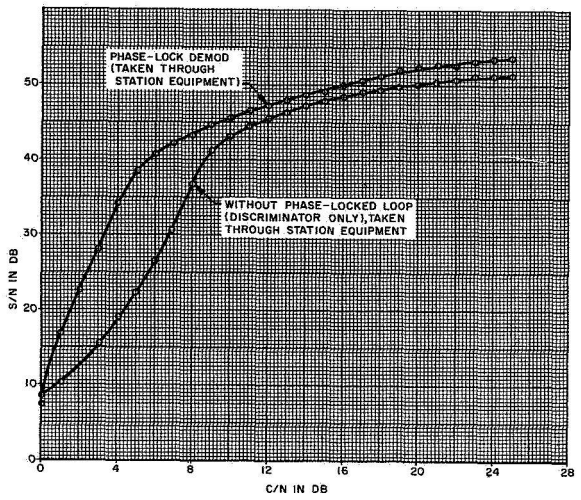


FIGURE 12–6.—S/N vs. C/N, channel 12, communications receiver.

Operational Results

S/N measurements made through the satellite show S/N ratios which are in every case lower than those measured through the station equipment. This is to be expected since the signal passes through the satellite transponder which adds its own noise contribution. Also, the variation in antenna gain around the spin axis introduces an additional noise component.

As the satellite spins (at about 167 rpm) the power radiated by it, as seen by a ground antenna, varies with the same fundamental frequency. This has the effect of moving the C/N ratio up and down, which in turn causes the S/N ratio in any particular band to vary at the spin frequency. That the RMS noise increases can be seen by considering the noise with spin modulation to be given by

$$n'(t) = n(t)\ [1 + \gamma \cos \Omega_s t]$$

where:

γ = Amplitude of spin modulation
Ω_s = Spin frequency

Consider the noise voltage to be described by the Gaussian process,

$$P(n) = \frac{e^{-n^2/2\sigma^2}}{\sigma \sqrt{2\pi}}$$

from which

$$P(n') = P(n)\left|\frac{dn}{dn'}\right|$$

$$\left|\frac{dn}{dn'}\right| = \frac{1}{1 + \gamma \cos \Omega_s t}$$

$$\therefore P(n') = \frac{e^{\left[\frac{-(n')^2}{2\sigma^2 (1 + \gamma \cos \Omega_s t)^2}\right]}}{(1 + \gamma \cos \Omega_s t) \sqrt{2\pi\sigma^2}}$$

The RMS value is seen to be increased by $\sqrt{1 + \gamma^2/2}$ The instantaneous statistics of the noise are still Gaussian.

For example consider a sinusoidal spin modulation of 6 db (peak-to-peak). Then,

$$\frac{P \max}{P \min}\left(= \frac{V \max}{V \min}\right)^2 = 4$$

$$\therefore \frac{V \max}{V \min} = 2$$

Then,

$$\frac{1 + \gamma}{1 - \gamma} = 2$$

$$\gamma = 0.33$$

Therefore, the increase in RMS noise is about 0.2 db. The actual difference between station performance and performance through the spacecraft is generally larger than this. The assumption of sinusoidal modulation is, of course, approximate. In many cases, the spin modulation brings the carrier near threshold where the noise increases precipitously. Thus, a larger difference is to be expected.

System Noise Performance With and Without Pre-Emphasis Through Station Loop

Figure 12–7 shows two curves of baseband noise versus frequency. The data for these curves were taken using a tuned voltmeter having a bandwidth of 340 cps. The noise shown represents the residual noise of the system with the receiver locked to an unmodulated carrier. If only FM noise was present, the curves would reduce to a straight line with a slope of 20 db/decade, which is the classical triangular FM noise spectrum. If the curve taken without de-emphasis is examined, it can be seen that between 50 and 250 kc the curve closely follows a line of 20 db/decade slope. Below 50 kc, the slope decreases and finally becomes negative. This change in slope is due to the addition of noise produced by incidental FM originating in the RF circuitry. Above 250 kc the slope increases slightly and then falls off. This behavior is a function of the phase-locked loop used in the receiver whose frequency response with signal tends to peak around 350 kc and then drops off sharply.

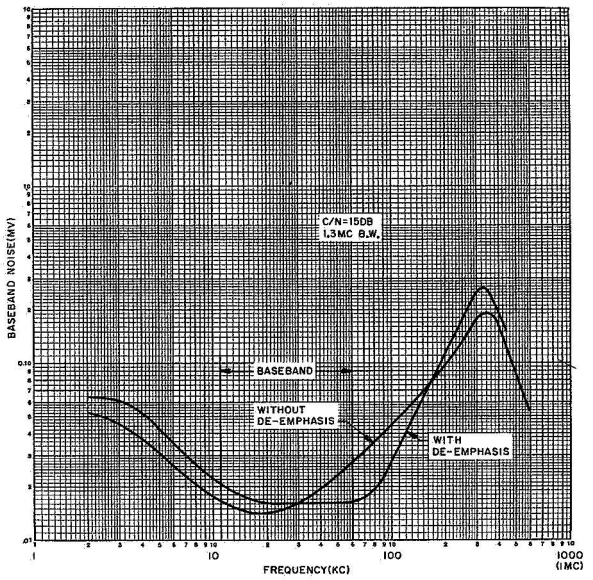


FIGURE 12–7.—Baseband noise vs. frequency, monitor receiver.

The curve of baseband noise versus frequency taken with de-emphasis differs from the flat curve by the response of the de-emphasis network. It can be seen that the noise in the 12 to 60 kc baseband is much flatter with de-emphasis than without. The curve with de-emphasis shows a variation of only 2 db over the band (12 to 60 kc) while the curve without de-emphasis shows a variation of 6 db. It should be noted that

the noise begins to increase below 20 kc. This correlates with *S/N* measurements taken in multiplex channels. Channel 1 (12 to 16 kc) will always show a lower *S/N* ratio than either channel 6 (32 to 36 kc) or channel 12 (56 to 60 kc). The difference between channel 1 and channels 6 and 12 *S/N* is dependent upon the carrier level. Near threshold the difference is only about 1 db or less. However, at a *C/N* of 25 db, differences of 8 db are noted. The crossover point of the de-emphasis network, which is the frequency at which the gain with the network inserted equals the gain in the "flat" position, occurs at 36 kc. The two curves of baseband noise versus frequency cross at 30 kc which agrees closely with the network crossover point.

Figure 12–8 shows a curve of baseband noise versus frequency taken on Relay I orbit 1376 with a comparison curve through the station equipment prior to the pass. At the time these experiments were run, there was a spurious 15-kc component caused by a ground loop in the exciter video amplifier input circuit. This peak should be disregarded when examining the curves since this condition has been eliminated. The components

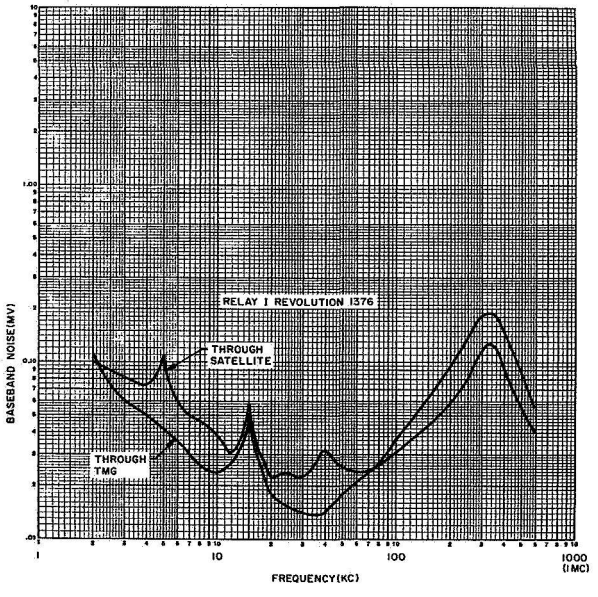


FIGURE 12–8.—Baseband noise vs. frequency, flat response.

appearing at 5 kc and 40 kc, however, appear only in the curve taken through the satellite and thus must originate in the satellite. The 5-kc component has been observed previously and may be due to the spacecraft inverter.

Noise Intermodulation, Thermal Noise, and Deviation

The design of an FM–FDM system is, in part, a compromise between intermodulation distortion and the degradation due to thermal noise. It is well known that the thermal *S/N* in an FM system is proportional to the square of the deviation ratio. However, as the deviation is increased, the effects of nonlinearity cause the resultant total *S/N* in an FDM system to degrade. In this section relationships between *S/N* and deviation are studied.

Procedure

Data was taken through an RF loop under a number of system conditions in order to display the effects of pre-deemphasis and threshold extension by phase locked detection. These were:

Case 1. Discriminator detection with and without pre-deemphasis; $C/N = 26$ db

Case 2. Phase locked detection with and without pre-deemphasis; $C/N = 26$ db

Case 3. Phase locked detection with pre-emphasis; $C/N = 10$ db

In each case the modulating signal was flat Gaussian noise over the baseband. The peak-to-peak deviation (18 db above RMS) was varied from 200 kc to 1.1 Mc. Thermal noise and intermodulation plus thermal noise were measured.

The high *C/N* (26 db) is used to suppress thermal noise so as to obtain a true indication of intermodulation effects.

Thermal noise was measured in the absence of modulation to determine the point at which *S/N* improvement with deviation ceases, and intermodulation distortion predominates.

Results

Figures 12–9 and 12–10 show the noise intermodulation and thermal noise obtained

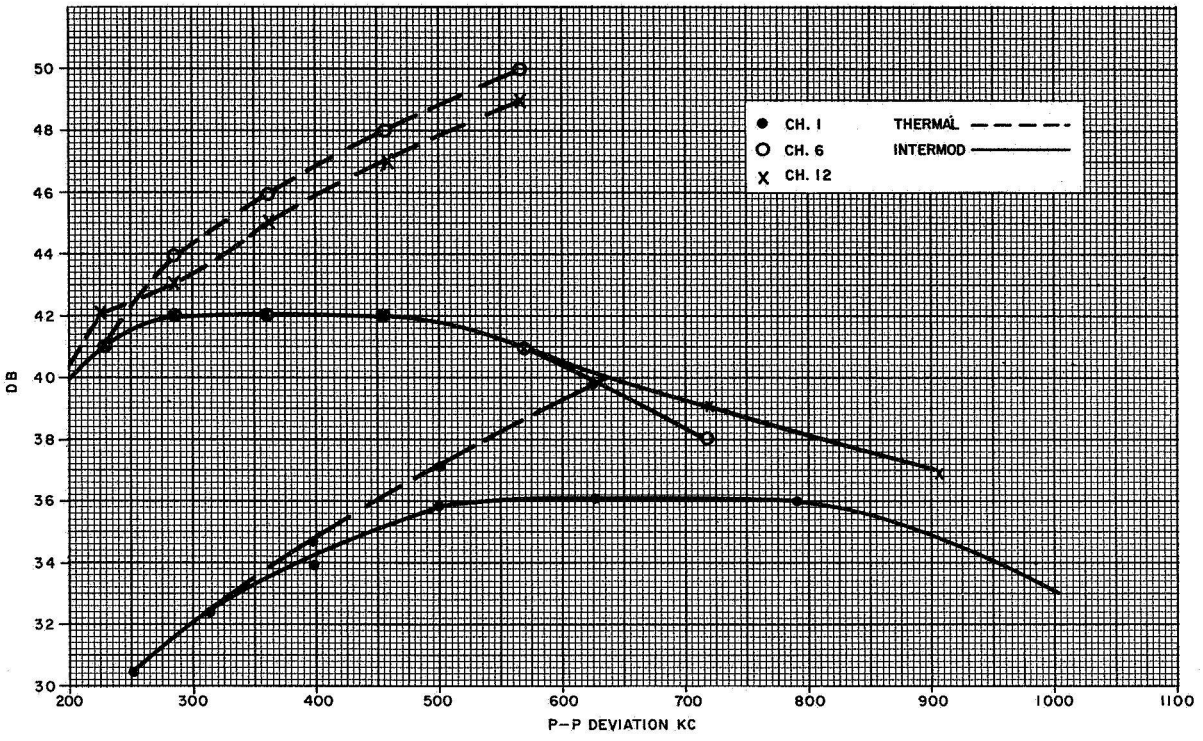


FIGURE 12–9.—Noise power ratio $C/N = 26$ db, discriminator detection without pre-deemphasis.

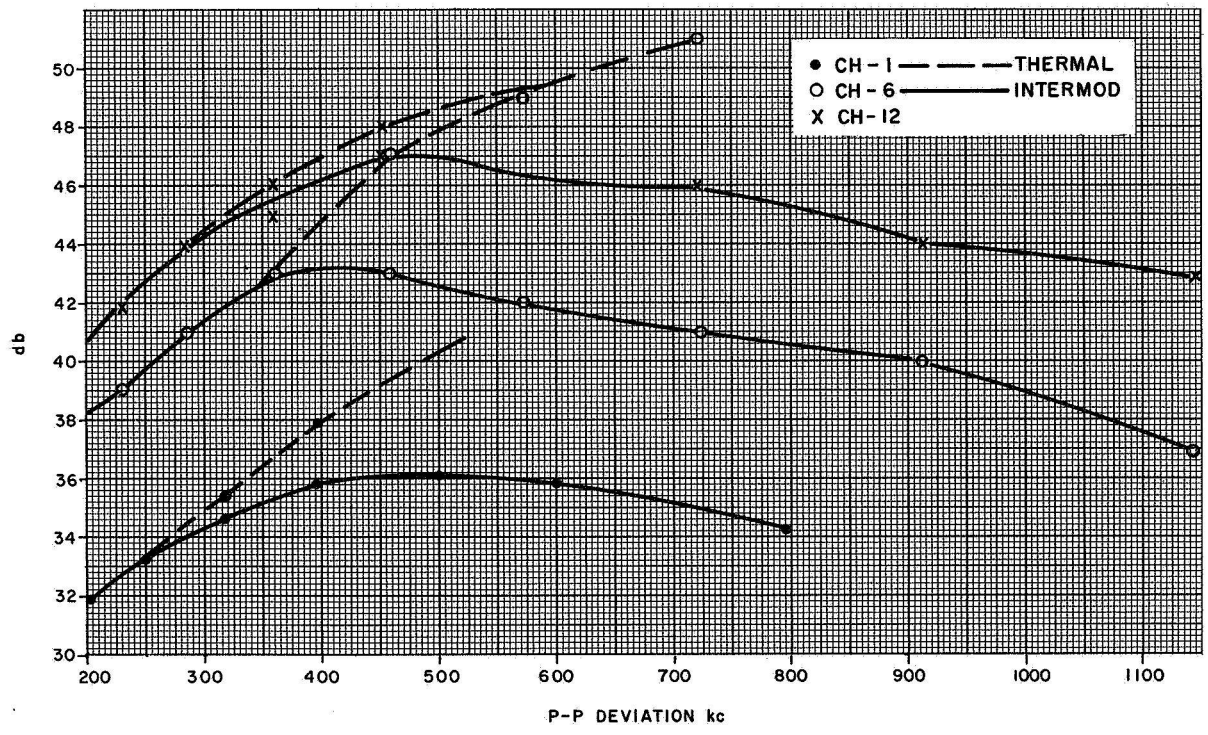


FIGURE 12–10.—Noise power ratio $C/N = 26$ db discriminator protection with pre-deemphasis.

using a typical limiter discriminator circuit, without and with pre-emphasis, respectively. Signal to noise is also plotted for comparison.

In Figure 12–9, taken at $C/N = 26$ db without pre-deemphasis, it appears that thermal S/N in channel 1 is about 11 db poorer than channels 6 and 12. In a theoretical FM system without pre-deemphasis, the low channel S/N should be better than that of the high channel, because of the classical triangular noise spectrum out of a discriminator under high C/N conditions. The observed phenomenon results from the residual FM in the system which becomes apparent at high C/N ratios. Because of the very high C/N (26 db), thermal noise in the top (60 kc) channel is about 55 db below the RMS test tone. Bottom channel (12 kc) noise then should be theoretically 14 db below this. However, the baseband amplifier noise and the noise power of local oscillators contained in both the exciter and receiver mark the thermal noise at this level. The power spectra of these components generally increase close to the nominal output frequency.

If the residual low channel noise were absent, the intermodulation curves for all three channels would be nearly the same. Note also, that for high deviations, the S/N curves approach each other. This indicates that, regarding intermodulation distortion, the effect is fairly uniform over the baseband. This would be expected from a system where intermodulation noise from amplitude and phase nonlinearities are essentially equal.

Comparison of Figures 12–9 and 12–10 shows that with pre-deemphasis the intermodulation in the top channel is improved by about 5 db. Note that with discriminator detection the peak of intermodulation performance is quite broad.

Figures 12–11 and 12–12 show performance without and with pre-emphasis but with

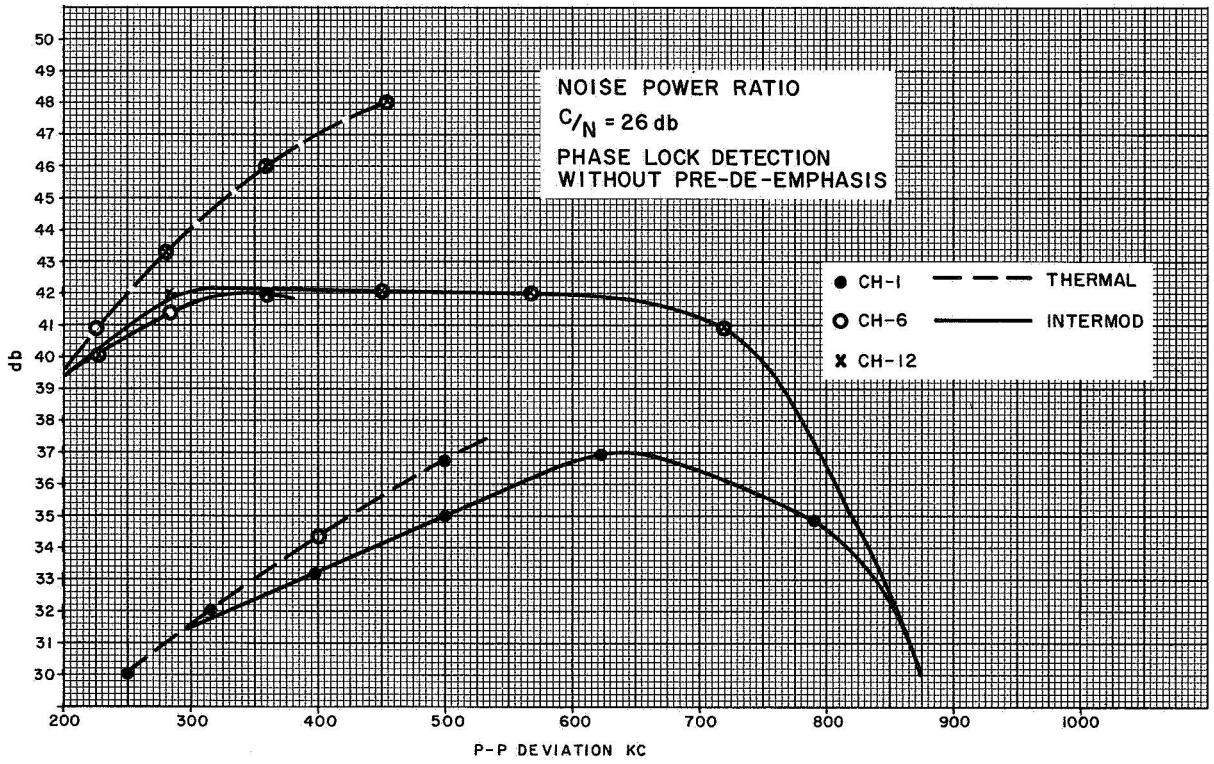


FIGURE 12–11.—Noise power ratio $C/N = 26$ db, phase lock detection without pre-deemphasis.

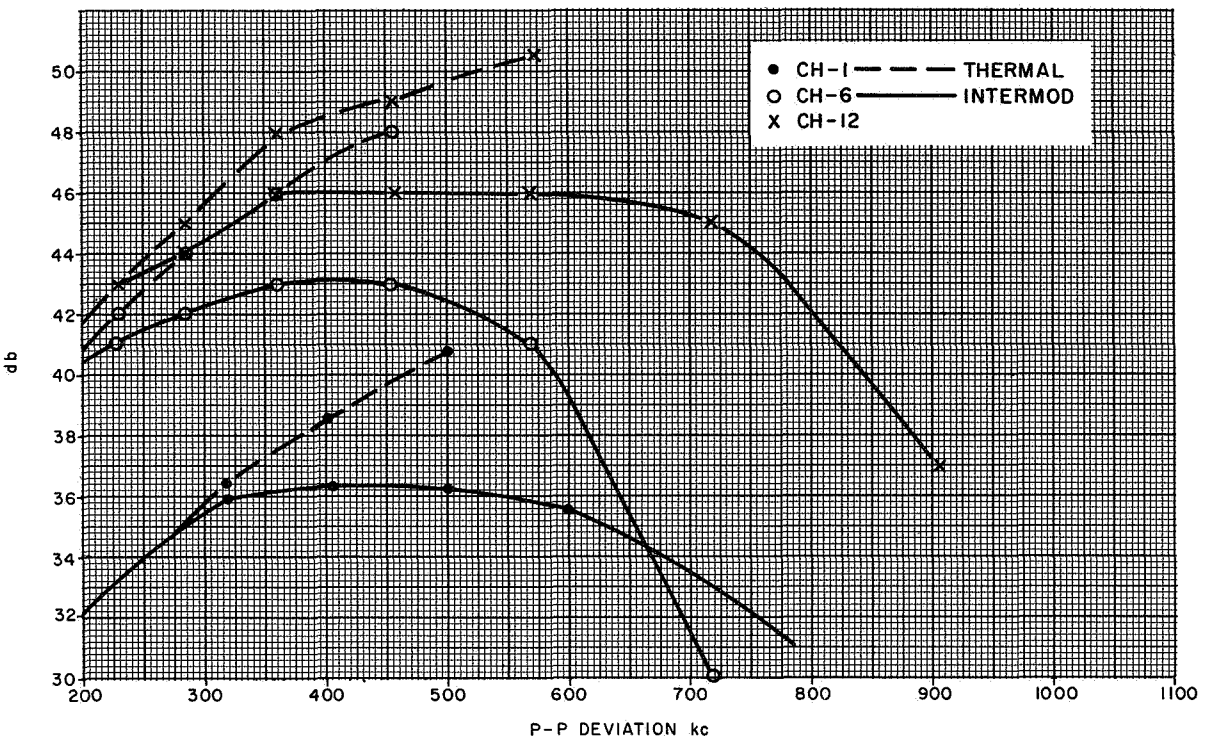


FIGURE 12–12.—Noise power ratio C/N = 26 db, phase lock with pre-deemphasis.

phase lock detection. The most marked difference between Figures 12–11 and 12–12 and Figures 12–9 and 12–10 is the rapid degradation in intermodulation performance as deviation is increased. This is to be expected, since both the maximum phase excursion and phase rate are limited by the phase lock loop dynamics. If these limitations are exceeded, the phase error increases precipitously as does distortion. Top channel intermodulation improvement with pre-deemphasis is about 4 db.

Figures 12–13 and 12–14 show intermodulation performance without and with predeemphasis at a typical operational C/N of 10 db. From these curves it appears that 1 or 2 db could be gained by increasing deviation to about 450 kc peak-to-peak instead of 390 kc.

The top channel improvement with predeemphasis is about 5 db. This is typical for systems where amplitude and phase nonlinearities generate approximately equal noise intermodulation.

The degrading effect of pre-deemphasis on the low channels is quite marked at deviations above 400 kc peak-to-peak. This can be attributed to the effect of baseband amplitude nonlinearities. With pre-emphasis, the high frequency terms begin overdriving the demodulator sooner than without pre-emphasis, and as a result, the low frequency channels receive a considerable amount of intermodulation power. The second and third order products of baseband amplitude nonlinearities are generated by successive convolutions of the input power spectrum with itself. The result is increasing intermodulation power with decreasing frequency. However, until the linear portion of the demodulator is exceeded (at 400 kc) ; the intermodulation in the bottom and middle channels are essentially equal with and without pre-emphasis.

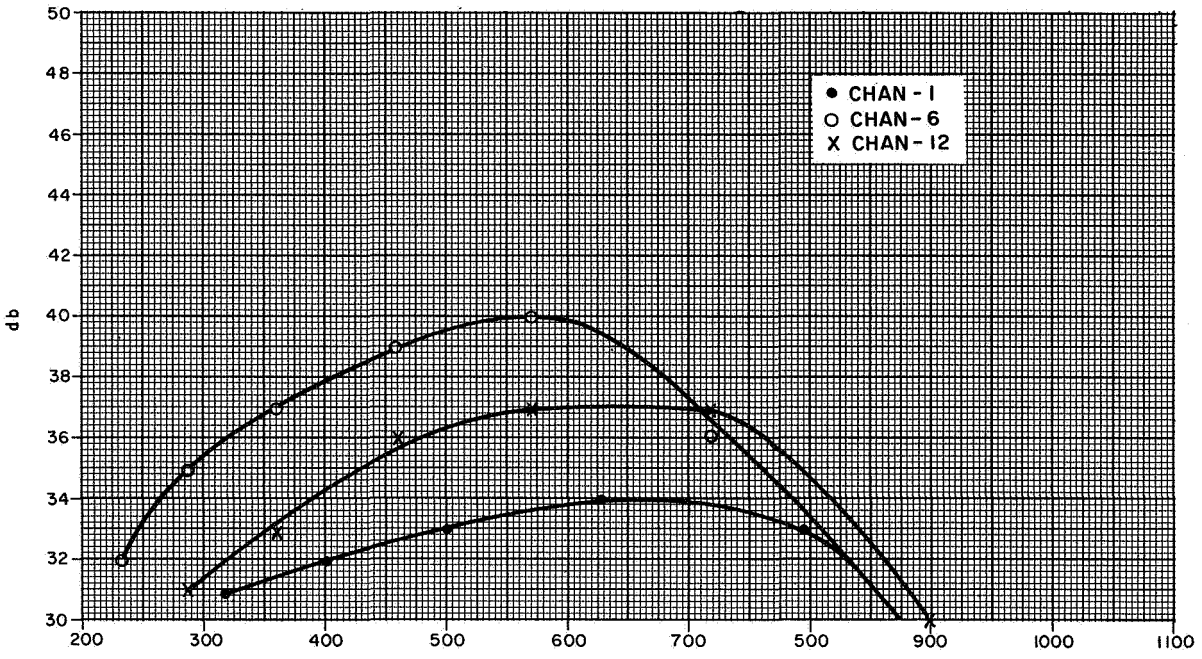


FIGURE 12–13.—Noise power ratio $C/N = 10$ db, phase lock detection without pre-deemphasis.

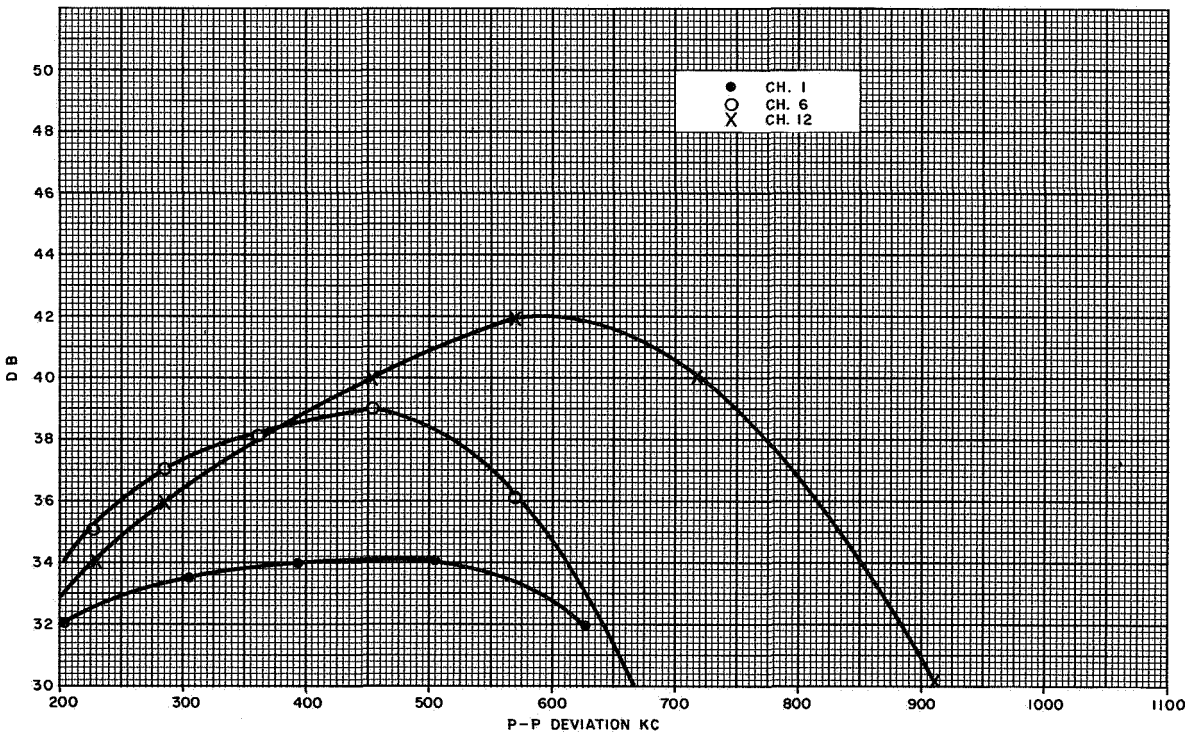


FIGURE 12–14.—Noise power ratio $C/N = 10$ db, phase lock detection with pre-deemphasis.

SPACECRAFT NOISE FIGURE IN NARROWBAND MODE

Introduction

On 26 October 1963, tests were conducted at COMNUT with the Relay I spacecraft to obtain data for calculations leading to spacecraft receiver noise figure in the narrowband mode.

This report deals with the theory behind the measurements and the calculations leading to the spacecraft noise figure evaluations.

Experiment Outline

During the experiment COMNUT measured (on orbit 2465) the receiver signal-to-noise ratio in multiplex channel 12 as a function of transmitted power. The transmitted power was successively set to 10 kw, 5 kw, 3 kw, 2 kw, 1 kw, 500 w, 100 w, and 50 w. The channel signal-to-noise ratio is a function of the RF carrier-to-noise ratio and is determined at critical points in the communications system (e.g., receiver inputs where thermal noise is a significant portion of the total input). In the Relay I Satellite-COMNUT System there are two such points: (1) at the spacecraft receiver input, and (2) at the COMNUT receiver input. These noise sources are commonly expressed as noise power densities and are represented mathematically by ϕ_v watts per cycle of bandwidth for the satellite and ϕ_g watts per cycle of bandwidth for the COMNUT receiver. Also ϕ_v can be expressed as a noise figure:

$$NF = 10 \log \left[1 + \frac{\phi_v}{(K)\,(290)} \right] \text{ db} \qquad (12.11)$$

where

NF = noise figure (db)
ϕ_v = spacecraft receiver noise power density (watts/cycle)
K = Boltzmann's constant (1.38×10^{-23} joules/°K/cps)
290 = reference temperature (degrees Kelvin)

The relationship between noise power densities and received single channel signal to noise is given by:

$$\frac{P_{s_o}}{P_{n_o}} = \left(\frac{\Delta f}{f_m}\right)^2 \frac{P_{s_v \rho}}{2b\,(n^2 \phi_v + \frac{\phi_g}{G})} \qquad (12.12)$$

where

P_{s_o}/P_{n_o} = channel signal to noise power ratio
$\frac{\Delta f}{fm}$ = top channel modulation index
b = multiplex channel bandwith (cps)
ρ = pre-emphasis factor
P_{s_r} = carrier power level entering spacecraft receiver (watts)
n = noise increment factor due to frequency multiplication in spacecraft
G = net gain between satellite receiver input and COMNUT receiver input
ϕ_r = spacecraft receiver noise power density (watts/cps)
ϕ_g = ground receiver noise power density (watts/cps)

With the exception of G and n, all factors in the equation $P_{s_o} P_{n_o}$ are known and remain constant during the experiment.

Determination of G

AGC circuitry in the spacecraft controls the main IF amplifier gain and consequently the net gain G, by maintaining the total output of the IF amplifier constant.
For example:

or

$$G\,(P_{s_v} + B_r \phi_r) = K \qquad (12.13)$$

$$G = \frac{K}{P_{s_r} + B_r \phi_r} = \frac{K'}{\frac{P_{s_v}}{B_r \phi_r} + 1} \qquad (12.14)$$

where B_v = spacecraft transponder bandwidth (cps) and $K' = K / B_v \phi_v$.
When $P_{s_v} << B_r \phi_r$, equation (12.13) reduces to

$$K = GP_{s_v} = P_{s_g}$$

where P_{s_g} = signal power at ground receiver.

Thus, K can be determined for a specific system: (1) by illuminating the spacecraft at a level whereby the relationship $P_{s_v} >> B_v \phi_v$ is satisfied, and (2) by measuring P_{s_g}.

For the system under consideration, $P_{s_{v\,max}} = -70$ dbm when COMNUT transmits 10 kw. For a typical spacecraft noise figure of 14 db, $B_v \phi_v = -97$ dbm. Therefore the inequality can be satisfied and K can be determined. Once K is determined, the net gain G is determined from Equation (12.14) as a function of P_{s_v} with spacecraft noise power density (ϕ_v) as a parameter.

As an example, when COMNUT transmitted 10 kw, P_{s_g} was measured as −99 dbm. Therefore, $K = -99$ dbm.

Determination of N

After entering the satellite transponder, carrier power, S_v, and noise power undergo a frequency translation and enter a frequency tripler. Being a nonlinear device, the tripler mixes the carrier and noise power causing additional noise products. Equation (12.15), which follows, demonstrates the tripling process affecting the carrier and noise voltage amplitudes:

$$V_o = K\,(S_i + N_i)^3 \qquad (12.15)$$

where

V_o = tripler output voltage
S_i = tripler input signal amplitude
N_i = tripler input noise amplitude

Expanding,

$$\frac{V_o}{K} = S_i^3 + 3\,S_i^2\,N_i + 3\,S_i N_i^2 + N_i^3$$

Here, S_i^3 represents the amplitude of the tripled carrier frequency. The other terms represent noise contributions. The noise-to-signal ratio at the output of the tripler can, therefore, be written as:

$$\frac{N_o}{S_o} = \frac{3\,S_i^2\,N_i}{S_i^3} + \frac{3\,S_i N_i^2}{S_i^3} + \frac{N_i^3}{S_i^3}$$

$$= 3\frac{N_i}{S_i} + \frac{3\,N_i^2}{S_i^2} + \frac{N_i^3}{S_i^3}$$

$$\frac{N_o}{S_o} = \frac{N_i}{S_i}\left(3 + 3\frac{N_i}{S_i} + \frac{N_i^2}{S_i^2}\right) \qquad (12.16)$$

where

$\frac{N_o}{S_o}$ = tripler output noise-to-signal voltage ratio

and

$\frac{N_i}{S_i}$ = tripler input noise-to-signal voltage ratio

The term $\left(3 + 3\frac{N_i}{S_i} + \frac{N_i^2}{S_i^2}\right)$ is the factor by which input noise to carrier is increased due to the frequency tripling process. The noise power increase resulting from frequency tripling of a carrier is obtained by squaring Equation (12.16) resulting in:

$$\frac{N_o^2}{S_o^2} = \frac{P_{n_o}}{P_{s_o}} = \left(3 + \frac{3\,N_i}{S_i} + \frac{N_i^2}{S_i^2}\right)^2 \frac{N_i^2}{S_i^2}$$

$$= n^2 \frac{N_i^2}{S_i^2} = n^2 \frac{P_{ni}}{P_{si}} \qquad (12.17)$$

where n^2 is defined as the noise power increment factor.

Figure 12–15 shows the relationship between S_i/N_i and n^2.

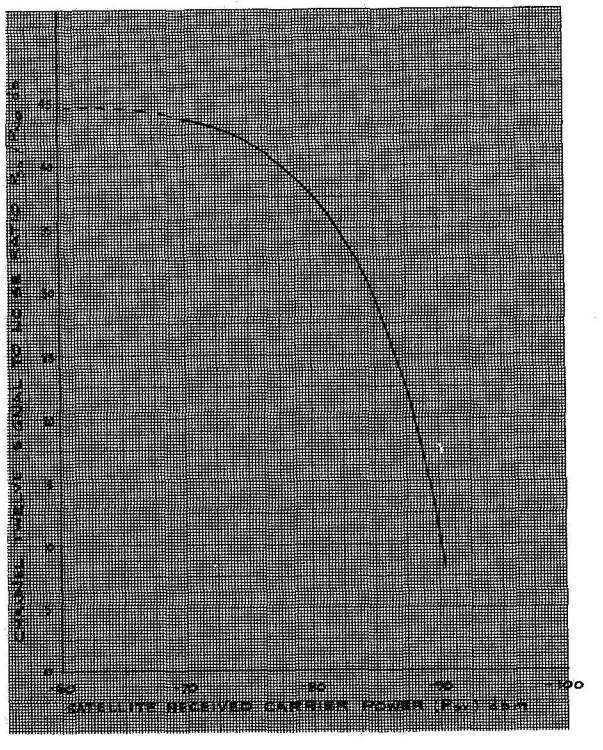


FIGURE 12–15.—Signal to noise characteristics of multiplex channel 12 Relay I orbit 2465.

Note that for large carrier-to-noise values the square of the increment factor approaches nine which is the square of the frequency multiplication factor. The values of G and n^2 can then be used in Equation (12.12) to obtain theoretical values of $(P_s/P_n)_o$.

Determination of Spacecraft Noise Figure

The theoretical values of signal to noise $(P_s/P_n)_o$ with ϕ_v as a parameter can be presented as a family of curves. Empirical values of $(P_s/P_n)_o$ can then be superimposed upon these theoretical curves. The theoretical curve most closely matching the empirical one determines noise figure.

Experiment and Calculations

Experiment Procedure

The previous section discussed the theory and relationships needed to determine spacecraft noise figure. Channel signal-to-noise measurements were conducted to provide the information for calculating G and empirical signal-to-noise values.

Signal-to-noise measurements were performed for orbit 2465 as described in the Relay Communication Experiment Plan Test IIIB1 (R1–0521) except that transmitted power was programmed in steps descending from 10 kw to 50 watts. The signal-to-noise ratio in Multiplex Channel 12 was measured at each power level.

Calculation of Parameters

This section presents typical calculations which lead to spacecraft receiver noise figure.

Path loss between COMNUT and the spacecraft at 1,733.33 Mc: Up-link path loss is given by:

$$a = 32.1 + 20 \log f + 20 \log d$$

where

a = path loss (db)
f = frequency (Mc)
d = distance (km)

Range variations for orbit 2465 cause only a ±0.1-db change in path loss, so only one range calculation is necessary. At 1,723.33 Mc, the path loss for an average range of 7,977 km is:

$$a = 32.9 + 20 \log 1723.33 + 20 \log 7977$$
$$a = 176 \text{ db}$$

Carrier power P_{s_v} arriving at the satellite:

$$P_{s_v} = P_T + A - a + A_v \text{ dbm}$$

P_T = transmitted power (dbm)
A = COMNUT's antenna gain (37.6 db)
a = path loss (db)
A_v = spacecraft antenna gain (db)

When COMNUT transmitted 10 kw, the carrier power arriving at the satellite was:

$$P_{s_v} = +70 + 37.6 - 176 - 3 = -71.4 \text{ dbm}$$

Theoretical Signal-to-Noise ratio $(P_s/P_n)_o$ to be expected in multiplex channel 12: Tabulated below are terms and their values to be inserted in Equation (12.12). These are obtained from known system parameters.

Δf = 126 kc peak
$\frac{\Delta f}{fm}$ = 2.21 = 3.44 db
b = 3×10^3 cps = 34.8 db above 1 cps
ϕ_y = −170.6 dbm/cycle for a system temperature of 350°K
ϕ_v = assumed parameter
n^2 = function of S_i/N_i
G = to be determined
B = effective system noise bandwidth (controlled by the phase locked loop in COMNUTS communications receiver.)
B_r = bandwidth of spacecraft in the narrowband mode (2×10^6 cps or 63.2 db above 1 cps*)
K = −99 dbm

The following steps are used to calculate the theoretical signal to noise ratio $(P_s/P_n)_o$ to be expected at COMNUT as a function of carrier power $(P_s)_v$ entering the spacecraft receiver. A typical set of calculations is also presented for an assumed spacecraft re-

*"Relay System Data Book," Space Technology Laboratories, Inc., Los Angeles, 5 February 1962.

ceiver noise figure of 12 db and carrier (P_{s_v}) power of −72 dbm.

$$\phi_v = KT_n = 10 \log K + 10 \log 290 + NF$$
$$= -174 + 12 = -162 \text{ dbm/cps}$$
$$B_g \phi_v = 56 - 162 = -106 \text{ dbm}$$
$$B_v \phi_v = 63.2 - 162 = -98.8 \text{ dbm}$$
$$K' = \frac{GP_{s_v}}{B_v \phi_v} = -99 + 98.8 = -0.2 \text{ db}$$
$$\frac{P_{s_v}}{B_v \phi_v} = -72 + 98.8 = 26.8 \text{ db}$$
$$G = \frac{K'}{\frac{P_{s_v}}{B_v \phi_v} + 1} = \frac{K'}{\frac{P_{s_v}}{B_v \phi_v}}$$
$$= -0.2 - 26.8 = -27 \text{ db}$$
$$\frac{P_{s_o}}{P_{n_o}} = \left(\frac{\Delta f}{f_m}\right)^2 \frac{1}{2b} \cdot \frac{P_{s_v} \rho}{n^2 \phi_v + \frac{\phi_g}{G}}$$
$$= 6.88 - 72 - 37.7 - 10 \log \left(n^2 \phi_v + \frac{\phi_g}{G} + \rho\right).$$

For this particular case,

$$n^2 = 9 = 9.5 \text{ db}$$
$$n^2 \phi_v = 152.45 \text{ dbm/cps}$$
$$\frac{\phi_g}{G} = 143.6 \text{ dbm/cps}$$
$$10 \log n^2 \phi_v + \frac{\phi_g}{G} = -143.6 \text{ dbm/cps}$$
$$\frac{P_{s_o}}{P_{n_o}} = (40.8 + \rho) \text{ db}$$

Figure 12–16 is a plot of $\frac{P_{s_o}}{P_{n_o}}$ vs P_{s_v} in channel 12 as measured during orbit 2645. Figure 12–17 is a plot of calculated P_{s_o}/P_{n_o} vs. P_{s_v} with ϕ_v (or spacecraft noise figure) as a parameter, considering $\rho = 0$. It is seen in Figure 12–17 that for $P_{s_v} \geq -60$ dbm, P_{s_o}/P_{n_o} is essentially independent of ϕ_v.

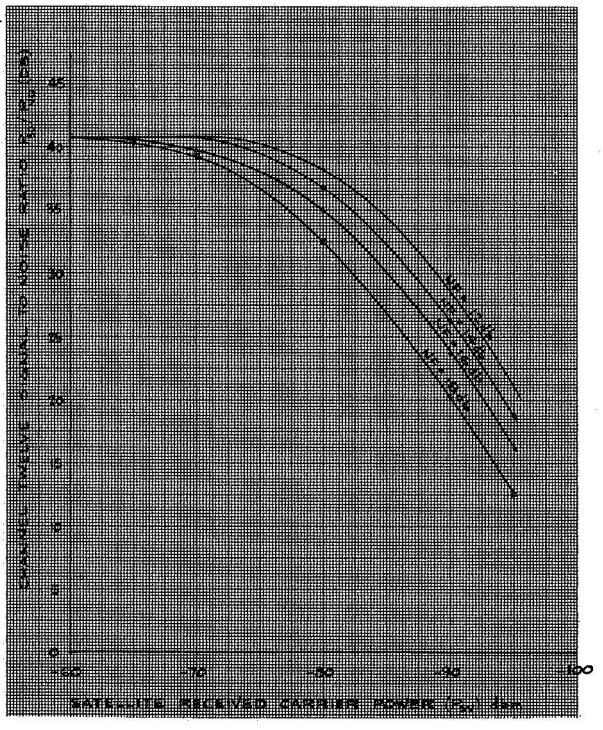


FIGURE 12–16.—Expected signal to noise characteristics of channel 12 with spacecraft noise figure as a parameter.

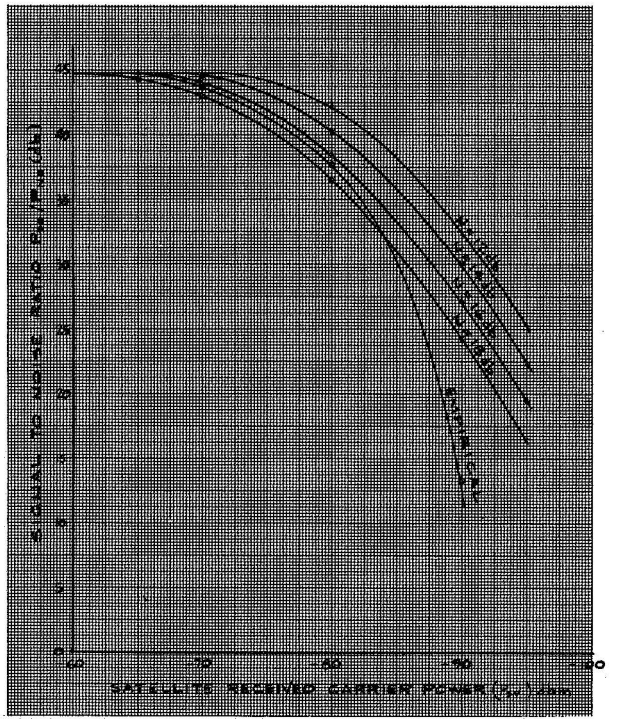


FIGURE 12–17.—Composite empirical and normalized theoretical signal to noise characteristics for Relay I orbit 2465.

This enables one to normalize the theoretical curves so that a comparison can be made between empirical and theoretical values. Figure 12–17 shows the normalized theoretical curves superimposed on the empirical curve in such a manner as to give equal results at $P_{s_v} = -60$ dbm. This has been done, in effect, by assuming $\rho = 4$ db which is the normal value for pre-emphasis improvement.

Conclusions

Figure 12–17 shows the empirical values of signal-to-noise in Multiplex Channel 12 superimposed on the family of theoretical curves. At $P_{s_v} = -70$ dbm, the empirical signal-to-noise ratio corresponds essentially to the theoretical signal-to-noise for a 16-db spacecraft receiver noise figure. At $P_{s_v} = -85$ dbm, the empirical signal-to-noise ratio corresponds to the theoretical values for a spacecraft noise figure of 18 db. Therefore, the spacecraft receiver noise figure is a function of carrier power arriving at the satellite's receiver, as shown in Table 12–3. This agrees with prelaunch measurements, which are shown for comparison.

TABLE 12–3.—*Satellite Receiver Noise Figure as a Function of Received Carrier Power*

Carrier power (P_{s_v})	Noise figure (from Orbit 2465 tests)	Noise figure (from prelaunch tests)
(dbm)	(db)	(db)
−70	16	14.2
−80	17	16.8
−85	18	—

It appears that the noise performance of the spacecraft has degraded from the prelaunch performance. For a typical operating point of −70 dbm the degradation is seen as 1.8 db worsening in noise figure.

NEAR-ZENITH TRACKING EXPERIMENT

Near-zenith passes are among the most severe tests on an az-el tracking mount because of the high azimuth velocity and acceleration capabilities required to maintain proper antenna pointing. A typical near-zenith pass was Relay I orbit 1137. Figure 12–18 is a polar plot of the near-zenith portion of this pass which occurred between 0033Z and 0034Z. From this plot it can be

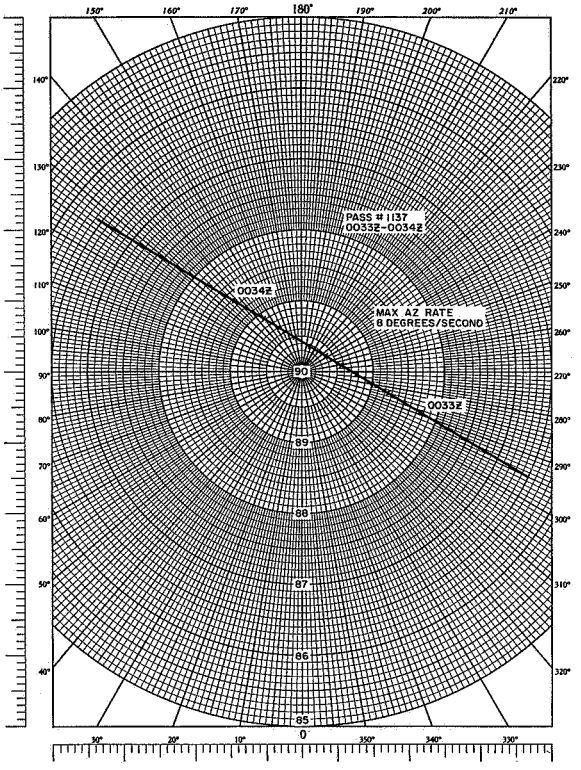


FIGURE 12–18.—Relay I orbit 1137, polar of zenith part of pass.

seen that the maximum elevation angle was 89.6 degrees. The maximum azimuth rate was 8 degrees/second.

Figure 12–19 is a section of the strip chart recording taken during the pass. The trace of azimuth error shows a maximum error voltage of 150 mv. This value of error is compatible with the peak rate of 8 degrees/second. The autotrack system has an error slope of 1 volt/degree; this error voltage corresponds to an angular difference of 9 minutes between the electrical axis of the azimuth error channel and the azimuth direction of the satellite.

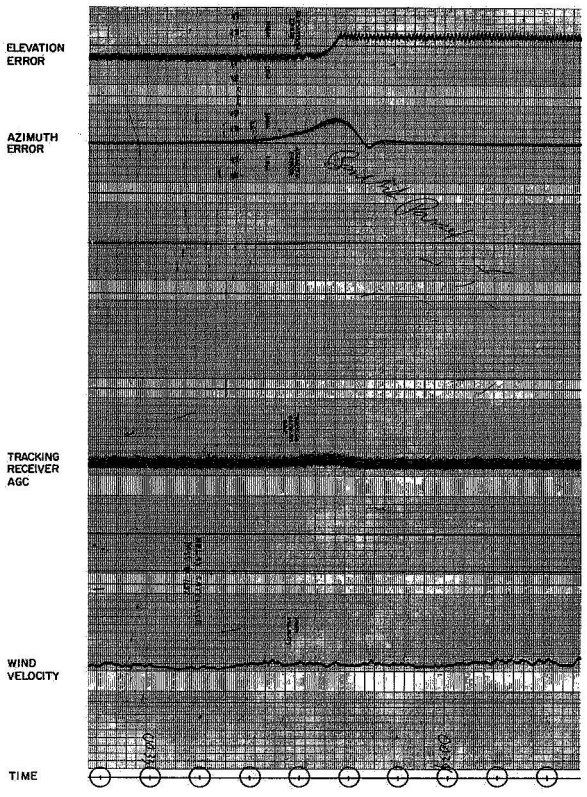


FIGURE 12–19.—Typical zenith path Relay I orbit 1137.

GENERAL CONCLUSIONS

The purpose of this report has been to present an analysis of selected experiments performed by COMNUT on Relay I during 1963. Wherever possible, measured performance has been compared with theoretical performance to establish the validity of both the analytical and empirical results.

Measurements of envelope delay and NPR have shown good agreement with their calculated values. However, work is continuing on improving measurement techniques and the interpretation of data.

It has been successfully demonstrated that the two tone test provides a means for separately predicting the contributions of amplitude and phase nonlinearities to noise intermodulation.

It has been shown that measured and calculated values of signal-to-noise ratio agree quite well, and that the phase-locked detection system used in COMNUT's receivers provides a threshold improvement of 4 db.

The results of the measurement of satellite noise figure show degradations of about 2 db from prelaunch values.

Investigations are continuing on each of the areas covered in the report to provide additional data on system performance as well as changes in performance with time.

AUTHORS. *This chapter was written by personnel of the International Telephone and Telegraph Federal Laboratories, Nutley, New Jersey, U.S.A. under contract NAS 5–2056 with NASA/Goddard Space Flight Center.*

APPENDIX A: DEVELOPMENT OF SECOND AND THIRD ORDER HARMONIC COMPONENTS

The input-output relationship is:

$$V_{oa} = V_i(t) + m_2 V_i^2(t) + m_3 V_i^3(t) + m_4 \frac{d}{dt}\left[\left|V_i^2(t)\right|\right] + m_5 \frac{d}{dt}\left[V_i^3(t)\right]$$

For two-tone tests:

$$V_i = g\left[\sin \omega_1 t + \sin \omega_2 t\right]$$

$$V_i^2 = g^2\left[\sin^2 \omega_1 t + \sin^2 \omega_2 t + 2 \sin \omega_1 t \sin \omega_2 t\right]$$

$$\frac{d(V_i^2)}{dt} = g^2\left[\omega_1 \sin 2\omega_1 t + \omega_2 \sin 2\omega_2 t + (\omega_1 + \omega_2)t - (\omega_1 - \omega_2) \sin (\omega_1 - \omega_2)t\right]$$

$$V_i^3 = \frac{9}{4} g^3 \sin \omega_1 t + \frac{9}{4} g^3 \sin \omega_2 t - \frac{g^3}{4} \sin 3\omega_1 t - \frac{g^3}{4} \sin 3\omega_2 t - \frac{3}{4} g^3 \sin (\omega_1 + 2\omega_2)t - \frac{3}{4} g^3 \sin (\omega_2 + 2\omega_1)t - \frac{3}{4} g^3 \sin (\omega_1 - 2\omega_2)t - \frac{3}{4} \sin g^3 (\omega_2 - 2\omega_1)t$$

$$\frac{d}{dt}\left[V_i^3\right] = \frac{9}{4} g^3 \omega_1 \cos \omega_1 t + \frac{9}{4} g^3 \omega_2 \cos \omega_2 t - \frac{3}{4} \omega_1 g^3 \cos 3\omega_1 t - \frac{3}{4} \omega_2 g^3 \cos 3\omega_2 t - \frac{3}{4} g^3 (\omega_1 + 2\omega_2) \cos (\omega_1 + 2\omega_2)t - \frac{3}{4} g^3 (\omega_2 + 2\omega_1) \cos (\omega_2 + 2\omega_1)t - \frac{3}{4} g^3 (\omega_1 - 2\omega_2) \cos (\omega_1 - 2\omega_2)t - \frac{3}{4} g^3 (\omega_2 - 2\omega_1) \cos (\omega_2 - 2\omega_1)t$$

Collecting terms of like frequency the amplitudes are tabulated below.

Term	Amplitude (output)
ω_1	$Ag\left[(1 + \frac{9}{4} m_3 g^2)^2 + (\frac{9}{4} m_5 g^2 \omega_1)^2\right]^{\frac{1}{2}} \cong Ag$
ω_2	$Ag\left[(1 + \frac{9}{4} m_3 g^2)^2 + (\frac{9}{4} m_5 g^2 \omega_2)^2\right]^{\frac{1}{2}} \cong Ag$
$\omega_1 \pm \omega_2$	$Ag^2\left[m_2^2 + m_4^2 (\omega_1 \pm \omega_2)^2\right]^{\frac{1}{2}}$
$2\omega_1$	$Ag^2\left[\frac{m_2^2}{4} + m_4^2 \omega_1^2\right]^{\frac{1}{2}}$
$2\omega_2$	$Ag^2\left[\frac{m_2^2}{4} + m_4^2 \omega_2^2\right]^{\frac{1}{2}}$
$\omega_1 \pm 2\omega_2$	$A\frac{3}{4} g^3\left[m_3^2 + m_5^2 (\omega_1 \pm 2\omega_2)^2\right]^{\frac{1}{2}}$
$\omega_2 \pm 2\omega_1$	$A\frac{3}{4} g^3\left[m_3^2 + m_5^2 (\omega_2 \pm 2\omega_1)^2\right]^{\frac{1}{2}}$
$3\omega_1$	$A\frac{1}{4} g^3\left[m_3^2 + 9m_5^2 \omega_1^2\right]^{\frac{1}{2}}$
$3\omega_2$	$A\frac{1}{4} g^3\left[m_3^2 + 9m_5^2 \omega_2^2\right]^{\frac{1}{2}}$
	$A \cong 0.7$ (baseband gain factor g is defined as peak input volts gA = peak output volts

PART III

N66-10251

Chapter 1

GSFC Demonstrations

INTRODUCTION

For the purposes of this report, a demonstration is defined as an operation with the spacecraft at the request of an individual or organization, not necessarily associated with test operations, for the purpose of exhibiting the capability of the spacecraft as a worldwide communication link. Within this definition, several demonstrations can be conducted during one revolution of the spacecraft, and several types of operations can be performed within the limits of one demonstration. For these reasons it is not incorrect to state that 112 revolutions were used, during which 133 demonstrations were conducted, consisting of the following elements:

- 80 television operations including 4 failures
- 14 facsimile operations including 2 failures
- 7 teletype operations including 1 failure
- 35 voice operations including 13 failures
- 5 special operations including 2 failures

Demonstration participation by the several ground stations is shown in the following chart.

Station	Type demonstration				
	TV	Fax	TTY	Voice	Special
COMAND	75	2	1	14	
COMBOD	32	2		1	2
COMGEB				2	
COMHIL	42	6		13	3
COMIBA	5				
COMMOJ	5				
COMNUT		12	6	19	5
COMRIO		5	3	18	1
COMTEL	1	5	4	2	

*See Appendix C, Page 556 for location of ground stations.

Several significant firsts in the field of satellite communications were accomplished during this period. The earliest was during revolution 267 on 17 January 1963 when the continent of South America was welcomed into this type operation through COMRIO, the "Radional" station at Jacarepaguá in suburban Rio de Janeiro, Brazil. Voice and teletype messages were transmitted in both directions in English, Portuguese and Spanish.

On 8 November 1963, during revolution 2566, greetings were exchanged between Mr. James Webb, NASA Administrator, and Mr. Richard Stuecklen of the Deutsche Bundespost. These greetings were exchanged via the COMAND and COMGEB stations. Thus was Germany welcomed into the field of space communications.

Japan was first contacted via satellite on 22 November 1963 when a prepared inaugural television program was transmitted to COMIBA from COMMOJ.

On 28 September 1963 during revolution 2722 material was transmitted from COMBOD to COMAND. The European material

was then augmented by more material in the United States and was later transmitted from COMMOJ to COMIBA. Of prime significance in this operation was the demonstration of the truly international characteristic of satellite communication. Material was taped in France, Italy, Russia, England and other European countries by the British Broadcasting Company and transmitted from the French ground station to the United States. The material added here was from Canada and Mexico as well as from the United States. Reports indicate that the material was enthusiastically received in Japan.

TELEVISION

The four television attempts which failed were as follows:

1. Revolution 1353 when the network pool coordinator did not order lines between Paris and Pleumeur-Bodou.

2. Revolution 1500 due to an equipment failure at COMHIL.

3. and 4. During revolution 1516 and 1523 where the BBC experienced trouble in their equipment at London.

The subject material of these demonstrations was quite varied, ranging from the opening ceremonies of the Mona Lisa display in Washington to the opening ceremonies of the annual TV "Emmy" awards program. There were isolated individual programs such as the conferring of United States citizenship on Sir Winston Churchill and there were subjects which received mass coverage such as the nine transmissions associated with the death and election of the Pope, seven concerning the MA–9 launch, nine on President Kennedy's trip to Europe and seventeen on President Kennedy's assassination and funeral.

Selected demonstrations are discussed and pictures taken of the monitors during those demonstrations are exhibited in Appendix A of this chapter. The selection of demonstration for Appendix A was based upon availability of photographs and for video tapes as well as the desire to present an example of each normal operating combination, i.e., COMAND to COMBOD, COMHIL to COMAND, etc.

The material used during revolution 749 on 20 March 1963, although not planned as a demonstration, was used on a National Broadcasting Corporation network program. It consisted of ten minutes, in color, from the "Kidnapped" story presented on Walt Disney's "Wonderful World of Color" program. The material originated in New York, was looped through the spacecraft at COMAND and was sent back to New York where it was taped.

FACSIMILE

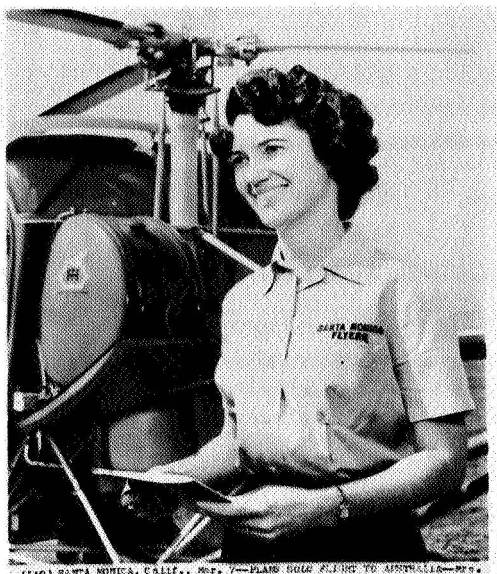
The two attempts at facsimile demonstrations which failed were during revolution 664 when the spacecraft could not be commanded properly and revolution 1044 when COMRIO could not operate.

The subject material for these demonstrations consisted mainly of news photographs and descriptive material for magazine articles. Of special interest were the following:

1. Revolution 657 on 8 March 1963 during which a photograph of Mrs. Betty Miller, a woman pilot, was transmitted from COMNUT for simultaneous reception at COMBOD, COMHIL and COMTEL. The Associated Press offices in Rome and in London retransmitted, via cable, back to New York the results of the demonstration. These photographs and the original are reproduced in Figure 1–1.

2. Revolution 997 on 21 April 1963 during which color facsimile was transmitted from COMNUT to COMTEL. The results of this transmission were used by several publication in Italy. A copy of the three black and white masters for this particular pass are shown in Figure 1–2.

3. Revolutions 1035 on 25 April 1963 when color facsimile was transmitted from COMNUT to COMHIL and 1073 on 30 April 1963 when the same picture was transmitted back from COMHIL to COMNUT. A reproduction of the picture was used on the cover of "Electronics" magazine.



Picture transmitted from New York to London, Rome and Paris.



Picture received in New York from Rome



Picture received in New York from London

FIGURE 1–1.—COMNUT to COMBOD, COMHIL, and COMTEL, revolution 657, 8 March 1963.

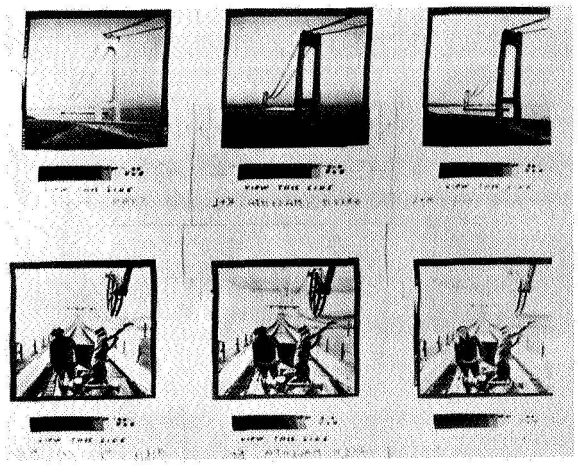


FIGURE 1-2.—COMNUT to COMTEL. Revolution 997, 21 April 1963.

QUANDO O SATELITE DE COMUNICACOES RELAY PASSAVA POR SOBRE A AMERICA DO NORTE HA ALGUNS DIAS, UMA MENSAGEM RADIFONICA DO SATELITE FOI CAPTADA PELO CENTRO DE VOO ESPACIAL DE GODDARD, PERTO DE WASHINGTON D.C. AO LER A MENSAGEM, JACK FLAHERTY, DIRECTOR DO PROGRAMA DE LANCAMENTO DESS SATELITE, OBSERVOU PARA UM DE SEUS ASSISTENTES: O SATELITE ESTA FRIO. A TEMPERATURA CAIU PARA 12 DEGREES C. VAMOS CANCELAR TODAS AS COMUNICACOES EXPERIMENTAIS COM O BRASIL NAS PROXIMAS ORBITAS E ESPERAR QUE AS BATERIAS DO SATELITE SE CARREGUEM NOVAMENTE.

UMA VEZ RECARREGADAS, AS BATERIAS COMECARAM A GERAR CALOR E A TEMPERATURA INTERIOR DO RELAY LOGO ATINGIU 22 DEGREES C, QUANDO OS DELICADOS INSTRUMENTOS DO RELAY PUDERAM VOLTAR A FUNCIONAR, NORMALMENTE, DENTRO DO MAXIMO CONFORTO.

MULTIPLIQUE ESTE PEQUENO PROBLEMA PELOS 120 SATELITES QUE OS ESTADOS UNIDOS JA LANCARAM COM EXITO NOS ULTIMOS CINCO ANOS, E DEPOIS MULTIPLIQUE ESSE RESULTADO PELOS MILHARES DE DADOS QUE CADA UM DESSES SATELITES NOS TRANSMITE, E E FACIL AVALIAR A TRABALHEIRA QUE NOS, AQUI EM TERRA, TEMOS COM ESSA MARAVILHOSA ERA DO ESPACO, DIZ JACK FLAHERTY.

OS CIENTISTAS ESPACIAIS ESTADUNIDENSES FORAM AUTHORIZADOS A SOLICITAR ASSISTENCIA E COOPERACAO DE CERCA DE VINTE PAISES PARA A CONSTRUCCAO DE SUAS QUATRO REDES DE ESCUTA, QUE HOJE CONTAM COM 27 ESTACOES DOS ESTADOS UNIDOS, EM 19 PAISES DIFERENTES, SENDO SEIS NA AMERICA LATINA.

TELETYPE

Of the seven teletype demonstrations, COMAND participated in one, COMNUT in six, COMTEL in four and COMRIO in three. The only failure was during revolution 407 on 4 February 1963 when an equipment malfunction at COMNUT necessitated termination of transmission after one demonstration had been completed, but prior to the start of a second.

The material used was press copy and magazine article material as well as some interchange of greetings. A portion of the message transmitted during the first half of revolution 407 on 4 February 1963 is reproduced herein as received at COMRIO and retransmitted to Goddard Space Flight Center. The message is in Portuguese and is part of an article for "Visão" magazine, a Brazilian publication.

VOICE

Of the 35 voice transmissions, COMAND participated in 13, COMHIL in 14, COMTEL in 2, COMNUT in 19, COMRIO in 18, and COMGEB in 2. The thirteen failures were as follows.

1. through 7. were during revolutions 383, 391, 796, 797, 812, 813, and 827 when COMRIO was unable to support.

8. and 9. during revolution 1027 when the command encoder failed at COMCON.

10. during revolution 1044 when COMRIO was unable to support.

11. and 12. during revolution 1392 when there was an antenna steering failure at COMHIL.

13. during revolution 2248 when a telephone operator opened the circuit because no one was speaking.

The material comprising all these demonstrations was quite varied, ranging from telephone calls between engineers to evaluate the quality of transmission to greetings of address between heads of government agencies.

Because there is no way to present in print the results of voice transmission for subjective analysis, none of these demonstrations are herein discussed in detail. It must be said, however, that the great majority of participants, whose opinions have been made known to the writer, are in agreement that satellite voice communication is generally of excellent quality.

A special engineering test, not planned as a demonstration but of public interest, was

that on 13 September 1963 during RELAY revolution 2131/32, a telephone conversation was completed from Mr. Howard Miller, a NASA/GSFC representative on board the USNS "KINGSPORT" in the harbor at Lagos, Nigeria to João Carlos Fonseca, the station manager at COMRIO in Brazil. The routing of the conversation was from the "KINGSPORT" to Fort Dix, New Jersey via SYNCOM thence to COMNUT, in Nutley, New Jersey via normal telephone circuits and from COMNUT to COMRIO via Relay.

SPECIAL

Of the five special transmissions all were participated in by COMNUT, two by COMBOD and three by COMHIL. The two failures were during revolution 1291 when an operator somewhere between the Mayo Clinic and COMNUT attempted to clear the "noise on the line" which was an electroencephalogram calibration, and revolution 1392 when COMHIL was unsuccessful in transmitting automatic typesetting data to COMNUT.

The success consisted of transmission of an electroencephalogram from the Mayo Clinic to the Burden Neurological Center during revolution 1035 on 25 April 1963, a fetal electrocardiogram from the Mt. Sinai Hospital in Milwaukee, Wisconsin to the C.N.R.S. in Paris, during revolution 1291 on 28 May 1963, automatic typesetting from Chicago, Illinois to London and Rio de Janeiro and from Rio de Janeiro to Chicago during revolution 1392 on 10 June 1963, and automatic typesetting from London to Chicago during revolution 1423 on 14 June 1963.

AUTHOR. *This chapter was contributed by* G. BULLOCK, *NASA/Goddard Space Flight Center, Greenbelt, Maryland, U.S.A.*

APPENDIX A

Of the 80 television demonstrations, six have been selected for further elaboration. The selection of these six was based upon availability of photographs and/or video tapes as well as the desire to present an example of each normal operating combination, i.e., COMAND to COMBOD, COMHIL to COMAND, etc. The selected six are:

Rev. 207—COMAND to COMBOD
Rev. 910—COMAND to COMHIL
Rev. 1189—COMAND to COMTEL
Rev. 1508—COMBOD to COMAND
Rev. 1531—COMHIL to COMAND
Rev. 2677—COMMOJ to COMIBA

Revolution 207 on 9 January 1963 was the first demonstration of any type via the Relay I spacecraft. It consisted of the transmission from COMAND to COMBOD of the program associated with the opening to the public of the *Mona Lisa* display in Washington, D.C. (See Figure 1–3).

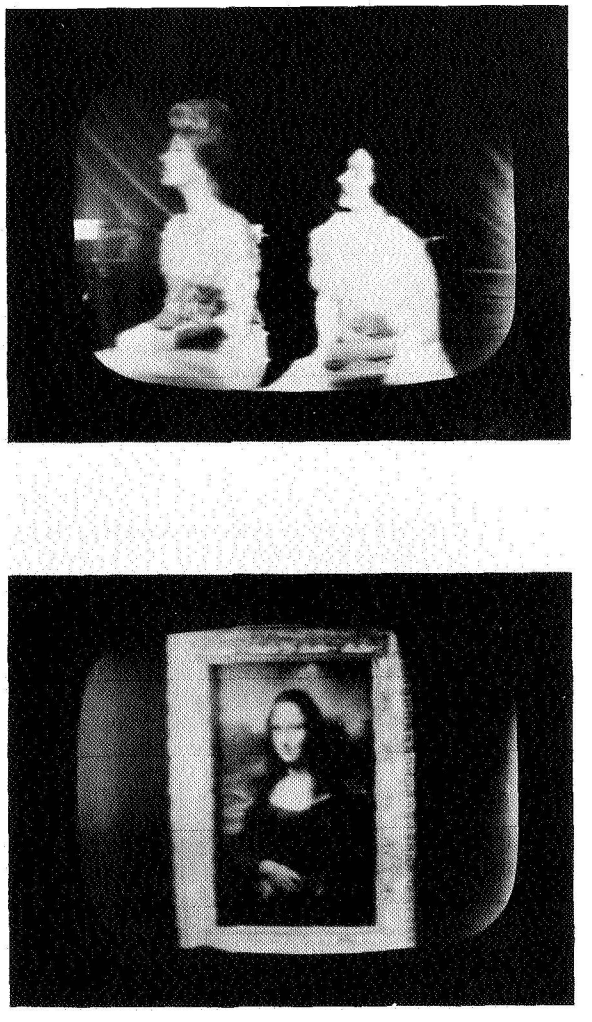


FIGURE 1–3.—First demonstration via Relay I spacecraft, COMAND to COMBOD, revolution 207, 9 Jan. 1963.

Revolution 910 on 9 April 1963 was a demonstration transmission involving Relay I and the English station. The transmission was from COMAND to COMHIL and consisted of the ceremonies during which President Kennedy bestowed honorary United States citizenship on Sir Winston Churchill. (See Figure 1–4.)





FIGURE 1–4.—COMAND to COMHIL, revolution 910 on 9 April 1963.

Revolution 1189 on 15 May 1963 was a COMAND to COMHIL program of miscellaneous studio pictures and material associated with the MA–9 launch. COMTEL monitored the transmission and sent pictures of their reception to Goddard Space Flight Center. (See Figure 1–5).

Revolution 1508 on 25 June 1963 was a COMBOD to COMAND transmission of events associated with President Kennedy's visit to Frankfurt, Germany. The material was recorded at COMAND. These photographs were made from the COMAND video tape recording. (See Figure 1–6.)





FIGURE 1–5.—COMAND to COMHIL, revolution 1189, 15 May 1963.



FIGURE 1–6.—COMBOD to COMAND, revolution 1508, 25 June 1963.





FIGURE 1–7.—COMHIL to COMAND, revolution 1531, 28 June 1963.



Revolution 1531 on 28 June 1963 was a COMHIL to COMAND transmission of President Kennedy's speech to the Irish Parliament. This program was used live on the National Broadcasting Company network. These photographs were made from the COMAND video tape recording. (See Figure 1–7).

Revolution 2677 on 22 November 1963 marked the first Japanese demonstration and consisted of a COMMOJ to COMIBA transmission of a program of welcoming messages to inaugurate operation at the Japanese terminal. These photographs are from the video tape recording made at COMIBA. (See Figure 1–8).

APPENDIX B

This appendix is a tabulation of all the demonstrations performed. Each revolution used and the date it occurred is listed. Tabulated versus the number listing is the type of demonstration performed. The attempt number (under A) success number (under S) and failure number (under F) is listed by type and total for each revolution.

TABLE 1–1.

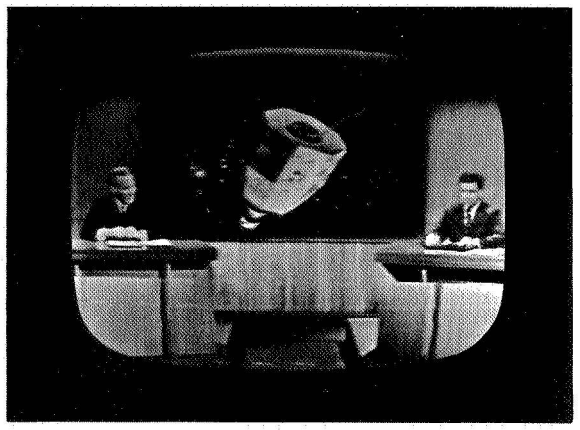
Rev.	Date	TV			Fax			TTY			Value			Special			Total		
		A	S	F	A	S	F	A	S	F	A	S	F	A	S	F	A	S	F
207	1- 9-63	1	1														1	1	
208	1- 9-63				1	1											2	2	
267	1-17-63							1	1		1	1					3	3	
275	1-18-63							2	2		2	2					4	4	
285	1-19-63	2	2														5	5	
363	1-29-63										3	3					6	6	
383	2- 1-63										4		1				7		1
391	2- 2-63										5		2				8		2
407	2- 4-63							3	3								9	7	
407	2- 4-63							4		1							10		3
440	2- 8-63										6	4					11	8	
440	2- 8-63										7	5					12	9	
440	2- 8-63										8	6					13	10	
657	3- 8-63				2	2											14	11	
663	3- 9-63										9	7					15	12	
664	3- 9-63				3		1										16		4
757	3-10-63				4	3											17	13	
789	3-25-63				5	4					10	8					18	14	
795	3-26-63	3	3														19	15	
796	3-26-63										11		3				20		5
797	3-26-63										12		4				21		6
812	3-28-63										13		5				22		7
813	3-28-63										14		6				23		8
827	3-30-63										15		7				24		9
828	3-30-63										16	9					25	16	
874	4- 5-63	4	4														26	17	
905	4- 9-73	5	5														27	18	
910	4- 9-63	6	6														28	19	
926	4-11-63	7	7														29	20	
927	4-12-63	8	8														30	21	
967	4-17-63										17	10					31	22	
967	4-17-63				6	5											32	23	
982	4-19-63				7	6		5	4		18	11					33	24	
983	4-19-63				8	7					19	12					34	25	
997	4-21-63				9	8		6	5								35	26	
1013	4-22-63										20	13					36	27	
1027	4-24-63										21		8				37		10
1027	4-24-63										22		9				38		11
1035	4-25-63				10	9											39	28	
1035	4-25-63				11	10											40	29	
1035	4-25-63													1	1		41	30	
1044	4-26-63				12		2										42		12
1044	4-26-53										23		10				43		13
1073	4-30-63										24	14					44	31	
1073	4-30-63				13	11											45	32	
1160	5-11-63										25	15					46	33	
1174	5-13-63	9	9														47	34	
1181	5-14-63	10	10														48	35	
1189	5-15-63	11	11														49	36	
1191	5-16-63	12	12														50	37	
1191	5-15-63	13	13														51	38	
1197	5-16-63	14	14														52	39	

TABLE 1–1.—*(Continued)*

Rev.	Date	TV			Fax			TTY			Value			Special			Total		
		A	S	F	A	S	F	A	F	S	A	S	F	A	F	F	A	S	F
1199	5–16–63	15	15														53	40	
1206	5–17–63	16	16														54	41	
1253	5–23–63	17	17														55	42	
1260	5–24–63	18	18														56	43	
1291	5–28–63										26	16		2	2		57	44	
1291	5–28–63													3		1	58		14
1307	5–30–63	19	19														59	45	
1315	5–31–63	20	20														60	46	
1329	6– 2–63	21	21														61	47	
1345	6– 4–63	22	22														62	48	
1345	6– 4–63	23	23														63	49	
1353	6– 5–63	24		1													64		15
1392	6–10–63													4		2	65		16
1392	6–10–63										27		11				66		17
1392	6–10–63										28		12				67		18
1415	6–13–63										29	17					68	50	
1415	6–13–63							7	6								69	51	
1423	6–14–63													5	3		70	52	
1423	6–14–63										30	18					71	53	
1462	6–19–63	25	24														72	54	
1469	6–20–63	26	25														73	55	
1477	6–21–63	27	26														74	56	
1485	6–22–63	28	27														75	57	
1492	6–23–63	29	28														76	58	
1500	6–24–63	30		2													77		19
1508	6–25–63	31	29														78	59	
1516	6–26–63	32		3													79		20
1523	6–27–63	33		4													80		21
1531	6–28–63	34	30														81	60	
1539	6–29–63	35	31														82	61	
1547	6–30–63	36	32														83	62	
1554	7– 1–63	37	33														84	63	
1562	7– 2–63	38	34														85	64	
2100	9– 9–63	39	35														86	65	
2162/63	9–17–63	40	37														87	66	
2248	9–28–63										31		13				88		22
2342	10–10–63	41	38														89	67	
2403	10–18–63				14	12											90	68	
2404	10–18–63	42	38														91	69	
2436	10–22–63	43	39														92	70	
2442	10–23–63	44	40														93	71	
2449	10–24–63										32	19					94	72	
2459	10–25–63	45	41														95	73	
2513	11– 1–63	46	42														96	74	
2551	11– 6–63	47	43														97	75	
2560	11– 7–63	48	44														98	76	
2566	11– 8–63										33	20					99	77	
2589	11–11–63										34	21					100	78	
2637	11–17–63	49	45														101	79	
2667	11–21–63	50	46														102	80	
2677	11–22–63	51	47														103	81	
2678	11–77–63	52	48														104	82	

TABLE 1–1.—*(Continued)*

Rev.	Date	TV			Fax			TTY			Value			Special			Total		
		A	S	F	A	S	F	A	S	F	A	S	F	A	S	F	A	S	F
2681	11–23–63	53	49														105	83	
2681	11–23–63	54	50														106	84	
2682	11–23–63	55	51														107	85	
2682	11–23–63	56	52														108	86	
2683	11–23–63	57	53														109	87	
2683	11–23–63	58	54														110	88	
2684	11–23–63	59	55														111	89	
2684	11–23–63	60	56														112	90	
2689	11–24–63	61	57														113	91	
2690	11–24–63	62	58														114	92	
2691	11–24–63	63	59														115	93	
2691	11–24–63	64	60														116	94	
2699	11–25–63	65	61														117	95	
2700	11–25–63	66	62														118	96	
2701	11–25–63	67	63														119	97	
2715	11–27–63	68	64														120	98	
2721	11–28–63	69	65														121	99	
2722	11–28–63	70	66														122	100	
2724	11–28–63	71	67								35	22					123	101	
2808	12– 9–63																124	102	
2893	12–20–63	72	68														125	103	
3017	1– 5–64	73	69														126	104	
3086	1–14–64	74	70														127	105	
3094	1–15–64	75	71														128	106	
3102	1–16–64	76	72														129	106	
3109	1–17–64	77	73														130	107	
3293	2– 9–64	78	74														131	108	
3689	3–31–64	79	75														132	109	
3712	4– 3–64	80	76														133	110	



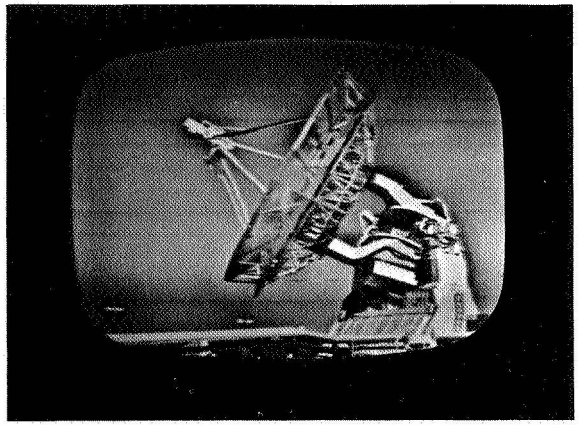


FIGURE 1–8.—COMMOJ to COMIBA, revolution 2677, 22 Nov. 1963.

APPENDIX C

COMAND—Ground Station of the American Telephone and Telegraph Company in East Andover, Maine.

COMBOD—Ground Station of the French Ministry of Posts and Telecommunications in Pleumeur-Bodou, France.

COMGEB—Ground Station of the Deutsche Bundespost in Raisting, Germany.

COMHIL—Ground Station of the British General Post Office in Goonhilly Downs, England.

COMIBA—Ground Station of the Kokusai Denshin Denwa Company in Juo-Machi near Tokyo, Japan.

COMMOJ—NASA test and operations station at Goldstone, near Barstow, California.

COMNUT—Ground Station of the International Telephone and Telegraph Company in Nutley, New Jersey.

COMRIO—Ground Station of the Companhia Rádio Internacional do Brasil in Jacarepagua, near Rio de Janeiro, Brazil.

COMTEL—Ground Station of the Telespazio organization in Fucino, Italy.

N66-10252

Chapter 2

Rio de Janeiro Space Communications Station

10252

The Rio de Janeiro Space Communication Station is being used to conduct two-way telephone, teletype and data transoceanic experimental communications by satellite, between North America, Europe and South America.

Designed and engineered by the Space Communications Laboratory of ITT Federal Laboratories, Rio de Janeiro Ground Station is operated by Companhia Rádio Internacional do Brasil by authority of the Brazilian Administration, which is cooperating with the U. S. National Aeronautics and Space Administration (NASA) on the Project Relay Experiments.

The Station can handle two-way, 12 simultaneous telephone conversations or 12 teleprinter of high speed data per voice channel or 144 total circuits whenever speech is not being transmitted.

This chapter describes the general station setup, the general design of the equipment, and operational procedures.

GENERAL STATION DESCRIPTION

COMRIO Station, standing for COMMUNICATIONS RIO DE JANEIRO, is located on the southern part of the city in a non-industrial zone shielded by mountains. It covers 108,000 square feet of flat, dry, sandy soil. The layout of the Station is shown in Figure 2–1.

The following factors were considered in the selection of a site: horizon profile, accessibility, microwave and TV interference and proximity of Brazil's international Traffic center (see Figure 2–2).

The choice of horizon profile was made considering maximum operational time utilization during a pass as well as shielding from nearby ground microwave and TV stations.

Microwave links and TV stations are listed in Table 2–1. No interference has been noticed to date from these sources.

A polar plot of the horizon profile is shown in Figure 2–3 as well as the percentage of of utilization of the azimuths during satellite communications. It can be seen that the azimuths utilized during 70% of time occur between 330° and 30°, with a maximum elevation obstacle in the range of 4.6°. The highest obstacle, however, is at 7° 42″ elevation, occurring in a 10° utilization sector.

Coordinates of the reference mark are Latitude South 22°57′ 06.5″ ± 1.2″; Longitude 43°22′20.7″ ± 1.3″; Altitude 4.478 m above mean sea level, as determined by geodetic survey. Distance of station site to downtown Rio de Janeiro is approximately 20 miles served by paved road.

A record of 1962 station weather is listed on Table 2–2. Annual averages are 27.4 to 17.6° C temperature variation, 80.3% relative humidity, 112.0 mm³ precipitation and 1.3 m/s wind velocity.

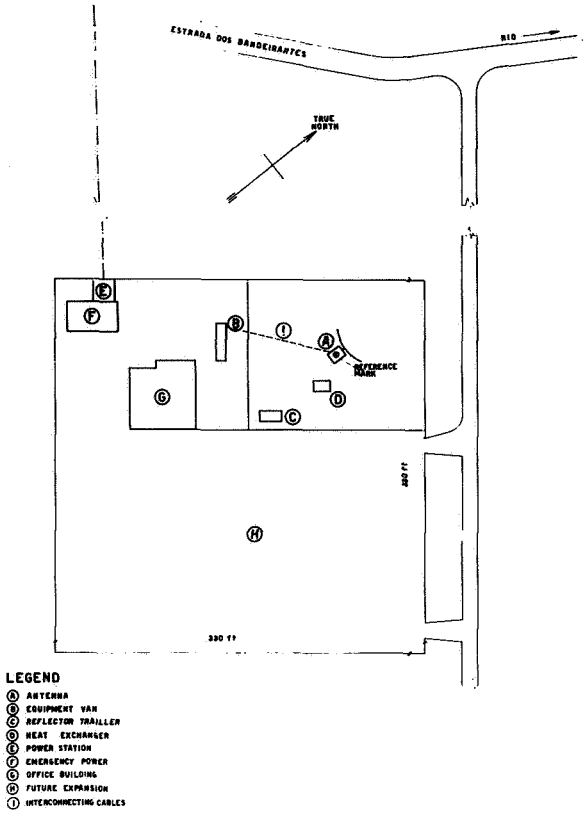


FIGURE 2–1.—Station layout.

The whole communications terminal consists of a 31′ × 8′ × 11′8″ equipment van weighing 20,000 lbs., 11′6″ × 8′ × 9′9″ antenna trailer weighing 26,000 lbs., 114″ × 100″ × 48″ heat exchanger trailer weighing 3,000 lbs., and 11′6″ × 8′ × 17′ antenna panel trailer weighing 4,500 lbs.

The equipment arrived in Rio de Janeiro December 8, 1962 by aircraft. It was erected and system checked so that by December 13, Satellite Relay I, orbit 1, was manually tracked by its 136 Mc VHF beason. On January 12, first voice and TTY message was relayed through Satellite Relay, orbit 229, to a similar ground station located at Nutley, New Jersey, U.S.A.

Primary power comes through a 25 KV aerial feeder, 50 cps, stepped down to 208V, 4 wires with 300 KVA capacity each. They are protected by 30 KV 1,000 MVA circuit breaker. Four 208V feeders are distributed with the following installed capacity: VAN

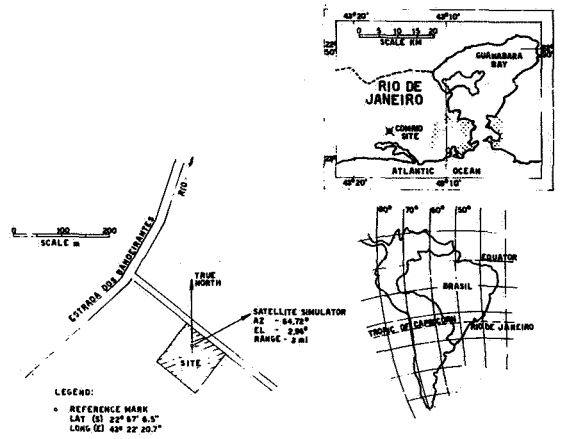


FIGURE 2–2.—Station site location.

140 KVA, Antenna 70 KVA, Heat-Exchanger 40 KVA and Supporting House 550 KVA. Emergency power is provided by one 125 KVA and one 50 KVA Diesel engines. Supporting facilities consist of a main building covering 3470 ft² with office warehouse, bedroom, kitchen, power substation and an emergency power building as shown in Figure 2–1. The Administration Building is shown in Figure 2–4.

A satellite simulator, that is, a transponder corresponding electrically to the satellite, is located 3 miles away on a hill with available access road and primary power. It is viewed from the station reference mark at azimuth 64.72° and elevation 2.96°.

Support communications facilities include one 50 Bauds, double current operation teletype connected by land-line to a TELEX international network; one standard 4 wire telephone channel for demonstration and service purposes connected to downtown in-

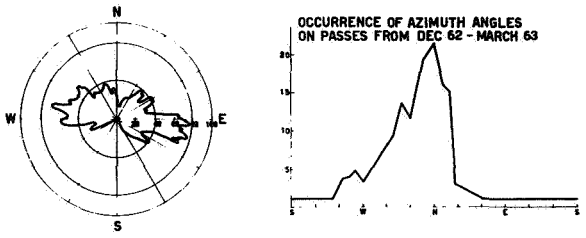


FIGURE 2–3.—Horizon profile.

TABLE 2-1.—*Microwave and TV Links*

Type of station	Location	Distance of COMRIO (Km)	Frequencies (Mc)	Power output (W)
Microwave link	Mendes	81	3,928.75 3,971.25	1 1
Microwave link	Caxias	21	3,891.25 4,008.75	1 1
Microwave link	Petropolis	60	3,810 3,920	5 5
TV station	Sumaré	12	82–88 7,036 7,250 10,900	30,000 1 1 1
TV station	Sumaré	12	186–192 7,030 6,897.5 6,950	20,000 1 1 1
TV station	Sumaré	12	210–216 6,170 6,330 6,845 6,795 6,895	30,000 1 1 1 1 1

TABLE 2-2.—*Weather Data—1962*

Month	Monthly average temperatures (°C)		Relative humidity (%)	Precipitation (mm^3)	Wind	
	Max.	Min.			Velocity ($m/^3$)	Direction
Jan	29.5	21.1	83	412.6	1.3	SE
Feb	29.9	21.7	82	249.6	1.2	SE
Mar	32.4	22.4	73	40.0	1.1	SE
Apr	28.5	19.3	75	29.0	1.4	SE
May	23.5	17.1	76	69.7	1.3	SE
Jun	23.1	12.9	77	21.1	1.4	NE
Jul	25.9	13.9	78	49.7	1.3	SE
Aug	26.7	9.7	83	44.8	1.6	SE
Sep	26.6	17.8	78	69.1	1.1	NE
Oct	26.6	15.2	91	77.5	1.4	SE
Nov	28.0	19.7	87	95.1	1.5	SE
Dec	28.7	20.9	79	183.3	1.4	SE
Annual average	27°.4	17°.6	80.3	112.0	1.3	--------

ternational telephone exchange through amplified land-lines; one two-wire crank-up telephone connected to local suburban network, operated via manual switchboard; and one simplex voice channel 136 Mc VHF connection between equipment van and satellite simulator location.

GENERAL DESIGN OF STATION

Rio de Janeiro Space Communication Terminal is characterized by a 10 Kw transmitter, a 30 ft. antenna reflector, and a system noise temperature of 420° K.

The receiving front-end, transmitter frequency generating stages, and power amplifier are housed in an antenna-mounted electronic package which is mechanically interchangeable so as to match the operating frequencies of the respective satellite for which the terminal is to be used.

COMRIO Station is presently equipped to participate primarily in Project Relay, but also suitable for modification and extension as required for later experiments.

The receiving IF and final stages, the transmitter power supply, the modulator, the terminal equipment, as well as control and testing facilities, are van mounted. The equipment van is shown in Figure 2–5. This arrangement eliminates the need for rotary joints. Suitable cabling interconnects van and antenna mounted components. Solid state components are used extensively throughout the equipment with corresponding reduction of size and total heat to be dissipated.

The communication terminal includes an antenna system, a tracking system, an antenna servo system, a communication receiver, a transmitter, a terminal equipment system and instrumentation.



FIGURE 2–4.—Administration building.

The Antenna System

The main reflector is a 30-foot parabolic dish of solid panel construction supported and oriented by an elevation over azimuth tracking mount. Azimuth coverage is restricted mechanically from +300° to −300° and elevation from −2° to +92°. A photograph of the antenna is shown in Figure 2–6.

The 30 foot aperture is illuminated by the microwave feeds employing a 6 ft. hyperboloid sub-reflector in a cassegrain arrangement which places the apparent focus of the antenna system at the vertex of the parabolic reflector.

The feed horn cluster includes 1700 Mc dual teflon polyrod transmitting horns and 4000 Mc four-horn simultaneous lobe comparison tracking feed. The four horns are also used for satellite signal reception. Circular polarization is obtained from screws positioned at 45° with respect to the plane surface of the wave guide. A pair of crossed dipoles mounted behind the sub-reflector is used for receiving 136 Mc VHF beacon from the satellite.

The antenna system is designed to be transported and operated in a flat bed trailer. The tracking mount is secured to a retractable tower which collapses on the trailer bed. The main reflector is assembled from 24 individual solid aluminum panels and major truss sections which are carried for transportation in a second flat-bed trailer. Sur-

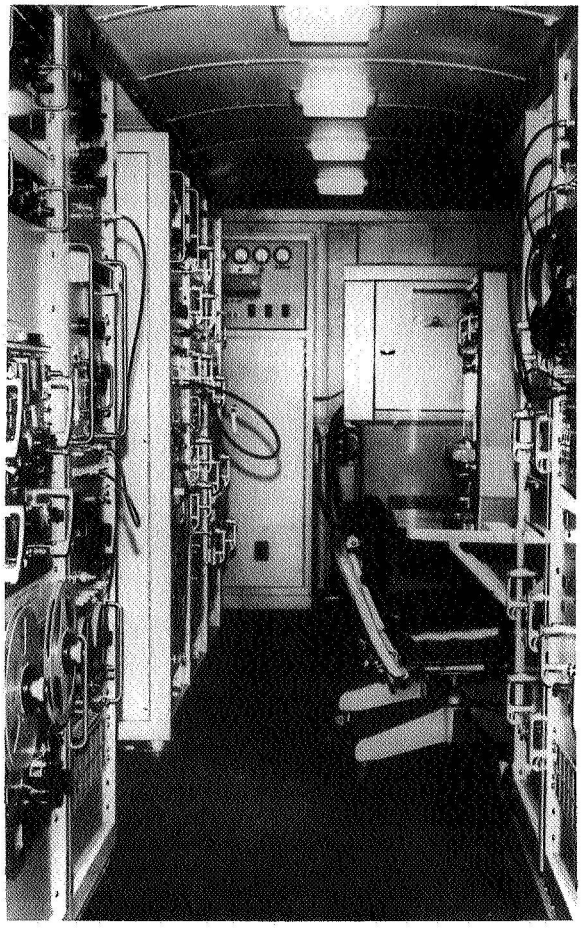


FIGURE 2–5.—Equipment van.

vival is designed for a maximum wind up to 35 mph with a gust factor of 1.5. The focal length over diameter ratio is 0.417 giving a focal length of 12.5 feet. The main reflector is manufactured to an accuracy of +0.080″ peak from true parabolic contour and will permit operation between 100 and 8500 Mc. The dish is attached to a cylindrical hub, which in turn is bolted to a trunnion box providing internal clearance for a 60″ × 40″ × 51″ electronic package which slides out on telescoping tracks whenever servicing is required.

The tracking mount incorporates the trunnion box and is supported by a four-foot diameter tubular tower the inside of which is used for wrapping all power signal, coaxial, and high-voltage cables. Water coolant

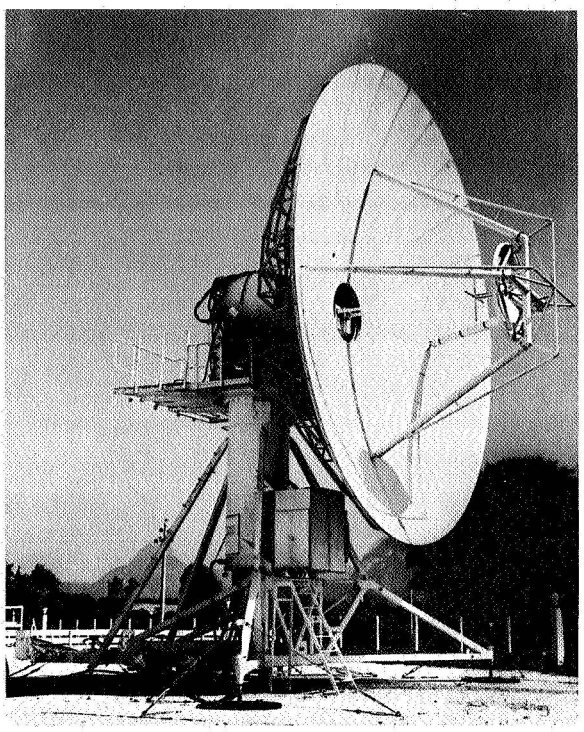


FIGURE 2–6.—Antenna.

lines for the transmitter and hydraulic lines to the servo drive are also located inside of the tower.

The Tracking System

Tracking is performed by a monopulse of split-beam amplitude sensing system, which senses instantaneous azimuth and elevation position of the satellite with respect to the antenna boresight axis. A 4079.73 Mc beacon signal is received by the four-horn arrangement. Signals between left and right or up and down horns are compared in phase through several magic tees producing elevation, azimuth and sum channels. The sum channel receives the added signal coming from the four horns and is, within limits, independent of the relative angular position of the satellite with respect to the boresight axis. This channel also provides range and Doppler shift correction signals, which are fed to the difference channels so as to keep them sensitive to angular tracking errors only.

A diplexer consisting of two preselectors is used in the sum channel output to separate the 4079.73 Mc tracking signal from the 4170 Mc communication signal. After filtering, the difference and sum signals go to ortho-mode type mixers which send, via pre-amplifiers, an IF of 70 Mc to the equipment van. The noise figure of the front end of the tracking receiver is in the order of 8 db. Tracking receiver IF is designated to accommodate from —87 to —57 dbm variations maintaining an effective AGC correction of 1 db for the difference channels output.

The tracking receiver rack, van mounted, obtains the 70 Mc signal from the front end and processes it to give 0.1 vdc correction per 0.1 degree angular error to be applied on the corresponding servo channel.

Frequency variations caused by Doppler effect and mixer oscillator instability are overcome by changing the local oscillator mixer frequency according to the frequency error. This is accomplished by using a phase-lock loop. A phase detector gives a dc error proportional to signal frequency variations which is applied, through a dc amplifier, to a local variable controlled oscillator on the mixer stage. Mixer steps down 70 Mc to 9.8 Mc signal which closes the loop through an 80 db gain IF strip, with the Phase Detector.

A similar arrangement exists to provide AGC correction. The output of the 9.8 Mc IF amplifier is applied to AGC Phase Detector, giving a dc error proportional to signal amplitude variation, which modifies, through a dc amplifier, the IF strip amplifier gain.

Azimuth and elevation output errors are obtained from phase detectors on the difference channels. A common 9.8 Mc crystal controlled oscillator is used as reference for all phase detectors.

A frequency search and acquistion circuit allows ± 120 kc Doppler shift during acquisition time. A saw-tooth signal fed to the local variable controlled oscillator will be interrupted by a trigger coming from the AGC phase detector as soon as its output is greater than a pre-set value. At the same time, the output of the difference channels is connected to the antenna servo system, starting the automatic tracking mode.

Antenna Servo and Control System

The two basic configurations of Antenna Servo and Control System are the automatic tracking mode and manual positioning mode as shown in Figure 2–7. Azimuth and elevation servos are similar in design.

Power to steer the antenna is provided by a 40 HP, 1750 RPM, 3 phase, 208v, 50/60 cycles, induction motor directly driving a 3000 psi pressure compensated, variable flow pump with a maximum displacement of 4.5 in.^{3} per revolution.

The elevation drive employs a 10 HP fixed stroke, axial piston, hydraulic motor, through a 3600:1 gear box; the azimuth drive utilizes a similar 20 HP hydraulic motor associated

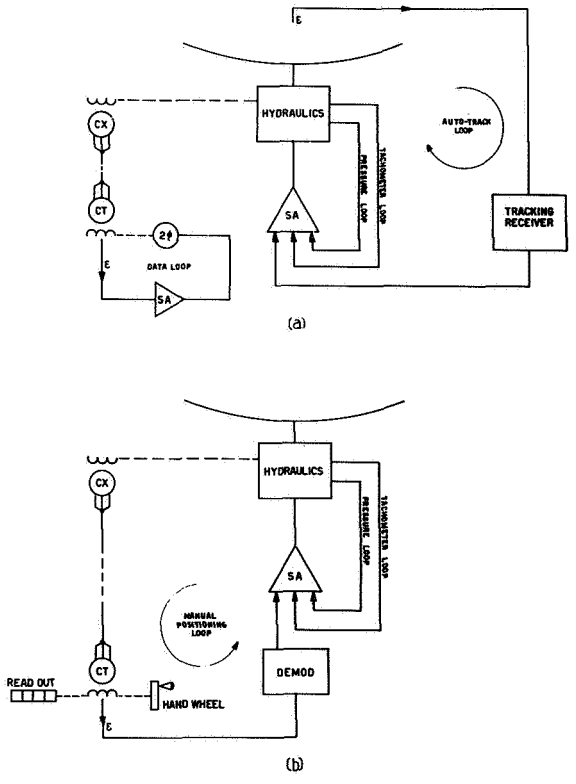


FIGURE 2–7.—Antenna basic configuration.

with a 1800:1 gearbox; both with flow independently controlled by electrohydraulic transducers or servo valves.

Hydraulic pump and drive motor, as well as the jog control, hydraulic antenna erection control, and protective and metering components are in a steel enclosure fastened to the antenna tower base. These constitute the antenna local control.

On automatic tracking mode, signal error, from the tracking receiver is fed to a servo-amplifier tray, van mounted, which controls the output of the hydraulic motors through the servo valve.

Associated with the antenna movements, a data gear box drives the rotors of a two-speed synchro transmitter system which are connected to corresponding synchro transformers on the equipment van. An error corresponding to the antenna position is fed out of the synchro transformer rotor to a servo amplifier associated with a two-phase motor which in turn positions the synchro transformer rotor, therefore closing the data servo loop. A mechanical counter connected to the synchro transformer shaft provides read-out indication.

In the manual positioning mode, which employs the same basic components as the auto-track mode, error is originated from the rotor of the synchro control transformer by rotating its shaft with a hand-wheel. Antenna position read out is directly obtained from the mechanical counter connected to the transformer rotor. The ac error is demodulated by a vibrating type device and fed to the servo amplifier. The loop then closes as in the automatic tracking mode.

The system is a type two, zero error, constant velocity servo, with a velocity and an acceleration loop, fed back into the servo amplifier. The signal for the velocity loop originates in a dc tachometer geared to the antenna. It increases the damping of the main servo loop and is also used for remote rate indication in the van. Acceleration loop signal is obtained from two pressure transducers on the hydraulic motor feed lines, and is used to increase the damping ratio of the motor-valve combination.

All antenna functions are monitored and controlled from the radio equipment van. Additional features include azimuth scan and rate memory facilities, provision for remote and programmed track modes, joysticks slew control, electrical limit stops, azimuth van controlled stow lock mechanism, error and rate meters, as well as warning indicators of malfunctions on the hydraulic system. The control console is shown in Figure 2–8.

Typical servo operating limits and performances are included in Table 2–3.

Transmitting System

Transmitting System consists of van mounted 71.5 Mc FM Modulator, a 17 KV beam power supply, control and protective circuitry, and antenna mounted 1726.67 Mc exciter unit driving a 10 KW, klystron power amplifier, water cooled by a separate, trailer mounted heat exchanger.

Baseband signals out of the multiplex terminals are first applied to a 70 cps to 10 Mc bandwidth, 3 stage video amplifier, with an adjustable gain from 16 to 32 db, followed by an optional pre-emphasis network which gives, for 12 channels, −3 db at 10 kc and +3 db at 60 kc tending to flatten the radio noise level over the frequency band of the FM transmitted signal.

Sensitivity of the modulator is 0.266 VRMS per Mc with an input impedance of 230 ohms and a minimum output level of +10 dbm. Modulation is obtained by applying the signal to a diode on the oscillator tank circuit. Different signal levels will change the oscillator frequency accordingly. The 71.5 Mc modulated signal, amplified and limited to minimize amplitude modulation, is fed to the exciter unit. A stable output is ensured by comparing the signal with a crystal controlled oscillator feeding back a reference potential to the modulator.

The exciter comprises an oven mounted crystal oscillator unit, a varactor multiplier chain and a strip-line type mixer. Frequency is generated at 49.949074 Mc and is multi-

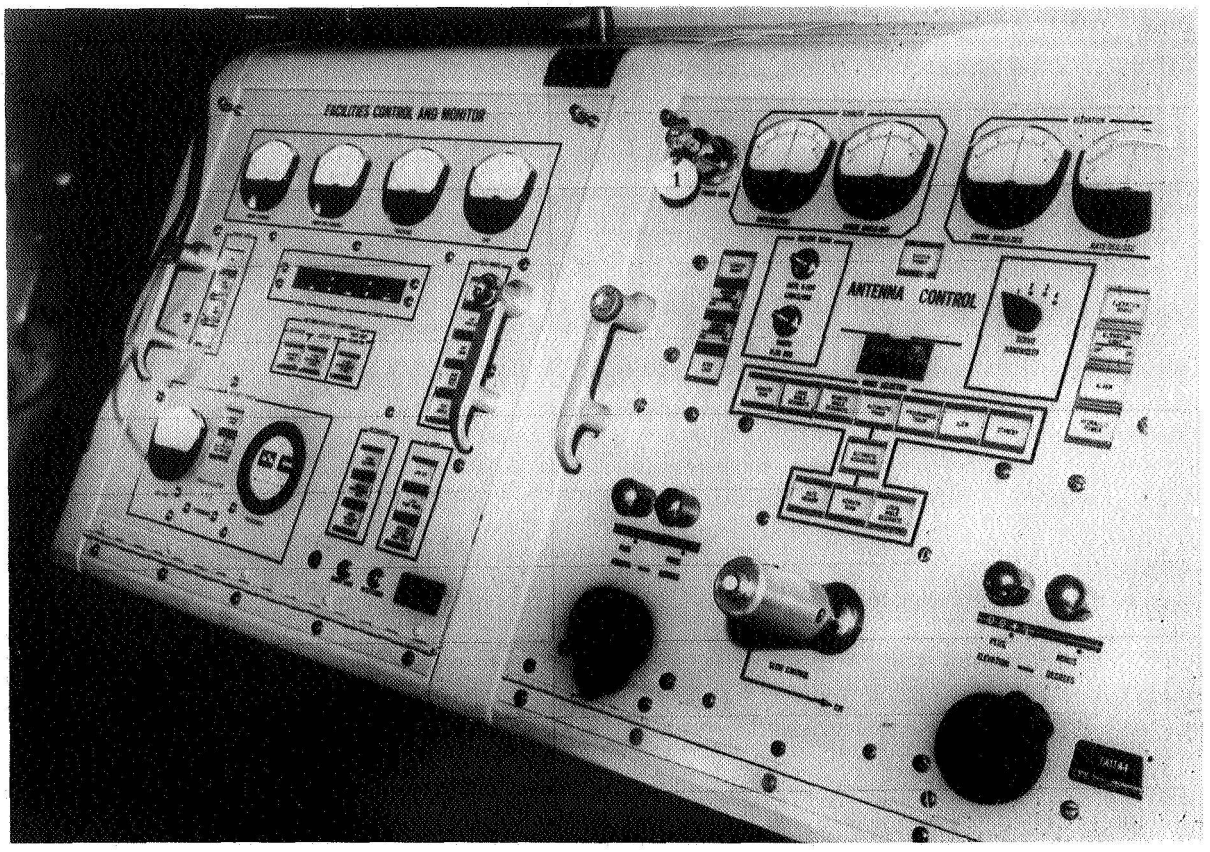


FIGURE 2–8.—Control console.

TABLE 2–3.—*System Performance*

Transmission system		
Modulator	Output frequency (Mc)	71.5
	Sensitivity (volts RMS per Mc)	0.266
	Output level (minimum dbm)	+10
	Impedance input (ohms)	230
	Impedance output (ohms)	75
	Max deviation (Mc)	± 8
Exciter	Exciter frequency (Mc)	1726.67
	Local oscillator (Mc)	1798.1667
	Crystal frequency (Mc)	49.949074
	Multiplying factors	2×6×3
	Local oscillator output (dbm)	+25
	Exciter output (dbm)	+20
Power amplifier	Frequency (Mc)	1726.67
	Frequency range (kmc)	1.7 to 2.4
	Tuning range (Mc)	700
	Power output (kw)	10
	Beam voltage (kv)	16
	Beam current (amp dc)	2.5
	Body current (with drive ma dc)	60
	Heater voltage (v)	3.5
	Heater current (amp)	16.5
	Number of cavities	4
	Tuning	Synchronous

Transmission system (*Continued*)		
Heat exchanger	Capability (kw)	38
	Coolant flow (gpm)	9–10
	Discharge pressure (psi)	135

Receiving system		
Tracking	Beacon frequency (Mc)	4079.73
	Lock-in threshold signal level (dbm)	−125
	Front end gain (db)	40
	Front end noise figure (db)	8.5
	Local oscillator frequency (Mc)	4009.73
	Mixer Type	Orthomode
	First IF frequency (Mc)	70.0
	Second IF frequency (Mc)	9.8
	Voltage controlled oscillator frequency (Mc)	60.2 ± 0.12
	Reference oscillator frequency (Mc)	9.8
	Output error slope (v per deg)	0.1 per 0.1
Communications	Modulation type	FM
	Com channel frequency (Mc)	4064.72
	Mon channel frequency (Mc)	4074.72

TABLE 2–3.—*System Performance (continued)*

Receiving Station (*Continued*)		
Communications (*Continued*)	Threshold carrier signal level (dbm)	−104
	Lock-in threshold signal level (dbm)	−113
	Front end gain (db)	45
	System noise temperature (°Kelvin)	420
	Local oscillator frequency (Mc)	4014.72
	IF frequency (Mc)	70
	Bandwidth (Mc)	1.3
	Voltage controlled oscillator (Mc)	70
	Demodulator sensitivity (VRMS per Mc)	0.055
	Baseband bandwidth (kc)	60
VHF	Beacon frequencies (Mc)	136.14 or 136.62
	Threshold signal level (dbm)	−140
	First local oscillator frequencies (Mc)	157.64 or 158.12
	First IF frequency (Mc)	21.5
	Second IF frequency (Mc)	4.5
	Reference oscillator (Mc)	4.5
	Voltage controlled oscillator sensitivity (kc per V)	12
	Doppler shift correction (kc)	±30
HF	Modulation type	AM, CW
	Operating ranges (Mc)	0.5 to 30.5
Terminal equipment		
Multiplex	Multiplexing type	Frequency division single-sideband
	Modulation type	Suppressed carrier
	Number of channels	12
	Output frequency (kc)	12 to 60
	Frequency response flat within 1 db (cps)	300 to 3400
	Signaling pilot frequency (cps)	3.825
	Send level, 4-wire, 600 ohms balanced (dbm)	−16 (minimum)
	Receive level, 4-wire, 600 ohms balanced (dbm)	+7 (maximum)
Teletype	Signaling frequency (words per minute)	66
	Selector magnets (ma)	20 to 60
Tone keyer	Center output frequency (cps)	1105
	Frequency shift (cps)	±50
	Input current (ma)	60
Demodulator	Center input frequency (cps)	1105
	Output current (ma)	30 to 100
Antenna system		
Electrical	Type	Parabolic with Cassegrain
	Frequency range (Mc)	100 to 8500
	Minimum gain at 4100 Mc (db)	+48.3
	Minimum gain at 1725 Mc (db)	+40.3
	Beamwidth, 3 db, at 4100 Mc (deg)	0.6

Antenna system (*Continued*)		
Electrical (*Continued*)	Beamwidth, 3 db, at 1725 Mc (deg)	1.4
	First side lobe maximum (db)	−15
	Collimation accuracy (deg)	±0.1
Mechanical	Paraboloid diameter (ft)	30
	Hyperboloid diameter (ft)	6
	Focal length per diameter	0.42
	Parabolic surface tolerance (m)	±0.08
	Hyperbolic surface tolerance (in)	±0.03
	Height of center of radiation (ft)	23
	Max wind survival (MPH)	35
	Wind gust factor	1.5
	Elevation travel (deg)	−2 to +92
	Azimuth travel (deg)	−300 to +300
Servo	Static pointing accuracy (deg)	±.04
	Azimuth:	
	Max tracking velocity (deg/sec)	10
	Max angular acceleration (deg/sec²)	6
	Elevation:	
	Max tracking velocity (deg/sec)	5
	Max Angular acceleration (deg/sec²)	3
	Dynamic pointing accuracy (deg)	±.1

plied successively by 2, 6, and 3 times, maintaining one part in 10^6 stability. A quarter wavelength coaxial line input in the final multiplier is coupled through a varactor to an open tuned coaxial cavity peaked to the third harmonic of the input frequency. Inputs to the mixer are 1798.16667 Mc, 300 mw, CW signal from the final multiplier and a 71.5 Mc signal from the modulator. Output is a 100 mw 1726.67 Mc FM signal applied to the klystron power amplifier. The mixer interrupts the carrier at the same rate as the modulating signal, causing a double sideband, −20 db suppressed carrier output.

The mixing element is a varactor diode which goes from near open to near closed as the 71.5 Mc signal is applied to it, meanwhile a 1798 Mc signal fed through a double-stub, micro-strip coaxial line tuner changes the effective impedance of the diode. Mixing occurs after suppressing the higher sideband. The 1726.67 Mc signal is applied to a four

cavity synchronous tuned klystron which delivers a rated 10 kw output power.

The unregulated beam power supply comprises a 3-phase 17 kc, Δ–Y power transformer, a conventional diode vacuum tube full wave rectifier, delivering 2.0 amp, followed by a choke input filter. The high tension negative side is applied to the klystron cathode, via an x-ray cable running from van to the antenna. The positive side of supply is lifted from ground by thyrite as a safety measure in case of an eventual ground.

Sequential application of power, protection of components and monitoring of the high voltage are controlled by solid state logic, actuating through an AND beam gate card on the high voltage circuit breaker. Logic functions are: beam application time delay, blower off delay, ac interlock for personnel protection, wave guide arc detector, low RF and mismatch, beam and body overloads, coolant flow, coolant temperature and air flow.

Regulated filament and 28v focusing magnet power supplies are also van mounted. Beam voltage and current, body current, magnet current, filament voltages and current, RF forward and reflected output and exciter output indications are provided. Beam voltage, klystron cavity tuning, RF input can be remotely performed from the equipment van. The waveguide between power amplifier and antenna is pressurized and dehumidified.

A 135 psi, 10 gpm, water to air heat exchanger, connected by flexible hoses to the klystron, remotely controlled from the van, affords up to 38 kw heat dissipation.

Terminal and Testing Equipment

A 12 voice channel multiplex equipment, teletype facilities, order-wire unit, recording unit and patch panels, provide the ultimate input and output of the communication terminal.

The 0 to 60 kc audio baseband is divided in a zero to 4 kc order-wire channel, an 8 kc guard band and 12 four kc voice channels. Twelve external land lines can be connected to the van.

An all transistor multiplex system comprising two redundant power supplies, twelve normal and twelve standby receiver-amplifiers, normal and standby 128 kc master oscillator with switching unit, filters, twelve channel modulator and alarm circuits affords two-way communications.

A −16 dbm minimum, 4 wire, 600 ohm, balanced transmit level and +7 dbm maximum, 4 wire, 600 ohm balanced receive voice frequency level are specified.

Teletype facilities include a teletypewriter unit, page printer, typing perforator and typing reperforator unit providing signaling frequency of 66 words per minute or 50 bauds.

A tone keyer and demodulator translates 5 unit code, 60 milliamp neutral signals to 1105 ± 50 cps frequency shifted tones, providing the connection between teletype and multiplex facilities.

Two telephone handsets, panel mounted, provide a 0 to 4 kc order wire and any 12 to 60 kc baseband channel voice communication.

A 3 speed, .3 to 3 kc, dual mixed inputs, magnetic tape recorder affords recording or pre-recording of voice, teletype, facsimile or data information. An audio amplifier and loud speaker can be used for demonstration purposes.

A patch panel permits the interconnection of modulation, receivers, land-lines, voice and teletype terminal equipment, audio amplifier and recording equipment. A back-to-back configuration, that is sending the received baseband back to the distant station can be performed with this arrangement.

Tests and recording equipment are rack mounted for maintenance, adjustment and station operating parameter determination. Coaxial fittings at each rack and antenna package provide connection of test equipment to the major units of the system.

A local time standard is included, consisting of a counter with logic designed to recycle as a clock drives a time digital dis-

play on the control console with 1 part in 10^7 stability. Synchronization is obtained by received local radio signals, checked against the Astronomical Observatory cesium atomic clock.

A noise tube, permanently installed in the waveguide front end, is used in conjunction with a measuring test set in the van, giving the noise figure of the receivers directly.

A multi-channel paper recorder gives a permanent record of AGC voltages, antenna position and servo error voltages. Event markers give one second and one minute pulses, transmitter ON, VHF receiver locked, and antenna acquisition indications. Recording is made by a hot type stylus on plastic coated paper in rectangular coordinates, driven at selected speed, ranging from .25 mm/s to 100 mm/s.

General purpose measuring and maintenance equipment includes a 0 to 510 Mc frequency counter with plug-in units, and three separate signal generators with, respectively, 10 to 420 Mc, 3.8 to 7.6 Mc, and 10 cps to 10 Mc coverage. A sweep generator and an oscilloscope are included for general testing purposes. The oscilloscope has a sweep range of 0.2 msec/cm to 12.5 sec/cm, a bandwidth of 2 cps to 300 kc.

Receiving System

The receiving system comprises two microwave fixed frequency receivers, a fixed frequency VHF receiver, and a general purpose HF receiver. One microwave receiver monitors the local transmission via the satellite, the other processes the transmission from a distant communication terminal.

The 4164.72 Mc monitor and the 4174.72 Mc communication frequencies signals are separated from 4080 Mc tracking sum channel, using a 20 Mc band pass diplexer, centered at 4,120 Mc. The receiver's 4,170 Mc signal goes to a non-degenerated parametric amplifier, maintained at package temperature of 20°C by an antenna mounted 6,000 Btu per hour air conditioner. The parametric amplifier uses a varactor as reactive element, a 16,256 Mc klystron reflex as a pump source, and a ferrite circulator. Maximum noise figure of 2.7 and minimum gain of 15 db over 15 Mc bandwidth referred to the 1 db points are achieved. Pump power varactor bias can be remotely controlled from van for noise figure improvement.

The 4170 Mc signal is further mixed-down in a mixer-preamplifier unit with a local carrier of 4104.72 Mc producing a 65 Mc IF signal sent to equipment can. The 4104 Mc local oscillator is similar in design to the transmitter exciter unit except for the final multiplier, which is a septupler rather than a quadrupler. The mixer is of varactor diode type which also incorporates a vacuum tube, cascode preamplifier. The unit presents a 7 db noise figure with 25 db gain and 20 Mc bandwidth referred to 1 db points.

A converter diplexer, in the van, separates 65 Mc centered IF signal into components respectively, 60 Mc monitor channel and 70 Mc communication channel. The 60 Mc monitor signal is further converted to 70 Mc. Receivers from this point are similar for both channels.

The receivers comprise a 60 db, variable gain vacuum tube, 70 Mc IF amplifier; 2 Mc bandpass filter; a conventional limiter; a phase lock loop; a conventional FM limiter demodulator; a 60 db gain base amplifier accommodating from 0 to 60 kc.

Automatic gain control in the IF strip accounts for signal strength variations due to varying satellite distances.

Phase lock loop consists of phase detector, narrow band loop filter, and voltage controlled oscillator. Up to 4 db signal to noise improvement is obtained due to FM threshold extension. Phase detector compares the IF 70 Mc FM signal and a 70 Mc signal from a voltage controlled oscillator. Output of the phase detector is filtered and the loop closes through a voltage controlled oscillator.

Output of the oscillator already presents threshold improvement effect and by processing it in a conventional limiter phase demodulator and a 60 db gain baseband amplifier the final audio baseband signal is obtained.

Carrier frequency variation due to Dop-

pler effect and frequency instability correction is obtained by sampling the 70 Mc FM signal out of the voltage controlled oscillator. The sample is transformed into a dc voltage correction by a limiter-discriminator AFC unit, which is fed back to the voltage controlled oscillator of the converter diplexer unit. Similar feedback is taken from the communication receiver to the mixer preamplifier unit front end. Provisions are made for manual frequency search, AGC measurement, and lock status indication.

The VHF receiver is a fixed tuning, dual frequency operation, van mounted unit for 136.14 and 136.62 Mc satellite beacon reception.

Double conversion occurs at 21.5 Mc and 4.5 Mc. A 3 kc bandwidth filter, and an IF conventional amplifier bring the signal to a correlation detector giving the audio output.

A frequency following loop allows for Doppler and instability frequency variations, by comparing in a phase detector unit the 4.5 Mc IF signal and a local 4.5 Mc reference source. Phase detector output controls a variable oscillator on the 21.5 Mc first mixer, closing the feedback loop.

Provisions are made for automatic frequency search, lock status indicator and Doppler signal output.

A conventional HF communication receiver covering from .5 to 30 Mc, is used for time signals and general reception purposes.

OPERATIONAL PROCEDURES

COMRIO Satellite Station has as a major objective, to contribute to the development of satellite communication by accomplishing multi-channel, two-way telephone transoceanic tests and demonstrations, the gathering of operational experience, and investigation of station functional environmental and operational performance.

Scheduling and tracking data for experiments with the Relay satellite are received in advance from the NASA satellite operations center. Tracking data include for every minute interval, AZ, EL, pointing coordinates, range in km, for all the visible period. Data are employed for initial antenna pointing before satellite acquisition, back-up in case of automatic tracking failure, checking of antenna pointing accuracy, and predicted signal strength calculations.

Subsystems and systems are checked prior, during and after each pass, so as to furnish correlation parameters for experiment analysis. The system block diagram is shown in Figure 2–9.

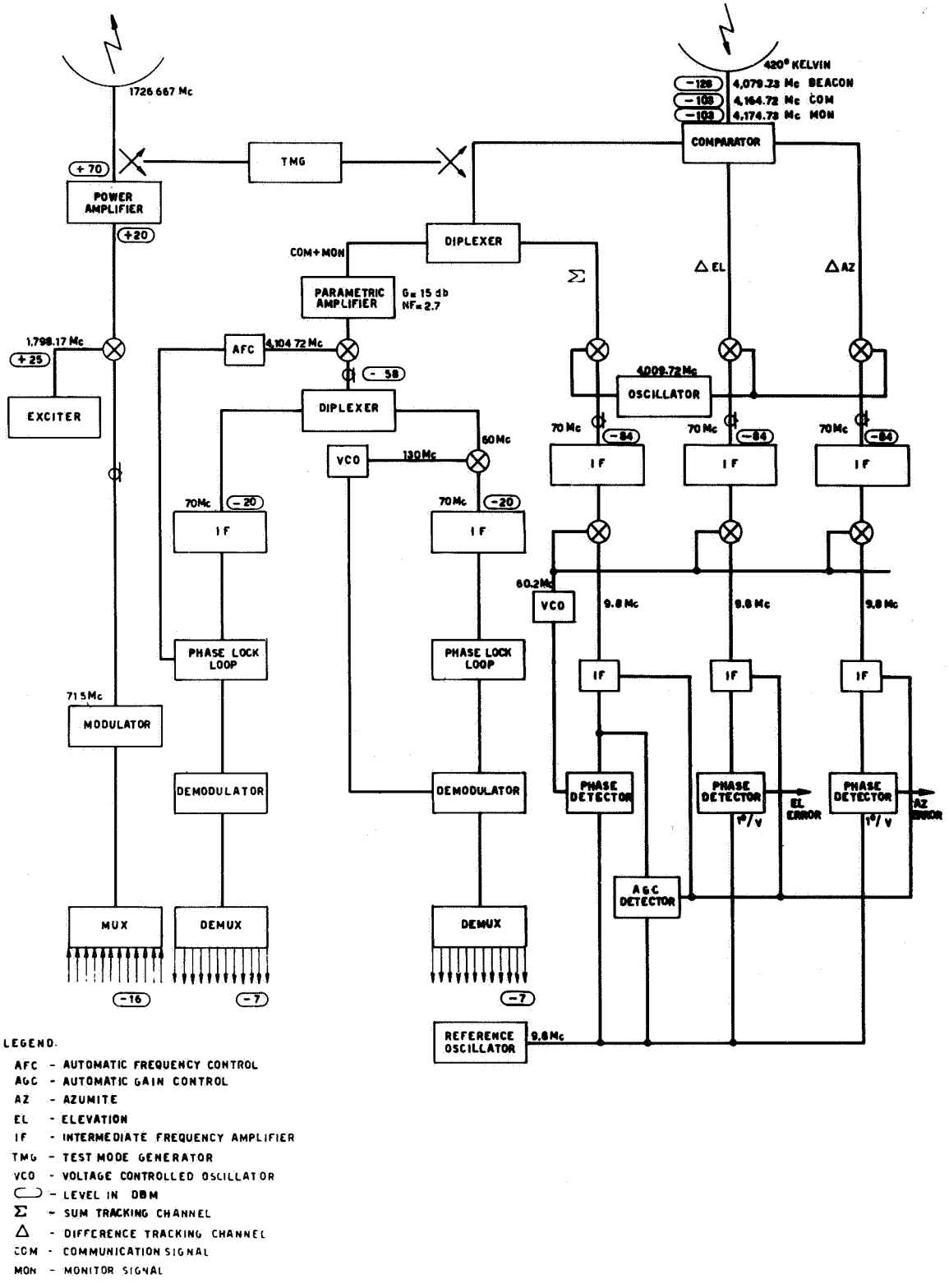
Basic checks for the system performance can be made using the following configurations: built-in station loop, satellite-simulator loop, satellite-short loop, station-to-station experiments, and back-to-back station loop.

Built-in station loop takes a 1726.667 Mc sampling from klystron output, feeding it back to the receiver front and using a van mounted test mode generator (TMG) unit. Actual performance of the transmitting and receiving system can be checked in this manner.

The TMG furnishes a calibrated 4079.73 Mc beacon carrier with or without a 4164.740 or 4174.740 Mc signal simulating the monitor and communication receiver spectrum. Beacon signal is obtained by mixing a 100 Mc crystal generated signal with the third harmonic of the 1326.57 Mc signal which is generated by a 73.6987 Mc crystal oscillator, multiplied successively by 2, 3 and 3 times in an amplifier varactor chain. Communication receive signals are simulated by mixing the 3rd harmonic of 1726.666 Mc sampled signal from the transmitter with either 1015.256 Mc or 1005.258 Mc. These two signals come, respectively, from 112.8063 Mc and 111.695 Mc crystal oscillator multiplied 9 times by a two stage varactor amplifier unit. Beacon output ranges from —25 to —65 dbm and signals output from —25 to —45 dbm for 0 dbm sampled input.

Satellite simulator or transponder loop evaluates transmitting - receiving systems, and tracking performances of the antenna.

The simulator can furnish the same frequency spectrum of the Test Mode Generator. Available beacon input power to the



LEGEND.

AFC - AUTOMATIC FREQUENCY CONTROL
AGC - AUTOMATIC GAIN CONTROL
AZ - AZUMITE
EL - ELEVATION
IF - INTERMEDIATE FREQUENCY AMPLIFIER
TMG - TEST MODE GENERATOR
VCO - VOLTAGE CONTROLLED OSCILLATOR
⊂⊃ - LEVEL IN DBM
Σ - SUM TRACKING CHANNEL
Δ - DIFFERENCE TRACKING CHANNEL
COM - COMMUNICATION SIGNAL
MON - MONITOR SIGNAL

FIGURE 2–9.—System block diagram.

transponder antenna ranges from +20 dbm to —80 dbm. As a repeater receiver, for an input ranging from +20 to —40 dbm, it gives back a +40 to —60 dbm, satellite to ground monitor signal.

The transponder consists of a beacon transmitter, a wide and narrow band receiver-repeater unit, an amplifier and power supply unit, and an antenna unit.

A beacon signal obtained from a 113.3258 Mc crystal controlled oscillator further multiplied 4 and 9 times through a varactor-amplifier chain and a signal from the receiver repeater unit are input to the amplifier unit. The received signal is mixed down to 70 Mc IF signal with 1655 Mc. The carrier comes from a 113.3258 Mc crystal oscillator multiplied 4 and 4 times in an amplifier varactor unit. The 68.333 Mc signal is selected by a 1.5 Mc over 1 db points bandpass filter network, trebled by a solid state varactor module and again mixed up to 4164.72 Mc. The signal for the high level balanced mixer is obtained from a 109.99 Mc crystal oscillator, multiplied 4, 3 and 3 times in a varactor amplifier chain.

Amplifier unit has a range capability from 4.05 to 4.25 kMc with RF gain of 33 db for an input power of 5.5 mw employing a traveling wave tube working in the saturation mode. High voltage power supply consists of an ac to dc converter, step-up transformer, and rectifier circuit, using a regulated 22.5 vdc input, giving ± 1 kv output.

The transmitting antenna is left-hand, circularly polarized, presenting 3.69 db gain with VSWR of 1.6 to 1. The receiving antenna is right-hand, circularly polarized, with 2.5 db gain.

The performance of the tracking system is evaluated by offsetting the antenna boresight ± .1° from the simulator beacon transmitter and measuring the corresponding azimuth and elevation dc voltage correction error. Servo response is checked by manually offsetting the antenna ± 3° from the simulator beacon transmitter and then recording automatic acquisition performance. Position readout accuracy can also be checked against the satellite simulator AZ and EL coordinates.

Built-in station and satellite simulator loops conclude with front-end noise figure measurements, clock synchronization, terminal equipment set-up and adjustments, and typical pre-pass operational procedures.

The satellite shot loop station to station and back to back station loops are configurations employing actual spacecraft.

Satellite acquisition is made by directing the antenna at a pre-determined bearing and time. Spacecraft arrival is first signaled by 136 Mc VHF receiver acquisition and further by detection of the 4,080 Mc beacon signal when automatic acquisition occurs. Tracking will then proceed automatically.

Satellite-short loop, the station-to-station experiments and the back-to-back station loop, constitute three sequential stages for performance evaluation, whereby the station communicates via the satellite with itself, with the distant station, and with itself through the distant terminal.

Time of events, AGC signals from the receiving system, antenna read-out, transmitter parameters, results of terminal equipment tests and from specific purposes tests data are recorded during the pass. System demonstrations include interconnection of local telephone and satellite communication system, teletype, and facsimile messages. During each communication pass, voice is used to coordinate experiments between participating stations.

AUTHORS. *This chapter was contributed by* J. C. FONSECA *and* C. H. MOREIRA, *Cia. Rádio Internacional de Brasil—ITT, Rio de Janeiro, Brazil.*

N66-10253

The Pleumeur-Bodou Space Communications Station

The Pleumeur-Bodou ground station is the research unit of the National Center for Telecommunications Studies (CNET) in the field of space communications. This installation makes possible the study of all the experimental problems connected with transmissions by active satellites: link performance, acquisition, tracking, telemetry, command, and operations. It is also capable of being adapted to commercial operation when the occasion arises for such operation.

INTRODUCTION

A ground station is the basic tool for experimental study of space communication systems. With the Pleumeur-Bodou ground station, CNET (Centre National d'Etudes des Telecommunications) has available a complex of equipment which enables it to acquire in-depth experience in the field of transmissions by active satellites.

This complex, however, was not intended only for experimentation. Operational use of the station was envisioned, and it is capable of being adapted as required to implement a commercial system of satellite communication.

The creation of a ground station at Pleumeur-Bodou was decided upon within the framework of the American Relay and Telstar projects. In the spring of 1961 the French government signed an agreement with NASA under which France participated in Project Relay by setting up a station with the capability of servicing communications links through the satellite.

In order to meet the very short schedule set by the planned launch date of the satellite, the Ministry of Posts and Telecommunications decided to request the cooperation of the AT&T. This company had undertaken to establish an original project for active satellite communications, Project Telstar, which included the development of a specially designed ground station at Andover. In December 1961 the AT&T signed a contract with the Administration of Posts and Telecommunications, undertaking to provide the essential elements of a station identical to the one at Andover as well as technical assistance. CNET was given responsibility for overall direction of the project, and CGE (Compagnie Generale d'Electricite) participated in the capacity of architect-engineer. After a preparatory period, the first construction work was started in October 1961 on the site selected at Pleumeur-Bodou. On 8 July 1962 all the elements were installed and on 9 July the system tests demonstrated that the station was in operating condition. The satisfactory operation of the station was confirmed by the historic communications effected with Telstar I. The equipment was subsequently completed in the autumn of 1962 to provide for operation with Relay I (see Figure 3–1).

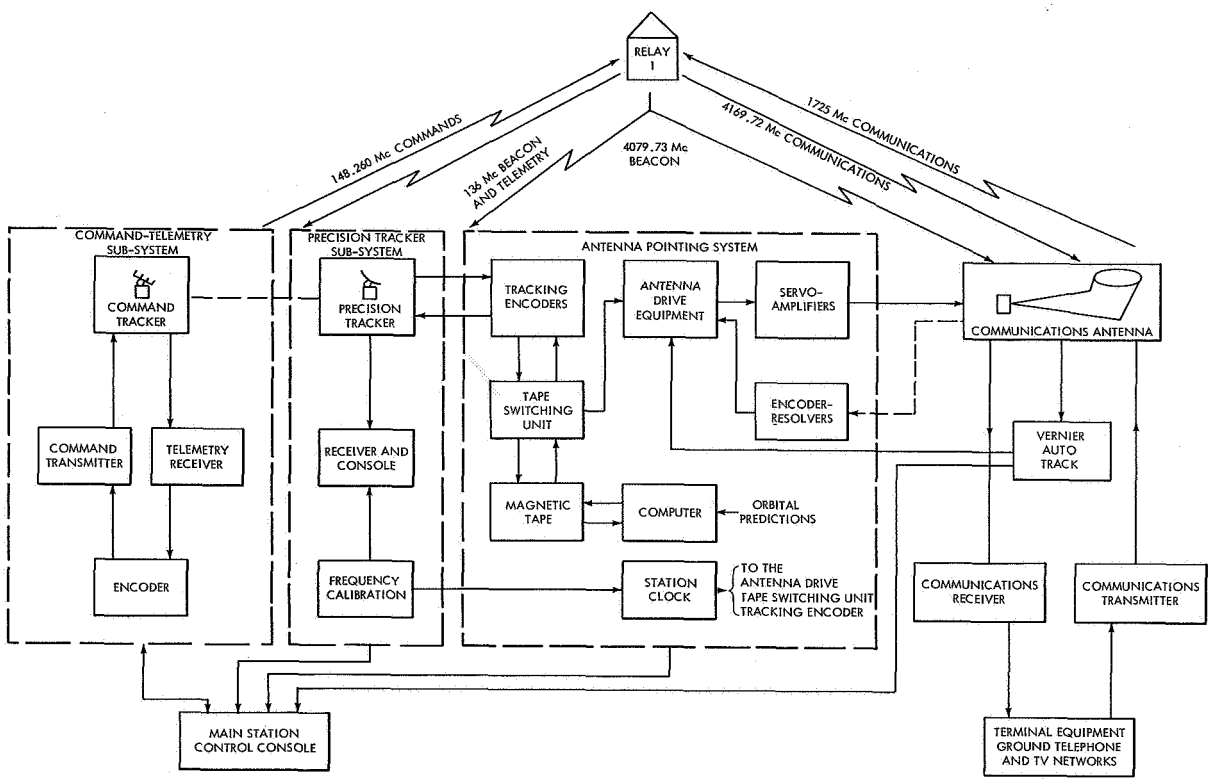


FIGURE 3–1.—General block diagram of the Pleumeur-Bodou Ground Station.

OVERALL DESIGN OF THE STATION

Communications Antenna

The communications antenna is the basic element of the station; its characteristics were determined by the performance characteristics of the Telstar and Relay satellites and by the desired link performance.

The aim is to achieve transatlantic transmission of high-quality television with sound, or of the equivalent of 600 one-way telephone channels, or of 12 channels of two-way telephony.

The satellite is at a high altitude in order to provide satisfactory mutual visibility between stations on both sides of the Atlantic, while the weight of the satellite, being limited by launch constraints, permits only a few watts of transmitter output. The received signal is extremely weak and the receiving antenna must have a very large gain and low noise. The horn antenna at Pleumeur-Bodou has the largest dimensions which can be achieved while still maintaining sufficient pointing accuracy.

Receiving

The horn antenna, having very low gain outside of the main lobe, receives a minimum of noise originating on the ground; the advantage of this low characteristic noise is utilized to the maximum by a maser cooled by liquid helium. The signal-to-noise threshold is further lowered by a frequency-compression demodulator.

Pointing

The antenna must locate and track the satellite with high reliability, which is obtained by a complex system of acquisition and tracking in which the capability of the antenna itself is complemented by a precision tracker. The use of digital intermediate equipment, plus automatic tracking, provides for pointing the antenna with the required accuracy.

Radome

The antenna was designed to operate while protected from atmospheric effects which could degrade the precision of its construction or perturb the pointing. This is provided by a radome, a flexible spherical envelope kept erect by air under pressure.

Telemetry and Command

In order to take advantage of all the experimental possibilities of the system, the station has equipment for receiving telemetry from the satellite and a ground command setup. A command tracker is able to track the satellite automatically and facilitate acquisition if required.

Equipment

The Pleumeur-Bodou station was equipped, after construction, with the following principal items of equipment:

1. Under the radome, a horn antenna with the communications transmitter and receiver, antenna drive, and the servo group for the pointing motors.
2. A precision tracker with antenna.
3. A command tracker with antenna.
4. In a central building, antenna steering equipment including a computation center, and terminal equipment providing connections with the telephone and television networks.
5. A boresight tower with satellite simulator for the horn antenna and a test tower for the trackers.
6. Auxiliary equipment for heating, air-conditioning, and radome inflation.

OPERATIONAL EQUIPMENT

Horn Antenna

The antenna is a horn reflector made up of a conical HF horn 36.5 m long, a parabolic reflector whose focus coincides with the apex of the cone, and a cylindrical screen with an opening of 344 m^2 (see Figure 3–2). Orientation in elevation is accomplished by rotating the horn about its horizontal axis. The entire structure rests on four trucks on two

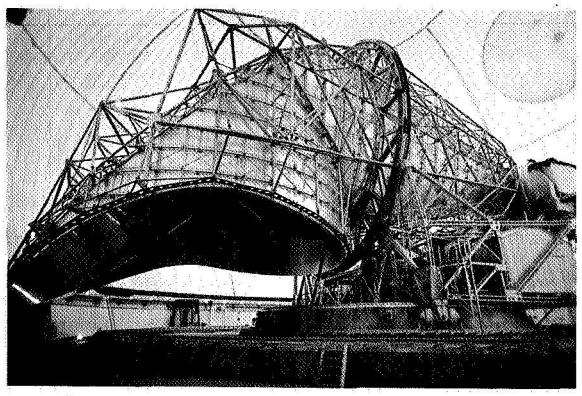


FIGURE 3–2.—Horn antenna.

concentric rails, and rotates in azimuth about the pivot, the only function of which is to assure perfect centering. The equipment is mounted in two cabins which form part of the rotating structure (see Figure 3–3). The apex of the horn is in the upper cabin, with a rotary joint providing the link between the stationary portion and the rest of the horn, which is movable in elevation. The reflecting surfaces were adjusted with the highest accuracy; the paraboloid differs from the theoretical paraboloid by ± 1.5 mm at most. The entire system is designed for great rigidity.

The characteristics are as follows:

	Gain (db)	3-db Beamwidth (deg)
Receiving 4170 Mc	57	0.23
Transmitting 1725 Mc	50	0.5

The 1 db radius of the beam for receiving is 0.06 degree. This value defines the maximum acceptable pointing error in azimuth and elevation; pointing error should not cause a decrease in gain greater than 1 db.

Antenna Pointing

The pointing accuracy defined above is difficult to attain because of the large inertia of the antenna (mass 340 metric tons). This degree of accuracy is obtained by the use of digital computation equipment and particu-

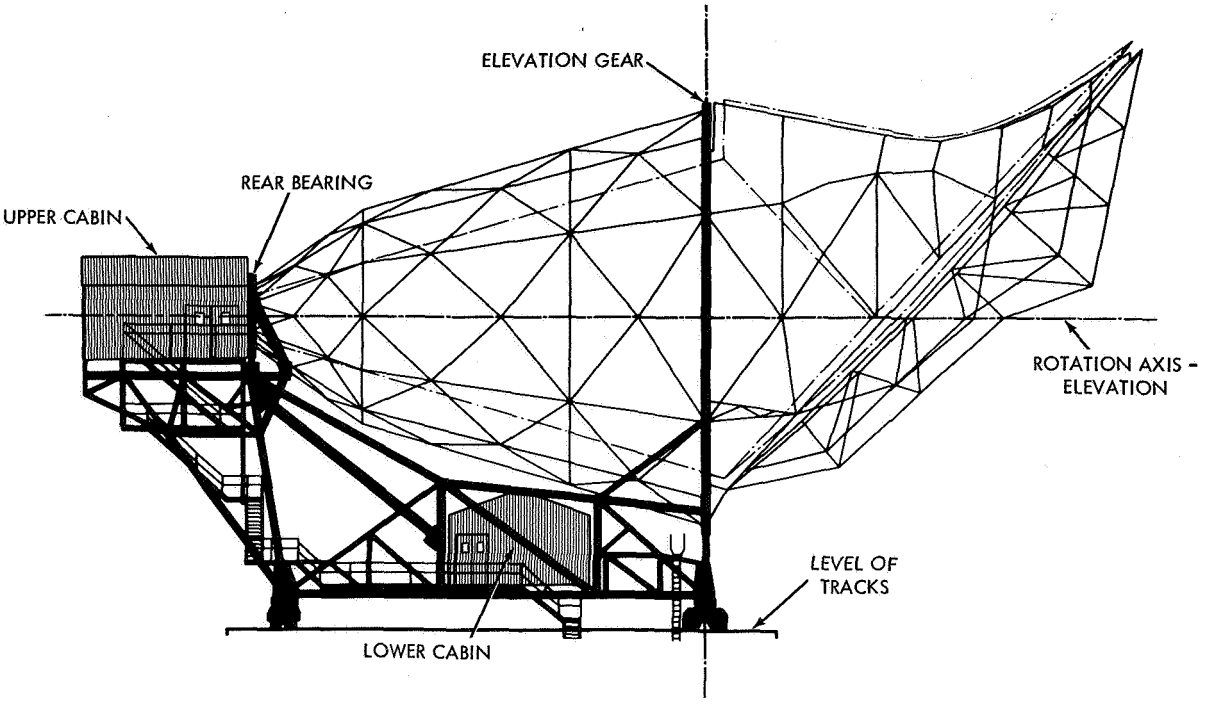


FIGURE 3–3.—Lateral view of the horn antenna.

larly by the use of a pointing error detector which provides vernier corrections or permits automatic tracking.

The equipment for measuring antenna position in azimuth and elevation is of high accuracy (+ 0.003 degree), corresponding to the desired pointing accuracy.

Normal Pointing Mode

In normal operation, the computing center develops antenna pointing data from topocentric coordinates. The data points are at 4-second intervals. They are recorded on a magnetic tape which is placed in a tape reader. At the selected moment, given by the station clock, a block of data is transferred to the antenna command where it is checked, stored in the memory, and interpolations are made at the rate of 128 intermediate points per second. The equipment adds to these points any automatic or manual corrections and compares the result with the actual position of the antenna to derive error voltages which drive the servo loops of the drive motors.

The topocentric coordinates which enable the ephemerides of the Relay satellites to be established are provided by the NASA computation center.

Vernier Autotrack (VAT)

The vernier autotrack (see Figure 3–4) operates on the 4079.73 Mc signal radiated by the satellite beacon and provides antenna pointing errors referred to an electrical axis. This provides automatic correction of mechanical deformations of the antenna. It makes use of the propagation conditions in a circular waveguide in which only the TE 11 and TM 01 modes are propagated.

The circular waveguide which extends the apex of the horn has two sets of coupled cavities arranged along two perpendicular diameters. Each set is coupled to two rectangular waveguides, making a hybrid junction. The cavities along the vertical diameter provide for extraction of the vertical component of TE 11 and TM 01. The cavities along the horizontal diameter provide for extraction of the horizontal component of

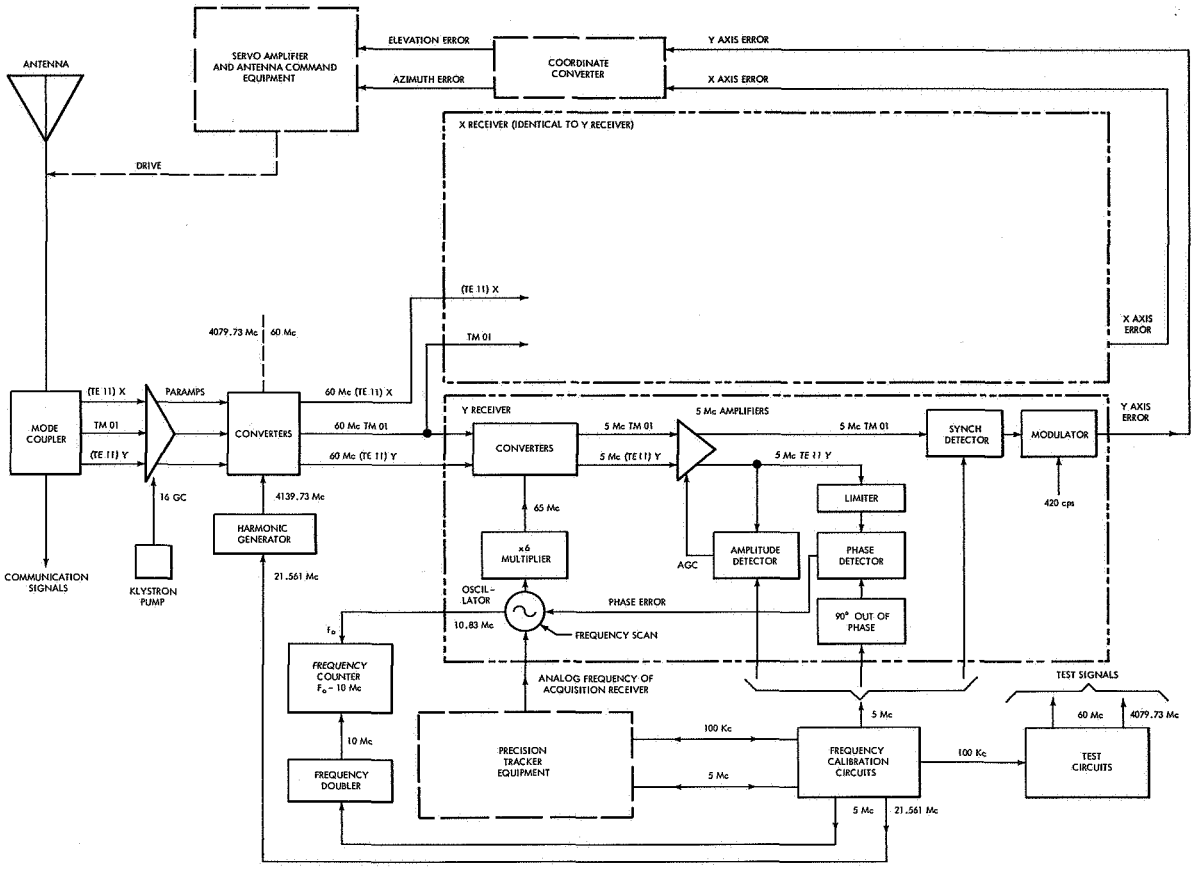


FIGURE 3–4.—Block diagram of vernier autotrack.

TE 11. Three amplification channels provide error voltages in azimuth and elevation.

The conversion of coordinates is performed by means of the coordinate converter which is included in the servo system. The error signals may drive the servo loops directly (autotrack) or they may correct the computed data after encoding (vernier).

The pointing angle accuracy obtained with the VAT is better than 0.005 degree. The pass band is 3 kc. The maximum angle for acquisition is 0.2 degree in all directions.

Servo Group

The servo group controls the hydraulic motors which position the antenna. Azimuth positioning is accomplished by two Vickers sets, each composed of a 25 hp electrical motor driving a pump, plus two receivers. Each receiver is connected through two reduction gears to a pinion which meshes with a rack mounted on a parapet sized to the foundations. One receiver operates as a brake and the other as a motor.

The elevation drive is also accomplished by two similar groups, but these are of 10 hp each (Figure 3–5). These groups are mounted on the azimuth structure; the bullgear is bolted around the elevation wheel.

The Vickers systems, driving through the reduction gears, provide a remarkable flexibility of response; the azimuth rate can vary from 0 to 1.5 deg/sec and the elevation rate from 0 to 1.4 deg/sec.

Each group includes several servo loops. Excessive torques due to the wind are eliminated by the radome. Antenna pointing is accomplished with the desired stability, since

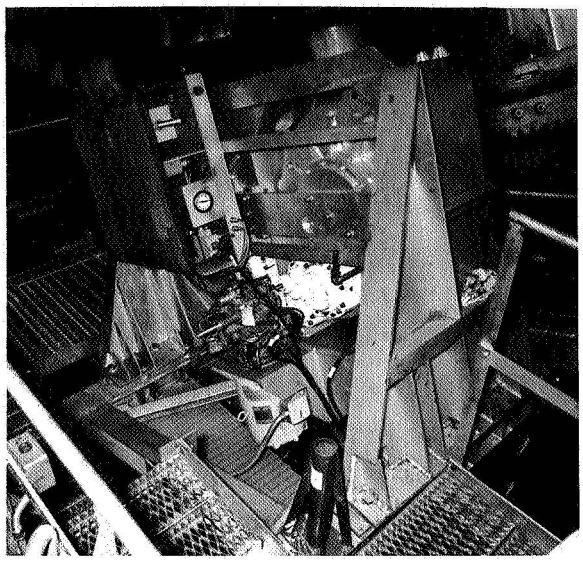


FIGURE 3–5.—Elevation drive.

the characteristic resonance of the antenna structure is relatively high (1.8 cps in azimuth).

The Relay Transmitter

The transmitter (Figure 3–6) has an output power of 10 kw at 1725 Mc. The signal, amplified at baseband, frequency modulates the reflex klystron 1 which oscillates at the frequency of 6174.13 Mc. Klystron 2 oscillates at 6100 Mc, so that beating the two signals in the mixer gives an intermediate frequency of 74 Mc. An automatic frequency control system using a quartz reference maintains the intermediate frequency at the nominal value.

The IF signal produced is amplified and transposed by mixer 2 to the transmitting frequency of 1725 Mc. The resulting signal goes through the exciter amplifier consisting of a traveling wave tube of 30 db gain, and then through the power amplifier, a 5-cavity klystron.

The transmitted signal at 1725 Mc is coupled into the antenna at the conical section immediately following the point of the apex. Two signals of equal amplitude and 90 degree phase difference are coupled at right angles and produce a signal of right-hand circular polarization in space (Figure 3–7).

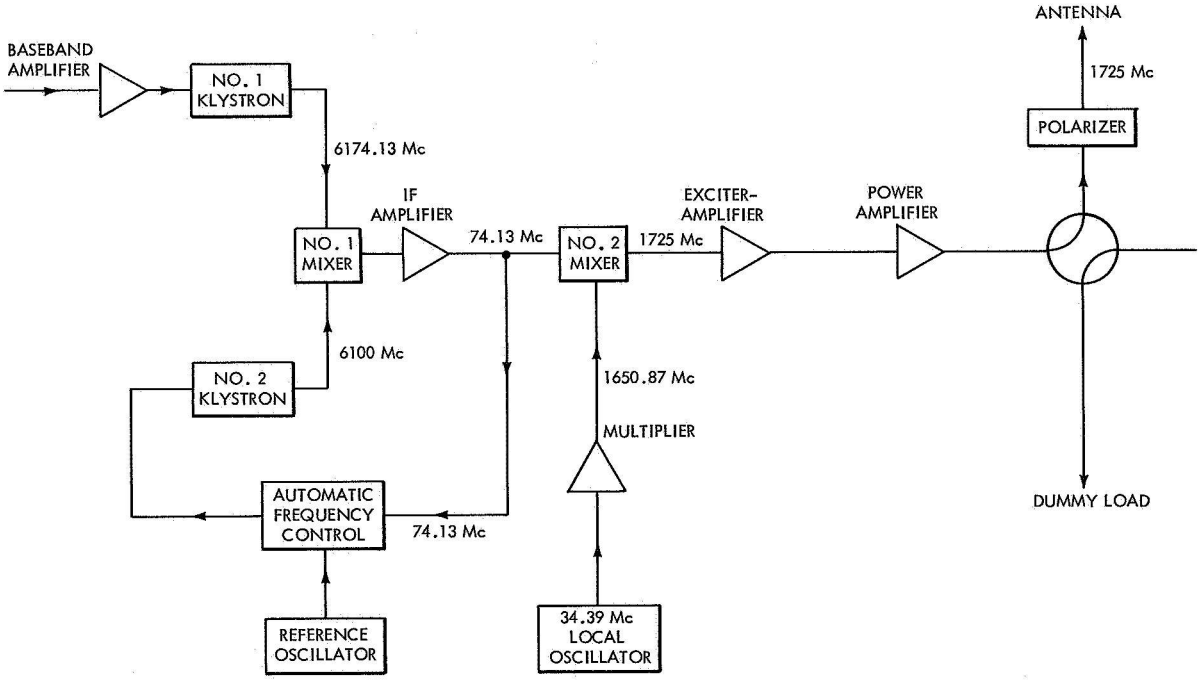


FIGURE 3–6.—Block diagram of Relay transmitting system.

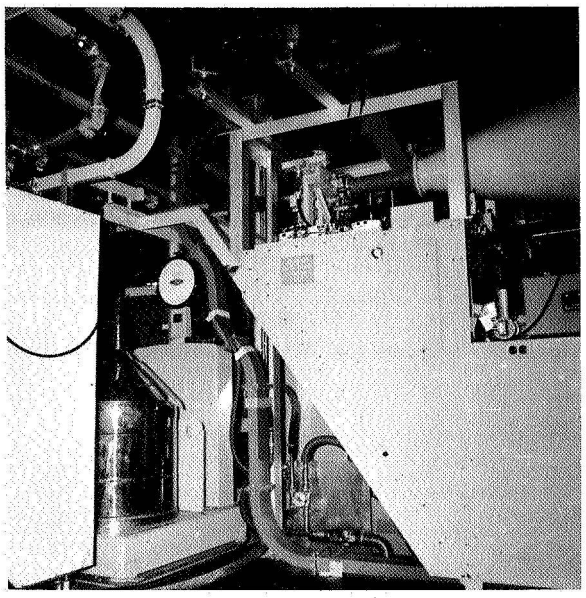


FIGURE 3–7.—View of the apex of the horn showing VAT and 1725 Mc transmitter coupling.

Receiver

The maser located behind the apex of the cone (see Figure 3–8) is connected to the antenna by the diplexer. The loss in the waveguides is kept to a minimum (0.2 db). The single tuned ruby maser is placed in liquid helium; it has a nominal frequency of 4170 Mc, gain of 42 db, 3-db bandwidth of 16 Mc, and noise temperature of 4°K. The pump frequency is 30,180 Mc and is stabilized automatically.

The amplitude is perfectly linear. The bandwidth is extended to 25 Mc by insertion of an IF equalizer installed just following the frequency converter. The signal converted to the intermediate frequency of 74 Mc is amplified up to a level of +1 dbm, maintained constant by automatic gain control. Since the frequency deviation of the received signal is very large, the threshold of the receiver is reduced to a minimum value by the process of frequency compression. The demodulator operates at an input frequency of 6123 Mc. The initial modulation index is reduced by this feedback device to a low value, and the noise spectrum in the loop is reduced to its minimum value. The threshold of the receiver is improved by 4 to 5 db.

Radome

The radome plays an important part in the achievement of the horn antenna performance. It protects the antenna against dust and atmospheric phenomena such as heat of the sun, wind, snow, rain, and ice. If the antenna were in the open air it would be subject, because of temperature variations, to deformations which would, in the case of the reflecting surfaces, reduce the

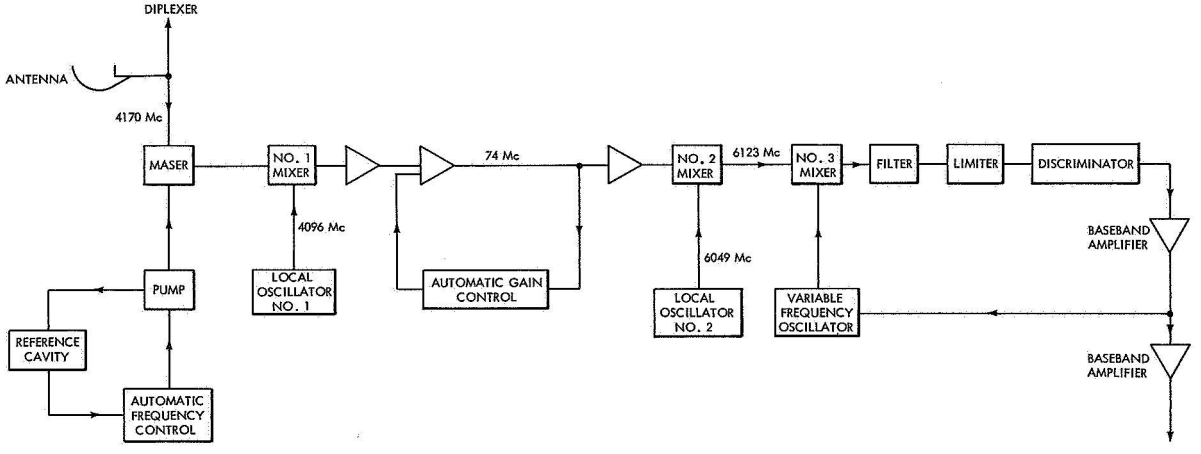


FIGURE 3–8.—Block diagram of receiving system.

gain and degrade the radiation pattern. The pointing accuracy would be reduced. The wind would be very harmful to tracking performance; a moderate wind would cause instabilities and strong wind would prevent pointing the antenna with the desired accuracy. Rain and snow would result in accumulations of water difficult to drain off. For these reasons, the radome made it possible to lighten the antenna structure and the drive system.

The envelope is a section of a sphere 64 m in diameter. The material is two layers of dacron with the fibers crossed at 90 degrees and coated with a synthetic rubber hypalon. The thickness is 1.8 mm ± 0.05 mm. This material produces the minimum of radioelectric losses and has minimum permeability to moisture.

The installation of the radome is a delicate operation (see Figures 3–9 and 3–10).

Precision Tracker

The precision tracker is a radio theodolite basically intended for measuring the azimuth and elevation of the satelite as functions of time during a pass (see Figure 3–11). It uses the signal from the 4079.73 Mc satellite beacon. In fact, it serves several functions in relation to the communications antenna; for one thing it assures acquisition in cases where the computed pointing data may be uncertain, by virtue of its 2 degree beam-



FIGURE 3–9.—Erection of the radome over the construction shelter.

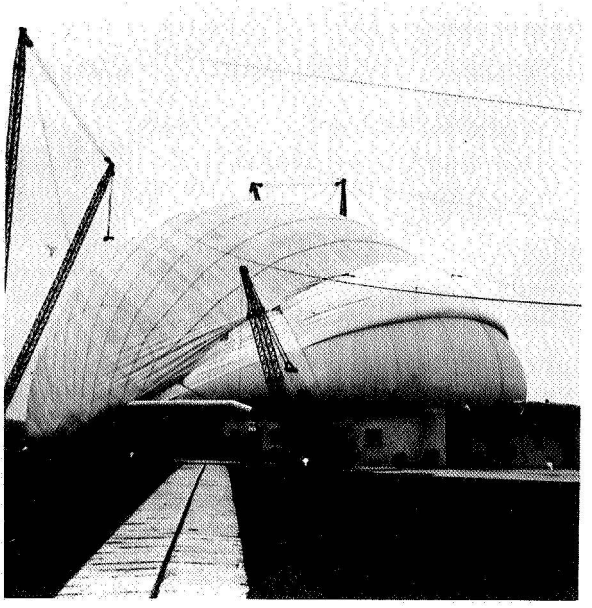


FIGURE 3–10.—Initial inflation of the radome over the construction shelter.

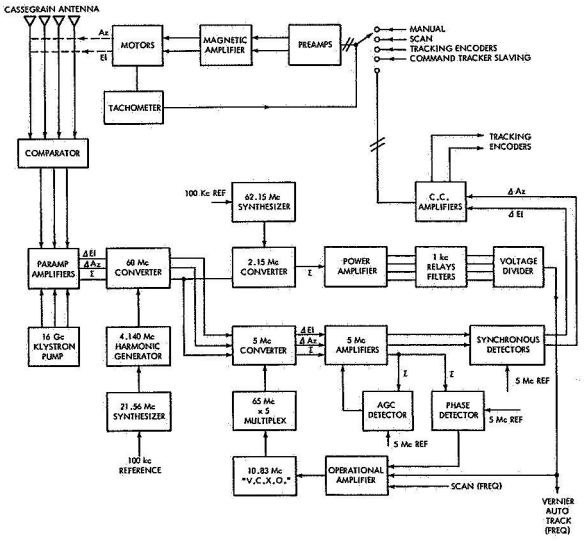


FIGURE 3–11.—Simplified block diagram of precision tracker.

width. It makes acquisition more rapid by the use of an acquisition receiver which determines the frequency received from the beacon. It is possible to slave the horn antenna to the precision tracker through digital tracking equipment. Lastly, it provides time and frequency references.

The antenna is a Cassegrain reflector 2.45 m in diameter; the principal reflector is a parabolic aluminum surface over which a molded fiberglass truncated cone structure is placed, serving as support for the subreflector. The secondary reflector is hyperbolic, 91 cm in diameter, and consists of a grid of horizontal aluminum wires. The antenna therefore accepts only the vertical component of the received signal. In front of the principal surface is placed a grid of wires oriented 45 degrees from the vertical, providing focusing at the apex after reflection. The signal is received in four horns placed at the apex of the parabola and then processed in four hybrids by addition and subtraction to give three signals (sum, azimuth difference, and elevation difference). The signals are amplified directly by three parametric amplifiers with high gain and low noise.

An acquisition receiver determines from the sum signal the exact frequency received; the pass band is $\pm$ 150 kc about the nominal frequency. The receiver consists of 300 channels each of 1 kc bandwidth. A set of 300 filters performs a spectrum analysis of the frequency, and the activated filter gives a signal which activates a digital device. The channel is identified and the other channels are switched off. An analog voltage proportional to the frequency deviation positions the quartz oscillator of the tracking receiver and triggers an automatic sweep about the frequency. When frequency lock is achieved the digital input is disconnected. The phase-lock loop keeps the sum signal in phase with a reference 5-Mc frequency. The difference signals are converted to 5 Mc and kept in phase coherence; coherent detection is performed in the error angle demodulators. The amplified error signals are used to drive the servo loops of the steering motors.

The mechanical accuracy of the system is 0.005 degree, and the maximum of pointing errors due to instability is 0.015 degree.

The acquisition of frequency enables the phase-coherent loops of the VAT to be preadjusted.

The frequency standard includes a very accurate 1-Mc crystal oscillator which supplies the 100 kc and 5 Mc references as well as a 1-sec timing signal to an accuracy of 1 part in 10^{11}. It is checked by the 18 kc signal received from the NBA station of the American Navy.

ARRANGEMENT OF THE OPERATIONAL EQUIPMENT

The equipment required for the operation of the station will be described in connection with their respective locations.

Communications Antenna

The antenna is located under the radome, with the complete structure mounted on two concentric rails. The equipment is mounted in two cabins; the upper cabin behind the horn, and the lower cabin in a position as close as possible to the axis of rotation in azimuth.

Upper Cabin

The throat of the horn is enclosed in the upper cabin, with a rotary joint to provide continuity between the apex and the rest of the horn. The following equipment is located in the upper cabin (see Figure 3–12).

1. Near the horn, the VAT equipment, mode coupler, and 4080 Mc receiver.
2. The communications receiver with maser, hyperfrequency pump, liquid nitrogen and liquid helium coolers, IF amplifier, frequency-compression loop.
3. The Telstar communications transmitter.
4. Measurement equipment, radiometry equipment, antenna command group equipment (encoder, resolver, VAT coordinate converter).

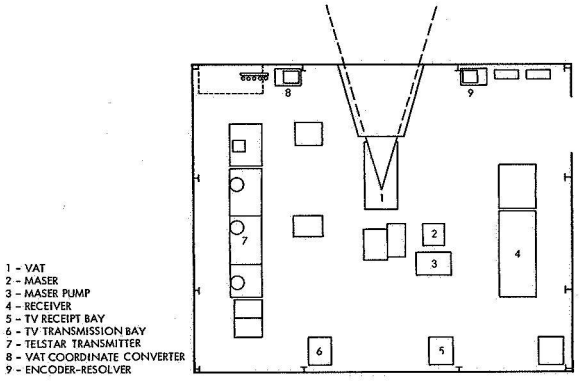


FIGURE 3–12.—Plan view of the upper room.

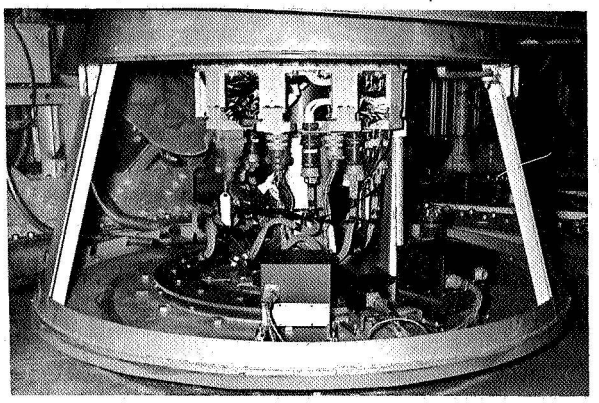


FIGURE 3–14.—View of the slip ring.

Lower Cabin

The lower cabin contains essentially the antenna steering equipment (see Figure 3–13).

Slip Ring—Cable Links

The antenna pivot carries a set of slip rings providing for transmission of signals and energy between the movable antenna and the cables which terminate in the radome (Figure 3–14).

Between the radome and the main building there are the following cable links:

1. 1 cable carrying six coaxial pairs 1.2/4.4 and 69 0.9 quads
2. 1 cable of 100 0.9 shielded pairs
3. 74 RG 11 A/U coaxial cables

In the radome annex is a rack containing an equalizer (amplifier) and a switching system for television signals.

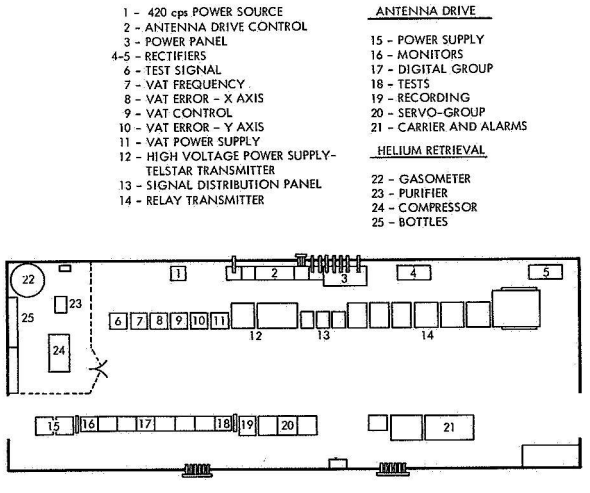


FIGURE 3–13.—Plan view of the lower room.

Main Building—Trackers

The antennas for the precision tracker and command tracker are located near the central building. This building brings together the controls for the whole complex and provides for connections with the national television and telephone networks.

Control and Tracking Room

At the center (see Figure 3–15), the station control console receives the data from the various systems and directs the acquisition and tracking operations. (Figure 3–16).

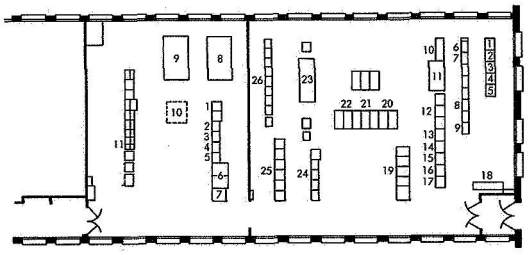
Three video monitors (two for transmission, one for receiving) provide for monitoring the television transmission link.

The precision tracker equipment includes:

—the frequency acquisition receiver
—the tracking receiver
—the frequency standard and station clock
—the 4080 Mc test signal generator
—the digital tracking equipment which is also part of the steering system for the horn antenna

The telemetry and command equipment includes:

—the antenna tracking receiver and the servo circuits



TERMINAL EQUIPMENT

1 - STILL PICTURE ANALYZER
2 - 60 cps CABINET-SYNCHROSTABILIZATION
3 - VIDEO SWITCHING
4 - TRANSMISSION MONITOR
5 - RECEIVING MONITOR
6 - MEASURING EQUIPMENT
7 - FRENCH RADIO-TV NETWORK BAY
8-9 - AMPEX VIDEO RECORDER
10 - AMPEX FR 100 RECORDER
11 - TELEPHONE RACK

TRACKING

1 - CLOCK OSCILLATOR
2 - CLOCK POWER SUPPLY
3-4-5 - TRACKING ENCODER GROUP (T.E.G.) POWER
6 - CLOCK
7 - T.E.G. TESTING
8 - T.E.G.
9 - AUXILIARY STATION CONTROL CONSOLE BAY
10 - PRECISION TRACKER - POWER SUPPLY
11 - PRECISION TRACKER CONSOLE
12 - COMBINED FILTERS
13 - PRECISION TRACKER LOGIC ELEMENT
14 - PRECISION TRACKER RECEIVER
15 - PRECISION TRACKER FREQUENCY ACQUISITION RECEIVER
16 - PRECISION TRACKER FREQUENCY GENERATOR
17 - PRECISION TRACKER TEST SIGNALS
18 - LINK WITH THE BORESIGHT TOWER (SATELLITE SIMULATOR)
19 - POWER PANEL
20 - STATION CONTROL CONSOLE
21 - RECORDERS
22 - TV RECEIVERS
23 - CABLE DISTRIBUTION FRAME
24 - TELEMETRY COMMAND CABINETS
25 - COMMAND TRACKER AUTOMATIC TRACKING
26 - N 1 CARRIER - 43 A TELEGRAPH

FIGURE 3–15.—Main building plan view of area for terminal equipment, tracking and control.

—the telemetry receiver, with FR–1100 magnetic tape recorder

—the command encoder and transmitter

Lastly, the 43 A1, N-carrier multiplex telegraph equipment permits the exchange of information with the antenna by a small

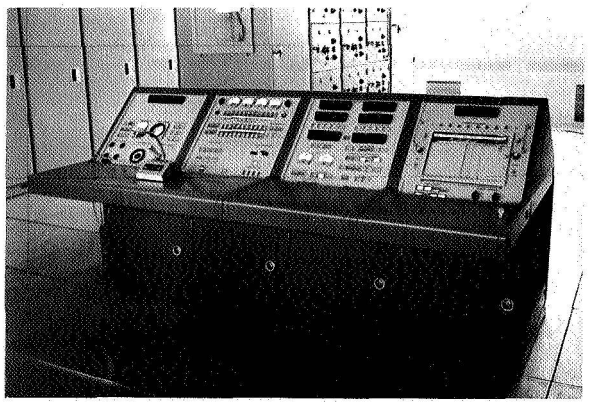


FIGURE 3–16.—Station control console.

number of circuits, reducing the number of slip rings on the antenna pivot. Special equipment provides radio links with the boresight tower on Losquet island.

Terminal Equipment Room

The television rack provides for distribution of the signals and performance of measurements (Figures 3–17 and 3–18). It is connected by two coaxial cables to the microwave links in Pleumeur-Bodou village for

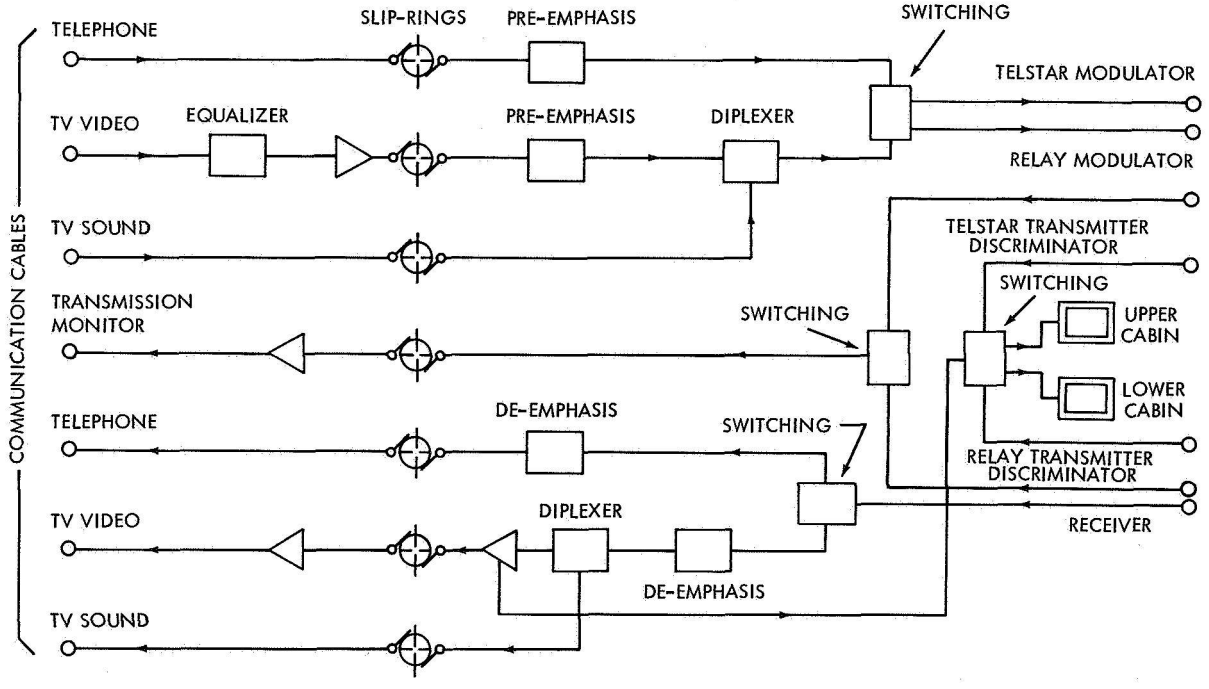


FIGURE 3–17.—Functional block diagram of terminal equipment.

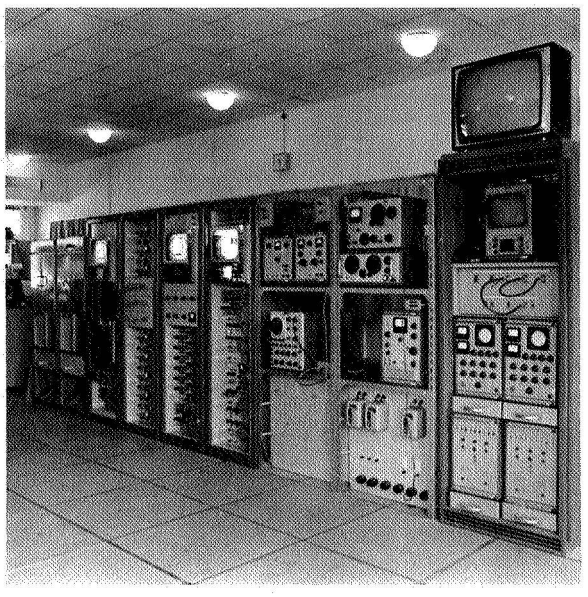


FIGURE 3–18.—View of the video rack.

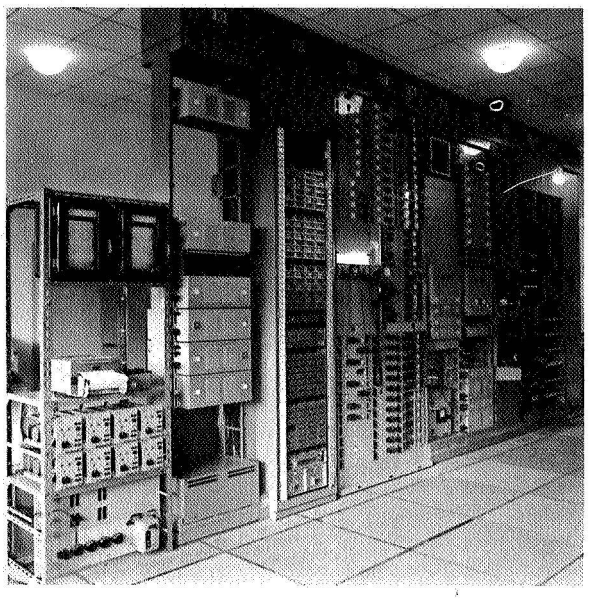


FIGURE 3–19.—View of the telephony rack.

transmission of pictures. The sound is carried by telephone channels.

Two Ampex tape recorders permit recording and retransmission of the television signals handled by the station.

The telephone terminal equipment provides the following links:

- 60 circuits between the Pleumeur-Bodou station and the Andover station through the satellite
- 24 circuits between Pleumeur-Bodou and Brest
- 12 circuits beween Pleumeur-Bodou and Paris via Brest (these use the Pleumeur-Bodou villiage to Brest microwave link)

Between the main building and the radome, the 60 Andover circuits use two pairs of the 6-pair coaxial cable; three other pairs are used for television video, with the sound sent through a quad.

Two self-carried coaxial cables provide the link between the station and the Pleumeur-Bodou microwave terminal, permitting establishment of 60 circuits.

The equipment rack includes: (Figure 3–19)

—a main generator
—primary group carrier generators
—secondary group carrier generators
—generators and transmitters of the 60 and 308 kc pilot signals

All the items constituting the telephony equipment are classic; their arrangement only was realized in a special way, so as to make easy the transmission tests and the measurements. The telephony rack is completed with an AMPEX FR 100—8 tracks —recorder.

Figure 3–20 shows how the station is connected to the national telephone and television networks. The frequency plan for the microwave links between the village of Pleumeur-Bodou and the relay at Roc Tredudon is as follows:

	Receive	Transmit
Telephony	2264 Mc	2136 Mc
Television	3543.5 Mc	3752 Mc

Computation Center

The IBM 1620 computer with special floating decimal point is supplemented by an auxiliary IBM 1623 memory (Figure 3–21). Input and output of large quantities of information is handled by an IBM 1622 card reader-perforator. The computer can be

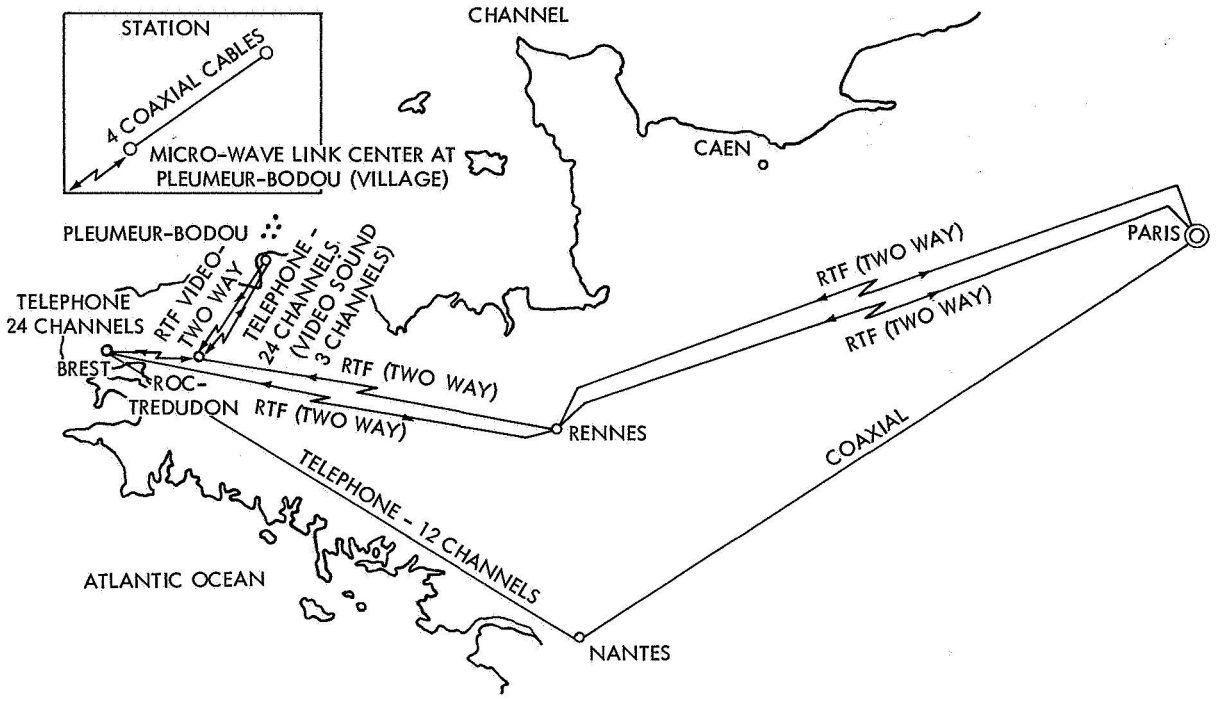
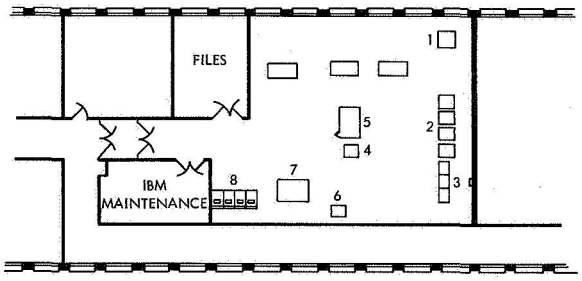


FIGURE 3–20.—Connections between the station and the telephone and television networks.



1 - IBM 046 UNIT
2 - IBM MAGNETIC TAPE UNITS
3 - TAPE SWITCHING UNIT
4 - TAPE SWITCHING CONSOLE
5 - COMPUTER
6 - IBM 026 UNIT
7 - TABULATOR - IBM 421 OR 407
8 - POWER DISTRIBUTION PANEL

FIGURE 3–21.—Plan view of the computation center.

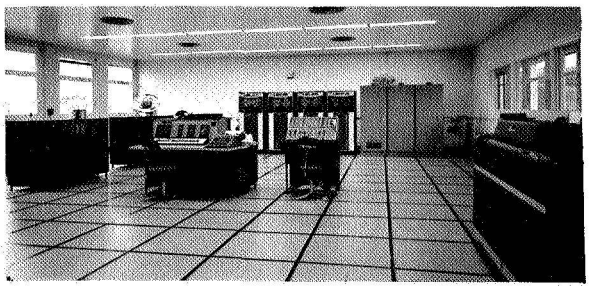


FIGURE 3–22.—View of the computation center.

connected to four Model 729 II magnetic tape units. A system of switching provides great flexibility in the use of the tapes.

Auxiliary Equipment—IBM 026 alphabetic multiperforator, IBM 407 tabulator, IBM 046 tape perforator (Figure 3–22).

SITE—FOUNDATIONS—BUILDINGS

Site

The search for a site was begun in the spring of 1961, and was limited to Brittany because of its location in the extreme west of France, providing the longest periods of mutual visibility across the Atlantic. The temperate climate of this region was also an attractive feature.

The Pleumeur - Bodou site was finally chosen for the following reasons (see Figures 3–23 and 3–24):

1. Proximity to the CNET laboratories in the Lannion region (Research Center—Flight Tests Center).

2. Easy access to telephone and television networks.

3. Quick acquisition in sparsely populated

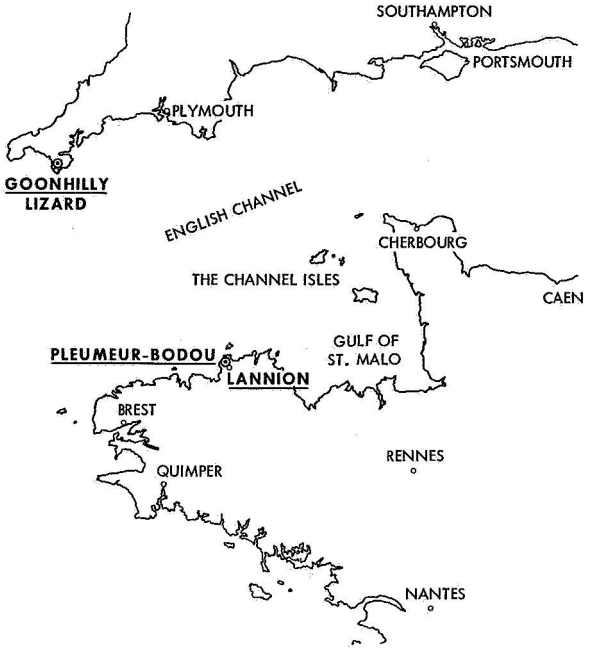


FIGURE 3–23.—Location of the ground station in Brittany.

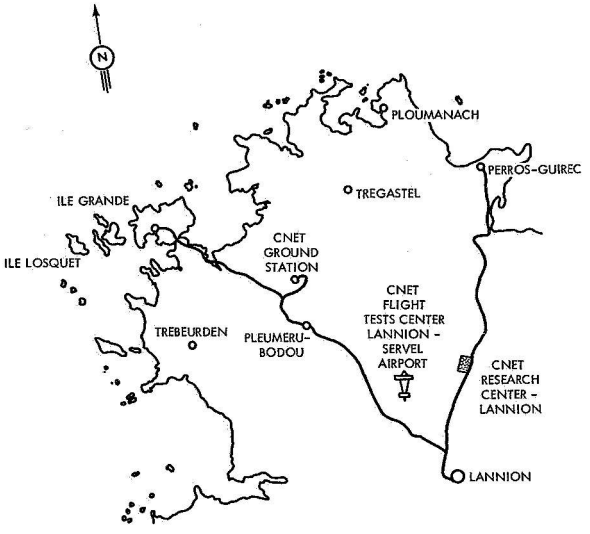


FIGURE 3–24.—The Pleumeur-Bodou region.

moors of a large area which was flat enough, offered stable granite layer, and allowed for future expansion.

4. Absence of RF parasites (distant from microwave links, airports, ports, and sea lanes), monitored by systematic measurements.

5. Configuration of the terrain in the form of a basin, with the rim providing improved RF protection without raising the horizon excessively (less than 5 degrees).

6. Convenient access roads and facilities for power and water supply.

7. Nearness to a coastal resort area providing good living conditions for personnel.

The site is 259.5 acres in area.

The geographic coordinates of the center of the antenna are:

Latitude 48° 47′ 13″ N

Longitude 03° 31′ 20″ W

Mean altitude is 40 m. Figure 3–25 gives an overall view.

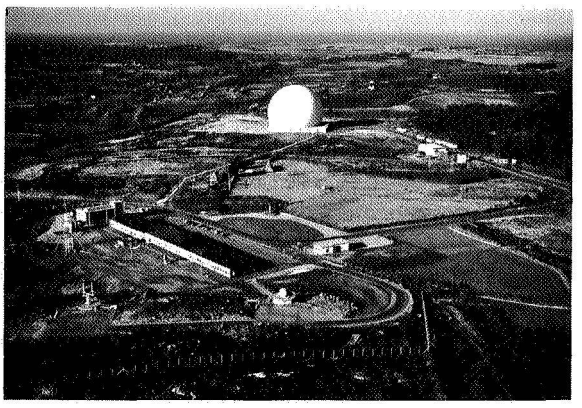


FIGURE 3–25.—Overall view of the station.

Layout of the Site

The present installations on the site leave ample room for future expansion (see Figures 3–26 and 3–27). The tracker antennas, the main building, and the heating plant are placed in a central location with respect to the radome and the sites of future antennas.

Radome

Erected on an open site, the radome area provides a very stable footing for the antenna (diameter of the circular tracks: 22 and 41 m). (See Figures 3–28 and 3–29). The track beds are integral with the pivot through radial arms of reinforced concrete.

The foundations of the pintle, the track beds, and the wall are large sole plates an-

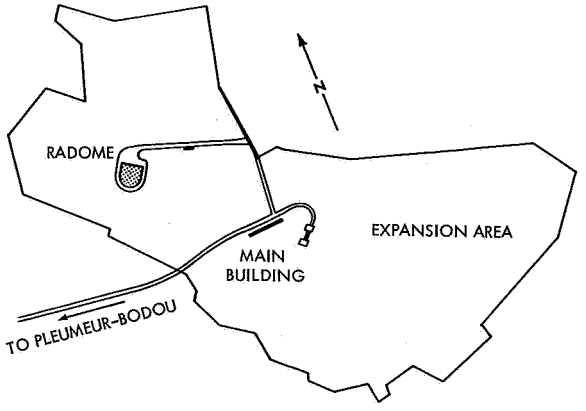


FIGURE 3–26.—General plan of the station.

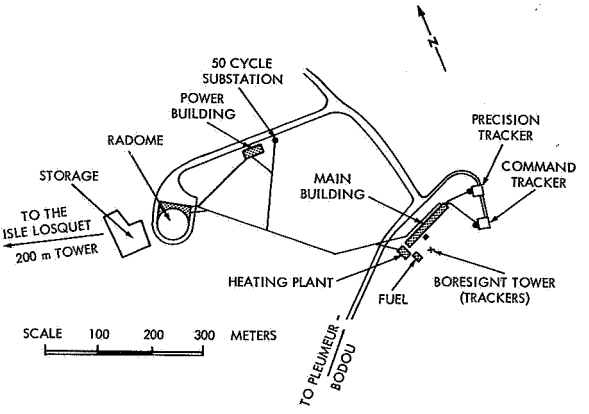


FIGURE 3–27.—Location of the buildings.

chored in 0.5 m of solid granite. Figure 3–30 shows the general appearance of the concrete structures.

The radome envelope is kept erect by air under a normal pressure of 3.8 cm of water; it can withstand winds up to 160 km/hr with the pressure raised to 14 cm of water.

A radome annex adjacent to the radome (500 m^2) contains the air locks, for both personnel and vehicles, and the following equipment:

1. The five blowers for radome inflation, with their emergency generator.
2. The electrical power switchboard.
3. The bay for the cables connecting the radome to the main building.
4. Equipment for chilling and circulating the cooling water (4°).
5. Heat exchangers supplying the 8 aerotherms for radome heating.
6. Storage for liquid helium and liquid nitrogen.

Main Building—Trackers

The two tracker antennas, located on a granite rise which is especially unobstructed, are mounted on concrete piles forming part of two small buildings. (See Figure 3–31.)

The main building is built at the foot of the rise and is a one-story building on one level. It has an area of 1500 m^2 (111 × 14 m). (See Figures 3–32 and 3–33.)

The two main parts of the building, the Equipment Room and the Computation Center, have special features. The floor is 30 cm from the ground and is made of (75 × 75 cm) movable sections of wood lath covered with plastic, supported by a metallic structure mounted on adjusting screws. The open space under the floor is used for cabling and for air-conditioning. The windows are fixed. A central air-handling system including two refrigerating units recycles the air through two supply and return systems; one serves the computation center and the other the equipment room.

Other areas of the main building are the commercial power room, the power switchboard, the batteries, the long-lines switchboard, the communications areas with the telephone switchboard and teletype sets, a storeroom, conference room, and offices for the engineers and the administrative services.

Near the central building is a very rigid 25-m tower (motion of the top less than ± 1.5 mm in winds of 120 km/hr) on the top of which are mounted the antennas for

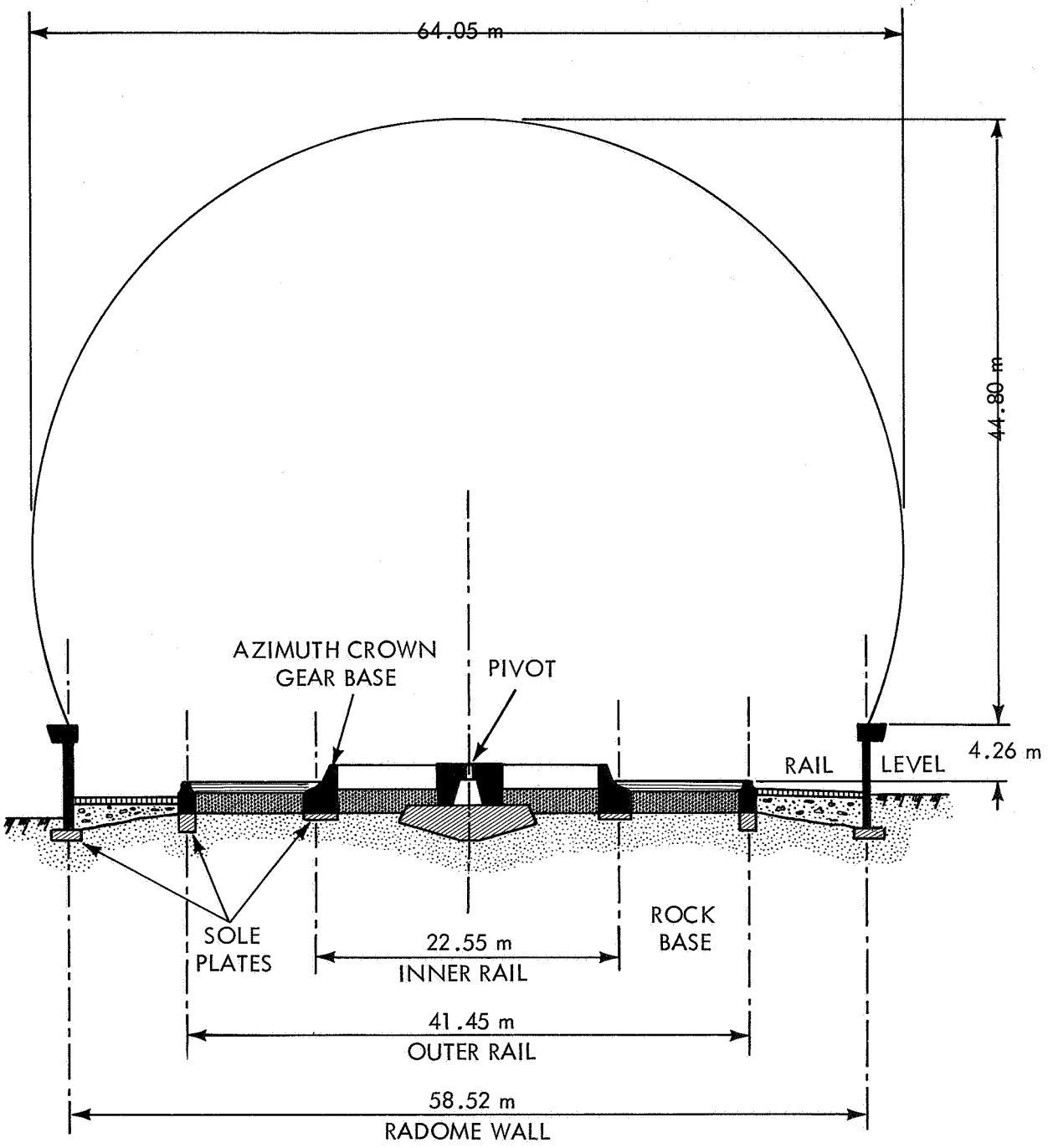


FIGURE 3-28.—Section of the radome foundations.

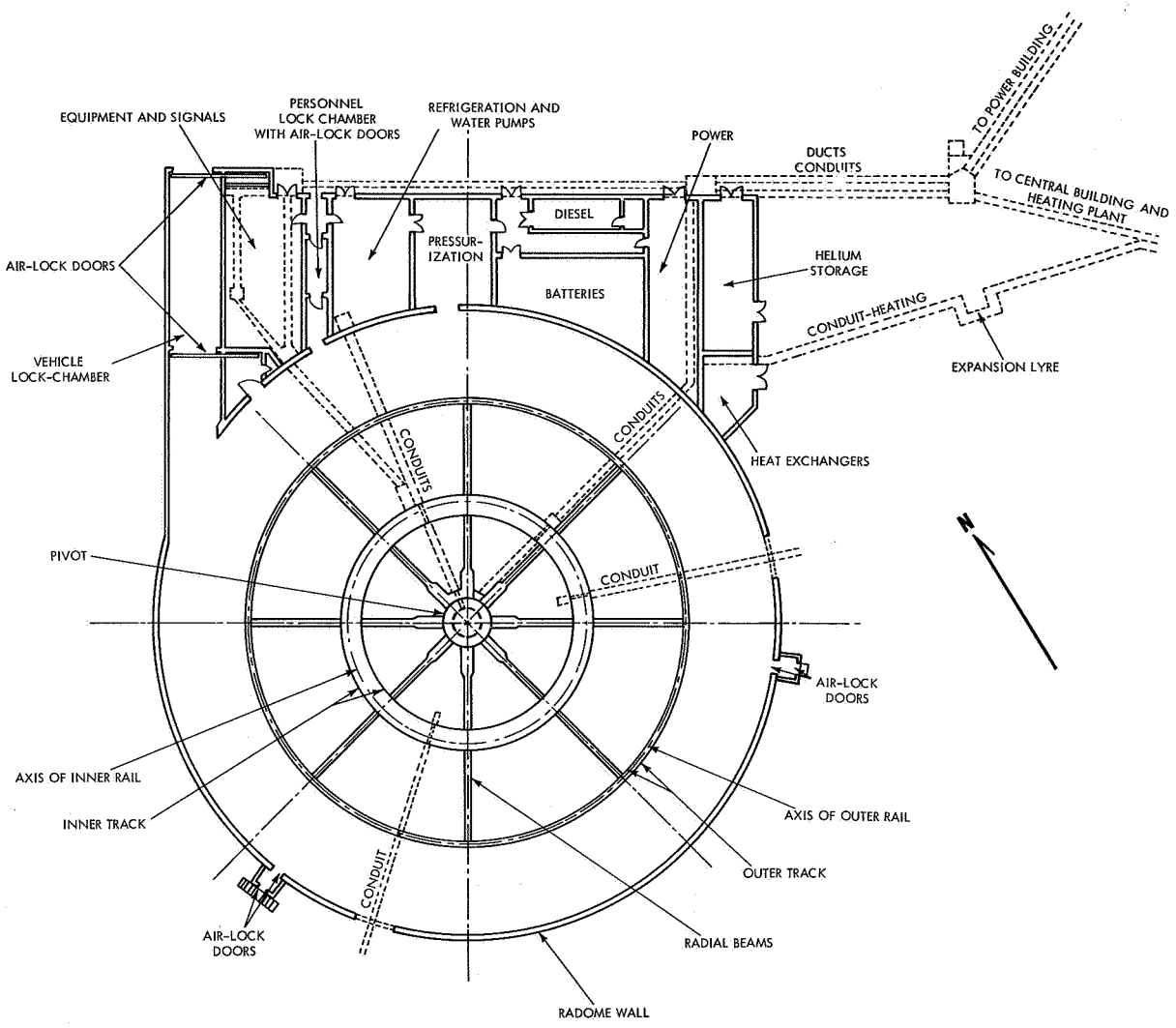


FIGURE 3–29.—Plan view of the radome and utility building.

testing the trackers as well as the anemometer which controls the inflation pressure of the radome.

Three poles support the antenna which receives the 18-kc signals for synchronizing the clock.

Power Building—Substation

The substation receives the two power supply lines from the national power network (see Figures 3–34 and 3–35).

The power building is 35 × 12 m, 5 m high. It contains essentially a 50-cycle substation, two 50/60 cycle converters, and four 60-cycle motor-generators. A 5-ton overhead crane is used in working on the motors.

Heating Plant

The heating plant (see Figure 3–36) is in a building 22 × 10 m, 6 m high. It contains two boilers providing superheated water under pressure (180°C and 10 kg/cm²)

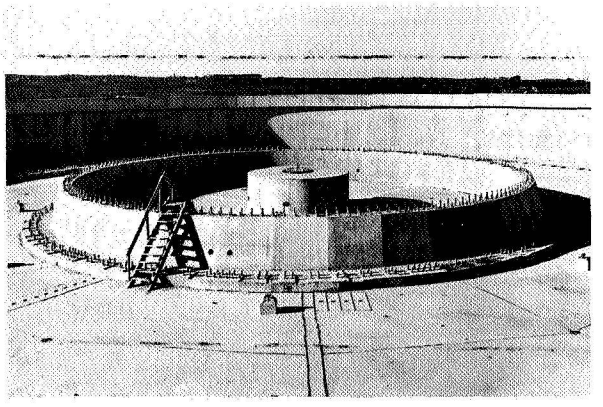


FIGURE 3–30.—General appearance of the concrete structure.

which is brought to the radome heat exchangers through a conduit 125 mm in diameter.

The power, 3×10^6 calories/hr., is ample to provide adequate heating in winter and to prevent accumulation of snow or frost.

External Conduits and Cableways

External conduits with special compartments connect the various buildings (see Figure 3–37); they are used by:

1. The medium and low-tension electrical power cables
2. The command, communication, and telephone cables
3. The water and heating pipes

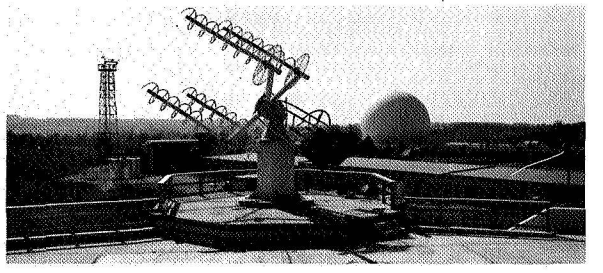


FIGURE 3–31.—Command tracker-boresight tower-main building.

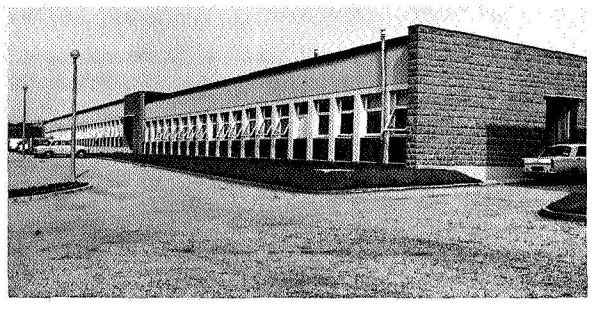


FIGURE 3–32.—Main building.

Suspended cableways connect the two tracker antennas, the test tower, and the main building.

Boresight Tower on Losquet Island

The satellite simulator (beacon and transponder) is mounted on a tower 200 m high situated on a small uninhabited island 6342

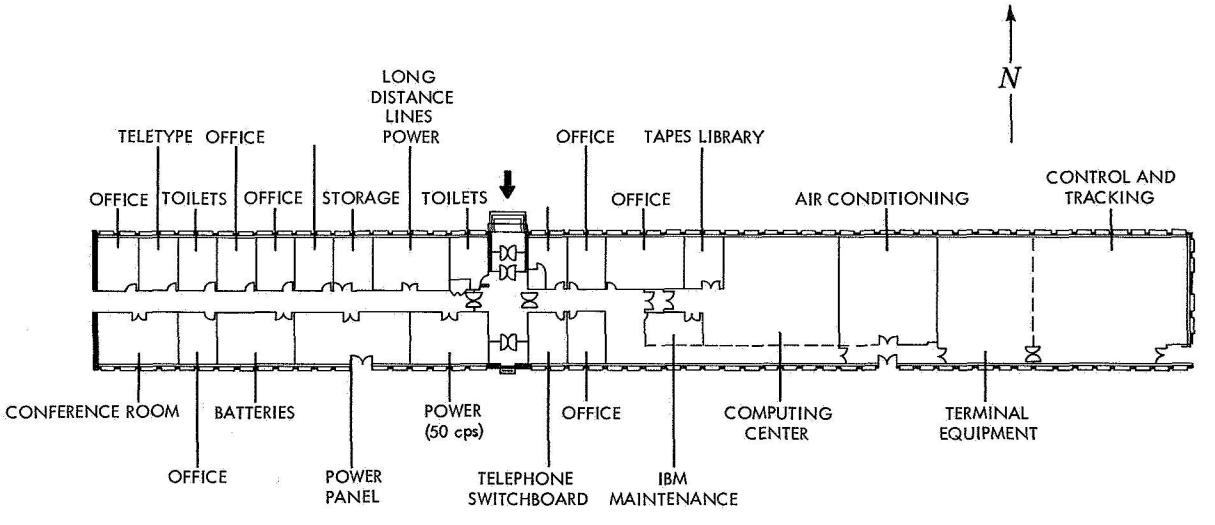


FIGURE 3–33.—Plan view of the main building.

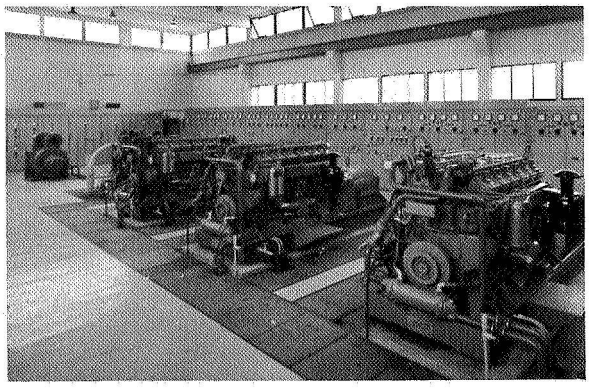
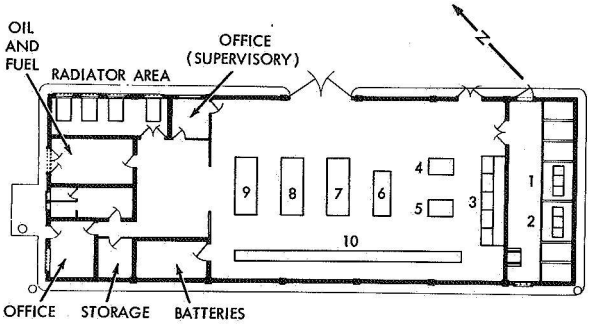


FIGURE 3–34.—View of the inside of the power station.



1,2 15,000/380-220 V - 630 KVA TRANSFORMERS
3 50 cps PANEL
4,5 50/60 cps CONVERTERS
6 GE1 - 60 cps - 75 KVA - EMERGENCY GENERATOR
7,8,9 GE2 - GE3 - GE4 - 60 cps - 250 KVA GENERATORS
10 60 cps DISTRIBUTION PANEL

FIGURE 3–35.—Plan view of the power building.

m from the center of the antenna (Figure 3–38). In this way it was possible to obtain an angle of 1.4 degree elevation for the direction from the axis of the horn antenna to the simulator.

The isolation of the island made necessary the installation of an independent power supply. The equipment on the tower is controlled and monitored by a radio link.

Service Communications

Teletype

Three semi-duplex units with tape perrators provide links with:
—the NASA network through London

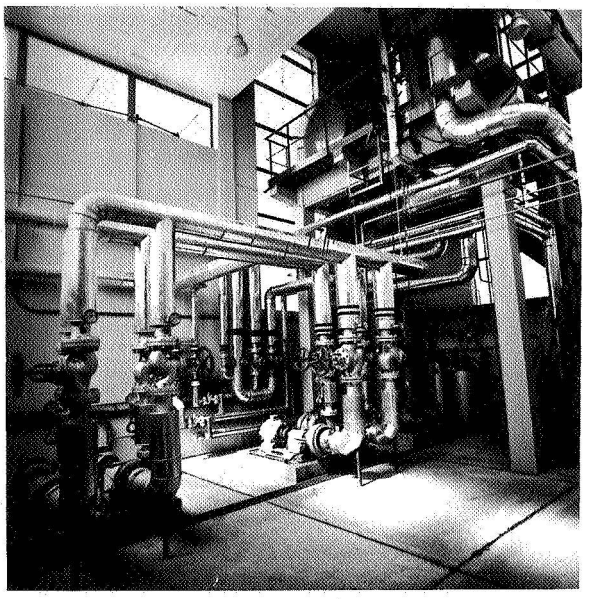


FIGURE 3–36.—View of the heating plant.

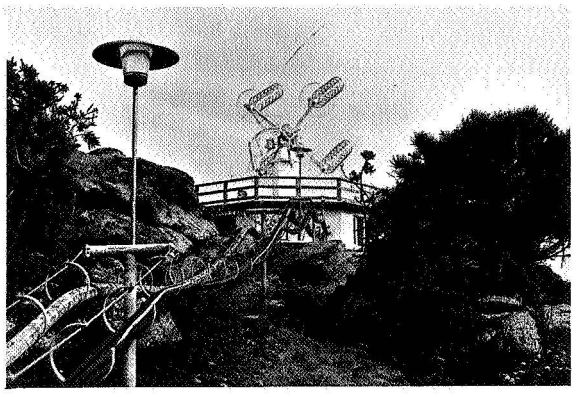


FIGURE 3–37.—External cableways.

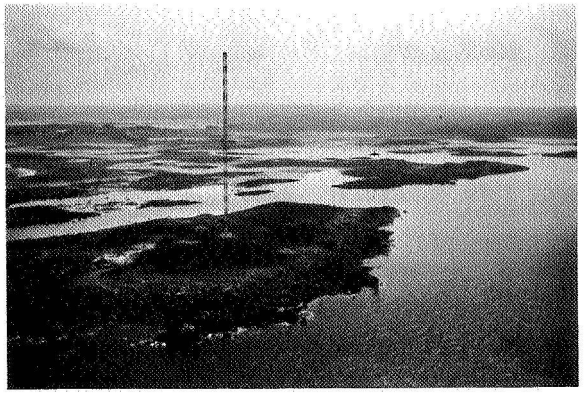


FIGURE 3–38.—Boresight tower on Losquet Island.

—BTL at Andover
—the French Telex network

Telephone

The telephone switchboard is connected to the French network and has direct lines to CNET in Paris, to Goddard Space Flight Center of NASA, and to the Andover earth station. An automatic internal system serves the entire complex.

ELECTRICAL POWER SYSTEM

The electrical power system (see Figure 3–39) is fairly complex because of the existence of two feed frequencies (50 and 60 cycles) and because of the requirements of reliability and quality imposed by the electronic equipment.

50 Cycle Alternating Current

The 50 cycle power from the national network is brought in on two medium-tension 15,000 volt lines, one normal and one standby, terminating at the substation. Since the main building is over 500 m from the power building, it was decided to install transformers at both locations. These units, of 630 and 1260 kva capacity respectively, provide the 220/380 v supply. They are supplemented by two voltmeter-balanced induction regulators which supply a voltage regulated to ± 2 percent for the electronic equipment of French origin.

60 Cycle Alternating Current

Power Supply for Radome Inflation

In the power building, two 50/60 cycle converters provide the normal power on two lines, one a spare. An emergency diesel generator (GE 1, 75 kva) starts automatically in case of failure of the normal power. A second spare generator (GE 5) of the same power is located in the radome utility building.

60 Cycle General Supply, 272/470 V

Three diesel generators in the power building provide continuous power. These units (GE 2, GE 3, and GE 4), are of 250 kva capacity. In normal operation the power is supplied by GE 2 or GE 3, which are started manually, with GE 4 started automatically as a spare. At critical periods GE 2 or GE 3 is coupled in parallel with GE 4.

The frequency tolerance of ± 1 percent is obtained by a speed regulator of the wattmeter type. The generators have a voltage regulator controlling the voltage to ± 1 percent.

The power is distributed to the radome by two separate special circuits (one for motors and one for electronic equipment), and to the main building where two transformers reduce the voltage to 120/208.

60 Cycle Special Supply

Certain elements of the antenna require a continuous power supply at 230 v, 60 cycles, single phase, with the ratio of sub-harmonics less than 0.5/1000. Two 60/60 cycle converters operating at 1800 rpm, with a capacity of 8 kva, provide this supply. They are started automatically. One unit is supplied from the 60-cycle current provided by the 50/60 conversion and the other from the 60-cycle general supply. At critical times both units are in operation, one under load and the other unloaded as a standby; the load can be transferred automatically in less than 0.25 second.

Antenna Power Supply

The power for the rotating structure is carried through the 28 power slip rings of the pivot. The neutral of the three-phase ac current is omitted, which does not affect the motors but requires a 45 kva transformer in the lower cabin for the single-phase circuits.

420–400 Cycle Supply

In the antenna there are two 0.3 kva units which supply a single-phase, 120 v, 420 cycle ± 0.25 percent current to the servo loops of the antenna.

In a small building near the main building are two units which provide 400-cycle ± 2 percent current at 120/208 v for the trackers.

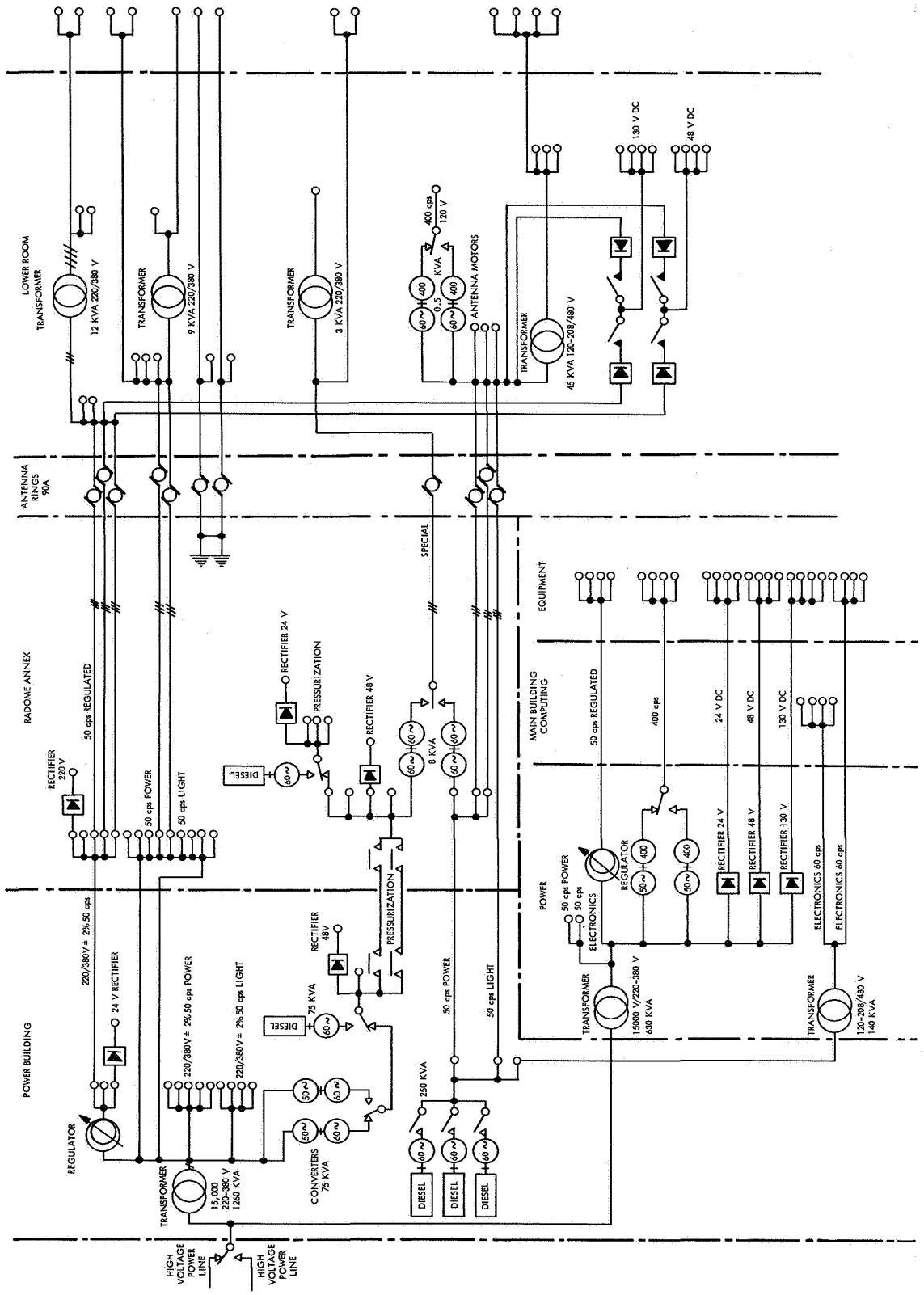


FIGURE 3-39.—General diagram of electrical installation.

Direct Current Sources

Two batteries in the main building supply the station clock and the telephone central with direct current at 24 v ± 5 percent with 1/1000 degree filtering.

One battery in the main building and two rectifiers in the antenna lower room supply 130 v ± 4 percent, 1/1000 filtering, for electronic equipment.

Telephone Equipment Power Supply

The telephone terminal equipment of the main building is served by a special system (battery-standby generator-switchboard) of the standard type for long lines equipment.

Boresight Tower on Losquet Island

An independent power supply is provided for the boresight tower equipment. It consists of continuous single-phase 220 v 50-cycle current provided by three generator sets rotated in service daily. A battery supplies the switchboard and the RF monitoring equipment. The battery can also provide emergency power for the tower light beacons.

CONCLUSION

The Pleumeur-Bodou station has operated practically without failure for all passes where its participation was called for. Operation of the station has enabled CNET to acquire, in addition to the experimental results, valuable experience in the characteristics of operation of such a new and complex system. It has afforded full justification for the decision of the CNET to equip the first French ground station with complete facilities.

The CNET has in this way gained a solid background for future operations with a commercial satellite communications network and for developing the present station into a fully operational one.

AUTHOR. *This chapter was contributed by* M. J. DAUTREY, *Centre National d' Etudes des Telecommunications (CNET), Issy-les-Moulineaux, France.*

N66-10254

Chapter 4

Results of Tests Performed with Relay I at the Pleumeur-Bodou Space Communications Station

10254

A description is given of the tests performed at the French satellite communications station at Pleumeur-Bodou with the Relay I satellite.

An analysis is given of the means for acquiring and tracking a satellite and of the characteristics of the resulting communication link. The tests were extremely satisfactory and provided the experience necessary for the commercial exploitation of future satellite communication links.

INTRODUCTION

Tests were performed at the Pleumeur-Bodou station using 123 passes of the Relay I satellite covering the entire period from the beginning of its operation to the time of writing. Acquisition and tracking tests were performed for the purpose of studying the various ways of using a large antenna for these functions, and the good and bad features of the communication link established through the satellite were determined.

The tests which will be described in this paper have shown that the operation of the station was perfect, and that the quality of the link was extremely satisfactory. It will be seen that it has been possible to determine the optimum characteristics and the operating limits of each of the station subsystems and to acquire the necessary experience for the exploitation of future satellite communication links. It has been shown that such links are technically feasible at the present time.

ACQUISITION AND TRACKING TESTS

During the first year of operation of the Relay I satellite, namely from 14 December 1962 to 14 December 1963, the Pleumeur-Bodou space station made use of 123 passes of the satellite, corresponding to 46 hours of transatlantic traffic. The links used for tests, whether communication tests or technical tests, were never interrupted or delayed because of a failure of equipment or personnel, of the antenna drive, or of the communication equipment.

For the entire group of satellites Relay I, Telstar I, and Telstar II, the percentage of time during which satellite tracking was successful reaches 99.5 percent for a total number of passes of 315, corresponding to 126 hours of operation. It should be noted that this figure includes the first hours of space communications, which must from many points of view be considered part of an experimental period. No disabling equipment failure occurred during any pass.

The primary purpose of the antenna drive is to keep the horn reflector antenna pointed accurately in the direction of the satellite in order to permit the transmission of communications of related tests. Accordingly, particular efforts were made, during those passes used, to establish the acquisition ca-

pabilities of the various types of equipment and their capacity to maintain contact with the satellite in the various modes of operation. On the basis of the results of these observations, we made a few alterations or additions to the equipment.

It should be kept in mind that the antenna drive equipment, except for the 136-Mc telemetry and command equipment which we will call the "command tracker," was built by CNET from components provided by Bell Telephone Laboratories and is identical to the equipment used at the Andover station.

We will analyze in turn the various subsystems shown in the block diagram of Figure 4–1.

Tests With the Command Tracker

Tracking Tests

The tracking equipment receives the signal from the satellite beacon which is transmitting on a frequency of about 136 Mc. In the case of Relay I, only the 136.14 Mc frequency was used from the first day.

It is noteworthy that despite the change in polarization characteristics of the satellite signals as a function of the look angle of the spin axis, no major difference in tracking performance was found with respect to the performance with Telstar I.

The many measurements made showed that the satellite could be acquired at the moment of its apparent rise above the horizon. Allowing for the refraction phenomena at elevations causing the first beacon signals to be received at geometric elevations from —0.5 to —1.0 degree, and for the time required for frequency lock of the receiver, it is still possible to drive the antenna in the automatic tracking mode for elevations below 2 degrees. This was even achieved on the day of launch, when on the third pass (with no mutual visibility with the U.S.) we were able to track the satellite at elevations below 5 degrees and to verify that the levels of the signal radiated by the satellite were satisfactory.

Nevertheless, because of ground reflections and the beamwidth of the antenna (20 de-

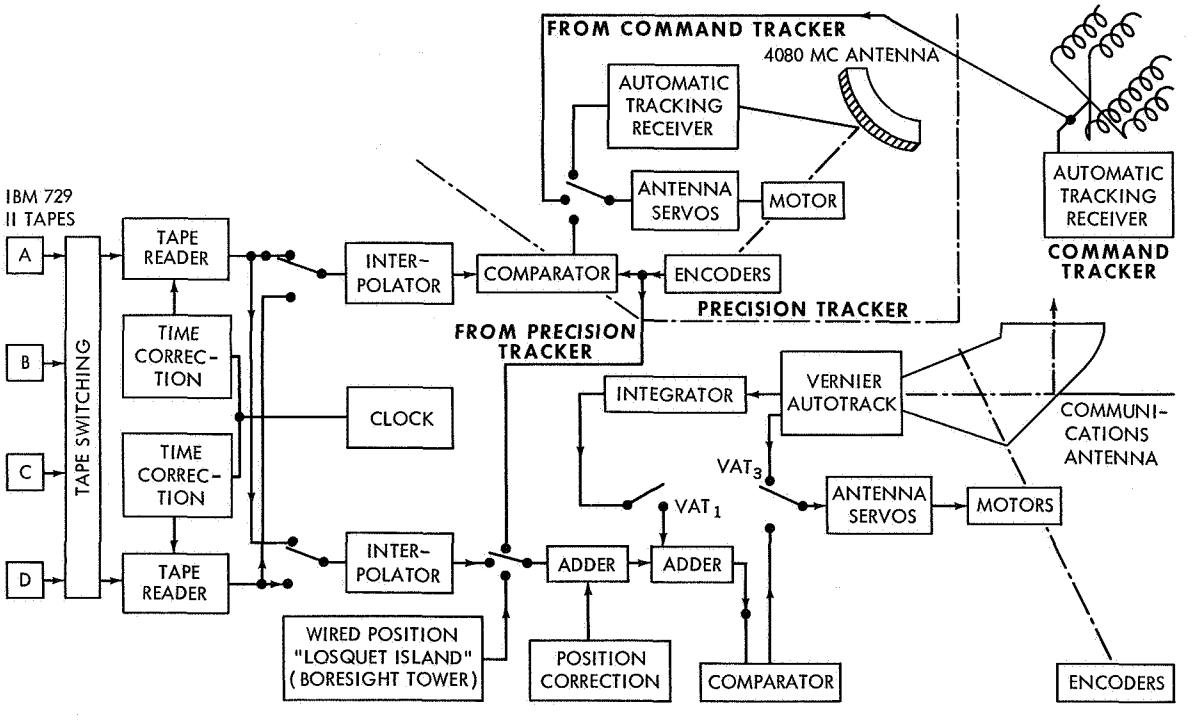


FIGURE 4–1.—Antenna drive—functional block diagram.

grees at 3 db), there are significant errors in the position information provided by the equipment encoders and the actual position of the satellite. These errors are most in evidence in elevation for angles below 20 degrees; the rapid fluctuations of the antenna may reach ±5 degrees, although the automatic track still does not lose lock. For higher elevations the pointing accuracy improves, reaching ±1 degree at 40 degrees. The azimuth information is only slightly affected by reflections, but because of the dimensions of the antenna and its mechanical structure, errors of about 2 degrees may occur as a result of wind gusts above 60 km/hr. Because of the very open site of the antenna, these wind speeds were observed fairly often during the winter of 1962–63.

Figure 4–2 is a reproduction of the recording of one tracking operation. During this pass the S/N ratio was 25 db and the wind speed 50 km/hr. This recording was made with the tracker encoder group of the precision tracker. With the precision tracker slaved to the command tracker, the position data from its encoders is compared at each instant to the precomputed tape for this pass. The validity of the tape data is continuously verified by the position information from the horn-reflector antenna tracking the 4080 Mc beacon. In addition, at the 15 degree, 20 degree, and 30 degree positions a check was made by transfer of the precision tracker to automatic tracking.

As indicated by the above results, the use of the command tracker for acquisition of the satellite by the communications antenna was limited to confirming the presence of the satellite and the time of its rise. The accuracy of the precomputed tape positions was, as will be seen later, greater than that of the tracking by the command tracker.

Telemetry

Telemetry data from Relay I was always correctly received and all the recorded magnetic tapes could be decoded without difficulty. Time information conforming to the NASA 36-bit time code was recorded on one track of the tape from a time encoder built at the station. When used with a decoder, this equipment makes it possible to know at each moment the state of the various satellite subsystems. The code is reproduced in Figure 4–3. The quality of the data would have permitted its use for surveillance of the satellite during the various command cycles.

Tests Performed With the 4080 Mc Precision Tracker

Acquisition

The acquisition of the 4079.73 Mc satellite beacon by the precision tracker is effected in two steps: a) acquisition in position; b) acquisition in frequency.

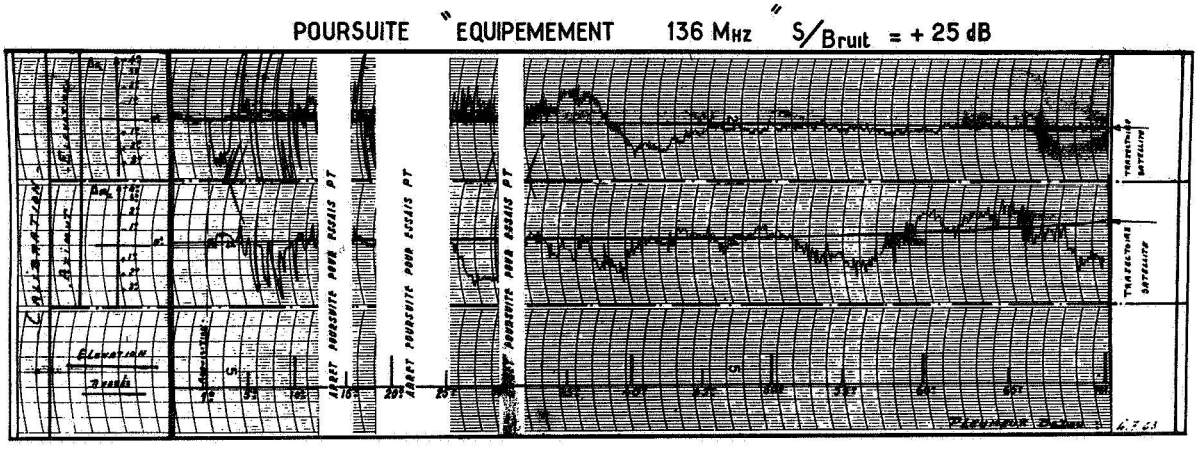


FIGURE 4–2.—136 Mc tracking—S/N = +25 db.

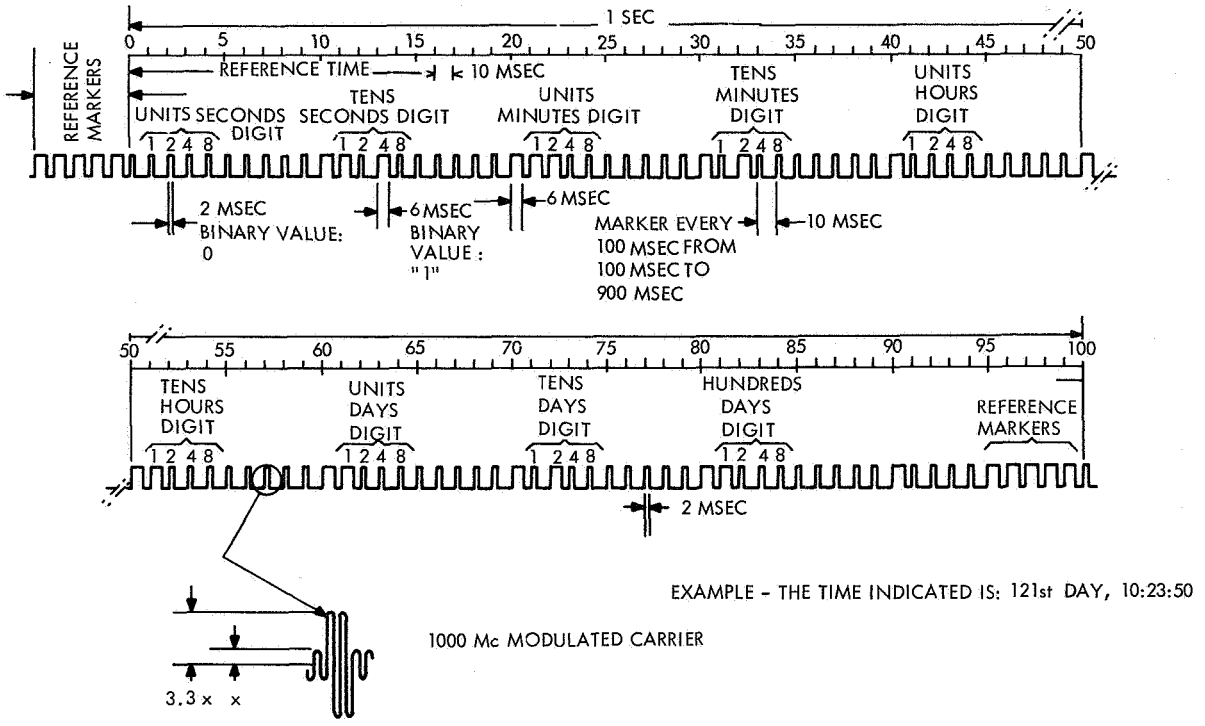


FIGURE 4–3.—NASA 36 bit time code.

Acquisition in Position—This acquisition is considered completed when the pointing of the antenna corresponds to the actual position of the satellite to within 0.5 degree. Since the 3-db beam-width of the antenna is 2 degrees, a pointing error of 0.5 degree corresponds to a loss of 1 db in the link.

Several series of tests were carried out with a view to adapting the method of acquisition to the circumstances and to the training of the operators.

It became apparent that the problem is not the same when the beacon is radiating at the time the satellite rises above the horizon as when acquisition is made at nonzero elevations. In the first case, acquisition can be effected in one of two ways:

1. By the use of precomputed magnetic tapes driving the azimuth and elevation motors through the tracking encoder; this method can be used when the time and position information provided are considered accurate.

2. By manually positioning the tracker antenna in elevation at 0 degree by using a slow, small-amplitude (about 2 degrees) sweep in azimuth about the calculated position. This method has the great advantage of virtually eliminating the time parameter for acquisition, since a trajectory which is correct but slightly shifted in time still permits successful acquisition.

It should be noted that acquisition by slaving to the command tracker was not used. In the event that there is any doubt about the pointing information, the presence of the satellite is confirmed by the command tracker, so that any gross error is avoided.

In the second case, where the beacon is not radiating when the satellite rises, acquisition is effected by slaving the precision tracker to the precomputed tapes, with a search in azimuth and elevation about this position.

Some tests were carried out with the precision tracker slaved to the command tracker, but because of the rapid variations of about ± 5 degrees it was not possible to obtain satisfactory results for elevations below 20

degrees. On the other hand, for elevations near or above 30 degrees, a trained operator may effect acquistion by this mode of operation.

It should be added that in practice the 4080 Mc beacon is always radiating at elevations below 20 degrees.

Acquisition in Frequency—When the satellite has been acquired in position, the automatic frequency control oscillator of the 4080 Mc tracking receiver must be locked in phase. Depending on the level of the received signal, this operation is automatic and nearly instantaneous, or else it requires the intervention of the operator. Taking into account Doppler effect, thermal drift of the beacon, or any other perturbation within the satellite, the range of frequencies within which the beacon frequency is found may be 150 kc about the nominal value.

The automatic method, making use of the 300-output comb filter, can in practice be used for received powers at the parametric amplifiers of −139 dbm, corresponding to a S/N ratio of +2 db for the receiver circuit used. This mode of acquisition was always used for Relay I, for which the range at acquisition varied from 5000 to 12,000 km, corresponding to received signal levels of −125 dbm to −132 dbm.

In cases of lower signal levels (Telstar II), it is necessary to have recourse to a systematic manual acquisition which consists of setting the 3-kc bandwidth channel of the receiver on the frequency received. Taking account of the Doppler frequency data supplied by the computer center, one can make a small-amplitude search about the predetermined frequency and at the same time make an auditory analysis of the beat signal; in this way it is possible to effect acquisition for S/N ratios in the 3-kc band as low as −8 db. As soon as frequency acquisition is achieved, the phase locking of the oscillator reduces the equivalent pass band to 100 cps, reducing the noise level to −151 dbm.

It should be noted that the frequency of the 4080 beacon appeared to vary, after allowance for Doppler shift, from 4079.730 Mc to 4079.750 Mc for different passes, making a variation of from 0 to +20 kc with respect to the nominal frequency. These deviations were noticeable especially during the first six months.

Another fact of interest is that with allowance for refraction at 4080 Mc (discussed indetail on page 610) final acquisition allowing transfer to automatic tracking by the precision tracker is achieved almost certainly for geometric elevations below 2 degrees for any of the methods used, whether automatic or manual, always assuming that the beacon is radiating when the satellite rises.

Tracking

Once the satellite beacon is acquired, the accuracy with which it will be tracked is a function of random variations in the tracking and of systematic errors resulting from mechanical imperfections of the system.

Random Errors—Random tracking errors are a function of both the elevation above the horizon and the S/N ratio in the receiving channel after phase lock. The direction of the received signal is much less subject to perturbations that the command tracker. Since the width of the antenna lobe is 2 degrees, ground reflections are appreciably reduced at low elevation angles. The accuracy is thus about 0.2 degree for elevations below 2 degrees. For higher elevations this accuracy improves rapidly until at 3 degrees it depends only on the S/N ratio.

The fluctuations due to ground reflections were detected by recording on magnetic tape the output data from the position encoders and comparing it to the theoretical path. Measurement of tracking characteristics for elevations above 3 degrees was carried out through the use of the horn reflector antenna associated with its vernier autotrack. These tests were made by taking advantage of the fact that the precision of the angular measurements of the horn reflector antenna is clearly greater than that of the precision

tracker. This difference reflects the larger dimensions of the horn reflector antenna and the fact that the S/N ratio in the receiver channel of the vernier autotrack system is always 10 db better than that of the precision tracker. On the other hand, the overall position response characteristics of the two systems are essentially comparable in the zone used.

With the horn antenna slaved to the antenna of the precision tracker through the encoders and digital equipment, the angular deviation between the pointing of the precision tracker antenna and the true position of the satellite is measured at each instant by the vernier autotrack circuits operating in open loop (see Figure 4–4).

Figure 4–5 reproduces recordings made with S/N ratios of 27 and 12 db for a servo noise bandwidth of 0.2 cps. Analysis of these results yields an rms noise

$$10^{-4} \text{ radian for S/N} = 27 \text{ db}$$
$$3 \times 10^{-4} \text{ radian for S/N} = 12 \text{ db}$$

In the case of Relay I the S/N ratio varied essentially between 27 and 20 db. It should be noted that these measurements include thermal noise as well as the resolution of the encoders (0.5×10^{-4} radian) and the mechanical errors about the given position.

We have also shown in the same figure recordings made during the same passes of the vernier autotrack output errors with the vernier autotrack operating in closed loop.

Systematic Errors—Systematic errors may result from imperfections in fabrication, from wear of the elevation and azimuth drive mechanisms and their associated encoders, or from variations in the setting of the antenna base. The only systematic checks of the base were those of level; these showed a piling up of the foundations over the first

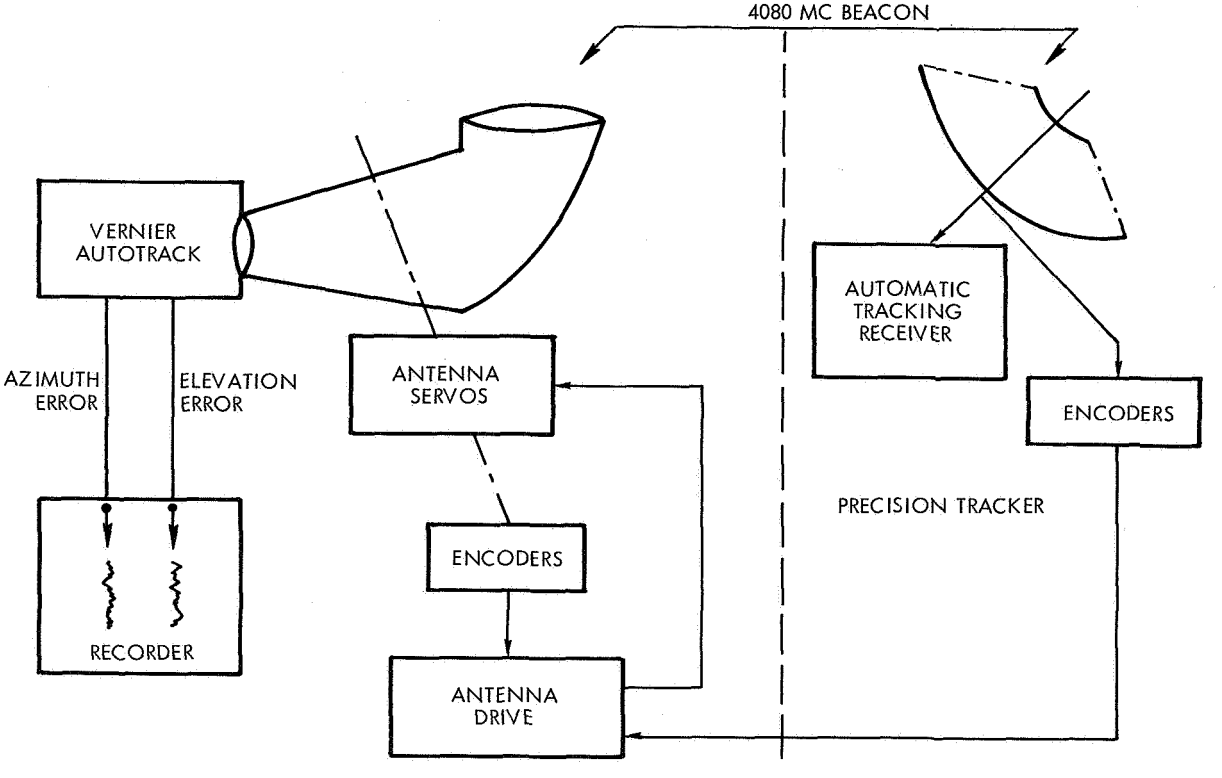


FIGURE 4–4.—Horn reflector antenna.

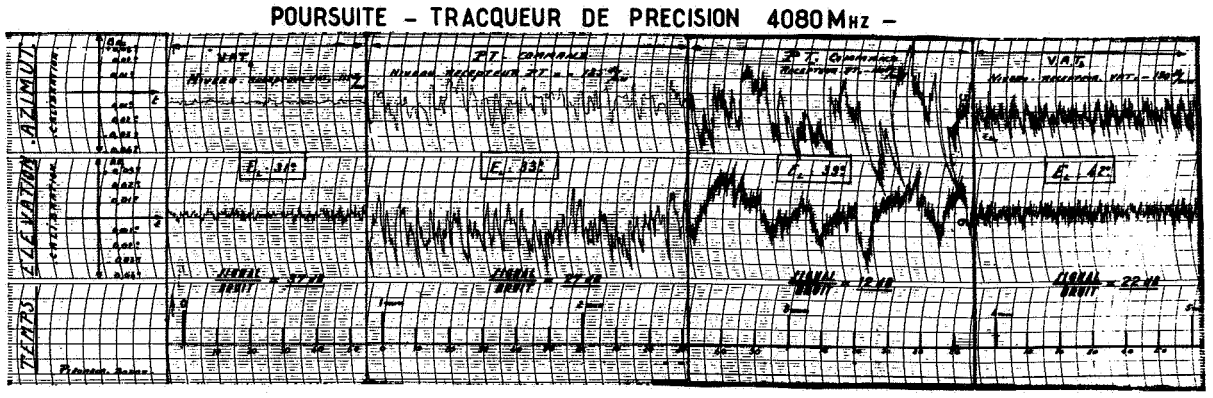


FIGURE 4–5.—4080 Mc precision tracker recording.

three months, leading to an angular variation of the reference plane of 0.015 degree. The monthly measurements presently being made do not require any adjustments of the base.

Optical sightings on the North Star have shown that the calibration of the encoders was correct to within ±0.01 degree about this position. In any case, we were not able to detect any systematic errors of consequence in relation to variations in azimuth and elevation during the passes we examined.

Utilization

For all the operational passes used at the station, the precision tracker was put into operation. The reliability and accuracy of this unit, together with its relatively wide field of acquisition (beamwidth of the antenna together with the search about the computed position), led us to consider it an element of operational reliability even though not essential to the satisfactory conduct of operations.

The data acquired and recorded on magnetic tape during the passes was not used in a systematic fashion for the determination of orbital parameters. It should be noted that the average length of passes, including the acquisition phase, was 20 minutes.

In order to facilitate use of the equipment and to reduce the operating personnel of the station, we installed the main controls of the tracking encoder group in the console of the precision tracker operator.

Information on the difference between the position commanded by the tape and the pointing of the antenna was displayed on the central console of the station. This information, shown on a meter after conversion into analog form and amplification, enables the chief of operations to know this difference to within 0.01 degree. A time correction adder identical to that used in the antenna drive group in the lower cabin under the radome permits time corrections to be made on the tape associated with the tracking encoder. This arrangement makes it possible to use the error indications provided at the central console to optimize the time and position information of the tape driving the horn antenna and thus facilitates establishment of the link.

A computer device which can be inserted between the precision tracker and the antenna drive group was designed and built at the station; this device makes possible correct pointing of the RF beam carrying the communication information despite any deformations of the antenna, when the horn antenna is directly slaved to the precision tracker antenna through the encoders. The principle of operation of this device will be described on page 610. The diagrams of the digital positioning circuits of the precision tracker antenna and of the communications antenna are shown in Figures 4–6 and 4–7.

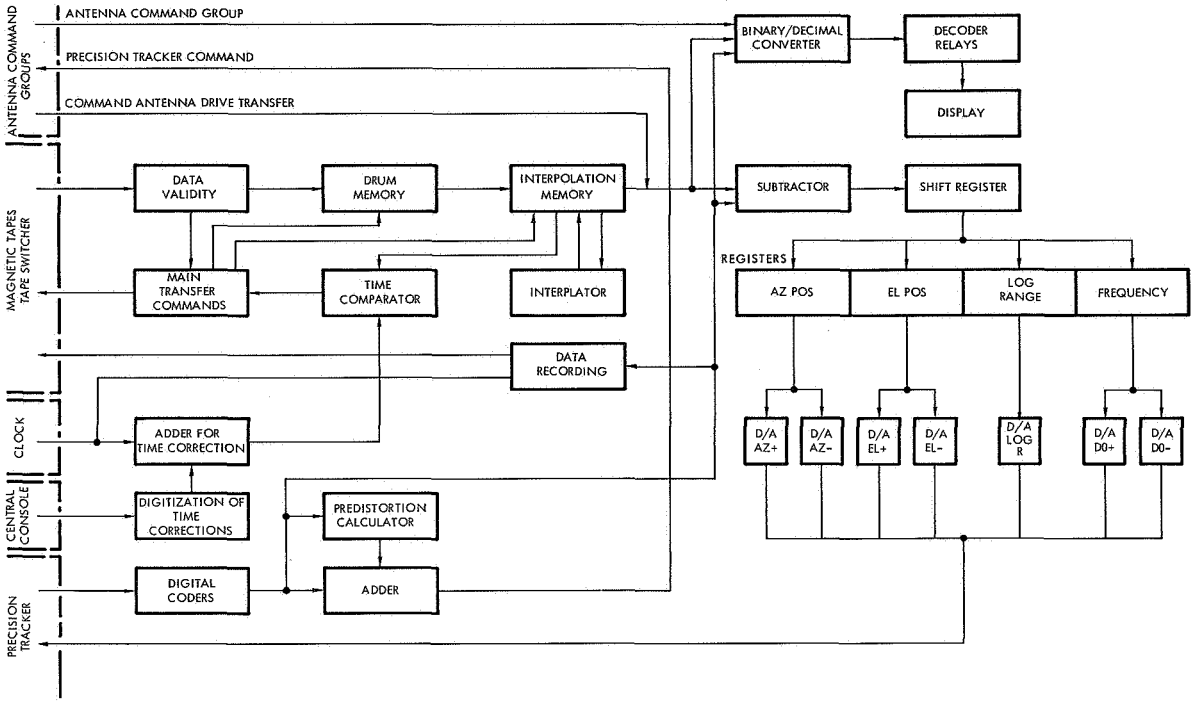


FIGURE 4–6.—Block diagram of precision tracker digital positioning.

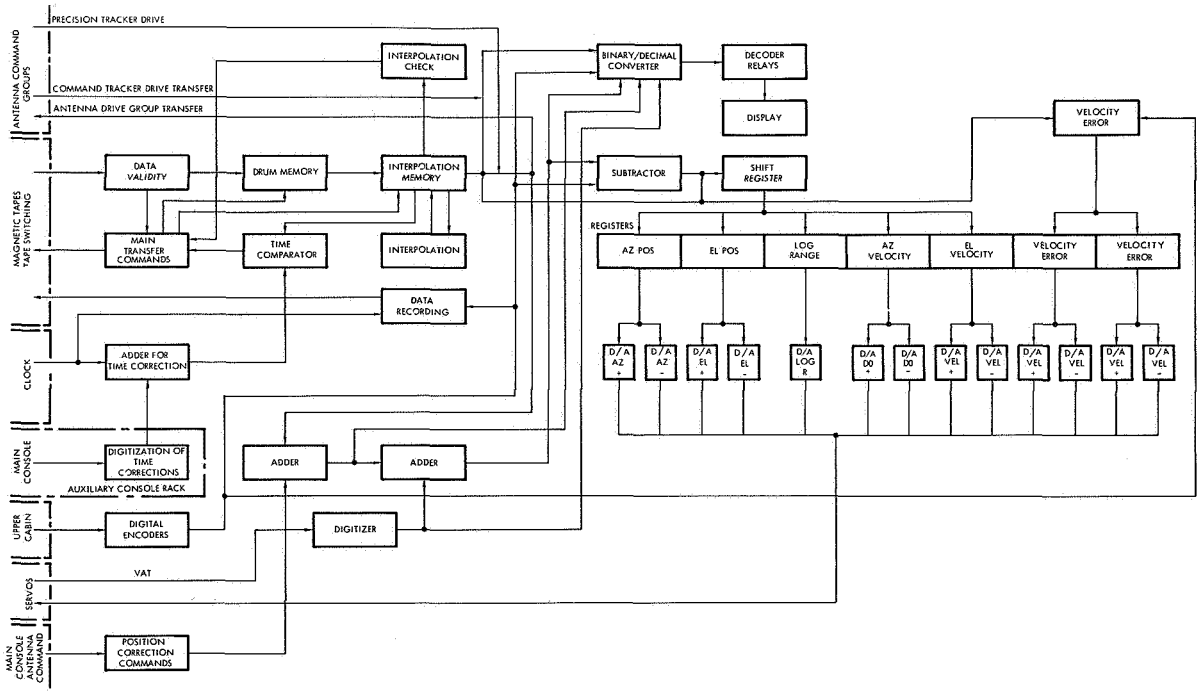


FIGURE 4–7.—Block diagram of communications antenna digital positioning.

Tests With the Communications Antenna

Tests made with the communications antenna concerned the various possible modes of acquisition and tracking, involving measurements of the characteristics of the antenna itself in relation to the particular conditions in which the mission is being carried out. We made studies of the following types:

- Radiation patterns of the horn reflector antenna in the reception band for communications centered on the normal 4169.72 Mc frequency and the 4079.73 Mc vernier autotrack frequency.
- Azimuth errors as a function of elevation.
- Refraction at low elevations.

Tests were also performed to determine the slant range of the satellite from the communication antenna.

Antenna Patterns

These tests were performed in order to determine the secondary lobes near the antenna and to verify that when the satellite is being tracked with the vernier autotrack, the pointing corresponds to the maximum of radiation at the communications reception frequency.

These measurements were performed while the satellite signal was being received at antenna elevations between 15 and 25 degrees. These values are a good compromise, permitting virtual elimination of ground noise so that the full sensitivity is available for measurements; the "cone effect" is negligible for the pattern measurement. It was not possible to take these patterns using the simulator on the boresight tower, because the angle at which the horn reflecter antenna sees the simulator is 1.35 degrees and ground effects are not negligible at this angle.

Method of Measurement—The satellite is illuminated by an auxiliary station radiating a pure frequency. At Pleumeur-Bodou the communications equipment receives the 4170 Mc frequency and the auto-track equipment receives the 4079.73 Mc beacon frequency. Because of the output power of the Relay I TWT, which provides a signal level at the maser input of —84 dbm at a range of 6000 km, we could reduce the receiver bandwidth to 700 kc, corresponding to a noise level of —126 dbm for a noise temperature of 30.5°K so that the patterns could be taken at —42 db with respect to the maximum radiation.

The tracking of the satellite is performed by magnetic tape. Correction for the relative deviation between the position of the satellite and the pointing of the antenna is made by insertion of position corrections in the antenna drive system. The tape is first checked to see that it is correct; if not, fixed position and time corrections are made to cause the actual and computed trajectories to coincide. This is a dynamic test, with the received signal levels recorded continuously. The position change (error) signals are applied at a constant rate of 0.6576 degree/minute in the area of the radiation maximum; more distant (2 to 10 degrees) radiation is measured at the rate of 42 degrees/minute. The received signal levels in both the vernier autotrack and communications channels are detected by means of the previously calibrated AGC level; the zero of the vernier autotrack corresponding to the pointing direction in automatic track is obtained by recording the "errors" in the azimuth and elevation channels. Relative variations in distance on the order of 0.01 per minute are neglected during the test. The power radiated by the satellite is assumed constant over the duration of a pointing movement.

After each pattern is taken, the zero level at the radiation maximum is taken again. The accuracy of measurement which depends on the precision calibration of the recording and on the accuracy of reading the recording, is on the order of $\pm$ 0.25 db.

Results—Figures 4–8 and 4–9 show the patterns obtained for the communications frequency. Pointing varied from — 10 to + 10 degrees from null; only those angles for which the received signal level is detectable are plotted. Several sets of measure-

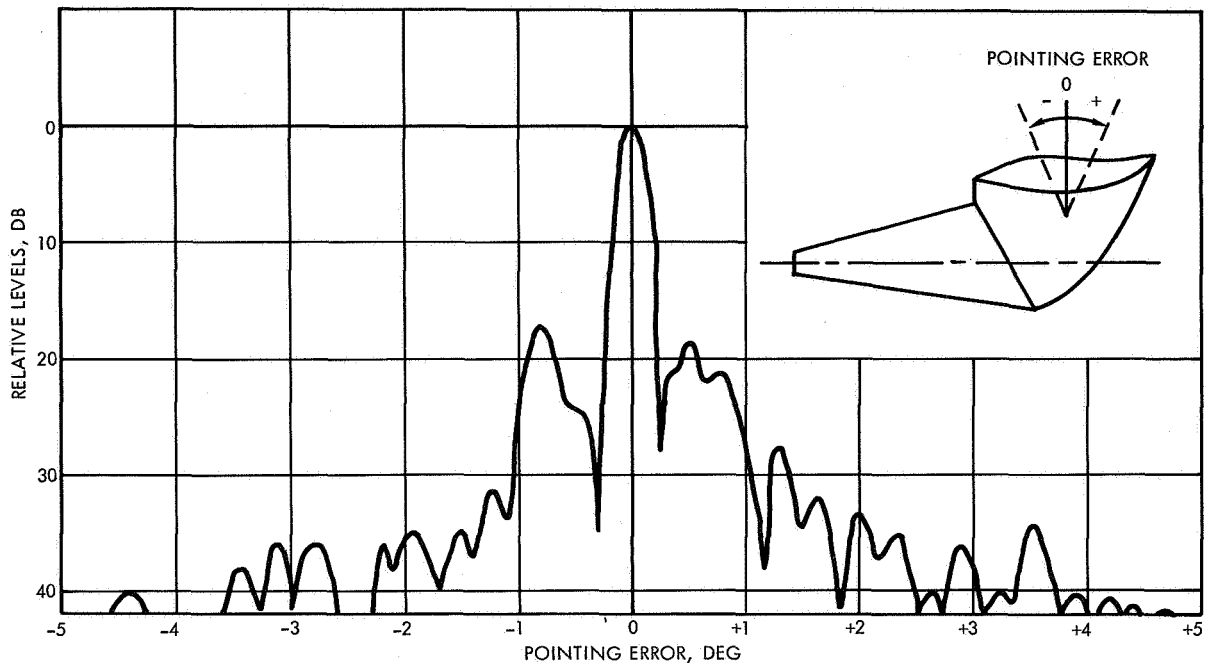


FIGURE 4–8.—Radiation pattern, azimuth plane—communications antenna.

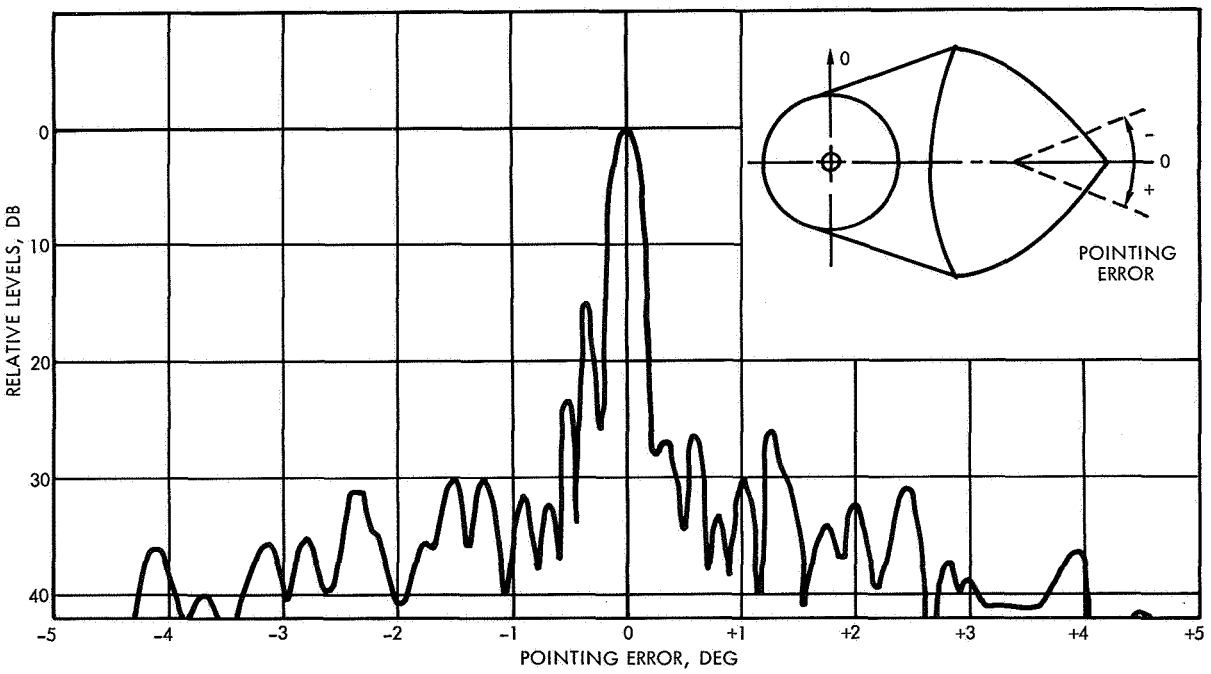


FIGURE 4–9.—Radiation pattern, elevation plane—communications antenna.

ments have permitted establishment of half-power widths.

a. Elevation variable, zero azimuth pointing error. Allowing for the recording and readout accuracy of ± 0.25 db, the beamwidth for three different tests was found to be:

$$0.208 < 3 \text{ db BW, deg} < 0.225$$
$$0.208 < 3 \text{ db BW, deg} < 0.23$$
$$0.205 < 3 \text{ db BW, deg} < 0.225$$

Taking the mean value, we obtain

$$3 \text{ db beamwidth} = 0.215 \text{ degree}$$

b. Azimuth variable, elevation pointing error zero. As above, for three different tests we found:

$$0.235 < 3 \text{ db BW, deg} < 0.25$$
$$0.235 < 3 \text{ db BW, deg} < 0.25$$
$$0.241 < 3 \text{ db BW, deg} < 0.26$$

The mean value is:

$$3 \text{ db beamwidth} = 0.245 \text{ degree}$$

Comparison of the commanded null of the vernier autotrack with the maximum radiation shows that within the accuracy of measurement these two points coincide. Figure 4–10 shows the patterns as seen by the x and y channels of the vernier autotrack. The range of measurement was limited to 15 db by the signal strength and sensitivity of the equipment.

The patterns taken at the 4080 Mc frequency differ appreciably from those taken at 4170 Mc. This difference corresponds to a slight misadjustment of the hyperfrequency circuits, involving inadequate decoupling of the TM01 and TE11 channels. The low amplitude of this perturbation affects in no way the overall operation of the system.

Study of Azimuth-Elevation Coupling

After the first month of operation of the station, it appeared that there was a systematic azimuth error when the elevation was above the horizon. A verification test performed by calibration on the stars indicated an error of about 0.20 degree for an elevation of 62 degrees. A series of measurements was then taken to plot the curve of azimuth-elevation coupling, with a view to introducing a distortion correction in the drive tapes of the communications antenna.

The method used consisted of tracking the satellite separately with the precision tracker and the large antenna, with the position of the latter controlled by the vernier autotrack. The positions were recorded during the entire pass, and the data was compared later. The information obtained in this way, together with star calibrations and the precomputed satellite trajectories, enabled us to plot a curve showing the azimuth errors as a function of elevation. Tests carried out for different azimuths showed that this law of variation remains valid for all azimuths. (See Figure 4–11).

Results: A first series of tests performed up to 15 December 1962 enabled us to establish the following relation: $\tan az = 1/570 \tan el$ (See Figure 4–11) which is eqivalent to the variation resulting from the radiation from the antenna in a plane shifted 0.1 degree from the perpendicular to the axis of rotation in elevation. A check of the antenna structure did not reveal any error of this order, but revealed that a very large percentage of the structure bolts were loose, resulting in excessive deformation as a function of variations in elevation.

A general overhaul of the structure was carried out in April 1963. Using the Relay I satellite, a systematic study was then made to define the new law of variation. It was possible to perform these measurements between 0 and 80 degrees: higher elevations were never reached with the satellite repeater radiating. Mathematical analysis of these results permitted us to derive an azimuth correction to be applied to the antenna as a function of elevation. This correction has the form

$$az = -0.06\left(\frac{1}{\cos el} - 1\right) - 0.05 \sin el$$

These corrections are systematically applied to the drive tape of the antenna and added in the digital azimuth information equipment.

This law of variation may be compared

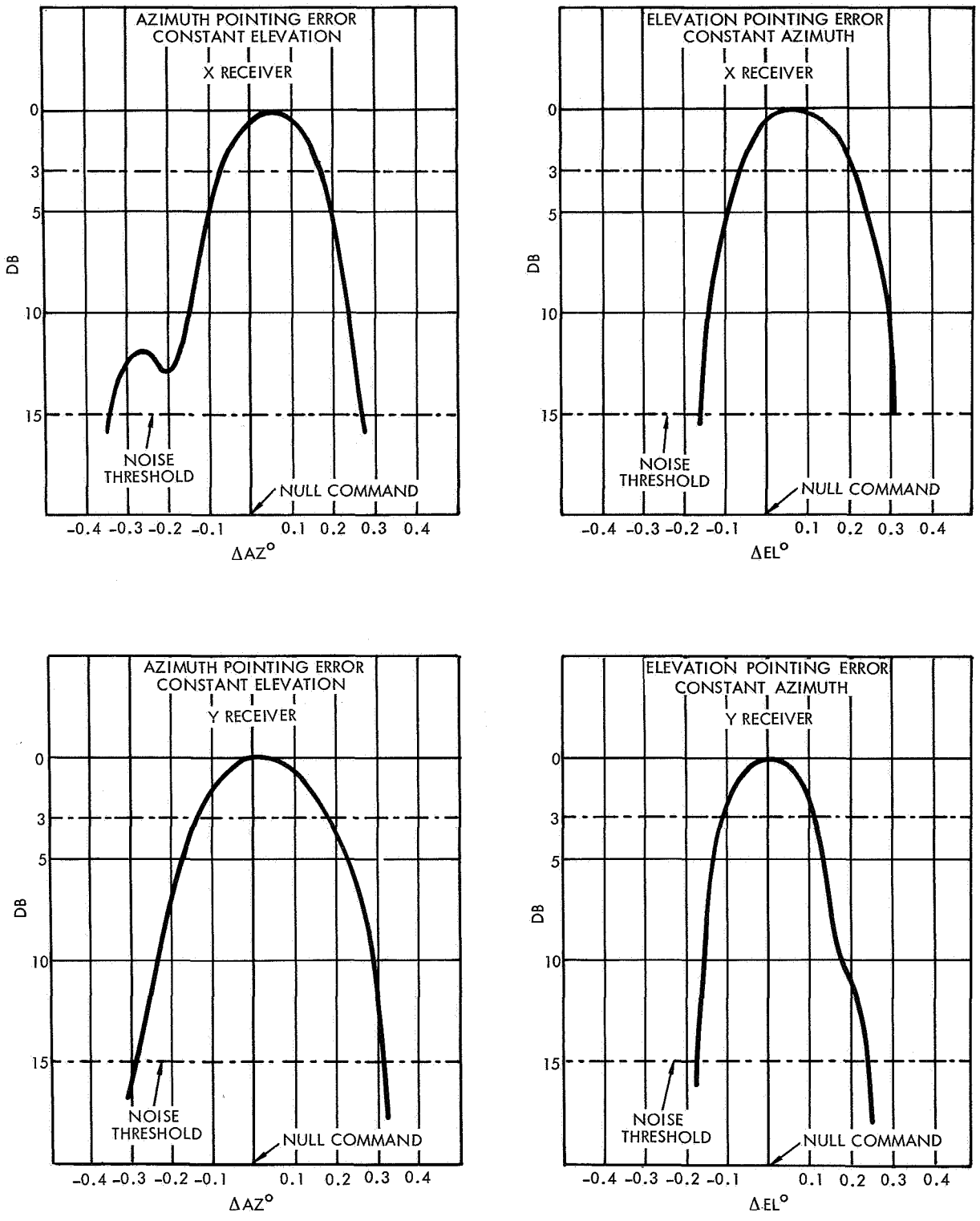


FIGURE 4–10.—Vernier autotrack receiver levels.

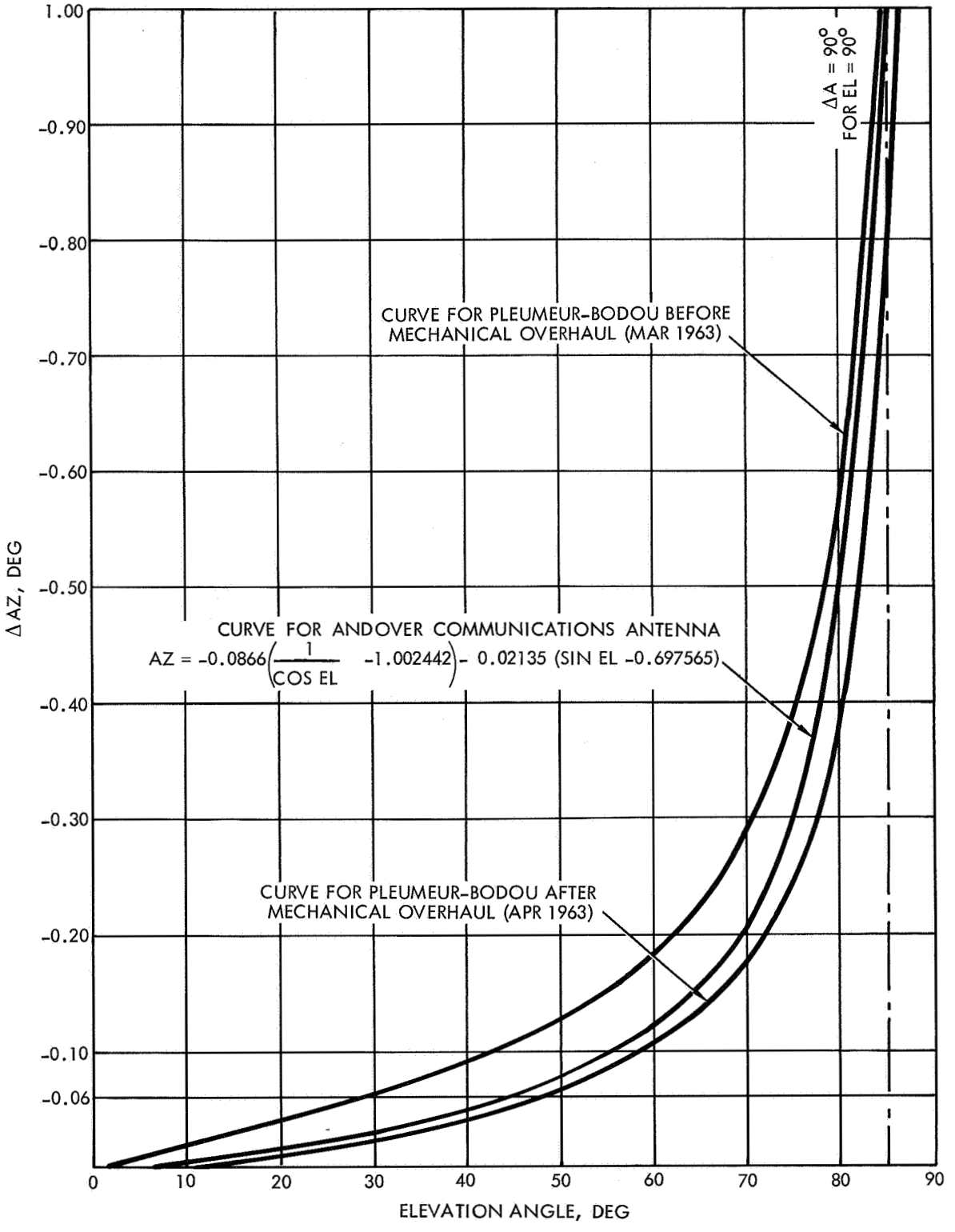


FIGURE 4-11.—Azimuth errors as a function of elevation—communications antenna.

with that provided to us by BTL and used on the Andover antenna (tracking program document, October 15, 1962—Program Description):

$$az = -0.0866\left(\frac{1}{\cos el} - 1.002442\right) - 0.02135\ (\sin el - 0.697565) = -0.0866$$

Note: This azimuth correction is to be applied to the "apparent width" of the radiation pattern for a rotation in a horizontal plane; for each value of the elevation the "apparent width" of the pattern is, because of the coning effect, equal to the actual width of the pattern (0.23 degree at 3 db) multiplied by 1/cos *el*.

In the present case, if no correction terms are introduced into the antenna drive equipment the communication link loss remains less than 1 db for any elevation.

Because of this coupling there appeared to be some difficulty associated with slaving the antenna directly to the precision tracker, since the positions indicated by the encoders of the two antennas did not have the same value while the satellite was being tracked. We therefore assembled a computer which would provide for making this correction between the encoders of the precision tracker and the antenna drive group.

The purpose of this device, which was mounted in available racks in the tracking encoder unit, is to provide automatic correction by means of a wired program which determines the value to be added to the azimuth information:

$$az = -a\left(\frac{1}{\cos el} - 1\right) - b \sin el$$

with $a = 0.06$ and $b = 0.05$, which corresponds to measurements made for values of elevation up to 85 degrees.

The series-type computer calculates the successive powers of the elevation, expressed in radians, up to the seventh term. It then modifies these terms as a function of the coefficients a and b and then adds the partial results. A complete cycle is performed in one sixty-fourth of a second.

The polynomial selected is of the form

$$az = \frac{5}{3}bx + \frac{b}{6}x^3 - \frac{b}{120}x^5 - \frac{45a}{720}x^6 + \frac{b}{7040}x^7$$

The deviations between this function and the theoretical one are always lower than the noise in the information provided by the precision tracker.

Study of Refraction

Since the satellite is commanded from the Nutley station, the relative positions of the Pleumeur - Bodou and Nutley stations and the direction of motion of the satellite are such that the satellite TWT is very often already operating at the time the satellite rises above the theoretical horizon at Pleumeur-Bodou. The advantageous position of the station, for which the proximity of the ocean makes the theoretical horizon coincide with the real horizon in many directions, has enabled us to perform tests on the refraction of signals at low elevations. These measurements were made at frequencies near 4000 Mc.

Many passes were used for these tests. It is noteworthy that no appreciable variation in the results was observed with respect to the seasons. This stability must be considered to result from the proximity of the sea over which the satellite rises and the small climatic variation of the region.

Two test methods were selected:

1. For elevations above 1 degree, we used magnetic tape recordings of antenna positions during automatic tracking of the satellite. This procedure requires the close attention and skill of the operators because of the fluctuation of received signal levels up to elevations of 3 degrees. The resulting information, corresponding to the apparent elevations, is later compared to the geometrical elevations of the theoretical pass, reconstructed from trajectory readouts during the entire pass.

This reconstruction of the trajectory was especially easy for Relay I, since the computed trajectories were very close to the actual trajectory. The accuracies obtained after reconstruction were of the order of 0.01 degree.

2. For elevations below 1 degree, the antenna is preset in elevation to the value selected for the measurement and is servoed in azimuth to the tape. Because of this latter condition, an attempt is made to select a pass for which the azimuth varies only slightly with time, in order to eliminate any time error in pointing. When the satellite rises, the time of passage across the antenna lobe prevents determination of the geometrical elevation corresponding to this apparent elevation.

Both methods enabled us to plot point by point the correction curve for refraction as a function of geometrical elevation (see Figure 4–12). This law of variation enabled us, once it had been introduced into the program for producing the antenna drive tapes, to acquire the satellite at apparent elevations of 0.2 degree, corresponding to a geometrical elevation of −0.6 degree. This acquisition does not assure the quality of the communication link, which is subject to large variations in level at these low elevations.

We have plotted on the same figure the following three curves:

1. The law of light refraction
2. The law in $(n-1)$ cot *el*, with $(n-1) = 3.3 \times 10^{-4}$
3. The law as plotted at Pleumeur-Bodou for 4000 Mc.

Analysis of these results shows the following:

1. The refraction measured at 4000 Mc, slightly greater than light refraction up to 3 degrees, is clearly greater for lower angles, reaching a limit of 1.05 degree for 0.55 degree elevation.

2. The measured refraction law coincides with the law in $(n-1)$ cot *el* with $(n-1) = 1/3000$ for angles greater than 7 degrees.

3. Use of the $(n-1)$ cot *el* law limited to the value $el = 3$ degrees corresponds for the rise of the satellite to an error of 0.6 degree, delaying acquisition with tapes which have been calculated with allowance for this information.

Range Measurements

The theory of the method used to measure ground antenna to satellite range is that from a knowledge of the propagation velocity of electromagnetic waves in the atmosphere and the propagation times in the various items of equipment used one can determine the range. This is done by measuring the time required for a signal transmitted by the ground station to return to the same station after frequency conversion by the satellite.

Measurement Setup — In addition to the station transmitting and receiving equipment, the measuring equipment includes a

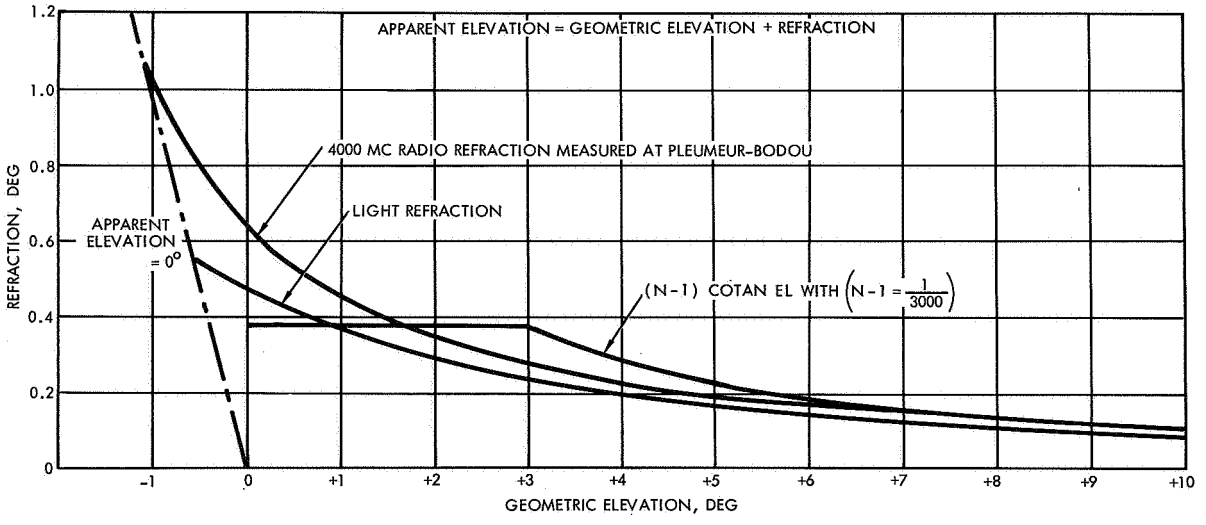


FIGURE 4–12.—Tropospheric refraction.

pulse generator and a time measuring device (Figure 4–13). The pulse generator receives pulses from the station clock (pulse frequency 1 cps, pulse width 0.5 sec) and provides pulses of the same frequency with a 3-volt amplitude and adjustable width. The pulse width adopted for the measurement is 500 microseconds with a rise time of 0.06 microsecond. Each pulse is fed both to the transmitter modulator and to one of the inputs of time measuring unit.

The equipment operates as follows: a pulse applied to one of the inputs ("start") starts the counter, which stops when a second pulse reaches the other input "(stop"). The counter measures the time separating the two pulses. The precision of the unit is 0.1 microsecond. The pulse fed to the transmitter modulator reappears after going through the satellite at the receiver output Δt seconds later and stops the counter, which then indictates the value of this Δt.

The results of the measurement were automatically recorded by a printer which records the values shown by the counter as well as the time each pulse leaves (every second on the second).

Measurements—The general expression giving the ground-to-satellite range must take into account the following:

1. The velocity of electromagnetic waves in free space. The velocity used is taken equal to the velocity of light:

$$C = 299{,}792.5 \pm 0.4 \text{ km/sec}$$

This is a figure arrived at after a series of

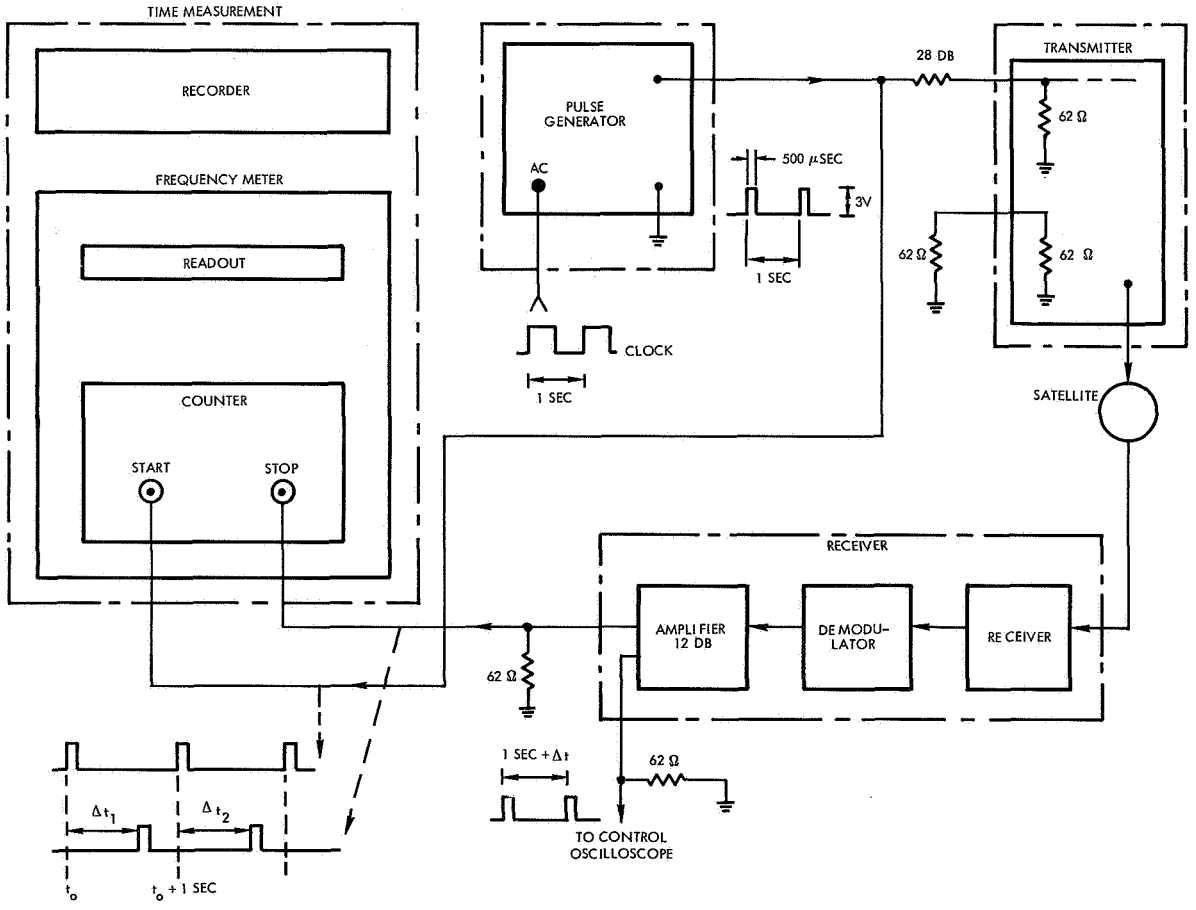


FIGURE 4–13.—Block diagram of range measuring equipment.

tests on reconstructed trajectories for Relay I.

2. The propagation time in the equipment. A satellite simulator in the boresight tower, at a known distance of 6344.4 m from the center of the antenna taken as a reference, permits determination of the propagation time in the set of equipment being used in relation to the theoretical time required to traverse the same distance at the velocity of propagation of electromagnetic waves. We assume in addition that the propagation time within the satellite is identical to that in the corresponding simulator.

We therefore have:

$$\Delta t_0 = t_m - \frac{2d}{v}$$

where

Δt_0 = Total propagation time in the equipment
t_m = Measured time
d = Reference distance
v = Propagation velocity

For Project Relay and the frequency compression demodulator this yields

$$\Delta t_0 = 44.1 - 42.3 = 1.8 \text{ microseconds}$$

3. The difference between the time recorded and the time of measurement. Since Δt is the time required by the signal to make the round trip from antenna to satellite to antenna, this difference is Δt. Allowing for the radial velocity of the satellite with respect to the station, the correction term to be introduced into the range measurement because of this time difference will be

$$-\frac{dD}{dt} \cdot \frac{\Delta t}{2}$$

4. The variation of the signal propagation velocity with respect to that existing in space and the curvature of the signal in the atmosphere. The cause of these phenomena is the variation in the index of refraction of the atmosphere. Using the 1620 computer, we undertook a theoretical study giving the deviation between the apparent measured distance and the actual distance.

In making this study we assumed the following expression as characterizing the law of variation of the index of refraction as a function of altitude from the ground:

$$n(h) = 1 + (n_0 - 1)\, e - 0.135\, h$$

for

$$(n_0 - 1) = \left(77.6\frac{p}{T} + 3.73 \times 10^5 \frac{Es}{T^2} U\right) \times 10^{-6}$$

where

p = Atmospheric pressure in millibars
T = Absolute Temperature, degrees K
Es = Saturated vapor pressure at temperature T
U = Relative humidity
h = Altitude in km

The results of this calculation are plotted in Figure 4–14.

Results: Taking into account the above considerations, we can write

$$R = \frac{1}{2} C\,(\Delta t - \Delta t_0) - \frac{dD}{dt} \cdot \frac{\Delta t}{2} - \epsilon_{(n)}$$

where

R = Antenna to satellite range
C = Propagation velocity of electromagnetic waves
t = Measured time
t_0 = Propagation time within the equipment
dD/dt = Radial velocity of the satellite
$\epsilon_{(n)}$ = Range correction as a function of the index of refraction (Figure 4–14)

The estimated accuracy of such a measurement appears, on the basis of an error calculation, to be on the order of a few tens of meters.

Figures 4–15 and 4–16 show curves plotted on passes 903 and 2669 of Relay I. The deviations between the measured range and the range calculated from the theoretical trajectory enable us to conclude, after a comparison with the radial velocity of the satellite, that the time error is 0.5 sec in one case and 2 seconds in the other. A reconstruction of the trajectory performed from precision tracker data confirms this deviation.

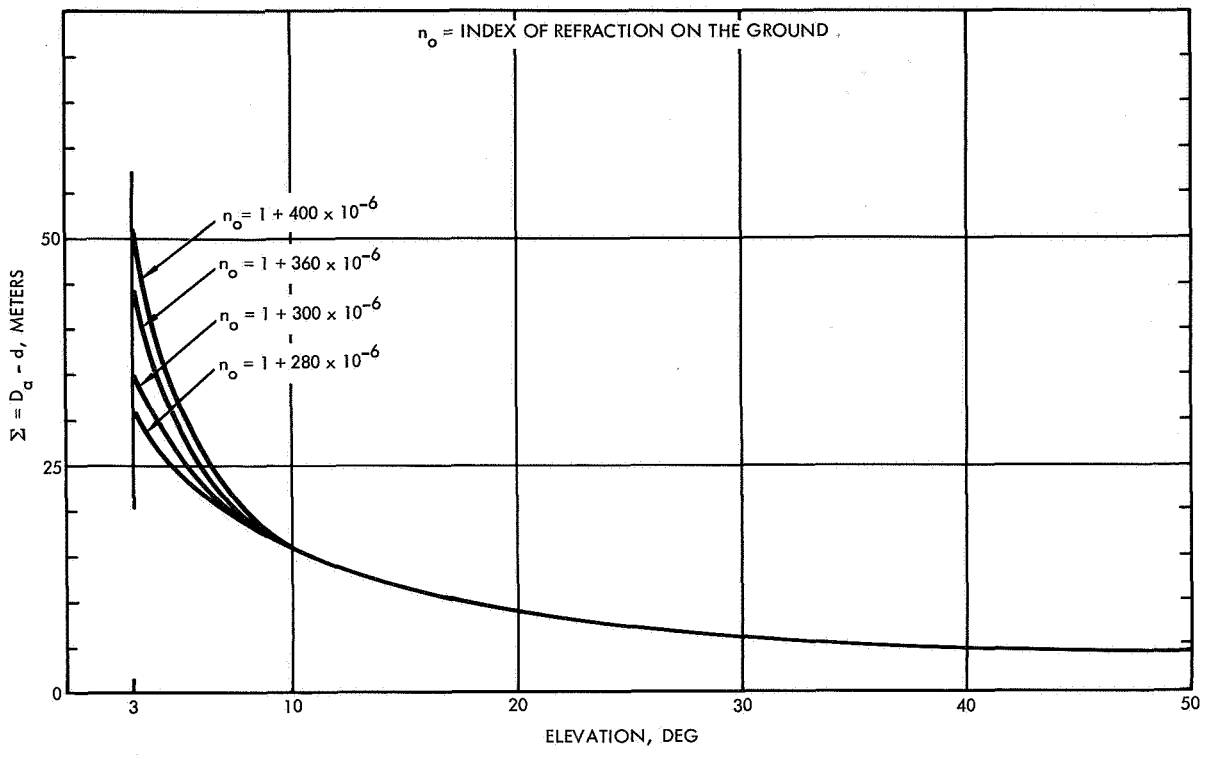


FIGURE 4–14.—Deviation between the apparent distance D_a and the geometrical distance d.

Method of Acquisition and Tracking

This section summarizes the experience we have acquired which enables us to define a general mode of operation suitable for the various circumstances which may occur.

Acquisitions—During the phase of waiting for the satellite to rise, or in case the beacon is not radiating when the satellite rises, for the beacon to be turned on, the antenna is driven by the precomputed tape prepared from the data received from Goddard Space Flight Center in the form of topocentric XYZ coordinates and transformed by the Pleumeur-Bodou computing center into az-el-range coordinates.

During the 133 passes conducted with Relay I, with the exception of the very first days of the satellite life in orbit, it has appeared that the accuracy of the received data is always better than ± 0.05 degree; this error is generally eliminated by the insertion of time corrections on the tape. These corrections are never greater than 3 seconds and are generally about 1 second.

On the other hand, the "mean orbital parameters" determined by NASA do not allow us, with the machine programs in our possession, to drive the antenna in a usable fashion; the results of the computation are not close enough to the actual positions.

The criterion of acquisition is the phase lock of the frequency drive oscillator in the vernier autotrack receiver, assuming satisfactory operation of the system as a whole. There are two ways in which this acquisition can be effected:

1. The precision tracker acquires the satellite first, and transfers to automatic track. The delay in acquisition by the horn antenna may arise either from a poor frequency in the phase lock oscillator of the vernier autotrack receiver or from drive tape data which does not correspond to adequate pointing ac-

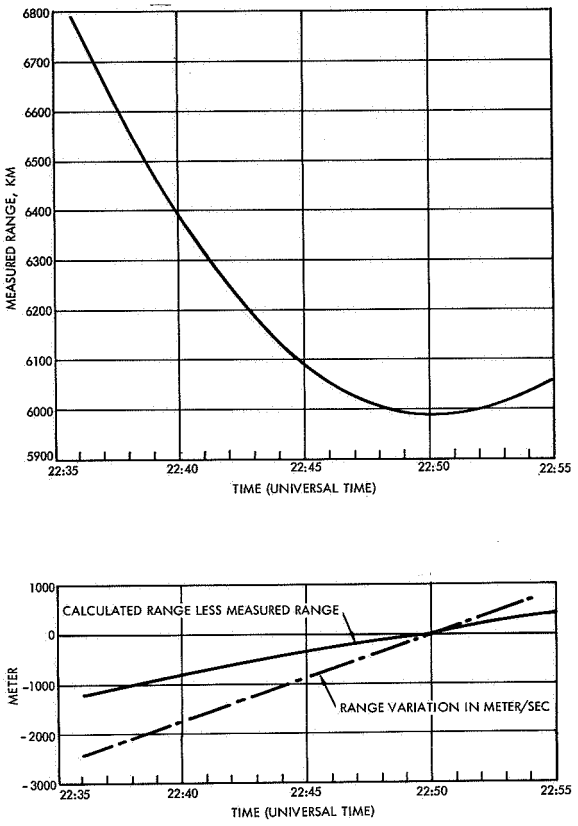


FIGURE 4–15.—Relay revolution 903—range measurement.

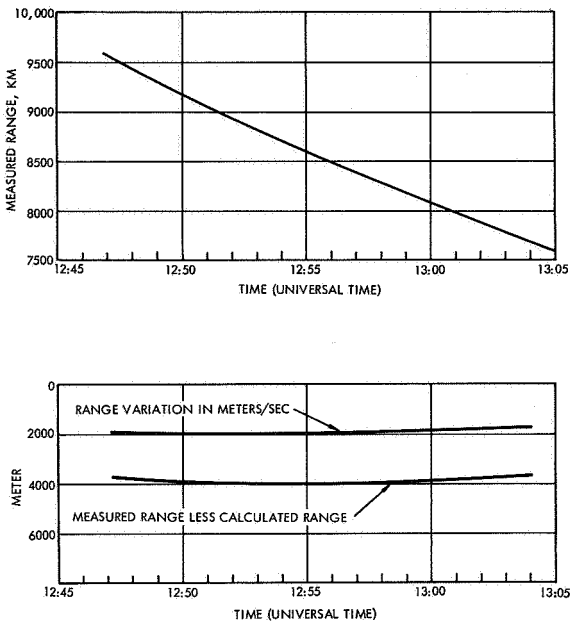


FIGURE 4–16.—Relay revolution 2669—range measurement.

curacy for the antenna. In either case, the oscillator does not lock on in phase.

The chief of operations can determine which of these errors is involved by looking at the AGC level of the communications receiver, as displayed on the central console. Two actions are taken:

(a) The vernier autotrack transfers to frequency servo on the precision tracker

(b) The error between precision tracker and tape, displayed on the console, is reduced as much as possible by insertion of time corrections.

If after these two steps are taken the satellite still has not been acquired, and if the elevation of the satellite is greater than 2 degrees, the horn antenna is slaved to the precision tracker. The 2 degree limit reflects the fact that below this elevation the oscillations of the precision tracker do not permit extended slaving of the horn reflector antenna to the precision tracker. With this arrangement, acquisition is normally effected very quickly.

2. The satellite is acquired by the vernier autotrack first or simultaneously with the precision tracker. In this case the tracking mode starts immediately.

It should be noted that acquisition by spiral scan about the position given by the tapes has never been used. Use of this mode of operation assumes that the precision tracker has not acquired, and results in a simultaneous search in frequency and position. Considering the spiral scan rates and the range of frequencies to be explored, the problem is virtually insoluble.

Tracking—As soon as the satellite beacon is acquired in frequency, the method generally used is transfer to the tracking mode called VAT 3. In this mode the antenna is slaved directly to the satellite without the tapes in the servo loop. It is therefore possible to compare the pointing data for the satellite with the tape data and to apply time

and position corrections to make them identical. Once this is done it is possible to remain in this tracking mode or to use mode VAT 1, which makes use of both the tape data and the pointing errors provided by the vernier autotrack. This mode has the advantage of greater reliability, since any interruption of reception by the vernier autotrack does not interrupt tracking; the tracking continues as commanded by the updated tapes.

In practice, both modes (VAT 1 and VAT 3) were used during the Relay tests without any loss of the satellite being attributable to them.

Tracking by means of direct slaving of the antenna to the precision tracker was used by way of test. This method gave very good results after insertion of the antenna distortion computer described on page 610. The oscillations introduced by the tracking noise in the precision tracker (see Figure 4–5) do not result in any fluctuation in the communication signal, since the angular deviations are comparable to the 3-db width of the lobe (0.23 degree). This tracking mode may on occasion be used in a case where the drive tapes have not yet been prepared, although the satellite has been acquired by the precision tracker. In order to facilitate the tests, the circuits of the antenna drive group were modified to provide for insertion of position corrections between the precision tracker encoders and the horn antenna.

Makeup of the Operating Crew—During the operational periods corresponding to satellite passes and the one-hour period preceding each pass, the antenna drive is manned by the following crew:

- One technician at the command tracker (if telemetry data are taken)
- One technician at the precision tracker
- One technician at the vernier autotrack
- One technician at the servo group
- One operator at the computing center
- One digital circuit technician able to work on both the precision tracker and communications antenna circuits.

The antenna drive crew is supervised from the central console (G.S.C.C.) by the chief of operations.

Conclusion

All the above tests have shown that the acquisition of the satellite is nearly certain and that subsequent tracking is such that communication links can be established and tests performed with them with no difficulties attributable to pointing errors. In particular, the tests have shown that it would be possible to reduce the amount of equipment and the computation time, while using only present techniques, by making use of the vernier autotrack associated with a rendezvous technique. With this technique it would be necessary to compute only the position of acquisition of the satellite, with the digital antenna drive equipment commanding the appropriate position and the vernier autotrack automatically taking over tracking as soon as the satellite is acquired.

In the case of a stationary or nearly stationary satellite, the use of the vernier autotrack as the main element of the antenna drive would probably have to be re-examined.

With well trained personnel who are familiar with the equipment, it is possible to cope with any slight incidents which might occur during satellite passes without interrupting the link, by making appropriate use of the various circuits for pointing the antenna in the direction of the satellite.

COMMUNICATIONS TESTS

The Pleumeur-Bodou station utilized 113 passes of the Relay I satellite for communication tests during the period from the launch of the satellite (14 December 1962 to 15 December 1963). Tests of a technical nature were made during 74 of the passes. In most of the cases the satellite was used in loop tests, where the station received back the signal it had transmitted. Such tests are nearly identical to straightaway tests, and much easier to perform. In the course of some of these tests, however, the Pleumeur-Bodou station worked in collaboration with

the Andover, Nutley, or Rio stations. System tests or demonstrations were carried out on 51 additional passes, with some technical tests accompanying or preceding the system test or demonstration on these passes as well.

The technical tests concerned measurements of received signal power, receiving system noise, noise in the communications channel, and distortions of the received signal. Some measurements were also made of the effects which are peculiar to satellite communications. We will conclude with a description of some of the system tests.

Received Carrier Power

The power level of the received signal was systematically measured during each pass used for tests. The measurement was made by recording the circuit variations in the receiver AGC. The measurement was calibrated prior to each pass by applying to the receiver input a signal of known power supplied by a hyperfrequency generator. The absolute accuracy is ± 1 db.

The results of these measurements were compared with values calculated from the range of the satellite. The following mean values were used in the calculations:

- Level of signal radiated by the satellite: 40 dbm for a one-way link, 37 dbm for a two-way link
- Satellite antenna gain, 0 db
- Station antenna gain at 4170 Mc, 58 db
- Receiving system attenuation, 0.4 db

The recordings of received carrier power enabled us to study both the mean value and the fluctuations of this parameter.

Mean Value of Received Carrier Power

Figures 4–17 and 4–18 show typical examples of the results for one-way and two-way links. The mean value of received carrier power is plotted as a function of satellite range, together with the theoretical

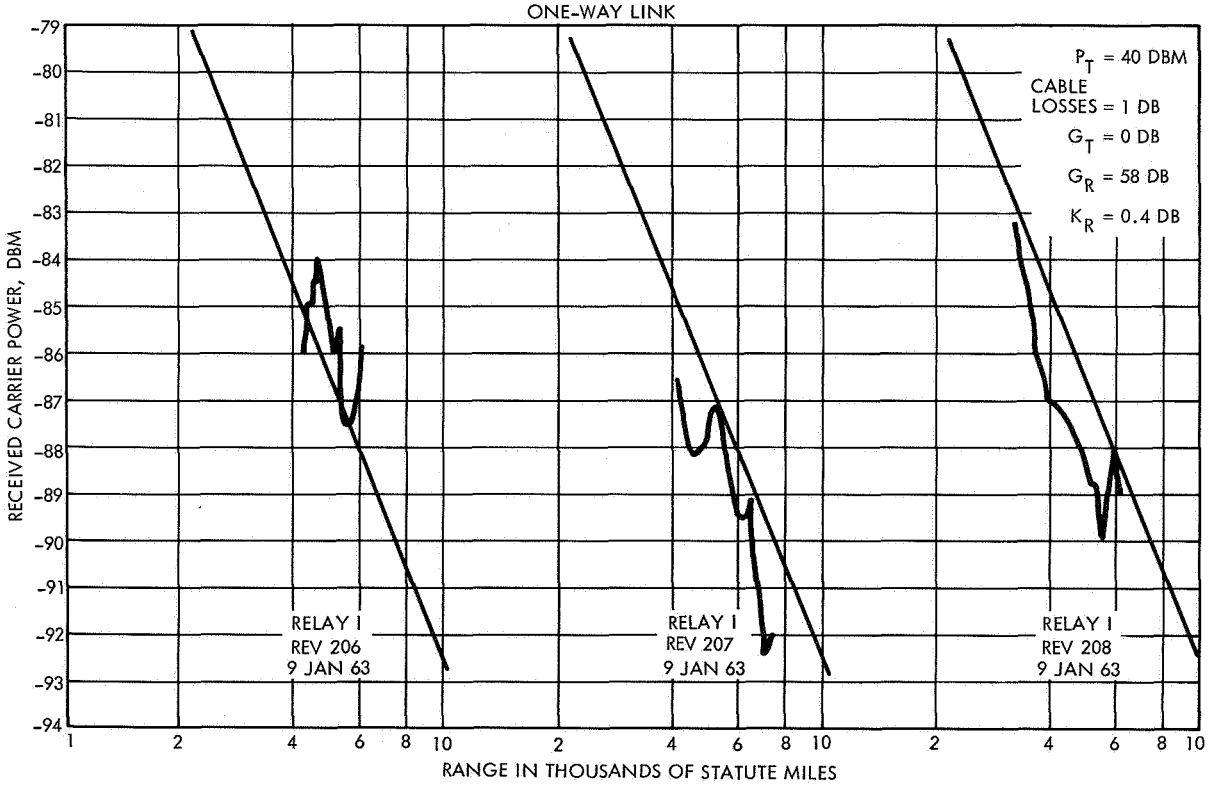


FIGURE 4–17.—Received carrier power at maser input, one-way link.

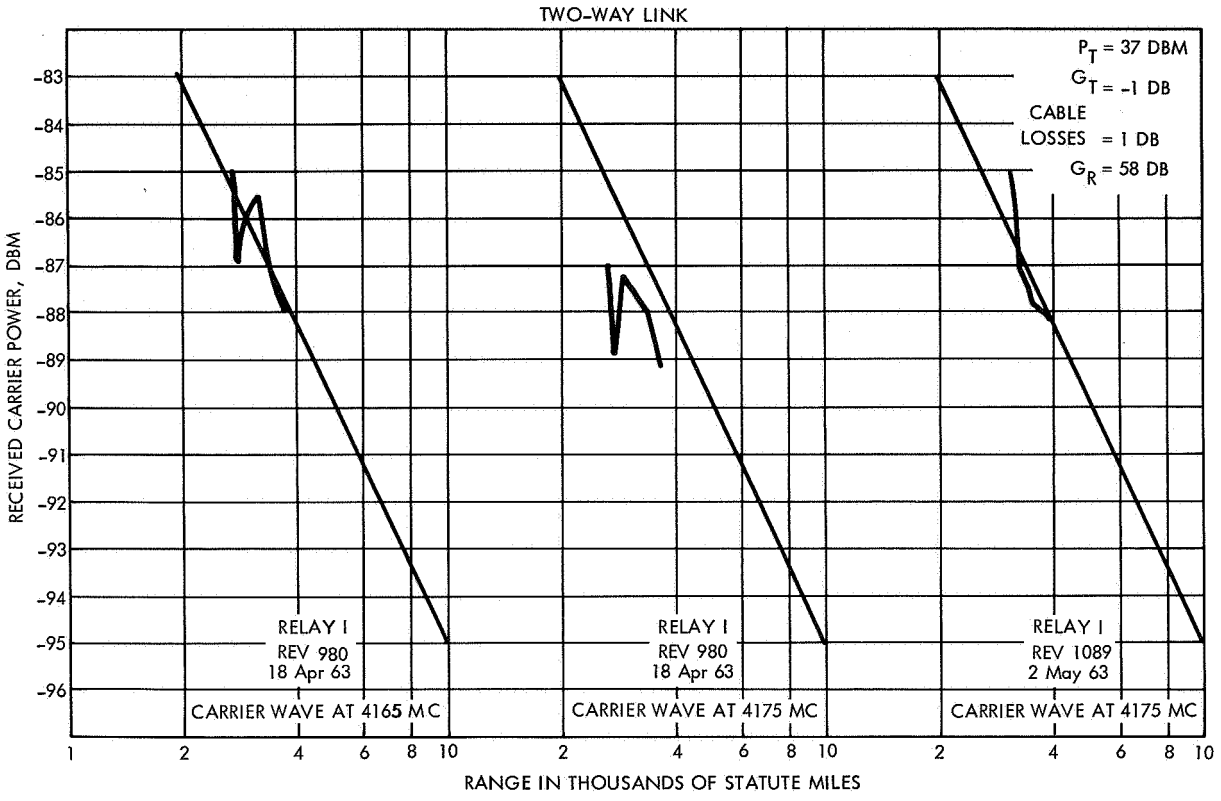


FIGURE 4–18.—Received carrier power at maser input, two-way link.

curve. The calculated values do not allow for variation of the satellite antenna gain as a function of look angle (the angle made by the satellite spin axis with the direction of the station), nor for the smaller variations in the output power of the satellite TWT. Good agreement can be seen between the theoretical and experimental results.

Fluctuations in the Received Carrier Power

One cause of large fluctuations in the received carrier power is the rotation of the satellite on its axis, combined with the irregularity of its radiation pattern. This rotation, however, does not explain adequately the very large variations noted at low elevations (Figure 4–19). We believe that in this case the observed fluctuations are due to multipath propagations caused by rapid changes in the homegeneity of the atmospheric layers traversed by the signal as well as by reflection of the signal from the ground at points near the antenna, where the radiation lobes are not yet formed. Figure 4–20 is a reproduction of a recording of received carrier power made with a high paper speed on the recorder; the elevation of the antenna was great enough so that only fluctuations due to the spin of the satellite appear. From this recording one can deduce that the spin rate of the satellite at that time was 2.6 rps. The fluctuations can be seen to be large, on the order of 3 db, and to have an apparent period twice that of the satellite spin rate. This is in agreement with the effect that could have been predicted from examination of the satellite antenna pattern taken before launch.

Noise Temperature of the Receiving System

Measurement of the noise temperature of the receiving system is performed at a point after the maser amplifier and the first IF stages. The noise contributed by the equip-

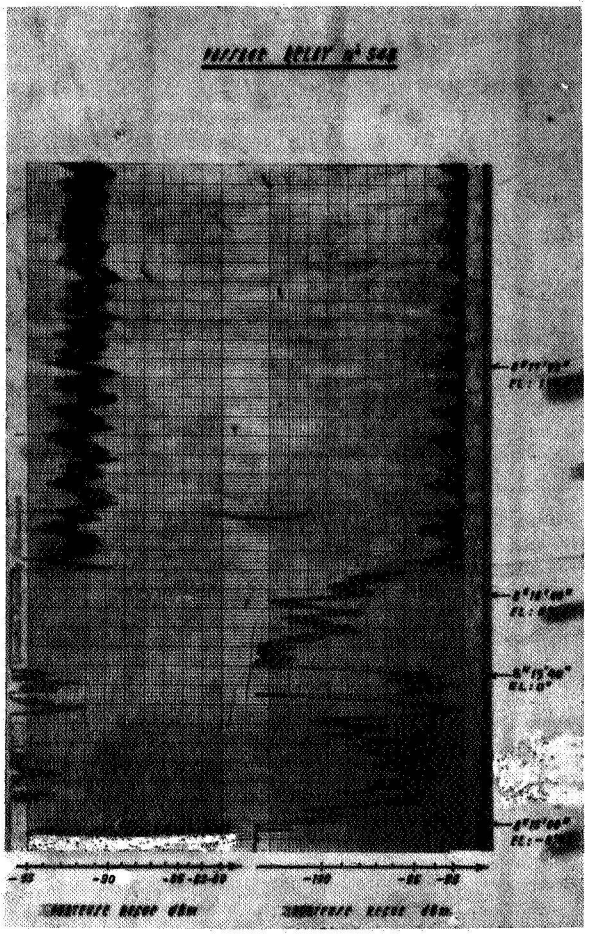


FIGURE 4–19.—Recording of received carrier power, pass 548.

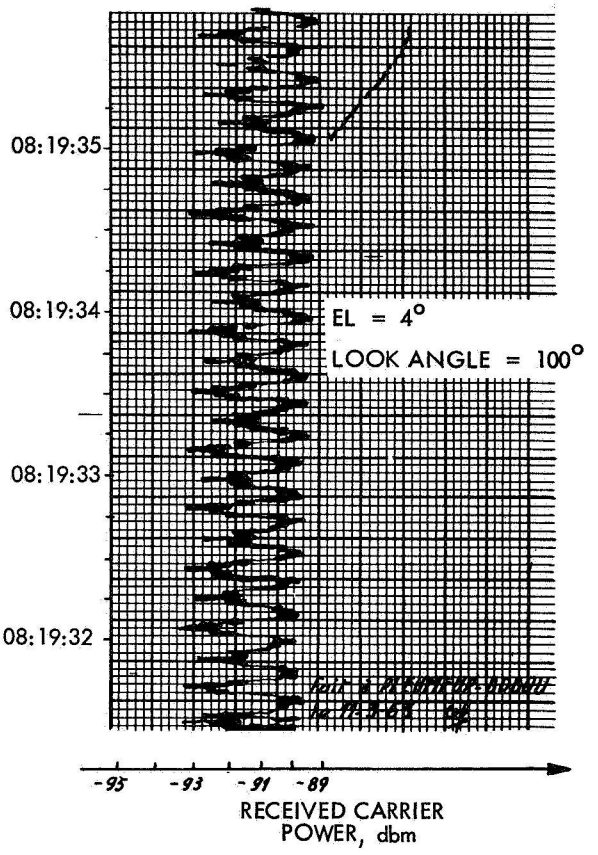


FIGURE 4–20.—High-speed recording of received carrier power, pass 548.

ment downstream of this point may be considered negligible; it will be seen later that this is not always the case, and that some parts of the baseband equipment are responsible for a significant part of the noise affecting the demodulated signal. This noise, however, is in equipment which is not peculiar to satellite communications and could be made negligible by improvements to the equipment.

The noise measurement is performed by determining the difference in power level of the noise contributed by the receiving equipment alone and the receiving equipment plus a known source of noise. A calibrated white noise generator is coupled in at the maser input to provide the second measurement. The presence of the satellite is not required for this measurement; it is performed before and after each pass utilized and each time the receiving system is ready for operation.

At the time of publication of the results of tests made with Telstar I we gave some statistical data on the noise temperature measured at the zenith. In the present report this information is supplemented by results from tests with Relay I. The data is based on 487 measurements performed during the period 1 September 1962 to 28 November 1963. The data obtained in July and August 1962 has been excluded, because the precision of those measurements is poorly defined.

It can be seen from Figure 4–21 that the great majority of receiver noise tempera-

tures at the zenith are in the vicinity of 33°K, but that a much smaller grouping of measurements falls between 50 and 60°K. These two points of concentration of measurements correspond respectively to the case of a dry radome and the case of a wet radome. Finally, a small number of measurements are above 70°K and appear to correspond to very unusual weather conditions such as heavy rain or snow.

The distribution curve was also plotted, as shown in Figure 4–22. It is seen that the mean value is 33°K, that in 85 percent of the cases the noise power deviates by less than 1 db from the mean values, and that in 99 percent of the cases it deviates by less than 4 db.

Noise in the Communication Channel

Since a low noise level is required if a communication channel is to be of sufficiently good quality, we determine the spectrum as well as the effect of noise in the telephone channels and in the video and audio channels of the television signal.

Analysis of Noise in the Communications Channel

The analysis of noise as a function of frequency in the communications channel is performed with a selective analyzer having an equivalent pass band of 4 kc. Figure 4–23 shows the noise power level as a function of frequency at a zero relative level point, corresponding to an effective frequency deviation of 675 kc for the satellite-ground link per 4-kc channel. We have plotted both the measured level of the signal and the theoretical straight line (broken line on the graph) corresponding to a triangular noise spectrum computed from the measured values of received power and noise temperature. We have also plotted on the same graph the same curves for the link formed by a loop on the satellite simulator (dashed lined). In this latter case the agreement between measured and theoretical values is excellent; for the satellite loop a triangular noise is still observable, but the measured noise power is about 3 db above the theoretical value (noise contributed by the ground-satellite direction is not taken into account).

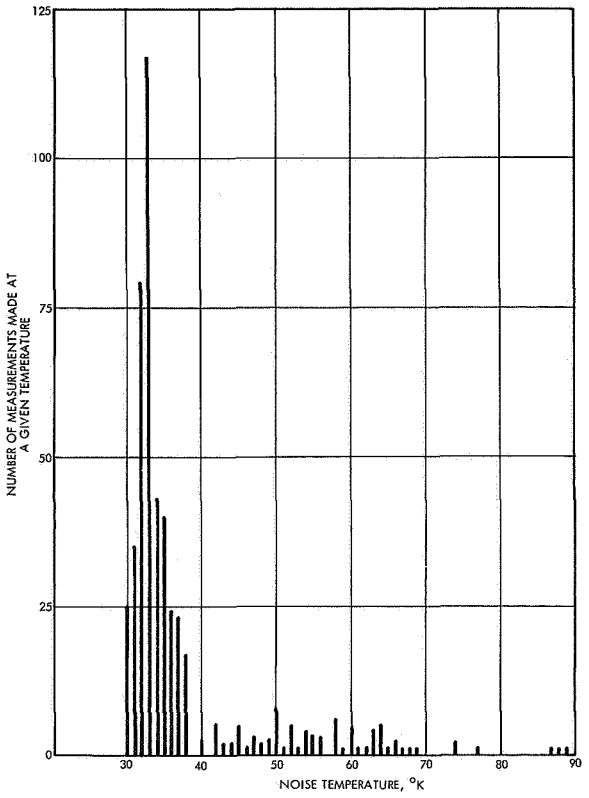


FIGURE 4–21.—Distribution of noise temperatures at the zenith over 487 measurements made from 1 Sept. 62 to 28 Nov. 63.

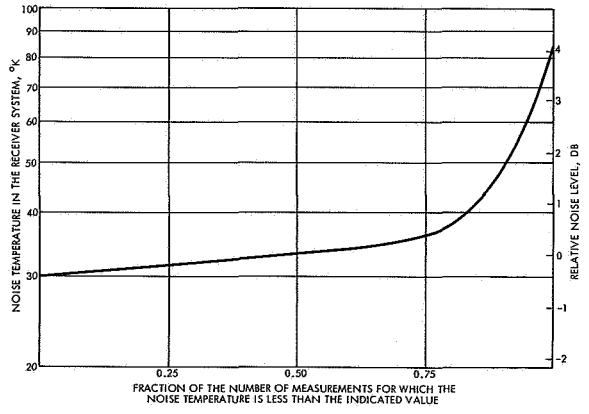


FIGURE 4–22.—Distribution of noise temperatures measured at the zenith (September 1962 to November 1963).

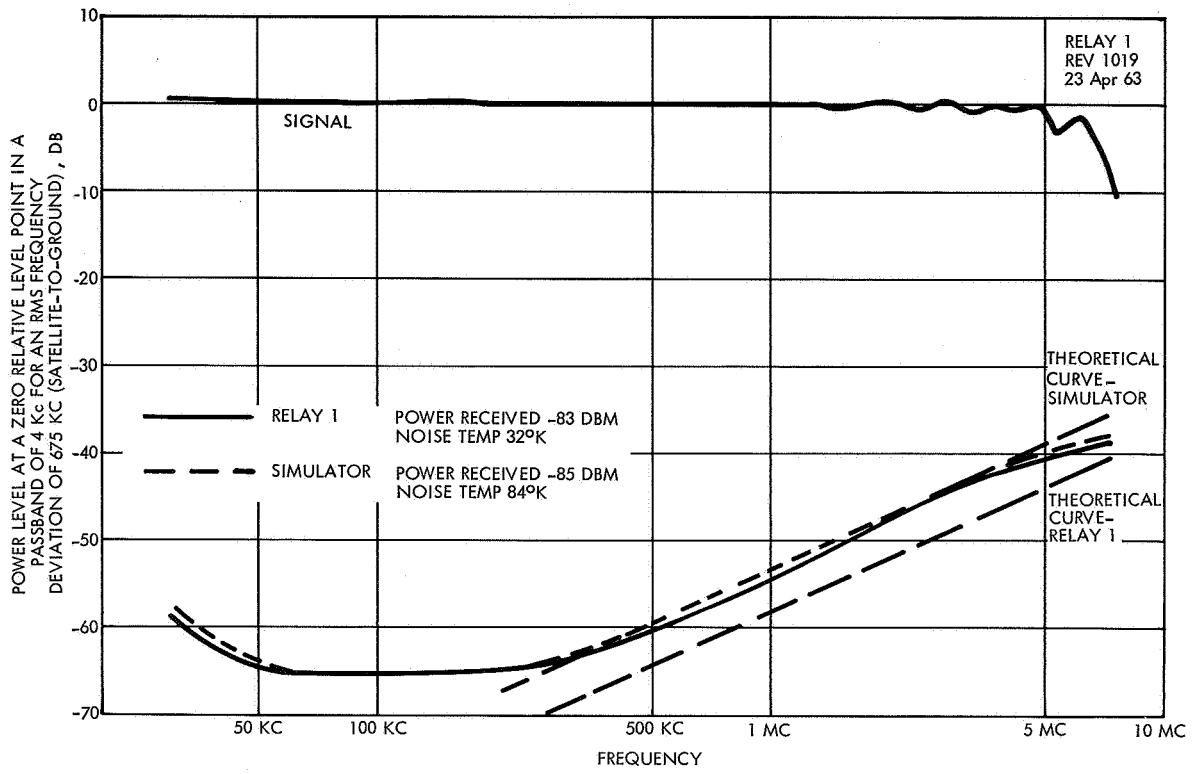


FIGURE 4–23.—One-way wideband link-analysis of baseband noise (at classical demodulator output).

For the low frequencies there is an increase in noise with respect to the theoretical curve which is due to the equipment; for these low frequencies the modulation gain is such that the portion of the noise created before demodulation becomes negligible in comparison to the noise of the baseband equipment. Beyond about 6 Mc the noise power decreases because of limiting of the pass band. In this connection it should be noted that the measurement was made directly at the output of a classical demodulator. The same measurement repeated at a telephony test point in the central building showed that the 3-db pass band after the signal entered the baseband equipment and the connecting cable was reduced to about 4 Mc. The connecting cable is not equalized beyond 3 Mc.

Noise in the Telephone Channels

Telephone Channel Noise for One-Way Links—From the above-described measurements, made at a telephony test point, it is possible to plot the curve representing the unweighted signal-to-noise ratio in a 4-kc telephone channel as a function of the center frequency of the given channel (Figure 4–24). It can be seen that the unweighted S/N ratio is greater than 44 db for channels having center frequencies as high as 2.5 Mc. It should be noted that at the time of this measurement, receiver noise temperature was abnormally high and the received signal power only average.

Telephone Channel Noise for Two-Way Links—In collaboration with the Nutley and Rio stations, communications tests were made of a group of 12 two-way telephone channels in the 12–60 kc frequency band. The S/N ratio in the channels was measured by means of a psophometer conforming to CCITT recommendations. Table 4–1 gives the results obtained with the Nutley station; it can be seen that the weighted thermal noise power

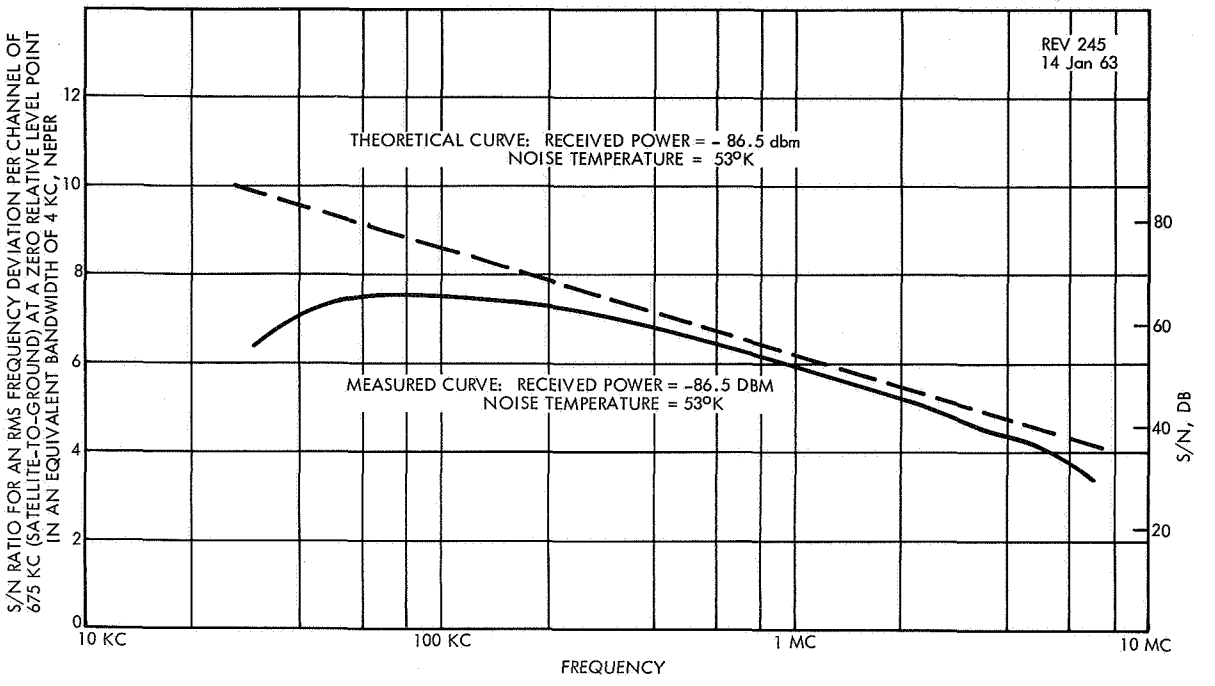


FIGURE 4–24.—Signal-to-noise ratio at baseband, one-way wideband link.

at a zero relative level point remained below 30,000 pw (weighted S/N ratio greater than 45 db). The reception conditions were average, the received power was on the order of —92 dbm, the receiver noise temperature was on the order of 38°K, and the rms frequency deviation per channel was 29.5 kc for the ground-satellite direction.

The same table shows the results of measurements taken when the link was looped on the simulator, which was then receiving only one carrier. These results are comparable to those obtained with the satellite; the gain obtained as a result of the greater received signal power was balanced by the increase in noise temperature for the low antenna elevation.

The same tests were repeated in collaboration with the Andover station in the 60–108 kc frequency band, with the rms frequency deviation per channel 104.7 kc for the ground-satellite direction. Table 4–2 gives the results of measurements made under average conditions of reception, with a received signal power of —92 dbm and receiver noise temperature of 34°K. The

TABLE 4–1.—*Transmission of 12 Telephone Channels (12–60 kc band)*
[Signal to Weighted Noise Ratio] db

Type of link (channel)	1	2	3	4	5	6	7	8	9	10	11	12
Two-way with Nutley	47	47	46	48	48	45	49	50	49	48	48	47
Looped on the simulator	41	42	51	50	45	39	49	52	46	52	52	53

TABLE 4–2.—*Transmission of 12 Telephone Channels (60–108 kc band)*
[Signal to Weighted Noise Ratio] db

Type of link (channel)	1	2	3	4	5	6	7	8	9	10	11	12
Two-way with Andover	53	60	58	60	58	60	60	60	60	54	61	61
Looped on the simulator	60	60	60	60	61	61	61	61	60	61	60	60

results obtained with a loop test on the simulator are practically identical. The weighted S/N ratio is about 10 db greater than that obtained in the 12–60 kc band, corresponding to the difference in modulation gains for the respective frequency deviations of 29.5 and 104.7 kc.

Television Noise

Noise in Video Channel — Measurements were made of the ratio of the complete peak-to-peak signal to rms noise in television, with the noise limited by a low-pass filter at 3 Mc and by a high-pass filter at 10 kc, fabricated in conformity to CCIR recommendations for the 405-line standard.

Table 4–3 gives the results of measurements taken under varying conditions of received power and noise temperature. An appreciable difference can be seen between the measured and calculated values. In addition, the improvement due to weighting as recommended by the CCIR for the 405-line standard does not reach the theoretical 12.3 db calculated for a triangular noise spectrum. These differences are largely due to ground equipment noise, especially in the link between the receiver under the radome and the central building. No difference is seen between values obtained above threshold with the frequency-compression demodulator and with the classical demodulator.

No impulsive noise was observed.

Noise in the Audio Channel

Measurements were made of the ratio of peak signal to rms noise in the television audio channel for one-way television, at a +3 dbm level point for a 1000-cps sinusoidal signal modulating the 4.5 Mc audio subcarrier with a peak frequency deviation of 17.7 kc; the peak frequency deviation produced on the carrier by the audio subcarrier was 1.4 Mc. Under these conditions the frequency deviation of the peak of the complex sound signal, which is by definition 9 db greater than the effective power of the 1000-cps sinusoidal signal, is 50 kc.

The measurements were made with an rms voltmeter measuring the effective unweighted noise and with a psophometer in the audio band giving the value of the effective weighted noise. For some measurements a pre-emphasis network of the RC type, favoring the highs and with a time constant equal to 75 microseconds, was used. Table 4–4 shows the results obtained during four passes. A large deviation can be seen between the measured values and those calculated in neglecting the noise contributed by the ground-satellite direction. This devia-

TABLE 4–3.—*Video S/N Ratio for One-Way Television*

Received power (dbm)	Noise temp (°K)	P–P signal/r.m.s. noise (db)					
		Calculated values without pre-emphasis		Measured values			
				Unweighted		Weighted	
		Unweighted	Weighted	With pre-emphasis	No pre-emphasis	With pre-emphasis	No pre-emphasis
−84	44	51.4	63.7	44.2	----------	50.2	
−82.5	43	52.9	65.2	45.2	----------	50.2	----------
−83.5	54	51	63.3	----------	42.5	----------	50.5
−84.5	67	49.1	61.4	----------	48.2	----------	57.2
−87	43	48.4	60.7	----------	44.2	----------	52.2
−88	40	47.7	60	----------	44.2	----------	52.2

TABLE 4–4.—*Audio S/N Ratio for One-Way Television*

Rev No.	Received power (dbm)	Noise temp (K)	Peak signal to r.m.s. noise (db)				
			Calculated	Measured			
			Unweighted, no pre-emphasis	Unweighted, no pre-emphasis	Unweighted, with pre-emphasis	Weighted, no pre-emphasis	Weighted, with pre-emphasis
448	−87.5	56	60	46	48	----------	----------
633	−87.1	32	62.8	51	58	----------	----------
873	−85.5	32	64.4	----------	----------	47.5	----------
2271	−89	30	61.2	----------	----------	----------	49.8

tion is due to ground equipment noise. In any case the quality of the link remains adequate.

No impulsive noise was observed.

Distortions in the Communications Channel

The distortions to which the signal is subject during transmission take the form chiefly of video signal and synchronization signal deformations in television or interchannel intermodulation noise in telephony. A main cause of distortion in FM is the variation of group propagation time in relation to intermediate frequency. We studied this phenomenon and its consequences for the transmission of multiplex telephony or a television signal.

GROUP DELAY DISTORTION AS A FUNCTION OF INTERMEDIATE FREQUENCY

This distortion is measured by applying to the modulator input a 50-cps sinusoidal signal which causes a frequency deviation of ± 10 Mc about the center frequency; on this signal is superimposed a 200-kc sinusoidal wave causing an additional frequency deviation of low amplitude (about 100 kc). At the receiving end the 50-cps signal is filtered out and the 200-kc wave is sent to a phase discriminator which gives an instantaneous voltage proportional to the deviation between the instantaneous phase of the 200-kc signal and the mean value of this phase, for a value of the intermediate frequency determined by the instantaneous amplitude of the 50-cps signal. This error voltage is applied to the vertical deviation plates of an oscilloscope whose horizontal sweep is at the rate of the 50-cps sinusoidal signal.

Figure 4–25 is a reproduction of the curve observed on the oscilloscope screen. A peak-to-peak distortion of about 60 nsec can be seen for a 20-Mc frequency band. In Figure 4–26 this distortion has been broken down into a linear distortion of 16 nsec peak-to-peak, a parabolic distortion of 40 nsec peak-to-peak, and a residual undulating distortion of 18 nsec peak-to-peak. Since the curve being studied is not a rigorous mathematical

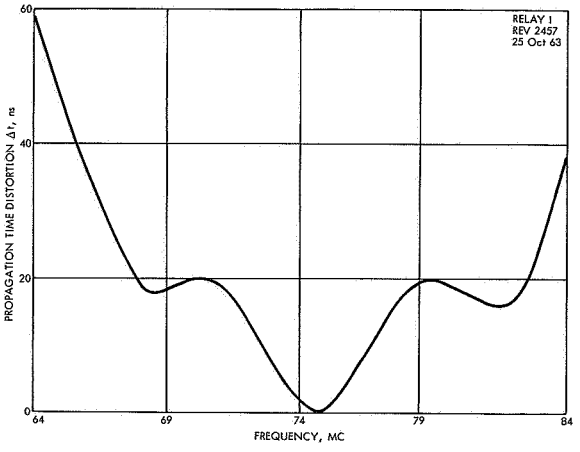


FIGURE 4–25.—Delay distortion as a function of the intermediate frequency.

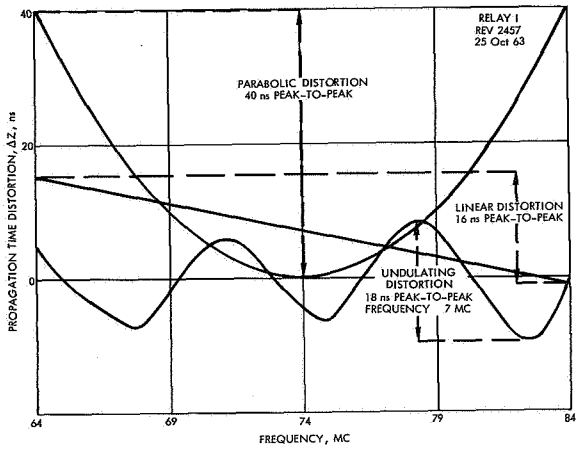


FIGURE 4–26.—Delay distortion as a function of intermediate frequency (separate components).

representation of the sum of these three types of function, this analysis has a certain arbitrary element in it.

Considering the accuracy of the measurement, about 2 nsec, no difference was observed between the results obtained with a classical demodulator and the frequency-compression demodulator, whether the link was looped on the satellite or on the simulator.

Intermodulation Noise in One-Way Telephony

Intermodulation noise is measured in the channels centered on 70, 1248, and 2438 kc of a 600-channel telephony multiplex. To make the measurement the transmission link is loaded by a continuous-spectrum signal conforming to CCIR notice No. 294. The rms frequency deviation per channel was varied on both sides of the nominal value of 512 kc. A pre-emphasis network conforming to CCIR notice No. 275 for 600 channels was used for some measurements.

The curves of Figure 4–27 indicate the results obtained with and without pre-emphasis; direct indication is given of the ratio of signal to unweighted noise at a zero relative level point in a 4-kc band. The dashed lines represent the measured value of the S/N ratio with no modulation present (thermal noise alone).

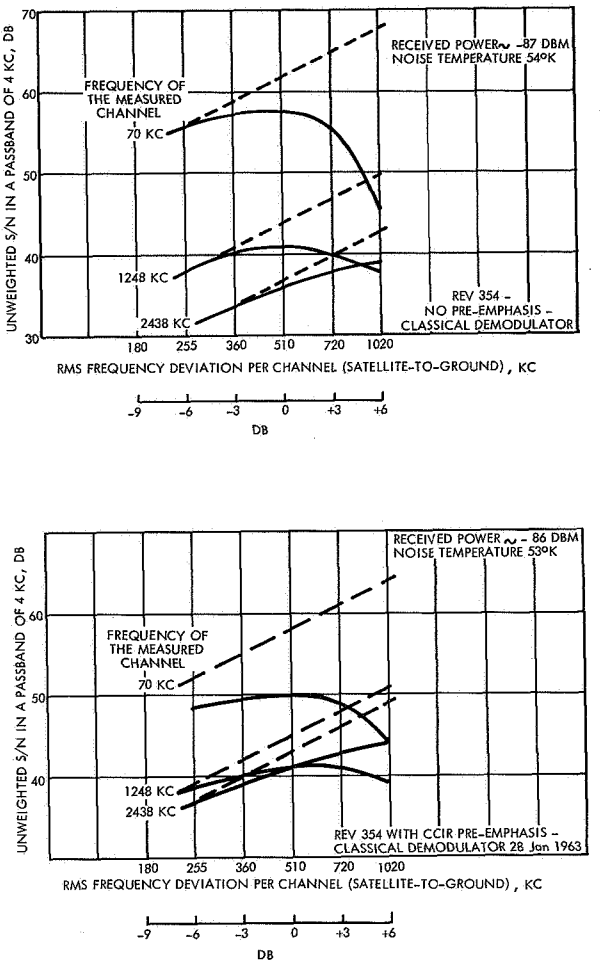
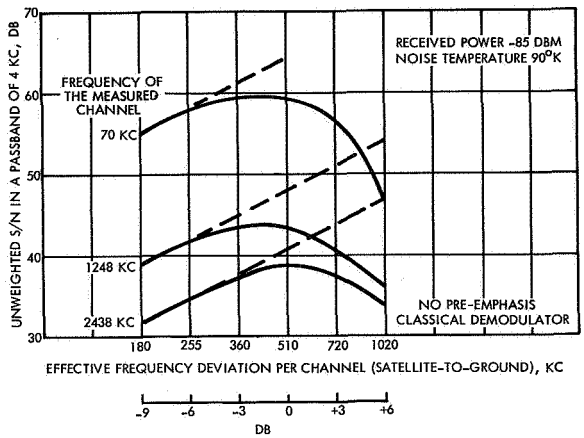


FIGURE 4–27.—Intermodulation noise for 600 one-way channels.

It can be deduced from these measurements that it would be possible, when pre-emphasis is not used, to choose an effective frequency deviation per channel on the order of 800 kc to obtain in the worst channel an optimum ratio of signal to unweighted noise of 39 db. When pre-emphasis is used, on the other hand, we observe as would be expected, an improvement in overall S/N ratio with an optimum value as high as 41 db for an effective frequency excursion per channel of about 650 kc. Under these conditions the total psophometric noise power is as high as 35,000 pw.

Figure 4–28 shows the same curves plotted for a link looped on the satellite simulator,



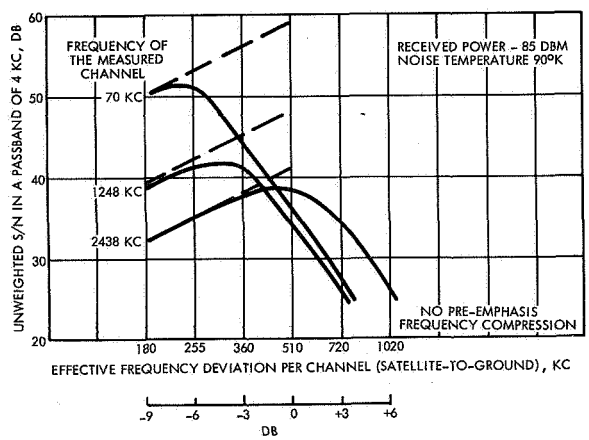
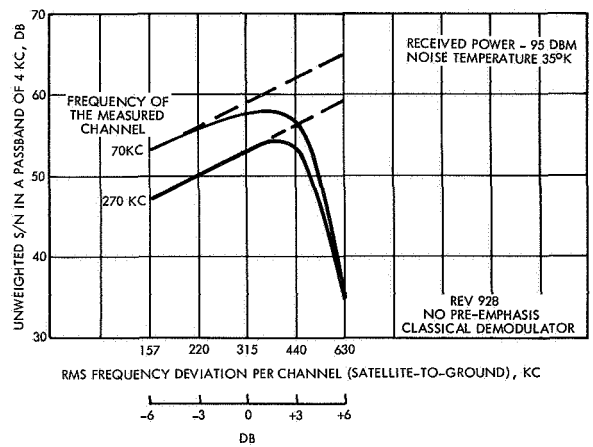


FIGURE 4–28.—Intermodulation noise for 600 one-way channels (in loop on the simulator).

with demodulation by a classical demodulator and by the frequency-compression demodulator. No pre-emphasis was used. The results obtained with the classical demodulator are comparable to those seen with the satellite, but with the frequency-compression demodulator the intermodulation noise is much greater. It is still possible with this demodulator, however, to obtain a signal to unweighted noise ratio in the worst channel of 38 db by reducing the effective frequency deviation per channel to about 400 kc. Under these conditions the use of the frequency-compression demodulator could be valuable whenever the receiving conditions were near threshold. Other measurements made using this same demodulator with the pre-emphasis network showed that the intermodulation noise was very large, even for very low values of frequency deviation per channel. This demodulator should therefore definitely not be used under those conditions.

Intermodulation Noise in Two-Way Telephony

Crosstalk measurements were made for a group of 60 two-way telephone channels in cooperation with the Andover station. No pre-emphasis was used. Figure 4–29 shows, as a function of rms frequency deviation per channel, the overall S/N ratio (thermal and



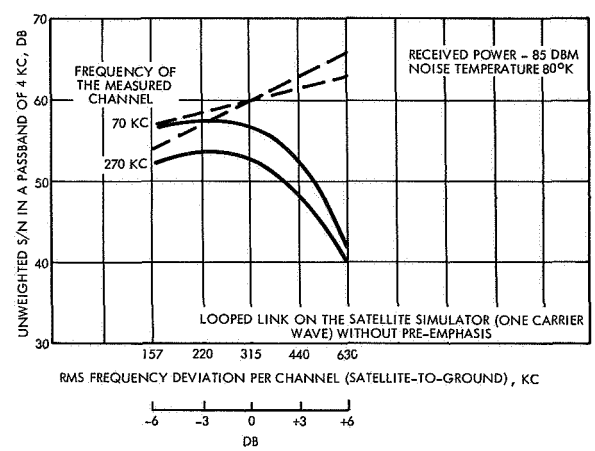


FIGURE 4–29.—Intermodulation noise for 60 two-way channels.

intermodulation noise) and the S/N ratio for thermal noise alone (dashed line). The conditions for the measurement were average, the received power —95 dbm, and the receiver noise temperature 35°K. It can be seen that with an rms frequency deviation per channel near 390 kc in the satellite-ground direction, the signal to unweighted noise ratio in a 4-kc pass band is 54 db in the worst channel (psophometric noise at a zero relative level point, 4000 pw). It is therefore possible to transmit with excellent quality 60 two-way telephone channels.

The same series of tests was performed with the link looped on the simulator, which was receiving a single carrier; the received power was in this case —85 dbm. Under these conditions the ratio of signal to thermal noise alone is higher than in the preceding case, and the intermodulation noise appears to be greater. With this observation in mind, the results shown on the same Figure 4–29 are comparable to those obtained with the link looped on the satellite. The abnormal shape of the variations of thermal noise alone in the window at 70 kc is due to the presence of equipment noise at low frequencies; this noise is no longer negligible when the noise contributed by the rest of the link is low.

Intelligible Crosstalk in Two-Way Telephony

Several passes of the satellite were used for measurement of intelligible intermodulation. Table 4–5 shows the results obtained in collaboration with the Andover station; the receiver RF bandwidth was limited by a filter of 6 or 3 Mc bandwidth. The Pleumeur-Bodou station transmitted a pure carrier wave at 1723.33 Mc and for the same carrier as received measured the noise in the channels centered at 100, 200, and 400 kc, while at the same time the Andover station transmitted a pure carrierwave at 1726.67 Mc (thermal noise alone). Then the Andover station transmitted this same carrier modulated by the center frequency (100, 200, 400 kc) of the channels measured at Pleumeur-Bodou (thermal noise plus intermodulation noise). The peak-to-peak frequency deviation at the receiver was 500 kc, 1 Mc, and 2 Mc.

With a 6 Mc RF band, a significant intermodulation is observed which appears to be independent of the frequency deviation chosen and which increases by about 6 db per octave as the frequency of the measurement channel increases. (It is possible to neglect in the total noise the portion due to thermal noise, since the ratio of signal to thermal noise alone is about 10 db greater than the overall S/N ratio.)

When the RF band is only 3 Mc, the intermodulation noise decreases by about 5 db, but still remains large and independent of the frequency deviation. It still increases essentially by 6 db per octave as a function of the frequency of the measured channel.

This latter characteristic is that of a noise generated after the first demodulation by

TABLE 4–5.—*Intelligible Crosstalk Signal to Unweighted Noise, No Pre-Emphasis*
[Δ F at receiver]

Measurement channel frequency (kc)	6 Mc RF band				3 Mc RF band			
	500 kc peak-to-peak		1 Mc peak-to-peak		1 Mc peak-to-peak		2 Mc peak-to-peak	
	Signal to thermal noise ratio (db)	Signal to total noise ratio (db)	Signal to thermal noise ratio (db)	Signal to total noise ratio (db)	Signal to thermal noise ratio (db)	Signal to total noise ratio (db)	Signal to thermal noise ratio (db)	Signal to total noise ratio (db)
100	52.3	44.5	----------	----------	58	49.5	63.5	49.5
200	50	39	55.5	38.5	----------	----------	60	44
400	44	34	50	32	----------	----------	56	38

the addition of white noise to the carrier prior to final demodulation. In order to explain the independence of intermodulation noise from the frequency deviation of the modulated carrier, additional measurements would be required for lower frequency deviations.

It should be noted the modulation of a carrier by a sinusoidal signal does not correspond to the reality of transmission of a telephone multiplex. Measurements made by simulating a 60-channel telephone multiplex with white noise have shown that the quality of the transmission was very good.

Distortions of the Television Signal

The study of distortions in the video channel of the television signal was performed by using the standard signals recommended by the CCIR. In the audio channel measurements were made of the overall distortion of a sinusoidal signal varying in frequency over the entire band used (20 to 8000 cps). Finally, a study was made of the intermodulation which could occur between these two channels.

Distortion in the Video Channel—Linear distortions in the video channel were measured at the frame frequency, the line frequency, and high frequencies. At the frame frequency the signal used was the CCIR test signal No. 1, to which was added frame sync pulses. A significant distortion was noted in the level of the sync pulses; this distortion, which was as high as 25 percent, was observed when the link was looped in baseband and is generated on the ground in the video equipment. At the line frequency, no distortion was observed in the CCIR test signal No. 2 when the classical demodulator was used; when the frequency-compression demodulator was used there was initially a distortion as high as 20 percent which was reduced to less than 5 percent after adjustment of the linearity of the slope of the demodulator. The measurement of the rise time of this same CCIR signal No. 2, calibrated at 166 nsec when transmitted, saw some distortions at high frequencies. The rise time of the reconstituted signal was as high as 200 nsec, whether the link was looped in baseband or on the satellite. This corresponds to the limiting of the frequency band used by a low-pass filter at 3 Mc.

Nonlinear distortion at average frequencies was measured by means of CCIR test signal No 3 with a 1-Mc sinusoid superimposed. The peak-to-peak amplitude variations of the 1-Mc sinusoid, filtered out from the rest of the signal and observed on an oscilloscope screen, do not exceed 5 percent; this value is comparable to that obtained when the link is looped in baseband. The same test signal was used to measure nonlinear distortion of the line sync signals when the video portion of each intermediate line, or three lines out of four (between the lines carrying the sawtooth signal), was set at the black, gray, or white level. The observed distortion does not exceed 10 percent.

No intermodulation of the audio channel on the video channel was detected.

Distortion in the Video Channel—Linear overall distortion of the sinusoidal signal of frequency varying from 30 to 8000 cps was measured with the loops closed at baseband, through the simulator, and through the satellite itself. The peak frequency deviation caused by the sinusoidal signal on the subcarrier was 17.7 kc; the subcarrier modulated the carrier with a peak frequency deviation of 1.4 Mc.

With the baseband loop the overall distortion for all frequencies between 30 and 8000 cps was less than 2 percent. The results obtained with the loop through the simulator or the satellite are comparable, with the overall distortion never exceeding 3 percent.

Intermodulation of the video on the audio channel was studied by measuring the peak signal to rms noise ratio while the video carrier was either unmodulated or modulated by the various signals used for video tests as well as by a test pattern or an actual tape recorded television program. The results obtained with the Andover station receiving, in loop test on the satellite, or through the simulator are identical, indicat-

ing that the distortions are as one would expect to be produced in the ground equipment. When no pre-emphasis is used the deterioration of the S/N ratio is large, reaching values often below 25 db rather than the average 50 db value when the carrier is unmodulated. With the use of a pre-emphasis network for the video signal conforming to the CCIR recommendation for the 405-line standard, the ratio is improved by about 5 db. The effect of pre-emphasis of the audio signal is even more pronounced; in this case the S/N ratio remains practically always above 40 db. With pre-emphasis for both signals the ratio is always above 45 db, and the link can then be considered to be of good quality.

Absolute Measurement of Propagation Time

Absolute measurement of propagation time was performed in loop on the satellite by measuring the interval of time which separates the transmission and reception of a square pulse with a very steep leading edge (rise time less than 1 microsecond). The whole video frequency band is used for this transmission; the accuracy obtained is $\pm$ 0.2 microsecond over the round-trip time, of $\pm$ 30 meters in satellite range. It is possible to compare the measured value with the value derived from the satellite range as determined from the orbital data. Figure 4–30 shows the deviation between these two values. It is seen that the agreement is good, with the maximum deviation of 15 microseconds corresponding to a range error relative to the computed range of about 5×10^{-4}.

System Tests

A large portion of the Relay I passes utilized at Pleumeur-Bodou were devoted to system tests or to demonstrations. During the period 4 January to 30 November 1963, 13 passes were used for system tests or demonstrations of telephony and 36 were used for television system tests or demonstrations.

SYSTEM TESTS FOR TELEPHONY

System tests of two-way telephony were performed in both the 12–60 kc and 60–108 kc bands. Eleven passes altogether were used for these tests in the January-November 1963 period. For several of these passes the link was actually used to re-transmit telephonic communications between subscribers in Europe and subscribers in the United States. The link was always excellent with respect to the contact established and the noise in the telephone channels. The results of quality tests which took into account the influence of propagation time and the operation of the echo suppressors are not yet available.

When the link is used for a telephone multiplex, one of the channels can be used for facsimile transmission. Figure 4–31 is a reproduction of the first facsimile transmission sent from Washington and received in Paris via the Relay satellite. Some deformation can be seen; it is caused by the variation in propagation time during the transmission, which has the effect of breaking the relative synchronization of the facsimile transmitter and receiver. This effect, which is tolerable in the case shown here, is nevertheless sufficiently large to be troublesome in the case of transmission of newspaper pages or drawings.

System Tests of Television

During the period 4 January to 30 November 1963, 36 passes were devoted to system tests of one-way television. Eighteen of these passes were used in the U.S.-Europe direction and 16 in the Europe-U.S. direction, while on two passes the link was used in each direction in turn. The received pictures were always of excellent quality and were often retransmitted over the Eurovision network. Figures 4–32, 4–33, 4–34 and 4–35 are reproductions of pictures received at the Pleumeur-Bodou station; Figure 4–34 was received during the first operational pass of the satellite and Figure 4–35 during a public demonstration on the occasion of the showing in the U.S. of the famous painting, "La Gioconda" (Mona Lisa).

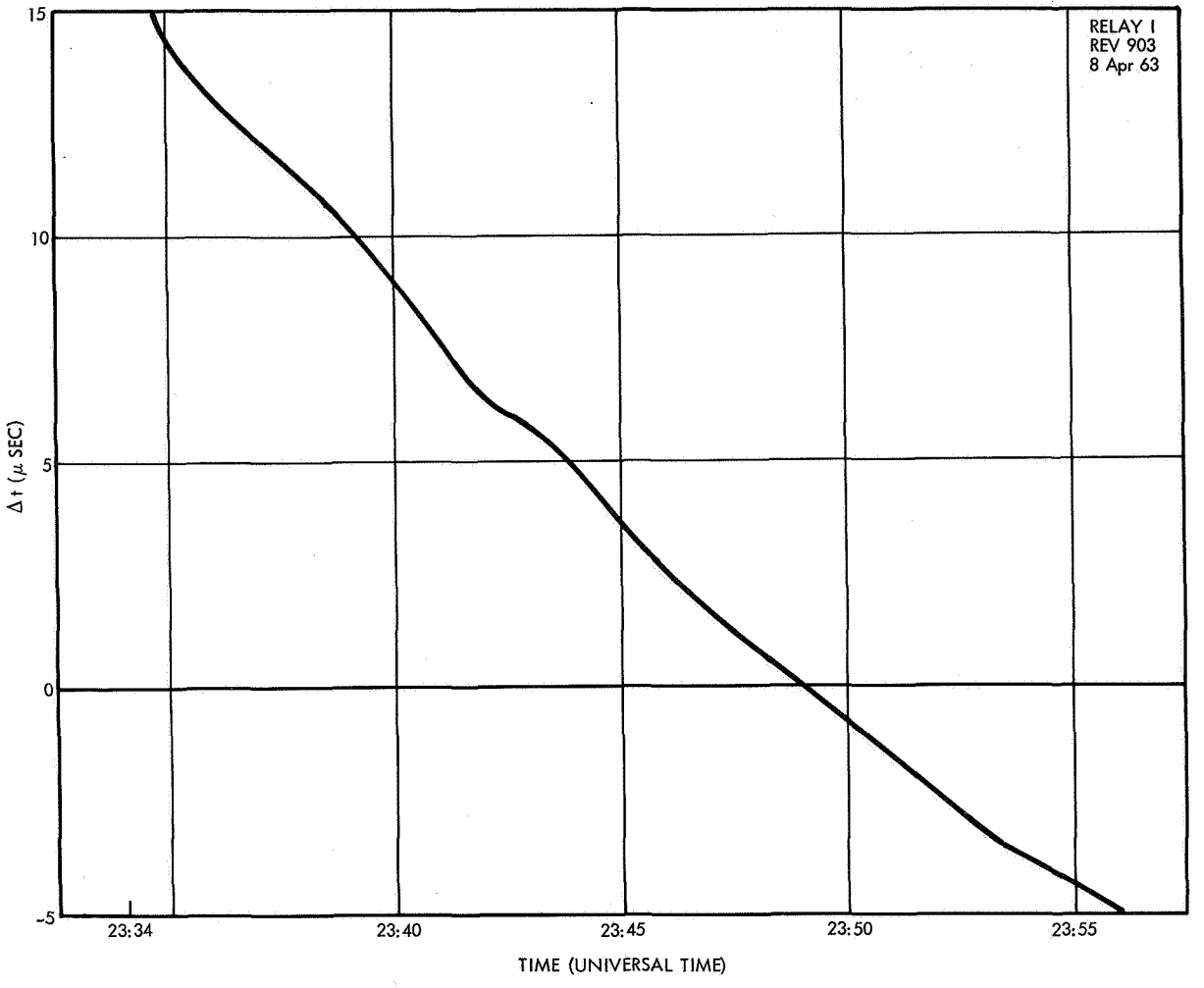


FIGURE 4–30.—Measurement of propagation time (deviation of measured value from calculated value).

CONCLUSION

The results of acquistion and tracking tests and of communications tests performed with the Relay I satellite were extremely satisfactory. They showed that it is possible to point a large antenna at a moving satellite with great accuracy, and that acquisition does not present any special problems. The wideband link established with the satellite is of excellent quality and the transmission of a telephone multiplex signal of 600 channels or a 525-line television signal was readily accomplished.

AUTHORS. *This chapter was contributed by* L. BOURGEAT, A. DYEVRE, *and* J. P. HOUSSIN, *Centre National d' Etudes des Telecommunications (CNET), Issy-les-Moulineaux, France.*

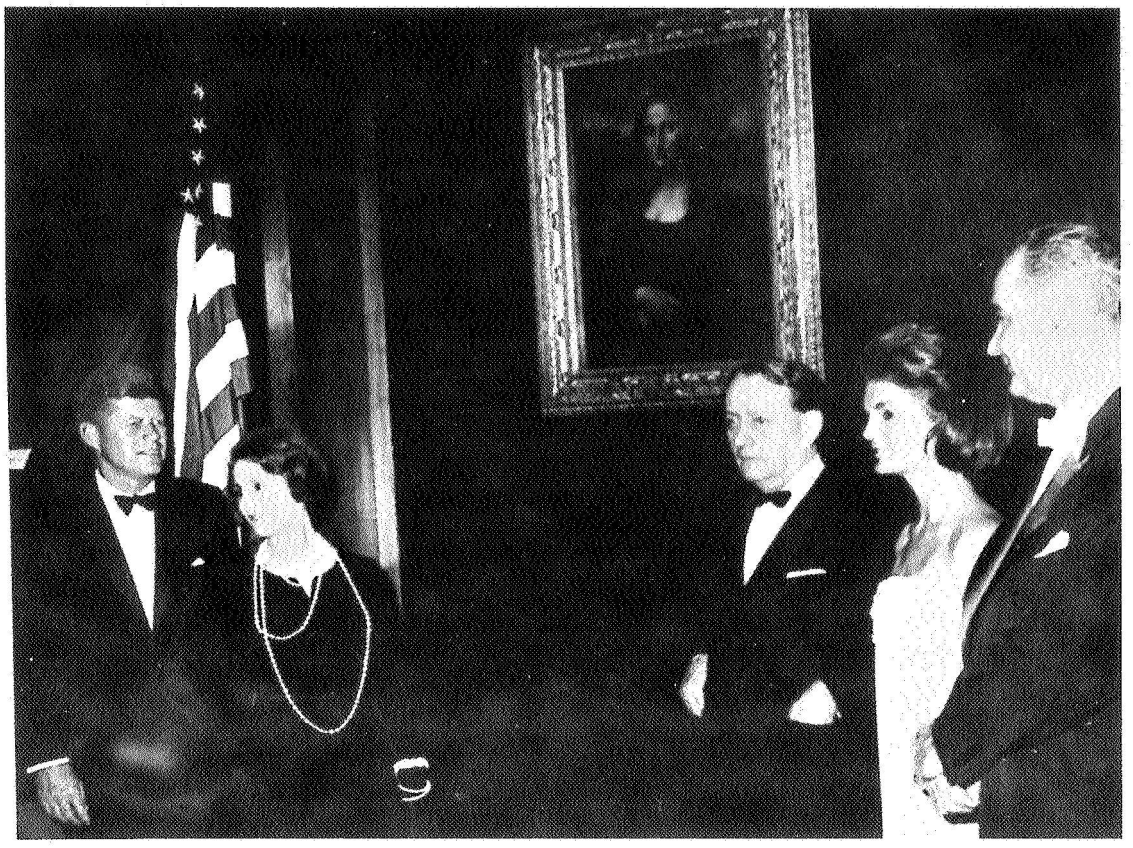


FIGURE 4–31.—First facsimile transmitted from Washington to Paris.

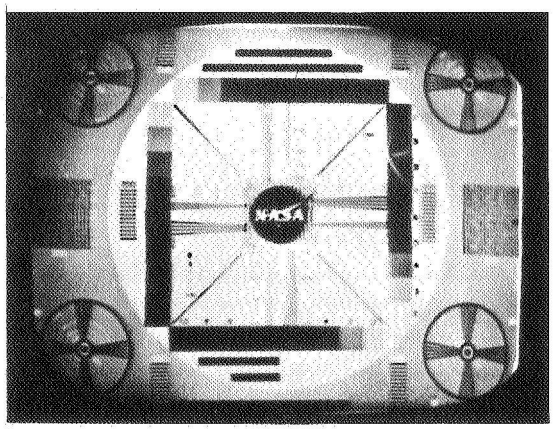


FIGURE 4–32.—Test pattern received at Pleumeur-Bodou from Andover pass 200.



FIGURE 4–33.—Picture received at Pleumeur-Bodou from Andover pass 206.

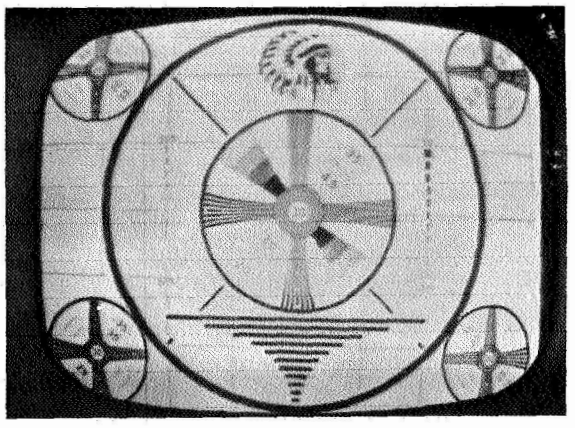


FIGURE 4–34.—Test pattern received at Pleumeur-Bodou during first operational pass of Relay I.



FIGURE 4–35.—Picture received at Pleumeur-Bodou during first public demonstration.

N66-10255

Chapter 5

The Raisting Space Communications Station

GENERAL

In 1961 the Deutsche Bundespost decided to take part in the international experiments for the transmission of communications via artificial satellites and in 1962 began to erect an earth station near Raisting (Upper Bavaria).

On 8 November 1963, a narrowband installation for 12 telephone channels (4-wire) was already put into operation, which enabled the Deutsche Bundespost to participate in the experiments performed within the scope of the NASA project Relay and the ATT project, Telstar. The results of these tests are compiled in Chapter 6.

By autumn, 1964, a wideband installation will be available, allowing the transmission of some one hundred telephone calls or one television program over satellites of the Relay or Telstar type.

Selection of the site for an earth station was particularly difficult because there is a very dense radio-relay network in the Federal Republic of Germany. A site near Raisting proved to be suitable since it is rather a long way off the main radio-relay links, and, as may be seen in Figure 5–1, the ridges of hills surrounding the terrain on all sides prevent interferences caused by other radio services. Figure 5–2 shows the horizon around the earth station.

There are two 2 Gc radio-relay links connecting the earth station with the long-distance network of the Federal Republic of Germany.

Raisting is about 10 km from the Olympia highway and has a railway depot (Figure 5–3).

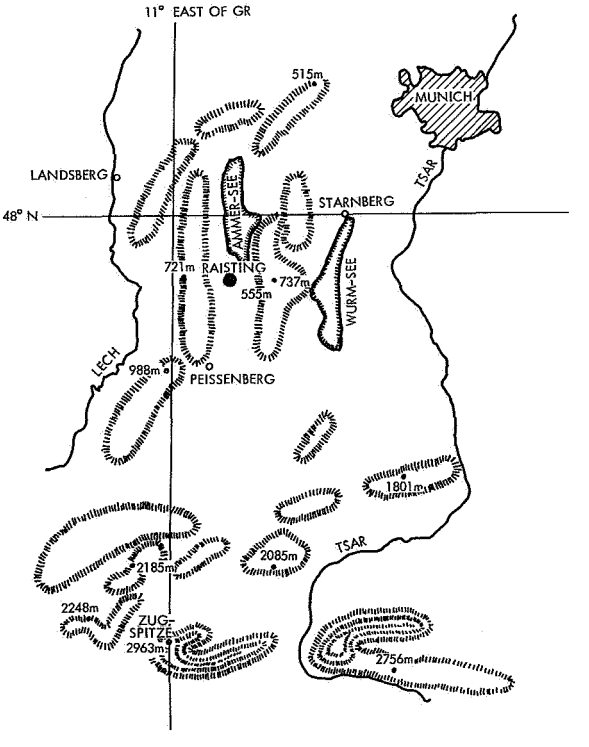


FIGURE 5–1.—Topology of Raisting earth station.

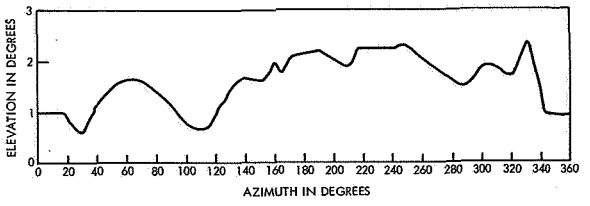


FIGURE 5–2.—Optical horizon at Raisting.

The environs of Raisting with the outline of the mountains defined against the sky and the close-by lake (Ammersec) allowing all kinds of aquatics, are a lovely place for the residential quarters of the staff members of the earth station.

NARROWBAND INSTALLATION

This installation was designed and constructed by the International Telephone and Telegraph Federal Laboratories at Nutley, New Jersey (USA). It consists mainly of a radio van with one trailer for the antenna support and another one for the heat exchanger. Figure 5–4 shows how the equipment and the additionally required huts are set upon the Raisting site.

Antenna

Use is made of a collapsible 9 m Cassegrain antenna, the gain of which is about 48 db at 4 Gc and about 51 db at 6 Gc. The beamwidth of the main lobe is at about 0.5° (3 db points). Immediately behind the antenna there is a trunnion box which is permanently connected with the reflector and which transmits the elevation motion to the antenna. The box contains, among other things, the RF units of the 2 Gc and 6 Gc transmitters, and of the 4 Gc receiver and the mixers (Figure 5–5).

The slewing range of the antenna covers —2° to +92° in the elevation and ± 300°

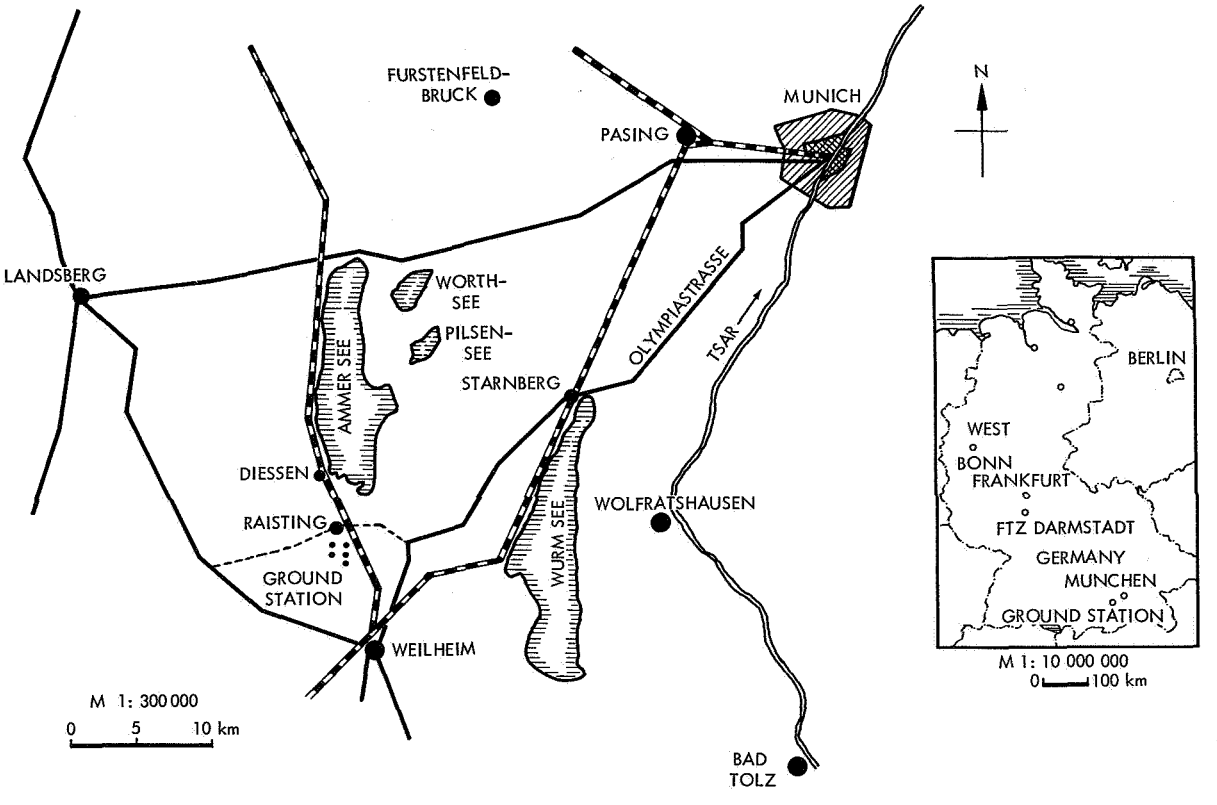


FIGURE 5–3.—Location of Raisting earth station.

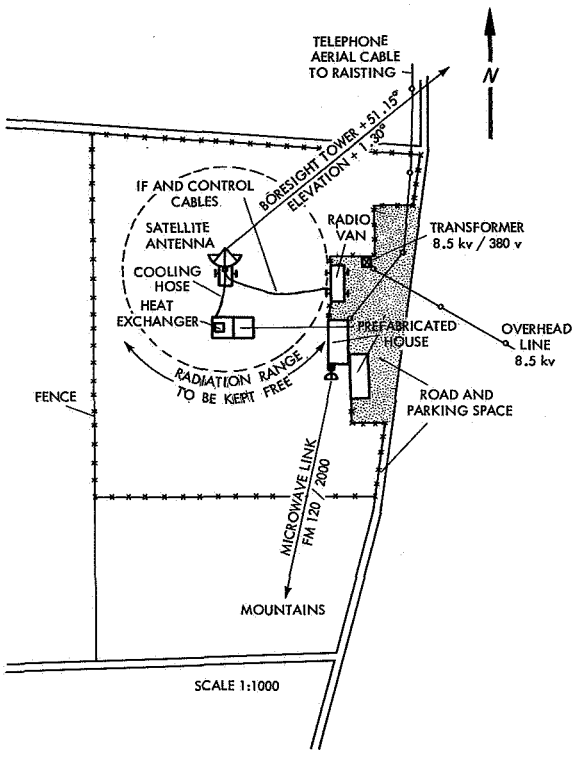


FIGURE 5–4.—Transportable satellite earth station Raisting (upper Bavaria).

in the azimuth. Its maximum slewing velocity is 5 degrees per second in the elevation and 10 degrees per second in the azimuth. The minimum slewing velocity amounts to 0.004 degrees per second, i.e., about 360 degrees per day. The antenna can still operate at wind velocities of up to 56 km/h.

Transmitter System

Each transmitter uses a 4-cavity klystron and supplies the antenna with a power of 10 kw. The klystrons are remotely controlled from the radio van. The klystrons and waveguides at the transmitter output are cooled by heat exchangers. The carrier baseband 12–60 kc provided for transmission purposes is fed to the FM modulator housed in the radio van, where it is converted into the IF-position 71.5 Mc (center frequency). Feeding to the RF box of the antenna is done via an interconnecting cable.

Receiver System

The communication signal received from the satellite is fed, via a frequency filter, to an uncooled parametric amplifier which has a gain of about 20 db and a noise figure of about 2.5 db. The pump frequency of the oscillator klystron in the receiver is 13.92 Gc. The signal converted into the IF position of 65 Mc is fed via an interconnecting cable to the receiver units housed in the radio van. A FM demodulator with feedback is used to improve the carrier-to-noise ratio. A carrier baseband of 12–60 kc is available at the demodulator output.

Antenna Pointing

Rough acquisition of the satellite is effected by manual positioning of the antenna, using orbital data calculated beforehand. Later on, antenna pointing is done by a beacon receiver. The beacon signal is fed via a 4-horn element in the antenna to a device effecting a separation in phase of a sum channel and two difference channels for azimuth and elevation. Filters ensure a good selection of the azimuth and elevation channels. In the sum channel, the communication signal is separated from the tracking signal and fed to the communication receiver. The separated tracking signals are fed to a 3-channel demodulator accommodated in the radio van.

When the antenna points to the satellite, a phase detector, after having made a phase comparison between the sum channel and the difference channels, supplies a direct current voltage proportional to the antenna pointing error. The error signal is used to correct the position of the antenna automatically. Because of the Doppler effect and the frequency instability, the sum channel receiver is equipped with a device for automatic frequency search and phase- lock. The receiver input voltage is continuously indicated for monitoring purposes.

THE WIDEBAND INSTALLATION

As mentioned before, this installation (Figure 5–6) will presumably be available

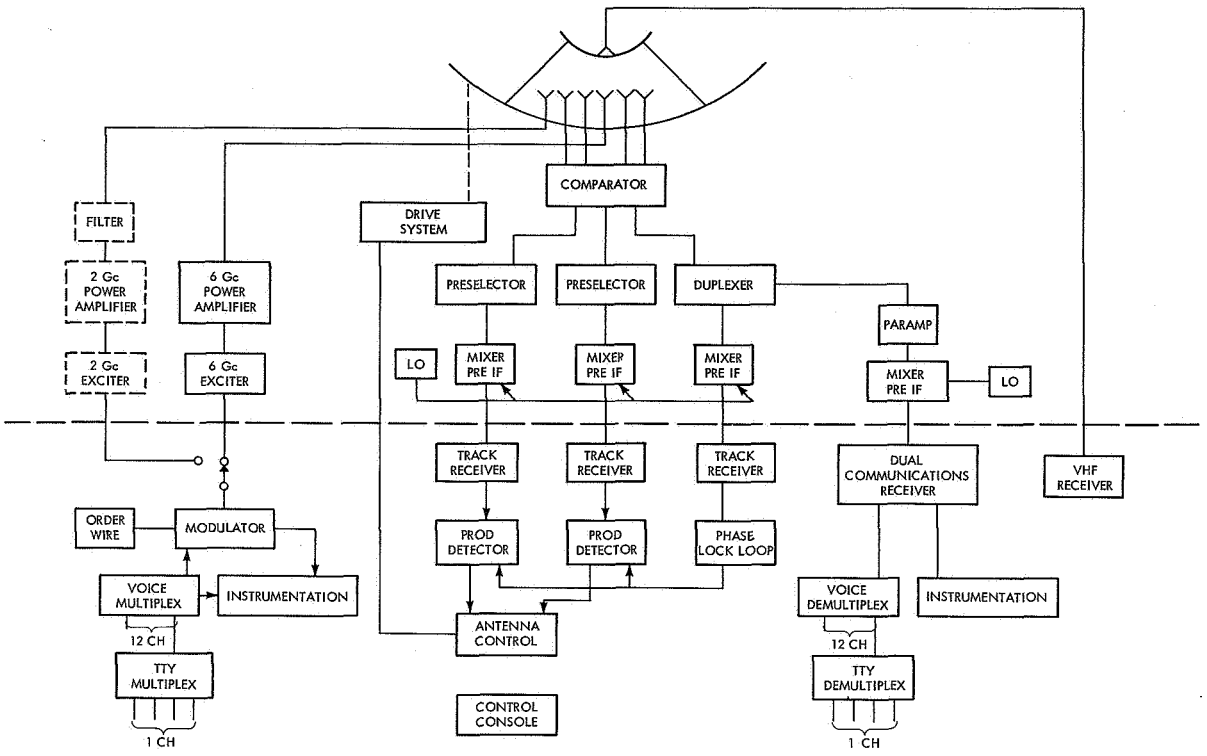


FIGURE 5–5.—Narrowband satellite earth station, Raisting, block diagram.

for transmission via communication satellites by autumn, 1964.

Antenna

This installation will use a 25 m parabolic reflector (Figure 5–7), which will be illuminated via a 2.5 m sub-reflector. The sub-reflector in turn will be excited by a small horn type parabolic antenna (Cassegrain principle). The focal length/diameter ratio is $f/D = 0.26$. The rim of the reflector is provided with a 0.5 m cylindrical shield to increase the front-to-back ratio.

Measurements at 34.7 Gc carried out on a scaled-down model (parabolic antenna 3 mϕ) indicated that in the 4 Gc range the antenna gain will be about 57 db. The measured beamwidth was 0.25° (3 db points).

The slewing range of the antenna covers ± 380° in the azimuth and —1° to +125° in the elevation.

An air-supported radome, having a diameter of 48.8 m and a height of 39 m, protects the antenna from the effects of the common elemental conditions.

Transmission System

The antenna system comprises a 6 Gc transmitter suitable for transmission tests via Telstar type satellites. The transmission system consists of an FM modulator, an exciter and a power amplifier designed for a maximum output of 2 kw. A water cooled traveling wave tube is used as power amplifier.

Receiving System

The receiving system comprises a maser, a low-noise amplifier and a FM receiver with FM feedback (Figure 5–8). The maser is cooled with liquid helium so as to obtain a noise temperature of about 4.5° K. For elevation angles exceeding 7°, the equivalent noise temperature of the entire receiving system will presumably be 54° K.

The FM receiver has three outputs, viz.,

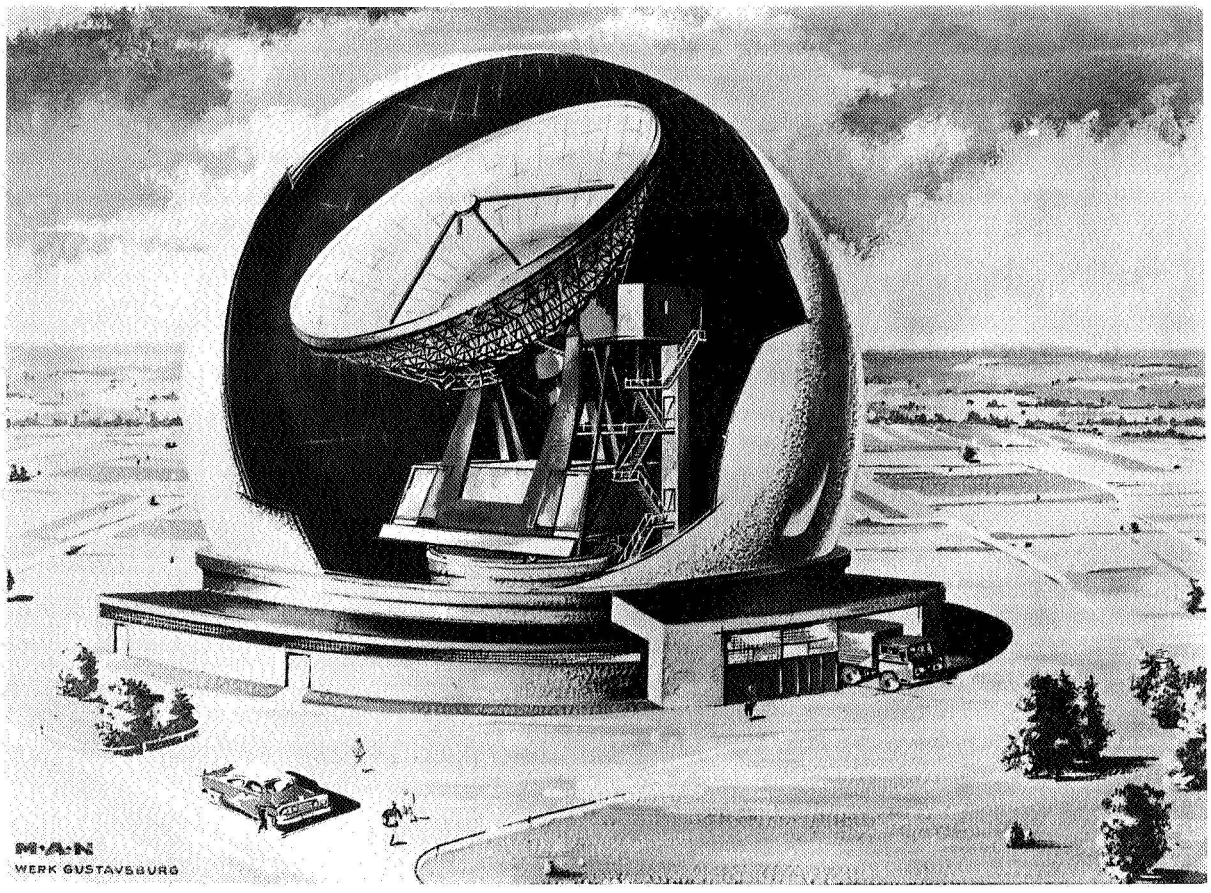


FIGURE 5–6.—Wideband installation at Raisting.

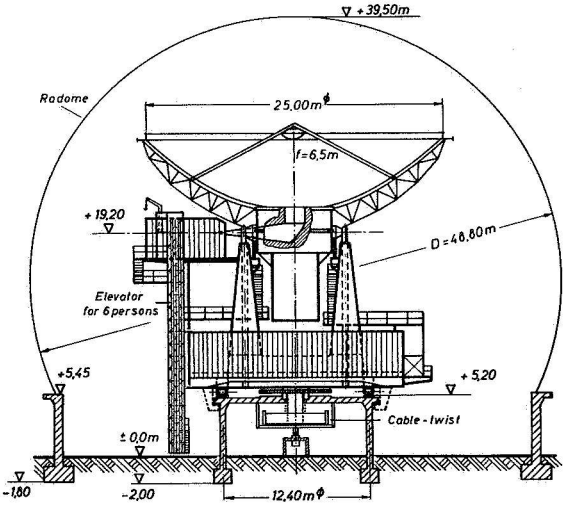


FIGURE 5–7.—Antenna Raisting—25 mØ Cassegrain.

one for the baseband, one for the television picture, and one for the sound. The receiving system allows reception of signals from Telstar and Relay type satellites. Both satellites use transmission frequencies in the 4 Gc range.

Helium Installation

Fifteen liter of liquid helium are required for a 24-hour operation of the maser. This demand is met by self-recovery and liquefying equipment, which is set up in the rotunda of the antenna building. From the upper antenna room the evaporated helium is immediately returned via a flexible pipe system to the helium treatment room, where it is stored in a gas tank. From there the helium

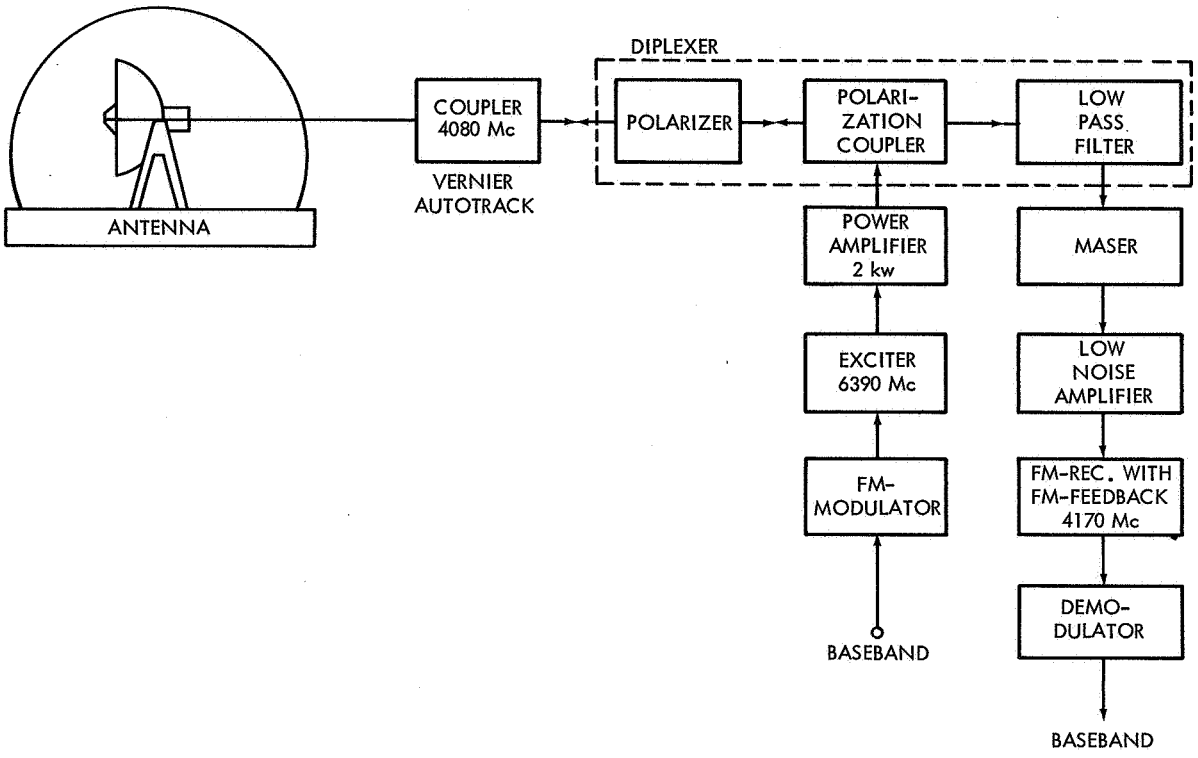


FIGURE 5–8.—Wideband satellite earth station Raisting, block diagram.

gas is fed via a preliminary filter to the liquefying equipment.

The installation operates fully automatically so that it does not need to be attended to at night.

Antenna Pointing

Prior to an expected satellite pass, data points, which are stored on magnetic tapes, are used to point the antenna to the satellite rise point on the horizon. An electronic computer (type IBM 1620/II) computes the data points from orbital data. At the beginning, these orbital data are supplied by NASA in the form of topocentric Cartesian coordinates.

The satellite emits beacon signals on 4080 Mc to be used for autotracking of the earth antennas. Upon reception of the beacon signal by the earth antenna, there is an automatic change-over to the antenna autotrack. Higher order modes of the 4080 Mc signal are developed in the horn reflector of the earth antenna. In the automatic precision tracking system these modes produce analog error signals which indicate the satellite position relative to the center of the antenna beam. These error signals are fed to the pointing system comprising the hydraulic drive system, the antenna and the digital equipment and can be used to position the antenna.

In order to increase the reliability, the magnetic tape is continuously running in support.

CENTRAL BUILDING

The central building, set up at a distance of about 300 m from the wideband installation, houses the equipment for recording testing, etc. In the test room there is, for instance, a magnetic tape recorder (Ampex FR 100 B) for recording the signals of facsimile, telegraph and data transmission tests. Moreover, a monitor is available for monitoring the picture quality of facsimile transmissions. A television standards converter converting the 625-line standard into

TABLE 5-1.—*List of the Equipment of the Raisting Earth Station*

	Narrowband installation			Wideband installation		
1. Parabolic antenna	9 m diameter. Angle of aperture 140° Distance between reflector and subreflector . . . 3 m. Cassegrain principle, without radome.			25 m diameter. Angle of aperture 180°. Distance between reflector and subreflector 6.5 m. Cassegrain principle radome 49 mϕ and 39 m height.		
1.1 Driving	Used for transmission and reception. Azimuth ± 300°, (10°/sec), Elevation −2 to +92° (5°/sec) Hydraulic drive.			Used for transmission and reception. Azimuth ± 380° (2°/sec) Elevation −1° to +125° (2°/sec) Hydraulic drive.		
1.2 Performance	Half-power width (3 db)	Gain	Equivalent noise temperature at 7.5 elevation	Half-power width (3 db)	Gain	Equivalent noise temperature at 7.5° elevation
4170 Mc	0.6°	48.4 db	350°	0.245	57.5 db	54°
6390 Mc	0.39°	51 db	----	----	61 db	----
1725 Mc	1.4°	41.0 db	----	----	----	----
2. Transmitter						
Frequency	1725 Mc. 6390 Mc.			----		
Feature	Water-cooled klystron amplifier.			6390 Mc. Water-cooled traveling wave tube.		
Performance	10 kw, bandwidth 1 Mc.			2 kw, bandwidth 25 Mc.		
3. Receiver						
Frequency	4170 Mc.			4170 Mc.		
Feature	Uncooled parametric amplifier.			Helium cooled maser.		
Performance	Noise temperature 290°K.			Noise temperature 4.5°K.		
4. Tracking system						
Frequency	4080 Mc.			4080 Mc.		
Feature	Communication antenna Monopulse mode.			Communication antenna Monopulse mode.		
Performance:						
Minimum tracking signal level	−130 dbm.			−130 dbm		
Pointing accuracy of the antenna	0.02°			0.003°		
5. Antenna pointing system						
Structure	Manual servo system.			Computer IBM 1620/II Magnetic tape, digital system, digital analog converter, servo system.		
	Autotracking of the antenna.			Autotracking of the antenna.		
Mode of operation	Manual, automatic.			Magnetic tape, automatic.		
6. AC Power supply	180 kva			800 kva.		
Emergency	----			Battery 2×2304 Ah/10h and Diesel driven generator set.		

the American 525-line standard and vice versa is set up in the control room of the central building. An RCA video recorder allows the recording of television programs. In addition there are German and American test pattern generators.

Two radio relay links, FM–120/2000 and FM 960–TV/1900, connect the Raisting earth station with the Deutsche Bundespost long-distance network. The FM 120/2000 link is used for internal telephone and teleprinter channels and for connection of 12 voice channels of the German domestic network to the terminal equipment of the narrow-band and wideband installations. The FM 960–TV/1900 link connects the Raisting earth station with the television network. Table 5–1 lists the equipment at the Raisting earth station.

Power Supply

The power supply of the Raisting earth station, accommodated in the central building, has a connecting load of 1000 kva and is, for the time being, only designed for test operation with a wideband and a narrowband installation. About 800 kva are required for the wideband installation and about 200 kva for the narrowband installation.

The wideband installation is connected to the 25 kv overhead power line of the Isar-Amper electric power company. The narrowband installation is at present supplied from a 7.5 kv transformer station at Raisting. Since the public power supply network is subject to voltage fluctuations and short-term mains failures, the power supply for the wideband installation was designed so as to attain a test service as free of failures as possible. To this end, a battery has been provided having a capacity of 2×2304 Ah/10h and in the case of a main power failure, allowing trouble-free operation for about 1 hour. In addition, there are three rotary converters, converting the dc voltage of the battery into ac voltage.

AUTHORS. *This chapter was contributed by personnel of the Deutsche Bundespost, Darmstadt, Germany, under the overall direction of* E. DIETRICH, *DBP.*

N66-10256

Chapter 6

Results of Tests Performed With Relay I at the Raisting Space Communications Station

INTRODUCTION

In 1963 a narrowband installation with 9 m parabolic Cassegrain antenna was set up at the Raisting earth station.

The station was expected to be ready for operation by 1 October 1963. However, a faulty 10 kw klystron caused some delay. Therefore, only monitoring experiments were carried out during the first days.

Upon replacement of the tube on 23 October 1963, COMGEB was also able to transmit on 1.7 kMc. Table 6–1 shows the test program carried out via Relay I:

Table 6–2 shows the azimuth, elevation, loop angle and slant range from COMGEB earth station to Relay I at the beginning and end of the experiments.

Deviation of Angle Readouts

Table 6–3 shows typical deviations of angle readouts from predicted pointing data supplied by Goddard Space Flight Center, NASA.

Test Results

The test duration per revolution of the experiment between COMGEB and COM-

TABLE 6–1.—*Test Program*

Rev	Test period	(GMT)	Content	Circuit
2403	63Y 10M 18D	1542–1559	Test 352	COMNUT-COMHIL*
2411	10M 19D	----------	----------	Satellite not available
2418	10M 20D	1342–1403	Test 221, 231	COMAND-COMGEB†
2426	10M 21D	1408–1420	Test 321	COMNUT-COMRIO*
2443	19M 23D	1920–1938	Test 221, 231	COMNUT-COMGEB
2449	10M 24D	1310–1325	Test 351, 321	COMNUT-COMGEB
2496	10M 30D	1420–1445	Test 221, 241	COMNUT-COMGEB
2558	11M 7D	1353–1358	Test 221, 231	COMAND-COMGEB
2563	11M 8D	1415–1440	Test 321	COMAND-COMGEB
2567	11M 8D	1739–1801	Test 254	COMNUT-COMGEB
2589	11M 11D	1320–1330	Test 321	COMAND-COMGEB
2614	11M 14D	1857–1903	Test 221, 231	COMNUT-COMGEB
2628	11M 16D	1330–1345	----------	Loop for COMNUT
2629	11M 16D	1650–1710	----------	COMNUT-COMGEB
3055	64Y 1M 10D	1030–1049	Test 231	COMNUT-COMTEL*
3094	1M 15D	1033–1048	----------	COMAND-COMHIL‡

*COMGEB monitored only. †COMGEB received only. ‡COMGEB tracked only.

TABLE 6–2.—*Position of Relay I During the Experiments*

Rev	AZ (deg)		EL (deg)		Range (km)		Loop angle (deg)		Circuit
	Beg	End	Beg	End	Beg	End	Beg	End	
2403	268	272	17	55	9705	5426	-------	-------	COMNUT-COMHIL*
2411	-------	-------	-------	-------	-------	-------	-------	-------	SATELLITE not available
2418	246	246	25	58	9400	6300	-------	-------	COMAND-COMGEB†
2426	256	258	2	14	12000	10500	-------	-------	COMNUT-COMRIO*
2443	-------	-------	-------	-------	-------	-------	-------	-------	COMNUT-COMGEB
2449	258	250	18	37	10346	8405	-------	-------	COMNUT-COMGEB
2496	273	275	17	56	10030	5906	-------	-------	COMNUT-COMGEB
2558	279	274	50	65	6660	5726	129	137	COMAND-COMGEB
2566	285	278	16	54	10287	5112	103	134	COMAND-COMGEB
2567	301	263	5	26	9644	5794	114	119	COMNUT-COMGEB
2589	280	277	38	57	8081	6411	118	132	COMAND-COMGEB
2614	280	263	5	5	7525	6717	113	105	COMNUT-COMGEB
2628	287	282	22	45	9602	7127	110	127	Loop for COMNUT
2629	302	269	7	24	9921	6294	115	118	COMNUT-COMGEB
3055	275	239	18	13	10094	9244	102	87	COMNUT-COMTEL*
3094	293	275	6	8	11624	11081	101	96	COMAND-COMHIL‡

*COMGEB monitored only. †COMGEB received only. ‡COMGEB tracked only.

NUT or COMAND was in general 15 to 20 minutes. The following narrowband tests were conducted:

221 Insertion gain stability

TABLE 6–3.—*Relay I—Revolution 3055*

NASA pointing data		Deviation (deg)	
AZXX	ELXX	AZ	EL
27260	1831	−0.10	−0.03
27118	1840	−0.08	+0.02
26973	1847	−0.08	−0.03
26827	1850	−0.09	−0.03
26679	1851	+0.06	−0.02
26529	1847	−0.06	+0.03
26378	1841	+0.07	+0.04
26226	1831	−0.06	−0.04
26071	1817	+0.06	−0.03
25916	1800	−0.07	−0.05
25759	1779	−0.09	+0.02
25601	1754	−0.09	−0.04
25442	1725	+0.07	−0.05
25282	1693	−0.10	+0.04
25120	1657	−0.06	−0.05
24958	1617	+0.08	−0.07
24795	1573	−0.09	−0.08
24632	1524	−0.09	+0.05
24467	1472	+0.08	−0.05
24302	1416	−0.12	−0.06
24137	1356	−0.10	−0.05

231 Continuous random noise

241 Amplitude-frequency characteristic-baseband

254 Intelligible crosstalk

321 Two-way telephony

351 Teletype transmission

352 Facsimile transmission

The experiments performed are shown in Table 6–4.

Insertion Gain Stability (221)

The tests were made to determine system insertion gain and gain stability for several telephone channels. The results of the measurements made on channels 1, 6 and 12 are indicated in Table 6–5.

Continuous Random Noise (231)

The purpose of this test was to determine the ratio of rms signal power to rms noise power existing in the telephone channels. In this case, too, measurements were made on channels 1, 6, and 12 (See Table 6–6).

Amplitude-Frequency Characteristic—Baseband (241)

The experiments were made to determine

TABLE 6–4.—*Narrowband Tests Conducted at COMGEB*

Rev	Experimental item							Circuit
	221	231	241	254	321	351	352	
2403	----	----	----	----	----	----	X	COMNUT-COMHIL*
2411	----	----	----	----	----	----	----	----------
2418	X	X	----	----	----	----	----	COMAND-COMGEB†
2426	----	----	----	----	X	----	----	COMNUT-COMRIO*
2443	X	X	----	----	----	----	----	COMNUT-COMGEB
2449	----	----	----	----	X	X	----	COMNUT-COMGEB
2496	X	----	X	----	----	----	----	COMNUT-COMGEB
2558	X	X	----	----	----	----	----	COMAND-COMGEB
2566	----	----	----	----	X	----	----	COMAND-COMGEB
2567	----	----	----	X	----	----	----	COMNUT-COMGEB
2589	----	----	----	----	X	----	----	COMAND-COMGEB
2614	X	X	----	----	----	----	----	COMNUT-COMGEB
2628	----	----	----	----	----	----	----	Loop for COMNUT
2629	----	----	----	X	----	----	----	COMNUT-COMGEB
3055	----	----	----	----	----	----	----	COMNUT-COMTEL*
3094	----	----	----	----	----	----	----	COMAND-COMHIL‡

*COMGEB monitored only.
†COMGEB received only.
‡COMGEB tracked only.

TABLE 6–5.—*Insertion Gain Stability Tests*

Rev	221		Circuit
	Gain	Variation	
2418	+4.8	----------	COMAND-COMGEB
2443	+0.5	----------	COMNUT-COMGEB
2496	−0.4	----------	COMNUT-COMGEB
2558	−0.1	----------	COMAND-COMGEB
2614	----------	----------	COMNUT-COMGEB

TABLE 6–6.—*Random Noise Measurement*

Orbit	231	Circuit
	Signal-to-noise ratio average (db)	
2418	40	COMAND-COMGEB
2443	34	COMNUT-COMGEB
2558	37	COMAND-COMGEB
2614	36	COMNUT-COMGEB

the useful system baseband. The measured characteristic is shown in Table 6–7. The measuring set was connected to the baseband output jack of the communication receiver.

Intelligible Crosstalk (254)

On orbit 2567, a 1726 Mc modulated signal with 100 kc was transmitted for COMNUT. The signal deviation was 100 kc peak to peak. A signal from COMNUT could not be measured due to receiver problems. The same happened on orbit 2629.

Two-Way Telephony (321)

The COMNUT-COMRIO two-way telephony test was monitored on orbit 2426. Voice on channels 3, 4, and 12 was recorded on tape from both receivers (communications monitor receivers). The voice quality was good. Spin modulation was found to exist on the channels transmitted from COMNUT.

During orbit 2449 (COMNUT-COMGEB) the first talk was made with COMNUT on channels 2, 4, and 5. The quality of channel 4 was good. Echos were heard on channels 2 and 5.

On orbit 2566 (COMAND-COMGEB) a two-way telephone conversation took place between Mr. Webb (Administrator of NASA) and Mr. Stücklen (Bundesminister für das Post- und Fernmeldewesen) on channel 2. Voice quality was not good due to noise on this channel. An attempt was made to switch over to channel 12, but there the same noise was also present. However, voice quality on channel 4 was good.

On orbit 2589 (COMAND-COMGEB) a two-way telephone demonstration was made by the German Press Agency DPA. Channels 2 and 12 were used for this purpose. Voice quality on channel 2 was good, but on channel 12 it was insufficient due to noise.

Teletype Transmission (351)

The purpose of this test was an evaluation of the quality of telegraph transmission via

TABLE 6–7.—*Orbit 2496 COMNUT-COMGEB*

Frequency (kc)	10	20	30	40	50	60	70	80	100	120
Level (db)	−10.5	−9.5	−10.0	−9.8	−10	−10.4	−10.1	−9.9	−10.4	−9.8

satellites. This transmission was performed on Relay I revolution 2449.

A FMVFT system (FM 120-24 channels) was used for transmission. A tape recorder Ampex FR–100 B was to receive the same signal which was looped through COMNUT. The COMGEB station was connected by means of a land and microwave line to the FMVFT equipment at Frankfurt/Main.

The results of this experiment are shown in Table 6–8.

Facsimile Transmission

This test was made to compare the performance of medium speed facsimile using the satellite with that of other existing media.

The transmission on Relay I orbit 2403 was performed when the COMNUT-COMHIL pass was monitored. The received signal was fed to Frankfurt/Main and recorded on an Ampex FR–100 B tape recorder. Figure 6–1 shows the received picture.

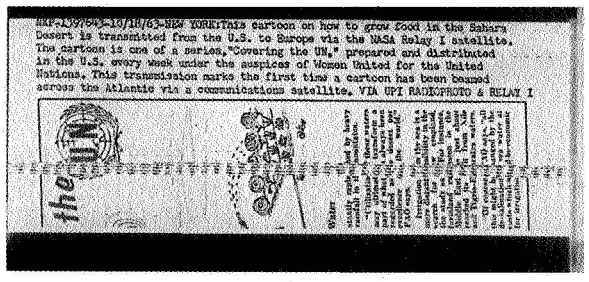


FIGURE 6–1.—Facsimile picture.

Due to late acquisition (this was the very first pass) only the second half of the picture was received. A channel reversal in the demux equipment caused the black and white frequencies to be also reversed. Thus the received picture was negative. During the recording, one interruption occurred when COMGEB lost track for 20 seconds.

Technical details were:

Index of cooperation: 352

Drum speed: 60 rpm

Landline signal: FM 800 ± 400 cps

Received Signal Power

The receiver AGC voltage was recorded during all passes. Table 6–9 shows the received signal strength at the beginning, in the middle and at the end of each pass:

Noise Temperature

The noise figure of the receiver system was measured prior to and after each pass with the antenna pointing at 45° elevation. The noise temperature referred to a 3-Mc bandwidth was calculated. Some meteorological conditions were also considered. All the data are shown in Table 6–10.

The participation of COMGEB in Relay I experiments was limited to 6 weeks duration. In addition to the test results, valuable oper-

TABLE 6–8.—*Evaluation of Teletype Transmission*

Channel	Signal	FMVFT syst. loop	Loop through ampex FR100B	Loop through COMGEB	Loop through COMNUT	
2	2:2	1	1	1	8	Isochr. distortion
4	Text	−4/+1	−4/+3	−4/+3	−18/+20	Ref. distortion*
6	1020 cps	1021.9	1021.9	1021.9	1022.6	
			−1022.2	−1022.2	−1022.7	
8	CCITT test chart	1	2	2	16	Isochr. distortion
10	1500 cps	1503.2	1503.2	1503.2	1503.1	
			−1503.3	−1503.3	−1504.1	
13	Text	−5/+2	−6/+4	−6/+3	−25/+25	Ref. distortion*
14	CCITT test chart	4	5	5	20	Isochr. distortion
18	CCITT test chart	2	3	3	18	Isochr. distortion
19	80-baud signals	10	14	13	50	Isochr. distortion
22	2:2	1	2	1	14	Isochr. distortion

1. Figure = early reference distortion. 2. Figure = late reference distortion.

ating experience was gained, which is one of the basic requirements for future operations.

AUTHORS. This chapter was contributed *by personnel of the Deutsche Bundespost, Darmstadt, Germany, under the overall direction of* E. DIETRICH, *DBP.*

TABLE 6–9.—*Received Signal Strength*

Orbit	Received signal power (dbm)			Circuit
	Begin	Middle	End	
2403	---	---	---	COMNUT-COMHIL*
2411	---	---	---	---
2418	---	---	---	COMAND-COMGEB†
2426	---	---	---	COMNUT-COMRIO*
2443	−109	−108	−102	COMNUT-COMGEB
2449	−107	−105	−106	COMNUT-COMGEB
2496	−105	−102	−100	COMNUT-COMGEB
2558	−106	−103	−103	COMAND-COMGEB
2566	−104	−104	−102	COMAND-COMGEB
2567	−107	−107	−105	COMNUT-COMGEB
2589	−103	−105	−105	COMAND-COMGEB
2614	−105	−104	−104	COMNUT-COMGEB
2628	−115	−115	−115	Loop for COMNUT
2629	−110	−107	−107	COMNUT-COMGEB
3055	---	---	---	COMNUT-COMTEL*
3094	---	---	---	COMAND-COMHIL‡

*COMGEB monitored only.
†COMGEB received only.
‡COMGEB tracked only.

TABLE 6–10.—*Noise Compensation of Receiver System*

Orbit	Noise temp (°k)	Meteorological conditions			
	EL=60° AZ=0°	Precipitation rate	Temp. (°F)	Humidity (%)	Wind velocity (m/sec)
2403	490	0	44		2
2411	500	0	46		0
2418	510	0	50		0
2426	500	0	45	Measuring	3
2443	500	0	48	equipment	0
2449	500	0	46	not yet	0
2496	470	0	44	available	4
2558	530	0	54		8
2566	500	0	59		0
2567	500	0	46		4
2589	470	0	59		3
2614	465	0	36		2
2628	510	15mm/day	41		4
2629	510	15mm/day	35		2
3055	410	---	20		4
3094	460	---	24		6

N66-10257

Chapter 7

Description and Results of Tests Performed at Fucino Earth Station with Relay I

INTRODUCTION

The Italian earth station, owned by Telespazio, is located in the Fucino Valley, about 135 km. east of Rome (80 statute miles).

Geographical coordinates are:

Latitude 41° 58′ 40.55″ North
Longitude 13° 36′ 04.21″ East
Altitude above mean sea level 650 m.

The site is surrounded by mountains, the maximum elevation angle of which is less than 6°. Figure 7–1 shows the portion of the optical horizon around the station.

Manufacturing of the telecommunication equipment started in March 1962 and the work on site began in early June of the same year. The station (Figure 7–2) was completed at the end of November for the receiving side and has been able to participate in many experiments performed with Relay I.

During 1963, 160 communication experiments were carried out, as shown in Table 7–1. Other experiments have since been conducted.

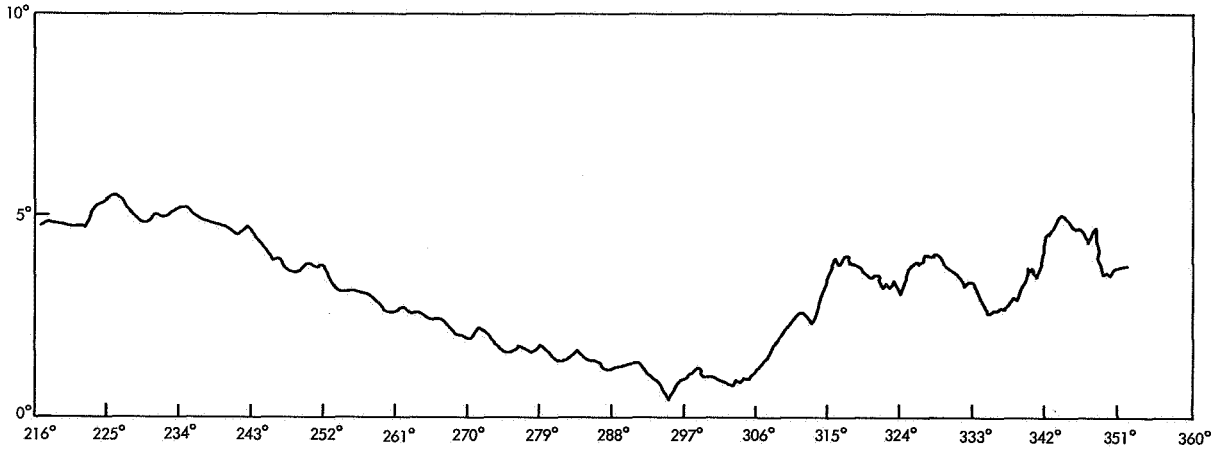


FIGURE 7–1.—Optical horizon, Fucino earth station.

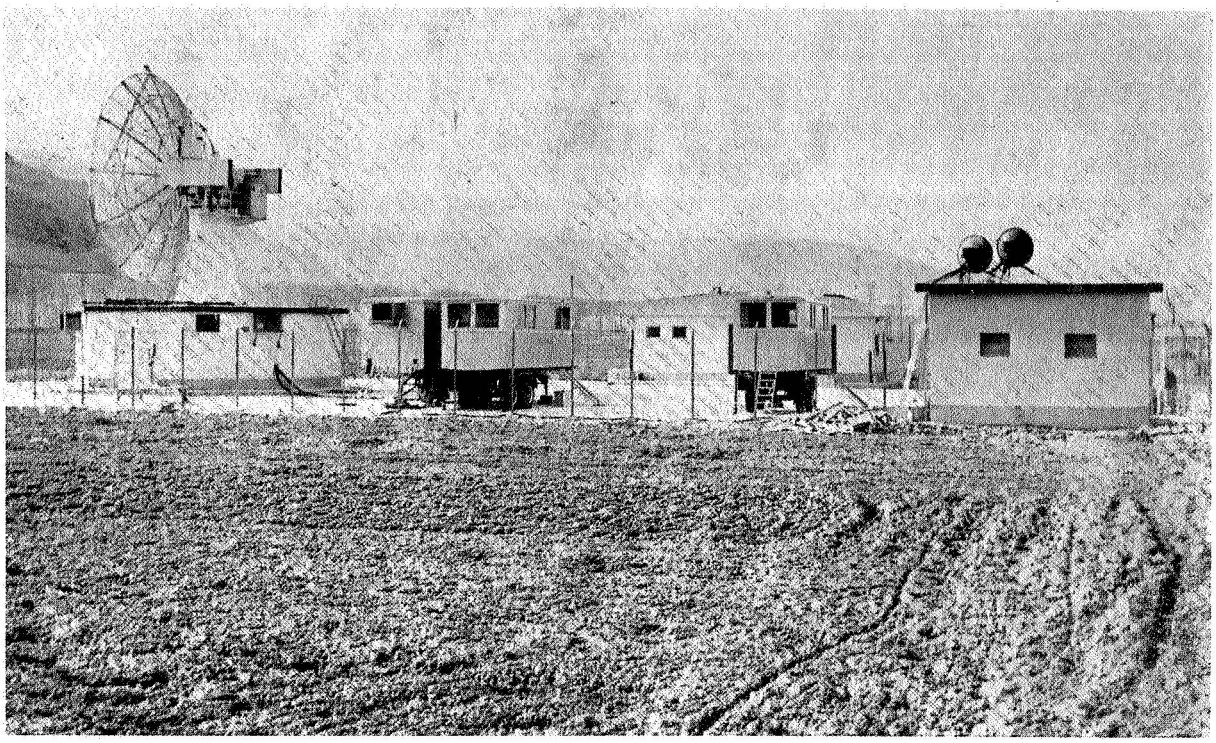


FIGURE 7–2.—General view of Telespazio station.

TABLE 7–1.—*Relay I Experiments Performed During 1963*

Wideband TV tests and demonstrations		Narrowband		Total	
No. experiments	Minutes	No. experiments	Minutes	No. experiments	Minutes
80	1515	80	1659	160	3174

DESCRIPTION OF THE EARTH STATION

Communication and tracking facilities with their main characteristics are listed below.

The station is equipped with fully steerable 30 ft parabolic dish, with a Cassegrainian sub-reflector, a four port horn feed assembly for 4 kMc band used both for 4 kMc beacon auto-track and communication receiver.

The communication receiver consists of a two stage parametric RF amplifier, the first stage being liquid nitrogen cooled.

The incoming signals are converted to 70 Mc and the IF amplifier is followed by either of two FMFB demodulators, for wideband and narrowband experiments respectively.

The tracking receiver is an amplitude sensing monopulse type. The initial acquisition is achieved by manually pointing the antenna on the predicted position of the satellite, according to the ephemerides received from NASA.

When the 4 kMc beacon is acquired by the tracking equipment, the servosystem is switched on autotrack mode. The station is also equipped with instrumentation and test equipment. Figure 7–3 is a block diagram of receiving system.

EQUIPMENT PERFORMANCE

Antenna

Gain at 4170 Mc.....48.7 ± 0.5 db
Half power beamwidth.....0.55
Side lobes.....—19.7 db min.

Parametric Amplifiers

Overall gain .....28.5 db
Bandwidth (3 db point).....25 Mc

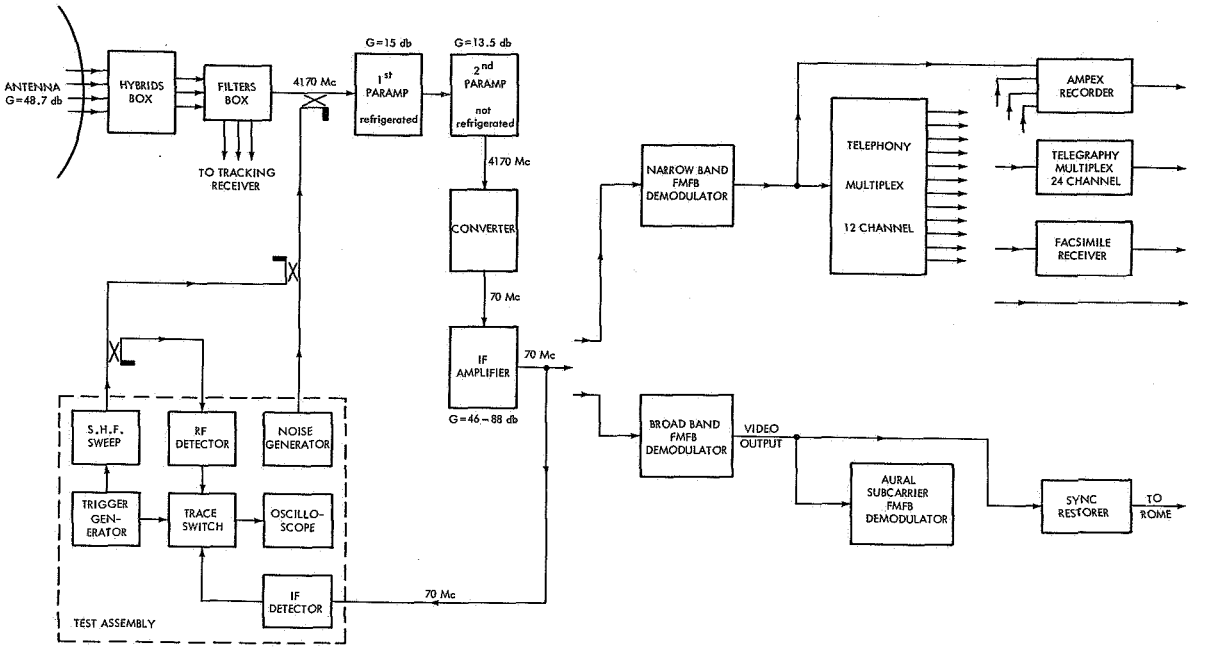


FIGURE 7–3.—Communications receiver system.

Noise bandwidth .....26 Mc

System Noise Temperature
(Measured with antenna pointed at zenith in normal weather conditions)

Receiver .....110° K
Hybrids, waveguides,
rotary joint, diplexer.....60° K
Sky temp. radome, spillover.....50° K

Overall system noise temperature...220° K

A minimum value of 195° K has been measured. The maximum value is approximately 250° K, 260° K having been measured in two passes. It is possible that a contribution to the measured variations of about 20° K is due to weather conditions, the remaining variation being attributable to the instability of the parametric amplifier.

Wideband Threshold

The actual threshold occurs when the carrier-noise power ratio is equal to 18 db in 1 Mc bandwidth. In these conditions the received power is about —97.5 dbm and the weighted video S/N ratio is about 39 db.

Narrowband Threshold

It occurs when the carrier to noise ratio equals 6.75 db for the group A (12–60 kc) and 10 db for the group B (60–108 kc) in 1 Mc bandwidth. Under these conditions the received power is, for group A, —108.5 dbm and the S/N ratio on the highest channel is about 35 db.

Using the CCIR emphasis and psophometrically weighting the noise, this ratio is about 41 db, which corresponds to a 80,000 pw noise in every channel.

For group B and S/N ratio in the highest channel at the threshold is about 44.0 db; using the CCIR emphasis psophometrically weighting the noise, this ratio becomes 50 db and the relative noise 10,000 pw.

The above values have been calculated theoretically, but a very good approximation to the same value has been found with the actual tests.

Tracking Threshold

The overall noise figure is about 9 db for the sum, azimuth and elevation channels. The minimum S/N ratio for acquisition is

about 10 db, which corresponds to a threshold power of —129 dbm.

ANALYSIS OF RESULTS

Received Carrier Power

Figure 7–4 shows some values of the received carrier power referred to the theoretical levels, corresponding to a satellite transmitting antenna gain of 0 db. Each dot represents a measurement.

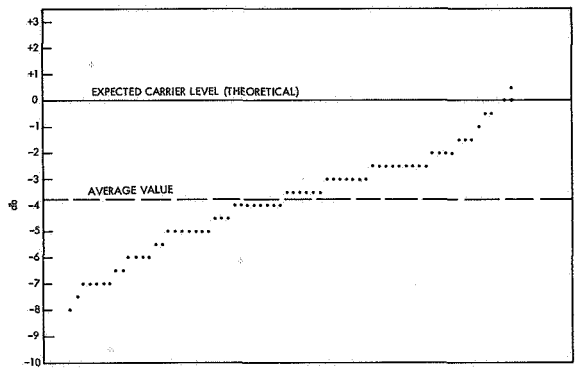


FIGURE 7–4.—Differences between theoretical and measured carrier power.

The measured power level differs from the expected one as far as —8 db. The average value is about —4 db. These differences may be partially attributed to errors in the power test system, particularly for low signal levels, to the spacecraft look-angle and to imperfect steering of the antenna.

It has been also observed that, at low elevation angles, the difference between theoretical and measured value is generally greater than the same difference for high elevation angles (about 1 db average). This fact is likely due to multipath propagation losses.

These discrepancies have been carefully investigated. The present conclusions are that a major loss other than the expected one (0.15 db) is due to the small styrofoam resin radome over the feed assembly. It was also recently discovered that the misalignment of the sub-reflector from the original position was due to deformation of the tripod spars and also to imperfect mounting of the sub-reflector.

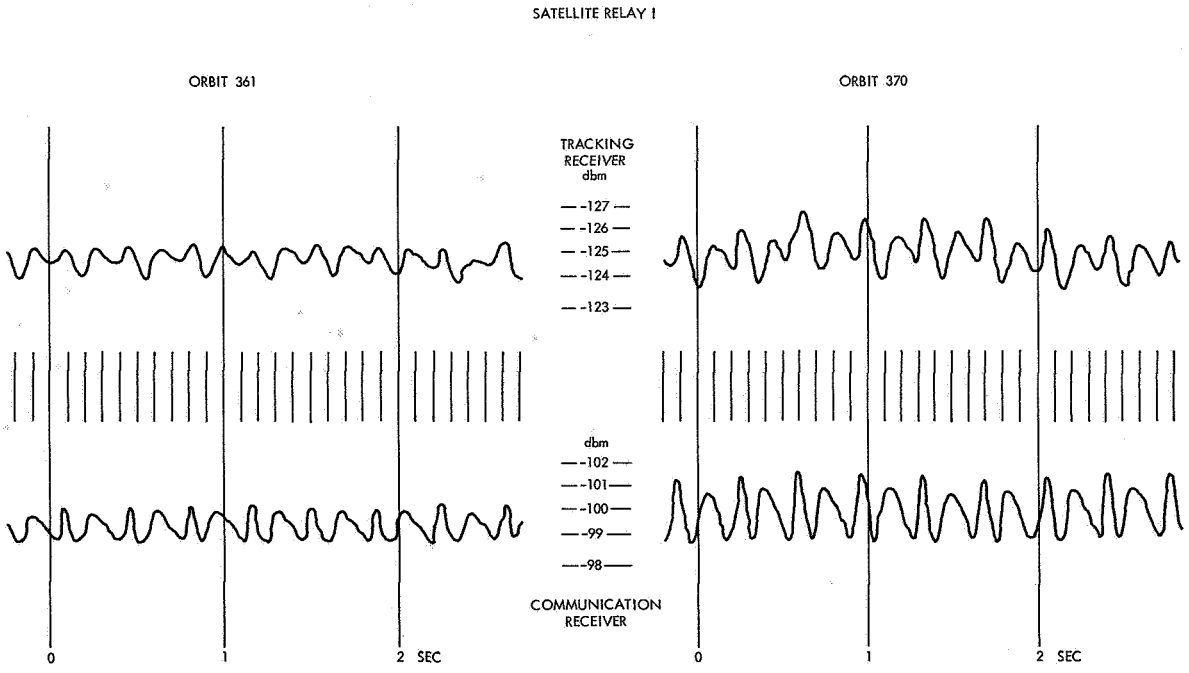


FIGURE 7–5.—AGC recording.

The maximum observed spin modulation was about 3 db, as seen in Figure 7–5, where the diagrams of the AGC levels versus time are represented for two passes.

Narrowband Experiments

1. *Baseband Characteristics*—The measurements were conducted during pass 191, 864 and 865. For Group A the obtained results are listed in Table 7–2 and plotted in Figure 7–6.

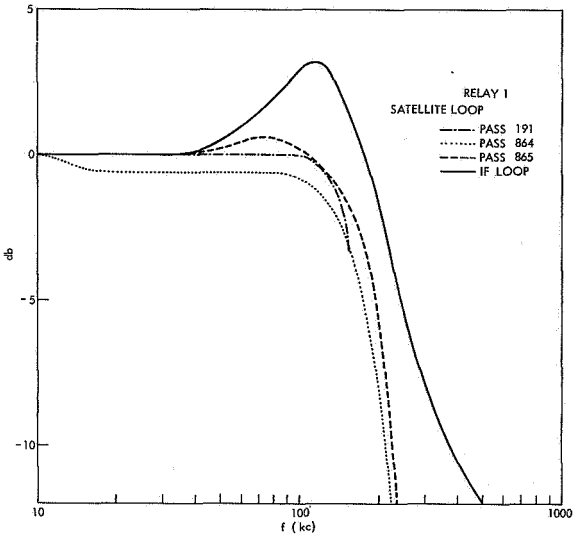


FIGURE 7–6.—Narrowband—group A, baseband characteristics.

TABLE 7–2.—*Results of Baseband Characteristic Measurements*

Frequency kc	Relative level (db)		
	Pass 191	Pass 864	Pass 865
10	0	0	0
20	0	−0.6	0
40	0	−0.6	0
80	0	−0.6	+0.4
160	−2.5	−3.5	−2.2
250	n.m.	−15.2	−16
350	n.m.	−26	n.m.

2. *Continuous Random Noise*—Some typical results of the channel 12 noise test for different values of the received carrier power are shown in Table 7–3. The values given are the actual received levels; the results are generally in good agreement with the expected values.

TABLE 7–3.—*Noise Test Results*

Received carrier power dbm	Psophometric noise (pw)		Pass number
	Expected	Measured	
−107	60,000	70,000	757
−105	40,000	55,000	585
−104.5	35,000	80,000	772
−104	30,000	28,000	734
−104	30,000	40,000	865
−104	30,000	44,000	881
−103	23,000	31,000	275
−103	23,000	38,000	881
−101	15,000	30,000	275
−101	15,000	18,000	864
− 99	9,000	14,000	2550

3. *Intermodulation Noise*

(a) *Noise Loading*—For this test pass 864 was considered because the carrier power received from Nutley was almost constant. The noise loading measured on channel 12 is —10 dbm0, which corresponds to the normal loading of speech.

The thermal noise on the same channel was measured 18,000 pw psoph. The total unweighted noise (thermal + intermodulation) with noise loading introduced on the other channels was —45.5 dbm0, that is about 16,000 pw psoph. Taking into account the measurement accuracy, we may conclude that the intermodulation noise is insignificant.

(b) *Harmonic Performance*—The results of three passes (864, 896, 1066) are shown in Table 7–4. The two modulation tones are 22 and 37 kc, with different modulation factors. The considered intermodulation and harmonic products are 15 and 44 kc.

TABLE 7–4.—*Harmonic Performance*

Tones	Pass 1066	Pass 864	Pass 896
22 kc	−2.5 dbm0	+4.2 dbm0	+ 6 dbm0
37 kc	−2 dbm0	+5 dbm0	+ 5 dbm0
15 kc	<−50 dbm0	−46 dbm0	−45 dbm0
44 kc	<−50 dbm0	−42 dmb0	−43 dbm0

For the pass 416 we obtained the following results:

Modulation tones: $f_1 = 15$ kc, $f_2 = 20$ kc

Nominal peak deviation: 200 kc corresponding to +4 dbm0

Harmonic and intermodulation products:

$f_2 - f_1 = 5$ kc ..... —45.1 dbm0
$2f_1 = 30$ kc ..... —42.3 dbm0
$f_1 + f_2 = 35$ kc ..... —46.2 dbm0
$2f_2 = 40$ kc ..... —47.2 dbm0

In the pass 587 we have measured

Modulation tones: $f_1 = 17$ kc $f_2 = 21$ kc

Rms deviations: + 0.2 db + 5.5 db respect to 88.8 kc

Harmonic and intermodulation products:

$f_2 - f_1 = 4$ kc..... —51 dbm0
$2f_1 = 34$ kc..... —43 dbm0
$2f_2 = 42$ kc..... —51 dbm0

We may conclude that the harmonic distortion is less than 1 percent (40 db) also for modulation factor of 200 percent (6 db).

4. *Insertion Gain*—This test is typical of the loop configuration, in which the earth station itself checks the transmitted and received signal levels.

Considering that the Fucino Station is not equipped with the transmitter, this test is not very significant. However, the results have been fairly good, as shown in Table 7–5

5. *Narrow Band Demonstrations*—A voice message from Dr. Dryden of NASA was received in a very high quality circuit on pass 275 (18 Jan. 1963). On the same pass a TTY message of about 1000 words was received without errors. The reception of facsimile pictures was very successful. The photograph of President Kennedy, reproduced in Figure 7–7 was received on pass 757.

A good result was also obtained in restoring colors with the three superimposed pictures of Bridge Giovanni da Verrazzano, received on pass 997 (21 April 1963).

Several other narrowband tests were performed very satisfactorily.

Wideband Experiments

1. *Wideband Technical Tests*—Although the Fucino Earth Station is not designed for wide band operation, TV test signals and demonstrations were received. As a matter of fact, when the Relay I Satellite was used for the first time on January 4th in a communication experiment, Fucino earth station monitored pass 169, and received on its monitor the first picture transmitted from Andover.

Only in some cases, under particularly favorable conditions, was reception above the

TABLE 7–5.—*Insertion Gain Test Results*

Channel	Measured level –(dbm)										
	Rev. 416	Rev. 750	Rev. 757	Rev. 772	Rev. 825	Rev. 826	Rev. 897	Rev. 2550	Rev. 2598	Rev. 2806	Rev. value
1	−0.6	0	0	+0.3	−0.4	−0.3	0	+0.3	0	−1.0	−0.17
2	−0.3	0	−0.2	0	−0.4	0	0	+1.0	−1.0	+0.2	−0.07
3	+0.9	+1.5	+1.0	+1.5	+0.4	+1.1	+1.0	+1.3	+1.0	−0.5	+0.92
4	+0.4	−0.5	n.m.	+1.0	+0.7	+1.1	+1.0	+0.5	+1.0	−0.3	+0.54
5	−0.1	+1.5	+1.1	+1.8	+1.3	+1.7	+1.2	−0.4	+0.2	0	+0.83
6	+0.3	+1.5	+1.2	+1.8	+1.3	+1.7	+1.8	−0.5	+0.9	+0.1	+1.01
7	+0.2	+1.0	+1.1	+1.2	+1.4	+1.8	+1.0	−0.35	0	−0.4	+0.70
8	+0.2	+1.0	+0.8	+1.8	0	+1.5	+1.0	−0.6	0	+0.8	+0.65
9	+1.2	+1.0	+1.1	+1.3	+0.8	+1.0	+1.8	−0.6	+0.2	+0.8	+0.86
10	+0.2	+0.3	+0.2	+1.3	+0.5	+0.9	+0.5	+0.5	0	+1.3	+0.57
11	−0.1	+0.3	+0.2	+0.6	+0.6	+0.8	+0.3	+0.9	+0.1	+0.5	+0.42
12	0	+0.5	+0.3	+0.8	+1.2	+1.7	+0.5	+0.9	+0.2	+1.1	+0.72



FIGURE 7–7.—Relay I revolution 757, 21 March 1963.

threshold; however, it was also possible to get some interesting results when the signal was near or slightly below the threshold.

Figure 7–8 shows the curve of the video weighted S/N ratio measured during three passes (316, 330, 338) with the received carrier power below the threshold. The slope of this characteristic is about 2.5 db/dbm.

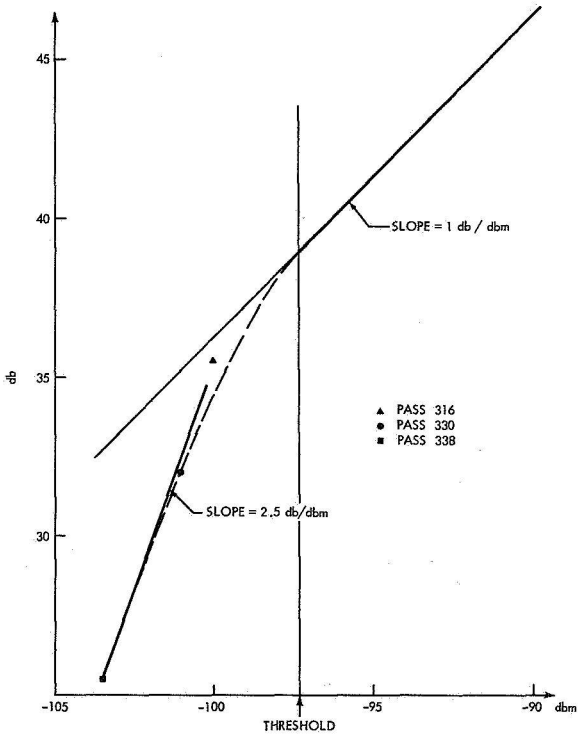


FIGURE 7–8.—Weighted video noise vs. received carrier power.

Some interesting comparison tests were conducted with the FMFB video demodulator and a phase-lock FM demodulator loaned by NASA.

It was observed that the phase-lock demodulator gives an improvement of 5–6 db with respect to a standard demodulator. In this way it is possible to get an acceptable

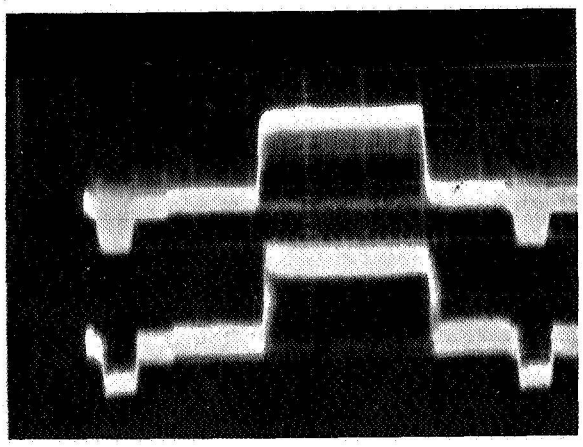


FIGURE 7–9.—Relay I revolution 330, video signal received on 25 January 1963.

picture even if the C/N ratio is only 2 db (i.e., for C/N—17 db in 1 Mc bandwidth), especially if the video signal has no sharp edges in its waveform. In Figure 7–9 a comparison between the two modulators is shown. The upper waveform represents the signal coming out of the FMFB demodulator, and the lower, from the phase-lock demodulator. This last signal is less noisy but it is affected by losses of lock in correspondence of sharp variations.

In order to facilitate the picture synchronization a sync restorer was developed. The sync restorer reforms and reinserts the sync pulses on incoming video signals affected by noise. The effects of this device are shown in Figure 7–10.

2. *Wideband Demonstrations* — Many TV demonstrations have been received: some of them have been relayed by means of a mobile microwave link to RAI's studios in Rome where they have been converted to 625/50 TV standard and broadcast on Italian television network or recorded on magnetic tape.

A picture received from Andover on pass 285 (19 January 1963) is shown in Figure 7–11.

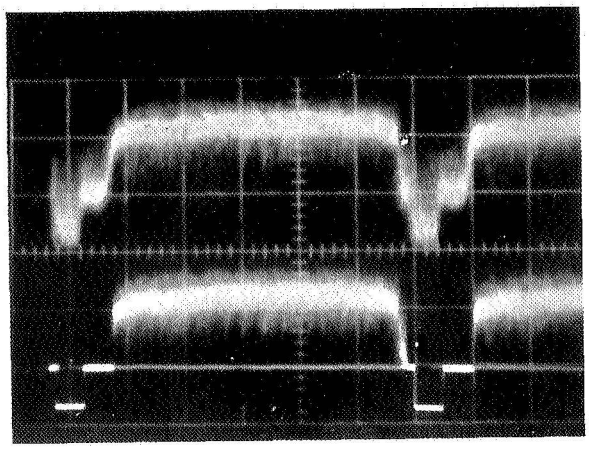




FIGURE 7–11.—Relay I revolution 285—19 January 1963.

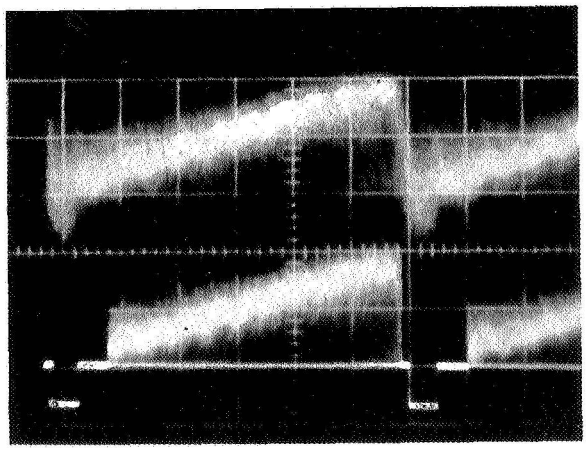


FIGURE 7–10.—Relay I revolution 285, 19 January 1963. Video signals without restoration of sync pulses.

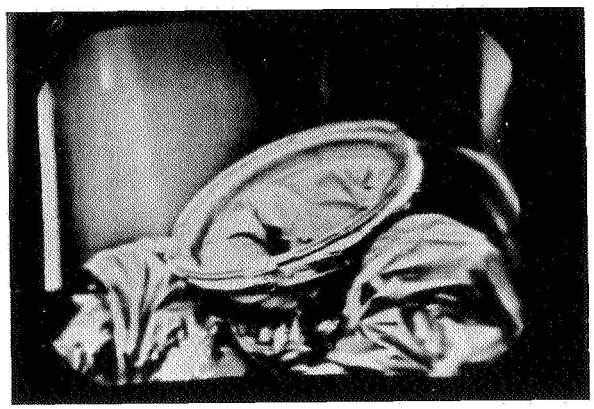


FIGURE 7–12.—Relay I revolution 1189—15 May 1963.

The photo presented in Figure 7–12 was taken during pass 1189 (orbital flight of Mr. Cooper, 15 May 1963).

AUTHORS. *This chapter was contributed by personnel of Telespazio, Rome, Italy, under the overall direction of* P. FANTI, *Telespazio.*

N66-10258

Chapter 8

The KDD Space Communications Station

GENERAL DESCRIPTION

In view of the fact that space communication is one of the most useful systems enabling us to handle the international communication, Kokusai Denshin Denwa Co., Ltd. (Japan's Overseas Radio and Cable System) began in 1961 the preparation of its earth station to promote the study thereof. The site of the station was selected in Juomachi, Taga-gun, Ibaraki-ken, Japan, which is 150 km north-northeast from Tokyo.

It is enclosed by a mountainous region on the west side so that mutual interference between the station and domestic microwave relay stations can be avoided. It is opened to the Pacific Ocean in the east side. The location is outside of normal airline routes as seen in Figure 8–1 and is also in a good weather area free from snowfall.

Figure 8–2 shows an airview of the KDD Earth Station (COMIBA) at the final stage of construction. There are two radomes separated by 260 m. The big radome contains communication facilities including a 20-m diameter Cassegrain antenna, and the small one contains tracking facilities having a 6-m diameter parabola antenna. Between them is a control building in which a control device and terminal equipment are provided. Two sets of simulators and a collimation tower are installed on the top of a mountain called Mt. Sekison in the southwest of the station as seen in Figure 8–3.

The tracking equipment and control device were partly completed at the end of June 1963. The first series of tracking tests were successfully carried out in July 1963 by re-

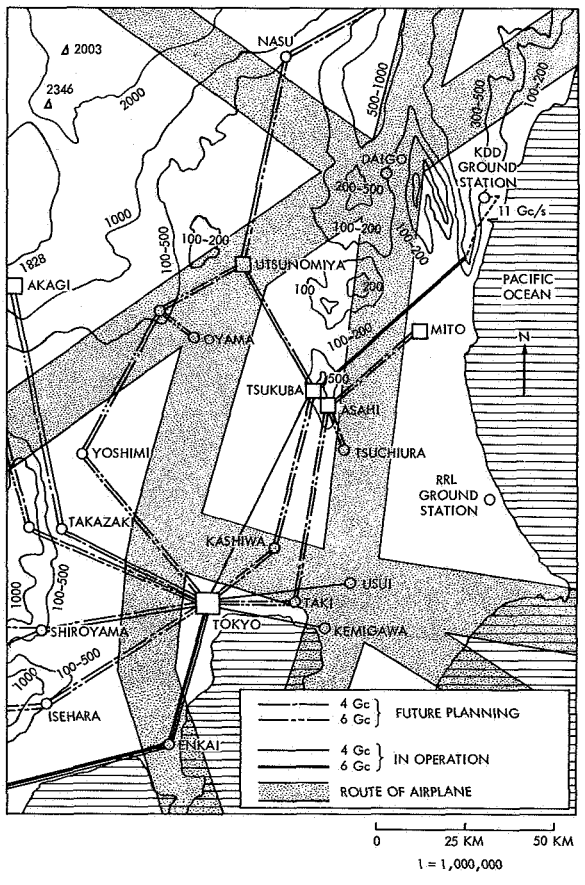


FIGURE 8–1.—Location of KDD earth station showing nearby airline routes.

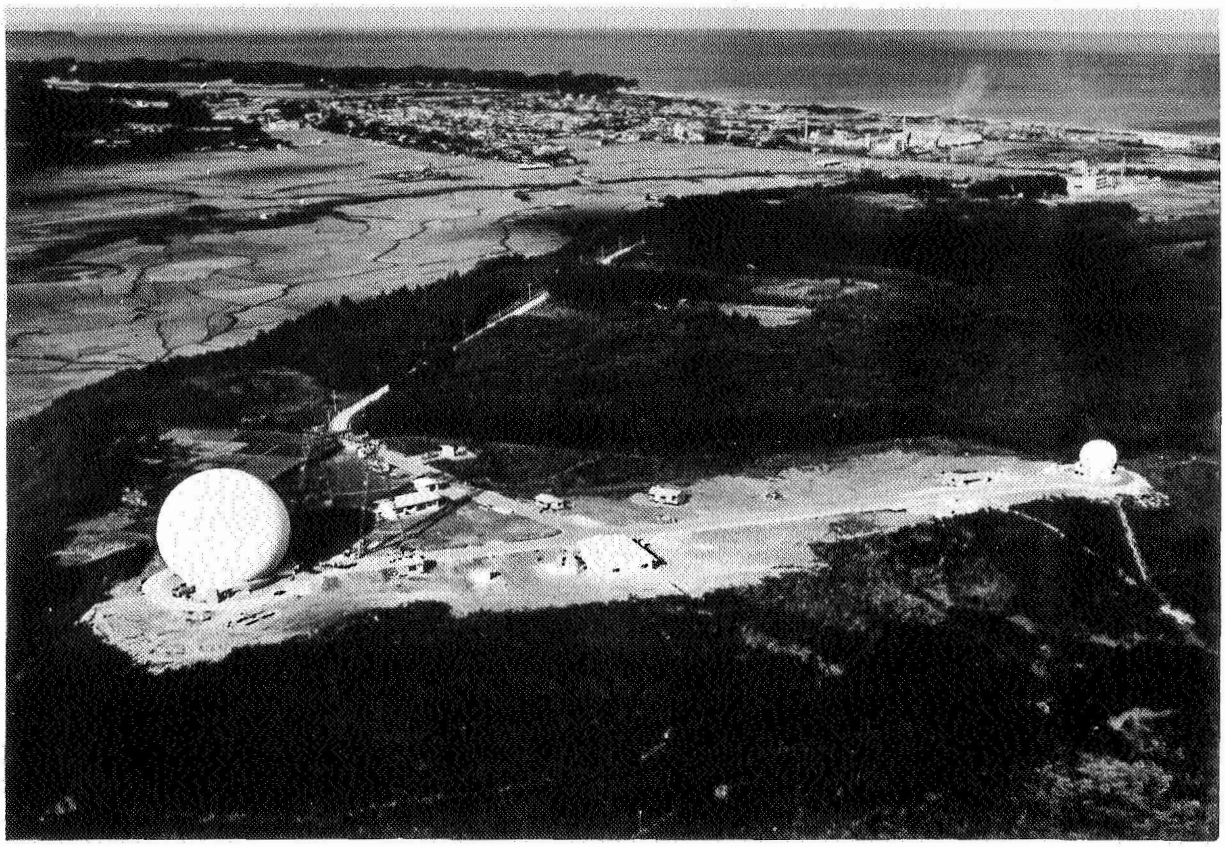


FIGURE 8–2.—Aerial view of KDD earth station.

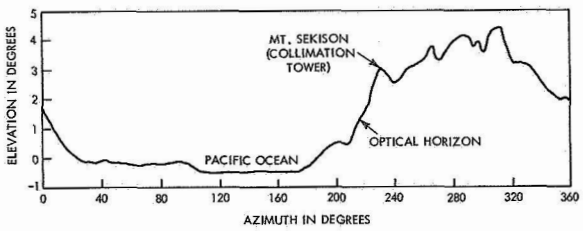


FIGURE 8–3.—Optical horizon.

ceiving a beacon signal emitted from a communication satellite, Telstar II, with the Andover earth station commanding the satellite. After the full completion of wideband receiving facilities, the first TV transmission over the Pacific Ocean was conducted from Mojave test station of NASA to KDD earth station on November 23, 1963 by using communication satellite Relay I. Technical tests were carried out ten more times between the station and Mojave and Andover station via Relay I and Relay II.

In addition to a transmitter for Telstar which was installed in November 1963, a transmitter for Relay was also completed on March 20, 1964.

A microwave link on 11 Gc for TV transmission and cables for telephone communication are to be provided between the station and the existing networks connecting to Tokyo central communication offices.

Details of principal communication facilities of the station are given in the following sections.

ANTENNA SYSTEM

A 20-m diameter, azimuth-elevation mounted Cassegrain (parabolic-hyperbolic) antenna is used in common for both transmission

and reception. A diplexer and filters are employed to separate transmitting and receiving frequencies. This antenna is driven with hydraulic motors and is positioned by slaving to the steering controller or by manual controlling. Both azimuth and elevation angles are displayed in digital form. Two horn projectors, which are mutually interchangeable, are provided corresponding to the projects, i.e., Relay and Telstar.

The whole structure is covered with a 30-m diameter single-walled soft radome to keep the high pointing accuracy in any weather condition.

Details are given as follows:

1. Reflectors
   (a) Main dish: Paraboloid, 20 m in diameter, 135° in aperture angle, 3 mm (rms) in surface accuracy.
   (b) Subreflector: Hyperboloid, 2 m in diameter.
2. Feeding system
   (a) Bandwidth: 25 Mc approximately for 4,170 Mc and 6,390 Mc, 16 Mc for 1,725 Mc.
   (b) Isolation of transmitting frequency at the receiver terminal: 120 db approximately.
   (c) Polarization: Righthand circular for transmission, lefthand circular for reception.
   (d) VSWR: 1.05 at 6,390 Mc, 1.14 at 4,170 Mc and 1,725 Mc.
   (e) Total loss: 0.5 db at 6,390 Mc, 0.55 db at 4,170 Mc, 0.3 db at 1,725 Mc.
3. Performance characteristics
   (a) Gain: 58 db at 6,000 Mc, 55 db at 4,000 Mc, 47 db at 1,725 Mc.
   (b) Front-to-back ratio: More than 60 db at all frequencies.
   (c) Noise temperature: 58° K on 4,170 Mc to the zenithal angle with radome.
4. Operating rate
   (a) Maximum velocity: 3°/sec (azimuth), 1°/sec (elevation).
   (b) Maximum acceleration: 3°/sec^2 (azimuth), 1°/sec^2 (elevation).
5. Radome
   (a) Form: Composed of 3/4 parts of a sphere 30 m in diameter, at the groundwork.
   (b) Structure: Single-walled, made of Vinylon (synthetic fabric) coated with Neoprene (synthetic rubber).
   (c) Loss: 0.2 db at 4,170 Mc, 0.3 db at 6,390 Mc (8° to 16° K with angle of elevation on 4,170 Mc.)
   (d) Wind load: Endurable under 60 m/sec in instantaneous wind velocity. (The first radome was split by wind of 26 m/sec, on January 20, 1964. The second one is being redesigned.)

TRANSMITTING EQUIPMENT

This equipment is for transmitting a high-power frequency-modulated signal at either one of the two frequencies, 6,390 Mc and 1,725 Mc. In order to minimize losses in the feeding system, the main parts of the equipment, two power amplifiers and a common modulator, are installed in a room on the antenna mount which can rotate in the azimuth plane along with the antenna. Two power supplies for the power amplifiers are located on the floor in the antenna tower and are led to the respective amplifiers through flexible cables.

Details of characteristics are given as follows:

1. Bandwidth: 25 Mc (1 db down) for 6,390 Mc, 16 Mc (1 db down) for 1,725 Mc.
2. Frequency stability: 1×10^{-5}.
3. Modulation: FM of ± 10 Mc in deviation, a baseband up to 7.5 Mc with pre-emphasis, 5% in differential nonlinearity.
4. Output power: 3 kw (at dummy load) for 6,390 Mc, 10 kw for 1,725 Mc.
5. VSWR: 1.05 (using isolator).
6. Harmonic suppression: 55 db.
7. Power requirement: 3-phase, 50 cps, 200 v, 40 kva for 6,390 Mc and 60 kva for 1,725 Mc.

RECEIVING EQUIPMENT

This equipment is for receiving and demodulating a wideband FM signal (carrying one TV system or 600 telephone channels)

transmitted from a communication satellite. In order to minimize losses in the feeding system, the receiver is placed in a room on the antenna mount which can rotate in the azimuth plane along with the antenna.

The equipment consists of three sections, a low noise amplifier whose first parametric amplifier is cooled by liquid nitrogen, a TWT amplifier with converter, and a demodulator adopting a negative feedback phase detector system having an improvement of about 4.5 db in threshold level. The threshold level is —98 dbm in case of incoming noise of 80° K into the equipment. Each section has its own power supply.

Details of the equipment are given as follows:

1. Low noise amplifier
   (a) Center frequency: 4,170 Mc.
   (b) Bandwidth: 100 Mc (3 db down).
   (c) Gain: 32 db
   (d) Receiver noise temperature: 82° K. (System noise temperature 140° K, at zenith, with radome)
2. TWT amplifier with converter
   (a) Input frequency: 4,170 Mc
   (b) Output frequency: 7,000 Mc
   (c) Bandwidth: 50 Mc (2 db down).
   (d) Gain: 74 db
   (e) Frequency stability of local oscillator: 1×10^{-5} (15° C to 45° C).
   (f) Conversion loss: 13 db.
   (g) AGC characteristics: +10 dbm ±1.5 db at the output in a range of input levels between —49 and —31 dbm
3. Demodulator
   (a) Input frequency: 7,000 Mc
   (b) Input level: +10 dbm ±1.5 db
   (c) Deviation: ±8 Mc
   (d) Video bandwidth: 4.5 Mc
   (e) Frequency response of video amplifier: ±1.5 db (60 cps to 4.5 Mc.)
   (f) Output impedance: 75 ohm ±7.5 ohm.

TRACKING FACILITIES

The tracking facilities are to provide precise angle information with which the 20-m antenna is to be pointed to a communication satellite. With the aid of approximate satellite-orbit information pre-calculated by a computer, it achieves initial acquisition by locking on an SHF beacon transmitted from the satellite, as it appears on the radio horizon. Then the equipment automatically tracks the satellite, providing the antenna with precise pointing information through an antenna steering controller.

Details of these facilities are given as follows:

1. System
   (a) Tracking mode: Simultaneous lobing adopting amplitude sensing monopulse technique.
   (b) Angular encoding: Binary coded decimal code, six digits (least significant digit being 0 or 5 only).
   (c) Accuracy: 0.017° (RMS)
2. Antenna
   (a) Form: Azimuth / elevation type parabola antenna, 6 m in diameter, 150° in aperture angle, ±3 mm in surface accuracy.
   (b) Range of rotation: ±400° (azimuth), —5° to 90° (elevation).
   (c) Drive: Oil pressure drive of valve control system.
   (d) Maximum velocity: 8°/sec (azimuth), 1°/sec (elevation).
   (e) Maximum acceleration: 8°/sec² (azimuth), 2°/sec² (elevation).
   (f) Polarization: Righthand or lefthand circular polarization (changeable).
3. Radome
   (a) Form: Composed of 3/4 parts of a sphere 11 m in diameter.
   (b) Structure: Dual-walled, made of Vinylon (synthetic fabric) coated with Neoprene (synthetic rubber).
   (c) Loss: 0.1 db at 4,000 Mc.
   (d) Maximum wind velocity: 60 m/sec.
4. Radio Receiver
   (a) Type: Phase-sensitive detection with voltage controlled oscillator.
   (b) Minimum tracking level: —140 dbm (bandwidth 150 cps).
   (c) Noise figure: 3 db (parametric amplifiers).

(d) AGC characteristic: Deviation less than 2 db at the output in a range of input levels between −170 and −90 dbm.

ANTENNA STEERING DIGITAL CONTROLLER

The antenna steering digital controller, containing parametrons as its stable logical elements, controls communications and tracking antennas at the earth station in time sharing control with stored programs.

Details of the antenna steering computer, the main part of this controller, are given as follows:

1. Logical element: 3,600 parametrons, excited by 2.3 Mc quenched by 25 kc.
2. Code: Binary coded decimal as external code, excess three as internal code.
3. Arithmetic: Bit parallel, digit serial, fixed decimal point.
4. Operation times: 0.8 ms. for addition and subtraction 50 ms. max. for multiplication, 54 ms. max. for division.
5. Transmission form: Parallel.
6. Word construction: 7 decimal digits + sign = 29 bits.
7. Instruction: One and one-half address, 41 instructions.
8. External switches: 32.
9. Control system: Stored program, overlapping control, acceptable external interruption.
10. Memory: Core matrix using dual frequency control, 512 word capacity.
11. Input-output selector: Magnetic-modulator matrix using small ferrite toroidal cores, 16 input-output with 29 bit parallel lines at the maximum speed of 1,250 words per second.
12. Power requirement: 200 v, 50 cps, 1 kva.

AUTHORS. *This chapter was contributed by personnel of the Kokusai Denshin Denwa Co. Ltd. (Japan's Overseas Radio and Cable System), Tokyo, Japan, under cognizance of the Japanese Ministry of Posts and Telecommunications.*

N66-10259

Chapter 9

Results of Tests Performed with Relay I at the KDD Space Communications Station

INTRODUCTION

Wideband receiving experiments were performed at the Earth Station (COMIBA) of Kokusai Denshin Denwa Co., Ltd. (KDD), Ibaraki, Japan.

As the Relay I satellite was expected to die in the middle of December 1963, the experiments were scheduled to come to an end during the first ten days of the month, and were carried out immediately after the completion of receiving facilities of the station. Since the satellite did not die, however, the experiments were extended one more week.

Details of the experiments are shown in Table 9–1. The change of the transmitting

TABLE 9–1.—*List of Wide Band Communication Tests and Demonstrations*

Orbit	Test period -UT)	Contents	Circuit
2677	63Y 11M 22D, 2027:42–2048	TV demonstration No. 1	COMMOJ→COMIBA
2678	22D, 2357:38–0015	TV demonstration No. 2	
2700	25D, 1904:42–1917:32	TV demonstration No. 3	
2701	25D, 2249:37–2305:16	TV demonstration No. 4	
2708	27D, 1959:04–2009	Test—A2, B1, D2, D3, H	
2709	27D, 2334:02–2347	Test—A2, B1, C1, D1, D2, D3, H	
2724	28D, 2139:39–2156	Test—H	
2731	29D, 1903:47–1916:06	Test—A2, B1, D2, D3, H	COMAND→COMIBA
2762	12M 3D, 1840:12–1851:00	Test—B1, C1, H	
2777	5D, 1637:45–1649:00	Test—A2, C1, D2, D3	
2785	6D, 1724:41–1736:00	Test—A2, B1, C1, H	
2816	11D, 1700:37–1713:57	Test—A2, B1, C1, C2, H	
2839	13D, 1546:40–1601:01	Test—A2, C1, C2	
2870	17D, 1519:21–1528:00	Test—A2, C1	

NOTE: Performance of command—COMMOJ (Mojave, Calif., USA). Transmission—COMMOJ and COMAND (Andover, Maine, USA.)
Contents of TV Demonstrations:
No. 1—The first official TV transmission from USA to Japan. Greeting for the first satellite communication.
No. 2—Record, life of the late President John F. Kennedy, simultaneously broadcast in USA and Japan.
No. 3—News.
No. 4—News, the state funeral of the late President John F. Kennedy.

station was due to a trouble with the transmitter at COMMOJ. The duration of the experiment per orbit was in general 15 to 20 minutes. As shown in the table, TV demonstrations were made four times, and technical tests designated by the Relay communication experimental plan (R1–5021) were performed ten times.

POSITION OF RELAY I DURING THE EXPERIMENT

The azimuth, elevation, slant range and look angle viewed from the earth station (COMIBA) to Relay I at the beginning and end of the experiment are given in Table 9–2.

EXPERIMENTAL RESULTS

Results of technical tests and demonstrations are summarized in Table 9–3.

Insertion Gain Stability (II–A2)

This test is to measure the system insertion gain and gain stability for baseband-to-baseband television transmission. Since the reference value of insertion gain variation in a medium period (10 seconds) is 1.0 db, the results of measurement satisfy the performance objectives.

Noise Measurement (II–B)

This test is to determine the weighted video signal-to-noise ratio, defined as the ratio of the peak-to-peak amplitude of the picture signal to the rms amplitude of the noise betwen 10 kc and 3.0 Mc with the video removed. The reference value of S/N is 43 db, so the measured values in general satisfy the performance objectives.

Line-Time Non-Linearity Distortion (II–C1)

This test is to determine variation in amplitude and phase of a level signal when the video level progresses from black to white within a line scan interval. The reference value of the m/M ratio should be greater than 0.80. All the values measured satisfy the requirement.

TABLE 9–2.—*Position of Relay I During the Experiments*

Orbit	Azimuth (deg.)		Elevation (deg.)		Slant range (km)		Look angle (deg.)		Circuit
	B	E	B	E	B	E	B	E	
2677	66.9	53.2	31.1	6.0	9300	10540	128	136	COMMOJ→COMIBA
2678	56.0	66.8	37.4	2.2	7620	8740	150	127	
2700	85.5	68.2	34.9	25.0	9030	9840	109	122	
2701	57.3	61.8	32.2	4.2	8300	9300	146	132	
2708	68.0	60.2	34.6	23.8	9140	9740	126	133	
2709	58.5	66.3	35.6	10.7	7800	8530	148	132	
2724	57.2	58.1	29.5	4.3	8880	9920	143	133	
2731	57.5	50.7	14.3	1.2	10610	11460	130	132	COMAND→COMIBA
2762	55.8	50.6	12.6	0.9	10800	11580	----	----	
2777	62.8	53.0	9.4	1.7	11200	12060	----	----	
2785	59.6	51.8	13.3	3.5	10870	11750	----	----	
2816	57.8	50.0	12.5	0.8	10940	12030	----	----	
2839	61.3	50.2	10.5	0	10960	12240	----	----	
2870	62.3	55.0	12.2	5.6	10600	11540	114	119	

NOTES:
1. Data—supplied by GSFC, NASA.
2. Earth station—COMIBA.

TABLE 9-3.—*Results of Measurement in Wideband Communication Tests*

Orbit	IIA2 (db)		IIB1	11C1	IIC2	IID1	IID2	IID3		II H	IV A		Circuit
	Gain	Variation						2T	T		Pic.	Test pat.	
2677	−0.14										4+	4+	COMMOJ→ COMIBA
2678											3−	4+	
2700											3−	4	
2701											3+	4	
2708	−0.26						0.031	0.021		4−			
2709	0		43	0.893(1)		0.05	0	(2)		4			
2724										4			
2731	+0.12		46				0.015	0.33(3)		4+/4−(4)			COMAND→ COMBA
2762			46							4			
2777	−0.26	±0.1		0.875			0.045	0.18(3)	0.35(3)				
2785	0	±0.1	43	0.875(1)						3+			
2816	0		(2)	0.92	0.9					(2)			
2839	−0.4			0.89	1.12								
2870	−0.2			0.9									

NOTES:

II A2 Insertion gain stability (measuring period—10 sec)
II B1 Signal to continuous random noise ratio in video channel
II C1 Line-time non-linearity distortion (rating: 0. 8)
II C2 Synchronization non-linearity distortion (allowance: 0.64-1.57)
II D1 Field time linear waveform distortion (rating factor: 0.05)
II D2 Line time linear waveform distortion (rating factor: 0.05)
II D3 Short time linear waveform distortion (rating factor: 0.05)
II H Grade of receiving TV picture (test pattern)
IV A Grade of receiving picture in TV demonstration

1. Estimated value.
2. Measurement was impossible.
3. Amplitude of transmitted pulse seemed to be lower than the specified.
4. All II H and IV A tests were conducted without emphasis except on Orbit 2731.

Grade of picture with emphasis on Orbit 2731 was 4−, worse than 4+ without emphasis on the same pass.

Synchronization Non-Linearity Distortion (II–C2)

This test is to determine variations in amplitude of the synchronizing signal as the video level is switched from black to white. The measured value Sa/Sb are within the objective limits, which are designated as the reference values of the ratio Sa/Sb, i.e., 0.64 to 1.57.

Field-Time Linear Waveform Distortion (II–D1)

This test is to determine the transient response of the system to field-time waveforms. It was made only on orbit 2709. The measured value is within the performance mask shown in paragraph 3.5.1 of CCIR Rec. 267 (Los Angeles, 1959).

Line-time Linear Waveform Distortion (II–D2) and Short-Time Linear Waveform Distortion (II–D3)

These tests are to determine distortions mainly due to the video transmission characteristics in the medium frequency range and in the high frequency range. The measured results satisfy the reference rating factor of 0.05, except in cases where amplitudes of transmitted pulses were lower than that specified.

Television Test (II–H)

This test is to provide the subjective evaluation of the system performance and to permit alignment of the system for television use.

All tests were conducted without pre-emphasis except on orbit 2731. Almost all of the results were good (grade 4) as shown in Table 9–3. The quality of the received pattern and picture was estimated according to the following score adopted by NHK (Japan Broadcasting Corporation):

5—Excellent (disturbance undetectable)

4—Good (disturbance detectable, but not annoying, and tolerable for high quality transmission)

3—Fair (disturbance annoying, intolerable for high quality transmission)

2—Bad (disturbance severely annoying and intolerable even for the general service), and

1—Unusable (information undetectable).

Signs + and — to the figures in Table 9–3 mean higher and lower in grade, respectively, compared with the original figure in the estimation. Grade of picture on orbit 2731 was 4— with emphasis, whereas it was 4+ without emphasis on the same orbit.

Received Signal Power (II–F)

The measurement of the received signal power is one of the most fundamental measurements for all performances of the communication systems. This was made in parallel at the same time as the experiments mentioned previously. The signal power received by the 20-meter antenna is represented in Table 9–4 in values at the beginning, in the middle, and at the end of each orbit.

It is found that the average received signal power closely relates to look angle of the satellite. Figure 9–1 shows the above relation, slant ranges on orbits 2677 to 2870 being normalized to a range of 10,000 km.

In case of a low signal power received, degree of spin fading in general tends to increase. The fading rate of spin fading was 2.58 cps.

The result of measurement of 4080 Mc beacon signal by a 6-meter antenna is shown in Table 9–5.

TABLE 9–4.—*Received Signal Power and System Noise by 20-Meter Antenna*

Orbit	Signal power (dbm)			Spin fading, p-to-p (db)	Noise temp. zenith (km)	P is percipitation; h is humidity. Weather cond.			Circuit
	B	M	E			P	t(°C)	h(%)	
2677	−92	−92.5	−93.5	5	160*	0	12	80	COMMOJ→COMIBA
2678	−95	−92.5	−91	6	145	0	15	72	
2700	−91.5	−91	−94	3	147	0	10	83	
2701	−96.5	−94.5	−93	7–2	144	0	14	65	
2708	−92	−93	−91.5	3	140	0	4	69	
2709	−98	−92	−91	8–3	139	0	9	60	
2724	−92.5	−92.5	−91.5	4–2	138	0	5.5	75	
2731	−92	−90.5	−94.5	3–4	137	0	3	72	COMAND→COMIBA
2762	−92.5	−93	−93.5	3	140	0	9	85	
2777	−91.5	−93	−94	3	140	0	8	95	
2785	−92	−91	−91.5	4–3	138	0	4	82	
2816	−94	−94	−94	5–7–5	136	0	6	95	
2831	−93.5	−95	−95	4	136	0	5	75	
2870	−92	−92	−93.5	3	137	0	5	80	

NOTES:

1. Effective noise bandwidth of communication receiver is 8 Mc.
2. Rate of spin fading was 2.58 cps.
3. *Radome was wet.

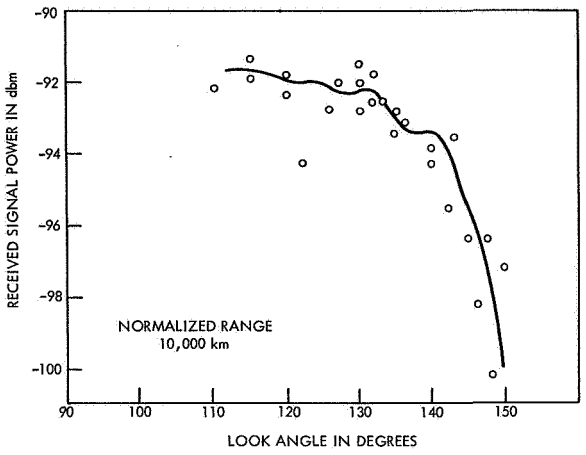


FIGURE 9–1.—Look angle directivity of Relay I antenna on 4170 Mc measured on revolution 2677 to 2870 (November 23 to December 18, 1963).

TV DEMONSTRATION (IV–A)

As shown already in Table 9–1, TV demonstrations were held four times during the period of this experiment. Grades of received pictures in these demonstrations are shown in Table 9–3. Estimation of test pattern was always better than that of the picture, because some original pictures transmitted were not of high quality. Quality of audio signal was not always so good, being markedly affected by spin fading. Figures 9–2 and 9–3 are typical of TV pictures received at the first demonstration between the U.S.A. and Japan on orbit 2677 on November 23, 1963.

NOISE TEMPERATURE

System noise temperature of the communication facility was measured immediately after each revolution at the zenithal angle. It is shown in Table 9–4 with the meteorological conditions. The value was about 140°K in the average during the period of the experiment.

TABLE 9–5.—*Received Signal Power by 6-Meter Antenna*

Orbit	Signal power (db)			Spin fading, p-to-p (db)	Remarks	Circuit
	B	M	E			
2677	−126	−125	−125	Not accurately measured	Due to a large time constant employed in the recording circuit	COMMOJ→COMIBA
2678	−128	−126	−128			
2700	−119	−118	−119			
2701	−120	−117	−116			
2708	−120	−118	−116			
2709	−120	−115	−116			
2724	−123	−122	−122			
2731	−120	−120	−126			COMAND→COMIBA
2762	−120	−120	−130		10 db drop in the last 1 min	
2777	−120	−124	−125	7	4 db drop at 1638:03	
2785	−122	−122	−121	7		
2816	−120	−123	−127	6	4 db drop at 1701:28	
2839	−117	−117	−129	6	4 db drop at 1554:05	
2870	−116	−120	−122	7	4 db drop at 1522:02	

NOTES:
1. All measurements were made on 4080 Mc beacon signal.
2. Bandwidth of receiver—500 cps.
3. Minimum signal level for tracking— −138 dbm.

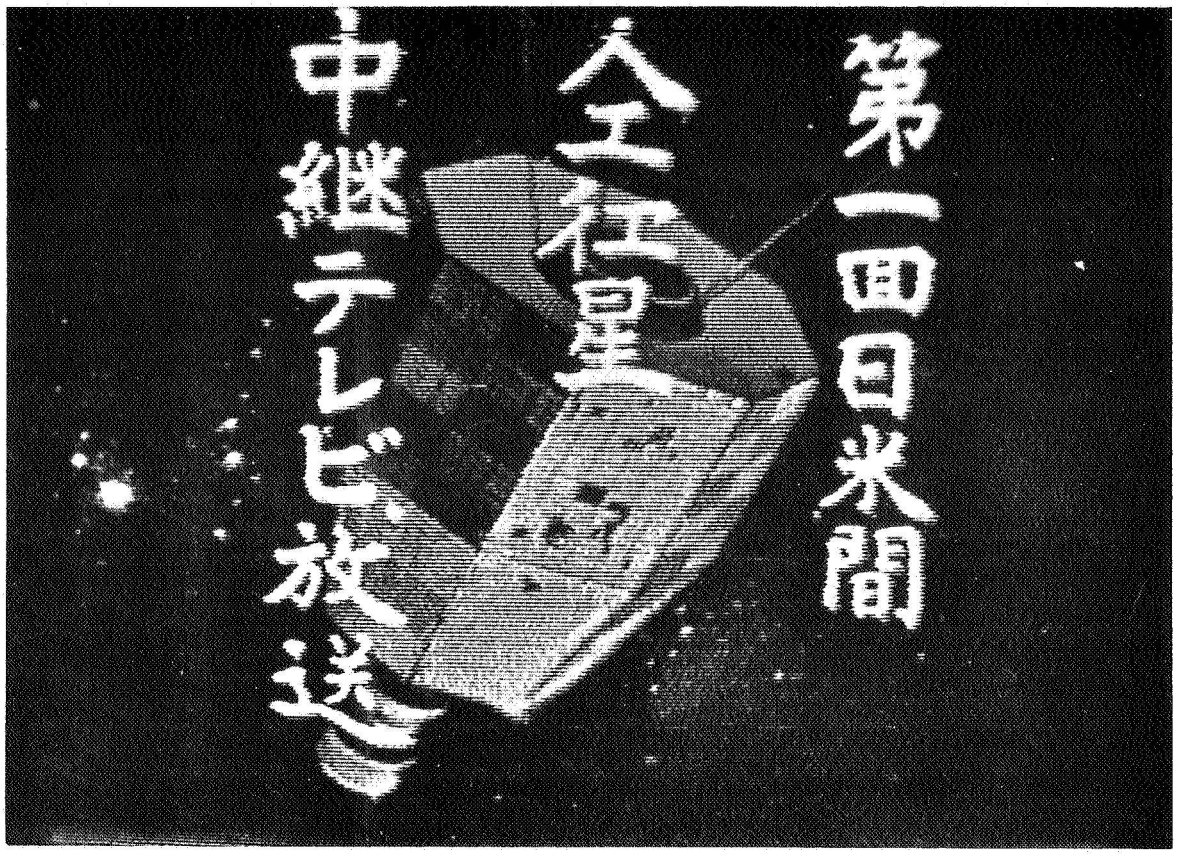


FIGURE 9–2.—TV picture received at COMIBA, first demonstration between U.S.A. and Japan.

COMPARISON BETWEEN CALCULATED AND MEASURED DATA

A comparison between the calculated and measured orbital data on each orbit is given in Table 9–6. Figure 9–4 shows azimuth and elevation errors in orbital prediction for Relay I with angle of elevation. Elevation error in general increases with decrease of elevation with a tendency indicated by a calibration curve given by NASA, whereas azimuth error is comparatively small and independent of angle of elevation.

CONCLUSION

As the experiment was limited to a short period, it is difficult to draw a decisive conclusion, but the experimental results may be summarized as follows:

1. As regards the insertion gain stability (II–A) and various transmission distortions (II–C1, II–C2, II–D1, II–D2 and II–D3), the measured values almost always satisfy the reference values. In other words, it may safely be said that the transmission characteristics of satellite-borne relay instruments and the ground-based receiver were fairly good.

2. The received power (II–F) fluctuated, in general, within a range of —91 to —94 dbm. Expressing the random noise (II–B) in a ratio of S/N, these values varied in a range from 43 to 46 db and satisfied the reference value of 43 db. The spin fading varying from 3 to 7 db peculiar to a satellite, however, was observed frequently.

3. The quality of TV video was fairly good generally, i.e., 3 or 4 expressed in the score adopted by NHK.

4. Audio signals were not very good and

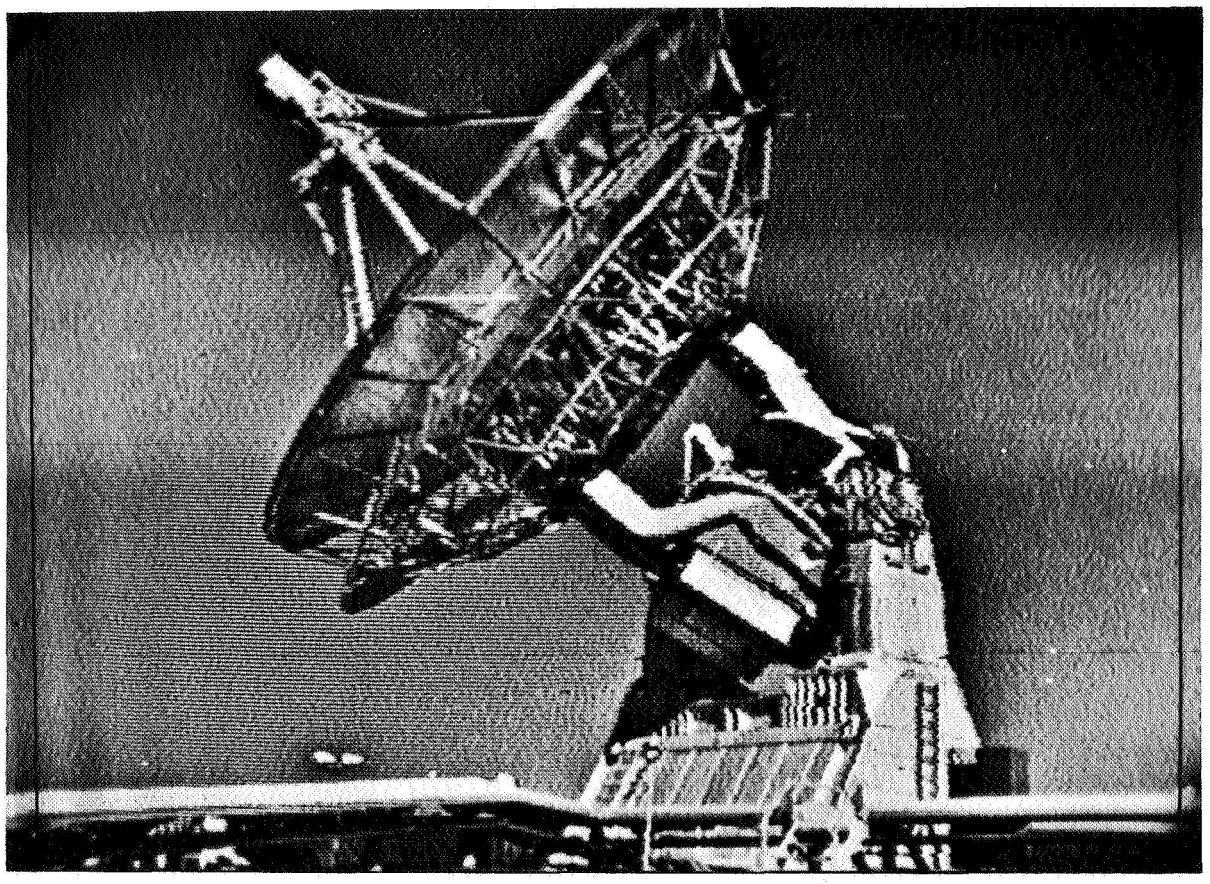
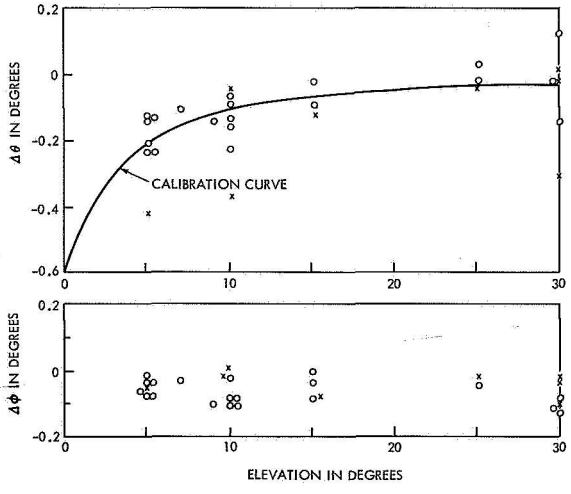


FIGURE 9–3.—TV picture received at COMIBA, first demonstration between U.S.A. and Japan.



Note—Cross marks among above errors gave a good coincidence with prediction by shifting time by 8 seconds.

FIGURE 9–4.—Azimuth and elevation error in orbital prediction for Relay I measured during revolutions 2677 to 2870.

an effect of spin fading was markedly observed.

5. The comparison between the predicted and measured orbital data was generally good, and there was no serious problem concerning satellite tracking.

6. As regards the phase-lock demodulator of the receiver, there still remain several technical problems, e.g., no improvement took place by the use of emphasis for TV reception.

7. As there was little rain during the period of experiment, the meteorological effect on noise temperature was not made clear.

AUTHORS. *This chapter was contributed by personnel of the Kokusai Denshin Denwa Co. Ltd. (Japan's Overseas Radio and Cable*

TABLE 9–6.—*Comparison Between Calculated and Measured Orbital Data*

Orbit	Calculated		Δ Az (degrees)	Δ El (degrees)	Circuit
	Azimuth (degrees)	Elevation (degrees)			
2677	65.72	30.00	−0.13	−0.14	COMMOJ → COMIBA
	54.58	10.00	−0.09	−0.21	
2678	59.41	30.00	−0.01	−0.30	
	64.85	10.00	0	−0.36	
2700	75.17	30.00	−0.03	−0.02	
	68.16	25.00	−0.02	−0.03	
2701	57.67	30.00	−0.10	+0.02	
	60.85	10.00	−0.10	−0.08	
2708	64.10	30.00	−0.08	−0.01	
	60.80	25.00	−0.04	−0.01	
2709	60.44	30.00	−0.12	+0.13	
	65.04	15.00	−0.08	−0.08	
2724	57.24	25.00	−0.03	+0.04	
	58.05	5.00	−0.03	−0.14	
2731	57.96	15.00	0	−0.01	COMAND → COMIBA
	52.44	5.00	−0.02	−0.13	
2762	54.48	10.00	−0.09	−0.13	
	52.24	5.00	−0.07	−0.24	
2777	62.12	9.00	−0.10	−0.14	
	56.72	5.00	−0.08	−0.20	
2785	56.54	10.00	−0.10	−0.15	
	52.85	5.00	−0.06	−0.24	
2816	59.98	15.00	−0.09	−0.12	
	52.42	5.00	−0.06	−0.42	
2839	60.57	10.00	−0.02	−0.04	
	54.80	5.00	−0.04	−0.12	
2870	59.40	10.00	−0.01	−0.06	
	56.08	7.00	−0.02	−0.10	

NOTES:
1. Δ = calculated value—measured value by 6-meter antenna.
2. Accuracy of measurement is ±0.01 degree.
3. Correction by effect of atmospheric refraction is not contained.

System), Tokyo, Japan, under cognizance of the Japanese Ministry of Posts and Telecommunications.

N66-10260

Chapter 10

The Goonhilly Downs Space Communications Station

INTRODUCTION

The initial purpose of the Post Office satellite system earth station at Goonhilly Downs, Cornwall, was to obtain information on the performance of experimental communication satellite systems; such information will be of great importance to the designers of systems for commercial operation. To facilitate this end, the United Kingdom and USA Governments prepared and signed, in February 1961, a Memorandum of Understanding regarding collaboration between the British Post Office and the United States National Aeronautics and Space Administration (NASA) on the testing of experimental communication satellites to be launched by NASA. The first phase of the tests covered projects Telstar and Relay, both using active satellites.

The understanding with the United States covers full interchange of technical information, makes clear that the collaboration relates to experimental tests only and is not concerned with commercial exploitation, and does not preclude the use of the Post Office experimental earth station for tests outside the cooperative projects outlined. Similar agreements between the United States and France, Federal Republic of Germany, Italy, and Brazil have since been approved.

The Goonhilly satellite system earth station has been planned and equipped, not only for participation in projects Telstar and Relay and similar experimental projects, but also with a view to possible operational use at a later date.

The Station and its Facilities

The site of the Goonhilly radio station, Figure 10–1, has been chosen to be particularly suitable for transatlantic communication in view of its westerly location; also, its southerly latitude is convenient for satellites in equatorial orbits. It is remote from the majority of microwave links in the United Kingdom, so that frequency-sharing with such links is facilitated. The horizon angles are predominantly negative with a maximum positive value of about 0.5°, so that satellite orbits involving low angles of elevation can be used. The main station building is located near the center of the site, the aerial being close to one corner. The site is large enough to accommodate additional aerials for experimental purposes or later for operational use.

The present equipment for participation in projects Relay and Telstar includes the following facilities:

1. An 85 ft diameter paraboloidal-reflector dish aerial with full steerability over the hemisphere above the horizontal plane.
2. Means for steering the aerial automatically from predicted orbital data.
3. A 10 kw transmitter operating at 1725 Mc for project Relay.
4. A 5 kw transmitter operating at 6390 Mc for project Telstar.
5. Low-noise receiving equipment for the

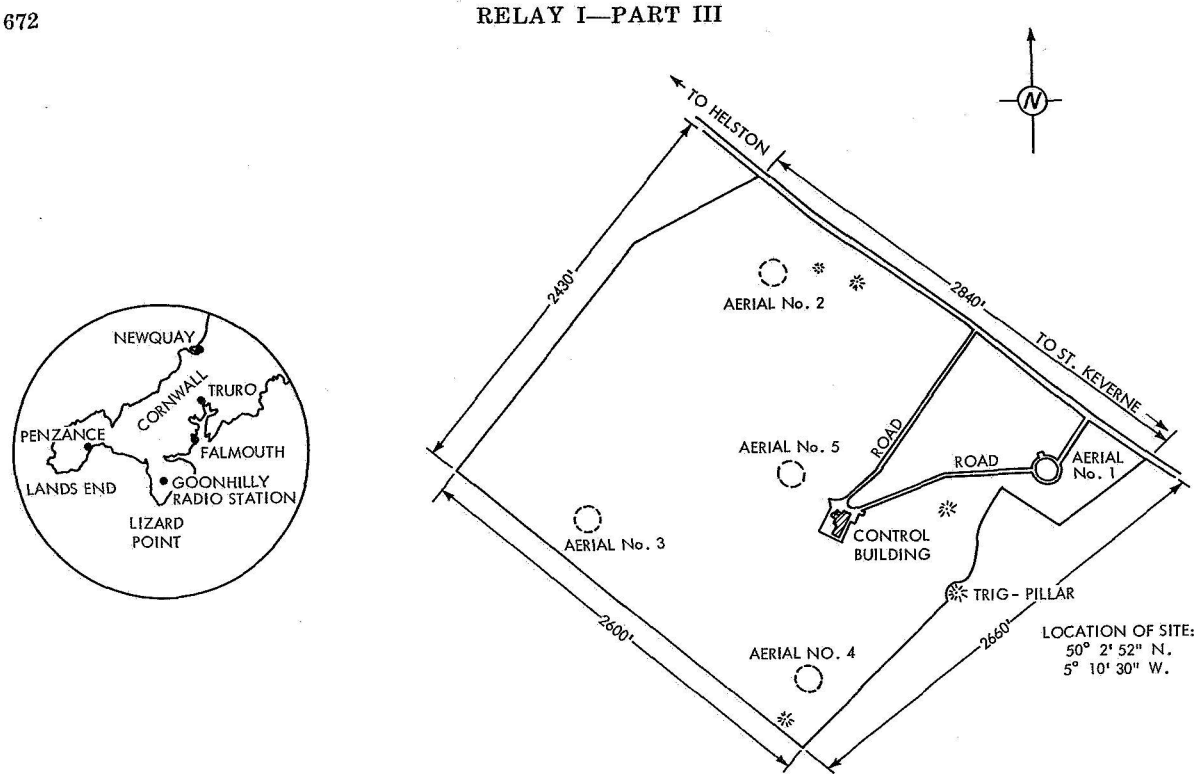


FIGURE 10–1.—Location of Goonhilly earth station.

4170 Mc communication and 4080 Mc beacon signals transmitted by the Telstar and Relay satellites.

6. Terminal equipment for transmission and reception of multi-channel telephone, telegraph and television signals.

7. Video and multi-channel telephone and telegraph links to the trunk network.

8. Support communications, including teleprinter and voice circuits to the USA, for the transmission of data and other information concerning the tests.

The Steerable Aerial

The steerable dish aerial, Figure 10–2, is designed for operation up to at least 8000 Mc, at which frequency the beamwidth is only about 0.1°. Since the satellites move rapidly across the sky, the aerial is required to track a rapidly moving satellite to within a few minutes of arc. The aerial rotates as a whole on a turntable to provide changes in azimuth, and the dish is rotated about a horizontal axis for elevation changes. In

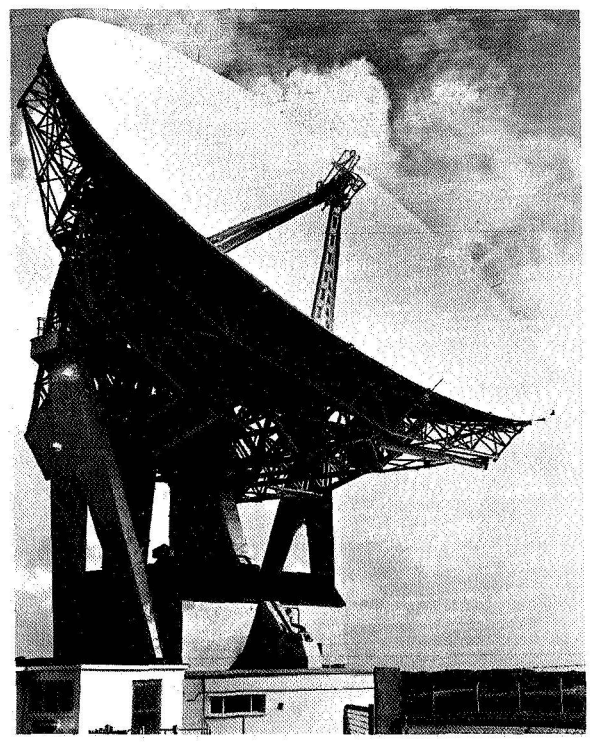


FIGURE 10–2.—The steerable antenna.

addition, small variations (up to a degree) of beam direction are possible by remotely-controlled movements of the feed at the focus of the dish. The feed for the dish is in the plane of the aperture, an arrangement which, with appropriate feed design, reduces the levels of the minor lobes of the radiation diagram. This is of great importance since, unless the minor lobes are very small, noise can be picked up from the terrain surrounding the aerial which would significantly degrade the signal-to-noise ratio of the very weak signals received from a satellite.

Since the aerial is not protected by a radome, stability under high wind conditions is achieved by a heavy, sturdy construction using reinforced concrete supporting members, and powerful driving motors. The weight of the movable part of the aerial structure is some 870 tons, and the structure is designed to operate in wind velocities up to 65 mph.

The aerial is automatically steered, using predicted orbital information derived from the NASA worldwide network of "Minitrack" stations, one of which is operated by the Department of Scientific and Industrial Research at Winkfield, near Slough. This data is received in digital form over a teleprinter circuit from the NASA Goddard Space Flight Center, U.S.A.; it has to be processed in an electronic computer at Goonhilly to give the aerial steering instructions in the appropriate form. In order to correct for small errors in prediction and errors arising from other causes, the manually- or automatically-controlled aerial beam swinging facility previously referred to is used. This operates from the 4080 Mc beacon signal transmitted by the satellite; by causing the aerial beam to scan circularly over a few minutes of arc, information is thereby derived which enables the appropriate corrections to be applied, initially on a manual basis and later automatically on a lock-on basis. A spiral scan of up to 1° is available, if required, to aid in satellite beacon acquisition, but has not in practice been found necessary.

Immediately behind the reflector dish there are two apparatus cabins; one of these accommodates the travelling-wave maser amplifier operating at 4170 Mc. The necessary low temperatures for this device are obtained by using liquid helium and liquid nitrogen, evaporated helium being recovered, stored, and compressed by equipment housed in a cabin on the horizontal turntable.

A cabin behind the reflector also accommodates filters for separating the satellite beacon signal from the satellite communication signal, so that the latter may be amplified separately in the maser. Means for determining the system noise-temperature are also provided. Waveguide assemblies with rotary and flexible joints connect the feed at the focus of the reflector with equipment in the cabins at the back of the reflector and on the aerial turntable.

On the horizontal turntable is an apparatus room accomodating the high-power stages of the Relay and Telstar transmitters, the low-power drive equipment for the transmitters, and equipment for translating signals to and from radio frequency and an intermediate frequency of 70 Mc.

A cylindrical enclosure in the middle of the apparatus room accommodates loops of flexible cable used to make connection between the equipment in the moving apparatus room and fixed equipment in the main control building and elsewhere. Rotation of the turntable around the vertical axis is restricted to ± 250°, so that cable loop rather than slip-rings can be used. Beneath the horizontal turntable and beyond it there is a chamber and tunnel for the inter-connecting cables.

Main Control Building

In the main buildings, Figure 10–3 and 10–4, from which all experiments are controlled, the principal rooms are equipped with:

1. control and experimental apparatus,
2. telegraph equipment,
3. computer and data processing equipment,

4. aerial steering equipment and precise time and frequency standards,

5. aerial steering console,

6. auxiliary test apparatus, including telecine and television equipment.

Control and Experimental Apparatus Room

A console is provided for the control of experiments, Figure 10–5, enabling the availability of the transmitting, receiving and test equipment and the aerial to be determined at all times, together with voice communication facilities to the operating staff concerned. A similar console is provided for aerial steering purposes, the latter including visual presentation on cathode-ray tubes of the incoming wave direction from the satellite.

The equipment in this room includes:

1. Baseband and intermediate-frequency equipment forming part of the transmitting and receiving communication system

2. Receivers for the "off-the-air" reception of television broadcast signals

3. Test equipment

4. Magnetic tape and other recorders

5. Satellite beacon signal receivers

6. Video and multi-channel telephony terminals

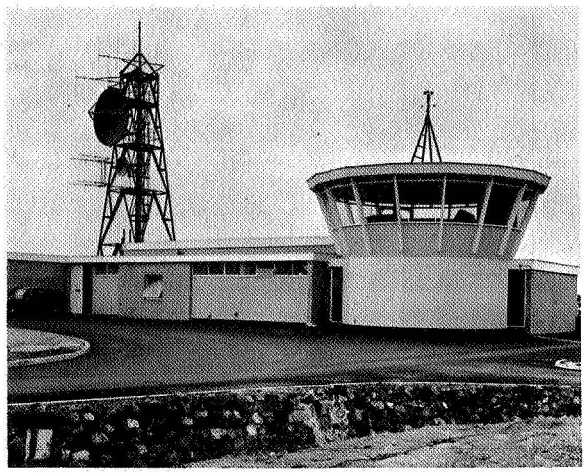


FIGURE 10–3.—External view of control building.

Telegraph Room

Separate teleprinters are provided for:

1. Operational traffic with, and reception of orbital prediction data from the Goddard Space Flight Center, USA

2. Communication with the satellite ground station at Andover, Maine, USA, on a private wire basis

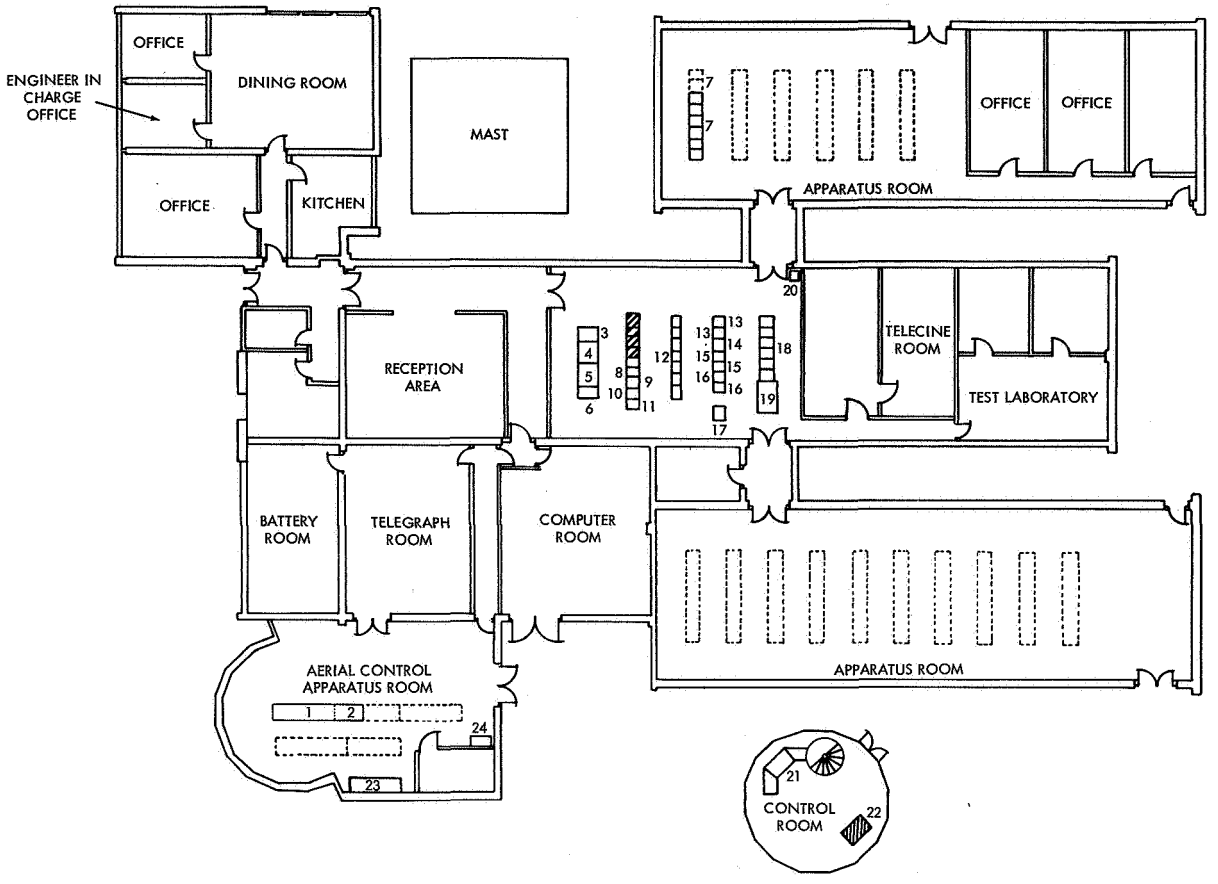
3. Telex facilities

4. The receipt of local meteorological information (to enable aerial safety precautions to be taken if necessary).

Computer Room

The prinicpal item in this air conditioned room, Figure 10–6, is a National-Elliot Type 803 electronic computer. As noted earlier, orbital data is received in digital form from the USA; this data provides predicted X, Y, Z versus time coordinates at one-minute intervals and is recorded on punched tape. The computer processes the data to provide aerial steering instructions also in punched-tape form, the output information for each one-second interval including time, azimuth bearing, rate of change of azimuth, elevation, rate of change of elevation and the slant range to the satellite. The computer program also makes allowance for changes of apparent satellite bearing due to atmospheric refraction. Telegraph-type tape readers and data recording equipment are provided for processing the received orbital data and for the preparation of the serial steering tapes.

Figure 10–7 shows the manner in which instructions from the computer are passed into the aerial steering equipment in the form of a punched paper tape. This tape is "read" by the equipment one second in advance, one second at a time. The tape-reading equipment positions the tape for each reading operation from the single "cycle start" hole marking the commencement of each sequence. The time to which the start of each sequence refers is punched into the tape as hours, minutes and seconds in a code which can be read by inspection. This is followed by instruction, in binary code, defining the azimuth and elevation directions required at that time.



ITEM	DESCRIPTION
1	AERIAL No. 1 CONTROL EQUIPMENT
2	AERIAL No. 2 CONTROL EQUIPMENT
3	CONTROLLER'S CONSOLE
4	CIRCUIT SWITCHING CONSOLE
5	BEAM SWINGING EQUIPMENT
6	TX AND RX SUPERVISORY CONSOLE
7	INLAND MICROWAVE LINK EQUIPMENT
8	TIME EQUIPMENT
9	EQUIPMENT RACK FOR CIRCUIT SWITCHING CONSOLE
10	MISC. APPARATUS RACK
11	D.P.U. RECEIVERS
12	BASEBAND AND IF EQUIPMENT
13	RECORDERS
14	WHITE NOISE TEST EQUIPMENT
15	MISC. TEST EQUIPMENT
16	T.V. TEST EQUIPMENT
17	CABLE TERMINATING RACK
18	CARRIER AND TRANSMISSION EQUIPMENT
19	DISTRIBUTION FRAME
20	VOLTAGE REGULATOR FOR ITEM 18
21	CONTROL CONSOLE AERIAL No. 1
22	CONTROL CONSOLE AERIAL No. 2 (PROPOSED)
23	CABLE TERMINATIONS AERIAL No. 2
24	MISC. APPARATUS RACK

FIGURE 10–4.—Plan view of control building.

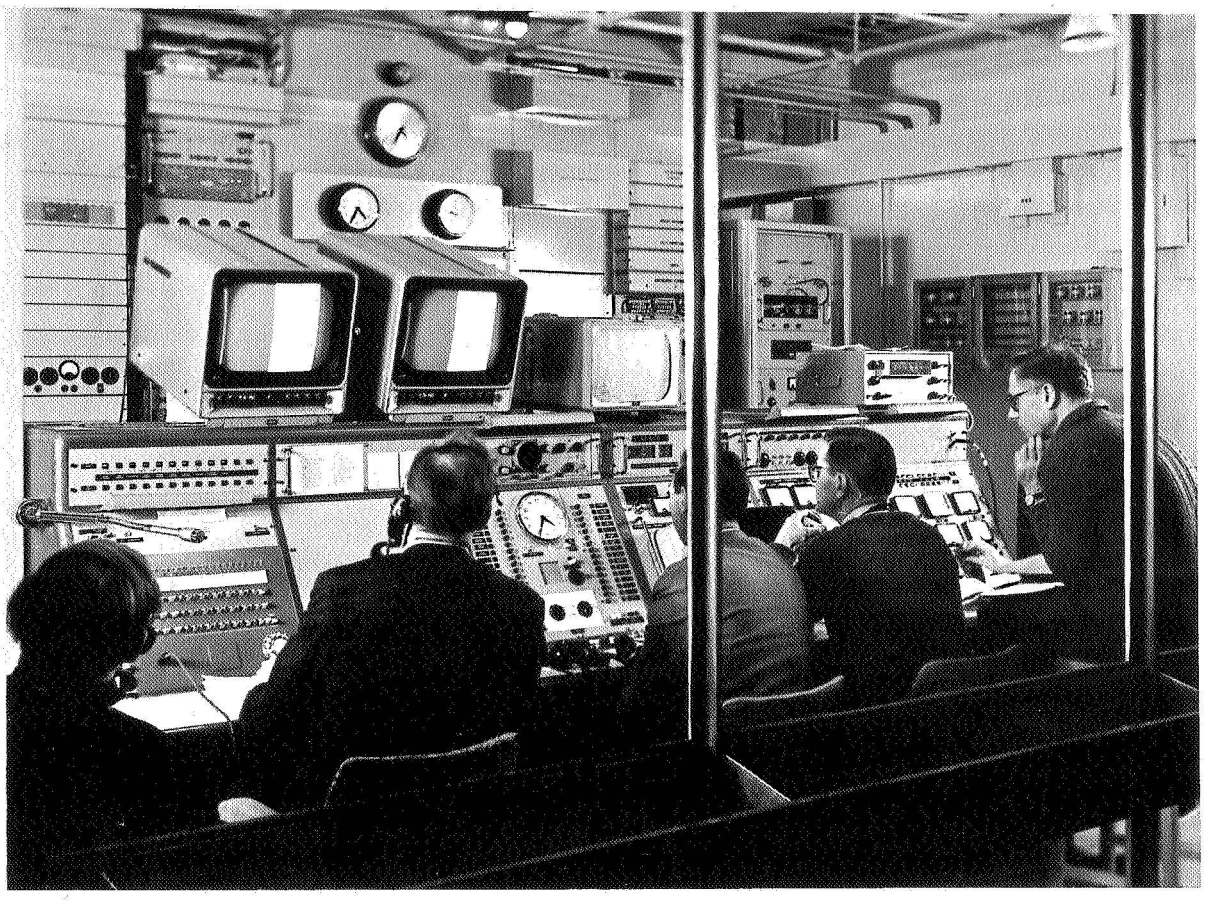


FIGURE 10–5.—The control console suite.

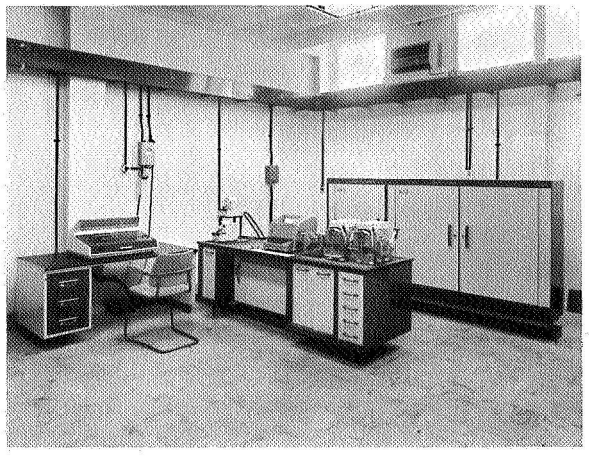


FIGURE 10–6.—Computer room.

With the exception of a short portion of tape giving a tape identification number, also in a simple code which can be read by inspection, the remainder of the one-second sequence contains a series of increments to the initially demanded aerial directions which enables the equipment to keep the driving motors running at the correct rates for the next demanded position to be reached with minimum error.

Aerial Steering Apparatus Room

The apparatus in this room enables a comparision to be made between the aerial steering input data in digital form and digital signals derived from readout units on the

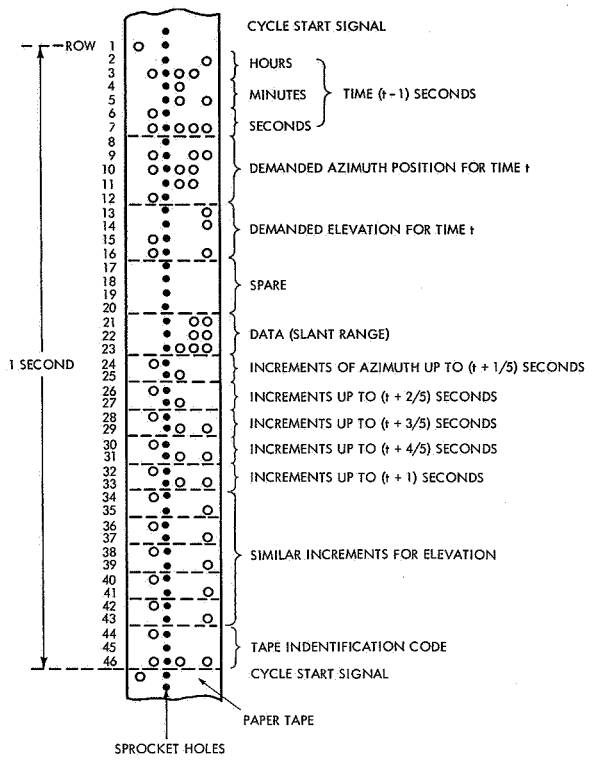


FIGURE 10–7.—Steering instructions on a punched paper tape.

aerial azimuth and elevation drives, thus enabling the servo feedback loops to be completed.

A temperature-controlled annex to this room accommodates quartz-crystal oscillators of high accuracy which, in conjunction with time signal radio receivers, provide a precise time source adjustable to Universal Time 2.

Steering tapes are received from the computer room for application to the input of the aerial steering apparatus, initiation of aerial movement being dependent upon synchronism between time as recorded on the tape and as generated by the precise time source.

Aerial Steering Console Room (Control Tower)

The aerial steering console room in the Control Tower, Figure 10–8 has been designed and placed to give uninterrupted visibility over the whole of the site. Though every precaution has been taken to ensure safety of personnel, by the provision of mechanical and electrical interlocks, it has been considered desirable that those controlling the movement of the aerial should have full visual surveillance. The aerial is floodlit at night.

Though aerial steering is fully automatic, it has been arranged so that the mechanical and electrical conditions of the aerial are displayed to an operator who can observe fault conditions, apply corrections and override the automatic system should any abnormality occur.

Power Supplies

The power supply for Goonhilly radio station is obtained at 11 kv from an electricity substation four miles distant, together with an alternative supply from Helston, eight miles distant. Both supplies are via overhead lines, except for a distance of some 400 yards on site, which is via underground cable. Changeover facilities are provided to enable the second supply to be used in the event of failure of the first. The present supply capacity is 450 kva; this will ultimately be increased to 800 kva.

The supply terminates at three transformers. At the aerial site a 250 kva transformer supplies power for driving motors and a 100 kva transformer supplies power for electronic equipment, etc. The third transformer, at the control building, is of 100 kva to provide power for the whole building.

Because of the very small risk of failure of both electricity supplies simultaneously, and because of the large amount of power required, no local standby power is provided except that derived from a 50 volt battery to operate emergency lighting, clocks and telephones.

System Checking Facilities

It is necessary to be able to check periodically the mechanical alignment of the aerial, the electrical bearing of the aerial beam and the performance of the transmitting and re-



FIGURE 10–8.—Aerial steering position in the control tower.

ceiving equipment, independently of a satellite. For these purposes the aerial is fitted with a boresight telescope for ranging on local and distant points of accurately known bearing. In addition, there has been installed at Leswidden, some 21 miles away, apparatus capable of simulating the Relay and Telstar satellites, thus enabling comprehensive overall system tests including tests of the aerial gain and radiation diagram to be made. Measurements of the aerial tracking characteristics are made using the radio star Cassiopeia A.

Transmission Equipment

The radio transmission equipment at a satellite system earth station differs markedly from that used in conventional radio-relay systems, for the following reasons:

1. The need for high-power earth station transmitters—with outputs of kilowatts instead of a few watts.
2. The very small signal power, of the order of micro-microwatts, received from satellites, and the resulting low signal-to-noise ratio in the intermediate-frequency passband of the ground station receiver.
3. The use of circularly polarized waves, as compared with linear polarization in most radio-relay systems.
4. The presence of Doppler frequency shifts on the received signals due to the motion of the satellite relative to the earth stations.

The earth station transmission equipment, shown in block schematic form in Figure 10–9, enables signals to be transmitted in a 5 Mc-wide baseband. Such a baseband could

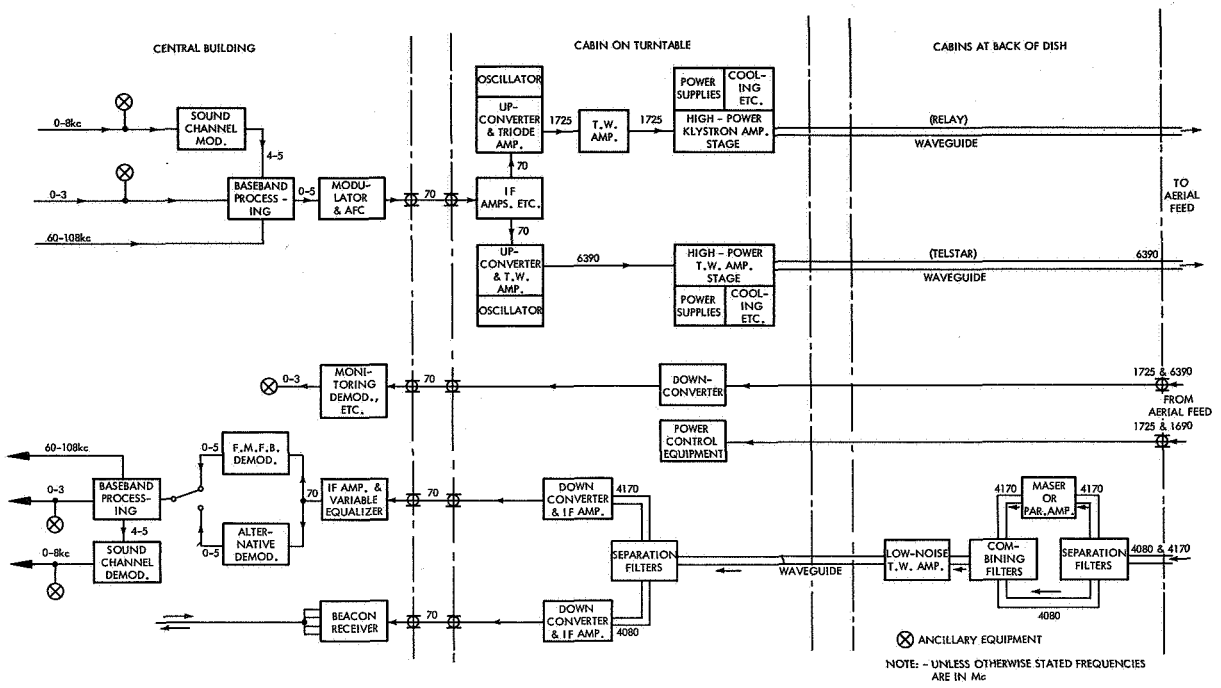


FIGURE 10–9.—Earth station transmission equipment, block diagram.

accommodate several hundreds of telephony channels or a television signal of up to 625-line definition or high-speed data transmissions. Multi-channel telegraphy and facsimile signals could alternatively be transmitted in the telephony channels.

The baseband input signals are applied to a 70 Mc frequency-modulator, the wide-deviation output of which is then passed to up-conversion equipment for translation to the desired radio frequency, a low-power driver stage and a high-power transmitting amplifier. As the ground-station transmitter frequencies for Relay and Telstar are very different, being 1725 and 6390 Mc respectively, separate up-conversion, driver, and high-power equipment are provided for the two projects. The Telstar high-power transmitter uses a 5 kc traveling-wave tube developed specially by the Services Electronics Research Laboratory, while that for Relay uses an Eimac 10 kw multi-cavity klystron amplifier.

Signals received from a satellite include a CW beacon emission on 4080 Mc for tracking purposes, as well as a communications signal on or near 4170 Mc. In view of the limited bandwidth of the maser used as a low-noise first-stage amplifier in the receiver, only the communications signal is amplified in the maser though both signals are amplified in a second-stage comprising a low-noise traveling wave tube. The beacon signal is selected by a waveguide filter and, after frequency-changing, is applied to a narrowband beacon receiver.

The communications signal is frequency-changed in a down-converter to an IF of 70 Mc and is then applied to one of three FM demodulators. One demodulator is of the conventional limiter/discriminator type and is suitable for use only when the received signal-level is relatively high. The second demodulator is of the frequency-modulation negative-feedback type; it is particularly suitable for multi-channel telephony. The third demodulator comprises a tuned circuit which instantaneously follows the frequency of maximum signal energy, the bandwidth being automatically adjusted according to

the received signal level. The second and third demodulators reduce the effective noise bandwidth and thus enable relatively weak signals to be satisfactorily received.

Tests and Testing Equipment

Although objective tests, i.e., measurements of transmission characteristics between earth station "baseband input" and "baseband output" via the satellite, can provide information on which the suitability of the system for any form of signal transmission can be assessed, it is nevertheless of value also to make subjective assessments. To this end facilities have been provided so that either one-way television pictures or two-way telephony signals can be transmitted for demonstration purposes.

One-way transmission tests via a satellite are carried out either between pairs of similarly equipped earth stations or "in loop." In the latter arrangement, the signals transmitted from a given earth station are received back at the same station.

Under two-way transmission conditions both of a cooperating pair of earth stations energize the same satellite at slightly different frequencies. For two-way telephony transmission the Relay satellite includes two separate receivers operating on slightly different frequencies, but in the Telstar satellite there is only a single wideband receiver. When working on a two-way basis via the Telstar satellite the transmitter powers of the cooperating earth stations must be continuously adjusted so that the signal levels at the input to the satellite receiver are essentially equal regardless of the distances of the respective earth stations from the satellite.

Many items of test equipment have been provided for the objective tests. These permit the measurement of insertion-gain stability, selective fading, noise levels, television signal transmission characteristics, telephone and telegraph signal transmission characteristics, received carrier power levels, Doppler frequency shifts and receiving system noise-temperatures, etc. For multi-channel telephony tests, white-noise signals simulating up to 600 telephone channels are available.

In the case of subjective telephony tests, baseband equipment has been provided so that twelve two-way circuits assembled in the ranges 12–60 kc or 60–108 kc may be set up. For subjective tests of television transmission, telecine equipment and high-grade picture monitors, suitable for 405, 525, and 625-line standards have been provided.

For telephony demonstrations the audio circuits are connected to the Post Office trunk telephone network. The audio circuits are also available for carrying out telegraphy, facsimile and data transmission tests via the Post Office Telegraph Branch Laboratories in London. In the case of television demonstrations, the video circuit is connected to the Post Office television distribution network, use being made when necessary of line-standards conversion equipment provided by the broadcasting organizations. The comprehensive network of inland communications provided for such demonstrations and tests is shown in Figure 10–10.

Conclusion

The station will undoubtedly play a useful part in the acquisition of the information and experience needed for the design and construction of successful operational satellite communication systems. It is of interest to note that the whole of the equipment and facilities provided, including the large steerable aerial, are of British design and manufacture, with the exception of Eimac klystron used in the Project Relay transmitter.

Acknowledgments

The thanks of the authors are due to their colleagues in the Post Office who contributed to the planning, design and provision of the Goonhilly satellite communication radio station, and in particular to the staff of the S. W. Region of the Post Office for their help in the installation phase.

Tribute is also due to the British telecommunications industry for its part in provid-

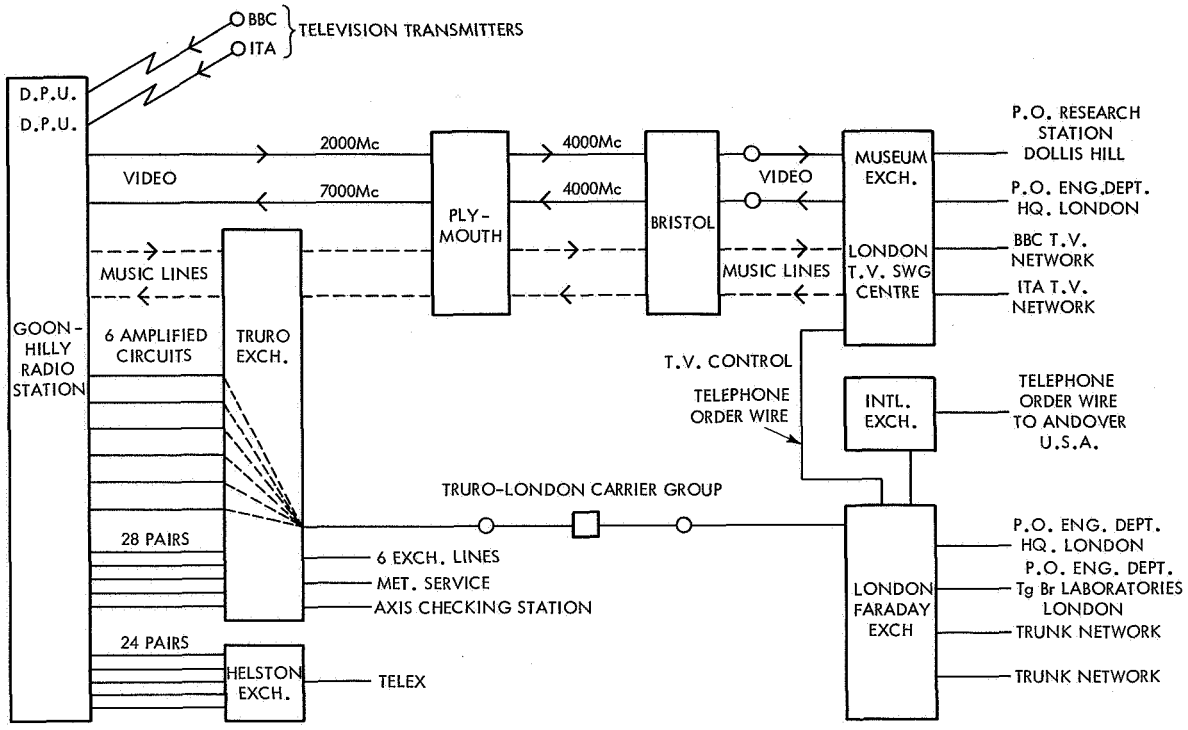


FIGURE 10–10.—Support communications for tests and demonstration.

ing much of the electronic equipment, to the Services Electronics Research Laboratory for the development of the 5 kw traveling wave tube, and to Husband & Company and associated contractors for the design and construction of the large steerable aerial. Special mention should be made of the contractors' staff who worked long hours on the aerial construction, often under extremely adverse weather conditions.

The permission of the Engineer-in-Chief of the Post Office to make use of information contained in this chapter is gratefully acknowledged.

This paper is, with minor modifications, as first published in *British Communications and Electronics,* August 1962, pp 574–479 and is reproduced by kind permission of the editor.

AUTHORS. *This chapter from the United Kingdom was contributed by the General Post Office, London, England. The foregoing Introduction section was authored by* W. J. BRAY *and* F. J. D. TAYLOR *of the GPO.*

THE GOONHILLY 85 FT. STEERABLE DISH AERIAL

Introduction

The choice of the basic type of aerial for a satellite communication ground station is of major importance in view of its influence on the overall performance, cost and time to complete the installation.

In the case of the Post Office satellite communication earth station at Goonhilly Downs, Cornwall, a decision was made early in 1961 to use an 85-foot diameter steerable paraboloidal dish aerial, without a radome, for tests with the Telstar and Relay and other communication satellites.

Tests with smaller paraboloidal dish aerials with the feed in the aperture plane had shown that a satisfactory electrical perform-

ance could be obtained, and experience with the 250-foot diameter radio-telescope at Jodrell Bank had shown that the mechanical problems could be overcome.

An important factor in the present case was the limited time—less than one year—available for the design, manufacture, construction and testing of the aerial.

Design Requirements

To specify for design purposes the requirements for such an aerial, it was necessary to know the frequency range and aerial gain required, the feed arrangements and radiation patterns needed, the orbits of the satellites and the proposed method of tracking, the nature of the ground on which the aerial was to be built and the weather under which it must operate.

Radio waves in the spectrum 1000 to 10,000 Mc are suitable for satellite communication and the Post Office decided for the Goonhilly aerial to limit its interest to the range up to 8000 Mc. In the case of Projects Telstar and Relay it had been decided that the critical satellite-to-ground link would operate at about 4000 Mc, the ground-to-satellite link operating at about 6000 Mc (Telstar) and 1700 Mc (Relay). System study showed that an aerial gain of the order of 55 to 60 db was desirable at 4000 Mc and an 85-ft diameter 90° dish was chosen, giving a theoretical gain of 58 db.

By careful design of the feed unit mounted at the focus in the aperture plane, the noise picked up on minor lobes could be minimized. As this would mean some fall-off in illumination toward the edge of the reflector, the profile tolerance could be eased in the outer zone. The tolerance $\pm \lambda/16$, i.e., $\pm$ 3/16 inch in this case, was applied to the central area out to 50-foot diameter, and twice this tolerance between 50-foot and 85-foot diameter. These tolerances were to be maintained under all weather conditions and angles of elevation. Combined feed units for transmitting and receiving were expected to weigh several hundred pounds, and to hold them at the focus, quadrupod legs were favored straddling the center of the reflector, leaving it free, if desired, for later conversion to Cassegrain feed. Model tests showed that the shadow cast by four legs 90° apart and springing from the bowl on a 35-foot diameter circle would be acceptable. Two of these legs at 90° and 270° could provide direct waveguide access to apparatus cabins at the back of the bowl near its horizontal axis while the other two legs at 0° and 180° could carry other services.

To cater for all likely orbits (circular and elliptical) in equatorial, polar or inclined planes and to follow satellites with periods as short as two hours and heights of only a few hundred miles at perigee, the aerial had to provide hemispherical coverage and be able to move rapidly. For the experimental aerial the velocity and acceleration were limited to 2° per sec and 1.33° per sec respectively, sufficient to track satellites not passing through or near the zenith. The beam-width at 4000 Mc being only 0.2° at the half power points, a tracking accuracy of one-third the beam-width was called for. Steering was to be from punched tape derived from orbital data transmitted to the Goonhilly Radio Station from the Goddard Space Flight Center, U.S.A. Time information was to be provided by a high precision quartz clock with the facility for checking against radio time signals.

The aerial site on Goonhilly Downs, Cornwall, is on the highest part of the Lizard peninsula with all-round freedom from obstruction above 1/2° elevation. According to Geological Survey Department, records the whole area for at least half a mile beyond the site boundaries rests on solid rock over 1000 ft deep which forms the largest single mass of Serpentine in Cornwall. The rock is tough, has indistinct cleavage, and is a very suitable base for reinforced concrete foundations on which to mount a precision instrument.

A study of wind records for the Lizard Peninsula for the last forty years showed that although high winds peaking up to 90 mph for short periods could be expected

almost annually, higher figures were most unlikely, and winds above 100 mph virtually unknown. Using a gust factor of 1.4 appropriate to the terrain it was therefore required that the aerial should have the following properties:

1. Be fully operational in winds up to 55 mph mean $\times$ 1.4 = 77 mph peak.
2. Be structurally and mechanically suitable for working in winds up to 65 mph mean $\times$ 1.4 = 91 mph peak.
3. Safely withstand winds up to 75 mph mean $\times$ 1.4 = 105 mph peak.

Design Considerations

If a radome is used to protect an aerial from the weather, the aerial itself may be relatively light in construction and the drive/control requirements will be correspondingly less stringent. However, energy losses in receiving through the radome, especially when the latter is wet, may lead to a significant increase of the overall noise temperature of the receiving system. The cost of a light aerial with a radome may also be greater than that of a heavier and more stable unprotected aerial.

The alternative approach, which was adopted for the Goonhilly aerial, is to use a heavy, stiff and stable supporting structure together with a well balanced, stiff dish to minimize deflections in high winds, driven by motors normally working well below their maximum capacity. The application of these principles has resulted in an aerial of good accuracy and radio efficiency, at relatively low cost.

So far as wind speeds are concerned the first requirement is that the aerial must be designed to survive the maximum winds it can be expected to encounter. Next, consideration must be given to the maximum wind speed at which the aerial must remain fully operational, i.e., maintain accuracy of shape when moving at full speed and within the specified following accuracy. The torque required to rotate the aerial in wind is proportional to the square of the wind speed, and the driving horsepower is proportional to the product of torque and angular speed, so that size of the driving motors will increase rapidly as the *full operational speed* maximum wind requirement is raised. It was not considered necessary, at least initially, to provide drives able to continue rotating the Goonhilly aerial at full speed in winds gusting above 77 mph with the dish at the angles corresponding to maximum wind torque.

The expected satellite orbits were such that operational speeds in excess of 2° per second were unlikely except when a satellite passes over or nearly over the earth station zenith.

The selection of the azimuth speed required careful consideration since this speed, combined with the selected maximum operational wind speed, determines the required horsepower of the azimuth motor. The combined horsepower of the azimuth and elevation drives must also be considered with respect to the total electrical power supply to be provided. For most of the time the aerial was expected to be operating in winds considerably below the maximum and at speeds below its maximum operational speed, i. e., the drive horsepower normally required would be very much below the maximum which may be occasionally required. If the specified maximum azimuth speed or the maximum operational wind speed were higher than was strictly essential, the electrical power requirements and the capacities of the various transformers, switches, etc., would be correspondingly increased.

The azimuth speed was fixed at 2° per sec giving a theoretical maximum drive motor size of 75 hp. The torque/speed calculations for elevation motion, after allowing for unbalanced moving parts, gearbox losses, etc., indicated that a 100 hp drive motor was required. In practice, both elevation and azimuth drives were eventually standardized at 100 hp.

The accuracy with which the aerial can be made to follow a satellite when under automatic control depends on the following factors:

1. The accuracy, rigidity and stability of the structure as a whole and of its major component parts.

2. The accuracy with which the actual angular position in azimuth and elevation can be determined at any time.

3. The reduction to a minimum of any backlash or uncontrolled motion in the drives.

4. The achievement of a stable and accurate but fast-responding servo-control system for the drive motors.

5. The provision of reliable and accurate control signals to control the servo in accordance with the demands of the satellite orbit to be tracked.

Having regard for these factors, and for the fact that orbital information would be available already processed into demanded azimuth and elevation angles at given times, the following basic decisions were made to enable the required tracking accuracy to be achieved:

1. The dish supporting structure would be of reinforced concrete, having a relatively high moment of inertia so as to give a steadying effect in gusty winds and high structural stability against deflections from all wind pressures.

2. Shaft angular position determination would be by use of 16-bit optical shaft encoders, giving a basic resolving power of 1 in 65536 (approx. 20 seconds).

3. The servo-control system would be of the digital type, receiving incoming demanded angle information on punched tape, comparing the demanded angle for each motion with the actual angle and finally passing an analog error signal to the servo-system.

The results of the dependent structural, mechanical and electrical decisions emanating from the basic decisions described above are detailed in the following paragraphs.

General Description of the Aerial

The general arrangement of the aerial is shown in Figure 10–11, and the components are described below.

The Dish

Both the structure and the membrane plating of the dish are of steel. The membrane is an 8-gauge Corten sheet, having good corrosion resistant properties, individ-

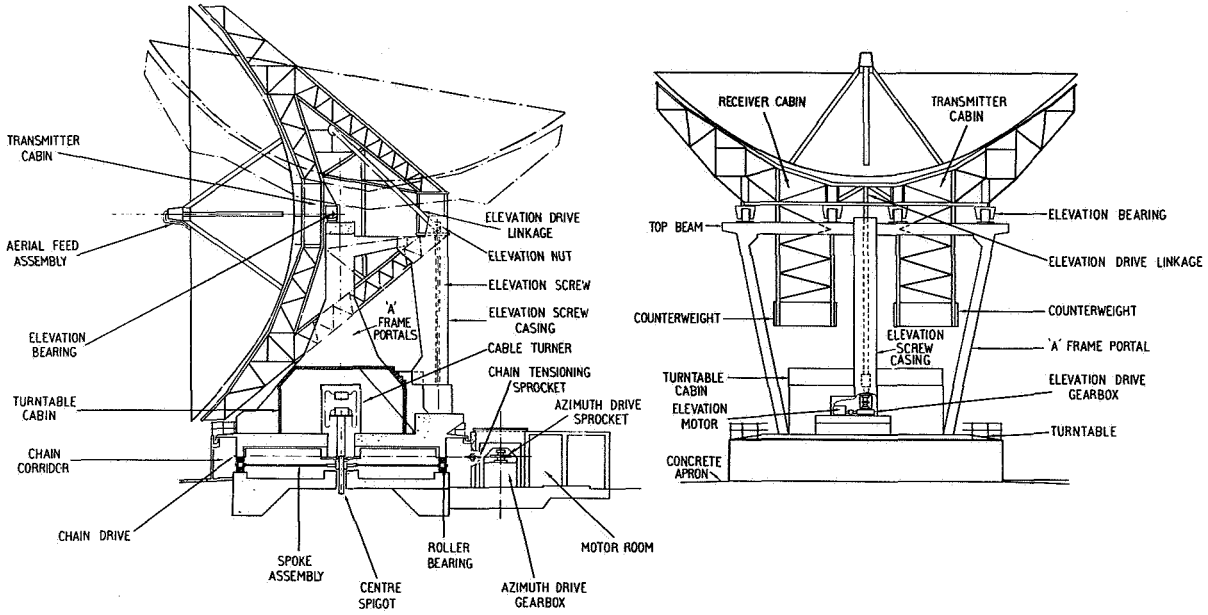


FIGURE 10–11.—General arrangement of the antenna.

ual plates being screwed to the supporting structure and then continuously welded to give good electrical continuity. Steel was chosen as giving the optimum combination of good strength and rigidity, and relatively low co-efficient of expansion with the minimum cost.

The balancing of the dish* is such that the natural tendency of the dish upper and lower edges to droop downwards as the dish moves from the zenith toward the horizon is automatically opposed by forces in the balance-weight supporting structure. A drainage system is provided for removal of rainwater, and snow may be removed by depressing the dish. The provision of a de-icing system for an installation in southwest Cornwall was considered unnecessary in view of the generally favorable weather conditions.

There are two steel cabins built into the structure behind the dish for housing radio apparatus as near to the focus as possible.

The dish is supported on a pre-stressed horizontal concrete beam via four large split roller bearings of the self-aligning type, one of the center pair of these being arranged to take axial thrust. The elevation optical shaft angle encoder is driven directly from the thrust bearing by an arm and pin arrangement.

The Dish Supporting Structure

The dish supporting structure comprises a horizontal concrete beam supported in turn by three reinforced concrete portal frames the outer two of which were precast and lifted into position, and the inner frame cast in situ. These portal frames stand on a circular reinforced concrete turntable base, which also carries a large cabin housing radio apparatus and accommodating the main cable-turning device. The latter enables connections to be made between equipment in the moving part of the structure and fixed equipment elsewhere without using slip-rings. The concrete cabin is fully screened with continuous copper sheeting.

The lower fixed portion of the mount is also of reinforced concrete, taken down to the rock.

Azimuth Mount

The moving part of the azimuth mount is carried on 54 tapered rollers, running between an upper and lower track of manganese steel, the tracks being 42 ft 6 in. in diameter, pre-assembled and accurately machined to the correct conical taper as complete rings. The rollers are carried in a built up circular frame held in position by 27 tubular spokes with a central hub revolving round a fixed center pivot. The hub is carried on the center pivot by a heavy spherical roller bearing, and a second similar but larger bearing on the pivot locates the moving part of the mount about the pivot. The arc of travel in azimuth is $\pm$ 250° from true south providing a 140° overlap on the azimuth circle. Located vertically on the fixed center pivot post is a rigid tubular tower structure on top of which the body of the azimuth shaft angle encoder is carried. The rotating disk of this encoder is driven from the rigid concrete roof of the turntable cabin previously mentioned. It is thus a feature of the design that both encoders are mounted with their axes on the relevant axis of rotation of the instrument and are driven from the axes of rotation.

The rotating part of the azimuth mount is fitted round its periphery with 46 teeth which engage with a 5 in. pitch, cranked-link roller driving chain of accuracy 0.015 percent on length and 140 tons breaking load. This form of drive was chosen to avoid the use of large gear wheels or toothed racks while providing greater capacity for resisting transient shocks. The chain is provided with tensioning sprockets on both sides of its free length; tension can be adjusted readily by screwing the sprocket mounting blocks in or out in slides. The driving sprocket is mounted on the vertical output shaft of the final bevel gear box; heavy steel frames set in the concrete floor carry an outrigger bear-

*Husband & Company Provisional Patent No. 12807/61.

ing for the drive sprocket and support the tension sprocket assemblies. The moving part of the aerial, weighing approximately 900 tons, moves silently and smoothly at all speeds, less than 2 hp being required to rotate the aerial at full operational speed in conditions of no wind.

The azimuth final bevel gear box is 8 ft 6 in. high and is preceded by a triple-reduction double-helical unit. The overall reduction ratio from drive motor to aerial is 3000:1 and all couplings are of the oil-filled gear type. The chain has an automatic lubrication system, and phosphor bronze slide supports under the whole of its free length. There is also a combined automatic greasing system for the 108 spherical roller bearings in the taper rollers, the two center pivot bearings, and for the manganese steel track surfaces.

Elevation Mechanical Drive

The bowl is rocked over its 100° arc in elevation by a steel connecting rod attached to a large nut on a 4-start 10 1/2-inch outside diameter vertical screw, 32 ft long over the screwed portion. The nut is split and has adjustment to enable backlash to be eliminated.

The screw is located inside a fabricated steel box and is carried in bearings at its upper and lower ends. The screw box is attached to the revolving part of the concrete mount and the center concrete portal frame at its lower end, and its upper end is attached to a concrete cantilever built out at right angles to the horizontal prestressed concrete beam. The screw is driven at its lower end by a single reduction worm box, preceded by a single-reduction double-helical box; the overall reduction between motor and dish being again 3000:1. The reduction ratio of the screw, nut and connecting rod system itself is 181.5:1. This form of elevation drive avoids the use of large gear wheels or heavy circular racks for the final drive, allows the dish to be supported by a number of bearings along the full length of the supporting structure, eliminates backlash and gives complete rigidity in the highest winds.

Azimuth and Elevation Electrical Drives

The two identical 100 hp dc driving motors for azimuth and elevation are of the traction type with skew slots, fan cooling, and a tachometer generator attached to the non-driving end of the shaft. Each motor has a top speed of 1000 rpm at 480 volts, full load current of 160 amps can be continuously sustained in the stalled condition, and smooth-speed range is 720:1. The couplings between the motors and the first gearboxes also carry brake drums on each of which two solenoid operated brake shoes operate. The azimuth motor shaft is equipped with a manually operated disk brake for parking. Each of the two motors has its own separate Ward Leonard motor-generator set, mounted side by side in a house built at the side of the mount; the same enclosure houses the two azimuth gearboxes and the azimuth drive motor. The Ward Leonard room also contains the ac panel for the two sets and a dc desk for manual control of both aerial motions. One part of the Ward Leonard room has been separated off and houses helium recovery plant and storage dewars. The room is entirely shielded with copper sheeting to all walls, roof and floor and copper gauze over the windows.

The Ward Leonard system and servo-loop are orthodox but the speed range of 720:1 is considerably greater than that normally used in this class of plant. The servo-amplifiers and control gear are located in the main control building approximately 1/4 mile from the motor-generator sets.

Control System

The digital control system is fully transistorized and there is a separate system for each motion. The aerial can be driven from the control desk either manually or under automatic control from a punched tape (Figure 10–12). When under automatic control, motion commences when the tape-start time and actual time coincide. Thereafter, demanded angle information read from the tape is stored, passed to an arithmetic unit,

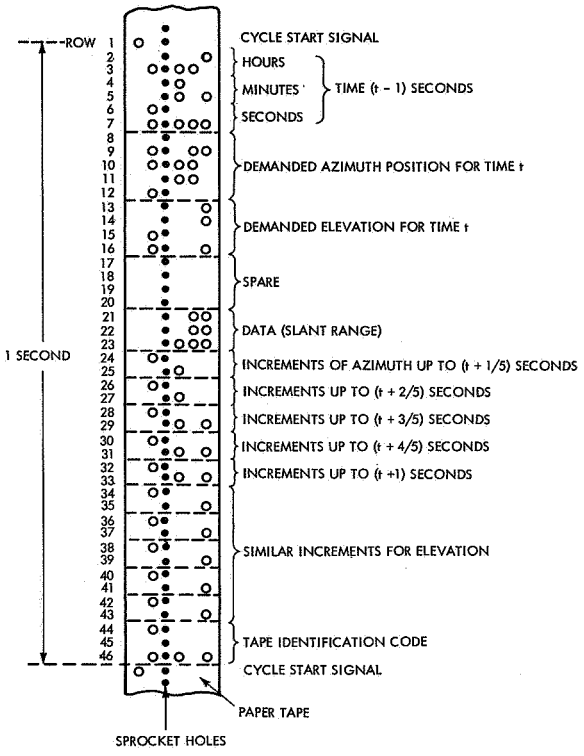


FIGURE 10–12.—A section of control tape.

and then on to the comparator unit, which also receives a statement of the actual angular position from the 16-bit optical shaft angle encoder. The difference between demanded and actual angle is ultimately converted to analog form and fed into the servo-amplifier equipment which responds accordingly. There is also a facility whereby the differential (rate of change) of error is used to eliminate hunting and overshooting by reducing the rate at which the error is reduced as the value of the error moves towards zero.

The aerial control desk (Figure 10–13) carries digital and analog displays of actual position, a digital display of demanded position, and manual speed controls for both motions, together with drive-motor voltage and current meters. When the aerial is under automatic (tape) control the normal speed controls change their function and can be used to apply a positive or negative correction to the motion so that the actual angular position of the aerial is the selected amount in front of or behind the position demanded by the tape. The desk also carries wind-speed and direction instruments, motor start/stop controls and colored-lamp signaling systems indicating the state of all safety interlocks of vital parts of the drive equipment. There is also a digital display of control-clock time and another of the time on the tape corresponding to the displayed demanded angles. If synchronism between clock and tape time is lost, the aerial stops at the last demanded position. The control desk also carries signal-lamp systems indicating the condition of the drive brakes, drive motor fans and lubrication systems on both motions and also red warning lights indicating that the limit of travel has been reached in either direction on either motion.

In addition to lighting the red signal lamp, operation of a limit switch at the end of the arc of travel also switches off the driving power on that motion and so stops the motion. To restart, a button in a special locked cabinet must be operated, when the aerial will automatically move out a certain distance from the limit switch and then stop, after which normal driving procedure may be resumed.

Calibration and Testing

Profile measurements on the completed dish were made with slip gauges against two accurate templates, one for the inner area and a second for the outer zone. About 1000 measurements were plotted on probability graph paper and showed 99 percent of the measurements within the tolerances specified with random distribution of error.

Before the dish was moved from its position as built with axis pointing to the zenith, an optical telescope was fitted in one of the cabins behind the dish with its axis truly vertical within 0.2 minutes. This then became the 90° reference condition for the elevation encoder. With the dish set to 60°, 45° and 0° in turn by the encoder, theodolite checks were made of the angle of the peripheral



FIGURE 10–13.—Antenna control desk.

plane, and agreement obtained to ± 15 seconds.

The azimuth zero on a true south bearing, and checks of the azimuth setting accuracy were obtained by viewing known points at 5 to 15 miles range through the telescope fitted to the dish. The true bearings of those points were computed by the Ordnance Survey Department to an accuracy better than one second.

First indications that the finished aerial would point accurately were obtained from successive transit observations through the optical telescope of Alpha Ursa Major. Smooth curves of the azimuth and elevation angles against time as this star moved across the sky, showed that under calm conditions a tracking accuracy of the order of one minute could be expected.

When radio equipment became available for testing the aerial, the horizontal radiation diagram was obtained by measuring the incoming signal strength from a 4000-Mc transmission from a test site at Leswidden some 21 miles from Goonhilly. The measured beamwidth was found to be 13 minutes, compared with a theoretical value of 12 minutes, and the first side lobes were correctly spaced on either side of the main beam.

Conclusions

Work was commenced on site on 1 June 1961, and the aerial had been tested and provisionally calibrated so that it was in full

operation on 10 July 1962. In the first eighteen months of its working life the aerial has worked satisfactorily with little attention. The British concept of a stiff dish on a sturdy mount without a radome has yielded an aerial of high performance at relatively low cost.

Acknowledgments

Special mention should be made of the excellent cooperation between the prime contractors: Cleveland Bridge and Engineering Co., Ltd., for foundations and reinforced concrete; Markham and Co., Ltd., for turntable and mechanical drives; The Brush Electrical Engineering Co., Ltd., for electric drives and control gear; John Brown Land Boilers, Ltd., for the dish structure; and N. G. Bailey and Co., Ltd., for cabling.

The aerial was designed and construction supervised by Husband and Company, Consulting Engineers.

The permission of the Engineer-in-Chief of the Post Office to use information contained in the paper is gratefully acknowledged.

AUTHORS. *This chapter from the United Kingdom was contributed by the General Post Office, London, England. The foregoing section on the Goonhilly 85 Ft. Steerable Dish Aerial was authored by* C. N. KINGTON *of Husband & Co., England and* H. E. PEARSON *of the GPO.*

COMPUTING AND DATA TRANSMISSION FOR THE PREDICTION STEERING OF THE GOONHILLY SATELLITE-COMMUNICATION AERIAL

Introduction

During a satellite pass, the aerial must be steered so that its axis points continuously, and with high accuracy, in the direction of the satellite. Of the various possible methods of achieving this result, that based on prediction of satellite position has been adopted for the first transatlantic communication experiments using the Telstar and Relay satellites. The process by which orbital predictions originating in the U.S.A. are converted to substantially continuous real-time azimuth and elevation pointing instructions at Goonhilly is described herein.

Planning Considerations

The following considerations influenced the planning of the system. On the one hand, data on the observed position of the satellite at known times would be received at the Goddard Space Flight Center, U.S.A. from various sources, including the world-wide Minitrack network of tracking stations, and would be processed there to derive the basic parameters of the satellite orbit, from which the future position of the satellite could be predicted. On the other hand, the need at Goonhilly would be to present to the inputs of the azimuth and elevation control systems, 50 times per second throughout a satellite pass, statements of the azimuth and elevation required at each instant (the "demanded" azimuth and elevation) in digital form to the nearest 2^{-16} revolution (0.33 minute of arc).

The passage from orbital elements known in advance at GSFC to angular demands in real-time at Goonhilly would involve considerable computation and, at some stage in the process, transmission of data across the Atlantic. The computation could be begun in advance at GSFC, continued in advance at Goonhilly, and completed in real-time at Goonhilly; the division of the work between these three stages was a matter for practical compromise. Advance computation at GSFC would reduce the computing load at Goonhilly (and at any other stations that might use similar data) but would increase the volume of data to be transmitted. At Goonhilly, the experimental nature of the project would make it appropriate to carry out as much of the remaining computation as possible in advance; for this purpose it would be possible to employ a general-purpose computer of well-established design, which could

also be used part-time for other work such as the analysis of records. The results of the advance computations could be checked before the time of the satellite pass. However, the need for subsequent data storage (e.g., on punched paper tape) would set a limit here, and it would be convenient to leave some simple computing to be carried out in real-time by special-purpose apparatus in the aerial control equipment.

Description of the Process

The considerations previously mentioned have led to the following arrangements: at GSFC the satellite position is predicted for intervals of one minute throughout each pass, and is expressed in topocentric Cartesian coordinates, i.e., in a rectangular coordinate system with axes in the directions east, north and vertical and origin at the center of motion of the Goonhilly aerial. Predictions in this form are transmitted to Goonhilly over a transatlantic telegraph circuit, and the receiving teleprinter produces simultaneously a page print and a perforated tape (the "Predictions Tape"). The data for each minute occupy one line of the page print and are accompanied by a "sum of digits" check. The data message includes a statement of the time to which the first prediction for each pass refers, and is sent in a standard format covering not only features visible on the page print but also the incidence of all functional characters (carriage return, shifts, etc.) that will be punched on the predictions tape. The time taken in transmission is about six seconds for each minute of a satellite pass. When the orbital elements for a particular satellite are well established, predictions can be sent once a week, to cover all the time during the ensuing week that the satellite will be above the Goonhilly horizon.

At Goonhilly, advance computations are carried out by a small general-purpose computer. The predictions tape is used directly at data input to the computer, and the first operation is to check the validity of the whole data message (normally covering many passes), applying the "sum of digits" check and examining the tape for errors in format. This operation is quite quick (0.13 seconds for each minute of pass) and is preferably concurrent with the reception of the data; if an error is detected, all the data for the pass affected are transmitted again.

For those parts of selected passes that are to be used for communication experiments, a further run on the computer, with the predictions tape as data input, calculates and prints azimuth, elevation and range for one-minute intervals. This run takes 1.2 seconds of computer time for each minute of pass. The print is useful to show the general nature of each pass. Specifically, it enables the operator to make a decision that is needed because the aerial is not designed to rotate continuously in azimuth, but has a range of movement limited to 500 degrees, so that over a range of 140 degrees any direction has two alternative numerical values; therefore two sets of azimuth values are printed and if one set shows a discontinuity the other must be selected. This decision accompanies the input data to the computer for the next operation.

The next stage represents the main computing operation undertaken at Goonhilly, and comprises the preparation by the computer of a punched paper tape—the "Control Tape"—bearing detailed azimuth and elevation data for the passes of interest. The predictions tape again constitutes the data input to the computer. Working in the rectangular coordinate system, fifth-order interpolation is used to derive values for one-second intervals from the one-minute data received from GSFC. Azimuth and elevation are then deduced for the one-second intervals. Finally, second-order interpolation is used to obtain the full details required on the control tape (see page 692), and the tape is punched.

The computer program is so arranged that corrections whose values are predictable can be applied to the calculated quantities in the course of this operation. An obvious need is for a correction in elevation to take account of the effect of atmospheric refraction; this correction is based on prior knowledge and

has been included from the outset. If operational experience brings to light any systematic departure of the electrical axis of the aerial from its mechanical axis* suitable corrections can be added later.

Certain calculations not concerned with aerial steering are included at this stage, to avoid the need for a separate computing operation; these are:

1. Calculation of slant range. The value is punched on the control tape for one-second intervals, so that a real-time display can be given, or automatic control of transmitter power can be effected.

2. Calculation of Doppler shift to facilitate the adjustment of the radio receiver; this information is required only in printed form.

Concurrently with the punching of the control tape the computer prints, for one-minute intervals, all the information needed by the operating staff during a pass, namely demanded azimuth and elevation, slant range, and Doppler shift.

The computations described, and the punching of the control tape, occupy 80 seconds for each minute of a pass; in other words, this work takes 1.3 times real-time.

When the control tape has been punched, it is checked in the computer; although it is impossible to guarantee that the aerial will never receive erroneous steering instructions, a check at this stage is desirable because incorrect tape punching is the most likely source of error. Checking based on repetition of the computations would take too long, and checking against output data stored in the computer would make excessive demands on storage. The check therefore takes the form of an examination of the tape for plausibility and self-consistency, as described on page 693. Checking takes 15 seconds for each minute of a pass.

To complete the description, it is necessary to mention the operations carried out in real-time in the aerial control equipment. To economize in paper tape, and equally important, tape-punching time, the azimuth and elevation information punched is largely in the form of increments of angles rather than complete angles (see page 692). In the aerial equipment, the control tape that has been prepared in advance as previously described is read in real-time, and the data are stored for periods of the order of one second. The equipment includes arithmetic units which add increments to accumulated values so as to make available, every 1/50 second, the full values of demanded azimuth and elevation.

Some Features of Computer Programing

The computer at Goonhilly is the version of the National-Elliott 803 with 4096 words of storage, two tape readers, and two tape punches. The double input and output is used for example when punching a control tape: the main data tape is the predictions tape, which is read by one reader; the other reader reads a data tape which specifies, among other things, which pass and which part of the pass is to be selected from the predictions tape. On the output side, one punch produces the control tape and the other punches a tape for print-out of operating data.

The 4096 words of storage are available for either instructions or numbers and there is complete freedom of choice between compact, but possibly slow, programming and fast, but possibly voluminous, programming; generally speaking, the latter has been chosen. The control tape punching program, for example, uses about 2000 words of storage.

An example of the choice of a method giving speed at the expense of fairly lavish storage is the calculation of the refraction correction for elevation. This could have been achieved by calculating some function, say a polynominal, which approximates the exact function; this would have involved storing, say, half a dozen constants. Instead, a critical table of 213 constants is stored, which allows the correction to be obtained much more quickly.

*In this context, the term "mechanical axis" means the direction defined by the readings of the shaft-angle encoders that measure the "actual" position of the aerial.

One of the main steps in the control tape calculation is interpolation to derive values for one-second intervals from those for one-minute intervals as given by the Predictions Tape. Six consecutive one-minute values of any particular variable define a fifth-degree polynominal from which one-second values are calculated for the interval between the third and the fourth of the six one-minute values. Of the many methods of evaluating this polynomial, building up from differences is the fastest since it uses the relatively fast operation of addition, the relatively slow operation of multiplication being used only for the calculation of leading differences. The operation can sometimes be speeded up even more by replacing the exact fifth-degree polynomial by an approximating fourth or even third-degree polynomial, depending on the smoothness of the original data as indicated by the maximum value of the fifth or fourth difference respectively. With Telstar, fourth differences are small enough to allow a third-degree polynomial to be used.

Although the current programs are reasonably satisfactory, they are not necessarily the best. For example, the control tape punching program requires the calculation of arctan and cosine functions. Standard Elliott library sub-routines have been used for these which calculate to the full precision of the computer word, namely 38 bits. Since azimuth and elevation are required to a precision of only 16 bits, these sub-routines could be replaced by less precise, and consequently faster, versions.

Details of Control Tape

The ultimate requirement is to present to the inputs of the azimuth and elevation control systems of the aerial, in real-time 50 times per second, a complete statement of the demanded azimuth and elevation in digital form to the nearest 2^{-16} revolution. This represents 17 bits for azimuth (the range of azimuth motion being 500 degrees = 1.39 revolution) and 15 bits for elevation (100 degrees = 0.28 revolution). It is impractical to store all these data on punched paper tape, and incremental operation must be adopted.

Suppose that, to describe the demanded azimuth (or elevation), a single incremental value is specified and that this is added to an accumulated number every 1/50 second. The result, assuming that the 1/50 second discontinuities are smoothed, will be a quantity increasing linearly with time, representing a demand for a constant angular velocity. A real demand, in which the velocity will not in general be constant, can be approximated by changing the value of the increment from time to time; the real curve of angular position as a function of time will then be approximated by a series of chords. The process is analogous to linear interpolation between given values in a mathematical table, and it can be shown that the maximum error that could be incurred (i.e., the maximum possible departure of the chord from the true curve) is given by:

where

e = $1/8\ a\ T^2$
T = time-interval over which a constant increment is added repeatedly
a = maximum acceleration during this interval
e = upper limit to error during this interval

The solution adopted is to prescribe increments on the tape for intervals of 1/5 second, so that any one increment is added 10 times. The formula shows that the error will not exceed 0.4 minute of arc at the maximum acceleration assumed in the structural design of the aerial (1.33 degrees per second per second).

Such increments of azimuth and elevation constitute the main content of the control tape. However, a complete specification of demanded azimuth and elevation is essential at the beginning of an automatic run, and is very desirable at intervals afterwards, so that any casual error may not be perpetuated. The complete demanded azimuth and elevation are therefore punched on the tape for intervals of one second. This has the desirable result that the concept of a specific

starting condition is avoided; automatic control can begin at any desired time (within about one second) during the period for which a control tape has been prepared. The scheme lends itself to a one-second cycle in the punching of the control tape and the operation of the digital part of the aerial control equipment.

A 5-track tape is employed; four of the tracks are used for numerical data, the fifth being reserved for a signal indicating the beginning of each one-second cycle. The complete punching scheme for one cycle is shown in Table 10–1.

TABLE 10–1.—*Punching of Control Tape*

Item	Number of rows
Cycle-start signal	1
Time (hr, min, sec)	6
Demanded azimuth	5
Demanded elevation	4
Slant range	3
Five increments of azimuth	10
Five increments of elevation	10
Tape code	3

Checking of Control Tape

The program which checks a control tape determines that:

1. Cycle-start signals appear as prescribed.

2. Time, azimuth, elevation, and tape code are within appropriate limits; e.g., the hours in a time must be less than 24, and the minutes and seconds less than 60. For azimuth and elevation this check is applied not only to the completely punched values but also to those that will subsequently be formed in the aerial control system by adding the increments.

3. Time, azimuth, and elevation are continuous: i.e.,

(a) each time is one second later than the previous time

(b) each azimuth (or elevation) agrees with that formed by summing the azimuth (or elevation) value and increments of the previous second, due allowance being made for the effects of rounding-off in calculation.

Acknowledgments

The National Aeronautics and Space Administration, U.S.A., evolved the scheme for the telegraphic transmission of data, and has supplied the remarkably accurate predictions on which the steering of the Goonhilly aerial has been based.

AUTHORS. *This chapter from the United Kingdom was contributed by the General Post Office, London, England. The foregoing section on Computing and Data Transmission for the Prediction Steering of the Goonhilly Satellite-Communication Aerial was authorized by* E. C. H. SEAMAN *and* W. E. THOMSON *of the GPO.*

BEAM-SWINGING FACILITIES FOR THE GOONHILLY SATELLITE-COMMUNICATION AERIAL

Introduction

The mode of satellite tracking adopted at the Goonhilly earth station is to steer the aerial primarily by means of predicted data computed from the satellite orbital parameters and to superimpose, during the passage of the satellite, corrections to remove any prediction errors or aberrations due the transmission path. Predictions have proved to be highly accurate for satellites having a high mass to projected area ratio orbiting at altitudes of which air drag is very small; hence the corrections are small and infrequent.

System Design

Aberrations in the predicted steering data are likely to be greatest during the acquisition phase when the aerial elevation is near zero and when, in consequence, tropospheric-ray bending is greatest. It was assessed initially that a beam swing of 1° in all direc-

tions from the boresight axis would adequately meet the most extreme condition, i.e., at the time of the earliest satellite passes and prior to refinement of the orbital parameters. Provision was therefore made in the original design for a swing of 1° but experience proved this to be in excess of requirement and it was subsequently reduced to 1/2°. The corresponding shift in the position of the feed unit in the focal plane of an 85-ft focal-plane paraboloid is 3 in.

A beam deviation of 1/2° is equivalent to 2 1/2 beamwidths (3 db) at the frequency, 4080 Mc, at which tracking of the Telstar and Relay satellites is performed. At this deviation a degradation in aerial gain of about 2 db is incurred and some beam distortion is present in the form of a coma lobe on the boresight-axis side of the beam. It was envisaged, therefore, that corrections to the predicted steering data would be needed, at least in the initial phase of a satellite pass, to ensure that large beam offsets were removed.

The feed-shift mechanism at the aerial focus, by which the beam is offset from the axis, is controlled through a hydro-electric servo system from a console in a control room about 1/4 mile from the aerial. This form of control has the advantages, as compared with an all-electric system, of lower weight at the focus, a safer stalling condition and the removal of most of the moving parts requiring maintenance to positions where they are more easily reached.

After approximate acquisition, the deviations of the satellite from the predicted course are followed by means of a conventional radar mode of tracking. No satisfactory adaptation of the static-split feed (monopulse) system is obvious when diplexed signals with circular polarization are utilized in a focal-plane dish. A conical-scan feed system is therefore used. The requirements, however, are notably different from those common to radar applications in which pulsed signals are generally received from a target whose course is likely to be erratic and evasive. In contrast, the course of a satellite is closely predictable and smooth and the target is a cw beacon on the satellite itself. A slow-speed scan in which the beam rotates about a point 1 db or less from the peak is therefore adequate. A slow speed is essential also to minimize the centrifugal forces encountered in spinning a heavy diplexed feed. The scanning speed is adjustable to avoid synchronism or harmonic relationship with the ripples in the aerial-radiation pattern of a spin-stabilized satellite.

The optimum offset of the rotating beam about the boresight axis depends on the sensitivity of the display equipment and on the allowable loss from the peak gain of the aerial. The latter is of particular importance when, as in Project Telstar, the ground transmit frequency in the diplexed signal is higher than the receive frequency. The transmit beam is then narrower and, for a given offset, introduces a greater loss into the transmit path than in the receive path. For the aperture illumination employed, Table 10–2 shows the approximate losses in the transmit and receive paths as the offset is varied. The transmitter frequency for Telstar is nearly 6390 Mc and that for Relay 1725 Mc. The beacon frequency is the same for both projects, 4080 Mc.

TABLE 10–2.—*Effect of Feed Offset in an 85-ft Focal-Plane Paraboloid*

Beam offset deg	Feed offset in.	Beacon signal loss db	Transmit loss	
			Telstar db	Relay db
0.061	0.36	1.0	2.5	0.25
0.041	0.24	0.5	1.25	0.12
0.027	0.16	0.25	0.62	0.06

The system was provided initially with a conical-scan radius for 1 db loss in the beacon signal. It was found, however, that the sensitivity of the equipment was sufficient to allow the radius to be reduced to the 1/4 db point. The transmit loss and signal modulation at the conical-scan frequency were reduced by this means.

Description of Equipment

Beam-Swinging Mechanism

The general arrangement of the beam-swinging mechanism is shown in Figure 10–14. The tube marked "Aerial Feed Unit" points towards the apex of the dish and in the central position its aperture is at the focus. The frame, shown as cut away, is mounted on a platform situated about 2 feet outside the focal plane. Two motions of the feed are provided; one is the major beam-swing motion in which the feed aperture can move to any position within a circle originally of 6 in. radius but later limited to 3 in.; the other is the conical-scan motion in which the feed moves circularly with a radius (in the final modification) of 0.16 in. about an axis fixed by the beam-swing motion. The radius of the conical-scan motion is modified simply by changing an eccentric in the motor drive.

The beam-swing motion pivots about gimbals at the rear and is effected by two hydraulic pistons mounted orthogonally in the plane of the main frame. The gimbals have an internal clearance sufficient to allow the waveguide components to be withdrawn through them, without dismantling the main structure. The rear section of the waveguide is flexible to allow movement of the feed relative to the external fixed feeder. The hydraulic pistons are controlled by servo-operated oil valves fed at 800 lb/in.^{2} by a pipeline from a hydraulic pump mounted on the roof of the cabin on the azimuth turntable of the aerial.

The gimbals for the conical-scan motion are placed midway on the feed support tube, the far end of which is given a circular motion by a motor mounted outside the beam-swing gimbals. The central disposition of the conical-scan gimbals results in this part of

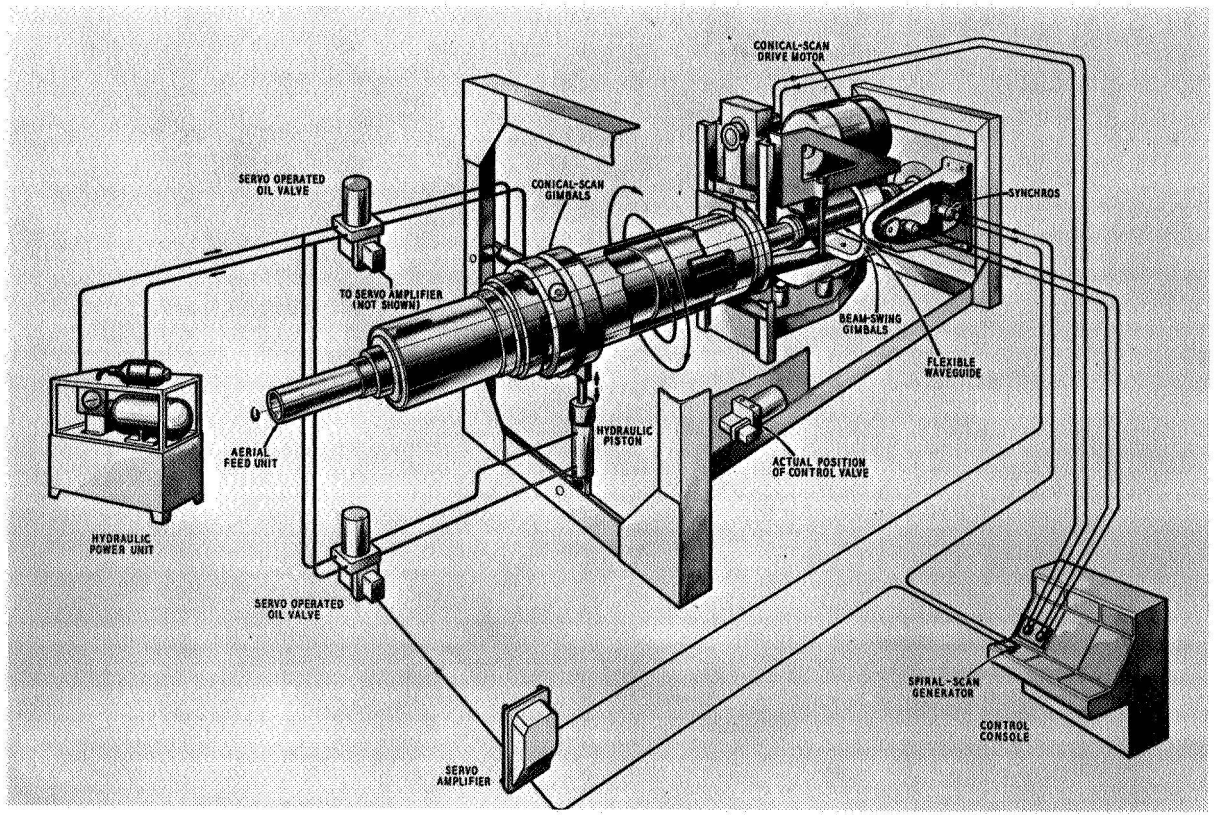


FIGURE 10–14.—Schematic of waveguide feed system.

the mechanism being sensibly in mechanical balance. Counterbalance collars are placed on the support tube fore and aft of the gimbals to balance completely particular feed assemblies. The conical-scan drive motor is fed from a small dc control set, originally of the Ward-Leonard type but which is shortly to be changed to the silicon-controlled-rectifier type to minimize space, weight, and the need for maintenance. The control set is mounted in one of the cabins behind the dish and allows the scanning speed to be regulated between 1/2 and 5 cps by remote control.

The whole assembly is designed for minimum maintenance and to withstand the weather conditions encountered at Goonhilly Downs. The weight of the mechanism, exclusive of the external waveguide feeders, is about 900 lb.

Conical-Scan Control Display

A cathode-ray tube display is associated with the conical-scan system to indicate the divergence of the satellite from the scanning axis in direction and angular magnitude up to 8 minutes. When the direction of the incoming beacon is off the axis of the conical scan by a small amount, the output of the beacon receiver is modulated at the scan frequency. The depth of modulation increases as the deviation off axis increases and determines the length of a radial trace on the CRT. The direction in which the satellite is off axis determines the phase of the modulation and hence the angular position of the trace. Erroneous indications of direction due to the modulation of the beacon by the satellite spin are readily eliminated by adjusting the conical-scan speed to be nonsynchronous with the spin-stabilization speed. A block diagram of the equipment is shown in Figure 10–15.

A 50 cps magslip link relays the rotary motion of the feed to the control console where a resolver is driven to provide the phase reference for the incoming beacon signal. The 2-phase output of the resolver is fed directly to the magnetic deflection coils of the CRT and the input of the resolver is derived from the beacon signal in the following way. The modulated dc output of the beacon receiver is detected, amplified and fed to a modulator which is so biased that only the positive tips of the input ac wave

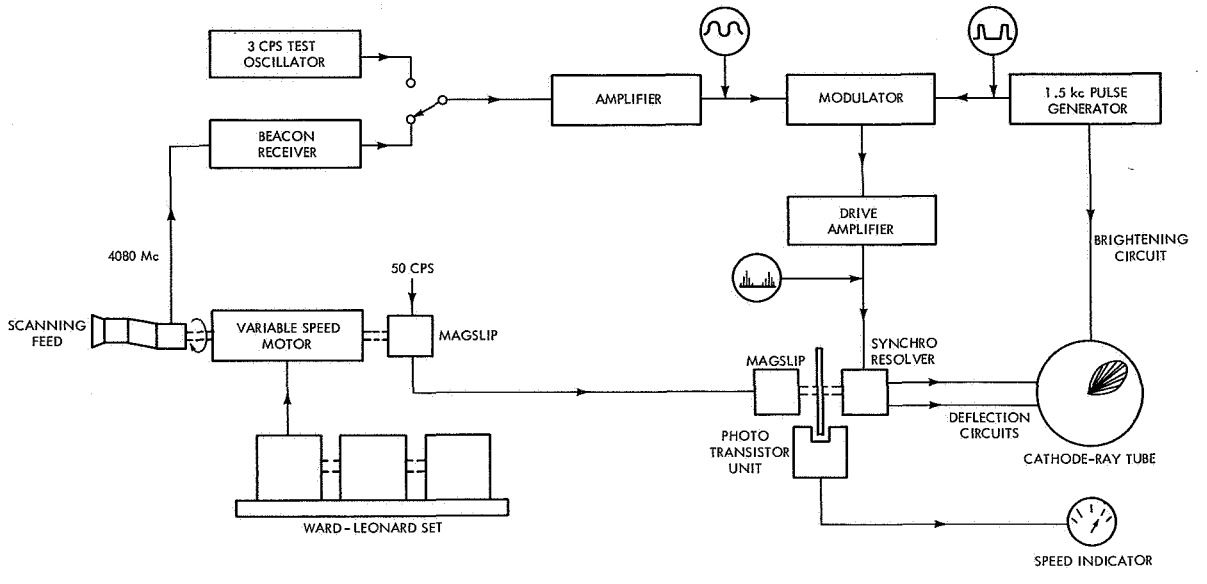


FIGURE 10–15.—Conical scan control and display.

produce an output. The carrier source to the modulator is a 1.5 kc pulse generator in which the pulse width is small. The pulsed output of the modulator is fed to the input of the synchro resolver through a drive amplifier. The necessity for pulsed modulation is twofold; firstly, adequate transmission through the resolver cannot be obtained at the low conical-scan frequency in use, so translation to a higher frequency is necessary; secondly, it affords a simple means of deriving a radial trace on the CRT without dc restoration when the input is alternating current. The tips of the forward pulses are brightened to improve the presentation and to blank the small backward pulses. The result is a lobe as shown in the sketch in Figure 10–15.

A 3 cps test oscillator is provided in the unit to simulate the output of the beacon receiver when the equipment is non-operational. The magslip-resolver link is also used to provide an indication of the conical-scan speed. A perforated disk mounted on the coupling between the magslip and the resolver modulates a light beam focused on a photo-transistor. The output of the transistor is measured on a meter in terms of the conical-scan speed.

Beam-Position Control and Display

The beam-positioning equipment is shown diagrammatically in Figure 10–16. The angular offset of the satellite relative to the aerial boresight axis is displayed on two meters calibrated respectively in terms of angular deviation in azimuth and elevation up to 30 minutes on each side of the central position. The meter display is derived from aerial feed-position indicators (linear transformers) mounted orthogonally on the beam-swing gimbals. The outputs of the transformers are rectified and fed to the relevant center-zero meter.

Indication that the satellite is acquired is shown on 3 lamps triggered at predeter-

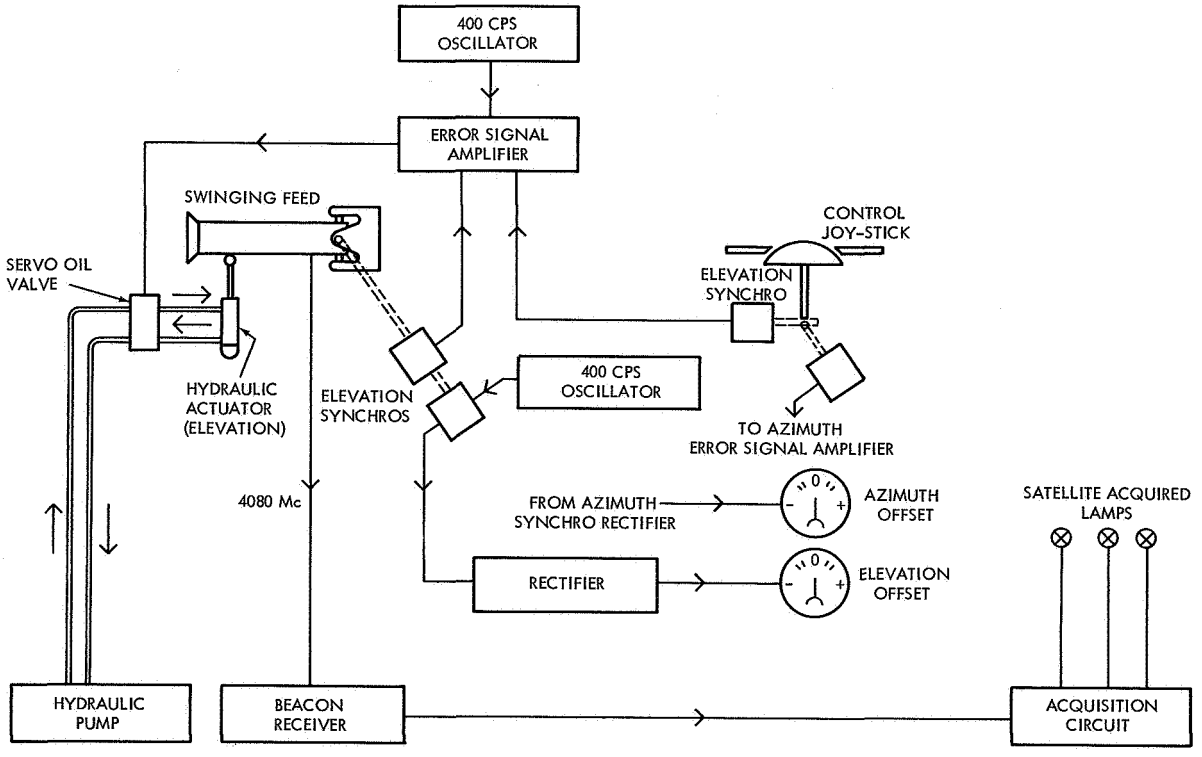


FIGURE 10–16.—Beam position control and display.

mined stages of acquisition by the depth of modulation imposed on the beacon signal by the conically scanned beam. Indication of complete acquisition is extended to other lamps at points in the earth station where the information is required.

Control Console

A two-position console, part of a suite of six used for experiment control, houses the conical-scan and beam-position presentation units. A photograph of the two positions is shown in Figure 10–17. The conical-scan display CRT is under the hood on the left-hand position. Test facilities for the conical-scan unit, the scan speed indicator and beacon output meter are placed immediately above the hood. The aerial position is displayed digitally on the top panel. The hand control for positioning the aerial beam is on the desk below the CRT. The original version of this control incorporated a spiral-scan generator for wide-angle search but the high accuracy of the predicted data supplied by the GSFC made the provision superfluous and it has been replaced by a "finger-tip" ball-type control.

The righthand bay of the console houses the beam-position unit and the satellite acquisition circuits. The digital switches, by which the corrections to be applied to the predicted course of the aerial are signalled to the aerial controller, are situated at the bottom lefthand corner of the panel.

The operational procedure is:

1. The functioning of the presentation

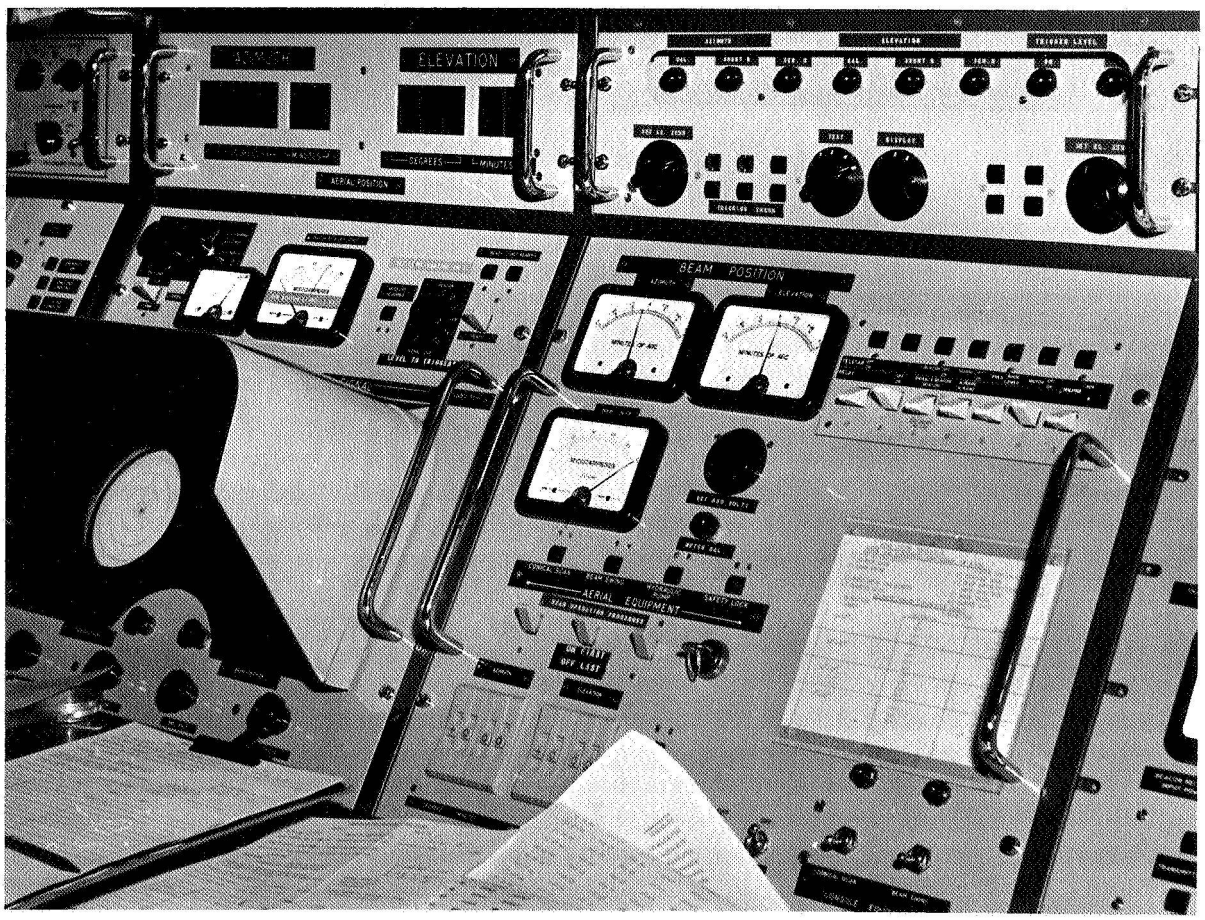


FIGURE 10–17.—Beam swinging console.

units and the scanning mechanism is checked before each satellite pass in conjunction with the Leswidden test station about 22 miles away.

2. The conical-scan motion is applied at the commencement of the pass and the radial display reveals any offset of the satellite from the aerial beam.

3. The hand control is used to steer the beam exactly on to the course of the satellite.

4. If the divergence of the beam from the boresight axis of the aerial, as displayed on the beam-position meters, is more than about 4 minutes (one-third beamwidth) then azimuth and/or elevation corrections to the predicted course of the aerial are demanded of the aerial controller to restore the beam to its on-axis position. As the corrections take effect the hand control is adjusted to follow the satellite to its on-axis bearing. This process is repeated as required during the period of the pass.

Operational Experience and Conclusions

Experience in Project Telstar showed that the tracking facilities, as originally provided with an extensive beam-swing capability and automatic spiral-scan facility, were more than adequate. These features have now been modified. It had been expected that acquisition would not be possible until the aerial elevation was about 5° to 7 1/2° but, in a very large proportion of the passes the satellite has been sighted while the aerial was waiting at zero elevation, i.e., when the satellite was yet below the horizon. Only very occasionally has acquisition been delayed until the elevation has reached 2°. This fact, and the accuracy of subsequent tracking, reflects very favorably the high accuracy of the predicted data obtained from the Goddard Space Flight Center. After superimposing standard corrections on the predicted steering data, to account for tropospheric refraction at low elevations, the remaining corrections necessary during the period of a pass have generally totalled no more than 5 minutes. Corrections in azimuth have been a littel larger, totalling up to 10 minutes. Adjustments in tracking by the beam-swing equipment and by over-riding the predicted data have, so far, been applied manually. Equipment to track the beam-swinging mechanism automatically has now been developed; further development to provide auto-track facilities for correcting the predicted data from the conical-scan equipment is in hand.

AUTHORS. *This chapter from the United Kingdom was contributed by the General Post Office, London, England. The foregoing section on Beam-Swinging Facilities for the Goonhilly Satellite - Communication Aerial was authored by* C. F. DAVIDSON *and* W. A. RAWLINSON *of the GPO.*

CIRCULARLY-POLARIZED DIPLEXER FOR THE GOONHILLY SATELLITE-COMMUNICATION AERIAL

Introduction

The diplexer described transmits some 4 to 5 kilowatts of microwave power and simultaneously receives a signal of the order of a micro-microwatt from a communication satellite, when used in conjunction with the earth-station aerial at Goonhilly.

The earth-station transmitter and receiver frequencies are 6.39 and 4.17 Gc respectively, the sense of polarization of the transmit signal into the dish aerial being lefthanded circularly polarized and that of the received signal from the dish aerial being right-handed. Thus a broadband reciprocal polarizer is required in addition to the diplexer. The details of the diplexer and the broadband polarizer, which constitute one integral unit, Figure 10–18, are discussed below.

The Diplexer

The transmitter power is launched in the TE_{11} mode in 2-inch circular guide through a linear taper from a rectangular waveguide (WG14). With the TE_{11} mode, separate regions of maximum and minimum power density are produced at 90° intervals around

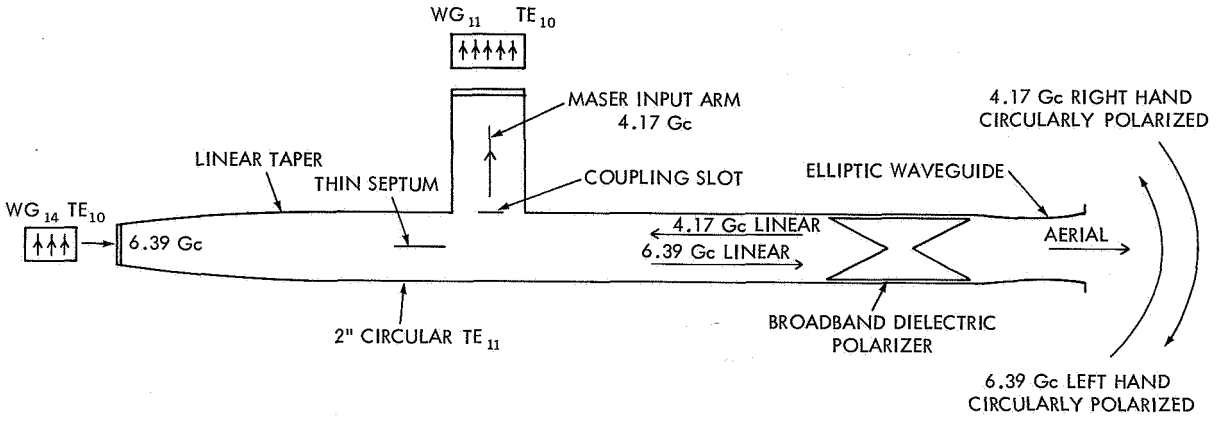


FIGURE 10–18.—Diplexer assembly.

the periphery of the circular guide. If a region of minimum power density due to the transmitted signal is chosen, the received signal may be launched so that its plane of polarization is transverse to that of the transmitted signal in this region. This can be achieved by suitable orientation of the broadband polarizer axis in relation to the axis of the transmit field electric vector. Under these circumstances the minimum coupling region due to the transmit field is the maximum coupling region due to received field, and the transmit electric vector is orthogonal to the received field electric vector.

If a narrow slot is cut in this region of the circular guide, it will be non-radiating so far as the transmit field is concerned but will be excited by the received field, since the slot is transverse to the received field electric vector. The coupling slot is common to the round guide and the transverse plane of the rectangular waveguide (WG11). The slot will not couple the whole of the received energy to the branched rectangular waveguide, but if a thin polished metallic septum is placed in the circular guide so that the received field electric vector is co-planar with the septum, then the entire received energy will be reflected and coupled to the rectangular waveguide. The field configurations and a cutaway view of the diplexer are shown in Figure 10–19.

Considering the diplexer as a third-order waveguide junction Figure 10–19, it is noted that there is a plane of symmetry across the terminals of arm 3. If the septum is placed at appropriate distance from the terminal plane of this arm, then the maser input arm (i.e., the waveguide 11 arm) and the aerial arm will behave as a perfect transmission line provided that the impedance in the branched guide is suitably adjusted in rela-

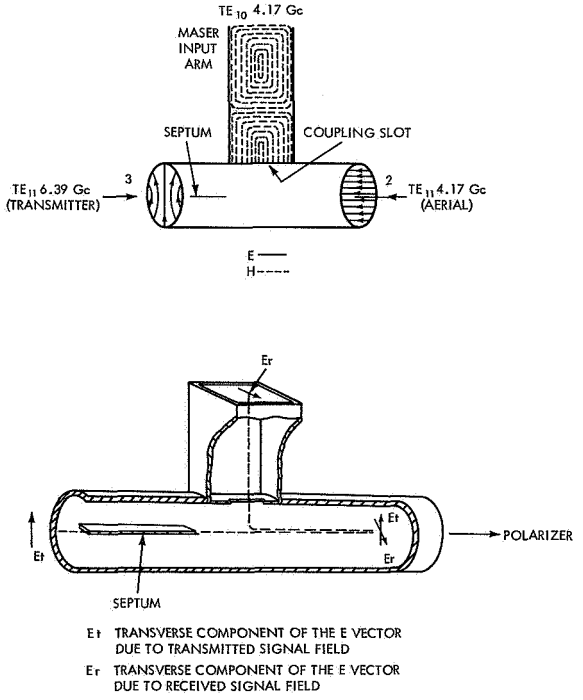
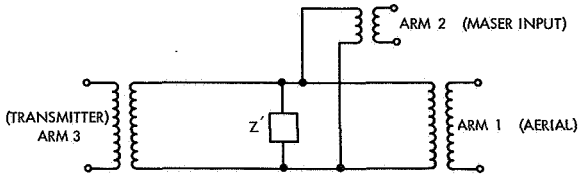


FIGURE 10–19.—Field configuration of the orthogonal TE_{11} modes and cutaway view of diplexer.

tion to the slot impedance Z, as shown in the transformer representation of the diplexer, Figure 10–20.



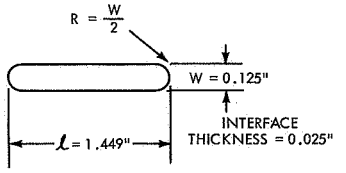


FIGURE 10–20.—Transformer representation of the diplexer and dimension of the coupling slot.

The coupling between the aerial arm and maser input arm is achieved through a narrow rounded slot centered in the transverse plane of the rectangular waveguide 11. The interface thickness between the round and the rectangular waveguide is extremely small. The effect of this slot on the fundamental mode of a waveguide may be computed from an equivalent circuit in which the diaphragm is represented by a two terminal impedance shunted across a transmission line which is assumed to carry a fundamental mode of the waveguide. For all practical purposes the reactance function of such a slot is given by the expression:

$$X = \frac{4\pi MZo}{ab\,\lambda_g} \qquad (10.1)$$

where M is the magnetic polarizability of the slot, Zo is the characteristic impedance of the waveguide, a and b are the width and the height of the guide, λ_g is guide wavelength.

The approximate value of the magnetic polarizability is

$$M = \frac{\pi}{16}\ell\, w^2 \qquad (10.2)$$

where ℓ is the length of the slot and w is the width of the slot.

According to Slater* the approximate resonant length of a thin slot centered on the transverse plane of the rectangular waveguide is given by the expression

$$\ell = \frac{\lambda_o}{2}\sqrt{1 + \frac{2aw^2}{b\,\lambda_g}} \qquad (10.3)$$

where λ_o is the free space wavelength. For a rounded slot having w/ℓ less than 0.11, equation (10.3) can be further simplified to

$$\ell = \frac{\lambda_o}{2} + 0.273w \qquad (10.4)$$

This empirical relationship agrees well with the experimental measurements and the slot is found to be resonant within the desired frequency range.

Experimental Results

From Equation (10.4), the following data are obtained for the slot shown in Figure 10–20.

For a center-frequency of 4170 Mc,

Length of the slot ℓ... $= 1.449'' \pm 0.003''$

Width of the slot w... $= 0.125'' \pm 0.003''$

Wall thickness between the rectangular and round waveguide... $= 0.025'' \pm 0.001''$.

Figure 10–21 shows the insertion loss and the VSWR between the aerial and maser input arm as well as the discrimination between the transmit and maser input arm. The discrimination achieved over the transmit frequency band exceeds 50 db.

The Broadband Polarizer

The principles of the broadband polarizing device may be best understood by considering the characteristics of a circularly polarized wave. Consider two linearly polarized waves, propagating in a positive Z di-

*J. C. Slater, "Microwave Transmission," 1942, pp 185–187, McGraw-Hill Book Co., Inc., New York.

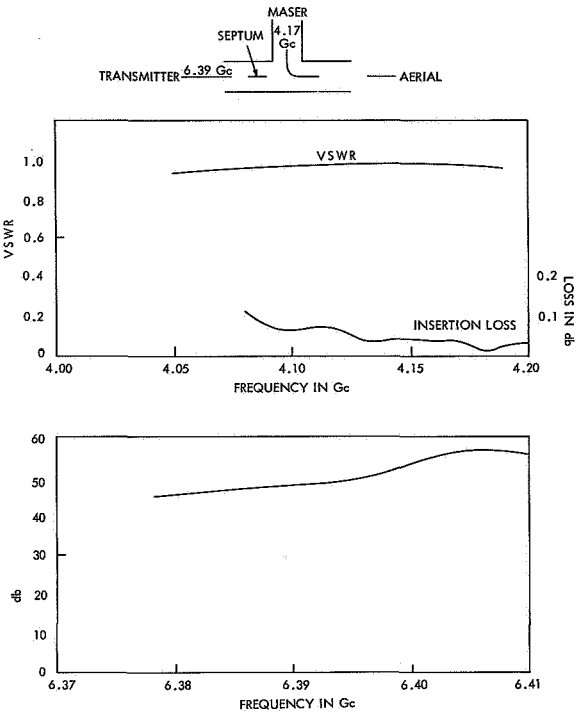


FIGURE 10–21.—Insertion loss between aerial and maser input arm and discrimination between transmit and maser input arm.

rection in space quadrature as shown in Figure 10–22, and described by

$$E_1 = E_0 \sin(\omega t - \beta Z),$$
$$E_2 = \gamma E_0 \sin(\omega t - \beta Z + \theta) \qquad (10.5)$$

where γ = constant; β = phase constant = $2\pi/\gamma_g$.

If one considers $\theta = \pi/2$ at a plane $Z = 0$, then

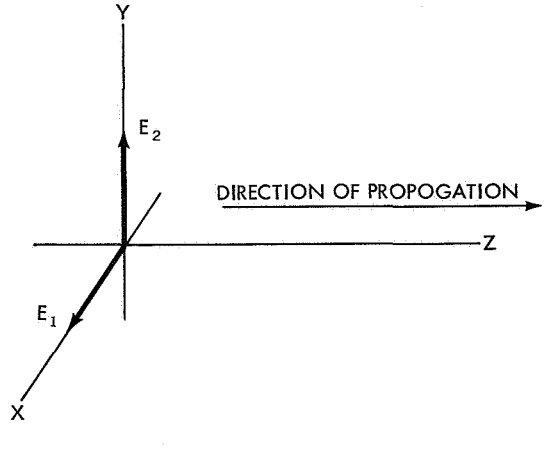
$$E_1 = E_0 \sin \omega t \text{ and } E_2 = \gamma E_0 \cos \omega t \qquad (10.6)$$

eliminating the time dependence gives the locus of these waves:

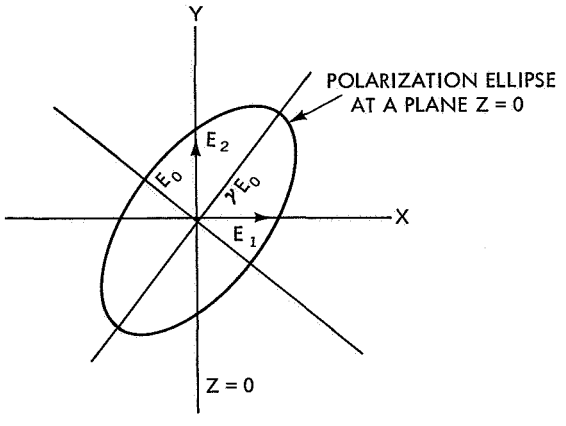
$$\frac{E_1^2}{E_0^2} + \frac{E_2^2}{\gamma^2 E_0^2} = 1 \qquad (10.7)$$

This is the equation of an ellipse with axes $2E_0$ and $2\gamma E_0$.

The resultant of these two components traces out this ellipse as it rotates in time. Such a rotating wave is termed an elliptical polarized wave, the polarization elipse at a plane $Z = 0$ being shown in Figure 10–22. A special case arises if $\lambda = 1$, when the locus reverts to a circle giving a circularly polarized (C. P.) wave. Circular polarization is therefore an ideal case of elliptic polarization, and is generally approximated in practice by elliptical polarization with an axial ratio approching unity. Such a wave is also referred to as Circularly Polarized without further qualification. The most usual man-



LINEARLY POLARIZED COMPONENTS OF AN ELLIPTICALLY POLARIZED WAVE.



POLARIZATION ELLIPSE

FIGURE 10–22.—Eliptically polarized waves.

ner of denoting the quality of such a wave is by the following ratio:

$$\frac{\text{Minimum of the transverse component of the electrical field}}{\text{Maximum of the transverse component of the electrical field}} = \frac{E_0}{\gamma E_0} = \frac{1}{\gamma} \qquad (10.8)$$

Sense of Polarization

It should be noted that the sense of polarization is ambiguous unless one clearly states the reference plane. The C. C. I. R. adopted, at its Xth Plenary Assembly (Geneva, 1963)* a definition according to which a righthanded circularly polarized wave is one in which an observer, looking in the direction of propagation, sees the electric vector rotating clockwise in a fixed plane.

Design of the Dielectric Plate

The two orthogonal components given in Equation (10.6) may be generated by establishing a linearly polarized wave E, Figure 10–23, at an angle of 45° to a differential phase shift section, such as a waveguide partially filled with dielectric.

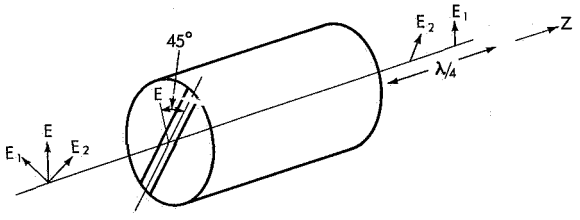


FIGURE 10–23.—Generation of a C. P. wave.

Consider the incident wave E splitting into two orthogonal components E_1 and E_2. Assuming the dielectric plate thickness to be considerably smaller than the length of the plate ℓ, the wave E_2 in the plane of the plate will be retarded in phase compared to E_1, the differential phase shift between E_1 and E_2 will be governed by the following relationship:

$$\phi = 2\pi\ell\left(\frac{1}{\gamma_{g2}} - \frac{1}{\gamma_{g1}}\right) \qquad (10.9)$$

where γ_{g1} and γ_{g2} are the guide wavelengths for the two orthogonal linearly polarized waves E_1 and E_2. Clearly the effective dielectric constant ϵ_2 corresponding to wave E_2 will be greater than the effective dielectric constant ϵ_1 corresponding to wave E_1 and consequently

$$\phi = 2\pi\ell\,\frac{\sqrt{\epsilon_2 - \left(\frac{\lambda_o}{\lambda_c}\right)^2} - \sqrt{\epsilon_1 - \left(\frac{\lambda_o}{\lambda_c}\right)^2}}{\lambda_o} \qquad (10.10)$$

where λ_c is the cut-off wavelength of the dominant mode, and λ_o is the free space wavelength.

For broadband operation the differential phase shift ϕ must remain approximately equal to 90° throughout the entire frequency spectrum of interest. The effective dielectric constants ϵ_1 and ϵ_2 are not directly computable and hence the length ℓ can only be calculated by finding the propagation constants for the two orthogonal waves E_1 and E_2. In order to do this one must solve a transverse eigen-value equation for each wave which is due to the boundary conditions at the dielectric-air interfaces. Such a calculation has been made for a polarizer in square guide, and it has been found experimentally that the results hold good in a circular guide having the same cut-off frequency as that of the square guide.

Consider two orthogonal H-waves propagating in the Z direction in a partially dielectric-filled square guide as shown in Figure 10–24, E and H being of the form:

$$E = E_o e^{j(\omega t - \beta Z)}, \quad H = H_o e^{j(\omega t - \beta Z)} \quad \text{and } E_Z = 0.$$

E_y is assumed to be continuous over the air-dielectric media I and II and dielectric-air media II and III. The phase shift for the component of the circularly polarized

*Documents of the Xth Plenary Assembly of the C. C. I. R. (Geneva, 1963).

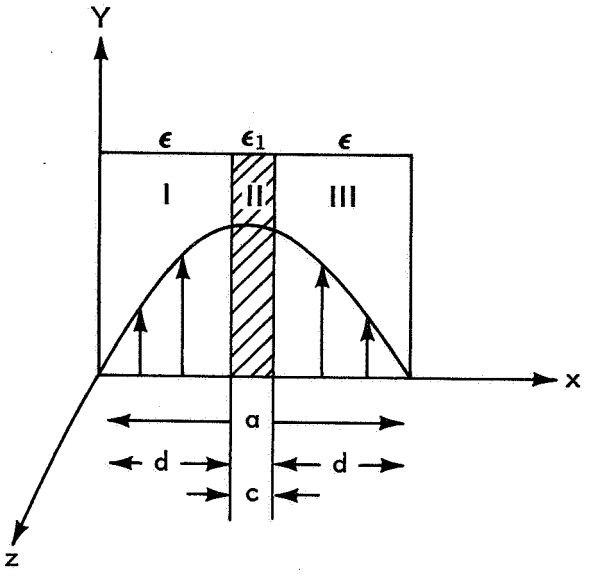


FIGURE 10–24.—Partially dielectric filled waveguide.

wave which travels parallel to the plane of the dielectric wedge is:

$$\gamma_2 = \sqrt{k^2 - \left(\frac{p}{d}\right)^2}, \qquad (10.11)$$

where

$$k = \frac{2\pi}{\lambda_o}$$

$$\frac{\tan p}{p} = \frac{s}{d} \cdot \frac{\cot q}{q}, \qquad (10.12)$$

where p and q are unknown and $s = C/2$.

It has been shown* that p and q satisfy the following equation:

$$\left(\frac{p}{d}\right)^2 = k^2 - \beta^2; \left(\frac{q}{s}\right)^2 = K k^2 - \beta^2 \qquad (10.13)$$

where $K = \frac{\epsilon_1}{\epsilon_o}$

$$\therefore q = s\sqrt{k^2 (K-1) + \frac{p^2}{d}} \qquad (10.14)$$

A similar analysis can be made for the perpendicular component but in view of the fact that the thickness of the dielectric wedge is considerably smaller than the length, it can be assumed that the phase shift for the perpendicular component is $\gamma_1 = 2\pi/\lambda_g$ per unit length where λ_g is air filled guide wavelength.

The following parameters were used for computation of the differential phase shift ϕ; see Equation (10.9).

$f = 4170$ Mc
$a = b = 1.75''$
$c = 0.125''$
$s = \frac{C}{2} = 0.0625''$
$d = 0.8125''$

For a dielectric consisting of P. T. F. E.
$K = 2.01$ and
$k = \frac{2\pi}{\lambda_o} = 0.873$ radian.

Solution of p is obtained from equations (10.12) and (10.13).

$$y = \frac{\tan p}{p} = \frac{s}{d} \cdot \frac{\cot q}{q}$$
$$p = 73.2° = 1.27 \text{ radian},$$

$$\therefore \gamma_2 = \sqrt{\left(\frac{2\pi}{\lambda_o}\right)^2 - \left(\frac{p}{d}\right)^2} = 0.615 \text{ radian/cm},$$
$$\gamma_1 = \frac{2\pi}{\lambda_g} = \frac{2\pi}{12.2} = 0.515 \text{ radian/cm},$$
$$\therefore \phi = \gamma_2 - \gamma_1 = 0.1 \text{ rad/cm} - 14.6°/\text{inch}.$$

According to the above calculation the required length of the dielectric wedge is approximately 6.2 inches. However, the preceding calculation does not take into account the effect of tapering, and this is difficult to allow for precisely. In order to determine the shape of the wedge, see Figure 10–25, the following procedure has been adopted.

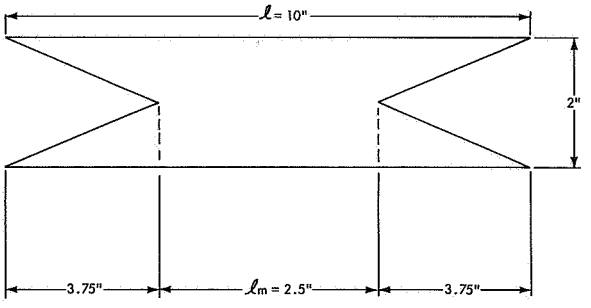


FIGURE 10–25.—Dimensions of the polarizer.

*L. Pincherle, "Electromagnetic Waves in Metal Tubes Filled Longitudinally with Two Dielectrics," Phys. Rev., Sept., 1944, Vol. 66, pp 118–130.

Assuming a length of the wedge $= \ell$ inches, then

minimum tapered length 0.75 λ_g at 4170 Mc $= 3.75$ inches,

diameter of the circular guide $= 2$ inches,

mid-section length of the wedge $\ell_m =$ $(\ell - 7.5)$ inches,

The overall effective area of the wedge is $(\ell \times 2) - 7.5 = 12.4$; hence $\ell = 9.95$ inches.

Based on the foregoing a wedge was prepared with an overall length of 10 inches and 3.75 inches tapered length; the measured ellipticities were found to be better than 0.8 over the band 4 to 6.5 Gc.

The P. T. F. E. wedge is held in position inside the 2-inch circular guide by means of eight dielectric pins penetrating slightly into the narrow dimension of the wedge. These dielectric pins are in turn sealed by thin metal sleeves.

Dispersion in Dielectric Plates

In general the thicker plates have better dispersion characteristics but the discontinuity introduced by a quarter-inch thick plate is sufficient to cause generations of higher order modes at the transmitting frequency (6.39 Gc), and a one-eighth inch thickness has therefore been used. This overcomes the difficulties due to overmoding but increases dispersion, the differential phase shift then being no longer constant over the required bandwidth. This has led to the investigation of means for providing compensation for dispersion.

Chu* has shown analytically that a slightly distorted circular guide can propagate two distinct transverse electric modes along the two axes of the ellipse. These two modes are usually known as the odd transverse electric (OH_1) and the even transverse electric (EH_1) waves. If a small section of elliptic guide (slightly distorted circular guide) is used in tandem with the polarizer and by giving proper orientation of the axes of the elliptic guide with reference to the dielectric plate it is possible to give slightly different phase velocities to the two orthogonal components of the circularly polarized wave.

The values of relative phase difference between the even and the odd mode in elliptic guide have been calculated for various values of Δ. Ellipticities better than 0.9 over the band 4 to 7 Gc have been obtained as shown in Figure 10–26, using the elliptical guide compensating section in tandem with the dielectric plate polarizer.

The loss of the polarizer comprises two parts, i.e., loss due to dielectric absorption and loss due to imperfect circularity of polarization, the noise temperature due to the polarizer being about 1.5° K.

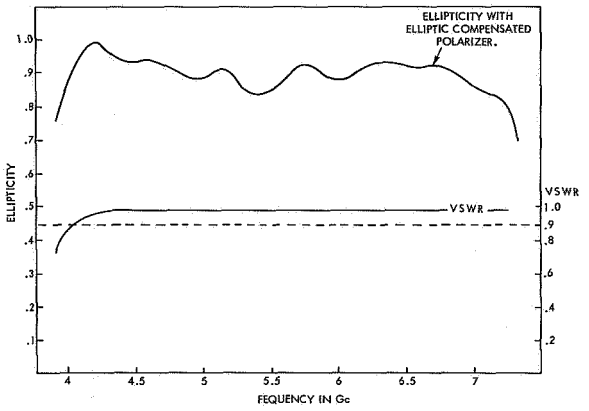


FIGURE 10–26.—Polarizer characteristics.

Establishment of Field Vectors

Returning to the question of establishing two orthogonal fields for the transmitted and received signal (E_t and $E\gamma$, Figure 10–19), consider the situation where the received signal from the aerial is to be right-handed circularly polarized and the transmitted signal into the dish aerial is to be lefthanded. In both cases the component with suffix 2, Figure 10–27, is phase delayed. The polarizing section must then be oriented with reference to the transmit field electric vector E_t, while the receiving field electric vector $E\gamma_2$, is delayed by 180° with respect

*Lan Jen. Chu, "Electromagnetic Waves in Elliptic Hollow Pipes of Metal," J. Appl. Phys., September 1938, Vol. 9.

to E_{γ_1}, the resultant E_γ then being orthogonal to E_t.

Conclusion

The diplexer and the broadband polarizer system described have been successfully used in the Goonhilly earth station installation for tests with the Telstar satellite.

A slightly modified version has been used in a combined feed assembly to provide communication via both Telstar and Relay satellites; in this modified version of the diplexer the transmitter power (1.7 Gc) for Relay propagates through a 5-inch circular waveguide enclosing the 2-inch waveguide diplexer used for Telstar. This combined feed assembly is described in detail in the following chapter.

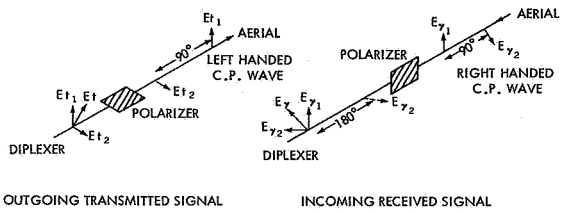


FIGURE 10–27.—Establishment of two orthogonal fields at the diplexer.

AUTHORS. *This chapter from the United Kingdom was authored by the General Post Office, London, England. The foregoing section on the Circularly Polarized Diplexer for the Goonhilly Satellite-Communication Aerial was authored by* D. CHAKRABORTY *and* G. F. D. MILLWARD *of the GPO.*

PRIMARY FEEDS FOR THE GOONHILLY SATELLITE-COMMUNICATION AERIAL

Introduction

The 85 ft diameter aerial at Goonhilly Downs, Cornwall uses a focal-plane paraboloidal reflector illuminated from a primary feed at the focus. Circularlly polarized waves are transmitted and received. For optimum gain and uniformity of the aerial radiation patterns, circular symmetry of the primary feed radiation pattern is desirable. The primary feed has therefore been made circularly symmetric.

The following terms, which are particularly applicable to large-aperture low-noise parabolic reflector type aerials, are used in the following account of the feed design:

Aerial gain factor (G); the ratio of the actual gain obtained to that of a uniformly illuminated aperture of the same area.

Illumination efficiency (e); the ratio of the energy illuminating the reflector to the total energy radiated by the feed.

Radiation spillover; the energy radiated by the feed, not illuminating the reflector.

System figure of merit; the ratio of aerial gain to the total receiving system noise-temperature in degrees Kelvin.

Other terms and symbols used are given in Table 10–3.

TABLE 10–3.—*List of Symbols*

G = Aerial gain factor
e = Illumination efficiency
ψ = Angular half-aperture of aerial, i.e., angle subtended by reflector periphery to the focus
ϕ = Angle subtended to focus
$G_f(\phi)$ = Gain function of primary feed radiation pattern
G_o = Primary feed gain when $\phi = 0$
$G_{\pi/2}$ = Aerial gain factor when $\psi = \pi/2$
β = Phase constant $= \frac{2\pi}{\lambda}\sqrt{1 - \frac{\lambda^2}{\lambda_c^2}}$
$k = w(\mu\varepsilon)^{1/2}$
$k_m = \sqrt{k^2 - \beta^2}$
μ = Permeability of medium (Henrys)
ε = Dielectric constant of medium (Farads)
λ = Free space wavelength
λ_c = Waveguide cut-off wavelength
λ_g = Guide wavelength
$w = 2\pi \times$ frequency
α = Radius of waveguide
θ = Angle subtended to center of waveguide aperture
$J_n(\chi)$ = Bessel's Function of nth order

Primary feed radiation patterns usually have a field intensity which is maximum in the direction of the vertex and which tapers towards the periphery of the reflector. Spillover is normally permitted to obtain an optimum gain factor. However, for the recep-

tion of low-level signals, when the aerial is pointing towards a low-temperature sky, some consideration must be given to spillover which results in the reception of thermal radiation from the earth. The spillover permitted with a receiving aerial may then be less than that with a transmitting aerial for optimum working conditions. The optimum spillover for reception also varies with the aerial elevation, but 5 degrees is an appropriate elevation for consideration since then the sky temperature has the fairly low figure of about 20 degrees Kelvin (°K)* and the spillover noise temperature is very nearly maximum. At low angles of elevation, approximately one-half of the spillover energy is at the average sky temperature (assumed to be 6° K) and the other half at the temperature of the earth.

The experiments with the Telstar and Relay satellites require transmitting frequencies at the ground stations of about 6390 and 1725 Mc respectively, and a common receive frequency of about 4170 Mc. The initial time available for development made it imperative to consider at the outset a separate primary feed design for each experiment. However, a composite feed unit capable of accommodating all three frequencies is now in use.

Aerial Gain Factor and System Figure of Merit

The gain factor of a parabolic aerial is given by*:

$$G = \cot^2\frac{\psi}{2} \left| \int_0^{\psi} \left[G_f(\phi)\right]^{1/2} \tan(\phi/2)\, d\phi \right|^2 \qquad (10.15)$$

Classes of primary feed patterns considered analytically by Silver are given by:

$$G_f\phi = G_o \cos^n \phi \qquad (10.16)$$

between the limits $\phi = +\pi/2$ and $-\pi/2$, and where $n = 2, 4, \ldots$ etc.

When $n = 2$, the optimum aperture ψ is about 66° and the gain factor obtained is about 0.83. The primary feed illumination at the reflector periphery is then about −10 db relative to that at the vertex.

In the case of the focal plane paraboloidal reflector, the angular aperture, ψ, is $\pi/2$ and the gain factor is:

$$G_{\pi/2} = \left| \int_0^{\pi/2} [G_f(\phi)]^{1/2} \tan(\phi/2)\, d\phi \right|^2 \qquad (10.17)$$

For the feed pattern given by Equation (10.16), the gain factor is only 0.57. To obtain a higher value therefore it is necessary to broaden the feed pattern allowing some spillover. This can be considered analytically by assuming a primary feed pattern given by:

$$G_f(\phi) = G_o \cos^n m\phi, \ldots \qquad (10.18)$$

between the limits $m\phi = +\pi/2$ and $-\pi/2$, and where m lies between 0.5 and 1.0.

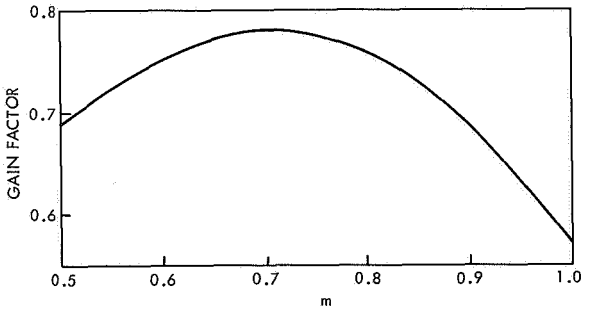


FIGURE 10–28.—Variation of aerial gain factor with m.

When the gain factor obtained from Equation (10.17) is plotted against the parameter m, the curve in Figure 10–28 is obtained for $n = 2$. This curve indicates that an optimum gain factor of about 0.78 is obtained with $m = 0.7$.

When the effects of radiation-spillover are considered, the following approximate for-

*D. C. Hogg: Problems in Low Noise Reception of Microwaves, I. R. E. Trans., Nat. Symp. on Space Electronics and Telemetry, 1960, p 8–2.

*S. Silver: Microwave Antenna Theory and Design, M. I. T. Radiation Laboratory Series No. 12.

mula for the system noise temperature is obtained:

$$T_S = T_1 + eT_2 + \frac{(1-e)}{2} T_3 + \frac{(1-e)}{2} T_4$$

where

T_1 = noise temperature of the receiving equipment (apart from the aerial)
T_2 = sky temperature seen by the aerial main lobe (20°K is assumed at 5° elevation)
T_3 = average sky temperature, assumed to be 6°K
T_4 = effective ground noise-temperature

Curves are plotted in Figure 10–29, giving values of figure of merit for an 85 ft diameter focal-plane aerial with various values of ground noise-temperature and with a receiving apparatus noise-temperature of 50° K. A ground temperature of 280° K is the figure assumed where the reflection coefficient of the earth is zero, i.e., the earth is regarded as a black body radiator. A temperature of 180° Kelvin is where the ground reflection coefficient is about 0.6, as estimated at Goonhilly Downs, and the case of 6° Kelvin is where the use of an earth-screen is possible, giving an image of the sky in the lower hemisphere of radiation. The latter is an interesting case because the spillover temperature is lower than that of the main lobe. The condition for maximum figure of merit is then very nearly coincident with the requirements for maximum gain factor, and the effective aerial temperature is less than that of the main lobe. Optimum figures for the three ground temperatures and for apparatus temperatures of 50° and 30° K are summarized in Table 10–4.

TABLE 10–4.—*Optimum Performance Figures of the Focal-Plane Paraboloid for Various Ground Noise Temperatures*

Equipment temperature = 50°K
Sky temperature = 20°K

Ground temperature (degrees K)	m	System Figure of merit (db)	Aerial gain factor	System noise temp. (degrees K)
280	0.8	41.2	0.758	73.1
180	0.77	41.3	0.77	72.8
6	0.69	41.6	0.777	68.6
280	0.815	42.6	0.75	52.5
180	0.78	42.7	0.765	52.4
6	0.68	43.1	0.777	48.7

Primary feed radiation patterns for m values of 0.8 and 0.69 are shown in Figure 10–30.

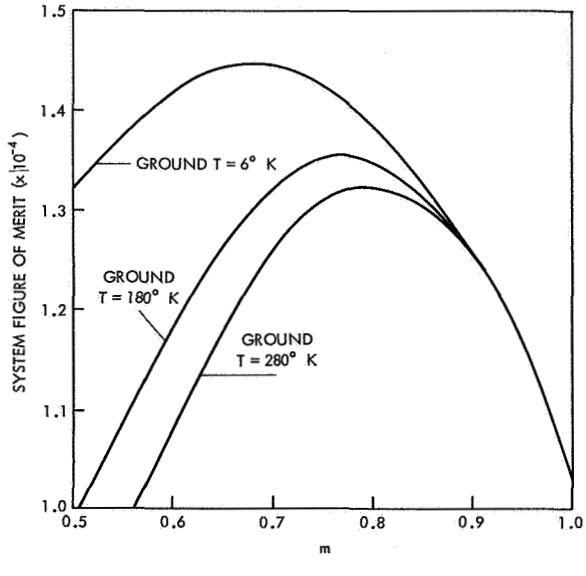


FIGURE 10–29.—Dependence of system figure of merit on the radiation pattern of a primary-feed illuminating an 85 ft diameter reflector.

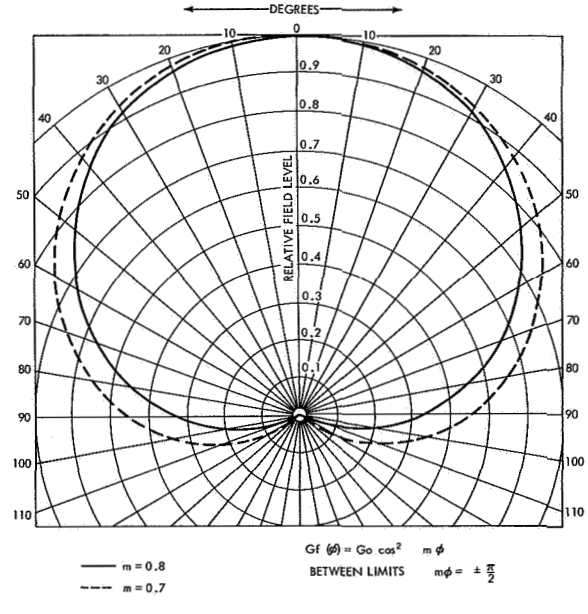


FIGURE 10–30.—Primary feed radiation pattern.

Radiation from a Small Aperture

The radiation patterns of a TE_{11} wave from an open-ended circular waveguide have been calculated by Chu*, and the normalized patterns are given by:

The E-plane field

$$E_{(\text{E-plane})} = \frac{2\left(1 + \frac{\beta}{k} \cdot \cos\theta\right) J_1 (ka \sin\theta)}{\left(1 + \frac{\beta}{k}\right) ka \sin\theta} \qquad (10.19)$$

and the H-plane field,

$$E_{(\text{H-plane})} = \frac{\left[\frac{\beta}{k} + \cos\theta\right]\left[J_o (ka \sin\theta) - J_2 (ka \sin\theta)\right]}{\left[1 + \frac{\beta}{k}\right]\left[1 - \frac{k^2 \sin^2\theta}{k^2_m}\right]} \qquad (10.20)$$

At 4170 Mc, the E and H Radiation patterns from a 2-inch circular waveguide (Figure 10–31) show that for use as a primary source of a low-temperature aerial the rearward radiation is excessive. It could be reduced by increasing the waveguide aperture, but then the breadth of forward radiation would not be obtained.

A circular flange placed about the waveguide aperture has a marked effect upon both the rearward radiation and the shape of the forward lobe. A feed with a 3–1/2-inch diameter flange about a 2-inch aperture has measured radiation characteristics showing reduced rearward radiation although increased directivity. The aerial gain factor and noise temperature obtained with this feed are estimated to be 0.53 and 5°K respectively. Improved radiation patterns were, however, obtained by placing the flange at critical distances behind the aperture, and further improvements were made by using two or more flanges. Experiments resulting in 3-inch and 4–1/2-inch diameter flanges, positioned 1/4 and 1–1/2 inches respectively behind the aperture, yielded the radiation patterns shown in Figure 10–32. Since the waveguide wall adversely affected the pattern, its thickness beyond the 3-inch flange was reduced to a knife-edge. The Telstar feed is based on the above, but the Relay and composite feeds with 5-inch diameter tubes have alternative flange assemblies.

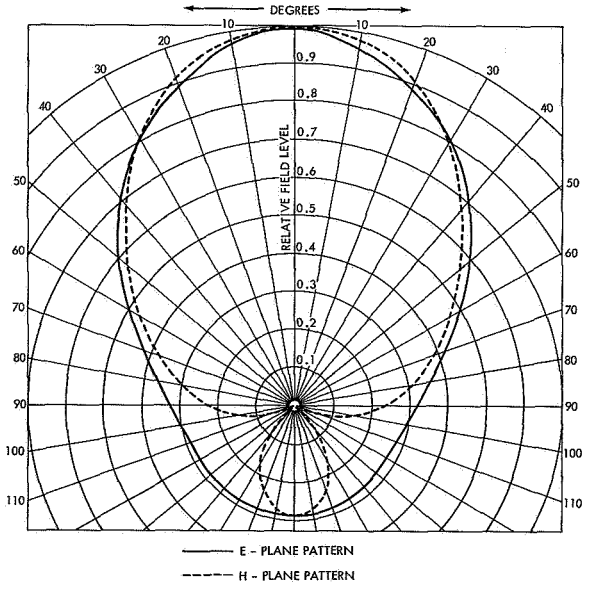


FIGURE 10–31.—Radiation pattern (theoretical) of open ended 2 inch diameter circular waveguide.

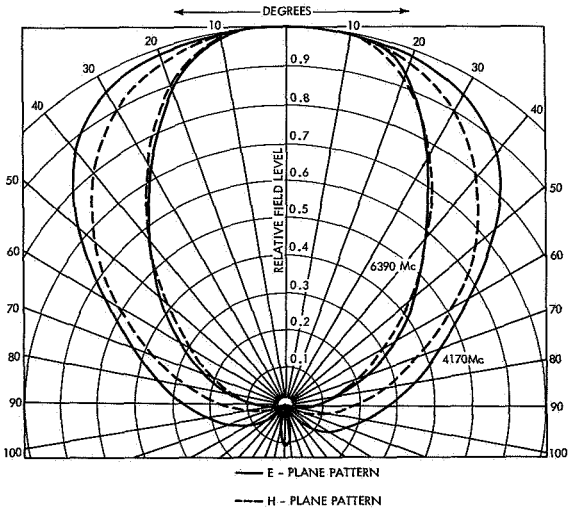


FIGURE 10–32.—Radiation patterns of Telstar feed.

*L. J. Chu: Calculation of the Radiation Properties of Hollow Pipes and Horns, Journal of Applied Physics, September 1940, (2, p 603–610).

Telstar Feed

General

The Telstar feed is in the form of a diplexer, the transmit frequency being higher than the receive frequency. Greater emphasis has been given to obtaining optimum operation over the receiving band about 4170 Mc. But since the minimum usable aperture at this frequency has a diameter of about 2 inches, a more directional feed pattern is obtained at the transmit frequency, resulting in slight aerial beam broadening and reduced gain factor. Since the flanges used for pattern shaping and noise reduction at 4170 Mc affect only slightly the 6390 Mc pattern, the form of aperture used in the Telstar feed (Figure 10–33) is that referred to in the description of the Telstar feed on this page.

Matching

The impedance discontinuity at the feed aperture without compensation is greater at 4170 Mc giving a VSWR of about 0.74 compared with 0.96 at 6390 Mc. Matching is provided by interposing within the waveguide a section of guide of different impedance. The waveguide section is realized in practice by fitting a dielectric sleeve of the required dimensions within the 2-inch diameter guide. The sleeve has only a small effect on the matching at 6390 Mc as the length is about 0.5 λ g at this frequency. The position of the sleeve and its thickness are such that improved matching is obtained at 4170 Mc.

A VSWR of greater than 0.97 was thus obtained over the transmit and receive frequency bands.

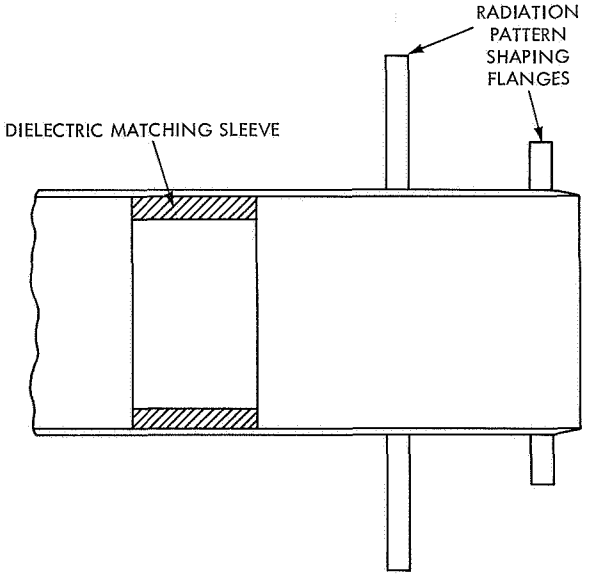


FIGURE 10–33.—Telstar feed.

Description

The Telstar feed (Figure 10–33) has the circular brass flanges soldered on the outside of the waveguide, the aperture end of which has been chamfered. The dielectric matching cylinder is of P.T.F.E. and is set into a slight undercut in the waveguide. Adjustments to the position of the aperture on assembly are made by inserting circular waveguide spacers between the connecting flanges of the primary feed and the waveguide feeder.

Feed Performance

The radiation patterns of the Telstar feed (Figure 10–32) show that at the receive frequency the average illumination taper is about —13 db at ± 90°. The aerial gain factor obtained from the feed pattern and the use of Equation (10.17) is estimated to be 0.66. The illumination efficiency is about 0.966 and with a noise-temperature of 180°K due to the surrounding terrain, the effective increase in system temperature due to spillover is 2.5°K with the aerial at 5° elevation. The pattern at 6390 Mc is considerably more directional and yields a gain factor of 0.51 and an illumination taper of about —21 db in the focal plane.

Aerial radiation patterns, calculated from the average primary feed patterns, have half-power beamwidths of 12.2 and 8.2 minutes at 4170 and 6390 Mc respectively.

Relay Feed

General

In the case of the Relay feed, with the lower transmitting frequency of 1725 Mc, compared with the Telstar feed, a larger

feed aperture was necessary. Since, however, maximum aerial efficiency and low noise temperature was again required at the receive frequency, it was imperative to consider the design of individual primary sources for transmission and reception. Of the types of feed investigated, a coaxial aperture was considered effective, the 1725 Mc signal being transmitted through a coaxial waveguide in the TE_{11} coaxial mode, and the 4170 Mc signal being received in the associated hollow inner conductor and supported in the TE_{11} circular-waveguide mode. Since the cut-off wavelength of the inner guide is less than the transmit wavelength, the high-power signal is rapidly attenuated along the receiving guide.

Description

The feed assembly (Figure 10–34) has waveguide size WG8 coupled to a power divider which divides the waveguide into two half-section guides. These diverage to allow the inclusion of a WG11 binomially-stepped corner in a waveguide combining section. The transducer following transforms the WG11 waveguide to 2-inch circular guide and the two half-section WG8 waveguides to septate 5-inch diameter coaxial guide. The wedges through the transition provide mechanical rigidity as well as continuity of mode transformation. The septate coaxial guide is coupled to a coaxial section in which the transmitted signal is converted from linear to circular polarization through a matched pair of dielectric quarter-wave plates of P.T.F.E., having low-loss and a high melting point. The principle of operation of this polarizer, although in coaxial guide, is similar to that used in the Telstar feed, which has been described in the previous section of this chapter. A dielectric filter near the coaxial aperture, while permitting low-loss transmission at 1725 Mc provides substantial reflection at the receive frequency thus reducing radiation of noise from the high-temperature transmit aperture. The filter is positioned relative to the aperture to obtain a broad radiation pattern at the receive frequency consistent with low-level spillover. Circular flanges about the outer conductor provide pattern shaping at the transmit as well as the receive frequency.

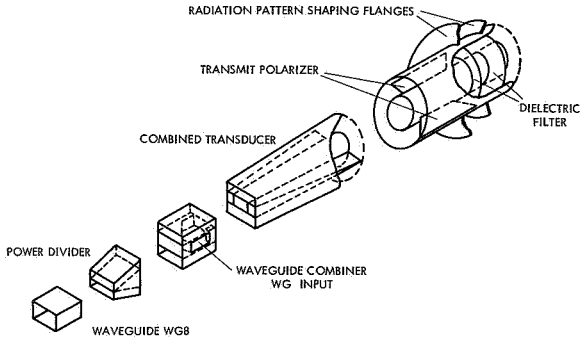


FIGURE 10–34.—Relay feed.

The dielectric polarizer and the matching in the inner waveguide are similar to those in the Telstar feed.

Composite Feed

Description

The composite feed (Figure 10–35 and 10–36) comprises the component parts of the Relay and Telstar feeds. The Relay transducer is, however, separated to perform the waveguide transformations at different parts of the assembly.

The waveguide from the Relay transmitter is again coupled to a power divider to provide the two half-section guides allowing the inclusion of a WG14 bend. The components in the center guide are then in the same sequence as in the Telstar feed and comprise a WG14/2 inch circular waveguide transducer, WG11/2 inch circular waveguide diplexer,* dielectric polarizer and the aperture matching section. In the transmitting outer guide the two half sections of WG8 sandwich the inner guide as far as the second transducer, where the rectangular guides are transformed to septate coaxial guide. The coaxial section is then similar to that in the Relay feed.

*D. Chakraborty and G. F. D. millward: A 4/6 Gc Circularly-Polarized Diplexer for the Goonhilly Satellite Communication Aerial.

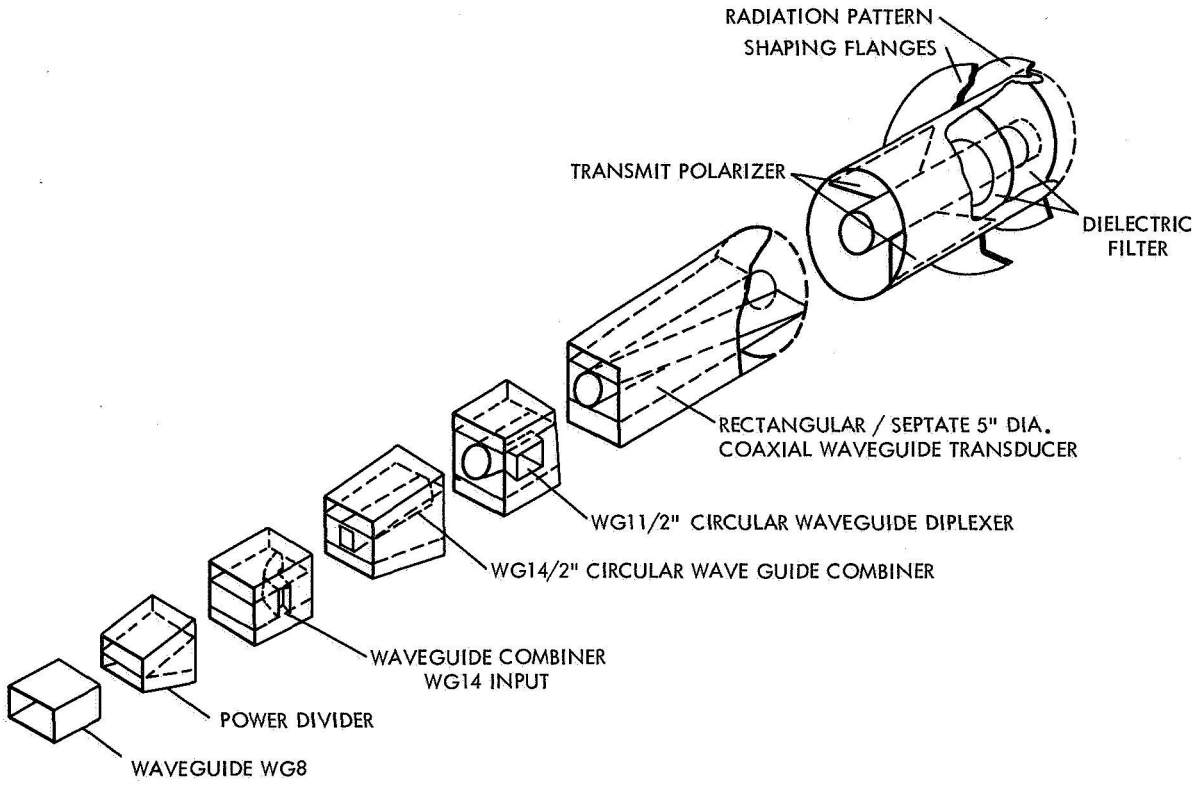


FIGURE 10–35.—Telstar/Relay composite feed unit.

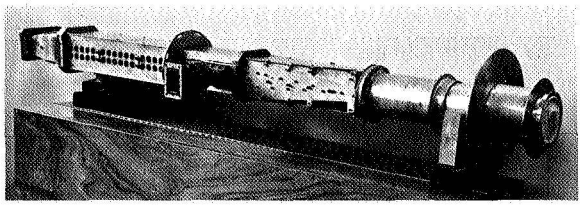


FIGURE 10–36.—Composite feed.

In the Telstar experiments the inner guide and its components are used, the 5 inch diameter aperture and flanges functioning only to shape the radiation pattern. In the Relay experiments, the WG8/5 inch diameter coaxial guide carries the transmitting signal, and the internal circular guide receives the satellite signal, the diplexer transferring it to the main receive waveguide feeder.

Performance

The impedance matching into the composite feed gives a VSWR of 0.97 at 1725 Mc. The matching characteristic measured over a frequency range is that shown in Figure 10–37.

The ellipticity ratio of the circularly polarized fields within the coaxial waveguide is about 0.98. The radiation pattern at the transmit frequency has a field intensity taper of —10db in the focal plane, and gives an aerial gain factor of about 0.67. The receive pattern is very similar to that of the Telstar feed and gives a gain factor of 0.66 and an illumination efficiency of 0.967.

Model Aerial Tests

During the period of feed development, some considerable experience was obtained

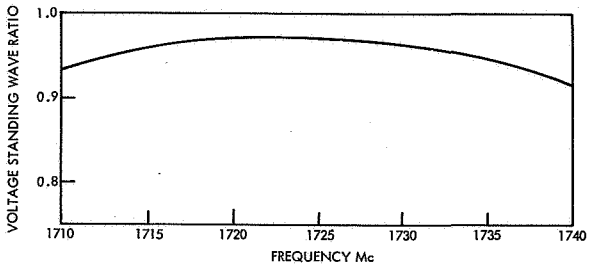


FIGURE 10–37.—Composite feed—overall matching characteristics.

with a 10 ft diameter focal-plane reflector modeled on the Goonhilly aerial. The model primary feeds were scaled to operate at about 11 Gc. A typical radiation pattern obtained with a model Telstar feed, vertically polarized (Figure 10–38) shows that apart from the main lobe and immediate side lobes,

1. At bearings up to ±20° relative to the electrical axis, the radiation is largely due to scatter from the tetrapod structure. This was shown by measurements with the tetrapod removed and the feed supported by thin nylon cords .

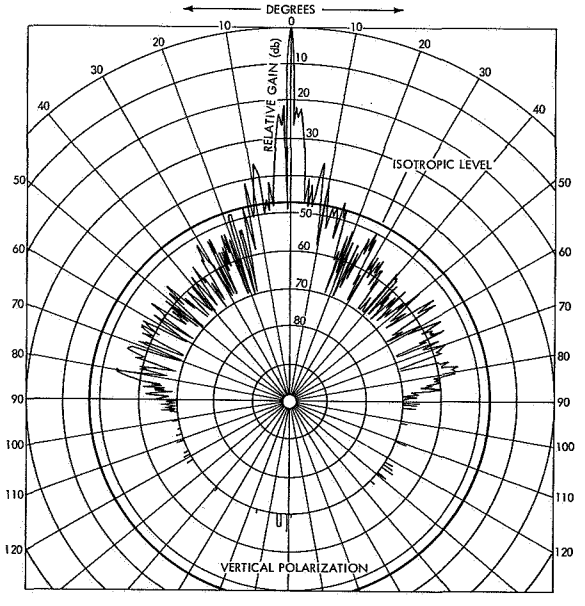


FIGURE 10–38.—H-plane radiation pattern of model aerial with Telstar feed scaled to operate at 11.1 Gc.

2. At bearings between ±20° to ±90° the radiation is predominately primary feed spillover.

The pattern with horizontal polarization showed a greater level of primary feed spillover consistent with the larger level measured in this plane in the primary feed radiation pattern (Figure 10–30).

Conclusions

Using idealized primary feed radiation patterns for guidance, it is evident that the permissible spillover is dependent upon the effective noise-temperature of the surrounding terrain, and to a lesser extent on the noise-temperature of the system receiving equipment. Where the equipment and ground temperatures are about 50 and 180°K respectively, a primary feed illumination taper of about —15db is required for an optimum figure of merit at low angles of aerial elevation. The effect of spillover is then to increase the system noise temperature by about 2.8 degrees, the gain factor being 0.77. However, if it were possible to reduce the effective ground temperature further, then the spillover could be increased to provide a greater aerial gain factor.

Experiments with circular flanges about a circular-waveguide aperture have resulted in primary feed patterns giving a gain factor of about 0.65 and an effective noise temperature increase of about 0.65 and an effective noise temperature $= 180°K$). The illumination taper at the reflector periphery is about 19db. If it were possible to broaden the feed pattern further to increase the gain factor, a closer approach to the ideal could be obtained.

AUTHOR. *This chapter from the United Kingdom was authored by the General Post Office, London, England. The forgoing section on Primary Feeds for the Goonhilly Satellite-Communication Aerial was authored by* I. A. RAVENSCROFT *of the GPO.*

WAVEGUIDE FEEDER SYSTEM

Introduction

There are two features which distinguish the feeder arrangements at a satellite earth station from those used in conventional microwave line-of-sight links. The first is the importance of low loss in all waveguides and components and the second is the need for rotating joints. Losses are important in the receive direction because they contribute signficantly to the overall system noise temperature while, in the transmit direction, not only do they waste expensive transmitter power but localized points of high loss can give rise to the formation of arcs when the power is applied. Rotating joints are required on the elevation axis of the aerial to permit waveguide connection between apparatus in the turntable cabin and on the dish.

In the installation at Goonhilly, three separate waveguide connections are required between the turntable cabin and the focus platform; one each for the Telstar and Relay transmitters operating at 6390 and 1725 Mc respectively, and one for the receiver feed, routed via the maser cabin on the back of the dish and operating at 4170 and 4080 Mc. Dominant-mode rectangular waveguide is used for these runs, and the components and installation practices used follow normal practice as far as possible.

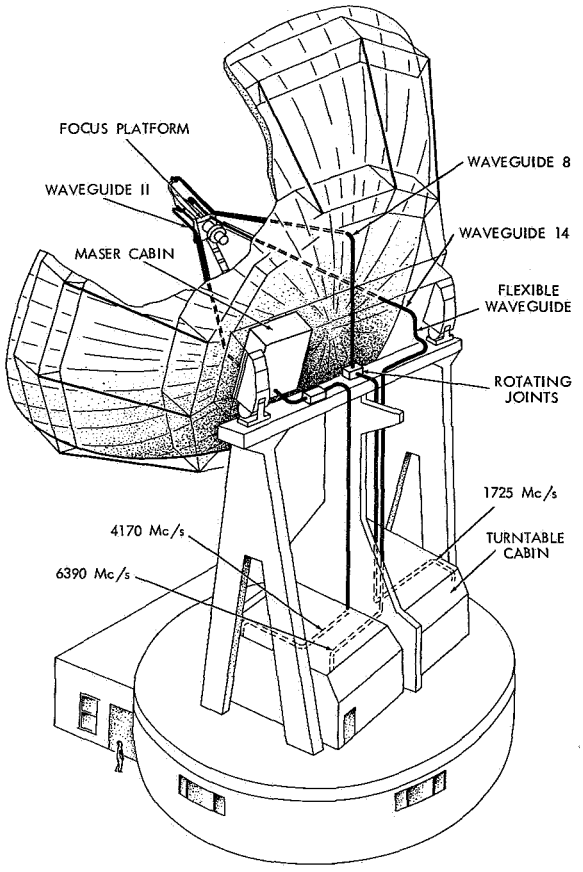


FIGURE 10–39.—Layout of main waveguide runs.

Main Waveguide Runs

Figure 10–39 shows the layout of the main waveguide runs. Rectangular waveguide is used in sizes WG 8, 11 and 14 for the 1725, 4170 and 6390 Mc guns, respectively. Copper waveguide, using electrolytic copper, is employed to minimize the losses.

It can be seen from the sketch that a relatively large number of bends or corners are required on each waveguide run, including some at special angles as at each end of the tetrapod legs. Fabricated corners of the simple mitred type are used in the WG 8 run. Typically, these give a measured VSWR of 0.995 at band center (1725 Mc), the VSWR remaining greater than 0.99 over a bandwidth of ± 20 Mc. In the WG 11 run, binomially-matched fabricated corners are used because the required bandwidth is greater—the beacon signal at 4080 Mc must be accommodated in addition to the communication signal at 4170 Mc. The VSWR of these corners is typically 0.995 at 4170 Mc and greater than 0.99 at 4080 Mc. In the WG14 run, the compactness of the fabricated corner is of less importance than in the larger sizes and also the high power-density of the transmitted signal makes the use of fabricated corners inadvisable. Bends which are made by blending copper waveguide on a suitable mandrel are therefore used. The VSWR of such bends is typically 0.985 at 6390 Mc.

The use of large mean powers in waveguide systems is less common than the use of large peak powers. However, experience has shown that waveguide systems carrying large mean powers are subject to the formation of arcs at power levels of more than an order of magnitude below those which might be expected to give trouble from voltage breakdown. No adequate theory exists for this type of breakdown but it is known that one cause is localized overheating of particles such as dust, swarf or shreds from rubber sealing rings. A consequence of the lack of an adequate theory of cw breakdown is that it is not possible to design a component with any assurance that it will not break down in service unless it has been tested at full power. Special precautions were taken during the installation of the waveguide runs to ensure that the interior surfaces of all waveguide and all components were kept scrupulously clean, particularly in the case of the WG14 installation where the power density is very high. The flange joints on the WG8 runs were improved by using metallic gaskets.

The performance of the WG11 and WG14 runs was measured after installation with the following results. The WG11 between the maser cabin and the focus platform gave a VSWR of between 0.91 and 0.96 in the frequency range 4070–4185 Mc. The attenuation, calculated from VSWR measurements with a short-circuiting plate over the guide, was 0.262 db compared with the theoretical figure of 0.188 db for plain copper guide of the same length. The WG11 run between the turntable cabin and the rotating joint on the elevation axis gave a VSWR of between 0.89 and 0.98 over the frequency range 4060–4175 Mc and the attenuation was 0.67 db compared with a theoretical figure of 0.52 db. The WG14 run between the turntable cabin and the focus platform gave a VSWR of between 0.82 and 0.97 over the frequency range 6350–6430 Mc and the attenuation was 1.94 db as compared with a theoretical figure of 1.76 db.

Rotating Joints

Rotating joints were required at the elevation axis of the aerial to permit the waveguide connections from the dish to be extended down to the apparatus in the turntable cabin. A separate joint is required for each frequency band but the basic principle is the same for all. This is that the TE_{01}-mode wave in rectangular guide is converted to a circularly polarized (or rotating) TE_{11}-mode wave in circular guide. The joint itself is in the circular guide and uses a simple choked flange, the rubbing contact occurring at the high-impedance junction between the two quarter-wave sections of the choke. After the joint, the wave is converted back again to the dominant mode in rectangular guide. This class of rotating joint was chosen for economy in design effort as some of the components used in it are also required for other purposes.

The 6390 Mc version of the rotating joint was not completed in time for the initial installation at Goonhilly and a length of flexible (twistable) rectangular waveguide was installed instead. This was arranged so that it is straight when the aerial elevation is 45°, the maximum bending thus being ± 45°. This arrangement has proved so successful that it is doubtful whether it is worthwhile replacing it with the more complex rotating joint.

Figure 10–40 shows a sketch of the 4170 Mc rotating joint. To minimize the axial

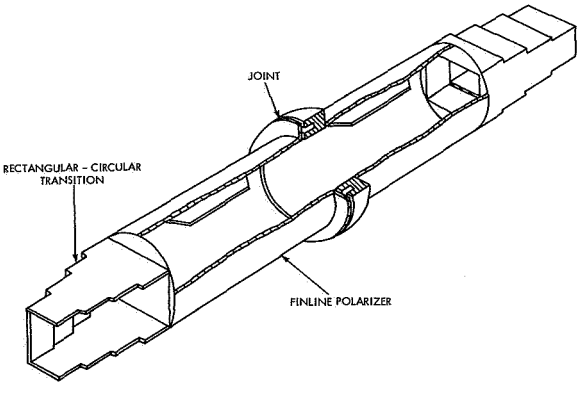


FIGURE 10–40.—Rotating joint.

length of the unit, a binomially corrected stepped transition is used to convert the TE_{01} wave in rectangular guide to a TE_{11} wave in circular guide. A constant guide-width is maintained throughout the intermediate rectangular steps of the transition to simplify the problem of obtaining a theoretical starting point for the design. The final dimensions are, however, obtained by experimental modifications of the initial design. In its final form the transition has a VSWR in excess of 0.98 from 4070 Mc to greater than 4300 Mc, the figure for 4170 Mc being about 0.99. The TE_{11} wave in the circular guide is converted to a circularly polarized wave by the finline polarizer. This contains a copper fin inserted into circular guide at an angle of 45° to the plane of polarization of the linearly polarized incident TE_{11} wave, and retards the phase of the resolved component of the incident wave which is parallel to the fin by 90° with respect to the component which is at right angles to the fin. The circularly polarized wave which emerges has the necessary circular symmetry to permit the joint to be rotated without introducing variations in its transmission properties. The joint itself is of the simple choke-flange type with a rubbing contact at the current null in the choke. Time did not permit the investigation of more sophisticated joints but present indications are that the simple type is quite adequate. Following the joint, another polarizer and stepped transition convert the circularly polarized wave back to the normal TE_{01} wave in rectangular guide. The insertion loss of the complete rotating joint is 0.035 db at 4170 Mc and the VSWR is nearly constant at 0.95 over the range of angles of rotation which are used and over the frequency range 4080–4183 Mc. The rotating joint for the 1725 Mc waveguide run is similar in principle to that just described but uses waveguide turnstiles to convert from rectangular guide to circularly polarized waves in circular guide. This arrangement leads to a shorter axial length. Initially, some doubts were experienced about the bandwidth of this type of joint but the performance has proved to be adequate. At mid-band frequency, 1725 Mc, the VSWR is about 0.99 irrespective of angle of rotation while at ± 20 Mc the VSWR varies between 0.95 and 0.99 with angle of rotation.

Waveguide for Receiver Input

The losses which occur between the primary feed at the focus of the dish and the input port of the maser are of particular importance because they contribute significantly to the overall system noise temperature. Unfortunately, a large number of waveguide components is required in this part of the system in addition to the plain waveguide, and this increases the difficulty in making the total loss small. The path between the primary feed and the maser includes the broad-band polarizer and diplexer (described elsewhere), flexible waveguide to permit the feed to be moved, some 31 ft of waveguide between the diplexer and the maser cabin and the rather complex assembly of components within the maser cabin which is illustrated in Figure 10–41. The assembly in the maser cabin is required to provide the

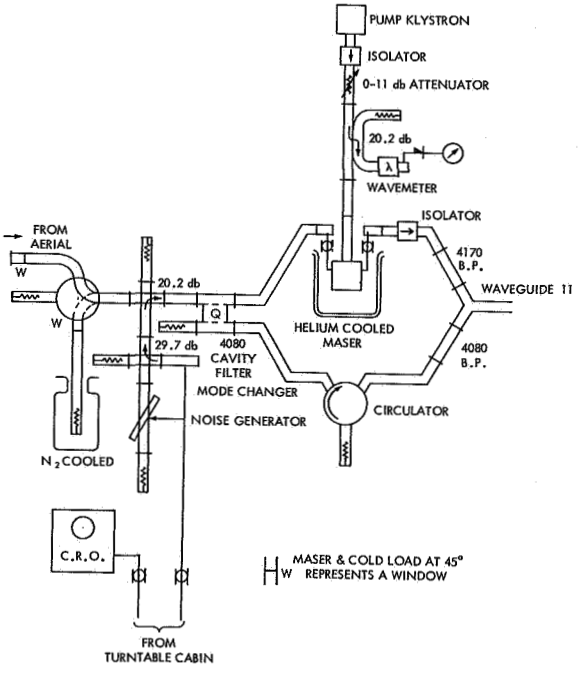


FIGURE 10–41.—Schematic of equipment in aerial cabin.

desired test facilities and to provide an alternative path for the beacon signal which lies outside the pass band of the maser.

Of the components in the maser cabin, the filter which separates the beacon signal from the communication signal could have the greatest potential for introducing loss in the communication channel. However, by employing a resonant cavity coupler for the beacon channel, this loss is only 0.033 db at 4170 Mc, and the loss in the beacon path is 1.3 db at 4080 Mc. The coupling loss between the beacon guide load and communication channel output is 33 db so the extra contribution to system noise is negligible.

The filter pair which combines the communication and beacon signals at the output of the maser and a similar pair which is fitted in the turntable cabin and feeds the two receivers, are of straightforward design and use three quarter-wave-coupled triple-post cavities. The isolator which follows the maser and the circulator in the maser by-pass are provided to ensure that the filters, which are designed on an insertion loss basis, are correctly terminated and so give their design performance.

In view of the importance of knowing the very small losses introduced by individual components, an experimental equipment for measuring very small losses has been developed. An analysis of the loss figures for the pre-maser waveguide components is given in Table 10–5.

It can readily be shown that a matched network of loss L (input/output power ratio) at a temperature T_o, inserted between an aerial of noise temperature T_a and a low-noise receiver (e.g., maser) as a temperature T_r, increases the effective aerial temperature by $T_o\ (L-1)$. Thus the total effective noise temperature of the system referred to the aerial is:

$$T_a + T_o(L-1) + LT_r.$$

Using the figures of Table 10–5 this becomes:

$$(T_a + 42 + 1.14\ T_r)\ °\text{K},$$

TABLE 10–5.—*Analysis of Losses in Pre-Maser Waveguide Components*

Component	Loss—db
Diplexer (incl. polarizer)	0.100
Connecting section (incl. twist and 1 corner)	0.074
External WG11 (incl. flexible section and 2 corners)	0.232
Internal WG11 (incl. 1 window and 2 corners)	0.021
Waveguide switch	0.028
Directional coupler	0.048
Internal WG11 (incl. 5 corners)	0.047
Beacon separation filter	0.033
Total	0.583

or referred to the maser input:

$$(0.87\ T_a + 37 + T_r)\ °\text{K}.$$

As the system noise temperature measured at the maser input, with the aerial pointing at zenith, is 56°K and the effective maser noise temperature is of the order of 13°K, the component of the noise temperature due to the waveguide losses cannot differ very much from the estimated figure of 37°K. While this figure is large, it can be seen from the table that there is not much scope for a substantial reduction unless the first-stage amplifier can be placed nearer the feed. The largest single component is the waveguide run between the diplexer and the maser cabin. Consideration is being given to using oversized rectangular and even circular guide, for the straight portion of the run down the tetrapod leg, but the maximum saving would only be some 7°K. Cooling of the waveguide run has been investigated, but it is not considered worthwhile.

Conclusions

The special features of the waveguide installation on the aerial at Goonhilly have been outlined and performance data have been given. The installation and all its components have functioned successfully in the manner expected. The most significant feature is the relatively large contribution which the waveguide installation between the pri-

mary feed and the maser makes to the system noise temperature. This is not due to any one cause but arises partly from the distance involved and partly from the necessary complexity of the arrangements. While it can be expected that further work will lead to a reduction in the losses in this part of the system, it seems unlikely that any very large reduction will prove possible unless the first-stage amplifier can be placed nearer the feed.

AUTHORS. *This chapter from the United Kingdom was contributed by the General Post office, London, England. The foregoing section on the Waveguide Feeder System was authored by* I. F. MACDIAMID *and* S. C. GORDON *of the G.P.O.*

THE 1700 MC TRANSMITTER

In order to achieve flexibility, unit cabinet construction is used for the transmitter, the heart of the equipment being a klystron. The transmitter has, in fact, been designed to operate with either of two types of klystron, viz, the new Eimac 5KM70SF (Figure 10–42) mentioned above, or the Varian VA 800 (Figure 10–43). This latter tube has been extensively used in tropospheric scatter links, being tunable from 1700 to 2400 Mc, and having an output power of 10 kw with a bandwidth of only 8 Mc to the —3 db points.

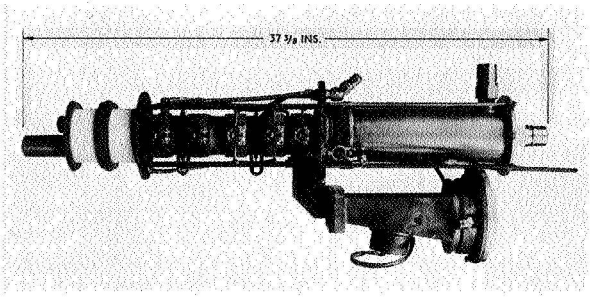


FIGURE 10–42.—The Eimac klystron type 5KM70SF used in the transmitter.

Klystron Operation

In case the reader is not familiar with the klystron tube, its operation is dependent upon the transit time of an electron beam, and is briefly as follows: A plentiful source of electrons produced at the tube cathode either by conventional radiation heating from a filament or by cathodic bombardment from a high voltage source. These electrons are drawn off to form an electron beam using an anode in the form of an annular ring situated close to the cathode. The electrons pass through the anode and are concentrated into

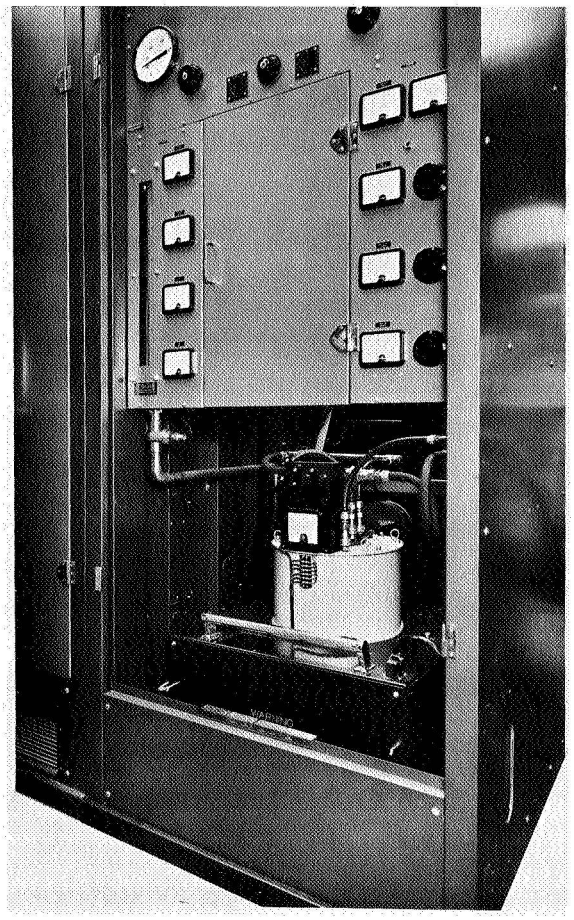


FIGURE 10–43.—The Varian klystron in position on its trolley.

a narrow parallel beam flow inside a tube, known as the drift tube, using a powerful magnetic field generated by external focusing magnets. The drift tube may be several feet long depending on the operating frequency of the klystron (about 14 in. long in the present case), and terminates in a collector electrode which absorbs those electrons remaining in the beam which are not drawn off earlier as RF power. At intervals along its length the drift tube has gaps in it across which the electrons have to pass. Each gap is surrounded by a cavity which can be made to resonate at the radio frequency of the klystron. The Eimac 5KM70SF has five such cavities.

The first cavity along the tube from the cathode has an RF probe inserted, to which is applied the RF drive from the drive unit at the required output frequency. The effect of injecting RF power into the resonant cavity is to alternately reverse the polarity of the potential across the gap in the drift tube at radio frequency thus alternately speeding up and slowing down the electron flow. Beyond the gap the electron flow will now consist of electrons traveling at different speeds, which in turn will produce bunching of electrons at a certain distance past the gap. If, at this point, a further cavity is inserted, a cumulative effect can be produced. As many as six cavities have been used, and the result is that a very large RF field can be produced in the final cavity, from which substantial power can be extracted using a suitable probe. As stated earlier, the remaining electrons are absorbed in the collector. As considerable power is dissipated in this collector it has to be cooled either by water or forced air. For larger klystrons, the losses in the drift tube wall are considerable and the drift tube also has to be cooled.

Equipment Composition

The transmitter itself consists of four main cabinets (i.e., drive unit, klystron unit, heat exchanger and power control unit), together with an extra high tension supply (e.h.t.) enclosure, as shown in the overall photograph (Figure 10–44) and the block diagram (Figure 10–45).

The drive unit supplies modulated RF power of approximately 0.5 w to the output klystron. Since it incorporates a number of facilities peculiar to the satellite project, it has been manufactured independently of the main transmitter, and is being provided by the GPO and not by STC.

The power control cabinet contains the auxiliary supplies, protection devices, fault signalling lamps, voltage regulator and main isolator.

The output klystron mounts on a special, easily removable, trolley in the klystron cabinet. The tube is seated in its focusing unit, together with the cavity tuning arrangements, on top of the trolley; while the filament and getter transformer, with their associated meters, are mounted in the lower compartment for the safety of personnel. Meters for the e.h.t. and focusing magnet supplies are mounted on panels on either side of the cabinet. Mounted at the cabinet rear are the RF output waveguide to the aerial, cross-coupler, and a water-cooled artificial load. Checking of the RF power fed into the latter is accomplished using dial thermometers and a flow meter on the cabinet front panel.

The main e.h.t. supply is generated in an enclosure at the rear of the power control and drive unit cabinets, using an e.h.t. transformer-rectifier, smoothing and an air cooling system.

The heat exchanger cabinet is shown in Figure 10–46 and contains an air-to-water heat exchanger, dual pumps and blowers, and control panels mounting flow meters, temperature gauges, water flow control valves, and motor starters.

Transmitter Operation and Facilities

Power Control Circuits

The equipment operates from a 415v three-phase 50/60 cps supply which is fed to the main isolator, from which it is distributed to various subcircuits via their protective overload switches.



FIGURE 10–44.—The transmitter assembly.

The main isolator is mechanically interlocked with all doors so that power cannot be switched on until they are closed and locked. In addition, the isolator is interlocked by a key with the door giving access to the aerial system.

The whole transmitter and heat exchanger is switched on and off by push-buttons on the control panel in the power control cabinet. Individual control of the heat exchanger, if required, is provided for by means of the push-buttons mounted on its central panel. Following "switch on" all the circuits are automatically operated in sequence up to the application of the e.h.t and are so interlocked that the failure of any one of them, or of the water and air supplies, instantly removes the e.h.t. A fault occurring in any of the major circuits is immediately indicated by the signalling lamps mounted on the cen-

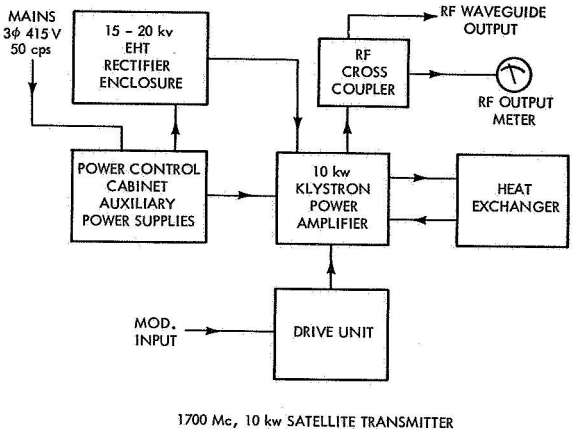


FIGURE 10–45.—1700 Mc, 10 kw satellite transmitter.

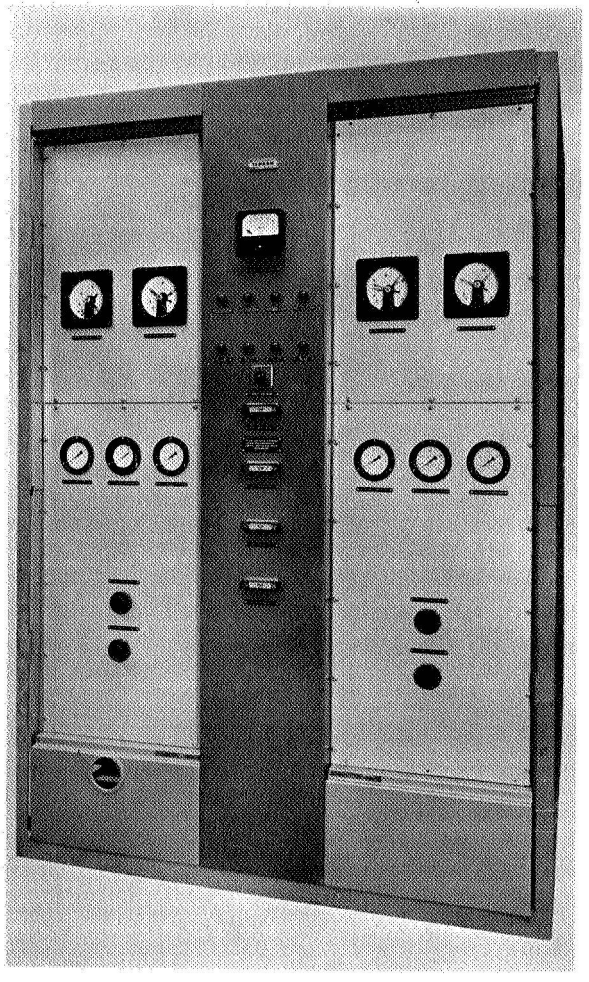


FIGURE 10–46.—The heat exchanger cabinet.

ter panel of the control cabinet. Special care has been taken in the design of fault protection circuits, especially for the e.h.t so that, under fault conditions, power can be removed from the klystron in a fraction of a second and there is no discharge from the smoothing condenser into the klystron.

The extra-high-tension supply is switched on and off by two pushbuttons mounted on a panel above the klystron. They are electrically interlocked with the voltage control, so that power can only be applied at near zero voltage. A smooth application of voltage is effected by a specially designed rotary stud switch, acting as a potentiometer, which varies the grid bias of a triode vacuum tube (STC 3J/232E) in series with the positive supply, from cutoff to a predetermined position value, corresponding with minimum anode dissipation. Three off-load taps on the rectifier transformer give output voltages of 0–10–16–20 kv. Thus at a predetermined positive grid voltage, corresponding to the maximum voltage on each range, the anode loss of the triode is kept to approximately 1–1.5 kw.

Klystron Amplifier Circuits

Approximately 0.5 w of RF output from the drive unit is applied to the input probe of the klystron which, as stated earlier, will normally be the Eimac type 5KM70SF, having five cavities. This tunes over the frequency range 1710–1800 Mc. It supplies 20 kw maximum power when driven to saturation, or 10 kw over a 15.5 Mc band, measured to the —0.5 db points. The overall unsaturated power gain is approximately 50 db with an efficiency of approximately 30 percent. The e.h.t. input to the klystron is between 16–18 kv at 3.5–4 amps.

Both the collector and drift tube are water-cooled, and, in the case of mains failure with resultant failure of the heat exchanger, there is enough water available to absorb the residual heat in the tube without further cooling.

The klystron beam is focused by a powerful electromagnet, requiring a dc power input of approximately 2.0 kw. The magnet also

requires water cooling. In the case of the Varian tube, tuning of the cavities is carried out by a tuning unit located on the top of the focusing magnet, and RF power output is read directly on a meter mounted on this unit. With the Eimac tube, the tuning controls are mounted on the side of the klystron assembly.

When using the Varian klystron, which requires bombardment of its cathode to maintain emission, it is necessary to control the filament and bombardment power accurately, and a magnetic amplifier is provided for this purpose.

The klystron RF output is fed into a waveguide, and thence via a cross-coupler to the aerial. By suitably calibrating the cross-coupler, the standing wave ratio in the waveguide is measured. If it exceeds a certain value, a protection unit operates, switching off the e.h.t. supply. A direct reading of the VSWR can be obtained by plugging a meter into a jack on a meter panel in the klystron cabinet. The cross-coupler also feeds a calibrated meter on the klystron tuning unit giving direct indication of RF output power.

Special precautions are also taken to protect the klystron against any arcs which might occur in the waveguide, causing damage to the klystron output window. A photoelectric cell is used to detect arcing and shut down the e.h.t supply.

Heat Exchanger

The purpose of the heat exchanger is to stabilize the temperature of the water supply cooling the klystron drift tube, collector, and focusing magnet, to within fairly close limits over a wide temperature range. It also keeps the water circulating around the artificial load at the same temperature when checking the RF power output of the transmitter. It is capable of handling a power dissipation of up to 65 kw. The coolant used is distilled water in a closed circulating loop. All the flow feeds are metered: each meter being fitted with contacts, so that a failure in any feed trips off the main e.h.t. supply. Similarly the water outlet temperature of the klystron is monitored by a temperature gauge, which operates a trip in the e.h.t. supply should the temperature reach dangerous limits due to pump or blower failure.

Flow control of the outlet feeds can be controlled by water valves located on the front panel. Water filters are used in appropriate parts of the cooling system to guard against blocking up the tubes of the klystron.

Conclusion

The aim in the design of this transmitter has been reliability which is of the utmost importance for work of this kind. It is hoped that its record will equal that of similar equipment operating in a quadruple diversity tropospheric scatter system, in which case the total "outage" time attributable to equipment failure during a year's continuous service was less than twenty minutes.

AUTHORS. *This chapter from the United Kingdom was contributed by the General Post Office, London, England. The foregoing section on the 1700 Mc Transmitter was authored by* E. A. RATTUE *and* D. L. COOPER-JONES *of Standard Telephones and Cables Limited, England.*

LOW-TEMPERATURE THERMAL NOISE SOURCE

Introduction

A matched waveguide termination was required as part of the noise temperature calibration facility in the receiving system at the Goonhilly earth station. For routine measurement of overall system noise temperature, this termination is at ambient temperature. For other noise measurements, and in particular for the measurement of the effective input noise temperature of the maser, the waveguide termination is cooled to 77°K by immersion in liquid nitrogen.

Design of the Termination

The termination consists of an absorptive

pyramidal load mounted inside a length of thick-walled copper waveguide, which provides an approximation to a constant temperature enclosure, even when only partially immersed in refrigerant. The adjacent section of waveguide has thin walls, made of an alloy of low thermal conductivity, in order to reduce the rate at which heat leaks into the refrigerant. A thin internal layer of silver ensures adequate electrical conductivity. The internal dimensions of the waveguide are those of R.C.S.C. waveguide No. 11, (i.e., 2.372 in. by 1.122 in.) Figure 10–47 shows two slightly different mechanical constructions of waveguide structure.

Before deciding on the type of absorptive material to be used, samples of various materials were tested by repeated cycles of immersion in liquid air. Of the two materials which were found suitable, one was a suspension of iron powder in a synthetic resin ("poly-iron"), cast in the laboratory, in a suitable mould, and the other was a commercial material, machined into the appropriate shape.

The samples were alternately cooled and warmed for several days, until it was established that when the temperature changes were not too sudden, serious cracking was unlikely, provided that water was excluded. However, if the samples were wet, the surface of the material became crazed and eventually broke up. It was therefore necessary to take suitable precautions to exclude condensed water vapor from the completed termination.

The shape chosen for the poly-iron load is shown in Figure 10–48. A symmetrical pyramidal shaped load, mounted centrally in the waveguide was found to be preferable to an assymetric, wedge-shaped load attached to the side of the guide. The pyramidal load

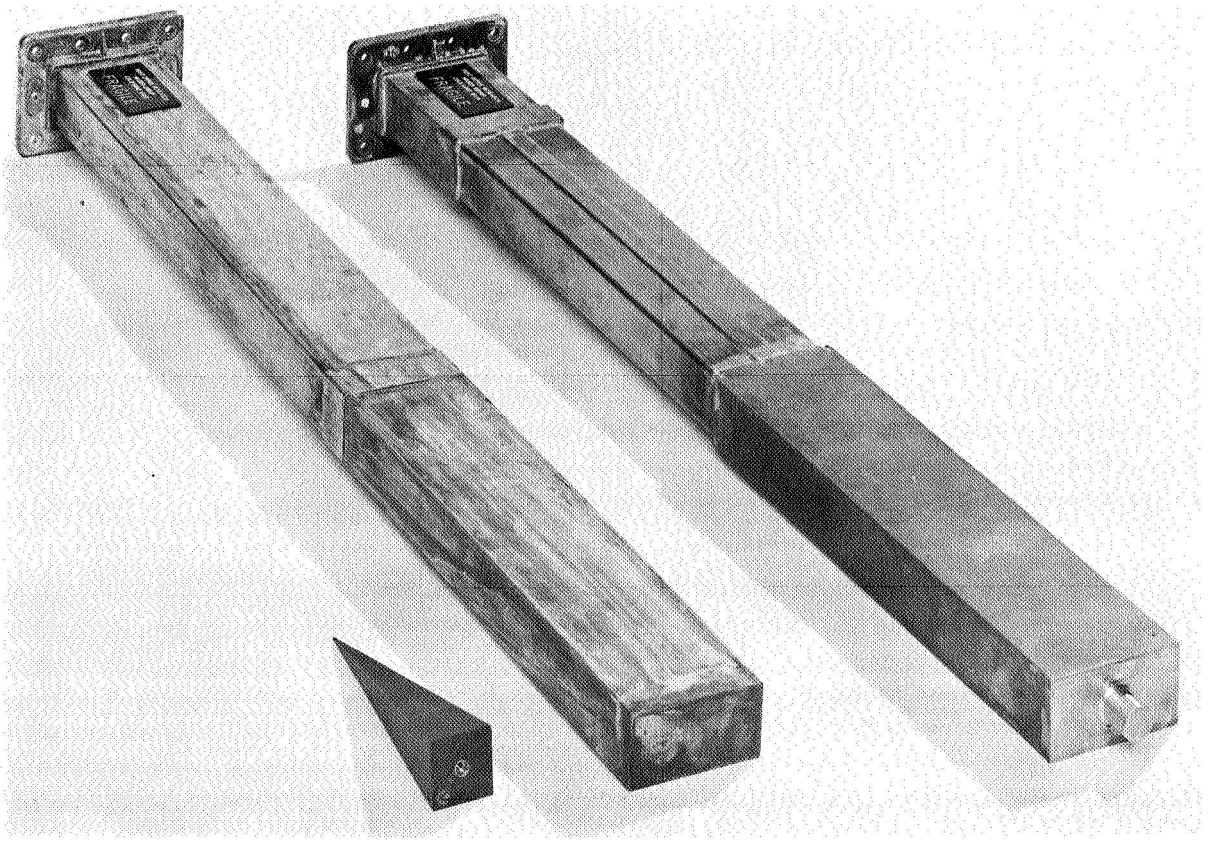


FIGURE 10–47.—Alternative types of cold termination and a poly-iron pyramid load.

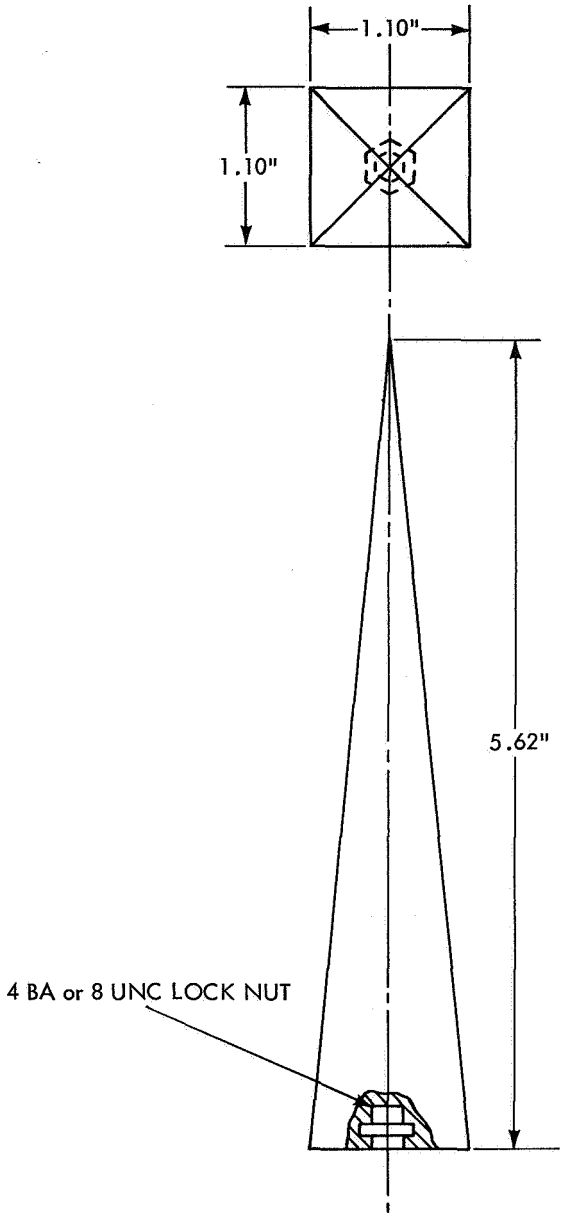


FIGURE 10–48.—Poly-iron pyramid load.

appears to be less likely to introduce small changes in impedance due to the absorptive material twisting or warping when cooled. The mounting screw is sealed with solder to prevent refrigerant leaking into the waveguide.

The residual VSWR of a termination using this type of load is, in general, better than 0.99 across the 3.8–4.3 Gc band.

Installation at Goonhilly

The general arrangement of the installation at Goonhilly Radio Station is shown in Figure 10–49. The equipment is located in the receiver cabin on the back of the parabolic reflector. The termination is mounted beneath the upper floor which is used for

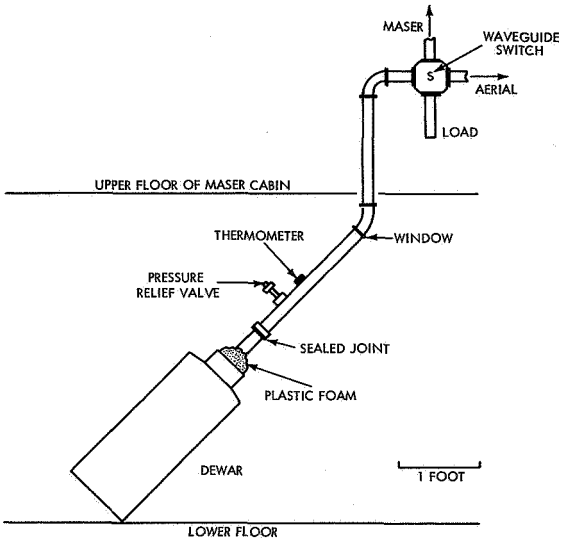


FIGURE 10–49.—Layout of cold load at Goonhilly.

maser operation. To prevent loss of liquid nitrogen when the aerial is moved in elevation, the termination and the metal dewar vessel surrounding it are mounted at 45° to the axis of the aerial. A binomially-corrected 45° waveguide corner was designed (with optimum performance at the receiver center frequency of 4.17 Gc) to connect the termination to the remainder of the waveguide.

To prevent the continuous entry of water vapor and oxygen which would condense in the cooled section of waveguide, a window is required. A simple uncorrected window of "Melinex" (I.C.I. trademark for polyethylene teraphthalate film) was found suitable. A thickness of 0.004″ introduced less than 0.005 db of attenuation, and no measurable change in the VSWR of the termination. The flanged joints between the window and the load were sealed with neoprene gaskets. A

spring-loaded relief valve was provided to prevent an excess pressure accidentally arising inside the waveguide and possibly rupturing the window and damaging the maser.

The VSWR of the termination was measured at the waveguide switch, at a frequency of 4.17 Gc. The value, 0.970, remained constant when the termination was cooled from 290°K to 77°K.

When the termination is used for the two-temperature method of measuring the maser noise temperature, it is necessary to correct for the additional thermal noise generated in the uncooled waveguide between the load and the maser. This amounts to 10°K.

The second termination for the two-temperature measurements is provided by a second pyramidal load at ambient temperature. This can be temporarily installed in the main waveguide in place of the usual flexible connection to the aerial feed. The thermal noise from the two loads can thus be compared by rotating the waveguide switch.

Conclusion

A waveguide-mounted thermal noise source for operation either at 77°K or at ambient temperature has been devised and installed as part of the receiver equipment at Goonhilly earth station, and used for noise temperature calibration throughout the experiments with the Telstar and Relay satellites.

AUTHOR. *This chapter from the United Kingdom was contributed by the General Post Office, London, England. The foregoing section on a Low-Temperature Thermal Noise Source was authored by* H. N. DAGLISH *of the GPO.*

THE HELIUM SYSTEM OF THE MASER INSTALLATION

Introduction

A traveling-wave solid-state maser amplifier is used to provide the first stage of amplification in the receiving system at the communication-satellite earth-station at Goonhilly Downs. While the maser itself was built by an industrial research laboratory, the auxiliary supplies and equipment essential for the operation of the maser were designed and built by staff of the Post Office Research Station. A major part of this auxiliary equipment consists of apparatus for handling the helium refrigerant.

General Description

The maser is a microwave amplifier in which the amplification takes place in a single crystal of "pink" ruby-crystalline alumina containing a small percentage of chromium. Microwave power, at a frequency of about 30 Gc, is injected into the crystal and temporarily disturbs the thermal equilibrium of outer electrons in the chromium ions in the crystal. Some of the energy stored in this way is available to amplify a low-level signal at a frequency of 4.17 Gc. The particular frequencies involved are determined by an applied steady magnetic field. The particular property of the amplifier which makes it so important for use in satellite communication is its ability to amplify extremely weak radio signals while introducing a negligible amount of additional background noise. A disadvantage is that it will only operate at very low temperatures. The present equipment requires a temperature lower than 2°K (i.e., −271°C) and the only possible method of obtaining such a low temperature is to immerse the amplifier in liquid helium. This normally boils at 4.2°K, but the lower temperature required for the maser can be produced by causing the helium to boil at a reduced pressure. A large vacuum pump must therefore be incorporated into the apparatus.

If the maser and all the associated equipment could have been mounted in close proximity, the installation would have been relatively straightforward. However, to make use of the unique low-noise properties of the maser, it was essential that it be mounted as near as possible to the focus of

the 85 ft. parabolic reflector, while the remainder of the equipment had to be mounted in the rotating cabin or at ground level.

It was not practicable to mount the maser actually at the focus because of its weight and because there was already a considerable amount of aerial-feed equipment at the focus. The maser was therefore housed in a cabin constructed on the back of the parabolic reflector, and connected by waveguide to the feed equipment at the focus.

Thus the complete installation consists of the helium control equipment associated with the maser, a vacuum line along and down the aerial structure to the vacuum pump, together with the equipment for controlling the flow of helium gas from the vacuum pump and storing this helium for return to the liquefaction plant. The location of the various items is indicated in Figure 10–50.

During operation, the axis of the aerial may be tilted between horizontal and 10° beyond vertical, and consequently all the equipment in the maser cabin, including the klystron and magnet power supplies, a small oscilloscope, a nitrogen-cooled reference load and the maser itself, must operate satisfactorily when tilted by 100°. To prevent refrigerant from spilling from the maser as the aerial tilts, it was mounted at an angle of 45° to the axis of the aerial, so that the maser axis is never more than 55° from vertical. However, access to the aerial cabin to fill the maser with refrigerant is only possible when the aerial axis is horizontal, so that the maser must be capable of being tilted in its cradle from the normal operating position through 45° to the vertical position for filling. The helium-gas handling system must also provide for the maser to be tilted inside the cabin, and, when the aerial is in use, for the cabin to tilt with respect to the ground without restricting the flow of helium gas. Sections of corrugated stainless steel tube are used to provide this flexibility.

Special quick-release waveguide flanges were designed to permit the maser to be tilted through 45° into the filling position, as shown in Figure 10–51.

Liquid Helium and Liquid Nitrogen

Liquefied gases are usually contained in metal dewar vessels, which are spherical flasks with a double wall, the space between the walls being evacuated to provide thermal insulation. The latent heat of helium is so

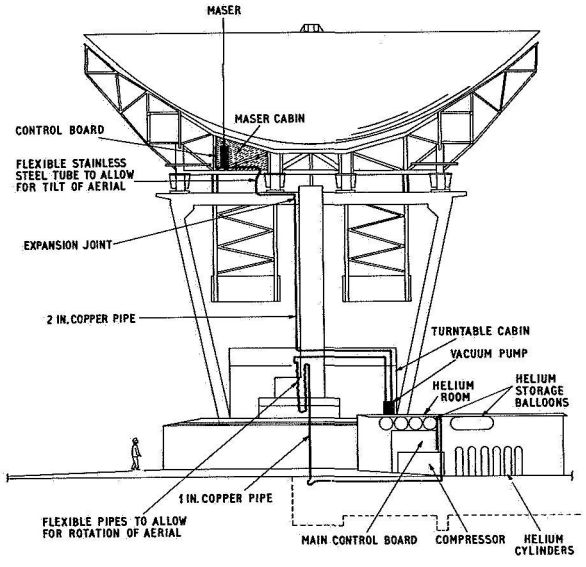


FIGURE 10–50.—Position of the maser and helium equipment on the Goonhilly aerial.

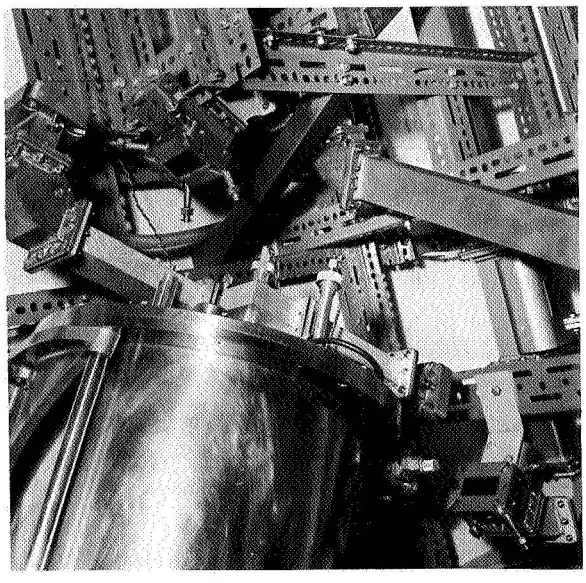


FIGURE 10–51.—The top of the maser tilted to show the quick release flanges.

low that this form of thermal insulation is inadequate. The maser is therefore mounted inside a double vacuum-insulated dewar, with the outer vessel containing liquid nitrogen. Equipment was provided for re-evacuting the insulating spaces in the maser dewar when necessary.

Double dewars must also be used for transporting and storing liquid helium. All supplies of liquid nitrogen and liquid helium are delivered by rail from a liquefaction plant in London to Cornwall two or three times a week.

The temperature of liquid helium is lower than the freezing point of both oxygen and nitrogen, and it is necessary to take precautions to prevent air from freezing inside the neck of the dewar vessels. A non-return valve must therefore be fitted to the dewars, allowing helium gas to boil away from the liquid, but preventing air from entering.

Cooling the Maser

The maser is mounted in its tipping cradle on one wall of the maser cabin, as shown in Figure 10–52. Above it on the wall is a control panel that enables the flow of helium gas to be regulated, and the pressure in the maser to be measured. A flexible stainless steel tube connects the maser to the control panel. Electrical monitoring equipment is also mounted on this panel, indicating the output of the klystron oscillator and the level of helium in the maser.

Figure 10–53 shows dewars of liquid helium and liquid nitrogen being lifted by a hydraulically-operated platform to the portal beam of the aerial, from which they can be carried to the maser cabin. Here, the liquid-nitrogen dewar is connected to an insulated transfer tube permanently installed in the cabin. Compressed nitrogen from a cylinder is used to force the liquid nitrogen along the thermally-insulated tube into the outer part of the maser dewar.

When the outer vessel of the maser dewar is full of liquid nitrogen, the inner vessel is filled with liquid helium. The helium-storage dewar is placed on a hydraulically-operated lift-platform beside the maser dewar, and a transfer tube is inserted into the two dewars. This transfer tube, which can be seen in Figure 10–54, has a vacuum-insulated double wall, to prevent the boiling of helium inside the transfer tube due to heat entering through the walls. A bladder attached to the helium-storage dewar is used to start the helium transfer. A gentle squeezing action agitates the liquid in this dewar, causing increased evaporation. The gas pressure so produced forces the liquid helium through the transfer tube. As the level of the helium rises in the maser dewar, the storage dewar and transfer tube are raised to keep the outlet of the transfer tube above the liquid surface in the maser dewar.

Great care must be exercised during the transfer to prevent air or water entering the dewars. When the dewar containing the maser is full, the transfer tube is rapidly removed

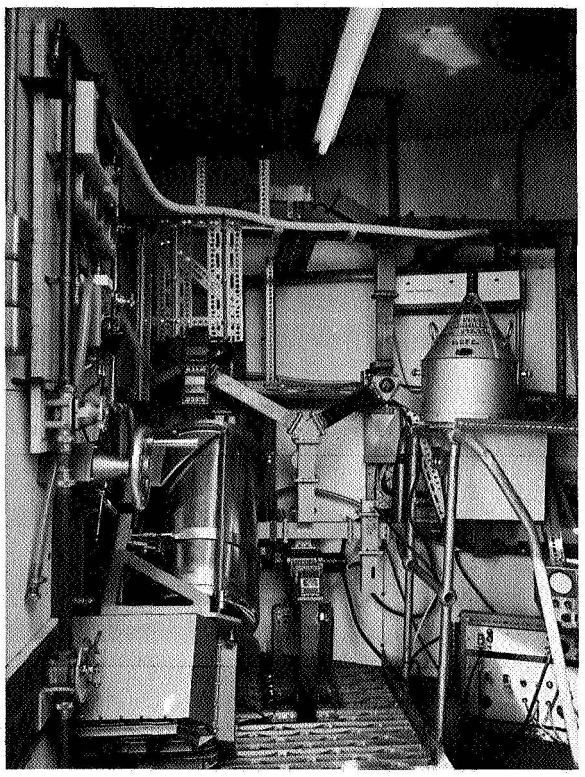


FIGURE 10–52.—The maser in the operating position showing the 12 liter dewar.

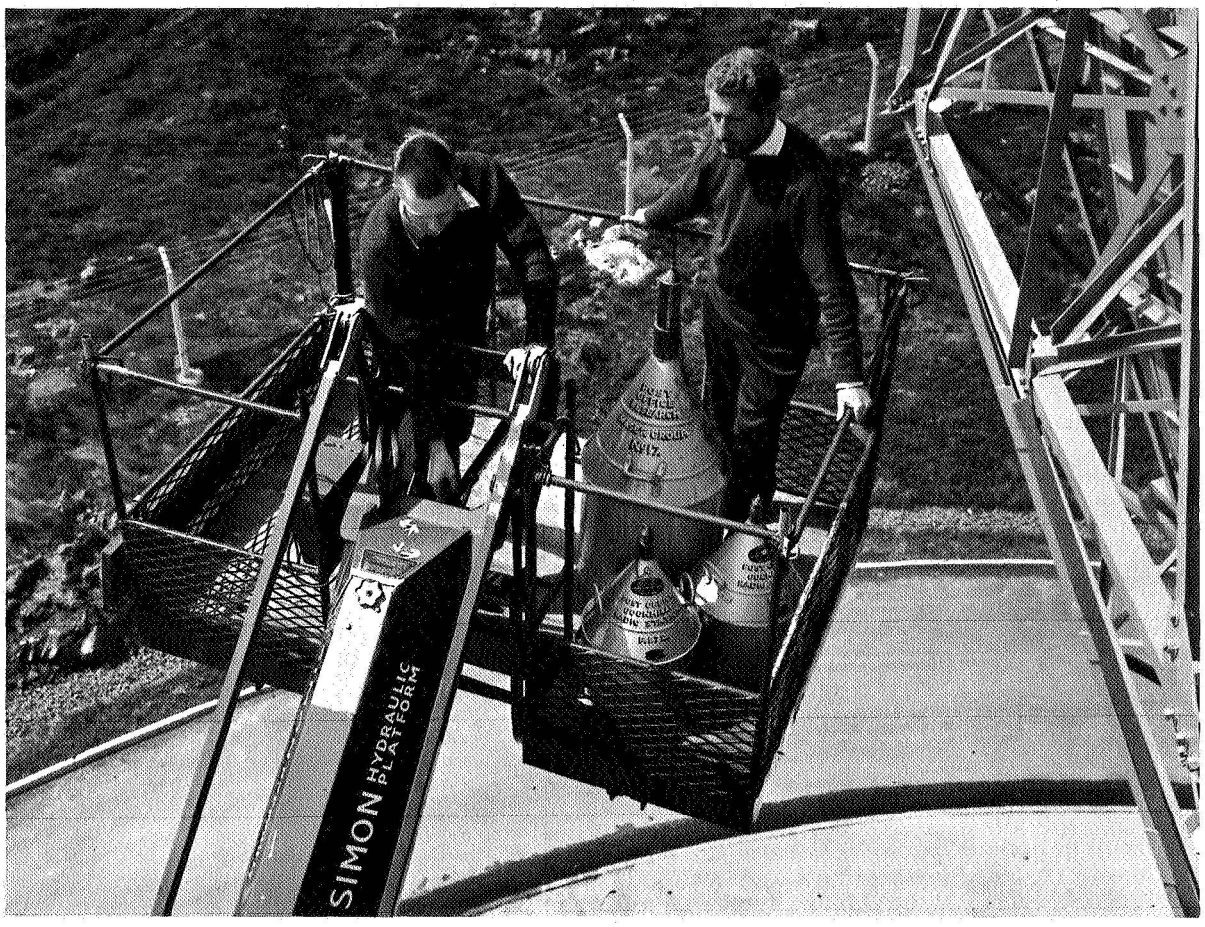


FIGURE 10–53.—Dewars of liquid helium and liquid nitrogen being lifted to the maser cabin.

and the entry port sealed. During the helium transfer, a considerable amount of liquid is evaporated in cooling the structure to 4.2°K. The helium gas so evolved passes along the flexible tube to the control panel, and thence into the helium collection system.

Immediately the maser dewar has been filled and the filling port sealed, the pressure must be reduced to a few torr (mm mercury) in order to lower the helium temperature from 4.2°K. The rate of change in the pressure must be controlled carefully in order to prevent damage to the maser. A special adjustable throttle valve was designed to control the rate of change of pressure during the initial stage of pump-down.

The version of the maser installed initially was built into a relatively small commercial helium dewar. More recently, a new dewar has been installed to give an extended maser operating life. This dewar, shown in Figure 10–52, holds approximately 12 liters of liquid helium.

The operating procedures devised for the small dewar have proved quite adequate for the new installation. The principal change has been an increase in the time needed to fill the dewar because of the greater volume of liquid, and the increased mass of metal to be cooled. Operationally, the increased helium capacity has enabled several successive Telstar and Relay passes to be used without refilling the maser. It has also been possible to carry out the maser filling some hours in advance of a satellite experiment, when this has been desirable.

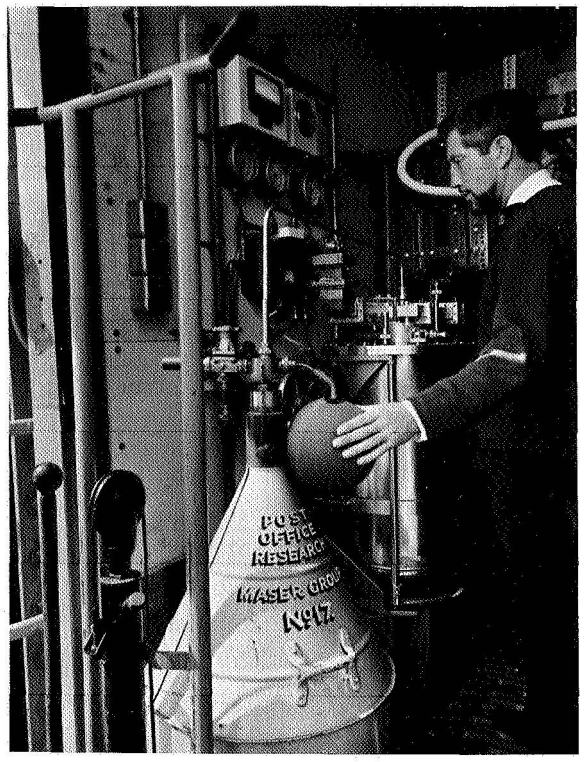


FIGURE 10–54.—Helium transfer into the maser.

The Main Vacuum Line

As already mentioned, the nearest position to the maser which could be used for the vacuum pump was in the turntable cabin. The main vacuum line between the maser cabin and the pump therefore had to be about 80 ft in length. Two-inch diameter copper pipe was used, with joints and bends assembled from commercial fittings, silver soldered into position. The pipeline was constructed in sections on the ground and these sections were joined by vacuum flanges sealed with rubber rings and bolted together by stainless steel bolts.

A great deal of care was taken in assembling the system, to eliminate possible sources of contamination or leakage. Apart from directly reducing the purity of the recovered helium, any volatile contamination in the pipeline would increase the background pressure in the system, making subsequent detection of possible leaks much more difficult. The success of the whole installation depends upon the quality of the silver-soldered joints and upon the cleanliness of the system, therefore elaborate cleaning and leak-testing procedures were devised and followed during the installation.

The 2-in. pipe is supported by a series of brackets fixed to the waveguide ladder which runs alongside the vertical center member of the concrete aerial structure. The weight of the pipe is taken on a special flange located near the base of the ladder and a flexible stainless steel section near the top permits small residual movements.

The Vacuum Pump

In order to handle large quantities of helium, a vacuum pump of large capacity is needed. The rate at which helium gas would be evolved could not be known in advance, as it depends upon the constructional details of the maser structure. A large margin of safety was therefore desirable when specifying the required pump performance. A pump with a capacity of 36 ft^3/min. was fitted; this was the largest available air-cooled vacuum pump, air cooling being very desirable to avoid the necessity for an additional water-circulation system on the aerial.

A remotely controlled valve is used to provide a low impedance path round the pump while the maser is being filled.

The Helium Recovery Apparatus

The output from the vacuum pump cannot be exhausted to the atmosphere in the usual way, but must be piped away for recovery. Accordingly, a 1 in. diameter copper pipe is connected to the output of the pump to carry the helium over the transmitting equipment to the rotating joint at the center of the turntable cabin. To carry the helium through this rotating joint four 17 ft lengths of nylon-reinforced P.V.C. tube are used, hanging as U-loops, connected in parallel. As the aerial rotates, the loops wind round a central pylon, permitting a movement of $\pm$ 250° from the central position. From the bottom of the central pylon the copper pipe goes through underground ducts to the helium room, which

is part of the building housing the aerial control gear.

The total length of the 1-in. pipe is about 120 ft and the same care over cleanliness was observed in its fabrication as for the 2-in. vacuum section.

The helium room, shown in Figure 10–55, contains a large control panel to handle the helium gas which is now at atmospheric pressure. This panel is fitted with over 20 vacuum-type valves to interconnect the pipe which brings the helium gas from the vacuum pump, the temporary gas store, and the compressor. A flowmeter is included, to monitor the rate of evolution of helium gas from the maser.

The helium store consists of rubberized canvas balloons suspended beneath the ceiling, each balloon holding up to 17 ft of helium. The initial installation of six balloons has been increased to 16, to give adequate storage for extended periods of maser operation.



FIGURE 10–55.—The helium collection room.

For return to the liquefaction plant, the contents of the balloons must be compressed into steel cylinders. A modified commercial air compressor is used to compress the helium to 1000 lb/in^2. Additional facilities are required to collect gas released from the pump and the starting bypass valve, which are normally open to the atmosphere in an ordinary air compressor. Helium, which is a monatomic gas, becomes hotter than diatomic oxygen or nitrogen during compression. To avoid damaging the compressor by overheating, it must not be used for more than 10–15 minutes at any one time when compressing helium. The full cylinders are returned by rail to the liquefaction plant in London, for the cycle to begin again.

Also visible in Figure 10–55 is the continuous chart recorded, connected to the resistance thermometers in the maser dewar. A continuous indication of helium level is thus always available.

Conclusion

The helium system at Goonhilly was commissioned on 25 June 1962, having been completely designed and constructed in four months. The general features of the system have proved satisfactory in operation, requiring little modification to the original conception, although a number of changes have been introduced to simplify the filling of the maser with liquid helium.

The great care taken in construction and operation of the helium system has been justified by the high level of purity attained for the returned gas.

AUTHORS. *This chapter from the United Kingdom was contributed by the General Post Office, London, England. The foregoing section on the Helium System of the Maser Installation was authored by* H. N. DAGLISH, M. R. CHILD, *and* A LEVITT *of the GPO.*

DEMODULATING TECHNIQUES

Introduction

As part of the program of experimental and development work to determine the optimum demodulating techniques for communication satellite systems, three types of demodulators have been investigated at the Goonhilly earth station; these are:

1. A conventional demodulator of the type used in 960-channel telephony or television microwave radio-relay links.
2. A frequency modulation feed-back demodulator in which the deviation of the signal is reduced before it reaches the final discriminator.
3. A variable-bandwidth "dynamic-tracking" demodulator in which the resonant frequency of a narrow bandwidth tuned circuit is moved rapidly to follow the nominal instantaneous frequency of the incoming signal.

The conventional demodulator will not be discussed in detail here; however, information is given on two specialized demodulators.

Up to a point, the baseband signal-to-noise ratio at the output of a broadband frequency-modulated microwave system can be improved by increasing the deviation. To accommodate the wider deviation signal, increased receiver bandwidth is required. If the noise temperature and gain of the receiver remain constant, the increased bandwidth will result in more noise reaching the limiter stage which precedes the discriminator. Thus, for the same received signal level the effective signal-to-noise ratio will be decreased.

So long as the instantaneous peaks of noise at the limiter input always remain a decibel or two below the carrier level, normal operation of the demodulator is maintained, i.e., changes of x db up or down in the carrier level will result in corresponding changes of approximately x db in the ratio of signal-to-basic noise measured at the baseband output. But when the peaks of noise are approximately equal to the carrier, a threshold condition is reached where any further decrease in carrier-to-noise ratio results in a much more than directly corresponding decrease in baseband signal-to-noise ratio.

For signals above the threshold level, good conventional demodulators of the types used in line-of-sight microwave links perform quite satisfactorily and nothing is to be gained by using more complex demodulating equipment. This will probably be the state of affairs under normal conditions in operational satellite systems. But when abnormally low-level signals have to be received, or when the noise level is unusually high, e.g., due to heavy rainfall, it is highly desirable that the demodulator should have the lowest possible threshold level. That is to say the demodulator should continue to operate down to the lowest practicable signal level before the output signal-to-noise ratio crashes catastrophically; under these conditions very complex demodulating equipment is justified, even if it lowers the operational threshold by only a few decibels.

A number of techniques are known or have been proposed for obtaining a lower threshold, but the basic principle of all involves either enhancement of the carrier or restriction of the effective bandwidth before demodulation. Baseband signal processing after demodulation (e.g., low-pass filtering) can effect the overall signal-to-noise ratio obtainable with any form of demodulator, but will normally have only a second-order effect on reliative performance of various demodulators and a virtually neglible effect on attainable threshold levels.

Frequency Modulation Feedback Demodulator

Design Features

The frequency modulation feedback demodulator follows the general principles laid down by Enloe* and is shown in block schematic form in Figure 10–56. It accepts an input signal at a mean frequency of 70 Mc, up-converts to a mean frequency of 3590 Mc

*L. H. Enloe: "Decreasing the Threshold in F.M. by Frequency Feedback", Proc. I.R.E., January 1962.

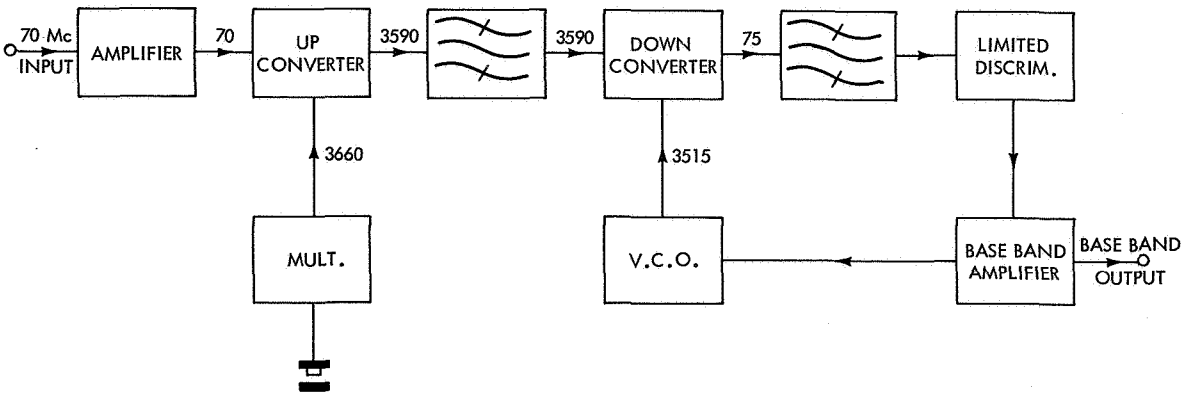


FIGURE 10–56.—FMFB demodulator, block diagram.

and then down-converts again to 75 Mc. The local oscillator for up-conversion is crystal controlled; but the oscillator used for down-conversion is a klystron which is frequency modulated in such a manner that the deviation of the final IF signal is reduced. The modulating signal for the klystron is obtained from the output of the final 75 Mc demodulator.

The version of this demodulator which is installed at Goonhilly normally operates at one or other of two fixed bandwidths; however, experiments have been carried out using continuously variable bandwidth facilities, so that the operating conditions can be more accurately adjusted to optimum for the signal level or modulation being received.

Performance

For television signals the threshold of the FM feedback demodulator is some 4 to 5 db below that for a conventional demodulator when operated at adequate bandwidth to allow satisfactory reception of both the video signal and the sound subcarrier.

The performance for 240-channel telephony signals is indicated by the curves in Figure 10–57. It will be noticed that the FM feedback demodulator provides appreciable improvement over a conventional demodulator (No. 6B) at values of IF signal-to-noise ratio below 10 db; however, a further improvement in this region would be required to meet accepted international standards of performance.

Figure 10–58 shows the baseband frequency response under open and closed-loop conditions.

Dynamic-Tracking Variable-Bandwidth Demodulator

Principles Involved

Automatic control of the IF bandwidth prior to limiting is already quite well known as a method of improving threshold performance of a receiver demodulator in fairly low deviation FM systems. In essence such an arrangement maintains normal receiver bandwidth until the input signal drops to a level close to threshold, but for still lower levels of signal the effective bandwidth of the receiver is progressively reduced. This reduced bandwidth lowers the total noise and hence the threshold, at the cost of rapidly rising distortion. The occasional rises in intermodulation noise which result from restricted bandwidth are generally to be preferred to the relatively severe bursts of noise which occur when a fading signal drops below threshold—especially in lightly-loaded telephony systems.

An automatic bandwidth control arrangement of this type is particularly useful for rapidly fading signals and was used very successfully in Post Office tests on a tropospheric-scatter link during 1959–1960; but

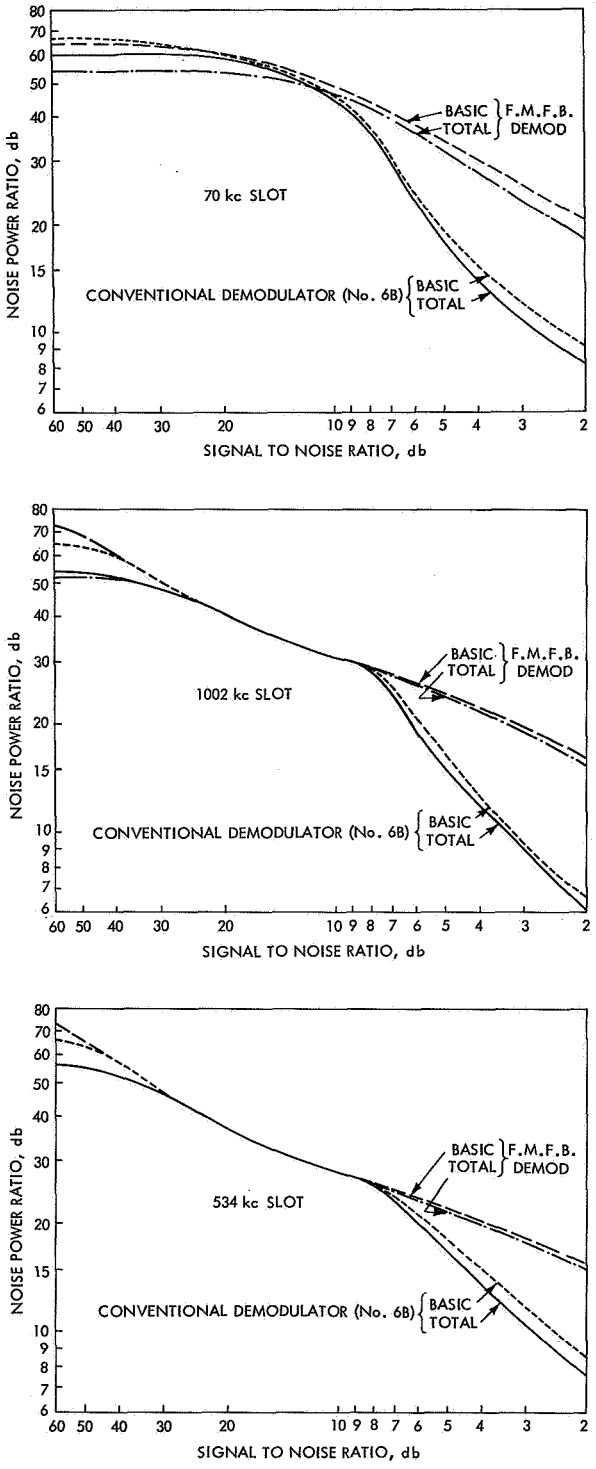


FIGURE 10–57.—FMFB demodulator, comparison with conventional demodulator (No. 6B).

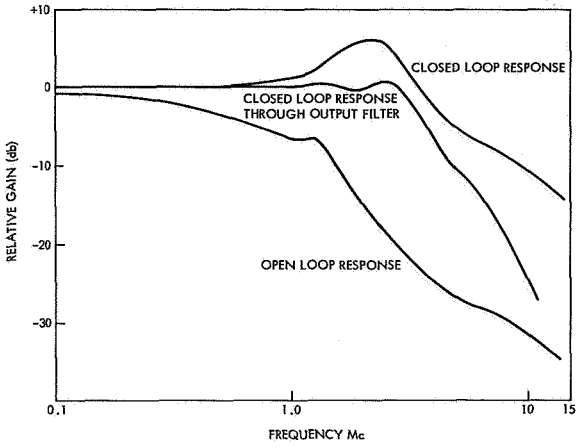


FIGURE 10–58.—FMFB demodulator, baseband frequency response.

it is not suitable for use in wide-deviation television systems.

It has been pointed out by Baghdady* that in many wide-deviation FM systems, only limited parts of the total signal bandwidth are carrying essential information at any specific moment, and that it should be possible to improve the threshold by a narrow-band IF filter provided that the filter could be tuned rapidly enough to follow the changing location of the main energy in the signal spectrum. Baghdady describes such a system in outline and calls the device a dynamic selector.

Design Features

A simplified block diagram of the demodulator is shown in Figure 10–59. A single tuned circuit is used as the variable filter, and a varactor diode forms the tuning element. Variation of the bandwidth is accomplished by alternating dc current through a thermistor bead.

The relationship between frequency and voltage which the varactor diode provides is non-linear, but this is compensated by shaping networks in the video amplifier.

A number of different ways of varying bandwidth were tried; but the majority of

*E. J. Baghdady: "Lectures on Communication System Theory," 1961, Chapter 19.

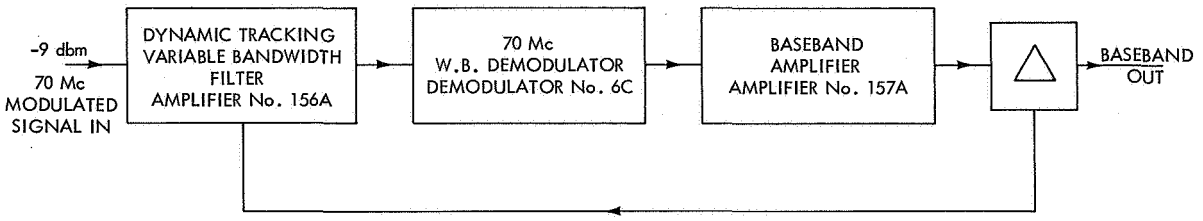


FIGURE 10–59.—Goonhilly radio station: dynamic tracking demodulator.

these resulted in tuning changes, and a thermistor was found to be the most satisfactory device.

The 3 db bandwidth of the tuned circuit is adjustable from about 2 to 20 Mc, but the narrowest bandwith is rarely useable in practice. A useful feature of the arrangement is that, under wideband (i.e., high signal level) conditions, the overall performance becomes virtually that of the associated high-grade conventional demodulator. The automatic bandwidth control is adjusted to maintain full bandwidth until the signal falls to within a decibel or two of threshold, and then decreases bandwidth at a rate of approximately 2 to 1 for a 3 db drop in signal.

Performance

For television reception under the usual conditions used for tests on Telstar and Relay, this modulator gives an average threshold improvement of about 4 or 5 db. The improvement is greatest on fairly uniform areas of grey, or on areas of slowly changing brightness; but is limited by noise in regions where there is a sudden change in brightness, due to inability of the narrow-band circuit to follow fast enough. This feature can result in some roughness of vertical edges under conditions of very low signal-to-noise ratio, which can be considerably reduced by fly-wheel synchronization, or synchronizing-pulse restoration.

The dynamic-tracking demodulator gives optimum results only if the incoming television signal includes a dc component, i.e., when specific frequencies correspond to the synchronizing pulse, black and white levels in the video waveform. It is less effective if the earth-station transmitter originating the signals uses no pre-emphasis and mean-frequency automatic frequency control. Furthermore, if the bandwidth restriction is excessive, cross modulation from the video channel into the sound-subcarrier channel may occur.

The variable-bandwidth dynamic tracking demodulator is considered unsuitable for multi-channel telephony, and it is probable that a simple variable-bandwidth system (i.e., without the tracking feature) may be preferred.

Possibilities for Further Improvement of Demodulator Performance

Noise Limiting Techniques

At the output of a wideband demodulator operating at or just below threshold, the noise peaks are very narrow. It is suggested that a peak-clipping device might be used at that point to restrict the video signal to limits appropriate to the white and synchronizing pulse levels, and if the bandwidth is subsequently restricted, (e. g., to 3 Mc) the amplitude of the noise peaks will be still further reduced. The clipping must take place before the video bandwidth is restricted.

It is possible that still further suppression of these short duration noise peaks could be obtained by arranging for automatic variation of the clipping levels, especially if the main signal can be very slightly delayed and advance information on its levels obtained from an earlier part of the circuit.

Alternatives Sound Channel Arrangement

The use of a sound subcarrier at 4.5 Mc necessitates, for television a minimum IF

bandwidth of slightly over 9 Mc. If this subcarrier is eliminated an IF bandwidth of just over 6 Mc would give a full bandwidth video response. In difficult reception conditions some restriction of video bandwidth is permissible and the effective IF bandwidth could then be further reduced. For example, a 2.5 Mc IF bandwidth would represent an improvement of about 10 db in threshold relative to a conventional demodulator of 25 Mc bandwidth.

Conclusions

When the carrier/noise ratio is appreciably greater than that corresponding to threshold conditions, a conventional demodulator is to be preferred. At carrier/noise ratios (measured in 25 Mc bandwidth) less than 10 db, there is some benefit from the specialized demodulators, and at carrier/noise ratios less than 6 db there is a marked benefit.

It is possible that further development work on noise limiting techniques in demodulators might result in yet better performance, and there is no doubt that elimination of the sound subcarrier, e. g., by transmission of the sound on pulses within the synchronizing interval of the television signal, would greatly increase the threshold margin for television under difficult conditions.

AUTHORS. *This chapter from the United Kingdom was contributed by the General Post Office, London, England. The foregoing section on Demodulating Techniques was authored by* R. W. WHITE *and* R. J. WESTCOTT *of the GPO.*

THE TRAVELING WAVE MASER AMPLIFIER

Introduction

The design and performance of the 4170 Mc Traveling Wave Maser at present installed at the G.P.O. Radio Station, Goonhilly Downs, is described. Means of increasing the bandwidth of the device are discussed.

System Requirements and Maser Specification

The signal entering the first stage of the Goonhilly receiver is very small, about 10^{-12} watts, and the bandwidth of the system is some tens of megacycles. If the received signal is to be amplified and detected with an acceptable signal to noise ratio then it is essential that the noise contribution made by the first stage amplifier should be as small as possible. It was therefore decided that the first stage amplifier should be a solid state traveling wave maser having sufficient net gain to make the noise contribution of the second stage amplifier insignificant. The specification for this traveling wave maser is as follows:

Signal frequency	4170 Mc
Gain (minimum)	20 db
Bandwidth to 3 db points	25 Mc
Noise temperature	15°K
Input VSWR	0.666 over the operating band
Operating life per filling of liquid helium	8 hr.

Design of the Maser

The overriding consideration in the design of this maser was the need to produce an engineered and operating device within some six or seven months of the initiation of the project. Sophistication in the design therefore was subordinate to expediency and as far as possible use was made of immediately available materials and techniques.

Active Materials

Because of its ready availability in large single crystals and also because of its proven characteristics, synthetic ruby was selected as the active material. Previous experience indicated that the best orientation for maser operation at frequencies below 7 kMc is that in which the applied magnetic field is at right angles to the c-axis of the ruby. In this orientation the ground state of the Cr^{3+} ion is split by the combined action of the crystal fields and the applied magnetic field accord-

ing to the energy level diagram in Figure 10–60.

It has been found experimentally that when the separation of levels 1 and 2 corresponds to a frequency of 4170 Mc the greatest inversion of the populations of these levels can be obtained if the pump is applied between levels 1 and 4, i.e., at a frequency of 30,150 Mc. In ruby having a Cr to Al ratio of 0.05 atoms percent we find that 1–4 pumping produces an inversion ratio of 2.7 at 1.4°K.

Operation at 1.4°K involves reduction of the liquid helium bath pressure to about 2.5 mm Hg. In practice this is accomplished within less than half an hour of filling and in an experimental system such as this where operation over more than three successive satellite passes is rarely required, this is no disadvantage.

Assuming that the excitation at the signal frequency is by an RF magnetic field circularly polarized in the plane perpendicular to the applied field (a condition which is closely approximated in practice) and using the tables of transition probabilities prepared by Chang and Siegman* we calculate that 1–4 pumping in 0.05% ruby at 1.4°K will produce a value of Q_m of $-15/\eta$.** Q_m is the magnetic quality factor of the structure and is essentially a measure of the ratio of the energy stored in the structure to the power absorbed by the maser material, η is the filling factor of the maser and is the ratio of the mean square RF magnetic field over the volume of the maser crystal to that over the volume of the propagating structure. Although filling factors up to 0.5 are theoretically possible in a traveling wave maser, experience suggests that 0.2 is a practical figure. Taking $\eta = 0.2$ we have $Q_m = -75$ as a basis for design.

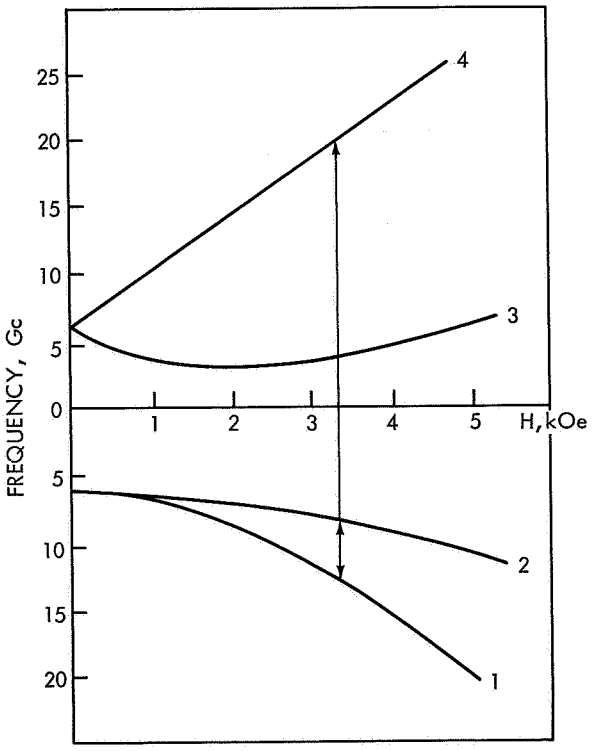


FIGURE 10–60.—Energy level diagram (Ruby, $\theta = 90°$).

Non-Reciprocity

A traveling wave maser exhibits some nonreciprocity by virtue of the fact that circularly polarized fields of opposite sense interact to different extents with the active ions.*** However, additional non-reciprocal backward loss must be provided if a completely stable device is to be obtained. Polycrystalline yttrium iron garnet is a suitable material for this purpose as its absorption line width is reasonably narrow (c. 150 oersteds) even at liquid helium temperature. Because of its high susceptibility only a small volume of this material needs to be incorporated in the maser. The dimensions of the yttrium iron garnet (Y.I.G.) are adjusted in order that resonant interaction at the signal frequency can be obtained with the same applied field as is required to give the correct ruby energy level splitting. In the present case the field is 3280 oersteds and an appropriate shape for the Y.I.G. is a flat disk of aspect ratio 0.1 with the plane of the disk perpendicular to the applied field.

*W. S. C. Chang, and A. E. Siegman, Stanford Technical Report 156–2, 1958.

**J. C. Walling, "Low Noise Electronics" (ed. K. Endressen) p. 225, Pergamon Press, 1962.

***J. Osborne, Phys. Rev., *67*, 351, 1945.

Obviously it is necessary that the Y.I.G. disk should be incorporated in the traveling wave maser in such a way that they are acted upon by a substantially circularly polarized RF field of opposite sense to that acting upon the ruby. This is accomplished by making use of a comb slow wave structure as described in the following section.

Slow Wave Structure

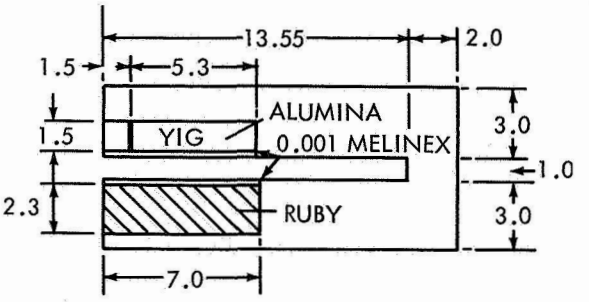
The small signal gain of a traveling wave maser can readily be expressed in terms of two quality factors, Q_m, the magnetic Q discussed above, and Q_o, the intrinsic Q of the propagating structure determined by ohmic and dielectric losses and also the forward loss of the Y.I.G. If r is the slowing factor (the ratio of the group velocity in the propagating structure at the signal frequency to the free space velocity of light) and N is the number of free space wavelengths in the structure, the net gain of the device, expressed in decibels is:

$$G = 27.3\, rN \left(\frac{1}{Q_m} - \frac{1}{Q_o} \right)$$

A structure having a slowing factor of 100 and an active length of 1.6 free space wavelengths (which is a convenient figure at a frequency of 4170 Mc) will therefore give an electronic gain of 58 db if $Q_m = -75$.

A suitable slow wave structure for the traveling wave maser then is one having this slowing factor and containing regions in which the RF magnetic field is circularly polarized, the structure must also allow propagation of the pump frequency, not necessarily in a slow mode.

All these requirements can be met by structures consisting essentially of an array of parallel conductors in which the RF magnetic field is substantially circularly polarized, the senses of polarization on the two sides of the array being opposite.



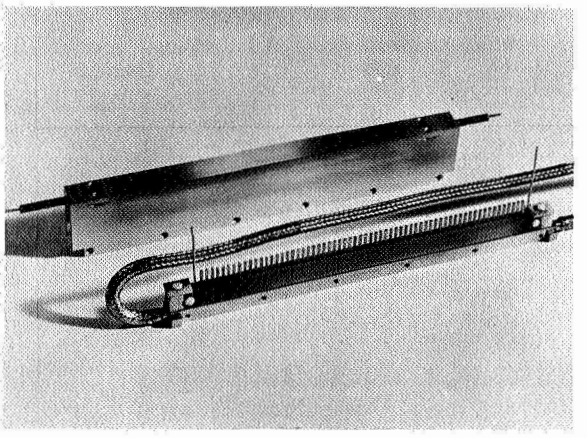


FIGURE 10–61.—4170 Mc comb structure.

A comb structure* is used in the present maser and has dimensions as indicated in Figure 10–61, the positioning of the ruby, dielectric and Y.I.G. disk in the structure is apparent from this figure.**

The dispersion characteristic for this structure when containing liquid helium is similar to that shown in Figure 10–62, and the slowing factor at the signal frequency is 110. The comb is milled from a block of high conductivity copper. This form of construction tends to minimize conductor losses. (The

*R. W. DeGrasse, E. O. Schulz du Bois, and H. E. D. Scovil, Bell Syst. Tech. J., *38*, 305, 1959.

**P. N. Butcher, Proc. I. E. E., *107B*, 341, 1960.

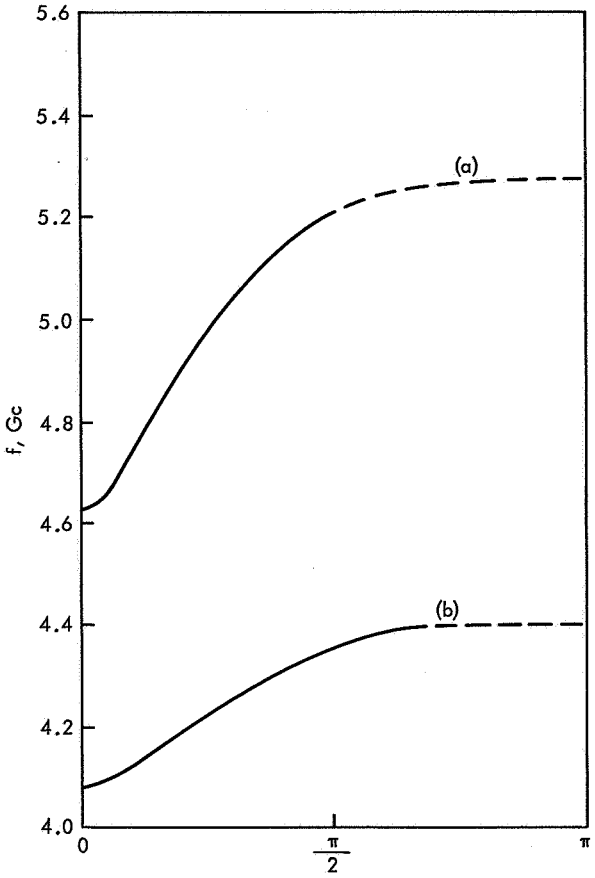


FIGURE 10–62.—Phase change per conductor.

slowing factor of 110 quoted above was inferred from the observed pass band of the structure, subsequent measurements of the ω-β characteristic of a similar comb suggest that this is over-estimated by about 10 percent.)

Input Leads

The input and output leads to the maser are air dielectric coaxials of low thermal conductivity (silver plated copper nickel). The leads have an outside diameter of 15 mm and a characteristic impedance of 72 ohms. It is important that these leads have a low electrical loss as they make the main contribution to the maser noise temperature. At the cryostat head these leads terminate in vacuum sealed waveguide to coaxial transitions. At their lower end the leads have tapered transitions to 5 mm OD coaxials having P.T.F.E. dielectric. These latter coaxials are matched to the comb by means of the arrangement shown in Figure 10–63. Some adjustment of the separation between the matching conductor and the first finger of the comb is necessary if the optimum match is to be secured over the pass band of the structure.

The pump power at 30,150 Mc is supplied by way of thin walled (0.2 mm) copper nickel waveguide with the internal dimensions of WG22. Approximately 40 mw is required to saturate the pump transition, this output power is obtained from selected R9518 klystrons.

In this connection we may note that operation at 1.4°K calls for substantially less pump power than does operation at 4.2°K and thus, although with a given pump source, pump frequency stabilization may be necessary for 4.2°K operation, it is not necessary for 1.4°K operation. No pump frequency stabilization is provided in the present maser.

Maser Packaging

The final form of the maser package depends on the form of magnet used. Superconducting magnets by virtue of their light weight and very high stability are attractive for use with masers operating at liquid helium temperatures and at the outset of the development of the Goonhilly maser it was hoped to make use of superconducting magnets. It soon became apparent, however, that the construction of a superconducting mag-

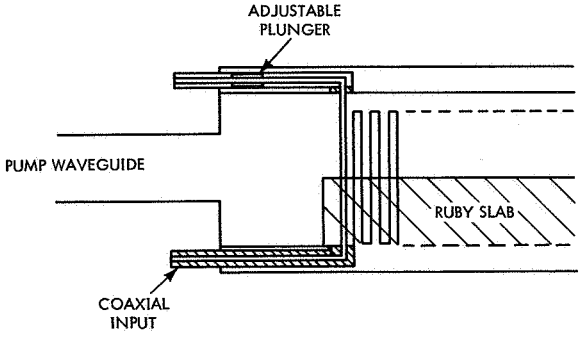


FIGURE 10–63.—Matching unit (schematic).

net giving the requisite field homogeneity was a matter of some difficulty and in view of the short time available for development, a permanent magnet version of the maser package was constructed as a parallel development. The permanent magnet version of the maser is illustrated in Figure 10–64 in which the trimming coils used to adjust the field of the permanent magnet are clearly visible.

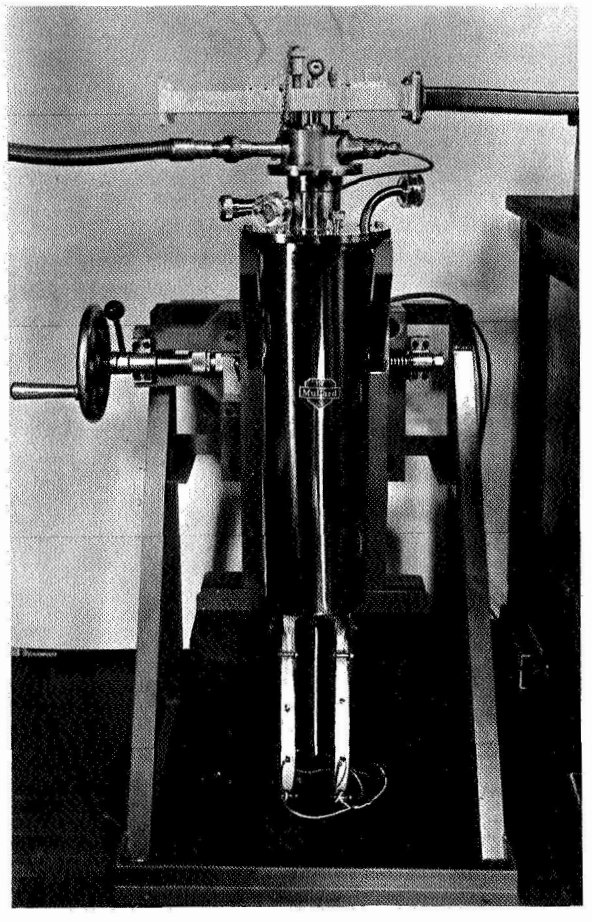


FIGURE 10–64.—Maser package with permanent magnet.

Following the work of Cioffi* on the use of superconducting screens in magnetic circuits, a superconducting magnet has been developed in which satisfactory operation of this maser in the laboratory has been obtained. Superconducting magnet masers have not been employed in the Goonhilly system.

Maser Performance

Laboratory Operation

In the permanent magnet shimmed to provide a field of 3280 oersted uniform to better than 0.1 percent over the volume of the ruby, the maser gives in the laboratory the performance summarized below:

Field	3,280 oersteds
Pump frequency	30,150 Mc
Operating temperature	1.4°K
Electronic gain	50 db
Bandwidth to 3 db points	16 Mc
Noise temperature	15 ± 4°K
Isolator backward loss	60 db
Isolator forward loss	3 db
Structure loss	8 db
Net forward gain	39 db
Input VSWR	1.4
Operation life/filling of He	8 hr.

Saturation effects become apparent at an input power of −65 dbm. The effect of possible breakthrough from the Goonhilly 6390 Mc transmitter on the maser performance was investigated in the laboratory and with the maximum power available (100 mw) at this frequency incident on the maser the performance at 4170 Mc was unaffected, and subsequent site experience confirmed this.

The recovery time of the maser after saturation at 4170 Mc is 150 milliseconds.

Bandwidth

The specification bandwidth of 25 Mc is slightly greater than can be achieved in a T.W.M. in a uniform magnetic field and giving a net gain in excess of 20 db (Figure 10–65). This was realized at the outset of the project and the maser was therefore designed to give a higher gain than the specified 20 db in a uniform field in order that ultimately the bandwidth could be increased, for instance, by field staggering. (Another reason why the maser was designed for high gain was that the operating temperatures which would be obtained at Goonhilly were uncertain in view of the considerable length

*P. P. Cioffi, J. A. Phys., *33*, 875, 1962.

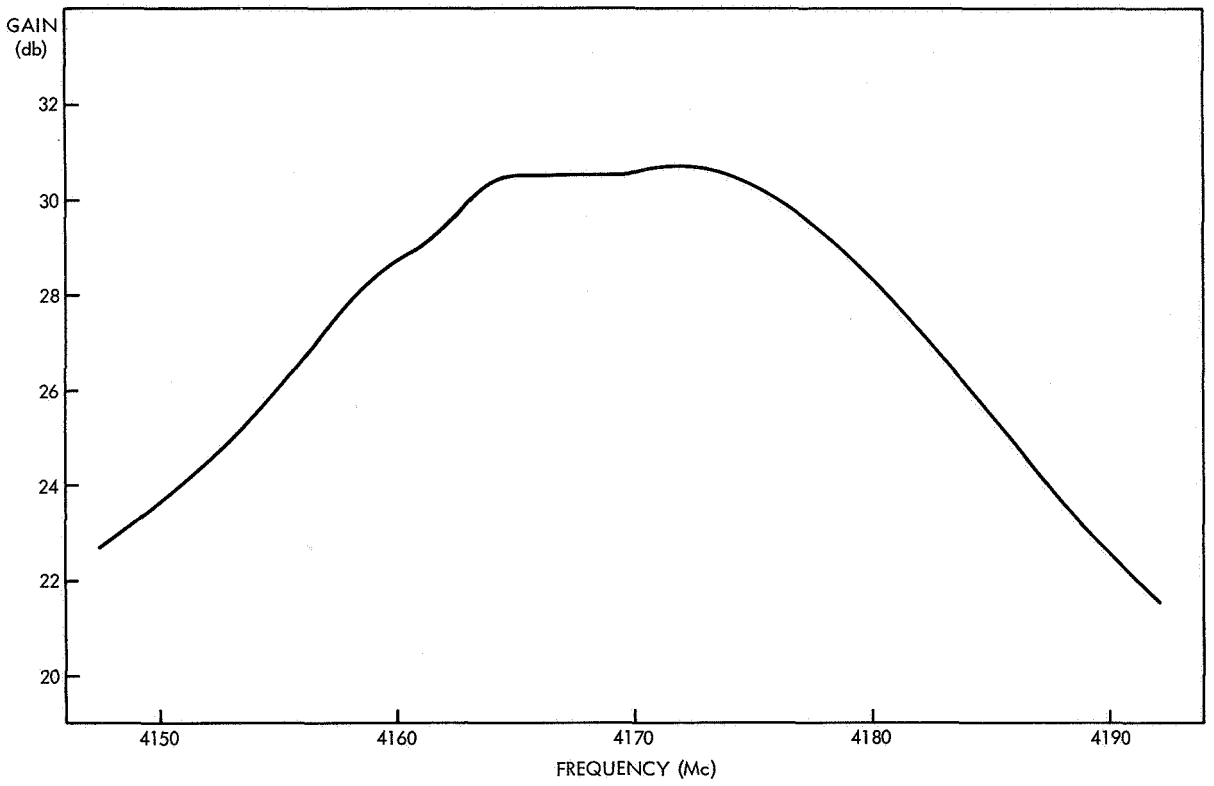


FIGURE 10–65.—*Bandwidth vs. electronic gain (G_0) for TWM in uniform field.*

of pipe between the maser and the helium pump—in the event 1.4°K was readily achieved.)

The bandwidth of a T.W.M. can be increased in practice by staggering either the crystal orientation or the magnetic field along the length of the maser. Orientation staggering is undesirable as it results in an unfavorable exchange of gain for bandwidth.

The bandwidth resulting from various forms of field staggering has been calculated on the assumption of a Lorentzian line shape and is plotted against peak electronic gain in Figure 10–66. Clearly a substantial increase in bandwidth can be obtained by the simple expedient of introducing a step in the magnetic field by suitably shimming the magnet.

In Figure 10–67 the observed gain of the maser is plotted against frequency for the case in which a step is introduced in the magnetic field by means of 0.006″ steel shims on the magnetic pole faces (magnet pole gap = 2.25″).

Site Operation

The uniform field permanent magnet version of the maser was installed in the Goon-

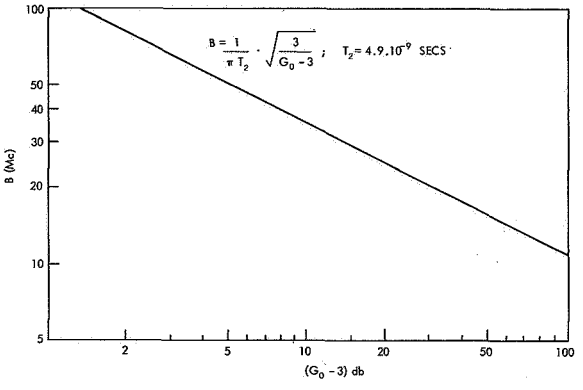


FIGURE 10–66.—*Bandwidth curves for maser with electronic gain of 50 db in uniform magnetic field, temperature 1.4° K.*

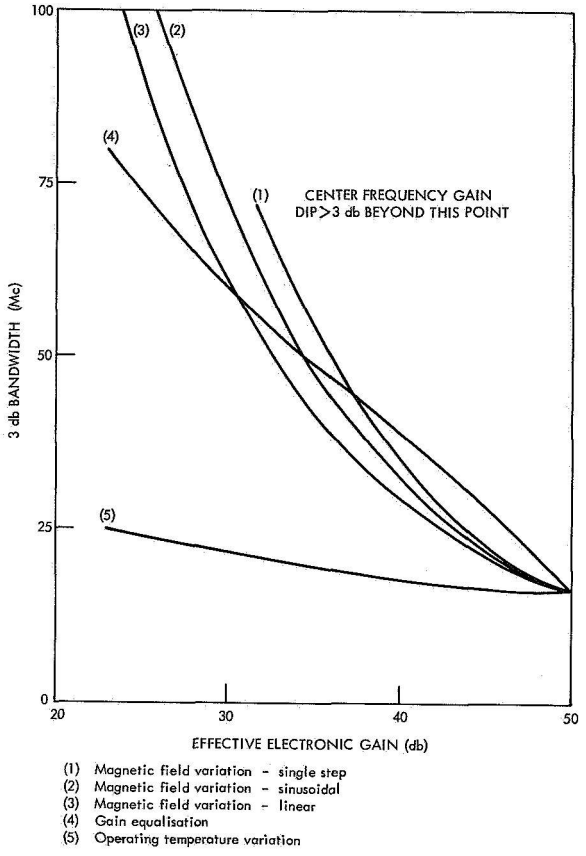


FIGURE 10–67.—Net gain—frequency characteristic of broad band maser.

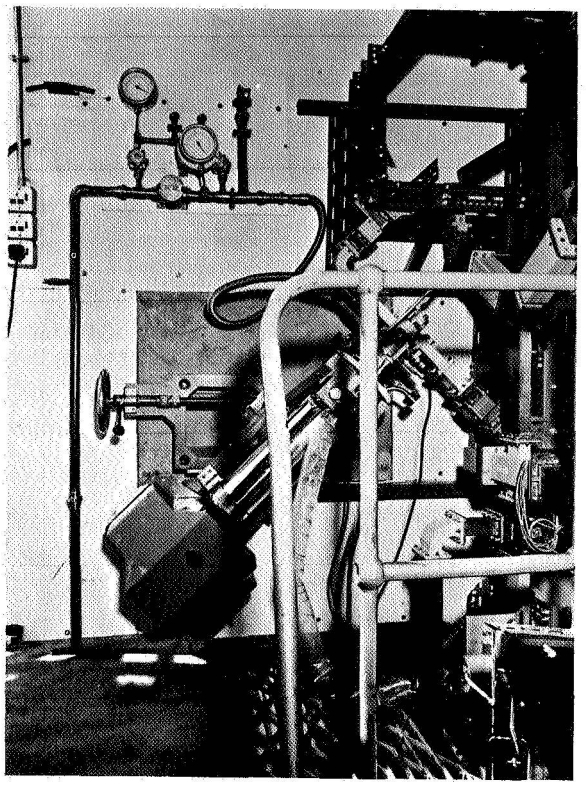


FIGURE 10–68.—Maser installed at Goonhilly.

hilly aerial in June 1962 (Figure 10–68) in a cabin at the back of the dish and gave a similar performance to that measured in the laboratory. It was not possible to obtain consistently an operating life of eight hours per filling of liquid helium when operating at 1.4°K, this being presumably due to the continuous movement of the aerial during satellite tracking. Changes in elevation of up to 100° are possible and for this reason the maser is mounted at 45° to the vertical when the dish is pointing to the horizon (Figure 10–65).

Following the initial Telstar experiments which were carried out using the maser in a uniform magnetic field, the bandwidth of the device was increased by shimming the magnet as previously described. A further improvement made has been the replacement of the small helium dewar vessels illustrated in Figure 10–64 by substantially larger vessels as shown in Figure 10–69. The use of the larger vessel has increased the continuous operating time per filling of liquid helium from less than eight hours to about 2 days.

Acknowledgment

The design, construction, and testing of this maser was completed in six months. This rapid development would not have been possible without the enthusiastic and able cooperation of Messrs. J. M. W. Cook, J. D. A. Day, E. L. Hentley, D. G. Stevenson, M. C. Kite and other of the authors' colleagues at Mullard Research Laboratories, which they gratefully acknowledge. The authors would also like to acknowledge the generous assistance in respect of equipment and installation given by Dr. H. N. Daglish and Mr. M. R. Child of the G.P.O. Research Establishment, Dollis Hill.

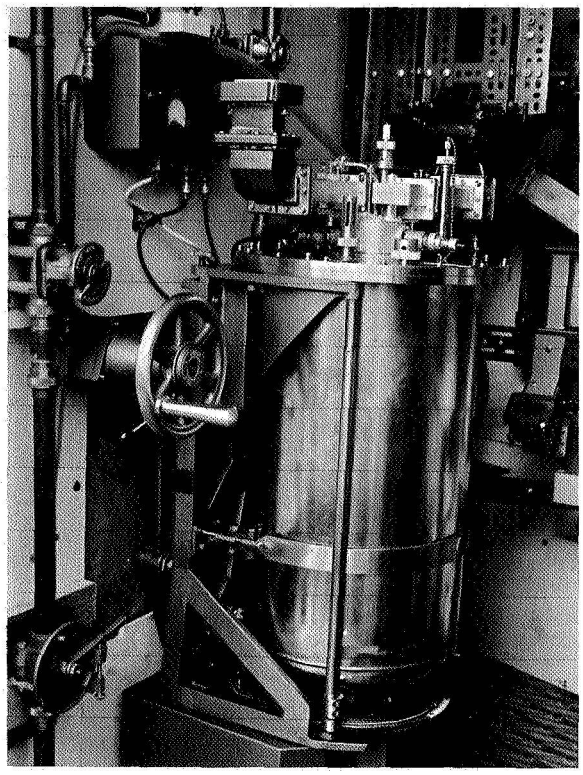


FIGURE 10–69.—Maser with large dewar at Goonhilly.

AUTHORS. *This chapter from the United Kingdom was contributed by the General Post Office, London, England. The foregoing section on The Traveling Wave Maser Amplifier was authored by* J. C. WALLING *and* F. W. SMITH, JR., *of the Mullard Research Laboratories, England.*

DIGITAL TECHNIQUES USED IN THE AERIAL STEERING

Summary

A description of the logic design for the digital control equipment is followed by further descriptions of items of particular interest. The means of applying offsets to the demanded aerial position for overcoming possible inaccuracy of the predicted orbit; and to demand accurately determined velocities manually; means of conversion from pure binary form to provide displays in terms of angles, and the derivation of analog voltages for the servo-amplifiers are discussed in detail.

A critical analysis of the equipment in the light of operational experience concludes this chapter.

Introduction

The prime function of the digital control apparatus was to position the steerable aerial in both azimuth and elevation axis in response to information on a punched tape.

Due to the need for efficient use of the tape, a system of linear interpolation over 200 millisecond intervals was used.

The digital equipment performed the interpolation process and calculated the angular position error signal fifty times per second.

Actual positions were determined by an optical Gray Code shaft encoder, suitably decoded, and applied to the error arithmetic unit.

Displays were provided showing aerial position, the angle demanded by the tape, control clock time, the angular corrections which might prove necessary to cancel out inaccuracies of the predicted trajectory. The other requirements of the digital apparatus were to provide accurate velocity signals, set manually, and to produce punched paper tape

records of aerial performance. Further signals, concerned with the G.P.O. communication equipment were recorded on the same tape via a digital logger.

System Design

Design Parameters

The following parameters were given:

1. A sample rate of fifty times per second.
2. Accuracy of digital equipment from tape reader to error better than two minutes of arc.
3. A ten-volt range in analog corresponding to ±42 minutes of arc error.
4. A standard frequency source of 2 kilocycles per second.
5. Tape information.

Items 1, 2, and 3 were determined by the servo design. Item 4 was a G.P.O. standard. Item 5 will now be discussed in greater detail.

Control Tape Information

The tape information is given in cycles, of a second duration. The demanded azimuth and elevation angles are stated in full form once per second.

Increments to be used for linear interpolation are stated in the following form: each increment corresponds to one tenth of the change in position over 200 milliseconds. There are five such increments for each axis. Each increment is used ten times, making in all fifty calculations per second of demanded angle, for each axis.

As the information is renewed once per second, any errors occurring in the arithmetic cannot endure longer than part of a second. A code identifying the tape is stated once per second.

Information corresponding to the aerial gain appropriate to the range of the satellite is given once per second.

Standard resistor-transistor printed circuit logic elements are used throughout.

Waveform Generation

It is convenient to use the standard 2 kilocycle signal to define the digit periods directly.

Waveforms are derived by division of the 2 kilocycle waveform and subsequent grouping using AND gates, see Figure 10–70.

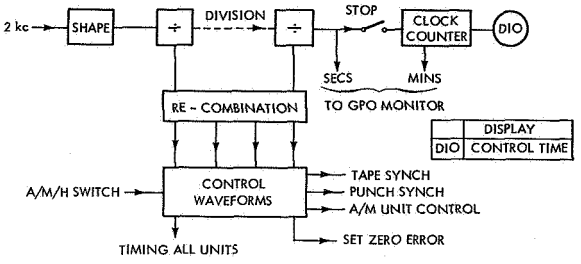


FIGURE 10–70.—Control diagram.

Each digit period is divided into four noncontagious phases. The phase waveforms are used as strobes to avoid spurious spikes caused by the AND operation on adjacent edges—this is established technique.

Operational Mode

In order to obtain the greatest reliability, pure binary serial arithmetic is used for the interpolation and error calculation.

The use of serial arithmetic requires serial to parallel conversion for error and tape punching. This is accomplished by the use of shift-registers. The only parallel conversion occurs in the Gray to Binary Conversion of the actual position transducers. Simple serial decoding would result in the most significant digit being produced first in time which is inconvenient for the subsequent arithmetic operations.

Peripheral Equipment

Logic design for tape reading and tape punching is well established, and will not be treated here in detail. The decoding techniques for the mechanical encoders used for correction and velocity increments is described later in detail.

Accuracy

The accuracy of two minutes of arc of the digital system is made up of several parts.

1. The accuracy of the shaft encoder
2. Rounding errors in the arithmetic
3. Drift in the digital to analog converter

The order of 1 and 2 are approximately the quantum step chosen and 3 can be improved by technique. The choice of a 16 bit system—i.e., 216 quanta equivalent to 360° of arc gives a quantum size of 19.77 seconds of arc. This value enables the design figure of 2 minutes to be improved upon under normal circumstances and leaves error in hand, so to speak, for the rest of the control design.

For accurate interpolation it was necessary to specify the incremental information on the control tape to $2^{-20} \times 360°$, the difference in accuracy of the resultant demanded angle and the 16 bit accuracy of actual position is referred to above as rounding error.

System Diagram

The final realization of the requirements is shown in Figure 10–71. The functions of each black box will be briefly described and the more interesting aspects will be treated in detail.

Tape Reading

The control tape advances one cycle per second in response to a control signal. This control signal occurs only when the following conditions apply:

1. When there is coincidence between the control clock and the time last read from the control tape.
2. When switching from manual to automatic operation so that the store can be "primed" with sensible information.
3. After the absence of one time coincidence to prevent the reader stopping in the event of a single mis-read or mis-punch. (This is extremely rare, of course.)

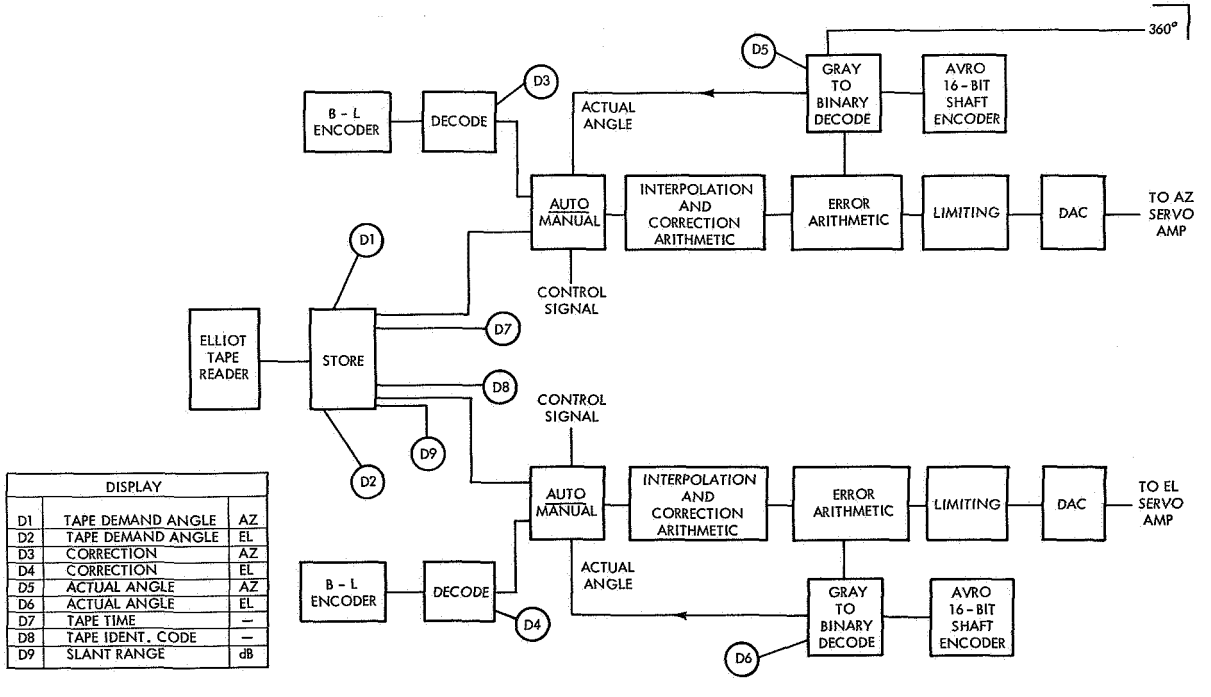
Tape Store

The data from the tape-reader occurs in sets of four parallel digits, the other track of the five track tape being used for synchronization.

Each set of digits is routed, using gating logic derived from counting rows, into an appropriate store.

Correction Logic

A mechanical encoder with a control knob on its input shaft at the control desk is used to derive parallel signals to be used for cor-



DISPLAY		
D1	TAPE DEMAND ANGLE	AZ
D2	TAPE DEMAND ANGLE	EL
D3	CORRECTION	AZ
D4	CORRECTION	EL
D5	ACTUAL ANGLE	AZ
D6	ACTUAL ANGLE	EL
D7	TAPE TIME	—
D8	TAPE IDENT. CODE	—
D9	SLANT RANGE	dB

FIGURE 10–71.—System diagram.

rection when on AUTOMATIC control. The same parallel signals are used as increments of position for MANUAL control. The mechanical shaft encoder outputs are in coded form to minimize ambiguity of readout. A decode unit converts to parallel signals representing signal and magnitude.

Auto/Manual Unit

This unit selects inputs to the arithmetic unit appropriate to the control mode.

On automatic mode the following operations are performed:

1. From the store are transferred demanded angle at 1 second intervals and increments at appropriate times to the arithmetic units.
2. From the correction logic the parallel signals are transferred fifty times per second in serial form to the correction arithmetic.

On manual mode the sequence is:

1. On first switching use actual angle as initial demanded angle.
2. Use the correction signal as an increment to be added fifty times per second—this will give rise to a uniform velocity; in order to maintain smooth minimum velocity the significance of the parallel digits is reduced by a factor of 2^{-7}.

Interpolation and Correction Arithmetic

The interpolation arithmetic performs the function of adding each tape demanded increment ten times to the accumulated angle. The value of the increment is renewed five times per second as previously explained. On manual control the increment remains at a constant value until the encoder shaft at the desk is turned. To avoid ambiguity due to sampling the parallel output while rotating the shaft, a 50 microsecond sampling interval is used.

While the correction signals are used for manual velocity setting, their use as corrections as used on "auto" are inhibited.

Error Arithmetic

The difference between the actual and corrected accumulated angles is calculated in the error arithmetic. Negative errors are prefixed by a bar digit.

Limiting

As the range of errors is small compared with a full revolution, the digital input to the D.A.C. is limited. In the event of a large error the appropriate end limit of the D.A.C. is demanded. This enables the D.A.C. to have a sensible dynamic range.

Digital to Analog Conversion—D. A. C.

The limited parallel digit signal is transferred 50 times per second into the D.A.C. and a signal of $\pm$ 5 volts about a $+5.0$ volts level is produced. This is appropriate to an error range of $\pm$ 42 minutes approximately ($\pm$ 128 quanta).

Shaft Encoders

Avro sixteen-bit gray-code shaft coders are connected to each axis. The encoders have their own amplifiers which apply signals to the coaxial lines from the aerial site to the steering apparatus room. As the azimuth motion exceeds 360°, a signal indicating positive rotation beyond due south is derived from a trip switch. This signal is combined logically with the 180° encoder track signal to produce the digit of significance $360° \times 2$ when a full rotation has taken place. This digit is referred to as the 17th bit.

Gray to Binary Decoder

This converts the sixteen parallel digits from the encoder to pure binary form and adds on the 17th bit where appropriate.

On elevation of course the 180° track would not normally be used as the maximum rotation is only 100° of arc, but for reasons of compatibility the full information is used. The azimuth and elevation channels are made as identical as possible to make testing and fault finding straight forward.

Displays

The displays shown on the diagram are situated on the control desk with the exception of Slant-Range db display which is on the Beam-Swingers console. The derivation

of all desk displays is considered in detail later. The slant range display is derived from an accurate dc voltage produced by a digital to analog converter.

Control Tape Reading Scheme

The control techniques for operating the Elliott high speed tape reader have been described elsewhere. A buffer tape reader was used in order to maintain a loop at the input to the high speed reader. This prevents snatching of the tape by the high speed reader which would give rise to reading errors.

Record Tape Punching

The information to be punched once per second is as follows:

1. Time in hours, minutes and seconds
2. Demanded angles at start of second
3. Error in full form at start of second
4. Tape identity code
5. Applied correction
6. Data derived from the data logger

(1) and (2) endure for a second and need not be stored again. (2) and (3) and (5) occur for less than one-fiftieth of a second and are stored. The data logger information is held in a store until punching has occurred.

The punch drive scheme was the one recommended by the manufacturer.

The record punch was used on manual operation also. This enabled check of the equipment to be made conveniently.

Logic Techniques

Much of the logic design uses well-established technique. While no novelty is claimed for the items which are now described, it was considered that they are sufficiently interesting to be described in further detail.

Design of Interpolation and Error Arithmetic

With reference to Figure 10–72, it will be seen that the demanded angle accumulator is a 24 bit shift register. The most significant digit is the one referred to as the 17th bit, the next 16 in significance are the digits appropriate to the 16 working bits, and the

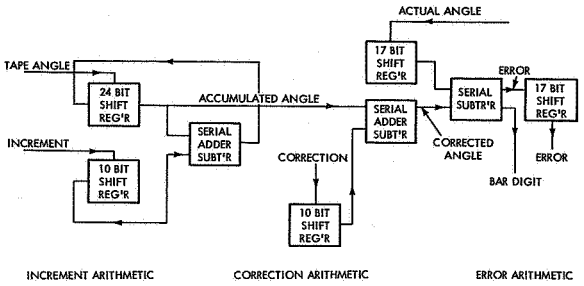


FIGURE 10–72.—Arithmetic scheme.

remaining digits are necessary to prevent coarseness of demanded angle after the addition of several increments.

The ten bit shift register recirculates to preserve the increment value for succeeding additions. The result of adding or subtracting increments to the demanded angle via the add-subtract unit is recirculated into the 24 bit accumulator. The serial accumulated angle has added to it the correction which has been converted to serial form in the shift register shown. The resultant angle is the complete demanded angle.

The actual angle serialized after the Gray to Binary conversion is subtracted from the demanded angle in a subtractor and the result stored in a 17 bit shift register and used in parallel for the digital to analog conversion.

Logic (not shown in the diagram) inspects the magnitude of the 17 bit number stored in the shift register. If it is less than $+128$ quanta, digital-to-analog conversion takes place and produces an error analog for normal control of the aerial. If the value exceeds $+128$ quanta but is less than ± 256 quanta, limiting occurs in the D.A.C. as previously described. If the value exceeds ± 256 quanta, protective logic causes the aerial to ignore this gross error condition and to coast for one or two seconds after which emergency stopping action is initiated if the gross error still persists.

Techniques for Generating a Parallel Ten-Bit Bi-Polar Number

As it is impossible to accurately predict the trajectory of a satellite during the initial

orbits, it was necessary to enable corrections to be made to the predicted angles on the control tape.

Any errors in the predicted time of arrival can be corrected in advance, the actual launch time then being known, by advancing or retarding the control clock by means of switches on the control desk as shown in the control logic diagram (Figure 10–70).

The correction signal is generated digitally in terms of sign and magnitude for the following reasons:

1. For convenience of calculation in the arithmetic
2. For convenience of display generation

The two shaft encoders for each motion consisted of an 8 bit Gray fine-encoder and a binary encoder which had lagging and leading contacts to overcome ambiguity of readout due to the gear-box between the encoders. The fine encoders were driven by hand control knobs, one for each motion, on the control desk. (See Figure 10–73.)

The encoders were capable of generating a 12-bit parallel number. The 10 least significant tracks were used for the 10-digit number and the most significant track for sign. The other track was not used, but was an alternative sign track should it be needed.

In this form, of course, negative numbers will not be correctly represented, but by inverting the ten least significant digits when the first track indicates a negative sign (0 for negative, 1 for positive, say) it is possible to approximate to negative numbers, the inaccuracy being one quantum. However, there is an advantage in retaining the inaccuracy of negative magnitudes in this form as the representation of zero is now two quanta wide. This is convenient as it allows zero correction to be set more readily. This is also important on manual control where the 10-bit number is used, with the significance of the digits reduced, to produce a velocity signal by accumulation of equal increments. It enables zero velocity to be obtained and held with greater reliability.

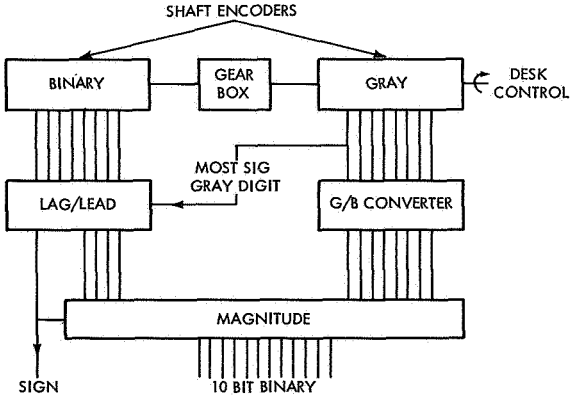


FIGURE 10–73.—Binary code converter.

As the display of correction was to the nearest minute it was necessary to provide an additional indication of true zero. This was achieved by surrounding the display zero with a green-field.

Means of Obtaining Displays

Elevation and Azimuth Applied Correction Display: The display logic converts two 10-digit dinary numbers into degrees and minutes. Angles up to a maximum of 5 degrees are converted and displayed at intervals of 0.5 second.

A simplified diagram of the system is shown in Figure 10–74.

System Outline—A negative pulse sets the binary counter B and the degree and minute counter D to zero and at the same time a positive pulse puts the input binary number into stores, S1.

A start pulse sets the binary output F to "1" allowing 4 kc pulses to pass through the gate G into the binary counter B and through M into the degree and minute counter D.

When a binary number counted in B and the input binary number stored in S1 are identical, the output from the coincidence logic C becomes "0" resetting the binary output F to "0". This inhibits the input gate G preventing any further count.

A positive pulse transfers the completed count in the degree and minute counter D to the stores S2 leaving the system free to make the next conversion. During the next conversion, the angle stored in 4, 2, 2, 1 code

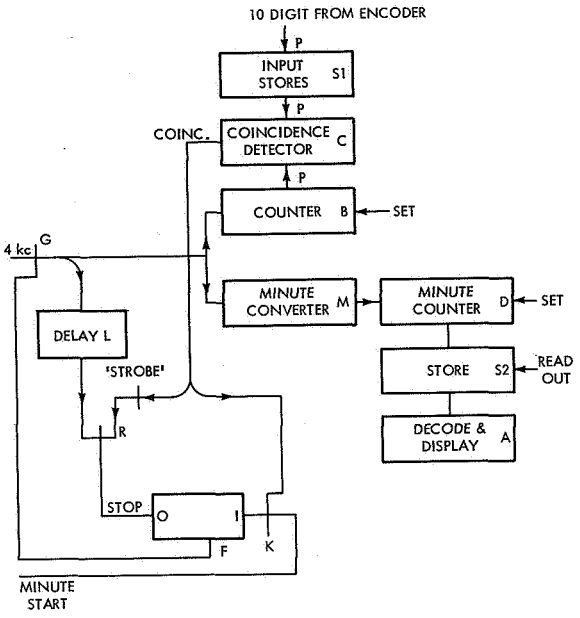


FIGURE 10–74.—Display logic for azimuth and elevation correction.

in S2 is decoded by amplifiers A and displayed as illuminated figures.

The binary to minute conversion is obtained by running counter D slightly less than three times slower than counter B. The minute converter M gives an output minute pulse for every three input pulses except for the 10th minute pulse and every subsequent 29th minute pulse which require four input pulses each.

In the special case of zero binary input the coincidence logic output would be "0" as soon as B had been set to zero. This would not prevent F from going to "1" and a maximum count being obtained. To avoid this the "0" on the coincidence logic is used to present this starting pulse from passing through gate K. The edges of the square waves applied to the coincidence logic C from the binary counter B have finite rise and fall times. Because of this there is the possibility that spurious coincidences could occur at the edges of these waveforms. These momentary coincidences would result in negative spikes from the coincidence logic C.

The spikes are prevented from passing through the gate R by strobe pulses which are obtained by delaying the 4 kc pulses at L. The delay time is such that strobe pulses are at "0" whenever a spike is present.

When the display reads 0° 0′ the correction signal may be one or two binary digits causing a slow drift on manual control. The outputs of the three zero amplifiers and the zero outputs of the stores for the two least significant input digits are connected to a 3 gate. When all the inputs to the gate are "1", the output is a "0"; this inhibits the sign amplifiers and gives a "1" on the input to an amplifier whose output is connected to the display. This gives a green field in place of the + or − sign on the display indicating that the manual correction is at true zero.

Elevation Readout—The elevation logic converts a 15-digit binary number into degrees and minutes up to a maximum of 100 degrees. The conversion is repeated at one second intervals.

The conversion is done in two stages:

1. The four most significant binary digits are counted; each unit representing an angle of 11 degrees 15 minutes

2. The remaining 11 binary digits are converted using the method described under Applied Correction Readout. A simplified diagram of the system is shown in Figure 10–75.

System Outline—A positive pulse puts the binary input number into stores S1, S2 and at the same time a negative pulse sets the counters B1, B2, M and D to zero.

A positive pulse starts the degree counter which for each single pulse into B2, counts 11 pulses into D via "or" gate B, and 15 pulses into M via "or" gate A.

When 60-minute pulses have been counted in M the degree pulse carried over to D is delayed at L1 to prevent it reaching the "or" gate B at the same time as one of the degree pulses from the degree counter.

When the binary number counted in B2 is identical to the number stored in S2 the output from the coincidence logic C2 becomes a "0" stopping the degree counter.

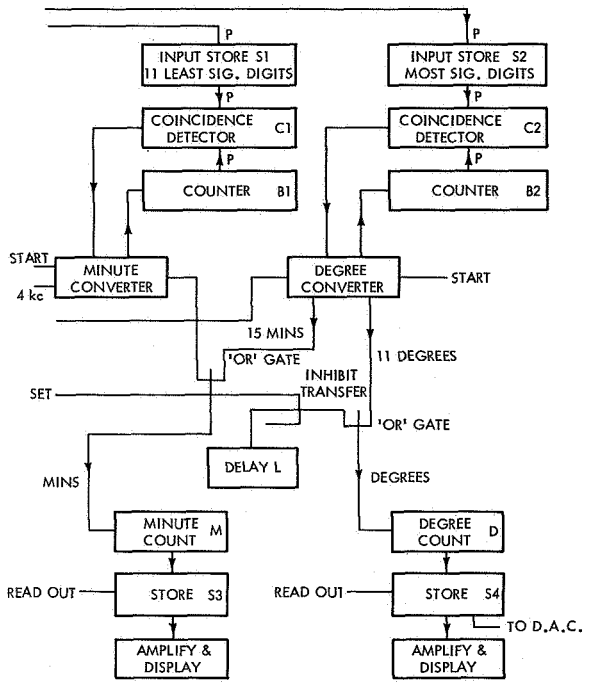


FIGURE 10–75.—Display logic for demanded and actual elevation.

Sufficient time is allowed for a full count of 15 in B2 if necessary. A negative pulse starts the minute converter which counts out the remaining 11 binary digits. The minute pulses pass the "or" gate A into minute counter M.

After sufficient time has been allowed to complete the conversion a positive pulse stores the count in S3 and S4.

The angles stored in 4, 2, 2, 1 code in S3 and S4 are decoded by amplifiers A and displayed by digilites.

The degree output from S4 is taken in 4, 2, 2, 1 code to a digital analog converter which drives a meter display.

When M is set to zero a delayed pulse is set up in L. This set is prevented from passing into D by inhibiting the gate G with the set pulse. The set pulse is of longer duration than the delayed pulse.

When coincidence occurs this prevents any further count. The degree and minute counters M and D will then contain a multiple of the angle 11 degrees 15 minutes. The minute converter is described under Applied Correction Readout.

Azimuth Readout Tape Demanded and Actual—The azimuth readout converts a 17-digit binary number into degrees and minutes. The angle is displayed in the range ± 250 degrees at one-second intervals.

The conversion is done in three stages:

1. The binary number 01011000111000111 (250 degrees) is subtracted from the input binary number.

2. The five most significant binary digits are counted, each unit representing 11 degrees 15 minutes, as described under Elevation Readout.

3. The remaining 11 binary digits are converted using the method described under applied Correction Readout.

The last two stages in the conversion are identical to the elevation readout for the added digit, the subtractor unit and the replacement of the input stores by a shift-register. A simplified diagram is shown in Figure 10–76.

System Outline—The binary number to be subtracted (250 degrees) is set in the shift

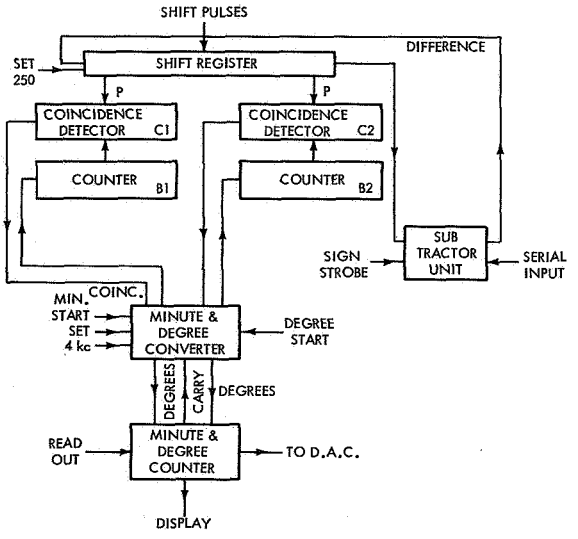


FIGURE 10–76.—Display logic for demanded and actual azimuth.

register H. This number and serial input are then shifted into the subtractor unit, and the difference replaced in H as it becomes vacated.

When the serial input is greater than 250, the difference (0—250) is positive and is stored in H. The sign from the subtractor is positive.

When the serial input 0 is less than 250, the difference (0—250) is negative. This is recirculated into the subtractor unit and subtracted from the input which is held at zero. The new difference (250—0) is positive and stored in H for the rest of the second.

The binary number in H is converted into degrees and minutes as described under Elevation Readout.

Digital to Analog Conversion Techniques

The error voltage to be applied to the input of the servo-amplifier is in the range 0 to 10 volts, 5 volts representing zero error. This voltage is derived from the output of a summing amplifier of better than 1 percent linearity and drift, which is enclosed in a small constant temperature enclosure—a modular.

The input currents to the summing amplifier are derived from a precision voltage source, and precision resistors, also enclosed in the temperature controlled oven.

Parallel transistor switches, with saturated collector-emitter voltages of the digits matched, are driven from stores into which have been transferred the parallel representation of the error.

The representation of the error is in bar notation, that is, the sign digit has significance similar to bar $\overline{1}$, etc., of the familiar logarithm table notation.

The error has been generated in this form as it simplifies unipolar switching. In the absence of a bar-digit, an input current appropriate to half-scale deflection is applied. In the absence of the least significant digits, this is equivalent to zero error.

Full scale positive is produced by energizing all switches, full scale negative by all switches being open.

Operational Experience

A critical analysis of the design of the digital equipment in the light of operational experience would perhaps best be made by others but the following points are worth making.

Reorganization of tape-format and the need for linear interpolation over 200 millisecond periods could well be investigated further when a full analysis of all likely orbits is made. This would enable longer periods of tape operation and would reduce storage and simplify the logic. Control under manual operation could be improved by resetting the demanded accumulator angle to the actual angle once per second. This would prevent an occasional gross error from being perpetuated on manual control.

There is insufficient data yet for prediction of future reliability of the digital equipment but the incidence of reading errors and inaccuracies from other sources is extremely low and augurs well for the future. It is extremely difficult to design digital compensation networks unless the servo parameters are accurately known. Now that the mechanical parameters are well defined it is thought that digital compensation techniques are worthy of further consideration.

Conclusions

The digital steering apparatus installed at the G.P.O. Radio Station has been described and discussed in detail where it was thought appropriate. This was an example of a digital and analog servo mechanism of the type where the sample rate was high compared to the band-width of the control system. The design of the apparatus was extremely interesting not only for its obvious technical and national interest but for the stimulation it gave to further investigation into the digital control field.

Acknowledgments

The work which this paper described was performed under subcontract to the Brush Electrical Engineering Co., Ltd. We acknowl-

edge with gratitude the help of our colleagues at Hawker Siddeley Dynamics, those associated with the project at Brush Electrical Engineering Company, and the G.P.O., W. S. Branch and Goonhilly Site personnel of the G.P.O. and the encouragement of Mr. C. N. Kington of Husband and Company.

Permission of the Institute of Electrical Engineers to reprint this article is acknowledged gratefully.

AUTHORS. *This chapter from the United Kingdom was contributed by the General Post Office, London, England. The foregoing section on Digital Techniques Used in the Aerial Steering was authored by* J. E. MARSHALL, R. J. COULTER, J. K. BINKS, K. J. CLARKE, T. STEVENAGE, *and* G. E. WILLETTE *of Hawker Siddeley Dynamics, Ltd., England.*

N66-10261

Chapter 11

Results Of Tests Performed With Relay I At The Goonhilly Downs Space Communications Station

INTRODUCTION

The first active communication satellite—Telstar I—was launched from Cape Canaveral by the U. S. National Aeronautics and space Administration (NASA) in July 1962, and was followed in December 1962 by satellite Relay. Since then many tests and demonstrations of television, multi-channel telephony and telegraphy, facsimile and data transmission have been made via this experimental satellite. In addition, much data has been accumulated on microwave propagation, earth-station receiving system noise temperatures and satellite tracking accuracy. Such tests and data will be of considerable value for the planning and design of future operational communication-satellite systems.

This section reviews the results obtained from the tests with the Relay satellite and draws some broad conclusions as to their implications. Since it will not be possible to present all the data, a representative selection has been made.

Several communication-satellite earth stations, including those at Andover (Maine), Nutley (New Jersey), Pleumeur-Bodou (France), Rio de Janeiro (Brazil), and Fucino (Italy), took part in the tests. The results presented, however, are mainly those obtained from measurements made at the British Post Office earth-station at Goonhilly, Cornwall. It is to be noted that much additional data on the performance of the communication satellite has been obtained by NASA via telemetry transmissions from the satellite.

The cooperative program of tests between the various earth stations has been coordinated by a Ground Station Committee. This committee, which is chaired by NASA, includes representatives of NASA, the administrations concerned with operation of the stations, and the satellite designers.

Before discussing the tests it will perhaps be of value to outline briefly the characteristics of satellite Relay and its orbit, and the characteristics of the Goonhilly earth station.

The Relay Satellite and Its Orbit

The main characteristics of the Relay satellite are shown in Table 11–1.

Characteristics of the Goonhilly Earth Station

In its present form the Goonhilly earth station has been designed and built primarily to enable tests to be made with experimental communication satellites, and also to be capable of development into an operational station at a later stage if required. For this reason it incorporates extensive testing equipment and other facilities that would not necessarily be part of an operational station.

TABLE 11–1.—*Main Characteristics of the Relay Satellite*

Date of launch	13 December 1962
Present status (Nov., 1963)	Operational
Transmission characteristics:	
Transmit frequency (Mc)	4170
Beacon frequency (Mc)	4080
Receive frequency (Mc)	1725
Radiated power (watts)	10
Transponder bandwidth (Mc)	25 and 2×2
Orbit:	
Perigee (statute miles)	840
Apogee (statute miles)	4600
Inclination (rel. to Equator)	47.5°
Period (minutes)	185

Steerable Aerial

The steerable aerial at Goonhilly employs an 85-ft diameter parabolic reflector with a feed in the aperture plane, Figure 11–1. Unlike the aerials at Andover and Pleumeur-Bodou, the Goonhilly aerial is designed to operate without a radome. The dish can be rotated in azimuth through ± 250 degrees, and in elevation from 0 to 100 degrees, by servo-controlled motor drives. The aerial is steered on the basis of predicted orbital data, with either manual or automatic fine correction of any residual errors in the data. The predicted data, which corresponds to the X, Y, Z coordinates of the satellite position at 1-minute intervals of time, is supplied over a teleprinter link from the Goddard Space Flight Center, U.S.A., up to a week or so in advance of each satellite pass. From it is derived, via a computer at Goonhilly, azimuth and elevation angle pointing data at 1-second intervals of time. The latter data is recorded on punched tape and used to control the aerial steering system.

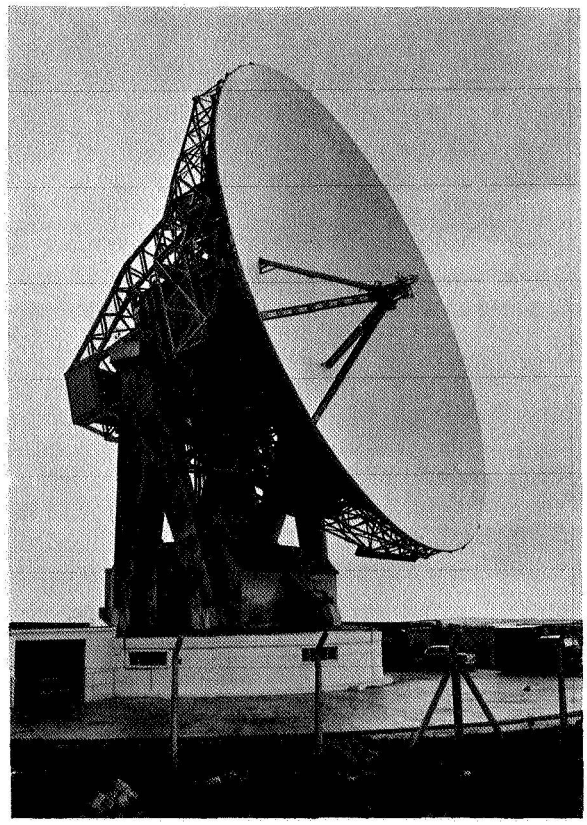


FIGURE 11–1.—Goonhilly aerial.

Any errors in aerial pointing are determined by causing the aerial beam to scan conically over a very small angle, e.g., 0.03 degree. The resulting amplitude modulation of the microwave beacon signal received from the satellite is detected and used to correct the aerial pointing, by either manual or automatic remote-control of the position of the feed at the focus.

Aerial Gain and Radiation Diagram

The accurate measurement of the gain of large-aperture microwave aerials is a matter of some difficulty, since the test transmitter or receiver must be located at least several miles away if a sufficiently plane wave is to be achieved. If tower-mounted test aerials are used, undesirable ground reflections are liable to arise, thus causing errors. However, the radio star Cassiopeia A provides a source of known and stable amplitude free from such limitations. Measurements of the gain of the Goonhilly aerial at 4170 Mc using Cassiopeia A indicate a gain of 55.6 db (excluding waveguide losses) relative to an isotropic aerial, as shown in Table 11–2:

The gain of 4170 Mc is some 3.5 db less than that of an ideal aerial with the same feed radiation pattern, the loss being mainly due to dish profile inaccuracies (these being

TABLE 11–2.—*Characteristics of Goonhilly Aerial*

Characteristic	Gain or Loss (db)		
Frequency (Mc)	1725	4170	6390
Gain of ideal aerial:			
Gain with uniform illumination	53.4	61.1	64.8
Loss due to tapering	1.8	2.0	3.0
Gain with tapered illumination	51.6	59.1	61.8
Additional losses due to:			
Feed support shadowing	1.5	1.5	1.5
Reflector profile inaccuracies	0.4	2.0	4.8
Total	1.9	3.5	6.3
Gain of actual aerial	49.7	55.6	55.5

less than 3/16 inch over the area of the dish within the 45-ft diameter); the remaining losses are due to scattering from, and aperture blocking by, the feed supporting structure. It is to be noted that the feed pattern is heavily tapered, the radiation intensity at the rim of the dish being some 18 db below that at the center, in order to reduce noise pick-up from the ground. The aerial gains at 1725 and 6390 Mc are 49.8 and 55.5 db, the losses being 1.8 and 6 db respectively, relative to an ideal aerial. The larger losses at 6390 Mc are due to the greater effect of profile inaccuracies as the frequency is increased.

The aerial radiation diagram at 4170 Mc, for angles up to ± 6° from the main lobe, is shown in Figure 11–2. For angles between ± 10° and ± 90° the minor lobes are at least 50 db below the main lobe, and beyond ± 90° they are at least 70 db below. The high discrimination provided by such aerials is, of course, a major factor in avoiding interference to and from terrestrial

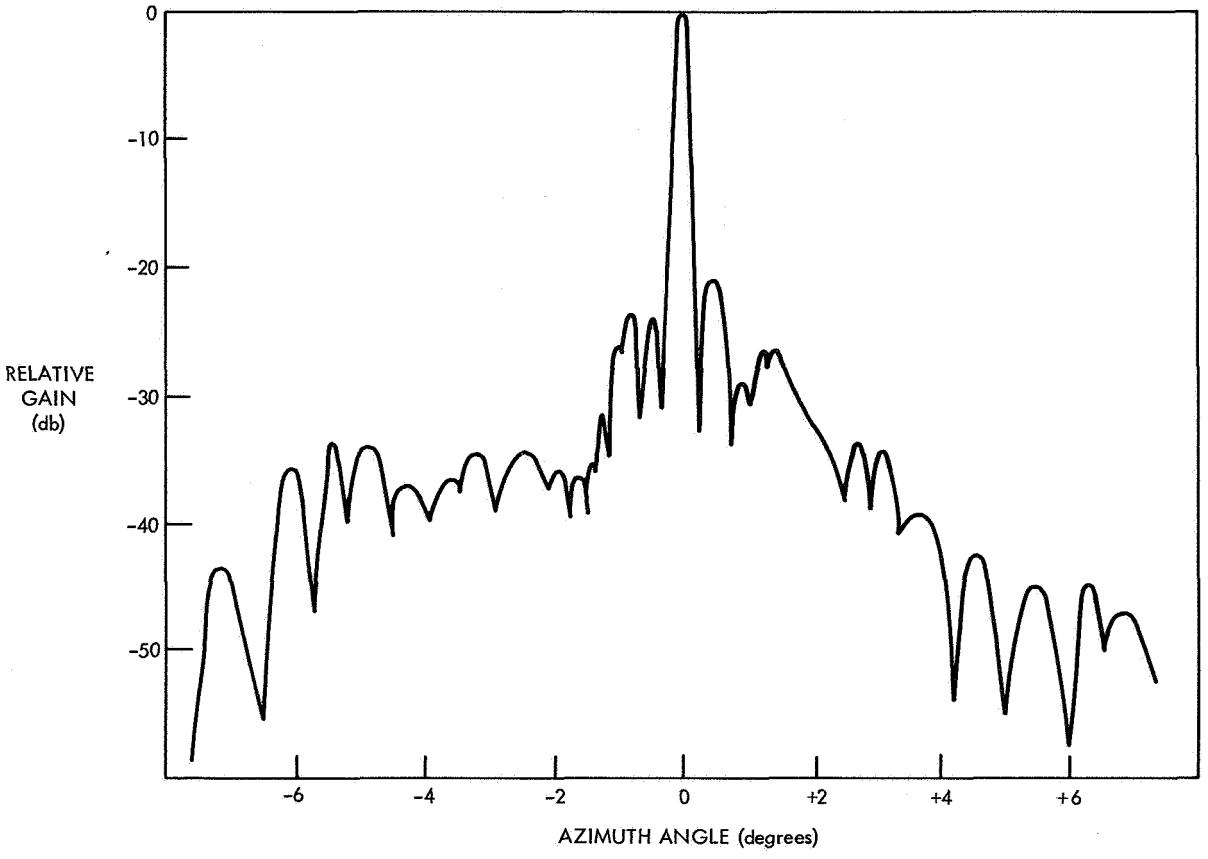


FIGURE 11–2.—Goonhilly aerial horizontal radiation diagram (4170 Mc).

radio-relay systems, and other satellites, using the same frequency bands.

The main lobe of the radiation diagram at 4170 Mc is shown in greater detail in Figure 11–3, which gives a comparison between the measured and computed values. The amplitudes of the first pair of minor lobes are somewhat larger than the computed values, due to scattering from the feed supporting structure. The width of the main lobe, 3 db below the maximum amplitude at 1725 Mc, is about 24 minutes of arc; it is 12 minutes of arc at 4170 Mc and only nine minutes at 6390 Mc; thus pointing accuracies of less than a few minutes of arc are essential if significant losses of received signal strength at earth station and satellite are to be avoided.

Receiving System Overall Noise Temperature

The signals received from Relay—even allowing for the gain of the 85-ft aperture aerial—may be only of the order of a micro-microwatt, and a low-noise receiving system is therefore essential. The Goonhilly receiver incorporates a liquid-helium cooled maser operating at about 2°K, the equivalent noise temperature at the maser input being about 12°K. However, the losses in the waveguide feeders, filters and other components between the maser and the aerial feed increase the overall receiving system noise tempera-

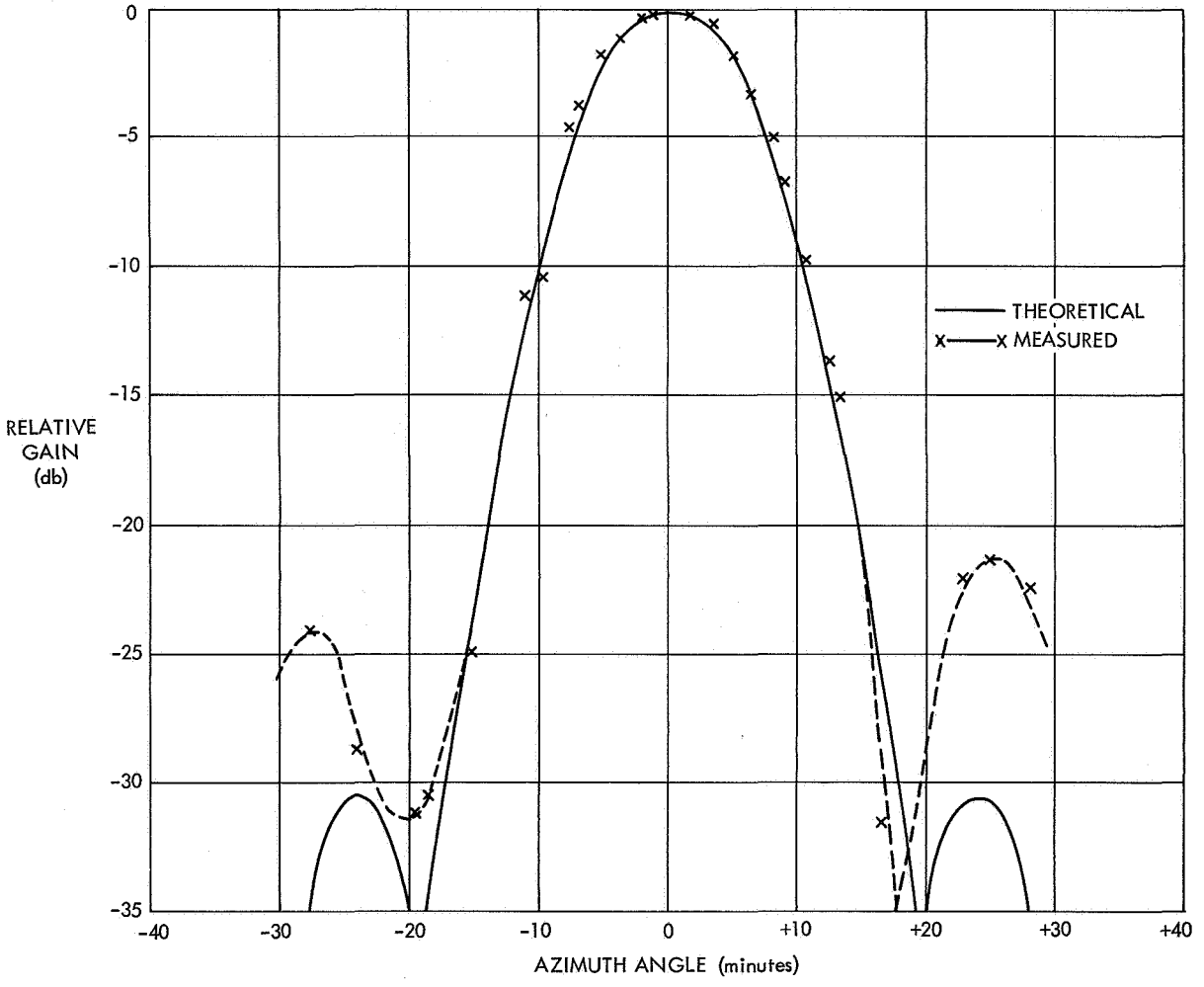


FIGURE 11–3.—Goonhilly aerial horizontal radiation diagram main lobe (4170 Mc).

ture to about 55°K when the aerial is pointing at the zenith, as shown in Figure 11–4. As the aerial moves from the zenith towards the horizon, additional noise is picked up from the atmosphere and, for angles of elevation below a few degrees, from the ground via the minor lobes of the radiation diagram. Figure 11–4 shows, curve (c), the calculated noise contribution from a "standard" atmosphere. The difference between the measured overall noise temperatures shown in curves (a) and (b) represents an improvement of some 15°K due to a reduction of the feeder system losses by 0.2 db. Of particular interest is the limited range of variation of the overall noise temperature at given angles of elevation over a period of some two months with changing atmospheric conditions, i.e., clear skies interspersed with rain, cloud, and occasional ground mist. It is believed that this small range of variation is in part due to the absence of a radome, which when wet could contribute significantly to the overall noise temperature.

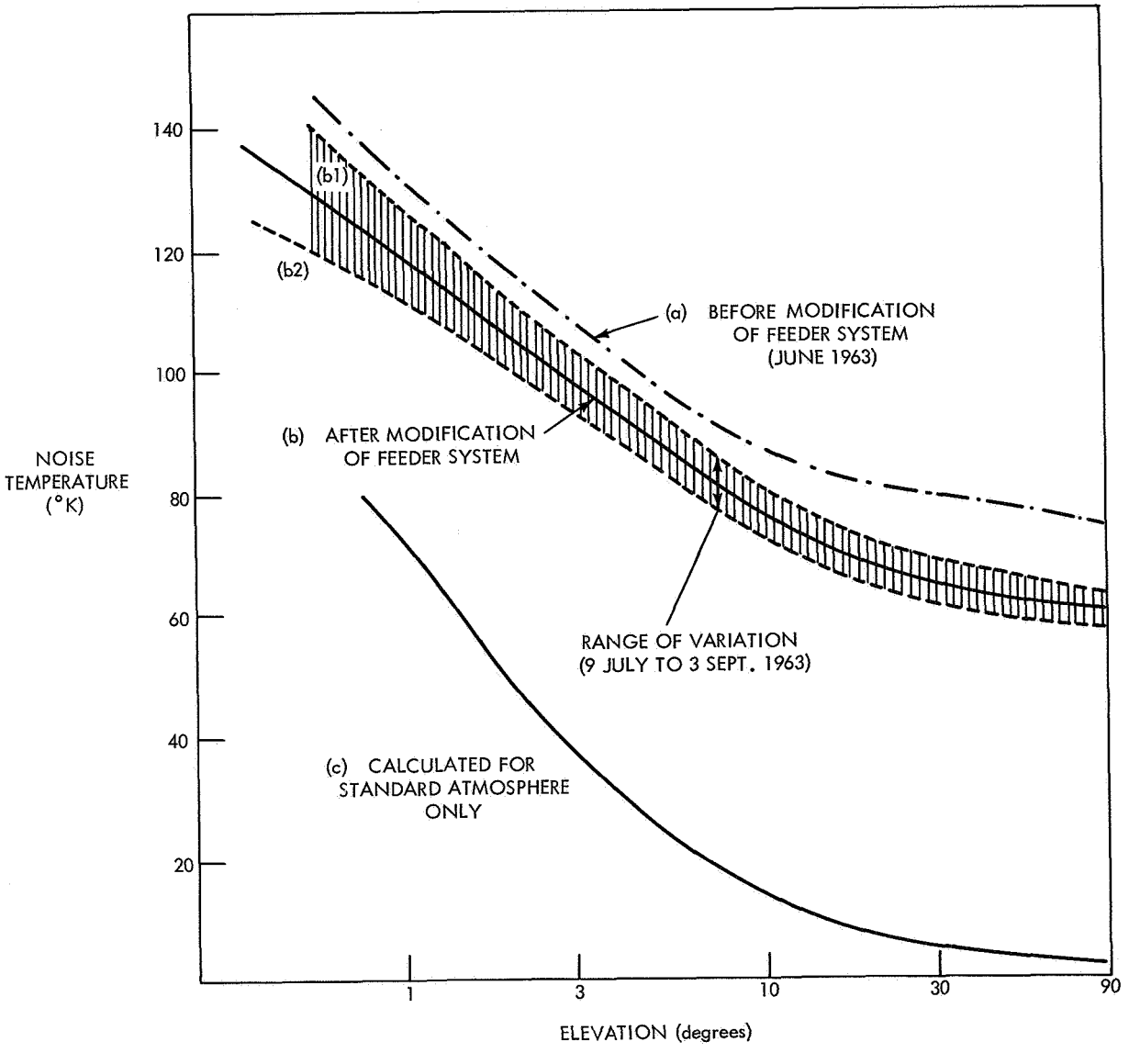


FIGURE 11–4.—Goonhilly overall noise temperature (measured) 4170 Mc.

Transmitters

The transmitter used at Goonhilly for tests with Relay produces an output of up to 10 kw at 1725 Mc. The corresponding maximum effective radiated power, allowing for the aerial gain and the feeder losses, is some 700 megawatts.

Results of Tests and Demonstrations

Characteristics of Received Carrier

The characteristics of the received carrier of primary interest are:

1. The variation of level during a satellite pass, especially at low angles of elevation.
2. The Doppler frequency shift due to the motion of the satellite relative to the earth stations.

The variation of received carrier level during a typical pass of Relay is shown in Figure 11–5. It indicates:

1. Acquisition of the satellite with the aerial beam only 0.5 degree above the horizontal.
2. Fluctuations of level of a few decibels for angles of elevation up to about three degrees, due to tropospheric layers and irregularities.
3. A steadily increasing level from about three degrees elevation, to the end of the pass.

Study of the variations of received carrier level for low angles of elevation is of considerable importance for the design of operational communication satellite systems, since the coverage obtainable and therefore the number of satellites required depends on the minimum angle of elevation at which signals can be consistently received. The fact that the horizon at Goonhilly is not more than 0.5 degree above the horizontal has facilitated such studies. Statistical data of the variation of received carrier level at low angles of elevation, obtained during a number of satellite passes, is shown in Figure 11–6. It is considered that reliable operation can be achieved for angles of elevation down to about three degrees; however, more data are needed to confirm this provisional result.

For angles of elevation above about three degrees, the received carrier level can be calculated with good accuracy from the free-space transmission equation, allowance being made for the satellite "look angle", i.e., the angle which determines the effective gain (or loss) of the satellite aerial along the direction between the satellite and the earth station.

Figure 11–7 shows a comparison between the measured and calculated received carrier powers for a typical pass of Relay. It also shows the Doppler frequency shift of the carrier during the pass, due to the rate of change of path length between the earth stations via the satellite. The varying small difference between the measured and calculated values is due to frequency drift of the oscillators in the satellite and earth stations.

The Doppler frequency shift may be up to some 80 kc on the 4170 Mc received carrier, i.e., up to 2 parts in 10^5, in the case of the

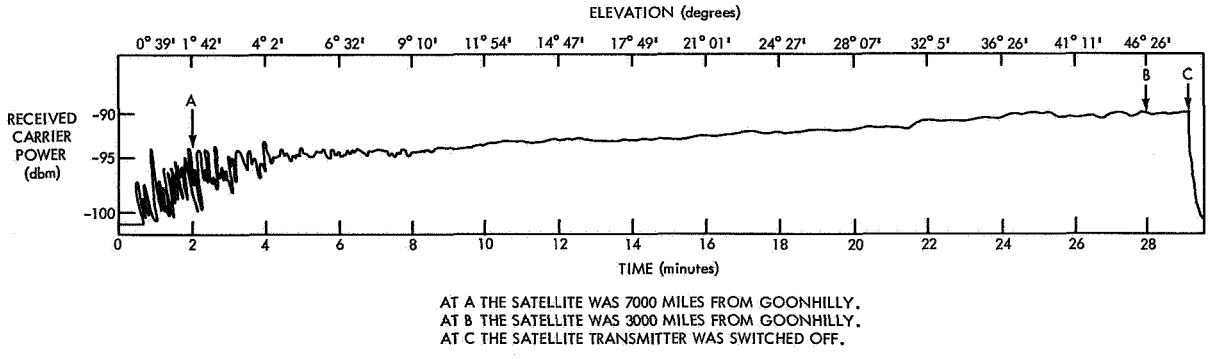


FIGURE 11–5.—Variation of received carrier power with angle of elevation and time.

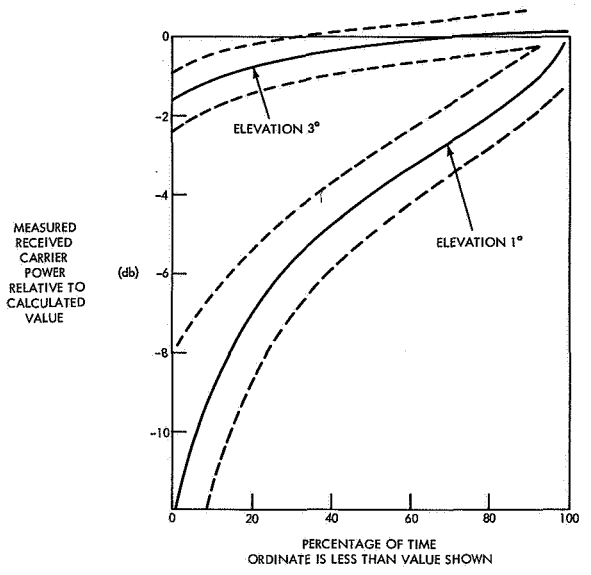


FIGURE 11–6.—Variation of received carrier level at low angles of elevation.

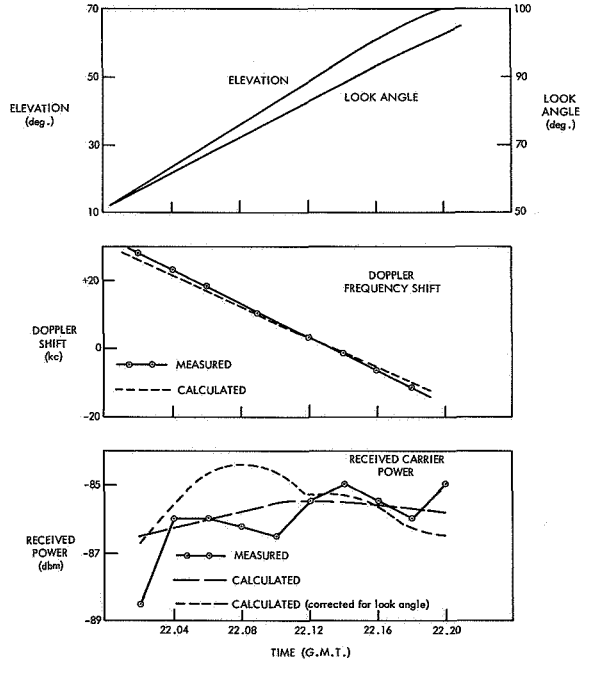


FIGURE 11–7.—Comparison of measured and calibrated received carrier power and Doppler shift.

Relay satellite, for a loop connection via the satellite, i.e., from one earth station to the satellite and back to the same earth station.

For earth stations on opposite sides of the Atlantic the Doppler shift rarely exceeds 1 part in 10^5, and is generally appreciably less. Such shifts of the carrier frequency are not significant in the wideband RF or IF channels of the FM communication system; they are important, however, in the narrow-band beacon channel which has to be tuned to allow for the shift. Doppler frequency shifts of up to 1 or 2 parts in 10^5 also occur in the baseband signals; the effects for various types of baseband signal will be discussed later.

Selective Fading and Multi-Path Effects

Observations have been made on many occasions to determine whether frequency selective fading or multi-path effects, e.g., due to partial reflections from tropospheric layers, are present. Such effects might be expected to occur, for example, at low angles of elevation with glancing incidence on the tropospheric layers.

Frequency selective fading can be investigated by transmitting a frequency-modulated carrier with a deviation of several megacycles per second and observing the received signal on an IF spectrum analyzer; multi-path echo signals can be investigated by transmitting a narrow pulse, e.g., 0.2 microsecond pulsewidth, and observing the received baseband signal.

Although many observations have been made, no evidence of selective fading or multi-path effects within the limits of resolution of the equipment have been detected for angles of elevation above about three degrees. This favorable result is attributable in part to the very high directivity of the earth-station aerial, which discriminates markedly against any tropospheric reflections more than a fifth of a degree off-beam, and partly to the smaller reflection coefficients for angles of incidence of greater than a few degrees relative to the mainly horizontal layers.

Below about three degrees elevation of the earth-station aerial beam, the received carrier level fluctuations indicate reflections

from tropospheric discontinuities. However, even in this region, the relative delays of such signals are so small that they do not give rise to significant selective fading or echo effects.

The foregoing observations are confirmed by the excellent transmission quality of the satellite link for television and multi-channel telephony signals, referred to later.

Satellite Tracking Accuracy

For angles of elevation above about three degrees, errors in uncorrected aerial pointing relative to the wave arrival direction rarely exceed 10 minutes of arc, and are generally less than 5 minutes of arc for satellite orbits predicted up to two weeks in advance. The manual or auto-track fine correction systems enable even these small errors to be reduced to one or two minutes of arc.

These results indicate the practicability in operational systems of using aerials with beamwidths of only 10 minutes of arc, i.e., with gains of up to about 60 db, provided that such regular operation does not extend below about three degrees elevation relative to the horizon. Below about three degrees elevation, ray bending due to atmospheric refraction plays an increasingly important role; in the case of a satellite, the true direction of which is horizontal, the aerial must be pointed about 0.6 degree above the horizontal, for a "standard" atmosphere. In practice the amount of refraction varies somewhat about the "standard" value and small fluctuations of wave arrival direction occur at low angles of elevation.

Television Transmission

It is to be noted that a sound channel is normally provided with the television channel, using a 4.5 Mc frequency-modulated subcarrier in the baseband. This requires that a 3 Mc low-pass filter be inserted in the television channel; the results reported are with such a filter in use, except where indicated otherwise.

Video Channel Transmission Characteristics—Typical video channel gain and delay/frequency responses, measured at Goonhilly, via the Relay satellite in loop, are shown in Figure 11–8. As would be expected in a frequency-modulation system, the loop-gain stability is good, the variation being generally less than ± 0.2 db.

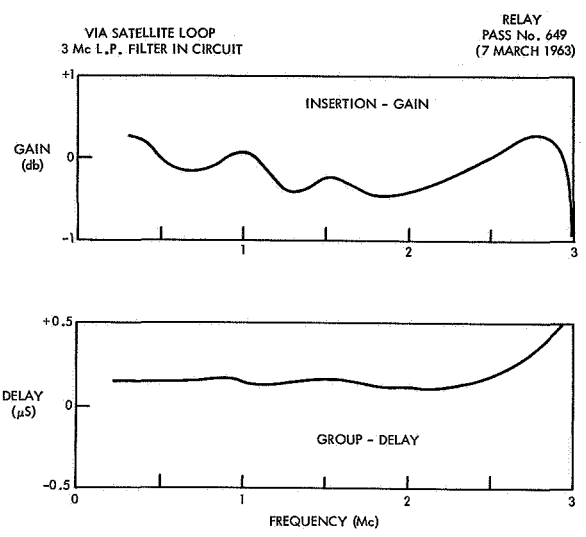


FIGURE 11–8.—Insertion-gain and group delay/frequency characteristics of video channel.

The video waveform response, measured with a sine-squared pulse ($2T = 0.3\ \mu S$) and bar signal with the satellite in loop is shown in Figure 11–9. The corresponding K-rating factor, which defines the waveform distortion, is less than 2 percent.

The good quality of the satellite video channel is shown by Figure 11–10, a typical test card on the U.S. 525-line television standard transmitted from Andover, Maine, to Goonhilly via Relay. Multipath and echo signals are imperceptible; such imperfections as are apparent on close examination of the received test card are due to the bandwidth restriction imposed by the 3 Mc low-pass filter on the nominal 4.5 Mc bandwidth video signal.

Doppler frequency shifts have no effect on the quality of the received monochrome video

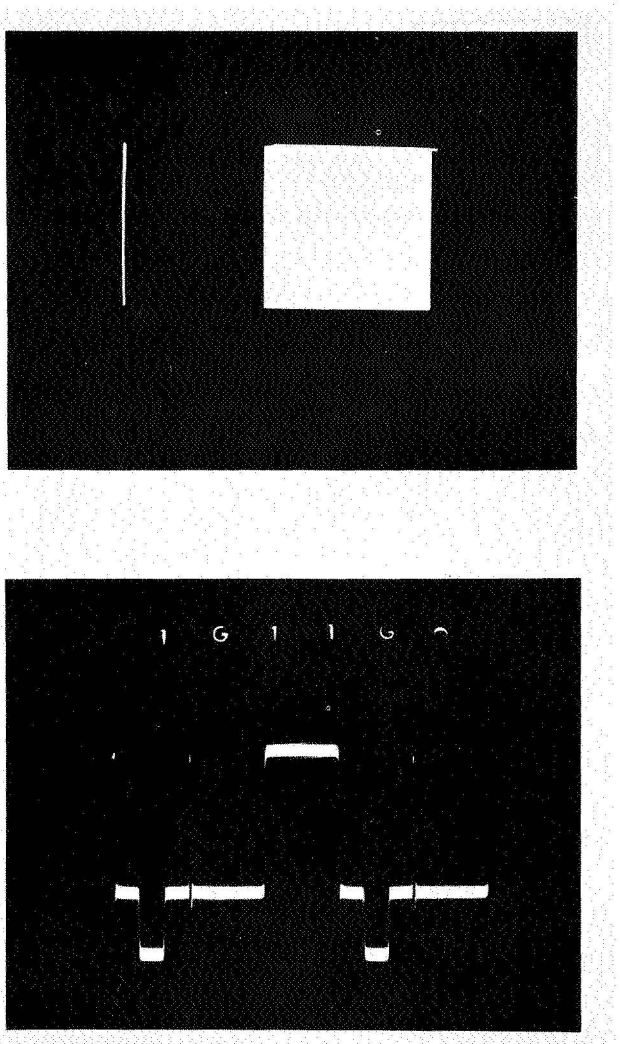


FIGURE 11–9.—Video waveform via satellite loop (3 Mc) L. P. filter in circuit.

signals, since they correspond to a slow variation of transmission time of a few tens of milliseconds during each pass and this is imperceptible to viewers.

Video Signal-to-Noise Ratio—For most passes of the Relay satellite, and for angles of elevation above a few degrees, the measured overall weighted video signal (peak-to-peak, black-to-white) to RMS noise ratio has been in the range from about 40 to 50 db, corresponding received carrier-to-noise ratios in a 25 Mc IF band exceeding some 10 db. The measured values have agreed, within one or two decibles, with the calculated values allowing for satellite range and look angle, the receiving system noise temperature and other characteristics.

Under the above conditions it is possible to use a normal frequency modulation demodulator to recover the video modulation from the carrier; however, occasionally due to the abnormally long distance to the satellite, unfavorable satellite look angles or low angles of elevation at the earth station, the received carrier-to-noise ratio has been less than 10 db. Under these conditions a frequency-following negative-feedback (FMFB) demodulator, or a variable-bandwidth dynamic-tracking demodulator (DTVB) can be used and have been shown to give satisfactory results for carrier-to-noise ratios, measured in a 25 Mc band, of only 6 db and useable results at even smaller ratios. The DTVB demodulator uses a narrowband filter, the center-frequency of which follows the instantaneous frequency of the FM carrier, the filter bandwidth being adjustable to suit the prevailing noise conditions. Figure 11–11 shows a comparison of the performance of the FMFB and DTVB demodulators with a normal FM demodulator under conditions of low carrier-to-noise ratio.

Use of Video Pre-emphasis and De-emphasis—It has generally been preferred at Goonhilly to use video pre-emphasis and de-emphasis, since this reduces the mean deviation of the frequency modulated carrier without reducing the overall signal-to-noise ratio. The smaller mean deviation has two advantages.

1. It reduces crosstalk from the video channel into the subcarrier audio channel due to residual non-linearity of the FM system

2. It improves the overall performance of the video channel under low-carrier-to-noise ratio conditions by minimizing effects due to maser bandwidth limitations.

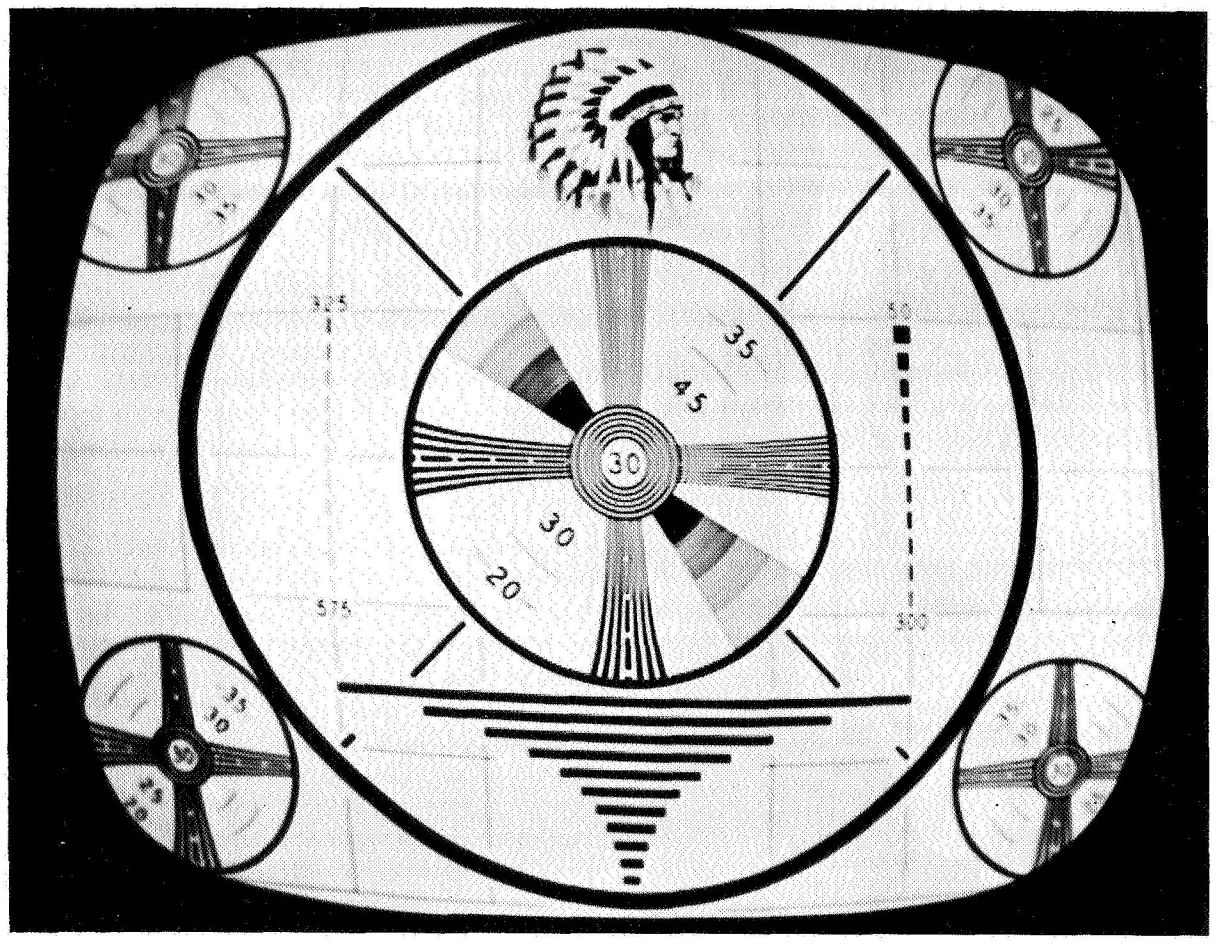


FIGURE 11–10.—Typical test card received at Goonhilly.

Video-to-Audio Crosstalk—Without video pre-emphasis the audio noise due to crosstalk from the video channel has varied from about —30 to —40 dbm (weighted), depending on picture content; with video pre-emphasis, values ranging from —44 to —48 dbm have been obtained.

Multi-Channel Telephony Transmission

Multi-channel telephony tests are especially important since the economic viability of communication satellite systems will depend to a considerable degree on their ability to accommodate large numbers of telephone channels, subdivided into both small and large blocks of channels.

The multi-channel telephony tests carried out with the Relay satellite have been of two types:

1. Two-way tests, e.g., demonstrations between telephone subscribers, using blocks of 12 or 24 channels in the baseband from 12 to 108 kc

2. One-way tests of 300 or 600 simulated telephone channels, using white noise in the baseband from 60 to 2540 kc.

12/24 Channel Two-way Telephony Tests—For two-way transmission of 12 or 24 telephone channels the transmissions from the two earth stations are spaced by 3.33 Mc, received in the satellite in separate narrow-band receivers, frequency-tripled at the intermediate frequency, and transmitted via a

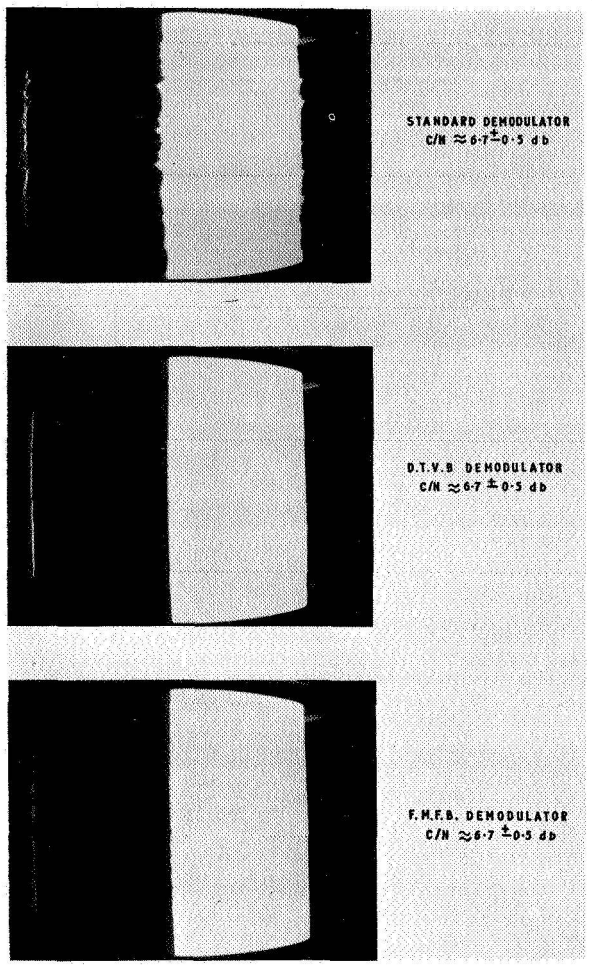


FIGURE 11–11.—Comparison of FMFB, D. T. V. B. and normal demodulators.

common broadband output amplifier, the carrier spacing then being 10 Mc. This represents a somewhat inefficient use of bandwidth, but the arrangement is convenient for experimental purposes in that only one transponder is needed in the satellite for two-way tests.

The weighted noise in the 3.1 kc wide telephony channels, measured at a point of zero relative level, ranges in general from about —55 dbm0 to —65 dbm0, when working with the larger earth stations.

The two-way telephone channels have been used for many subjective tests and demonstrations between telephone subscribers and the results have been fully comparable with other high-quality long-distance transmissions systems. In one series of tests six telephone channels in a 12-channel group were looped via the Relay satellite to provide a 45,000 mile transmission path in space, the one-way transmission delay then being about a quarter of a second. The telephone speech over this long path was of satisfactory quality and substantially free from noise and interference; the effect of the transmission delay was, however, noticeable as an occasional difficulty in interrupting the distant speaker.

One-Way Tests with 300/600 Simulated Telephone Channels—As mentioned earlier, large numbers of telephone channels carrying speech and other signals may be conveniently simulated by white noise with a uniform spectrum occupying the same frequency range as the telephone channels, e.g., 60 to 1300 kc for 300 channels and 60 to 2540 kc for 600 channels.

In order to determine the performance of a transmission system, narrow slots are inserted in the spectrum of the white-noise test signal, the slots being centered on 70, 534, 1248 and 2438 kc. The slots enable any noise, whether basic, i.e., of thermal origin, or due to intermodulation between the signals in the telephone channels, to be measured at the output of the transmission system under test. The loading of the transmission system, i.e., the RMS frequency deviation produced in a frequency-modulation system, by the multi-channel signal, can be varied by adjusting the level of the white-noise test signal at the input of the system. As the loading is increased, the level of basic noise in the slot channels at the output of the system decreases and the inter-modulation noise increases. Thus, an optimum loading condition giving the best overall signal-to-noise ratio can be determined.

Furthermore, the effect of pre-emphasis of the multi-channel signal before transmission can be readily assessed by means of a white-noise test signal. Pre-emphasis is useful in frequency modulation systems for

multi-channel telephony, since in the absence of pre-emphasis the basic noise spectrum tends to be "triangular", the signal-to-basic noise ratio in the high-frequency baseband channels being worse than in the low-frequency channels; with pre-emphasis a more uniform distribution of signal-to-noise ratio in the baseband can be obtained. However, in choosing the amount and shape of the pre-emphasis characteristic, a compromise is necessary, since too much pre-emphasis introduces excessive intermodulation noise in low-frequency telephone channels.

White-noise test signals are also useful for comparing the multi-channel telephone performance of FMFB and standard demodulators under conditions of low received carrier-to-noise ratio.

The application of these principles to simulated multi-channel telephony tests using the Relay satellite will now be discussed. Figures 11–12 and 11–13 respectively show the results of 300 and 600 channel white-noise loading test with Relay, the loading being varied about a "normal" value for the simulated multi-channel signal, the deviation produced by a test-tone of 1 mw at zero level point in a telephone channel then being 675 kc RMS. The results indicate that the "normal" deviation was nearly optimum with the single exception of the lowest channels and only under 600 channel loading. The effect of pre-emphasis was, as expected, to improve the high-frequency channels, e.g., at 2438 kc, at the expense of the low-frequency channels, e.g., at 70 kc. The pre-emphasis used was the standard characteristic for conventional radio-relay systems with a range of 8 db.

The tests have also shown that with a standard FM demodulator the system threshold occurs for a carrier-to-noise ratio, in a 25 Mc band, of about 10.5 db; with the FMFB demodulator the corresponding ratio is about 6.5 db, an improvement of 4 db.

In an operational system meeting international circuit standards, the test tone-to-weighted noise ratio would be expected to exceed 50 db, compared with the values of 46 to 56 db shown in the 300-channel tests

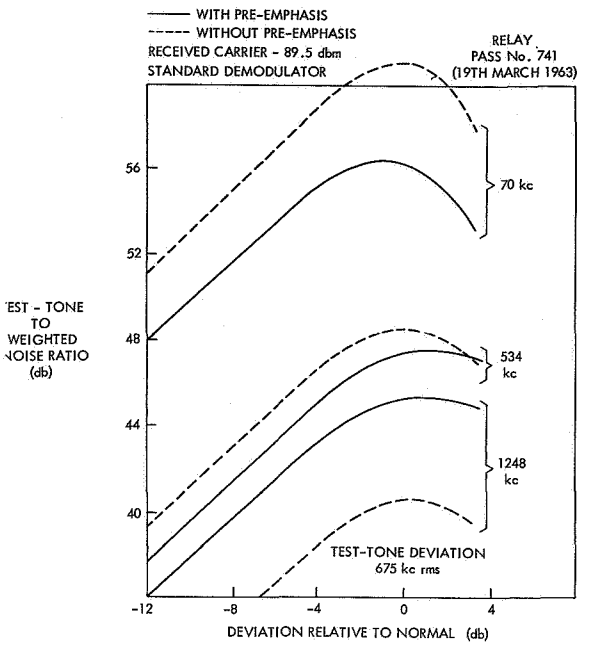


FIGURE 11–12.—300 channel white noise loading test.

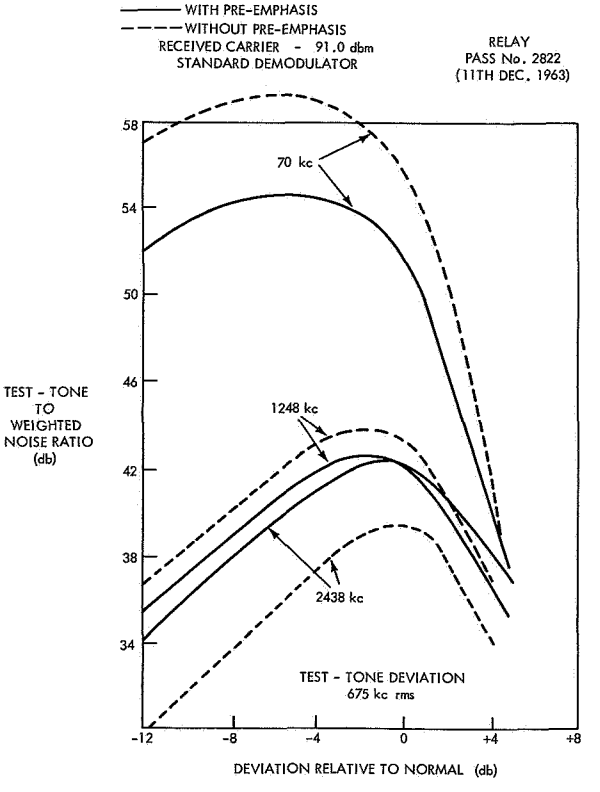


FIGURE 11–13.—600 channel white noise loading test.

and 37 to 45 db in the 600-channel tests. However, it should be borne in mind that the experimental satellite Relay does not employ significant aerial gain at the satellite; in an operational system using attitude-stabilized satellites, aerial gains of up to 15 db would be possible and would yield a corresponding improvement in signal-to-noise ratio. Furthermore, the linearity of the experimental system is by no means optimum; improved RF/IF delay equalization and more linear modulators and demodulators should be possible with further development. Given such improvements, it is expected that at least 1000 telephone channels to international circuit standards should be achievable on each radio carrier, using satellite transmitter powers of no more than a few watts. With large blocks of telephone channels, correction of Doppler frequency shifts would be necessary, as discussed later.

Facsimile Transmission

A number of tests of facsimile transmission have been made via the Relay satellites, using individual audio channels in the 12/24 channel groups and standard facsimile transmitters and receivers.

1. A double-sideband amplitude modulated audio tone, e.g., 1300 cps.
2. A frequency-modulated audio tone, e.g., with 1500 cps for white and 2300 cps for black.

In general, the amplitude-modulated transmissions are more susceptible to impairment due to noise or variations of loss in the transmission path, than are the frequency-modulated transmissions, and are thus a more searching form of test.

Figure 11–14 shows CCITT test charts transmitted via Relay, the upper chart with frequency modulation and the lower chart with amplitude modulation.

The principal defect likely to occur in facsimile transmission via a satellite link, unless special means are taken to prevent it, is "skew" of the received picture due to the gradually changing transmission delay as the path length via the satellite changes. For typical Relay orbits, which are highly, elliptical, this might be up to 10 milliseconds in a picture transmission time of 7.5 minutes, i.e., up to 2 parts in 10^5 compared with the CCITT recommended limit for skew of 1 part in 10^5.

In an operational satellite system using a medium-altitude circular equatorial orbit the rate of change of transmission delay would be less than for the Relay orbits, and would be within the CCITT limit for skew.

V. F. Telegraphy and Data Transmission

Many tests of V.F. telegraphy transmission have been made via Relay satellite, using individual audio channels in the 12/24 channel groups. Standard frequency-modulation V.F. telegraph terminal equipments were used with the following characteristics:

1. 120 cps channel spacing and a frequency deviation of ± 30 cps (CCITT standard)
2. 170 cps channel spacing and frequency deviation of ± 35 cps (U. S. standard)

The tests were in three main classes:

1. Demonstrations, in cooperation with American telegraph common carriers, between Telex subscribers in London and New York.
   Although some difficulties were encountered initially, apparently due to differences between British and American V.F. telegraph equipments, most of the demonstrations were successful and it was concluded that the satellite link did not contribute any significant adverse factor.
2. Tests over the loop London-Andover-London, using 50-baud signals and CCITT standard terminal equipment.
   On a number of passes, even when the signal-to-noise ratio was lower than would normally be expected, the start-stop distortion and the basic error rate was about the same as that of a long distance circuit provided by conventional means.
3. One-way tests between New York and London using U.S. standard terminal equipment.

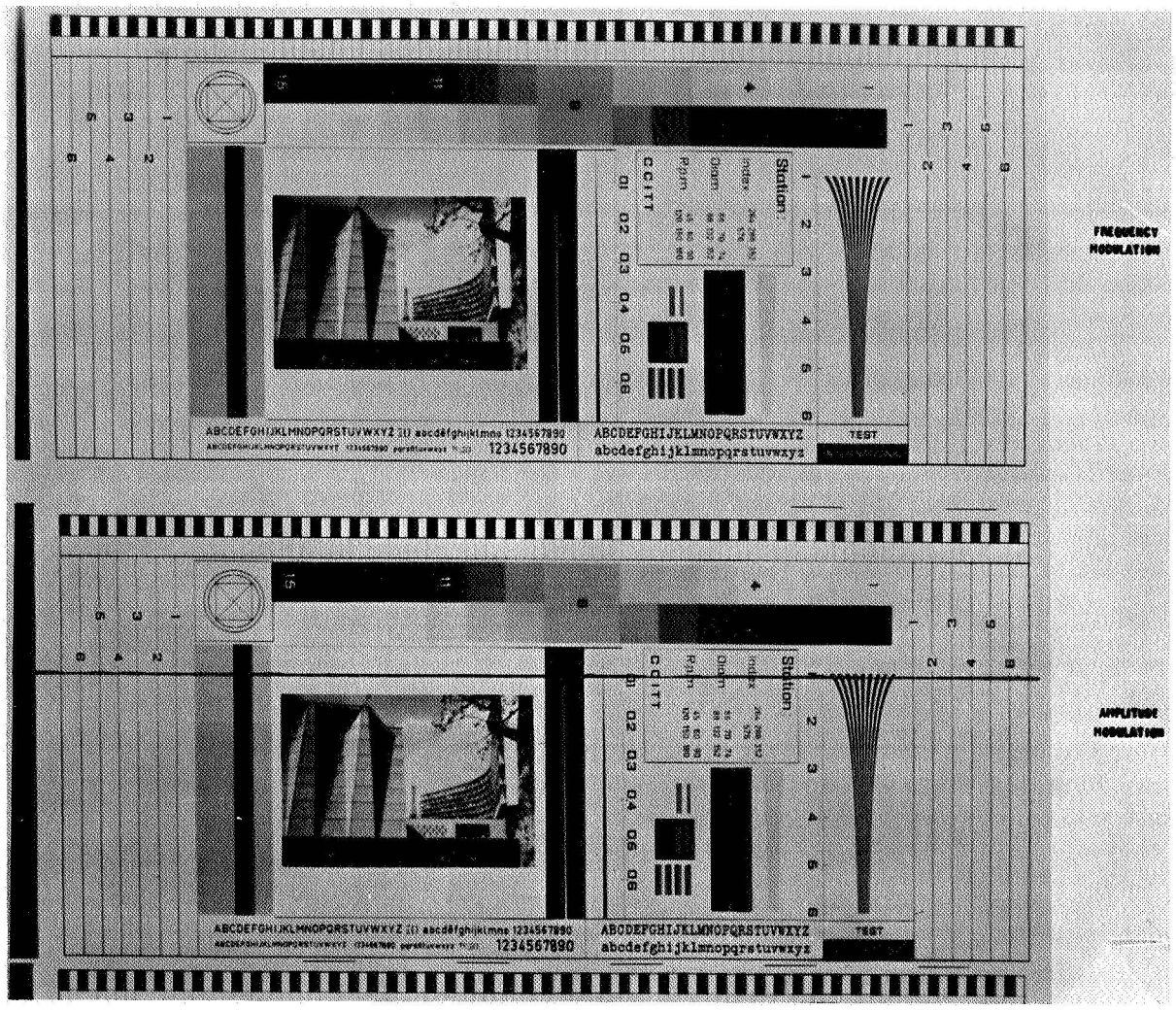


FIGURE 11–14.—Facsimile transmission, Relay I.

For the channels in the 12/24 channel groups used for the various telegraph tests, Doppler frequency shifts were less than 1 or 2 cps, and thus did not present a major source of distortion. However, it was noted that, while the gradually changing transmission time causes no difficulty for start-stop teleprinter systems, an adequate range of automatic speed correction is necessary for isochronous systems. In future operational satellite communication systems using larger blocks of channels with higher baseband frequencies than the 12/24 channel groups used in the tests it will be necessary to correct for Doppler frequency shifts, e.g., by the use of pilot reference frequency carriers, path-delay correction or by other means. Consideration will also need to be given to compensation for the change of transmission delay in switching from satellite-to-satellite, which may be up to 10 or 20 milliseconds, equivalent to one element of a 50-baud teleprinter signal, in some types of satellite system.

Conclusions

In this broad survey it has only been possible to present representative results from the considerable volume of experimental data that has been accumulated since the launch of Relay I. Nevertheless, the results obtained

from the tests and demonstrations to date have confirmed the expectation that active communication satellites could provide high-quality stable circuits for television, multichannel telephony, V.F. telegraphy and facsimile picture transmission. The very good results obtained in the tests with 600 simulated telephone channels, are particularly noteworthy. With further development it is considered that it will be possible to transmit at least a thousand telephone channels, of international circuit performance standards, on each radio carrier; communication satellites with twice or three times this capacity can be envisaged.

The propagation results obtained at Goonhilly have been particularly interesting since they have revealed the possibility of reliable operation down to elevation angles of only a few degrees. This conclusion has a marked bearing on the coverage provided by a communication satellite and the numbers of satellites required to provide worldwide coverage. It is also of interest that at no time has interference, e.g., from radio-relay systems sharing the same frequency band or from other man-made sources, been detected on the satellite link.

The practicability of tracking satellites, to within some ten minutes of arc, from orbital data predicted up to a fortnight in advance, with automatic fine correction to within a minute or two of arc, has been established.

Finally, it is believed that the results obtained at Goonhilly and the other earth stations participating in the NASA cooperative program of communication satellite tests will be of considerable value for the design of future operational systems.

Acknowledgments

The authors would like to thank their colleagues in the Post Office Engineering Department who contributed to the tests and demonstrations described in this section, and in particular the staff of the Telegraph Branch who provided information on the V.F. telegraphy and facsimile tests. Thanks are due to the BBC. and I.T.A. for their help in the television demonstrations, the staff of the cooperating earth stations at Andover and Nutley, and to NASA and members of the Ground Station Committee for their help in planning many of the tests. They also wish to acknowledge the cooperation of the American Telephone & Telegraph Company and other U.S. common-carriers in telephony, V.F. telegraphy and television transmission tests.

The permission of the Engineer-in-Chief, General Post Office, to make use of information contained in this chapter and the permission of the Institute of Electrical Engineers to reproduce it is gratefully acknowledged.

AUTHORS. *This chapter was contributed by* W. J. BRAY, F. J. D. TAYLOR, *and* R. W. WHITE *of the General Post Office, London, England.*

☆ U.S. GOVERNMENT PRINTING OFFICE: 1965—771-349

"The aeronautical and space activities of the United States shall be conducted so as to contribute . . . to the expansion of human knowledge of phenomena in the atmosphere and space. The Administration shall provide for the widest practicable and appropriate dissemination of information concerning its activities and the results thereof."

—NATIONAL AERONAUTICS AND SPACE ACT OF 1958

NASA SCIENTIFIC AND TECHNICAL PUBLICATIONS

TECHNICAL REPORTS: Scientific and technical information considered important, complete, and a lasting contribution to existing knowledge.

TECHNICAL NOTES: Information less broad in scope but nevertheless of importance as a contribution to existing knowledge.

TECHNICAL MEMORANDUMS: Information receiving limited distribution because of preliminary data, security classification, or other reasons.

CONTRACTOR REPORTS: Technical information generated in connection with a NASA contract or grant and released under NASA auspices.

TECHNICAL TRANSLATIONS: Information published in a foreign language considered to merit NASA distribution in English.

SPECIAL PUBLICATIONS: Information derived from or of value to NASA activities. Publications include conference proceedings, monographs, data compilations, handbooks, sourcebooks, and special bibliographies.

TECHNOLOGY UTILIZATION PUBLICATIONS: Information on technology used by NASA that may be of particular interest in commercial and other nonaerospace applications. Publications include Tech Briefs; Technology Utilization Reports and Notes; and Technology Surveys.

Details on the availability of these publications may be obtained from:

SCIENTIFIC AND TECHNICAL INFORMATION DIVISION

NATIONAL AERONAUTICS AND SPACE ADMINISTRATION

Washington, D.C. 20546